

The Reaction of Nitrogen with, and the Diffusion of Nitrogen in, Beta Zirconium¹

M. W. MALLETT, JACK BELLE, AND B. B. CLELAND

Battelle Memorial Institute, Columbus, Ohio

ABSTRACT

The rate of reaction of nitrogen with high-purity zirconium was determined for the temperature range of 975° to 1640°C at 1 atm pressure. The reaction followed a parabolic law and the parabolic rate constant in (ml/cm²)²/sec was calculated to be

$$k = 5.0 \times 10^3 e^{-48,000/RT}$$

where 48,000 ± 1500 cal/mole is the activation energy for the reaction. The rate of diffusion of nitrogen in beta zirconium was obtained for the temperature range of 920° to 1640°C at 1 atm pressure. Diffusion-rate calculations based on a solution of the usual diffusion equation gave a diffusion coefficient,

$$D = 1.5 \times 10^{-2} e^{-30,700/RT} \text{ cm}^2/\text{sec.}$$

The energy of activation of diffusion, 30,700 cal/mole, has a probable error of 1000 cal/mole. The calculated entropy of activation for diffusion is 3.5 cal/mole degree. The limiting solubilities of nitrogen in beta zirconium were determined from the diffusion data. The heat of solution of nitrogen in beta zirconium is 12,900 ± 500 cal/mole.

INTRODUCTION

Kinetic studies of gas-metal reactions have gained great impetus since Pilling and Bedworth (1) published their classic paper on the oxidation of metals at high temperatures. The various laws of film growth have been adequately treated in the literature (2-11) and will, therefore, not be discussed here. The purpose of the present investigation was twofold: (a) to study the over-all kinetics of the zirconium-nitrogen reaction, and (b) to study the interstitial diffusion of nitrogen in zirconium.

The reaction of nitrogen with zirconium has been described by Gulbransen and Andrew (12) in the temperature range 400° to 825°C, and by Dravnieks (13) at 860° to 1050°C. Both investigations showed that the zirconium-nitrogen reaction follows the parabolic law. Rates of diffusion of nitrogen in beta zirconium with a high hafnium content (1.8-2.2%) were reported in a paper from this laboratory (14). When the purer zirconium (0.015% hafnium) became available, it was decided to repeat the diffusion studies in conjunction with kinetic studies of the zirconium-nitrogen reaction at high temperatures.

EXPERIMENTAL

Method

To determine the rate of reaction between zirconium and nitrogen, the rate of consumption of

nitrogen by a specimen of metal at high temperature was measured. The apparatus used was a modified Sieverts type, consisting of a Vycor reaction tube, sealed by means of a greased, ground-glass ball joint to a glass manometer system, which was connected through stopcocks to a vacuum system and a gas buret. The system was evacuated by a 2-stage glass mercury-diffusion pump backed by a mechanical pump. A cold trap, cooled with a dry ice-acetone mixture, was placed between the diffusion pump and the reaction system. The sample was heated by high-frequency induction, using a 2-kw Lepel converter. The temperature was controlled to ± 5°C by adjustment of a V20 Variac in the converter input line and by use of an external variable resistance connected across the power leads in parallel with the work coil.

The zirconium specimens were machined cylinders about 4 cm long by 0.7 cm in diameter. A hole was drilled through the sample about 1/8 in. from one end, using a No. 46 drill. A graphite tube, which extended about 1/16 in. on either side of the sample, was inserted in the drilled hole. The tube served to prevent interaction between the zirconium sample and the thermocouple. A platinum-platinum + 10% rhodium thermocouple was threaded through the graphite tubing, and the butt-welded bead was located at the center of the sample diameter. The thermocouple ends were soft soldered to similar leads which were permanently sealed in the reaction-tube cap. The thermocouple was used both to measure the sample temperature and to suspend the sample in the reaction tube.

It was found necessary to correct the thermo-

¹ Manuscript received June 18, 1953. This paper was prepared for delivery before the Wrightsville Beach Meeting, September 13 to 16, 1953. Work done under Contract No. W-7405-eng-92 for the United States Atomic Energy Commission.

couple temperature readings because, in using induction heating with the specimen suspended by the thermocouple, the thermocouple wires conducted heat from the hot junction, causing the readings to be low. This correction was made for work in an atmosphere of nitrogen in the temperature range 975° to 1640°C. The thermocouple was calibrated against a Pyro optical pyrometer² sighted on a hohlraum in the sample through a Pyrex window. The differences in temperatures between the thermocouple and the calibrated pyrometer readings were considerable. At 975°C, the thermocouple reading was 75 degrees low, and at 1650°C, the thermocouple reading was 140 degrees low.

The specimens were abraded with kerosene-soaked 240-, 400-, and 600-grit silicon carbide papers and washed in successive baths of naphtha, ether, and acetone. Care was taken to keep the specimens under acetone until they were placed in the reaction tube.

With the specimen at the desired temperature, purified nitrogen was admitted from a gas buret. Further nitrogen additions were made, as needed, to keep the pressure at 500 to 760 mm. Pressure measurements were made every 2 min at the start of each run and at longer time intervals as the reaction rate decreased. Nitrogen, present in the apparatus as a gas phase, was determined from pressure measurements on a full-length open-end mercury manometer and the calculated dead space of the system. The difference between the amount of nitrogen added and that remaining in the gas phase was the amount absorbed by the specimen.

To convert total quantity reacted to quantity per unit area, the geometric dimensions of the specimen were used. Upon completion of a run in which nitrogen was reacted with zirconium for a predetermined time, the system was evacuated, and the specimen cooled rapidly. Rapid cooling was necessary because of the diffusion studies. This was easily accomplished since the heating was done by induction. When the high-frequency converter was shut off, the temperature fell from 1000° to about 400°C in 2 min.

After a reaction-rate run was completed, lengths equal to the radius of the cylindrical sample were cut from the ends of the specimen and discarded. The rest of the sample was machined radially into several layers of equal weight which were then analyzed for nitrogen content by a modified Kjeldahl method. The concentration in the surface layer, including the alpha and gamma layers, was

²The pyrometer was calibrated for reading through the Pyrex window over a range of temperature up to 1800°C against a ribbon-filament tungsten lamp standardized at 100-degree intervals by the National Bureau of Standards.

not used in the calculations. The remaining layers contained only nitrogen which had diffused as solute through the beta zirconium core. Diffusion coefficients were determined by the graphical method (14), using the average nitrogen concentrations of each layer, the average radius of the layers, and the time of diffusion.

Materials

The pure zirconium used in these experiments was iodide crystal bar produced by the de Boer process, double arc melted, and cold rolled into a $\frac{3}{8}$ -in. diameter rod. Test specimens were machined from this rod. Impurities in the zirconium were determined by spectrographic, chemical, and vacuum-fusion analyses. The weight percentages of the principal impurities detected were: iron, 0.025; hafnium, 0.015; silicon, 0.01; tin, 0.01; oxygen, 0.005; nitrogen, 0.001; and hydrogen, 0.0005.

The nitrogen used was prepared by passing pre-purified tank nitrogen (The Matheson Company) over zirconium turnings, heated at 850°C. The gas was then dried by passing through a dry ice-acetone cold trap. Mass spectrographic analysis showed that the only measurable impurity was 0.2% argon.

SURFACE REACTION

The rate of the surface reaction of zirconium with nitrogen was measured in the range 975° to 1640°C at 1 atm pressure. Adherent golden-yellow films of ZrN were observed throughout the temperature range in agreement with the observation of Dravnieks (13). Results of the measurements for several runs are shown in Fig. 1 and 2. The square of the amounts (ml STP) of nitrogen consumed per unit surface area of the metal are plotted against time. It was found that, in all cases, the reaction conformed to the parabolic rate law, $w^2 = kt$, with occasional deviations in the direction of a slower initial rate. This initial slower rate was attributed to a contaminating layer of oxide. This effect was less evident at higher temperatures because of the solution of the oxide film in the metal. The induction period varied from 0 to 20 min at temperatures 975° to 1305°C and from 0 to 5 min at temperatures 1305° to 1640°C. Also, the slight thermal fluctuations of the dead space, both in the reaction zone and the room-temperature parts of the apparatus, may result in slight deviations in measurements of the amount of nitrogen absorbed. Again, such deviations tend to have a more marked effect when the volumes of gas absorbed are relatively small, as is the case in experiments carried out below 1100°C.

A plot of the logarithm of the amount of nitrogen consumed per unit surface area vs. the logarithm of

time should give a straight line with a slope equal to 0.5 if the parabolic law is obeyed. As can be seen from Table I, such behavior was observed.

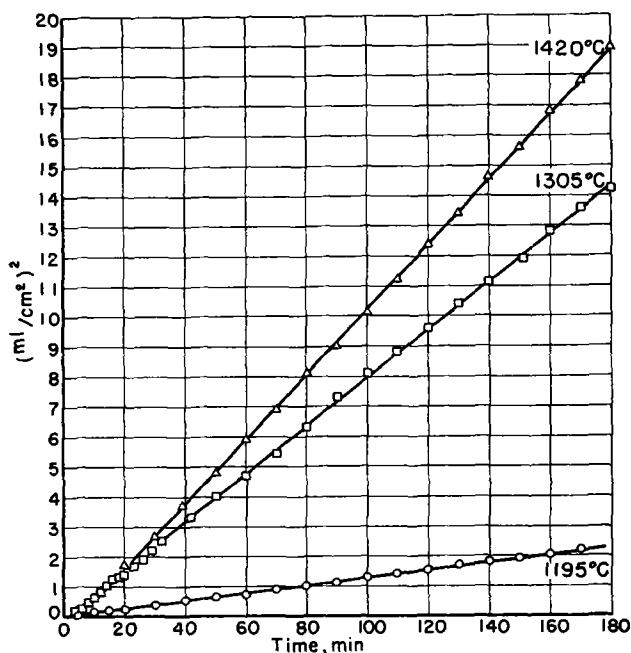


FIG. 1. Reaction of zirconium with nitrogen (ml N_2 consumed per cm^2 metal surface) 2 vs. time.

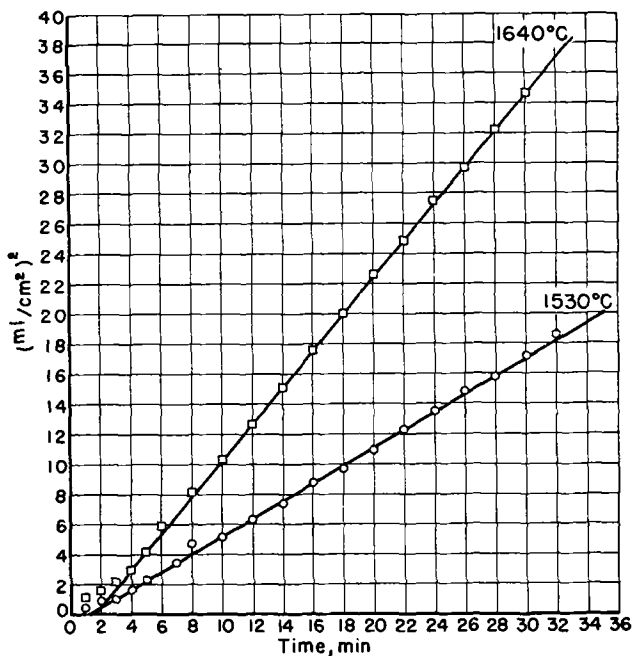


FIG. 2. Reaction of zirconium with nitrogen (ml N_2 consumed per cm^2 metal surface) 2 vs. time.

The rate constants (k) calculated from the various plots and the slopes of the log-log plots are given in Table I, together with the temperature and the length of each run. The reproducibility of the measurements is evident. In most cases, there

was a variation of about 25% in the constants. The variation between runs at constant temperature

TABLE I. Parabolic rate constants for the reaction of zirconium with nitrogen

Temp, $^{\circ}\text{C} \pm 5^{\circ}$	Length of run, min	Rate constant (k), $(\text{ml}/\text{cm}^2)^2/\text{sec}$	Slope of log-log plot
975	300	2.0×10^{-6}	0.47
1030	300	5.4×10^{-5}	0.55
1085	180	1.7×10^{-4}	0.54
1085	180	5.9×10^{-5}	0.61
1085	300	1.1×10^{-4}	0.60
1140	240	1.2×10^{-4}	0.62
1195	170	2.1×10^{-4}	0.51
1195	180	3.2×10^{-4}	0.56
1195	180	7.0×10^{-4}	0.55
1305	180	1.3×10^{-3}	0.52
1305	120	7.5×10^{-4}	0.57
1420	180	1.8×10^{-3}	0.53
1420	180	3.2×10^{-3}	0.48
1420	60	1.7×10^{-3}	0.54
1475	60	7.2×10^{-3}	0.54
1530	180	7.1×10^{-3}	0.48
1530	60	1.1×10^{-2}	0.51
1530	32	9.7×10^{-3}	0.54
1640	30	2.0×10^{-2}	0.55

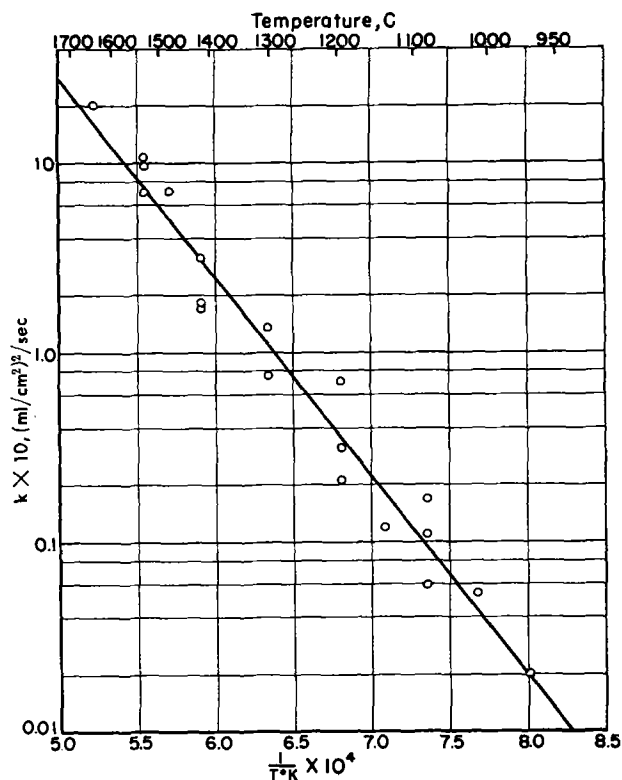


FIG. 3. The zirconium-nitrogen reaction—variation of reaction rate constant with temperature.

may be due, in part, to differences in the surface roughness from one sample to another.

Fig. 3 is a plot of $\log k$ vs. $1/T$. The equation of the best straight line through the points from 975 $^{\circ}$

to 1640°C was determined by the method of least squares; and the experimental energy of activation and the frequency factor were calculated by the Arrhenius-type equation, $k = Ae^{-Q/RT}$. The energy of activation for the low-hafnium pure zirconium is $48,000 \pm 1500$ cal/mole, as compared with the value of 52,000 cal/mole obtained by Dravnieks (13) for the high-hafnium zirconium. The rate constant in $(\text{ml}/\text{cm}^2)^2/\text{sec}$ is $k = 5.0 \times 10^3 e^{-48,000/RT}$.

DIFFUSION WITHIN THE METAL

As defined previously (14), c_0 is the constant concentration maintained at the surface and a is the radius of the cylinder. The values Dt/a^2 and c_0 , and the diffusion coefficients obtained from them graphically (14), are listed in Table II. The temperature variation of the diffusion coefficient can be evaluated

TABLE II. Diffusion coefficients of nitrogen in zirconium

Time, min	Temp, °C ± 5°	c_0 , wt %	Dt/a^2	$D \times 10^7$, cm ² /sec
600	920	0.13	0.013	0.55
300	975	0.12	0.008	0.72
300	1030	0.21	0.015	1.3
180	1085	0.22	0.01	1.5
300	1085	0.28	0.015	1.3
240	1140	0.21	0.017	1.9
170	1195	0.27	0.024	3.4
180	1195	0.30	0.02	3.1
180	1195	0.34	0.042	6.3
127	1305	0.41	0.042	7.7
180	1305	0.47	0.09	11.0
120	1305	0.44	0.028	6.3
60	1420	0.47	0.035	14.0
180	1420	0.56	0.15	17.0
60	1475	0.72	0.055	25.0
60	1530	0.82	0.10	35.0
32	1530	0.70	0.055	39.0
30	1640	0.92	0.055	51.0

by the equation, $D_\beta = D_0 e^{-Q/RT}$. Fig. 4 is a plot of $\log D_\beta$ vs. $1/T$ for the low-hafnium zirconium. The equation of the best straight line through the points from 920° to 1640°C was determined by the method of least squares. The experimental energy of activation is $30,700 \pm 1000$ cal/mole, and the diffusion coefficient in cm²/sec is $1.5 \times 10^{-2} e^{-30,700/RT}$. This is in fair agreement with the earlier value reported, $3 \times 10^{-2} e^{-33,600/RT}$, from this laboratory (14) on high-hafnium zirconium.

The entropy of activation for diffusion can be estimated from the experimental value of D_0 and the approximation suggested by Wert and Zener (15). Nitrogen diffusion through beta zirconium is assumed to be interstitial. Furthermore, the assumption is made that as the solute atom moves from one interstitial position to an adjacent interstitial position its potential energy varies in a simple sinusoidal manner. Then, from Wert and

Zener (15), the vibration frequency γ is given by the approximation

$$\gamma = \left(\frac{E}{2m\lambda^2} \right)^{1/2},$$

where E is assumed approximately equal to the energy of activation, m is the mass of the solute atom, and λ is the distance between the interstitial positions. From the expression for *bcc* lattices, $D_0 = \frac{1}{6} a_0^2 \nu \exp(\Delta S/R)$ (a_0 , the lattice constant = 3.62 Å for beta zirconium), ΔS can be evaluated. λ is assumed to be $a_0/2$ (15) and ΔS was calculated to be 3.5 cal/mole deg in agreement with Zener's prediction that a low positive value for the entropy

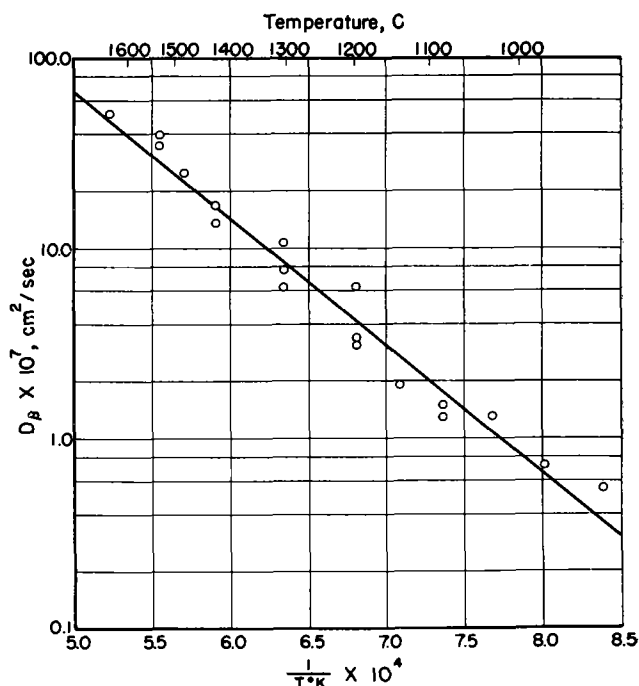


FIG. 4. Diffusion of nitrogen in zirconium—variation of diffusion coefficient with temperature.

of activation suggests that diffusion occurs through the lattice and not through grain boundaries or other short-circuiting paths. A similar calculation was made for the diffusion of nitrogen in beta titanium. Using the results of Wasilewski (17), $D_\beta = 3.5 \times 10^{-2} e^{-33,800/RT}$, the entropy of activation for diffusion was calculated to be 5.3 cal/mole deg. However, for the diffusion of nitrogen in thorium, data from this laboratory (18) indicate that a negative entropy of activation for diffusion is also possible. From $D = 2.1 \times 10^{-3} e^{-22,500/RT}$, ΔS was calculated to be -4.4 cal/mole deg.

SOLUBILITY OF NITROGEN IN BETA ZIRCONIUM

As pointed out previously (14), the solubility limit of nitrogen in beta zirconium is the concentra-

tion just inside the interface between the beta and alpha phases. The calculated c_0 is, then, the approximate limiting solubility of nitrogen in beta zirconium at the given temperature. The calculated c_0 's are listed in Table II and a plot of the c_0 values is given

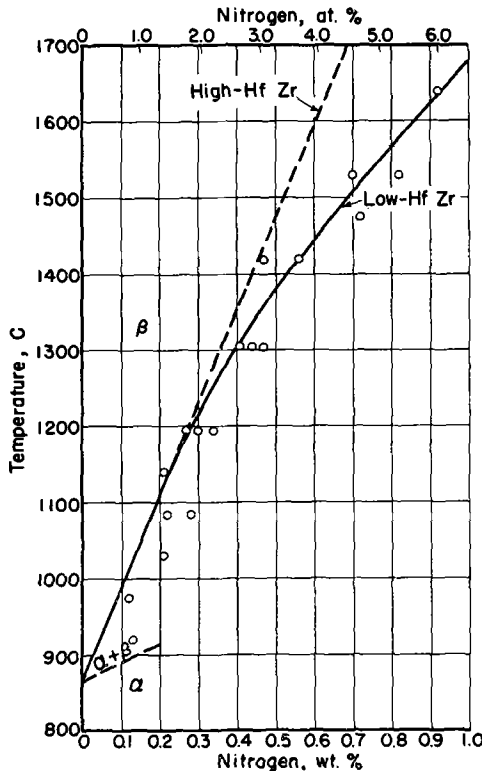


FIG. 5. Solubility limits (c_0 's) of nitrogen in beta zirconium

in Fig. 5. A smooth curve, which is considered the approximate boundary between the beta and alpha-plus-beta phases, was drawn through these points. The solubility limit previously (14) determined for high-hafnium zirconium is also shown. The dashed

line is suggested to indicate the possible boundary between the alpha and alpha-plus-beta phases.

The solubility in weight per cent nitrogen in zirconium over the temperature range 920° to 1640°C can be expressed as

$$\log c_0 \text{ (in wt \%)} = -\frac{2810}{T} + 1.42.$$

The heat of solution for nitrogen in zirconium obtained from this equation is $\Delta H = 12,900 \pm 500$ cal/mole.

Any discussion of this paper will appear in a Discussion Section, to be published in the December 1954 issue of the JOURNAL.

REFERENCES

1. N. B. PILLING AND R. E. BEDWORTH, *J. Inst. Metals*, **29**, 529 (1923).
2. C. WAGNER, *Z. physik. Chem.*, **B21**, 25 (1933).
3. T. P. HOAR AND L. E. PRICE, *Trans. Faraday Soc.*, **34**, 867 (1938).
4. J. BARDEEN, W. H. BRATTAIN, AND W. SHOCKLEY, *J. Chem. Phys.*, **14**, 714 (1946).
5. D. CUBICCIOTTI, *J. Am. Chem. Soc.*, **72**, 2084 (1950).
6. E. A. GULBRANSEN, *Trans. Electrochem. Soc.*, **81**, 327 (1942).
7. E. A. GULBRANSEN AND K. F. ANDREW, *This Journal*, **96**, 364 (1949).
8. H. A. MILEY, *Trans. Electrochem. Soc.*, **81**, 391 (1942).
9. N. F. MOTT, *Trans. Faraday Soc.*, **36**, 472 (1940).
10. N. F. MOTT, *Trans. Faraday Soc.*, **43**, 429 (1947).
11. J. T. WABER, *J. Chem. Phys.*, **20**, 734 (1952).
12. E. A. GULBRANSEN AND K. F. ANDREW, *J. Metals*, **1**, 515 (1949).
13. A. DRAVNIKIS, *J. Am. Chem. Soc.*, **72**, 3568 (1950).
14. M. W. MALLETT, E. M. BAROODY, H. R. NELSON, AND C. A. PAPP, *This Journal*, **100**, 103 (1953).
15. C. WERT AND C. ZENER, *Phys. Rev.*, **76**, 1169 (1949).
16. C. ZENER, *J. Applied Phys.*, **22**, 372 (1951).
17. R. J. WASILEWSKI, Private communication.
18. A. GERDS AND M. W. MALLETT, To be published.

The Reaction of Silver Alloys with Sulfur in Mineral Oil

II. Examination of Reaction Films and Mechanism of Reaction¹

H. O. SPAUSCHUS, R. W. HARDT, AND R. T. FOLEY

Materials and Process Laboratory, General Electric Company, Pittsfield, Massachusetts

ABSTRACT

Reaction product films grown on silver alloys by reaction with sulfur in mineral oil were examined by spectroscopic, X-ray, and electron-diffraction techniques. Interpretation of the results leads to a mechanism of reaction in which the rate-determining step during the steady phase is diffusion through a strained interfacial zone of constant thickness, comprised of the sulfide of the alloying element dissolved in β -silver sulfide, altering the number of normal lattice defects. The sulfide of thallium, which, unlike all the other alloying elements, yields a sulfide with a cation/anion ratio similar to silver sulfide, is exceptional.

INTRODUCTION

A study of the kinetics of the reaction between many silver alloys and sulfur dissolved in mineral oil demonstrates that the solution of an alloying element in silver causes a retardation in the steady-state reaction rate (1). Generally speaking, the whole reaction may be broken down into two phases: the initial reaction similar to that with silver alone; the later reaction differs from that of silver (except for silver-thallium alloys) and follows a linear weight gain-time pattern. The linear relationship which describes this later steady state seems not to be particularly dependent on the chemical nature of the alloying element dissolved in silver.

To explain this unusual behavior, an understanding of how the composition and structure of the reaction films formed on silver alloys differ from that of "normal silver sulfide," is required. Of particular concern is the final disposition of the alloying element.

The purpose of this paper is to report the analyses of these tarnish films, and to formulate a mechanism of reaction.

EXPERIMENTAL

Spectrographic examination of films.—Samples of stripped sulfide films were diluted with nine parts of a buffer composed of equal parts of barium nitrate and ammonium sulfate and analyzed with a Zeiss Medium Quartz Spectrograph. Quantitative estimations of the amounts of alloying elements in the films were made by comparison with standards prepared with silver nitrate and salts of the alloying elements (usually the nitrate). The thicknesses of the stripped films varied from 10,000–50,000 Å. These are described as "thick" films in the discussion below.

¹ Manuscript received February 27, 1953. This paper was prepared for delivery before the Wrightsville Beach Meeting, September 13 to 16, 1953.

X-ray diffraction examination.—"Thick" films were stripped, powdered, and analyzed by the powder method with a General Electric XRD-1 instrument employing a cylindrical camera and copper or cobalt radiations.

Electron diffraction examination.—The electron diffraction analyses were made with a General Electric electron diffraction instrument. Both "thin" films (1000–4000 Å) and "thick" films were examined on the alloy panels by a reflection technique. "Very thin" films (less than 1000 Å) were also stripped and examined by transmission.

Film stripping technique.—A strip of a silver alloy which had reacted with sulfur was made the anode in a solution of 0.8N nitric acid solution at room temperature and electrolyzed for 5 min with a current density of 4 amp/dm². The strip was transferred to warm dilute nitric acid solution, rinsed, and then transferred to water. In water, the film was shaken loose, rinsed with water, then acetone, and finally dried.

A separate sample of the same silver alloy was given the same electrolytic treatment to determine whether objectionable anodic films were formed by this treatment.

RESULTS

Spectrographic examination.—The results from the spectrographic analyses of the reaction films are summarized in Table I. The sulfide films grown on the silver alloys of aluminum, magnesium, and manganese contain only a trace of the alloying element. However, an appreciable amount of the alloying element was found in the films grown on alloys of antimony, cadmium, indium, thallium, and zinc. It is significant that in every case the alloying element was evident. It was not possible to get reproducible values from a single sample of the film grown on the cadmium alloy. Deviations of $\pm 40\%$

from the 7.0% value were observed. This non-uniformity indicates that there were local concentrations of cadmium in the film, some regions being richer in cadmium than others. The precision of the results reported for the other films is better, being of the order of $\pm 10\%$, with $\pm 20\%$ for the zinc and $\pm 25\%$ for the indium alloy.

X-ray diffraction examination.—The x-ray examination of the films from silver and silver alloys gave only the pattern for β -silver sulfide, which has been assigned a monoclinic (pseudo-orthorhombic) structure by Ramsdell (2). The pattern for the film from the 9.6% Zn alloy was an exception in that extra lines were observed which were not identifiable, e.g., not ZnS or ZnO. None of the other patterns gave any indication of the presence of alloying element, the sulfide of the alloying element, or any compound of the alloying element in these films.

Electron diffraction examination.—Both thin and thick films were examined by electron diffraction

TABLE I. Spectrographic examination of films

Alloy from which film was stripped	Emission line (or lines) used	Estimated amount of alloying element present in film
%		%
Pure Ag	2721.8	0
4.0 Al-Ag	2568.0	0.015
1.8 Sb-Ag	2877.9	0.45
30.0 Cd-Ag	2265.0	7.0
11.8 In-Ag	2710.3	0.4
0.4 Mg-Ag	2776.7, 2779.8	0.04
4.3 Mn-Ag	2605.7	0.01
2.9 Tl-Ag	2918.3, 3229.8	0.9, 0.6
5.9 Tl-Ag	2918.3, 3229.8	0.95, 0.7
9.6 Zn	3302.9, 3345.0	0.5

using the reflection technique. Only patterns for β -silver sulfide were observed. However, the interplanar spaces in the patterns obtained from some of the films deviated from the X-ray spacings for pure β -silver sulfide. These deviations are believed to be indicative of distortions in the silver sulfide lattice. To make a quantitative estimation of this distortion, a "deviation" was calculated by subtracting the X-ray spacing from the electron diffraction spacing for each line. The deviations for all the lines in a given pattern were then averaged and this "average deviation" is given in Table II.

It is apparent that the distortion is, in general, not only greater for the thin films, but decreases or disappears as the film grows outward. The maximum error involved in the measurement of the deviation is less than 0.01 \AA per line, so the deviation for the thin films is considerably more than that possible by an accumulation of experimental errors. On the other hand, most of the deviations observed in the

thick films could be accounted for by experimental error.

Films on several high alloys gave greater distortions. The deviation observed with the sulfide film from pure silver was quite small and of the order of experimental error in the measurement.

Further measurements on films of the order of thickness of 500 \AA which had been stripped from the basis metal were made by a transmission

TABLE II. Film distortions from deflection measurements

Basis alloy composition	Average deviation ($\text{\AA} \times 10^2$)
Thin films	
%	
24.4 Zn-Ag	+3.86
15.3 In-Ag	+3.75
0.8 Mg-Ag	+2.67
1.2 Pb-Ag	+2.58
1.6 Al-Ag	+2.40
19.8 Cd-Ag	+2.17
Ag	+0.75, +0.91
3.2 In-Ag	+0.71
2.9 Tl-Ag	+0.60
5.1 Zn-Ag	+0.08
5.9 Tl-Ag	0.00
9.4 In-Ag	-0.41
Thick films	
12.6 Zn-Ag	+1.79
1.2 Pb-Ag	+1.00
Ag	+0.47
0.8 Mg-Ag	+0.40
2.1 Sn-Ag	+0.33
5.1 Zn-Ag	+0.16
1.6 Al-Ag	-0.13
15.3 In-Ag	-0.42
3.2 In-Ag	-0.47

TABLE III. Film distortions from transmission measurements

Basis alloy composition	Average deviation ($\text{\AA} \times 10^2$)
%	
Ag	-0.06
3.2 In-Ag	-0.09
30.0 Cd-Ag	-0.92
12.6 Zn-Ag	-1.60

technique. Only the pattern for silver sulfide was recorded. The measured distortion is reported in Table III, and it is significant that the distortion present in the film when the film was attached to the alloy disappeared, or the deviation shifted in a negative direction.

DISCUSSION

The spectroscopic examination of the films showed that sulfide films grown on silver alloys of

cadmium, antimony, indium, thallium, and zinc contained an appreciable quantity of the alloying element. The films grown on aluminum, magnesium, and manganese alloys contained only a trace of the alloying element. Nevertheless, the X-ray diffraction analysis in all cases indicated only the pattern for β -silver sulfide. This was confirmed by electron diffraction examination both with a reflection technique and a transmission technique. Therefore, the conclusion was drawn that when alloying elements are present in the film they exist in the form of their sulfides dissolved in β -silver sulfide.

This conclusion is limited by the fact that all but the reflection electron diffraction measurements were made on stripped films, i.e., the system studied had been disturbed before the actual measurements. An examination of the surface (metallic) of the alloy after reaction would contribute greatly to our knowledge of the system. We would be able to determine whether or not there was a concentration of the alloying element on the surface of the alloy hindering reaction through the formation of a diffusion barrier. But, here again, to examine the reacted surface the sulfide film must be stripped. In so doing we would alter completely the system we would study. Another limitation imposed is that of the lack of sensitivity of diffraction measurements to minor constituents in mixtures. The electron diffraction apparatus is probably the best instrument now available for the study of surface reactions. However, various experimenters claim that a concentration of less than 5% would remain undetected in a mixture. The system here under investigation, by virtue of the well-formed silver sulfide crystals, is particularly suited for examination by diffraction techniques.

The electron diffraction analyses show that usually the film just formed is distorted. As the film grows the extent of distortion decreases and largely disappears as the thick film is attained. If the film is stripped from the silver alloy, the distortion is relieved or the positive deviation is shifted to a negative value.

The thick films appear similar in structure to that of "normal" silver sulfide which would suggest that the cause of the observed steady-state rate is located at the metal-film interface.

Mechanism of Reaction

A postulated mechanism of reaction of the silver alloys with sulfur must account, first, for the rapid reaction during the early stage of the reaction life, and, second, for the decreased rate exhibited during the steady-state phase which constitutes the greater part of the reaction. The behavior of the

silver-thallium alloys, which differ from the main body of alloys, must also be explained.

The analyses of the reaction films indicate that the sulfide of the alloying element exists in the films in solution in the silver sulfide lattice. There is a concentration of the sulfide of the alloying element near the interface. This is the interpretation placed on the distortion observed in the sulfide lattice in the very thin film, but not in the thick film. This distortion is also associated with the attachment of the sulfide film to the alloy surface as shown by the relief of the distortion when the very thin films are removed from their metallic support.

More weight is given to the results obtained from the electron diffraction examination because, in this case, we dealt with an undisturbed system.

Thus, during the first rapid stage of the reaction, an interfacial layer comprised of the alloying element sulfide dissolved in β -silver sulfide is developed, giving a strained lattice. The rate-determining step during this stage is the diffusion of dissolved sulfur to the alloy strip surface. This distorted zone achieves a given thickness for a specific alloy. From then on the growth is slow, with the rate-determining step being diffusion through this interfacial zone.

The process by which silver sulfide grows has been demonstrated to be one of diffusion of silver cations and electrons through a film which contains cation vacancies, the gradient of which vacancies governs the diffusion (3). Solution of the sulfide of the alloying element in the silver sulfide lattice changes the number of lattice defects. All of the sulfides of lower cation/anion ratio than Ag_2S decrease the rate of reaction after about 100 hr. These are Al_2S_3 , Sb_2S_3 , PbS , CdS , In_2S_3 , MgS , PdS , MnS , SnS , and ZnS . Films grown on silver-thallium alloys behave much like those grown on unalloyed silver. The thallium sulfide, Tl_2S , with the same cation/anion ratio as Ag_2S , enters into the Ag_2S lattice without disturbing it and also without affecting the steady-state rate.

The distortion observed in the majority of the films is more than that to be expected from the growth of a sulfide lattice with certain lattice spacings on an alloy with different lattice spacings, since such distortion was not observed in thin films grown on thallium alloys.

The rate-determining steps for the two phases of the reaction are: (a) the diffusion of sulfur in solution to the metallic strip; and (b) the diffusion of silver cations and electrons through an interfacial zone of constant thickness. The interfacial zone is comprised of an alloying element dissolved in silver sulfide.

The reaction rates are of an order accountable for by hindered diffusion through silver sulfide. However, experimental work reported here does not discount the formation of a barrier zone of alloying element at the interface between the metallic strip and the film. As suggested above, the presence of this zone would be difficult to prove experimentally. The possibility of the alloying element remaining in solution in silver and diffusing backward as a significant step in the mechanism is unlikely.

The expected rate of diffusion of many of these alloying elements in silver may be approximated with data collected by Jost (4). The observed rate of reaction is 10^3 – 10^5 times that expected by this process.

On the other hand, the extrapolated diffusion rates for silver in lead and aluminum are sufficiently rapid to account for the rates of reaction with sulfur.

Any discussion of this paper will appear in a Discussion Section, to be published in the December 1954 issue of the JOURNAL.

REFERENCES

1. R. T. FOLEY, M. J. BOLTON, AND W. MORRILL, *J. Electrochem. Soc.*, **100**, 538 (1953).
2. L. S. RAMSDELL, *Am. Mineralogist*, **28**, 401 (1943).
3. C. WAGNER, *Z. physik. Chem.*, **21B**, 25 (1933); in "Atom Movements," p. 153, American Society for Metals, Cleveland, Ohio (1951).
4. W. JOST, "Diffusion, In Solids, Liquids, Gases," Academic Press Inc., New York (1952).

The Rate of Dissolution and the Passivation of Titanium in Acids with Ammonium Fluoride Added¹

M. E. STRAUMANIS AND C. B. GILL

University of Missouri, School of Mines and Metallurgy, Department of Metallurgy, Rolla, Missouri

ABSTRACT

Although Ti is very resistant to the action of all acids, except HCl, H₂SO₄, and especially HF, its resistance breaks down if soluble fluorides are added to the acidic solutions. It was found that the HF liberated by acids partially dissolves the protective film that is always present on the surface of Ti. Hydrogen ions then are discharged at the local cathodes, which are now exposed to the acids through the pores of the film. In agreement with this concept, the rate of dissolution of Ti increases only slightly with increased concentration of a strong acid (HCl, H₂SO₄), at a constant concentration of NH₄F, but it increases greatly with increased concentration of NH₄F (at a constant concentration of the strong acid).

If the concentration of NH₄F is increased still further, the Ti becomes passive, and simultaneously its potential decreases to -0.94 volt (hydrogen scale). This passivation could be explained by formation of a partial salt film on the surface of the dissolving Ti, and by increase of hydrogen overvoltage on local cathodes, because of the NH₄F present.

INTRODUCTION

Titanium dissolves readily in pure hydrofluoric acid, slowly in hydrochloric acid, and more slowly in sulfuric acid (1, 2). In all other acids titanium is nearly insoluble, but it reacts with many of these acids if some water-soluble fluoride is added to the acid. In the presence of such a fluoride, titanium is attacked by strong acids such as nitric, hydrobromic, hydroiodic, and perchloric; acids of medium strength (phosphoric); and even by weak dilute acids such as formic and acetic acids. Trifluoroacetic acid also reacts violently with titanium if the acid is diluted with water.

The intention of this investigation was to collect data concerning the proceedings and the rate of dissolution processes in the presence of soluble fluorides, in order to get some insight into the mechanism of this kind of dissolution.

The experiments were made with Remington Arms 1.6 mm thick rolled titanium sheet of a purity of ~97.6% (1). Squares of 1 cm² surface area were cut, imbedded in Bakelite, and without any heat treatment, only 1 cm² of the titanium plates was exposed to the action of the acid. The rate of dissolution was computed from the volume of hydrogen evolved. Purest NH₄F was added to the solutions. The experimental arrangement was the same

as described previously (1), and duplicate sets of experiments were made in each instance.

RATE OF DISSOLUTION OF TITANIUM AT A CONSTANT CONCENTRATION OF AMMONIUM FLUORIDE

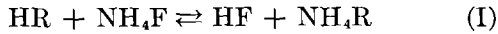
In Fig. 1, the rate of dissolution of Remington Arms titanium in hydrochloric and sulfuric acids of increasing concentrations at a constant concentration of ammonium fluoride (0.05M) is shown.

The lowest curve shows the rate of dissolution of Ti in purest sulfuric acid. The rate of dissolution increases if ammonium fluoride is added, but increases only slightly, in all cases, with the concentration of the acid, even though 10N hydrochloric acid is already a nearly concentrated acid. Each experimental point is the mean value of two experiments, and represents the maximum rates of dissolution. The dissolution usually began with a short period (or no period) of induction, then came a flat maximum, and finally the rate decreased slowly. The duration of each run was from 4-10 hr. As compared with the rate of dissolution in purest sulfuric acid, the rate is greatly increased by the presence of ammonium fluoride, and it is still higher with the dissolution in hydrochloric acid. However, the increase of the rate with the concentration of the acids is nearly the same in both cases. This is proved by the slopes of the straight portions of the curves, which are very nearly equal.

Some of the experiments were continued in the acids over a period of from 50-70 hr, in order to find out whether or not the rate of dissolution de-

¹ Manuscript received May 29, 1953. This paper was prepared for delivery before the Montreal Meeting, October 26 to 30, 1952. Based on a thesis submitted by C. B. Gill in partial fulfillment of the requirements for the Ph.D. degree to the Graduate School of the University of Missouri.

depends on the absolute amount of hydrofluoric acid liberated by the displacement reaction, assuming that the reaction goes to



completion. It was found that the dissolution continues at a considerable rate after a time, when, according to reaction (I), all the HF available was used up. This fact clearly shows that hydrochloric

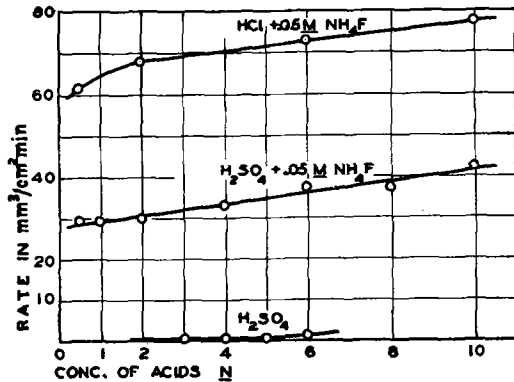


FIG. 1. Rate of dissolution of Ti in pure sulfuric acid, and in hydrochloric and sulfuric acids, at a constant concentration of NH_4F (0.05M), 1 mm³ of hydrogen corresponds to 0.001424 mg Ti.

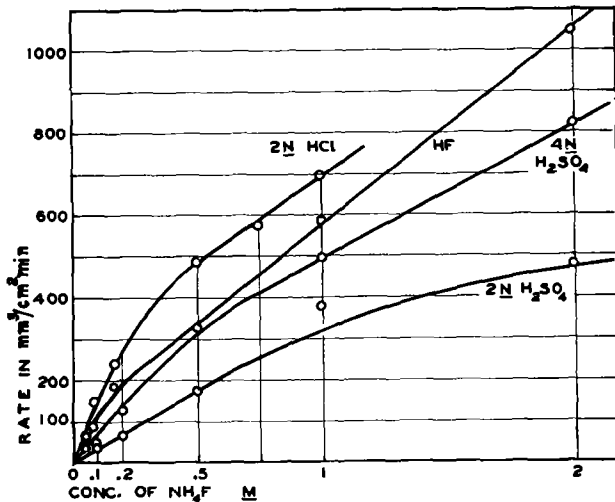


FIG. 2. Dissolution rates of Ti in constant concentration of HCl and H_2SO_4 , plus increasing amounts of NH_4F ; 1 mm³ of hydrogen corresponds to 0.001424 mg Ti.

and sulfuric acids attack titanium at a much faster rate in the presence of F^- than when F^- is not present.

RATE OF DISSOLUTION OF Ti IN ACIDS AT AN INCREASING CONCENTRATION OF NH_4F

The rates of dissolution of titanium in 2N hydrochloric acid, in 2N and in 4N sulfuric acid, in the presence of increasing amounts of NH_4F are

shown in Fig. 2. For comparison, the rates obtained in pure hydrofluoric acid are shown in the same diagram. The rates of the previous diagram, at 2N acid with 0.05M ammonium fluoride, are represented by the first points on this graph. There is a considerable increase in the rates with increasing concentration of NH_4F , from 0.05 to 2 molar, while in the previous diagram the rate in hydrochloric acid increased only from 62 to 77 mm³/cm² min, while changing the concentration of the acid from 0.5 to 10N. This behavior again shows the great influence of NH_4F , or of F^- , on the acceleration of the process of dissolution. The fact that the rate in the mixtures of 2N hydrochloric acid and ammonium fluoride was found to be greater than in hydrofluoric acid alone, again testifies to the increased reactivity of hydrochloric in the presence of fluoride ions.

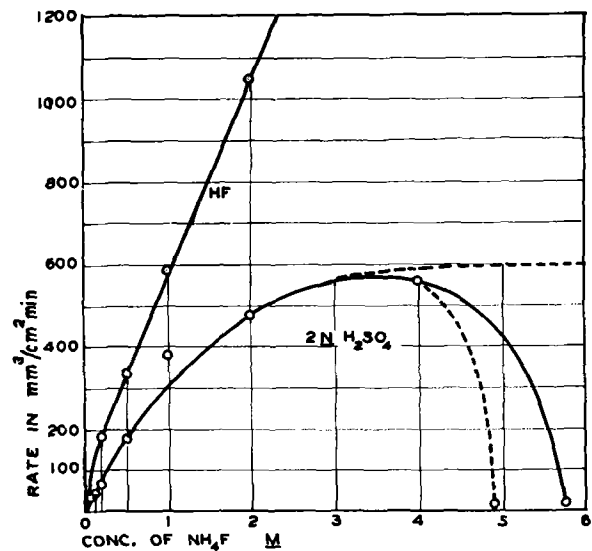


FIG. 3. Rates of dissolution of Remington Arms Ti in 2N H_2SO_4 , with increasing amounts of NH_4F added. The HF curve is drawn for comparison.

It was of interest to know how a further increase in ammonium fluoride concentration would influence the rate of dissolution. The effect of increasing additions of ammonium fluoride to the 2N sulfuric acid is shown in Fig. 3. We would expect that the rate of dissolution should increase and approach some constant value, as shown by the horizontal dashed curve. Instead of this, the rate dropped quickly as soon as the concentration of ammonium fluoride in the solution exceeded 4M (two experiments are represented by the descending portion of the solid curve, and by the dashed curve). The drop in the rate was so severe that it is justifiable to speak of passivation of the titanium. The same phenomenon also occurred in hydrofluoric and in other acids, with the rate sometimes dropping down to 0, and then increasing slightly. Table I shows the degree

of passivation of titanium by ammonium fluoride. The final rate of dissolution in the presence of large amounts of ammonium fluoride was only $\frac{1}{35}$, or less, of the maximum rate.

POTENTIAL MEASUREMENTS

In order to find out the reasons for the passivation observed, potential measurements of titanium in the presence of large amounts of ammonium fluoride were made in air and in nitrogen. Table I shows the normality of the acid and the molarity of the ammonium fluoride. There were 30 grams of the salt in a total volume of 158–160 cm³ of the acid.

In every case, when the investigation was being made in air, after the aforementioned quantity of ammonium fluoride was added to the acid being used, whether sulfuric or hydrofluoric, the potential of the titanium electrode dropped to very negative values (down to -0.94 volt) within 20–60 min. Simultaneously, the titanium electrode turned dark, and the rate of hydrogen development fell off to

TABLE I. Passivation of Ti by NH_4F ; N_2 atmosphere

Acid	$[\text{NH}_4\text{F}]$ <i>M</i>	Rate in mm ³ /cm ² min	Final rate/maxi- mum rate
2 <i>N</i> H_2SO_4	0	0.0	—
2 <i>N</i> H_2SO_4	3.5	580	—
2 <i>N</i> H_2SO_4	5.8	84 → 17	1/34
2 <i>N</i> H_2SO_4	4.9	34 → 0 → 17	1/34
1 <i>N</i> HF	0	590	—
1 <i>N</i> HF	5.9	26 → 0 → 17	1/35
1 <i>N</i> HF	4.9	34 → 17	1/35
1 <i>N</i> HF	4.9	25 → 17	1/35

nearly a complete stop. Then, within the next 60 min, the potential rose, and after some time dropped again more slowly, finally reaching a potential of approximately -0.78 volt, which is roughly the potential of a titanium electrode in pure hydrofluoric acid. Nevertheless, the rate of dissolution was still very low, although it did rise slightly from its lowest reading (Table I). All of these potential fluctuations were probably related to the formation and breakdown of some kind of films on the titanium surface. This conclusion followed from the fact that in every case in air the acid mixture first turned greenish-yellow until the maximum negative potential was reached, indicating the formation of the complex ion $[\text{TiFe}_6]^{3-}$; then at the constant potential reading the solution became colorless, which indicates the formation of the colorless complex ion $[\text{TiF}_6]^{2-}$, because of the presence of oxygen (oxidation of the trivalent titanium ion of the complex to tetra-

valent).² Each salt present might be in equilibrium with a separate kind of film on the titanium.

This view was supported by the behavior of titanium in the same mixtures, but in a nitrogen atmosphere. The drop of the potential was as severe as in the first case, but then the potential stayed fairly constant after some initial fluctuations (Fig. 4). However, the potential was far below that reached in pure hydrofluoric acid. The rate of dissolution was very low (Table I). The color of the solution was greenish-yellow throughout the whole experiment. The electrodes were bright and shiny when removed from the flask after the runs and did not display any discoloring surface film, although the presence of a thin salt film was not excluded. The surface of the titanium soon turned dark, especially when it was washed with water. The behavior of the electrical potential of this

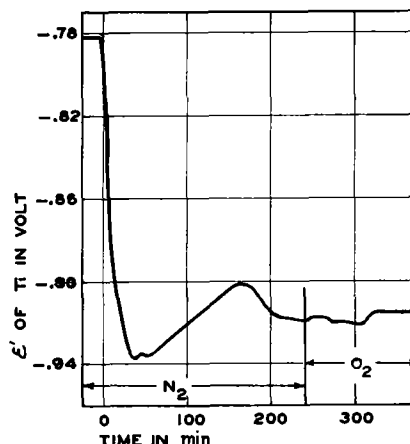


FIG. 4. Potential of Ti in HF in the presence of large amounts of NH_4F (Table I).

oxidized electrode, in the ammonium fluoride-acid mixture in air, was very similar to that already described. Strangely enough, if the nitrogen was replaced by air, as shown in Fig. 4, the potential did not change appreciably.

There is a fundamental difference in the passivation phenomenon just described, and the passivation of many other metals. While, in the latter case, the potential of the metal becomes more positive during passivation, the potential of titanium and of a few other metals (8) becomes less positive, accompanied by a decrease in the rate of dissolution. Under respective conditions, titanium also shows the usual anodic passivation (9).

Attempts were made to prove the increase of resistance of the titanium electrode during passivation. For this purpose the internal resistance of a

² The difficultly soluble, dark violet crystals of $(\text{NH}_4)_2[\text{TiF}_6]$ were not obtained (7).

Ti|HF, NH₄F|Pt cell, just after switching off the current, produced by the cell itself, was measured. In the case of the presence of a salt film, a greatly increased internal resistance should be expected. However, the measurements revealed that the resistance on the titanium surface increased only slightly when the ammonium fluoride concentration exceeded 4*M*. This increase in resistance was not sufficient to explain the whole drop in the rates of dissolution (Table I), and revealed the porosity of such a salt film if it was present on the dissolving surface.

OVERPOTENTIAL IN PRESENCE OF AMMONIUM FLUORIDE

In order to get some further clue to the passivation observed and, as the dissolution of titanium in hydrofluoric acid is an electrochemical process (1), it was of importance to know the behavior of the

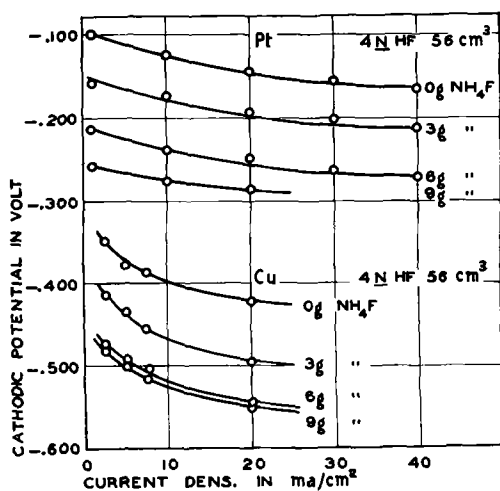


FIG. 5. Overpotentials on a platinized Pt and Cu electrode (covered with finely divided Cu) in 4*N* HF, in the presence of NH₄F.

local cathodes on the titanium in the presence of large amounts of ammonium fluoride.

For the measurement of hydrogen overvoltage, the cell Ti|HF, NH₄F|Pt (or with a copper cathode) was again chosen. The necessary current density was produced by the cell itself, in order to avoid complications which might be caused by anodically developed oxygen, using an external current. The cathodic potential was measured during the flow of the current by a 1*N* calomel reference electrode, whose capillary was touching the cathode. Thus, the overvoltage measurements were performed by the direct method (3), and the current density was adjusted by manipulating an exterior resistance (resistance box).

The cathodic potential curves were obtained at different current densities in 4*N* hydrofluoric acid

(56 cm³), to which, subsequently, amounts of ammonium fluoride in 3-gram increments were added. The results obtained are shown in Fig. 5.

All the measurements made show definitely that the hydrogen overvoltage of the metals, platinum and copper, increases with the increasing concentration of ammonium fluoride in the electrolyte. As all the curves in Fig. 5 follow Tafel's equation, the increase in overvoltage can be characterized by the increase of the constant, *a*, of Tafel's equation (4-6). This equation, as applied to the calculation of the negative cathodic potential, η (or overvoltage in volt), is as follows:

$$\eta = -(a + b \log i)$$

Here *a* and *b* are constants and *i* is the current density in milliamp/cm². Table II shows that the

TABLE II. Cathodic potential of platinized platinum in 4*N* HF, with NH₄F added; volume of the HF: 56 cm³

<i>i</i> in m amp/cm ²	NH ₄ F in mole/l	<i>a</i>	<i>b</i>	η in volt calc.	η in volt obser.	Δ
10	0	0.089	0.0523	-0.141	-0.127	-0.014
20	0	0.089	0.0523	-0.157	-0.161	+0.004
30	0	0.089	0.0523	-0.166	-0.175	+0.009
40	0	0.089	0.0523	-0.173	-0.191	+0.018
10	1.4	0.156	0.0270	-0.183	-0.174	-0.009
20	1.4	0.156	0.0270	-0.191	-0.189	-0.002
30	1.4	0.156	0.0270	-0.196	-0.200	+0.004
40	1.4	0.156	0.0270	-0.199	-0.213	+0.014
10	2.7	0.213	0.0301	-0.243	-0.235	-0.008
20	2.7	0.213	0.0301	-0.252	-0.245	-0.007
30	2.7	0.213	0.0301	-0.257	-0.263	+0.006
40	2.7	0.213	0.0301	-0.261	-0.271	+0.010
10	3.9	0.255	0.0219	-0.277	-0.275	-0.002
15	3.9	0.255	0.0219	-0.281	-0.283	+0.002

potential calculated from the equation is in good agreement with those obtained experimentally, and that the constant, *a*, increases from 0.089 up to 0.255, with increasing ammonium fluoride additions.

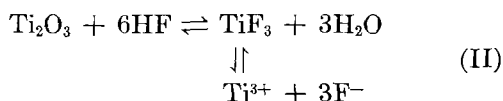
In the case of copper, there was still better agreement between the calculated values of the cathodic potential and those actually obtained experimentally. The constant, *a*, increased from 0.335 to 0.455, while the concentration of ammonium fluoride (in the hydrofluoric acid) increased from 1.4 to 3.9*M*. The increase of the constant, *a*, with the concentration of the ammonium fluoride, was linear in both cases. The constant, *b*, of the copper overvoltage curves, fluctuated between 0.064 and 0.084, indicating a steeper slope of the straight lines than for those of platinum. The influence of sodium fluoride additions upon the overvoltage had a similar, if not stronger, effect. The behavior of agar-

agar solutions added to the acid in separate experiments was analogous, although not so strong. It is also very possible that other metals would exhibit a similar cathodic behavior in the presence of ammonium fluoride.

DISCUSSION

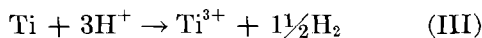
There is some difficulty in trying to explain the phenomena observed, but on the basis of the experiments performed, the following conclusions were developed concerning the mechanism of the dissolution of titanium in acids, in the presence of soluble fluorides.

It cannot simply be assumed that the rate of dissolution of titanium is proportional to the concentration of the hydrofluoric acid liberated according to reaction (I) because the dissolution of titanium continues with a considerable rate after the hydrofluoric acid has been used up. However, the increased action of hydrochloric, sulfuric, and many other strong and weak acids can be explained as follows. It was previously shown that the phenomena observed in the dissolution of titanium in acids can only be explained by the presence of a protective film on the titanium surface, this film being soluble in hydrofluoric acid, but nearly or completely insoluble in other acids (1). The film, which frequently is even clearly observable on the surface of the metal, probably consists of lower oxides of titanium (Ti_2O_3 ?), or of some basic salts. Only free hydrofluoric acid is capable of partially dissolving the film on titanium, and so the film is always in equilibrium with the hydrofluoric acid displaced according to equation (I), by the acid HR:



As hydrofluoric acid is a weak acid, reaction (I) becomes possible with very many acids, even weak acids, according to the law of mass action.

The film becomes thinner, with increasing concentration of the hydrofluoric acid, the pores increase, and the metal subsequently goes into solution at a greater rate, according to:



The dissolution of the metal in the pores proceeds because of the action of local elements. The formation of basic salts, or of an oxide film, which otherwise would occur during the dissolution process, is prevented by the hydrofluoric acid present. Thus, the thickness of the protective film is determined by the concentration of the hydrofluoric acid.

In agreement with this concept is the slow increase in the rate with increasing concentrations of

HR, at a constant concentration of ammonium fluoride (Fig. 1), for, according to the law of mass action, the concentration of hydrofluoric acid increases only slowly with appreciable increase of [HR]. Therefore, the thickness of the film is reduced slightly, which in turn accounts for only a small increase in the rate of dissolution. Hydrochloric acid is more active than sulfuric acid because of the higher hydrogen ion concentration.

The gradual tapering off of the dissolution reaction (although the hydrogen ion concentration of the acid solution is still high) is explained by the possibility of the binding of F^- by Ti^{3+} :



as the $[Ti^{3+}]$ increases steadily during the dissolution process, and the $[F^-]$ decreases. With decreasing HF concentration, the film becomes thicker, the pores narrow, and the rate of dissolution decreases.

If the $[NH_4R]$ is now increased, with a constant [HR], then, of course, the [HF] increases strongly (Fig. 2), as can be shown by applying the mass action law. The thickness of the film decreases, and the rate of dissolution of titanium increases appreciably with increasing $[NH_4F]$.

Increasing the concentration of ammonium fluoride still more should have made the rate independent of $[NH_4F]$. Instead, the rate decreased sharply as soon as the 4*N* concentration was exceeded.

The explanation, according to the theory of local currents, is as follows. The rate of dissolution, V , as calculated from the increase of hydrogen volume, Δv (developed on the surface area, A) during the time Δt is given by equation (V), which was derived by one of the authors in 1930 (10). This equation is slightly modified here to obtain the correct (positive) sign for the rate of dissolution:

$$V = \frac{\Delta v}{\Delta t A} = kz^1 \frac{\eta - \epsilon^1}{r} \quad (V)$$

k being a constant, ϵ^1 the dissolution potential, η the overvoltage (potential) of the local cathodes, r the average resistance of each local cell, and z^1 the number of local cathodes per surface unit (1). Equation (V) was used in 1933 to discuss the possibilities of protection of metals from corrosion, and especially the case of increased hydrogen overvoltage was emphasized (11). A similar equation for the same purpose was used by Mears (12) and Mears and Brown (13) in 1949 and 1950.

At passivation, the rate V drops to low values, and usually can be explained by the shift of ϵ^1 toward positive potentials. The difference $\eta - \epsilon^1$ then becomes small, and the corrosion current drops to nearly zero. However, for passivity in the case of

titanium, the other three variables (z^1 , η , and r) are responsible, because of the very strange potential behavior of the passivated titanium (Fig. 4), the potential becoming more negative. Consequently, this passivation is different than with most of the other metals, and cannot be explained by the change in potential.

A noteworthy reason for the passivity of titanium is the formation of the thin salt layer, as already mentioned. However, because of the low electrical resistance of this layer, it must have large pores, so that the dissolution can proceed in these pores at a rather high rate. Therefore, the salt layer, by shielding and blocking a part of the number of active cathodes (z^1), decreases the rate of dissolution, but only partially explains the reason for passivation.

The real reason for passivation of the titanium lies in the increase of the hydrogen overvoltage on the local cathodes (or decrease of the cathodic potential) because of the presence of the ammonium fluoride, as is clearly demonstrated by Fig. 5. The emf of the local elements in the pores drops, and a very low current density results. This condition is contrary to the behavior of metals where the passivity is the result of a high current density in the pores of the protective film present on the surface of the passivated metal. In this case, the current density is very low, and is the reason, probably together with the extremely low $[\text{Ti}^{3+}]$, for the very negative potential of Ti. The $[\text{Ti}^{3+}]$ is low because of a complex ion formation with the ammonium fluoride which has been added.

The conclusion is that the passivation of titanium by ammonium fluoride is caused by the decrease in the number of active local cathodes

(covered by the salt film), and by the increase of overvoltage (polarization) on the free cathodes. Evidently these two effects overbalance the increase in the rate of dissolution, expected from the lowering in the anodic potential and the decrease in the resistance of the electrolyte, and as a result the rate of dissolution of Ti drops sharply.

Thus this case of passivation is in agreement with the theory developed by one of the authors (10, 11), and recently by Mears (12).

Any discussion of this paper will appear in a Discussion Section, to be published in the December 1954 issue of the JOURNAL.

REFERENCES

1. M. E. STRAUMANIS AND P. C. CHEN, *This Journal*, **93**, 234 (1951).
2. M. E. STRAUMANIS AND P. C. CHEN, *Corrosion*, **7**, 229 (1951); *Metall*, **7**, 85 (1953).
3. C. F. PRUTTON AND S. R. MARON, "Fundamental Principles of Physical Chemistry," p. 586, Macmillan Co., New York (1947).
4. J. TAFEL, *Z. phys. Chem.*, **50**, 645 (1905).
5. G. KORTUM AND J. O. M. BOCKRIS, "Textbook of Electrochemistry," Vol. II, pp. 420, 426, Elsevier Publishing Co., New York (1951).
6. M. E. STRAUMANIS, in G. M. Schwab's, "Handbuch der Katalyse," Vol. VI, 166 (1943).
7. A. PICCINI, *Atti Linc.*, **1**, 47 (1885); *Gazz. chim. ital.*, **16**, 106 (1886).
8. R. B. MEARS, *This Journal*, **95**, 1 (1949).
9. C. D. HALL, JR., AND N. HACKERMAN, *J. Phys. Chem.*, **57**, 262 (1953).
10. M. STRAUMANIS, *Z. physik. Chem.*, **A148**, 349 (1930); *Korrosion u. Metallschutz*, **9**, 1 (1933).
11. M. STRAUMANIS, *Korrosion u. Metallschutz*, **9**, 229 (1933); *ibid.*, **11**, 49 (1934).
12. R. B. MEARS, *This Journal*, **95**, 1 (1949).
13. R. B. MEARS AND R. H. BROWN, *This Journal*, **97**, 75 (1950).

The Electrolytic Preparation of Molybdenum from Fused Salts

I. Electrolytic Studies¹

SEYMOUR SENDEROFF AND ABNER BRENNER

National Bureau of Standards, Washington, D. C.

ABSTRACT

Potassium hexachloromolybdate (III), K_2MoCl_6 , dissolved in molten alkali halides may be electrolyzed to deposit pure molybdenum at the cathode. The effect of the operating variables on the nature of the deposit is discussed.

INTRODUCTION

In recent years, interest in the refractory metals has been stimulated by the need for materials for use at exceptionally high temperatures. Much attention has been given to molybdenum because of its availability in this country (1) and its favorable mechanical and physical properties at elevated temperatures (2).

In view of this interest, a research program was initiated to determine the feasibility of an electrolytic method for its production. Not only was the production of pure molybdenum powders of interest, but, further, the possibility of producing coherent molybdenum electrodeposits was explored. This latter is of particular interest since it would provide a means of by-passing the rather complicated powder-metallurgy techniques now used for producing molybdenum objects. When only surface properties are important, a coating of molybdenum may be applied to an object, thus conserving much of this critical metal and further enabling one to take advantage of the structural properties of the basis metal. In addition, electroforming with molybdenum would result in elimination of not only powder metallurgy but also many difficult and expensive fabrication steps.

Historical

The present commercial method of producing the metal consists of reducing pure molybdic oxide with hydrogen to form a fine powder which is then worked by powder metallurgy methods. Recently, a method of producing ingots by vacuum arc-melting has been brought to a stage of pilot-plant operation (3). A method for producing molybdenum deposits on objects has recently been described (4) which

¹ Manuscript received April 7, 1953. This paper was prepared for delivery before the Philadelphia Meeting, May 4 to 8, 1952. Based on a thesis submitted by Seymour Senderoff to the Faculty of the Graduate School of the University of Maryland in partial fulfillment of the requirements for the Ph.D. degree.

involves the reduction of molybdenum pentachloride vapor by hydrogen in a sealed vessel at about 20 mm Hg total pressure and at 800° to 1100°C. Another method for producing molybdenum deposits (5) employs the thermal decomposition of molybdenum carbonyl at about 600°C below 0.1 mm Hg.

A thorough analysis of the literature and many attempts to duplicate published claims lead to the conclusion that pure molybdenum has not heretofore been electrodeposited from aqueous solutions, organic solvents, or from molten salts.

Deposits containing as much as 50% Mo alloyed with iron, nickel, or cobalt, as the second element, may be obtained by electrolysis of acidic or slightly alkaline citrate solutions (6), and deposits of somewhat lower Mo content alloyed with iron or cobalt can be obtained from concentrated alkali solutions (7); but examination of the properties of these deposits, when built up to a thickness of 0.001 in. to 0.002 in., shows that, when the molybdenum content exceeds about 25–30%, the deposits have a high oxide content, are very weak, and usually crumble on stripping of the basis metal. Further, the phase diagrams for the binary systems of molybdenum with nickel (8), iron (9), and cobalt (10) indicate that alloys containing less than about 90% molybdenum would not have satisfactory properties at elevated temperatures.

Much work has been done in attempts to obtain pure molybdenum from organic and other low-temperature nonaqueous systems, but little has been published because of the lack of positive results (11–13).

The work of Ksycki and Yntema (14) is the most recent paper on electrodeposition of molybdenum from aqueous systems. Deposits from their bath [Reference (14) p. 55] whose thicknesses were 0.1 and 0.4 microns were analyzed² and found to

² Microanalysis performed by R. A. Paulson of this Bureau.

contain 74 and 80% molybdenum, respectively. MoO_2 contains 75% molybdenum. Electron diffraction studies³ indicated the possible presence of small amounts of free molybdenum in the deposits.

The literature on the electrolysis of aqueous solutions of molybdenum compounds contains a large amount of conflicting information. After a thorough analysis of the literature and many attempts to duplicate claims (14–20), it can be stated with certainty that no electrodeposit whose major constituent is molybdenum metal has been obtained by the electrolysis of aqueous or organic electrolytes, with the possible exception of deposits which grow to only a few microns in thickness and then cease forming. The properties and composition of deposits as thin as these are extremely difficult to determine. This opinion is in agreement with Childs and coworkers (4) and Lander and Germer (5).

An interesting process is described in Gmelin (21) with references to two review articles (22), one of which is clearly a translation of the other, and neither of which gives reference to the original publication. In this process, molybdenum pentachloride, silica, and sodium chloride are heated, and the effluent vapors passed through molten sodium chloride, which is electrolyzed. Molybdenum is said to deposit at the cathode, which may be either copper or molten lead. This process may be that originally described by Gin (23).

Another process recommended a mixture of calcium molybdate and molybdenum carbide dissolved in bauxite (24), while still another recommended the electrolysis of molten calcium molybdate (25). Kratky and Bruckner (26) electrolyzed a melt of barium or calcium chloride and, after the electrolysis had begun, a water-free molybdenum salt was added. The calcium or barium metal already present in the bath from the initial electrolysis is said to reduce the molybdenum salt to molybdenum metal. Forland recommended a mixture of equimolar proportions of molybdenum pentachloride, sodium chloride, and aluminum chloride which melts below 200°C (27). He claims that the low melting point of the mixture permits electrolysis at 200°C without appreciable volatilization of the molybdenum pentachloride. This electrolysis was performed here, using a U tube as described by the inventor. Copious evolution of fumes both of the molybdenum pentachloride and the aluminum chloride occurred. The cathodic deposit was a very fine spongy black powder which reacted with water with the evolution of gas.

Andrieux reported the cathodic deposition of

³ Electron diffraction studies performed by M. Swerdlow of this Bureau.

molybdenum from a molten bath consisting of borax, sodium fluoride, zinc oxide, and molybdic acid at about 1000°C (28). In the same paper, rather similar solutions and conditions with other metals are said to produce borides rather than the free metal.

As a result of work which appears later in this study, it seems highly improbable that pure molybdenum metal can be deposited from an oxygen-containing melt, and that reports indicating this has been accomplished should be carefully checked.

EXPERIMENTAL PROCEDURES AND APPARATUS

Scope.—In determining the scope of this study it seemed, from an examination of the literature, and from some experience with the electrolysis of molten titanium compounds (29), that the most promising solvent would be mixtures of alkali chlorides. Therefore, practically all of the work was done in this medium. The molybdenum compounds chosen for investigation were those of greatest stability in each oxidation state of molybdenum. Of the hexavalent compounds, the molybdates are undoubtedly extremely stable, so sodium molybdate was the compound chosen. No hexachloride is known to exist, and the hexafluoride boils at 35°C.

The most stable of the quinquivalent compounds is the pentachloride, which boils at 268°C. However, it has an appreciable vapor pressure above 150°C. In addition, it is rapidly hydrolyzed by atmospheric moisture at room temperature. Since a fair amount of work with this compound in molten salts has already been done, no further study of it, other than the check of the Forland patent described above, was undertaken.

Of the tetravalent molybdenum compounds, the complex octacyanide is probably the most stable. It was prepared here and its properties were checked. The tetrahalide decomposes before melting and is decomposed by air, light, etc. Of the trivalent molybdenum compounds, the complex hexachloride is the most stable, and proved to be particularly suited to accomplish the purpose of this study. Most of this paper deals with the electrolysis of solutions of this compound. The divalent chloride is the most stable of the simple molybdenum halides and was chosen as the divalent compound for study in this work.

The electrolytic studies presented in this paper are concerned mainly with the reactions at the cathode. Insoluble anodes, diaphragms, etc., for electrowinning are now under study.

Equipment.—Since it was decided, on the basis of previous work with titanium, to do all electrolyses in an inert atmosphere, it was necessary to design equipment for that purpose. The requirements which were set for the equipment included: (a) upper

temperature limit of 1000°C; (b) automatic temperature control; (c) manipulable electrodes in a closed system; (d) visibility of electrodes and electrolyte during operation; (e) cathode agitation; and (f) sufficiently leak-proof apparatus to maintain an internal pressure of 1 mm and to maintain an adequate protective atmosphere under a reasonably small flow of argon.

It became apparent that the design of such equipment could be greatly simplified if induction heating were used. A photograph of the equipment as finally assembled is shown in Fig. 1, and a schematic detail drawing in Fig. 2. A Pyrex glass cylinder, (A), 2¾ in. in diameter and 18 in. high, closed at the bottom, was placed in the furnace coil, (B), which was about 6 in. high and mounted on a transite platform. Inside the Pyrex tube was placed a ceramic cylinder, (C), made from "Alfrax" body

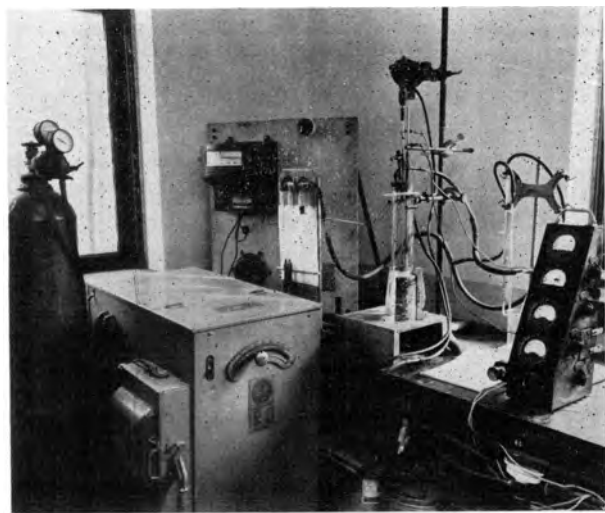


FIG. 1. Apparatus for electrolysis of fused salts

and a small amount of binder, the purpose of which was mainly that of thermal insulation. Inside the ceramic cylinder was placed the machined graphite crucible, (D), made of AGR⁴ graphite. The crucible was 6 in. high, 2 in. O.D., and had a ¼-in. wall thickness. A thin sheet of mica was used between the Pyrex envelope and the furnace coil since it was found that this reduced the tendency to arc through the glass and crack it. A rubber bung, (E), was used to close the top of the Pyrex cylinder. One central and five peripheral holes were drilled through the bung, 5-in. lengths of tightly fitting glass tubing were inserted in four of the holes, and short lengths of rubber tubing were fitted to the tops of the glass tubes. A rod, ¼ in. in diameter and 2 ft long, (F), was inserted through the center hole and served as a cathode. It was connected at the top to a variable

⁴ National Carbon Company, Cleveland, Ohio.

speed stirring motor, (G), by a tightly fitting rubber coupling. Through the holes around the periphery of the bung were inserted a McDanel refractory thermocouple protection tube (glazed), (H), long enough to reach the bottom of the crucible, and a ¼-in. diameter tungsten rod which served to hold the rod or sheet anode, (I), by means of a molybdenum connector, (J). A third peripheral outlet was used as an escape chimney, (K), and was fitted with a screw clamp, while in the fourth (which had no glass tube) was inserted a stainless steel tube, (L), extending to within 2 or 3 in. of the top of the crucible. It served as a gas inlet or

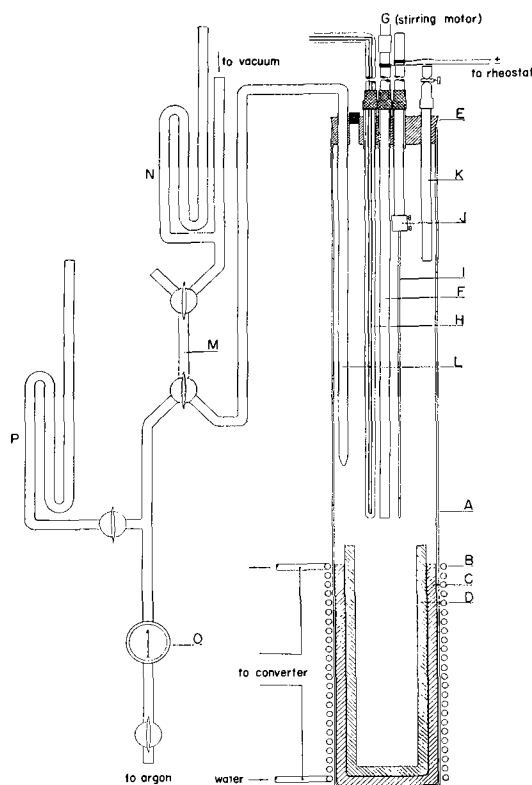


FIG. 2. Schematic diagram of electrolysis cell and auxiliary equipment.

evacuation port. The fifth hole was closed with a rubber stopper and was used only for potential and polarization studies. The furnace was supplied with power by an Ajax-Northrup 3KVA mercury spark-gap converter, which was controlled by a chromel-alumel thermocouple and a Brown controlling pyrometer, placed in the input circuit of the converter. The heating rate was rapid, the melt reaching a temperature of 900°C in about ten minutes. An air-cooling coil was placed around the top of the Pyrex cylinder near the rubber bung; thus the area around the bung was always kept cool to the touch. With the water cooling in the furnace coil around the glass and the ceramic crucible separating the glass

from the heated crucible, the thermal gradient was sufficiently large to permit long periods of operation with the charge at 900°C without softening the glass.

General procedure.—The procedure is as follows.

Electrolysis.—The electrolytes consisted of a mixture of alkali chlorides and a salt of molybdenum. The alkali chloride mixture henceforth is called the "halide solvent." A typical electrolysis run was performed in a manner designed to exclude, insofar as was possible, traces of moisture or contamination by air. The procedure began with the purification of the "halide solvent" by fusing it at a temperature a few hundred degrees above its melting point in the crucible in which the electrolysis would be done. It was then allowed to cool in an argon atmosphere. The Pyrex vessel was then opened and the previously dried molybdenum compound quickly added on top of the solid halide solvent. (The method of drying the molybdenum compound was determined by the properties of the compound itself.) The bung and attached equipment were then set in place, with the anode and cathode withdrawn above the crucible. The system was evacuated, filled with argon to 3 or 4 cm above atmospheric pressure, and the argon flow continued. After flushing the system, the heating was started, and, as soon as the salts melted, the thermowell was inserted into the melt. At the desired operating temperature, the anode and cathode were inserted into the melt, the cathode connected to the stirring motor, the electrical leads connected, and the electrolysis begun. The flow rate of the argon was set at any value between 200 and 3000 cc/min as desired during the run, but the outlet chimney was always adjusted to maintain a pressure above atmospheric inside the system throughout the run.

When very hygroscopic material, such as lithium chloride, was present, the following additional pretreatment before electrolysis was required in order to expel all moisture and oxycompounds. The bath was heated to 900°C at the same time that the argon flow was increased to about 3000 cc/min. This rapidly drove out any released moisture and volatile oxycompounds, and reduced their opportunity to attack the solution. After 15–30 min at this temperature, the solution was cooled to the operating temperature, the argon flow reduced to the usual value of about 300 cc/min, and the solution electrolyzed at low current density until the deposits showed no oxide present.

At the end of a run, the cathode, anode, and thermocouple were withdrawn from the melt and allowed to cool in the inert atmosphere, while the electrolyte itself cooled and froze. The system was not opened until the temperature inside was below

100°C. After removing the bung with the anode and cathode, an auxiliary bung was quickly replaced, the system evacuated and filled with argon, and the electrolyte stored in an inert atmosphere for later runs. The rubber sleeves through which the electrodes and thermocouple well were passed were lubricated with silicone stopcock grease and all stationary joints were sealed with Unichrome⁵ stop-off lacquer No. 323, as was the joint between the Pyrex envelope and the large rubber bung.

The cathode deposit was separated by first soaking the cathode in boiling 10% hydrochloric acid. Contrary to some statements in the literature this does not appreciably attack molybdenum. After the adhering salts from the electrolyte were dissolved, the deposit, if powder, was removed by scraping, hammering, chiseling, or whatever procedure was required by the nature of the deposit. This was then lightly ground in a mortar and washed with distilled water. Fines and any impurities lighter than molybdenum remained suspended while the molybdenum settled out. The liquid was decanted, and this was repeated until the supernatant liquid was practically clear. The molybdenum was then filtered, washed with acetone, and dried.

Except where otherwise indicated, the cathode was a 1/4-in. diameter tungsten rod immersed to a depth of about 3 in., giving a cathode area of 0.15 dm² (2.3 in.²). It was rotated at 300 rpm. The anode was a pure commercial molybdenum⁶ sheet, 0.5 in. x 0.030 in., immersed to the same depth.

The molybdenum anode was used mainly to simplify the investigation of the cathode reactions. It was found early in the work that molybdenum dissolves with 100% current efficiency in the molten chloride electrolyte. As a result, there were no complications introduced by anodic products, oxidation of the electrolyte, or any other factors usually associated with an insoluble anode. In electrowinning, a divided cell with an insoluble anode and some convenient anolyte may be required.

Analysis.—Many analyses for molybdenum were performed using the volumetric Jones reductor method (30) and a few using the gravimetric method of precipitation in acid solution with α -benzoin oxime (31).

Metallography.—The microstructure of the molybdenum deposits was investigated by mounting specimens in Bakelite or Lucite and polishing by standard methods.⁷ The samples were etched with Murakami's reagent, which consists of 10 grams of

⁵ United Chromium, Inc., New York, N. Y.

⁶ Fansteel Metallurgical Corporation, North Chicago, Ill.

⁷ The metallographic specimens were prepared by F. P. Brodell of this Bureau.

potassium ferricyanide and 6 grams of sodium hydroxide dissolved in 200 ml of water.

ELECTRODEPOSITION

General Considerations

Potassium hexachloromolybdate (III), K_3MoCl_6 , (for preparation see Part II of this series), was the most satisfactory electrolyte for electrodepositing molybdenum from fused baths. The salt was used in two types of halide solvents: (a) 1:1 mixture (by weight) of sodium chloride and potassium chloride, and (b) the eutectic mixture⁸ of lithium chloride and potassium chloride. Preliminary tests, with baths containing different concentrations of the molybdenum salt, indicated that the best deposits were obtained with baths nearly saturated with the molybdenum salt at the temperature of deposition.

longed electrolysis, a quantity of current equivalent to about 1 amp-hr/gram of bath was passed through a small batch of bath (B). This was enough current to replace the initial quantity of molybdenum in the bath about 20 times. The bath was still in operating condition after this experiment, and no evidence of deterioration was observed.

The deposits from bath (A) usually consisted of rather coarse powders, with an average diameter of about 0.01 in. In many instances, however, a layer of the deposit immediately next to the cathode, about 0.001 in. in thickness, was adherent to the cathode and appeared quite dense. A typical deposit from bath (A) is shown in Fig. 3, and a cross section of the adherent molybdenum layer next to the cathode is shown in Fig. 4. It was about one crystallographic grain thick.

TABLE I.—Deposits from K_3MoCl_6 —KCl—NaCl Solution

No.	Conc. mole %	K_3MoCl_6 wt %	Current density (amp/dm ²)	Plating time (hr)	Wt of deposit collected (g)	Type of deposit
1	2.0	12	30	1.0	0.25	Nonmetallic black powder
2	2.0	12	100	0.5	—	Nonmetallic black powder
3	3.3	18	3	1.5	—	Nodular superficially coherent Mo deposit overlying thin coherent layer
4	3.3	18	100	0.5	6.7	Dendritic Mo powder overlying adherent layer (see Fig. 12)
5	4.9	25	3	1.5	0.86	Superficially coherent nodular deposit overlying adherent layer
6	4.9	25	30	1.0	2.8	Powder agglomerates consisting of trees and large multifaceted crystals of molybdenum over an adherent layer
7	4.9	25	100	0.5	8.5	Granular metallic powder over adherent layer (see Fig. 3 and 4 and col. 3, Table IV)
8	4.9	25	Periodic reverse 30 direct 60 reverse	1.0	3.2	Powder consisting of small platelets over about 0.002 in. of adherent plate

All deposits were prepared at 900°C.

The deposition was carried out over a range of current densities from 3 to 100 amp/dm² and over a range of temperatures from 600° to 900°C. The lithium chloride-potassium chloride melt had an advantage over the sodium chloride-potassium chloride melt in that it could be operated at a lower temperature, and coherent deposits, as well as powders, could be obtained from it. It had the disadvantage of being very hygroscopic, and required somewhat more care. The compositions, in weight per cent, of the two baths used for most work were: (A) NaCl 37.5%; KCl 37.5%; K_3MoCl_6 25%, at 900°C; (B) LiCl 34%; KCl 41%; K_3MoCl_6 25%, at 600°–900°C. The composition of other baths tried is given in Table I.

To demonstrate the life of the bath under pro-

⁸ The composition by weight of this mixture is 45.5% lithium chloride, 54.5% potassium chloride.

The deposits obtained from bath (B) at 900°C (Fig. 5 and 6) were similar to those from bath (A), except that the grain-size of the deposit was somewhat finer and the coherent layer of molybdenum under the powder was thicker than with bath (A).

At 600°C and 3 amp/dm² coherent deposits (Fig. 7 and 8) were produced which could not be obtained from either bath at 900°C. Fig. 9 shows a coherent tubular deposit of molybdenum from which the cathode has been dissolved. It was about 2 in. long, 0.25 in. in diameter, with a wall thickness of 0.02 in. The tube was hard and brittle, but mechanically sound. Its external surface was quite rough. The density was 9.6 g/cm³ or about 94% of the theoretical density of molybdenum. In comparison, powdered molybdenum, which has been pressed and sintered, has a maximum density of about 92% of the theoretical density (32). The

tube was deposited on a tubular steel cathode coated with 0.001 in. of silver, and closed at the end. Neither iron nor copper cathodes could be used as they were attacked by the solution, ap-

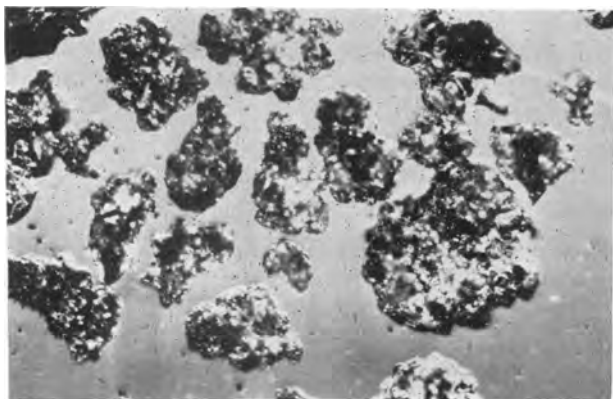


FIG. 3. Deposit of molybdenum powder—bath A. 50X



FIG. 4. Cross section of adherent molybdenum layer after removal of overlying powder—bath A. 500X.

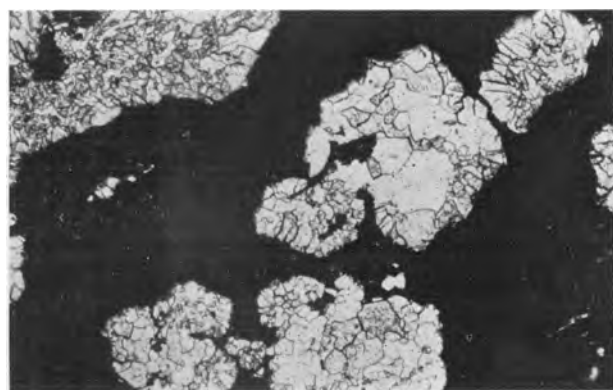


FIG. 5. Granules of Mo powder etched to show grain structure—bath B. 100X.

parently chemically displacing molybdenum from the melt. At 600°C and 100 amp/dm², the fine grain powder deposits shown in Fig. 10 and 11 were produced.

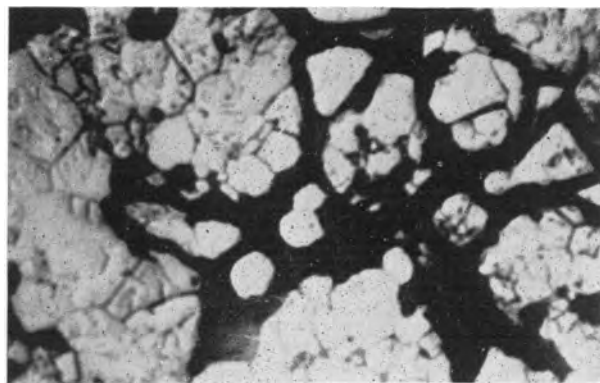


FIG. 6. Cross section of molybdenum deposit adjacent to cathode after removal of loose powder—bath B, 900°C. 500X.

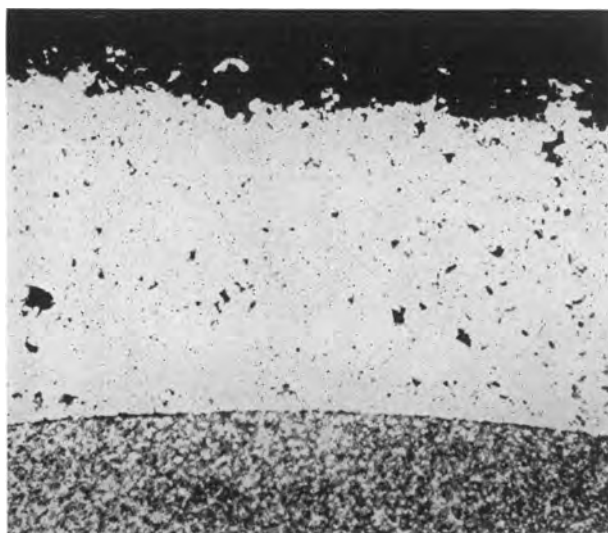


FIG. 7. Cross section of coherent molybdenum deposit from bath B, 600°C. 100X.

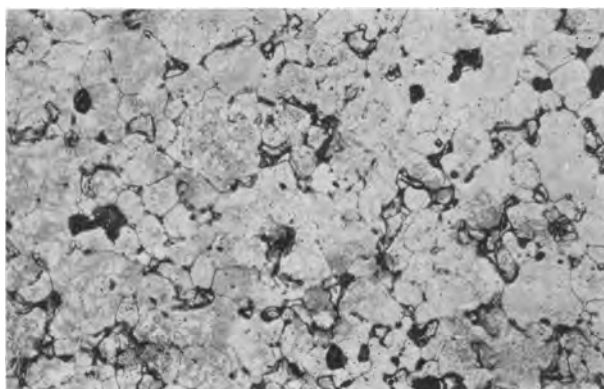


FIG. 8. Same as Fig. 7, etched to show grain structure. 500X.

The purity of the molybdenum deposits was established by chemical and spectrochemical analyses as discussed below.

Variables Involved in the Deposition of Molybdenum

The study of the variables involved in the deposition of molybdenum was made for the purpose of determining how they affected the purity and the physical nature of the deposit. The most important factor in obtaining pure deposits of molybdenum was the purity of the reagents and the atmosphere above the electrolytic cell.

Oxygen and moisture.—The exclusion of air and moisture from the salts composing the melt and the



FIG. 9. Electroformed molybdenum tube and cup



FIG. 10. Molybdenum powder from 100-gram batch produced at 600°C from bath B. 50X.

atmosphere above the cell was of extreme importance for producing pure molybdenum deposits. Before this was recognized, impure deposits were obtained which contained oxide. Such deposits usually consisted of a layer of black powdery material adjacent to the cathode with a layer of molybdenum crystals over it. A black powder was also formed in the melt. X-ray diffraction analyses⁹ established

⁹ Analyses performed by F. A. Mauer and H. E. Swanson of this Bureau.

that these black powders were largely Mo_2O_3 mixed with a small proportion of metallic molybdenum.

During runs with contaminated melts or atmospheres, volatile blue and white products condensed on the upper walls of the glass envelope. These were probably oxymolybdenum compounds of valence 4 or 5 formed by oxidation of the K_3MoCl_6 . Bath (B), containing the hygroscopic lithium chloride, was particularly prone to give such results until the procedure previously described for pretreating the melt before electrolysis was worked out.

The importance of maintaining an oxygen-free melt was demonstrated by two additional experiments: (a) a bath which was operating satisfactorily

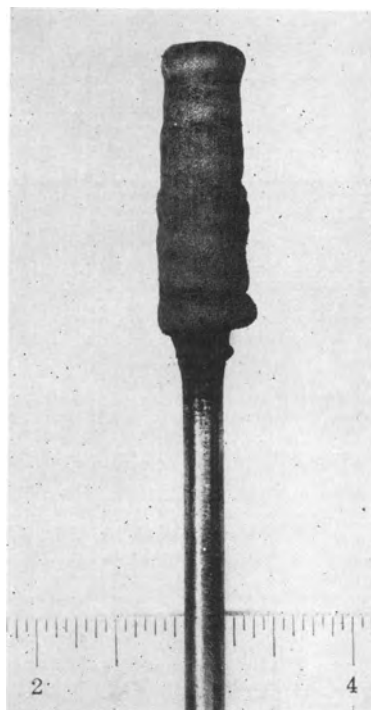


FIG. 11. Molybdenum powder deposit on cathode, as it appears after immersion in dilute HCl to dissolve adhering electrolyte.

was opened briefly to the air; the resulting deposit and melt contained black oxide; and (b) the introduction of about 0.1% by weight of sodium molybdate into a melt completely stopped the deposition of molybdenum. The changes of cathode potential occurring during the experiments will be discussed in Part III of this series.

Composition of melts.—The main difference between the two baths, (A) and (B), is that the latter may be operated at a lower temperature. More coherent deposits were obtained from bath (B) at 600°C than from bath (A) at 900°C. Apparently temperature is the most important variable in this case, as the deposits obtained from bath (B) at 900°C, although somewhat more coherent than those from bath (A), were nevertheless powdery in

nature. However, a careful comparison of a number of deposits from the two baths at 900°C indicates that the presence of the lithium salt does have a beneficial effect on coherence and reduction of grain size apart from the temperature effect. This is not necessarily a specific effect of the lithium ion itself, but may be because of the presence of a trace of moisture which could not be removed from this very hygroscopic material. Moisture, although harmful in large quantities, might be beneficial in trace amounts. Both baths operated at about 100%

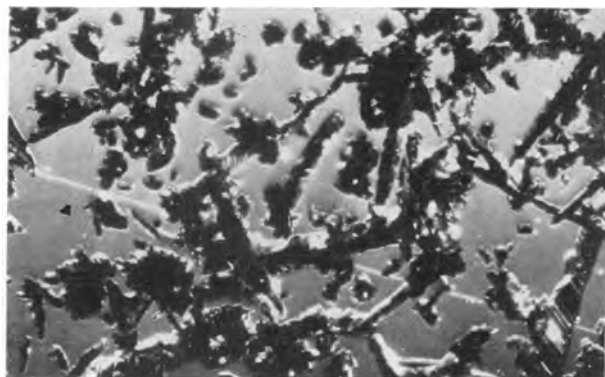


Fig. 12. Dendritic molybdenum powder—bath A. 50×

point than (B), two halide melts containing aluminum chloride were tried, but as the solubility of K_3MoCl_6 was not very high in these melts below 600°C, no further work was done with them. A comparison of these halide melts with bath (B) is given in Table II.

Current density.—The current densities used varied from 3 amp/dm² to 100 amp/dm². Adherent and coherent deposits were obtained only from bath (B) at 3 amp/dm². At higher current densities the deposits from both bath (A) and bath (B) were noncoherent, consisting of either dendrites or granular powder. The effect of current density on the deposits from baths (A) and (B) is shown in Tables I and III.

Periodic reversal of current was used with bath (A) in an attempt to obtain smooth coherent deposits. No improvement was noted, although a wide range of direct and reverse cycles was tried. The forward cycles ranged from 20–60 sec duration with current densities from 30 to 100 amp/dm². The reverse cycles ranged from 6–15 sec duration with current densities from 60 to 200 amp/dm². No smoothing was obtained on periodically reversing current when depositing coherent molybdenum from bath (B) at 600°C and 3 amp/dm².

TABLE II. Solubility of K_3MoCl_6 in low melting halide solvents

No.	Bath composition*				Temp, °C			
	AlCl ₃	KCl	LiCl	K_3MoCl_6	300	400	500	600
1†	—	2.7	2.3	1.7	Solid	Solid	Dark red liquid mixed with small solid phase	Uniform dark red liquid
2	4.3	1.2	—	1.1	No solubility of Mo compound. Clear melt above red salt	Melt above solid Mo compound very slightly colored	Reddish brown solution with some solid phase	Same as at 500°C with only small solid phase remaining
3	4.0	—	0.8	1.1	Same as 2	Clear melt above Mo compound	Similar to 2 but more solid present	Similar to 2 but solid phase larger

* The concentration of K_3MoCl_6 in the three mixtures is in the range of 4 to 5 mole %.

† Composition No. 1 corresponds to bath (B).

cathode current efficiency over a wide range of current density.

Only a few variations in bath compositions were studied. A few tests were made with the KCl-NaCl halide solvent with lower concentrations of molybdenum than in bath (A). The data are given in Table I, No. 1–4. The dendritic deposit of No. 4 (Fig. 12) consisted of needles 0.5 to 1.5 mm long and was characteristic of the solution of intermediate concentration of molybdenum. The needles were practically monocrystalline except for small crystals growing at edges, points, or other irregularities on the needles. To find a bath with a lower melting

Anode.—In all of the electrolyses, a molybdenum anode was used. The anodes corroded cleanly with 100% efficiency. This is an advantage if this process is used for electroplating or electrorefining, but electrowinning would require either a soluble anode other than molybdenum, or more likely an insoluble anode. Insoluble anodes would require a divided cell since the molybdenum compound is very easily oxidized anodically. This was shown by an experiment in which the molybdenum anode touched the carbon crucible, thus making it anodic. The current efficiency of the anodic solution of molybdenum was considerably reduced, and the content

of molybdenum in the melt dropped considerably. The experiment indicated that anodic oxidation of the K_3MoCl_6 to volatile molybdenum compounds at a graphite electrode occurred about as readily as anodic solution of the molybdenum anode.

Voltage.—The voltage required for deposition of molybdenum was very low when using molybdenum anodes. It varied from about 0.045 volt at a current density of 3 amp/dm² to about 1.5 volt at 100 amp/dm². This indicates that the electrolytic deposition and solution of molybdenum occurs with

TABLE III. Deposits from K_3MoCl_6 -KCl-LiCl solution

Temp, °C	Current density (amp/dm ²)	Plating time (hr)	Wt deposit collected (g)	Type of deposit
600	3	5	2.9	Coherent rough plate, 0.02 in. thick (see Fig. 7, 8, 9)
900	3	5	—	Superficially coherent powder covering about 0.01 in. of badly cracked and porous plate (see Fig. 6)
600	6	4	—	Powder composed of microscopic dendrites over coherent plate
600	30	1	5.7	Fine-grained powder (5.3 g) over approximately 0.0015 plate (0.43 g)
600	100	1.75	29.0	Very fine-grain powder (see Fig. 10 and 11 and col. 1, Table IV)
900	100	1	17.9	Malleable nodular powder deposit (see Fig. 5 and col. 2, Table IV)

The composition of all solutions is that of bath (B).

very little polarization. The cathode polarization is discussed more fully in Part III of this series.

Characteristics of Deposits

Purity of the deposits.—The purity of molybdenum is an important matter, since the ductility of molybdenum, particularly at low temperatures, is believed to depend upon the absence of certain impurities such as oxygen and nitrogen. The molybdenum content of the electrolytic powders was over 99% as determined chemically. Spectrochemical analyses of three specimens of electrolytic powders (No. 1, 2, and 3, Table IV) are compared with three specimens of commercial molybdenum, one of which is a spectrochemical standard, and with a sample of specially purified molybdic oxide. The electrolytic powders compare favorably in purity with the standard specimens and commercial products.

The oxygen content of the electrolytic powders was determined by heating in dry hydrogen at 1060°C and noting the loss in weight.¹⁰ The specimens prepared under the best conditions had an oxygen content of about 0.026%. With further improvement in the atmosphere of the electrolytic cell and in the purity of the compounds, this should be capable of being reduced further. A qualitative test showed that the chloride content of the powders was negligible. Powders of columns 2 and 3, Table IV, are at least 99.9% Mo.

Properties of the deposits.—The appearance of the deposits has already been described. The electroformed tube previously mentioned was brittle, but some nodular powders obtained by electrolysis at 900°C (see Fig. 5) were somewhat malleable, as they could be slightly flattened with a hammer. The hardness of the powders ranged from 245 to 285 Vickers hardness number. Some of the powder was compacted in a mold under a pressure of 30 ton/in.² The compact, a cross section of which is shown in Fig. 13, was strong and had a density of 8.36 g/cm³. Further work will be done to determine the properties of the molybdenum after being subjected to sintering and rolling.

Electrolysis of Other Molybdenum Compounds

Molybdenum dichloride.—The interest in molybdenum dichloride stems from the fact that it is the most stable of the molybdenum halides. It is inert in moist air at room temperature and may be heated at 600°C in an inert atmosphere without decomposition. It is only slowly attacked even by nitric acid or aqua regia. Its great stability is attributed to its existence as the trimer, Mo_3Cl_6 , or hexamer, Mo_6Cl_{12} .

Twelve grams of molybdenum dichloride (for preparation, see Part II of this series) was dissolved in 100 grams of the lithium chloride-potassium chloride eutectic mixture to make a 4 mole-% solution of $MoCl_2$. This was electrolyzed in an inert atmosphere as described previously.

The conditions of electrolysis were the same as those used with K_3MoCl_6 in the KCl-LiCl solvent, i.e., 600°C, 100 amp/dm² for 30 min. The results of the run were inconclusive and the experiment may need to be repeated. A rough treed deposit of molybdenum was obtained with a cathode current efficiency of only 37% based on Mo^{2+} and 55% based on Mo^{3+} . The solidified melt remaining after the run appeared similar to those obtained with K_3MoCl_6 , and analyses showed that all the molybdenum present was in the trivalent state. These

¹⁰ The method used was kindly communicated to the authors by H. E. Hostetter, Climax Molybdenum Company, Detroit, Michigan.

TABLE IV. Spectrochemical analysis of electrolytic and commercial molybdenum powders†

Impurity	Sample No.						
	1	2	3	4	5	6	7
Aluminum	W	VW	VW	VW	VW	—	W
Barium	—	—	—	—	VW	—	—
Calcium	VW	—	T	T	T	T	—
Cobalt	VW	—	VW	VW	VW	—	VW
Chromium	T	—	—	VW	T	—	—
Copper	VW	T	T	VW	VW	VW	T
Iron	W	VW	VW	W	VW	VW	W
Magnesium	VW	T	T	VW	VW	T	T
Manganese	VW	—	—	W	VW	W	VW
Nickel	VW	—	—	VW	VW	—	VW
Lead	VW	T	T	T	T	—	T
Silicon	W	VW	VW	W	VW	W	W
Silver	T	—	—	—	—	—	—
Tungsten	—	—	—	—	—	W	—
Oxygen*	0.257%	0.026%	0.068%	0.268%			

Col. 1—part of 110-g batch from LiCl-KCl solution.

Col. 2—sample from LiCl-KCl solution produced with specially purified melt.

Col. 3—sample from NaCl-KCl solution.

Col. 4—Commercial molybdenum powder (Westinghouse Corp.).

Col. 5—Commercial molybdenum sheet used as anodes (Fansteel Corp.).

Col. 6—Specially purified MoO₃ used as spectroscopic standard.

Col. 7—Molybdenum powder (Hardy) used as spectroscopic standard.

W, weak = 0.01–0.1%.

VW, very weak = 0.001–0.01%.

T, trace = 0.0001–0.001%.

* Not determined spectroscopically.

† Spectrochemical analysis performed by E. M. Krumrine of this Bureau.

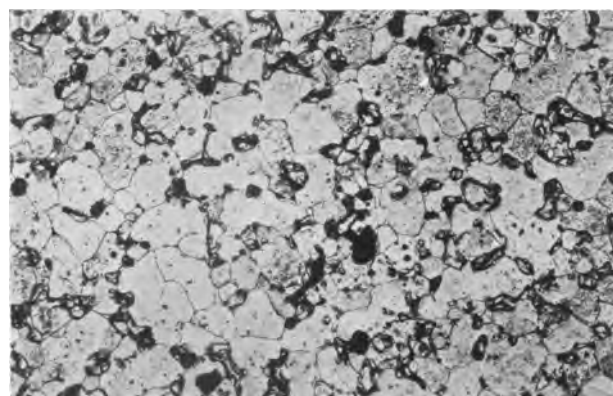


FIG. 13. Cross section of compacted and presintered molybdenum bar prepared from electrolytic molybdenum powder. 100X.

results indicate: (a) that Mo²⁺ in the melt is anodically oxidized to Mo³⁺ quite readily; and (b) that Mo²⁺ is not reduced to metal at the cathode readily, if at all. To confirm these indications a molybdenum dichloride melt would have to be

electrolyzed with separate anode and cathode compartments.

Sodium molybdate.—In previously published attempts to electrodeposit molybdenum from fused electrolytes, the alkali molybdates have been favored salts because they melt readily without decomposition. Mention was made above that small quantities of molybdates in a K₃MoCl₆ bath inhibited the deposition of pure molybdenum. Therefore, the production of pure molybdenum from fused molybdates is not to be expected.

Two molybdate melts were electrolyzed at 900°C and 100 amp/dm² with a molybdenum anode as was done with the K₃MoCl₆ in the KCl-NaCl solvent. They were: (a) pure anhydrous sodium molybdate, and (b) sodium molybdate, 13 grams dissolved in 100 grams of a melt consisting of equal parts by weight of sodium and potassium chloride. The results with both melts were similar. The bulk of the reaction product was found dispersed throughout the melt as a black, water-insoluble powder containing about 77% molybdenum, corresponding

to MoO₂ (75% Mo). Only a very thin, somewhat metallic looking film, covered by a black powder, remained on the cathode. An x-ray diffraction examination of the material on the cathode indicated that it contained molybdenum metal, Mo₂O₃, and Mo₂C. The latter must have been deposited from a secondary product resulting from the reaction of a molybdenum compound with the carbon crucible. The black cathode product was estimated to contain about 50% free Mo. Electrolysis of the sodium molybdate melt at 3 amp/dm² produced no deposit at all at the cathode.

Potassium octacyanomolybdate (IV).—Preliminary experiments with potassium octacyanomolybdate, K₄Mo(CN)₈, indicated that it was not sufficiently stable at elevated temperatures to permit it to be electrolyzed. The compound was prepared by the method of Bucknall and Wardlaw (33) and dehydrated without decomposition at 110°C. The pure salt, when heated in a sealed tube at 625°C, did not melt, but decomposed into gases and a black residue. Analysis by x-ray diffraction showed that the residue contained, among other substances, KCN and gamma-Mo₂N in about equal proportions. Since it may be expected that the cyanide complex would be more compatible with a molten cyanide solvent than with a molten chloride, a melt was made with about equal parts of KCN, NaCN, and the octacyanide, and heated in a sealed tube to 625°C. This mixture also did not melt, although KCN-NaCN alone has a melting point slightly above 500°C. The change in color, mainly to black, indicated that the molybdenum compound had decomposed.

SUMMARY AND CONCLUSIONS

This study of the electrolysis of molybdenum compounds in fused salts has shown that a solution of potassium hexachloromolybdate (III) dissolved in a mixture of alkali halides can be electrolyzed in an inert atmosphere to produce deposits of pure molybdenum at the cathode.

The recommended compositions and operating conditions for the deposition of pure molybdenum are:

	grams		grams
(A) KCl	50	(B) KCl	54.5
NaCl	50	LiCl	45.5
K ₃ MoCl ₆	33	K ₃ MoCl ₆	33
900°C		600°-900°C	

The solutions may be operated at any current density up to 100 amp/dm² with a cathode current efficiency of 100% to produce deposits of 99.9+ % molybdenum. No information at higher current densities has been obtained. At high current densities, powders are obtained from both baths, but

with solution (B) operated at 600°C and 3 amp/dm², coherent dense deposits of molybdenum up to 0.02 in. thick have been produced. It is believed that this is the first reported instance of the production of coherent massive electrodeposits of molybdenum.

ACKNOWLEDGMENTS

The authors express their sincere appreciation to Dr. William Blum, National Bureau of Standards, and to Dr. W. J. Svirbely, Professor of Chemistry, University of Maryland, for their advice and guidance during the course of this work, and to the United States Army Ordnance Department for their financial support.

Any discussion of this paper will appear in a Discussion Section to be published in the December 1954 issue of the JOURNAL.

REFERENCES

1. H. W. DAVIS, "Molybdenum," from "Minerals Yearbook," U. S. Bureau of Mines, p. 785 (1949).
2. R. M. PARKE, *Metal Progress*, **60**, 81 (1951); J. J. HARWOOD, *Product Eng.*, **23** (1), 121 (1952).
3. R. M. PARKE AND J. L. HAM, *Trans. Am. Inst. Mining & Met. Engrs.*, **171**, 416 (1947).
4. W. J. CHILDS, J. E. CLINE, W. M. KISNER, AND J. WULFE, *Trans. Am. Soc. Metals*, **43**, 105 (1951).
5. J. J. LANDER AND L. H. GERMER, *Trans. Am. Inst. Mining & Met. Engrs.*, **175**, 648 (1948).
6. H. J. SEIM AND M. L. HOLT, *Trans. Electrochem. Soc.*, **96**, 205 (1949).
7. L. F. YNTEMA, U. S. Pat. 2,428,404 (1947).
8. R. M. PARKE, in "Metals Handbook," p. 1230, American Society for Metals, Cleveland, Ohio (1948).
9. W. P. SYKES, *ibid.*, 1210.
10. M. HANSEN, "Der Aufbau der Zweistofflegierungen," J. Springer, Berlin (1936).
11. K. WOLF, Dissert. Aachen Tech. Hochschule (1917); Gmelin's "Handbuch der Anorg. Chem.," 8th ed., Syst. 53, Molybden, p. 155 (1935).
12. WOLFRAM-LAMPEN, A. G., German Pat. 237,014 (1910).
13. H. S. BOOTH AND M. MERLUB-SOBOL, *J. Phys. Chem.*, **35**, 3319 (1931).
14. M. J. KSYCKI AND L. F. YNTEMA, *Trans. Electrochem. Soc.*, **96**, 48 (1949).
15. A. CHILESOTTI, *Z. Elektrochem.*, **12**, 146, 173, 197 (1906).
16. C. G. FINK AND C. H. ELDRIDGE, Canadian Pat. 274,429 (1927).
17. L. F. YNTEMA, *J. Am. Chem. Soc.*, **54**, 3775 (1932).
18. E. POKORNY AND K. SCHEIDER, German Pat. 582,528 (1934).
19. W. P. PRICE AND O. W. BROWN, *Trans. Electrochem. Soc.*, **70**, 423 (1936).
20. K. A. PAUL, Russian Pat. 53,756 (1938); *C.A.*, **35**, 1326 (1941); A. S. MININ, Russian Pat. 59,863 (1941); *C.A.*, **39**, 873 (1945).
21. GMELIN'S "Handbuch," *op. cit.*, p. 35.
22. H. ALTHERTUM, *Z. angew. Chem.*, **42**, 4 (1929); G. M. DYSON, *Chem. Age, London*, (Monthly Metallurgical Section) **18**, 33 (1928).
23. G. GIN, *L'Electricien*, **32**, 107 (1906).
24. *Metallborse*, **18**, 1155 (1928).

25. J. W. BECKMANN, U. S. Pat. 973,336 (1910).
26. A. KRATKEY AND W. BRUCKNER, German Pat. 263,301 (1911).
27. T. R. FORLAND, U. S. Pat. 1,305,350 (1919).
28. J. L. ANDRIEUX, *Ann. chim.*, [10] **12**, 499 (1929).
29. A. BRENNER AND S. SENDEROFF, *This Journal*, **99**, 223C (1952).
30. SCOTT'S "Standard Methods of Chemical Analysis," (N. H. Furnam, Editor) 5th ed., Vol. 1, p. 594, D. Van Nostrand Co., Inc., New York (1939).
31. *Ibid.*, p. 591.
32. C. G. GOETZEL, "Treatise on Powder Metallurgy," Vol. 1, p. 668, Interscience Publishers, Inc., New York (1949).
33. W. R. BUCKNALL AND W. WARDLAW, *J. Chem. Soc.*, **1927**, 2983.

The Electrolytic Preparation of Molybdenum from Fused Salts

II. The Preparation of Reduced Molybdenum Halides¹

SEYMOUR SENDEROFF AND ABNER BRENNER

National Bureau of Standards, Washington, D. C.

ABSTRACT

An improved method for the preparation of potassium hexachloromolybdate (III), K_3MoCl_6 , is described. Potassium molybdate is dissolved in hydrochloric acid and the solution electrolyzed in a divided cell. Hydrogen chloride gas is then added to the catholyte to precipitate K_3MoCl_6 .

A new method for preparing molybdenum dichloride, $(MoCl_2)_x$, is described. Molybdenum pentachloride is reduced with molybdenum powder to the trichloride. This is then heated to produce the molybdenum dichloride by thermal dissociation.

INTRODUCTION

The methods in the literature for preparing potassium hexachloromolybdate (III), K_3MoCl_6 , and for molybdenum dichloride, $(MoCl_2)_x$, were found to be unsatisfactory for the preparation of large quantities of material, and so new procedures were developed which are described herein.

POTASSIUM HEXACHLOROMOLYBDATE (III)

Potassium hexachloromolybdate (III), K_3MoCl_6 , was first prepared by Chilesotti (1) and later by Bucknall and coworkers (2). The latter's procedure is based on an electrolytic reduction of a solution of molybdic acid in strong hydrochloric acid, followed by addition of potassium chloride. The method yielded a pure anhydrous product, but since it involved very dilute solutions and evaporations under reduced pressure, it was inconvenient for the preparation of large amounts of the salt. Modifications were introduced which eliminated these defects and gave a very interesting insight into the chemistry of the formation of this compound.

The procedure used in this laboratory for preparation of potassium hexachloromolybdate (III), K_3MoCl_6 , is as follows. Potassium molybdate, 480 g, was dissolved in 1050 ml of water, and this solution was added to 1050 ml of 12*N* hydrochloric acid in a 3-liter beaker. (Note: If the acid is added to the molybdate solution, molybdic acid precipitates and is very difficult to redissolve.) The beaker was loosely covered with a plastic disk into which had

been drilled one large central hole, two smaller holes near the outer edge at both ends of a diameter, and a third smaller hole near the outer edge. A porous alundum cylinder, closed on the bottom, was filled with 200 ml of 12*N* hydrochloric acid and inserted through the central hole of the cover. This cylinder served as a diaphragm between the anolyte it contained and the catholyte around it. Two sheets of platinum, used as cathodes, were held by platinum wires through corks placed in the two opposite holes in the cover, and a glass tube connected to a nitrogen tank was inserted through a cork in the third outer hole of the cover. A 1/2-in. diameter graphite rod, serving as anode, was inserted into the anolyte and the level of the anolyte was adjusted to the same height as that of the catholyte.

The solution was electrolyzed with a current of 20 amp (cathodic current density, about 7 amp/dm²) for 8 hr.

The course of the electrolysis was followed by taking samples of the catholyte, adding them to excess ferric alum solution, and titrating with potassium permanganate. When the reducing power of the catholyte became constant, the electrolysis was stopped. The catholyte was agitated during the electrolysis by a stream of nitrogen, and the anolyte received periodic additions of concentrated hydrochloric acid to replace that lost by electrolysis and as spray. The temperature of the catholyte rose during the electrolysis to 65°C, and the solution became dark red. The catholyte was removed, heated to 95°C, and saturated with hydrogen chloride gas. As the solution cooled, more hydrogen chloride gas was added and crystals of K_3MoCl_6 separated. These were filtered, washed with 1600 ml of 12*N* hydrochloric acid, 1600 ml of 1:1 12*N* HCl-alcohol mixture, and 1600 ml of methanol. The red crystals

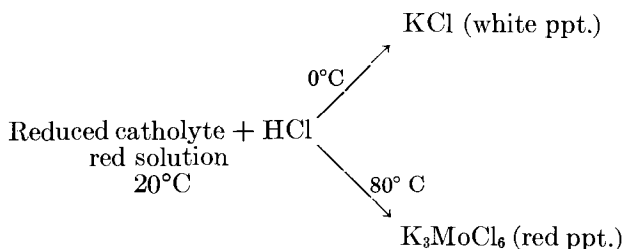
¹ Manuscript received April 7, 1953. This paper was prepared for delivery before the Philadelphia Meeting, May 4 to 8, 1952. Based on a thesis submitted by Seymour Senderoff to the Faculty of the Graduate School of the University of Maryland in partial fulfillment of the requirements for the Ph.D. degree.

were dried by heating under reduced pressure, and analyzed.

The analysis gave Mo, 22.6% and Cl, 50.2% (theoretical—Mo, 22.5% and Cl, 49.9%). A yield of 400 grams or about 70% of calculated was obtained.

Properties

During the development of this method a series of reactions were observed which demonstrate that the $[\text{MoCl}_6]^{-3}$ ion is extremely stable in acid solution and not subject to rapid reversible dissociation and formation at room temperature. If the catholyte is reduced and saturated with hydrogen chloride gas without permitting its temperature to rise, and then cooled to near 0°C , potassium chloride precipitates. If instead of cooling after saturation with hydrogen chloride, the solution is heated at this point to above 80°C , K_3MoCl_6 precipitates, i.e.,



This conclusively demonstrates that the reduced catholyte, before heating, contains potassium ions, cations containing trivalent molybdenum, and chloride ions, and little, if any, complex molybdenum anions.

On cooling, the potassium chloride crystallizes because of its insolubility in concentrated hydrochloric acid. On heating, however, the reaction $\text{Mo}^{3+} + 6\text{Cl}^- \rightarrow [\text{MoCl}_6]^{-3}$ occurs and K_3MoCl_6 precipitates. On cooling the mother liquor from this precipitation, more K_3MoCl_6 separates but no KCl, because most of the K^+ has been removed in the precipitation of the complex salt. Were $[\text{MoCl}_6]^{-3}$ in equilibrium with Mo^{3+} and Cl^- , as is the case with complexes such as $[\text{Ag}(\text{CN})_2]^-$ or $[\text{Ag}(\text{NH}_3)_2]^+$, the K_3MoCl_6 would have precipitated immediately on saturating the reduced catholyte with hydrogen chloride. Probably the major function of the evaporations used by previous investigators to prepare this salt was the formation of the complex ion by heating, rather than merely concentrating the salts.

The salt, K_3MoCl_6 , is a brick-red stable salt. It precipitates without any water of crystallization, but, if insufficient hydrogen chloride is added before precipitation, an aquo complex, possibly $\text{K}_2[\text{MoCl}_5\text{H}_2\text{O}]$ (2), may precipitate. The water cannot be removed from this compound by heating without decomposing the compound. The K_3MoCl_6

may be heated in air at 110°C without any decomposition. In the dry state it is stable to light and not hygroscopic. It may be heated in vacuo to at least 600°C for 20 hr without observable decomposition or melting. This is particularly significant when one remembers that MoCl_3 is unstable above 340°C (4) and that at 650°C it is completely decomposed to MoCl_2 and Mo metal. This further demonstrates that the K_3MoCl_6 is not a double salt which may be represented by the formula $3\text{KCl} \cdot \text{MoCl}_3$, but that it is a salt of the highly stable complex anion, $[\text{MoCl}_6]^{3-}$. When very hot its color darkens slightly, but it lightens again on cooling. It is rapidly decomposed at 600°C , however, if in contact with air or moisture. The standard procedure finally adopted for removing the last traces of adsorbed water from the compound before using it in a molten electrolyte was to heat it in vacuo at 250°C for two to three hours and then to store it in a desiccator.

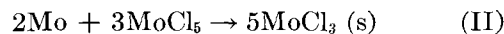
MOLYBDENUM DICHLORIDE

Molybdenum dichloride, $(\text{MoCl}_2)_x$, where the x has been shown by various investigators to be 3 or 6 (3), was first prepared by Blomstrand (5) by the thermal decomposition of molybdenum trichloride which he obtained by the hydrogen reduction of molybdenum pentachloride. The difficulties in this procedure were noted by Liechti and Kempe (6) and others who suggested various precautions and modifications. The hydrogen reduction of molybdenum pentachloride is particularly difficult and attempts here to accomplish this resulted in impure products with poor yields. Lindner and co-workers (7) describe what is alleged to be a superior method in which molybdenum powder is chlorinated by reaction with phosgene at 610°C .

This reaction was attempted both as directed and with a number of modifications but was unsatisfactory for the preparation of appreciable amounts of pure material. After consulting the thermodynamic data on the molybdenum halides collected by Quill (4), a method was devised which proved quite successful. According to Quill, the reaction:

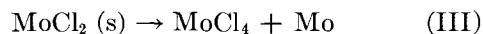


at 340°C at 1 atm total pressure reaches equilibrium with MoCl_4 at a partial pressure of 0.7 atm and MoCl_5 at a partial pressure of 0.3 atm. Further, at 330°C the reaction:



goes practically to completion with the MoCl_5 at 1 atm pressure.

Lastly, the reaction:



does not begin until 530°C is reached and at 600°C the equilibrium pressure of MoCl₄ is only 1 atm.

By heating molybdenum powder with an excess of molybdenum pentachloride in a sealed tube at 350°C, reaction (II) may be accomplished while reaction (I) is suppressed. When the molybdenum powder is all used up, the excess molybdenum pentachloride may be removed and the molybdenum trichloride heated at some temperature below 600°C to form MoCl₂, without reaction (III) occurring to a large extent.

An attempt to reduce molybdenum pentachloride to molybdenum dichloride by reduction with molybdenum at high temperature in one step did not give a pure product. This was probably due to the molybdenum powder being coated over with MoCl₂ which prevented further reaction of the molybdenum metal. The two-step procedure, however, was quite successful, although it was necessary to perform the final step at 650°C, resulting in slight contamination of the MoCl₂ by molybdenum powder. Below this temperature the disproportionation of the trichloride proceeded somewhat slowly.

The following was the procedure used: 7.6 g of Mo powder was mixed with 36.6 g of MoCl₅ (4.6 g MoCl₅ excess) and charged into a Pyrex gauge glass tube 1.5 cm diameter and 30 cm long. The tube was evacuated, sealed, and placed in a steel pipe closed at both ends. The entire assembly was allowed to stand in a furnace at 350°C for 48 hours. The tube was tilted during this heating so that most of the product would be at one end. After cooling, the other end was opened and a "condensing angle" was sealed onto the open end. The "condensing angle" was a 12-in. length of the same gauge glass, bent in the middle to an angle of about 120°. The tube was again evacuated and sealed and set in the furnace with the 6-in. length beyond the bend protruding out of the furnace. The temperature was brought up slowly and the excess molybdenum pentachloride collected in the cold end.

When most of the pentachloride had distilled over (at about 300°C) the temperature was raised to 650°C and held there for 24 hours to effect the disproportionation and further purification. Although the hot end softened and flattened considerably, the glass did not collapse or break, and the bright yellow dichloride, (MoCl₂)_x, remained in the hot portion of the tube. Fourteen grams of relatively pure material were obtained for a yield of 65% based on the molybdenum powder used. Analysis showed it to contain 58.3% Mo and 43.7% Cl. Theoretical composition for MoCl₂ is 57.4% Mo and 42.6% Cl. A slight excess of molybdenum may be present in the product and is probably due to free molybdenum metal formed by decomposition of the MoCl₂. This could have been avoided by

heating for a much longer time at about 600°C instead of 650°C, but since a small amount of free molybdenum metal would not be harmful in an electrolysis test, it was not considered necessary to do this.

Properties

The material must be used in the condition in which it is produced. Attempts to remove the free metal with dilute nitric acid resulted in the formation of a hydrate, $x\text{MoCl}_2 \cdot y\text{H}_2\text{O}$ from which the water could not be removed without decomposing the salt. The (MoCl₂)_x is slightly soluble in alcohol, but an alcoholate is formed, and attempts to drive off the alcohol also resulted in decomposition.

A sample of MoCl₂ was mixed with a portion of a eutectic mixture of lithium chloride and potassium chloride which had been previously fused and ground. The mixture had the following composition in weight per cent: MoCl₂, 12.3%; LiCl, 40.3%; KCl, 47.4%; and was a 4.4 mole per cent MoCl₂ solution. On heating this mixture in an evacuated sealed tube to 600°C, the charge became completely fluid and, on freezing, it was observed to have become a uniform bright red. A complex halide had evidently formed.

SUMMARY

A simplified method for the preparation of potassium hexachloromolybdate (III) and a new method for the preparation of molybdenum dichloride has been described.

ACKNOWLEDGMENTS

The authors express their sincere appreciation to Dr. William Blum, National Bureau of Standards, and to Dr. W. J. Svirbely, Professor of Chemistry, University of Maryland, for their advice and guidance during the course of this work, and to the United States Army Ordnance Department for their financial support.

Any discussion of this paper will appear in a Discussion Section, to be published in the December 1954 issue of the JOURNAL.

REFERENCES

1. A. CHILESOTTI, *Atti reale accad. Lincei*, [5] **12** II, 67 (1903); *Gazz. chim. ital.*, **33** II, 354 (1903).
2. W. R. BUCKNALL, S. R. CARTER, AND W. WARDLAW, *J. Chem. Soc.*, **1927**, 513.
3. N. V. SIDGWICK, "Chemical Elements and Their Compounds," Vol. II, p. 1061, Oxford (1950).
4. L. L. QUILL, "The Chemistry and Metallurgy of Miscellaneous Materials," paper 8, p. 276 ff, McGraw Hill Book Company, New York (1950).
5. C. W. BLOMSTRAND, *J. prakt. Chem.*, **77**, 97 (1859).
6. L. P. LIECHTI AND B. KEMPE, *Liebigs Ann. Chem.*, **169**, 354 (1873).
7. K. LINDNER, E. HALLER, AND H. HELWIG, *Z. anorg. v. allgem. Chem.*, **130**, 209 (1923).

The Electrolytic Preparation of Molybdenum from Fused Salts

III. Studies of Electrode Potentials¹

SEYMOUR SENDEROFF AND ABNER BRENNER

National Bureau of Standards, Washington, D. C.

ABSTRACT

Polarization and equilibrium potential studies in molten halide solutions are described. A new reference half-cell, i.e., Ag, AgCl, was used. It was found that molybdenum is rather noble (between copper and silver) in the emf series in this system, but that oxides are preferentially deposited if oxycompounds are present. Evidence for ionic association and complex formation in molten halides at 600°C is discussed.

INTRODUCTION

In order to obtain some insight into the electrochemistry of the fused salt systems (1), measurements of cathode potentials were made on some of them, and the static potentials of a number of metal-metal salt systems in the same halide were measured.

EXPERIMENTAL

Reference Electrode

To measure electrode potentials, a reference electrode, which is constant, reproducible, and reversible, is required. Yntema and his students (2) described a reference electrode for use in molten salts between 100° and 200°C which consisted of an aluminum rod in a ternary mixture of AlCl₃-NaCl-KCl. This was not suitable in the range of interest, i.e., 600°-900°C, mainly because of the volatility of AlCl₃. An ideal molten electrolyte for this range of temperature is silver chloride, which melts at 455°C, boils at 1550°C, and is easily prepared with high purity. No other stable valence states of silver exist to provide ambiguity of composition, and, in the absence of light, the chloride undergoes no visible decomposition when heated for long periods of time. Oxide contamination, which is a serious problem in most molten systems, does not occur in silver chloride because silver oxide decomposes at about 300°C, and, if formed during filling of a cell, would be destroyed when the cell is brought up to temperature.

That the Ag, AgCl(l) cell is reversible and

practically nonpolarizable was shown by Aten, den Hertog, and Westenberg (3) who reported that silver dissolved anodically and deposited cathodically from molten silver chloride at 475°C, and that the polarization voltage was only 0.5 mv at a current density of 1 amp/dm². This was confirmed in tests described below.

In the design of a cell, one serious disadvantage of the Ag, AgCl(l) electrode had to be considered. Since silver is quite noble, its presence in an electrolyte in which the potential of a base-metal electrode was being measured would cause a serious error. On the other hand, the presence of a foreign electrolyte, containing a base-metal ion, in the molten AgCl would have a minor effect on the potential of the reference electrode as its effect would be dependent only on the slight decrease in the concentration of AgCl in the cell. The cell was designed, therefore, to minimize diffusion and convection, and to cause the direction of flow of molten liquid, if any, to be toward the molten silver chloride rather than toward the electrolyte, and to have a large amount of silver chloride present so that small impurities of base-metal electrolyte entering it would cause negligible changes in its potential.

The reference electrode cell is shown in Fig. 1. It is made of fused silica and consists of two tubes (A, D) of 9-mm bore connected by a heavy walled capillary (B) of 1.5-mm bore. Another capillary tube (C) is fitted as shown, onto one of the larger tubes. The end of this capillary is bevelled to an angle of about 60°, and is the equivalent of the Luggin capillary used as a probe for measuring potentials in aqueous solution. At the point where capillary (B) enters tube (D), there is a constriction which is tightly packed with asbestos. Molten silver chloride is poured into tube (A) and suction is

¹ Manuscript received April 7, 1953. This paper was prepared for delivery before the Philadelphia Meeting, May 4 to 8, 1952. Based on a thesis submitted by Seymour Senderoff to the Faculty of the Graduate School of the University of Maryland in partial fulfillment of the requirements for the Ph.D. degree.

applied to tube (D) [while stopping up the opening of (C)] until a tiny bead of silver chloride is drawn through the asbestos plug. A clean $\frac{1}{8}$ -in. rod of silver is inserted into the molten chloride to within one inch of the bottom of tube (A) and held in that position by a silver disk fitting over the top of the tube. A silver wire is silver-soldered to the top of the silver rod. The entire cell was anchored at the top in an aluminum fixture in which it was rigidly held by spring-loaded set screws. This fixture also held the cathode in contact with the end of capillary (C). A strip of molybdenum sheet serving as anode was bent to a half-cylinder and placed over the outside of tube (A). It was held by a clamp, to

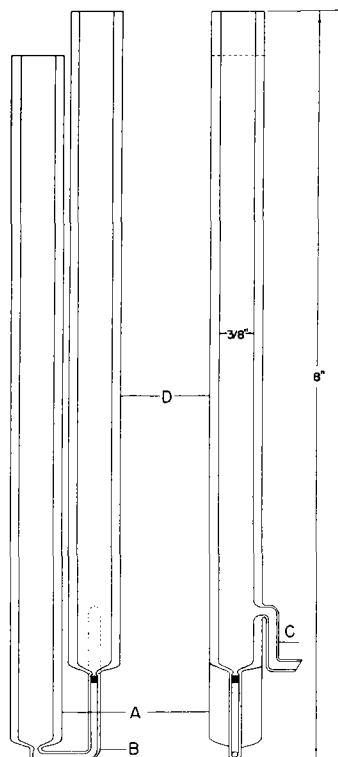


Fig. 1. Detail of reference electrode half-cell

which a heavy plastic-insulated wire was attached. This wire was wound as a helix and served as an anode lead.

The entire assembly was suspended by the cathode from the electrode connector, (J),² the anode lead wire and the wire from the silver reference electrode were drawn through holes in the rubber stopper in the bung, (E),² and the system closed. After the procedure described earlier (1) for establishment of an inert atmosphere was followed, the electrolyte in the crucible was melted and the electrode assembly lowered into the crucible. The electrolyte then entered tube (D), through capillary (C), and formed a liquid junction with the silver chloride at the

² See Fig. 2, Reference (1).

asbestos plug. The levels of the solutions were adjusted so that the level of the electrolyte in (D) was slightly higher than that of the silver chloride in (A). The asbestos plug was tight enough to prevent flow of solution through it except under applied vacuum, as when filling the cell, but the levels were adjusted in this manner so that if flow did occur it would be toward the silver chloride rather than toward the electrolyte. Current was passed through the cell (cathode area = 0.1 dm^2) as for plating. The current was set and held at each value for about one minute while the potential between the cathode and reference electrode was measured using a potentiometer and high-sensitivity galvanometer. Zero current values were taken before and after each run, and they usually agreed fairly well.

When measuring equilibrium potentials, the anode was not used, and the cathode hung above capillary (C) rather than in contact with it. The same procedure for maintaining an inert atmosphere was followed. Potentials were read at half-hour intervals, and when the potential remained constant within 1 mv for 3 hr, that value was taken as the equilibrium potential.

The reproducibility and reversibility of the reference electrode was confirmed in the following manner. Silver chloride was poured into both sides of the quartz cell, capillary (C) was sealed, and silver rods inserted in both legs of the cell. The entire unit was immersed in molten potassium chloride-lithium chloride eutectic mixture which was maintained at 600°C . The immersed area of the electrodes was 0.025 dm^2 . The initial potential difference of 3.0 mv fell in 1 hr to 0.4 mv, at which point the potential difference became constant. This potential difference is probably due to some small asymmetry in the two electrodes, contact potentials, etc. The cell was then polarized by passing current through it for 5-min periods. The circuit was then opened and the potential read.

After passing 1 ma through the cell, the 0.4-mv potential was re-established in less than 30 sec after opening the circuit. With 2.5 ma, 1 min was required, and with 5 ma (equivalent to 0.2 amp/dm^2) the cell was permanently polarized, its potential being 1 mv 30 min after opening the circuit. Since full-scale deflection of the galvanometer used during the measurements corresponded to a current of $0.6 \mu\text{amp}$, the possibility of polarizing the cell while balancing the potentiometer was negligible. That the cell is reversible is demonstrated by the fact that one of the silver rods was anode, and the other cathode during polarization, and, up to 2.5 ma, the cell reverted rapidly to normal on stopping the polarizing current. The reversibility of the molybdenum electrode in the K_3MoCl_6 -alkali halide melt

was demonstrated by the electrodeposition and anodic solution of the metal at low current densities and low polarization.

Cathode Potential Measurements

A solution of K_3MoCl_6 in LiCl-KCl eutectic mixture of a standardized composition (4.1 mole % K_3MoCl_6) was prepared and purified by thermal and electrolytic means (1). The reference electrode cell, with molybdenum anode and cathode, was inserted into the melt and allowed to stand until the static potential became fairly constant. Readings were then taken at 20 points in the current density

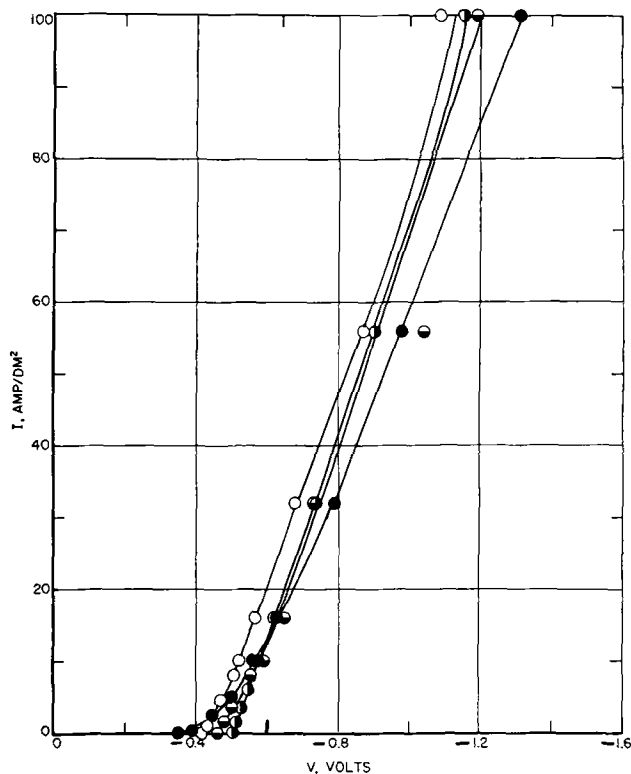


Fig. 2. Cathode potential curves for solution of K_3MoCl_6 in LiCl-KCl (0-100 amp/dm²) measured against silver-silver chloride electrode. ●—600°C; ○—700°C; ◐—800°C; ◑—900°C.

range from 0-100 amp/dm². Fewer points were taken in the upper than in the lower part of the range because, at high current density, the nature of the cathode surface changes very rapidly and makes the values obtained less reliable. Current density-potential curves were determined at 600°, 700°, 800°, and 900°C. Duplicate runs were made for each temperature, no two runs at the same temperature being done consecutively. In addition, the runs at different temperatures were done in random sequence, so that the effects of time or systematic variation in the solution would not be confused with a temperature effect. The average value of the two

determinations of cathode potential for each current density and temperature was used in plotting the isothermal cathode potential curves. Fig. 2 shows these over the entire range of 0-100 amp/dm². Fig. 3 shows the 0-10 amp/dm² range on an expanded scale. On the whole, the values are reproducible to about ± 10 mv.

The static or equilibrium potentials range from 0.349 volt to 0.501 volt between 600° and 900°C with a temperature coefficient of $+5 \times 10^{-4}$ volts/deg. The silver reference electrode is the positive (noble) pole.

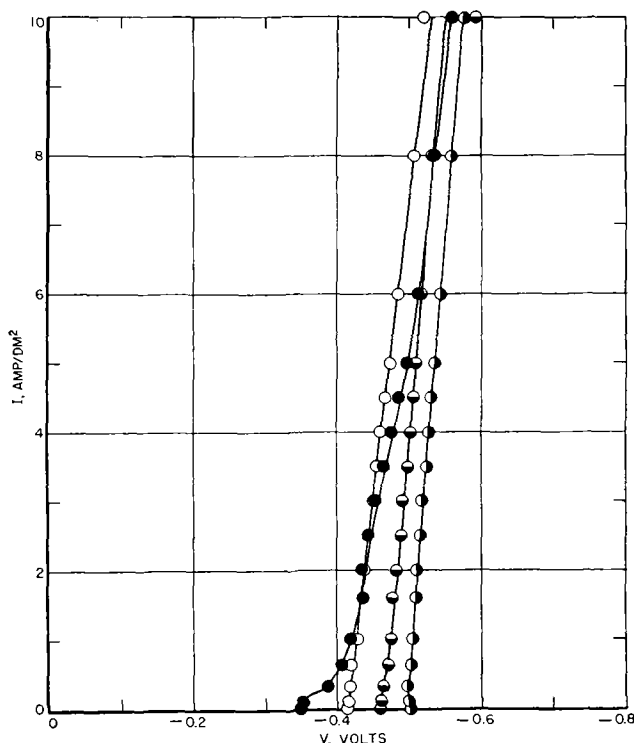


Fig. 3. Low current density portion of curves of Fig. 2 (0-10 amp/dm²) measured against silver-silver chloride reference electrode. ●—600°C; ○—700°C; ◐—800°C; ◑—900°C.

When the same solutions were contaminated by exposure to air, the current density-potential curves shown in Fig. 4A were obtained. The equilibrium potentials ranged from 0.071-0.034 volt between 600° and 800°C with a temperature coefficient of -2×10^{-4} voltage. Heating to 900°C and/or electrolysis restored the solution to its original condition.

These results show conclusively that air contamination ennobles the potential of a molybdenum electrode in the solution by about 0.3-0.4 volt.

In order to study the cathode potentials in a system containing potassium molybdate, a solution consisting of 45.5 grams of LiCl, 54.5 grams of KCl, and 18.5 grams of K_2MoO_4 (4.1 mole % K_2MoO_4) was prepared and current density-voltage curves run

under inert atmosphere, with usual precautions for drying the salts. The initial values of equilibrium potentials varied from 0.75–1.25 volts, with no reproducibility between the zero current potential at the beginning and end of the run. The silver electrode was still the positive pole. In any event, this unstable potential showed the electrode to be much less noble than in the trivalent molybdenum solution. The solution was then electrolyzed, after which stable equilibrium potentials were obtained. The values were 0.029 volt at 600°C and 0.052 volt at 900°C, or about the same as in a melt con-

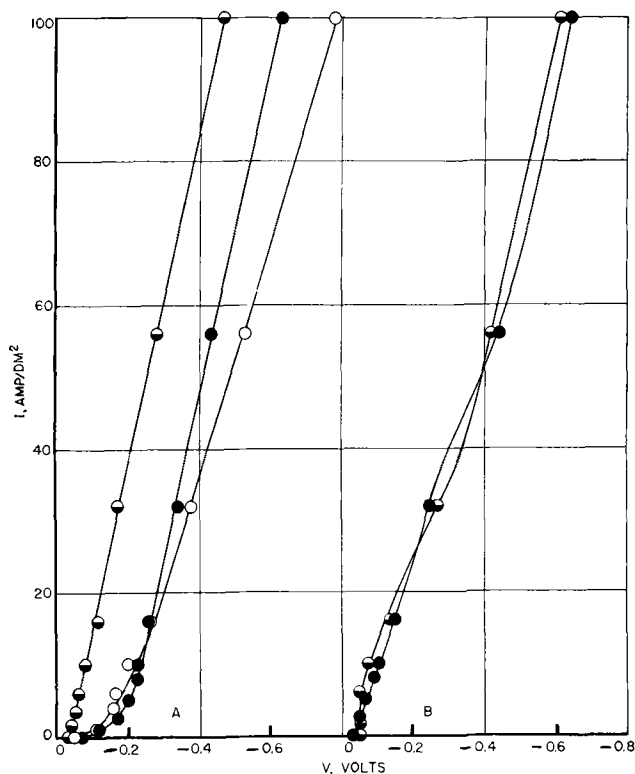


FIG. 4A. Cathode potential curves for air-contaminated K_3MoCl_6 solution. ●—600°C; ○—700°C; ◐—800°C.

FIG. 4B. Cathode potential curves of solution of K_2MoO_4 in LiCl-KCl. ●—600°C; ◐—900°C. (Both measured against silver-silver chloride reference electrode.)

taminated with air. The temperature coefficient was $+8 \times 10^{-5}$ volts/deg in this range. These values remained in this range despite heating, electrolysis, or other treatment. The cathode potential curves for this solution are shown in Fig. 4B. The potential values obtained in this solution are not as reproducible as in the uncontaminated trivalent molybdenum solution.

Equilibrium Potentials of Other Metals in Molten Lithium Chloride-Potassium Chloride

To obtain some information about the emf series in molten halide melts at 600°C, and particularly

the position of molybdenum in this series, equilibrium potential data were obtained for zinc, ferrous iron, cuprous copper, and silver, each in 4.1 mole per cent solutions of their chlorides in the KCl-LiCl eutectic mixture in the absence of air. The anhydrous salts were prepared in the following manner. Commercial anhydrous C.P. zinc chloride and ferrous chloride, $FeCl_2 \cdot 4H_2O$, were dried in a current of dry hydrogen chloride at 400°C for two hours. Cuprous chloride was washed free of cupric compounds with water and dried at 450°C in a stream of dry hydrogen chloride. Since zinc was molten at the temperature of the experiments, the zinc electrode consisted of a pool of zinc in the bottom of the vessel. Electrical contact was established with a tungsten rod sealed in glass. Measurements were made as described earlier.

Table I gives the equilibrium potentials found for these systems.

Also included in the table is the equilibrium potential found for molybdenum under conditions similar to those used for the other metals. This

TABLE I. Potential, E , of M electrode in 4.1 mole % M chloride dissolved in KCl-LiCl (eutectic composition) against the Ag, AgCl (pure) reference electrode at 600°C

M	E (volt)
Zinc.....	-1.277
Iron (divalent).....	-1.033
Copper (monovalent).....	-0.626
Molybdenum (trivalent).....	-0.349
Silver.....	-0.312

table represents the emf series for these elements at 600°C at a concentration of 4.1 mole per cent in LiCl-KCl eutectic mixture as solvent.

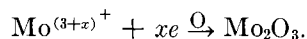
DISCUSSION OF RESULTS

Current Density-Potential Curves

One of the most important facts demonstrated previously (1) was the inability to obtain a pure molybdenum deposit from solutions containing oxygenated salts or even from solutions of non-oxygenated salts which have been slightly contaminated with air or moisture. Whenever oxygenated compounds were present, the current efficiency for molybdenum deposition was reduced and molybdenum oxides were formed in the deposit, as shown by x-ray diffraction. A consideration of the potential measurements with the pure trivalent molybdenum, air-contaminated trivalent molybdenum, and molybdate solutions clearly demonstrates the cause of this behavior. In addition, it gives some insight into the electrochemistry of these systems. The equilibrium potential of a molybdenum electrode in

an air-contaminated trivalent molybdenum solution is about 0.4 volt lower (more noble) than in a pure trivalent molybdenum solution. A difference of this magnitude indicates that the electrode reactions occurring in the two systems must be entirely different. Not only is this shown by the magnitude of the difference in potential but by the fact that the temperature coefficient of the potentials differs in magnitude and sign.

Consider the manner in which oxides deposit on the cathode from contaminated solutions. Since the trivalent molybdenum salt is easily oxidized by air at these temperatures, one of the effects of the contamination must be to produce oxygenated compounds of molybdenum in which the molybdenum has a valence higher than three. The potential measurements showed that the reduction of these intermediate valence molybdenum compounds to the trivalent oxide proceeds at a more noble potential than does the reduction of trivalent molybdenum to molybdenum metal. That is, the higher, more negative potential is characteristic of the electrode reaction, $\text{Mo}^{3+} + 3e \rightarrow \text{Mo}$; and the more noble potential is characteristic of a reaction which may be written:



It is apparent that oxygen must be absent from the system in order to obtain pure molybdenum. Therefore, from a contaminated bath at low current density one would expect no molybdenum deposit at all, only oxides, and at high current density, when the cathode has become sufficiently polarized to reach the deposition potential for molybdenum metal, both processes should occur. At 600°C, the cathode in a contaminated bath does not reach the potential at which molybdenum can codeposit with the oxide until a current density of 30–40 amp/dm² is attained, and, at 900°C, it barely reaches it at 100 amp/dm².

In the initial potential measurements on the potassium molybdate solution no equilibrium potential at all was obtained with a molybdenum electrode. The unstable potential observed was more than 0.5 volt less noble than that for reducing trivalent molybdenum to metal. This suggests that a molybdate solution is actually not in equilibrium with a molybdenum electrode, that is, the reaction $\text{MoO}_4^- + 6e \rightarrow \text{Mo} + 4\text{O}^-$ either does not occur or never reaches equilibrium. The very high initial potential observed is of no consequence with regard to electrode reactions since, after electrolysis for a short while, it changes to a stable potential of about the same value as that obtained with an air-contaminated trivalent solution.

The molybdate solutions and the contaminated

trivalent molybdenum solutions turn blue during electrolysis, which confirms the presence of molybdenum compounds with a valence of 4 or 5, and it is these, rather than the hexavalent molybdenum, which are in equilibrium with the electrode. Breaks in the curve occur in the vicinity of 0.3 volt at about 30 amp/dm², and these probably represent the beginning of the reduction of trivalent molybdenum to metal. Since the potentials measured in the electrolyzed molybdate solution and in the air-contaminated trivalent molybdenum solution are about the same, the same reaction may be occurring. This is confirmed by x-ray diffraction which identified Mo_2O_3 in the deposit from the molybdate and in the deposit from the trivalent molybdenum solution.

The potentials of a molybdenum electrode in dilute solutions of K_2MoO_4 and K_3MoCl_6 in AlCl_3 - NaCl - KCl mixture at about 200°C were reported (4) to be about the same. They are the same because those experiments were all run with the solutions exposed to air and all of the solutions were purified by electrolysis. Therefore, this compared electrolyzed molybdate solution with an air-contaminated trivalent molybdenum solution, solutions which were shown here to give very similar cathode potential curves. Neither of these solutions, however, gives pure molybdenum deposits, so the deposition potentials which were reported cannot be ascribed to any definite electrode reaction.

Relation Between Cathode Potential Curves and the Nature of the Deposit

The cathode potential curves for deposition of molybdenum at the various temperatures were examined to determine whether they correlated with the physical form of the deposit. The molybdenum deposits obtained from the fused baths were powdery or dendritic, with the exception of the deposits obtained from the 600°C bath below a current density of 3 amp/dm²; it is of interest to inquire whether this is related to the observed cathode potential curves. In deposition from aqueous solution, the production of fine-grained smooth deposits is often associated with a higher polarization than that attending the deposition of the coarsely crystalline or spongy deposits from solutions of simple salts. The smoother deposits may not necessarily be caused by the higher polarization, but apparently the same conditions that yield the smoother deposits also cause the higher polarization.

The cathode potential curve for molybdenum deposition at 600°C (Fig. 3) has a slight change in curvature at about 3.5 amp/dm², which corresponds approximately to the change of deposit from the coherent to the powdery form. However, this break

is so slight that it is barely beyond the precision of measurement, and may be considered as the effect of the change in surface area of the deposit on the cathode potential, rather than a change in the nature of the electrode reaction. The slope of the curve for 600°C is somewhat flatter than the curves obtained for the higher temperatures over the whole range of current density from 0–100 amp/dm² thus indicating a higher polarization. It is only from the 600°C bath that smooth coherent deposits are obtained at low current density. They became powdery above 3 amp/dm², but this is probably the usual "burning" which is observed with all plating solution at high current densities.

The main difference between the current density-potential curve for deposition at 600°C and at the higher temperatures appears to be the presence of a break in the 600°C curve at about 0.25 amp/dm². This break indicates that a change in the electrode reaction occurs at this point and that it may be the source of the polarization observed in this bath. It is suggested that this represents the current density at which the slow dissociation of the (MoCl₆)³⁻ becomes the rate-controlling step of the reaction. Below this point, the deposition of molybdenum may occur by discharge of the Mo³⁺ ion, but above this point the concentration of the simple molybdenum ion in the cathode film is essentially zero, and deposition proceeds by discharge of the complex anion.

At 900°C, the rate of dissociation of the complex anion is sufficiently great to permit deposition to occur from the simple cation over the full range investigated and so the deposits are powdery at all current densities. When operating at 600°C, as the current density is decreased from high values to 3 amp/dm², the deposit changes from powdery to coherent. On lowering the current density still further, the deposit changes back to powdery at a current density corresponding to the observed break in the curve at 0.25 amp/dm². This hypothesis is in accord with observations on the thermal stability of the salt K₃MoCl₆, which is quite stable at 600°C (in vacuo), but at 900°C produces a slight sublimate. This is indicative of a slight dissociation of the complex into MoCl₃, which, in turn, is not stable at that temperature. Other evidence for the slow dissociation of (MoCl₆)³⁻ are its reactions in water solution (5) and its magnetic susceptibility which indicates that it exists as the very stable octahedral structure with a *d²sp³* bond type. Further evidence for the view that the molybdenum is present as a stable complex in the fused salt bath comes from observations of the potentials of other metals in fused electrolytes, as described in the following section.

Static Potentials of Molybdenum and Other Metals in Fused Electrolytes

The equilibrium potentials of molybdenum and four other metals in a fused KCl-LiCl melt containing each metal in a concentration of 4.1 mole per cent are given in Table I. The point of most interest is that molybdenum is relatively noble, being very close to silver in potential. Thus, it is not surprising that iron and copper displace molybdenum from a molten plating bath. The noble position of molybdenum in this series also suggests that these baths might be very well suited for electrowinning. This prediction requires caution with respect to particular metallic impurities, since the various metals might not take the same positions in this series as they do in the aqueous system. It appears that nickel may be more noble than copper in this fused halide system.

Metal salts appear to form complexes in fused baths just as they do in aqueous solutions. A comparison of the emf series in three types of fused baths and in water solution is shown in Table II.

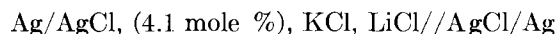
All the potentials have been calculated with reference to a silver electrode immersed in a solution of a silver salt at the same concentration as the other metals in the series. For example, column 4 is obtained from Table I by taking the potential of silver in a 4.1 mole per cent solution (potential 0.312 volt) as the reference electrode instead of silver in pure molten silver chloride. Column 1 is calculated from the data of Verdick and Yntema (6) for one mole per cent solutions of salts of the indicated element in AlCl₃-KCl-NaCl solvent at 200°C. Column 2 was calculated from the measured values of the potentials of Daniell cells consisting of: M/pure molten chloride of M//pure molten chloride of N/N, where M and N are metals, at 600°C given by Lorenz [(7) Vol. III]. (The value for tin is at 350° but the author states that the temperature coefficient of the potential is very small in this case.) Column 3 is the familiar emf series for electrolytes of unit activity in aqueous systems, taking the silver instead of the hydrogen electrode as zero.

The potentials in columns 1 and 2, for the aluminum chloride type solvent and the pure fused halides, respectively, are quite close. The potentials in the fused KCl-LiCl bath in column 4 are between those in an aqueous media in column 3 and those in columns 1 and 2. A significant difference between the pure molten salt system, column 2, and the aqueous system, column 3, is the absence of solvation in the former, since there is no solvent; and the existence of extensive solvation of the ions by water in the latter. If this is the cause of the differences in the two series, then the salts dissolved in the aluminum chloride mixture (column 1) are in a

condition very similar to the pure molten state, while the salts dissolved in the KCl-LiCl mixture (column 4) are to some extent solvated.

The calculation of the activity of metal ions in fused salt baths of the type in column 4 lends support to the view that salts therein are solvated. The voltage, E , of the following cell was calculated from data of Lorenz (7) and from the data given here: Zn/ZnCl₂ (4.1 mole %) KCl, LiCl//ZnCl₂ (pure)/Zn; $E = 0.850$ volt at 600°C. Substituting this value of emf in Nernst's equation gives the activity³ of zinc in the 4.1 mole per cent solution as 10⁻⁸ mole per cent. This shows that zinc is rather tightly complexed in the alkali halide melt. Lorenz has demonstrated the existence of a complex chloroplumbate anion in the molten mixture of KCl-NaCl-PbCl₂ and in KCl-PbCl₂ by transference measurements [(7) Vol. II]. However, all metal salts apparently do not form complexes in molten alkali halides.

A similar calculation for silver dissolved in a KCl-LiCl melt shows that silver, in contrast to zinc and lead, does not form complexes to any extent. From the data of Table I, the voltage of the following cell:



is 0.312 volt. Calculation of the activity of silver in the alkali halide melt yields 1.6 mole per cent as compared to the actual concentration of 4.1 mole per cent, thus indicating very slight complexing. A calculation on a similar silver chloride concentration cell was made with data taken from Suchy (8) who, however, did not give complete data on the mole per cent silver in his alkali halide melt. The results of this calculation confirmed the above, which shows that silver chloride does not appreciably form complexes in the alkali halide melt. In all of these calculations, liquid junction potentials have been neglected.

The comparison between the potentials in the aluminum chloride-alkali halide melt and the pure metallic halide melts indicated that complexing of metal compounds did not occur in the aluminum chloride melt. The explanation of the difference between the aluminum chloride type melt (column 1, Table II) and the alkali halide melts (column 4, Table II) is that all of the potassium chloride and sodium chloride in the former melt has been complexed by the aluminum chloride which is present in excess to form stable ions of the form, (AlCl₄)⁻, so that no alkali halide remained for the complexing of the other metals. From these results it seems that

³ The standard state of unit activity is taken to be that of the metal ion in the pure salt.

solvents for molten salts may be compared as to their relative tendency to accept or donate anions just as solvents in acid-base phenomena are compared as to their tendency to accept or donate protons.

Studies of complex formation in molten salts may be of considerable interest in problems of electrodeposition of metals from these systems, since it is known that in aqueous systems many metals are better deposited from complex ions than from simple ions.

SUMMARY AND CONCLUSIONS

Potential and polarization studies have shown that the inability to obtain pure molybdenum deposits from systems containing oxygenated salts stems from the fact that the deposition of oxides occurs at a potential of about 0.3 or 0.4 volt more noble than the reduction to metal. As a result, even slight contamination of the electrolyte by air, moisture, or oxycompound results in gross con-

TABLE II. *EMF series in various media*
E (volt)

Type of electrolyte	1. Fused AlCl ₃ -KCl-NaCl	2. Fused pure salt	3. Aqueous	4. Fused KCl-LiCl
Element				
Zinc.....	0.42	0.43	1.6	0.97
Lead (ous).....	0.30	0.32	0.92	—
Iron (ous).....	0.19	—	1.2	0.72
Tin (ous).....	0.17	0.07	0.93	—
Copper (ores).....	0.04	—	0.28	0.31
Molybdenum.....	—	—	—	0.04
Silver.....	0	0	0	0

tamination of the deposit with oxides, even when operating at high current densities.

Polarization studies have shown that the cathode polarization is small at the higher temperatures, but somewhat greater at 600°C. There is also some evidence that the reaction mechanism differs at 600°C from the mechanism at higher temperatures. It is believed that the production of coherent deposits results from the higher polarization involved in plating from a stable complex anion of molybdenum and from the fact that the operating temperature is well below the recrystallization temperature of molybdenum.

The relative position of zinc, iron, copper, molybdenum, and silver in the emf series in molten lithium chloride-potassium chloride eutectic mixture as solvent at 600°C has been established. Molybdenum has been shown to be more noble than all but silver. The values for the potentials obtained indicate that these metals tend to form complexes in this solvent and are present mainly as the chloro-metal anion.

The use of potential measurements such as these in determining solvation or complex-formation in molten electrolyte solvents has been explored.

A new reference electrode for measuring potentials in molten salts has been described. It consists of silver in pure molten silver chloride contained in a suitable cell to reduce contamination of the electrolytes due to diffusion and convection. The reference electrode has been shown to be stable, constant, and reversible. It is easy to prepare and may be used over a wide range of temperature.

ACKNOWLEDGMENTS

The authors express their sincere appreciation to Dr. W. Blum, National Bureau of Standards, and to Dr. W. J. Svirbely, Professor of Chemistry, University of Maryland, for their advice and guidance during the course of this investigation and to the

U. S. Army Ordnance Department for their financial support.

Any discussion of this paper will appear in a Discussion Section, to be published in the December 1954 issue of the JOURNAL.

REFERENCES

1. S. SENDEROFF AND A. BRENNER, *This Journal*, **101**, 16 (1954).
2. R. G. VERDIECK AND L. F. YNTEMA, *J. Phys. Chem.*, **46**, 344 (1942).
3. A. H. W. ATEN, H. J. DEN HERTOOG, AND L. WESTENBERG, *Trans. Electrochem. Soc.*, **47**, 265 (1925).
4. E. E. MARSHALL AND L. F. YNTEMA, *J. Phys. Chem.*, **46**, 353 (1942).
5. S. SENDEROFF AND A. BRENNER, *This Journal*, **101**, 28 (1954).
6. R. G. VERDIECK AND L. F. YNTEMA, *J. Phys. Chem.*, **48**, 268 (1944).
7. R. LORENZ, "Die Electrolyse Geschmolzener Salze," Vols. 1 and 2 (1905) and Vol. 3 (1906), W. Knapp, Halle A. S.
8. R. SUCHY, *Z. anorg. Chem.*, **27**, 165, 193 (1901).

The Acid Dissociation of the Aquoscandium Ions

II. Effect of Temperature and of Ionic Strength¹

MARTIN KILPATRICK AND LEWIS POKRAS²

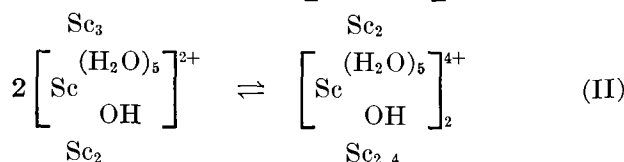
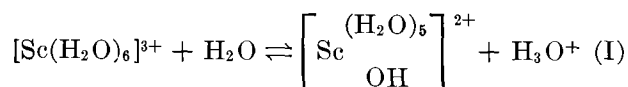
Department of Chemistry, Illinois Institute of Technology, Chicago, Illinois

ABSTRACT

The first dissociation constant of hexaaquoscandium ion and the dimerization constant for the hydroxypentaaquoscandium ion have been determined over the temperature range 10°–40°C in aqueous solutions, whose ionic strengths were adjusted with sodium perchlorate. From these data, approximate values of ΔH and ΔS have been calculated. The effect of electrolyte concentration on the above equilibrium constants is also reported.

INTRODUCTION

In an earlier publication (1), it was shown that the acidity of the aquoscandium ion in perchlorate systems may be explained by assuming the following equilibria to be of major importance:

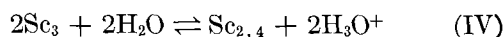


It was found convenient to define the hydroxyl number:

$$n \equiv (3 - a) + \frac{C_{\text{NaOH}} - C_{\text{HClO}_4}}{C} \quad (\text{III})$$

where a is the ratio of perchlorates to scandium atoms in the solid scandium perchlorate hydrate employed to prepare the buffer solutions studied; C , C_{HClO_4} , and C_{NaOH} are stoichiometric molar concentrations of total scandium salt, perchloric acid, and sodium hydroxide, respectively; and n represents the stoichiometric number of hydroxyl groups per scandium atom in the systems studied.

Representing the equilibrium constants for equations (I) and (II) by K_1 and K_d , respectively, and defining the constant for the over-all process:



¹ Manuscript received January 20, 1953. A portion of this paper was prepared for delivery before the New York Meeting, April 12–16, 1953. Paper was abstracted from a part of the dissertation presented by Lewis Pokras to the Faculty of the Graduate School of Illinois Institute of Technology in partial fulfillment of the requirements for the Ph.D. degree.

² Present address: J. T. Baker Chemical Company, Phillipsburg, N. J.

as K_0 , it follows that:

$$K_0 = C_{\text{H}}^2 C_{2,4} / C_3^2 = K_1^2 K_d \quad (\text{V})$$

where C_{H} , C_3 , C_2 , $C_{2,4}$ are the equilibrium concentrations of H_3O^+ , Sc_3 , Sc_2 , and $\text{Sc}_{2,4}$, respectively.

On substituting data obtained by study of buffer systems at 25°C and an ionic strength of 1.00₀, principally NaClO_4 , in the equation:

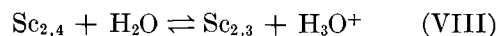
$$\frac{C_{\text{H}}(Cn + C_{\text{H}})}{C(1 - n) - C_{\text{H}}} = K_1 + \frac{2[C(1 - n) - C_{\text{H}}]}{C_{\text{H}}} K_0 \quad (\text{VI})$$

the constants given in Table IV for 25°C and $\mu = 1.00_0$ were obtained. When these constants are, in turn, substituted in the equation:

$$C_{\text{H}}^3 + C_{\text{H}}^2(Cn + K_1 - 2K_0) + C_{\text{H}}[C(1 - n)(4K_0 - K_1)] - 2K_0[C(1 - n)]^2 = 0 \quad (\text{VII})$$

values of C_{H} are obtained which may be compared with experimental values. At $n < 0.5$, agreement between experimental and calculated values of $-\log C_{\text{H}}$ was found to be excellent.

Since at higher values of n the agreement became progressively poorer, it was suggested that further polymerization by steps such as:



becomes increasingly important at higher values of n . Similar equilibria are proposed by Pedersen (2), Graner and Sillén (3), and Ahrlund (4) in explaining the acidity of $\text{Cu}(\text{NO}_3)_2$, $\text{Bi}(\text{ClO}_4)_3$ and $\text{UO}_2(\text{ClO}_4)_2$ systems, respectively.

It is the purpose of the paper which follows to present experimental data obtained under other experimental conditions, to discuss the effect of ionic strength and of temperature on the equilibria, and

to develop the thermodynamic constants for the system.

Experimental Method

Details of the experimental method, purification of reagents, and methods of calculation have been described previously (1). The data which follow are comparable in every respect with those presented for 25°C and $\mu = 1.00_0$.

EXPERIMENTAL DATA

The experimental data obtained are summarized in Tables I through III. Values of $-\log C_H$ as a function of n for scandium buffers at $C = 1.00 \times 10^{-2}M$, $\mu = 1.00_0$, and $t = 10.0$ and 40°C are presented in Table I. Table II summarizes similar data for buffers with $C = 1.25 \times 10^{-3}M$, while Table III includes all data obtained at $t = 25^\circ C$ and $\mu \approx 1.00_0$. The effect of temperature is also illustrated by Fig. 1 which is based on data from Table I. The effect of ionic strength is illustrated in Fig. 2, taken from data in Table III.

The method employed to evaluate equilibrium constants for the several sets of experimental conditions studied was essentially that described in the earlier publication. However, it was necessary to modify the method slightly because of the considerably smaller number of buffers studied under conditions other than $t = 25^\circ C$ and $\mu = 1.00_0$.

In calculating constants from the data on the effect of ionic strength, two equations of the form of equation (VI) were evaluated at each ionic strength, employing experimental data for buffers at $C = 1.25_0 \times 10^{-3}$ and $n = -0.013$ and $+0.187$. The resulting pairs of equations when solved simultaneously led to the sets of constants presented in Table IV.

Since considerably more data are available at $\mu = 1.00_0$ and $t = 10^\circ C$ or $40^\circ C$, five equations were employed for the evaluation of each set of constants. The resulting equilibrium constants are also given in Table IV.

It was pointed out previously that values of the constants depended markedly on the n values chosen as a source of data in setting up equation (VI). In addition, there is a much less marked dependence on C . Therefore, if values of the constants for different experimental conditions are to be compared, they must be derived from data obtained at comparable values of n and C .

In order that this comparison have the greatest possible validity, we have therefore recalculated the constants for $t = 25^\circ C$ and $\mu = 1.00_0$ from two additional groups of data. In one case, the data group was chosen to be comparable with data employed in

calculating constants at varying ionic strength; in the other case, to be parallel with constants at varying temperatures. These constants are also given in Table IV.

When the several sets of constants are employed to calculate values of $-\log C_H$ for the buffer systems examined, the values given in the "calculated" columns of Tables I to III are obtained. The differences

TABLE I. $-\log C_H$ for Sc Buffers at $C = 1.00 \times 10^{-2}M$, $\mu = 1.00_0$

n	$-\log C_H$ at $t = 10^\circ C$			$-\log C_H$ at $t = 40^\circ C$		
	exp.	calc.	diff.	exp.	calc.	diff.
-0.213	2.622	2.672	-0.050	2.588	2.622	-0.034
-0.0130	3.235	3.322	-0.087	2.986	2.996	-0.010
+0.187	3.865	3.867	-0.002	3.332	3.329	+0.003
0.387	4.148	4.151	-0.003	3.594	3.585	+0.009
0.527	—	—	—	3.739	3.762	-0.023
0.587	4.365	4.416	-0.051	3.807	3.842	-0.035
0.787	4.578	4.771	-0.193	4.025	4.194	-0.169
0.933	4.719	5.412	-0.693	4.174	4.733	-0.559
1.033	4.820	5.689	-0.869	4.253	5.064	-0.881
1.181	4.959	4.978	-0.019	4.373	4.397	-0.024

TABLE II. $-\log C_H$ for Sc buffers at $C = 1.25 \times 10^{-3}M$, $\mu = 1.00_0$

n	$-\log C_H$ at $t = 10^\circ C$			$-\log C_H$ at $t = 40^\circ C$		
	exp.	calc.	diff.	exp.	calc.	diff.
-0.117	3.822	3.684	+0.138	3.505	3.476	+0.029
-0.067	3.868	3.785	+0.083	3.536	3.527	+0.009
-0.0170	3.963	3.893	+0.070	3.583	3.580	-0.003
+0.103	4.188	4.131	+0.057	—	—	—
0.209	—	—	—	3.821	3.811	+0.010
0.260	4.445	4.378	+0.067	3.887	3.876	+0.011
0.327	4.508	4.470	+0.033	—	—	—
0.419	—	—	—	4.044	4.054	-0.010
0.527	4.734	4.734	0.000	4.167	4.184	-0.017
0.577	—	—	—	4.202	4.250	-0.048
0.696	4.922	4.993	-0.071	—	—	—
0.780	—	—	—	4.423	4.595	-0.172
0.827	5.023	5.280	-0.257	—	—	—
0.933	5.131	5.721	-0.590	4.524	5.151	-0.627
0.949	—	—	—	4.579	5.273	-0.694
1.033	5.167	6.183	-1.016	4.591	5.482	-0.891
1.181	5.244	5.470	-0.266	4.638	4.777	-0.139

between experimental and calculated values are of the same magnitude as was observed for the much larger number of buffers studied previously, and exactly the same trends in the differences are noted at all temperatures and ionic strengths studied.

Effect of Ionic Strength on the Equilibrium Constants

While it would be most desirable to obtain thermodynamic values of the dissociation constants at infinite dilution from the values of the constants given

stants of weak electrolytes as a function of T , and for computing the thermochemical functions. . . .” (5) the authors have chosen to employ the relationships due to Harned and Robinson (6). On substituting data from Table IV into their equation:

$$-\log K = A/T + B + CT \quad (\text{XI})$$

the following relationships are obtained for $\mu = 1.00_0$ mostly in NaClO_4 :

$$-\log K_1 = -4408.3T^{-1} + 41.163 - 0.0724T \quad (\text{XII})$$

$$-\log K_0 = +4937.3T^{-1} - 15.593 + 0.0170T. \quad (\text{XIII})$$

The related equations below, given by Bates and Pinching (7), were then employed in calculating values of the thermochemical properties of the system.

$$\Delta F = 2.3026R(A + BT + CT^2) \quad (\text{XIV})$$

$$\Delta H = 2.3026R(A - CT^2) \quad (\text{XV})$$

$$\Delta S = 2.3026R(-B - 2CT) \quad (\text{XVI})$$

$$\Delta C_p = 2.3026R(-2CT) \quad (\text{XVII})$$

However, since the equilibrium constants derived here are not the thermodynamic values at $\mu = 0$, the parameters A , B , and C of equations (XII) and (XIII) will not lead to true thermodynamic properties of the system. Furthermore, since no valid method of evaluating the activity coefficients of the species involved in the equilibrium constants is apparent, it is not possible to calculate the thermodynamic dissociation constants.

Nevertheless, the standard state for the systems could be defined as the state in which the solutions are essentially one molar in NaClO_4 ; the thermochemical properties calculated could then be considered to be referred to a standard state. The calculation is, therefore, based on this definition, instead of infinite dilution as the standard state. The superscript zero in equations (XIV) to (XVII) has been omitted in order to avoid confusion of the symbols with those defined in the more customary manner.

Employing for R the Birge value of $1.9869 \text{ cal mole}^{-1} \text{ deg}^{-1}$, the values of the above properties have been calculated. They are presented in Table V, along with related properties for the dimerization reaction calculated as follows. Values of ΔF and ΔH were obtained by appropriate addition of equations and energy terms; ΔS for the dimerization was then calculated from ΔF and ΔH values by substitution in the fundamental equation:

$$\Delta F = \Delta H - T\Delta S \quad (\text{XVIII})$$

While the values are given to two significant figures in Table V it must be emphasized that these figures are somewhat questionable. When the entire calculation is repeated, employing different but parallel groups of data to calculate the constants, one obtains equilibrium constants and thermochemical properties which differ from those presented in the table. However, the signs, orders of magnitude, and trends exhibited in the recalculated values are similar in every respect to those presented in Table V.

TABLE IV. *Equilibrium constants for the acidic dissociation of the aquoscandium ion at various experimental conditions*

Temp, °C	Ionic strength, μ	Equilibrium constants		
		$10^5 K_1$	$10^6 K_0$	$10^{-3} K_d$
25	1.00 ₀	1.17 ₂	1.01 ₆	7.38
10	1.00 ₀	0.808	0.221 ₄	3.39 ₃
25	1.00 ₀	1.62 ₃ *	0.927*	3.51 ₈ *
40	1.00 ₀	3.87 ₃	3.20 ₁	2.13 ₄
25	0.0100 ₀	2.45 ₃	4.47	7.43
25	0.100 ₀	1.81 ₀	2.15 ₄	6.58
25	0.500	1.25 ₈	1.26 ₈	7.99
25	1.00 ₀	1.18 ₃ †	0.889†	6.35†

* Employed only in determining effect of temperature on the equilibria.

† Employed only in determining effect of ionic strength on the equilibria.

TABLE V. *Thermochemical properties of the aquoscandium ion acid system in 1M NaClO₄*

Reaction	Temp °C	ΔF kcal mole ⁻¹	ΔH kcal mole ⁻¹	ΔS Cal mole ⁻¹ deg ⁻¹	ΔC_p Cal mole ⁻¹ deg ⁻¹
First acid Dissociation K_1	10	+6.6	+6.4	-0.7	+190
	25	6.5	9.3	+9.	200
	40	6.3	12.	19.	210
Over-all K_0	10	8.6	16.	27.	-44
	25	8.2	15.	25.	-46
	40	7.9	15.	22.	-49
Dimerization K_d	10	-4.6	3.6	28.	—
	25	-4.8	-2.9	6.	—
	40	-4.8	-9.7	-15.	—

For example, on carrying out three independent calculations, leading to three independent sets of thermochemical properties, the signs of ΔS exhibit the same reversal of sign for the first acid dissociation and dimerization steps as indicated above, although the magnitudes of ΔS may vary considerably.

In the previous paper (1) it was pointed out that dependence of the constants on n and C undoubtedly reflected contributions from higher dissociation and polymerization steps. These contributions are, in turn, probably responsible for the variations in equilibrium constants discussed above. However, if one

employs parallel data at the several temperatures in evaluating the constants, one may assume as a first approximation that the contributions of higher steps are essentially equal and, therefore, are cancelled out on evaluation of the temperature coefficients.

To the extent that these assumptions are correct, and since no comparable data have yet been presented for an aquometal ion, the authors feel that these data may be of considerable interest to workers in the field.

Note added in proof. The neglect of the equilibria for the higher polymers $\text{Sc}_{3,5}$; $\text{Sc}_{4,6}$; $\text{Sc}_{5,7}$; $\text{Sc}_{6,8}$, etc., may well explain the dependence of ΔH and ΔS on the C and n values used, and may also explain the trends in the thermodynamic quantities. Sillén, at the Symposium on Co-ordination Chemistry held in Copenhagen, August 9 to 13, 1953, presented a method for calculating the equilibrium constants involved in polynuclear complexes, and preliminary

calculations for scandium, on the assumption of repeated reaction, show reasonable agreement with the experimental data.

Any discussion of this paper will appear in a Discussion Section, to be published in the June 1954 issue of the JOURNAL.

REFERENCES

1. M. KILPATRICK AND L. POKRAS, *J. Electrochem. Soc.*, **100**, 85 (1953).
2. K. J. PEDERSEN, *Kgl. Danske Videnskab. Selskab. Mat-fys. Medd.*, **20** (7), 27 (1943).
3. F. GRANER AND L. G. SILLÉN, *Acta Chem. Scand.*, **1**, 631 (1947); *Nature*, **160**, 715 (1947).
4. J. AHRLAND, *Acta Chem. Scand.*, **3**, 374 (1949).
5. H. S. HARNED AND B. B. OWEN, "The Physical Chemistry of Electrolytic Solutions," 2nd ed., p. 509, Reinhold Publishing Company, New York (1950).
6. H. S. HARNED AND R. A. ROBINSON, *Trans. Faraday Soc.*, **36**, 973 (1940).
7. R. G. BATES AND G. D. PINCHING, *J. Am. Chem. Soc.*, **71**, 1274 (1949).

Equivalent-Circuit Model of the Transference Cell¹

GEORGE W. MURPHY²

Argonne National Laboratory, Lemont, Illinois

ABSTRACT

An equivalent-circuit model characterized by remarkable pictorial simplicity is proposed for a cell with reversible electrodes in contact with a solution of a suitable binary electrolyte, nonuniform in concentration. The capacitance part of the circuit is related to the free energy change of the dilution process, while the resistance parts are related to the cation and anion transports. On the basis of the model, correct equations are derived for (a) the conductance of the solution, (b) the diffusion of the electrolyte (Nernst equation), and (c) the concentration cell with transference. In addition, equations, which have not been subjected to experimental test, are derived for (d) capacitance of the condenser, (e) current as a function of applied potential difference, and (f) concentration difference as a function of applied potential difference. Mixtures of electrolytes are considered briefly. On the basis of the model, a method is proposed for the determination of thermodynamic properties of electrolytes by transference cell measurements which does not involve a measurement of the transference number. The range of applicability of the model to various aspects of electrochemistry is discussed, and the concept of diffusion potential is critically re-examined.

INTRODUCTION

Electrode and ion-transport processes are both essential elements of every electrochemical cell. It is sometimes possible to study one of these processes with negligible interference from the other. For example, in electrical conductance and moving-boundary experiments, the ion-transport processes of interest are isolated from electrode phenomena by appropriate experimental technique. Conversely, in electromotive force measurements, carried out for the purpose of deriving thermodynamic properties, careful experimental design can sometimes reduce ion-transport processes to a position of negligible significance. Generally speaking, the interpretation of data is facilitated when the reversible and irreversible processes are not intermingled.

The great bulk of electrolytic processes occur, however, with just such intermingling. A simple classical illustration of this is the concentration cell with transference, where the diffusion of ions is unavoidably present during emf measurements. Also in this category is the inverse of the concentration cell with transference, i.e., a concentration gradient is generated by electrode and ion transport processes upon application of an external voltage.

¹ Manuscript received January 26, 1953. This paper was prepared for delivery before the New York Meeting, April 12 to 16, 1953. This research was completed at Argonne National Laboratory during a leave of absence from the Univ. of Wisconsin under the Participating Institutions Program. Based on portion of ANL Report 5104, Jan. 1953.

² Present address: New York State College for Teachers, State University of New York, Albany, N. Y.

The same arrangement results when convection is eliminated from the electrogravitational process described by Murphy (1) by operating with horizontal electrodes. It is discussed by Murphy and Batzer (2) as an example of a type *H* (for horizontal) cell. Many other examples of cells in which electrode and ion-transport processes must be treated together can be found throughout the field of electrochemistry.

We propose herein an equivalent-circuit model of a cell which involves integrated electrode and ion-transport processes, including the specific types mentioned above. This model emphasizes the importance of time-independent or steady states in cells where current is flowing and concentration gradients are present. From the model, long-established equations for conductance, for the diffusion of ions, and for the concentration cell with transference are derived, as well as some others which have not been subjected to experimental test. It thus serves as a quantitative basis of reference for a number of experimental facts, and it is so simple that it possesses considerable pedagogical appeal. The model is heuristic in nature, suggesting, for example, a new approach to the determination of the thermodynamic properties of electrolytes.

The term "transference cell" refers to a system with two identical reversible electrodes in contact with an electrolytic solution, one or more ions of which participate in the electrode reaction. By "reversible" it is meant that the clearly specifiable reaction at one electrode occurs in exactly the reverse manner at the other, and that there is no activation or resistance overpotential at the elec-

trodes. The applied or measured potential is always less than that required for decomposition of the solution, i.e., concentration gradients, but no changes in composition are established in the cell as a result of passage of current. The familiar "concentration cell with transference" is a special case of the transference cell when there is a concentration gradient, but no external current.

Throughout the article, the silver-silver chloride electrode, chloride ion system is adopted for illustration. Complete dissociation of the electrolyte, e.g., KCl, is assumed. Three aspects of this cell are shown in Fig. 1. In section (a) the system is in

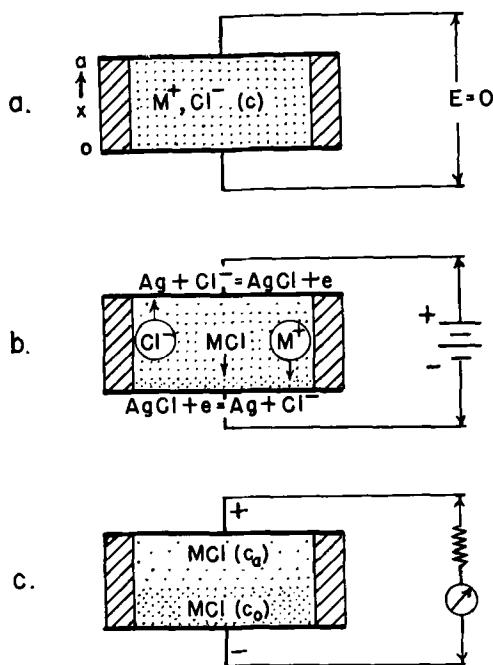


FIG. 1. Cross sections of the transference cell. Heavy horizontal bounding lines represent silver-silver chloride electrodes; cross-hatching, insulating spacer; density of dots, concentration of electrolyte. (a) Cell in equilibrium, concentration uniform; (b) cell with external applied voltage, representing "charging" of the cell; and (c) concentration cell with transference, emf being measured with high resistance voltmeter.

equilibrium, with a uniform concentration and no external voltage. In section (b) an external voltage has been applied, but changes in concentration have occurred near the electrodes only. This corresponds to a Hittorf transference experiment. Because of the density differences which arise, the cathode is situated at the bottom to avoid convection currents. In section (c) the concentration difference between the top and bottom electrodes leads to an external emf; this is a concentration cell with transference. The external battery of (b) has been replaced by a high-resistance voltmeter. In (b) a substantial current in the external circuit

passes, while in (c), for a measuring instrument of infinite sensitivity, there is no external current at all.

It is evident that continued passage of current in (b), followed by removal of the external current source, leads to a concentration cell with transference (c). It has been shown (3, 4) that the steady-state concentration distribution reached after prolonged current passage is linear for the ideal case.

EQUIVALENT CIRCUIT

The application of equivalent-circuit models to electrochemical problems is not new. Electrical double-layer phenomena at mercury-solution interfaces in particular have been interpreted by this means. Grahame (5, 6), in his capacitance studies, noted the presence at certain polarizing potentials of a very large capacity effect due to oxidation-reduction phenomena at the electrodes. He called this a "pseudocapacity" to distinguish it from true double-layer capacity. Breyer and Gutman (7) referred to this as a "dynamic capacitance."

The condenser and other elements of our equivalent circuit are similar to those utilized by Grahame and by Breyer and Gutman in that they involve oxidation-reduction at the electrodes, but differ in that they also involve concentration gradients throughout the solution. Moreover, we have restricted ourselves to the simplest types of electrode processes and are primarily concerned with the time-independent or steady state achieved by steady application of a d-c voltage. These states would have no chance of attainment with the a-c methods employed by Grahame and other investigators, who were primarily interested in double-layer phenomena. The "steady states" in a-c work are time averages over a number of cycles, but the variables are changing during periods of the order of one cycle.

Equivalent-circuit models are also important in the interpretation of the dielectric properties of crystals. According to MacDonald's model (8), charge carriers within the crystal may be responsible for a large part of the capacitive reactance.

The postulated equivalent circuit of the transference cell is given by Fig. 2a and 2a'. The latter circuit diagram, which contains two condensers in one arm, illustrates the complete blocking action to the external circuit of charges passing through R_+ , which is analogous to the blocking action of positive ions by the electrodes in the transference cell. On the other hand, the mathematical treatment is simplified if a single condenser is retained in the left arm; the capacitance of the condenser in Fig. 2a is obtained by series addition of the capacitances of the two condensers in Fig. 2a'.

Qualitative considerations which lead to the model are as follows:

<i>Cell</i>	<i>Equivalent Circuit</i>
Current is carried by parallel movement of two charge carriers, M^+ and Cl^- ions, with different ionic conductances l_+ and l_- .	There are two parallel arms in the circuit with different resistances R_+ and R_- , where $R_+/R_- = l_-/l_+$.
The electrodes are "permeable" to Cl^- ions. (The electrode reaction consumes or liberates Cl^- ions.)	Negative charge passes directly from the external source through R_- .
The electrodes are blocking to M^+ ions. (The electrode reaction does not involve M^+ ions.)	Charges passing through R_+ are blocked from the external circuit by condensers (Fig. 2a').
A concentration gradient generates an external voltage.	A charged condenser leads to an external voltage.
A concentration gradient is self-equalizing by diffusion in the absence of an applied voltage.	In the absence of an applied voltage, a charged condenser will automatically discharge through R_+ and R_- .

Further details of correspondence between the cell and circuit are restricted to the steady state:

<i>Cell</i>	<i>Equivalent Circuit</i>
The chemical potential of the electrolyte varies with position in the cell, but is invariant with respect to time. Cl^- ions are flowing continuously through the cell, while M^+ ions are stationary.	The electrical potential varies with position, but is invariant with respect to time. Negative charges are flowing continuously through R_- , but no charge flows through R_+ .

A virtual transfer of dQ/F equivalents of M^+ (and hence of MCl) from the anode, contacting solution of activity a_a , to the cathode, contacting solution of activity a_c , leads to an increase in free energy of the system of $dG = 2(dQ/F)RT \ln(a_a/a_c)$ (G is the free energy of the system and F is the faraday constant.)

If the circuit is indeed electrically equivalent to the cell, it follows from elementary thermodynamic considerations that

$$E_c = 2(RT/F) \ln(a_a/a_c). \quad (I)$$

It is to be noted that E_c is the potential difference at the electrodes with steady-state current flowing in the external circuit; but during internal discharge of the cell (Fig. 2c) with no current flowing in

the external circuit, the measured potential difference will be less than E_c .

Referring to Fig. 2b, it is stressed that dQ is the charge passed through the left-hand side of the circuit only. Concurrently with this process, an additional charge dQ' passes through the right-hand side in a purely dissipative manner; therefore, this feature of the circuit is consistent with the lack of reversibility in the cell as a whole. The model clearly specifies that all reversible phenomena of the cell are to be associated with the condenser, and all irreversible phenomena with the resistances.

Each of the three circuit elements of Fig. 2a is nonlinear; that is, the currents through the resistance are not proportional to the potential drops, and the charge on the condenser is not proportional to the voltage across its plates. For steady-state operation and ideal behavior of the cell, suitable

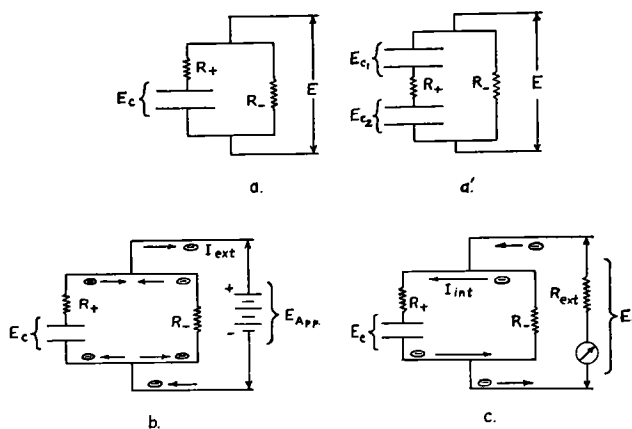


FIG. 2. Equivalent circuit corresponding to cells of Fig. 1. (a) Basic circuit; (a') alternate basic circuit with dual condensers; (b) charging with external source; and (c) internal discharge (free diffusion).

mathematical relations between emf, current, and concentration are readily found.

In Fig. 2b, the current corresponding to Fig. 1b is analyzed. The flow of negative charge through the right-hand side is electrically equivalent to a positive charge flowing in the opposite direction. The current in the external circuit is the sum of these two.

The current during internal discharge of the cell is shown in Fig. 2c. The internal current is equivalent to free diffusion of the salt, with the flux of positive ion equal to the flux of negative ion, as required by the electroneutrality condition. From the electrical circuit standpoint, this means that the current through the left must be equal to that through the right. Only an infinitesimal current flows through the external circuit to actuate the potentiometer. The internal current is fictitious in the sense that it cannot be measured as an electric

current, but it is by no means a new concept. As early as 1888 Nernst (8) postulated that the diffusion of the ions of an electrolyte constituted an internal electric current, and he was led thereby to the concept of "diffusion potential," which arises because of the different mobilities of ions. Although the diffusion potential has had many applications since Nernst's time, it is an objectionable concept from the operational viewpoint, since it cannot be measured directly. We propose in this treatment to express the physical behavior of the system in terms of the external potential applied to, or generated by, the cell.

Discharge of the cell of Fig. 2c could also occur by short-circuiting the voltage measuring device. This can be referred to as "external discharge," in contrast to the "internal discharge" of free diffusion, which occurs irreversibly whether an external circuit is present or not.

MATHEMATICAL TREATMENT

The Cell Resistance

In order to demonstrate electrical equivalence of cell and circuit in quantitative fashion, the further assumptions are made that activities may be replaced by concentrations and that conductances are linear functions of the concentration. These assumptions, together with those made earlier, characterize what will be referred to as an ideal transference cell. In this case the mathematical conditions for equivalence of cell and circuit are:

$$E_c = (2RT/F) \ln C_o/C_a \quad (\text{II})$$

$$R_+ = (l/A l_+) \int_0^a (1/C) dx \quad (\text{IIIa})$$

$$R_- = (l/A l_-) \int_0^a (1/C) dx \quad (\text{IIIb})$$

where a is the distance between the parallel electrodes of area A , C is the local concentration in equivalents per cc, and l_+ and l_- are the mobilities (equivalent ionic conductances). In the case of the linear concentration distribution which is attained in the steady state,

$$R_+ = \{a/A l_+ (C_o - C_a)\} \ln (C_o/C_a) \quad (\text{IVa})$$

$$R_- = \{a/A l_- (C_o - C_a)\} \ln (C_o/C_a) \quad (\text{IVb})$$

When the ratio C_o/C_a is close to unity, these equations reduce to

$$R_+ = a/A l_+ C_o; R_- = a/A l_- C_o. \quad (\text{Va, b})$$

The true cell resistance, as seen by the external circuit, is evidently obtained by parallel combination of these elements:

$$R_{\text{cell}} = R_+ R_- / (R_+ + R_-) \\ = \{a/A \Lambda (C_o - C_a)\} \ln (C_o/C_a) \quad (\text{VI})$$

where $\Lambda = l_+ + l_-$ is the equivalent conductance of the salt. In the limit as $C_o \rightarrow C_a$,

$$R_{\text{cell}} = a/A \Lambda C_o, \quad (\text{VII})$$

which is just the cell resistance that would be measured with a uniform electrolyte by an a-c method. On the other hand, examination of Fig. 2 shows that the apparent resistance in the steady state is

$$R'_{\text{cell}} = a/A l_- C_o, \quad (\text{VIII})$$

since no net current flows through the left-hand side.

Self-Discharge of the Cell—Verification of Nernst's Diffusion Equation

During the self-discharge of the cell (free diffusion, Fig. 2c), the internal current density, I_{int} , produces a difference of potential $A I_{\text{int}} (R_+ + R_-)$ across the series combination of resistances, which is equal in magnitude, but opposed in sign, to E_c . Combining this relation with equations (II) and (IV),

$$I_{\text{int}} = (2RT/F) \{(C_o - C_a)/a\} \\ \cdot \{l_+ l_- / (l_+ + l_-)\} \quad (\text{IX})$$

However, I_{int} is also equal in magnitude, but opposed in sign, to the product FJ of the faraday constant and the diffusion flux J , for which Fick's law of diffusion

$$J = I_{\text{int}}/F = D(C_o - C_a)/a \quad (\text{X})$$

is valid, where D is the diffusion coefficient. It follows from equations (IX) and (X) that

$$D = (2RT/F^2) l_+ l_- / (l_+ + l_-) \quad (\text{XI})$$

which is Nernst's equation (8). Ample experimental verification for this equation has been provided in cases where ideal conditions are approached.

The measured emf of the self-discharging cell is just E_t , that of a concentration cell with transference. In terms of the potential drops across the resistors, E_- and E_+ ,

$$E_t = E_- = E_c - E_+ = E_c - \frac{l_-}{l_+} E_c,$$

whence

$$E_t = \frac{l_+}{l_+ + l_-} E_c = t_+ E_c. \quad (\text{XII})$$

This is a verification of another long-established equation. Equations (VII), (XI), and (XII) are a concise summary of the known properties of the ideal transference cell. The accuracy of the equivalent circuit model has, therefore, been

established by the derivation of these equations on the basis of it.³

Capacitance of the Condenser

On charging the condenser, the potential difference across its plates increases, corresponding to an increasing concentration gradient in the transference cell. By equation (II), the minimum work done in transferring the infinitesimal quantity of electrolyte $dy = dQ/F$ is

$$FE_c dy = 2RT \ln \frac{C_o}{C_a} dy. \quad (\text{XIII})$$

The energy dissipated in the right-hand resistor is not included in this calculation; furthermore, the transfer may be imagined to occur infinitesimally slowly, so that there is no energy dissipation in the left-hand resistor. Under these conditions, the system is always in a steady state, with a linear concentration gradient. The concentration at the mid-point between the electrodes remains constant, and the electrolyte transfer takes place across this dividing line.

The concentration at any point and the number of moles transferred are connected by the relation

$$CV = 4y \left(\frac{2x}{a} - 1 \right) + n_0, \quad (\text{XIV})$$

where V is the volume of the cell and n_0 the number of moles of electrolyte. Since C cannot be less than zero at the anode, y is limited to values between zero and $n_0/4$ for the linear concentration distribution.

Equation (XIII) may be integrated after substituting (XIV):

$$\begin{aligned} \text{work} &= 2RT \int_0^y \ln \frac{C_o}{C_a} dy \\ &= 2RT \int_0^y \ln \frac{n_0 + 4y}{n_0 - 4y} dy \\ &= \frac{RT}{2} \left\{ (n_0 + 4y) \ln \left(1 + \frac{4y}{n_0} \right) \right. \\ &\quad \left. + (n_0 - 4y) \ln \left(1 - \frac{4y}{n_0} \right) \right\} \end{aligned} \quad (\text{XV})$$

When $n_0 \gg 4y$, corresponding to a low emf, this equation reduces to⁴

$$\text{work} = \frac{8RTy^2}{n_0}. \quad (\text{XVI})$$

³ The derivation of equation (VII) started with the assumption that the ionic conductances are independent of one another; since this assumption leads to the correct result for the concentration dependence of cell resistance [equation (VII)], the law of independent ionic migrations is verified.

⁴ The first two terms in the series expansion of $\log(1 + 4y/n_0)$ and $\log(1 - 4y/n_0)$ are retained.

In transporting y equivalents, Fy coulombs are passed through the left-hand side of the circuit. Thus, the work done in charging the condenser, in the region where equation (XVI) is valid, is proportional to the square of the charge transferred, a characteristic of a normal condenser. The capacitance of the condenser is evidently $n_0 F^2 / 16RT$. Unlike a normal condenser, the capacitance is directly proportional to the number of moles of electrolyte, but independent of the electrode separation or area.

The capacitance for a typical case is enormous by any ordinary standard. Suppose, for example, that $n_0 = 10^{-4}$ equivalent, a quantity which would be contained in a decinormal solution filling a 1 cm^3 cell. At room temperature, the capacitance is

$$\frac{10^{-4} \times (9.65)^2 \times 10^8}{16 \times 8.316 \times 298.1} = 21.2 \text{ farad}$$

This exceeds by many powers of ten the capacitance of any radio condenser of comparable size.

Current as a Function of Applied Voltage

Since all of the components in the equivalent circuit model are nonlinear, the cell as a whole will not be expected to follow Ohm's law. For any point within the cell, equation (II) becomes

$$dE/dx = (2RT/F) d \ln C/dx \quad (\text{XVII})$$

in the steady state. Since $I = t_- C \Delta E/dx$ [compare equation (VIII)], it follows that

$$I = (2RT/F) t_- \Delta C/dx \quad (\text{XVIII})$$

While dC/dx is constant throughout the cell, dE/dx is obviously not so, being greater at the points of lower concentration. The E of this equation is the total potential difference measured by Ag-AgCl electrodes, but, as indicated previously, it is also the potential difference across the condenser plates under steady-state operation.

Upon integrating equation (XVIII), and noting that when $x = a/2$, $C = C_{or}$, the original uniform concentration of electrolyte, there results the equation

$$C = \frac{IF}{2t_- RT} \left(x - \frac{a}{2} \right) + C_{or} \quad (\text{XIX})$$

Substituting (XVII) into (XVIII), integrating over x , and solving for I , one obtains

$$I = \frac{4C_{or} t_- \Delta RT}{aF} \tanh EF/4RT \quad (\text{XX})$$

The E in this equation is the total applied potential. By expanding the hyperbolic tangent and retaining only the first term, we obtain an equation valid for small applied potentials:

$$I = C_{or} t_- \Delta E/a \quad (\text{XXI})$$

Ohm's law is, therefore, satisfied under this con-

dition; however, the conductance measured under steady-state operation is t_- times the value measured under uniform concentration conditions.

When $EF/4RT$ becomes very large, the hyperbolic tangent approaches unity, equation (XX) becomes

$$I = 4C_{or} t_- \Delta RT/aF, \quad (XXII)$$

and the current density is independent of applied potential.⁵

Equation (XX) has also been obtained in a mathematical analysis by Piguet, Kuhn, and Kuhn (10). The assumptions inherent in their derivation lead, however, to an incorrect result for the emf of a concentration cell with transference.

Concentration as a Function of Applied Voltage

The concentration difference between the electrodes may be expressed in terms of the current density by application of equation (XIX):

$$C_o - C_a = \frac{IFa}{2t_- \Delta RT} \quad (XXIII)$$

Substituting (XX) into (XXI), we have

$$C_o - C_a = 2C_{or} \tanh \frac{EF}{4RT} \quad (XXIV)$$

This equation has also been obtained by Piguet, Kuhn, and Kuhn (10). According to equation (XXIV), the ratio $\frac{C_a - C_o}{C_{or}}$ is dependent only on the applied potential for the system under study, but independent of transference number and conductance. The elimination of terms characteristic of irreversible processes from the concentration-potential relation is relevant to our discussion below.

For small values of E , equation (XXIV) becomes

$$\frac{C_a - C_o}{C_{or}} = \frac{EF}{2RT} \quad (XXV)$$

For practical purposes this is equivalent to equation (XIV). For large values of E , equation (XXIV) leads to the result

$$C_o - C_a = 2C_{or} \quad (XXVI)$$

Since the total number of moles is conserved, this equation shows that the limiting condition at high applied potential is reached when the concentration at $x = 0$ has doubled, while that at $x = a$ has fallen to zero.

Extension of Theory to Mixtures

While the foregoing mathematical treatment has been applied to only the simplest case, a 1-1 elec-

⁵ A potential difference between the electrodes of 0.6 volt, corresponding to a $\tanh (EF/4RT)$ of 0.9999, is regarded as large. Above this voltage, decomposition of the solution with cathodic evolution of hydrogen may occur. Equation (XIX) is no longer valid at such voltage.

trolyte in an ideal transference cell, a single electrolyte of any other valence type could be handled easily. The treatment of mixtures is more complex, requiring the introduction of additional elements into the electrical circuit model, and additional parameters in the equations. The detailed treatment will be deferred to a later paper, but it is worthwhile here to outline the procedure for a relatively simple case: electrodes again reversible to the chloride ion, electrolyte a mixture of two chlorides, e.g., NaCl and KCl. The equivalent circuit of this

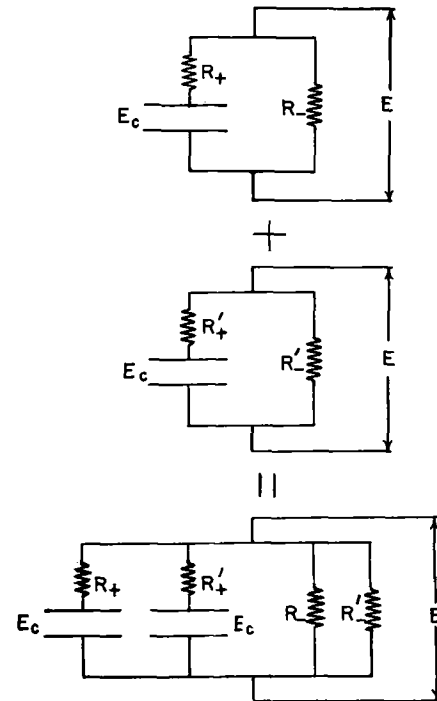


FIG. 3. Diagrams illustrating parallel additivity of circuit elements for two single electrolytes to obtain equivalent circuit for mixture.

cell is obtained by parallel combination of circuits for each salt, as if the other were absent (Fig. 3).

It is assumed in this treatment, as before, that the system is thermodynamically ideal, and that Kohlrausch's law of independent ionic mobilities is obeyed. Since these conditions will not be met in a practical case, the equations based on this model are intended merely as illustrative of the approach.

Application of a polarization potential will produce, in the steady state, a solution with a concentration ratio C_o/C_a which is the same for each constituent. When this potential is released, the emf of the resulting concentration cell with transference is given by

$$E_t = [(t_+)_1 + (t_+)_2]E_c, \quad (XXVII)$$

$$(t_+)_1 = (C_+)_1(l_+)_1 / [(C_+)_1\Lambda_1 + (C_+)_2\Lambda_2]$$

$$(t_+)_2 = (C_+)_2(l_+)_2 / [(C_+)_1\Lambda_1 + (C_+)_2\Lambda_2]$$

In general, when an indefinite number of cations are present in the system with the common chloride ion:

$$E_t = E_c \sum_i (t_+)_i \quad (\text{XXVIII})$$

$$(t_+)_i = (C_+)_i (l_+)_i / \sum_i (C_+)_i \Lambda_i$$

$(C_+)_i$ = concentration of the i th cation species
 $(l_+)_i$ = mobility of the i th cation species
 Λ_i = equivalent conductance of the chloride salt of the i th cation species.

It is evident that the nonsteady states prevailing in the general classical problem of junction potentials will involve much greater mathematical complexity. Nevertheless, the pictorial simplicity of the equivalent circuit model should be of assistance in setting up equations for a particular junction potential problem. Diffusion problems in multi-electrolyte systems are also accessible to the model.

DISCUSSION

*What is Diffusion Potential?*⁶

The equivalent circuit model of Fig. 2 contains three elements, each characterized by its own potential difference when the solute is diffusing freely from an initial steady-state concentration distribution; moreover, each is directly measurable in principle by appropriate experimental technique, if electrodes reversible to the desired ion can be found. Thus, the potential across R_- is obtained directly from the circuit of Fig. 2. If the electrolyte were HCl, the potential across R_+ would be directly measurable through reversible hydrogen electrodes (Fig. 4). None of these potentials is equivalent to Nernst's diffusion potential, which is postulated to arise in a solution because of different rates of migration of ions across a concentration gradient. This potential difference is not directly measurable in principle, but must be calculated on the basis of assumptions in the Nernst theory from measurements on the emf of the cell as a whole. For non-ideal solutions, these assumptions are inexact; furthermore, cell emf's in the case of mixtures are strongly dependent on the structure of the junction, and it must be emphasized that all such measurements involve the use of electrodes with characteristic properties on which the magnitude of the measurement depends. Diffusion potential, however, is postulated to be a property only of a solution containing a diffusing electrolyte.

This problem, and the equivalent one of single ion activities, has been dealt with at length by Guggen-

⁶ The terms "junction potential" and "diffusion potential" are used interchangeably.

heim (11), who sums up the situation as follows: "The electric potential difference between two points in different media can never be measured, and has not yet been defined in terms of physical realities; it is therefore a conception which has no physical significance."

Taylor (12) arrives at a similar conclusion, pointing out that single ion activities or free energies, and the potential at a liquid junction, are not thermodynamically defined, but are "purely mathematical devices, which may indeed be employed safely with considerable freedom."

MacInnes and Longworth (13) discuss several types of liquid junctions, and, in agreement with Guggenheim and Taylor, take the position that only the observed cell emf has real thermodynamic significance. Nevertheless, these writers follow the general practice of ascribing a definite numerical value to the junction potential in the simpler cases, where the assumptions involved in their mathematical treatment are reasonably secure.

The concept of diffusion potential in simple

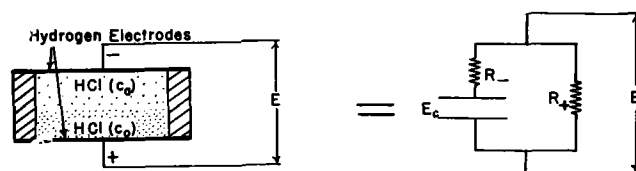


FIG. 4. Transference cell with electrodes reversible to cation and its equivalent circuit.

systems, when properly interpreted, does lead to correct results. On the other hand, the extensive body of literature which has accumulated around this interpretation suggests that it is not wholly satisfactory, even as a mathematical device. Classical electrochemical problems now interpreted in terms of diffusion potential seem to call for a new approach which involves only operational concepts. The equivalent circuit model of this paper might serve as a starting point. It will have to be shown, of course, that the model can be extended to non-ideal systems; this point is considered in the next section.

Non-ideal Systems

The successful results obtained in the case of the ideal transference cell are a strong temptation to take the general premises of the model as valid for non-ideal systems as well. Equation (II) would be replaced in this case by

$$E_c = \frac{2RT}{F} \ln \frac{(a_{\pm})_o}{(a_{\pm})_a} \quad (\text{XXIX})$$

where a_{\pm} is the mean activity of the electrolyte. The conductance would no longer be proportional to concentration, but this is unimportant to our

discussion; in the steady state, the applied potential difference is the same as E_c , the significant quantity from the thermodynamic standpoint, irrespective of the dependence of conductance on concentration. Clearly, we have a new means for determining activities of electrolytes. The technique of MacInnes and coworkers (14) for determining activity coefficients through transference cell measurements make use of equation (XII), but this requires, in addition, a different kind of experiment to determine the transference number. The method suggested here seems to offer a real advantage in economy of experimental effort. However, it has to be admitted that at the present time the validity of our model cannot be guaranteed by theoretical arguments for the non-ideal case, and no data by which a decisive experimental test can be made appear to have been recorded in the literature.

In designing a critical experiment, it would be unsafe to take the potential applied to the working electrodes as a measure of the cell emf. Any irreversible electrode effects due to slow kinetics of the electrode reaction, or resistance of the silver chloride film, would yield a value too high, if these factors are not negligible. Such effects are representable as an unknown series resistance added to the circuit of Fig. 2a. The difficulty could be circumvented by the use of probe electrodes at appropriate points in the cell, which would carry only the infinitesimal current required for potentiometric measurements.

A different cell design from that illustrated in Fig. 1 would be necessary. Figure 5a shows a suitable basic design, which differs from the previous one in having perforated or mesh electrodes close together and surrounded by electrolyte solution. Electrolyte is then free to pass through the electrode system. In the steady state, the concentration gradient is between the electrodes, while above and below the electrodes are solutions of uniform concentration, into which the probe electrodes may be inserted. The positioning of the latter is not critical. Both the working and the probe electrodes are silver-silver chloride. The former are visualized as being large with a copious supply of silver chloride on the cathode. The probe electrodes can be very small.

The equivalent circuit of this cell is shown in Fig. 5b, and is to be compared with that of Fig. 2a', which has dual condensers. The heavy lines represent the working circuit, and the light lines within the dotted areas, A and B, the additional circuit elements required for correspondence with the solution above and below the working electrodes, in which the probe electrodes are situated.

This equivalent circuit is evidently more complex than that of Fig. 2a', but the steady-state behavior is the same. If it is assumed that the measuring instrument requires only a vanishing current, in the steady state the two circuits A and B contribute nothing to the measured voltage. Irreversible over-voltage effects are representable as unknown resistance R_1 , R_2 , R_3 , and R_4 . In the measuring circuit, the voltage drops across R_3 and R_4 will be small, but in the working circuit the voltage drops across R_1 and R_2 could be large.

The optical methods of analysis now extensively employed in electrophoresis, diffusion, and ultracentrifuge investigations would be suitable for concentration determinations in such an experiment, or the solutions could be drained from their compartments and subjected to chemical analysis. It is well to bear in mind that attainment of the steady state

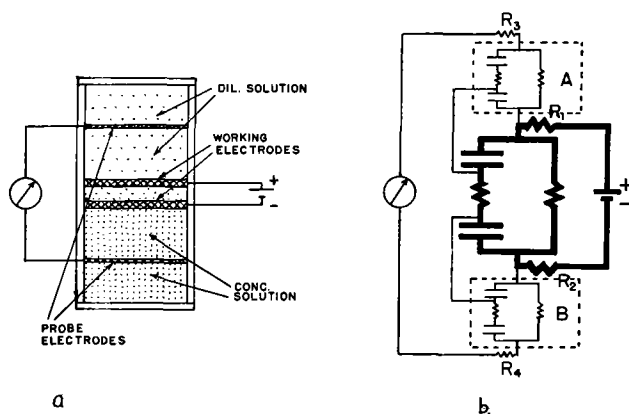


FIG. 5. Basic cell design (a) and equivalent circuit (b) for the determination of thermodynamic properties of the electrolyte MCl.

from a uniform solution would be a matter of hours or days; this time could be shortened by commencing the experiment with all conditions approaching those of the steady state as closely as possible.

It may be argued that the introduction of another irreversible process—steady current flow—on top of diffusion would introduce more uncertainty into the interpretation of emf measurements than is encountered where diffusion alone is present (concentration cell with transference). The equivalent circuit model suggests, however, that when two concurrent irreversible processes are properly balanced (coupled), interpretation of the reversible part of the system is facilitated. This point is to be considered further in a later paper, where the transference cell is treated by the methods of thermodynamics of the steady state.

Any discussion of this paper will appear in a Discussion Section, to be published in the December 1954 issue of the JOURNAL.

REFERENCES

1. G. W. MURPHY, *This Journal*, **97**, 105 (1950).
2. G. W. MURPHY AND D. BATZER, *This Journal*, **99**, 520 (1952).
3. H. J. S. SAND, *Phil. Mag.*, (6), **1**, 45 (1901).
4. T. R. ROSEBRUGH AND W. L. MILLER, *J. Phys. Chem.*, **14**, 816 (1910).
5. D. C. GRAHAME, *J. Am. Chem. Soc.*, **63**, 1207 (1941).
6. D. C. GRAHAME, *This Journal*, **99**, 370C (1952).
7. B. BREYER AND F. GUTMAN, *Trans. Faraday Soc.*, **43**, 785 (1947).
8. J. R. MACDONALD, *Bull. Am. Phys. Soc.*, Cambridge, Mass., Meeting, 1953. Details to be published.
9. W. NERNST, *Z. physik. Chem.*, **2**, 613 (1888).
10. J. PIGUET, W. KUHN, AND H. KUHN, *Helv. Chim. Acta*, **34**, 1183 (1951).
11. E. A. GUGGENHEIM, *J. Phys. Chem.*, **33**, 842 (1929).
12. P. B. TAYLOR, *J. Phys. Chem.*, **31**, 1478 (1927).
13. D. A. MACINNES AND L. G. LONGSWORTH, *Cold Spring Harbor Symposia Quant. Biol.*, **4**, 18 (1936).
14. A. S. BROWN AND D. A. MACINNES, *J. Am. Chem. Soc.*, **57**, 1356 (1935).

Anodic Behavior of Aluminum and Its Alloys in Sulfuric Acid Electrolytes¹

RALPH B. MASON AND PHYLLIS E. FOWLE

Aluminum Research Laboratories, New Kensington, Pennsylvania

ABSTRACT

This paper deals with the main factors affecting the rate of solution of anodic oxide coatings on aluminum as they are being formed in sulfuric acid electrolytes. Conditions favoring high coating ratios or thick, hard abrasion-resistant coatings have been investigated. Low temperatures, high current densities, which permit a shorter time of immersion in the electrolyte, and the addition of substances such as oxalic acid to the electrolyte, favor the formation of such coatings. This has been mainly an investigation of the competition between the rate of formation and the rate of solution of the coatings.

INTRODUCTION

The physical characteristics of the thick commercial anodic coatings on aluminum are markedly affected by the rate at which the coatings dissolve during formation. Some of the factors affecting the efficiency of anodic coating formation in sulfuric acid electrolytes have been discussed in several papers (1-3). The present paper extends previous work (3) to include conditions favoring higher coating efficiencies which result in improved physical properties.

It has been shown (4) that a high purity aluminum (99.95%) anode in a coulometer reacts electrochemically in a sulfuric acid electrolyte with an efficiency of 100% even though the operating conditions are varied over a wide range. On the other hand, the anodic oxide coating is slowly attacked by the sulfuric acid electrolyte and the efficiency of coating formation decreases as those factors which favor chemical solution of the coating predominate. There is always competition between the rate of formation and the rate of solution of the coating and, if the coating is not formed rapidly enough, little or no oxide coating remains on the surface under unfavorable conditions.

As a measure of the efficiency of oxide coating formation, some investigators (1, 2, 5) used the ratio of the weight of coating to the theoretical weight of aluminum oxide that should be formed from the weight of aluminum reacting. In the case of oxide coatings formed in sulfuric acid electrolytes, however, the coating ratio or the weight of coating divided by the weight of aluminum reacting appears to be a more practical figure to use for the

evaluation of the efficiency of coating formation (6), since coatings formed in sulfuric acid electrolytes are known to contain an appreciable percentage of sulfate (7-9). Oxide coatings formed on 99.95% aluminum in a 15% (by weight) sulfuric acid electrolyte under certain standard conditions of operation contain about 12-14% SO₃ (calculated from the sulfate determination), some water, and the remainder alumina. In addition, oxide coatings formed on aluminum alloys may contain other substances derived from the alloying elements.

It has been demonstrated, within certain limits, that the coating ratio (weight of coating divided by the weight of aluminum reacting) is increased by decreasing the concentration of the electrolyte or the temperature, or by increasing the current density (3). These factors have an appreciable effect on the amount of coating dissolved by the electrolyte during formation. Lowering the temperature of the electrolyte is especially effective in reducing the solution of the anodic oxide coating during formation (3, 10, 11). Thus, by changing the conditions of treatment so as to decrease the rate of solution of the oxide coating, the coating ratio is increased. If all the aluminum reacting were converted to aluminum oxide and none of the oxide were dissolved by the electrolyte, the coating ratio would be 1.89 (6). When the coating contains 14% SO₃, the theoretical coating ratio would be about 2.2. Because of the solvent action of the sulfuric acid electrolyte on the coating, however, a coating ratio of 2.2 has not been observed as yet. In these experiments, it is shown that, by selecting suitable conditions for forming the coating, it is possible to approach, but not actually reach, a coating ratio of 2.2.

While it is possible to reduce the rate of attack of the oxide coating during treatment by lowering the concentration of the electrolyte, it is not always

¹ Manuscript received July 1, 1953. This paper was prepared for delivery before the Wrightsville Beach Meeting, September 13 to 16, 1953.

practical to do so, especially at lower operating temperatures. In the present experiments, the electrolytes which were used contained from 12% to 25% (by weight) sulfuric acid; the one used in the majority of cases contained 15% (by weight) of sulfuric acid.

PROCEDURE

Specimens of 0.064-in. (1.63 mm) aluminum sheet were cut to size, cleaned, weighed, and anodically treated in 12–15% (by weight) sulfuric acid electrolyte for 10, 20, and 30 min, or other convenient times, at temperatures of 34°, 50°, 60°, and 70°F (1.1°, 10.0°, 15.6°, and 21.1°C). After washing and drying, the specimens were weighed. The coatings were then stripped in a phosphoric-chromic acid solution, according to a suggestion of Mason (12), and they were washed, dried, and weighed again. From these measurements, the weight of aluminum reacting and the weight of the coating was calculated.

The specimen dimensions were so chosen that, with 1 amp of current flowing, the desired current density could be obtained. For example, the area of the surface for the specimen used at 12 amp/ft² (1.3 amp/dm²) was 12 in.² (77.4 cm²), for the specimen used at 48 amp/ft² (5.2 amp/dm²) the area was 3 in.² (19.4 cm²). In all cases, the area of the cut edges of the specimens was included in the total area.

The specimens were suspended in the electrolyte by means of a tantalum clip between two pure lead cathodes. Suitable agitation of the electrolyte was obtained by means of an electrically driven glass stirrer. When a high current density is used, a higher voltage is necessary, and this results in considerable heat which must be removed rapidly in order to minimize attack of the coating or burning. The electrolyte for the experiments at all but the lowest temperature was held in a rectangular Lucite tank 4 in. x 8 in. x 8 in. (10.2, 20.3, and 20.3 cm), and was cooled by passing ice water through a lead coil immersed in one end of the tank. A sensitive mercury thermoregulator in conjunction with a delayed-action vacuum tube relay was used to control the centrifugal type pump which circulated the ice water. It was possible to hold the temperature of the electrolyte constant to about 0.1°F (0.06°C).

For the experiments at 34°F (1.1°C), a rectangular lead tank holding about 9 liters of electrolyte was placed within a larger iron tank and surrounded with cracked ice. An electrically driven glass stirrer was used for agitation. Since the maximum current used was only 1 amp and the volume of the electrolyte was relatively large, it was possible to hold the temperature of the electrolyte constant.

EXPERIMENTAL WORK

All results obtained in the experiments on coating ratios are shown in graphical form. Coating ratios have been plotted against the weight of metal removed by electrochemical action or the approximate time of treatment.

High purity aluminum (99.95%) was anodically treated in a 15% sulfuric acid electrolyte at 70°F (21.1°C) using various current densities and times of treatment. The family of curves in Fig. 1 shows the effect on the coating ratio of varying the current density from 6 to 72 amp/ft² (0.65 to 7.8 amp/dm²) for coating periods up to about 40 min. As the time of treatment increases, the coating ratio decreases. This indicates that for a given current density there is more chemical solution of the coating as the thickness or time of treatment increases. This solution takes place on the outer surface and on the pore walls. All the curves at 70°F (21.1°C) have about the same slope. As the current density is increased beyond 12 amp/ft² (1.3 amp/dm²), it is more difficult to obtain consistent coating ratio values, and it is usually necessary to make several check determinations.

Effect of Lowering Temperature

When the temperature of the sulfuric acid electrolyte is reduced to 50°F (10°C), the rate of solution of the coating is decreased (see Fig. 2). The slope of the curves for 6, 12, and 24 amp/ft² (0.65, 1.3, and 2.6 amp/dm²) is less steep than at 70°F (21.1°C), indicating less over-all solution of the coating. The curves for 36 and 48 amp/ft² (3.9 and 5.2 amp/dm²) are approximately parallel to the *X* axis and show that, under these conditions, there is no decrease in the coating ratio with increasing times of treatment. However, at 72 amp/ft² (7.8 amp/dm²) the coating ratio increases with time of treatment. This higher coating ratio may be explained by a continued decrease in the rate of solution of the coating at the bottom or base of the pores because of a build up of solution products within the pore channels. This effect becomes more pronounced as the length of the pore or the path of travel for the dissolved aluminum increases.

Coating ratio curves for 99.95% aluminum anodically treated in 15% sulfuric acid at 34°F (1.1°C) are shown in Fig. 3. At this low temperature, even the coating ratio curve for 6 amp/ft² (0.65 amp/dm²) is very nearly parallel to the *X* axis, indicating no substantial increase in rate of solution of coating with time of treatment. The curve for 48 amp/ft² (5.2 amp/dm²) starts to turn up at 30 min. At 72 amp/ft² (7.8 amp/dm²) the coating ratio rises rapidly to a value of 1.90 at 43 min.

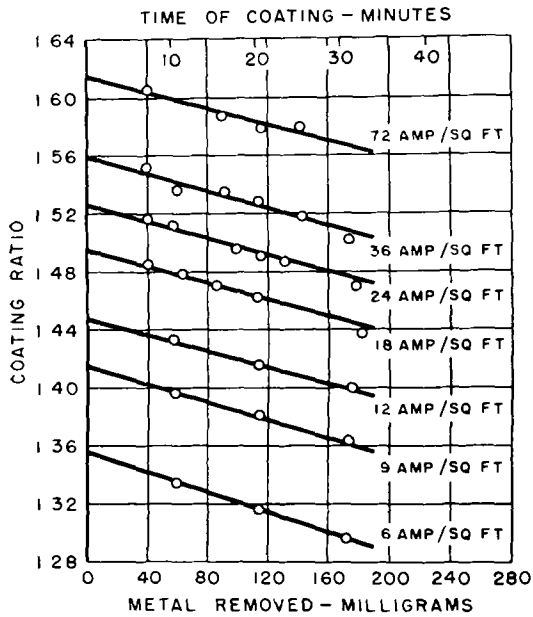


FIG. 1 Effect of current density on coating ratio for 99.95 aluminum treated anodically in 15% H₂SO₄ at 70°F (21.1°C).

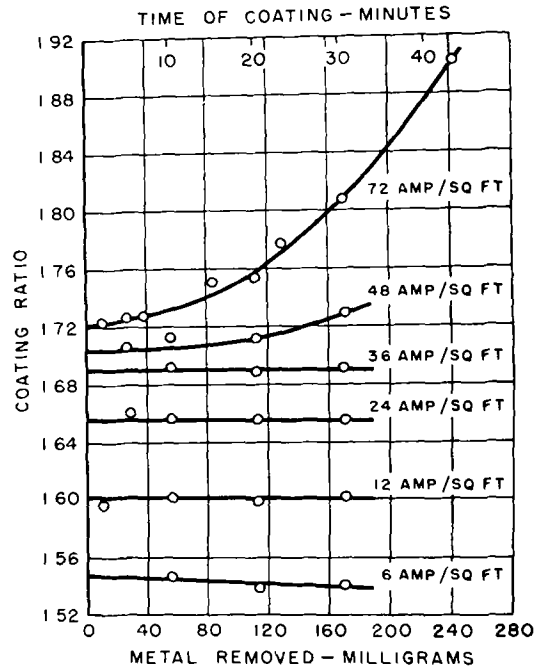


FIG. 3 Effect of current density on coating ratio for 99.95 aluminum treated anodically in 15% H₂SO₄ at 34°F (1°C).

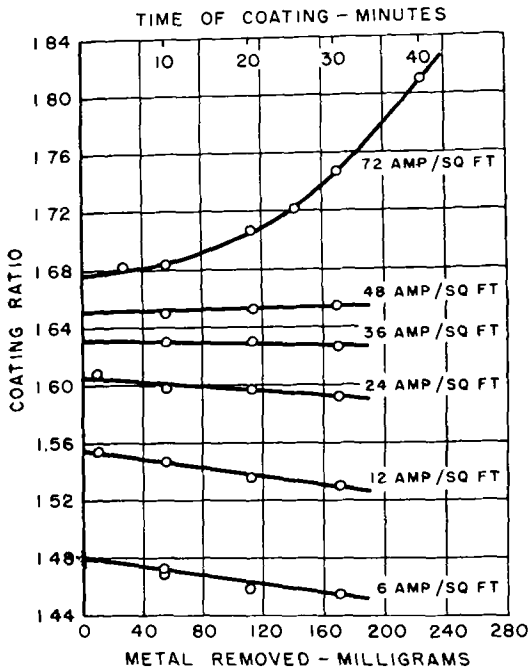


FIG. 2 Effect of current density on coating ratio for 99.95 aluminum treated anodically in 15% H₂SO₄ at 50°F (10°C).

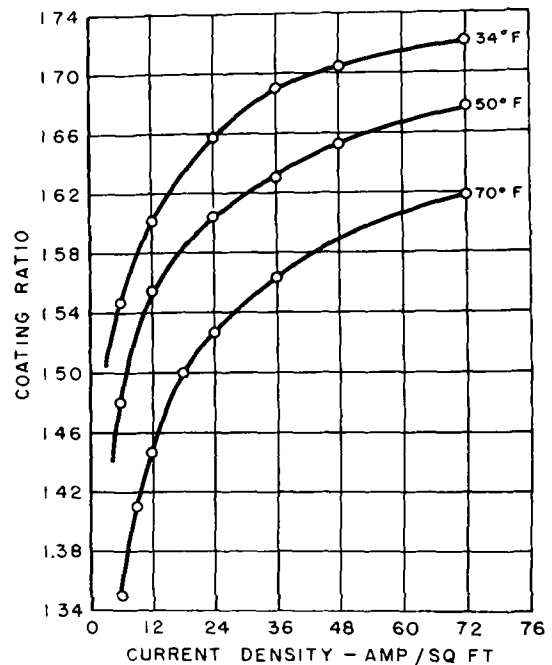


FIG. 4. Effect of current density on coating ratio at 1 min for 99.95 aluminum treated anodically in 15% H₂SO₄.

Effect of Time and Current Density

The coating ratios obtained by extending the curves to cut the Y axis at zero time should be the maximum for a given pore size since there should be the minimum chemical attack of the coating already formed. In Fig. 4, the coating ratios at one minute (from Fig. 1-3) are plotted against current density.

Judging from these curves, increasing the current density from 36 to 72 amp/ft² (3.9 to 7.8 amp/dm²) at 70°F (21.1°C) would have slightly less effect on increasing the coating ratio than lowering the temperature 20°F (11°C), while increasing the current density from 12 to 24 amp/ft² (1.3 to 2.6 amp/dm²)

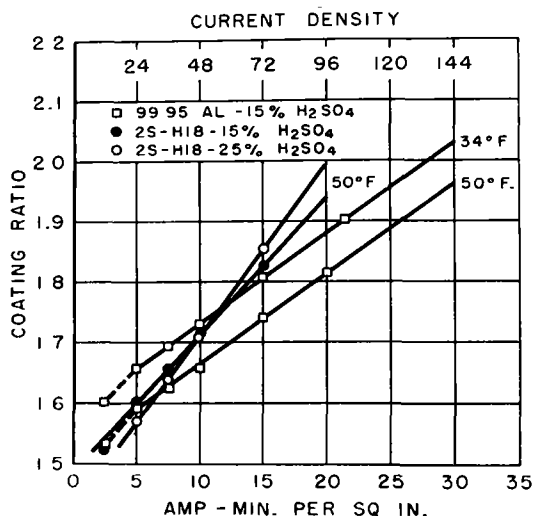


FIG. 5. Effect of current density and temperature on the coating ratio.

at 50°F (10°C) would have slightly more effect on increasing the coating ratio than decreasing the temperature about 16°F (9°C).

The family of curves of Fig. 4 indicates that, depending on high current densities and low temperatures alone, it is exceedingly difficult to obtain a coating ratio greater than about 1.80. In order to take advantage of the rapid increase in coating ratio values with time or thickness of coating when formed at low temperatures and high current densities, the coating ratios for 30 or 40 min coatings taken from Fig. 1, 2, and 3 are plotted against ampere minutes per square inch (or equivalent current densities) in Fig. 5. The total time that each specimen re-

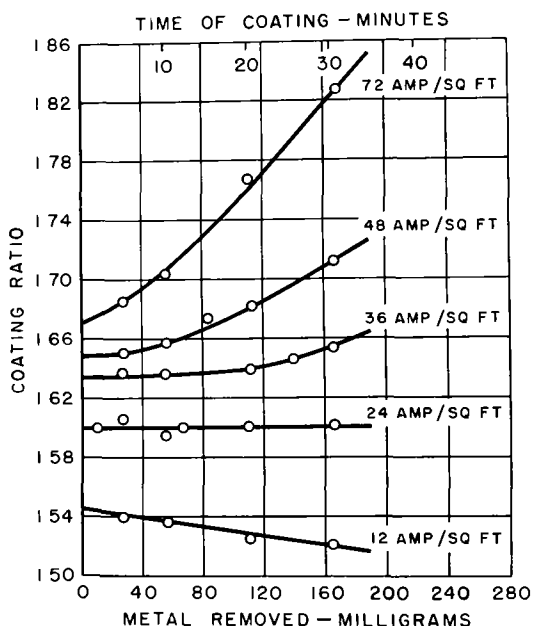


FIG. 6. Effect of current density on coating ratio for 2S-H18 alloy treated anodically in 15% H_2SO_4 at 50°F (10°C)

mained in the electrolyte was approximately the same, so the amount of oxide dissolved per square inch from the outer surface should be about the same. As the ampere minutes per square inch are increased beyond 5, the curves appear to be straight lines which, if extended far enough, would give the postulated theoretical coating ratio at some current density higher than 144 amp/ft² (15.6 amp/dm²) or 30 amp min/in.² (4.65 amp min/cm²). Because of experimental difficulties, no coating ratio higher than 1.90 was obtained at this time. This is perhaps about the highest value that can be obtained experimentally, since the solution of the outer surface cannot be prevented entirely and the pores which are necessary for continued growth are equivalent in volume to the oxide coating which has been dissolved.

In Fig. 5, the curves for 99.95% aluminum at 34°F (1.1°C) and 50°F (10°C) are parallel and indicate that the oxide surface dissolved more rapidly at 50°F (10°C) than at 34°F (1.1°C). The rate of solution of the oxide coating decreased as the concentration of dissolved aluminum in the pores increased with current density.

Behavior of Aluminum Alloys

The coating ratio curves for the common aluminum alloys differ somewhat from those for high purity metal. Coating ratio curves for 2S-H18 anodically treated in 15% sulfuric acid at 50°F (10°C) are shown in Fig. 6. The curve for 24 amp/ft² (2.6 amp/dm²) is parallel to the X axis. Several of the curves for the higher current densities turn upward, indicating a decrease in the rate of solution of the coating at the bottom or base of the pores. This effect takes place at a lower current density

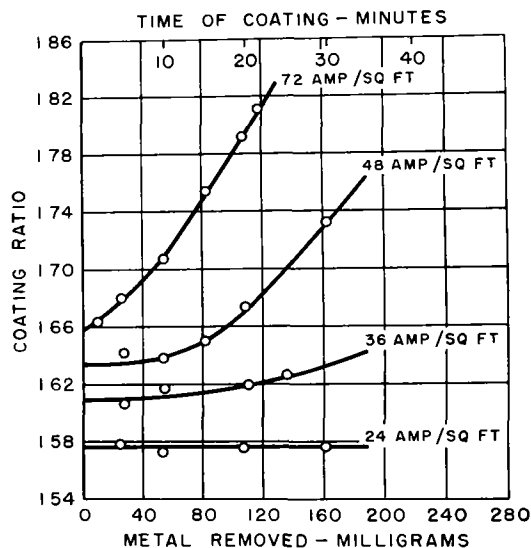


FIG. 7. Effect of current density on coating ratio for 61S-T6 alloy treated anodically in 15% H_2SO_4 at 50°F (10°C).

with 2S than with high purity metal (see Fig. 2). Increasing the acid concentration from 15 to 25% at 50°F (10°C) has only a slight effect on the coating ratio curves. Although the values are slightly lower in the 25% sulfuric acid for normal current densities, increasing the concentration of the acid by 10% has less effect than raising the temperature 10° or 20°F (5.5° or 11°C).

Referring again to Fig. 5, where the 30-min coatings on 2S have also been plotted, it will be noted that the curve for 2S is steeper than the corresponding curve for 99.95% aluminum. Either the pore walls of the coating on 2S are less soluble than the pore walls of the pure aluminum (99.95%) because of the impurities, or the pores are fewer in number because of a higher voltage across the primary or barrier layer (13). At current densities greater than 48 amp/ft² (5.2 amp/dm²), the solvent action of 25% sulfuric acid on the pore walls appears to be less than 15% sulfuric acid.

Since the rapid increase in coating ratio values with time is always accompanied by an abnormal increase in voltage, an investigation of the higher coating ratio values is mainly of theoretical interest. To produce hard abrasion-resistant coatings in the sulfuric acid electrolyte, conditions should be chosen that will give a coating ratio curve parallel to the X axis (or time of coating).

Although coating ratio curves for 52S-H34, 61S-T6, and 75S-T6 were determined, only the values for 61S-T6 have been plotted in Fig. 7. The curves for 52S and 61S are very similar to those for 2S (Fig. 6), but have somewhat lower coating ratio values at the lower current densities, as might be expected. In the case of 61S-T6, the curves for 48 and 72 amp/ft² (5.2 and 7.8 amp/dm²) turn up more rapidly than the corresponding 2S and 52S curves, and actually higher coating ratio values are obtained at 20 or 30 min.

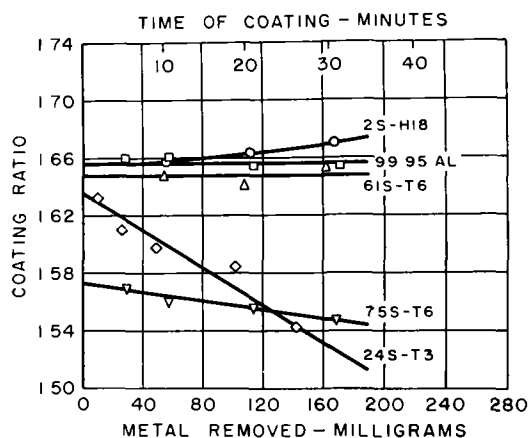


FIG 8. Coating ratios for various alloys anodically treated in 15% H₂SO₄ at 34°F (1.1°C) and a current density of 24 amp/ft² (2.6 amp/dm²).

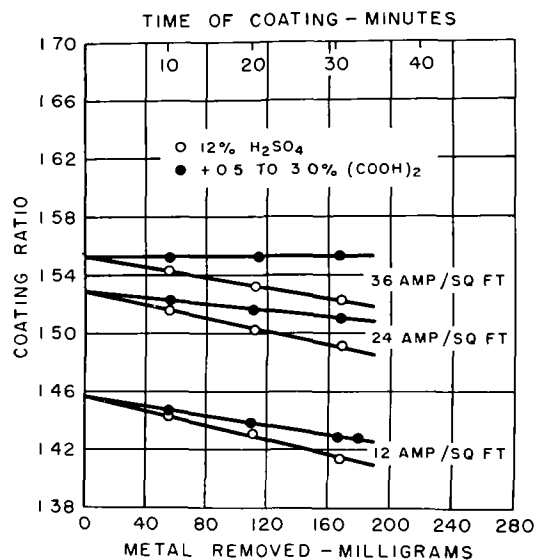


FIG 9 Effect of addition of oxalic acid to 12% H₂SO₄ electrolyte at 70°F (21.1°C) on coating ratio of 2S-H18. Average results have been plotted for the various additions of oxalic acid

No values have been shown for the 75S-T6 alloy at 50°F (10°C) since the coatings appear to be appreciably more soluble than those on the other two alloys. The slope of the curve for 36 amp/ft² (3.9 amp/dm²) is still noticeably steep.

In Fig. 8 are shown a few coating ratio curves for some of the alloys anodically coated in 15% sulfuric acid at 34°F (1.1°C). A single current density of 24 amp/ft² (2.6 amp/dm²) was used for this particular test. The curves are very similar for 99.95% Al, 2S-H18, and 61S-T6. The curve for 2S shows a tendency to turn upward at 30 min, indicating a slight decrease in the rate of solution of the coating. The curve for 75S-T6 is less steep than the corresponding one at 50°F (10°C). The curve for 24S-

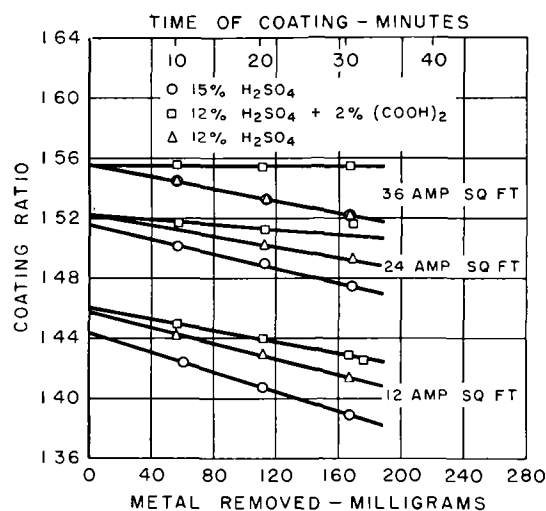


FIG 10. Effect of decreased concentration and addition of oxalic acid to a sulfuric acid bath at 70°F (21.1°C) on coating ratio of 2S-H18

T3 is noticeably steep, indicating substantial solution of the coating in the electrolyte as the time of treatment increases. It is very difficult to treat 24S-T3 anodically for 30 min at a current density of 24 amp/ft² (2.6 amp/dm²) and obtain a uniform

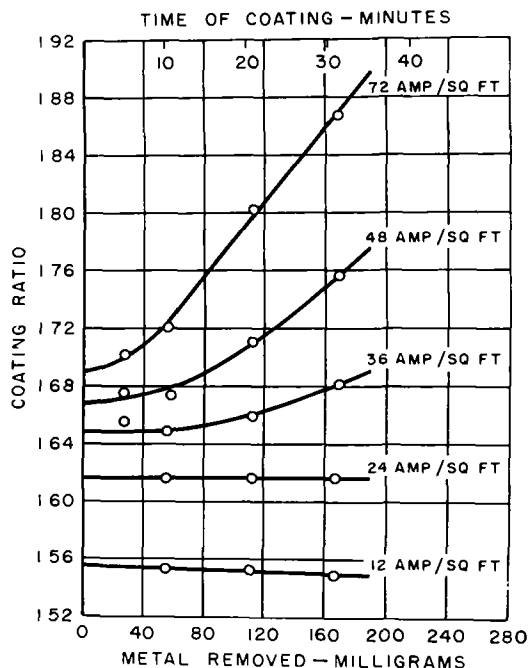


FIG. 11 Effect of current density on coating ratio for 2S-H18 alloy treated anodically in 12% H₂SO₄ + 1% (COOH)₂ at 50°F (10°C)

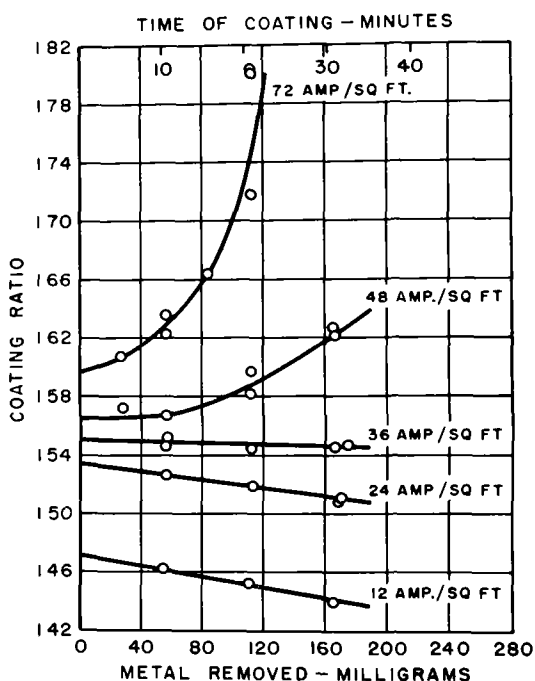


FIG. 12 Effect of current density on coating ratio 75S-T6 alloy treated anodically in 12% H₂SO₄ + 1% (COOH)₂ at 50°F (10°C)

coating. Several 30-min samples were discarded because of burning.

Addition of Oxalic Acid

One of the most effective addition agents known for decreasing the solubility of the anodic oxide coating in sulfuric acid is oxalic acid. The coating ratio curves for 2S-H18 in 12% sulfuric at 70°F (21.1°C) plus small amounts of oxalic acid are shown in Fig. 9. It is apparent that small amounts of oxalic acid are effective in reducing the rate of solution of the coating as the time of treatment increases. The smallest addition (0.5%) appeared to be as effective as the addition of 3.0%, and average values have been plotted. Because of the decomposition of oxalic acid in use, it is more practical to use 1 or 2% as the addition agent.

Coating ratio curves for 2S-H18 in 12% sulfuric acid, 15% sulfuric acid, and 12% sulfuric acid plus 2% oxalic acid are compared in Fig. 10. The differences between 12 and 15% sulfuric acid are less pronounced as the current density is increased to 36 amp/ft² (3.9 amp/dm²). The curve for 12% sulfuric acid plus 2% oxalic acid at 36 amp/ft² (3.9 amp/dm²) is parallel to the X axis even though the temperature is 70°F (21.1°C).

Coating ratio curves for 2S-H18 and 75S-T6 anodically coated in 12% sulfuric acid plus 1.0% oxalic acid at 50°F (10°C) have been plotted in Fig. 11 and 12. Here the effect of the oxalic acid addition is about as pronounced as at 60° or 70°F (15.6° or 21.1°C). The presence of 1% oxalic acid in 12% sulfuric acid is especially effective in reducing the solubility of the oxide coating in the case of the 75S-T6 alloy. It is possible that the addition of oxalic acid to the sulfuric acid electrolyte decreases the solution of the pore walls, resulting in a smaller total pore volume than would be obtained normally.

For practical use, the sulfuric-oxalic acid electrolyte at 50°F (10°C) is as good as the plain 15% sulfuric acid at 34°F (1.1°C). A higher operating temperature is permitted since the oxalic acid decreases the rate of solution of the pore walls. A slightly longer time of treatment would be required to obtain the same weight of coating at the higher temperature because of the somewhat greater coating ratios obtained at 34°F (1.1°C).

SUMMARY

Coating ratios have been determined for aluminum and its common wrought alloys in sulfuric acid under various operating conditions. The rate of solution of the oxide coating from the pore walls and the outer surface is a determining factor for the value of the coating ratio. The highest coating ratio

values are found where the conditions of coating are adjusted to give the minimum rate of solution of the coating.

For a coating containing 14% SO_3 , the postulated theoretical coating ratio would be 2.20 and not 1.89 (Al_2O_3 only) when the efficiency is 100%. It is possible to approach, but never reach, the theoretical value because the volume of the coating represented by the pores has been dissolved as well as some of the outer surfaces.

When high current densities and low temperatures are employed to produce thick oxide coatings, it appears that the rapid formation of solution products in the pores causes a decrease in the rate of solution of the oxide coating, which in turn produces higher coating ratio values.

Any discussion of this paper will appear in a Discussion Section to be published in the December 1954 issue of the JOURNAL

REFERENCES

1. B CHANDA, *Trans Indian Inst Chem Engs*, **1**, 67 (1947-1948)
2. J. D. EDWARDS AND F. KELLER, *Trans Electrochem Soc*, **79**, 135 (1941)
3. R. B. MASON AND C. J. SLUNDER, *Ind Eng Chem*, **39**, 1602 (1947).
4. M. TOSTERUD AND R. B. MASON, *Trans Electrochem Soc*, **90**, 221 (1946)
5. O. F. TARR, M. DARRIN, AND L. G. TUBBS, *Ind Eng Chem*, **33**, 1575 (1941)
6. S. ANDERSON, *J Applied Phys*, **15**, 477 (1944)
7. F. LIECHTI AND W. D. TREADWELL, *Helv Chim Acta*, **30**, 1204 (1947)
8. K. NORDEN, *Z. Elektrochem*, **6**, 159, 188 (1899)
9. N. D. PULLEN, *Metal Ind (London)*, **54**, 327 (1939)
10. J. KRONSBELN, *Trans Electrochem Soc*, **94**, 353 (1948)
11. N. D. TOMASHOV, *Vestnik Inzhenerov i Tekh*, **2**, 59 (1946)
12. J. D. EDWARDS, *Proc Am. Soc Testing Materials*, **40**, 959 (1940)
13. W. BAUMANN, *Z Physik*, **111**, 708 (1939)

The Mechanism of the Anodic Formation of Lead Chromate¹

CARL WAGNER

Department of Metallurgy, Massachusetts Institute of Technology, Cambridge, Massachusetts

ABSTRACT

This paper deals with the interplay of diffusion and convection processes governing the anodic formation of lead chromate during the electrolysis of a solution of sodium chromate and sodium chlorate between lead electrodes. At sufficiently high current densities, the boundary layer contains excess lead ions and flows downward in virtue of its higher density. Lead chromate is formed, in part, at a distance of 0.01 to 0.1 cm from the anode by counterdiffusion of lead ions and chromate ions and, in part, at the lower edge of the anode by mixing of boundary layer and bulk solution.

INTRODUCTION

The electrolysis of a dilute solution of sodium chromate between lead electrodes leads to the formation of a thin adherent layer of lead chromate and lead dioxide at the anode, and subsequently oxygen is evolved. On the other hand, according to a patent by Luckow (1) and a fundamental investigation by Le Blanc and Bindschedler (2), the electrolysis of a solution containing a mixture of sodium chromate and sodium chlorate yields a precipitate of lead chromate appearing at some distance from the surface of the anode and falling down to the bottom of the trough, provided that the excess of sodium chlorate is sufficient and the current density is appropriately chosen. Thus, lead chromate is formed with a current efficiency close to 100% without passivation of the anode. This process is of industrial importance, since the crystals of lead chromate produced in this way have a well-defined size, which is appropriate for use of the product as a pigment. The same principle may be employed for the production of other nearly insoluble lead salts such as lead sulfate and basic lead carbonate, as has been shown by Luckow (1), Isenburg (3), and others.

The striking difference between the electrolysis of a solution containing only sodium chromate and the electrolysis of a solution containing a mixture of sodium chromate and sodium chlorate has been explained by Le Blanc and Bindschedler (2) in the following manner. In a solution of sodium chromate there are only chromate ions as anions, and thus a noticeable concentration of lead ions can nowhere be expected in view of the extremely low solubility of lead chromate. Consequently, formation of lead chromate can take place only at the surface of the anode and, thereby, the anode is passivated after some time. In a solution containing a mixture of sodium chromate and sodium chlorate, however, a thin layer of the solution near the anode may con-

tain lead, sodium, and chlorate ions, but practically no chromate ions. When lead ions migrating away from the anode encounter chromate ions migrating from the bulk solution toward the anode, a precipitate of lead chromate is formed. The local depletion of chromate ions in the vicinity of the anode is due to the fact that in a mixture of sodium chromate and sodium chlorate only a small portion of the electrical current is carried by chromate ions, and the larger portion of chromate ions required for the formation of lead chromate approaches the anode by diffusion rather than by electrolytic migration. The prevalence of lead ions in the solution near the anode has been ascertained with the aid of potential measurements by Just (4).

It remains open to question why the chromate ions reach the vicinity of the anode but not its surface. To find a solution of this paradox, one has to take into account not only diffusion processes, but also convection caused by local concentration and density differences according to Levich (5), Agar (6), Wagner (7), Keulegan (8), and Wilke, Tobias, and Eisenberg (9).

At the beginning of the electrolysis of a solution of sodium chromate and sodium chlorate, chromate ions are, of course, present at the surface of the anode and, therefore, initially lead chromate at the surface of the anode is formed under all conditions. The following events, however, depend on the current density applied and the concentration of chromate.

STRUCTURE OF THE BOUNDARY LAYER IF AN ADHERENT LAYER OF LEAD CHROMATE IS FORMED

When, for a given concentration of chromate, the current density is relatively low, depletion of chromate at the anode will not be complete, for the depleted solution has a lower density and, thus, flows upward. Since the effective thickness and the average flow velocity of the boundary layer increase

¹ Manuscript received July 14, 1953.

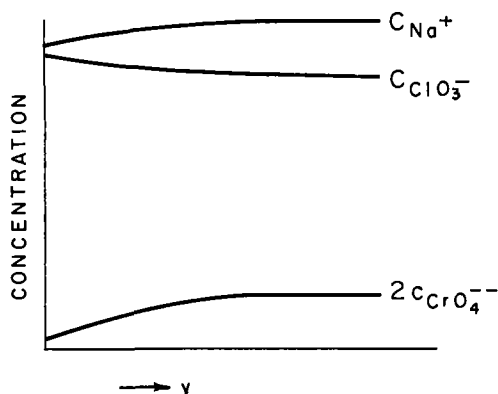


FIG. 1 Concentration distribution in the boundary layer when an adherent layer of lead chromate is formed

in the flow direction (7), fresh solution flows toward the electrode and supplies chromate ions. Thus lead chromate is formed at the surface of the anode until the anode is passivated by too thick a layer of lead chromate. Conditions in the boundary layer are shown schematically in Fig. 1.

If a lead electrode in a solution of sodium chromate with an excess of sodium chlorate is kept at a potential at which all chromate ions approaching the electrode react with lead but practically no Pb^{++} ions leave the electrode, the thickness of the boundary layer and the value of the limiting current density may be calculated from equations derived in a previous paper (7). The concentration of chromate ions, c_1 , as a function of the distance from the electrode, y , from the electrode may be approximated by the relation

$$c_1 = c_{1(0)}[1 - (1 - y/\delta)^2] \quad (I)$$

where $c_{1(0)}$ is the concentration of chromate ions in the bulk solution and δ is a parameter of the dimension of length as a measure of the thickness of the boundary layer. Since the mobilities of the other ions, Na^+ and ClO_3^- , do not differ considerably from the mobility of the chromate ions, the parameter δ may be used for the representation of the concentration distribution of all ions and likewise for the velocity profile. Then δ (cm) is found to be

$$\delta = \left[\frac{120D_1\nu x}{gc_{1(0)} \left(\frac{\partial \ln \rho}{\partial c_{Na_2CrO_4}} - \frac{\partial \ln \rho}{\partial c_{NaClO_3}} \right)} \right]^{\frac{1}{2}} \quad (II)$$

where D_1 (cm²/sec) is the diffusion coefficient of chromate ions, ν (cm²/sec) is the kinematic viscosity of the solution, x (cm) is the distance from the lower edge of the electrode, $g = 981$ cm/sec² is the gravitational acceleration, ρ (g/cm³) is the density of the solution, and the concentrations in mole/cm³ are designated by c with the respective subscripts.

The average current density $(I/A)_H$ for an electrode of height H is obtained as

$$\left(\frac{I}{A} \right)_H = \frac{16FD_1c_{1(0)}}{3} \cdot \left[\frac{gc_{1(0)}}{120D_1\nu H} \left(\frac{\partial \ln \rho}{\partial c_{Na_2CrO_4}} - \frac{\partial \ln \rho}{\partial c_{NaClO_3}} \right) \right]^{\frac{1}{2}} \quad (III)$$

At 25°C the following numerical values hold: $D_1 = 1.1 \cdot 10^{-5}$ cm²/sec corresponding to a mobility of chromate ions of $0.88 \cdot 10^{-3}$ (cm/sec)/(volt/cm); $\nu = 0.90 \cdot 10^{-2}$ cm²/sec; $\partial \ln \rho / \partial c_{Na_2CrO_4} = 140$ (mole/cm³)⁻¹; $\partial \ln \rho / \partial c_{NaClO_3} = 70$ (mole/cm³)⁻¹ (10); $F = 96,500$ coulomb/equivalent. Le Blanc and Bindschedler (2) investigated a solution containing 12 grams $NaClO_3$ /liter and 3.0 grams Na_2CrO_4 /liter corresponding to $c_{1(0)} = 1.9 \times 10^{-5}$ mole Na_2CrO_4 /cm³. For this solution equation (II) gives a value of $\delta = 0.1$ cm at a distance of $x = 10$ cm from the upper edge of the electrode, and equation (III) gives an average current density of 1.15×10^{-3} amp/cm² for an electrode of 10 cm height.

STRUCTURE OF THE BOUNDARY LAYER WHEN LEAD CHROMATE IS FORMED WITHIN THE BOUNDARY LAYER

The current density of 0.006 amp/cm² applied in most runs reported by Le Blanc and Bindschedler (2) exceeds the limiting current density for formation of $PbCrO_4$ at the surface of the anode. At higher current densities and under steady-state conditions, lead ions enter the solution near the anode and migrate across the boundary layer up to a certain distance δ_p where they encounter chromate ions and form a precipitate of $PbCrO_4$ as is shown schematically in Fig. 2. Since the solution near the anode is rich in lead chlorate, its density is higher than that of the bulk solution. The solution near the surface of the anode will, therefore, flow downward. The

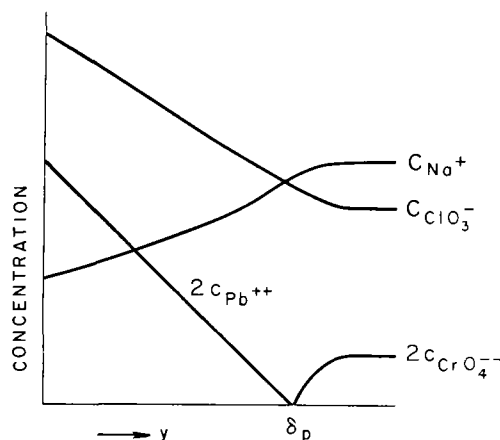


FIG. 2 Concentration distribution in the boundary layer when lead chromate is formed within the boundary layer

thickness and the average flow velocity of the boundary layer increase with increasing distance from the upper edge of the anode. Accordingly, bulk solution flows into the boundary layer. Thereby chromate ions are transported toward the anode at a rate beyond that accounted for by electrolytic migration and diffusion. The amount of chromate ions entering the boundary layer, however, cannot be equivalent to the amount of lead ions formed at the anode, for the mechanism suggested in this paper presupposes a definite thickness and a definite flow velocity of the boundary layer involving excess lead ions at the lower edge of the anode. Consequently, lead chromate is formed not only at some distance δ_p in front of the anode, but also in a mixing zone of lead-rich boundary layer and bulk solution below the lower edge of the anode. In this respect, the present analysis differs from that given by Le Blanc and Bindschedler (2).

EXPERIMENTAL

A lead foil coated with lacquer on one side was tilted by 15° vs. the vertical direction, the free surface facing downward. The electrolyte contained 12 grams NaClO_3 and 3 grams Na_2CrO_4 per liter. In accordance with Le Blanc and Bindschedler (2), a current density of 0.006 amp/sec was applied. The precipitate of PbCrO_4 formed within the boundary layer settled downward, and separated from the tilted electrode. In addition, fringes of precipitated lead chromate were observed at the lower edge of the electrode. This confirms the conclusion that a sizable amount of lead chromate is formed at the lower edge of the electrode by virtue of mixing of the lead-rich boundary layer with bulk solution.

CONCLUDING REMARKS

Approximate calculations indicate that the amount of lead chromate formed in the mixing zone at the lower edge of the anode is a substantial fraction of the total amount of lead chromate. Calculations are omitted in this paper since the effect of PbCrO_4 moving downward has been disregarded

and an estimate of this neglect is not possible. For this reason, only a qualitative discussion of the interplay between diffusion and convection is given.

A somewhat different situation is encountered when the electrolyte is stirred, and thereby the effective thickness of the diffusion boundary layer is determined. This case has been considered by Aten (11) with special reference to the anodic formation of silver halide at a silver electrode for the electroanalytic determination of halogen. In this case, silver halide has to be formed virtually only at the surface of the anode. Thus, the current density must not exceed the limiting value for exclusive formation of silver halide at the anode. The limiting current density is proportional to the concentration of halide in the bulk solution and, therefore, tends to zero when the electrodeposition of halogen is close to completion. An appropriate value of the current density at any time may be obtained by confining the electrode potential to such a value that the concentrations of both silver and halide ions at the anode are sufficiently low and accordingly the migration of silver ions into the boundary layer is negligible.

Any discussion of this paper will appear in a Discussion Section to be published in the December 1954 issue of the JOURNAL.

REFERENCES

- 1 C LUCKOW, D R P 91, 107 (1894)
- 2 M LE BLANC AND E BINDSCHEDLER, *Z Elektrochem*, **8**, 255 (1902)
- 3 A ISENBURG, *ibid*, **9**, 255 (1903)
- 4 G JUST, *ibid*, **9**, 547 (1903)
- 5 B LEVICH, *Acta Physicochim URSS*, **19**, 117 (1944), *Discussions Faraday Soc*, **1**, 37, Gurney and Jackson, London (1947)
- 6 J N AGAR, *ibid*, **1**, 26 (1947), *Trans Electrochem Soc*, **95**, 361 (1949)
- 7 C WAGNER, *Trans. Electrochem Soc.*, **95**, 161 (1949).
- 8 G H KEULEGAN, *J Research Nat Bur Standards*, **47**, 156 (1951)
- 9 C R WILKE, C W TOBIAS, AND M EISENBERG, *This Journal*, **100**, 513 (1953).
- 10 LANDOLT-BORNSTEIN, *Physikalisch-Chemische Tabellen*, 5th ed, pp 1104, 136, 425, Springer, Berlin (1923)
- 11 A H W ATEN, *Z physik Chem*, **92**, 320 (1918).

Extractive Metallurgy of Zirconium by the Electrolysis of Fused Salts

II. Process Development of the Electrolytic Production of Zirconium from K_2ZrF_6 ¹

M. A. STEINBERG, M. E. SIBERT, AND E. WAINER

Horizons Incorporated, Cleveland, Ohio

ABSTRACT

An intensive investigation of the electrolysis of K_2ZrF_6 in an electrolyte of NaCl has been carried out to determine the optimum conditions for the production of zirconium metal by fused salt electrolysis

Cell designs and conditions of operation evolved are described, yielding a high purity zirconium powder which is ductile on consolidation. This metal can be fabricated with ease, and is comparable to Kroll zirconium sponge. Because of the stability of the raw materials, their ease in preparation and in electrolysis, coupled with lower cost equipment, it is felt that this process will yield a much lower cost zirconium metal.

INTRODUCTION

The historical and theoretical aspects of the double fluoride process for production of zirconium metal have been discussed in previous papers (1, 2). The basic concept of the process entails the electrolysis of a fused alkali halide-potassium zirconium fluoride mixture under a purified argon atmosphere. In this paper, a detailed operational procedure is given for the electrowinning of zirconium metal, including treatment of the raw materials, construction and operation of the electrolytic cell under an inert atmosphere, electrolytic procedures and conditions of current and voltage, and recovery of the metal from the deposits obtained.

A complete description of the effects produced by variations in the operating variables is given. Temperature, current density, voltage, and cell atmosphere are all significant variables in this operation. Purity of raw materials and concentration effects are of equal or greater importance.

Metal produced by this process has been thoroughly evaluated by chemical analysis and physical metallurgical techniques. A summation of this data and methods employed are included in this discussion.

EQUIPMENT AND CELL DESIGN

All electrolytic work done toward development of the fluoride process was done in cells of the type shown in Fig. 1, as compared to the work done in the small cells previously used. The design illustrated

takes a charge of 5 lb. Two modifications of the cell are used, but these differ only in details, and not in capacity or operation.

The process has been successfully adapted to cells of 30- and 250-lb capacity. A subsequent paper will deal with larger scale operation in detail.

The cell design is essentially a steel shell with all-graphite interior parts. Heating is accomplished by an a-c heated carbon resistance element. This element is supported by its leads inside of a graphite shell separated from the steel casing by lampblack insulation. Silica and firebrick have been alternatively employed as insulation. The crucible is seated on a graphite pedestal inside the heating element. An inner graphite liner separating the crucible from the element and serving as a safety measure in case of crucible leakage has previously been used with this cell, but is not shown in this design.

Water-cooled copper-to-graphite element leads are used. The crucible serves as the cell anode and the positive d-c connection is made directly to the cell casing.

The head is basically a graphite dish packed with insulation and fitted with a water-cooled steel top. The cathode and thermocouple are inserted through this head. A steel bumped head with a gasketed flange is also provided to cover the whole upper assembly for evacuation of the cell.

Cells of this type are operated almost indefinitely with no corrosion of inner graphite parts if the cell interior is kept dry and free of atmospheric contamination. Crucibles are replaced after four to six runs due to salt leakage problems with commercial CS graphite.

Also, this cell can be utilized with a water-cooled

¹Manuscript received June 15, 1953. This paper is based on a portion of the work carried out by Horizons Incorporated for the New York Operations Office of the Atomic Energy Commission under Contract No. AT(30-1)-1144

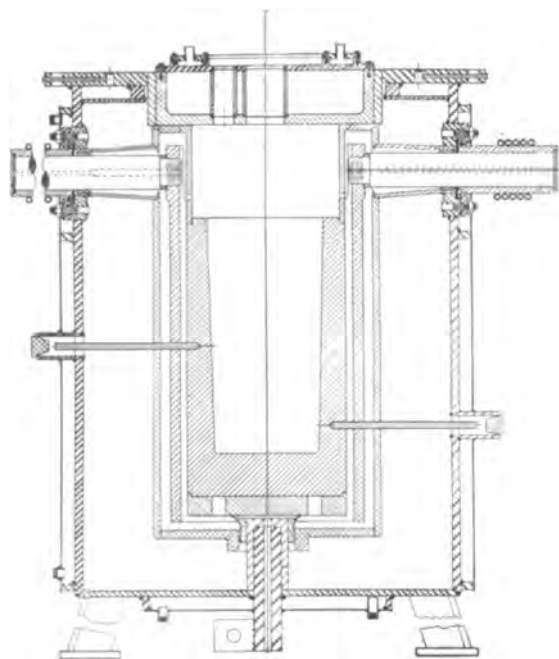


FIG. 1 Assembly drawing of inert-atmosphere zirconium electrolytic cell.

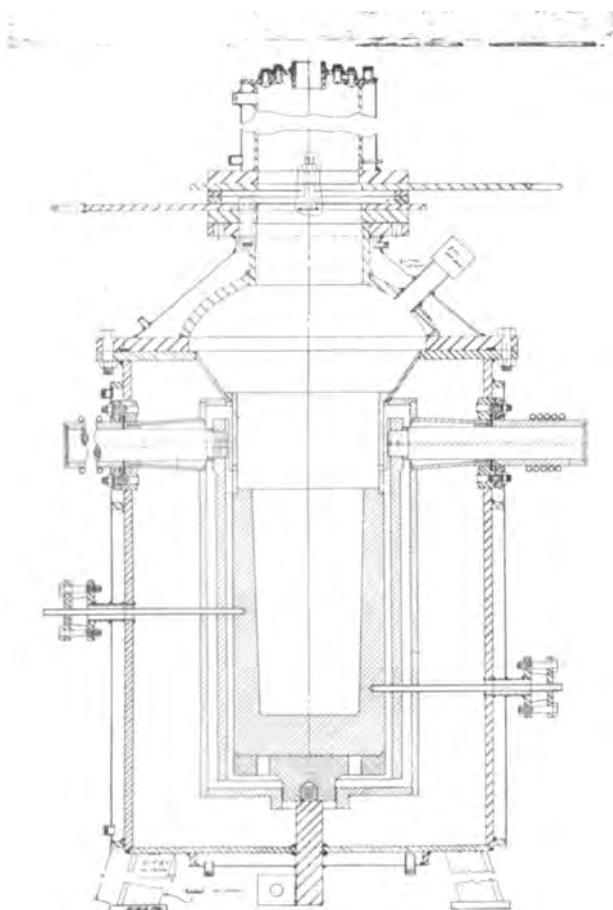


FIG. 2 Assembly drawing of modified electrolytic cell with bumped head, gate valves, and cathode removal chamber in place.

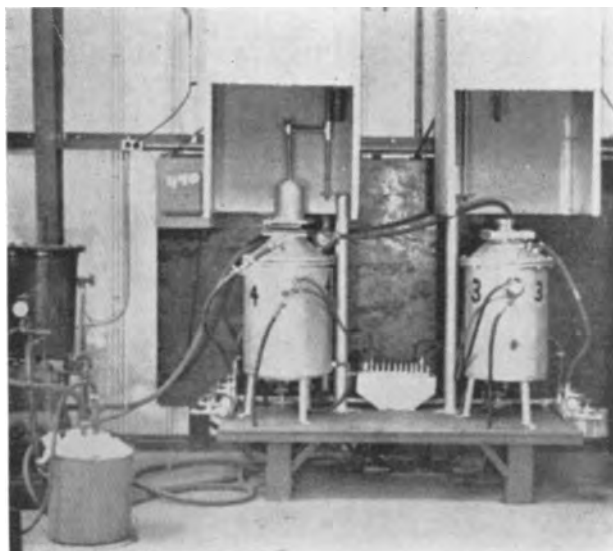


FIG. 3 External view of cells showing hood system and vacuum pump, cell 3 with vacuum head in place, and cell 4 with cathode removal chamber, cathode holder, and cathode in place.

cathode-removal chamber which fits onto the bumped head in place of the vacuum flange (Fig. 2). A photograph of two cells, one being evacuated (cell 3) and one with the bumped-head, cathode removal chamber and cathode in place is shown in Fig. 3. The two sliding gate valves shown in Fig. 2 close off both the cell and the cathode chamber so that the cathode chamber with the cathode and deposited metal can be removed from the cell proper and cooled under argon while the electrolyte and cell are sealed off under argon also. A second cathode removal chamber is placed on the cell and both gates are open, enabling a second electrolytic run to be made. A central panel board with a-c and d-c controls, temperature indicator, and argon flow-meters and valves for the operation of these cells, is shown in Fig. 4.

The argon is admitted through one of the element leads traveling down to the cell bottom, up around the crucible, and out through the head.

An a-c welding transformer has been used as a heating power source. A variety of d-c sources have been used with equal success. The most versatile is a motor generator set. A Hobart 400 amp a-c welder has been satisfactory as an a-c source. A Columbia 2000-amp motor generator has proved to be an extremely versatile and reliable d-c unit.

Linde Argon, $99.98 \pm 0.02\%$ in purity, is used as an inert atmosphere during operation. For further purification, the gas is passed through a column of phosphorus pentoxide to remove any residual moisture and then through a titanium sponge column

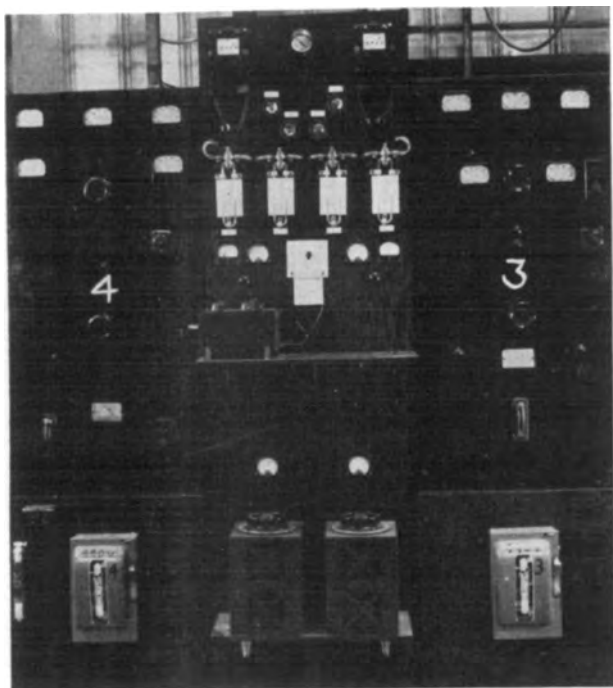


FIG 4 Front over-all view of panel board showing a-c and d-c controls and meters, temperature indicating equipment and argon pressure controls, and manometers for the two cells and the cathode removal chambers.

at 700°C to remove O_2 and N_2 . A sketch of this drying train is shown in Fig. 5 and is illustrated in Fig. 6.

OPERATIONAL PROCEDURES

Preparation of Cell and Materials

As will be later explained, it is essential that the cell and materials used be in an anhydrous condition; therefore, certain purification and cleaning steps must be taken. These include a hot evacuation of the cell and the vacuum drying of salts used in the electrolyte.

A new cell or one which has not been used for some time must be evacuated to remove moisture, hygroscopic salts, and certain organic materials. In the case of a new cell, insulating materials, particularly lampblack, and graphite parts contain large quantities of moisture and organic materials. The cell is first evacuated down to 100 μ or less at room temperature and then heated up to 100°–200°C above the normal operating temperature and pumped until the original pressure is again attained.

Raw materials must be pure and anhydrous. The sodium chloride used has been of reagent grade requiring, at most, an oven drying for 10–12 hr at 110°–120°C to remove surface occluded moisture. The K_2ZrF_6 is somewhat hygroscopic and is vacuum dried in a vacuum oven for 4–6 hr at 80°C at approximately 50 μ . The K_2ZrF_6 used has been of three

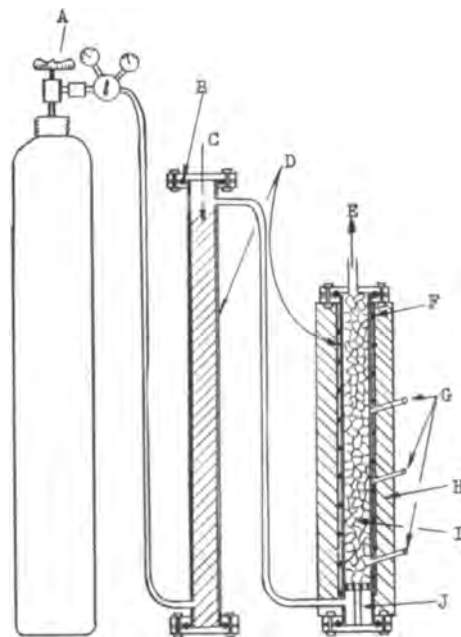


FIG 5. Sectional drawing of argon purification train used with zirconium electrolytic cells A—argon tank; B—copper O-rings, C— P_2O_5 packing; D—3-in. O.D. stainless steel tubes with steel flanges, E—to electrolytic cells; F—chromel "A" wire (14GA) embedded in refractory alundum cement; G—thermocouple wells; H—Kaylo pipe insulation; I—titanium sponge; and J—pedestal support

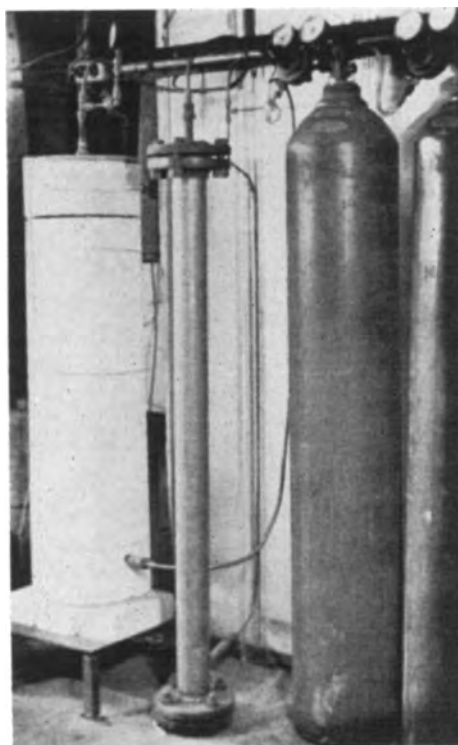


FIG. 6. Argon purification train with heaters, insulation, valves, etc., Ti column and P_2O_5 column.

types: (a) a C.P. grade, 99 + %, as supplied by the Kawecki Chemical Company, (b) a recrystallized 99.9% grade (Kawecki Chemical Company), and (c) a recrystallized 99.9% material produced in this laboratory.

Charging of Cell

The cell is initially heated to 850°–900°C under an argon atmosphere with the crucible in place. The dry salts are then charged and melted as rapidly as possible under a heavy argon flow.

When a fluid bath is obtained, the temperature is set at about 850°C using a chromel-alumel thermocouple embedded in the crucible wall. If purification of the bath is needed, a graphite cathode is inserted into the bath and d.c. applied to the circuit. Voltage is set at 1.5–2.0 volts. When moisture has been eliminated, a rise of 0.5–0.8 volt will be noted with a simultaneous current drop. Other more easily electrolyzable impurities are also broken down in this pre-electrolytic step. The bath is then ready for electrolysis.

Electrolysis

The cell temperature is dropped to 800°–850°C and a steel cathode with a nickel lead shaft inserted into the bath under low voltage (1–2 volts). This cathode shaft is protected by a graphite sleeve. Nickel is used as a lead because of its greater resistance to dry chlorine attack. A cylindrical cathode is used

to conform to the crucible configuration. A variety of cathode designs, including cones, disks, and strips, have been tried, but these produce no outstanding changes in results. When the cathode has reached bath temperature, the current is increased to a point where the initial current density is 250–400 amp/dm². At these temperatures this yields an actual bath voltage of 3.5–4.0 volts and an indicated voltage of 4–6 volts, including the voltage drop through the cell. All reported voltages are meter readings and not actual electrode voltages. Electrolysis is carried out for a calculated number of ampere-hours based on a deposition rate of 0.5 gram/amp-hr. This is equivalent to about 60% current efficiency which is normally encountered. When the bath is near exhaustion of the available zirconium, sodium is produced and will be observed burning at the sight hole of the cell. There is little visible action during the runs aside from the evolution of copious amounts of chlorine.

When the run is over, the cathode is raised from the bath with a small voltage still across the cell. It is clamped into position just above the bath or in a sealed cooling chamber above the cell and allowed to cool to room temperature in an argon atmosphere.

A typical cathode and deposit as cooled and removed from the cell is shown in Fig. 7. An operating data synopsis for three typical runs is given in Table I, along with a summary of characteristics of the deposited metal.

Metal Recovery

The deposit as recovered from the cell or cooling chamber is a gray to black rough surfaced metal-salt agglomerate. It is roughly one-third metal and two-thirds salts. These salts are principally NaCl, NaF, KCl, and KF, with small amounts of K₂ZrF₆, and possibly other lower zirconium chlorides or fluorides.

The deposit is broken off the cathode and jaw-crushed to coarse lumps. These are allowed to soak in water for a short time until soft. They are then wet mortared to break up salt agglomerates, washed in buffered hot water solutions, and kept just slightly acidic to prevent excessive precipitation of any hydrous oxides of zirconium. A series of washings and decantations are made until there is no evidence of residual salts and no test for halide ions in the wash water. The powder is then filtered and acetone dried.

Metal Consolidation

The metal as recovered from the washing step is a coarsely crystalline powder, brilliantly metallic. Typical granules and powder particles of as-recovered metal are shown in Fig. 8. This powder may either be sintered under argon or high vacuum, arc



Fig. 7 Typical electrolytic zirconium deposit. (Reduced one-third in reproduction)

TABLE I. *Electrolysis of K₂ZrF₆-NaCl-Salt Bath*

Run No	K ₂ ZrF ₆ %	Electrolysis			Amp hr	Yield %	C E %	Remarks
		T °C	E Volts	C D Amp/dm ²				
68-47	38	800	5.8	340	560	84	64	Commercial recrystallized K ₂ ZrF ₆
68-61	38	800	4.9	270	600	87	62	Commercial recrystallized K ₂ ZrF ₆
68-51	41	800	4.8	270	500	86	63	Horizons recrystallized K ₂ ZrF ₆

Screen analysis (% retained on screen)

Run No	+35 %	+100 %	+150 %	+200 %	+325 %	-325 %
68-47	2.9	30.0	21.0	14.8	17.0	14.3
68-61	1.4	30.1	18.4	12.7	19.8	17.6
68-51	13.7	50.2	14.9	7.6	8.4	5.2

Analysis for carbon, oxygen, and nitrogen

Run No	Zr %	C %	N %	O %	Hardness Rockwell B
68-47	99.9	0.047	0.011	0.038	82
68-61	99.8	0.030	0.0017	0.074	85
68-51	99.8	0.029	0.002	0.049	84

Amp hr = ampere hours of electrolysis

Yield % is based on total available Zr in electrolyte

C E = Current efficiency based on number of ampere hours of electrolysis and theoretical yield of 0.85 gram/amp hr.

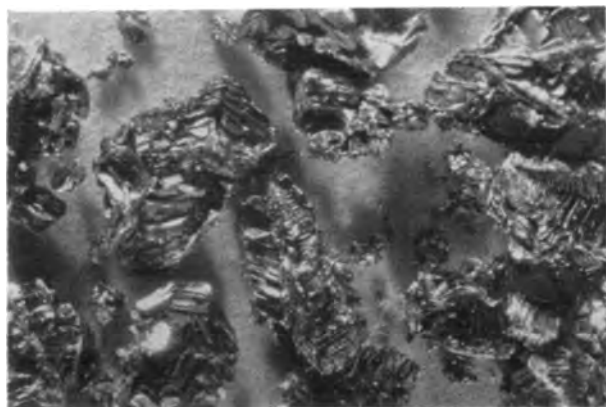


FIG. 8. As-recovered zirconium granules, water washed prior to compaction for arc melting 15X

melted, or sheath rolled. The usual procedure carried out at Horizons Incorporated for evaluation purposes has been arc melting.

A small laboratory arc-melting furnace has been used, employing a water-cooled copper hearth and a tungsten tipped electrode. The unit operates under a quarter atmosphere of argon. Arc-melted, cast ingots up to 50 grams in weight are melted from each electrolytic run for evaluation. These ingots are melted from the powder, cold-pressed into compacts at 10 tsi.

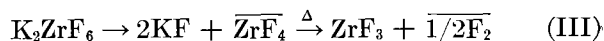
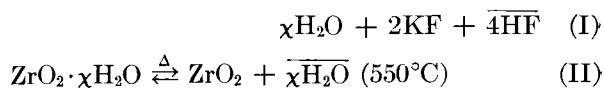
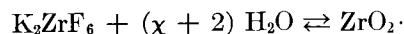
EVALUATION OF THE PROCESS

Mechanism of the Reaction

The mechanism of the reaction has not been conclusively established, but certain definitive facts are known which suggest a number of possibilities all leading to the same end result.

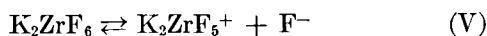
The fused salt mixture has been essentially standardized as one of NaCl and K₂ZrF₆. All the observed by-products and end products may be accounted for by consideration of the various chemical and electrochemical reaction possibilities through the purification and deposition cycles.

Considering only the double fluoride in a bath with some moisture present, the following chemical reactions might occur.

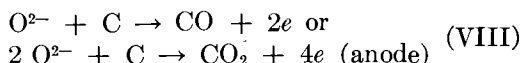
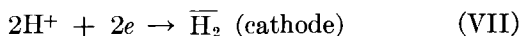
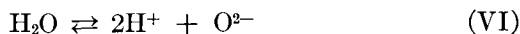


Reactions (I) and (II) probably occur to some extent during charging and melting of the salts. It is doubtful that reaction (III) occurs at all. Fluorine is apparently replaced by chlorine, and a similar decomposition does occur to some extent as the chloride when NaCl is melted with K₂ZrF₆.

Ionization may take place in the following manner:

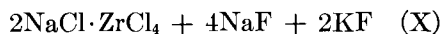
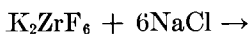


During the dehydration or purification step, a low voltage pre-electrolysis with a graphite anode can produce the following reactions,



These latter three reactions all occur as evidenced by gases evolved from the cell.

When NaCl is considered as part of the system, the chlorine replacement then can occur. Since no fluorine is evolved, this replacement is definitely known to take place, possibly according to one of the following reactions.

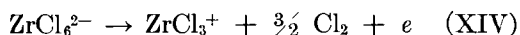
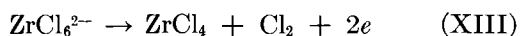


KCl is also found in the bath, so there is some replacement of fluorine in this instance.



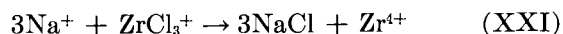
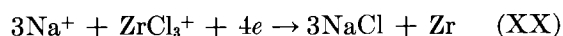
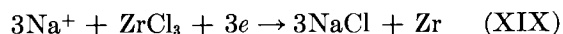
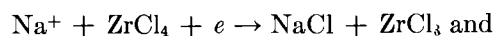
All ionic salts are of course present to a great extent as ions in a fluid melt.

On electrolysis the following anode reactions are possible, assuming elimination of moisture.



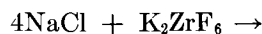
Reaction (XII) occurs throughout the process when the voltage is greater than 2.5 volts. There is no definite proof that (XIII) and (XIV) occur, but if reaction (IV) takes place, then reactions of this type could logically follow.

The exact mechanism of the reduction from 4^+ Zr(IV) to Zr^0 is in doubt. There is definite reason to believe it evolves through breakdown of a chloride, and some reason to think the reduction is stepwise going from 4^+ Zr(IV) through 3^+ Zr(III) to Zr^0 . The following cathode reaction types can be postulated.

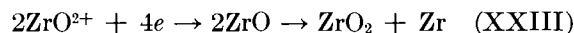


Reactions (XV) and (XVI) are relatively unimportant, occurring only when the zirconium concentration in the electrolyte is near exhaustion. It is doubtful whether (XVII) or (XVIII) occur, as there is no concrete evidence that the simple Zr ions exist. Reactions (XIX) through (XXI) are means by which Zr could be liberated. Any such mechanism could derive Zr(IV) or Zr(III) from the anode or from the bath and produce Zr at the cathode.

The over-all cell reaction is as follows:

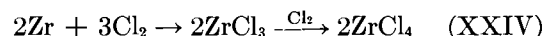


Certain side reactions enter under specific conditions. If significant oxygen remains in the bath and ZrO_2 is produced, then high oxygen deposits are produced.



This reaction also occurs during the purification cycle.

If the temperature is extremely high, chlorination can occur at the cathode, the chlorine being derived from the anode.



Disproportions are also possible at higher temperatures and extreme voltages as:



Finally, the process is definitely an electrolytic one and not a sodium reduction by secondary reaction at the cathode. There is no apparent reaction on melting of the two salts. Furthermore, metal may be produced below the decomposition potential of sodium chloride. The cathode deposit is a compact adherent one unlike a thermal reduction product. There is no evidence of sodium metal production during the reaction until the available zirconium is near depletion, or at extremely high voltages when some sodium may be codeposited.

The process is not operable when exposed to the air. Deposits made in air are mixtures of oxide and

TABLE II. Effect of K_2ZrF_6 concentration on the electrolytic production of zirconium

Run No	Concentration K_2ZrF_6 %	Yield %	Current efficiency	% >100 mesh	% C	% N	% O	Hardness Rockwell B
61-147	20	82.5	57.5	ND	ND	0.012	0.061	ND
61-164	20	80.5	61	ND	0.042	0.002	0.042	79
61-171	24	81	51.3	ND	0.034	0.0013	0.055	90
75-175	26.5	94	54	ND	0.034	0.0032	ND	ND
74-4	27	93	46	25.8	0.058	0.007	ND	ND
74-6	27	90	44	36.3	0.074	0.0139	ND	ND
68-35	33	86	50	27.6	ND	ND	ND	83
68-57	38	80	69	59.9	0.023	0.0002	0.060	87
68-51	41	66	63	63.9	0.029	0.002	0.049	84

E (volts) = 5-6 volts

Current density = 300-500 amp/dm².

Temperature = 830°-860°C.

ND = not determined

metal, very finely divided, and analyze at best around 85% Zr.

Effect of Concentration of K_2ZrF_6

This process is operable using K_2ZrF_6 concentrations up to 50%, but considerable difference is observed in operational characteristics. A high concentration is desirable from two standpoints, lower operating temperatures and longer runs without recharging.

Maximum yields of metal have been encountered using 25-30% by weight K_2ZrF_6 concentrations. Maximum current efficiencies are obtained using the 35-40% range. Thus a 30-35% concentration has been considered the optimum concentration range.

Pertinent data for runs of various concentrations are shown in Table II and illustrated in Fig. 9.

Some tendency has also been noted toward an increase in particle size with increasing concentration, but the observation is not conclusive at this time. Zirconium metal of comparable purity has been produced throughout the range of concentrations investigated.

Temperature Effect

Bath temperatures from 790° to 1000°C have been investigated. The melting point of the usual 30-35% K_2ZrF_6 -NaCl bath is just under 790°C and, at this minimum temperature, the bath is quite viscous giving poor deposition characteristics and low efficiencies. At 800°C, however, the efficiency climbs to a maximum. Beyond 870°C, it falls off to a point where it is only 40% at 1000°C. With other variables affecting the process considered, the optimum operating temperature appears to be about 850°C.

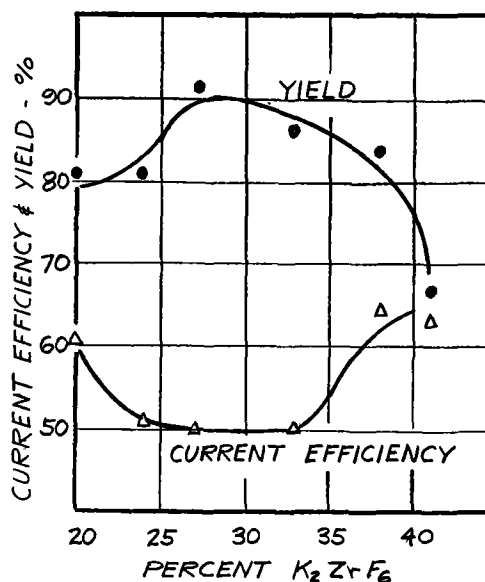


FIG. 9. Effect of initial K_2ZrF_6 concentration in the electrolyte on the metal yield and current efficiency.

TABLE III. Effect of temperature on the efficiency of zirconium metal production by fused salt electrolysis of K_2ZrF_6

Run No	Temp. °C	Yield %	Current efficiency %	% C	% N	% O	Hardness Rockwell B
61-142	790	71.5	43.5	ND	0.007	0.128	—
68-33	800	76	63	ND	ND	ND	86
61-164	860	80.5	61	0.042	0.002	0.042	79
61-191	920	70	43	ND	0.0015	0.033	ND
61-44	1000	90	40	ND	ND	ND	ND

E (volts) = 5-6 volts.

Current density = 300-500 amp/dm²

Concentration of 20% by weight of K_2ZrF_6 in NaCl.

At higher temperatures, the deposits are richer in salts and the crystals of zirconium are of a dendritic type. There is also a greater tendency for pick-up of impurities, and over-all metal quality is diminished.

Pertinent data for runs showing effect of temperature and efficiency are given in Table III and illustrated in Fig. 10.

Effect of Cell Feed Purity

Probably no other single factor is of greater importance in the fluoride process than is the purity of the salt bath. The most deleterious contaminants are water, oxides, and iron. Such impurities must either be absent or removed through pre-electrolysis and vacuum drying of salts. Otherwise the presence of these impurities is directly reflected in efficiency of the process and quality of the deposit.

In all experimental runs reported here, C.P. or

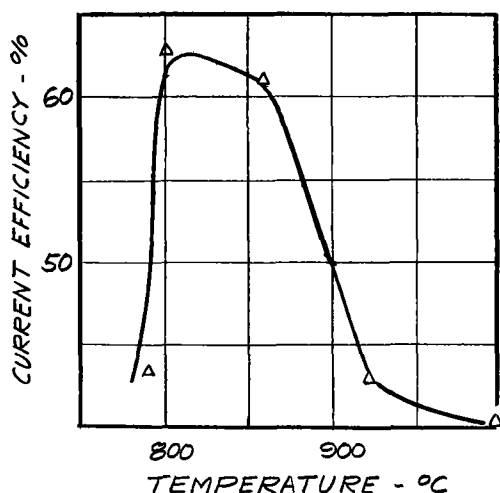


FIG 10. Effect of temperature on the current efficiency in the electrolytic production of zirconium from K_2ZrF_6

TABLE IV. Spectrographic analysis of typical K_2ZrF_6 (K_2ZrF_6 ignited to oxide for analysis)

Element	Per cent	Element	Per cent
ZrO ₂	Major	MoO ₃	—
SiO ₂	0.05	NiO	0.002*
Fe ₂ O ₃	0.005	Cr ₂ O ₃	0.005
Al ₂ O ₃	0.08	SnO ₂	—
HfO ₂	0.50	Ag ₂ O	—
CuO	0.0005*	CoO	—
TiO ₂	0.001	Ta ₂ O ₃	—
CaO	0.30	Cb ₂ O ₅	—
MnO	0.001*	B ₂ O ₃	0.0005*
MgO	0.001	V ₂ O ₅	0.003
WO ₃	—	Na ₂ O	—
PbO	0.01	K ₂ O	Major

* Less than.

Elements not detected. P, Bi, Ga, Cd, Y, Yb, In, Ge, Li, Ir, As, Os, Lu

Analytical Grade NaCl has been utilized. K_2ZrF_6 obtained from several sources and also prepared at Horizons Incorporated has been investigated. However, a major portion of the work reported has

been accomplished with K_2ZrF_6 with a purity as given in Table IV.

Water in the NaCl may be removed by high temperature air drying to a tolerable limit. That in the K_2ZrF_6 can be removed by a vacuum drying step. The cell of course must also be dry.

Iron in the salts can be removed by a low voltage pre-electrolysis. Since the crucible is anodic, any iron present is also removed in such a step if the amount is not excessive. No iron can be exposed in the cell or chlorination will result, and an FeCl₃ atmosphere will prevail in the cell. Iron serves to reduce the process efficiency and also cut down the particle size in addition to contaminating the deposit.

The presence of oxides or water in the bath is reflected in the oxygen analysis of the metal produced. This produces an extremely hard zirconium possessing little or no ductility.

Data illustrating effects of these various impurities are shown in Table V. The first six of these runs employed either a low grade zirconium source material or had a foreign substance added to the bath. Four satisfactory runs are appended for comparison.

Continuous Operation of the Process

Considerable work has been done toward extending the process beyond a single run batch-type procedure. Indications are that the process is adaptable to a semicontinuous operation. This has been done through reuse of a given bath and employment of a cathode cooling chamber. The design of such a cell was noted in Fig. 2 and 3. This cooling chamber is nothing more than a water-cooled gas tight container which can be removed from the cell with the cathode, allowing the insertion of a second cathode.

Theoretically a bath should be useful for a minimum of six runs. A bath is limited only by the buildup of NaF and KF which lowers the electrical conductivity and makes it more susceptible to polarization effects. Up to three runs have been made on a given bath with no noticeable effect on metal pro-

TABLE V. Effect of cell feed purity

Run No	Type Zr source	Zr concentration %	Yield %	Current efficiency %	% >100 mesh	C %	N %	O %	Hardness Rockwell B
68-39	Recrystallized commercial, Fe in cell	11	61	58	ND	ND	ND	ND	ND
92-27	Recrystallized commercial, +1% ZrO ₂	12	61	52	32.4	ND	ND	ND	R _C 34
92-29	Recrystallized commercial, +1% ZrO ₂	12	51	46	28.9	0.011	0.000+	1.23	97
75-5	K_2ZrF_6 , crude (contains ZrO ₂)	7.2	82	56	44.3	0.049	0.033	0.255	ND
75-23	Low Hf, crude	6.4	92	34	46.1	0.070	0.007	0.207	ND
75-26	Horizons, crude	3.9	86	24	32.4	0.261	0.057	0.457	ND
68-47	Vac. dried, recrystallized, no pre-electrolysis	12	87	62	32.9	0.047	0.011	ND	82
75-175	Vac. dried, recrystallized, no pre-electrolysis	8.5	94	54	ND	0.034	0.0032	ND	ND
61-164	Vac. dried, recrystallized, pre-electrolysis	6.4	80.5	61	ND	0.002	0.042	0.042	79
74-6	Commercial, as received, no pre-electrolysis	9	90	44	55.8	0.074	0.013	ND	ND

ND = not determined.

TABLE VI *Semicontinuous operation for electrolytic zirconium production*

Run No	K ₂ ZrF ₆ conc. %	Temp. °C	I Amp	E Volts	Yield %	Current efficiency %	% >100 mesh	C %	N %	O %	Hardness Rockwell B
68-31	25	850	150-200	4 5-4 2	86	43	23 9	0.027	ND	0 006	95
-33	25	800	200-60	5 3-4 1	76	63	ND	ND	ND	ND	ND
74-4	27	840	150	5 8	93	47	26 0	0 058	0 007	ND	ND
-6	27	860	120-95	7 8-5 3	90	44	36 3	0 013	0.013	ND	ND
-7	27	860	125	6 2	ND	60	ND	ND	ND	ND	ND
68-57	38	820	200	5	80	69	59 9	0 023	0 0002	0 060	87
-59	38	800	200-100	5.6-4 5	54	35	19.4	0 030	0 0017	0 112	85

ND = not determined.

duced. Certain adjustments are necessary however in temperature and operating current. Typical data for semicontinuous operation are shown in Table VI.

Effect of Other Variables

Other variables have only minor effects on the process in general. An argon atmosphere is of course important, but a highly purified argon is not necessary.

Current density has little effect within fairly large limits. The lower limit is fixed only by voltage, and a minimum of 2.0-2.5 volts must be maintained across the cell for a satisfactory deposit. The upper limit of current density is about 500 amp/dm². Beyond this point metal is produced, but particle size diminishes and the metal is more difficult to recover from the deposit.

• Electrode distance and cathode design have had little effect to this point. Investigation along these lines has of course been confined to the 5-lb cells with fixed dimensions.

EVALUATION OF METAL PRODUCED

Chemical Evaluation

Zirconium produced by the fluoride process has been evaluated by means of chemical analysis, screen analysis, and spectrographic analysis. The following analytical methods have been employed:

Total Zr: Pyrophosphate gravimetric method; HF or aqua regia solution of sample; precipitation with (NH₄)₂HPO₄ followed by ignition to ZrO₂.

Carbon: Combustion method and KOH absorption of CO₂. Standard Leco Semi-Automatic Determinator used.

Nitrogen: Kjeldahl Method using Micro Kjeldahl apparatus (Scientific-Glass Apparatus Co.—M-3074). HF solution of sample. Titration with 0.01N HCl

Oxygen: Chlorination method, ignition in purified

chlorine at 400°C, followed by ignition of residue and weighing as ZrO₂. Adapted from HCl volatilization method developed at Massachusetts Institute of Technology AEC Laboratory (3, 4). Average values obtained:

Zr and Hf — 99.6-99.9 % N — 0.002-0.004 %
C — 0.04-0.06 % O — 0.04-0.08 %

Samples have periodically been sent out for spectrographic analysis. Samples of such analyses are reported in Table VII.

Particle size analyses have been done using a Ro-Tap vibrator with a standard set of Tyler screens, 35, 80, 100, 150, 200, and 325 mesh.

Typical analyses are given in Fig. 11 for two samples in the form of distribution curves. Other analyses for representative runs are reported in Table VIII. It is not unusual to have >50% of +100 mesh.

TABLE VII *Typical spectrographic analysis of electrolytic zirconium*

(Reported in parts per million)

Element	Sample				
	6144-46 Powder	61-90 Powder	61-90 After double drip melting	Composite 1	Composite 2
Al	60	725	700	80	100
Ca	—	7	25	<50	<50
Cr	10	30	25	50	30
Cu	20	65	65	<5	<5
Fe	800	850	300	200	100
Hf	9400	—	—	15,000	15,000
Mg	<5	3	12	<10	<10
Mn	10	40	7	<10	<10
Mo	20	<10	<10	<10	<10
Ni	30	20	20	50	40
Pb	30	40	<5	<10	<10
Si	40	100	105	200	30
Sn	40	9	50	<10	<10
Ti	270	1015	690	500	500
V	—	<100	<100	ND	ND
W	100	ND	ND	ND	ND

ND = not determined

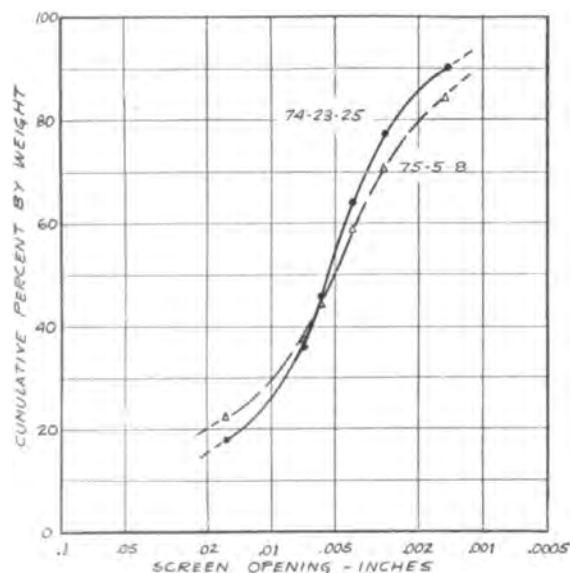


FIG. 11. Particle size and size distribution plot of two typical electrolytically produced zirconium metal powder products.

TABLE VIII. Particle size analysis

Run No	+35 %	+100 %	+150 %	+200 %	+325 %	-325 %	Remarks
68-57	11.7	48.2	15.5	8.4	10.0	6.2	
68-61	1.4	30.1	18.4	12.7	19.8	17.6	
92-27	1.7	30.7	23.1	14.1	23.3	7.1	
92-31A	5.4	49.6	21.8	8.7	10.6	3.9	
68-49	5.8	37.7	21.3	12.6	14.9	7.7	High K ₂ Zr- F ₆ conc.
92-39B	6.4	43.4	17.9	10.1	15.0	7.2	

Metallurgical Evaluation

In almost all of the electrolytic runs in which sizable amounts of zirconium powder were recovered, samples were taken for arc melting to produce small ingots on which hardness and workability data were obtained.

Cold rolling, in most cases, was carried out on the as-cast ingots without prior annealing, as this is the most drastic type of treatment for the determination of ductility in forming that can be carried out. Hot working, to strip of about $\frac{1}{8}$ -in. thickness followed by cold reduction, both with and without intermediate anneals, was also carried out. Sheath rolling of both melted ingots and cold-pressed powder was conducted using mild steel as the canning material. Wire-rolling to 0.030-in. diameter was conducted on selected ingots to determine the ease of fabrication of the electrolytically produced zirconium by this method.

In general, the zirconium powder was compacted

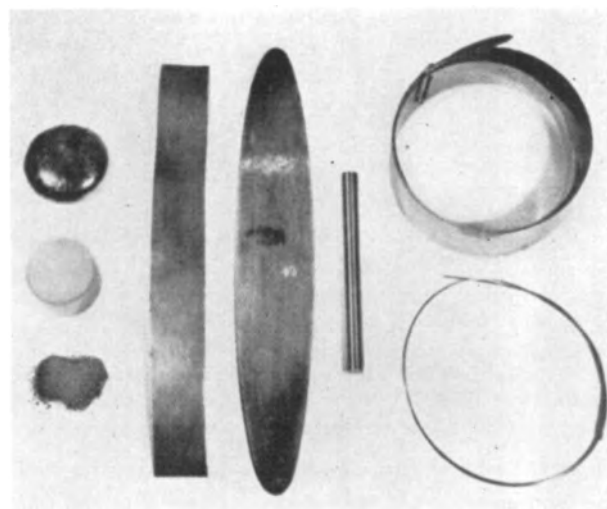


FIG. 12. Zr powder, Zr cold press compact, melted ingot, cold-rolled sheet, hot-rolled strip, machined Zr bar, coiled cold-rolled Zr foil 0.008 in. thick, and rolled Zr wire 0.03 in. diameter (Reduced to slightly less than one-half size)

in a 1-in. diameter die, by cold pressing at 10 tsi. Compacts of 20–50 grams in weight were prepared. These were melted in a small laboratory arc-melting furnace under an atmosphere of argon of approximately 20 cm pressure. A water-cooled tungsten electrode and water-cooled copper hearth were used, each ingot being turned over and remelted to insure complete fusion and homogeneity of the cast metal.

Rockwell A and B hardnesses were taken on both sides of the ingot after first grinding parallel flat surfaces on the faces. In the case of thin sheet, Vickers hardness readings using a 5 kg load were obtained.

Fig. 12 is a photograph showing the various stages of processing of the electrolytically produced zirconium. The powder pressed to a compact of about 70% density is arc-melted and a cast ingot is obtained, as shown. Cold-rolled strip, hot-rolled plate, and a cold-rolled and machined rod are also shown. A coil of cold-rolled sheet and wire, rolled to 0.030 in., are included.

Some of this zirconium powder was melted by an arc method, using a consumable electrode. The powder was extruded and sintered and the resulting rod melted to obtain the two-pound ingot shown in Fig. 13. This ingot had an average hardness value of Rockwell B-85

HARDNESS OF AS-CAST ZIRCONIUM INGOTS

In measuring the hardness of the cast ingots of zirconium an attempt has been made to correlate the hardness values to the oxygen contents determined on each batch of powder produced.

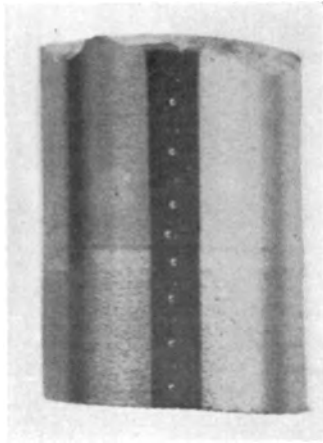


FIG 13 Small zirconium ingot, 2 lb, melted by consumable electrode method from the sintered powder. (Reduced to 1/2 size)

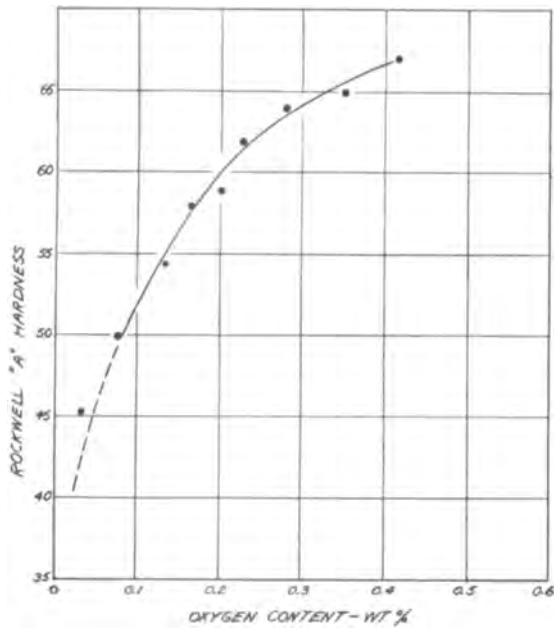


FIG 14 Hardness as a function of oxygen content for as-cast electrolytically produced zirconium, C \cong 0.05%; N $_2$ \cong 0.003%.

Only those runs with nitrogen contents between 0.002 and 0.005 weight per cent (0.003% average) and carbon contents between 0.02 and 0.07 weight per cent (0.05% average) were chosen. With this as a basis, the oxygen contents were plotted against the hardness values obtained and this variation is shown in Fig. 14.

DUCTILITY OF ELECTROLYTICALLY PRODUCED ZIRCONIUM

The workability of the as-cast zirconium ingots was determined by rolling to sheet and determining the hardness at certain stages in the reduction. Attempts were not successful, in general, to reduce the arc-melted ingots over 50% by cold-rolling if the

as-cast hardness exceeded Rockwell A 54-55. However, if the hardness of the ingot was lower than this, it was possible to cold roll strip directly from the ingot stage without intermediate anneals, provided care was taken to grind out any incipient edge-cracking that may occur. Cold reductions of up to 98% have been experienced on certain batches produced. However, almost all of the zirconium produced could be hot rolled at 700°-800°C to plate (0.125 in) and cold rolled to sheet (as thin as 0.006 in.) with no difficulty. Typical cold reduction vs. hardness data are given in Fig. 15. This material has working characteristics that compare favorably with sponge zirconium.

Sheath rolling has been attempted both with the cold-pressed powder and with cast ingots using a mild steel sheath. Hot rolling to a reduction of about 60%, followed by an additional cold reduction of

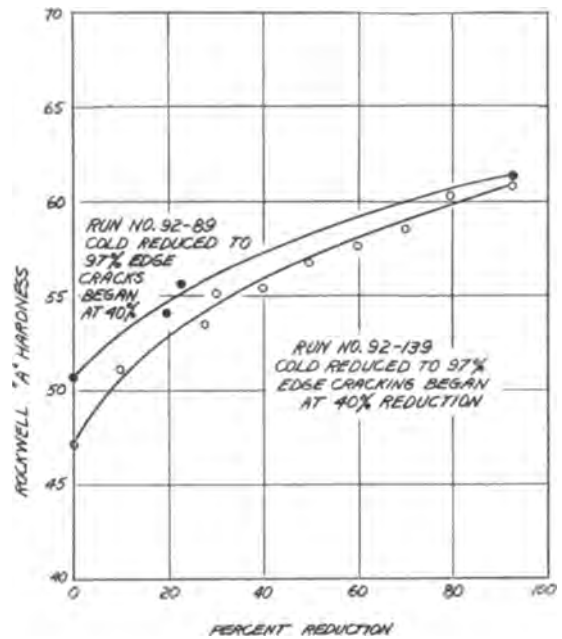


FIG 15. Hardness vs. reduction in rolling for electrolytically produced zirconium.

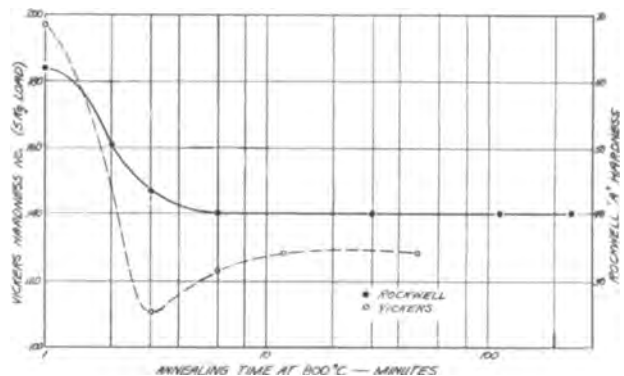


FIG 16. Hardness as a function of annealing time for 97% cold-rolled zirconium.

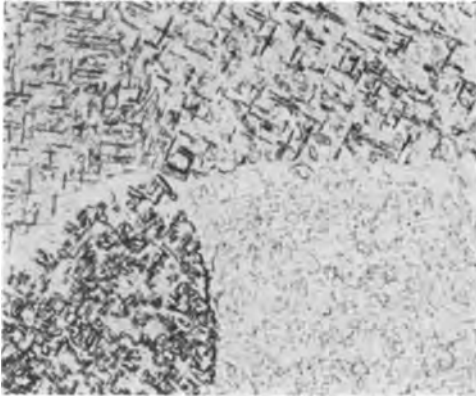


FIG 17. As-cast zirconium ingot showing typical Widmanstatten structure of cast zirconium electrolytically polished and etched Bright-field illumination 100X

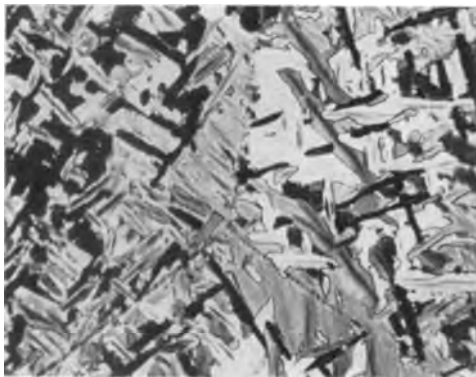


FIG 18 As-cast zirconium ingot similar to Fig 17, showing details of Widmanstatten structure electrolytically polished and etched Polarized light 250X

about 30%, was obtained. The zirconium is then removed from the steel sheath and further reduced cold to strip of the order of 0.006–0.010 in. in thickness.

The hardness variations as a function of annealing time for two different runs of zirconium, cold rolled approximately 97%, are given in Fig 16.

MICROSTRUCTURES OF ZIRCONIUM, ELECTROLYTICALLY PRODUCED

Typical microstructures of the as-cast, cold-worked, and annealed zirconium are shown in Fig. 17 through 25

The well identified as-cast structure of zirconium showing the Widmanstatten pattern is shown in Fig. 17 and 18, under bright light and polarized light illumination.

Specimens, cold pressed to a 17% reduction in thickness and annealed at 800°C, are shown in Fig. 19 and 20. In an annealing time of 5 min, only partial recrystallization has occurred, while 15 min at 800°C has resulted in complete recrystallization.

The structure of an as-cast ingot, cold-rolled 98% without intermediate anneal, is shown in Fig. 21.

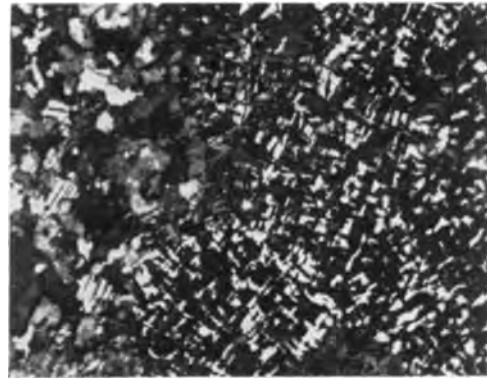


FIG. 19 Zirconium (cold reduced 17%) annealed 5 min at 800°C, showing partial recrystallization Polarized light. 100X

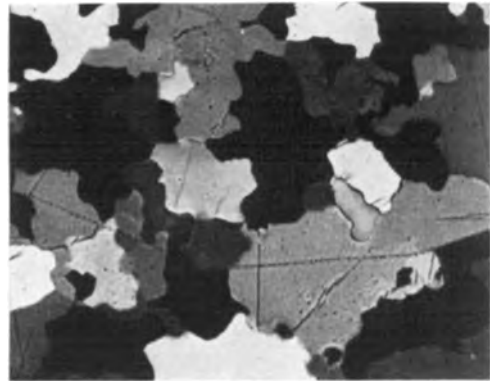


FIG 20. Zirconium, vacuum annealed 15 min at 800°C after 17% cold reduction Polarized light 250X

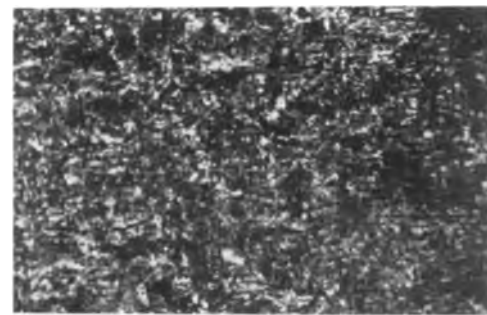


FIG 21 Zirconium ingot, cold rolled 98% without intermediate anneal Polarized light 250X

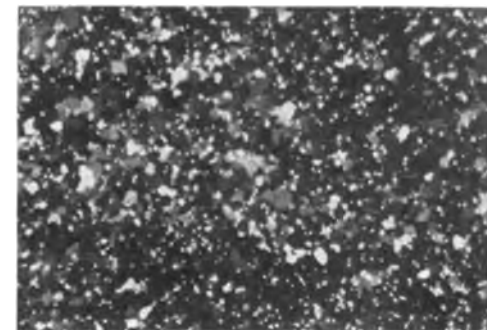


FIG 22 Same as Fig 21 but vacuum annealed 15 min at 800°C. Complete recrystallization has taken place. Polarized light 100X

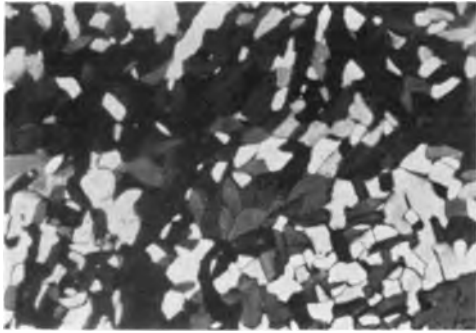


FIG 23 Same specimen as Fig 22 but vacuum annealed 4 hr at 800°C. Complete recrystallization and grain growth have taken place. Polarized light. 100X



FIG 24 Electrolytic zirconium metal, arc-melted and hot-rolled 80% from 0.375-0.07 in., at 700°C followed by 40% cold reduction from 0.070-0.030 in. Polarized light. 250X



FIG 25 Electrolytic zirconium metal, arc-melted and sheath-rolled at 900°C to 60% reduction, sheath-rolled, cold to an additional 30%, removed from sheath and cold-reduced to 0.008 in. sheet to a total of 98% reduction. Electrolytically polished. Polarized light. 250X

Annealing this specimen at 800°C for 15 min has resulted in complete recrystallization, while recrystallization and considerable grain growth has occurred in this specimen annealed at the same temperature for 4 hr.

The microstructure of a typical hot-rolled ingot, followed by a lesser amount of cold reduction is shown in Fig. 24. Fig. 25 shows the severely deformed structure of a sheath rolled zirconium specimen in which a substantial amount of cold reduction has taken place.

DETERMINATION OF PREFERRED ORIENTATION IN ROLLED SHEET AND WIRE

Cold-Rolled Sheet Texture

Pole figures were determined for cold-reduced zirconium sheet rolled from electrolytically produced metal, consolidated by both sheath rolling and by cold rolling. Samples of zirconium sheet, cold rolled to over 95%, were utilized for these determinations.

An abbreviated x-ray method was used for the determination of the pole figures. Although this method does not lend itself to high accuracy, it is wholly adequate for the purpose at hand, to determine the degree of preferred orientation obtained with electrolytically produced zirconium, cold-rolled 95% or better.

The sheet of zirconium is placed parallel to the x-ray beam, between the target and film, and bent slightly so that the x-ray beam strikes the surface at a low glancing angle and is diffracted onto the film. Only two glancing angle shots were made for each specimen, one being perpendicular to the rolling direction and the thickness direction of the sheet, and the other, perpendicular to the transverse and the normal direction of the sheet. Although it was not possible to estimate many degrees of intensity for the two poles plotted, (0002) and (10 $\bar{1}$ 0), the data were sufficient to give good approximations of the rolling textures. The average orientation is best described by representing the basal planes (0001) parallel to the rolling direction but inclined

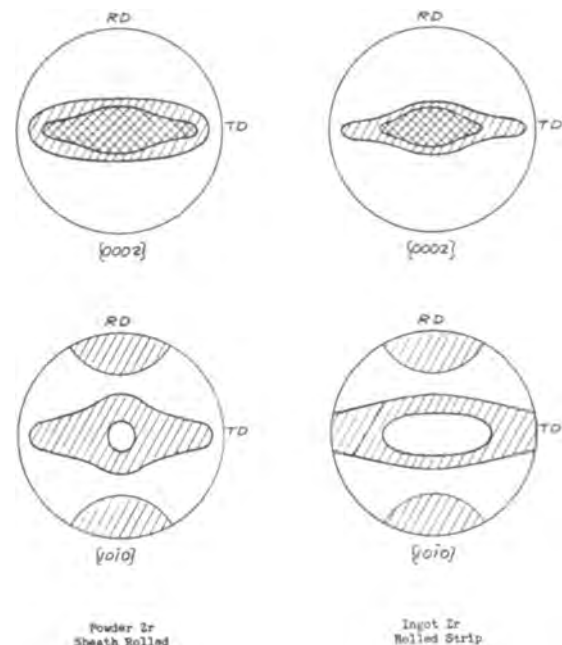


FIG 26 Pole figures for {0002} and {10 $\bar{1}$ 0} planes of electrolytic zirconium sheet produced by indicated methods.

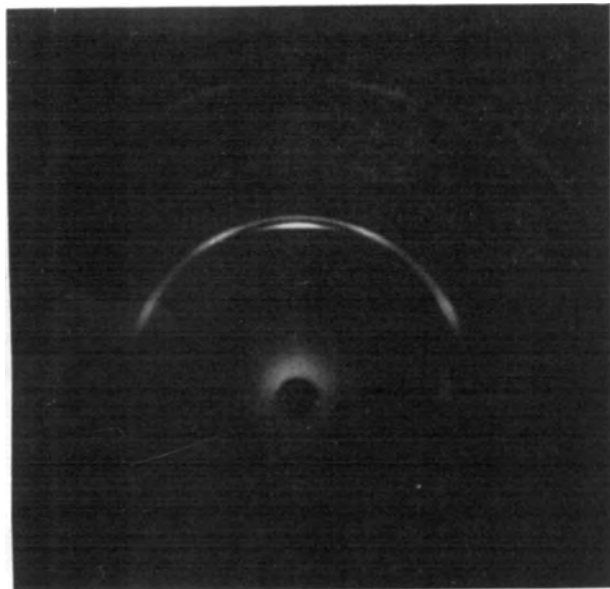


FIG 27 X-ray photogram of rolled zirconium wire produced from electrolytic powder—MoK α radiation

from the rolling plane by about 30° in the transverse direction and with a $\langle 10\bar{1}0 \rangle$ in the rolling direction.

Fig. 26 shows these pole figures for the sheath-rolled and the cold-rolled zirconium specimens.

Cold-Rolled Wire Texture

The texture of cold-rolled electrolytic zirconium wire was determined from the x-ray photogram in Fig. 27. It was found that the $\langle 10\bar{1}0 \rangle$ direction was parallel to the wire axis. This is in agreement with the result of other investigators (5).

The results of these brief studies of preferred orientation in cold-worked zirconium metal produced by the electrolytic method show that the metal behaves in the same manner as iodide and sponge zirconium (6).

PRESENCE OF "SECOND PHASE" IN ELECTROLYTICALLY PRODUCED ZIRCONIUM

A second phase has previously been reported in both iodide and sponge zirconium of high purity. This phase, present in the annealed structure of the equiaxed alpha grains of zirconium, is acicular in nature when the zirconium is in the annealed state and suggests a preferential precipitation out of solution from the HCP lattice of the alpha zirconium.

This second phase has been present in varying amounts in almost all samples of electrolytic zirconium produced. From recent work done on titanium, reported in the literature, there is good evidence that this second phase in zirconium is a hydride (7). Thus, some simple experiments were conducted to determine if the hydride phase was present in the zirconium metal produced by this

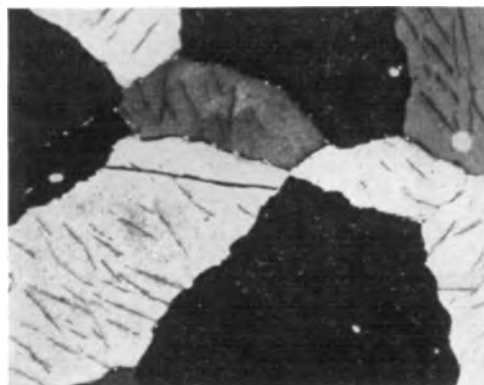


FIG 28 Zirconium, vacuum annealed 2 hr at 800°C , furnace cooled, revealing hydride precipitation phase. Polarized light $150\times$

process. Determinations of hydrogen content on representative samples of zirconium from time to time have yielded values of 0.01 to 0.025 weight per cent hydrogen present in the electrolytic zirconium.

These experiments consisted of first annealing small arc-melted zirconium ingots and slow cooling them, and then reheating to 310° to 410°C , followed by water quenching. The annealing was done at 800°C for 2 hr in a sealed-evacuated quartz tube. Fig. 28 is a photomicrograph of the structure resulting, revealing the acicular needles of the second phase in the alpha grains.

The photomicrograph of the specimen, heated to 310°C for 4 hr and water quenched, shows a decreased amount of this second phase (Fig. 29), while the one heated to 410°C for 1 hr and water quenched shows the complete absence of the phase. Only equiaxed alpha grains are present with a few mechanical twins resulting from polishing (Fig. 30).

To further substantiate this second phase, a second sample was annealed at 850°C for 5 hr in a sealed off-evacuated quartz tube, and furnace cooled. The acicular second phase is again present (Fig. 31). However, when this specimen is heated to

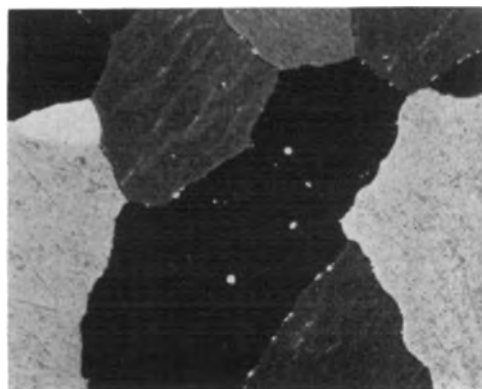


FIG 29 Zirconium, same as Fig 28 but 4 hr at 600°F and water quenched. Note decreased amount of hydride phase. Polarized light $150\times$

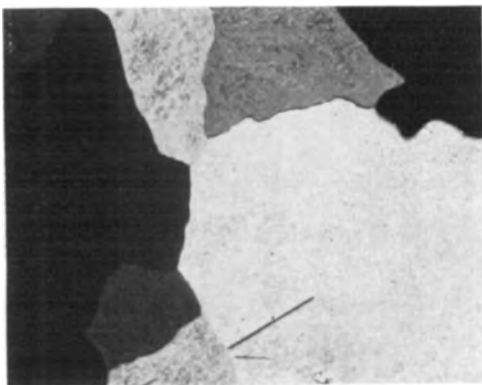


FIG. 30. Zirconium, same as Fig 28 but 1 hr at 800°F and water quenched. Note hydride phase completely dissolved and only one phase, α zirconium is evident. Polarized light 150 \times

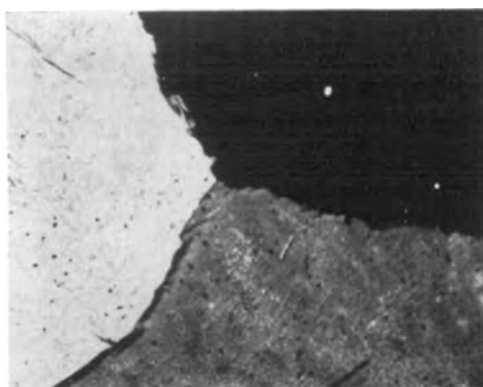


FIG. 31. Electrolytically produced zirconium metal, vacuum annealed 850°C for 5 hr, and furnace cooled. Hydride phase is still evident. 150 \times

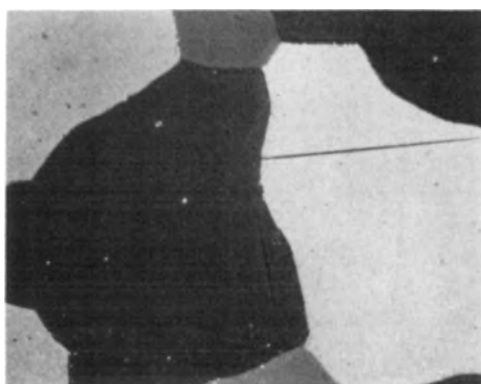


FIG. 32. Same as Fig 31. Heated in a vacuum at 850°C for 5 hr but degassed in an actively pumping system at 0.02 μ pressure for 5 hr. Hydride phase has disappeared. Polarized light. 250 \times

850°C in a vacuum system which is being actively pumped, and a pressure of less than 0.02 μ is obtained, and this specimen is then furnace cooled, this second phase has disappeared, as is shown in the photomicrograph of Fig. 32. The fact that the acicular phase, present in the annealed specimen, disappears on heating to a relatively low tempera-

ture followed by quenching and by degassing at a higher temperature in a vacuum, establishes this phase as a hydride. Neither the oxide, carbide, or nitride becomes soluble at these low-solution treatment temperatures, nor can zirconium be degassed of them by an 850°C vacuum treatment.

CONCLUSIONS

A practical electrolytic process has been evolved for the production of pure zirconium metal. The method entails the electrolysis of K_2ZrF_6 in molten NaCl under a protective argon atmosphere.

Metal so produced is in the form of coarse crystalline dendrites which may be consolidated by standard arc melting or powder metallurgical techniques. The resultant product is satisfactory from a purity, hardness, and ductility standpoint, and is comparable to sponge produced by magnesium reduction of the chloride. Improvements in purity of the starting material and refinements in the recovery procedure have made this possible.

The fluoride process utilizes readily available materials. The double fluoride itself is easily prepared from the oxide, silicate, or zirconate by normal chemical procedures.

Standard electrolytic equipment with some modification could be employed for commercial operation. Provision must be made for a protective atmosphere and elimination of chlorine corrosion.

The process may be run on a semicontinuous basis, a number of runs being made on the same salt bath simply by charging fresh K_2ZrF_6 to the electrolyte. The bath life is limited only by the buildup of NaF and KF in the salt system, making it more refractory and less conductive. A high fluoride bath is also more susceptible to polarization.

The process is operable within broad limits with respect to temperature, voltage, current, and zirconium concentration. The bath may be run from 790°–1000°C, but maximum efficiency is obtained from 800°–850°C. Voltages over 2.0–2.5 volts must be used to obtain a satisfactory deposit. An upper current density limit of about 500 amp/dm² is necessary to avoid a very fine particle size deposit. An optimum initial K_2ZrF_6 concentration lies in the range of 30–35 weight percent, although the process functions with less efficiency using baths of 1–40% K_2ZrF_6 .

Zirconium produced by the fluoride process is of 99.8–99.9% in purity with average values of about 0.05% carbon, 0.05% oxygen, and 0.003% nitrogen being obtained. It has a hardness of Rockwell B 80–85. Aside from titanium and hafnium, metallic impurities are very low.

The process, as developed to this point, gives a product satisfactory for most applications. The

prime factors contributing to this development are use of pure materials, a protective atmosphere, and a careful recovery procedure.

ACKNOWLEDGMENTS

The authors are grateful to the A.E.C. for continued support in the work and permission to publish the results obtained. Acknowledgment must be made to a number of individuals who have contributed to this work over the past three years. Assisting in the process work were Q. H. McKenna, G. J. Franke, and A. A. Topinka. Cell designs were executed by B. C. Raynes, J. A. DaMico, P. M. Rief, and A. A. Topinka. Analytical work was done by R. R. Brutton, K. Chatham, and F. Bizjak. Assisting with the metallographic examinations and physical property determination were F. C. Wagner, S. Kulchar, and E. D. Fisher. All personnel are members of the staff of Horizons Incorporated.

Any discussion of this paper will appear in a Discussion Section to be published in the December 1954 issue of the JOURNAL.

REFERENCES

1. M. A. STEINBERG, M. E. SIBERT, AND E. WAINER, "Zirconium and Zirconium Alloys," pp 37-72, American Society for Metals, Cleveland, Ohio (1953).
2. W. J. KROLL, W. R. CARMODY, AND A. W. SCHLECTEN, *U. S. Bur. Mines Report of Investigation 4915*, p. 23, November 1952
3. E. B. READ AND L. P. ZOPATTI, Massachusetts Institute of Technology-AEC Report 1038, Contract W7405-eng-175
4. W. C. LILLIENDAHL, D. M. WROUGHTON, AND E. D. GREGORY, *This Journal*, **93**, 235 (1948).
5. C. J. MCHARGUE AND J. P. HAMMOND, *J Metals*, **5**, 57 (1953).
6. R. K. MCGEARY AND B. LUSTMAN, *Trans Am Inst. Mining Met. Engrs.*, **191**, 994 (1951).
7. C. M. CRAIGHEAD, G. A. LENNING, AND R. I. JAFFEE, *J. Metals*, **4**, 1317 (1952).

Corrosion Inhibition in Acid Solution¹

CECIL V. KING AND EDWARD HILLNER

Department of Chemistry, New York University, New York, New York

ABSTRACT

Cylinders of iron, zinc, and cadmium were rotated in a highly corrosive solution of acid containing nitrate ion as a depolarizer, as described previously. Three kinds of inhibitors were added to the solution (a) dichromate ion plus complexing or chelating agents for metal ions; (b) a wetting or emulsifying agent which is strongly adsorbed; and (c) a reagent which forms a very insoluble precipitate with ferrous and ferric ions. Measurements of the effectiveness of these inhibitors are given

INTRODUCTION

As shown previously (1), iron, zinc, and cadmium dissolve at approximately the same diffusion or transport-controlled rate, in dilute hydrochloric acid with excess of a suitable depolarizer present. Low concentrations of dichromate ion reduce the dissolution rate considerably. Fluoride ion improves the inhibiting effect of the dichromate; presumably, it converts ferric and chromic ions formed to soluble complexes, and prevents precipitation of nonadherent or porous hydroxides

One objective of the present work was to find if complexing or chelating agents for ferrous, ferric, and chromic ions would be generally effective as inhibition "promoters" with dichromate, and if any would be superior to fluoride ion in this respect.

A second objective was to investigate the effect of emulsifying certain water-insoluble chelating agents, and other insoluble compounds which have been reported to confer low reactivity to solid surfaces by strong adsorption. The emulsifying agents were found to be just as effective when used alone, and experiments with one of them are reported below.

As a third objective of this exploratory work, a search was made for a reagent which would form a very insoluble, adherent precipitate with the first metal ions dissolved, since this should be an effective method of inhibition. With iron, cupferron was found to be a good inhibitor of this type, unfortunately, the compound is not very stable in acid solutions.

EXPERIMENTAL

The pure metals used were described previously (1). The cylinders varied from 1.75 to 2.0 cm in diameter, and were always rotated at 15000 ± 200

cm/min peripheral speed. Cylinder lengths were: iron 3.2 cm, zinc 2.5 cm, cadmium 2.6 cm.

The metals were abraded with No. 600 silicon carbide paper and weighed before each run; afterward, they were wiped with filter paper wet with water or alcohol, rinsed with alcohol, dried, and reweighed. Only total weight losses for the time specified are given. Most of the experiments were carried out at room temperature, as given in the tables.

For a reference corroding solution, a mixture containing 0.02M HCl, 0.06M KNO₃ was used. In each experiment with this and other mixtures, the solution volume was 250 ml. Since some of the reagents change the pH, measurements were made with a Beckman meter. All solutions were exposed to the air

Many of the experiments were repeated once or more, and the reproducibility was, in general, no worse than ± 0.2 mg. When longer runs were made, or when the cylinders were reimmersed in the same or a fresh solution after weighing but without polishing, the corrosion rate usually increased with time. This was especially true of iron, where pitting was quite evident, as noted below.

Dichromate of course cannot be used with reagents which reduce it. No such reduction was noticed except with cupferron, and dichromate was not needed in experiments with this compound.

Chemicals used were of the best commercial grades. Cupferron (the ammonium salt of *N*-nitroso-phenylhydroxylamine) is commonly available for analytical purposes. Sodium gluconate and glucono- δ -lactone were supplied by Charles Pfizer and Company, Brooklyn, N. Y. Ethylene diaminetetraacetic acid (EDTA) and diethylenetriaminepentaacetic acid (DTPA) were supplied by Alrose Chemical Company, Providence, R. I. Thionyltrifluoroacetone (TTA) was from the Dow Chemical Company, Pittsburg, Calif.

RESULTS

Table I shows the weight loss of the cylinders in the 0.02M HCl, 0.06M KNO₃ solution alone and

¹Manuscript received June 10, 1953. This paper was prepared for delivery before the Wrightsville Beach Meeting, September 13 to 16, 1953. From a Master's thesis submitted by Edward Hillner in the Graduate School of New York University. Work done under U. S. Atomic Energy Commission Contract No. AT (30-1)-816 with New York University.

TABLE I. Weight loss, mg in 5 min, in 250 ml 0.02M HCl, 0.06M KNO₃, 30 ± 1°C, 15,000 cm/min peripheral speed

K ₂ Cr ₂ O ₇	Fe	Zn	Cd
—	76	78	148
0.01M	5.7	4.8	6.7

TABLE II. Weight loss in mg, in HCl, 0.06M KNO₃, sodium gluconate, 28–30°C, 15,000 cm/min

	HCl M	Gluco- nate M	K ₂ Cr ₂ O ₇ M	Time	Wt loss	pH
Iron	0.02	0.01	—	5 min	2.3	2.1
	0.02	0.01	0.01	5	1.4	2.1
	0.02	0.04	0.01	5	1.4	3.5
	0.02	0.01	—	5	4.4	2.1
Zinc	0.02	0.01	0.01	15	2.3	2.1
	0.02	0.04	0.01	15	−0.3	3.5
	0.03	0.04	0.01	2 hr	−0.2	3.4
	0.04	0.04	0.01	3 hr	−0.2	2.6
	0.02	0.01	—	5	4.4	2.1

with added K₂Cr₂O₇ under the conditions of these experiments. Without dichromate, about 50% of the acid is used up in five minutes, and if the initial concentration were maintained, the weight loss would be about 30% greater.

Sodium gluconate is widely used as a complexing agent for iron and other metal ions. The salt increases the pH of the acid solution, and in some experiments additional HCl partly compensated for this. Results of experiments with gluconate are given in Table II.

The dissolution rate of iron is decreased by the gluconate alone, even more when dichromate is present. In the latter solutions, the cylinder became coated with a light orange film, which wiped off easily with alcohol. On longer runs the dissolution rate became higher and the iron cylinder started to form pits.

The gluconate-dichromate mixture was more effective with zinc than with iron, being fully protective for 3 hr at a pH of 2.6. The weight increases shown in Table II are probably due to an oxide film, although this was invisible and the metal surface remained bright. In the runs in which weight was lost the zinc acquired a very light yellow film.

In similar solutions containing dichromate and gluconate, a cadmium cylinder lost a few mg in 5 min.

Gluconic acid is easily formed by hydrolysis of glucono-δ-lactone. To obtain solutions containing gluconic acid with a pH of 1.8, the lactone was added to the 0.02M HCl, 0.06M KNO₃ mixture and the solution allowed to stand for about 2 hours. The corrosion rates with both iron and zinc were larger than those given in Table II at pH = 2.1.

TABLE III. Weight loss in mg, in HCl, 0.06M KNO₃, in solutions saturated with EDTA, 25°–28°C, 15,000 cm/min

	HCl M	K ₂ Cr ₂ O ₇ M	Time	Wt loss	pH
Iron	0.02	—	5 min	7.0	1.7
	0.02	0.01	5	2.8	1.7
	0.01	0.01	5	0	2.0
	0.01	0.01	15	0.7	2.0
	0.01	0.01	2 hr	5.5	2.0
Zinc	0.02	—	5 min	96	1.7
	0.02	0.01	5	10	1.7
	0.01	0.01	2 hr	0	2.0
	0.01	0.01	20 hr	0	2.0
Cadmium	0.01	0.01	5 min	3.1	2.0

EDTA is not very soluble in water (about 0.005M) and is commonly used in the form of the more soluble salts, as a sequestering or chelating agent in neutral or basic solutions. In the present experiments, the solutions were saturated with the acid form of the compound, and in some cases the hydrochloric acid was reduced to 0.01M to keep the pH near 2.0. Dissolution experiments with EDTA are summarized in Table III. With dichromate present the iron acquired a light yellow film, the cadmium a light brown film; both rubbed off easily with alcohol. The zinc remained bright when no weight was lost.

DTPA has been reported to be a more effective chelant for some metal ions in acid solutions than EDTA. Solutions to which it was added, with a pH of 1.9, proved to be somewhat more corrosive than those described in Table III.

Citric acid forms chelates with both bi- and tri-valent metal ions (2, 3). Experiments were run with citric acid in the corroding solution as shown in Table IV.

A number of substances, added to a hydrochloric

TABLE IV. Weight loss in mg in solutions containing citric acid, 0.06M KNO₃, 21°–25°C, 15,000 cm/min

	HCl M	K ₂ Cr ₂ O ₇ M	Citric acid M	Time	Wt loss	pH
Iron	—	—	0.2	5 min	2.4	1.85
	—	0.01	0.2	5	9.0	1.85
	0.01	—	0.01	5	4.4	2.1
	0.01	0.01	0.01	5	1.2	2.1
Zinc	0.01	—	0.01	5	7.4	2.1
	0.01	0.01	0.01	5	0	2.1
	0.01	0.01	0.01	1 hr	0.9	2.1
	0.01	0.01	0.01	3 hr	6.4	2.1
	0.01	0.01	0.01	23 hr	21	2.1
Cadmium	0.01	—	0.01	5 min	85	2.1
	0.01	0.01	0.01	5	31	2.1

TABLE V. Weight loss in mg, in 0.5M acetic acid, 0.06M KNO₃, pH = 2.5, 27°-29°C, 15,000 cm/min

	K ₂ Cr ₂ O ₇ M	Time	Wt loss
Iron	—	5 min	5.5
	0.01	5	0
	0.01	3 hr	75
Zinc	—	15 min	986
	0.01	15	-0.1
	0.01	48 hr	+0.1

acid-nitrate mixture or to nitric acid alone, decrease the dissolution rate of iron (4). Nitrate does not act well as a depolarizer with citric acid alone; the acid probably enhances protection by an air-formed oxide film. The same is true of sodium gluconate (Table II).

Citric acid has no such protective effect with zinc unless dichromate is present also.² The experiments with zinc in Table IV were repeated several times with different cylinders of both SP and reagent grade zinc, in runs of several hours duration. The weight loss averaged about 1 mg/hr, but it should be noted that an appreciable fraction of the acid is neutralized in 23 hr. The metal remained bright and shiny, but in every case two or three comparatively deep pits appeared near the lower end of the rotating cylinder. At first it was thought that there were flaws in the metal but in the repeated experiments this proved not to be the case.

Acetic acid.—It was shown by Abramson and King (4) that iron dissolves in acetic acid-potassium nitrate solutions about one-tenth as fast as in strong acids, indicating that the rate is not diffusion-transport controlled. It has also been shown by Hackerman and Hurd (5) that dichromate reduces the corrosion of iron in air-free acetic acid solutions of pH near 3. The experiments of Table V were run to test the effect of dichromate in more concentrated acetic acid with air and nitrate ion present, with both iron and zinc.

Dichromate protects iron temporarily in this solution, but the effect breaks down and pits appear on the surface. When the iron was removed and repolished after a 1 or 2 hr run, it was again completely protected for 5 or 10 min in the same solution. The zinc cylinder was left in the solution without dichromate for 15 minutes inadvertently. The

² Loss of dichromate is never important in the experiments. The concentration used, 0.01M, is twice the amount which gives maximum inhibition when used alone (1). While 15 meqs of dichromate was present in the solutions, 21 mg of zinc (Table IV) corresponds to only 0.64 meq, assuming that only dichromate was reduced. Nitrate may have been reduced as well, but there was no way of testing this.

protective effect of dichromate is remarkable; cadmium was not similarly protected.

Other complexing agents.—Many reagents form complexes or chelates with the metal ions concerned here, and some which looked more promising as inhibition "promoters" with dichromate were tried as mentioned below.

Sulfosalicylic acid forms soluble complexes with ferrous and zinc ions (2), with ferric ion (3), and a rather unstable complex with chromic ion (6). When added to the dichromate-containing corroding solution making the pH = 1.7, it increased the dissolution rate of all three metals.

Acetylacetone chelates with bi- and trivalent metal ions (3). When added in concentrations of 0.05 and 0.1M to the dichromate-containing corroding solution, it reduced the dissolution to about 2 mg in 5 min in all three cases. Visible films were formed; the chelates are apparently not very soluble.

TTA was originally made to assist in extracting metal salts into nonaqueous solvents (7). It is slightly soluble in water, and with a trace of ferric ion added to the saturated solution, a pink coloration and eventually a precipitate appear. When the HCl-KNO₃-K₂Cr₂O₇ solution was saturated with TTA, no effect was found on dissolution rates, however.

Emulsions of TTA were no more effective than the emulsifying agent alone. The same was true of emulsions of reagents which are reported to be strongly adsorbed and to deactivate the surface of metals. Two such reagents tried were perfluorodecanoic acid (8) and tricresylphosphate.

Aerosol OT (dioctyl ester of sodium sulfosuccinate) was one of the emulsifying agents used. When it alone was added to the HCl-KNO₃ solutions, the results shown in Table VI were obtained. Dichromate did not increase the inhibition. The results indicate that Aerosol is strongly adsorbed and that the metal surface becomes approximately saturated at a low concentration. However, the adsorbed film is not completely protective.

Cupferron.—This compound has long been used to precipitate ferric iron quantitatively (9). The

TABLE VI Weight loss, mg in 5 min, in 0.02M HCl, 0.06M KNO₃, with Aerosol OT; 25° ± 1°C, 15,000 cm/min

Aerosol wt %	Wt loss		
	Fe	Zn	Cd
0.001	67	60	126
0.005	2.5	11	4.8
0.01	2.9	1.7	0.9
0.05	2.9	1.6	1.5
0.10	2.5	1.5	2.5
0.20	2.7	1.5	5.7

TABLE VII Weight loss of iron cylinder, mg in 5 min, in 0.02M HCl, 0.06M KNO₃, with cupferron, 30°-33°C, 15,000 cm/min

Cupferron <i>M</i>	Wt loss	Cupferron <i>M</i>	Wt loss
0.001	69	0.0034	-0.1
0.0025	62	0.0038	-0.1
0.003	1.3	0.005	-0.1
0.0032	0.2	0.01	-0.2

TABLE VIII. Weight loss of iron cylinder in mg, in cupferron solutions with 0.06M KNO₃, 0.5 gram acetphenatidin/liter, 15,000 cm/min

Cupferron <i>M</i>	HCl <i>M</i>	Time hr	Wt loss	Temp, °C	pH
0.01	0.02	3	0.9	15-17	2.5
0.10	0.02	19	0	14-20	5.2
0.05	0.04	19	0.8	28-30	3.5
0.05	0.06	19	5.3	28-30	2.0

ferrous salt is similarly insoluble; both are no doubt chelates. Cupferron was found very effective in protecting iron in 5-min runs, as shown in Table VII. After each run the iron was covered with a golden brown film, most of which came off with alcohol, leaving a very shiny surface. The small weight gain at concentrations above 0.0032M must have been due to precipitate which was not removed.

The protective effect broke down in longer runs, apparently due to decomposition of the cupferron. The compound is more stable at lower temperatures, and is possibly stabilized by the addition of small amounts of acetphenatidin (acetophenetidine) to the solution, as suggested by F. G. Germuth. Some experiments with various concentrations of cupferron and HCl are given in Table VIII.

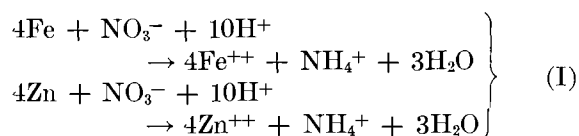
Cupferron does not act as an inhibitor with zinc or cadmium, since no insoluble compounds are formed.

Potentials of the corroding metals.—The potentials of the rotating cylinders were measured against a saturated calomel half-cell. In 0.02M HCl, 0.06M KNO₃ the values were as follows: iron, -0.48 volt; zinc, -0.98 volt, cadmium, -0.71 volt. On addition of 0.01M dichromate the potentials were decreased numerically (became less anodic) by 0.15 to 0.20 volt. The solutions which gave best inhibition showed no greater, and generally a smaller effect. The potentials were followed for 5 min only, since there was no evidence of a rapid drift. The behavior is quite different from that of iron in neutral or slightly alkaline, aerated solutions of oxidizing or non-oxidizing inhibitors (10).

DISCUSSION

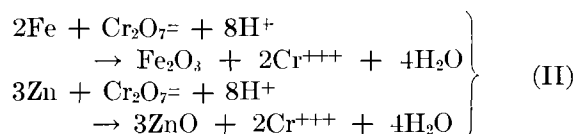
Previously the authors (1) followed the view of Mayne and Pryor (12) that chromate acts as an inhibitor by direct oxidation of iron to the oxide, probably after first being adsorbed on the metal surface. In the acid solutions employed here this would apply to the dichromate ion, and to zinc and cadmium as well as iron. To be protective, the oxide films would have to be of the anhydrous, crystalline types which are not easily dissolved by acids.

The ordinary dissolution of these metals has to be accompanied by a rise in pH at the surface, when nitrate is present, ammonium ion and other reduction products are formed (11):



It is quite possible that ferrous and zinc hydroxides precipitate and are later redissolved. In fact, it is almost certain that the surface of iron is never quite clean in such solutions, at least in the presence of air.

Direct oxidation of the metal by dichromate also increases the pH at the surface. Since Cr₂O₃ or Cr(OH)₃ is formed in only small amounts along with Fe₂O₃, even in chromate inhibition in neutral solutions (12), Cr⁺⁺⁺ is written in the following equations:



If any ferrous ion is formed by reaction (I) it would also be oxidized rapidly by dichromate, using up hydrogen ions.

The function of complexing or chelating agents is, then, to prevent precipitation of oxides or hydroxides by forming soluble complexes with ions not involved in forming the tightly adherent film of impervious oxide. An alternative view is that these reagents act to clean the surface of air-formed, less protective films, thus allowing free access of dichromate ion to be adsorbed. Since fluoride ion is an effective promoter with dichromate ion on zinc, its main action would appear to be to keep chromic ion in solution rather than to clean the surface. However, it has been reported that chromic and fluoride ions form a stable complex only very slowly (13). Gluconic acid and EDTA are rather nonselective; it would be useful to have rapid, specific chelants for each of the ions involved.

Chelants which form very stable complexes will probably prove to be the best promoters with dichromate. The chelates, however, must be soluble; acetylacetone forms moderately stable complexes, but is not very protective because a porous, adsorptive film is formed. Citric and sulfosalicylic acids form the least stable complexes of the reagents used. TTA is too insoluble in water, and chelates are formed too slowly in the very dilute solution. EDTA forms very stable compounds with ferrous and ferric ions. Not many stability constants with chromic ion are known.

It is possible that extremely stable chelates will prove undesirable in inhibition, since they may cause, rather than hinder, dissolution. It has been reported that inactive metals such as copper can dissolve, with evolution of hydrogen, in solutions of strong chelants for their ions [(3) p. 57].

The data show that protection is obtained more easily when the pH is above 2 than when it is lower. Gluconic acid, DTPA, and sulfosalicylic acid may have seemed more favorable at a somewhat higher pH . The effect of pH is evident with EDTA in Table III. At least two factors are involved: some chelants form weak acids, or chelate with hydrogen ion, and strongly acid solutions dissolve oxide films, or attack flaws in them, more rapidly.

Cadmium is less easily protected than iron and zinc in these acid solutions. This no doubt indicates that the oxide formed is more rapidly soluble in acids, or does not have a suitable crystalline form to be adherent and protective. The effect of a simple adsorption inhibitor (Aerosol) is at least as great as on zinc and iron (Table VI).

Iron is more difficult to protect than zinc, and

preliminary study shows that the reason lies in the nature of the iron surface as prepared for the experiments. The breakdown of protection in the best solutions (Table III) is accompanied by pitting, which is visible under a microscope at an early stage and in some cases definitely takes place along abrasion marks left in polishing. Finer polishing, or a short chemical etch, results in longer protection before pits become visible. This aspect of protection is under further study.

Any discussion of this paper will appear in a Discussion Section to be published in the December 1954 issue of the JOURNAL

REFERENCES

- 1 C V KING, E. GOLDSCHMIDT, AND N. MAYER, *This Journal*, **99**, 423 (1952).
- 2 F. J. WELCHER, "Organic Analytical Reagents," Vol II, D Van Nostrand Co, Inc, New York (1947).
- 3 A E MARTELL AND M CALVIN, "Chemistry of the Metal Chelate Compounds," Prentice-Hall, Inc, New York (1952).
- 4 M B ABRAMSON AND C V KING, *J Am. Chem Soc*, **61**, 2290 (1939).
- 5 N HACKERMAN AND R M HURD, *This Journal*, **98**, 51 (1951)
- 6 A M LIEBMAN AND R C ANDERSON, *J Am Chem. Soc*, **74**, 2111 (1952)
- 7 M CALVIN AND J. C REID, AEC Report, MDDC-1405 (1947), *J Am Chem Soc*, **72**, 2948 (1950)
- 8 F SCHULMAN AND W A ZISMAN, *ibid*, **74**, 2123 (1952)
- 9 J F FLAGG, "Organic Reagents," p 133, Interscience Publishers, Inc, New York (1948)
- 10 M J PRYOR AND M COHEN, *This Journal*, **100**, 203 (1953).
- 11 J G BROWN, *J Phys Chem*, **25**, 431 (1921)
- 12 J E O. MAYNE AND M J PRYOR, *J Chem Soc*, **1949**, 1831
- 13 A S WILSON AND H TAUBE, *J Am Chem Soc*, **74**, 3509 (1952)

Microstructure and the Corrodibility of Steel in Inhibited Hydrochloric Acid Solutions¹

P. H. CARDWELL

Dowell Incorporated, Tulsa, Oklahoma

ABSTRACT

In a study of the corrodibility of steels it was found that the degree of annealing as measured by the resolution of the pearlite, the grain size, and the presence of the Widmanstatten structure has considerable influence on the corrosion rate of the steels. Two acid inhibitors were examined in order to investigate materials which could be used satisfactorily to protect different grain structure steels during industrial applications of inhibited hydrochloric acid solutions.

INTRODUCTION

Heat treating a steel changes its resistance to corrosion by certain media (1). Under specific corrosive conditions a martensite steel may have a different corrodibility than other structures such as ferrite with lamellar pearlite or spheroidite, and tempered martensite. Since the corrosion of a metal takes place upon its surface, which is composed of crystal faces, edges, corners, boundaries, and disturbed crystal layers (2), and since the surface property of a metal is a composite of all the properties of these many types of exposed surfaces, it is understandable that the corrodibility is related to the surface property of the metal. Thus, it is not too surprising that a major change in the grain structure of steel, as from martensite to pearlite and ferrite, has an influence on the corrodibility of the steel, however, there seems to be very little information available as to the influence of only slight changes in the grain structure on the corrodibility of specific types of steel such as pearlite.

The studies reported in this investigation of microstructure and corrodibility were made on samples of steels which are in commercial use. In the examination of the steels the following items were studied: importance of the degree of annealing of steels, the influence of grain size, the effect of Widmanstatten and spheroidite structures, the significance of cold-worked metal, and the value of two different types of acid inhibitors to protect metals of various microstructures. It is realized that the preferred method of study is to vary only one variable, e.g., grain size, maintaining all others constant; however, the object of this investigation was somewhat different in that it was desired to know the effect of these various items in relationship to the other items upon the

steels in actual commercial use. It should be realized that, due to the nature of this investigation, definite conclusions as to the effect of any one variable could not be measured. However, certain indications can be pointed out when specific combinations of these items are present. Such information is of commercial importance.

DEGREE OF ANNEALING

Recently, it was reported (3) that the corrodibility of 16 different steels in 10% inhibited hydrochloric acid increased slightly with increase in carbon content. Many of the steels did not show this relationship as well as others, and, for this reason, the present study was made of microstructures to determine its influence on the relationship of the corrodibility to carbon content.

Experimental results.—The various steels investigated and their corrodibility in 10% inhibited hydrochloric acid are given in Table I. The steels were in the form of tubing, with the exception of the SA-70, SA-212A, and SA-105I which were plate stock, and SA-7 and SAE-1035 which were forged boiler hand-hole plates. This table regroups data previously reported (3).

The metals were then annealed and the corrosion rates redetermined. With the majority of the metals there was no change, but with two of the SA-83A samples, one of SA-192, one of SA-210, and with SA-53, SA-7, and SAE-1035, the annealed specimens gave lower corrosion rates. These last two steels might have been expected to give lower corrosion rates after annealing because of the change from a cold-worked structure produced from machining. The annealing was accomplished by heating the metal specimens for an hour at a temperature of 857°C in a neutral salt bath, followed by slow cooling to atmospheric temperature.

The inhibitor used in concentration of 0.4% in the hydrochloric acid solution was an aromatic nitrogen-

¹ Manuscript received July 3, 1952. This paper was prepared for delivery before the Detroit Meeting, October 9 to 12, 1951.

TABLE I. Corrosion rates, grain size, and magnification required to resolve pearlite of various steels

Metal	Corrosion rate 10% inhibited HCl, mdd	Percentage carbon	Grain size	Resolution of pearlite
SA-7	7320	0.21	Medium-fine ASTM No 5-6	Partially 500X
SA-7 annealed	1950	0.21	Fine ASTM No 6-7	Almost completely 500X
SA-53 annealed	2540	0.28	Fine ASTM No 7	Almost completely 500X
SA-70	1710	0.16	Medium ASTM No. 5	Partially 500X
SA-83A S 1	2780	0.17	Very fine ASTM No 8	Partially 1000X
SA-83A S 2	4300	0.16	Fine ASTM No 6-7	Not resolved 1000X
SA-83A S.2 annealed	2200	0.16	Fine ASTM No 7	Almost completely 500X
SA-83A S 3	7420	0.16	Very fine ASTM No 8	Not resolved 1000X
SA-83A S 3 annealed	3030	0.16	Medium ASTM No 5	Partially 1000X
SA-105I	2340	0.17	Fine ASTM No 7	Almost completely 1000X
SA-106A	2680	0.23	Fine ASTM No. 7-8	Partially 1000X
SA-192 S 1	1810	0.16	Fine ASTM No. 7-8	Partially 500X
SA-192 S 2	3180	0.17	Fine ASTM No 6-7	Not resolved 1000X
SA-192 S 2 annealed	2640	0.17	Fine ASTM No. 6-7	Partially 1000X
SA-210 S 1	4740	0.32	Very fine ASTM No. 8	Partially 1000X
SA-210 S 2	2780	0.29	Medium-coarse ASTM No. 3-4	Almost completely 500X
SA-210 S 2 annealed	2240	0.29	Very fine ASTM No 8	Almost completely 500X
SA-210 S 3	5270	0.35	Fine ASTM No. 6-7	Partially 1000X
SA-210 S 4	2680	0.24	Medium-fine ASTM No 5-6	Partially 750X
SA-212A	2440	0.28	Medium-fine ASTM No 6	Partially 500X
SAE-1035	7360	0.23	Fine ASTM No 6-7	Almost completely 500X
SAE-1035 annealed	2680	0.23	Medium-fine ASTM No. 5-6	Almost completely 500X
Boiler tube inner surface	31,100	0.15	Medium-fine ASTM No 5-6	Spheroidized
Boiler tube outer surface	2000	0.15	Medium-fine ASTM No 5-6	Spheroidized
Boiler tube outer surface annealed	1860	0.15	Medium-fine ASTM No 5-6	Almost completely 100X

sulfur coal tar material.² The inhibitor contained a saturated straight chain (average 10 carbon) hydrocarbon sodium sulfonate wetting agent to increase its efficiency (4).

In the investigation of the microstructure by means of metallographic examination, the steel specimens were mounted, polished, and etched with 5% nital. The specimens were examined under the microscope at various magnifications in order to resolve the pearlite. The results of this investigation are summarized in Table I.

Discussion.—In the metallographic study of the various boiler metals, it was found that of steels which were examined, all were pearlitic except the SA-53 which had a Widmanstatten structure. This is the structure obtained by heating to a relatively high temperature and then cooling rapidly. It is of interest to note that the Widmanstatten structure was changed to pearlite upon annealing, and this was accompanied by a decrease in corrosion rate.

In this study, the degree of annealing was determined by means of the magnification necessary to

resolve the pearlite. The lower the magnification necessary to resolve the pearlite, the more complete is the annealing. It was found that the degree of annealing varied considerably from steel to steel. In some of the steels, the pearlite was almost completely

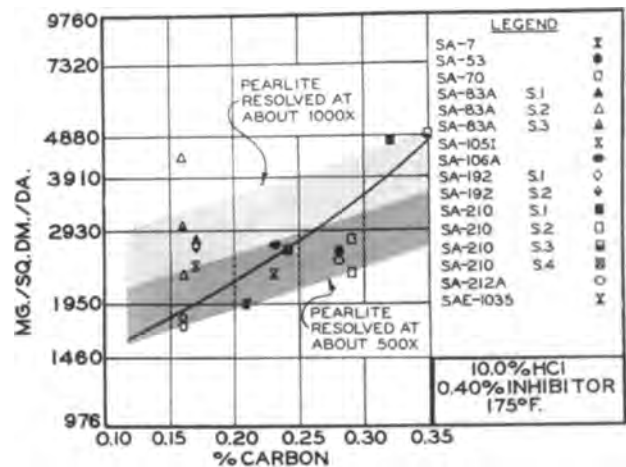


FIG 1 Influence of the degree of annealing on the corrodibility

² Dowell Incorporated A25.

resolved at 500 diameters while in others the pearlite was not resolved at 1000 diameters.

The influence of the degree of annealing on the corrodibility of the steels is given in Fig. 1, a previously published curve (3) to which have been added shaded areas of corresponding degrees of annealing. It shows that degree of annealing has considerable influence on the corrodibility of steels in inhibited hydrochloric acid solutions. The more complete the annealing, the lower is the corrosion rate of the metal in the acid. This graph indicates that the variation of these data from the mean curve when corrosion rates are plotted against carbon content is partly due to the difference in the degree of the annealing of the steel.

INFLUENCE OF GRAIN SIZE

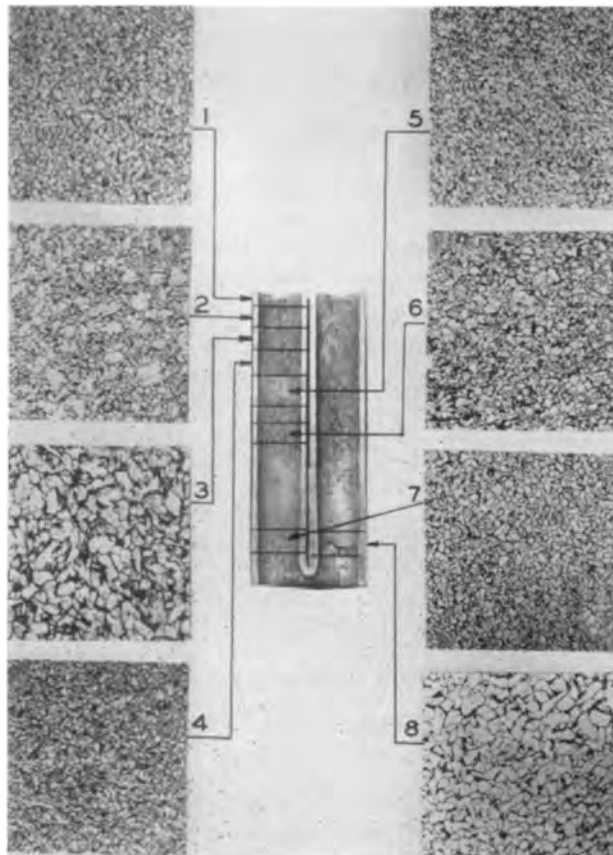
There has been considerable work (1, 5) reported as to the influence of grain size on corrodibility. At first glance, the work seems confusing, but, undoubtedly when the complete system of metal, microstructure, and corrosive media are taken into consideration, the results are not contradictory. While it would be expected that the large crystals would be more stable than the small ones, there are other factors which must be considered, such as

presence and location of the cementite. In addition to this, consideration has to be given as to which is the most susceptible to attack by the corrosive media, the grain boundaries or the grain itself. It would be expected that with inhibited hydrochloric acid solutions the crystals would be more susceptible to attack than the cementite grain boundaries. If this is the case, then the large grains will be attacked in preference to the fine grains.

In the study of the resolution of the pearlite of the boiler steels, the grain size was determined. The grain size of the majority of these steels varied from medium fine to fine (ASTM No. 5-8); the only exception was one of the SA-210 samples which had a medium-coarse (ASTM No. 3-4) grain. Upon annealing, this SA-210 sample had a very fine (ASTM No. 8) grain size and the corrosion rate was lowered slightly, from 2780 to 2240 mdd.

A considerable amount of information as to the effect of grain size has been obtained from a study of microstructure and corrodibility of bifurcate tubes. The metallographic examination of the metal showed that the structure beyond the weld-heat affected zone, that is, the normal nonaffected metal, was of a smaller grain size than were the grains in the heat affected zone. When such tubes were exposed to the nitrogen-sulfur coal tar inhibited hydrochloric acid solutions, pitting occurred in the areas of large grains. The microstructures of a tube are shown in Fig. 2 and 3

The upper part of the double tube end ([1], Fig. 2)



[[FIG 2 Microstructure of section of bifurcate tube

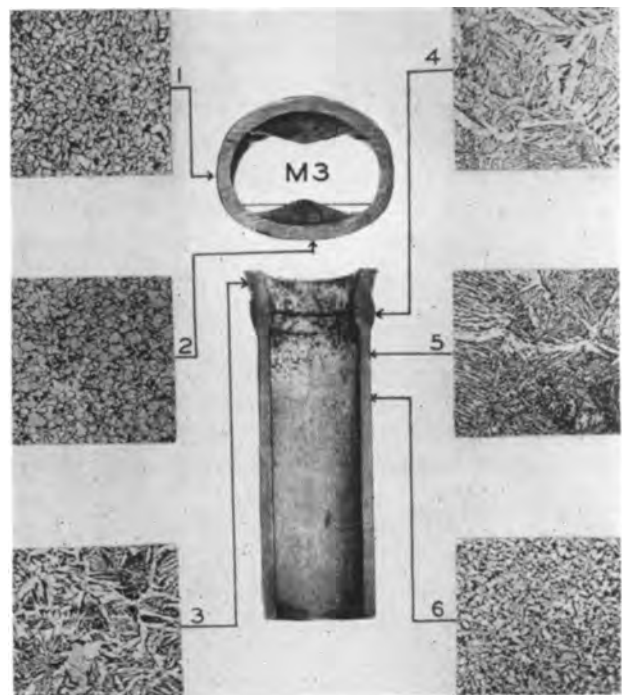


FIG 3. Microstructure of section of bifurcate tube

showed only a small amount of pitting and had a fine grain structure ASTM No. 8. The metal farther down the tube toward the juncture between the double and the single tube showed considerable pitting in the area of larger grain structure ASTM No. 6-7 ([2], Fig. 2) and ASTM No. 5-6 ([3], Fig. 2). Below the pitted area closer to the juncture was a section of the double tube which had a very fine grain structure, ASTM No. 8 ([4] and [5], Fig. 2). The fine grains of this area merged into an area of slightly larger grains, ASTM No. 7, ([6], Fig. 2) which were pitted. A large pit was noted in one of the tubes which was found to be in an area of medium-fine grain structure, ASTM No. 6, ([8], Fig. 2).

The section of the tube between the double and single tube was pitted and showed a fine grain structure, ASTM No. 7, ([1] and [2], Fig. 3). The single end of the bifurcate showed pitting at and around the welded area. The crystal structure of the weld metal is shown by [4], Fig. 3 and of the heat affected zone by [3] and [5], Fig. 3. Below this area was a very fine grain, ASTM No. 8, which was not pitted.

Whenever metal is welded together, there always seems to be a change in crystal structure (6) from that of the metal before welding, usually fairly fine grains going to a larger grain structure. The net result of the welding is to bring about an area of larger grain structure which merges on both sides into finer grain structures. The size, location, and amount of larger grain depends upon the temperature gradient brought about within the metal by the welding process (7).

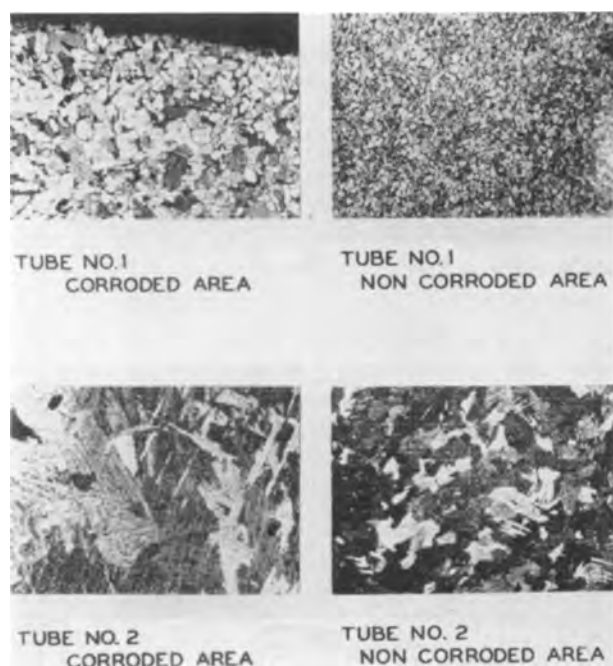


FIG 4 Corrosion adjacent to welds Magnification, approx 75X

This change in crystal structure has been found also in boiler tubes which have been welded. In such tubes, a pitting type of corrosion has been found. The corrosion in these cases was discovered adjacent to the welds as shown in Fig. 4. The corrosion took place in the areas of large crystals and, in addition, in tube No. 2, the Widmanstatten structure was also found in the corroded area.

Other investigations (8) have shown that in metals in which there is a variation of crystal sizes, the attack is in the areas of large grains. The steel tubing used in gas distillate wells is usually upset on the ends in order to reinforce the strength at the threaded areas. The process of upsetting changes the crystal structure, and, if the tube is not heat treated sufficiently, there are areas of coarse grain structure adjacent to fine grains. With the upset tubing, the corrosion has been found in the areas of coarse grain structure which are always adjacent to the fine grain zones.

The reason for the pitting in the areas of large crystals seems to be due either to the large grains being more susceptible to attack, or to a galvanic effect of dissimilar metal structures in contact with each other. In studies of corrodibility in inhibited hydrochloric acid solution of metals possessing uniform but different grain structure, only slight variations in corrosion rates are found. This is shown in Table II. These data were obtained at 74°C using SAE 1020 steel in nitrogen-sulfur coal tar inhibited 10% hydrochloric acid solution. Thus, it is believed that the corrosion is caused in the main by the presence of dissimilar metal structures and, secondarily, by larger grains.

EFFECT OF WIDMANSTATTEN STRUCTURE

The presence of Widmanstatten structure is fairly common in boiler steels. Such structures are usually found in tubes which have been welded and in forged handhole caps, as well as manhole plates. The presence of the Widmanstatten structure and its influence on corrodibility has already been mentioned in the SA-53 steel of Table I and the boiler tube of Fig. 4. Additional information on Widmanstatten structure is given in Fig. 5 which shows the photomicrographs of boiler handhole caps. The first

TABLE II Grain size and corrodibility

Crystal structure	Corrosion rate, mdd	Magnification to resolve pearlite
Medium—ASTM No 4 and 5	1560	500X
Fine—ASTM No 7 to 8	1270	1000X
Very fine—ASTM No 8	1320	Not resolved 1800X
Partially spheroidized ASTM No 6	1220	Not resolved 1800X

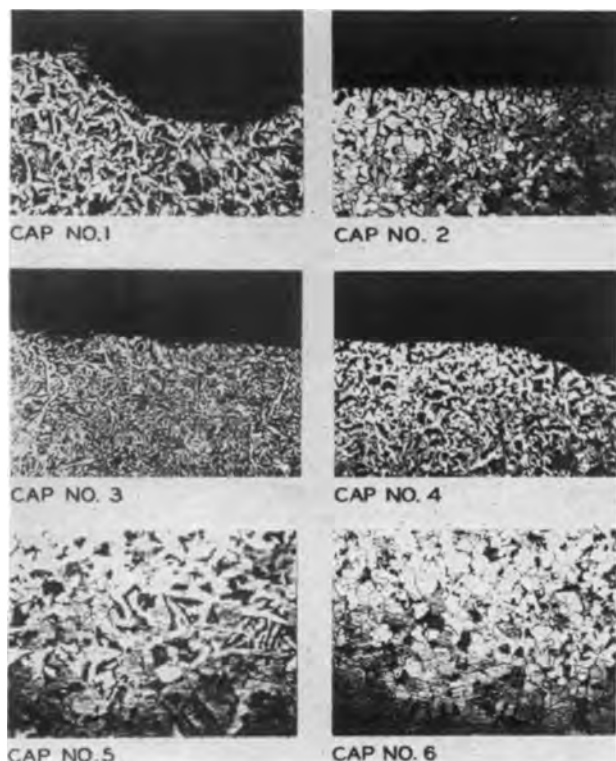


FIG 5 Microstructure of boiler handhole caps Magnification, approx 75X.

TABLE III Boiler handhole caps

Cap	Grain size ASTM	Corrosion rate, mdd	Magnification to resolve pearlite
1	5-6	585	Half at 1700X
2	5-6	391	Nearly all at 1700X
3	7	830	No resolution at 1700X
4	6	244	Nearly all at 400X

four caps were exposed to the nitrogen-sulfur coal tar inhibited 3.5% hydrochloric acid solutions for 6 hr at 65.5°C, and, of these, the only cap which showed any evidence of pitting was cap. No. 1. The corrosion rate, grain size, and magnification necessary to resolve the pearlite for the handhole caps are given in Table III.

The structure of the steel in cap No. 1 is chiefly pearlitic with the presence of some Widmanstatten structure. The grain size is medium fine (ASTM No. 5-6). In cap No. 2 the grain size is about the same as that of cap No. 1, whereas cap No. 4 has somewhat smaller grain size; but in both of these caps the crystals are more regular in shape and there is no Widmanstatten structure present. In the case of cap. No. 3, the grain size is fine and irregular. It appears that this cap may have been forged while fairly cool; as a result, the grains which were broken up by the forging had little or no opportunity to reform.

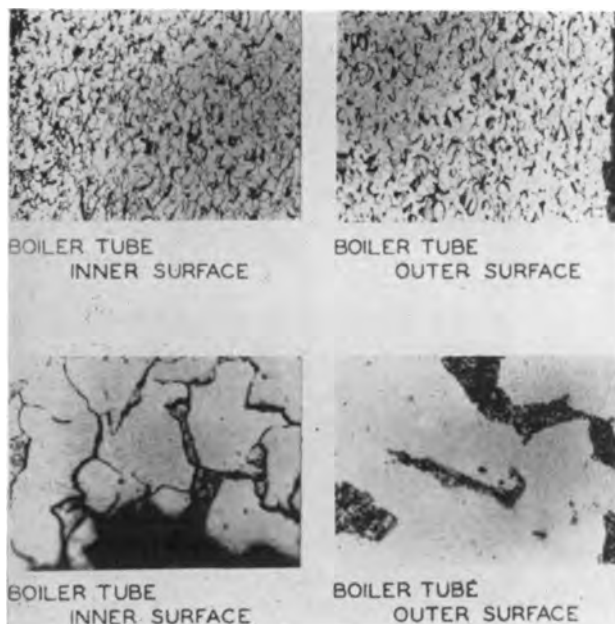


FIG 6 Intergranular oxidation and spheroidite Magnification, top, approx 25X, bottom, approx 500X

As in the case of the boiler metals discussed earlier, the degree of annealing as measured by the resolution of the pearlite has considerable influence on the corrodibility of the handhole caps.

SPHEROIDITE

When the corrosion rate of a boiler tube taken from a superheater header of a high-pressure boiler was measured in the nitrogen-sulfur coal tar inhibited 10% hydrochloric acid solution at 74°C, it was found that the inner surface of the metal had a higher corrosion rate than the outer surface. The corrosion rate of the inner surface was 31,100 mdd, whereas for the outer surface the corrosion rate was 2,000 mdd, this latter result being about what would be expected for a steel containing 0.15% carbon.

The photomicrographs of the inner and outer surfaces of the boiler tube are given in Fig. 6. The inner surfaces have been subjected to intergranular oxidation, which may account for the high corrosion rate. In regard to the outer surface, the pearlitic areas are spheroidized. If the metal was originally pearlite, then this indicates that the tube has been heated for a considerable period of time at a temperature of 590° to 700°C.

The spheroidite can be changed into normal pearlite by annealing. The corrosion rate of the annealed pearlite specimen was found to be 1860 mdd. This would indicate that the spheroidization of the pearlite does not have an appreciable effect upon the corrodibility of the metal in the nitrogen-sulfur coal tar inhibited hydrochloric acid at 79°C.

This conclusion agrees with the corrodibility of

laboratory-formed spheroidite as is given in Table II. In this connection, it is of interest to note that in the case of gas distillate well tubing (8, 9) the steel is more susceptible to attack when the pearlite becomes spheroidized. The reason for this was believed to be due to the corrosion protective film which, because of the crystal structure, gives better protection to pearlite than to spheroidite. It may be that the hydrochloric acid removes this protective film, resulting in spheroidite and pearlite steels having about the same corrosion rates in inhibited acid solutions.

PRESENCE OF COLD-WORKED METAL

In the construction of steel equipment, it is often necessary to use stressed metals. Boilers contain a considerable amount of cold-worked or stressed metals such as the rolled tube ends, the machined surfaces on the handhole caps, and the seats for these caps in the headers. When such metal is exposed to the usual inhibited hydrochloric acid solutions, pitting may occur in the stressed areas.

A handhole cap was subjected to 5% hydrochloric acid with the nitrogen-sulfur coal tar inhibitor for 19 periods of eight hours each at 65.5°C. It was mounted in a manner simulating boiler conditions so that acid contacted only the underside of the cap. The lip was pitted and a deep groove formed at the point of contact between the handhole cap and gasket. The crystal structure of the lip is given as cap No. 5 in Fig. 5. The grain size is rather large and angular, which indicates a stressed condition within the metal. It is possible to change the crystal structure of the handhole caps by annealing to give caps which are more resistant to corrosion.

A similar handhole cap was annealed and then subjected to the nitrogen-sulfur coal tar inhibited 5% hydrochloric acid solution. There was very little corrosion on the annealed plate. Its crystal structure is shown in Fig. 5, cap No. 6. Annealing reduced the grain size somewhat and the crystals are not angular.

EFFECT OF DIFFERENT TYPES OF INHIBITORS

Since industrial equipment is designed and built with steels containing different crystal structures which it is impossible to change once the unit is erected, it becomes necessary to select the inhibitor for the specific crystal structure conditions. In order to determine the effect of other inhibitors to prevent the pitting type of corrosion as obtained by the nitrogen-sulfur coal tar inhibited acid solutions, tests were performed using a rosin amine-ethylene oxide condensate as an inhibitor. This material polyethanol RAD-1112 (13) is surface active and

functions as a combination inhibitor and wetting agent to prevent the attack of acid more effectively.

Using the polyethanol amine inhibitor in 5% hydrochloric acid solution, an unannealed handhole cap was treated. It showed slightly more attack than the annealed one above, but was much better than the unannealed one exposed to the nitrogen-sulfur coal tar inhibited hydrochloric acid solution.

Another comparison between the nitrogen-sulfur coal tar and the polyethanol amine inhibitors was made using bifurcate tubes. Two bifurcates which had identical crystal structures were subjected for 16 periods of six hr each to 7.5% hydrochloric acid solutions inhibited with these two materials.

In the case of the nitrogen-sulfur coal tar inhibitor, the acid caused pitting in the areas of the large crystals, and in these same areas Widmanstatten structure was also present. The tube subjected to the polyethanol amine inhibited acid solution did not pit even though the tube had the same crystal structure. An investigation of other bifurcate tubes containing only dissimilar metal structures, medium and fine grain, but no Widmanstatten structure, has shown that the polyethanol amine inhibited hydrochloric acid solutions do not cause pitting, whereas the nitrogen-sulfur coal tar inhibited hydrochloric acid solutions do.

The reason why the polyethanol amine is a more satisfactory inhibitor for hydrochloric acid solutions than a coal tar material, when dissimilar grain sizes and Widmanstatten structure are present, is not understood at this time. Part of the explanation may be that the polyethanol amine molecule is both a wetting agent and an inhibitor, whereas in the case of the coal tar inhibitor two different chemical molecules are used, a wetting agent and an inhibitor.

CONCLUSIONS

This investigation indicates that the crystal structure of the metal has considerable influence on its corrodibility in inhibited hydrochloric acid solutions. The more complete the annealing, as measured by the resolution of the pearlite, the lower is the corrodibility. When there is a variation in the grain size, pitting occurs in the area of larger crystals. This may be due, in part, to the larger crystals, but what seems to be more important is the presence of two dissimilar metal structures. The corrodibility is increased by the presence of Widmanstatten structure and cold-worked metal, whereas very little if any effect is obtained by spheroidizing the pearlite. The degree of influence of these various crystal structures is dependent upon the inhibitor used in the hydrochloric acid solution. The effect is much more pro-

nounced in the case of a nitrogen-sulfur coal tar type inhibitor than with a polyethanol amine type.

ACKNOWLEDGMENTS

The author wishes to express appreciation to H. W. Schmidt and N. C. McClure of The Dow Chemical Company's Materials Engineering Service Laboratory and to C. L. Lunsford, A. H. Fries, and A. Park of Dowell's Chemical Research Laboratory for assistance in the preparation of this paper.

Any discussion of this paper will appear in a Discussion Section, to be published in the December 1954 issue of the JOURNAL.

REFERENCES

1. F. N. SPELLER, "Corrosion, Causes and Prevention," 2nd ed., pp. 79-87, McGraw-Hill Book Company, Inc., New York (1935)
2. A. T. GWARDNEY, "Corrosion Handbook," (H. H. Uhlig, Editor) p. 33, John Wiley & Sons, Inc., New York (1948)
3. P. H. CARDWELL AND S. J. MARTINEZ, *Ind. Eng. Chem.*, **40**, 1956 (1948)
4. P. H. CARDWELL AND L. H. EILERS, *Ind. Eng. Chem.*, **40**, 1951 (1948).
5. U. R. EVANS, "Metallic Corrosion Passivity and Protection," 2nd ed., p. 426, Edward Arnold & Company, London (1946).
6. C. F. COMSTOCK *Trans Am Inst Mining Met Engrs.*, **62**, 555 (1920)
7. S. W. MILLER, *Trans Am. Inst. Mining Met Engrs.*, **58**, 700 (1918)
8. M. E. HOLMBERG, *Corrosion*, **2**, 278 (1946).
9. R. W. MANUEL, *Corrosion*, **3**, 415 (1947).
10. E. A. BRIED AND H. M. WINN, *Corrosion*, **7**, 180 (1951).

Positive D-C Corona on Polyethylene-Insulated Wire in Air¹

D. S. RODBELL,² J. B. WHITEHEAD, AND C. F. MILLER

The Johns Hopkins University, Baltimore, Maryland

ABSTRACT

An investigation of an apparent anomaly in the electric strength of air about polyethylene-insulated wires, under atmospheric conditions, when direct voltages are applied to the wire is described. Results show that the air surrounding the wire does break down when the gradient, due to the applied voltage, exceeds the accepted value for the electric strength of air, but the discharge is not maintained. An explanation of this self-quenching action is given.

INTRODUCTION

The corona discharge has been known and studied for many decades (1). The major objective of these investigations was either to establish accurate quantitative laws governing this phenomenon, or to explain the mechanisms involved in terms of fundamental processes (2-6).

From the work done to the present, it is felt that the corona discharge, in principle, is understood in terms of fundamental processes (3-5). The "Law of Corona" has been established as a valid empirical criterion for corona formation.

Some recent work at the Naval Research Laboratory (Appendix I) indicates an anomaly in the formation of positive corona on polyethylene-insulated wire in air under atmospheric conditions. It is the purpose of this paper to explain this apparent departure from a heretofore well-established law.

For the relatively simple geometry of a coaxial arrangement of a bare, round wire and a conducting outer cylinder with a potential difference between them, the gradient at the surface of the central conductor is given by

$$E_r = \frac{V}{r \ln R/r}$$

where V = the applied potential difference, r = the radius of the inner conductor, and R = the inner radius of the outer cylinder.

It is known from the Law of Corona (1, 7, 8) that the voltage gradient, at the surface of a wire of radius, r , at which the initial formation of corona occurs is given by

$$g = Am\delta + Bm \sqrt{\frac{\delta}{r}} \quad \text{max kv/cm}$$

¹ Manuscript received June 26, 1953. This paper was prepared for delivery before the New York Meeting, April 12 to 16, 1953.

² Present address. General Electric Research Laboratory, Schenectady

where A and B are constants, m is an irregularity factor (= 1 for smooth uniform wires), and δ is the density factor (= 1 at STP).

So accurate is this law for predicting corona onset, that a Corona Voltmeter built upon this principle has been used as a secondary high voltage standard (9).

The theory of the positive corona discharge requires that there be one free electron in proximity to the corona-forming surface in order to initiate the avalanches (3, 4). The only requirement of the anode surface is that it establish an electric field at its surface which exceeds the dielectric strength of the air. Thus, assuming a smooth cylinder at atmospheric conditions, specification of only the radius of curvature establishes, by the Law of Corona, the critical gradient at the surface of the cylinder.

From the foregoing considerations, for a coaxial arrangement of cylinders with the outer being a conductor and the inner being at a positive potential with respect to the outer cylinder, and as long as the inner cylinder has quantitatively describable parameters, the field may be calculated, and prediction of the applied voltage that yields corona is possible. Corona onset is usually established by a visual glow, an audible hiss, or observing the abrupt increase in the average current flowing to the electrode. For polyethylene-insulated wire as the inner cylinder and positive direct voltage applied, no such indications can be observed (for alternating voltage no discrepancy is encountered). Direct voltages exceeding ten times predicted onset values fail to yield corona in this sense, and result in dielectric rupture of the polyethylene (see Appendix I).

This would indicate an anomaly in either the dielectric strength of air, or in the Law of Corona, both well-established. This paper will give experimental evidence that neither of these properties are, in reality, violated, and the explanation will be given which anticipated these results.

DESCRIPTION OF APPARATUS

The direct voltages required for the experimental work were obtained from two power supplies, both having outputs positive with respect to ground. The first was a (0-22.5)-kv doubler rectifier; the second d-c supply was a (0-30)-kv r.f. rectified type.

The 60 cps alternating voltage employed was obtained from a G.E. testing transformer. The step-up voltage ratio of this transformer is 150:1 when connected as used.

The polyethylene wire samples were in two sizes. One was the aircraft antenna wire on which the phenomenon was first observed; the outer diameter of this wire is 0.462 cm (0.182 in.), the central conductor diameter is 0.128 cm (0.0505 in.). The other polyethylene wire was obtained from the American Phenolic Corporation, and has an outer diameter of 0.292 cm (0.115 in.), and an inner conductor diameter of 0.08 cm (0.0315 in.). A bare brass rod of 0.3175 cm (0.125 in.) diameter and a bare copper rod of 0.203 cm (0.081 in.) diameter were also employed, as described in the next section.

The two outer cylinders used had inside diameters of 2.34 cm (0.910 in.) and 1.27 cm (0.50 in.). The 2.34-cm (0.910-in.) cylinder was 20.3 cm (8 in.) long; the 1.27-cm (0.50-in.) cylinder was 30.5 cm (12 in.) long. Both of these cylinders had, attached to their ends, cylindrical wooden fillets, flaring outward, with a radius of curvature of about 2.5 cm. The inner surface of these fillets was covered with several coats of Du Pont conducting silver paint (No. 4817) which was carried into the cylinder itself far enough to insure an equipotential surface. The purpose of these fillets was to decrease uniformly the gradient on the wire as it left the cylinder. The same conducting paint was also used to make a tight-fitting outer cylinder on the 0.462-cm (0.182-in.) polyethylene wire when examination of the polyethylene alone was made.

The central wire was used in lengths of about 61 cm (24 in.). It was mounted in a tower made of wood, Bakelite, and ceramic insulation. The members of the tower were coated with Dow-Corning four-silicone compound in order to minimize surface

leakage. Several small Lucite disks were made to assist the centering of the wire and cylinder. These disks had a central hole, 0.00254 cm (0.001 in.) larger than the wire diameter, and an outer diameter 0.00254 cm (0.001 in.) smaller than the cylinder with which they were to be used. When the wire was drawn tight by means of brass machine screws soldered to its ends, and the appropriate disks placed on the wire, the cylinder holder was adjusted until the Lucite disks dropped through the cylinder. The cylinder holder was then locked in place by suitably placed bolts.

A Tektronix 511 A.D. oscilloscope was used for observing the charging current wave form. Permanent records of these wave forms were made photographically using a DuMont Type 296 oscilloscope record camera. The oscilloscope was equipped with a 5CP11A cathode ray tube to obtain an easily photographed trace. Voltage applied to the oscilloscope was obtained from a voltage divider through which the charging current passed. This divider was constructed of forty 3.3 megohm resistors in series in the upper arm; the lower section was usually one 3.3 megohm resistor, but another could be paralleled with this to change the division ratio by a factor of approximately two. A very low capacity shielded cable (7 $\mu\text{mf}/\text{ft}$ at 1000 cps; 3-ft length) connected the upper and lower sections of the divider. The voltage divider was reasonably compensated for capacity without further adjustment, as was indicated by its attenuating a 100-kc square wave without noticeable change in wave shape. The voltages were applied directly to the vertical deflection plates of the cathode ray tube in order to avoid any distortion that might be caused by the transient response of the input amplifiers and associated circuitry.

The high voltage switching was obtained using a Western Electric Type 217-B rapid close relay. The relay was operated on 25 volts d.c. A secondary set of contacts on the relay was used to trigger the driven sweep of the oscilloscope, this allowed a time delay between the start of the sweep and the application of the high voltage to the specimen. The voltage wave obtained was a good approximation to a step function for the purposes of investigation.

Measurements of total charge were made using a ballistic galvanometer whose undamped characteristics are: sensitivity—0.002 microcoulombs/mm (on a scale 1 meter distant); C. D. R. X.—9000 ohms; period—30.5 sec; resistance—2325 ohms.

An Ayrton universal shunt with a resistance 10,000 ohms was used to obtain nearly critical damping resistance.

Also employed were a General Radio Type 716-B capacity bridge, and a General Radio beat frequency oscillator, Type 713-B.

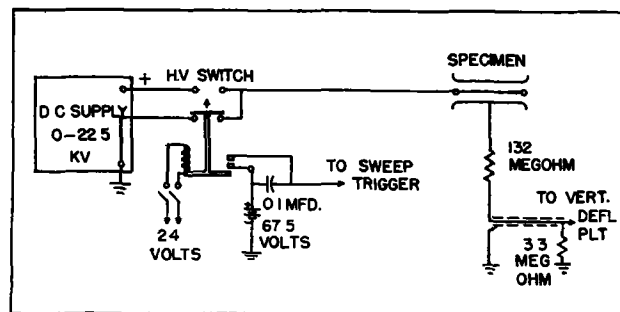


FIG 1 Circuit for current wave shape observations

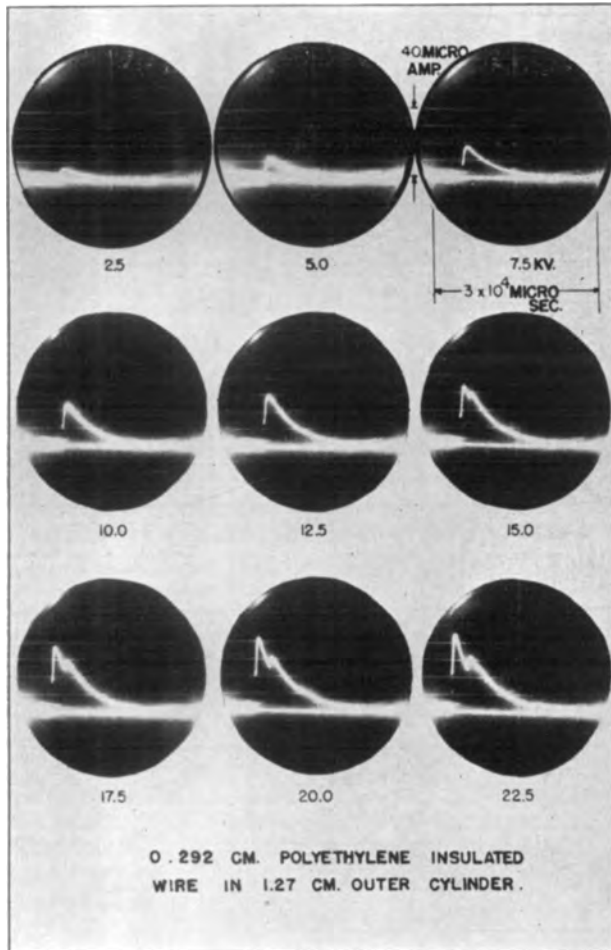


FIG. 2 Current vs. time—polyethylene-insulated wire in air; 0.292 cm polyethylene-insulated wire in 1.27 cm outer cylinder

MEASUREMENTS, OBSERVATIONS, AND RESULTS

Current Wave Shape

The circuit employed in observing current wave shape is shown in Fig. 1. The voltage supply available at the time these data were recorded had a maximum output of 22.5 kv. The current wave shapes shown throughout this paper have, for their axes, ordinates proportional to current, and abscissae proportional to time. The time between the left and right vertical grid lines (i.e., the 0 and 10th horizontal divisions), unless otherwise noted, is 3×10^4 microsec. The ordinate scale is of interest in relative magnitudes between wave shapes of a given set, and is the same for a given set, unless otherwise noted (its value is about 10 microamp/vertical division). These coordinate scales shall be referred to hereafter as "normal."

Fig. 2 shows a typical set of current wave shapes for polyethylene-insulated wire in a conducting outer cylinder. Fig. 3 shows current wave shapes for bare central wires.

To examine what primary contribution the poly-

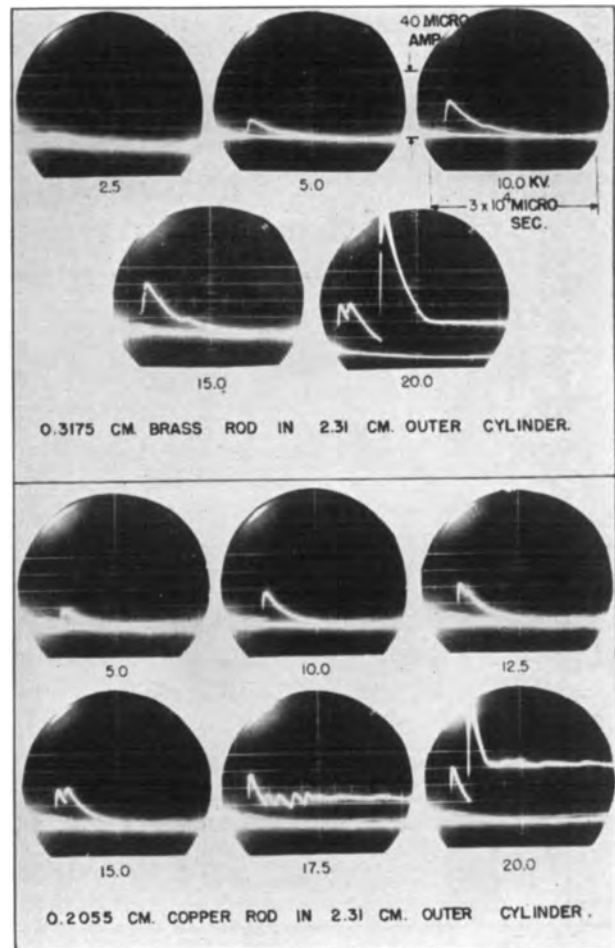


FIG. 3. Current vs. time—bare central conductors in air

ethylene might make to the wave shapes (in the sense of interfacial polarization, etc.) when it is part of the dielectric circuit, some observations of current wave shapes for polyethylene alone were made. This was accomplished by excluding air from the concentric arrangement. The 0.462-cm (0.182-in.) wire was covered along a central section, about 30.5 cm (12 in.) in length, with several coats of conducting silver paint. When dry, this painted surface was a tightly-fitting, outer conductor. With this arrangement as the coaxial specimen, photographs of the current wave shapes were made. These are given in Fig. 4.

Measurement of Total Charge

Employing a ballistic galvanometer, measurement of the total charge flowing to the coaxial arrangements of polyethylene wires in the two outer cylinders was obtained for various voltages up to 30 kv. The Ayrton shunt was used to assure a constant value of damping, and one which was very closely the critical damping resistance for the galvanometer used. The shunt was used throughout at a multiplying power of unity. Since, for a given arrangement,

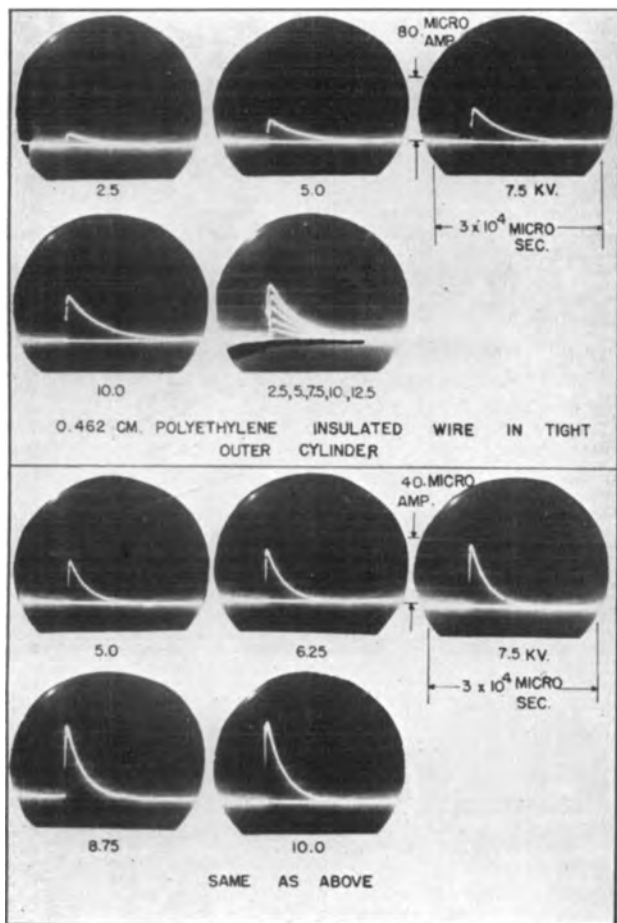


FIG 4 Current vs time—polyethylene-insulated wire in tight-fitting outer cylinder

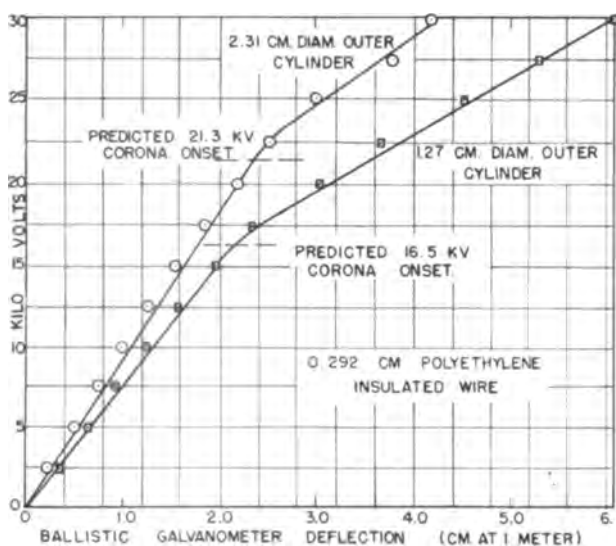


FIG 5 Voltage vs charge—polyethylene-insulated wire

the external circuit parameters are not changed, the deflection of the galvanometer is directly proportional to the total charge which flows, provided only that the time of charge flow is much less than the

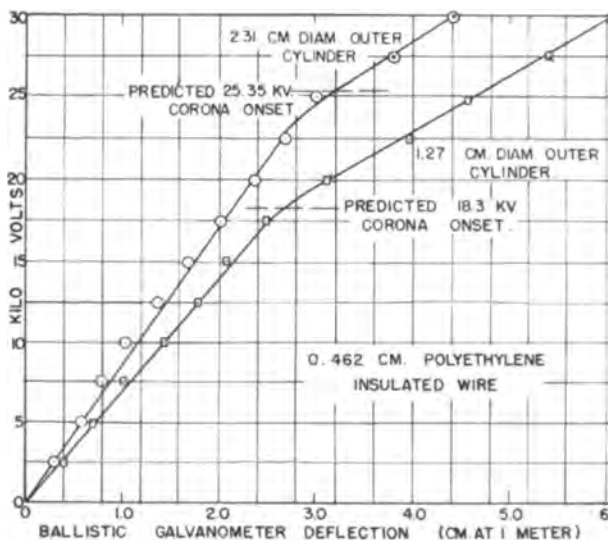


FIG 6 Voltage vs charge—polyethylene-insulated wire

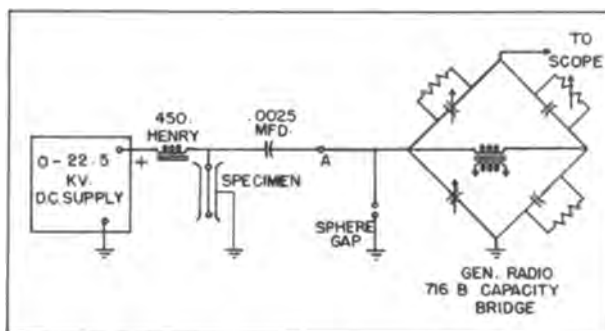


FIG. 7 Capacity bridge circuit

period of the galvanometer (10). This is realized in these measurements since the time for charge flow is of the order of 0.02 sec, and the period of the galvanometer is 30.5 sec.

Fig. 5 and 6 show plots of initial deflection of the ballistic galvanometer (in centimeter on a scale 1-meter distant) as abscissa vs. applied voltage as ordinate. The abscissa is directly proportional to total charge. Each point represents the average of at least three observations. The deviation is not greater than 3%.

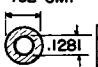
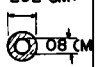
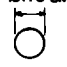
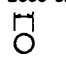
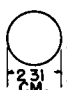

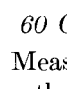
Auxiliary Observations

Using the General Radio 716-B capacity bridge, the General Radio beat frequency oscillator 713-B, and associated apparatus connected as in Fig. 7, capacity measurements were made using a substitution technique. With the circuit opened at [A], the bridge was balanced with the 0.004- μ f capacitor and the 500-kilohm resistor in parallel in the unknown arm. The specimen arm was then connected, and the capacitor, C_s , was readjusted to balance the bridge. The direct voltage was then slowly raised from 0 to 22.5 kv, while watching the oscilloscope for a change in the balanced condition.

In the case of the 0.318-cm (0.125-in.) brass rod in the 1.27-cm (0.5-in.) outer cylinder, the bridge became unbalanced at a voltage very close to theoretical corona onset value, the amount of unbalance (as estimated from the amplitude of the signal on the oscilloscope) increased as the voltage was increased. When the 0.292-cm (0.115-in.) polyethylene-insulated wire replaced the brass rod and the same procedure was followed, a momentary unbalance was observed as theoretical corona onset voltage was reached, but the balanced condition was reestablished in less than 1 sec. The bridge settings remained untouched. As the direct voltage was further increased, similar unbalances were observed, but these also returned to the balanced condition in a short time (less than 1 sec) without any external changes to the apparatus. These same observations were noted for bridge frequencies from 1000–20,000 cps.

TABLE I. Corona onset values in kv for the geometries investigated

(A-C values are given as peak, i.e., $\sqrt{2} \times$ rms) S.I.C. for polyethylene taken as 2.35

CENTRAL CONDUCTOR	POLYETHYLENE INSULATED 462 CM.	INSULATED 292 CM.	BRASS .3175 CM.	COPPER 2055 CM.
OUTER CYLINDER				
	CALC.		CALC.	
	25.35	21.3	17.3	15.0
	CALC.		CALC.	
	18.3	16.51	12.1	11.29
	MEAS.		MEAS.	
	A.C. 17.81, D.C. —	A.C. 15.7, D.C. —	A.C. 12.01, D.C. 12.0	A.C. 11.65, D.C. 11.1

60 CPS and D-C Corona Onset Measurements

Measurements of corona onset voltages were made for the configurations for which a normal type corona could be observed. The results are given in Table I along with the calculated values. Onset was determined by a microammeter in series with the specimen in the d-c case, and a neon bulb across part of a series resistance for the a-c case. An audible hiss accompanied the onsets observed.

DISCUSSION OF RESULTS

Examination of the charging current vs. time curves for the various configurations reveals that, for values of voltage well below calculated corona onset, the shape of the curve is the exponential form, anticipated for a capacitor in series with a resistor. In the ideal case, where there is no inductance present, the initial amplitude of such a current form is given by E/R , where E is the magnitude of the step function voltage wave, and R is the series resistance; furthermore, the rise is instantaneous and the exponential decay begins distinctly at the peak of the initial rise

with no rounding of the peak. However, due to the finite inductance present in any physical network, these ideal conditions are only approximated, and there is noted the rounded peak and initial slope of the leading edge. This departure from ideal is also contributed to by the form of the step function voltage wave, itself an approximation.

As the amplitude of the applied voltage approaches the predicted onset value for the configuration (see Table I), secondary peaks are observed. These occur, in time, a few milliseconds after the initial peak. It is to be noted here that the voltage actually appearing across the coaxial cylinders is not the step function voltage wave, but something of the form of an increasing exponential whose asymptotic amplitude is equal to the amplitude of the step function voltage applied. In fact, the voltage across the cylinders vs. time would closely resemble the current wave form inverted.

These secondary peaks occur in all cases when the applied voltage amplitude is in the vicinity of calculated corona onset. In the case of the bare center conductor, however, as the voltage exceeds the corona onset value, the current stops decreasing with time and assumes a steady value whose magnitude is determined by the applied voltage and the geometry. That is, the magnitude of the steady corona current is that value for which the potential drop in the series resistance, subtracted from the applied voltage amplitude, leaves a value of voltage across the cylinders which is equal to or greater than the critical corona onset value. For the insulated wires, no such steady-state value is ever observed; regardless of the form and number of the secondary peaks, the current magnitude tends toward zero with increasing time. From the time scale on the current vs. time curves, it is seen that the current is essentially zero within 3×10^4 microsec for the insulated wires (the value being somewhat different for each configuration due to small differences in geometric capacity).

Any steady current beyond this time would be due to interfacial polarization—d-c leakage and/or volume conduction in conjunction with a corona discharge.

That polyethylene has practically no interfacial polarization could be assumed after examination of the published data of dielectric constant vs. frequency, which is essentially constant from d.c. to well beyond 100 megacycles/sec.

Interfacial polarization manifests itself as a drop in the dielectric constant accompanied by an increase in the absorption (loss) (11). This occurs within the lower frequency end of the electromagnetic spectrum for materials with high resistivities (polyethylene has a resistivity of the order of 10^{15} ohm-cm).

The results obtained show that for polyethylene alone there is no indication of appreciable steady-state current.

The maximum voltages employed on the 0.462-cm (0.182-in.) polyethylene wire alone exceed the maximum stress when this wire is employed in the normal air-surrounded configurations. Hence, any contribution to the charging current wave shape by the polyethylene, in a primary sense, would be reproduced here for the polyethylene alone. There is no indication that anything of the correct order of magnitude is present from these data.

Surface leakage current over the specimen and apparatus would be observed on these same data. Examination reveals that if any surface leakage, volume conduction, and/or interfacial polarization exist in or on the dielectric circuit studied, their magnitude combined is too small to be observed by the techniques employed here, and for the purposes of this investigation they can be considered negligible.

From the data of the polyethylene alone, it is clear that any internal discharges (due to voids, for example) would appear on the current-time trace as discontinuities in the exponential decay. Austen and Hackett (12) report these void discharges in extruded polyethylene cable, occurring at a maximum stress of 46.9 kv/cm for 50 cps. This stress corresponds to 7.8 kv applied to the 0.462-cm (0.182-in.) polyethylene wire alone; from the data no such discharges are observed for the direct voltages employed. The discharges reported by Austen and Hackett occur in the order of 10^{-7} sec, and hence if these occur in the 0.462-cm (0.182-in.) wire used here, they might not be seen due to time considerations alone. Furthermore, it is quite likely that, since the mechanisms of the a-c and d-c discharges are somewhat different, the void discharges may not occur at all in the d-c case for this value of stress.

If the secondary peaks of the current wave shapes are not due to primary contributions of the polyethylene, then they must be due to temporary breakdown of the air surrounding the inner cylinder, this breakdown becoming permanent in the case of the bare center conductors when the applied voltage exceeds the corona forming gradient. In the case of the polyethylene-insulated wire, some mechanism exists which prevents permanent breakdown of the air for applied d-c potentials exceeding the critical value. The fact that the air molecules actually are ionized when voltages exceeding the critical value are applied should lead to an increase in the total charge that would flow in the circuit if they did not ionize. This is, in fact, verified by the results of applied voltage vs total charge (measured with a

ballistic galvanometer) for the configurations employing polyethylene wire and air.

The slope of the voltage vs. total charge plots is proportional to the reciprocal of the effective capacity of the configuration during the time of charge flow. It would be expected then that the capacity would be different at voltages above critical corona value. This was observed as a transient condition in the capacity measurement using the superposition technique described. When the charge stopped flowing, the effective capacity returned to its previous value. For the bare conductor as the central member, when the direct voltage exceeded the critical corona value, there was a maintained change in capacity as long as the direct voltage was applied.

THEORY AND CONCLUSIONS

The criterion for a self-sustained corona discharge about a conductor, at a positive direct voltage, may be written [after Loeb (3)] as

$$\beta f \left(\exp \int_r^{r+a} \alpha dx \right) = 1$$

Where f = factor giving the number of photons produced by an electron avalanche capable of photoionizing the gas; β = the geometrical chance factor that these photons will ionize the gas molecules and build up the discharge, the expression

$$\left(\exp \int_r^{r+a} \alpha dx \right)$$

represents avalanche formation due to ionization by a single electron as it moves from $a + r$ in the gap to r (the surface of the corona-forming electrode); α = the first Townsend coefficient, representing the number of ionizing collisions per unit path length in the direction of the field. The position $r + a$ is the location in the gap at which the field is great enough to give α a value different from zero.

When the electron avalanche arrives at the anode, it is absorbed; in its wake it has left many excited atoms and positive ions. Production of other electrons to initiate new avalanches is due, according to the classical Townsend theory, to positive ion bombardment of the cathode. Loeb (3, 5, 13) and English (14) present evidence that this is not necessary, but that photo-ionization of the gas due to photons emitted from excited gas atoms is sufficient to produce the required electron to trigger the next avalanche. This electron must occur in the gap at a distance $r + a$, or greater, in order to satisfy the previously mentioned criterion. The only further requirement is that the applied field be maintained in the gap so that α shall not become zero.

In the preceding sequence, the surface at r was a

conductor. If this conductor is now covered with a good insulator, such as polyethylene, then the electron avalanches reaching this surface cannot be absorbed, either conductively through the dielectric, or as absorbed charge in the interfacial sense. They must, therefore, reside on the surface and, as such, become a negative surface charge on the dielectric (perhaps a space charge very closely surrounding the dielectric). The field, due to this surface charge, will be superimposed on the field due to the applied system voltage. This clearly reduces the field strength in the gap. If the resultant field is still high enough to give α a value different from zero, so that another avalanche may follow, then this electron avalanche succumbs to the same fate as its predecessor, and the charge contained in it adds to the previous surface charge to further lower the electric field strength in the gap. By this process, a condition is reached where α is negligibly small, and no more avalanches are possible at the same applied voltage.

If the voltage is now increased, more negative charge builds up around the insulating surface, and equilibrium is again established in the gap. This process of increasing voltage is culminated when the dielectric strength of the insulation has been reached due to the resultant field. What is occurring in the configuration is that the electric field in the air gap is being maintained at a value just below critical (i.e., approximately 30 kv/cm) by the surface charge process, whereas the field in the dielectric is much greater than would normally exist without the surface charge. A simple calculation reveals that only 1 particle in 10^{12} need be ionized to supply sufficient charge to reduce the field strength below corona value for the configurations used here. The stress at breakdown for the N.R.L. data (Appendix I) is of the order of 3000 kv/cm in the polyethylene. Although this seems quite high, it is known that in highly uniform geometries the intrinsic dielectric strength may be approached, and this for good, solid dielectrics is in the range of 10^7 volts/cm. It is quite likely that this ratio of electric stresses of about 100:1 in the configuration is the answer to why the outer cylinder size of the N.R.L. data makes only a small difference in the rupturing value of applied direct voltage required for the concentric arrangement of polyethylene wire in air. When the dielectric breaks down, the surface charge in the vicinity of rupture is absorbed by the inner conductor, and breakdown of the total gap follows by the previously described mechanism.

The first pulse (after initial peak) observed on the current traces presented in the data corresponds, therefore, to the arrival of the voltage applied to the coaxial cylinders, to a value which allows an ava-

lanche to occur in the gap. The secondary pips on the current traces are secondary avalanches which may occur only for higher voltages since now a surface charge exists on the polyethylene (the voltage across the cylinders is increasing approximately in an exponential fashion, as noted earlier). The field in the gap is distorted due to surface charge; these secondary avalanches, therefore, are not as sharp or well-defined as the initial one.

In the case of the 60 cps applied voltage, normal corona is observed. This is in agreement with the theory set forth here since, in the a-c case, the d-c volume conductivity of the dielectric is not important, and the necessary current is of the displacement type, not requiring transport of charges through the dielectric, but only displacement of electrons or positive ions in the dielectric itself about their equilibrium positions.

For bare wires in air, with coaxial symmetry, pulses on the current vs. time curves are also observed. These are similar to those observed for the polyethylene-insulated wire, except that when the voltage across the cylinders exceeds the value corresponding to corona formation, corona is observed in the normal sense. Brown (15) reports that when a secondary cylinder is introduced between, and insulated from, a bare wire and its outer cylinder, the direct voltage applied between the wire and outer cylinder may exceed many times the predicted corona onset value without observing corona in the normal sense. This is, in fact, due to a lowering of the gradient about the central wire caused by the initial breakdown charge residing on the intermediate cylinder (the charge on the cylinder being of the same sign as the polarity of the central wire).

The pulses observed on the current traces presented here that occur at voltage values below critical corona onset magnitudes are probably what Loeb (3, 13) terms pre-onset streamers and burst pulses, due in part to ambient ionization below avalanche-forming gradients.

CONCLUSIONS³

From the arguments presented in this paper, the following conclusions may be drawn:

(A) There exists no gross discrepancy in either the

³ It is to be expected that insulators other than polyethylene should behave in a similar manner under the conditions described herein, provided they possess comparably high values of volume resistivity. No observations were made for the wire negative. Since the mechanisms for positive and negative corona are considerably different, no conclusions concerning the negative case can be made here. In speculation, knowledge of the behavior of polyethylene under positive ion bombardment is required. Such information is notably lacking in the available literature.

accepted d-c dielectric strength of air, or the Law of Corona as applied here.

(B) The phenomena described at the outset have been explained in terms of fundamental processes.

(C) The data obtained are in agreement with this explanation.

ACKNOWLEDGMENT

The authors express their appreciation to the Naval Research Laboratory for their cooperation in this problem.

Any discussion of this paper will appear in a Discussion Section, to be published in the December 1954 issue of the JOURNAL

REFERENCES

- 1 F W PEEK, JR, *Trans. AIEE*, **30**, 1889 (1911), *ibid*, **31**, 1051 (1912), *ibid*, **32**, 1767 (1913)
- 2 J D COBINE, "Gaseous Conductors," p 252, McGraw-Hill Book Co., New York (1941)
- 3 L B LOEB, *J Appl Phys*, **19**, 882 (1948)
- 4 J S TOWNSEND, *Electrician*, **71**, 348 (1913)
- 5 C G MILLER AND L B LOEB, *J. Appl. Phys*, **22**, 494 (1951)
- 6 C G MILLER AND L B LOEB, *J Appl. Phys*, **22**, 614 (1951)
- 7 J B WHITEHEAD, *Trans AIEE*, **29**, 1159 (1910), *ibid*, **30**, 1857 (1911), *ibid*, **31**, 1093 (1912)
- 8 F W. PEEK, JR, "Dielectric Phenomena in High Voltage Engineering," McGraw-Hill Book Co, New York (1920)
- 9 J B. WHITEHEAD AND M W PULLEN, *Trans. AIEE*, **35**, 809 (1916).
- 10 F A LAWS, "Electrical Measurements," Chap II, McGraw-Hill Book Co, New York (1938).
- 11 E J MURPHY AND S O MORGAN, *Bell System Tech J*, **16**, 493 (1937)
- 12 A E W AUSTEN AND W HACKETT, *J. Inst Elec Engrs. London*, **91**, (1944)
- 13 L B LOEB, *Phys Rev*, **73**, 798 (1948)
- 14 W N. ENGLISH, *Phys Rev*, **77**, 850 (1950)
- 15 W. S BROWN, "The Electric Strength of Air at Atmospheric Pressure Under Alternating and Continuous Potentials," Dissertation, The Johns Hopkins University (1916).

APPENDIX I

The following data⁴ represent direct kilovolts, wire positive, at which rupture of the dielectric occurs. No normal

⁴The presented data are extracted from a letter sent to Dr. C F Miller by Dr J E Dinger of the Naval Research Laboratory, Aerology Branch, Mechanics Division, Washington, D C

corona was observed during the measurements which were performed in air under atmospheric conditions. The wire is the 0.463-cm (0.182-in.) diameter polyethylene-insulated conductor used in the experimental work described in this paper.

Large cylinder (18 in. I.D., 36 in. long) —During these tests the voltage was increased from 0 to 240 kv at the rate of 100 kv/min, held at 240 kv for 2 min (if breakdown had not yet occurred), and then increased at 100 kv/min until breakdown occurred.

Breakdown voltage for wire kv	No. of samples
190	1
220	1
240	3
260	1
270	1
280	1
290	3
300	1
310	1
320	1

Small cylinder (0.68 in. I.D., x 8 in. long) —Rate of rise procedure same as that given above for large cylinder.

Breakdown voltage for wire kv	No. of samples
170	1
200	1
220	1
240	3
275	1
310	1
320	1
330	1

Small cylinder (0.68 in. I.D. x 8 in. long) —During these tests the voltage was increased from 0 to 240 kv at rate of 50 kv/min, held at 240 kv for 2 min (if breakdown had not previously occurred), and then increased at 50 kv/min until breakdown occurred.

Breakdown voltage for wire kv	No. of samples
240	5
260	1
275	2
280	1
285	1

In addition to the above, a few tests were made with a small cylinder having $\frac{3}{16}$ I.D. These tests gave a voltage scatter at breakdown in the same range as given for the two cylinders above. These data seem to indicate that the size of the cylinder is not much of a factor in the breakdown voltage.

The Preparation of Phosphor Screens for Color Television Tubes¹

SIDNEY LEVY² AND ALBERT K. LEVINE³

Physics Laboratories, Sylvania Electric Products Inc., Bayside, New York

ABSTRACT

A method is described for producing accurately registered, fine-detail patterns of color phosphors for use in making screens for color television cathode ray tubes. The method is photographic in nature, and the desired phosphor pattern is produced by irradiating a thin film of a photosensitive resin material containing dispersed phosphor with an appropriate light pattern and developing the pattern by suitable means.

INTRODUCTION

One of the important aspects of color television research is the development of practical and economical methods for the construction of color television kinescopes for picture display. The phosphor screen in color kinescopes is much more complex than the screen in any other type of cathode ray tube. This paper describes the preparation of color television screens by a novel method using commercially available materials and relatively inexpensive equipment.

REQUIREMENTS

Phosphor screens for color television tubes consist of finely detailed discrete patterns of three different color-emitting phosphors. These patterns may be in the form of circular dots or thin lines. On a screen measuring 9 in. x 12 in., these dots would have a diameter of about 12 thousandths of an inch. Similarly, a line screen would have lines of about this thickness. The location and size of these dots or lines must be accurate within a thousandth of an inch over the entire screen area. A tube employing the shadow mask principle is shown disassembled in Fig. 1. The screen for such a tube has a mosaic pattern of dots of three different phosphors. Details of the pattern are shown in Fig. 2. A short distance from the screen, toward the gun end of the tube, there is a thin, perforated metal mask which is parallel to the screen and of nearly the same area. For each hole in the mask there is a corresponding trio of phosphor dots. Three electron guns are mounted symmetrically about the axis of the tube. The guns, mask, and dotted screen are so positioned that the electron beam

from each gun, when deflected, is directed through the holes in such a way as to strike dots of one color only. Thus, by modulating the current in each beam, the relative magnitudes of the primary colors emitted by the tri-dot element can be adjusted so that the desired visual color for that element is produced by physical mixture. Satisfactory performance of the tube depends upon accurate registration of the electron guns, the perforated metal mask, and the dotted screen plate.

Several methods have been proposed for preparing such screens, e.g., settling phosphor through masks, silk-screen printing, letterpress printing, and electrostatic printing. To date, the silk-screen process is the only published method (1) which has been successfully applied to color-screen preparation. The photobinder process, which will be described in this paper, has also been used successfully to prepare screens for the shadow-mask tricolor kinescope. The method is photographic in nature, and the perforated shadow mask of the tube itself, or a photographic reproduction of the mask, is used as the master pattern.

In the photobinder process, a photosensitive resin binder is blended into a paste with one of the color-emitting phosphors. The paste is applied to the glass screen plate in a thin film by knife coating or other suitable means. Light from a suitable small-area source is allowed to pass through the openings of the master pattern in an exposure device, exposing portions of the film. The exposure device is positioned in such a way that the exposed portion of the film will constitute the desired dot pattern for the particular phosphor being used. Then the unexposed, and hence unfixed, areas are washed away by a solvent. The entire process is then repeated for each of the phosphors to be applied. When the dot patterns for all three colors have been obtained, the light-fixed photosensitive binder is removed by baking at 400°C, and a permanent silicate binder is applied by spraying.

¹ Manuscript received July 20, 1953. This paper was prepared for delivery before the New York Meeting, April 12 to 16, 1953.

² Present address: American Safety Razor Company, Brooklyn, N. Y.

³ Assistant Professor, Brooklyn College, Brooklyn, N. Y., Consultant, Physics Laboratories, Sylvania Electric Products Inc., Bayside, N. Y.

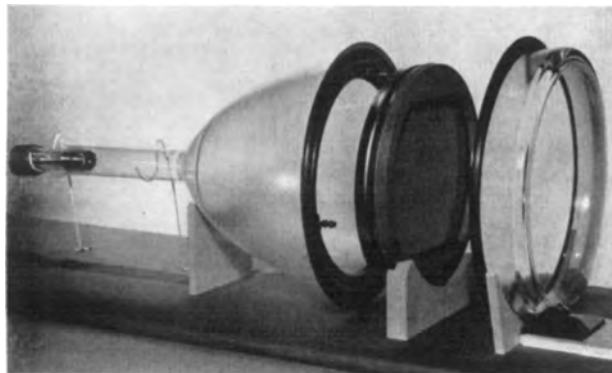


FIG 1. Exploded view of shadow mask color kinescope

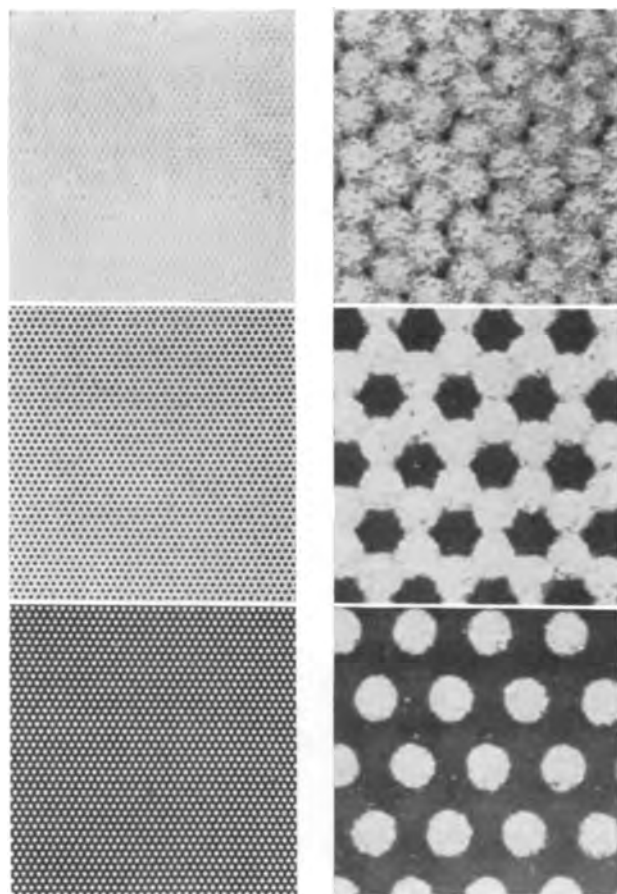


FIG. 2 Portion of tricolor phosphor screen with one-dot, two-dot, and three-dot patterns, showing successive stages of mosaic dot pattern, natural size, and enlarged.

Resist Materials

The use of photosensitive resist materials is well known, especially in the field of graphic arts. Photographically fixed gelatin-type materials are used to prepare halftone and line reproductions for press printing. Photo stencils, which are used extensively in silk-screen printing, and photo-offset printing are also based on the use of photographically set materials of various types.

It was proposed at these laboratories to use such resist materials directly on the glass screen plates either as a contact stencil or, if a suitable material could be found, as a photosensitive temporary binder for the phosphor, permitting direct photographic reproduction of the dot pattern on the glass screen plate. The method which was most promising, and which has been successfully developed, is the one using the photosensitive material as a temporary binder for the phosphor.

The criteria for a suitable photosensitive vehicle are: (a) adequate photosensitivity; (b) noninteraction with the phosphor materials; (c) suitable viscosity and other rheological properties to give stable dispersions of phosphor; (d) ease of incorporation into a practical coating system; (e) absence of interfering residue.

Several photosensitive materials were tested and one is being used successfully to prepare color screens. The materials tested were: (a) gelatin (photographic); (b) polyvinyl alcohol; (c) polyvinyl acetate; (d) Kodak Photosensitive Lacquer (an experimental material manufactured by Eastman Kodak and available on special order).

A number of other materials exhibit the photochemical sensitivity required, but the investigation was limited to the materials readily available. It is possible that additional research will lead to better and more effective systems. The material which was successfully used was Kodak Photosensitive Lacquer (KPL). All of the materials investigated were suitable in every respect except for the requirements that the material should leave no interfering residue and have no effect on the phosphor or tube life. However, a residue develops with all of the materials, other than KPL, since the required sensitization is effected by use of ammonium, potassium, or sodium dichromate, any one of which leaves a chromic oxide residue on ignition. In addition, these materials themselves leave a residue after firing at 400°-500°C.

Additional research is required on gelatin and the polyvinyl resins to find new sensitizers and to obtain high purity materials and thus make them useful systems. In contrast, the Kodak material has a volatile sensitizer incorporated, leaves no residue after bakeout at 400°C or lower, and has all the other required characteristics. KPL and polyvinyl acetate require an organic solvent such as trichloroethylene or a ketone for the process, whereas the others are water soluble.

A solution of KPL, which was 30% solids by weight, was used to make up the phosphor pastes. The composition of the paste was approximately 25% KPL (dry), 25% phosphor, and 50% solvent. After preliminary stirring, this mixture was blended by passing through a three-roll ink mill. The viscosity

of the resulting paste ranged from 1000–5000 centipoise, depending on the particular phosphor, and the paste offered no problems in knife coating.

The phosphors employed were Sylvania #160 green (zinc orthosilicate), #150 red (zinc phosphate), and #170 blue (calcium magnesium silicate).

Coating Process

The photosensitive resist materials which were used in this investigation are relatively unaffected by ordinary room illumination. Nevertheless, to avoid complications, all steps of the procedure through the development of the exposed pattern were carried out in darkened rooms under red safelight.

In the investigation of coating problems, a thin film of the phosphor paste made from one of the various photoresists was applied to a glass plate with one of the various types of knife coaters, and the coated plate was then allowed to dry in air. A Bradley blade was employed for some of the test work. To meet the requirements of television tube face plates, a special knife-coating fixture was designed for coating flat glass panels with curved outlines. The device, which is illustrated in Fig. 3, features a sliding flat plate with a concave curved end. With the coating blade resting on this plate, the knife coater is filled with the phosphor paste. As the blade slides toward the screen plate, the concave edge of the sliding plate meets the convex edge of the screen plate and is held there while the blade continues across the screen plate. This makes it possible to do the complete coating operation with a single stroke.

The knife-coating process occasionally resulted in nonuniform coating weights over large areas. This was traced to variations in glass flatness. To overcome this, a spray coating system is now under investigation that should produce more satisfactory coatings. The spray coating method uses a traversing

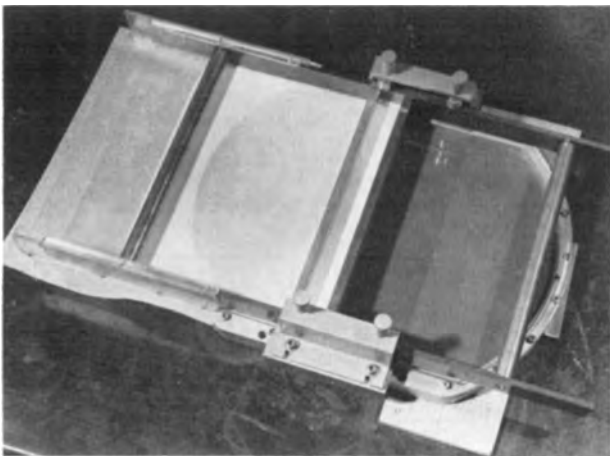


FIG. 3. Knife coater in use

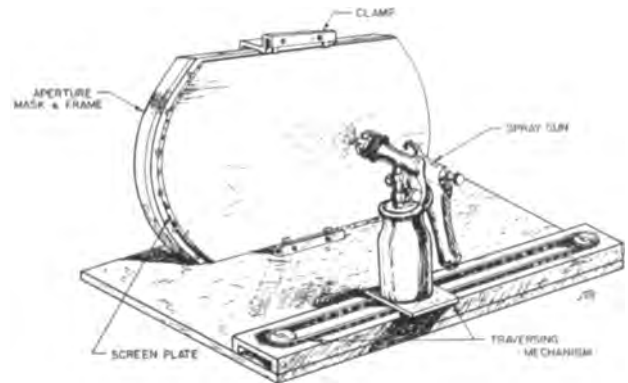


FIG. 4. Spray coating device

spray mechanism with a wide-angle spray gun and a pressurized can. As shown in Fig. 4, the fan-shaped spray is aligned across the panel, and the traverse moves the gun along at right angles to the alignment of the fan spray. By control of the can pressure and feed rate, a relatively uniform film can be attained.

Exposure and Development

Several different methods of exposure were employed. In the first, the panel was exposed with the emulsion side in contact with a negative of the required pattern. In the second, the panel was exposed from the emulsion side by point-light shadow projection, an optical analogy to the situation in the shadow-mask tube. In the third, the panel was exposed from the glass side by point-light shadow projection (see Fig. 5). This method gave the best over-all results because good adherence of film to glass resulted from the exposure at the glass-emulsion interface. In addition, the dot size was photographically reproduced. This was not the case in either method of emulsion-side exposure, probably because of light scattering in the emulsion.

Exposure from the glass side introduces a slight uncorrectable displacement in the pattern produced

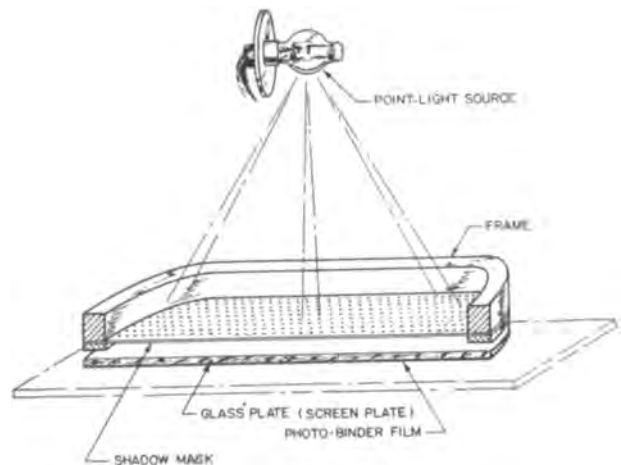


FIG. 5. Exposure arrangement in photobinder process

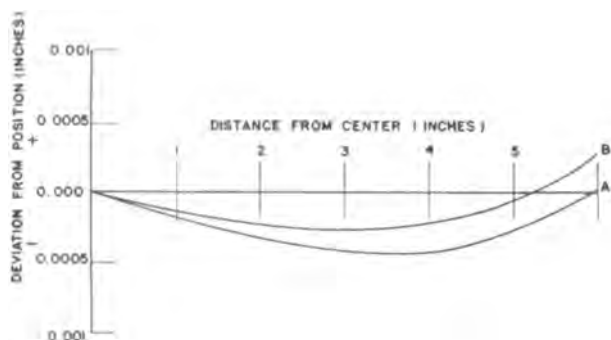


FIG. 6 Refractive error in shadow projection through glass. Curve A—compensated to zero at edge, curve B—compensated for minimum deviation

by the refraction in the glass. The magnitude of this displacement can be calculated. Fig. 6 gives the location error vs. distance from the center of the screen for a particular setting of the exposure device. The maximum error can be reduced to a value which is negligible by suitable design of the geometry of the exposure device. In the present case, the maximum error in dot location due to refraction is less than 0.0003 in.

The apparatus actually employed is shown in Fig. 7. It consists of a vertical optical bench with a precision milling machine table attached to the base. The light source is a Sylvania 300-watt zirconium,

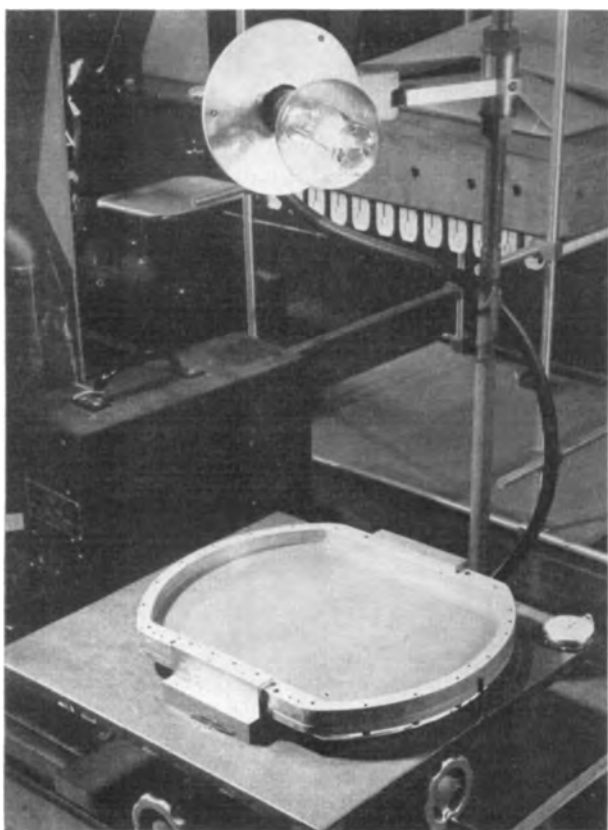


FIG. 7. Optical bench for point shadow projection

enclosed, concentrated arc lamp. This lamp has a crater 0.116 in. in diameter. A crater of this size produces shadowed dots of adequate size to be covered by the electron beam in the tube. The master pattern can be either the aperture mask or a photographic reproduction of it. The coating, exposure, and developing are carried out with the screen panel and aperture mask clamped together in such a way that the outside of the screen plate faces the side of the aperture mask which faces the guns in the finished tube. To position the dots for the different colors, the milling table is used to move the aperture mask and screen assembly relative to the arc lamp. The distance traversed by the milling table in this operation is about 0.3 in. and is measured to the nearest thousandth.

The distance from the arc lamp to the master (or aperture mask) is calculated from the desired pattern size, using the known spacing between the screen plate and the aperture mask and the thickness and refractive index of the screen panel. The refractive effects taking place at the glass-air interface enter into this calculation. When the spacings used are essentially those to be used in the color tube, the uncorrectable deviation due to refraction is less than 0.0003 in. (see Fig. 6).

The exposure time for each batch of each color phosphor is determined by a step exposure. The emulsion is exposed for the appropriate length of time and the film is developed by washing away the unexposed areas with a suitable solvent (trichloroethylene). The washing was done in several ways, including a condensing vapor type solvent wash, immersion in solvent, and a flush spray, the last was found most effective. The panel is recoated, the table is indexed to the position for the second set of dots, and the exposure is repeated for a time appropriate for the second phosphor. The procedure is repeated for the third phosphor.

After all three sets of dots have been developed, the photosensitive binder is removed by baking the plate at 400°C for several hours. The phosphor

TABLE I Color and brightness measurements for green phosphor No. 160 (zinc orthosilicate)

Binder	Relative brightness, % of control	Color*	
		x	y
Control	100	0.260	0.715
Kodak Photosensitive Lacquer	96	0.260	0.725
Polyvinyl alcohol	39	0.262	0.720
Gelatin	9	0.185	0.540

* Chromaticity values, based upon the color measurement system of the International Commission on Illumination.

deposit is very fragile at this point and the screen is sprayed with a 14% solution of potassium silicate, using an air brush, to form a permanent binder. The subsequent operations are: (a) floating on a lacquer film; (b) aluminizing by high vacuum evaporation, (c) baking out lacquer film. These operations have been summarized elsewhere in the literature (2).

Luminescence of Experimental Screens

Three sets of panels were prepared with the green phosphor (zinc orthosilicate), using Kodak Photo-sensitive Lacquer, polyvinyl alcohol, and gelatin, respectively, as binders. The luminescent output and color of the KPL sample were not significantly different from the control, a liquid-settled panel. However, the efficiency of the polyvinyl alcohol and gelatin panels were markedly reduced, being, respectively, 39% and 9% that of the control; the color of the gelatin panel was also changed as shown by the chromaticity values. These results are summarized in Table I.

Test runs on full-size color screens showed that the KPL screens can give uniform screens with brightness comparable to screens prepared by the silk-screen method. Registration of the several sets of dots was excellent, and the reproduction of the dot size and location was photographic within measureable limits.

CONCLUSION

The photobinder technique for the preparation of mosaic phosphor patterns for color kinescopes offers considerable promise. By its nature, it is more precise than the silk-screen method, and it may be useful in overcoming the lack of interchangeability of units in the matching tube members, particularly in the case of the aperture mask of the shadow-mask tube.

The technique is applicable to the production of other mosaic surfaces in tubes, e.g., memory tubes, where precisely registered and accurately sized areas of sensitive materials are required.

ACKNOWLEDGMENT

The authors wish to acknowledge the assistance of Julius T. Ragusin and Virgil C. Ragusin in performing the experimental work, and in preparing the drawings for this publication.

Any discussion of this paper will appear in a Discussion Section to be published in the December 1954 issue of the JOURNAL

REFERENCES

- 1 N S FREEDMAN AND K. M. McLAUGHLIN, *Proc I R E*, **39**, 1230 (1951)
- 2 N S FREEDMAN AND K. M. McLAUGHLIN, *Proc I R E*, **39**, 1230 (1951), D W EPSTEIN AND L PENSACK, *RCA Rev*, **7**, 5 (1946)

Electrolytic Reduction of Benzoic, Phenylacetic, and Cinnamic Acids and Esters at a Platinized-Platinum Cathode¹

SHINICHI ONO, TADAO HAYASHI, AND JYUNICHI NAKAYA

Department of Chemistry, Naniwa University, Osaka, Japan

ABSTRACT

A study has been made of the electrolytic reduction of certain aromatic carboxylic acids and esters at a platinized-platinum cathode (Pt-pt) in alcoholic sulfuric acid solution.

It was found that the reduction at a Pt-pt cathode was quite different from that pursued at a lead or a mercury cathode. At a Pt-pt cathode, the reduction of benzoic, phenylacetic, and cinnamic acids and esters gave rise to cyclohexyl compounds. In no case was the carboxyl group reduced.

A special study of the electrolysis at a Pt-pt cathode under elevated pressure was made. The results confirm the catalytic nature of the process.

INTRODUCTION

Numerous studies have been made of electrolytic reduction of benzoic (1), phenylacetic (2), and cinnamic (3) acids, using high hydrogen overvoltage cathodes, such as Pb, Cd, Hg, and Hg-Zn cathodes, but no attempt has been made to determine the effect of platinized-platinum cathode (Pt-pt) on them, except in the case of cinnamic acid (4).

This has now been done. It has been found that the reduction of these acids at a Pt-pt cathode in alcoholic sulfuric acid solution gave rise to cyclohexyl compounds, but no alcohols. The esters also gave the corresponding cyclohexyl compounds.

Earlier work showed that the reduction of benzoic (1) and phenylacetic (2) acids at a Pb cathode gave benzyl- and phenylethyl-alcohols, respectively. Cinnamic acid at a Hg or a Pb cathode produced bimolecular compounds as well as phenylpropionic acid, but no phenylpropyl alcohol. With cinnamic acid it has now been found that the reduction of the double bond took place first, and then that of the benzene ring. The carbonyl groups in these compounds were quite resistant to the catalytic action of a Pt-pt cathode. It is also of interest that the interposition of a CH₂ or a CH₂CH₂ linkage between phenyl- and carboxyl- groups has no essential influence on the course of reduction.

Differences in the electrolytic reduction using Pb and Pt-pt cathode are summarized in Table I.

It is apparent that the course of the reduction at a Pt-pt cathode contrasts sharply with that pursued at a Pb or a Hg cathode. The characteristic properties of the Pt-pt cathode have been mentioned by several authors as follows.

Fichter and Stocker (5) and also Bancroft and George (6) observed the formation of cyclohexanol by the electrolytic hydrogenation of phenol using a Pt-pt cathode, and it was stated that a Pt-pt cathode had a specific effect on the hydrogenation of phenol. Sitaraman (7) found that the 3-isomeric cresols gave the corresponding methylcyclohexanols and methylcyclohexanones.

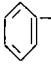
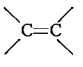
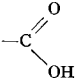
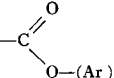
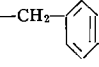
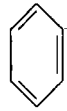
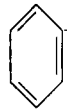
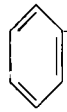
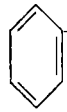
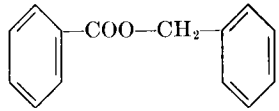
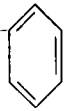
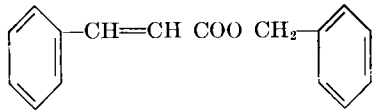
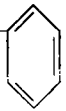
Wilson (8) suggested that there were close analogies between the prepared cathodes of Pt or Ni and catalytic hydrogenation in the reduction of sorbic acid and beta-vinylacrylic acid. Thus the reduction of sorbic acid at a Pt-pt cathode gave considerable amounts of 2-hexenoic acid and the fully saturated hexoic acid, whereas Hg or Pb cathode produced only a mixture of 3- and 4-hexenoic acid. This author pointed out that catalytic hydrogenation must proceed through electrically neutral intermediates, whereas electrolytic reduction may or may not, since it proceeds only in ionizing media. Much more important must be the condition of the hydrogen on the surface of the Pt-pt cathode.

In the present experiments, judging from the fact that (a) benzene rings were hydrogenated independently of the distance from the carboxyl group, and (b) both benzene rings in phenyl and benzyl esters were hydrogenated at the same time, it can be said that the reduction at a Pt-pt cathode takes place independently of the proton affinity of parts of the molecules. It is probable, therefore, that the reduction, under these conditions, involves the combination of an active center of the organic molecules with a chemisorbed hydrogen atom, in the manner envisaged by Horiuti (9).

Little attention has been paid in the past to the effect of external pressure on electrolytic reduction of organic compounds. Ipatiev, *et al.* (10) measured the

¹ Manuscript received January 7, 1952. This paper was prepared for delivery before the Detroit Meeting, October 9 to 12, 1951.

TABLE I. Effect of cathode on reduction of various groups

Group												
	Compound	Cathode	Pb	Pt-pt	Pb	Pt-pt	Pb	Pt-pt	Pb	Pt-pt	Pb	Pt-pt
 -COOH			-	+			+	-				
 -CH ₂ -COOH			-	+			+	-				
 -CH=CH COOH			-	+ ₂	+	+ ₁	-	-				
 -CH ₂ -COOC ₂ H ₅			-	+					-	-		
 -COO-CH ₂ - 			-	+ ₁					+	-	-	+ ₁
 -CH=CH COO CH ₂ - 			-	+ ₂	+	+ ₁			-	-	-	+ ₂

Note + and - indicate reducibility and nonreducibility, respectively, +₁ and +₂ give the order in which the groups are reduced.

overtoltage on the Pt-pt in acid and alkaline solutions under pressures up to 100 atm. They observed that the potential of the cell increased with pressure.

Assuming that the reduction at a Pt-pt cathode consists mainly in a catalytic mechanism, there could be a correlation between the reduction products and the external pressure. Since no data are available, the present series of experiments was designed.

EXPERIMENTAL

Materials.—Benzoic and phenylacetic acids (C. P. products) were purified by recrystallization. Cinnamic acid and esters were prepared by standard methods. The mp or bp of samples was as follows:

	Acid	Ethyl ester	Phenyl ester	Benzyl ester
Benzoic	122	87-8/10 mm	71	145-7/5 mm
Phenylacetic	76	124-5/18 mm	42	172-4/12 mm
Cinnamic	132	144-5/16 mm	72	195-8/5 mm

Reduction technique.—The catholyte was 75, 50, 40, and 28% of sulfuric acid to which ethyl alcohol had been added. A sheet lead anode was used. The platinized-platinum cathode was prepared as follows. A platinum (100 cm²) cylinder of gauze or sheet was platinized by electrolysis of platonic chloride solution (3 grams of platonic chloride in 100 ml of distilled water and 0.03 gram of lead acetate added).

The usual type of electrolytic cell was used. The porous cup (17 cm x 4.6 cm, Japan Chemical Ceramic Company, permeability, 3.94×10^{-4} cm/sec, porosity, 57.31) was used as a cathode compartment, and the cell was immersed in a water bath to maintain the desired temperature. The samples were dissolved in alcoholic sulfuric acid solution and placed in the cathode chamber. Sulfuric acid was used as an anolyte. Current density was varied between 0.5 and 6.5 amp/dm².

In the case of reduction under high pressure, the electrolytic cell was placed in an autoclave especially

designed for this purpose (Fig. 1) and hydrogen was allowed to enter to a little more than the desired pressure. The valve between the tank and bomb was then closed and current was switched on.

Isolation and characterization of products.—When the reduction was completed, the catholyte was diluted with water and extracted with ether. The ether extracts were collected, washed with water, and dried over anhydrous sodium sulfate. The ether was

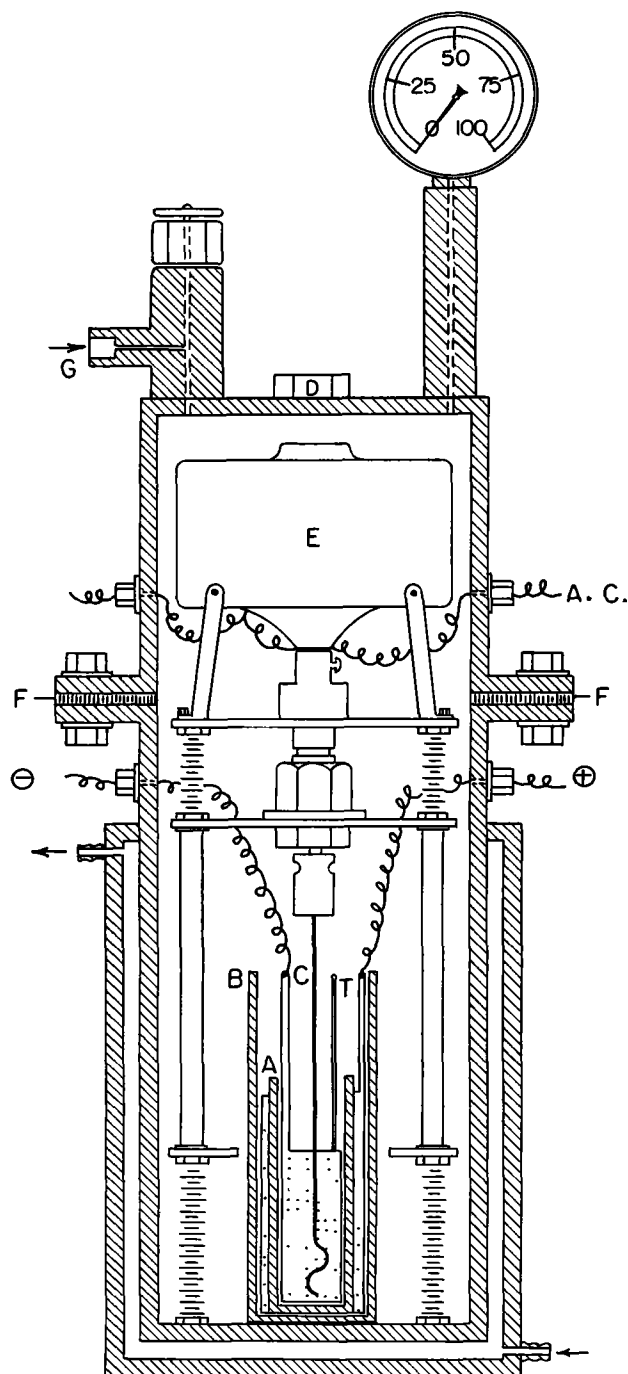


FIG 1 Autoclave specially designed for pressure electrolysis A—porous cup, B—electrolytic cell, C—cathode, D—safety disk, E—stirring motor, F—rubber packing, G—gas inlet, T—maximum thermometer

evaporated and the residue was distilled under diminished pressure. The fractions obtained were characterized and weighed. The physical properties of cyclohexyl compounds obtained are shown in Table II.

Typical Experiments

(a) *Phenylacetic acid.*—13.5 grams (0.1 mole) of phenylacetic acid was dissolved in 40 ml of ethyl alcohol and 40 ml of sulfuric acid (50%) and placed in the cathode chamber. Sulfuric acid (30%) was used as an anolyte. A current of 2.0 amp was passed for 14 hr (theoretical for 13.6 grams phenylacetic acid, 16.1 amp hr). The temperature was kept between 25°–30°C.

When the reduction was completed, the catholyte was diluted with 50 ml of water and extracted with ether. The ether extracts were washed with water and dried over anhydrous sodium sulfate. After evaporating the ether, the residue was distilled under diminished pressure giving two fractions: (f_1) 65°–80°/6 mm Hg (10.2 grams) and (f_2) 114°–119°/6 mm Hg. Redistillation of (f_1) gave ethyl cyclohexylacetate, bp 68°–70°/6 mm Hg, $D_4^{25} = 0.9475$, $n_D^{25} = 1.4472$,

TABLE II Physical constants of reduction products

Compound	M P (°C)	B P (°C/mm Hg)	D_4^{25}	n_D^{25}
$C_6H_{11}COOH$	29			
$C_6H_{11}CH_2COOH$	33			
$C_6H_{11}CH_2CH_2COOH$	16	132–3/9	0.9966	1.4658
$C_6H_{11}COOC_2H_5$	80	5–81 5/11	0.9525	1.4398
$C_6H_{11}CH_2COOC_2H_5$		68–70/6	0.9475	1.4472
$C_6H_{11}CH_2CH_2COOC_2H_5$		92–94/8	0.9674*	1.4488*
$C_6H_{11}COOC_6H_{11}$		60–62/7	0.9517	1.4395
$C_6H_{11}CH_2CH_2COOC_6H_{11}$		72–75/6	0.9741	1.4700
$C_6H_{11}CH_2COOCH_2C_6H_{11}$		70–73/8	0.9765	1.4510

* at 20°C

TABLE III Effect of current density—(a) ethyl benzoate

Catholyte ethyl benzoate, 10 g; ethanol, 50 ml, 75% sulfuric acid 30 ml, temp. 25°–30°C, quantity of current: 16 amp hr, cathode Pt-pt, gauze, (100 cm²)

Run No	Current density (amp/dm ²)	Yield† (%)	Current efficiency (%)
1	0.8	78.8	52.8
2	1.2	78.0	52.2
3	2.0	60.5	40.5
4	3.0	65.3	43.7
5*	4.0	74.0	49.5
6*	6.0	74.0	49.5

† Ethyl hexahydrobenzoate * Temp 35°–40°C Yield is calculated on consumed depolarizer. Current efficiency is the percentage of current used in producing the product.

and (f_1) was distilled again under diminished pressure giving bp 117°–119°/6 mm Hg, mp 30°C, identified as cyclohexylacetic acid.

(b) *Ethyl benzoate (under pressure)*.—Ten grams

TABLE IV *Effect of current density—(b) ethyl phenylacetate*

Catholyte ethyl phenylacetate, 10 grams; ethanol, 50 ml, 75% sulfuric acid, 30 ml; quantity of current: 16 amp hr (theory 9.8 amp hr), temp. 25°–30°C, cathode, Pt-pt, gauze (100 cm²)

Run No.	Current density (amp/dm ²)	Yield† (%)	Current efficiency (%)
1	0.5	76.0	46.6
2	1.0	56.8	34.8
3	2.0	56.8	34.8
4	3.5	63.6	39.0
5*	5.0	63.6	39.0
6*	6.5	66.5	40.7

† Ethyl cyclohexylacetate. * Temp 40°–45°C

TABLE V *Effect of current density—(c) phenylacetic acid*

Catholyte phenylacetic acid, 13.6 grams, ethanol, 40 ml, 50% sulfuric acid, 40 ml, quantity of current 28 amp hr (theory 16.1 amp hr), temp 30°–35°C, cathode, Pt-pt, sheet (100 cm²)

Run No	Current density (amp/dm ²)	Yield† (%)	Current efficiency (%)
1	1.0	76.5	44.0
2	2.0	80.2	46.1
3	3.0	74.6	42.9
4*	4.0	77.5	44.6
5*	5.0	75.5	43.4

† Cyclohexylacetic acid and its ethyl ester. * Temp 40°–45°C.

TABLE VI. *Effect of acid concentration—(a) benzoic, phenylacetic, and cinnamic acids*

Catholyte: compound, 0.1 mole; ethanol, 40 ml; sulfuric acid, 40 ml, temp 30°–35°C, cathode: Pt-pt, sheet, (100 cm²)

Run No.	Compound (g)	H ₂ SO ₄ (%)	Current density (amp/dm ²)	Product*		Yield (%)	Current efficiency (%)
				f_1 (g)	f_2 (g)		
1	Benzoic (12.3)	28	1.0	5.0	4.4	66.0	53.1
2	Benzoic (12.3)	75	1.0	8.1	1.8	66.0	53.1
3	Phenylacetic (13.6)	28	2.0	6.0	6.0	77.5	44.6
4	Phenylacetic (13.6)	50	2.0	9.5	3.0	77.5	44.6
5	Phenylacetic (13.6)	75	2.0	10.5	1.5	72.5	41.7
6	Cinnamic (14.8)	28	3.0	4.0	6.0	60.0	42.8
7	Cinnamic (14.8)	40	3.0	6.8	6.0	76.0	54.2
8	Cinnamic (14.8)	75	3.0	11.4	2.2	76.5	54.6

Quantity of current: Run No 1–2, 20 amp hr (theory 16.1 amp hr) 3–5, 28 amp hr (theory 16.1 amp hr) 6–8, 30 amp hr (theory 21.4 amp hr).

* Products f_1 , ethyl esters of cyclohexyl acids; f_2 , cyclohexyl acids

(0.67 mole) of ethyl benzoate was dissolved in 50 ml of ethyl alcohol and 30 ml sulfuric acid (75%) and placed in the cathode chamber. Sulfuric acid (50%) was used as an anolyte. The electrolytic cell was placed in the autoclave and hydrogen was admitted to 20 atm pressure. The reduction was carried out at a current density of 1.2 amp/cm² for 16 amp hr (theoretical for 10 grams ethyl benzoate, 10.7 amp hr).

During reduction, the temperature in the cell was uncontrolled, but a maximum thermometer inserted in the catholyte showed that this had not been higher than 25°C.

The catholyte was diluted with water, neutralized with sodium carbonate, and extracted with ether. The ether was evaporated and the residual solution was distilled under diminished pressure. The fraction bp 78°–82°/11 mm Hg was collected. Redistillation gave bp 80.5°–81.5°/11 mm Hg, $D_4^{25} = 0.9525$, $n_D^{25} = 1.4398$. Saponification with 20% alcoholic potassium hydroxide gave a hexahydrobenzoic acid, mp 28°C.

(c) *Cinnamic acid to hydrocinnamic acid*.—Cinnamic acid (7.5 grams) in 75% sulfuric acid and alcohol solution was electrolyzed with 6.0 amp hr of current (theoretical for 7.5 grams of cinnamic acid, 2.7 amp hr) and gave (f_1) 3.5 grams, bp 140°–54°/10 mm Hg, mp 48°C, (f_2) 1.5 grams, bp 159°–64°/10 mm Hg, mp 85°C, and (f_3) 1.3 grams, unchanged cinnamic acid. The (f_1) was recrystallized from ligroin, mp 49°C, identified as hydrocinnamic acid. It was shown that (f_2) was a mixture of hydrocinnamic and cinnamic acids.

(d) *Cinnamic acid to cyclohexylpropionic acid*.—

Cinnamic acid (7.5 grams) in 75% sulfuric acid and alcohol solution was reduced at 3.0 amp/dm² for 5 hr (theoretical for 7.5 grams cinnamic acid, 10.8 amp hr) and gave (a) bp 91°–94°/8 mm Hg, 5.7 grams, and (b) bp 124°–6°/8 mm Hg, 1.0 grams. The fraction

TABLE VII. *Effect of acid concentration—(b) ethyl benzoate*

Catholyte: ethyl benzoate, 10 grams, ethanol, 50 ml; sulfuric acid, 30 ml; temp 40°–45°C, quantity of current, 16 amp hr (theory 10.7 amp hr); cathode Pt-pt, gauze, (100 cm²)

Run No	H ₂ SO ₄ (%)	Current density (amp/dm ²)	Yield* (%)	Current efficiency (%)
1	40	2.0	58.7	39.3
2	75	2.0	64.5	43.1
3	80	2.0	65.4	43.7
4	96	2.0	64.5	43.1

* Ethyl hexahydrobenzoate

TABLE VIII. *Effect of temperature—(a) ethyl benzoate*

Catholyte ethyl benzoate, 10 grams, ethanol, 50 ml, 75% sulfuric acid, 30 ml; quantity of current 16 amp hr (theory 10.7 amp hr); cathode Pt-pt, gauze, (100 cm²)

Run No	Temp (°C)	Current density (amp/dm ²)	Yield* (%)	Current efficiency (%)
1	7–11	4.0	54.8	36.6
2	25–30	4.0	74.0	49.5
3	55–60	4.0	76.0	50.8
4	8–10	2.0	43.3	29.0
5	25–30	2.0	60.5	40.5

* Ethyl hexahydrobenzoate

TABLE IX. *Effect of temperature—(b) phenyl benzoate*

Catholyte phenyl benzoate, 10 grams, ethanol, 70 ml; 75% sulfuric acid, 30 ml; quantity of current: 20 amp hr (theory 16.2 amp hr); cathode Pt-pt, gauze, (100 cm²)

Run No.	Temp (°C)	Current density (amp/dm ²)	Yield* (%)	Current efficiency (%)
1	30–35	5.0	19.8	16.0
2	45–50	5.0	24.6	19.9
3	50–55	5.0	34.0	27.5

* Cyclohexyl hexahydrobenzoate.

TABLE X. *Effect of duration of reduction of ethyl benzoate*

Catholyte ethyl benzoate, 10 grams, ethanol, 50 ml; 75% sulfuric acid, 30 ml; current density: 4.0 amp/dm²; temp. 30°–35°C; theoretical amount of current 10.7 amp hr

Run No.	Duration of run		Yield* (%)	Current efficiency (%)
	(hr)	(amp hr)		
1	4.0	16.0	74.0	49.5
2	5.0	20.0	73.0	39.1
3	6.0	24.0	72.0	32.1
4	7.5	30.0	74.0	26.4

* Ethyl hexahydrobenzoate.

(a), $D_4^{20} = 0.9674$, and $n_D^{20} = 1.4488$, was identified as ethyl cyclohexylpropionate.

(e) *Phenyl cinnamate*.—Phenyl cinnamate (11.2 grams) in 75% sulfuric acid (30 ml) and alcohol (50 ml) was electrolyzed at a current density of 1.0 amp/dm² for 20 hr (theoretical for 11.2 grams of phenyl cinnamate, 16 amp hr) at 25°–30°C. The

TABLE XI. *Effect of pressure—(a) ethyl benzoate*

Catholyte ethyl benzoate, 10 grams, ethanol, 50 ml; 75% sulfuric acid, 30 ml, quantity of current 16 amp hr (theory, 10.7 amp hr), cathode Pt-pt, gauze, (100 cm²)

Run No	Pressure (atm)	Current density (amp/dm ²)	Temp (°C)	Yield* (%)	Current efficiency (%)
1	1 (H ₂)	4.0	30–35	74.0	49.5
2	10 (H ₂)	1.2	20–25	84.5	56.5
3	20 (H ₂)	1.2	20–25	85.5	57.2
4	10 (H ₂)	4.0	30–35	75.0	50.2
5	20 (H ₂)	4.0	30–35	75.0	50.2
6	30 (H ₂)	4.0	30–35	77.0	51.3
7	40 (H ₂)	4.0	30–35	73.1	49.0
8	20 (CO ₂)	2.0	25–30	64.5	43.2
9	40 (CO ₂)	2.0	25–30	58.6	39.2

* Ethyl hexahydrobenzoate.

TABLE XII. *Effect of pressure—(b) phenylacetic acid*

Catholyte phenylacetic acid, 13.6 grams, ethanol, 40 ml, 50% sulfuric acid, 40 ml, quantity of current 28 amp hr (theory 16.1 amp hr), temp 40°–45°C; cathode Pt-pt, sheet, (100 cm²)

Run No.	Pressure of hydrogen (atm)	Current density (amp/dm ²)	Yield* (%)	Current efficiency (%)
1	1	5.0	75.5	43.4
2	15	2.0	75.5	43.4
3	25	4.0	77.0	44.3
4	35	4.0	75.5	43.4
5	25	5.0	78.2	45.0
6	40	5.0	77.0	44.3

* Cyclohexylacetic acid.

TABLE XIII. *Effect of pressure—(c) cinnamic acid*

Catholyte cinnamic acid, 7.5 grams, ethanol, 60 ml; sulfuric acid, 20 ml, temp 25°–35°C, quantity of current: 15 amp hr (theory 10.8 amp hr), cathode Pt-pt, sheet, (100 cm²)

Run No.	Pressure of hydrogen (atm)	Current density (amp/dm ²)	Yield* (%)	Current efficiency (%)
1	1	3.0	60.3	43.4
2	15	3.0	62.8	45.2
3	30	3.0	69.3	49.9
4	1	5.0	74.5	53.6
5	35	5.0	74.5	53.6
6	45	5.0	70.5	50.8

Note: Concentration of sulfuric acid. Run No. 1–3 28%, Run No. 4–6, 40%.

* Cyclohexylpropionic acid.

reduction gave cyclohexyl cyclohexylpropionate, bp 72°–75°/6 mm Hg, $D_4^{25} = 0.9741$, $n_D^{25} = 1.4700$. Saponification with 20% alcoholic potassium hydroxide solution gave cyclohexylpropionic acid, mp 16°C, and cyclohexanol.

RESULTS AND DISCUSSION

Effect of current density—It was found that better yields could be obtained at lower current densities. This is shown in Tables III, IV, and V.

Effect of acid concentration—It may be seen from the data in Tables VI and VII that stronger acid solution caused the formation of esters, otherwise acid concentration had no noticeable influence on the reduction.

Effect of temperature—It is seen in Tables VIII and IX that the reduction was favored by high temperatures.

Effect of duration.—Table X shows that yield of product was almost independent of duration of the run. Current efficiency fell, of course, as the run was prolonged beyond the theoretical time.

Effect of pressure.—A special study was undertaken of the effect of high pressure in the course of the reduction. It is seen in Tables XI to XIII that the reduction was favored at high hydrogen pressure, although the effect was not great. Assuming that the reduction at a Pt-pt cathode proceeds by a catalytic mechanism, it would be expected that pressure would increase the rate of reduction of organic compounds. The results obtained, however, are irregular. More detailed conclusion must await further results.

ACKNOWLEDGMENT

It is with great pleasure that the authors responded to the invitation of Professor C. L. Wilson to submit a paper for the Symposium on Electro-Organic

Chemistry. The authors express their sincere thanks to him for his kind advice and encouragement.

Any discussion of this paper will appear in a Discussion Section, to be published in the December 1954 issue of the JOURNAL

REFERENCES

- 1 C. METTLER, *Ber*, **37**, 3692 (1904); **38**, 1745 (1905); **39**, 2933 (1906)
J. TAFEL AND G. FRIEDRICH, *Ber*, **37**, 3187 (1904)
E. BAUR AND E. MULLER, *Z. Elektrochem*, **34**, 98 (1928).
F. SOMLO, *Z. Elektrochem*, **35**, 264 (1929).
FR. FICHTER AND I. STEIN, *Helv. chim. Acta*, **12**, 821 (1929)
S. SWANN, JR., AND G. D. LUCKER, *Trans. Electrochem. Soc*, **75**, 411 (1939)
- 2 C. MARIE, R. MARQUIS, AND BIRCKENSTOCK, *Bull. soc. chim*, **25**, 512 (1919)
H. INOUE, *J. Ind. Eng. Chem. (Japan)*, **24**, 914 (1921).
3 H. INOUE, *J. Ind. Eng. Chem. (Japan)*, **24**, 916 (1921).
C. L. WILSON AND K. B. WILSON, *Trans. Electrochem. Soc*, **84**, 153 (1943)
C. L. WILSON, *ibid*, **92**, 369 (1947)
- 4 N. I. KOBOSEV AND L. L. KLACHKO-GURVICH, *Acta physicochim*, **10**, 1 (1939).
W. W. MONBLANOVA, N. I. KOBOSEV, AND P. S. PHILLIPPOVICH, *Zhur. Fiz. Khim*, **13**, 326 (1939), *Acta physicochim. (U R S S.)*, **11**, 317 (1939).
N. KOBOSEV, L. NIKOLAEV, I. ZUBOVICH, AND J. GOLDFELD, *Zhur. Fiz. Khim*, **19**, 48 (1945); *Acta physicochim (U R S S.)*, **21**, 289 (1946)
- 5 FR. FICHTER AND R. STOCKER, *Ber*, **47**, 2015 (1914).
- 6 W. D. BANCROFT AND A. B. GEORGE, *Trans. Electrochem. Soc*, **57**, 399 (1930)
- 7 M. V. SITARAMAN AND V. V. RAMAN, *Current Sci. (India)*, **16**, 23 (1947)
- 8 C. L. WILSON, *Trans. Electrochem. Soc*, **75**, 353 (1939).
- 9 J. HORIUTI AND G. OKAMOTO, *Bull. Chem. Soc. Japan*, **13**, 216 (1938)
J. HORIUTI AND G. OKAMOTO, *Sci. P. I. C. P. R. (Japan)*, **28**, 231 (1936)
- 10 V. V. IPATIEFF, JR., V. V. SHISHKIN, G. A. POLEV, AND I. A. DUBKOV, *J. Phys. Chem. (U R S S.)*, **5**, 1114 (1934)

Flexible Leads for Low-Frequency Electric Furnaces¹

M. EATON

Shawinigan Chemicals Limited, Shawinigan Falls, Quebec

AND

S. B. THOMAS

Northern Electric Company Limited, Montreal, Quebec

ABSTRACT

Special problems are encountered in designing cables to transfer power from the bus system to the electrodes of arc furnaces. The requirements for cable are outlined and a brief study made of the various types used. The development of water-cooled cables is traced, and data are given on construction, current ratings, life expectancy, and other characteristics. The conclusion is that this type of cable is a practical solution of the problems encountered.

INTRODUCTION

Water-cooled flexible leads, consisting essentially of a flexible conductor inside a flexible metal tube with suitable terminals and water passage, have been in use for many years. One of their most important applications pertains to calcium carbide furnaces.

The electrical resistance of a calcium carbide furnace is low (usually between 1200 and 2500 microhms, depending on the power taken and the nature of the charge). In order to obtain a satisfactory power factor, it is therefore necessary to limit the reactance to a corresponding value. Since reactance is directly proportional to frequency, it presents a greater problem in the design of 60-cycle furnaces than it does for furnaces with power supplied at lower frequencies. The reactance, X , equals $2 \pi fL$ ohms. The inductance, L , depends mainly on the size, shape, length, and arrangement of current-carrying parts.

Fig. 1 and 2, showing schematically the arrangement of low-voltage connections to the electrodes of a carbide furnace designed for low reactance, serve to show the advantage gained by the use of water-cooled flexible leads. Current supplied by transformer [2] is carried to the contact shoes, [10], on the electrodes, [11], [12], and [13], by interlaced bus bars, [3], and uninterlaced connections, [7], [8], and [9], including water-cooled flexible leads, [16]. Single circuits are indicated, whereas in practice multiple circuits, with a corresponding number of electrode contact shoes, are used. Minimum reactance is obtained mainly by (a) making all parts of the circuit as short as practicable, (b) the use of multiple circuits, (c) carrying the interlaced (alternatively

plus-minus) bus bars from the transformer to points as near the electrodes as practicable, and (d) by completing the delta connections at the electrodes. In this arrangement of current-carrying parts, the flexible leads are exposed to the radiant heat of the furnace and, therefore, they must be water-cooled. If, alternatively, flexible leads made with multiple thin copper strips or bare stranded conductors are located outside the furnace, the length of the uninterlaced connections is increased with a corresponding increase in reactance.

Further advantages are gained in the use of water-cooled flexible leads if they can be mounted in the form of an upright arch, as indicated in Fig. 2. The height of the horizontal connections between the interlaced bus bars, [3], and the electrode, [13], is determined by the amount of clearance under them that is required for furnace operation. Since flexible lead [16] is self-supported, when its terminal connections are arranged to hold it in an arched position it may be installed as indicated. In order to obtain the same clearance with a suspended flexible lead, it would be necessary to raise the interlaced bus bars, [3], together with the horizontal tube, [9], and to increase the length of tube [19]. The self-supported flexible lead of this design therefore provides means for reducing the length and, consequently, the reactance of the electric circuit. Another advantage of the arched position is that the flexible lead has a minimum exposure to the radiant heat of the furnace and to damage by tools used in the operation of the furnace.

The development of a self-supported water-cooled flexible lead suitable for low-frequency electric furnaces is the main subject of this discussion.

Consideration of means for making the flexible leads self-supported when mounted in an arched

¹ Manuscript received April 16, 1953. This paper was prepared for delivery before the New York Meeting, April 12 to 16, 1953.

position led to the choice of a design in which this characteristic is obtained by the use of one or more flat strips of resilient metal which make the leads flexible in a longitudinal plane at right angles to the flat surfaces of the spring strips and comparatively rigid in a transverse direction.

Four arrangements of the spring strips, comprising successive steps in the development, are illustrated by Fig. 3 to 6. The results of accelerated aging tests are tabulated in Table I.

Fig. 3 and 4 serve to illustrate the arrangement of the component parts of both flexible leads I and II, Table I. As indicated in Fig. 3, a conventional water-cooled flexible lead, consisting of flexible conductor [10] soldered in receptacle [9] of terminal [5], having water passages [6]-[7]-[8]-[15] and outer flexible metal tube [30], is provided with spring strips (phosphor-bronze), [20] and [25], firmly fixed to the terminals, [5], by means of silver solder. Fig. 4 is a sectional view of this arrangement. The spring strips make the flexible lead self-supported when its terminal connections are made to hold one end in the position indicated by Fig. 3, and the cable is looped around laterally to a similar parallel terminal in suitable spaced relation. Since in a bend of this shape one spring strip is longer than the other, a flexible lead of this design must be fabricated and maintained with a predetermined shape of bend, i.e., with suitably spaced terminals either parallel or inclined toward one another at a predetermined angle.

FLEXIBLE LEAD I

The first flexible lead of this design was made with only one spring strip located on the under side of the flexible conductor and having its ends brazed to the conductor strands at the terminals. An accelerated aging test was made on a test lead of this design with results as shown in Table I. The testing apparatus

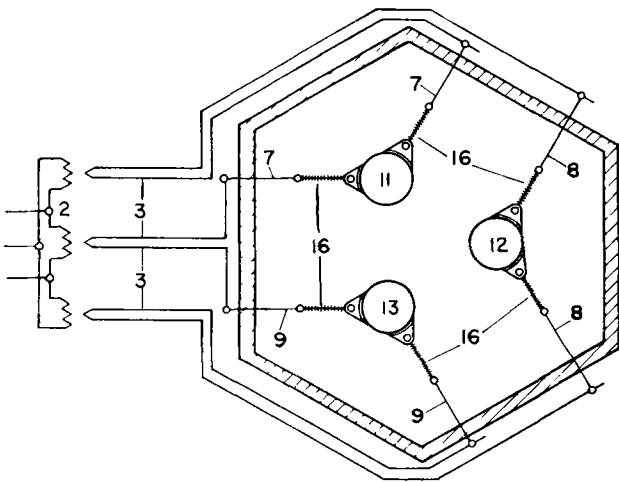


FIG 1 Low voltage connections for a calcium carbide furnace

was made to hold the terminals vertical and parallel and with a suitable bending diameter. With one terminal fixed, the other terminal was moved up and down a distance of 3 ft until failure occurred, water pressure being maintained throughout the test. The tabulated results show the number of cycles and the distance traveled by the moving terminal before leakage of the cooling water occurred.

Although measurement of the movement of carbide furnace electrodes indicated that flexible leads with a test performance equal to that of flexible lead I might remain in service two or three years without trouble, in practice it was found that leakage occurred after only about six months of operation. Through breakage of the conductor strands to which the spring strips were brazed and by other causes the spring strips became displaced, thus failing to support the flexible leads in a uniform arch and causing wear on the outer flexible tubes with final leakage.

The discrepancy between the actual life and the life expectancy based on test results is accounted for by the difference between furnace operating conditions and test conditions. The flexible lead on test

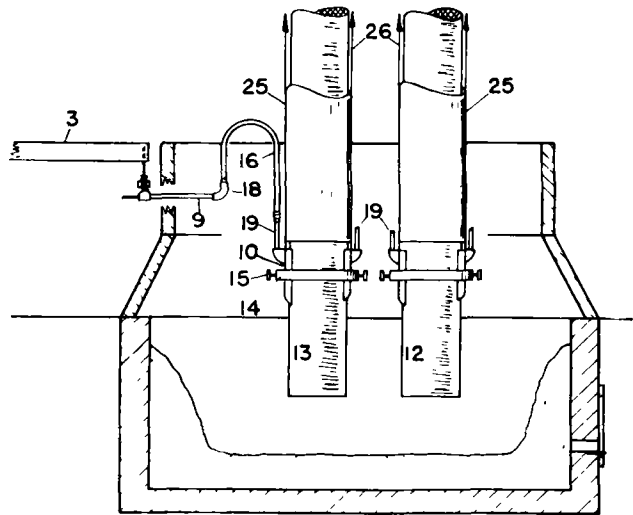


FIG 2 Low voltage connections for a calcium carbide furnace

TABLE I Results of accelerated aging tests on self-supported flexible leads

Ref No	Description	Cycles traveled free end	Traveled distance ft
I	1 spring strip in water passage	3,770	22,620
II	2 spring strips in water passage	12,616	75,696
III	Spring at center of 4-segment conductor	11,120	66,720
IV	Spring at center concentric design	31,594	189,564

was constantly held at the bending diameter for which it was made and with the spring strip flexing only in a vertical plane passing longitudinally through its center, whereas, because of limited horizontal movement of the electrodes at the elevation of the contact shoes, flexible leads in service were subjected to stresses resulting from changes in bending diameter and alignment.

FLEXIBLE LEAD II

The design of the flexible leads was then changed to that shown in Fig. 3 and 4. The use of two spring strips, firmly fixed to the terminals, served to give the flexible leads more adequate support and, at the same

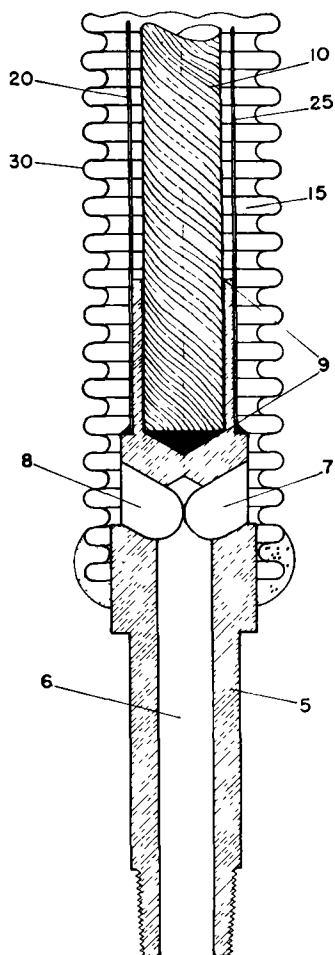


FIG. 3. Sectional views of self-supported flexible leads

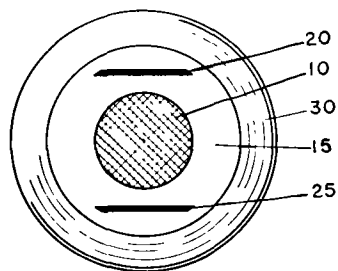


FIG. 4. Sectional views of self-supported flexible leads

time, the additional spring strip reduced wear on the outer flexible tube caused by relative motion between the flexible conductor and the flexible tube.

The accelerated aging test indicated considerable improvement as compared with flexible lead I. It has been found that the life of the lead in service was approximately doubled by the changes in its construction. However, the spring strips still tended to become displaced with results as described above. Improvement was only in the length of service obtained before leakage occurred.

FLEXIBLE LEAD III

A further development of the flexible lead was made by securing a single spring strip, [20], at the center of a flexible conductor, [10], made in four segments as shown in Fig. 5. The assembly was held together with a neoprene-insulated binding wire, [35], which was also designed to prevent frictional wear on the inner surfaces of the flexible tubing.

The accelerated aging test (see Table I) indicated that a flexible lead of this construction was not improved with respect to life expectancy. The test life was limited because of irregular bending of the outer flexible tube. The flexible tubing tended to bend sharply at two or three points, with final failure caused by leakage at one of them. It was later found that the irregularity of the flexing was caused by displacement of the binding wire, [35], Fig. 5. A wire braid is now used to hold the segments in place.

FLEXIBLE LEAD IV

Flexible lead IV (Fig. 6) includes a flexible conductor with a core of unusual construction. A strip of resilient metal, [20], is embedded at the center of

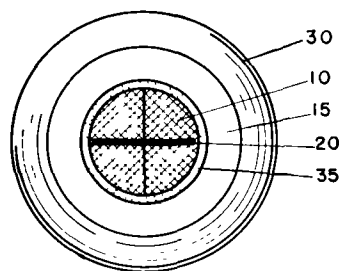


FIG. 5. Sectional views of self-supported flexible leads

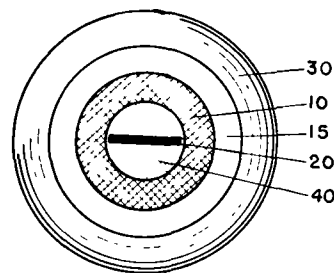


FIG. 6. Sectional views of self-supported flexible leads

an elongated core, [40], of circular cross section and made of elastic material such as neoprene. The flexible conductor, [10], is stranded around the core. The cored conductor is then soldered into the terminals and the outer flexible tubing is applied as indicated in Fig. 3. The results of the accelerated aging test are shown in Table I.

A number of advantages are derived from the concentric construction of this flexible lead, its essential characteristic being that the length of any element, except elastic parts, remains unchanged no matter how the flexible lead is bent in a longitudinal plane at right angles to the flat surfaces of the spring strip. (A) The flexible lead may be fabricated in straight lengths and supported in the form of an upright arch with its terminals either vertical or inclined toward one another at any desired angle, whereas a flexible lead having nonelastic elements of different bending radii must be fabricated and maintained with a predetermined shape of bend, i.e., with its terminals suitably spaced and parallel or inclined toward one another at a given angle (B) The flexible lead is adapted to accommodate changes in the shape of bends and alignment such as occur in service. Lack of this property in other flexible leads referred to above introduced internal stresses which greatly reduced their useful life. (C) The construction of the flexible lead is such that none of its elements can become displaced. Deficiency in this respect has been a source of trouble with other water-cooled flexible leads as already related. (D) The electrical characteristics of the flexible conductor are improved as a result of its cored construction. This feature is of particular importance because of the magnitude of the currents carried (5–8 amp/1000 cir mils).

Flexible leads of the concentric design have been in service for several months. Their length of life in service is not yet known, but the results of the accelerated aging test indicate that they should operate two to three years without trouble. Failure on test resulted from fatiguing of the metal in the outer flexible tube with final cracking and leakage of the cooling water.

It seems that any further improvement in the life of these flexible leads will depend on improving the resistance to metal fatigue in the outer flexible tubing. Flexibility is obtained by means of annular or helical corrugations and by the use of metal having suitable thickness and resilience.

It is suggested that the resistance to fatigue of the metal used in the construction of flexible tubing of this type might be improved by the use of metal having two or more laminations separated from one another by a film or films of a suitable lubricant. An inner lamination of thinner metal would provide greater flexibility without loss of mechanical

strength. The object is to obtain a tire-and-tube effect which will make the tubing still serviceable after cracks form in the outer lamination and until the equivalent of a "blow-out" occurs.

Flexible leads of the class referred to will operate without trouble for much longer periods if made with nonmetallic outer flexible tubing. Water-cooled flexible leads with neoprene outer tubes are being used. Unfortunately, nonmetallic tubes cannot continuously withstand the heat of flames or the radiant heat from furnace charges even when protected with asbestos fabric, as has been proven by trial.

It is found that if water-cooled flexible leads, with outer flexible tubing made of metal, are mounted in such a way that they may touch one another or other objects at a different electrical potential, they must be protected with insulation, such as that provided by asbestos sleeving, in order to prevent damage from arcing contacts.

The main sources of trouble with a self-supported flexible lead of the type described have been eliminated. A long-felt need for a water-cooled flexible lead suitable for low-frequency electric furnaces is therefore realized.

The previous portion of this paper dealt with the development, usage, characteristics, and advantages of self-supported, water-cooled furnace cables. The other aspects of these cables which are pertinent to this discussion are those of design and manufacture.

DESIGN

It has been found that the requirements vary to such an extent that a new design must usually be prepared for each application. However, while the designs are all basically similar, there may be considerable difference in details.

The designer must know, or must determine from the operating engineers, certain limiting conditions under which the cables are to function. These include the electrode current, the vertical travel required, the spacing between the bus bar and the electrode terminals, and any details regarding clearance, etc., which may be applicable.

Usually, more than one cable per electrode is required to carry the current. A 3-phase 20,000 kva furnace may draw as much as 75,000 amp/electrode, and a multiple cable system is obviously required. The number of cables is often limited by certain features of furnace design. If so, a preliminary choice of conductor size is made, using current densities of from 5–8 amp/1000 circular mils of copper area. These correspond approximately to current densities of from 6000 to 10,000 amp/in.² which are considerably higher than the average density of 1000 amp/in.² often used in bus bar design. However, these current densities, or even higher ones, are satisfac-

tory as long as there is sufficient cooling water available to carry away the heat resulting from conductor losses, and as long as the cost of this heat loss can be tolerated. Based on these values of current density, the closest standard conductor size to that required is calculated.

The method of designing the conductor is not of particular interest here except to provide good flexibility. This can be achieved by using a large number of wires of annealed copper stranded together in the conventional manner to form a flexible conductor.

If the furnace is totally enclosed and near-normal ambient temperature conditions prevail, it is advantageous to use a reinforced neoprene hose which has almost unlimited ability to withstand flexing. Tests similar to those previously described were carried out on a cable having a hose of this type, and were concluded after 100,000 cycles of flexing without the cable having failed. The reinforcing is necessary to operate the hose under water pressure and must be nonmetallic to prevent the flow of induced currents which would overheat the reinforcing material and damage the hose.

If the cable is to be subjected to excessive heat or if there is danger of "blow-outs" of molten material from the furnace, a metallic hose is used. The type which has proved most successful is a seamless, flexible phosphor bronze hose. No wire braid reinforcement is necessary on this hose because the ends are restrained against longitudinal expansion and because the pressures used are such that the hose itself has ample strength against radial stresses.

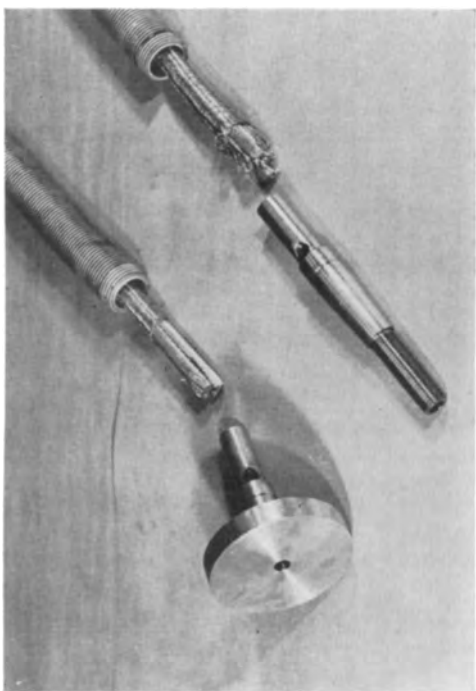


FIG 7 Component parts of a self-supported, water-cooled cable with segmental conductor

Knowing the conductor size, the designer can now calculate the approximate diameter of the terminals and decide on a size for the hose. This must be such that the hose can safely withstand continued flexing at the bending diameter corresponding to the required distance between the bus system and the electrode shoe. If this condition is not satisfied, the conductor size, and hence the number of cables required, must be revised.

The terminals are usually machined from copper rod and in general conform to the style shown in Fig. 3, although they may be modified somewhat to provide for different methods of making electrical and mechanical connections to the furnace. Clamps, tapered fittings, and solidly brazed connections are suitable connecting media. The cross-sectional area of the water passages, [6], [7], and [8], is made approximately equal to the area of the annular space, [15], between the conductor and hose. Only a moderate flow of water is required under a pressure of 30–60 psi. With current densities of the order previously mentioned, a water temperature rise of approximately 20° F above intake temperature is to be expected over the length of one cable.

The only main point left to consider is the length of the cable. This is dependent upon the vertical travel required. A simple arithmetical calculation involving the travel and mean bending diameter gives a minimum length for the hose. To this must be added a certain amount to insure that the hose is not subjected to bending at the point of connection to the terminals under extreme positions of travel. In practice, the length of a cable in its arched position is surprisingly short. The one with reinforced neoprene hose is 4 ft 9 in. in height. It has a 1,500,000 CM conductor, a 2 $\frac{3}{8}$ in. ID hose, and is capable of a maximum safe travel of 4 ft 9 in.

MANUFACTURE

It is evident from the preceding discussion that there are considerable differences in the various cables and, since relatively small numbers of these cables are made, mass production or assembly line procedures are not usually possible. Therefore, it is necessary to design tools, jigs, and methods of assembly.

Fig. 7 depicts the component parts of a cable. The larger terminal is intended for bolting to the electrode shoe, and the smaller one is intended to be fastened into a tapered fitting on the bus bar system. The conductor in this case is of segmental construction, two flexible segments being laid on either side of the supporting strip of spring phosphor bronze and held in position by a bronze wire braid. One end of this conductor is shown cut and prepared for insertion in the terminal. The conductor is soldered into the terminals while fixed in a jig of the correct

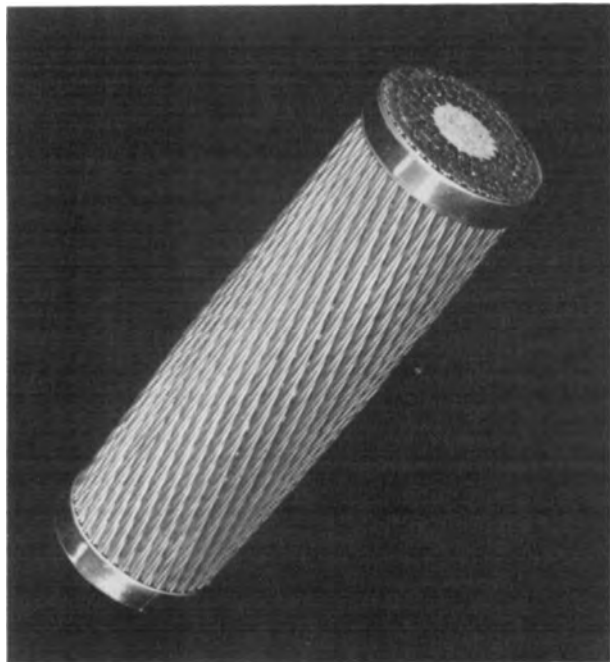


FIG 8 2,000,000 CM asbestos-cored cable

dimensions. For shipping, a clamp is fastened across the ends of the cable, between the two terminals, to maintain it at the proper bending diameter until installation is complete.

OTHER TYPES OF CABLES

Other types in use may be classified as: (A) water-cooled cables (a) supported by external means, and (b) unsupported, (B) bare cables (a) standard concentric stranded, and (b) special types, i.e., asbestos or spring cored

A cable is said to be self-supporting if it can be installed in the form of an upright arch without external means of support. This is the type of cable which has already been described. When external support is required, it usually takes the form of a system of pulleys and counterweights. Some cables are not supported and hang in a loop between the bus bar and electrode. In general, water-cooled cables of these types are subject to much the same limitations regarding current carrying capacity, length and bending diameters as are self-supporting cables.

Bare flexible leads are commonly used for electric furnaces. Obviously, a proportionately greater cross-sectional area of copper is required than for water-cooled cables. Sufficient copper area must be provided to maintain a heat balance such that the cable is not damaged by excessive temperature rise. The cable is heated by resistance losses and by radiant heat from the furnace, and this heat must be dissipated into the air. Damage of the copper conductor

from oxidation will result if its temperature exceeds 350°–400° F. There is thus a definite limit to the current which may be carried by a given cable under known conditions.

These cables may be of the usual concentric design, or they may be annular. The latter construction decreases alternating current losses and increases the surface area so that, for equivalent copper area, it has advantages over the standard concentric design. The annular construction is derived by stranding wires concentrically around a core of asbestos, a spiral spring, or similar material. Fig. 8 is a view of an asbestos-cored cable of 2,000,000 CM. It consists of 756 wires of #16 B&S annealed copper stranded around a $\frac{3}{4}$ -in. asbestos rope. There is little advantage to be gained from using this construction in sizes less than 2,000,000 CM. Both standard concentric stranded and annular cables must be fitted into suitable terminals for attachment to the furnace.

CONCLUSION

In this paper the writers have attempted to present certain data which have been accumulated over the past 15 years in designing, manufacturing, and operating self-supported, water-cooled furnace cables. Several patents have been granted as a result of this work. The authors do not contend, nor has experience shown, that this type of cable is to be preferred above all others for every installation. However, it is suggested that under certain conditions self-supported, water-cooled cables can be used to advantage.

The following characteristics have been mentioned:

- 1 The power factor of the furnace can be improved by the use of short, interlaced multiple bus circuits combined with short flexible connections between the bus system and the electrodes. High effective electrode travel and low electrical reactance can be achieved by the use of arched cables.

- 2 Further reductions in reactance can be achieved by maintaining these flexible cables in an upright arch so that the length of all associated connections can be reduced to a minimum.

3. Advantages are derived from supporting the cables in this manner because the cable is farther away from the heat of the furnace.

- 4 The need for any auxiliary supporting apparatus is eliminated by the use of self-supporting cables.

5. More space is available for furnace operations because fewer cables are required and because more space is available directly over the "melt."

These advantages can only be fully realized when the cables can be operated with a reasonable freedom from maintenance and when the operating life is at least comparable to that of bare flexible leads.

Development has now progressed to such an extent that the authors believe these conditions can be fulfilled. Several such installations are in use in Canada and others are contemplated in the future in Canada, the United States, and Europe.

ACKNOWLEDGMENTS

Credit is due to W. R. Tims, power cable design engineer of the Northern Electric Company, for

originating the idea of placing the spring strip at the center of the flexible lead as shown in the 4-segment-conductor design, Figure 5. The authors also wish to acknowledge the cooperation of other associates in the development of flexible leads suitable for electric furnaces.

Any discussion of this paper will appear in a Discussion Section, to be published in the December 1954 issue of the JOURNAL

Low-Temperature Electrolytes

Study of Some Physical Properties of the Calcium Halide-Water Systems over the Temperature Range of 25° to -60° C¹

FRED RAKOWSKY AND A. B. GARRETT

McPherson Chemical Laboratory, The Ohio State University, Columbus, Ohio

ABSTRACT

Data are given for electrical conductivity, freezing points, density, and viscosity of several solutions of calcium chloride, bromide, and iodide over the temperature range of 25° to -60°C. Halide solutions have the following eutectics: calcium chloride, -55°; calcium bromide, -83°; and calcium iodide, -77°C. The calcium iodide-water system has an incongruent melting point at -23.5°C. The electrical conductance-viscosity product shows considerable deviation from Walden's rule.

PURPOSE OF THE INVESTIGATION

The purpose of the investigation was to determine some of the physical properties of calcium halide-water systems over the temperature range 25° to -60°C. These systems show some promise as low-temperature electrolytes.

The phase diagram for the calcium chloride-water system has been determined by Rooseboom (1). Jones and Getman (2) have recorded some data on freezing points, electrical conductivities, refractive indices, and specific gravities of some dilute calcium halide solutions. No other data are available for these systems.

APPARATUS AND PROCEDURE

The constant-temperature cryostat used for density and viscosity measurements was similar to that of earlier work (3), except that the thermostat-bath medium was alcohol instead of air. Temperature was controlled within $\pm 0.2^\circ\text{C}$ over the entire temperature range.

Density, viscosity, and electrical conductivity measurements were made in the manner already described (3). Uncertainty of density values is less than ± 0.0002 g/ml. Uncertainty in relative viscosity values above -20°C is less than 0.5%; for lower temperatures (-20° to -60°C) uncertainty increases to about 3%.

Temperature readings were taken with a thermometer calibrated by a platinum resistance thermometer which was calibrated at the National Bureau of Standards.

The cryostat used for special conductivity measurements was similar to one previously used (3) except that the inner Pyrex tube was replaced by a 12-in. Pyrex test tube suspended in the Dewar after the desired temperature had been reached by add-

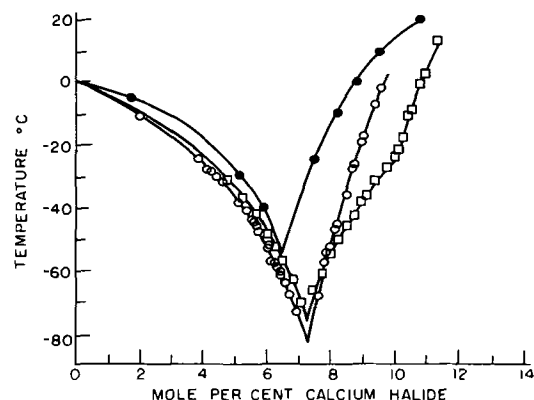


FIG. 1. Freezing points of calcium halide solutions. ●—CaCl₂-H₂O system (Rooseboom); ○—CaBr₂-H₂O system; □—CaI₂-H₂O system.

TABLE I. Melting points

Temp, °C	Mole %	Temp, °C	Mole %
Getman and Jones data		Data this investigation*	
Calcium bromide-water system			
-13.1	2.8	-14.5	2.8
-17.5	3.38	-17.7	3.38
-30.5	4.59	-31.0	4.59
-47	5.88	-49.0	5.88
Calcium iodide-water system			
-10	2.4	-11	2.4
-27	4.45	-28.0	4.45
-60	6.47	-56.5	6.47

* Data interpolated from Fig. 1.

ing dry ice to the bath liquid. A temperature control of $\pm 0.2^\circ\text{C}$ was easily maintained. Uncertainties in the measurements of conductivities are less than 0.1% above -20°C and less than 2% at -60°C .

Thermal analyses were made in the following

¹ Manuscript received August 13, 1953.

TABLE II. Density of calcium halide solutions

Temperature, °C	Density (g/ml)			
	Solutions of CaCl ₂			
	30.8 wt % 6.80 mole %	29.6 wt % 6.45 mole % (eutectic)	28.4 wt % 6.14 mole %	
25	1.2909	1.2784	1.2649	
20	1.2937	1.2808	1.2676	
0	1.3041	1.2909	1.2775	
-20	—	1.3011	1.2873	
-40	1.3261	1.3121	1.2971	
-60	Frozen	Frozen	Frozen	
Temperature, °C	Solutions of CaBr ₂			
	51.27 wt % 8.66 mole %	47.6 wt % 7.90 mole %	46.6 wt % 7.26 mole % (eutectic)	37.9 wt % 6.22 mole %
	25	1.6671	1.6191	1.5757
20	1.6715	1.6233	1.5787	1.5051
0	1.6870	1.6383	1.5937	1.5185
-20	1.7037	1.6542	1.6089	1.5325
-40	1.7213	1.6711	1.6255	1.5473
-60	1.7416	1.6900	1.6426	Frozen
Temperature, °C	Solutions of CaI ₂			
	57.4 wt % 8.31 mole %	56.6 wt % 8.21 mole %		
	25	1.9214	1.9114	
20	1.9259	1.9156		
0	1.9453	1.9350		
-20	1.9653	1.9546		
-40	1.9860	1.9752		
-60	—	1.9964		

apparatus contained in a clear glass Dewar filled with a dry ice-alcohol mixture: a 15-ml sample contained in a Pyrex test tube was partially insulated from the cooling bath by placing this test tube inside a larger test tube which gave a 0.3-cm air space between the two concentric test tubes. The outer tube was filled with enough ethanol so as just to touch the bottom of the inner tube. A spiral glass stirrer, driven by a variable speed motor, was provided. Freezing or melting points of solutions were determined by means of a calibrated toluene thermometer with one-degree centigrade divisions. Readings were accurate to within $\pm 0.5^\circ\text{C}$.

Materials

All salts were Baker and Adamson reagent quality. Solutions of calcium halides were standardized by calcium and halogen analysis according to procedures described by Pierce and Haenisch (4).

Standard solutions of sodium oxalate were made from National Bureau of Standards sodium oxalate. Solutions of potassium permanganate were standardized against National Bureau of Standards sodium oxalate.

TABLE III. Relative viscosity (relative to water at 25°C) of calcium halide solutions

Temperature, °C	Viscosity — $\eta = \frac{t_1 d_1}{t_2 d_2}$			
	Solutions of CaCl ₂			
	30.8 wt % 6.80 mole %	29.6 wt % 6.45 mole % (eutectic)	28.4 wt % 6.14 mole %	
25	3.150	2.928	2.765	
20	3.583	3.279	3.017	
0	6.072	5.527	5.087	
-20	12.42	11.47	10.25	
-40	35.04	31.09	27.91	
-60	Frozen	Frozen	Frozen	
Temperature, °C	Solutions of CaBr ₂			
	51.37 wt % 8.66 mole %	47.3 wt % 7.90 mole %	46.6 wt % 7.26 mole % (eutectic)	37.9 wt % 6.22 mole %
	25	4.667	3.490	2.950
20	5.180	3.888	3.309	2.478
0	8.738	6.425	5.341	4.001
-20	17.83	12.85	10.35	7.594
-40	50.94	34.62	27.11	19.18
-60	294.4	178.1	139.8	Frozen
Temperature, °C	Solutions of CaI ₂			
	57.4 wt % 8.31 mole %	56.6 wt % 8.21 mole %		
	25	4.142	4.092	
20	4.844	4.502		
0	7.428	7.300		
-20	14.65	13.84		
-40	37.72	34.83		
-60	163.2	151.1		

DISCUSSION

Data are shown in Tables I, II, III, and IV, and in Fig. 1.

Density-temperature relationships are linear for all three halides studied over the temperature range of -60° to 25°C . The density-concentration relationship for the calcium bromide-water system is linear over the range of 37.9–51.3 weight % calcium bromide.

Viscosity-temperature data of all three halide systems give the high increase at low temperature observed for many other salt solutions over this temperature range (3).

Electrical conductivity of all three halide systems at low temperature decreases to about 5 to 10 % of the values at room temperature.

Presumably because of their high concentration, these solutions show the expected deviations from Walden's rule (5) of the constancy of the conductance-viscosity product (over the temperature range studied).

Rooseboom (1) reports a eutectic temperature of

TABLE IV. Specific conductivity of calcium halide solutions

Temperature, °C	Specific conductivity (ohms ⁻¹ cm ⁻¹)			
	Solutions of CaCl ₂			
	30.8 wt % 6.80 mole %			28.4 wt % 6.14 mole %
25	0.1089			—
20	0.1027			0.1110
0	0.0750			0.0814
-20	0.0475			0.0524
-40	0.0214			0.0239
-60	0.0056			Frozen
Temperature, °C	Solutions of CaBr ₂			
	51.27 wt % 8.66 mole %	47.6 wt % 7.90 mole %	46.6 wt % 7.26 mole % (eutectic)	37.9 wt % 6.22 mole %
	25	—	—	—
20	0.1012	0.1129	0.1188	0.1275
0	0.0714	0.0819	0.0863	0.1275
-20	0.0413	0.0483	0.0536	0.0608
-40	0.0169	0.0223	0.0238	0.0303
-60	0.0035	0.0054	0.0065	0.0086
Temperature, °C	Solutions of CaI ₂			
	57.4 wt % 8.31 mole %			56.6 wt % 8.21 mole %
	20	0.0986		
0	0.0710			0.0718
-20	0.0431			0.0438
-40	0.0193			0.0198
-60	0.0053			0.0056

-55°C for calcium chloride-water (6.45 mole % salt). The calcium bromide-water system has a

eutectic at -83°C (7.26 mole % CaBr₂). This is the lowest of these three calcium halides (Fig. 1). The calcium iodide-water system has a eutectic at -77°C (7.25 mole % CaI₂) and an incongruent melting point at 23.5°C (9.95 mole % CaI₂) (Fig. 1). The solid phase, presumably a hydrate, was not identified. Iodide solutions decompose readily from air oxidation and must be protected with an inert atmosphere. Freezing point data of Getman (covering the range of 0 to approximately 6 mole %) are in good agreement with Rooseboom's data for calcium chloride and with the present data for calcium bromide and calcium iodide (see Table I).

A comparison of characteristics of these three halides indicated that calcium bromide has many desirable characteristics for a low-temperature electrolyte (6).

Any discussion of this paper will appear in a Discussion Section to be published in the December 1954 issue of the JOURNAL.

REFERENCES

1. H. W. B. ROOSEBOOM, *Z. physik. Chem.*, **4**, 31 (1889).
2. H. C. JONES AND F. H. GETMAN, *Z. physik. Chem.*, **49**, 385 (1904).
3. A. B. GARRETT AND S. WOODRUFF, *J. Phys. Chem.*, **55**, 477 (1951).
4. W. C. PIERCE AND E. L. HAENISCH, "Quantitative Analysis," pp. 300, 430, John Wiley and Sons, Inc., New York (1948).
5. O. WALDEN AND H. ULICH, *Z. physik. Chem.*, **107**, 219 (1923); H. ULICH, *Fortschr. Chem.*, **18**, 33 (1926).
6. A. B. GARRETT, J. WELSH, S. WOODRUFF, R. COPPER, AND J. HEIKS, *J. Phys. Chem.*, **53**, 505 (1949).

Radioactive Tracers in the Study of Pitting Corrosion on Aluminum

P. M. AZIZ²

Institute for the Study of Metals, University of Chicago, Chicago, Illinois

ABSTRACT

Radioactive cobalt and lead ions in solution have been used to study the distribution of local cathodes on aluminum alloy specimens which were actively pitting, and to study the processes of film breakdown and repair on aluminum alloy specimens after introducing them into a corrosive environment. In the study of pitting, radioactive ions were introduced into the solution after pitting of the sample had proceeded for a predetermined length of time. The tracer was then permitted to plate out onto local cathodes, and, after washing and drying, autoradiographs of the surface were prepared. Results indicate that after a pit is a few hours old it is surrounded by a ring of cathodic surface and outside this is an annular ring of passive surface which prevents lateral expansion of the corrosive attack, the remainder of the surface being cathodic. In the study of the mechanism of film breakdown and repair, samples with different surface treatments were placed in the solution and radioactive ions were introduced after various predetermined times, exchange permitted to take place, samples washed and dried, and autoradiographs prepared of the surface. Results indicate that, on contact with the solution, the surface oxide film breaks down and is then repaired by reaction with the solution.

INTRODUCTION

Passive metals, such as aluminum and its alloys, and the stainless steels are very slowly attacked even in the presence of oxygen by such media as natural waters and dilute solutions of fruit acids. The attack may be localized in the form of pits which can perforate thin sheet with potentially serious consequences.

Several investigations have been carried out on the nature of pitting corrosion, but these studies have dealt with either the electrochemical nature of the attack (1, 2), or phenomena such as the probability of pitting (3, 4), and have not been directly concerned with the reason for the localization of the attack. However, qualitative views concerning the cause of this localization are held, and it is generally thought to be due to an isolated breakdown in the protective oxide film leading to localized attack of the metal. If this is the case, local cathodes must be confined to an area near the pit mouth since most of the surface remains covered with an inert oxide film. Hence, if distribution of the cathodic elements on the surface of a pitting metal is determined, a clue to the mechanism of the localization may be obtained.

If the ion of a metal, more electropositive than

the corroding metal, is introduced into the solution, it will plate out electrochemically on the local cathodes, and a determination of distribution of the plated material will give the location of cathode elements. Radioactive tracers of heavy metals such as lead and cobalt are ideally suited for this application since they can be detected in trace amounts by means of the radiation which they emit and, hence, they may be introduced into the corrosive environment in only slight concentration, thereby reducing danger of altering the cathode distribution by the process of measurement. Radioactive isotopes have been used previously in the study of corrosion mechanisms (5, 6), and references can be made to the excellent review by Simnad (7) of literature dealing with the use of radioisotopes in the study of metal surface reactions in solution. None of these studies has dealt with the distribution of cathode elements on a pitting surface; the present work is concerned with the study of this distribution on pitting aluminum surfaces, using radioactive isotopes of the heavy metals, lead and cobalt, and its effect on the distribution of corrosion. Distribution was determined by preparing autoradiographs of metal specimens after exchange of the corroding surface with the radioisotope.

EXPERIMENTAL

Materials

The metal used in this investigation was "Super Purity" aluminum, (99.99% Al) alloyed with

¹ Manuscript received April 27, 1953. This paper was prepared for delivery before the Wrightsville Beach Meeting, September 13 to 16, 1953.

² Present address: % Aluminium Laboratories Limited, Box 84, Kingston, Ontario, Canada.

0.5% iron and 0.3% silicon. The finished metal was supplied in the form of cold rolled sheet 0.064 in. thick.

The radioactive isotopes used were Co^{60} and Pb^{210} in the form of chloride solutions in distilled water. The activity of the solutions was 1 microcurie per 0.1 ml of solution and the total cation concentration was 1 ppm.

Autoradiographs were prepared on Kodak no-screen x-ray film. Precautions recommended by Yagoda (8) for the prevention of spurious results were observed.

Chicago tap water was the corrosive medium used in all the work described herein. This is a moderately hard water with hardness reported as CaCO_3 of 140 ppm. It is filtered and chlorinated to a free chlorine content of 0.14 lb per million gallons of water.

Procedure

Metal samples, in the form of one-inch squares of sheet, were annealed one-half hour at 350°C and furnace cooled. They were then etched in 85% orthophosphoric acid at 70°C for two minutes and washed in six changes of tap water. Washing in tap water was necessary since it was found that using distilled water passivated the surface and no exchange with the tracer took place. Following this treatment, three types of experiment were carried out.

1. Samples were immediately transferred to a 200-ml crystallizing dish containing 150 ml of water, and pitting was permitted to proceed for the desired length of time. On these small samples it was found that pitting did not initiate spontaneously on all samples, and it was necessary to initiate pits artificially so by touching the point of a dissecting needle to the surface of the metal. Comparison of natural with artificially initiated pits showed no difference in their cathode structures, and artificial initiation was used throughout. After pitting had proceeded for the desired length of time, the sample was removed from the water in a horizontal position and 0.1 ml of the solution of radioactive tracer introduced into the film of water retained on the surface of the specimen. Exchange took place for ten minutes, the sample was washed with distilled water, dried with alcohol, and an autoradiograph prepared of the surface. The autoradiographic exposure employed was $1\frac{1}{2}$ hours, with one exception, which will be noted in the proper context. Distribution of local cathodes on the surfaces of samples, which had pitted for time periods of from 6 hours to 14 days, was examined in this manner using both Co^{60} and Pb^{210} .

2. Coarse-grained samples were etched, washed, and exposed to water for 24 hours, exchanged with Co^{60} , and autoradiographs prepared of the

surface to determine whether crystal structure had any effect on the distribution of local cathodes.

3. Two series of nine samples each were etched and washed as previously described, and one set was immediately placed in tap water, while the other set was permitted to oxidize in air for 24 hours and was then placed in the water. Samples were then removed from the water after the following periods of immersion: 30 sec, 5 min, 10 min, 20 min, 40 min, 90 min, 120 min, 3 hr, 24 hr. They were permitted to exchange with Co^{60} and autoradiographs prepared as described in section 1.

This series of experiments was designed to determine how the oxide film forms on a stripped active surface on immersion in a corrosive medium, and what happens to a protective oxide film on immersion in a corrosive medium.

RESULTS AND DISCUSSION

1. Fig. 1 shows autoradiographs of pits exchanged with Pb^{210} after pitting for six hours to fourteen days, while Fig. 2 shows autoradiographs of pits in

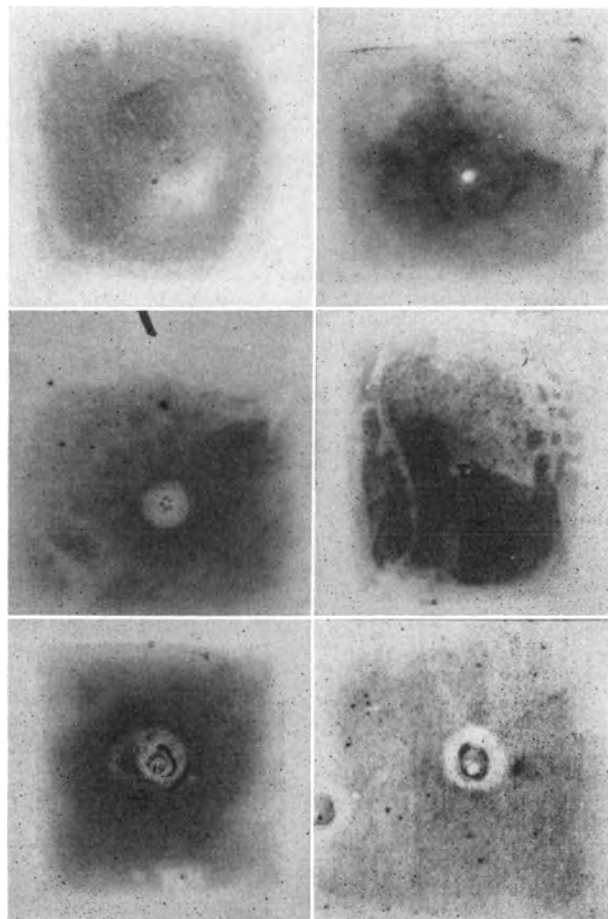


FIG. 1. Autoradiographs of pits of indicated age exchanged with Pb^{210} . Top left—6 hours old; top right—24 hours old; center left—3 days old; center right—5 days old; bottom left—7 days old; bottom right—14 days old.

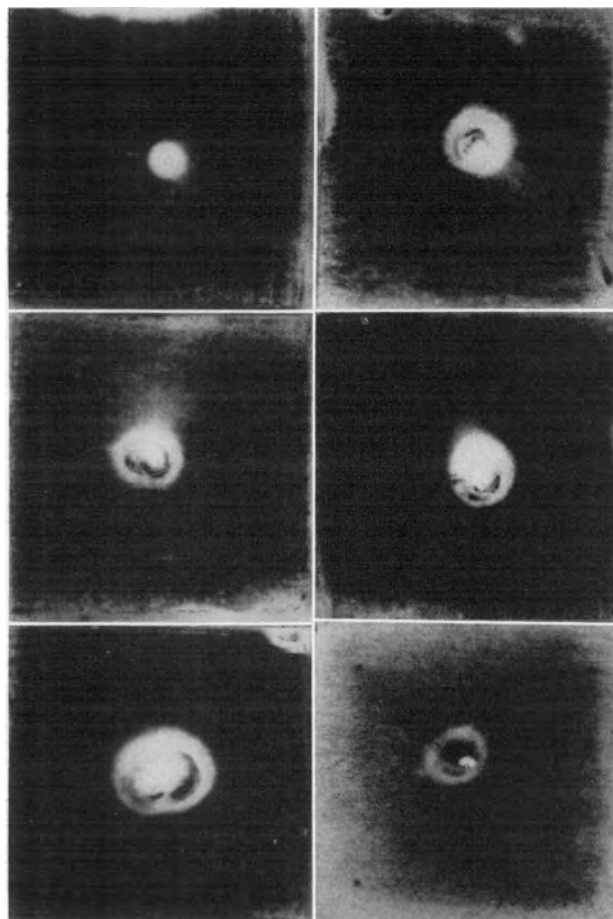


FIG. 2. Autoradiographs of pits of indicated age exchanged with Co^{60} . Top left—6 hours old; top right—24 hours old; center left—3 days old; center right—5 days old; bottom left—7 days old; bottom right—14 days old.

the same alloy and under the same conditions as Fig. 1 but exchanged with Co^{60} . Local cathode distribution is shown up in greater detail with the Pb^{210} than with the Co^{60} , but the general pattern obtained is the same with both radioisotopes. It was not found possible to detect any correlation between distribution of local cathodes on the surface and any detectable feature of the structure of the underlying metal.

The mouth of the pit is surrounded by an annular ring of cathodic surface, and about this is a ring of inert surface, neither anode nor cathode. The remainder of the surface is cathodic, since deposition of radioactive tracer had taken place over it. As shown by the Pb^{210} this distribution becomes more sharply defined as the pit grows older. Use of Co^{60} brings out this distribution at a much earlier pit age.

Microscopic examination of the inert area about the mouth of the pit showed that it was covered with a thick film, presumably of hydrated aluminum oxide. Fig. 3 is a photomicrograph taken in this

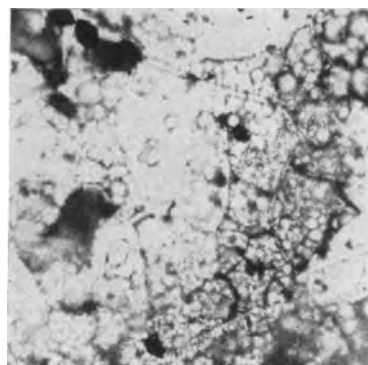


FIG. 3. Photomicrograph of inert area of 7-day old pit in Fig. 1.

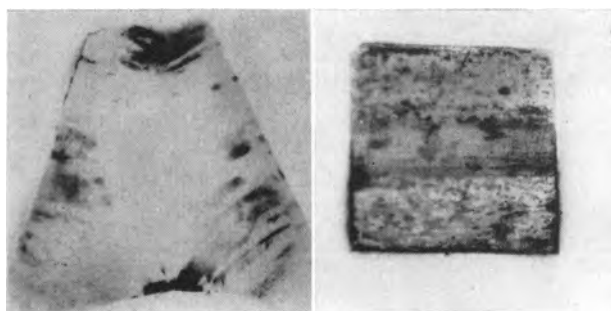


FIG. 4. Autoradiograph of coarse-grained aluminum, corroded, exchanged with Co^{60} . Left—ingot; right—sheet.

inert area of the sample from which the seven day old pit in Fig. 1 was prepared.

2. Specimens from which the autoradiographs of Fig. 4 were prepared were cut from a large-grained ingot and a sheet of high purity aluminum, respectively. The latter possessed a banded texture and the autoradiographs followed the general pattern of the crystal structure.

3. Fig. 5 shows autoradiographs prepared from phosphoric acid etched samples exposed to water for periods of 30 sec to 24 hr, while Fig. 6 shows autoradiographs prepared from samples which were oxidized in air previous to exposure in the water. The normal autoradiographic exposure of $1\frac{1}{2}$ hr gave negative results with the etched sample which had been immersed in water 24 hr (Fig. 5) and this autoradiograph was given a 24-hr exposure.

With both methods of preparation, etching and etching with subsequent air oxidation, the surface is highly reactive on initial immersion in the water and exchanges extensively with the radioactive ion but, as the period of exposure increases, activity decreases and after 24 hr the surface is passive. Because of a lack of reproducibility of behavior from sample to sample, the sequence of changes is not clear cut, but this general trend has been verified with experiments on a large number of specimens. It is interesting that the thin air-formed oxide film is not protective when the sample is immersed in

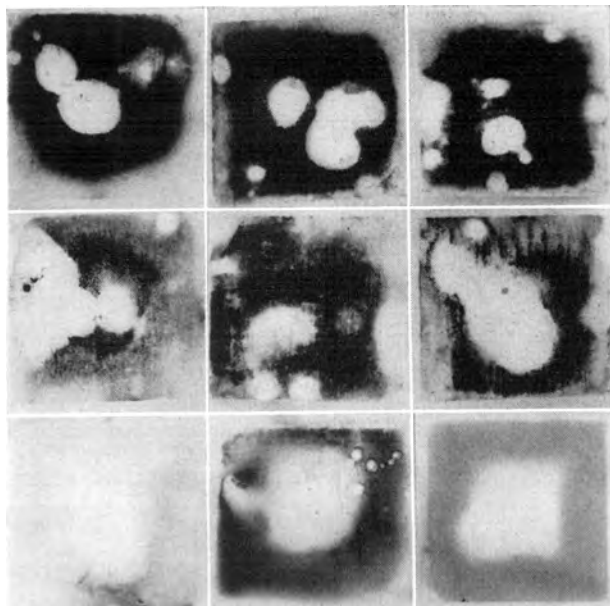


FIG. 5. Cobalt⁶⁰ autoradiographs of samples etched and exposed to water for the times shown. Top left—30 sec; top center—5 min; top right—10 min; center left—20 min; center center—40 min; center right—90 min; bottom left—120 min; bottom center—3 hours; bottom right—24 hours.

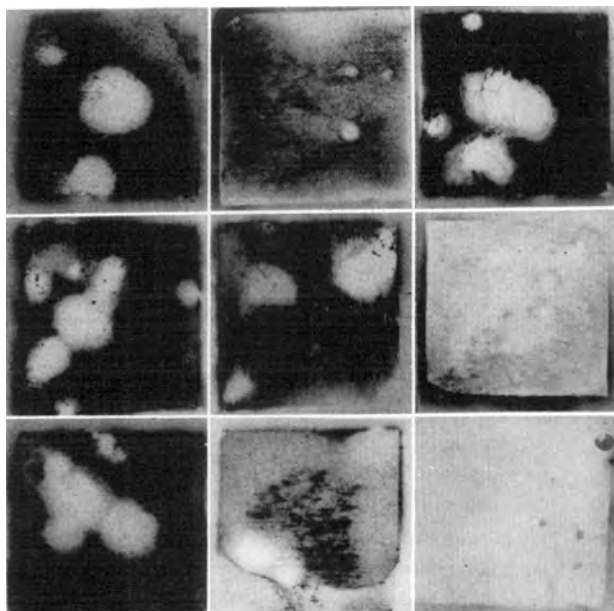


FIG. 6. Cobalt⁶⁰ autoradiographs of samples, etched, air-oxidized, and exposed to water for times shown. Top left—30 sec; top center—5 min; top right—10 min; center left—20 min; center center—40 min; center right—90 min; bottom left—120 min; bottom center—3 hr; bottom right—24 hr.

the water, but either breaks down and then repairs itself by reaction with the corrosive medium, or else is so thin that it permits the passage of electrical current and allows some corrosion to take place. A previous publication (9) has dealt with a probable mechanism of pitting corrosion in aluminum and

this may be amplified here in view of the present findings. In addition, Edeleanu and Evans (10) discuss a view of pitting corrosion which is in essential agreement with the present work.

When the specimen is immersed in the water any air-formed film present on its surface breaks down and general corrosion ensues, with anodic and cathodic reactions taking place at neighboring sites over the surface. These reactions result in the formation of alkali at the cathodes and in the passage of aluminum into solution at the anodes as aluminum ions. These aluminum ions hydrolyze, forming alumina with a resultant decrease in the pH of the solution. In time, the alkaline cathodic products of reaction and the acid products of reaction intermingle as a result of diffusion and convection; the pH of the anodic solution rises and when the solubility product of the alumina is exceeded it precipitates from solution. If the alumina is precipitated as an adherent protective film on the surface of the metal, corrosion reaction is stifled and the metal becomes passive as shown by the 24-hr autoradiographs of Fig. 5 and 6. However, if the surface is incompletely covered, the anodic and cathodic reactions are separated, precipitation of a film then takes place in the area between them, the anodic attack is localized, and a pit forms. As Fig. 1 shows, the configuration of local cathodes and of the passive localizing film about the anode take up circular symmetry, and in a sense the localization of the attack becomes autocatalytic.

ACKNOWLEDGMENTS

The author wishes to thank Professors C. S. Smith, N. H. Nachtrieb, G. V. Raynor, and C. S. Barrett for valuable discussion during the course of this work, and Aluminium Laboratories Limited for arrangements that made it possible to carry out this work at the Institute for the Study of Metals, University of Chicago.

Any discussion of this paper will appear in a Discussion Section to be published in the December 1954 issue of the JOURNAL.

REFERENCES

1. R. B. MEARS AND R. H. BROWN, *Trans. Electrochem. Soc.*, **74**, 519 (1938).
2. R. B. MEARS AND R. H. BROWN, *ibid.*, **81**, 455 (1942).
3. R. B. MEARS AND R. H. BROWN, *Ind. Eng. Chem.*, **29**, 1087 (1937).
4. P. M. AZIZ AND H. P. GODARD, *ibid.*, **44**, 1791 (1952).
5. M. T. SIMNAD, *This Journal*, **98**, 301 (1951).
6. M. T. SIMNAD, *Rev. met.*, **48**, 1 (1951).
7. M. T. SIMNAD, Institute of Metals Monograph, No. 13 (in course of publication).
8. H. YAGODA, "Radioactive Measurements with Nuclear Emulsions," John Wiley and Sons, Inc., New York (1949).
9. P. M. AZIZ, *Corrosion*, **9**, 3 (1953).
10. C. EDELEANU AND U. R. EVANS, *Trans. Faraday Soc.*, **47**, 1121 (1951).

The Mechanism of Metallographic Etching

I. The Reaction Potentials of a Two-Phase Brass in Various Etching Reagents¹

GEORGE L. KEHL AND MAX METLAY²

School of Mines, Columbia University, New York, New York

ABSTRACT

Potentials generated by reaction of portions of small, single grains of each of the two phases of alpha-beta brass with various etching solutions have been measured. The potential of beta phase is consistently 0.01 to 0.03 volt more anodic than that of the alpha phase in the same reagent.

INTRODUCTION

Preparation of metallic specimens for metallographic examination involves use of well-established polishing and etching techniques (1). Innumerable etching reagents described in the literature have all been evolved through methods of trial and error, since the existing understanding of mechanisms of etching processes is not sufficiently precise to permit prediction of appropriate compositions. Inasmuch as metallographic etching in the usual sense consists of reaction between a polished metal surface and a liquid reagent resulting in alteration of the polished surface, the process is essentially one of controlled corrosion, and knowledge provided by the extensive literature of corrosion research (2, 3) gives a rational clue to mechanisms of etching. However, details must still be determined, and this communication is the first of a series dealing with these details.

Corrosion (and hence etching) proceeds by electrolytic action attending structural differences that exist on the specimen surface. Some discrete surface portions are anodic to others and, in consequence, suffer dissolution electrolytically under appropriate circumstances. In pure metals and in single phase alloys an electrolytic potential (polarized) is established between grains of different orientation, between the matrix and tramp secondary phases, between grain boundaries and grains proper, and along concentration gradients in heterogeneous single phase alloys. In multiple phase alloys there exists in addition a sharp difference in composition between structural phases.

To determine the influence of surface structure variations on electrolytic reactivity during etching, potential generated during the process is measured at the various types of sites described. In this research an alpha-beta brass of appropriate composi-

tion is used as the material of interest, and potentials of each phase measured independently during etching in a variety of conventional etching reagents. In principle this is accomplished by isolating a portion of one phase on the surface of a metallographic specimen, and protecting the remaining surface from the etching reagent by a covering of insulating resin. The exposed surface portion is allowed to react with the etching reagent, and the potential generated is measured with respect to a saturated calomel cell. By making a large number of independent measurements on each phase during etching, average relative potentials of the two phases during reaction can be determined. Potential so measured is essentially the polarized potential attending local anodes and cathodes existing on the isolated surface area. Since metallographic etching generally takes place within a period of a few seconds to a few minutes, potentials at short times are of greatest interest. These are best obtained by use of a rapid recording potentiometer.

EXPERIMENTAL

Specimens

The metal used in this study is a commercial alpha-beta brass, or Muntz metal, of composition 60.75% copper, 38.55% zinc, remainder manganese, iron, silicon, and lead. Specimens were heated to 855°C for 15 min in argon and furnace cooled to enlarge grain size and to provide a nearly equilibrium structure.

Specimens are mounted in Bakelite by standard metallographic mounting methods. Both ends of a cylindrical mount are ground flat until the specimen is exposed. One side of the specimen is drilled and tapped; the other is ground and polished for metallographic examination. The specimen is very slightly relief-polished to reveal the structure, then coated with resin as described below. Mechanical support for the specimen, which also serves as the electrical contact, consists of a $\frac{3}{8}$ in. diameter brass rod ap-

¹ Manuscript received August 3, 1953.

² Present Address: Department of Chemistry, Harpur College, State University of New York, Endicott, New York.

appropriately threaded to fit into the tapped hole in the specimen.

Coating Technique

In order to make emf measurements on each phase, it is necessary to coat the entire specimen surface with a protective coating, except a portion of that phase whose potential is to be measured.

A previous method (4) for achieving this consisted of creating a hole with a specially shaped needle in a covering film of ethylcellulose applied to the specimen surface. This method has the disadvantage that the metal surface thus exposed may be cold worked to a degree significant with respect to subsequent potential measurements.

Two resin formulations have been used in these experiments, formulation No. I based on Epon resin 1001, and formulation No. II based on Vinylite resin VMCH. Formulation No. I has the advantage that it is extremely resistant chemically, and the disadvantage that it must be allowed to set overnight and that the minimum area left exposed is slightly larger than with formulation No. II. The latter formulation has the advantage of setting within an hour of coating, but is not quite as resistant chemically as No. I, and thus is not always successful in protecting the specimen, especially in longer runs. Results given in this communication were obtained with No. I, while No. II was used in subsequent experiments to be reported.

Formulation No. I.—Stock solution: Epon 1001³ or Devran 65⁴—6 parts by weight; acetone—1 part; toluene—1 part. Catalyst solution: diethylene triamine—10%; acetone—45%; toluene—45%.

Just before use, one part of catalyst solution is thoroughly mixed with two parts resin solution. This coating must be allowed to set overnight. It can be removed by soaking in acetone, then scraping with a dull instrument.

Formulation No. II.—Vinylite resin VMCH⁵ is mixed with a small amount of cyclohexanone. A little acetone is added until viscosity and flow properties of the mixture are adjudged satisfactory. This coating will set in about one hour, and can be removed by swabbing with acetone.

Either resin formulation is applied by placing a few drops on the Bakelite mount around the specimen edges and it is subsequently distributed over the surface by means of a spade-like tool actuated by a micromanipulator. A piece of Saran tubing cut to an appropriate shape and attached to an applicator

³ Product of the Shell Chemical Company.

⁴ Product of the Devco Reynolds Company.

⁵ Product of the Bakelite Division, Union Carbide and Carbon Corporation.

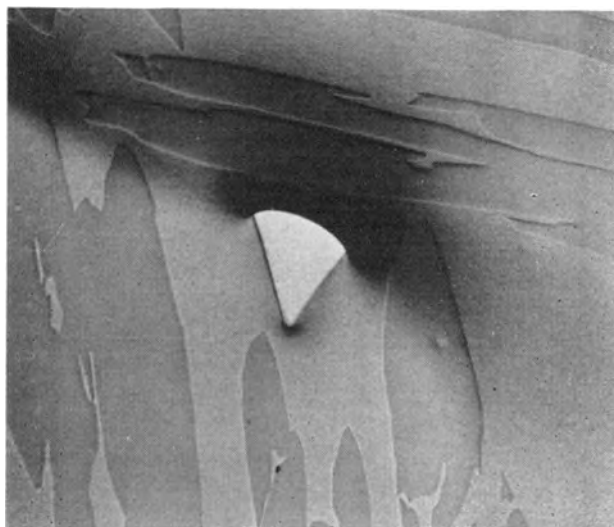


FIG. 1. Surface of alpha-beta brass as coated with resin except for an isolated portion of the beta phase (triangular area). Exposed area unetched. 150X.

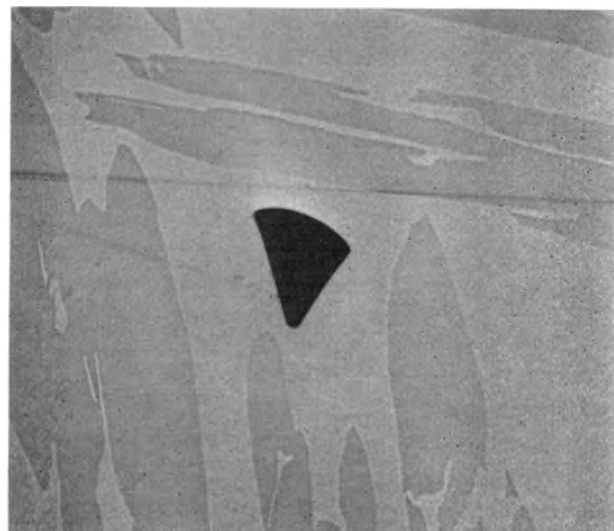


FIG. 2. Same as Fig. 1, except exposed area of beta phase is etched and the resin coating removed. 150X.

stick has been found convenient to serve as the distributing tool. During coating the specimen is observed by means of a low power microscope, so that the area to be left exposed can be kept free of resin, and the remainder of the sample can be thoroughly covered. A typical example of a coated specimen is shown in Fig. 1. The same specimen, after etching and removal of the resin coating, is shown in Fig. 2.

Apparatus

The electrical system used to measure electrode potentials consists of a Leeds and Northrup Type K-2 potentiometer with a Speedomax recording potentiometer connected across its galvanometer

leads. This system allows potential to be read as the sum of potentials indicated by the Type K-2 potentiometer and by the recorder. Therefore, the potentiometer is kept adjusted to supply a voltage within 50 millivolts of the reaction cell, so that the resultant emf remains within the recorder range. The recorder has a full scale travel time of two seconds, and is actuated at about 50 microvolts unbalance, with current drain of about 7×10^{-9} amp. This small order of current drain does not appreciably polarize the electrodes of the system, but if the emf is changing rapidly as it does at onset of the reaction, some external polarization undoubtedly takes place.

A saturated calomel cell is employed as the standard reference electrode. The design is conventional, except that a fritted glass disk of fine porosity separates the saturated KCl from the etching reagent.

Reagents

The reagents used in this study were in general the common etching reagents for brass (1):

[1] Ferric chloride reagent No. 1: 1 part FeCl_3 , 10 parts conc. HCl, 113 parts H_2O ; [2] ferric chloride reagent No. 2: 1 part FeCl_3 , 10 parts conc. HCl, 20 parts H_2O ; [3] ferric chloride reagent No. 3: 1 part FeCl_3 , 1 part conc. HCl, 4 parts H_2O ; [4] ammonium hydroxide—hydrogen peroxide reagent: 1 part conc. NH_4OH , 1 part 3% H_2O_2 , 1 part H_2O ; [5] copper ammonium chloride reagent: 10% copper ammonium chloride in water, plus NH_4OH to basicity; [6] ammonium persulfate reagent: 10% $(\text{NH}_4)_2\text{S}_2\text{O}_8$ in water; [7] ammonium persulfate—ammonium hydroxide reagent: 1.25 g $(\text{NH}_4)_2\text{S}_2\text{O}_8$, 25 cc conc. NH_4OH , 75 cc H_2O ; [8] ammonium hydroxide reagent: 1 part conc. NH_4OH , 2 parts H_2O ; [9] chromic acid reagent—10% CrO_3 in water, plus one drop

conc. HCl for each 25 cc reagent, added immediately before use.

Measurements

The reaction cell containing the etching reagent and the calomel cell are immersed in a thermostatically controlled water bath at 25°C . The fritted disk is immersed in the reagent one or two minutes

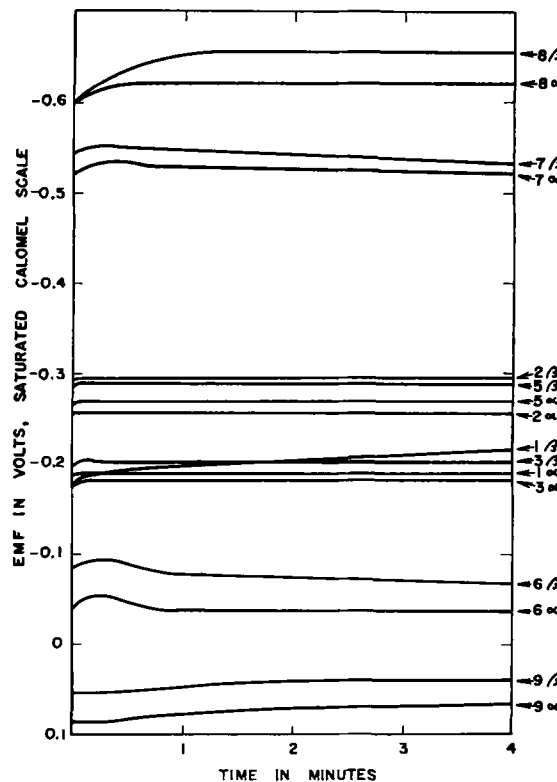


FIG. 3. Emf of isolated areas of alpha or beta brass on saturated calomel scale vs. time. Each curve is identified by number of the reagent, as listed in text, and by the phase exposed to reagent.

TABLE I. Potentials of isolated alpha and beta phases in 60-40 brass in various etching reagents, in reference to a saturated calomel electrode of 25°C

Reagent ^a	Range in potential, v		Usual potential spread in a single run, v		Average potential, v	
	Alpha	Beta	Alpha	Beta	Alpha	Beta
1. FeCl_3 No. 1 ^b	-0.17 to -0.20	-0.17 to -0.20	0.005	0.05 to 0.1	-0.185	-0.19 to -0.21
2. FeCl_3 No. 2.....	-0.245 to -0.265	-0.282 to -0.295	0.002 to 0.01	0.005	-0.256	-0.293
3. FeCl_3 No. 3.....	-0.175 to -0.193	-0.20 to -0.29	0.005	0.005	-0.180	-0.20
4. $\text{NH}_4\text{OH-H}_2\text{O}_2^c$	-0.41 to -0.45	-0.45 to -0.48				
5. $\text{Cu}(\text{NH}_4)_2\text{Cl}_4$	-0.26 to -0.27	-0.28 to -0.29	0.002	0.002	-0.267	-0.288
6. $(\text{NH}_4)_2\text{S}_2\text{O}_8$	-0.04 to -0.08	-0.07 to -0.11	0.01 to 0.03	0.03	-0.06	-0.08
7. $(\text{NH}_4)_2\text{S}_2\text{O}_8\text{-NH}_4\text{OH}$	-0.50 to -0.53	-0.54 to -0.55	0.01 to 0.03	0.01 to 0.03	-0.53	-0.545
8. NH_4OH	-0.62	-0.64 to -0.68			-0.62	-0.65
9. CrO_3	0.080 to 0.098	0.033 to 0.068	0.005 to 0.015	0.005 to 0.015	0.094	0.048

^a Reagents are described more fully in the text.

^b The potential for beta brass in this reagent rose gradually with time. Average potentials given indicate the range of the start of the runs. After about 10 min., the potential is about -0.25 to -0.27 volt.

^c $\text{NH}_4\text{OH-H}_2\text{O}_2$ reagent gave very erratic results due to rapid formation of gas bubbles on the metal surface. Potentials varied rapidly and erratically over 50 to 100 mv, and more. Values given may be considered an informed guess.

before the specimen is to be immersed. The potentiometer is set at some emf value, determined approximately by an initial trial, electrical connections are made, and the mounted specimen is immersed in etching reagent. Care is taken that the top of the mount and the supporting rod remain out of contact with the reagent. The potential difference between specimen and calomel cell is then recorded by the Speedomax recorder. When it appears that the potential is changing so that it will no longer be within the recorder range, the potentiometer slide wire is reset to keep recorded potential within the instrument's range. True measured potential is then the sum of the potentiometer setting and the potential indicated by the recorder.

RESULTS

A summary of results of potential measurements is given in Table I. For each reagent, the following information is given for each phase: (a) range of potential (with respect to saturated calomel) in volts, over all runs; (b) usual variation of potential in a single run; and (c) probable value of the potential in volts.

Fig. 3 shows variation of potential with time for several representative experiments with various etching reagents. Each curve is identified by the reagent number, as in the description above, and by the phase exposed.

DISCUSSION

It can be seen from inspection of Table I that an appreciable difference exists between reaction potentials of alpha and beta phases, generally in the range of 0.01 to 0.03 volt, with beta always anodic to alpha. Since the beta phase is rich in zinc compared to the alpha, this behavior can reasonably be expected. The consistent small difference in emf seems to indicate, at least for the system under consideration, that if the phases were to be coupled, etching would proceed in part by galvanic action with the beta phase anodic to the alpha phase. Data supporting this statement will be included in a forthcoming communication relative to closed circuit potential measurements between the two phases.

An attempt to obtain data of the same kind for other systems showed that the magnitude of potential difference between anode and cathode depends, among other factors, on the dissimilarity of electrodes, as expected. At one extreme, that is, using similar electrodes, some attempts were made to determine reaction potentials of grain centers and grain boundaries of a small-grained single phase 90-10 alpha brass in ferric chloride reagent No. 1. Here etching is characterized by preferential dissolution at grain boundary regions.

Experiments indicate that grain boundaries are anodic to the grains proper, although techniques were

not sufficiently sensitive to determine the difference with any accuracy. However, for other metals, it has been shown in several cases that grain boundaries are anodic to grain centers; for example, high purity (99.986%) aluminum in 20% HCl (5), 70-30 brass in 1% NH₄OH (6).

At the other extreme, potential measurements were made on an alloy possessing phases greatly dissimilar. Cadmium and bismuth are practically insoluble in each other in the solid state, and, as a consequence, alloys of this system consist essentially of two pure-metal phases. These alloys can be etched by means of a reagent consisting of one part I₂, three parts KI, and ten parts H₂O. This reagent preferentially attacks and darkens the cadmium phase. Measurements on selected compositions indicated the bismuth phase to have a potential of -0.09 ± 0.02 volt with respect to a saturated calomel electrode, while the corresponding potential for cadmium was -0.825 ± 0.001 volt, cadmium therefore being 0.735 volt anodic to bismuth.

All etching reagents employed in etching of alpha-beta brass, with the exception of ammonium hydroxide-hydrogen peroxide (reagent No. 4), have the characteristic of attacking the beta phase preferentially and darkening it metallographically relative to the alpha phase. As noted in Table I, emf values given for the ammonium hydroxide-hydrogen peroxide reagent can be considered only an informed guess, since there was a wide, rapid, and erratic variation of recorded potential, undoubtedly due to formation of oxygen bubbles on the metal surface. It is unfortunate that this situation exists, since it would be interesting to compare emf values in reagents which have opposite etching effects on the same alloy.

ACKNOWLEDGMENTS

This research was made possible through support of the Atomic Energy Commission under Contract AT-(30-1)-1006.

The assistance of Dr. Erica Wasilewski and of Mr. Arthur Bauer with the experimental work is gratefully acknowledged.

Any discussion of this paper will appear in a Discussion Section, to be published in the December 1954 issue of the JOURNAL.

REFERENCES

1. G. L. KEHL, "Principles of Metallographic Laboratory Practice," McGraw-Hill Book Co., Inc., New York (1949).
2. H. H. UHLIG, Editor, "Corrosion Handbook," John Wiley & Sons, Inc., New York (1948).
3. R. B. MEARS, *This Journal*, **97**, 316 (1950).
4. L. W. SMITH AND V. J. PINGEL, *ibid.*, **98**, 48 (1951).
5. E. H. DIX, JR., *Trans. Am. Inst. Mining Met. Engrs.*, **137**, 21 (1940).
6. R. B. MEARS AND R. H. BROWN, *Ind. Eng. Chem.*, **33**, 1001 (1941).

The Kinetics of Oxidation of High Purity Nickel¹

E. A. GULBRANSEN AND K. F. ANDREW

Westinghouse Research Laboratories, East Pittsburgh, Pennsylvania

ABSTRACT

The effect of time, temperature, and surface pretreatment on rate of oxidation of high purity nickel is studied for the temperature range of 400°–750°C using a vacuum microbalance technique. The data are compared to previous studies in the literature and with other metals. Oxidation data are interpreted in terms of the parabolic rate law and classical theory of diffusion.

Large deviations from the parabolic rate law are found to occur during the initial stages of reaction and smaller deviations over long periods of time, especially at low temperatures. However, reasonable values of heat and entropy of activation for the over-all reaction can be calculated; these are 41,200 cal/mole and –6.0 entropy units (eu), respectively. Parabolic rate law constants over the temperature range of 550°–700°C are given by

$$A = 3.8 \times 10^{-4} e^{-41,200/RT} \text{ cm}^2/\text{sec.}$$

The negative value for entropy of activation for the over-all reaction when corrected for entropy of formation of the vacancies leads to a value of 1.5 for entropy of activation for diffusion. Theoretical considerations suggest that the latter term should have a value of 1.7–3.3 eu. The good agreement between theoretical and experimental entropies of activation suggests that diffusion is occurring largely through the lattice of nickel oxide and not at grain boundaries, at least for the temperature and time region over which analyses were made.

A comparison of present data with older studies in the literature shows a large variation in parabolic rate law constants. These variations are interpreted in terms of impurities increasing the concentration of nickel ion vacancies.

INTRODUCTION

The work reported in this paper is part of a larger study on the mechanism of oxidation of nickel-chromium and nickel-chromium-iron alloys at high temperatures. To interpret oxidation of practical metals containing impurities and alloys, it is necessary to have detailed knowledge of rates of oxidation of high purity metals. Several studies have already been reported (1–5).

A number of studies have been made on oxidation of nickel of widely varying purity at temperatures above 600°C (6–8). These results were summarized in a paper by Kubaschewsky and Goldbeck (9) and correlated with their own measurements. This study shows variations of 100 in values found for the parabolic rate law constant at a given temperature.

Using a volumetric method, Moore (10) studied oxidation of 99.9% pure nickel over the temperature range of 400°–900°C. The parabolic rate law was found to represent the data, with the rate constant being given as

$$A = 3.09 \times 10^{-5} e^{-38,400/RT} \text{ cm}^2 \text{ sec}^{-1}.$$

Moore's values for A differ from those summarized

by Kubaschewsky and Goldbeck (9) by a factor of 20 to 2000.

In a recent work, Campbell and Thomas (11) found that time dependence of the oxidation rate of nickel in the temperature range up to 302°C could be fitted by a logarithmic rate law. Deviations from a parabolic rate law were explained on the basis of a space charge set up in very thin films.

A comparison of the various studies (9, 10) suggests a strong influence of alloying elements, impurities, and contaminants in the gas atmosphere. The fact that other surface reactions of nickel are difficult to reproduce in both liquid (12) and gaseous media is probably related to these same factors.

Evidence exists to show that certain alloying elements affect the rate of oxidation of nickel. Wagner and Zimens (6) have shown that the parabolic rate law constant of nickel is increased by addition of chromium and manganese. According to Horn (13), the oxidation rate constant for a 6% chromium-nickel alloy is increased by a factor of 16. Increase in rate is explained on the basis of an increase in number of nickel ion vacancies. Above 6%, the rate of reaction is found to decrease.

Lithium, on the other hand, is found to decrease the oxidation rate constant. This is reported by Hauffe and Pfeiffer (14) in a study of effect of Li_2O in vapor state on rate of oxidation in air. Other

¹ Manuscript received November 3, 1952. This paper was prepared for delivery before the Montreal Meeting, October 26 to 30, 1952.

elements, as impurities or in the gas atmosphere, will have their characteristic effects depending upon their charge, size of ion, electronegativity, and solubility.

Alloying elements and impurities in the metal or atmosphere may have an additional effect on the course of oxidation. Thus, if impurity or alloying element concentration changes during the reaction, and if vacancies of nickel ions in oxide are sensitive to the particular impurity, the parabolic rate law constant will change during the experiment. Wagner and Zimens (6) found in a study of nickel at 1000°C that the parabolic rate law constant decreased as the oxidation progressed.

The oxide formed on nickel over the temperature range of 300°–700°C was studied by Gulbransen and Hickman (15) and found to be NiO. Wyckoff (16) gives the structure of NiO as a unimolecular rhombohedron with $a_0 = 2.9459 \text{ \AA}$. Rooksby (17) found NiO to be rhombohedral at 18° and face-centered cubic at 275°C, with $a_0 = 4.1946$.

Nickel forms the stable oxide NiO in the temperature range of this work. Thermodynamic calculations show that at 1000°C the decomposition pressure of oxygen over nickel oxide and nickel is 10^{-11} atmospheres. The surface oxide, however, is readily reduced by hydrogen from a thermodynamic point of view at temperatures of 400° to 1000°C.

The purpose of this work is (a) to determine the time and temperature dependence of the rate of oxidation and how these values are affected by pretreatment and initial oxide formation, (b) to evaluate from this information the heat, entropy, and free energy of activation of the rate-determining process and to compare these values with other metals and alloys, and (c) to point out physical and chemical factors in the oxide and metal affecting the mechanism of reaction.

APPARATUS AND METHOD

All of the kinetic measurements were made using the vacuum microbalance and associated equipment (18, 19). The sensitivity of the balance was 0.91 micrograms per division (0.001 cm) and weight change could be estimated to 0.25 micrograms. The vacuum system and associated equipment have been described (19, 20, 21). A mullite furnace tube which was sealed directly to the all-glass vacuum system was also used. McLeod gauge pressures of 10^{-6} mm of Hg or lower were achieved over the entire temperature range.

The oxygen purification system has been described (18).

Since specimens were supported by a 2-mil nickel-chromium alloy wire from the balance, a direct measurement of specimen temperature was impractical. Temperature was measured using a

TABLE I. *Spectrographic analyses of nickel*

Element	Sponge, %	Strip, %
Cu	0.001	<0.0004
Ag	<0.0002	<0.0002
Mg	0.0002	0.0001–0.0005
Si	0.0005	0.0005–0.001
Fe	0.0002	0.0005–0.001
Mn	—	0.0001–0.001
Co	None	0.0002–0.002
Ca	—	0.00005–0.0001
Al	None	0.0002–0.002

platinum and platinum-10% rhodium thermocouple which was fastened to the mullite tube, the head of the couple being at the center of the length of the specimen. Temperature was controlled by an L&N Speedomax controller to within $\pm 2^\circ\text{C}$.

Samples.—Samples were prepared from 0.013-cm thick high purity strip purchased from Johnson, Mathey and Company, London. Table I shows the spectrographic analyses of nickel sponge from which the strip was rolled.

The following specimen preparations were used: *Semidegassed abraded specimens.*—Specimens were abraded through 4/0 polishing paper. The last two steps were made under purified kerosene. Specimens were then washed successively with soap and water, distilled water, petroleum ether, and absolute alcohol, and heated to the experimental temperature in a vacuum of 10^{-6} mm of Hg. Since they undergo degassing in this treatment, these samples are noted as semidegassed abraded specimens.

Vacuum annealed specimens.—Abraded specimens were annealed in a vacuum of 10^{-6} mm of Hg at 950°C for 24 hr and then lightly abraded under purified kerosene with 2/0 and 4/0 polishing papers. These are noted as degassed or vacuum annealed specimens.

Electropolished and hydrogen annealed.—Unabraded specimens were placed in a glycerol sulfuric acid bath at 62°C for 4 min at a current density of 1 amp/in.² Specimens were then washed in distilled water and heated for 12 hr at 900°C in a hydrogen furnace.

All specimens weighed 0.6830 gram and had surface areas of about 10 cm². All samples were stored in a desiccator.

RESULTS

High Vacuum Reaction

Behavior of nickel specimens in high vacuum was studied as a function of temperature to test (a) the quantity and composition of gas given off on heating to test temperature, and (b) extent of oxidation on heating to test temperature.

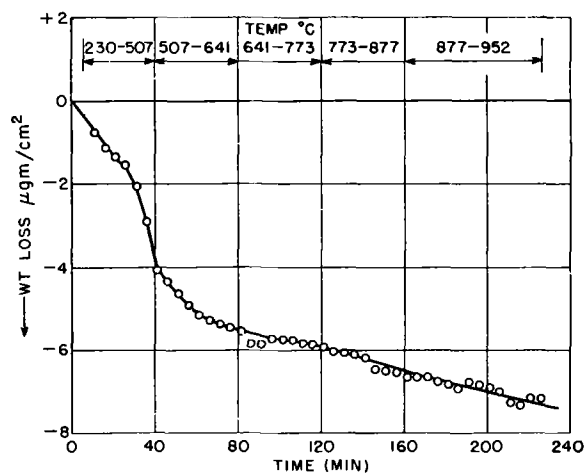


FIG. 1. Vacuum behavior of Ni 230°-952°C, vacuum $< 10^{-6}$ mm of Hg.

Fig. 1 shows the weight loss vs. time curve for the vacuum heating of an abraded specimen from room temperature to 952°C. The gas liberated on heating to 952°C weighed 6.8 micrograms/cm². This corresponds to a weight percentage of 100 ppm. A mass spectrometer analysis of the gas showed a mass peak at 28 which indicated that the gas was either CO or N₂, but the small amount of gas available made it impossible to determine which. This experiment suggested that CO or N₂ was the largest impurity in the metal, and that experiments should be made to test the effect of gas content on rate of reaction.

A visual examination of the specimen showed no evidence of an appreciable oxide film as judged by its temper colors. Electron diffraction analyses showed a pattern of nickel and nickel oxide which suggested that the film was very thin. The oxide formed on heating over a period of 10-20 min to the test temperature would be much less than that formed in this test.

Reaction with Oxygen

The reaction was studied as a function of time, temperature, gas content, surface preparation, and preoxidation. Results are shown in Fig. 2-10. Weight change was calculated in micrograms/cm² with thickness of oxide being related to weight gain by the relation: 1 microgram/cm² = 62.9 Å. This was based on the assumptions that surface roughness ratio = 1 and that the oxide was NiO.

Time and temperature.—Fig. 2 shows the effect of time and temperature on rate of oxidation of semi-degassed specimens at an oxygen pressure of 7.6 cm of Hg over the temperature range of 400°-750°C and over a period of oxidation of 6 hr. In order to test the time variation of the parabolic rate law constant, experiments in the temperature range of 400°-550°C were made over a 30-hr period.

The shapes of the oxidation curves in Fig. 2 are

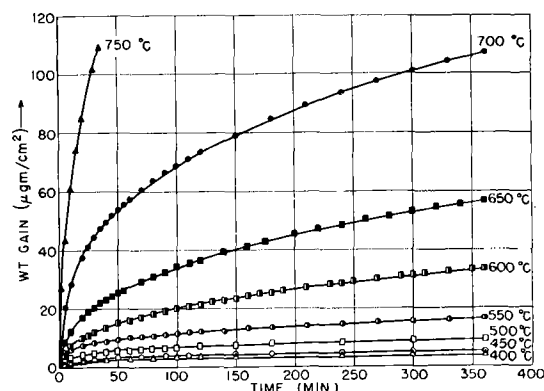


FIG. 2. Effect of temperature 400°-750°C, oxidation of nickel, 0.1 atm O₂.

TABLE II. Oxide film thickness vs. oxide color

Temp. °C	Thickness		Color
	μg/cm ²	Å ($\rho = 1$)*	
400	7.15	450	Gray mottled with straw crystallites
425	11.05	695	Light blue
450	8.25	519	Blue
475	16.7	1050	Gray
500	16.7	1050	Gray
550	30.6	1920	Gray
600	33.8	2120	Gray
650	56.9	3580	Gray
700	107.2	6750	Gray
750	109.0	6850	Gray

* Surface roughness ratio = 1.

similar to those found with other metals (1-5). A strong temperature dependence is noted.

The colors of the oxides formed in the oxidation of nickel were not well developed for this thickness range. Table II shows a correlation of oxide color and thickness of the oxide. No evidence was found for cracking of oxide film during the reaction or on cooling.

Parabolic rate law correlation.—Many empirical rate laws have been suggested to explain the time behavior of oxidation. The parabolic rate law based on principles of formation and diffusion of nickel ion lattice defects has been the most successful equation for explaining oxidation. The equation states that $W^2 = At + C$. Here W is the weight gain, t is the time, and A and C are constants.

To test agreement of the experiments with theory, plots were made of the square of weight gain vs. time. Fig. 3 and 4 show two such plots for the 475° and 650°C runs. The 475°C plot shows the slope or parabolic rate law constant A continually decreasing with time, while the 650°C plot shows a smaller decrease with time. Values of A were tabulated in the figure captions to illustrate this effect.

Results in Table II are in agreement with the

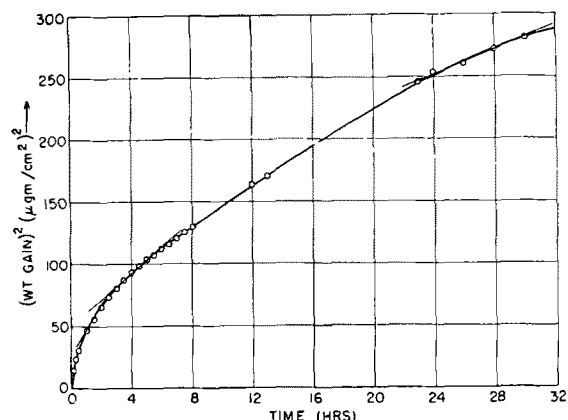


FIG. 3. Oxidation of Ni 475°C—0.1 atm O₂. Parabolic plot, 1–2 hr $A = 5.33 \times 10^{-15}$; 3–6 hr $A = 2.862 \times 10^{-15}$; 24–30 hr $A = 1.385 \times 10^{-15}$.

work of Wagner and Zimens (6) who found a similar behavior at 1000°C. The parabolic rate law can be fitted approximately to the data in the temperature range of 600°–750°C, while below 600°C it is impossible to make a reasonable fit. Experimentally, one must conclude that certain factors are operating between the metal and oxide which improve protective properties of the metal.

Temperature dependence.—The temperature dependence of the rate of oxidation has been interpreted by the Arrhenius law and the transition state theory (21). In previous papers the transition state theory was used for calculating entropy and heat of activation of the rate-controlling process. Since partition functions of the activated complex and normal lattice site were used in developing the theory, the free energy of activation ΔF^* was not defined by a physical process.

Following Zener's (22) restatement of the classical theory of diffusion, it was possible to clarify the processes involved in oxidation. In this theory, free energy of activation of diffusion, ΔF^* , was defined by the work required to produce a given distortion in the lattice. This enables one to apply rigorous thermodynamic operations on ΔF^* and to interpret the entropies and heats of activation. In this sense, the classical theory (22) has an advantage over the transition state theory, although the final equations are similar.

Processes occurring in oxidation are of two types: thermodynamic processes, such as the formation of vacancies which involves the free energy of formation of a vacancy, and rate processes, such as diffusion, which involve a free energy of activation. Thermodynamic functions for the rate processes are designated by an asterisk.

The theory of oxidation developed in an earlier paper (21) is used as a basis for deriving an equation for the parabolic rate law constant, A . The classical

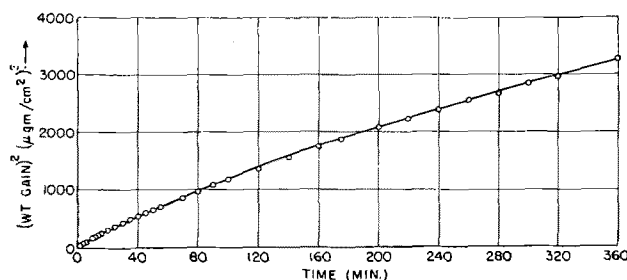


FIG. 4. Oxidation of Ni 650°C—0.1 atm O₂. Parabolic plot, 1–2 hr $A = 1.66 \times 10^{-13}$; 3–6 hr $A = 1.25 \times 10^{-13}$.

expression (22) is used for the diffusion coefficient, D , and the thermodynamic equilibria equations for the concentration of vacancies assuming the vacancies are formed by solution of oxygen in the NiO lattice.

$$A = \frac{2\gamma\nu a^2}{4^{1/3}} \Omega N (p_{O_2})^{1/6} e^{(\Delta S^0/3 + \Delta S^*)/R} e^{-(\Delta H^0/3 + \Delta H^*)/RT} \quad [1]$$

Here $\Delta S^0/3$ is the standard entropy of formation of a vacancy and ΔS^* is the entropy of activation of diffusion; $\Delta H^0/3$ is the standard heat of formation of a vacancy, and ΔH^* is the heat of activation of diffusion; a is the distance between diffusion sites, ν is the frequency of vibration along the direction leading across the saddle configuration; Ω is the volume of oxide formed per ion; N is the number of ions per cm³; R is the gas constant; T the temperature; γ a coefficient determined by the geometry of the atomic jumps; and p is the pressure of oxygen. For vacancy diffusion in a face-centered cubic lattice, $\gamma = 1$.

Although ν has usually been given a value of 10^{13} vibrations per second, a better value can be obtained from the characteristic Debye temperature. Assumptions made and details of the calculations are given in Appendix I. The results show a value of 8.5×10^{12} vibrations/sec for the Ni⁺⁺—Ni⁺⁺ bond in NiO. Calculations of Appendix II show that presence of a vacancy has only a minor effect on vibration frequencies of oxygen ions in the NiO lattice. A similar small effect would be expected for the Ni⁺⁺—Ni⁺⁺ bond. The normal lattice distance between Ni⁺⁺—Ni⁺⁺, 2.96 Å, is used for a .

Errors in choosing ν and a are less than experimental errors in the calculation of $(\Delta H^0/3 + \Delta H^*)$ from the data.

Substituting the values of the constants, equation [1] becomes

$$A = 7.5 \times 10^{-3} e^{(\Delta S^0/3 + \Delta S^*)/R} e^{-(\Delta H^0/3 + \Delta H^*)/RT} \quad [2]$$

Using this equation, the sums $(\Delta H^0/3 + \Delta H^*)$ and $(\Delta S^0/3 + \Delta S^*)$ are obtained. Unfortunately, there is no way to determine the separate quantities within the sums from oxidation studies alone. However, the entropy of formation of the vacancies can be

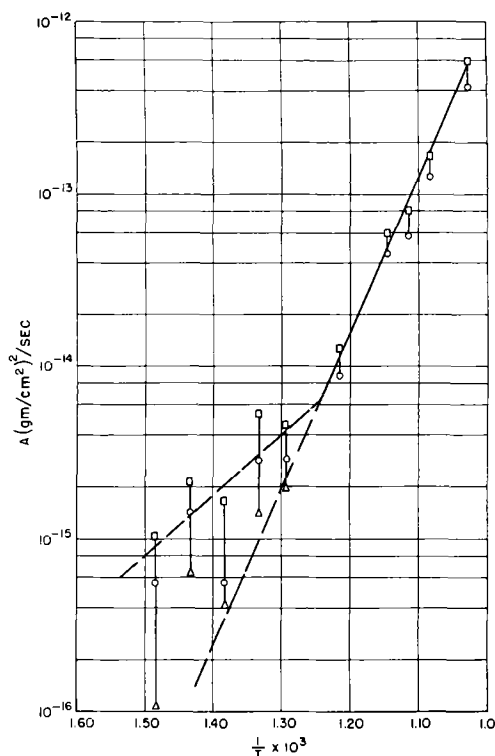


FIG. 5. Oxidation of semidegassed Ni; log plot A vs. $1/T \times 10^3$. \square —1-2 hr; \circ —3-6 hr; \triangle —24-30 hr. $\Delta H^* = 41,200$ cal/mole.

calculated, and it is therefore possible to evaluate ΔS^* . Values calculated from experimental data can be compared with values calculated theoretically from thermodynamic considerations. Such a comparison makes possible the testing of the mechanism of vacancy formation and, in a larger sense, the reaction mechanism.

Fig. 5 shows a plot of the logarithm of A vs. $1/T$. Since the rate constants change with time, these constants were evaluated and tabulated for the time periods of 1-2 hr, 3-6 hr, and in the lower temperature range at 24-30 hr. As was previously noted, a large uncertainty was found for the A values below 550°C. The data can be fitted by a straight line above 550°C. Below 550°C the time variation of A makes it impossible to determine the slope. However, values of A determined in the time range of 24-30 hr approach values given by an extrapolation of the straight line.

A heat of activation of 41,200 cal/mole was cal-

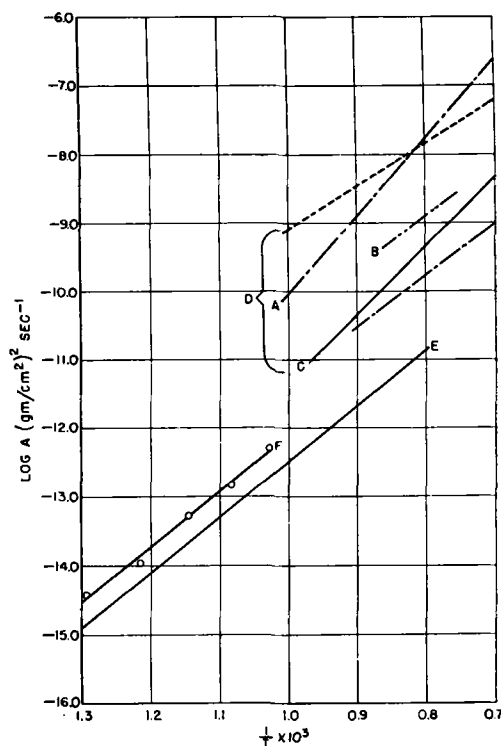


FIG. 6. Oxidation of Ni; log A vs. $1/T \times 10^3$. Curve A—Goldbeck; curve B—Pilling and Bedworth; curve C—Matsunaga; curve D—curves from Kubaschewski and Goldbeck; curve E—Moore [calculated to $(\text{gm}/\text{cm}^2)^2 \text{sec}^{-1}$]; curve F—present work.

culated from the slope for the temperature range of 500°–700°C. This value is nearly in agreement with the work of Moore (10).

The temperature independent factors, $e^{(\Delta S^0/3 + \Delta S^*)/R}$ were evaluated from equation [2]. Table III shows a summary of values of the parabolic rate law constants for 1-2 hr and 3-6 hr oxidation periods, average value of the parabolic rate law constants for the two periods, and heats, entropies, and free energies of the rate-controlling process in oxidation of nickel. Negative entropy values of -5.72 to -6.47 were calculated.

Comparison with the literature.—Fig. 6 shows a comparison of log A vs. $1/T$ with other values in the literature. The curves given by Kubaschewski and Goldbeck (9) summarizing older work at high temperatures were included. Where possible, the original source of data was given. Results of this study differ by a factor of 10 to 1000 from older results. How-

TABLE III. Parabolic rate law constants, entropies, heats, and free energies of activation for the oxidation of semidegassed nickel

Temp, °C	A (1-2 hr) (g/cm ²) ² /sec	A (3-6 hr) (g/cm ²) ² /sec	A (avg) (g/cm ²) ² /sec	$\frac{(\Delta S^0 + \Delta S^*)}{3}$ cal/mole/°C	$\frac{(\Delta H^0 + \Delta H^*)}{3}$ cal/mole	$-T \frac{(\Delta S^0 + \Delta S^*)}{3}$ cal/mole	ΔF^* cal/mole
550	1.28×10^{-14}	8.8×10^{-15}	1.08×10^{-14}	-5.92	+41,200	+4870	+46070
600	5.95×10^{-14}	4.51×10^{-14}	5.23×10^{-14}	-5.72	+41,200	+4990	+46190
625	8.00×10^{-14}	5.65×10^{-14}	6.83×10^{-14}	-6.47	+41,200	+5810	+47010
650	1.66×10^{-13}	1.25×10^{-13}	1.46×10^{-13}	-6.07	+41,200	+5600	+46800
700	5.96×10^{-13}	4.19×10^{-13}	5.08×10^{-13}	-6.02	+41,200	+5860	+47060

ever, agreement with recent work by Moore (10) in temperature dependence is good. In absolute value, the present work gives values differing by a factor of 2.5 from those given by Moore. Since Moore used preoxidized samples in an attempt to eliminate the initial part of the reaction, the difference between results is in the right direction. The effect of preoxidation on reaction rate is discussed later.

The reason for wide deviation in results is probably due to impurities present (13) in many samples of nickel used and in the method of surface preparation. The effect of impurities is to increase or decrease the number of vacancies and thus the rate of oxidation, the particular effect depending upon size, charge, and electronegativity of the added ion.

Horn (13) has shown that Th, Zr, Nb, Ce, W, Ti, Ca, Au, Cr, Mn, Ta, Mo, Cu, Al, and Si increase the rate of reaction at 900°C. However, to study the effect of impurities from a fundamental point of view, it is necessary to measure the rate of reaction at a series of compositions of one alloying component at a number of temperatures in order to see the effect of impurities on $(\Delta H^0/3 + \Delta H^*)$ and

$(\Delta S^0/3 + \Delta S^*)$. If the process of formation of vacancies is changed by addition of impurities, $\Delta H^0/3$ and $\Delta S^0/3$ of the formation process would change because of the different mechanism involved, while ΔH^* and ΔS^* of diffusion should not be so greatly affected.

Comparison with other metals.—Fig. 7 shows a comparison of rate of oxidation of nickel, chromium, and 80-Ni, 20-Cr alloy at 700°C and 0.1 atm of oxygen. In order of increasing rate of reaction the metals show the following relation: 80-Ni, 20-Cr alloy < chromium < nickel.

Effect of degassing.—Two sets of samples were tested, semidegassed, and degassed. Procedures for preparing the samples have been described. Fig. 8 shows a comparison of typical results. Degassed specimens show an eight- to tenfold increase in reaction rate for oxidation experiments below 500°C, while at temperatures above 600°C the increase is of the order of two- to threefold. Decrease of the effect with temperature is to be expected from the nature of the degassing curve (Fig. 1).

Experiments suggest that N₂ or CO in the nickel oxide lattice effectively reduces the number of nickel ion vacancies and thus reduces rate of oxidation. This effect will be reported in more detail in a future paper.

Fig. 9 shows the effect of electropolishing and annealing of the metal on rate of reaction. A strong increase in rate of reaction was observed at several temperatures. This increase may be explained in three ways: (a) effect of impurities left on the metal from the polishing bath, (b) possible addition of gases to the metal during electropolishing, and (c) changed nature of the surface resulting from electropolishing. Again, experimental difficulties make it impossible to study this effect thoroughly.

Effect of preoxidation.—A study of the effect of preoxidation is important for two reasons. First, it is

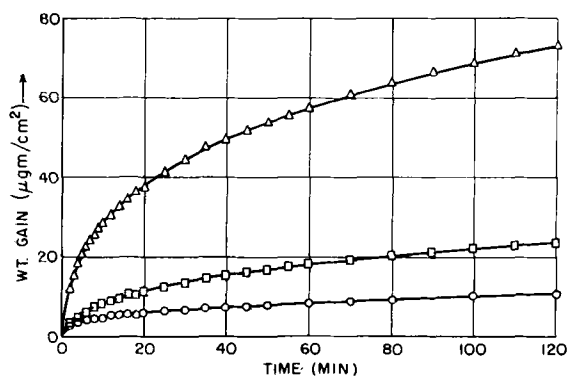


FIG. 7. A comparison of the oxidation of Ni, Cr, and Ni-Cr V at 700°C—7.6 0.1 atm O₂. Δ —Ni $A = 5.96 \times 10^{-13}$; \square —Cr $A = 6.38 \times 10^{-14}$; \circ —Ni-Cr V $A = 1.17 \times 10^{-14}$.

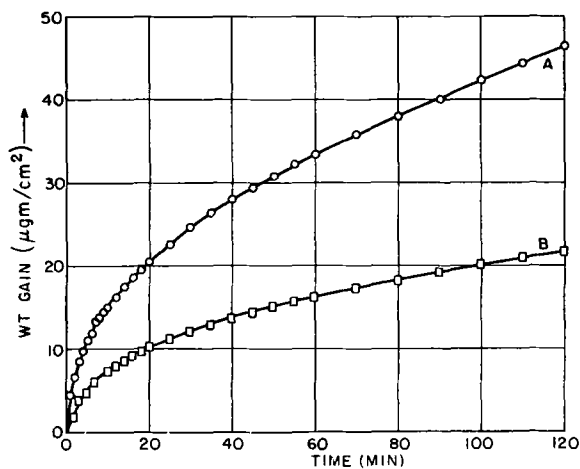


FIG. 8. Oxidation of Ni 600°C—0.1 atm O₂. Curve A—de-gassed; curve B—semi-degassed.

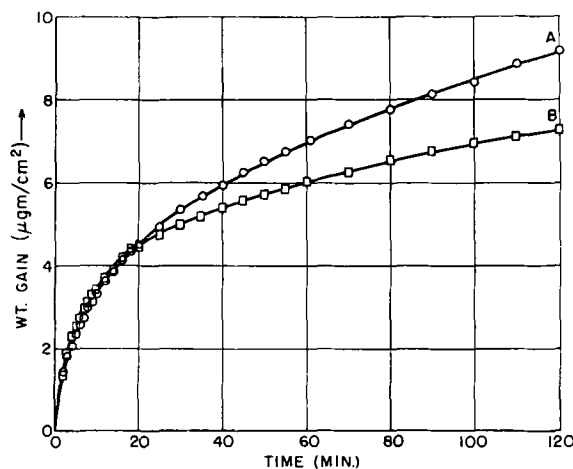


FIG. 9. Effect of pretreatment. Curve A—electropolished and annealed; curve B—abraded through 4/0.

of interest to test whether a set of experiments based on a preliminary preoxidation treatment would give oxidation curves similar to those determined at a single temperature. Second, the use of preoxidized surfaces may make possible the study of the effect of geometrical properties of oxide on rate of reaction. A preliminary set of experiments was made in this work. A series of specimens was oxidized at 600°C and 0.1 atm of O₂ to give an oxide of 15 micrograms/cm². After the oxygen was pumped off, the specimen was heated or cooled to the reaction temperature and a second oxidation made at the new temperature.

To evaluate the effect of preoxidation, the rate of reaction, dW/dt , was calculated at a total thickness W and compared to a similar calculation for a sample oxidized at a single temperature. Results show that preoxidation treatment gives smaller rates of reaction. Fig. 10 shows a parabolic plot of such a comparison at 750°C, while Table IV shows a summary of the effect of preoxidation on the parabolic rate law constant at temperatures of 550°–750°C. The effect was an important one and depends on the temperature difference between preoxidation and subsequent oxidation. These results

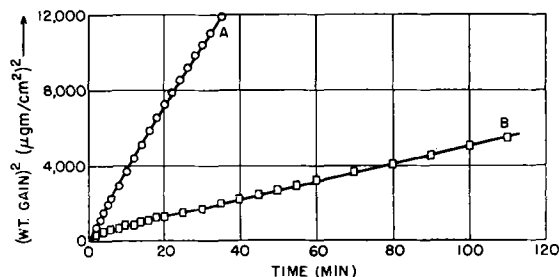


FIG. 10. Effect of preoxidation (600°C—7.6 cm O₂) on oxidation of Ni 750°C—0.1 atm O₂ abraded through 4/0. Curve A—no film; curve B—15 μg/cm².

TABLE IV. Effect of preoxidation on parabolic rate law constants

Temp, °C	A (g/cm ²) ² /sec	Condition	Ratio of $\frac{A \text{ normal}}{A \text{ preoxidized}}$
550	8.7×10^{-15}	Normal	1.39
550	6.25×10^{-15}	Preoxidized*	
600	6.8×10^{-14}	Normal	1.61
600	4.21×10^{-14}	Preoxidized*	
650	1.84×10^{-13}	Normal	1.79
650	1.035×10^{-13}	Preoxidized*	
700	9.32×10^{-13}	Normal	3.9
700	2.40×10^{-13}	Preoxidized*	
750	6.05×10^{-12}	Normal	7.6
750	7.96×10^{-13}	Preoxidized*	

* Preoxidized to 15 μg/cm².

may explain in part the difference in the results of Moore (10) and those of this work.

It should be noted that the effect depends on the difference at a given thickness between the physical structure of oxide film of the preoxidized specimen and that of the film produced at a single temperature. This is discussed in more detail later.

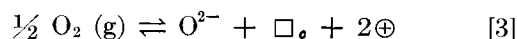
THEORETICAL

Four topics are considered: (a) experimental entropy of activation of diffusion, (b) theoretical entropy of activation of diffusion, (c) time dependence of the parabolic rate law, and (d) nature of the preoxidation effect.

Entropy of Activation of Diffusion

Previous studies on oxidation of metals (1–5) have shown that in many cases negative entropies of activation were observed. These values are in contrast to positive values which are predicted and found for self-diffusion processes in metals (22). However, the process of formation of vacancies in a metal occurs by removal of a metal atom from the interior to the surface. From simple considerations of loosening of the binding of metal atoms by the vacancy, this process should give a positive entropy change (22).

In NiO, vacancies were formed by a process of condensation of oxygen gas into the oxide lattice according to the reaction



to form new oxide, a vacant lattice site, \square_{e} , and two positive holes, \oplus . Essentially, we are condensing a gas to a solid oxide and a negative entropy change results.

Since the entropy of vacancy formation can be calculated, it was possible to determine the entropy of activation of the diffusion process. From elastic constant considerations, Zener (22) suggested that positive values should be found for the entropy of activation of diffusion.

The entropy of vacancy formation can be evaluated from an analysis of equation [3] if it is assumed that positive holes reside on Ni⁺⁺⁺ and that vacancies and positive holes are dissociated.

Simple electrostatic calculations show the attractive energy between a positive hole and a cation vacancy to be of the order of 10 times the thermal energy at 1000°K, assuming a dielectric constant of 10 for NiO. However, for low concentrations the $T\Delta S^0$ term in the free energy expression would be larger than ΔH^0 and thus make possible dissociation, since many sites were available for the cation and positive hole to occupy. Assumption of dissociation has been confirmed by experimental studies of the oxygen pressure dependence of conductivity (23)

and rate of oxidation (24) of nickel. At higher vacancy concentrations, association would be expected to occur.

Details of the entropy calculations are given in Appendix II. Results show a negative entropy of -7.5 cal/mole/°C to be associated with formation of one mole of vacancies.

Subtracting this value from the over-all experimental entropy term ($\Delta S^0/3 + \Delta S^*$) gives a value of 1.5 cal/mole/°C for the value of ΔS^* , the entropy of activation of diffusion. This value can now be compared to the theoretical value.

Theoretical Value for Entropy of Activation of Diffusion

Zener (22) has used the sign of the value for entropy of activation to determine whether diffusion is occurring through the lattice or at grain boundaries or other short-circuiting paths. Since a positive value of entropy of activation for diffusion was obtained for nickel oxidation, this would suggest that diffusion was occurring mainly through the lattice. To make such a prediction, it is necessary to ask what is the theoretical value of ΔS^* . This value may be estimated from theoretical considerations from the equation (22).

$$\Delta S^* = \frac{\lambda\beta\Delta H^*}{T_m} \quad [4]$$

Here λ is a numerical coefficient less than 1 and represents the fraction of free energy of activation or work that goes into straining the lattice. ΔH^* is the heat of activation of diffusion. T_m is the melting temperature of NiO, and β is defined as

$$\beta = -d(\mu/\mu_0)/d(T/T_m) \quad [5]$$

Here β is a dimensionless quantity involving the temperature coefficient of the appropriate elastic modulus μ , μ_0 is the value of μ extrapolated to absolute zero of temperature.

Zener (22) has determined the value of β from the temperature coefficient of Young's modulus or from the temperature coefficient of the shear modulus. Since data on the temperature coefficient of the elastic modulus were not available for oxides, β has been evaluated from the statistical thermodynamic expression for specific heat and the simple relationship between compressibility of a solid and characteristic frequency of the atoms. The calculations are presented in detail in Appendix III. β was found to have the value 0.345, while λ was assumed to take the value of 0.55.

It is now possible to place upper limits on values that ΔS^* of diffusion may take for NiO. A unique value was not possible to calculate since experimental data gave only the sum of the heat for forma-

tion of vacancies and the heat of activation for diffusion, while equation [1] requires ΔH^* of diffusion alone. However, a maximum value can be placed on ΔS^* by assuming that experimental heat of activation is equal to heat of activation of diffusion. Thus, assuming $\Delta H^* = 41,200$ cal/mole, ΔS^* is 3.3.

Assuming a more reasonable value for the ΔH^* of diffusion of 20,600 cal/mole, ΔS^* is equal to 1.7. Since the corrected experimental value is of the order of 1.5, agreement is well within experimental errors and assumptions made in calculations. An agreement of 1 in the value of ΔS^* means an agreement of 1.65 in the value of the parabolic rate law constants. Agreement between theory and experiment regarding the sign of ΔS^* suggests that, in high temperature oxidation of nickel, diffusion probably occurs mainly in the lattice and not at grain boundaries or other defects.

During the early part of the reaction in which the parabolic rate law does not apply and for low temperature experiments, the reaction occurs probably by grain boundary diffusion. This interpretation was suggested in a previous paper (26), although a detailed analysis of the entropy of vacancy formation was not included. Conditions for transition from grain boundary growth to growth by diffusion through the lattice depend upon the grain boundary area of oxide particles and upon the particular values of ΔH^* and ΔS^* for the processes.

Time Dependence of Parabolic Rate Law Constant

Two explanations may be given. The first is based on the assumption that concentration of impurities within the oxide is changing as oxidation proceeds, thus changing the number of vacancies for diffusion. Horn (13) has shown that most of the common alloying elements increase the reaction rate. As the reaction proceeds, the tendency is for impurity concentration to decrease because of the limited amount of material available in the metal. This factor could account for the decreasing of the parabolic rate law constant observed by Wagner and Zimens (6) and in this work.

The second explanation is based on assumption of a grain boundary diffusion mechanism for early stages of reaction. As the film thickens, oxide crystallites grow, and at some thickness the influence of grain boundary diffusion becomes small compared to lattice diffusion.

Certain evidence supports this point of view. Previous studies (27) on size of oxide grains in thin oxide films showed that oxide grains changed in size during reaction and that such changes were a function of both temperature and time of oxidation. In the case of Fe oxidized at 250°C for 5 min, the average particle size of oxide crystallites was 350 Å.

This increased to 1200 Å when oxidation was carried out for 30 min. Since the grain boundary area decreases as oxide crystallites grow, the parabolic rate law constant also decreases until at some thickness the reaction is controlled by lattice diffusion.

Nature of the Preoxidation Effect

The preoxidation effect is very difficult to explain if we accept the interpretation that the reaction is essentially controlled by lattice diffusion and that entropy calculations are correct. One may postulate that impurities may concentrate in the oxide during preoxidation treatment, which tends to lower oxidation rate at higher temperatures. Further experimentation, however, is necessary to understand and to explain this phenomenon.

SUMMARY

Reaction of high purity nickel with oxygen was studied using the vacuum microbalance method over the temperature range of 400°–750°C. Colored oxide films were formed even at the lowest temperatures after 30-hr oxidation periods.

A comparison of rate of oxidation showed that nickel oxidizes faster than chromium and 80-Ni, 20-Cr alloy. Data were fitted to the parabolic rate law, and it was shown that the rate law constant decreases with extent of oxidation, the greatest deviations occurring in the temperature range of 400°–550°C. For the temperature range of 550°–700°C, a $\log A$ vs. $1/T$ plot gave a straight line and a calculated heat of activation of 41,200 cal/mole.

A comparison with previous work in the literature showed the rate of oxidation of high purity nickel to be 1/10 to 1/1000 of that which other workers found on less pure nickel. The effect of impurities on the oxidation rate was discussed.

Using the classical theory of diffusion, entropies and free energies of activation of the rate-controlling process were calculated and compared to those of other metals. Experimental entropies of activation of -6.0 were corrected for the entropy of formation of nickel ion vacancies to give an entropy of activation of diffusion of $+1.5$ cal/mole/°C. On the basis of certain assumptions, theoretical considerations suggest that the entropy of activation for diffusion may have a maximum value of 3.3 eu, while a more reasonable assumption leads so a value of 1.7 eu.

This agreement of theory with experiment suggests that in the temperature range of 600°–700°C the reaction is controlled mainly by lattice diffusion.

The effect of a preoxidation treatment on rate of oxidation was studied. It was shown that preoxidation at 500°C greatly affects the rate of reaction at higher temperatures.

ACKNOWLEDGMENTS

The authors are indebted to Dr. C. Zener and Dr. R. Heikes for their helpful comments and suggestions on the classical theory of diffusion and the interpretation of negative and positive entropies of activation.

APPENDIX I

FREQUENCY OF VIBRATION OF Ni⁺⁺—Ni⁺⁺ BOND

Assume that the atoms in NiO are vibrating as harmonic oscillators and interacting according to Hooke's law, and that the calculated frequency is characteristic of movement of Ni⁺⁺ ions through the NiO lattice. The assumption of harmonic oscillations is a reasonable one since the atoms spend the great bulk of their time in these energy states.

The value of ν_{\max} is calculated from the characteristic Debye temperature:

$$\theta_D = \frac{h\nu_{\max}}{k} \quad [6]$$

Here ν is the maximum frequency, h is Planck's constant, and k is Boltzman's constant. For NiO, θ_D is 404 (25).

From the Debye temperature, $\nu_{\max} = 8.5 \times 10^{12}$.

APPENDIX II

ENTROPY OF VACANCY FORMATION

Change in entropy can be estimated from three considerations: (a) change associated with condensation of oxygen gas into the NiO lattice to form a new oxide following equation [3] and assuming no distortion; (b) change associated with distortion of the NiO lattice by cation vacancy alone; (c) change associated with distortion of the NiO lattice due to formation of two positive holes (Ni⁺⁺⁺ sites).

Change in Entropy Due to Condensation of Oxygen

At 1000°K the entropy of $\frac{1}{2}$ O₂ (g) (28, 29) is calculated to be 29.10 cal/mole/°C, while the entropy of NiO (28, 29) is calculated to be 18.08 cal/mole/°C.

The entropy, S , of O²⁻ in the NiO (s) lattice is assumed to be $\frac{1}{2}$ the entropy of NiO (s) or 9.04 cal/mole/°C.

Entropy Change Due to Distortion of the NiO Lattice

If a Ni⁺⁺ is removed from the NiO lattice and two positive holes are formed (Ni⁺⁺⁺ sites), the six oxygen ions surrounding each of these sites are disturbed. Assume that removal of a Ni⁺⁺ ion results in a displacement δ_c of oxygen ions toward and in line with adjacent Ni⁺⁺ ions, while formation of a positive hole results in a displacement δ_p of oxygen ions toward and in line with the positive hole. The effect of both displacements to a first approximation is to increase the binding of the oxygen ion to its nearest neighbors. This results in a decrease in entropy of oxygen ions in the lattice of NiO.

Relation between α_M and b .—In the calculations that follow it is necessary to calculate the relationship between the Madelung constant, α_M , and the constant b of the repulsive energy terms.

The equation for the lattice energy W of a mole of NiO crystal, neglecting Van der Waals energy and the zero point energy (31), is

$$W = N \left[\frac{-4e^2\alpha_M}{r_0} + 6w_{+-}(r) + 6w_{--}(r) + 6w_{++}(r) \right] \quad [7]$$

Here N is Avogadro's number, e is the electronic charge, and r_0 is the cation-anion distance. The first term refers to the electrostatic energy while the terms $w_{++}(r)$, $w_{--}(r)$, and $w_{+-}(r)$ refer to the repulsive or overlap energy terms of the respective bonds.

Each of the $w(r)$ terms is expressed as

$$w(r) = Cb \exp [(r_1 + r_2)/\rho] \exp [(-r/\rho)] \quad [8]$$

Here r is the distance between ions, r_1 and r_2 are ionic radii of the Ni^{++} and O^- , respectively, b is a fixed constant if C is defined by

$$C = \left(1 + \frac{Z_1}{n_1} + \frac{Z_2}{n_2} \right) \quad [9]$$

Here Z_1 and Z_2 are valences of the ions, and n_1 and n_2 are the number of electrons in the outer shell. Under these conditions, $\rho = 0.345 \times 10^{-8}$ cm. For NiO , $C_{+-} = 1$, $C_{--} = 0.5$, and $C_{++} = 1.5$.

Using 0.74 \AA as the ionic radius of Ni^{++} and 1.35 \AA for O^- , we have the following expression for the lattice energy:

$$W = N \left[\frac{-4e^2\alpha_M}{r_0} + 6C_{+-}b \exp [-(r_0 - 2.09)/\rho] + 6C_{--}b \exp [-(\sqrt{2}r_0 - 2.70)/\rho] + 6C_{++}b \exp [-(\sqrt{2}r_0 - 1.48)/\rho] \right] \quad [10]$$

The relation between α_M and b is found by differentiating and setting $W(r) = 0$. The result shows

$$b = \frac{0.49e^2\alpha_M\rho}{r_0^2} \quad [11]$$

Calculation of the displacement δ_c for a cation vacancy.—Total energy of an ionic lattice, W , containing a cation vacancy can be expressed by the following equation:

$$W = W_0 + \Delta W_1 + \Delta W_2 \quad [12]$$

Here W_0 is the initial energy without a vacancy, ΔW_1 is the change in energy due to a displacement δ_c of oxygen ions surrounding the vacancy, and ΔW_2 is the change in energy due to removing the Ni^{++} ion with the O^- ions in the displaced position.

Change in the electrostatic energy part of ΔW_1 associated with displacement alone can be shown to be negligible by a simple example. Consider the energy associated with an oxygen ion in the three ion system— Ni^{++} — O^- — Ni^{++} . Let the original cation-anion distance be r_0 and displace the ion a distance δ . If the two Ni^{++} are fixed, then change in the electrostatic energy part of ΔW_1 is

$$\Delta W_1 (\text{elec}) = \frac{-4e^2}{r_0 - \delta} + \frac{4e^2}{r_0} - \frac{4e^2}{r_0 + \delta} + \frac{4e^2}{r_0} \quad [13]$$

Expanding,

$$\Delta W_1 (\text{elec}) = \frac{-4e^2}{r_0} \left(\frac{2}{1 - (\delta/r_0)^2} \right) + \frac{8e^2}{r_0} \approx 0 \text{ for small } \delta/r_0 \quad [14]$$

Initial total energy of an ionic lattice remains in the form W_0 since it does not contain any term involving the displacement δ_c . To evaluate ΔW_1 , refer to Fig. 11A which shows a plane through the NiO lattice containing the vacancy together with spacings of nearest neighbor ions. Since it has been shown that the electrostatic part of ΔW_1 is negligible, it is necessary only to consider the following overlap repulsive terms in ΔW_1 : (a) interaction between

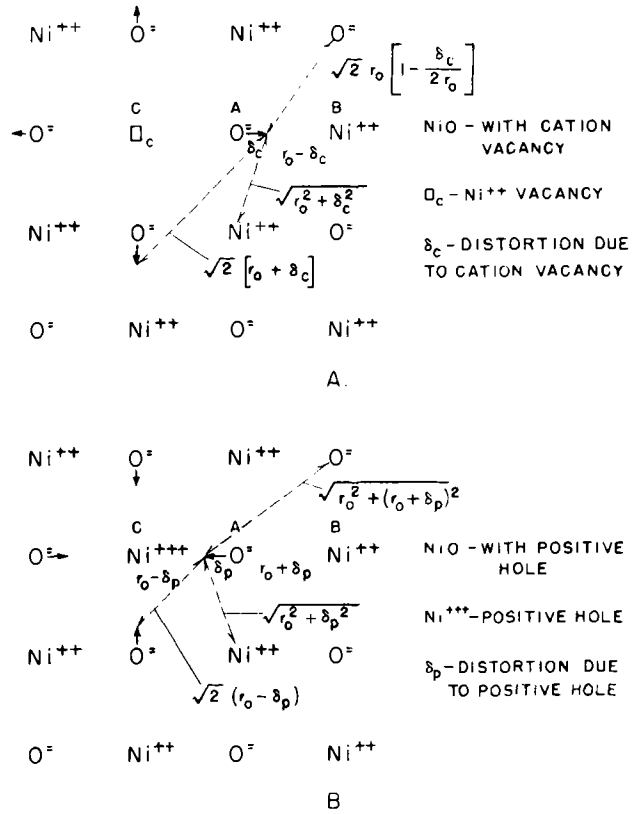


FIG. 11. Effect of vacancy and positive hole on nickel oxide lattice.

O^- at A and Ni^{++} at B; (b) interaction between O^- at A and 4 O^- in the plane of Ni^{++} at B and perpendicular to line AB; (c) interaction between O^- at A and 4 Ni^{++} in the plane of A and perpendicular to line AB; (d) interaction of O^- at A and 4 O^- in the plane of the vacancy at C and perpendicular to line AB; and (e) interaction between O^- at A and Ni^{++} at C. Part of the latter term drops out on removing Ni^{++} and forming a vacancy.

$$\begin{aligned} \Delta W_1 = & 6C_{+-}b[\exp -(r_0 - \delta_c - r_1 - r_2)/\rho - 1] \\ & + 24 C_{--}b \left[\exp - \left(\sqrt{2}r_0 \left(1 - \frac{\delta_c}{2r_0} \right) - 2r_2 \right) / \rho - 0.47 \right] \\ & + 24 C_{+-}b \exp - (\sqrt{r_0^2 + \delta_c^2} - r_1 - r_2)/\rho - 1 \\ & + 12 C_{--}b[\exp - (\sqrt{2}(r_0 + \delta_c) - 2r_2)/\rho - 0.47] \\ & + 6 C_{+-}b[\exp -(r_0 + \delta_c - r_1 - r_2)/\rho - 1] \end{aligned} \quad [15]$$

This equation represents change in energy produced by one vacancy, assuming 6 O^- are displaced for each vacancy.

Change in energy ΔW_2 due to removing the Ni^{++} ion can now be evaluated. The electrostatic energy change for one vacancy and six disturbed oxygen ions is evaluated from the potential at Ni^{++} .

$$V = \frac{-2e\alpha_M}{r_0} + \frac{12e}{r_0} \frac{-12e}{r_0 + \delta_c} \quad [16]$$

The first term is the Madelung potential while the latter terms represent the effect of O^- on the potential at Ni^{++} at the new distance, $r_0 + \delta_c$. The value of the electrostatic energy to remove the Ni^{++} after the O^- ions have been dis-

Repulsive energy terms in the total energy expression for disturbed and normal lattice cases were set up in a similar manner to that in the second section. Repulsive energy terms between nearest neighbors were used.

The following results were found:

$$\tilde{W}(N) = 2.70 \frac{b}{\rho^2} = \kappa_N, \quad [27]$$

and

$$\tilde{W}(D) = 3.39 \frac{b}{\rho^2} = \kappa_D. \quad [28]$$

Since

$$\frac{\nu_D}{\nu_N} = \left(\frac{\kappa_D}{\kappa_N}\right)^{1/2} = \left(\frac{3.39}{2.70}\right)^{1/2} = 1.12, \quad [29]$$

and since 6 O⁻ were involved, $\Delta S_e = -6R \ln \nu_D/\nu_N = -1.34$ cal/mole/°C.

Entropy of positive hole formation.—Following the method of the preceding section, consider the total energy of the lattice with positive holes present. Lattice situations for force constant calculations are shown in Fig. 12B. Again, ΔX represents the new displacement. Setting up the total energy expression in a similar manner to that of the third and fourth sections, and differentiating twice with respect to ΔX ,

$$\begin{aligned} \tilde{W}(D) &= 2.92 \frac{b}{\rho^2} \\ \frac{\tilde{W}(D)}{\tilde{W}(N)} &= \frac{2.92}{2.70} = 1.08 \end{aligned} \quad [30]$$

Thus,

$$\frac{\nu_D}{\nu_N} = \left(\frac{\kappa_D}{\kappa_N}\right)^{1/2} = \left(\frac{2.92}{2.70}\right)^{1/2} = 1.04 \quad [31]$$

$\Delta S_p = -6R \ln 1.04 = -0.47$ cal/mole/°C. Since two moles of positive holes are formed for each mole of vacancies,

$$\Delta S_p = -0.93 \text{ cal/mole/}^\circ\text{C.}$$

Calculation of over-all entropy change.—Entropy change of the NiO lattice for condensation of $\frac{1}{2}$ mole of O₂ and for formation of one mole of vacancies and two moles of positive holes at particular lattice sites in a large amount of NiO can now be evaluated. Entropy change on condensation without distortion of $\frac{1}{2}$ mole of O₂ gas is equal to to 29.10 - 9.04, or 20.1 cal/mole/°C. Since order was established in the process, the entropy change is negative or -20.1 eu. Entropy changes associated with the two types of distortion are -1.34 and -0.93 or a total of -2.3 cal/mole/°C. Thus, the total entropy change is -22.5 cal/mole/°C. Since 3 defects were formed, the entropy change per defect is -7.5 cal/mole/°C.

Subtracting this value from the experimental over-all entropy of activation, there is obtained a value of +1.5 cal/mole/°C for the entropy of activation of diffusion, ΔS^* .

APPENDIX III

ESTIMATION OF β

β can be estimated from the statistical thermodynamic expression for specific heat, C_p :

$$C_p = \frac{\partial}{\partial T} \left\{ RT^2 \left(\frac{\partial \ln Q_V}{\partial T} \right)_P \right\} \quad [32]$$

where

$$Q_V = \frac{kT}{h\nu}$$

Carrying out the necessary differentiation,

$$C_p = R \frac{\partial}{\partial T} \left\{ T - T^2 \left(\frac{d \ln \nu}{dT} \right) \right\} \quad [33]$$

According to Einstein (31) there is a simple relation between compressibility, χ , of a solid and characteristic frequencies of the atoms, ν_E . This relationship is $\nu_E \sim 1/\chi^{1/2}$. Since χ is related to the reciprocal of the elastic modulus μ , there results the relationship

$$\nu_E \sim \mu^{1/2} \quad [34]$$

$$C_p = R \frac{\partial}{\partial T} \left\{ T - \frac{T^2}{2} \left(\frac{d \ln \mu}{dT} \right) \right\} \quad [35]$$

Rearranging and substituting the value of β from [12],

$$C_p = R + \frac{RT}{T_m} \frac{\mu_0}{\mu} \beta \quad [36]$$

For three degrees of freedom,

$$C_p = 3R + 3 \frac{RT}{T_m} \frac{\mu_0}{\mu} \beta$$

To estimate β , substitute 2363°K for the melting point of NiO and a value of 7.4 cal/°C/gram atom (14.8/2) for the specific heat of NiO at 1000°K. Since the ratio of μ/μ_0 is 1 at $T = 0^\circ\text{K}$ and 0 at the melting point, a linear function of μ/μ_0 with temperature is assumed. This gives a value of μ/μ_0 of 0.6 at 1000°K.

By substituting and solving, it is found that $\beta = 0.345$.

Any discussion of this paper will appear in a Discussion Section, to be published in the December 1954 issue of the JOURNAL.

REFERENCES

1. E. A. GULBRANSEN AND K. F. ANDREW, *Trans. Am. Inst. Mining Met. Engrs.*, **185**, 515 (1949).
2. E. A. GULBRANSEN AND K. F. ANDREW, *ibid.*, **185**, 741 (1949).
3. E. A. GULBRANSEN AND K. F. ANDREW, *ibid.*, **188**, 586 (1950).
4. E. A. GULBRANSEN AND K. F. ANDREW, *This Journal*, **97**, 383 (1950).
5. E. A. GULBRANSEN AND K. F. ANDREW, *ibid.*, **98**, 241 (1951).
6. C. WAGNER AND K. ZIMENS, *Acta Chem. Scand.*, **1**, 574 (1947).
7. N. B. PILLING AND R. E. BEDWORTH, *J. Inst. Metals*, **29**, 529 (1923).
8. Y. MATSUNAGA, *Japan Nickel Rev.*, **1**, 347 (1933).
9. O. KUBASCHESKY AND O. GOLDBECK, *Z. Metallkunde*, **39**, 158 (1948).
10. W. J. MOORE, *J. Chem. Phys.*, **19**, 255 (1951).
11. W. E. CAMPBELL AND N. B. THOMAS, *Trans. Electrochem. Soc.*, **91**, 623 (1947).
12. R. PIONTELLI, Private communication.
13. A. L. HORN, *Z. Metallkunde*, **40**, 73 (1949).
14. K. HAUFFE AND H. PFEIFFER quoted in a paper by K. Hauffe, *Wissenschaftliche Zeitschrift der Universität Greifswald*, Jahrgang I, 1951/52, Mathematisch-naturwissenschaftliche Reihe Nr. 1.
15. E. A. GULBRANSEN AND J. W. HICKMAN, *Trans. Am. Inst. Mining Met. Engrs.*, **171**, 306 (1947).
16. R. W. G. WYCOFF, "Crystal Structures," 1, Table III, Interscience Publishers Inc., New York (1948).
17. H. P. ROOKSBY, *Acta. Cryst.*, **1**, 226 (1948).
18. E. A. GULBRANSEN, *Trans. Electrochem. Soc.*, **81**, 187 (1942).

19. E. A. GULBRANSEN, *Rev. Sci. Instruments*, **15**, 201 (1944).
20. E. A. GULBRANSEN AND K. F. ANDREW, *Ind. Eng. Chem.*, **41**, 2762 (1949).
21. E. A. GULBRANSEN, *Trans. Electrochem. Soc.*, **83**, 301 (1943).
22. C. ZENER, *J. Appl. Phys.*, **22**, 372 (1951).
23. H. H. VON BAUMBACH AND C. WAGNER, *Z. physik Chem.*, **B24**, 59 (1934).
24. C. WAGNER AND KARL GRÜNEWALD, *ibid.*, **B40**, 455 (1938).
25. H. SELTZ, B. J. DEWITT, AND H. J. McDONALD, *J. Am. Chem. Soc.*, **62**, 88 (1940).
26. E. A. GULBRANSEN, International Symposium on "The Reactivity of Solids," Gothenburg, June 1952. To be published.
27. R. T. PHELPS, E. A. GULBRANSEN, AND J. W. HICKMAN, *Ind. Eng. Chem.*, anal. ed., **18**, 391 (1946).
28. Nat. Bur. Standards Circular 500, "Selected Values of Chemical Thermodynamic Properties," Washington, D. C. (1952).
29. K. K. KELLEY, Bur. Mines Bulletin 476, Washington, D. C. (1949).
30. M. BORN AND J. E. MAYER, *Z. Physik*, **75**, 1 (1932).
31. N. F. MOTT AND H. JONES, "Theory of the Properties of Metals and Alloys," p. 13, Oxford Press, London, England (1936).

The Protective Action of Pigments on Steel¹

M. J. PRYOR

Kaiser Aluminum and Chemical Corporation, Spokane, Washington

ABSTRACT

The action of aqueous extracts from litharge, metallic lead, red lead, basic lead carbonate, zinc, and zinc oxide on the corrosion of steel was investigated. It was found that litharge extracts inhibited the corrosion of steel completely, that extracts from metallic lead and red lead inhibited for a short period, and that extracts from basic lead carbonate, zinc, and zinc oxide had no protective action. Protective properties of the decanted extracts were in the same order as their reserve alkalinities. Litharge, metallic lead, and red lead extracts protected only when they contained dissolved air; when deaerated, they attacked steel slowly. The passivity film formed in litharge extracts was found to be composed largely of γ -Fe₂O₃, no lead compounds being detected. It was considered that the lead in the litharge extracts was present partly in the ionic form, possibly as Pb(OH)⁺ ions, whereas the lead in extracts from metallic lead was present mainly as massive and colloidal lead hydroxide.

INTRODUCTION

Attention has previously been directed (1) to the fact that aqueous extracts from certain lead compounds, principally metallic lead, litharge, and red lead, had inhibitive actions on corrosion of steel. It was shown (2, 3) that the inhibitive action of the extract from red lead was of a temporary nature, while similar properties were ascribed to the extracts from metallic lead (4) and basic lead carbonate (5). Inhibitive properties of the extracts have been attributed alternatively to their alkalinity (6, 7), to adsorption of soluble lead compounds (1), and, in the case of red lead, to a combination of alkalinity and oxidizing power (2).

The present examination was carried out to investigate reactions occurring between steel and aqueous extracts from metallic lead powder, litharge, red lead, basic lead carbonate, metallic zinc powder, and zinc oxide. The investigation included determinations of potential-time data and weight losses in solutions freed from and containing dissolved air; the nature of the passivity films and of the aqueous extracts was also examined.

EXPERIMENTAL

Materials

The steel used in the partial immersion tests was annealed autobody steel 0.1 cm thick having the analysis: C—0.12%; Si—0.02%; P—0.014%; Mn—0.32%; S—0.01%; Sn and V—not detected. Steel used in experiments with deaerated solutions was in the form of annealed sheet 0.02 cm thick, the analysis of which was given in a previous paper (8).

¹ Manuscript received June 17, 1953. This paper was prepared for delivery before the Wrightsville Beach Meeting, September 13 to 16, 1953. Experimental work carried out at the National Research Council of Canada, Ottawa.

Pigments used in this investigation had the following compositions: metallic lead—98.4% Pb; litharge—95.7% PbO; red lead—99.1% Pb₃O₄; basic lead carbonate—80% Pb, 8.25% CO₂; metallic zinc—99.9% Zn; zinc oxide—99.7% ZnO. The balance of the litharge was mainly in the form of Pb₃O₄. All other chemicals were of C.P. quality.

Preparation of pigment extracts.—Extracts were prepared by exposing 50 grams of each pigment to 1 liter of distilled water in a stoppered flask for eight days. The flasks were shaken at frequent intervals to insure dispersion of pigment particles. After eight days the solutions were decanted from the residual pigments and stored in well-stoppered bottles.

Reactions between Steel and Pigment Extracts in Presence of Dissolved Air

Steel specimens measuring 5 x 2.5 cm, which had been degreased in benzene, abraded with 3/0 emery paper, and weighed, were partially immersed in the decanted extracts in such a manner that they did not come into direct contact with any residual particles of pigment. Partial immersion tests of five days' duration were carried out in 30 ml of each solution, an area of 12.5 cm² of specimen being immersed in each test solution. Control experiments in distilled water were also carried out. At the end of the experiments the specimens were pickled in inhibited hydrochloric acid, dried in acetone, and reweighed. The weight losses, which are the average of experiments in triplicate, together with the initial and final pH values of the solutions, are shown in Table I. The extract from litharge gave complete inhibition, while those extracts from metallic lead and red lead gave inhibition for 24 hours and six hours, respectively, after which time corrosion occurred at a lower rate than in distilled water. Extracts from basic lead

TABLE I. *Weight losses in extracts containing dissolved air*

Solution	Initial pH	Wt loss/cm ² mg	Average wt loss/cm ² mg	Final pH	Reserve alkalinity, ml	Observations
Fresh distilled water.....	5.5	0.96, 0.80, 0.93	0.90	6.6	—	General corrosion
Distilled water stored in glass bottles for 4 weeks.....	8.9	0.80, 0.80, 0.85	0.82	6.7	0.1	General corrosion
Decanted Pb extract.....	9.9	0.52, 0.27, 0.47	0.43	6.9	7.9	Inhibition for one day after which localized corrosion proceeds at a reduced rate
Pb extract filtered through glass wool.....	9.4	0.72, 0.68, 0.71	0.70	6.8	5.7	General corrosion at reduced rate
Pb extract filtered through Whatman No. 1 filter paper.....	8.6	0.70, 0.69, 0.69	0.69	6.9	0.6	General corrosion at reduced rate
Decanted PbO extract.....	9.7	<0.01	<0.01	7.5	15.2	Passivity
PbO extract filtered through glass wool.....	9.7	<0.01	<0.01	7.5	12.25	Passivity
PbO extract filtered through Whatman No. 1 filter paper.....	8.0	<0.01	<0.01	7.2	2.1	Passivity
PbO extract filtered through Whatman No. 42 filter paper.....	7.3	<0.01	<0.01	7.0	1.6	Passivity
Decanted Pb ₃ O ₄ extract.....	9.7	0.57, 0.58, 0.54	0.56	6.8	4.1	Passivity for a few hours after which time general corrosion proceeds at a reduced rate
Pb ₃ O ₄ extract filtered through glass wool.....	8.35	0.78, 0.61, 0.73	0.71	6.9	0.8	General corrosion at slightly reduced rate
Pb ₃ O ₄ extract filtered through Whatman No. 1 filter paper.....	7.3	0.70, 0.71, 0.69	0.70	6.7	0.3	General corrosion at slightly reduced rate
Decanted basic lead carbonate extract.....	8.95	0.85, 0.86, 0.86	0.86	6.5	0.3	General corrosion
Decanted Zn extract.....	8.6	0.81, 0.80, 0.81	0.81	6.7	0.15	General corrosion
Decanted ZnO extract.....	7.7	0.90, 0.93, 0.91	0.91	6.4	0.3	General corrosion

carbonate, zinc, and zinc oxide had no detectable inhibitive properties.

Potential time data were determined in 50 ml of each decanted extract. Control experiments in fresh distilled water and distilled water that had been stored in a stoppered glass bottle for four weeks were also carried out. The area of specimen exposed to each solution was 12.5 cm² and duration of the experiments was five days. Potential difference² readings against a standard calomel electrode were recorded continuously by means of a Leeds and Northrup Micromax recording potentiometer. To prevent contamination of the extracts by chloride, the calomel electrode was contained in a beaker of distilled water and bridged to the extracts under examination through a stopcock "greased" with a stiff paste of bentonite, glycerine, and water, and maintained in the closed position (9). The results are shown in Fig. 1. The effect of progressively finer filtration

² All potentials in this paper are expressed on the Standard Hydrogen Scale.

on the form of the potential time curves in extracts from litharge, lead, and red lead is shown in Fig. 2, 3, and 4.

Reactions between Steel and Deaerated Extracts

Determinations of weight loss and of the relationship between potential and time were carried out in deaerated extracts from metallic lead, litharge, and red lead. The deaeration technique previously described (10), based on the very large decrease in gaseous solubility on freezing solution, was employed.

Weight loss determinations (9) were carried out on degreased specimens measuring 4 x 3 x 0.02 cm; they were abraded with 3/0 emery paper and exposed to 50 ml of deaerated extracts which had been filtered through glass wool to remove massive pigment particles. Duration of experiments, which were carried out in triplicate, was five days; results are shown in Table II, from which it may be seen that the deaerated extracts do not inhibit corrosion of steel.

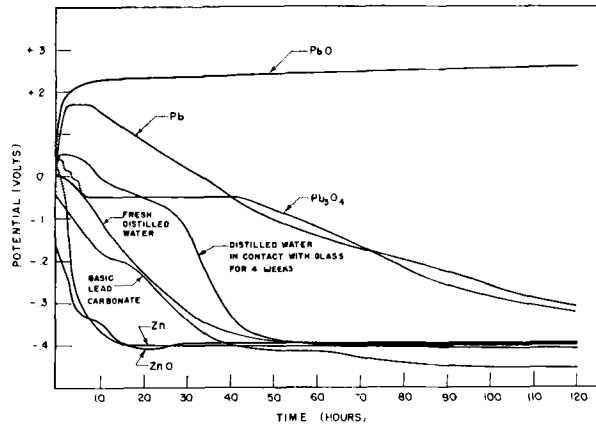


FIG. 1. Potential/time curves in decanted extracts containing dissolved air.

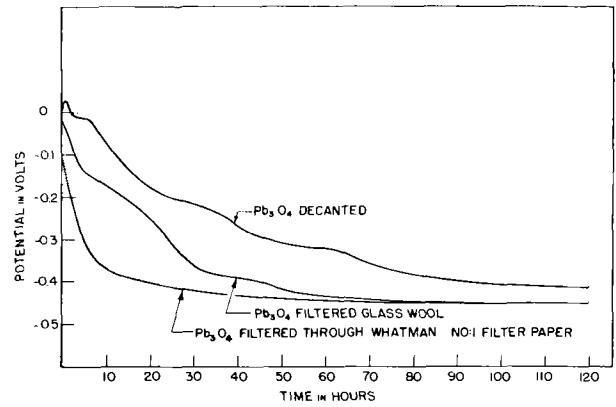


FIG. 4. Effect of filtration on potential/time curves in red lead extracts containing dissolved air.

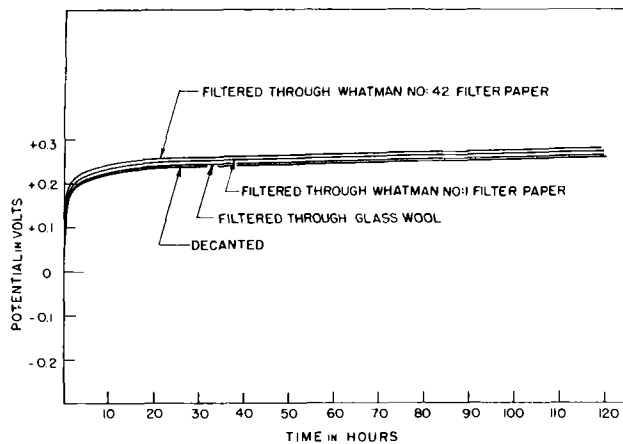


FIG. 2. Effect of filtration on potential/time curves in litharge extracts containing dissolved air.

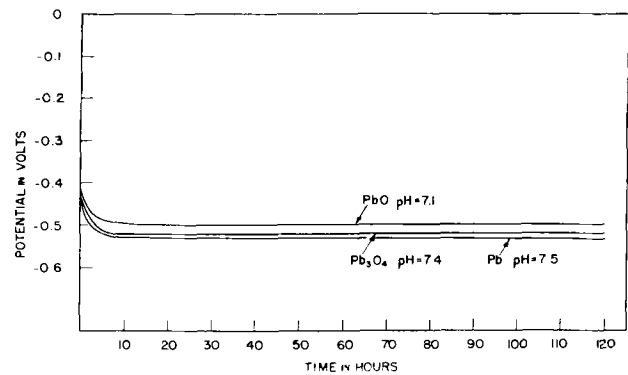


FIG. 5. Potential/time curves in deaerated decanted extracts.

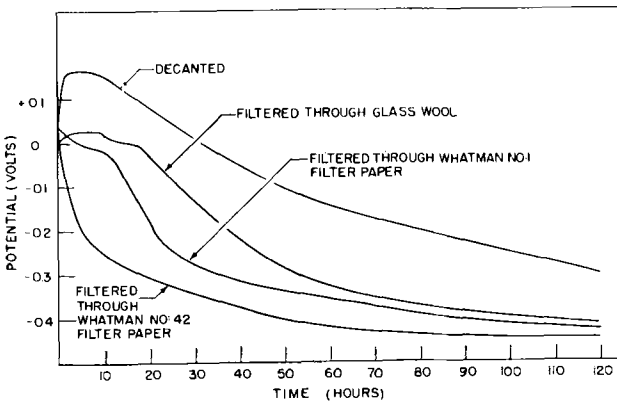


FIG. 3. Effect of filtration on potential/time curves in lead extracts containing dissolved air.

Potential determinations were carried out in apparatus described previously (10) in which a specimen measuring 2.5 x 0.5 cm was exposed to 10 ml of the deaerated decanted extract, to which had been added 10 ppm chloride ion, in order that the chloridized silver wire also contained inside the apparatus could take up a steady potential characteristic of the concentration of chloride in solution. Results,

TABLE II. Weight losses in deaerated extracts

Solution	Wt loss/cm ² mg	Average wt loss/cm ² mg
PbO extract filtered through glass wool..	0.024, 0.028, 0.028	0.027
Pb extract filtered through glass wool..	0.024, 0.024, 0.022	0.023
Pb ₃ O ₄ extract filtered through glass wool..	0.028, 0.036, 0.028	0.031

(Fig. 5), show that deaeration results in a large shift in potential in the negative (less noble) direction.

Examination of Extracts

Initial pH values of extracts were found to be distinctly alkaline (Table I) which confirms much previous work (6, 7, 11). It was, therefore, decided to determine whether passage of lead or zinc into solution had resulted in any appreciable buffering action. One hundred ml of each deaerated extract was titrated electrometrically with 0.01N HCl while being constantly stirred by means of an electromagnetic stirrer. Results (Fig. 6) show that extracts from litharge, lead, and red lead have a pronounced buffering action, whereas those from basic

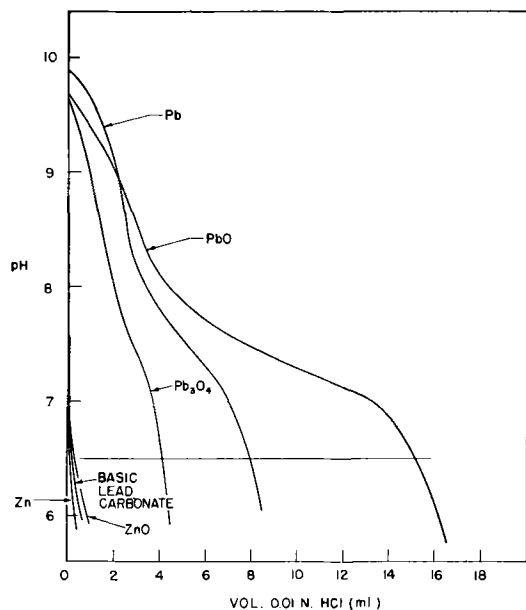


FIG. 6. Neutralization curves of decanted extracts

lead carbonate, zinc, and zinc oxide do not. Reserve alkalities, which are arbitrarily defined as volumes of 0.01N HCl required to bring the pH values of 100 ml of the extracts to 6.5, are shown in Table I.

Effect of filtration on the neutralization curves of extracts from litharge, metallic lead, and red lead was next investigated. Methods of filtration used included filtration through glass wool, through Whatman No. 1 filter paper, and through Whatman No. 42 filter paper which should remove progressively greater quantities of insoluble compounds from solution. In every case, progressively finer filtration progressively reduced reserve alkalities of the extracts (Table I).

Change in pH with time due to absorption of atmospheric carbon dioxide was determined by permitting decanted extracts to remain in contact with the atmosphere for five days. Measurements of pH were made on the solutions each day (Fig. 7).

An examination of the extracts from lead and from litharge was next undertaken to determine whether the superior inhibitive properties of extracts from litharge were caused by greater concentration of lead in solution or by lead being present in a different form than that in the lead extract.

In order to relate the reserve alkalities of the extracts to the total quantity of lead in solution, 50 ml of each extract was filtered through glass wool and the reserve alkalities determined. Total lead concentration of the same solutions was then determined gravimetrically with results as shown in Table III.

The weight of lead required to produce appropriate buffering action was calculated, assuming that it was present in the form of $Pb(OH)_2$. This is probably true for lead extract (12), although it has been

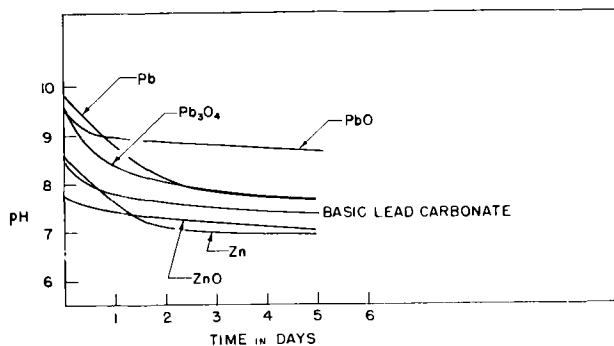


FIG. 7. Effect of atmospheric carbon dioxide uptake in the pH values of decanted extracts.

TABLE III

Solution	Reserve alkalinity ml 0.01N HCl	Wt of lead in solution, mg	Calculated wt of lead required to produce appropriate buffering action, mg	Wt of lead apparently not contributing to buffering action, mg
Pb extract filtered through glass wool....	6.2	3.8	3.2	0.6
Pb extract filtered through glass wool....	10.6	7.8	5.5	2.3

stated that the $Pb(OH)_2$ slowly transforms to the more insoluble lead dioxydihydroxide $Pb_3O_2(OH)_2$ (13). Since, in either case, one molecule of the lead compound requires two molecules of HCl for dissolution, the calculation is not affected by the transformation. Lead extract gives quite close agreement between calculated and measured weights of lead in solution, the error of 0.6 mg probably being due to the formation of basic carbonate which has little or no buffering action. There is, however, a marked disagreement between the calculated and observed weights of lead in the litharge extract which may mean that the lead is present in some form different from $Pb(OH)_2$ or $Pb_3O_2(OH)_2$.

Twenty-five ml of each extract were filtered through Whatman No. 42 filter paper and the ultraviolet absorption spectra determined in a Cary recording spectrophotometer (Model 11). Unfortunately concentrations of lead in solution, 0.8 mg/25 ml in the litharge extract and 0.35 mg/25 ml in the Pb extract, were rather low for this type of investigation. Results with lead extract indicated only scattering from particles probably of colloidal dimensions and no absorption bands were present. Results with litharge extract indicated less scatter, although the total lead concentration in solution was higher. There was an absorption band at 2080 Å which is not usually found in molecular litharge (14). Although this band is very near to the lower limit of the instrument it is considered to be significant. It should also be pointed out that a concentration difference of 100% would not cause its disappearance.

Twenty-five ml of the litharge extract were filtered through Whatman No. 42 filter paper and enclosed in a semipermeable membrane of untreated (non-waterproofed) cellophane. The "bag" of cellophane was then placed in 25 ml of distilled water to determine whether an appreciable quantity of the total lead in solution was present in the ionic state. Using the lead sulfide test, it was found that appreciable quantities of lead passed from the extract through the semipermeable membrane and into the surrounding water. A considerable proportion of the total lead was adsorbed by the cellophane so that after dialysis for one day, neither the solutions inside nor outside the membrane were completely inhibitive. Potential-time data subsequently obtained for steel specimens exposed to these solutions indicated that the solution from outside the membrane, containing lead in the ionic form, had temporary inhibitive properties at least equal to the solution from inside the membrane containing a greater total quantity of lead compounds, some presumably in the ionic state and the remainder in the colloidal state.

An attempt was made to repeat this examination using the extract from metallic lead, but it was found that the concentration of lead in solution was not sufficient to give significant results.

Nature of Passivity Films Formed in Litharge Extracts

Specimens passivated for five days in litharge extracts that had been decanted, or filtered through glass wool, through Whatman No. 1 filter paper, or through Whatman No. 42 filter paper, were then washed for 15 min in running distilled water, wiped with filter paper, and dried with methanol. They were then etched with dilute nitric acid to destroy passivity films; the acid was adjusted to a pH value of 2.0 with dilute sodium hydroxide and tested for the presence of lead by means of the lead sulfide test. In no case was a positive test for lead obtained and it was concluded that any lead that might be present in the passivity films was so small in quantity (less than 10^{-5} mg/cm² of specimen) that it could not be directly responsible for passivity.

The passivity film resulting from two days' exposure of an originally film-free steel specimen to a litharge extract that had been filtered through glass wool was isolated from the metal by a modification of the methanol-iodine method (15). The apparatus, shown in Fig. 8, permits passivity films to be isolated without bringing the specimens into contact with air after passivation. The specimen was suspended in the reaction chamber (R) which was partly filled with 0.1N ammonium chloride. The system was flushed with purified nitrogen³ and the specimen made

³ Nitrogen was purified by passing it through a column containing finely divided copper, deposited on Fullers earth, at a temperature of 200°C.

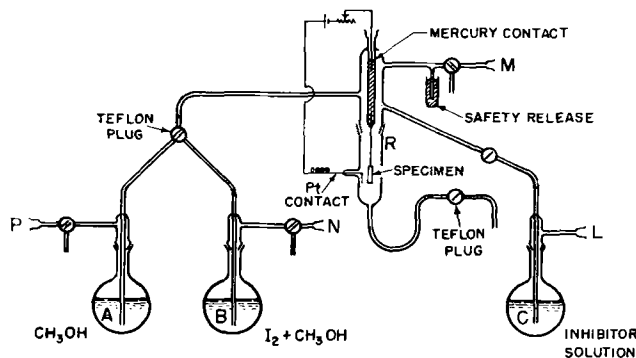


FIG. 8. Film stripping apparatus

cathodic for one minute at a current density of 1 milliamp/cm² in order to destroy the air-formed oxide film by cathodic reduction (16). Ammonium chloride was then forced from the reaction chamber by nitrogen admitted through (M) and replaced by the litharge extract, saturated with dissolved air, which was forced from the flask (C) by compressed air. To eliminate contamination by chloride, this solution was drained away and replaced by fresh inhibitor from (C). The apparatus was then opened to the air and the specimen allowed to stand in the inhibitor solution for two days. At the end of this period the apparatus was flushed with nitrogen and flask (A) filled with anhydrous methanol and (B) with 100 ml of anhydrous methanol in which had been dissolved 6 grams of anhydrous iodine. The iodine had previously been dried by standing over phosphorus pentoxide while the methanol was dried by refluxing with, and distilling from, magnesium turnings and a trace of iodine. Both solutions were deaerated by simultaneous boiling and bubbling of nitrogen. The solutions were cooled and the inhibitor solution forced from the reaction chamber. The specimen was washed several times with methanol forced from flask (A) by compressed nitrogen. The film stripping solution in (B) was then forced into the reaction chamber and left in contact with the specimen for approximately 30 min. At the end of this period, the film stripping solution was run from (R) and the specimen again carefully washed with methanol from (A). The specimen was finally removed from the apparatus and placed in a dish of methanol. The passivity film, which should be hanging loosely from the specimen, was detached by gentle agitation of the dish, and suitable samples were collected on copper grids for examination by electron diffraction.

Portions of stripped film were examined by electron diffraction and gave a diffuse ring pattern characteristic of either γ -Fe₂O₃ or Fe₃O₄ (Table IV). Portions of the films were dissolved in 1:1 HCl and tested for the presence of ferrous ions using the

TABLE IV. Ring pattern obtained from stripped passivity film

Ring radius	Spacing	Intensity	hkl
<i>cm</i>	<i>d</i> (Å)		
1.24	2.50	V.S. ^a	311
1.49	2.07	S ^b	400
1.94	1.60	W ^c	511, 333
2.10	1.49	S	440
2.63	1.20	W	444

^a V.S.—very strong; ^b S—strong; ^c W—weak.

di-2-pyridyl test (17). Failure to detect ferrous ions indicated that the passivity film was largely composed of γ -Fe₂O₃ which compound has been found to be the major constituent of passivity films formed in many anodic inhibitors (8, 18, 19).

DISCUSSION

It is evident that extracts from litharge, metallic lead, and red lead have definite inhibitive properties, whereas those from basic lead carbonate, zinc, and zinc oxide do not. Inhibitive properties of extracts from metallic lead and from red lead appear to be of a temporary nature, which is in accord with previous work (2–4). Similar temporary inhibitive properties have been previously ascribed to basic lead carbonate (5) but this was not confirmed in this examination. However, properties of these extracts may well depend on the method of preparation, which may explain discrepancies in the results of different investigators. The following discussion is, therefore, confined to the behavior of the extracts prepared in the manner described above.

Whereas the protective action of decanted extracts from metallic lead and red lead lasted for only 24 and six hours, respectively, extracts from litharge gave complete inhibition for prolonged periods; this protective action was not destroyed by filtering with a fine quantitative paper such as Whatman No. 42. It is proposed, therefore, to discuss first the protective action of litharge extracts and then to attempt to point out the reasons for the less effective protection afforded by the other extracts.

Protective Action of Litharge Extracts

From the form of potential-time curves in solutions containing dissolved air (Fig. 2) and from the fact that specimens were unchanged in appearance and had no detectable weight loss in five days (Table I), it appears that the litharge extract was behaving as an effective anodic inhibitor, a conclusion previously advanced by Mayne (1). Had the litharge been functioning as a cathodic inhibitor, the potential would have been more negative and some corrosion would have taken place before a protective film was formed.

Anodic inhibition may presumably be brought about either by adsorption of lead compounds from solution onto the anodic areas or by the oxide film mechanism, which has been proposed for such common anodic inhibitors as sodium hydroxide (18), sodium phosphate (10), sodium carbonate, sodium benzoate, and sodium silicate (19).⁴ Failure to detect even minute traces of lead compounds in passivity films makes it unlikely that inhibition is caused by adsorption of lead compound from solution. Passivity films isolated from initially film-free steel specimens passivated for two days in filtered litharge extracts were found to be composed largely of γ -Fe₂O₃, no second phase, neither lead compounds nor hydrated oxides of iron, being detected. It should be pointed out that the electron microscope-electron diffraction technique developed by Menter (18, 19) was not employed in this examination and so detection of small amounts of a second phase would not be expected. Chemical examination largely precluded the presence of lead compounds, but some hydrated oxides of iron, such as lepidocrocite (γ -FeO·OH), might well be present in small amounts.

Inhibitive properties of litharge extracts are dependent on the presence of oxygen dissolved in solution since it was shown that, when the extracts were deaerated, the potential became very much more negative (reactive) (Fig. 5) and the iron was slowly attacked (Table II). The form of the potential-time curve indicated that the corrosion was largely under cathodic control and that no film formation was occurring in deaerated solution. This behavior is identical to that of anodic inhibitors having non-oxidizing anions such as sodium hydroxide, carbonate, benzoate, acetate, and silicate previously investigated by the author (9). Inhibition is considered to be primarily due to oxygen dissolved in solution which adsorbs on the surface of the iron and takes part in a heterogeneous reaction with surface iron atoms to form a thin film of γ -Fe₂O₃, probably in a manner similar to that by which oxide films are formed in air. The thickness of similar films of γ -Fe₂O₃ formed in solutions of sodium phosphate and in air was found to be 100–200 Å (20).⁵ Since the formation of a protective film of oxide is not instantaneous, it is believed that the initial stages of film formation are accompanied by very slow corrosion which, on account of the very small size of the areas available for anodic reaction, is

⁴ It was previously suggested (21) that inhibition might be due to a dilute solution of sodium silicate formed by interaction of water with the glass vessels. Potential/time curves (Fig. 1) and weight loss determinations (Table I) in water that had been stored in glass bottles for four weeks show that this explanation is unlikely.

⁵ Calculated on the apparent surface area of the specimens.

mainly under anodic control, and leads to the formation of small inclusions of corrosion product in a matrix of $\gamma\text{-Fe}_2\text{O}_3$. It has been suggested that rate of formation of the oxide film should be independent of the $p\text{H}$ of the solution (10), but that the rate of the accompanying electrochemical corrosion decreased with a rise in the $p\text{H}$ value of the solution. Since factors tending to stimulate the rate of electrochemical corrosion should militate against passivity, high $p\text{H}$ values should be more favorable to passivity and low $p\text{H}$ values more favorable to corrosion. Formation of the inclusions of corrosion product, usually lepidocrocite (18), from ferrous ions, hydroxyl ions, and dissolved oxygen results in the local production of hydrogen ions which are detrimental to passivity; it has been suggested, therefore, that anodic inhibitors that have a high $p\text{H}$ value and are also well buffered are likely to be the most effective (19).

Protective Action of Other Extracts

Extracts prepared for this examination were all found to have $p\text{H}$ values higher than 7.0. In addition, however, their reserve alkalinities were determined (Fig. 6 and Table I). By comparison with the weight-loss results (Table I) it can be seen that the reserve alkalinities of the decanted extracts are related to their efficiencies as anodic inhibitors. The litharge extract with a reserve alkalinity of 15.2 ml protected completely; the metallic lead extract, reserve alkalinity 7.9 ml, protected for 24 hr, while the red lead extract, reserve alkalinity 4.1 ml, protected for 6 hr. The remaining extracts with reserve alkalinities of 0.3–0.15 ml had no detectable inhibitive properties.

In practice, these reserve alkalinities are further decreased by absorption of atmospheric carbon dioxide which leads to the precipitation of basic lead or zinc carbonates. Effect of prolonged exposure to the atmosphere on $p\text{H}$ values of the extracts is shown in Fig. 7. The $p\text{H}$ value of all extracts became lower but the proportionately greatest effect was noted with extracts from metallic lead and zinc.

Lack of protective action of the extracts from basic lead carbonate, metallic zinc, and zinc oxide is thus attributed to their lower $p\text{H}$, and to their low reserve alkalinities which makes them unable to counteract local drop in $p\text{H}$ at anodic areas.

Extracts from metallic lead and red lead have higher initial $p\text{H}$ values and greater reserve alkalinities than those extracts mentioned above. However, lead extract absorbed atmospheric carbon dioxide at an inordinately high rate which must result in a considerable decrease in its reserve alkalinity. Initial stages of passivation in these extracts are considered to be similar to those suggested above for

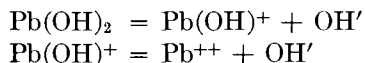
litharge. There is no evidence that the temporary protective action of red lead is in any way connected with its oxidizing properties, as suggested previously (2). The potential-time curve determined in deaerated solution (Fig. 5) showed that these oxidizing powers were insufficient to cause any detectable film formation. Furthermore, it was previously shown by Mayne (11) that lead dioxide, a more powerful oxidizing agent, had no inhibitive action on the corrosion of iron. One of the differences between these extracts and that from litharge is that their lower reserve alkalinities are able to maintain only a temporarily alkaline $p\text{H}$ value at pores in the oxide film where hydrogen ions are being generated due to the formation of corrosion product. Lead extract, having a higher reserve alkalinity, maintains the temporary protection for a longer time than that from red lead.

Nature of Extracts from Metallic Lead and Litharge

Apart from the fact that extracts from litharge, metallic lead, and red lead have appreciable reserve alkalinities, the composition of these extracts has not yet been discussed. Their reserve alkalinities are undoubtedly associated with the passage of lead into solution. Formation of the extract from metallic lead is, perhaps, most easily understood. It is believed that the lead corrodes in the normal electrochemical manner and that the interaction of the anodically formed lead ions with hydroxyl ions generated at the cathodes leads to the precipitation of sparingly soluble lead hydroxide. It has been stated (13) that this lead hydroxide then transforms into the less soluble lead dioxydihydroxide $\text{Pb}_3\text{O}_2(\text{OH})_2$ or $3\text{PbO}\cdot\text{H}_2\text{O}$ (13). That lead is present in solution largely as $\text{Pb}(\text{OH})_2$ [or $\text{Pb}_3\text{O}_2(\text{OH})_2$] is supported by the comparison of the calculated weight of lead, as lead hydroxide, required to produce the determined reserve alkalinity, with the observed weight of lead in solution (Table III). The slight discrepancy in results is probably due to action of atmospheric CO_2 which forms some basic lead carbonate which has a very low reserve alkalinity. Filtration with progressively finer filter papers reduces the lead content of the solution and the reserve alkalinity (Fig. 6 and Table I) by removal of greater quantities of insoluble material and probably also by adsorption of lead on the filter paper (1). A portion of the lead in solution appeared to be in colloidal form and was not removed by filtering with Whatman No. 42 filter paper. The ultraviolet absorption spectrum of such a solution was a curve characteristic of scatter from colloidal particles.

Appreciable quantities of litharge are known to be dissolved by distilled water (22) and the resulting solution is alkaline (11). The weight of litharge dissolved is said to be reduced in the presence of

carbon dioxide. Litharge was assumed to be in solution in the form of $\text{Pb}(\text{OH})_2$ by Glasstone (23) who quoted a value of 1.7×10^{-15} for its solubility product. According to Pleissner (13), however, the $\text{Pb}(\text{OH})_2$ had two stages of ionization, viz.:



for which α , the percentage degree of ionization, was 27% for the first step. This was supported by the observations of Berl and Austerweil (24) who found complete ionization of a solution of $\text{Pb}(\text{OH})_2$ containing 0.262 millimole/liter.

Several experiments were performed to determine whether litharge extract differed from lead extract because lead concentration in solution was higher, or because the lead in solution was present in some different form. It was first found (Table III) that, although the reserve alkalinity of the litharge extract was higher than that of lead extract, the proportion of the total lead, calculated as lead hydroxide, apparently contributing to reserve alkalinity, was lower. This appeared unlikely to be due to absorption of atmospheric CO_2 which was less readily absorbed by litharge extracts than by metallic lead extracts (Fig. 7). Furthermore, although the buffering power of decanted extracts accurately reflected their relative inhibitive powers, this was not so with filtered litharge extracts, some of which gave complete inhibition with reserve alkalinities as low as 1.6 ml (Table I). Dialysis experiments indicated that these extracts contained a proportion of lead in the purely ionic form rather than as colloidal $\text{Pb}(\text{OH})_2$; this conclusion was supported by the ultraviolet absorption spectrum, which showed that the filtered litharge extract, although containing a greater total weight of lead than the filtered lead extract, gave less random scatter (due to the presence of colloidal particles) but had an absorption band at 2080 Å. This band is not found in the spectrum of molecular PbO and is probably characteristic of some form of ionic lead.

No one section of the above evidence is conclusive in itself, but taken together these points indicate that the lead in litharge extracts is partly present in some different form from that in metallic lead extracts, which appear to contain lead mainly in the form of $\text{Pb}(\text{OH})_2$. Since $p\text{H}$ considerations largely preclude the formation of plumbite ions and lead ions themselves have no inhibitive properties (1), it appears that the lead may be partly present as $\text{Pb}(\text{OH})_2$ and also as $\text{Pb}(\text{OH})^+$ ions. These ions would be expected to have a greater mobility than colloidal $\text{Pb}(\text{OH})_2$ and would react more quickly with hydrogen ions formed at anodic areas and, therefore, produce more effective buffering. This may explain not only the superior buffering action, but

also the superior inhibitive properties of the litharge extracts. Since the $\text{Pb}(\text{OH})^+$ ions would be expected to have a low transport number their rate of migration away from anodic areas should not be high enough to detract from their local buffering action and hence from their inhibitive properties.

ACKNOWLEDGMENTS

The author wishes to thank Mr. J. Harris for supplying the pigments, Dr. D. S. Russell and Mr. P. Tymchuk for carrying out the analyses of the extracts and of the pigments, Dr. C. Sandorfy for determining the ultraviolet absorption spectra, and Dr. F. J. Bowen and Mr. W. E. Stump for their helpful comments.

Any discussion of this paper will appear in a Discussion Section to be published in the December 1954 issue of the JOURNAL.

REFERENCES

1. J. E. O. MAYNE, *J. Soc. Chem. Ind. London*, **65**, 197 (1946).
2. R. M. BURNS AND H. E. HARING, *Trans. Electrochem. Soc.*, **69**, 178 (1936).
3. K. G. LEWIS AND U. R. EVANS, *J. Soc. Chem. Ind.*, **53**, 25T (1934).
4. S. C. BRITTON AND U. R. EVANS, *ibid.*, **58**, 90 (1939).
5. J. C. HUDSON, 4th Report of Corrosion Committee, Iron and Steel Institute, London 199 (1936).
6. U. R. EVANS, "Corrosion, Passivity & Protection," p. 595, Arnold, London (1937).
7. J. E. O. MAYNE, *Research, London*, **6**, 278 (1952).
8. J. E. O. MAYNE AND M. J. PRYOR, *J. Chem. Soc.*, **1949**, 1831.
9. M. J. PRYOR AND M. COHEN, *This Journal*, **100**, 203 (1953).
10. M. J. PRYOR AND M. COHEN, *ibid.*, **98**, 263 (1951).
11. P. YORKE, *Phil. Mag.*, **28**, 17 (1846).
12. M. TRAUBE-MENGARINI AND A. SCALA, *Kolloid-Z.*, **6**, 240 (1910).
13. M. PLEISSNER, *Arb. kaiserl. Gesundh.*, **26**, 398 (1907).
14. R. W. B. PEARSE AND A. G. GADE, "Identification of Molecular Spectra," p. 206, John Wiley & Sons, Inc., New York (1949).
15. W. H. J. VERNON, F. WORMWELL, AND T. J. NURSE, *J. Chem. Soc.*, **1939**, 621.
16. U. R. EVANS AND H. A. MILEY, *Iron Steel Inst. London, Carnegie Schol. Mem.*, **25**, 197 (1936).
17. F. FEIGL, "Qualitative Analysis by Spot Tests," p. 96, Nordemann Publishing Co. Inc., New York (1939).
18. J. E. O. MAYNE, J. W. MENTER, AND M. J. PRYOR, *J. Chem. Soc.*, **1950**, 3229.
19. J. W. MENTER, *Compt. Rend. du Premier Congres International de Microscopie Electronique*, Paris 1950; *Editions de la Revue d'Optique*, Paris 1952.
20. M. J. PRYOR, M. COHEN, AND F. BROWN, *This Journal*, **99**, 542 (1952).
21. R. S. THORNHILL, Discussion to J. E. O. Mayne, *J. Soc. Chem. Ind.*, **67**, 199 (1946).
22. H. REMY AND A. KUHLMAN, *Z. anal. Chem.*, **65**, 161 (1924).
23. S. GLASSTONE, *J. Chem. Soc.*, **119**, 1689 (1921).
24. F. BERL AND G. AUSTERWEIL, *Z. Elektrochem.*, **13**, 169 (1907).

Measurement of Particle Size Distribution of Phosphors¹

MARTHA J. BERGIN AND KEITH H. BUTLER

Sylvania Electric Products Inc., Salem, Massachusetts

ABSTRACT

A quick method of calculating particle size distribution from optical measurements of sedimentation rates is described. It is shown that the apparent mean diameter is greatly influenced by degree of dispersion of the powder and that reproducibility requires careful control of dispersion.

INTRODUCTION

Use of a single mean value to express "particle size" of a nonhomogeneous powder does not adequately define coarseness or fineness of the powder. Depending on the particular method of measurement or calculation employed, there are several different average diameters. For a satisfactory definition of the powder, particle size distribution must be known.

Similarly, there is no universally applicable method for determining particle size distribution of powders because of the tremendous range of sizes encountered. Microscopic counting can be applied over a considerable range by using variable magnification, while extremely small size material may be measured by use of an electron microscope. However, at best, counting is an extremely tedious process.

Within a limited range of particle size, gravity sedimentation in a liquid medium is adequate, but the problem of measuring the amount of material settled in a given time presents some difficulties. Gravimetric methods, such as the Andreasen pipette or the Oden balance are accurate, but again the elapsed time from start to finish is quite long.

Measurement of optical transmission during sedimentation is a very convenient method experimentally, but interpretation of data has required rather slow and complex calculations (1) giving, finally, a histogram of distribution. A somewhat simpler method of calculation is described by Musgrave and Harner (2), but even this requires considerable time, which has limited its use.

The particle size of phosphors used in fluorescent lamps and television tubes lies inside the range for gravity sedimentation. Knowledge of their particle size distribution is valuable both for control of firing procedures and milling methods, as well as for development of new methods of making and proc-

essing these phosphors. Limitations of previously described methods have so restricted their general use that important differences between phosphors are frequently not recognized.

This paper presents a simplified method of calculation using optical transmission data, with which a distribution curve can be obtained in minutes rather than hours. It is thus suited for control work. The method is based on two postulates: first, the light scattering coefficient is independent of particle size, and second, the particle size distribution function can be represented adequately by a log-normal probability function.

Using optical transmission data, a simple slide rule calculation gives points for plotting on probability paper, and a simple graphical conversion gives distribution of particle size.

The method is limited by three requirements which are adequately met by most phosphors: (a) the distribution must contain few particles smaller than 2μ , because turbulence invalidates Stokes' law for smaller particles; (b) only a small percentage larger than 50μ should be present to avoid difficulty in obtaining transmission at zero time, as a result of excessively rapid settling; (c) there must be an adequate difference in refractive index between the particle and the medium to insure constancy of the light scattering coefficient.

Since the basic purpose of the work was development of a rapid method suitable for comparison measurements on similar materials, rather than that of a precision method for absolute values on a wide range of materials, no attempt was made to estimate absolute errors resulting from approximations used.

MATHEMATICAL DISCUSSION

Basic Principles

Several texts (3, 4, 7) discuss in detail the relationship between transmission and particle size. It should be pointed out that light is scattered by transparent particles suspended in a medium with a different refractive index. Light which enters the

¹ Manuscript received June 26, 1953. This paper was prepared for delivery before the New York Meeting, April 12 to 16, 1953.

slit and thence the photocell has two components: first, all of the unscattered light, and second, part of the scattered light. With the geometry of the Photometer, the correction for scattered light is small and will be only slightly changed by particle size or concentration.

The amount of light transmitted through the suspension is given by Beer's law which can be expressed in the form

$$L_t/L_\infty = e^{-KB} \quad (I)$$

where B is the sum of cross-sectional areas of the particles; K is the constant dependent on dimensions of the equipment and on scattering coefficient of the particles, L_t is light transmitted through the suspension at time t , and L_∞ is light transmitted through the system free of particles. The zero subscript (e.g., L_0) denotes the value at a settling time of $t = 0$. Formula (I) can be converted to natural logarithms

$$\ln (L_\infty/L_t) = KB \quad (II)$$

The assumption that a log-normal probability distribution of particle size is present holds for many industrial products prepared by firing or grinding. Both operations are common in the preparation of phosphors. Separation by centrifuging or elutriation, or in a few cases by screening, may significantly alter the distribution so that the log-normal law does not hold. However, these operations are not customary in phosphor preparation, so they should not affect the validity of the postulate. In any event, an inspection of plotted data shows whether a log-normal distribution does exist.

It is assumed that the constant, K , in Beer's law is independent of particle size. Its variation with particle size, index of refraction, and wave length of light has been thoroughly discussed in recent literature on optical scattering coefficients, with DeVore and Pfund (5) and Gumprecht and Sliepevich (6) giving excellent summaries.

DeVore and Pfund show a universal scattering curve in which the abscissa is the parameter $d/\lambda (m^2 - 1)/(m^2 + 2)$. When this parameter² is above 0.6, scattering remains constant at 2.0 over a very large range of parameter values; while, if the parameter falls below 0.6, the scattering coefficient deviates considerably from this constant value. Hence 0.6 may be chosen as a limiting value for the parameter. With zinc sulfide in water, the parameter drops to 0.6 at a particle size of $\frac{1}{2} \mu$. Since most television phosphors are above this size, it can be assumed that the scattering coefficient is constant.

For calcium halophosphates in water, because of

² d is the particle diameter, λ the wave length of light, while m is the ratio of refractive indices of particle and medium.

the different refractive index, the limiting value 0.6 of the parameter is reached at 2.0 μ diameter. In this case, deviations from Beer's law may be a little more pronounced, but, since these phosphors are usually large in particle size, the assumption that the scattering coefficient is constant seems valid. Even with xylol as the medium, Beer's law holds adequately for most phosphors.

Applying formula (II), it can be seen that the ratio of the total cross-sectional areas of particles in the suspension at time t , to that present at time $t = 0$, is given by:

$$B_t/B_0 = [\ln (L_\infty/L_t)]/[\ln (L_\infty/L_0)]. \quad (III)$$

This can be converted to common logarithms and simplified by setting $L_\infty = 1$, and expressing L_t and L_0 in terms of this unit, giving

$$B_t/B_0 = (\log 1/L_t)/(\log 1/L_0). \quad (IV)$$

This ratio can be quickly determined by a slide rule calculation after L_0 and L_t are known. Since B_t is the integral of the cross-sectional area of the particles which have not settled out at time t , while B_0 is the corresponding integral for the complete distribution, then plotting on logarithmic probability paper 100 B_t/B_0 against time of settling should give a straight line, if the log-normal law for particle size distribution is valid.

Conversion of Data

Having obtained the first graph of the function $(\log 1/L_t)/(\log 1/L_0)$ against time, conversion to a graph of $F(d)^3$ against diameter is quite simple. It is assumed that Stokes' law holds, and this may be written as:

$$d^2 = 18 \times 10^8 h\eta/(D_1 - D_2)gt \quad (V)$$

where d is diameter in microns, η is viscosity in poises, h is distance settled in centimeters, D_1 is absolute density of the particles in grams/cc, D_2 is density of the medium, g is 980 (the gravity constant), and t is time in seconds.

Using this formula, the diameter corresponding to a 100-min settling time is calculated. From the graph, the percentage settled at 100 min is determined, and this percentage plotted against calculated diameter. A point corresponding to 1-min settling time is plotted against ten times this diameter, and a straight line drawn through the two points. This plot can be made on the same sheet of log-probability paper used for the original data.

From this graph, it is possible to determine the median diameter, d_{op} , which is the 50% point and also the standard deviation, σ , which is given by $\sigma = \text{diameter at } 50.00\% / \text{diameter at } 15.87\%$.

³ $F(d)$ is the cumulative per cent of particles having diameters below diameter d .

The median optical diameter, d_{op} , is also the geometric mean optical diameter based on area.

The geometric mean diameter, d_g , as defined by DallaValle (5), is expressed as

$$\log d_g = \Sigma n \log d / \Sigma n \quad (\text{VI})$$

This diameter is based on length, as determined by microscopic counting. Similarly, d'_g , is the geometric mean diameter based on weight (or volume) in the case of a screen analysis. So there are three separate geometric mean diameters: d_g based on length, d_{op} based on area, and d'_g based on volume.

From the two parameters d_{op} and σ , thus obtained, any desired statistical diameter can be calculated using methods given by DallaValle (3) or Herdan (4). Some of these conversion formulas are listed below⁴ for the most commonly used diameters. The parameters d_g and d'_g are defined above; d_{vs} represents the mean volume-surface diameter, and d_w the weight mean diameter in DallaValle's notation.

$$\log d_g = \log d_{op} - 4.606 \log^2 \sigma \quad (\text{VII})$$

$$\log d'_g = \log d_{op} + 2.303 \log^2 \sigma \quad (\text{VIII})$$

$$\log d_{vs} = \log d_{op} + 1.151 \log^2 \sigma \quad (\text{IX})$$

$$\log d_w = \log d_{op} + 3.454 \log^2 \sigma \quad (\text{X})$$

It is sometimes convenient to have a frequency curve with per cent plotted against diameter or against log of the diameter. This is done by picking off appropriate points and plotting differences against the average of the diameters using uniform intervals. In the case of a plot against log diameter, a geometric progression of diameters is used, e.g., 0.5, 1, 2, 4, 8 μ , with the point being plotted at the geometric mean of the interval.

The probability chart method of representing particle size distribution is not commonly used in the pipette method of measurement. In the present application, the procedure used was very similar to that used for optical measurement. It was tested to confirm by another method the fact that the distribution present in phosphors conformed to the log-normal law. The weight of powder in a unit volume of suspension was determined at a fixed point after various times of settling and expressed as a percentage of initial concentration. These quantities were then plotted against time on log-probability paper, and, by Stokes' law, converted to a plot of diameter. A comparison of the two methods is shown in Fig. 1. It should be noted that in the optical method 100-min settling corresponds to 2.1 μ , while in the pipette method 100 min cor-

⁴ The authors wish to thank Mrs. Mary S. Jaffe, one of the reviewers of this paper, for clarifying the mathematics of this difficult subject and correcting some errors in the formulas.

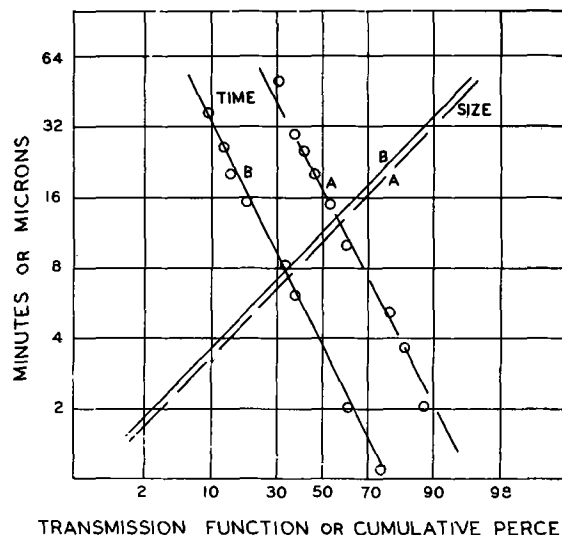


FIG. 1. Comparison of particle size distributions of halophosphates determined; curve A, by pipette method, curve B, by optical method.

responds to 4.4 μ , because of differences in the distance settled and in viscosity of the media. Both methods show that distribution was of the log-normal type.

EXPERIMENTAL DATA

In the present paper, data are intended to show application of the method to several phosphors, with some examples to show the effect of variables in the testing method on results.

Typical Experimental Run

Experimental data reported in this paper were obtained on the Photelometer.⁵ This instrument (1) consists essentially of a tungsten light source, a sedimentation cell, and a photocell whose response is measured on a microammeter. The amount of light which passes through the cell is recorded at predetermined time intervals. A reading of 100% transmission through the clear medium in a duplicate cell is used as reference. Although no provision is made for control of temperature around the cell itself, heat generated from the light source is eliminated by means of a heat absorber placed in the light path. A volume of 13 ml of suspension is normally placed in the cell. These conditions give a settling path of 3.4 cm.

To determine particle size, enough powder to give an initial transmission of between 20–40% (preferably 20–30%) is dispersed in a suitable medium. A more complete discussion of methods of dispersing is included in the next section. For most phosphors, a trisodium phosphate solution (1.0 g/100 ml water) accompanied by hand shaking of the cell for two minutes was found adequate to produce complete

⁵ Central Scientific Company.

deflocculation. The cell was then inserted into the Photometer and percentage of light transmitted recorded at various times.

The work sheet shown in Table I gives typical data as obtained on a zinc sulfide phosphor of the type used in cathode ray tubes. Data correspond to

TABLE I
Powder type—cathodoluminescent zinc sulfide
Dispersing solution—1% trisodium phosphate

Time (min)	Hand shaking (2 min)			Waring dispersion (5 min)		
	Photometer reading (L) [*]	Log (1/L)	100 B _t /B ₀	Photometer reading (L) [†]	Log (1/L)	100 B _t /B ₀
	%					
¼	42	0.376	95			
½	44	0.357	89			
¾	47.2	0.327	82			
1	51	0.282	71	35.5	0.450	86
1¼						
1½	61	0.224	56			
1¾	64	0.194	49			
2	68	0.168	42	41	0.388	74
3	83	0.081	20	45.4	0.342	66
4	92.5	0.034	8.5	49.2	0.308	59
5				53	0.276	53
6				55	0.260	49
7				57	0.244	47
8				60	0.222	43
9				62	0.208	40
10				64	0.194	37
15				70	0.156	30
20				72	0.144	27
25				74	0.131	24

* At zero time (by extrapolation), Photometer reading 40%.

† At zero time, Photometer reading 30%.

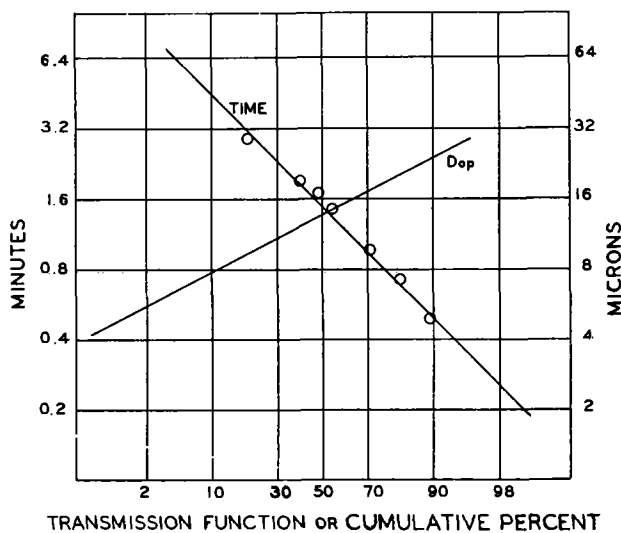
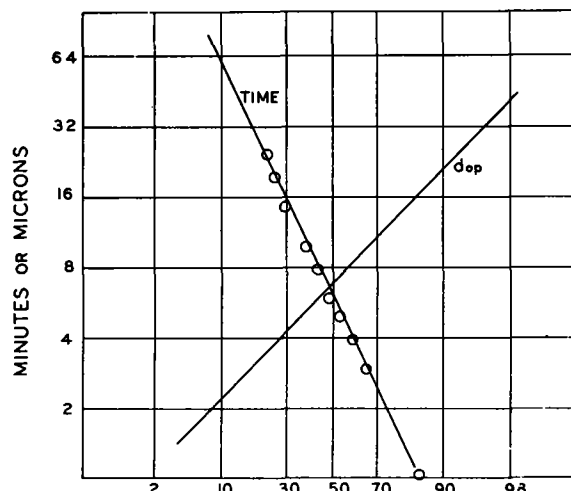


FIG. 2. Transmission function and derived particle size distribution of cathodoluminescent zinc sulfide; dispersed by hand shaking.



TRANSMISSION FUNCTION OR CUMULATIVE PERCENT

FIG. 3. Transmission function and derived particle size distribution of cathodoluminescent zinc sulfide, dispersed by Waring blender.

TABLE II. Data for Stokes' law calculation for ZnS

Temperature.....	25°C
Medium.....	Water
Viscosity.....	0.009 poises
Settling distance.....	3.4 cm
Particle density.....	4.10 g/cc
Medium density.....	1.00 g/cc
Time in seconds.....	6000
Calculated particle diameter.....	1.75 μ

Fig. 2 and 3. Table II gives necessary data for the Stokes' law calculation shown by formula (V).

Method of Testing Dispersion

In dealing with sedimentation, the effect of dispersion is vitally important. Since terminology is very poorly established, "primary particle," "aggregate," and "floculate" as used in this paper will be defined.

A "primary particle" is one which, when observed in the microscope, has well-defined boundaries and appears to be a single crystal.

An "aggregate" is a group of primary particles held together by some type of cementing agent so that mechanical work is needed to separate them.

A "floculate" is a group of primary particles or of aggregates present in a suspension, and held together by electrical charges, so that only a minute amount of mechanical work is needed to break them down into smaller particles. Such floculates are not present if the suspension is properly dispersed.

The major problem in preparing suspensions for any determination of particle size by sedimentation is that of preventing flocculation, since settling rate of a floculate is approximately that of an equivalent

spherical particle having the same total mass. To obtain accurate results, it is therefore necessary to use a dispersing agent to prevent flocculation.

To determine whether a suspension is deflocculated, a quick test is observation of a drop of the suspension magnified about 250 times. If sufficient dispersing agent is present, smaller particles will be in Brownian motion, and when two of these small particles come in contact, they will promptly separate rather than cohere. Use of an excess of agent may lead to reflocculation.

A more precise test is to determine particle size with varying amounts of dispersing agent present. If dispersion is good, particle size will be reproducible and will be smaller than the size obtained when either insufficient or excess agent is used.

Method of Dispersing Phosphors

Since phosphors as prepared and used are known to contain large numbers of aggregates of various sizes and band strengths, it is obvious that the method of dispersion may have a great effect on particle size distribution.

If severe mechanical work is applied to the suspension, all but the most firmly cemented aggregates will be completely separated and particle size distribution will approach that of primary particles. If this work is performed on a dilute suspension, for example by agitation with a Waring blender, it is improbable that any primary particles will be broken, but aggregates should be separated. This is discussed in more detail in a later section.

Fig. 4 shows the effect of various periods of agitation in the Waring blender with 0.2 gram of a fluorescent ZnS and 1.0 gram of phosphate per 100 ml of water. Effects of aggregation on settling rate are quite striking. The shaken suspension is apparently a mixture of coarse and fine material as shown by the break in curve A. The coarse fraction is quite uniform; i.e., on a particle size basis, σ is low. With increasing time of agitation in the blender this breaks down gradually. At one minute a mixture of coarse and fine exists as seen in curve B; at three minutes there is no evidence of coarse material (curve C); and at ten minutes the settling rate is still slower. Conversion of these data to particle size distributions shows that σ becomes smaller for the fine fraction as time of agitation increases.

Obviously, a great deal of care is needed in setting conditions of dispersion for powders of this type, if reproducible results are to be obtained.

Very gentle agitation, such as shaking by hand or by a wrist-action mechanical shaker, is sufficient to deflocculate the material without breaking down

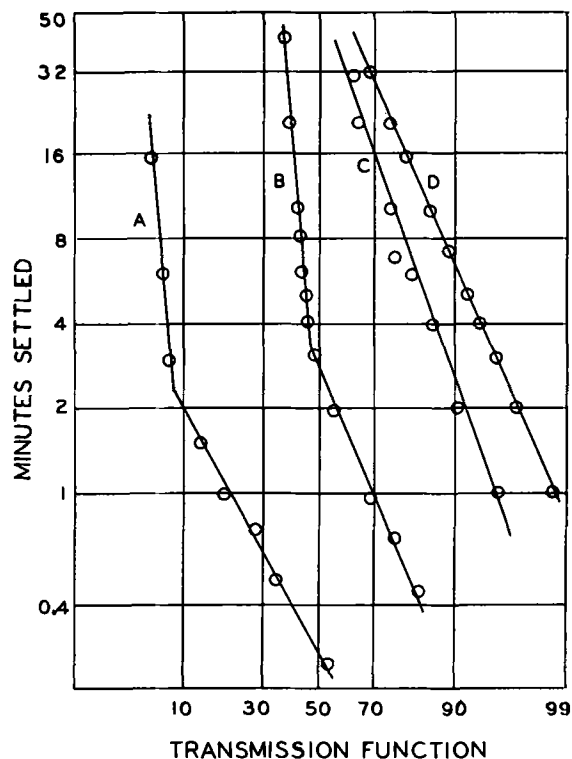


FIG. 4. Effect of dispersion time in Waring blender on transmission function 100 B_t/B_0 ; curve A, hand shaken; curve B, 1-min mix; curve C, 3-min mix; curve D, 10-min mix.

any aggregates except those with very weak bonding.

Particle sizes obtained have been designated: (a) aggregate particle size (D_{op}). This is the result obtained by hand shaking for two minutes; (b) ultimate particle size (d_{op}).⁶ This result is obtained using the Waring blender.

As was indicated in the experimental section, phosphors were dispersed with suitable agents in distilled water. Approximately 0.2 gram of phosphor was used per 100 ml of solution in the Waring blender tests. In hand shaking, sufficient phosphor was added to 13 ml of the solution to give an initial transmission reading of between 20–30%.

Data on Calcium Halophosphates

Several dispersing agents were tried with calcium halophosphates; of these, dilute ammonium hydroxide or dilute trisodium phosphate gave the most reproducible results. The effect of powder concentration during sedimentation was tested by runs with 0.5 gram/100 ml giving an initial transmission of 12% and 0.17 gram with an initial transmission of 39%. The results, shown in Fig. 5, in-

⁶ This "ultimate particle size" approximates that of primary particles, but a few aggregates may be present.

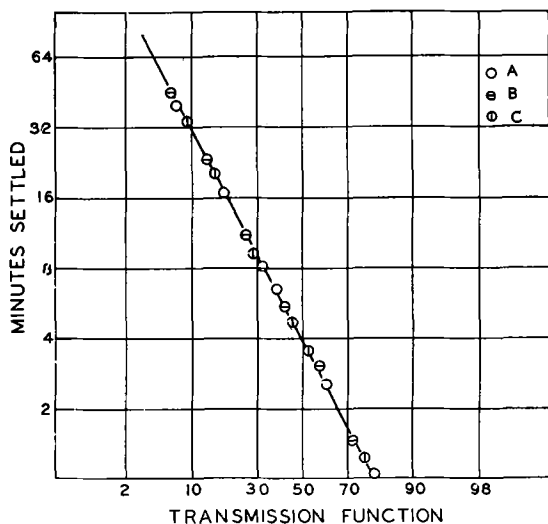


FIG. 5. Effect of concentration during sedimentation on transmission function with halophosphate phosphor.

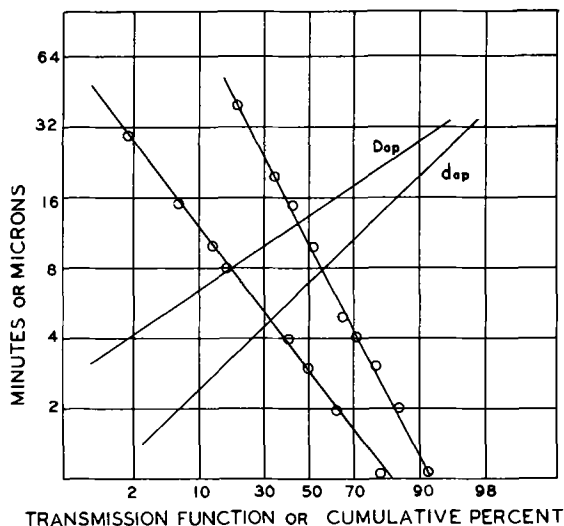


FIG. 6. Transmission function and derived particle size distribution of calcium tungstate; D_{op} , dispersed by hand shaking; d_{op} , dispersed by Waring blender.

indicate that concentration is not an important factor.

It has been found experimentally that the amount of work performed on the halophosphate suspension by the Waring blender does have some effect on particle size. The effect is, however, much less pronounced than with zinc sulfide. Aggregates are apparently separated in 3 min, and very little change in particle size results from further agitation. Change in amount of sample does have some effect with larger sample sizes leading to apparent smaller

particle sizes. This may be due to breaking by impact of one particle against another.

There is a striking difference in behavior of various phosphors when agitated in a Waring blender. Halophosphate phosphors show evidence of some aggregation, but the breakdown from mechanical work is slight. In contrast, the fluorescent zinc sulfide⁷ is composed of large aggregates, which are readily separated by the Waring blender, indicating that bonding forces are weak. Each particular powder must, therefore, be tested with varying degrees of mechanical work to determine how much dispersion is needed to give the ultimate particle size.

Data on Calcium Tungstate

Fig. 6 shows typical data on a calcium tungstate phosphor dispersed by two methods. The effect of mixing in the Waring blender was much like that observed with calcium halophosphate.

CONCLUSION

This paper has presented a quick method for determination of particle size distribution of phosphors by measurement of optical transmission during sedimentation. It has been assumed that Beer's law applies, and that distribution conforms to the log-normal law. Accuracy is more than adequate for many control and experimental applications. In addition to phosphors, the method is potentially useful for other powders with particle sizes between 2 and 50 μ .

Any discussion of this paper will appear in a Discussion Section to be published in the December 1954 issue of the JOURNAL.

REFERENCES

1. M. N. STATES, *A.S.T.M. Proc.*, **39**, 795 (1939).
2. J. R. MUSGRAVE AND H. R. HARNER, "Turbimetric Particle Size Analysis," Eagle-Picher Research Laboratories, Joplin, Mo. (1947).
3. J. M. DALLAVALLE, "Micromeritics," Pitman Publishing Co., New York (1943 and 1951).
4. G. HERDAN, "Small Particle Statistics," Elsevier Publishing Co., New York (1953).
5. J. R. DEVORE AND A. H. PFUND, *J. Opt. Soc. Amer.*, **37**, 826 (1947).
6. R. O. GUMPRECHT AND C. M. SLIEPCEVICH, *J. Phys. Chem.*, **57**, 90 (1953).
7. E. K. FISCHER, "Colloidal Dispersions," Chap. II, John Wiley & Sons, Inc., New York (1950).

⁷ The fluorescent zinc sulfide was New Jersey zinc # 2304, a fine partial size material intended for use in paints.

Electrothermal Heating of Solutions¹

KENNETH A. KOBE

University of Texas, Austin, Texas

AND

CARL J. CARLSON

Standard Oil Company of California, Avenal, California

ABSTRACT

For heating and evaporation of concentrated solutions of electrolytes, the solution itself can serve as a resistor to give uniform heating throughout. Solutions of salts having a negative temperature coefficient of solubility can be concentrated by electrical heating, provided electrodes are maintained at a temperature below that of the solution. Experimental details are given for solutions of sodium sulfate. The electrical conductivity of saturated solutions of Na_2SO_4 , Na_2CO_3 , Na_3PO_4 , and MgSO_4 has been determined from 25°C to 75° or 90°C.

INTRODUCTION

It is difficult to heat solutions of salts which have a negative temperature coefficient of solubility. These salts with an "inverted solubility curve" are well known as ones that form hard deposits of scale on heat transfer surfaces. Sodium sulfate, sodium carbonate, and calcium sulfate are salts of this type. Sodium sulfate is of particular importance because it usually is recovered from natural brines and industrial operations as sodium sulfate decahydrate, $\text{Na}_2\text{SO}_4 \cdot 10\text{H}_2\text{O}$, containing 56% water which must be removed before it is economical to ship the salt any distance. This problem of dehydration is one that has been attacked by many methods (1), of which submerged combustion, or internal heating with hot gases, has been the most successful (2). This process requires gaseous fuel which is not available in many localities.

One possible method of heating concentrated solutions has not been investigated. Little use has been made of the fact that the concentrated solution itself can be made the resistor in an electrical circuit and electrical power converted into heat uniformly within the body of the solution. The electric steam boiler is well known, but this has operated on dilute solutions. No work has been done on use of electrical energy for internal heating of saturated solutions, particularly solutions of those salts that are scale-formers.

SALT HYDRATES

Some salts that are dehydrated industrially to produce an anhydrous, or less hydrated, salt are

¹ Manuscript received April 17, 1953. The experimental work reported here was conducted in the laboratories of the Department of Chemical Engineering, University of Washington, Seattle, Washington.

$\text{Na}_2\text{SO}_4 \cdot 10\text{H}_2\text{O}$ (which contains 44.2% anhydrous salt), $\text{Na}_2\text{CO}_3 \cdot 10\text{H}_2\text{O}$ (37.1%), $\text{Na}_3\text{PO}_4 \cdot 12\text{H}_2\text{O}$ (43.2%), $\text{MgSO}_4 \cdot 7\text{H}_2\text{O}$ (48.9%), $\text{FeSO}_4 \cdot 7\text{H}_2\text{O}$ (54.7%). Although the feasibility of using electrical power for the dehydration process depends on economic considerations, the technical merit of the process warrants investigation, as does the action of scale-forming salts on electrodes. Fundamental data should be obtained which can be used for design purposes.

A large amount of data is available on electrical conductivity of dilute salt solutions, but few data are available on saturated solutions. Conductivity of saturated solutions of four salts (Na_2SO_4 , Na_2CO_3 , Na_3PO_4 , and MgSO_4) was determined from 25° to 75° or 90°C. Saturated solutions of an analytical grade of these salts were prepared by rotating a bottle containing a salt excess for 1 to 7 days in a thermostat set at the desired temperature. Concentration of the solution was determined to ascertain that it checked known solubility data. The saturated solution was transferred from the bottle to a calibrated conductivity cell immersed in the same thermostat, and conductivity of the solution was determined. Data are given in Table I and shown on Fig. 1. It undoubtedly is safe to extrapolate conductance curves for sodium sulfate and carbonate to their normal boiling points. For sodium phosphate and magnesium sulfate, both the solubility and conductance increase with temperature, so that extrapolation may not give a reliable value.

DEHYDRATION OF SODIUM SULFATE DECAHYDRATE

Because of the industrial importance of sodium sulfate and its well-known tendency to form scale, a small installation was built to study dehydration of sodium sulfate decahydrate to anhydrous salt.

TABLE I. Specific conductance of saturated solutions of four salts

Temp, °C	Specific conductance, mhos per cm ³			
	Na ₂ SO ₄	Na ₂ CO ₃	Na ₃ PO ₄	MgSO ₄
25.0	0.124	0.103	0.0702	0.0473
27.6	0.137	0.0984	0.0751	0.0494
30.0	0.147	0.0991	0.0821	0.0506
34.8	0.152	0.102	0.0867	0.0524
42.8	0.188	0.134	0.0973	0.0537
50.0	0.218	0.167	0.104	0.0545
64.0	0.278	0.234	0.187	0.0572
75.0	0.334	0.286	0.228	0.0588
90.0	0.394	0.366		

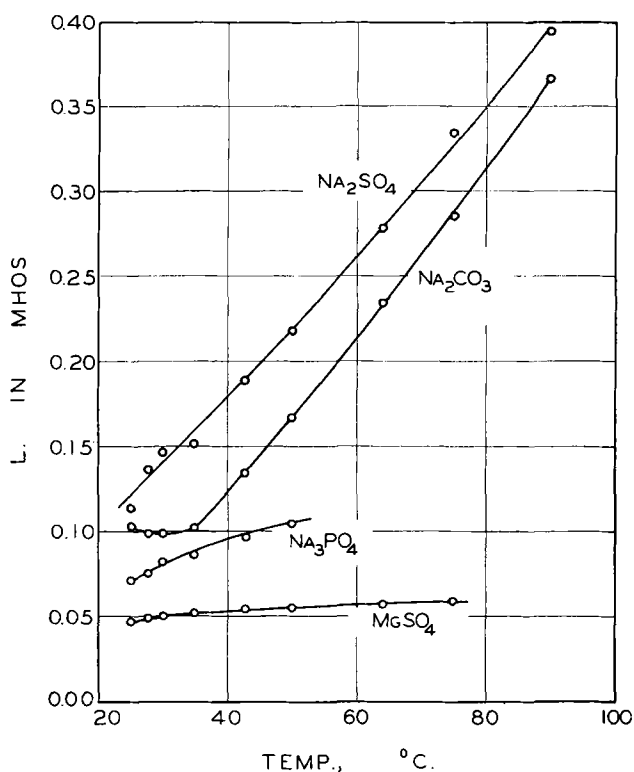


FIG. 1. Electrical conductivity of saturated salt solutions

The transition temperature of decahydrate to anhydrous salt is 32.4°C, above which sodium sulfate has a negative temperature coefficient of solubility. Solid sodium sulfate decahydrate added to a boiling solution will melt incongruently and immediately deposit part (47%) of the anhydrous sodium sulfate. The remainder of the sodium sulfate must be obtained by evaporating the water of hydration. A cycle of operations can be devised which will require a minimum of electrical energy by taking only the anhydrous sodium sulfate deposited on melting and returning the mother liquor to a natural pond for recrystallization of more decahydrate crystals. Such an operation calls for more pumping and handling of solids, so usually it is not practical for operations based on industrial production of decahydrate, or

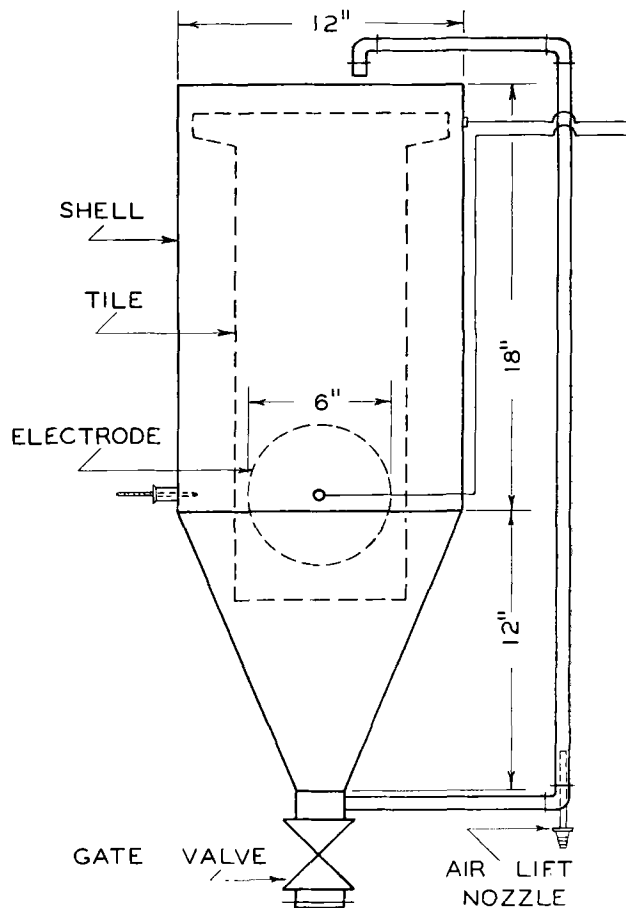


FIG. 2. Evaporator

where refrigeration is used to crystallize decahydrate from a solution.

An evaporator with a conical bottom was adapted for electrothermal heating. Fig. 2 shows the evaporator, 12 in. in diameter, body 18 in. high with a conical bottom 12 in. high terminating in a 2-in. ips coupling to which was attached a rapid opening gate valve. To circulate the solution, a $\frac{3}{4}$ -in. pipe was connected at the bottom with an air inlet to form an air-lift. Because of the relatively small diameter of the evaporator, a glazed sewer tile was hung centrally in the evaporator body and one electrode, a 6-in. diameter disk, was suspended within the tile. The evaporator body served as the other electrode and resistance of the system could be varied by changing the location of the central electrode. The 60-cycle electrical power was passed through a step-down transformer to give 150 amps at 32 volts. A wattmeter in the circuit measured power input to the evaporator. The evaporator body was covered with magnesia insulation to decrease heat losses. A preliminary experiment showed that evaporation was equivalent to 95.0% of power input.

Numerous runs were made varying the central electrode size and position and with various rates of feed of decahydrate to the evaporator and various

rates of circulation of solution within the evaporator. From these experiments it was concluded that the electrothermal method of heating was entirely satisfactory for saturated solutions of sodium sulfate. Boiling took place uniformly throughout the solution. Solid sodium sulfate decahydrate could be fed directly to the solution to take advantage of incongruent melting. Crystal size of anhydrous sodium sulfate deposited from solution depended on crystal size of the decahydrate feed. Large-size feed crystals formed larger crystals of anhydrous salt. In general, most of the anhydrous salt was retained on a 48 mesh screen. Circulation of solution using the air-lift caused a marked increase in size of the crystals formed, as would be expected from the Oslo system of evaporation and crystallization (3).

SCALE FORMATION AND CORROSION

In all runs with sodium sulfate, scale formed on the central electrode but none formed on the evaporator body which was the other electrode. Because of small area and high current density on the central electrode, its surface temperature undoubtedly was higher than the solution temperature, so that scale formation on the hotter surface was inevitable. Scale would decrease the amount of current that could pass through the electrode surface. At times the hard scale would crack and fall from the electrode, which would cause a surge of current into the solution, but continued operation would build up another layer of scale.

The problem of scale formation was studied along with electrode corrosion in a different electrolytic cell. This was a rectangular stone cell, 7 x 7 x 18 in., which was covered with thermal insulation. One electrode was a sheet iron box 5.5 x 4.5 x 0.5 in. In two hours this electrode was covered with an impervious coating of scale. A similar electrode was made, differing from the first only by placing copper inlet and outlet tubes so that water could be circulated through the box. On this new electrode, maintained at a temperature below that of the solution, no scale formed after six hours of operation (4). These electrodes after use are shown in Fig. 3.

Corrosion was found with mild steel electrodes, so a study was made of other materials. Electrodes

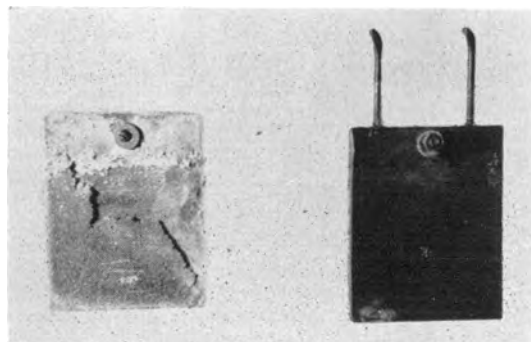


FIG. 3. Uncooled (left) and cooled (right) electrodes operating in boiling sodium sulfate solution.

TABLE II. Corrosion of electrode materials in ten hours in boiling sodium sulfate solution

Metal	Loss in wt, %
Galvanized iron.....	2.3
Copper.....	9.0
Tin.....	2.6
Stainless steel, KA2.....	0.0
Aluminum.....	13.4 (1 hr only)
Monel metal.....	2.4
Zinc.....	3.3
Lead.....	20.0
Cast iron.....	Nil

were cut approximately 5 x 6 in. and measured accurately as to area and weight. Current density was maintained at 4.4 amp/dm², and time of operation was 10 hr. Results are given in Table II. All metals showed marked corrosion except stainless steel, sheet tin, and cast iron. Monel metal showed deep grooves after ten hours. No quantitative measurements could be made on cast iron because of the weight of the electrode. After 20 hours of operation, no pitting or corrosion could be observed.

Any discussion of this paper will appear in a Discussion Section to be published in the December 1954 issue of the JOURNAL.

REFERENCES

1. K. A. KOBE AND C. W. HAUGE, *Can. Chem. Met.*, **18**, 177 (1934).
2. K. A. KOBE, C. J. CARLSON, AND C. W. HAUGE, *Ind. Eng. Chem.*, **28**, 589 (1936).
3. H. SVANOE, *ibid.*, **32**, 636 (1940).
4. K. A. KOBE, U. S. Pat. 2,272,345, Feb. 10, 1942.

Diaphragm Type Amalgam Caustic-Chlorine Cell¹

CHAS. POTTER² AND A. L. BISIO

Department of Chemical Engineering, Columbia University, New York, New York

ABSTRACT

An amalgam-type caustic cell was studied. It consisted of an anode compartment which contained brine and graphite anodes, and a cathode compartment which contained a mercury cathode, denuder water, and graphite chips. The compartments were separated by a horizontal "nylon" cloth diaphragm. Optimum operating characteristics of the cell were: denuder liquor velocity, 8.0 gal/hr/ft² Hg; brine velocity, 1.0 gal/hr/ft² Hg; brine temperature, 50°C; current density, 1.0 amp/in.² Hg, and a voltage drop of 3.70 volts. The cell produced 0.80 lb caustic soda/kwhr at a current efficiency of 90–91%. This indicates slightly improved efficiencies over present commercial operation.

INTRODUCTION

Most commercial amalgam caustic-chlorine cells employ flowing mercury in both the electrolyzer and decomposer sections of the cell. A cell with a stationary mercury pool supported between an electrolyzer section on the bottom and a decomposer section above should be effective. Since sodium amalgam is lighter than mercury, the amalgam should rise from the electrolyzer interface to the decomposer interface.

A similar cell may have been proposed earlier (1, 2). Operation of such a cell was apparently not successful due to failures of construction material. Patents (3–5) have been issued to cover this type of cell construction; however, no extensive studies have been reported.

EXPERIMENTAL

Cell

A diagram of the cell is given in Fig. 1.

Brine solution was kept in a two-liter glass vessel which contained a shelf built around its circumference. On the shelf, supported by rubber blocks, rested a glass cylinder of 350 ml capacity. A taut nylon cloth³ which acted as the diaphragm was stretched across its lower face. The cloth was fastened around the glass cylinder by a metal band; the edges of the cloth as well as the metal band were covered with de Khotinsky cement. A 0.135 cm thick mercury pool was placed on the diaphragm, and above the mercury pool rested 250 ml of water. Except where otherwise noted, graphite chips completely covered the mercury-water interface to pro-

vide a surface of low hydrogen overvoltage. Chip size was $-3.5/+4.0$ Tyler Standard Screens; there was 0.75 gram graphite/cm² mercury surface. The anode was a graphite plate which encircled the inner compartment at mercury level. Thus, electrolyzer and decomposer sections were created.

Electrolyzer or denuder solution could be added independently or removed by means of siphons and dropping funnels. Mechanical agitation was not employed in either compartment of the cell. Brine feed to the electrolyzer was saturated at the brine feed temperature. A standard selenium rectifier was used to provide power needed for experimental work. Auxiliary voltmeters and ammeters were placed in the electrical circuit of the cell as needed, in addition to meters contained in the rectifier assembly.

Ordinary electrode-grade graphite⁴ proved suitable for electrolysis of the brine. With proper control of brine composition at 324 ± 30 grams NaCl/liter H₂O, long anode life can be anticipated. Graphite anodes which were kept under 24-hr service for three months showed no change in weight, water displacement, electrical conductivity, or visual appearance. During prolonged electrolysis the cell showed no voltage trend, indicating absence of any significant change in surface characteristics of the electrode.

Contact to the mercury cathode was made by a Monel screen immersed in the mercury. The electrical contact was permanent and effective, and amalgamated after a few moments of operation.

Voltage Studies

Voltage drop across the cell depends upon the average current density at which the cell is operated, temperature, concentration of electrolyte, sodium content of the amalgam, cathode-anode spacing, diaphragm resistance, and means of removing chlorine bubbles. The voltage-current density relationship for the experimental cell is shown in Fig. 2.

⁴ Grade A6NX, National Carbon Company.

¹ Manuscript received May 15, 1953. The work reported in this paper is taken from the thesis of Attilio Bisio presented in partial fulfillment of the requirements for the degree of Bachelor of Science, June 1953.

² Present address: Amersil Company, Inc., Hillside, New Jersey.

³ "Vinyon N" cloth supplied by the Carbide and Carbon Chemical Corporation, New York, N. Y.

Exact slope of the curve is influenced by details of cell construction and by the extent to which parasitic resistances have been minimized. Voltage drop across the cell increased relatively slowly with increasing average current density. The fact that no gas is generated at the mercury cathode contributes substantially to this favorable relationship. High conductivity of brine solution is also a contributing factor.

Cell voltage was not influenced by brine flow rate over the range 0.0–10.0 gal/hr/ft² Hg. Flow rate is defined as the turnover in a chamber, in the sense that it is an indication of volumetric contact with the mercury surface. The geometry modifies effects of turnover. At flow rates higher than 10 gal/hr/ft² Hg and constant average current density, the voltage initially decreased with increasing flow rate, then finally levelled off. No quantitative measurements were made in this region. The denuder flow rate had no effect on voltage drop across the cell, which is shown as a function of temperature in Fig. 2.

Since decomposition voltages of brine solutions were not determined, caution should be exercised in extrapolation of these curves. Temperature coefficient of the voltage was 0.035 volt/°C at all current densities. Temperatures given in Fig. 2 are those of the brine; denuder temperatures were generally 5–10°C higher.

The cell was operated with a brine temperature of 50°C in all succeeding work.

Anode potential, cathode potential, and voltage

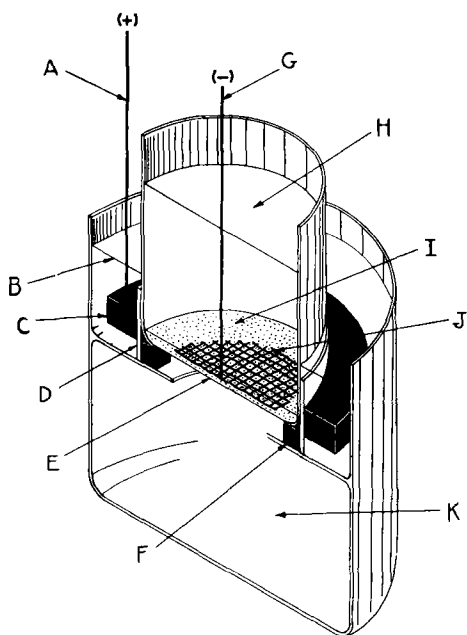


FIG. 1. Cell construction. A—anode lead; B—brine liquid level; C—anode (graphite ring); D—insulation; E—nylon diaphragm; F—rubber block supports; G—cathode lead; H—denuder section (pure sodium hydroxide solution); I—mercury pool; J—Monel screen contact; K—brine.

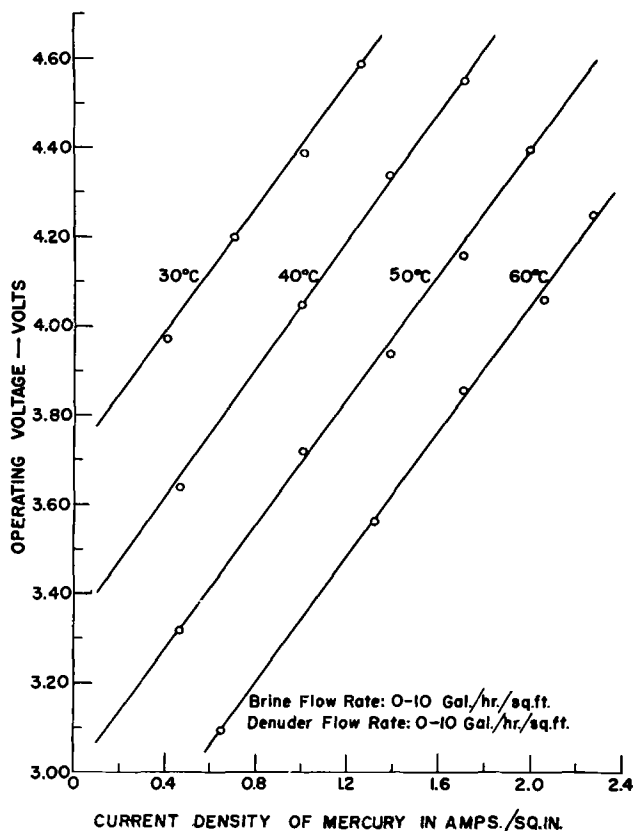


FIG. 2. Operating voltage as a function of current density and temperature.

drop across the diaphragm were determined with a calomel half-cell and tubulus (6–8); voltage drop in solution and contact drops were determined by difference. These potentials are plotted in Fig. 3. Probable error in each of the measured potentials is less than 0.01 volt.

Voltage drops across the solution, diaphragm, and contact were small in comparison to anode and cathode potentials (Fig. 3). Voltage drops across the diaphragm were of the same order of magnitude as comparable published measurements for the diaphragm of a Vorce cell (9).

Anode potential was an important item in voltage drop across the cell, since its variation with current density was greater than that of the other potentials. Factors governing anode potential in a mercury cell are the same as in a diaphragm cell except that brine concentration and current density are somewhat higher (10, 11). At 1 amp/in.² the anode potential is 1.580 volts. Assuming that chlorine discharge potential on platinum is 1.330 volts (12), a polarization of 0.25 volt results at a current density of 1 amp/in.² This value is a reasonable approximation of published measurements (9, 13).

Anode potential measured during prolonged electrolysis was somewhat lower than that found in short laboratory tests. This occurred repeatedly, the

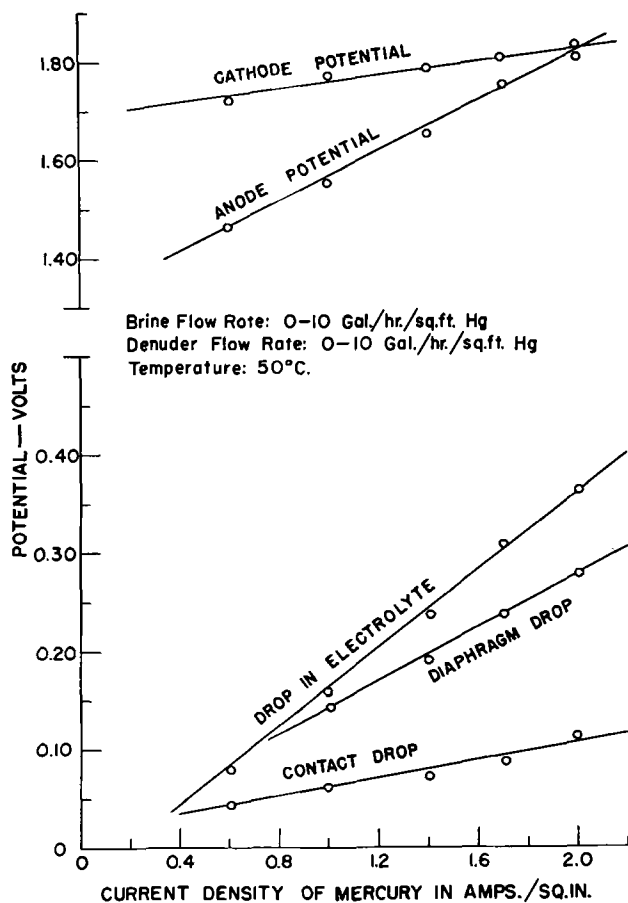


FIG. 3. Individual potentials as a function of current density.

depression being greater than the experimental error; at present no reason is advanced as to why this should occur. The effect, however, may be due to some type of anode conditioning by chlorine evolution.

Cathode potential is influenced only slightly by current density in comparison with anode potential. This is to be expected since polarization is effected by current density only in case of gas evolution (14). Changes in brine concentration influence cathode potential but slightly, whereas a change in amalgam concentration has a more pronounced effect (11).

Operating Current Density

Current efficiency of the cell over a wide range of brine and denuder velocities depended upon the average current density at which the cell was operated. Visible gas evolution at the cathode occurred above a current density of 1.2 amp/in.² It is also probable that incipient gas generation occurred at lower current densities. All succeeding work was carried out at a current density of 1 amp/in.² Operating voltage at 50°C was 3.70 volts.

Amalgam Denuder Studies

Graphite chips were floated on the mercury pool surface in an effort to provide low hydrogen over-

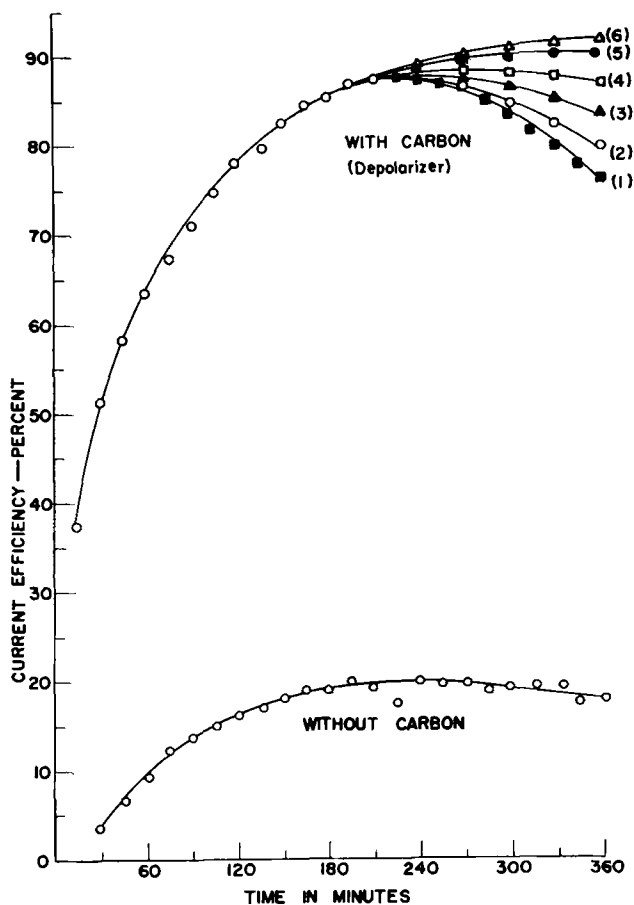


FIG. 4. Instantaneous current efficiency as a function of time of operation and denuder liquor velocity. Current density: 1 amp/in.² Hg; temperature: 50°C. Flow rates in gal/hr/ft² Hg; brine flow: 1.0; denuder flow: (1) 0.0, (2) 2.0, (3) 4.0, (4) 6.0, (5) 8.0, (6) 10.0.

voltage and promote the reaction of sodium amalgam with water (11, 13). Fig. 4 shows that at a denuder velocity of 0.0 gal/(hr/ft² Hg), presence of the depolarizer increased current efficiency approximately four times. The mechanism of amalgam decomposition has been studied previously (13).

Flow Rate Studies

Fig. 4 also shows instantaneous current efficiency to be a function of time of operation and of denuder liquor velocity. During the first 3½ hr of cell operation, there was a slow buildup of sodium amalgam in the mercury which caused a slow increase in current efficiency, irrespective of denuder liquor velocity. When the average caustic concentration reached 8.3% by weight, current efficiency at low denuder flows began to decrease with time. At higher denuder flows, however, the apparatus approached steady state as indicated by curves 5 and 6 of Fig. 4. Raising denuder liquor velocity above 10.0 gal/hr/ft² Hg when the average caustic concentration is less than 32% had no effect on current efficiency.

Decrease of current efficiency at low denuder liquor flows was due to concentration polarization at

the mercury-caustic interface which slowly increased with time. There were indications that caustic concentration at the mercury-caustic interface was over 25% by weight. Higher denuder liquor flow rates reduced this concentration polarization.

Although brine velocities were varied over the range 0.0 to 10.0 gal/hr/ft² Hg, this variation did not have any effect on the relationship between current efficiency and time as presented in Fig. 4. This was anticipated since the amount of brine consumed during a run amounted to less than 10% of total brine present. If electrolysis were continued for a longer period, however, cathodic polarization would be expected.

Inasmuch as turnover had no effect on early stages of amalgam buildup, one may speculate that rate of buildup was due to transfer of sodium controlled by a chemical step. After 3½ hr of operation, turnover did have an effect on rate of buildup, and here one may speculate that transfer of sodium was controlled by a convectional or diffusional process.

Steady-state cell operation after 3½ hr of buildup at a denuder velocity of 8.0 gal/hr/ft² Hg and a brine velocity of 1.0 gal/hr/ft² Hg permitted operation at a current efficiency of 90–91% and attainment of a caustic concentration of 32.0% by weight. Concentration polarization then increased to such a point that current efficiency was less than 90.0%. If at this time denuder liquor velocity was increased above 30 gal/hr/ft² Hg, caustic concentration could be built up to 40% by weight before concentration polarization increased to such a point that current efficiency was less than 90%. At this point, however, heavy gas generation occurred at the mercury-brine interface. Gas generation was probably due to sodium concentration in the amalgam being greater than 0.2%, thus raising the sodium ion discharge potential above the potential for hydrogen discharge. This was confirmed in other experimental work (8). Titration of the sodium amalgam indicated that concentration of sodium was above 0.25% under these conditions.

The necessary increase in denuder liquor velocity after onset of concentration polarization was eliminated by operating two cells in series at a denuder liquor velocity of 8 gal/hr/ft² Hg. Transfer between the two denuder compartments caused mixing to occur, thus decreasing the tendency for concentration polarization. A caustic concentration of 40% by weight was obtained at this velocity, whereas 30 gal/hr/ft² Hg was previously necessary.

CONCLUSIONS

Operation of the experimental cell with a two-stage denuder and denuder liquor velocity of 8.0 gal/hr/ft² Hg, brine velocity of 1.0 gal/hr/ft² Hg, current density of 1 amp/in.² Hg, and voltage drop of 3.70 volts, produced 0.80 lb caustic soda/kwhr (1600 kwhr/ton) at a current efficiency of 90–91%.

It is difficult to compare this cell to others reported in the literature, since complete operating data are rarely given. However, the following statements can be made: (a) brine and denuder velocities noted above were well below those reported in the literature (10); (b) circulation of mercury was eliminated; (c) current density and over-all voltage drop were about the same as those reported for commercial operating units (15); and (d) the cell had the same output per kilowatt hour as commercial units of both the amalgam and diaphragm types.

ACKNOWLEDGMENTS

The work presented here was greatly encouraged by the interest of Dr. Henry Linford and Dr. Edward Saubestre. The aid of Mr. David Feder and Mr. Edward Foley is also gratefully acknowledged.

Any discussion of this paper will appear in a Discussion Section to be published in the December 1954 issue of the JOURNAL.

REFERENCES

1. E. A. LESUER, *Trans. Electrochem. Soc.*, **63**, 315 (1933).
2. E. A. LESUER, *Trans. Am. Inst. Chem. Eng.*, **6**, 168 (1915).
3. V. ENGELHARDT AND N. SCHONFELDT, German Pat. 549,724, April 14, 1932.
4. B. CATALDI, U. S. Pat. 1,336,281, April 6, 1920.
5. T. MATAUSHIMA, U. S. Pat. 1,368,955, February 15, 1921.
6. U. R. EVANS, "Metallic Corrosion, Passivity and Protection," Chap. 1, Arnold, London (1948).
7. J. N. AGAR, as quoted by U. R. EVANS, *J. Iron Steel Inst.*, **141**, 220 (1940).
8. U. R. EVANS AND T. P. HAAS, *Proc. Roy. Soc.*, **A125**, 370 (1932).
9. W. W. STENDER, M. M. STRONGANOV, AND P. B. ZIVOTINSKY, *Trans. Electrochem. Soc.*, **65**, 189 (1934).
10. G. L. MANTELL, "Industrial Electrochemistry," 3rd ed., Chap. 17, McGraw-Hill Book Co., New York (1950).
11. R. B. MACMULLIN, *Chem. Eng. Progr.*, **46**, 440 (1950).
12. H. J. CREIGHTON AND W. A. KOHLER, "Electrochemistry," 4th ed., Vol. II, p. 194, John Wiley & Sons, Inc., New York (1943).
13. W. C. GARDINER, *Chem. Met. Eng.*, **52**, No. 7, 110 (1945).
14. S. GLASSSTONE, "An Introduction to Electro-Chemistry," p. 438, D. Van Nostrand Co., New York (1942).
15. J. H. PERRY, (Editor), "Chemical Engineers Handbook," 3rd ed., p. 1810, McGraw-Hill Book Co., New York (1950).



Anhydrous Ethylenediamine¹

R. M. CREAMER AND D. H. CHAMBERS

Bureau of Mines Eastern Experiment Station, College Park, Maryland

Ethylenediamine has been used frequently in electrochemical investigations as a nonaqueous ionizing solvent, as a chelating agent, and as a starting material for organic synthesis. One difficulty encountered in its use has been the preparation of a dry sample. Several methods have been advanced for drying ethylenediamine (1-3). These methods, however, are time consuming, present handling difficulties, and usually give a poor yield; therefore, an attempt was made to develop a more satisfactory method. Water removal by addition of a third material that forms a low-boiling azeotrope has been used extensively in other systems for dehydration. An effort was made to employ this procedure in dehydrating ethylenediamine.

The first agent used, isopropyl ether, was found to be capable of accomplishing the desired dehydration. The main objection to this dehydrating agent was the rate of reaction; it required about 25 hr to dehydrate 350 ml of 70% diamine. Benzene proved to be a much faster dehydrating agent than isopropyl ether, probably as a result of the larger percentage of water in the benzene-water azeotrope. It was also found that a total condensing, phase-separating stillhead permitted drying to be completed with only a small quantity of dehydrating agent. This stillhead retained a portion of the condensed vapors. The light benzene fraction of the distillate was returned to the column as reflux, and only the heavier immiscible water layer was removed from the system.

Ethylenediamine was dehydrated with benzene in the following manner: 100 ml of dry benzene was added to 500 ml of 70% ethylenediamine. This two-phase mixture was placed in a 1-liter flask at the bottom of a fractionating column 90 cm long and 30 mm in diameter that was filled with 3 mm glass helices. To permit rapid dehydration, the boil-up rate from the flask was adjusted close to the column's maximum capacity. A manometer that measured the pressure in the flask was useful in preventing column

flooding. The water and the small quantity of ethylenediamine that distills with it were separated from the benzene, the other component of the azeotrope, by means of the stillhead previously mentioned. The system was protected from the outside atmosphere by soda-lime tubes. During distillation, the stillhead temperature slowly increased from about 75°C to the boiling point of pure benzene, 80°C. Removal of water by the azeotrope was rapid until only the monohydrate remained, at which point the rate of water removal became slower. When the ethylenediamine was dry, a point indicated by collection of a distillate of only one phase, benzene was discharged from the stillhead and the dry diamine distilled from the column. The time required to dry 500 ml of ethylenediamine in the apparatus described was about 15 hr, a time that could probably be decreased by the use of a column of greater capacity. The concentration of ethylenediamine in the product was at least 99.5% and had a specific conductivity of 1×10^{-5} ohm⁻¹ cm⁻¹ or less. The yield was 88%. Most losses could be attributed to hold up in the fractionating column and still base.

This method gives a product that compares favorably in physical and chemical characteristics with the product obtained by the use of chemical methods of dehydration. The yield from the dehydration is high, the amount of dehydrating agent required is small and is easily recovered, and the dehydration and purification are completed in only a single piece of apparatus.

Any discussion of this paper will appear in a Discussion Section to be published in the December 1954 issue of the JOURNAL.

REFERENCES

1. G. L. PUTNAM AND K. A. KOBE, *Trans. Electrochem. Soc.*, **74**, 609 (1938).
2. W. H. BRAMLEY AND W. F. LUDER, *J. Am. Chem. Soc.*, **66**, 107 (1944).
3. J. T. CLARKE AND E. R. BLOUT, *J. Polymer Sci.*, **1**, 419 (1946).

¹ Manuscript received May 25, 1953.

Rate of Oxidation of Three Nickel-Chromium Heater Alloys between 500° and 900°C¹

EARL A. GULBRANSEN AND KENNETH F. ANDREW

Westinghouse Research Laboratories, East Pittsburgh, Pennsylvania

ABSTRACT

Rates of oxidation of three heater alloys of nominal composition 80% nickel-20% chromium were studied over the temperature range of 500° to 950°C and at a pressure of 7.6 cm of Hg of oxygen, using the vacuum microbalance method. Temper color films were obtained for all oxidations below 850°C, while gray or gray-green films were obtained at temperatures of 850°C and higher. No evidence was found for scaling or cracking of the oxide from the alloys on cooling at temperatures of oxidation up to 950°C.

The parabolic rate law was applied to the data. Reasonable agreement was found for temperatures above 650°C, while below this temperature the parabolic rate law constant varied with time. This time variation was explained in terms of composition changes in the oxide and growth of the oxide crystallite size.

The classical theory of diffusion was used to interpret effect of temperature on rate of oxidation, and heats, entropies, and free energies of activation for the over-all reaction were evaluated from the data.

Heats of activation varied from 38,150 cal/mole for alloy 12046 to 51,400 cal/mole for alloy 13246, while the entropies of activation varied from -15.8 entropy units (eu) for alloy 12046 to -3.5 eu for alloy 13246. On an absolute basis, alloy 12246 had the slowest rate of attack with oxygen under the given conditions. This was not in agreement with the results of A.S.T.M. life tests.

When compared to other metals, chromium reacted 4.1 times and nickel 12.6 times as fast with oxygen as alloy 13246.

Calculations were made on the entropy of vacancy formation assuming that the reaction follows a mechanism of positive ion diffusion through vacancies created by the solution of oxygen at the oxide-gas interface. This gives an entropy term of -7.5 eu which partially accounts for the negative entropy of activation observed. Agreement of the theoretical rate of reactions with experiment was within a factor of 10 for all of the alloys. This difference is discussed briefly.

INTRODUCTION

The high resistance to oxidation of the 80% nickel-20% chromium series of heater alloys is well known. One of the interesting developments in this series of alloys over the past 30 years has been the improvement in performance in cyclic oxidation tests. This is a result of changing the manganese and silicon contents as well as a result of addition of small quantities of zirconium, calcium, aluminum, cerium, etc., to the alloy. In spite of the great technical importance, no adequate scientific explanations have been put forward.

In a recent series of papers (1, 2, 3) from these laboratories, a systematic study was made of the crystal structures of oxide films using x-ray and electron diffraction methods on eight alloys of this nominal composition. It was shown that crystal structures of oxide films were a function of time and temperature of oxidation and the composition of the alloy, if manganese was present. For this

series of alloys there appeared no direct correlation between performance in cyclic oxidation tests and composition and crystal structure of the oxide film.

It is the purpose of this paper to study the rate of oxidation of three alloys of the 80% nickel-20% chromium composition as a function of time and temperature and to relate the data to the parabolic rate law and the classical theory of diffusion.

Literature

No published work has been reported on the rate of oxidation of the 80% nickel-20% chromium alloys. Scheil and Kiwit (4) studied the oxidation of a series of iron-nickel-chromium alloys. They find the best alloys were characterized by presence of a scale of Cr₂O₃ alone, while poorer alloys gave scales characterized by the presence of oxides of iron. Lustman (2) subjected a series of 80% nickel-20% chromium alloys to cyclic as well as constant temperature oxidation tests at 1175°C. Continuous oxidation tests showed little difference in oxidation rates, while A.S.T.M. life tests showed a sixfold

¹ Manuscript received April 6, 1953. This paper was prepared for delivery before the Wrightsville Beach Meeting, September 13 to 16, 1953.

variation. Cyclic oxidation tests showed a fair correlation with A.S.T.M. useful life tests.

The A.S.T.M. useful life test (5) is a cyclic test conducted on wire specimens in air atmosphere at 1175°C. Useful life is defined as the time required for a 10% change in the electrical resistance of the wire.

The effect of minor constituents on lifetime tests has been described by Hessenbruch (6). The effect of small quantities of magnesium, calcium, zirconium, cerium, thorium, of the order of 0.1% or less, was to greatly improve the performance.

In a recent work, Buckle, Jacquet, and Poulignier (7) applied metallographic and oxidation studies to the determination of service temperatures of 80 nickel-20 chromium alloy turbine blades. Details of this study are not available to date.

Thermodynamic Predictions

Gulbransen and McMillan (3) considered in detail the thermodynamic equilibria of several surface reactions occurring on nickel-chromium alloys. Six types of reactions were shown to occur. These were: (a) direct oxidation of the several metal components, (b) solid phase reactions of one oxide with another metal, (c) formation of spinels with either Cr_2O_3 or Fe_2O_3 , (d) formation of silicates between the oxides and SiO_2 , (e) reaction of carbon from the metal with the surface oxide to form CO and reduced metal and, (f) vaporization of the metals.

Calculations showed that all oxides of the major and minor components of the alloy were stable to direct decomposition up to 1200°C, except in neutral or reducing atmospheres. Solid phase reactions of NiO with Cr, Si, Mn, and Ca were possible at all temperatures. Spinel could form between NiO, MnO, FeO and Cr_2O_3 and Fe_2O_3 but not with CaO and SiO_2 . Reaction of carbon in the alloy with NiO was feasible at temperatures above 975°C. Formation of silicates was possible, while vaporization became important only at the higher temperatures under vacuum or inert and reducing atmospheres.

Gulbransen and McMillan (3) also considered the effect of minor components on composition and physical properties of the oxide and oxide-alloy interface.

EXPERIMENTAL

Method

A vacuum microbalance was used for all rate measurements. Its construction and use have been described (8, 9). The 0.0127-cm thick specimens have surface areas of 14 cm^2 and weigh 0.6840 gram. Sensitivity of the balance was 1 division (0.001 cm) per microgram and the weight change was estimated to $\frac{1}{4}$ of a division (0.25×10^{-6} gram).

Auxiliary apparatus containing the balance and specimen was evacuated to 10^{-6} mm of Hg or better. A quartz or mullite furnace tube (10) was used to contain the specimen and was sealed directly to the Pyrex glass apparatus.

Other auxiliary apparatus was used for the preparation of pure hydrogen and oxygen (8). Weight change during reaction was followed by observing a pointer on the balance beam by means of a micrometer microscope. Readings of the balance were taken in vacuo before reaction at the temperature, during the reaction in oxygen, and after the reaction in vacuo.

Samples

Specimens used in this study were specially prepared, analyzed chemically and spectrographically, the useful life tested, and were made available to us by the Driver Harris Company. The three alloys represent a 30-year improvement in the technology of heater alloy preparation. Alloy 12046 represents a modern high life heater alloy. Table I shows analyses of samples together with A.S.T.M. life tests.

Specimens were given the following surface preparation. Portions of the strip were abraded starting with number 1 grit paper and finishing through 4/0 paper. The last stage was carried out under purified kerosene to avoid oxidation. After abrading, samples were cleaned with soap and water, distilled water, petroleum ether, absolute alcohol, and stored in a dessicator.

A number of specimens were given an additional treatment by heating in hydrogen at 900°C for one-half hour before reacting with oxygen.

TABLE I. Composition and life tests, nickel-chromium alloys

Alloy	Composition %										Useful life (hr)	Test temp, °C
	C	Mn	Si	Cr	Ni	Fe	Zr	Ca	Mg	Al		
12046 New Ni-Cr Alloy V	0.08	0.01	1.39	19.91	Bal.	0.34	0.10	0.024		0.07	157	1175
12246 Old Ni-Cr Alloy V	0.08	0.01	0.30	19.98	Bal.	0.32	0.05	0.029		0.08	86	1175
13246 Old Ni-Cr Alloy V	0.12	1.70	0.30	19.98	Bal.	0.20	—		0.006		25	1175

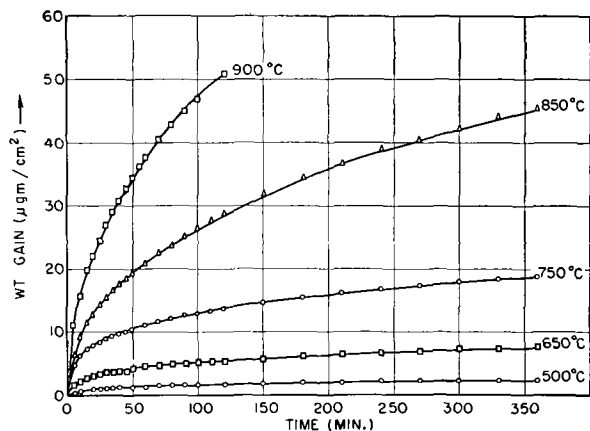


FIG 1 Effect of temperature oxidation of 12046 Ni-Cr alloy, 7.6 cm of Hg of O₂ abraded through 4/0

RESULTS

The reaction with oxygen was studied as a function of time and temperature and results are shown in Fig. 1 to 3. An oxygen pressure of 7.6 cm of Hg was used for all experiments. The weight change was plotted in $\mu\text{g}/\text{cm}^2$. The thickness of the resulting oxide in Angstroms was calculated from the crystal structure or density assuming a surface roughness ratio of unity. For Cr₂O₃ the relation was $1 \mu\text{g}/\text{cm}^2$ equals 61 Å. However, other oxides observed in the film would have different thickness values per microgram of oxygen reacted. For purposes of convenience the value for Cr₂O₃ was used in this paper.

Time and Temperature

Fig 1 to 3 show effect of time and temperature on the rate of oxidation for the three alloys over the temperature range of 500° to 900°C. Most of the experiments were run for a total of six hours. Thirty-hour experiments were made at the lower

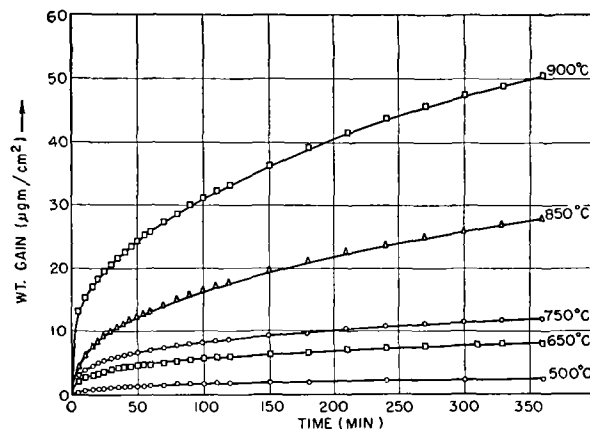


FIG 2. Effect of temperature oxidation of 12246 Ni-Cr alloy, 7.6 cm of Hg of O₂ abraded through 4/0

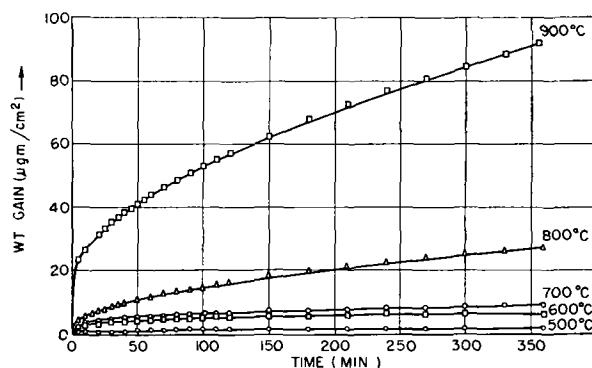


FIG 3 Effect of temperature oxidation of 13246 Ni-Cr alloy, 7.6 cm of Hg of O₂ abraded through 4/0

temperatures to test the variation of the parabolic rate law constant with time.

For all of the curves a rapid pickup of oxygen occurs in the first few minutes with the rate decreasing as the film thickens. Similar curves were found for other metals (11, 12).

Table II shows oxide film thickness vs oxide

TABLE II Oxide film thickness vs oxide color
7.6 cm of Hg of O₂, 6 hr of reaction except where noted

Temp	Alloy 12046			Alloy 12246			Alloy 13246		
	Thickness		Color	Thickness		Color	Thickness		Color
	$\mu\text{g}/\text{cm}^2$	Å($\rho = 1$)		$\mu\text{g}/\text{cm}^2$	Å($\rho = 1$)		$\mu\text{g}/\text{cm}^2$	Å($\rho = 1$)	
450	2.48	152	Lt straw						
500	6.2 ^a	378	Pink	5.9 ^a	360	Pink	4.56 ^a	278	Pink
550	5.13	312	Straw	5.45	332	Pink	6.50 ^a	396	Dk blue
600	11.5 ^a	701	Blue	8.86	540	Dark blue	8.01	490	Dk. blue
650	9.73	594	Blue	10.3	629	Blue	12.69 ^a	774	Lt blue
700							12.9	786	Lt. blue
750	20.6	1260	Straw	15.5	945	Straw-green	19.7	1200	Straw
800				22.6	1380	Straw-pink	31.2	1905	Green
850	50.4	3080	Gray	32.6	1990	Gray-green	58.1	3550	Gray
900	55.5	3380	Gray	50.4 ^b	3065	Gray	92.1	5610	Gray

Lt—light

^a 30-hr test

^b 2-hr test

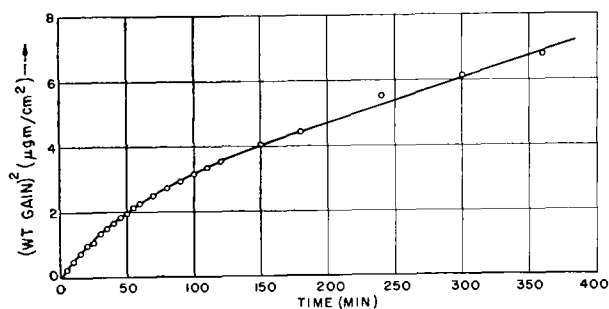


FIG. 4 Oxidation of 12246 Ni-Cr alloy, 500°C, 7.6 cm of Hg of O₂. Parabolic plot. 1-2 hr $K = 3.75 \times 10^{-16}$; 3-6 hr $K = 2.27 \times 10^{-16}$

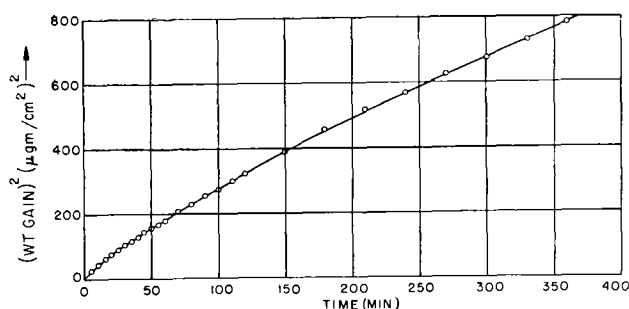


FIG. 5 Oxidation of 12246 Ni-Cr alloy, 850°C, 7.6 cm of Hg of O₂. Parabolic plot. 1-2 hr $K = 4.055 \times 10^{-14}$, 3-6 hr $K = 3.14 \times 10^{-14}$.

color for the three alloys as a function of temperature. Two series of temper colors were observed on the alloys. For alloy 12046, the first straw color was found at a thickness of 152 Å. This color appeared to be present also at a thickness of 312 Å. A second straw color was noted at 1260 Å. Above 2000 Å, all of the oxides were gray or green-gray. All of the oxides formed in this study were stable to cracking on cooling the alloy to room temperature. It should be noted that the temper colors produced were not only a function of the temperature but also of the time of oxidation and the composition of the alloy.

A comparison at 900°C of the total extent of oxidation showed alloy 12246 as the most resistant to oxidation. However, the differences between the rates of reaction of the three alloys were not large.

Parabolic Rate Law

Although many empirical rate laws have been suggested to explain the effect of time on the rate of oxidation, the parabolic rate law (13, 14) has been the most successful since its derivation was based on principles of formation and diffusion of ions in the oxide (14). The equation states $W^2 = Kt + C$. Here W is the weight gain, t is the time, and K and C are constants.

It was not expected that this rate law should hold for the initial part of the reaction or where the

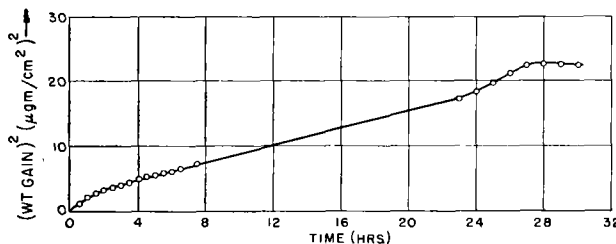


FIG. 6 Oxidation of 12046 Ni-Cr alloy, 500°C, 7.6 cm of Hg of O₂ abraded through 4/0

composition of the oxide film was changing appreciably.

To test the agreement of the experiments with the parabolic rate law, plots were made of the square of the weight gain vs. time. Fig. 4 and 5 show two such plots for alloy 12246 at 500° and 850°C, respectively. It was noted that the slope of the plot decreases rapidly with time for the first two hours of reaction at 500°C and that there was a smaller change at 850°C. Decrease in value of the parabolic rate law constant K with time is illustrated in the captions on the figures for the 1-2 hr and 3-6 hr time periods. Larger changes in the value of K were noted if the initial slope at time zero was compared to the 24-30 hr value.

Fig. 6 shows a parabolic rate law plot for the oxidation of alloy 12046 at 500°C for 30 hr. For this experiment the parabolic rate law constant K (slope of plot) was essentially constant between 4 hr and 22 hr of reaction. The value of K then increased and levelled off to zero value. In several experiments on other alloys, a weight loss after 28 hr of reaction was actually observed. This type of behavior is similar to the first stage of a stepwise oxidation process observed by Caplan and Cohen (15) in a study of the oxidation of iron-chromium alloys.

Levelling off of the rate of reaction shown in Fig. 6 could be explained by a change in the composition of the oxide film. Gulbransen and McMillan (3) noted from electron diffraction studies that NiO was the oxide formed after a two-hour oxidation, while Cr₂O₃ was found after a thirty-hour oxidation.

The strong dependence of the parabolic rate law constant K on the time of oxidation, as shown in Fig. 4 and 6, was probably due to two factors: (a) a process of composition change, and (b) a growth in the crystallite size of oxide particles. This latter effect has been discussed in detail in another work (16). In brief, the argument was that diffusion occurred for an oxide film of small crystallites at the grain boundaries, while for larger crystallites this grain boundary area was small and diffusion occurred throughout the crystal lattice.

The parabolic rate law could be fitted approximately to the data above a temperature of 650°C,

while below this temperature it was not possible to make a reasonable fit for reasons previously noted.

Temperature Dependence

In earlier papers the authors have used the transition rate law theory (17) and the classical expression for the diffusion coefficient as expressed by Zener (18) to interpret the parabolic rate law (19). In the latter treatment the parabolic rate law constant was given by the expression

$$K = 2 \gamma \nu a^2 e^{\left(\frac{\Delta S^\circ}{8/3} + \Delta S^*\right)/R} e^{-\left(\frac{\Delta H^\circ}{8/3} + \Delta H^*\right)/RT}$$

Here $\frac{\Delta S^\circ}{8/3}$ and $\frac{\Delta H^\circ}{8/3}$ are the entropy and heat of formation of the vacancies, while ΔS^* and ΔH^* are the entropy and heat of activation of diffusion, a is the interatomic distance between diffusion sites, ν is the frequency of vibration along the direction across the saddle configuration, R is the gas constant, T is the temperature, and γ a coefficient determined by the geometry of the atomic jumps. K has the units of $\text{cm}^2 \text{sec}^{-1}$.

To evaluate ν and γ it was necessary to assume a particular oxide and a mechanism for diffusion. According to the recent work of Gulbransen and McMillan (3), Cr_2O_3 was the predominant oxide on alloys 12046 and 12246 while $\text{MnO} \cdot \text{Cr}_2\text{O}_3$ was found on alloy 13246. Since the parabolic rate law holds only above 650°C , the appearance of NiO at lower temperatures was not of concern.

Before assuming a mechanism of diffusion, consider the details of the Cr_2O_3 structure. Cr_2O_3 has the rhombohedral structure (20) with $a = 5.38 \text{ \AA}$ and $\alpha = 54.83$. The oxygens are in approximately close-packed hexagonal array with Cr ions occupying two-thirds of available octahedral holes, i.e., sandwiched between planes of oxygens. The octahedral holes are situated in chains running vertically through the structure along [111], and along each chain is a succession Cr, Cr, hole, Cr, Cr, hole. In the horizontal metal atom planes, i.e., odd numbered (444) planes 1, 3, 5, etc., the metal atoms are slightly above or below the plane and the empty holes lie in these planes. Therefore, filled and unfilled holes form puckered sheets.

Each Cr has in its own puckered horizontal plane 3 Cr neighbors at 2.921 \AA and 3 unfilled holes at 2.876 \AA . Each Cr has either above or below it 1 Cr neighbor at 2.871 \AA and either below or above it 1 unfilled hole at 1.982 \AA . The easiest movement for a Cr is to the empty hole either above it or below it at only 1.982 \AA . Movement horizontally to the three holes at 2.876 \AA is more difficult because of the increased distance and because two barriers of oxygen triangles must be penetrated, while the

vertical movement requires only the penetration of one set of oxygen triangles.

This structure makes it difficult to evaluate precisely the geometry of atomic movements during oxidation as well as the distance moved per jump. In the evaluation of ν and γ it was assumed that the ν 's are equal for the various possible atomic jumps, that the distance between Cr atoms is equal, and that a random distribution of Cr atoms occurs in the structure. On this basis the average value for γ was calculated to be $\frac{1}{4}$.

The value of a was taken as 2.9 \AA . This could be high if diffusion occurs largely at the short spacing between the Cr atoms and the unoccupied position adjacent to it in the C direction.

The value of ν was calculated from the characteristic Debye temperature, $\theta_D = h\nu_m/k$ (19). ν_m is the maximum allowed frequency, h is Planck's constant, and k is Boltzmann's constant. θ_D for Cr_2O_3 was 362. To estimate the frequency ν_{Cr} along the path of the reaction, two fundamental relationships were used:

$$\nu = \frac{1}{2\pi} \sqrt{\frac{f}{m}} \quad (\text{I})$$

$$\nu_{\text{max}} = \sqrt{\nu_{\text{Cr}} \cdot \nu_0} \quad (\text{II})$$

The first equation relates the frequency, the force constant f , and the mass of the atom, while

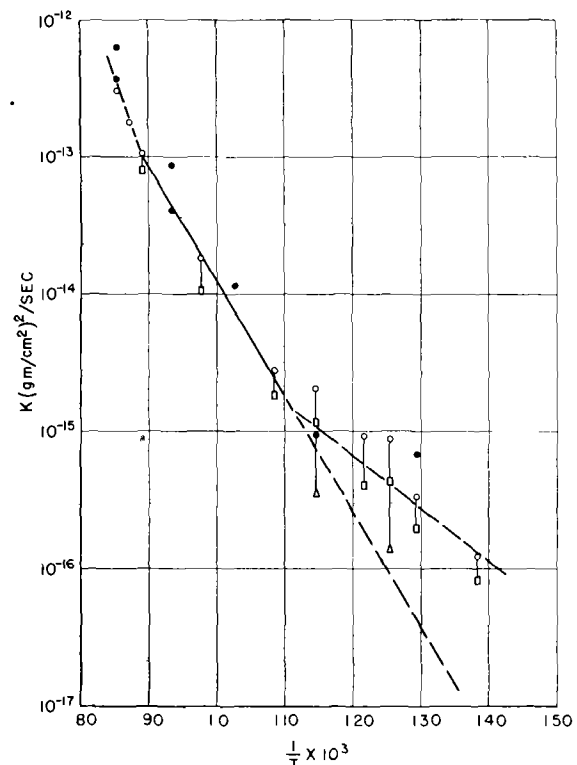


FIG 7 Oxidation of 12046 Ni-Cr alloy, log plot K vs $1/T \times 10^3$ \circ = 1-2 hr, \square = 3-6 hr, \triangle = 24-30 hr; \bullet = H_2 pretreated 30 min, 900°C , 1-2 hr, $\Delta H^* = 38,150 \text{ cal/mole}$

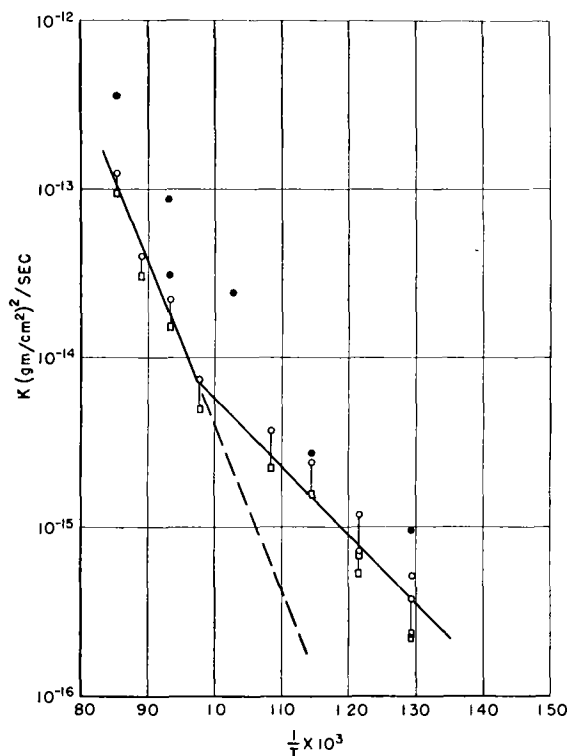


FIG 8 Oxidation of 12246 Ni-Cr alloy, log plot K vs $1/T \times 10^3$ \circ = 1-2 hr, \square = 3-6 hr, \bullet = H_2 pretreated 30 min, $900^\circ C$, 1-2 hr, $\Delta H^* = 44,400$ cal/mole

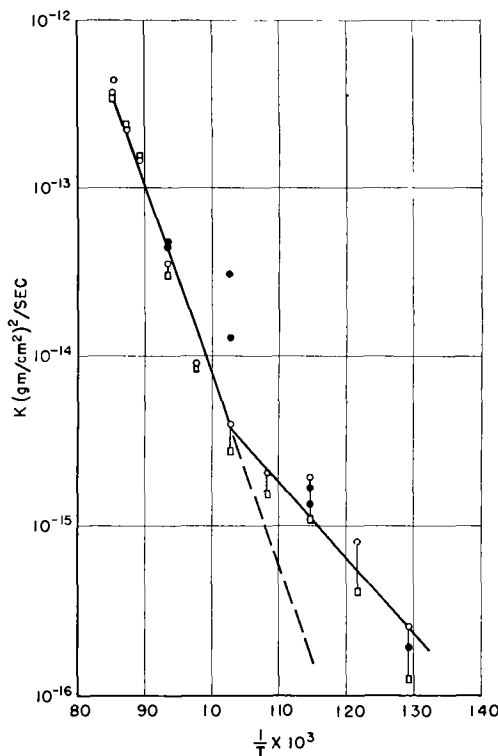


FIG 9 Oxidation of 13246 Ni-Cr alloy, log plot K vs $1/T \times 10^3$ \circ = 1-2 hr, \square = 3-6 hr, \bullet = H_2 pretreated 30 min, $900^\circ C$, 1-2 hr, $\Delta H^* = 51,400$ cal/mole

the second equation relates the maximum value of ν to the maximum values of ν for the atoms. ν_{Cr} was calculated to be 5.66×10^{12} .

Fig. 7 to 9 show plots of the logarithm of K vs. $1/T$ for the three alloys while Tables III to V show part of the experimental data on which the plots were made. Since the rate constants change with time, these constants were calculated and tabulated for the time periods of 1-2 hr, 3-6 hr, and at lower temperatures for 24-30 hr. Above $650^\circ C$ the data can be fitted by a straight line; below this temperature the time variation of K makes it impossible

to determine the slope. It may be noted that the values of K determined in the range of 24-30 hr approach values given by the extrapolation of the straight line relationship. The deviation of data below $650^\circ C$ from the parabolic rate law has been discussed in a previous section.

Table VI shows a summary of the experimental heats, entropies, and free energies of activation for the three alloys. In addition, the calculated value for entropy of activation of diffusion was tabulated. This is discussed in the next section. Using free energy of activation as a basis for comparison of

TABLE III Parabolic rate law constants, entropies, heats, and free energies of activation for oxidation of 12046 Ni-Cr alloy

Temp, $^\circ C$	$K(1-2 \text{ hr})$ (g/cm^2) ² /sec	$K(3-6 \text{ hr})$ (g/cm^2) ² /sec	$K(\text{avg})$ (g/cm^2) ² /sec	ΔS^* cal/mole/ $^\circ C$	ΔH^* cal/mole	$-T\Delta S^*$ cal/mole	ΔF^* cal/mole
650	2.78×10^{-15}	1.85×10^{-15}	2.315×10^{-15}	-15.7	38150	-14500	52650
750	1.832×10^{-14}	1.092×10^{-14}	1.462×10^{-14}	-16.2	38150	-16600	54750
850	1.082×10^{-13}	8.15×10^{-14}	9.485×10^{-14}	-15.8	38150	-17750	55900
875	1.805×10^{-13}	—	1.805×10^{-13}	-15.1	38150	-17300	55450

TABLE IV. Parabolic rate law constants, entropies, heats, and free energies of activation for the oxidation of 12246 Ni-Cr alloy

Temp, $^\circ C$	$K(1-2 \text{ hr})$ (g/cm^2) ² /sec	$K(3-6 \text{ hr})$ (g/cm^2) ² /sec	$K(\text{avg})$ (g/cm^2) ² /sec	ΔS^* cal/mole/ $^\circ C$	ΔH^* cal/mole	$-T\Delta S^*$ cal/mole	ΔF^* cal/mole
750	7.5×10^{-15}	4.90×10^{-15}	6.2×10^{-15}	-11.7	44400	-11980	56380
800	2.25×10^{-14}	1.573×10^{-14}	1.913×10^{-14}	-11.5	44400	-12300	56700
850	4.055×10^{-14}	3.14×10^{-14}	3.598×10^{-14}	-12.1	44400	-13600	58000
900	1.259×10^{-13}	9.49×10^{-14}	1.104×10^{-13}	-11.6	44400	-13600	58000

TABLE V. Parabolic rate law constants, entropies, heats, and free energies of activation for the oxidation of 13246 Ni-Cr alloy

Temp, °C	$K(1-2 \text{ hr})$ (g/cm ²) ^{1/2} /sec	$K(3-6 \text{ hr})$ (g/cm ²) ^{1/2} /sec	$K(\text{avg})$ (g/cm ²) ^{1/2} /sec	ΔS^* cal/mole/°C	ΔH^* cal/mole	$-\Delta F^*$ cal/mole	ΔF^* cal/mole
700	4.0 × 10 ⁻¹⁵	2.78 × 10 ⁻¹⁵	3.39 × 10 ⁻¹⁵	-3.5	51400	-3400	54800
750	9.16 × 10 ⁻¹⁵	8.8 × 10 ⁻¹⁵	8.98 × 10 ⁻¹⁵	-4.26	51400	-4360	55760
800	3.52 × 10 ⁻¹⁴	3.025 × 10 ⁻¹⁴	3.273 × 10 ⁻¹⁴	-4.04	51400	-4340	55740
850	1.185 × 10 ⁻¹³	1.332 × 10 ⁻¹³	1.259 × 10 ⁻¹³	-3.46	51400	-3900	55300
850	1.46 × 10 ⁻¹³	1.54 × 10 ⁻¹³	1.50 × 10 ⁻¹³	-2.92	51400	-3280	54680
875	1.805 × 10 ⁻¹³	2.28 × 10 ⁻¹³	2.043 × 10 ⁻¹³	-3.37	51400	-3860	55260
875	2.22 × 10 ⁻¹³	2.38 × 10 ⁻¹³	2.30 × 10 ⁻¹³	-3.14	51400	-3600	55000
900	2.565 × 10 ⁻¹³	2.92 × 10 ⁻¹³	2.743 × 10 ⁻¹³	-3.80	51400	-4460	55860
900	3.70 × 10 ⁻¹³	3.6 × 10 ⁻¹³	3.65 × 10 ⁻¹³	-3.22	51400	-3780	55180

TABLE VI. Comparison of the parabolic rate law constants and heats, entropies, and free energies of activation at 850°C

	12046	12246	13246
$K \text{ cm}^2/\text{sec}$	3.525 × 10 ⁻¹⁴	1.339 × 10 ⁻¹⁴	4.67 × 10 ⁻¹⁴
$\Delta H^* \text{ cal/mole}$	38150	44400	51400
$\Delta S^* \text{ cal/mole/deg}$	-15.8	-12.1	-3.46
$\Delta F^* \text{ cal/mole}$	55900	58000	55300
$\Delta S_D^* \text{ cal/mole/deg}$	-8.4	-4.7	+3.9

alloys, it is seen that alloy 12246 shows a lower rate of reaction than the other alloys. Alloys 12046 and 13246 were approximately equal in their over-all performance although entropies and heats of activation differ appreciably.

Table VII shows a comparison of the heats, entropies, and free energies of activation for chromium, nickel, and alloy 13246. Chromium reacts 4.1 times and nickel 12.6 times as fast as alloy 13246.

Effect of Hydrogen Pretreatment

A number of the specimens were heated to 900°C and given a pretreatment in 2.4 cm of purified hydrogen for 30 min before reacting with oxygen at 7.6 cm of Hg of O₂ at the given temperatures. Parabolic rate law constants are plotted in Fig. 7 to 9. Results are in good agreement with results from abraded samples for alloy 12046 and, with some exceptions, agreement was good for alloy 13246. Somewhat higher rates of reaction were

TABLE VII. Comparison of the parabolic rate law constants and heats, entropies, and free energies of activation at 700°C

	Cr	Ni	13246
$K \text{ cm}^2/\text{sec}$	2.38 × 10 ⁻¹⁴	2.06 × 10 ⁻¹³	1.261 × 10 ⁻¹⁵
$\Delta H^* \text{ cal/mole}$	70,400	41,200	51,400
$\Delta S^* \text{ cal/mole/deg}$	22.0	-6.0	-3.50
$\Delta F^* \text{ cal/mole}$	49,000	47,040	54,800

found for the hydrogen pretreated specimens for alloy 12246.

THEORETICAL

The experimental entropy of activation is made up of two terms: (a) entropy of formation of vacancies, and (b) entropy of activation of diffusion. Theoretical and experimental studies by Zener have shown that the entropy of activation of diffusion should be positive. In a previous paper (19) calculations were made for the oxidation of nickel and these verified Zener's prediction. The essential problem was to evaluate the entropy of vacancy formation.

To make these calculations for the nickel-chromium alloys, assume that diffusion in Cr₂O₃ occurs through cation vacancies. These form by the reaction



Here \square_c refers to the cation vacancy, \oplus to the positive electron hole, and O^- to the oxygen ion in the Cr₂O₃ structure.

Change in entropy can be calculated from the entropy of $\frac{1}{2}$ mole of O₂ gas and 1 mole of O^- in the Cr₂O₃ lattice and from the entropy change of distortion of the Cr₂O₃ structure due to the formation of positive holes and cation vacancies. Following the methods of a previous paper (19), we assume the entropy of the oxygen ions in Cr₂O₃ to be $\frac{1}{5}$ of the molal entropy.

Since Cr₂O₃ has a rhombohedral structure, the authors have not attempted to calculate the entropy of distortion. Instead, they assume the distortion entropy changes associated with the NiO lattice. For NiO, an entropy of distortion of -1.34 cal/deg was calculated for each mole of cation vacancies and -0.47 cal/deg for each mole of positive holes. Since only $\frac{2}{3}$ of a cation vacancy is formed in the reaction, total entropy of distortion is -1.8 cal/deg. Therefore, at 1000°K entropy change of condensation of $\frac{1}{2}$ mole of O₂ and the formation of $\frac{2}{3}$ mole of vacancies and 2 moles of positive holes at particular lattice sites in a large amount of Cr₂O₃ is $-(29.10 - 10.8 + 1.8) = -20.1$.

Since $2\frac{2}{3}$ defects are formed, entropy change per defect is -7.5 cal/mole/deg.

Since the entropy of activation term in the rate expression is made up of two terms, the entropy of formation of vacancies and the entropy of activation of diffusion, it is possible to evaluate the latter term. These values are tabulated in Table VI.

Alloy 13246 gave a positive entropy of activation for diffusion which agrees with theoretical predictions (18). However, alloy 12246 and 12046 gave negative values of -4.8 and -8.5 eu, respectively. Experimental errors in the determination of ΔH^* from the data may lead to errors in ΔS^* of diffusion of ± 2 . In addition, until the details of the mechanism of diffusion can be given, the values of a , ν , and γ may be in error. In this interpretation, these errors would show up in the entropy term and may lead to errors of ΔS^* of diffusion of ± 2 . The over-all error in ΔS^* was of the order of ± 4 .

In addition to these errors in the picture of diffusion and in the evaluation of ΔH^* , several other factors are of importance. First, the mechanism of vacancy formation is influenced by alloying elements and impurities which leads to different values for the entropy of vacancy formation. Second, the oxide was not Cr_2O_3 alone but a segregated mixture with SiO_2 , CaO , etc. Third, grain boundary diffusion phenomena may be of importance in this system. These effects would give in the correlation made here negative entropies of diffusion since all of the deviations from theory were thrown into the entropy term.

At present it is impossible to make a complete theoretical interpretation of the entropy term. It may be noted, however, that on an absolute basis the agreement of theory with the experimental rate is within a factor of ten for all of the alloys.

From a technical point of view, it is of interest to compare the results with the useful life test data. In this study alloy 12246 showed the lowest oxidation rate at constant temperature, while useful life

tests showed alloy 12046 was superior. This has been discussed by Gulbransen and McMillan (3) in a recent paper. They conclude that performance in useful life tests was not a measure of normal oxidation processes alone but of resistance to cracking of the oxide from the alloy.

Any discussion of this paper will appear in a Discussion Section to be published in the December 1954 issue of the JOURNAL

REFERENCES

- 1 J. W. HICKMAN AND E. A. GULBRANSEN, *Trans. Am. Inst. Mining Met. Engrs.*, **180**, 519 (1949)
- 2 B. LUSTMAN, *ibid.*, **188**, 995 (1950)
- 3 E. A. GULBRANSEN AND W. R. McMILLAN, *Ind. Eng. Chem.*, **45**, 1734 (1953).
- 4 E. SCHEIL AND K. KIWIT, *Arch. Eisenhuttew.*, **9**, 405 (1935-6)
- 5 F. E. BASH AND J. W. HARSCH, *Am. Soc. Testing Materials, Proc.*, **29**, Pt. II, 506 (1929)
- 6 W. HESSENBRUCH, "Metalle und Legierungen für hohe Temperaturen," Julius Springer, Berlin (1940).
- 7 C. BUCKLE, P. JACQUET, AND J. POULIGNIER, Abstract of paper delivered to 1952 Autumn Meeting of the Societe Francaise de Metallurgie
- 8 E. A. GULBRANSEN, *Trans. Electrochem. Soc.*, **81**, 187 (1942)
- 9 E. A. GULBRANSEN, *Rev. Sci. Instr.*, **15**, 201 (1944)
- 10 E. A. GULBRANSEN AND K. F. ANDREW, *Ind. Eng. Chem.*, **41**, 2762 (1949).
- 11 E. A. GULBRANSEN AND K. F. ANDREW, *This Journal*, **97**, 383 (1950)
- 12 E. A. GULBRANSEN AND K. F. ANDREW, *ibid.*, **98**, 241 (1951).
- 13 N. B. PILLING AND R. E. BEDWORTH, *J. Inst. Metals*, **29**, 529 (1923).
- 14 N. F. MOTT, *Trans. Faraday Soc.*, **36**, 472 (1940).
- 15 D. CAPLAN AND M. COHEN, *J. Metals*, **4**, 1057 (1952)
- 16 E. A. GULBRANSEN, Proceedings Gothenburg International Conference on Solid State Reactions, 1952, to be published
- 17 E. A. GULBRANSEN, *Trans. Electrochem. Soc.*, **83**, 301 (1943).
- 18 C. ZENER, *J. Appl. Phys.*, **22**, 372 (1951)
- 19 E. A. GULBRANSEN AND K. F. ANDREW, *This Journal*, **101**, 128 (1954).
- 20 R. W. G. WYCKOFF, "Crystal Structures," Interscience Publishers, Inc., New York (1951)

Surface Reaction between Oxygen and Thorium¹

A. F. GERDS AND M. W. MALLETT

Battelle Memorial Institute, Columbus, Ohio

ABSTRACT

The rate of reaction of oxygen with arc-melted and rolled iodide thorium has been found to obey the parabolic rate law in the temperature range of 850° to 1415°C at 1 atm pressure. The rate constant can be expressed as $k = 5.5 \times 10^7 e^{-62,800/RT}$ (ml/cm²)²/sec. The energy of activation, 62,800 cal/mole, has a probable error of 2400 cal/mole.

INTRODUCTION

Reactions between gases and metals generally have been found to obey a linear, parabolic, cubic, or logarithmic rate law. Factors controlling the various laws as well as their derivations have been adequately described in the literature (1-7) and are, therefore, not repeated here.

Levesque and Cubicciotti (8) studied the oxidation of thorium at 45 cm pressure in the temperature range of 250° to 700°C. They found the reaction to proceed in accordance with the parabolic rate law between 250° and 350°C and calculated the energy of activation to be 31,000 cal/mole. Between 350° and 450°C, the rates of oxidation were reported to be linear with time. An energy of activation of 22,000 cal/mole was found for this temperature range. Above 450°C, they reported that the temperature of the sample rose considerably above the temperature of the furnace, resulting in nonisothermal conditions.

The present investigation was made to study the reaction between oxygen and thorium for longer times and at higher temperatures and pressures than those studied by Levesque and Cubicciotti.

MATERIALS

The thorium used in this investigation was iodide crystal bar produced by the de Boer process. The crystal bar was arc melted, forged into a 1-in. square rod, and cold finished to a $\frac{5}{16}$ -in. cylindrical rod. Test specimens, each $1\frac{1}{2}$ in. long, were machined from this rod. Diameters of the specimens were reduced to slightly less than $\frac{5}{16}$ in. to remove surface contamination.

Thorium was analyzed by spectrographic, chemical, and vacuum-fusion methods. Principal impurities found were 300 ppm by weight each of carbon and oxygen and 100 ppm each of silicon and

molybdenum. All other impurities were present in concentrations of less than 100 ppm.

Oxygen used in this study was prepared from degassed potassium permanganate by the method described by Hoge (9). Gas was dried by passing through a dry ice-acetone cold trap prior to its reaction with the thorium specimen.

PROCEDURE

Experimental apparatus was similar to that described in an earlier paper (10) with a few modifications. Since the reaction being studied involved oxygen, it was necessary to use a zirconia tube to separate the thermocouple from the thorium specimen instead of a graphite tube liner. The dead volume of the reaction system was materially reduced by suspending a Vycor tube, sealed at both ends, from a hook in the cap of the reaction tube. A sketch of this arrangement is shown in Fig. 1.

A 4-kw tungsten-gap-type Lepel converter was used to heat the specimens. Temperature readings were made with a Pt-Pt + 10% Rh thermocouple calibrated against an optical pyrometer as in previous work (10).

A cylindrical thorium specimen to be used in a reaction rate study was abraded on 240-, 400-, and 600-grit kerosene-soaked silicon carbide papers. Kerosene minimized oxidation during abrasion and was removed by successively rinsing in naphtha, ether, and C. P. acetone. The specimen was then suspended in the reaction tube as noted above. The specimen was degassed by heating under a vacuum of less than 0.5μ at 1200° to 1400°C for at least 15 min to remove hydrogen prior to adding the oxygen. Oxygen was added to the reaction tube to atmospheric pressure in measured amounts from a 50-ml glass buret. Progress of the surface reaction was followed by observing pressure changes in the closed system with an open-end mercury manometer. Further measured amounts of oxygen were added from time to time to maintain the pressure between about $\frac{3}{4}$ and 1 atm. The system was evacuated and the specimen was cooled to room

¹ Manuscript received August 20, 1953. This paper was prepared for delivery before the Wrightsville Beach Meeting, September 12 to 16, 1953. Work was done under Contract No. W-7405-eng-92 for the United States Atomic Energy Commission.

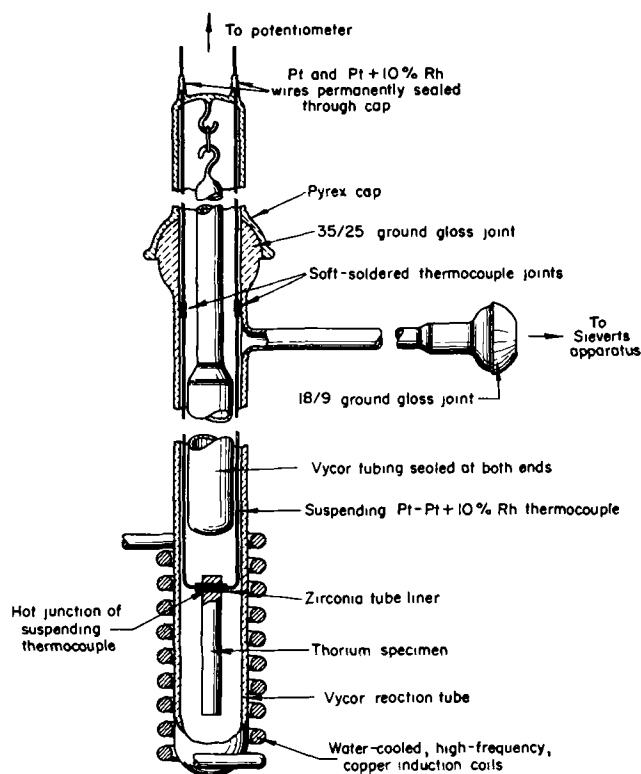


FIG. 1 Cutaway section of reaction tube assembly

temperature in vacuum after the reaction had been followed for the desired time.

The difference between the quantity of oxygen added to the reaction system and that remaining in the gas phase is a measure of the gas absorbed by the specimen at any time. Quantity of gas reacted per unit area was computed by using the original geometrical dimensions of the specimen.

RESULTS AND DISCUSSION

Solubility of Oxygen in Thorium

The solid solubility of oxygen in thorium is low even at elevated temperatures. Evidence of this can be obtained by observing the angular inclusions of oxide found in the microstructure of thorium. Magnesium-reduced thorium usually contains from 0.10 to 0.15 weight % oxygen and many oxide inclusions are evident. Arc-melted and rolled iodide thorium usually contains less than 0.05 weight % oxygen and, although fewer in number, discrete oxide inclusions can be noted in its microstructure. Even this lesser amount of oxygen in the arc-melted iodide thorium exceeds the solubility limit of oxygen in thorium at elevated temperatures. This was shown quite clearly by reacting a sample of this thorium with oxygen at 1415°C for 3 hr. The surface oxide layer was removed and the rest of the sample was analyzed for oxygen. A sample of the base material with no oxygen added was also analyzed. Both

specimens analyzed 0.028 ± 0.003 weight % oxygen. These results indicate that no oxygen was diffused into the specimen as a result of the reaction at 1415°C, and that the thorium previously had been saturated with oxygen at a temperature higher than 1415°C, probably during reduction or arc melting. This low oxygen solubility made it impossible to obtain diffusion data.

Rates of Reaction

The rate of surface reaction of oxygen with thorium was studied in the temperature range of 850° to 1415°C at atmospheric pressure. These reactions produced a tightly adherent surface film of ThO_2 which was dark-gray to black for the higher temperatures and tended to be lighter-gray for the lower temperatures. Plots of the experimental data for several of the oxidation runs are shown in Fig. 2. For clarity, some of the curves for intermediate temperatures, and curves which crossed or fell close to other curves, were omitted.

It was observed that, as the oxygen first contacts the thorium, an exothermic reaction occurs, increasing the temperature of the specimen instantaneously by as much as several hundred degrees Celsius. A similar observation was made by Levesque and Cubicciotti (8) for temperatures above 450°C. With the use of induction heating and continuous control of power available, this effect could be counteracted by reducing rapidly the heat input

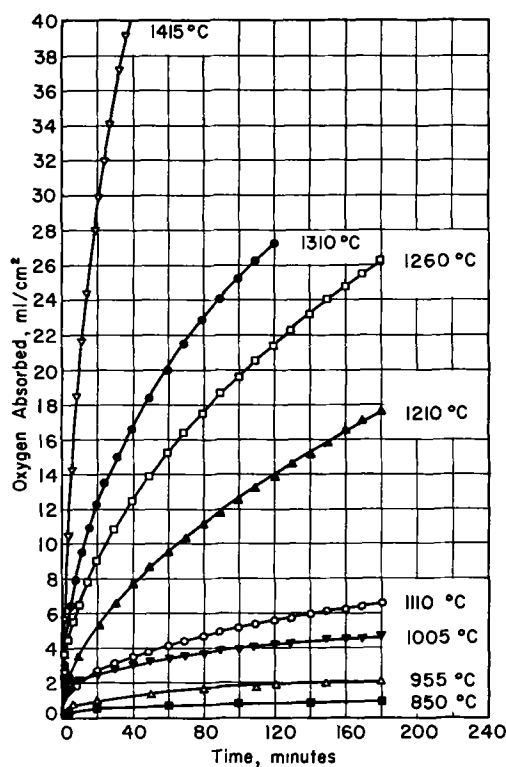


FIG. 2. Oxidation of thorium at 850° to 1415°C

from the converter. At higher temperatures, where the rate of reaction is quite rapid, the temperature could be effectively controlled by this technique. However, at lower temperatures, where the rate of reaction is normally quite slow, the amount of oxygen reacted during even a brief nonisothermal period is relatively large compared to the amount of gas reacted isothermally thereafter. This was especially significant at temperatures below about 1055°C where as much gas might be absorbed in the first fraction of a minute with the specimen at the elevated temperature as would be absorbed by the specimen at the desired temperature in several hours. It was obvious that in order to interpret the data, a correction for the non-isothermal period was required.

Moore (11) has described an equation for the parabolic law which provides for the discarding of initial deviations in reaction behavior. With the initial conditions, $y = y_0$ at $t = 0$, the integrated form of the equation is

$$y - y_0 = \Delta y = k(t/\Delta y) - 2y_0, \quad (\text{I})$$

where: y = experimental value for the amount of oxygen reacted, y_0 = amount of oxygen reacted nonisothermally, k = the parabolic rate constant; and t = time from origin at y_0 .

Using equation (I), the rate constant, k , for each

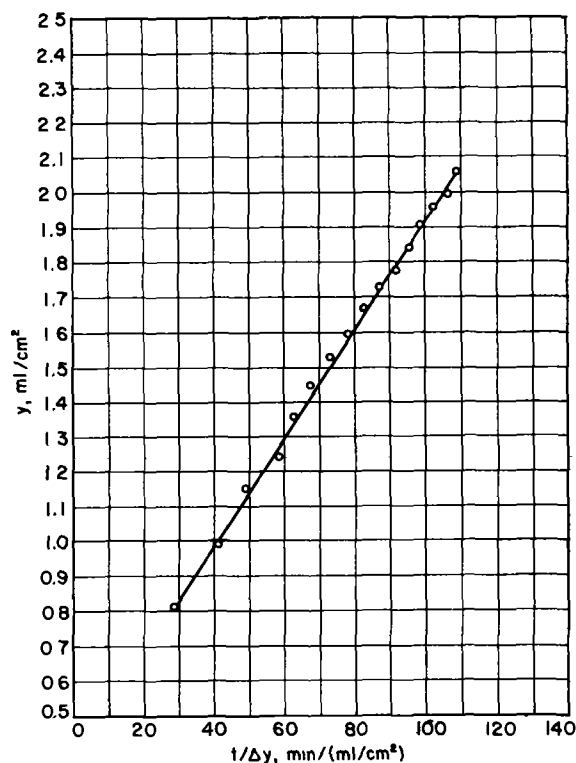


FIG. 3. Oxidation of thorium at 955°C

temperature was obtained from the slope of the straight line portion of a plot of y against $t/\Delta y$. Fig. 3 is an example of this type of plot.

Slopes obtained from log-log plots of the corrected data for the gas absorbed in milliliters per square centimeter vs. time for the 14 experimental runs in the temperature range of 850° to 1415°C are listed in

TABLE I. Rate constants, k , determined at various temperatures

Run No	Temp, °C	Total time, t , of run, min	Total oxygen absorbed in time, t , ml/cm ²	y_0 , ml/cm ²	$k \times 10^3$ (ml/cm ²) ² /sec	Slope of log-log plot*
1	850	180	0.99	0.36	0.040	0.55
2	900	180	2.13	0.82	0.181	0.53
3	955	180	2.12	0.66	0.259	0.58
4	1005	180	4.70	1.93	0.790	0.58
5	1055	180	6.52	1.09	2.70	0.51
6	1110	180	6.66	0	3.35	0.42
7	1110	180	5.46	0	2.18	0.42
8	1160	180	17.61	0	29.5	0.52
9	1210	180	17.69	0	33.9	0.52
10	1210	180	25.98	0	63.7	0.56
11	1260	180	26.33	0	62.3	0.50
12	1310	180	25.28	0	57.4	0.48
13	1310	120	27.32	0	95.2	0.44
14	1415	45	44.79	0	839	0.55

* Slope of corrected experimental data. The origin of time, $t = 0$, was set at amount of oxygen, y_0 , reacted in first stage of oxidation. Slope of 0.50 indicates a parabolic rate law is being obeyed.

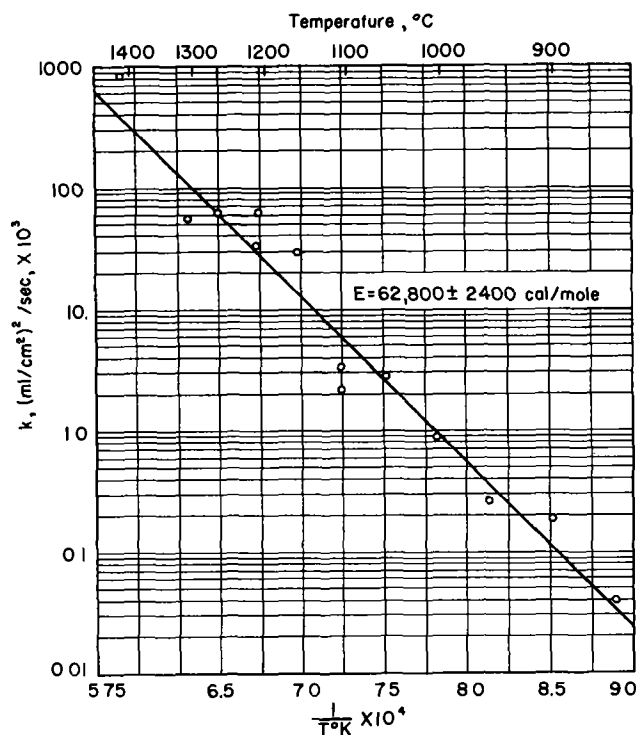


FIG. 4. Thorium-oxygen reactions; variation of rate constant, k , with temperature.

Table I. Slopes vary from 0.42 to 0.58, showing that corrected experimental data follow the parabolic rate law reasonably well. Values of the rate constants, k , calculated for the reactions are also listed in Table I. Fig. 4 shows a plot of these parabolic rate-law constants against $1/T$. The position of the best straight line through the experimental points was obtained by the method of least squares. Energy of activation of the reaction was calculated using the Arrhenius-type equation $k = Ae^{-Q/RT}$. The rate constant, k , in $(\text{ml}/\text{cm}^2)^2/\text{sec}$ can be expressed as:

$$k = 5.5 \times 10^7 e^{-62,800/RT} \quad (\text{II})$$

where $62,800 \pm 2400$ cal/mole is the energy of activation.

Levesque and Cubicciotti (8) reported an energy of activation of 31,000 cal/mole for the parabolic oxidation of thorium between 250° and 350°C . This value probably should not be compared with the value obtained in the present work because of the difference in level of temperature ranges involved. Another aspect of the oxidation of thorium at high temperatures is the relatively high activation energy for the reaction compared with those generally found for other metals. However, the reaction is not unique in this respect, since the activation energies for the parabolic oxidation of metals range from 18,000 to 62,000 cal/mole (12, 13).

ACKNOWLEDGMENTS

It is a pleasure to acknowledge the assistance of Mr. B. G. Koehl, who performed the reaction rate experiments, and Mrs. Mary Penn and Mrs. Margaret Thomas, who made the many tedious calculations of the data. The counsel of Mr. W. M. Albrecht and Dr. Jack Belle in interpretation of the experimental data is also greatly appreciated.

Any discussion of this paper will appear in a Discussion Section to be published in the December 1954 issue of the JOURNAL

REFERENCES

- 1 U. R. EVANS, *Trans. Electrochem. Soc.*, **91**, 547 (1947)
- 2 N. B. PILLING AND R. E. BEDWORTH, *J. Inst. Metals London*, **29**, 579 (1923)
- 3 N. F. MOTT, *Trans. Faraday Soc.*, **36**, 472 (1940)
- 4 C. WAGNER AND K. GRUNEWALD, *Z. physik. Chem.*, **40B**, 455 (1938)
- 5 E. A. GULBRANSEN AND K. ANDREW, *Trans. Am. Inst. Mining Met. Engrs.*, **185**, 515 (1949)
- 6 A. DRAVNIKS AND H. J. McDONALD, *Iron Age*, **164**, 78 (August 25, 1949), *ibid.*, **164**, 84 (September 1, 1949)
- 7 J. T. WABER, *Metal Prog.*, **62**, 76 (September, 1952)
- 8 P. LEVESQUE AND D. CUBICCIOTTI, *J. Am. Chem. Soc.*, **73**, 2028 (1951)
- 9 H. J. HOGE, *J. Research Natl. Bur. Standards*, **44**, 321 (1950)
- 10 M. W. MALLETT, J. BELLE, AND B. B. CLELAND, *This Journal*, **101**, 1 (1954).
- 11 W. J. MOORE, *ibid.*, **100**, 302 (1953)
- 12 A. DRAVNIKS, *ibid.*, **100**, 95 (1953)
- 13 D. CUBICCIOTTI, *J. Am. Chem. Soc.*, **72**, 2084 (1950)

Reaction of Nitrogen with, and the Diffusion of Nitrogen in, Thorium¹

A. F. GERDS AND M. W. MALLETT

Battelle Memorial Institute, Columbus, Ohio

ABSTRACT

Rates of reaction of nitrogen with thorium were determined for the temperature range of 670° to 1490°C at 1 atm pressure. The reaction follows a parabolic law and the parabolic rate constant in (ml/cm²)²/sec is $k = 5.9 e^{-24,300/RT}$. The activation energy of reaction has a probable error of 1300 cal/mole. Rates of diffusion of nitrogen in thorium were obtained over the temperature range of 845° to 1490°C at atmospheric pressure. The diffusion coefficient in cm²/sec is $D = 2.1 \times 10^{-3} e^{-22,500/RT}$. The activation energy of diffusion has a probable error of 1300 cal/mole. Limiting solubilities of nitrogen were determined from the diffusion data. The heat of solution of atomic nitrogen (from ThN) in thorium is $\Delta H = 11,000$ cal/mole.

INTRODUCTION

Thorium is one of a number of metals that tarnish at room temperature rather rapidly when exposed to the atmosphere. The tarnish film formed is largely oxide resulting from a reaction of the thorium with oxygen and moisture from the air. At elevated temperatures both oxygen and nitrogen react with thorium. In its fabrication, such operations as melting, forging, rolling, swaging, and the like are commonly employed. It would be of interest to know the precautions that must be observed to prevent contamination of the metal during the various operations. A study of the reaction of thorium with oxygen at atmospheric pressure in the temperature range of 850° to 1415°C was recently completed at this laboratory (1). Levesque and Cubicciotti (2) have reported on the oxidation of thorium in the temperature range of 250° to 700°C in an oxygen atmosphere at a pressure of 45 cm. It was the objective of the present investigation to study the rate of reaction of nitrogen with massive thorium and also to obtain data on the diffusion and solubility of nitrogen in the metal.

Thorium metal has a face-centered-cubic structure with a lattice constant of 5.088 Å. Three nitrides of thorium are reported in the literature. Matignon and Delépine (3) produced a yellowish-maroon powder by heating thorium in nitrogen, to which they assigned the formula Th₃N₄. Chiotti (4) identified the crystal structure of ThN as face-centered cubic with a lattice constant of 5.18 Å. Zachariasen (5) reported the crystal structure of

Th₂N₃ to be hexagonal, of the La₂O₃ type, with $a = 4.08 \pm 0.01$ Å and $c = 6.30 \pm 0.02$ Å.

No references have been found in the literature either to rates of reaction of nitrogen with thorium or to solubilities or rates of diffusion of nitrogen in thorium.

MATERIALS

Iodide crystal-bar thorium, produced at Battelle Memorial Institute, was used in the investigation. The crystal bar was arc melted, forged to a 1-in.-square rod and cold finished to a $\frac{5}{16}$ -in. cylindrical rod. Test specimens, each $1\frac{1}{2}$ in. long, were machined from this rod. Diameters of the specimens were reduced to slightly less than $\frac{5}{16}$ in. to remove surface contamination. Each specimen had a surface area of about 8 cm².

Impurities in the thorium were determined by spectrographic, chemical, and vacuum-fusion analyses. Principal impurities detected were carbon and oxygen, 300 ppm by weight each, and silicon and molybdenum, 100 ppm each. All other impurities were present in amounts less than 100 ppm by weight.

Nitrogen used in this study was prepared by passing prepurified tank nitrogen (The Matheson Company) over zirconium turnings heated at 850°C. The gas was then dried by passing through a dry ice-actone cold trap. Purified gas was analyzed by means of a mass spectrometer and found to contain 99.8 vol % nitrogen with 0.2 vol % argon as the only measurable impurity.

PROCEDURE

The modified Sieverts apparatus used to measure rate of reaction of nitrogen with thorium is similar to that described in a previous report (6). In this

¹ Manuscript received August 20, 1953. This paper was prepared for delivery before the Wrightsville Beach Meeting, September 12 to 16, 1953. Work was done under Contract No. W-7405-eng-92 for the United States Atomic Energy Commission.

investigation, the thorium specimen, suspended by a platinum-platinum + 10% rhodium thermocouple threaded through a hole drilled near one end, was separated from the thermocouple by a small graphite tube liner. The thermocouple was calibrated against a standardized optical pyrometer (6).

A Vycor tube sealed at both ends was used to reduce the dead volume of the reaction system. Specimens were heated inductively. Power was supplied by a 4-kw tungsten-gap-type Lepel converter.

Cylindrical thorium specimens used in these reaction rate studies were prepared as has been described in a previous paper (1). Specimens were degassed by heating under a vacuum of less than 0.5μ at 1150° to 1600°C for at least 10 min to remove hydrogen prior to adding the nitrogen.

Nitrogen was added to the reaction tube, containing the thorium specimen, to atmospheric pressure in measured amounts from a 50-ml glass buret. Progress of the reaction was followed by observing pressure changes in the closed system with an open-end mercury manometer. Further measured amounts of nitrogen were added from time to time to maintain the pressure between about $\frac{3}{4}$ and 1 atm. The system was evacuated and the specimen was cooled rapidly to room temperature in vacuum after the reaction had taken place for the desired period of time.

The difference between the quantity of nitrogen added to the reaction system and that remaining in the gas phase is a measure of the gas absorbed by the specimen at any time. The quantity of gas reacted

per unit area was computed by using the original geometrical dimensions of the specimen.

Specimens reacted with nitrogen in order to study the rates of reaction at various temperatures were also used to obtain diffusion data. Lengths equal to the radius were cut from the bottom end of the specimens and also from the lower edge of the hole that had been drilled near the top to suspend the specimens. The remainder was machined radially into layers of equal weight which were then analyzed for nitrogen by a modified Kjeldahl method. Diffusion coefficients and the energy of activation of diffusion were determined using the average nitrogen concentration of each layer, the average radius of the layers, the original radius of the specimen, and the time of diffusion.

RESULTS AND DISCUSSION

Surface Reaction

The rate of surface reaction of nitrogen with thorium was studied in the temperature range of 670° to 1490°C . The nitride film formed on the surface of the specimen is characterized by a golden-yellow color when the reaction takes place below 750°C . At higher temperatures, the surface film is a dark-gray color which seemed in some cases to be composed of discrete grains. However, the golden-yellow film, noted when the reaction took place at lower temperatures, was visible if the gray outer film was cracked away. Fig. 1 shows the microstructure at the surface of a sample of thorium reacted with nitrogen at 1370°C . At a magnification of $250\times$, the relatively thick dark-gray outer layer of Th_2N_3 can be distinguished easily from the inner, thin, golden-yellow layer. This golden-yellow material was reported to be ThN by Chotti (4). The discrete and somewhat dendritic-shaped inclusions, which are present abundantly, have the characteristic color of the mononitride. These can easily be distinguished from the few very dark-etching oxide inclusions which are also shown in Fig. 1. Both surface films appear to react at room temperature with moisture from the atmosphere to form the powdery gray oxide, ThO_2 .

The reaction between nitrogen and thorium was found to follow a parabolic law in the temperature range of 670° to 1490°C at atmospheric pressure. Experimental data for several representative runs are plotted in Fig. 2. At temperatures below 1255°C , some slight initial deviations were found in a few cases. Between 1370° and 1605°C , reactions were parabolic initially, and, after a short time, became linear (see Fig. 3). At 1370° and 1490°C , the initial period of parabolic reaction was 20 to 30 min. At 1605°C , the parabolic rate law was obeyed for only the first 5 min of reaction. Reaction then be-

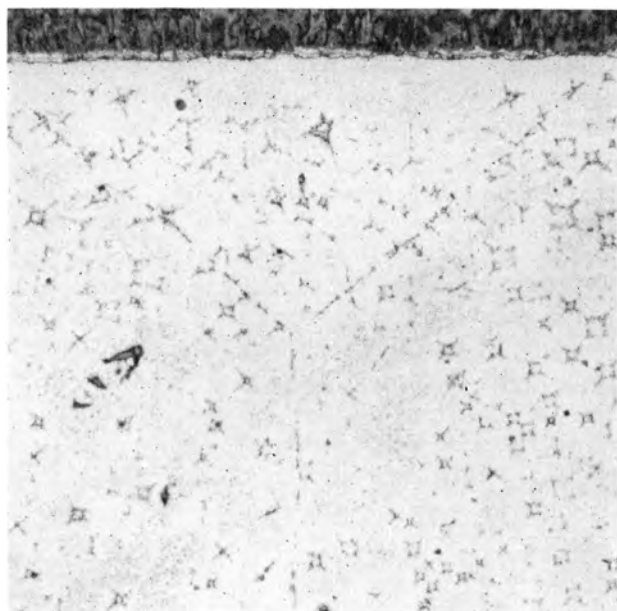


FIG 1 Structure at surface of thorium reacted with nitrogen at 1370°C $250\times$.

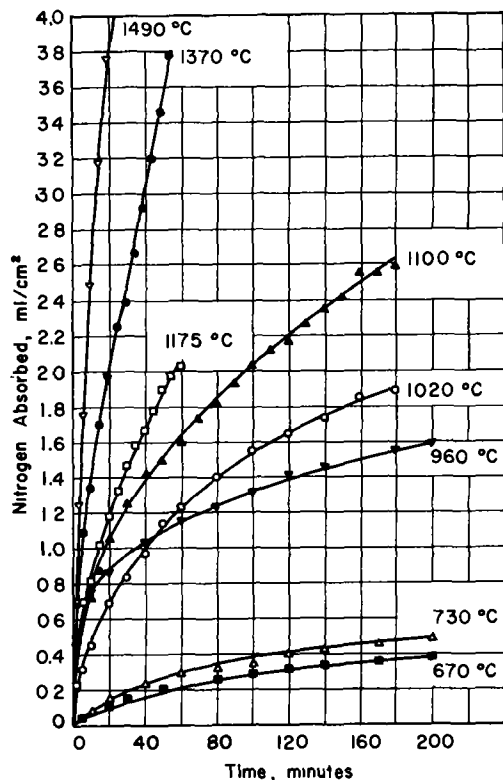


FIG 2 Reaction of nitrogen with thorium at 670° to 1490°C

came linear with time for at least 40 min longer. It is also rather interesting to note that the reactions at 1490° and 1605°C changed from parabolic to linear when about 6 mg of nitrogen per square centimeter of surface area had been reacted.

Cubicciotti noted a similar change in type of rate in the oxidation of uranium (7) at about 200°C and also in the oxidation of cerium (8) between 160° and 190°C. Gulbransen and Andrew (9) studied the reaction between nitrogen and beryllium and found a similar effect for the reaction at 925°C. In the three instances cited above, reactions proceeded parabolically with time initially and then increased to a rate faster than parabolic, becoming linear with time in two cases. Cubicciotti (7) explained this phenomenon by reasoning that, since the volume of the compound formed on the surface is larger than that of the metal reacted, the surface film must be under stress. When the film reaches a certain thickness, the stress becomes large enough that the film begins to crack or flake. At this point, the film is no longer protective and the reaction then is linear or faster than linear with time. As the temperature of the reaction is increased, cracking can occur sooner since the rate of reaction is more rapid. At some temperature, the entire reaction might appear to be linear. This hypothesis seems also to fit well data obtained in this study of the reaction between nitrogen and thorium.

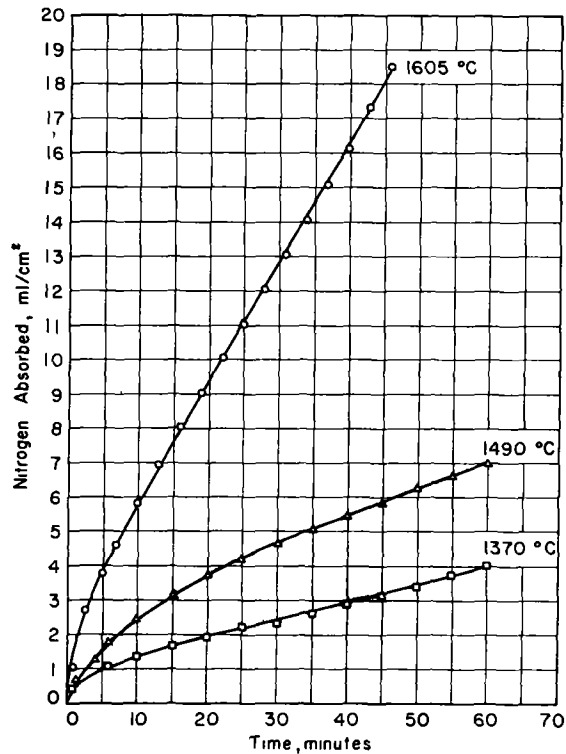


FIG 3 Reaction of nitrogen with thorium at 1370° to 1605°C

TABLE I Experimental rate constants, k , for the thorium-nitrogen reaction

Sample	Temp, °C	$k \times 10^4$, (ml/cm ²) ² /sec
1	670	0.13
2	730	0.28
3	900	2.94
4	900	4.00
5	960	1.97
6	1020	3.55
7	1100	6.00
8	1175	11.9
9	1200	6.62
10	1200	9.83
11	1255	22.3
12	1370	36.0
13	1490	130

The parabolic-rate constant, k , was calculated by determining the slope of the straight line resulting when the square of the amount of gas absorbed per unit area was plotted against time. Values of k determined in individual experiments at temperatures in the range of 670° to 1490°C are shown in Table I. A plot of $\log k$ vs. $1/T$ of these experimental points is shown in Fig. 4. The position of the best straight line through these points was determined by the method of least squares. The activation energy, obtained using the Arrhenius-type equation, $k = Ae^{-Q/RT}$, is $24,300 \pm 1300$ cal/mole. The correspond-

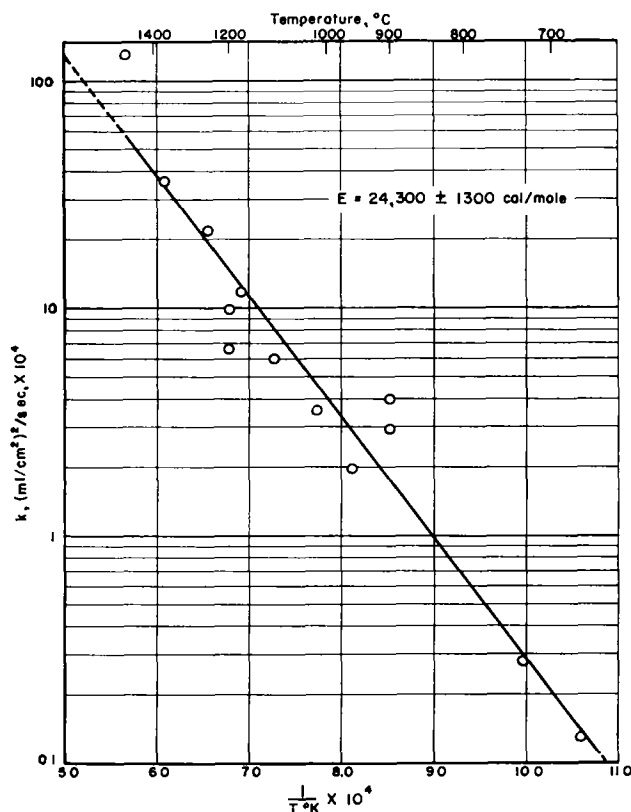


FIG 4 Thorium-nitrogen reactions, variation of parabolic reaction rate constant, k , with temperature

ing rate constant for the reaction in $(\text{ml}/\text{cm}^2)^2/\text{sec}$ is

$$k = 5.9 e^{-24,300/RT} \quad (\text{I})$$

where the frequency factor is 5.9.

The energy of activation of 24,300 cal/mole is much lower than the value obtained for the oxidation of thorium, namely, 62,800 cal/mole. Energies of activation for the reaction between various metals and nitrogen reported in the literature vary from 31,400 cal/mole for the reaction of vanadium with nitrogen (10) to 75,000 cal/mole for the reaction of beryllium with nitrogen (9). All of these activation energies are higher than that found in the present investigation.

Diffusion

Diffusion data for nitrogen in thorium were computed by the graphical method described by Mallett and coworkers (11). Values of the diffusion coefficient, D , obtained from the experimental data in the temperature range of 845° to 1490°C, are listed in Table II.

A plot of the logarithms of the diffusion coefficients vs. reciprocal temperature is shown in Fig. 5. The equation of the best straight line through the experimental points was determined by the method of least squares. The energy of activation of diffusion,

obtained from the Arrhenius-type equation, is $22,500 \pm 1300$ cal/mole. Diffusion coefficient, D , in square centimeters per second is

$$D = 2.1 \times 10^{-3} e^{-22,500/RT} \quad (\text{II})$$

Energy of activation of diffusion, 22,500 cal/mole, is in the range reported in the literature for the diffusion of nitrogen in other metals Wert and Zener (12), using internal friction measurements, calculated an activation energy of diffusion of 17,700 cal/mole for nitrogen in iron. Kê (13), using the same technique, obtained an activation energy of 44,000 cal/mole for the diffusion of nitrogen in tantalum. Mallett and coworkers (11), with the same method as used in the present investigation, report an activation energy of 33,600 cal/mole for the diffusion of nitrogen in a zirconium-2 weight % hafnium alloy. More recent work by Mallett,

TABLE II Experimental diffusion coefficients for nitrogen in thorium

Sample	Time, hr	Temp, °C	c_0 , wt % nitrogen	$D \times 10^7$ cm ² /sec
1	6½	845	0.048	0.530
2	3	900	0.079	1.09
3	6	960	0.097	2.19
4	3	1020	0.117	3.08
5	3	1100	0.159	6.61
6	1	1175	0.185	14.6
7	2	1200	0.177	8.65
8	1	1255	0.216	16.4
9	1	1370	0.276	17.0
10	1	1490	0.335	34.6

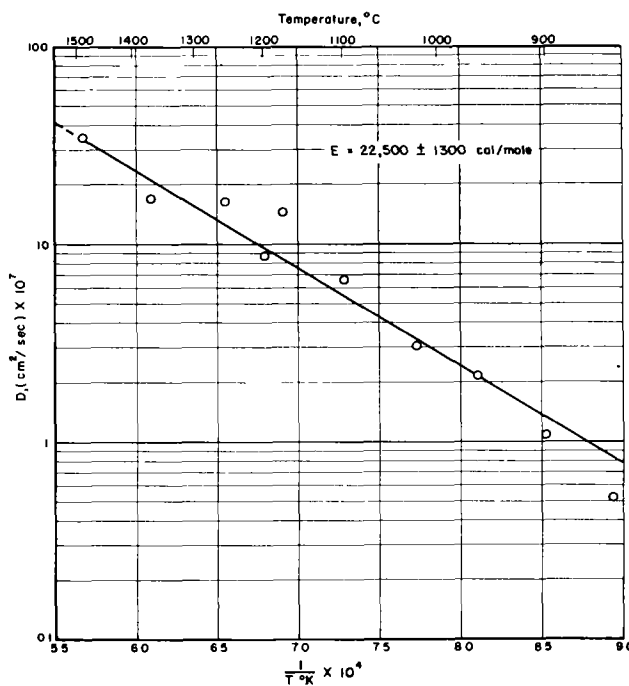


FIG 5 Thorium-nitrogen diffusion, variation of diffusion coefficient, D , with temperature.

Belle, and Cleland (6), with low-hafnium zirconium, yielded a value of 30,700 cal/mole.

Solubility

The limiting solubility (11), c_0 , of atomic nitrogen is the concentration of nitrogen just inside the interface between the ThN surface film and the thorium metal. This concentration may also be considered as the solubility of nitrogen at a partial pressure equal to the dissociation pressure of ThN. Since the surface layer is quite thin, no serious error is introduced in obtaining maximum solubility by extrapolating data to the outer surface of the specimen rather than the interface between the surface film and the specimen.

Values of c_0 at the various temperatures are listed in Table II. A plot of these values against temperature is shown in Fig. 6. The line described in this plot is a boundary between a single- and two-phase region on the thorium-nitrogen phase diagram. The course of the line below about 0.05 weight % nitrogen is not known, but it appears likely that the line may approach zero concentration asymptotically with decreasing temperature.

A plot of the values of c_0 , listed in Table II, on a logarithmic scale vs. reciprocal temperature is shown in Fig. 7. The slope of the best straight line through the experimental points was determined by the method of least squares. The solubility in weight per

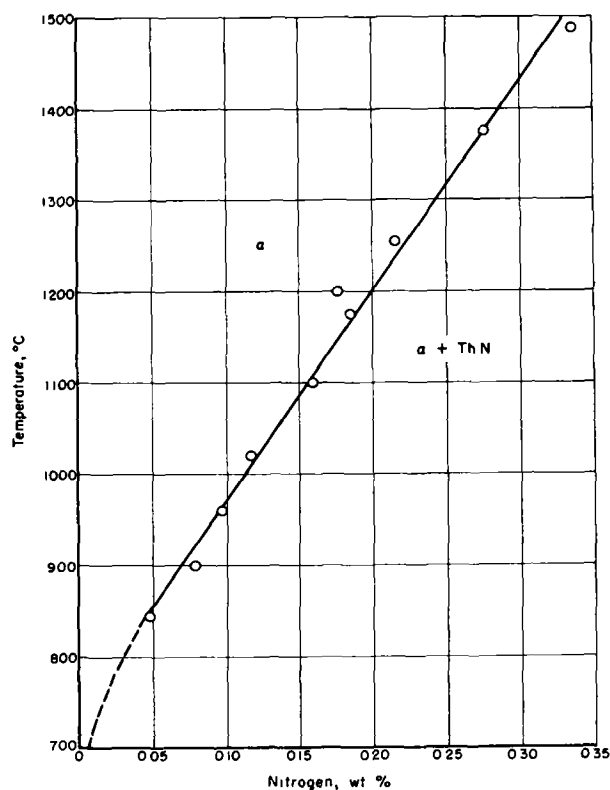


FIG 6 Solubility limits of nitrogen in thorium

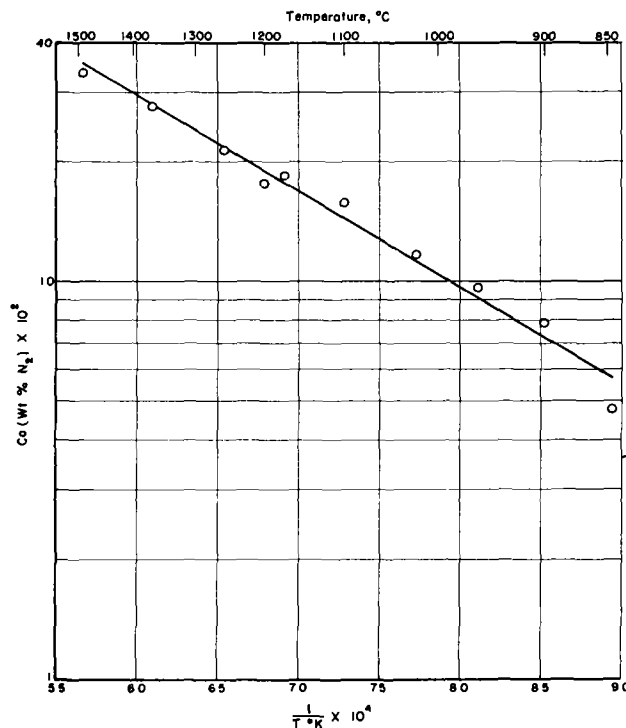


FIG 7 Variation of solubility of nitrogen in thorium with temperature

cent nitrogen in thorium over the temperature range involved, 845° to 1490°C, can be expressed as

$$\log_{10} c_0 = -2405/T + 0.9115 \quad (\text{III})$$

where T is the temperature in degrees Kelvin. From this equation, the heat of solution per mole of atomic nitrogen (from ThN) dissolved in thorium is $\Delta H = 11,000 \pm 400$ cal.

CONCLUSIONS

Reactions of thorium with nitrogen were studied, using a modified Sieverts apparatus, over the temperature range of 670° to 1605°C. Below about 750°C, a golden-yellow nitride film of ThN formed on the surface of the specimens. At higher temperatures, the surface film was the dark-gray Th₂N₃. Beneath this and adjacent to the thorium, the golden-yellow nitride was found. Both products reacted slowly at room temperature with oxygen and moisture from the air to form ThO₂.

Reaction-rate data were found to obey the parabolic rate law between 670° and 1490°C. At 1370° and 1490°C, reactions were parabolic the first 30 min and then became linear. The reaction at 1605°C became linear after only about 5 min of parabolic reaction. An activation energy of reaction of $24,300 \pm 1300$ cal/mole was calculated for the parabolic reaction between 670° and 1490°C. This value is lower than activation energies reported in the literature for the reaction of nitrogen with other metals.

The rate of diffusion of nitrogen in thorium was determined over the temperature range of 845° to 1490°C. An activation energy of diffusion of $22,500 \pm 1300$ cal/mole was calculated, which is in the range reported for the diffusion of nitrogen in other metals. Limiting solubilities of nitrogen in thorium were obtained from the diffusion data. From these solubility data, a heat of solution, $\Delta H = 11,000 \pm 400$ cal/mole for nitrogen in thorium, was calculated.

In the hot working of thorium below 850°C, no great difficulty would be expected by diffusion or solution of nitrogen into the metal. Even if such hot fabrication were carried out in a 100% nitrogen atmosphere, the principal contamination would be the formation of a thin surface nitride film. In working in air, the surface film is oxide rather than nitride.

ACKNOWLEDGMENTS

The authors wish to acknowledge the assistance of Mr. B. G. Koehl who performed the reaction-rate experiments, Mrs. Mary Penn and Mrs. Margaret Thomas who made the many calculations required to interpret the data, and Miss Betty Hannahs who

prepared the specimens for metallographic study. The counsel of Dr. Jack Belle in interpretation of the experimental data is also greatly appreciated.

Any discussion of this paper will appear in a Discussion Section to be published in the December 1954 issue of the JOURNAL.

REFERENCES

- 1 A F GERDS AND M. W. MALLETT, *This Journal*, **101**, 171 (1954)
- 2 P LEVESQUE AND D CUBICCIOTTI, *J Am Chem Soc*, **73**, 2028 (1951)
- 3 C A MATIGNON AND M DELÉPINE, *Ann chim et phys*, **8**, 10, 130 (1907)
- 4 P CHIOTTI, Atomic Energy Commission Declassified Report, AECD-3072, 48 (June 5, 1950)
- 5 W H ZACHARIASEN, *Acta Cryst*, **2**, 388 (1949)
- 6 M W MALLETT, J BELLE, AND B B CLELAND, *This Journal*, **101**, 1 (1954)
- 7 D CUBICCIOTTI, *J Am Chem Soc*, **74**, 1079 (1952)
- 8 D CUBICCIOTTI, *ibid*, **74**, 1200 (1952)
- 9 E A GULBRANSEN AND K F ANDREW, *This Journal*, **97**, 383 (1950)
- 10 E A GULBRANSEN AND K F ANDREW, *ibid*, **97**, 397 (1950)
- 11 M W MALLETT, E M BAROODY, H R NELSON, AND C A PAPP, *ibid*, **100**, 103 (1953)
- 12 C WERT AND C ZENER, *Phys Rev*, **76**, 1169 (1949)
- 13 T. S. KÉ, *ibid*, **74**, 917 (1948).

The Cathodic Reduction of Anions and the Anodic Oxidation of Cations¹

CARL WAGNER

Department of Metallurgy, Massachusetts Institute of Technology, Cambridge, Massachusetts

ABSTRACT

Anions approach a cathode by diffusion and convection rather than by electrolytic migration in view of the adverse potential gradient. The rate of transport of anions of valence z_i toward a cathode is decreased appreciably if the potential difference across the diffusion boundary layer is of the order of, or greater than, $kT/|z_i|e = 0.025/|z_i|$ volt. This effect may account for the prevention of the reduction of hypochlorite at a cathode covered by a diaphragm of chromium oxide. Similarly, the rate of transport of cations toward an anode is decreased appreciably if the potential difference across the diffusion boundary layer is of the order of, or greater than $kT/z_i e = 0.025/z_i$ volt.

INTRODUCTION

When a negatively charged ion X^- is reduced cathodically, it has to approach the cathode by diffusion and convection against an adverse potential gradient. If no other cathodic process takes place and the solution contains a large excess of other ions providing a high electrical conductivity, the adverse potential gradient is small and the transport rate of anions X^- is affected only slightly. If, however, in addition to the reduction of anions X^- , a second electrochemical reaction takes place and the total current density is sufficiently high, the adverse potential gradient may become significant and, thereby, the transport rate and the reduction rate of anions X^- may be decreased considerably.

If positively charged ions are oxidized anodically, e.g., $\text{Fe}^{2+} = \text{Fe}^{3+} + e^-$, they also have to approach the electrode against an adverse potential gradient. Thus one has a situation analogous to the reduction of anions at a cathode.

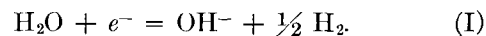
In the following, calculations are presented for idealized conditions. Since these ideal conditions are not easy to realize, theoretical conclusions have not been verified. The following analysis, however, is based only on well-established electrochemical principles which do not require verification. A comparison between experimental results and theoretical conclusions would, therefore, show only whether actual experimental conditions were sufficiently close to ideal conditions underlying the theoretical analysis.

Most important are certain qualitative results which are independent of idealizing assumptions. In particular, it is shown that the cathodic reduction of anions, e.g., hypochlorite in solutions with excess

sodium hydroxide, may virtually be prevented at high current densities.

REDUCTION PROCESSES IN A SOLUTION WITH EXCESS SODIUM HYDROXIDE

When a solution of sodium hydroxide is electrolyzed, hydrogen is evolved at the cathode,



The cathodic formation of hydroxyl ions leads to an enrichment of hydroxyl ions at the cathode. For the sake of simplification, we assume a stagnant boundary layer of thickness δ beyond which concentration differences are negligible, owing to vigorous stirring and turbulent mixing. In an ideal experiment, such a type of boundary layer may be realized by means of a diaphragm whose pores are so large that specific effects due to adsorption and the electrical double layer can be disregarded.

The transport rate of ions of type i per unit time per unit area in the direction of the x coordinate in a dilute aqueous solution at rest can be expressed as

$$\begin{aligned} \frac{1}{A} \frac{dn_i}{dt} &= -D_i \frac{\partial c_i}{\partial x} - \frac{D_i}{kT} c_i z_i e \frac{\partial \phi}{\partial x} \\ &= -c_i D_i \left(\frac{\partial \ln c_i}{\partial x} + \frac{z_i e}{kT} \frac{\partial \phi}{\partial x} \right) \end{aligned} \quad (\text{II})$$

where dn_i/dt is the number of moles of ions, i , passing cross section A per unit time, D_i the diffusion coefficient of ions of type i , c_i their concentration, z_i their valence (positive for cations and negative for anions), e the electronic charge, ϕ the electrical potential, k the Boltzmann constant, and T absolute temperature. The first term on the right-hand side of equation (II) accounts for transport due to the concentration gradient, whereas the second term accounts for electrolytic migration.

¹ Manuscript received August 3, 1953.

The "mobility" of ions i does not appear explicitly, since it is expressed in terms of the diffusion coefficient by using the Nernst-Einstein relation, $D_i = \text{mobility} \times kT$.

Under steady-state conditions, the concentration c of sodium hydroxide in a stagnant boundary layer is a linear function of the distance x from the surface of the electrode as follows by applying equation (II) to cations and anions, respectively, for an anion transport rate corresponding to the cathodic process formulated in equation (I), eliminating the potential gradient, and calculating the concentration c as a function of distance x from the cathode. Thus,

$$c = c_o[\gamma - (\gamma - 1)x/\delta] \quad (\text{III})$$

where c_o is the bulk concentration of sodium hydroxide and $\gamma = c_E/c_o$ is the ratio of the sodium hydroxide concentration c_E at the electrode to the bulk concentration c_o outside the boundary layer ($x > \delta$).

Upon substituting equation (III) in equation (II) for sodium ions whose transport rate is zero, it follows that

$$\frac{\partial \phi}{\partial x} = \frac{kT}{e} \frac{\gamma - 1}{\gamma \delta - (\gamma - 1)x} \quad \text{at } 0 \leq x \leq \delta. \quad (\text{IV})$$

Now we assume that in addition to sodium hydroxide the solution contains a small amount of ions of type j which are readily reduced at the cathode so that their concentration vanishes at $x = 0$. Applying equation (II) to ions j , we may show that the transport rate of ions j will be affected appreciably by the potential gradient only if the potential difference across the diffusion boundary layer is of the order of, or greater than, $kT/|z_j|e = 0.025/|z_j|$ volt. If the concentration of ions j is much less than the concentration of sodium hydroxide, equations (III) and (IV) remain approximately valid. The reduction rate, v_j , of ions j in moles per unit area per unit time is equal to the negative value of the transport rate in the direction of the x coordinate. Upon substituting equation (IV) in equation (II) for $i = j$, it follows that

$$v_j = D_j \frac{\partial c_j}{\partial x} + \frac{D_j z_j c_j (\gamma - 1)}{\gamma \delta - (\gamma - 1)x} \quad (\text{V})$$

where c_j , but not v_j , depends on x . Integrating equation (V) with respect to x and putting $c_j = c_{j(0)}$ for $x = \delta$ as the bulk concentration of ions j outside the boundary layer, we obtain

$$c_j = \frac{v_j \delta}{(z_j - 1)D_j(\gamma - 1)} \left[\gamma - (\gamma - 1) \frac{x}{\delta} \right] + \left[c_{j(0)} - \frac{v_j \delta}{(z_j - 1)D_j(\gamma - 1)} \right] \times \left[\gamma - (\gamma - 1) \frac{x}{\delta} \right]^{z_j} \quad \text{if } z_j \geq 1 \quad (\text{VIa})$$

$$c_j = \left\{ c_{j(0)} - \frac{v_j \delta}{D_j(\gamma - 1)} \ln \left[\gamma - (\gamma - 1) \frac{x}{\delta} \right] \right\} \times \left[\gamma - (\gamma - 1) \frac{x}{\delta} \right] \quad \text{if } z_j = 1. \quad (\text{VIb})$$

As mentioned above, we assume that ions of type j are readily reduced at the cathode if hydrogen is developed. Thus, letting $c_j = 0$ for $x = 0$ in equations (VIa) and (VIb), we find the reduction rate v_j to be

$$v_j = \frac{(z_j - 1)D_j(\gamma - 1)c_{j(0)}}{\delta} \frac{\gamma^{z_j}}{\gamma^{z_j} - \gamma} \quad \text{if } z_j \geq 1 \quad (\text{VIIa})$$

$$v_j = \frac{D_j(\gamma - 1)c_{j(0)}}{\delta \ln \gamma} \quad \text{if } z_j = 1 \quad (\text{VIIb})$$

If the sodium hydroxide concentration at the surface of the cathode differs only slightly from the bulk concentration, i.e., if $\gamma \cong 1$, it follows from equations (VIIa) and (VIIb), with the aid of series expansions, that the reduction rate is

$$v_j^{(0)} \equiv v_j(\gamma \rightarrow 1) = D_j c_{j(0)}/\delta. \quad (\text{VIII})$$

Under these conditions, the reduction rate of ions j is independent of the simultaneous evolution of hydrogen, since the total potential difference across the boundary layer is small as compared to $kT/e = 0.025$ volt. This relation is well-known in polarography.

If the concentration of sodium hydroxide at the cathode is much greater than the bulk concentration, i.e., if $\gamma \gg 1$, we have the following three cases.

1. For reducible cations with a valence z_j equal to or greater than 2, it follows from equations (VIIa) and (VIII) that

$$v_j/v_j^{(0)} \cong (z_j - 1)(\gamma - 1) \quad \text{if } \gamma \gg 1 \text{ and } z_j \geq 2. \quad (\text{IXa})$$

2. For univalent reducible cations it follows from equations (VIIb) and (VIII) that

$$v_j/v_j^{(0)} = (\gamma - 1)/\ln \gamma \quad \text{if } z_j = 1. \quad (\text{IXb})$$

3. For reducible anions ($z_j < 0$) it follows from equations (VIIa) and (VIII) that

$$v_j/v_j^{(0)} = -(|z_j| + 1)(\gamma - 1)\gamma^{-|z_j|}/(\gamma^{-|z_j|} - \gamma) \cong (1 + |z_j|)/\gamma^{|z_j|} \quad \text{if } \gamma \gg 1 \text{ and } z_j < 0. \quad (\text{IXc})$$

The value of γ is related to the current density, J , used for the evolution of hydrogen. According to Faraday's law and equation (I), J/F must be equal to the transport rate of hydroxyl ions per unit area. Substituting $J/F = (dn_{\text{OH}^-}/dt)/A$ in equation (II) for hydroxyl ions and combining with equation (II) for sodium ions with zero transport rate, we obtain

$$J/F = (c_E - c_o)(D_{\text{Na}^+} + D_{\text{OH}^-})/\delta \quad (\text{X})$$

whence

$$\gamma = c_E/c_o = 1 + J\delta/[c_o(D_{\text{Na}^+} + D_{\text{OH}^-})F]. \quad (\text{XI})$$

At high current densities, the value of γ is, therefore, virtually proportional to the current density.

From equations (IXa), (IXb), and (XI), it follows that at high current densities ($\gamma \gg 1$) the transport or reduction rate of positively charged ions j is essentially proportional to the current density, i.e., the electrical field in the boundary layer supports the diffusion of these ions toward the cathode.

On the other hand, it follows from equations (IXc) and (XI), that at high current densities ($\gamma \gg 1$) the transport or reduction rate of anions is essentially inversely proportional to the $|z_j|^{\text{th}}$ power of the current density. In this case, the adverse potential gradient in the boundary layer has a strong retarding effect on the reduction of ions j .

To satisfy the condition $\gamma \gg 1$, the potential difference across the boundary layer must be greater than $kT/e = 0.025$ volt. Since the effective thickness δ of the boundary layer is in general less than 0.05 cm, this condition is satisfied only if the potential gradient in the bulk electrolyte is much greater than 0.5 volt/cm. In most cases, such conditions are avoided, and, therefore, diffusion of anions toward the anode is hindered only to a small extent. However, locally high current densities and, thus, potential differences exceeding 0.025 volt across the boundary layer may occur at a cathode with a diaphragm as is discussed below.

OXIDATION PROCESSES IN A SOLUTION WITH EXCESS ACID

Analogous relations hold for the anodic oxidation of an oxidizable substance dissolved in acid when oxygen is evolved at the anode. Since the potential gradient has the opposite sign, z_j has to be replaced by $-z_j$ in equations (V) to (VIIb). Thus the oxidation rate of cations becomes inversely proportional to the $(z_j)^{\text{th}}$ power of the current density used for the evolution of oxygen, if $\gamma \gg 1$.

REDUCTION PROCESSES IN A SOLUTION WITH EXCESS ACID

Next, we assume conditions under which at the cathode a depletion of electrolyte occurs. As an example, we consider the reduction of ions j in a solution of excess hydrochloric acid when hydrogen is evolved. In this case, the acid concentration c_E at the surface of the cathode is less than the bulk concentration c_o and, thus, $c_E/c_o = \gamma < 1$. Equation (III) is, therefore, rewritten as

$$c = c_o[\gamma + (1 - \gamma)x/\delta] \quad (\text{XII})$$

where c is the acid concentration at distance x from the cathode. Upon substituting equation (XII) in equation (II) for Cl^- ions with $z_i = -1$ and zero transport rate, it follows that

$$\frac{\partial \phi}{\partial x} = \frac{kT}{e} \frac{1 - \gamma}{\gamma \delta + (1 - \gamma)x} \quad \text{at } 0 \leq x \leq \delta \quad (\text{XIII})$$

Upon introduction of equation (XIII) into equation (II) for $i = j$, the reduction rate of a reducible substance j at a sufficiently small concentration, equal to the negative value of the transport rate in the direction of the x coordinate, is found to be

$$v_j = D_j \frac{\partial c_j}{\partial x} + \frac{D_j z_j (1 - \gamma)}{\gamma \delta + (1 - \gamma)x} \quad (\text{XIV})$$

Integration with $c_j = c_{j(0)}$ for $x = \delta$ as the bulk concentration of ions j gives

$$c_j = \frac{v_j \delta}{(z_j + 1)D_j(1 - \gamma)} \left[\gamma + (1 - \gamma) \frac{x}{\delta} \right] + \left[c_{j(0)} - \frac{v_j \delta}{(z_j + 1)D_j(1 - \gamma)} \right] \times \left[\gamma + (1 - \gamma) \frac{x}{\delta} \right]^{-z_j} \quad \text{if } z_j \geq -1 \quad (\text{XVa})$$

$$c_j = \left\{ c_{j(0)} + \frac{v_j \delta}{D_j(1 - \gamma)} \ln \left[\gamma + (1 - \gamma) \frac{x}{\delta} \right] \right\} \times \left[\gamma + (1 - \gamma) \frac{x}{\delta} \right] \quad \text{if } z_j = -1. \quad (\text{XVb})$$

Assuming that ions j are readily reduced at the cathode and, therefore, putting $c_j = 0$ for $x = 0$, we obtain the reduction rate v_j from equations (XVa) and (XVb) as

$$v_j = \frac{(z_j + 1)D_j(1 - \gamma)c_{j(0)}}{\delta(1 - \gamma^{z_j+1})} \quad \text{if } z_j \geq -1 \quad (\text{XVIa})$$

$$v_j = \frac{D_j(1 - \gamma)c_{j(0)}}{\delta \ln \gamma^{-1}} \quad \text{if } z_j = -1 \quad (\text{XVIb})$$

If the acid concentration at the surface of the cathode differs only slightly from the bulk concentration, i.e., if $\gamma \cong 1$, equations (XVIa) and (XVIb) transform to equation (VIII), i.e., the reduction rate is proportional to the concentration $c_{j(0)}$ and independent of the current density.

If the current density is close to the limiting value of the current density due to concentration polarization with respect to hydrogen ions and thus $\gamma = c_E/c_o \ll 1$, we have the following three cases.

1. For positively charged ions j it follows from equations (XVIa) and (VIII) that

$$v_j/v_j^{(0)} \cong z_j + 1 \quad \text{if } \gamma \ll 1 \text{ and } z_j > 0 \quad (\text{XVIIa})$$

2. For univalent anions it follows from equations (XVIb) and (VIII) that

$$v_j/v_j^{(0)} \cong 1/\ln \gamma^{-1} \quad \text{if } \gamma \ll 1 \text{ and } z_j = -1. \quad (\text{XVIIb})$$

3. For anions with a valence greater than unity it follows from equations (XVIa) and (VIII) that

$$v_j/v_j^{(0)} \cong (|z_j| - 1) \gamma^{|z_j|-1} \quad \text{if } \gamma \ll 1 \text{ and } z_j \leq -2. \quad (\text{XVIIc})$$

According to equation (XVIIc) the reduction rate v , of divalent or trivalent anions is greatly diminished by applying a high cell voltage which results in a current density close to the limiting value due to concentration polarization with respect to hydrogen ions and, thus, gives a value of γ much less than unity. In general, such conditions are not likely to occur. This case is, therefore, only of academic interest.

OXIDATION PROCESSES IN A SOLUTION WITH EXCESS SODIUM HYDROXIDE

Relations analogous to equations (XII) to (XVIIb) can be derived for the anodic oxidation of oxidizable substances in a sodium hydroxide solution when oxygen is evolved at the anode. Since the potential gradient has the opposite sign, z , has to be replaced by $-z$, in equations (XIV) to (XVIb). Thus, the oxidation rate of cations with a valence greater than unity becomes proportional to the $(z, -1)^{\text{th}}$ power of the concentration ratio $\gamma = c_E/c_o$ of sodium hydroxide if $\gamma \ll 1$.

PREVENTION OF THE CATHODIC REDUCTION OF HYPOCHLORITE

When hypochlorite is produced by the electrolysis of a sodium chloride solution for industrial purposes, reduction of hypochlorite at the cathode must be minimized. This can be accomplished by a thin diaphragm at the surface of the cathode. According to Foerster and Bischoff (1) and others (2), a small amount of calcium or magnesium chloride is added to the electrolyte so that, at the cathode, a precipitate of calcium or magnesium hydroxide is formed. According to Muller (3), a small amount of chromate is added, which is reduced at the cathode and yields a very thin but effective diaphragm of chromium oxide.

If the current density in the pores of such a diaphragm is sufficiently high, cathodic reduction of hypochlorite will be minimized by the adverse potential gradient in the pores in view of conclusions drawn from equation (IXc).

It seems significant that the reduction of chromate takes place as long as the current density is relatively low, but will practically cease after a sufficient portion of the surface of the cathode has been covered by chromium oxide and, thus, a sufficient current density has been reached, for chromate ions are also rejected by an adverse potential gradient. This mechanism automatically gives a diaphragm which is effective, but does not cause an excessive IR drop or polarization potential.

According to this interpretation, no specific repulsing forces are needed in order to prevent the approach of hypochlorite toward the cathode, or its reduction. Specific adsorption in the pores of the diaphragm seems of minor importance because of the small thickness of the electrical double layer at high electrolyte concentrations.

Frumkin and Florianovich (4) have pointed out that reduction of anions at a cathode may also be prevented if the electrical double layer next to the cathode contains virtually no anions, as is characteristic of a cathode kept at a sufficiently negative potential with respect to a standard hydrogen electrode if the total electrolyte concentration is low. This effect, however, becomes insignificant at high electrolyte concentrations used for the electrolytic production of hypochlorite.

To summarize, the adverse potential gradient in pores of a diaphragm seems to be sufficient in order to account for the prevention of the reduction of hypochlorite ions.

Any discussion of this paper will appear in a Discussion Section to be published in the December 1954 issue of the JOURNAL.

REFERENCES

1. H. BISCHOFF AND F. FOERSTER, *Z Elektrochem*, **4**, 464 (1898).
2. F. OETTEL, *ibid*, **5**, 1 (1898), E. MULLER AND M. BUCHNER, *ibid.*, **16**, 93 (1910); P. PRAUSNITZ, *ibid*, **18**, 1025 (1912).
3. E. MULLER, *ibid*, **5**, 469 (1899); **7**, 398 (1900); **8**, 909 (1902).
4. A. N. FRUMKIN AND G. M. FLORIANOVICH, *Doklady Akad. Nauk. S. S. S. R*, **80**, 907 (1951).

Stability of 2,6-Di-Tertiary-Butyl-Para-Cresol Inhibited Transformer Oil in an Arc^{1,2}

R. NICHOLS HAZELWOOD, KAZUMI OURA,³ AND RAYMOND M. FREY

Line Material Company, Milwaukee, Wisconsin (A McGraw Electric Company Division)

ABSTRACT

Behavior in an arc of transformer oil inhibited with 0.3% by weight 2,6-di-tertiary-butyl-para-cresol was studied. It is shown that there is no essential difference between decomposition of inhibited and uninhibited transformer oil. By quantitative determinations and paper chromatography, it was found that there is no preferential destruction of the inhibitor itself by arcing. The path of arcing breakdown of transformer oil was studied, and it was found that the process was similar to thermal cracking of petroleum.

INTRODUCTION

Three years ago the electrical industry initiated use of inhibitors to prevent oxidation in transformer oil. This step had been advocated by Von Fuchs (1) who had shown that inhibitors increased the life of transformer oil in laboratory tests. Requirements of a satisfactory inhibitor are: (A) oxidation products of the inhibitor must be oil soluble. (B) The inhibitor should be relatively nonpolar, insoluble in water, and should not react directly with molecular oxygen. (C) The inhibitor should not be removed by oil reclamation procedures and should not be incompatible with regular grades of transformer oil.

Compounds known as "hindered phenols" were found to be excellent oxidation inhibitors for petroleum products (2). Many persons felt that earlier oxidation inhibitors of the phenylene diamine or aminophenol types were not as satisfactory because of their susceptibility to air oxidation and their high water solubility (3). The hindered phenols are characterized by tertiary butyl groups on the 2 and 6 positions of the aromatic ring and an *n*-alkyl group on the 4 position. Effectiveness of the inhibitor increases with increasing length of this alkyl group and decreases with decreased branching of groups on the 2 and 6 positions (4).

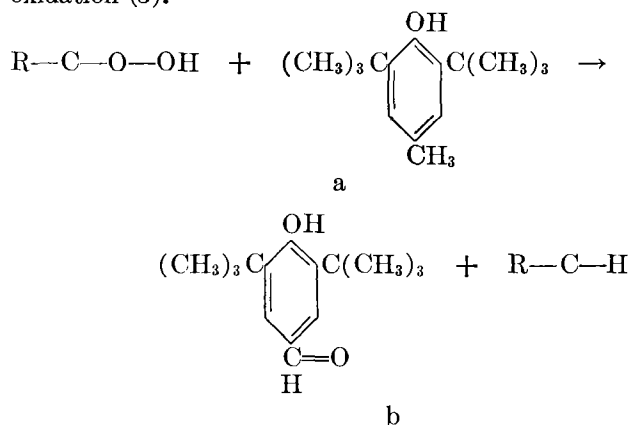
Commonest of hindered phenols in commercial practice is 2,6-di-tertiary-butyl-para-cresol, known as DBPC. DBPC is a clear white crystalline solid melting at 70°C and boiling at 265°C. Specific gravity at 20°C is 1.048. It is soluble in common organic solvents and insoluble in water and aqueous solutions (5). It does not react with alkalis or undergo any of the usual reactions of a phenol due to the shielding effect of the large tertiary butyl groups (6).

¹ Manuscript received July 24, 1953. This paper was prepared for delivery before the New York Meeting, April 12 to 16, 1953

² Second in a series of studies on inhibited transformer oil. For first paper see Reference (9)

³ Deceased (August 10, 1953)

The primary function of an oxidation inhibitor in mineral oil is to react with hydroperoxides formed by oxidation (3).



The aldehyde (b) has some anti-oxidant properties itself, although not to the extent that DBPC (a) has (4).

The function of an inhibitor is to interrupt a chain reaction. It is now thought that the reaction chain in hydrocarbons follows the sequence of: hydrocarbon → hydroperoxide → aldehyde → acid. This chain is interrupted at the stage of formation of hydroperoxide. The inhibitor is oxidized to the aldehyde (b). This aldehyde can be produced by chromic acid oxidation of DBPC (4), or by oxidation with bromine in alcohol solution (7). It has been isolated by chromatographic methods from oxidized inhibited oil samples (4).

Zwelling (8) has shown that DBPC-inhibited transformer oil decreases formation of sludge and maintains the transformer in better condition. Because of this and previous work,⁴ most of the electrical industry adopted inhibited oil for use in distribution transformers. Use of inhibited oil in switchgear and circuit interrupting devices was started in January 1951. Recent studies on small distribution oil circuit reclosers (9) and on large

⁴ Previous work done by Shell Oil Company.

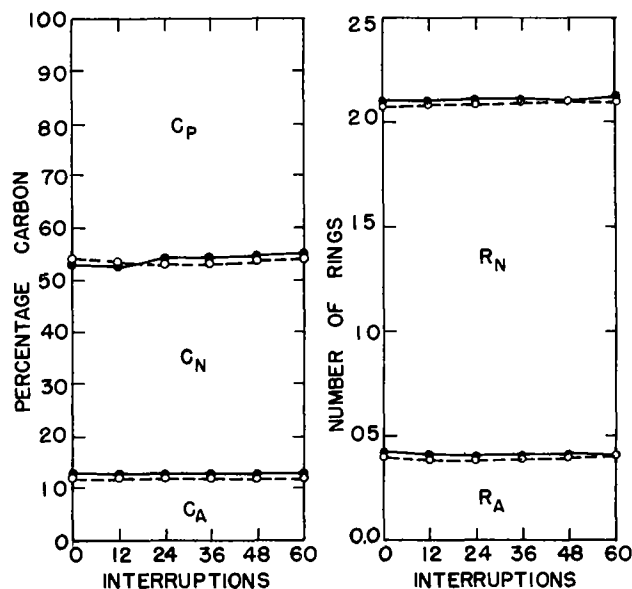


FIG 1 Carbon distribution and ring content for series 1 60 interruptions at 7.2 kv, 490 amp, 30% power factor. C_A = aromatic carbon, C_N = naphthenic carbon, C_P = alkyl carbon, R_A = aromatic rings, and R_N = naphthenic rings. —●— = inhibited oil, —○— = uninhibited oil

circuit breakers (10) have shown that there is no essential difference in behavior and size of carbon particles formed in inhibited and uninhibited oils, and that presence of inhibitor causes no apparent anomalies in performance of these devices

EXPERIMENTAL

Oil samples to be arced were placed in standard production Model KYLE Type H oil circuit reclosers. These reclosers had coil ratings of 5, 25, or 50 amp. Varying conditions of voltage, current, and power factor of the short circuit faults were then applied. Conditions chosen simulate extreme heavy duty field operation.

In each series of experiments, one recloser was filled with uninhibited transformer oil drawn from a newly received tank car. The other recloser was filled with oil inhibited in the laboratory with crystalline DBPC. The same base stock oil was used for all samples. Concentration of DBPC was 0.3% by weight (common concentration in commercial practice).

Viscosity of oil samples was measured using calibrated Ostwald-Fenske viscosity pipettes in constant temperature baths controlled at 37.8°C (100°F) and at 98.9°C (210°F). Densities were measured with a Leach pycnometer at 20°C. The pycnometer was calibrated at 20°C with distilled H₂O and then corrected to absolute density (20/4°C). Refractive index and refractive dispersion were measured with an Abbe refractometer at 20°C. The weight per cent of DBPC was determined colorimetrically by reduction of phosphomolybdic

acid to molybdenum blue (11). Molecular weights were measured by the cyroscopic method in benzene or by viscosity-density correlations (12). Data for various sample series were analyzed for carbon distribution and ring content by the *n-d-M* method (13). These data, combined with viscosity index and specific dispersion data, give a picture of reactions which take place in the arc.

RESULTS AND DISCUSSION

Fig. 1 is a plot of a series of 60 interruptions at 7200 volts, 490 amp, and 30% power factor. The recloser had a coil rating of 25 amp. In this and all subsequent cases, arcing time was approximately 1/2 to 1 cycle/interruption.

Results of this series of arcings show that there is a small but continuing decrease in aromatic content and an increase in naphthenic content. The alkyl carbon shows a decrease. These changes are seen in both carbon distribution and ring content. It is also notable that the method is sensitive enough to show the presence of the aromatic inhibitor (DBPC) in the inhibited oil.

Fig. 2 is a plot of a series of 64 arcings at 7200 volts, 700 amp, and 30% power factor in a recloser with a coil rated at 50 amp. In inhibited oil, the trend is similar to results shown in Fig. 1, that is, increased naphthenes and decreased aromatics and paraffins. However, the uninhibited oil appears to show just the opposite behavior. Fig. 3 shows specific dispersion which is another measure of aromatic content, for the series in Fig. 2. Here, the decrease for both samples indicates that the aromatic content is decreasing in each case.

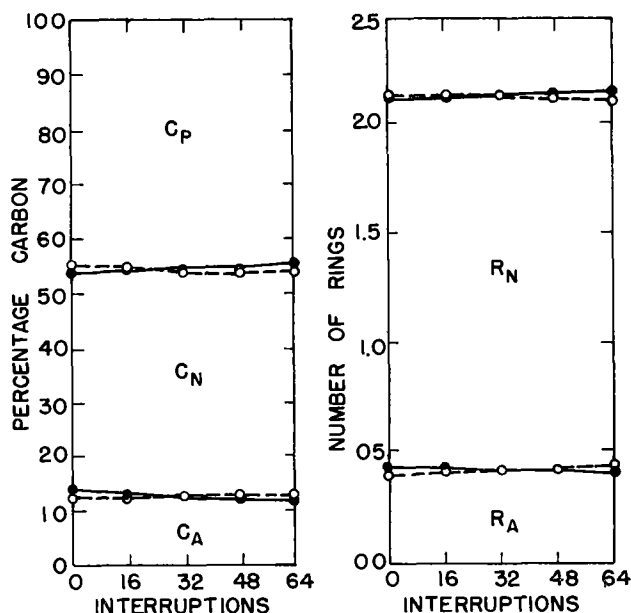


FIG 2 Carbon distribution and ring content for series 2 64 interruptions at 7.2 kv, 700 amp, 30% power factor. —●— = inhibited oil, —○— = uninhibited oil

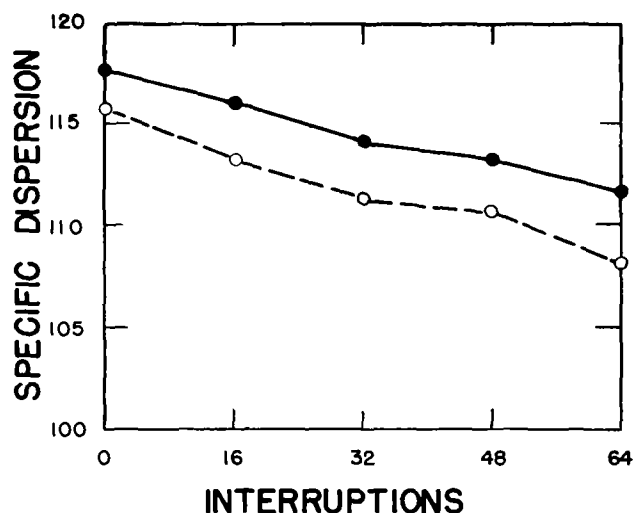


FIG. 3 Specific dispersion for series 2. Specific dispersion, δ , = $n_F - n_C/d_4^{20} \times 10^4$

A series of four reclosers having 5-amp coils was prepared for studies of oxidation stability of oil. Two of these had inhibited oil and two had uninhibited oil. A total of 20 interruptions at 13,200 volts, 100 amp, and 30% power factor was performed.

Table I shows the results of these conditions on carbon distribution and ring content.

The only statistically significant changes are in decreased aromatic content and increased naphthenic content of the inhibited oil, and decrease in paraffinic carbon of both oils. Decrease in aromatic content of the inhibited oil might be interpreted as inhibitor destruction. However, this was not found to be the case.

A 50-amp coil recloser was filled with an inhibited oil and arced 40 times at 7200 volts, 705 amp, and 30% power factor. Samples were drawn at 0, 20, and 40 operations. Table II presents results of this series.

Inspection of data presented indicates that the following changes occur when transformer oil is arced in a circuit recloser: aromatic content is decreased, alkyl chains are broken, and viscosity, molecular weight, and viscosity index are decreased.

These changes are in addition to formation of carbon, hydrogen, and hydrocarbon gases from complete breakdown of the oil. Cracking of oil to gaseous hydrocarbons, hydrogen, carbon, and acetylene polymers has been described by Salzer (14).

These changes are consistent with what would be expected in a thermal cracking process. In thermal cracking, side chains are cleaved, aromatics are reduced to cycloalkanes, and cycloalkyl rings may be broken. As the temperature of the thermal cracking process is raised, another phenomenon occurs. Aromatics are produced at the expense of saturated

TABLE I

No. of interruptions	Oil sample	% C _A	% C _N	% C _P	R _A	R _N
0	Inhibited	12.6	40.0	47.4	0.42	1.71
20	Inhibited	11.3	43.0	45.7	0.37	1.79
0	Uninhibited	11.2	42.1	46.7	0.37	1.81
20	Uninhibited	11.6	42.7	45.7	0.38	1.78

% C_A = % aromatic carbon, % C_N = % naphthenic carbon, % C_P = % paraffinic carbon, R_A = number of aromatic rings, R_N = number of naphthenic rings.

TABLE II

No. of interruptions	% C _A	% C _N	% C _P	VI*	n†	d ₄ ²⁰	M‡	% DBFC§
0	12.3	42.8	44.9	73	9.09	0.8869	267	0.30
20	12.0	43.7	44.3	67	8.93	0.8873	264	0.31
40	11.5	44.7	43.8	45	8.89	0.8884	260	0.32

* Viscosity index

† Centistokes at 37.8°C (100°F)

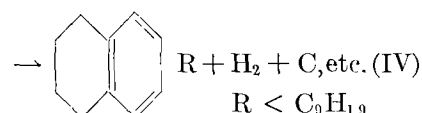
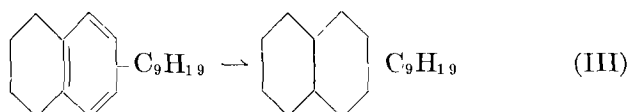
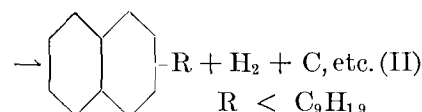
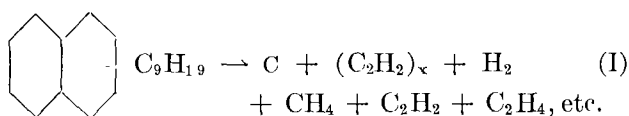
‡ Cryoscopic

§ All ±10%. Differences here not significant

molecules. The same thing happens in catalytic cracking, although the process is more selective and operates at a lower temperature.

From these considerations and from data presented above, a series of equations may be written to describe a portion of what happens to transformer oil in an arc. These equations make use of a so-called "average molecule" which merely represents approximate composition of the transformer oil.

Current theories of the composition of petroleum indicate that above the gasoline range, ring compounds are present primarily as 6-membered fused ring systems, with aliphatic side chains (13). In transformer oil, wax-free crudes are used, so there are no free paraffins present. Aromatics are thought to be part of a fused ring system along with naphthenic rings, rather than free (15). With these factors in mind, the following equations can be written:



Orientation and number of alkyl side chains is not specified, but, probably the chains are present in one long unbranched alkyl group. This is indicated from viscosity index and viscosity data. If there were more than one chain or branched chains, a lower viscosity index would be expected (13).

These equations lead to certain expected results. If equations (II) and (IV) are true, the molecules would become more spherical in shape. This would result in an increase in density and a decrease in molecular weight, viscosity, and viscosity index. All these have been shown experimentally.

Analysis indicates that there is no specific decomposition of DBPC in the arcing process. The phosphomolybdate method for determination of DBPC (11) is not specific but is characteristic of all cresols. However, it was found that alkyl cyclohexanols did not react in the phosphomolybdate spot test (6). To check further the possibility that some side chains might be cleaved from DBPC by the arc, thus destroying much of the antioxidant character (4), paper chromatograms were run on arced oil samples. With Whatman No. 1 paper, butanol saturated with ammonia served as a developing solvent for ascending or descending chromatograms. In this system, the R_f value of phenol is 0.78; of *p*-cresol, 0.31; of 2-*tert*-butyl-*p*-cresol, 0.2; and of DBPC, 0.00. No compound other than DBPC was found in the developed chromatograms, using a 1% phosphomolybdic acid solution in methanol as a spray reagent, followed by exposure to ammonia vapor for five minutes. It is, therefore, reasonable to conclude that, within the limits of detection, DBPC is not preferentially destroyed by arcing.

Further studies are in progress to determine more specific information about the effects of arc energy on cracking of transformer oil in an arc, on the effect of repeated arcing for a prolonged period, and on fractionation of arced oil.

CONCLUSIONS

1. There is no essential difference in the path of decomposition of uninhibited transformer oil and transformer oil inhibited with 0.3% by weight of 2,6-di-*tert*-butyl-*para*-cresol.

2. Decomposition of transformer oil by arcing is similar to thermal cracking. The process is characterized by side chain cleavage, hydrogenation of aromatics, and formation of the decomposition products carbon, acetylene polymers, hydrogen, and hydrocarbon gases.

3. There is no preferential destruction of the inhibitor by arcing.

Any discussion of this paper will appear in a Discussion Section to be published in the December 1954 issue of the JOURNAL.

REFERENCES

- 1 G. H. VON FUCHS, *ASTM Symposium on Insulating Oils* (3rd series), **1949**, 28.
- 2 D. R. STEVENS AND W. A. GRUSE, U. S. Pat. 2,265,582 (1941)
- 3 M. C. K. JONES, A. R. JONES, AND B. R. STRICKLAND, *Ind. Eng. Chem.*, **44**, 2721 (1952)
- 4 J. I. WASSON AND W. M. SMITH, *ibid.*, **45**, 197 (1953).
- 5 W. A. PARDEE AND W. WEINRICH, *ibid.*, **36**, 595 (1944)
- 6 G. H. STILLSON, D. W. SAWYER, AND C. K. HUNT, *J. Am. Chem. Soc.*, **67**, 303 (1945)
- 7 G. M. COPPINGER AND T. W. CAMPBELL, *ibid.*, **75**, 734 (1953).
- 8 M. I. ZWELLING, *Elec. World*, **134** [7] 73 (1950)
- 9 K. OURA, R. N. HAZELWOOD, AND R. M. FREY, *Trans. AIEE*, **72**, Part III, 297 (1953).
- 10 W. M. LEEDS AND R. F. SEUBERT, *ibid.*, **72**, Part III, 718 (1953)
- 11 Koppers Co. Method #C-520, Koppers Company, Chemical Division, Pittsburgh.
- 12 A. E. HIRSCHLER, *J. Inst. Petroleum*, **32**, 133 (1946)
- 13 K. VAN NES AND H. A. VAN WESTEN, "Aspects of the Constitution of Mineral Oils," Elsevier Publishing Co., New York (1951)
- 14 E. SALZER, "Fundamentals of AC Circuit Interruption," p. 36, Allis-Chalmers Mfg. Co., Milwaukee, Wis. (1950)
- 15 K. VAN NES, H. I. WATERMAN, H. A. VAN WESTEN, AND H. VAN KRANEN, *J. Inst. Petroleum*, **38**, 998 (1952)

New Manganese-Activated Fluoride Phosphors¹

ARTHUR L. SMITH

Tube Department, Radio Corporation of America, Lancaster, Pennsylvania

ABSTRACT

The following manganese-activated fluorides were found to exhibit efficient cathodoluminescence NaZnF_3 , KZnF_3 , K_2ZnF_4 , NaMgF_3 , KMgF_3 , K_2MgF_4 , CaF_2 , KCaF_3 , KCdF_3 , and the solid solutions formed between CaF_2 and AlF_3 . With MgF_2 and ZnF_2 , AlF_3 was found to be only a diluent, with CaF_2 , however, three compounds, $2\text{CaF}_2 \cdot \text{AlF}_3$, $\text{CaF}_2 \cdot \text{AlF}_3$, and $\text{CaF}_2 \cdot 2\text{AlF}_3$, were discovered, the first having a peak emission at 5380 \AA and the latter two at 5250 \AA . Emission of Mg and Zn compounds containing K or Na was almost identical with that of the original MgF_2 and ZnF_2 . Although $\text{CaF}_2:\text{Mn}$ has an efficient green and $\text{CdF}_2:\text{Mn}$ a weak green emission, their K-perovskites show strong yellow-orange emission. From the above results, a hypothesis is advanced relating a coordination number of six for the divalent cation in fluorides to orange emission, and a coordination number of eight to green emission.

INTRODUCTION

Manganese-activated fluorides of zinc, magnesium, and zinc-magnesium have been investigated previously from both practical and theoretical viewpoints. Because these fluorides have predominantly exponential decay, they have been used in cathode ray tubes designed for applications such as radar and loran requiring long-persistence phosphors (1, 2). They have also been used by Williams and co-workers in the formulation of basic concepts of the luminescence process (3-6).

Other manganese-activated fluorides have received scant attention. Calcium fluoride is a possible exception, although even it has not been studied in any systematic fashion. The only positive statement found in available literature was that $\text{CaF}_2:\text{Mn}$ has a green cathodoluminescence (7). Therefore, a program was begun to determine whether fluorides other than zinc and magnesium could be effectively activated by manganese.

Fluorides of the alkali metals are poor phosphors, probably because of ion charge differences. There is a lack of suitable sites at which the manganese ions can function as activators. Manganese activation also failed to produce luminescence in the fluorides of strontium and barium. It produced only an inefficient luminescence in cadmium fluoride, probably because the ions in these structures are too large to be replaced effectively by manganese. Perovskite-type fluorides of the class $\text{M}^{\text{I}}\text{M}^{\text{II}}\text{F}_3$, on the other hand, were found to be excellent base matrices. Spectral energy emission characteristics of this class of fluorides led to the formulation of a new hypoth-

esis concerning the role of manganese as an activator (8).

Compounds and solid solutions of aluminum fluoride and alkali or alkaline earth fluorides were also investigated. The combination of aluminum fluoride and calcium fluoride was the only combination which gave efficient phosphors. An x-ray investigation of this system led to the discovery of hitherto unreported compounds of $\text{AlF}_3-\text{CaF}_2$.

PREPARATION OF PHOSPHORS

All the simple fluorides were prepared in platinum vessels by reaction between excess C.P. H_2F_2 or $(\text{NH}_4)_2\text{F}_2$ and purified carbonates or oxides of the requisite cation. The slurry was carefully evaporated to dryness and then baked at 500°C to decompose any remaining acid or ammonium fluorides. Manganese fluoride was added to the simple fluorides (or, in cases where complexes were to be formed, to the suitable combination of the simple fluorides) in the amount of 1 mole %/mole of base matrix. Mixtures were then dry ground in a mortar and fired in either carbon crucibles or platinum crucibles surrounded by carbon to prevent oxidation. Firing temperature depended on the melting point of the final compound. For compounds melting above 1000°C that temperature was used; for compounds melting below 1000°C , the firing temperature was 50° below the melting point. All mixtures except those containing $\text{CaF}_2-\text{AlF}_3$ were fired for two half-hour periods and were ground between firings. $\text{CaF}_2-\text{AlF}_3$ mixtures were fired for three half-hour periods.

TESTING OF PHOSPHORS

X-ray diffraction analyses were made with nickel-filtered radiation from a copper-target tube

¹ Manuscript received October 1, 1953. This paper was prepared for delivery before the New York Meeting, April 12 to 16, 1953

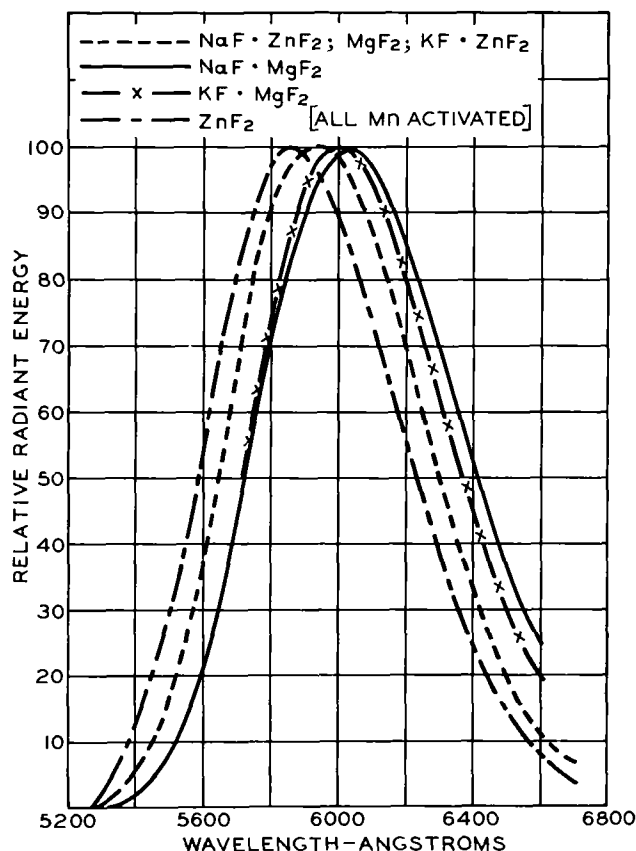


Fig. 1 Spectral energy distribution curves of manganese-activated zinc fluoride, magnesium fluoride, and their alkali fluoride perovskites.

operated at 40 kv and 15 ma. Phosphor samples were rotated within a circular camera 14.32 cm in diameter.

Cathodoluminescence efficiencies and emission spectra were determined with a defocused electron beam having a current density of $1.5 \mu\text{a}/\text{cm}^2$ and an accelerating potential of 8000 volts. Peak efficiencies and spectral distribution of energy were measured by the spectroradiometer and method described by Hardy (9).

SIMPLE FLUORIDES

The cathodoluminescence of the manganese-activated alkali fluorides and aluminum fluoride was of such low order that accurate readings were not possible. Because of differences in ion size and charge between these cations and manganese, the manganese probably cannot be built into the lattice in the proper manner to form active centers. Ion-size differences alone probably prevent the effective activation of fluorides of beryllium, strontium, and barium by manganese. No accurate data could be obtained for any of these mixtures.

Manganese-activated zinc, magnesium, and zinc-magnesium fluorides have been thoroughly de-

scribed (1-6). Their spectral-energy peak is approximately 5900 \AA , as shown in Fig. 1.

Calcium and cadmium fluorides are not as well known as the zinc and magnesium fluorides. Concurrently with the work described in this article, Ginther (10) was investigating properties of calcium fluoride activated by cerium and manganese. Results given here concerning the peak and shape of the spectral energy emission curves are in substantial agreement with his results. The peak value of 4950 \AA for calcium fluoride activated with 1 mole % manganese checks reasonably well with Ginther's value of 4900 \AA for this concentration. $\text{CaF}_2:0.01 \text{ Mn}$ is a moderately efficient phosphor having 30% of the efficiency of $\text{ZnF}_2:\text{Mn}$. The spectral energy emission curve for this mixture is shown in Fig. 4. Its persistence is the shortest of all the fluorides, although exact data are not yet available. $\text{CdF}_2:0.01 \text{ Mn}$ is a very poor phosphor; its efficiency is only 1% of that of zinc fluoride. It has essentially the same spectral energy emission characteristic and peak emission as calcium fluoride.

FLUORIDE PEROVSKITES

Structural Considerations

The perovskite structure is one in which large cations together with either O^- or F^- form a close-packed arrangement with smaller cations in the interstices of sixfold coordination. A definite relationship must exist between the ionic radii of the ions in order that this structure be formed. For fluorides, this relationship is expressed by the equation

$$r\text{M}^{\text{I}} + r\text{F}^- = t\sqrt{2} (r\text{M}^{\text{II}} + r\text{F}^-)$$

where t can have a value between 0.8 and 1.0 (11a). The large ions M^{I} and F^- form a close-packed arrangement with the smaller M^{II} ions in the interstices. The M^{II} ions are surrounded by six F^- in octahedral configuration. Substitution of the values of the ionic radii of Li, Na, K, Mg, Zn, Mn, Cd, and Ca in their proper places in the above equation indicates that Li should form no complexes at all, Na should form a complex with Mg, Zn, or Mn, but not with Ca or Cd, and K should form complexes with Mg, Zn, Mn, Ca, or Cd. All theoretically possible structures have been prepared in the laboratory except those of manganese, which were not tried. No compound formation occurred where theory indicated it was impossible. Potassium perovskites of Mg, Zn, and Ca have been reported previously and their x-ray diffraction pattern published (12). The compound $\text{NaF}\cdot\text{MgF}_2$ has also been investigated and was found to have a melting point of 1030°C (13). Although $\text{NaF}\cdot\text{ZnF}_2$ and $\text{KF}\cdot\text{CdF}_2$ are predicted by the above equation,

they have not been reported previously. These compounds were made, and were found to have x-ray diffraction patterns typical of the group.

Another complex fluoride, K_2MgF_4 , has also been reported (14). Although the diffraction pattern of this fluoride is available (12), its exact crystal structure has not yet been determined. The previously unreported zinc analogue, K_2ZnF_4 , was also prepared, and was found to have an x-ray diffraction pattern very similar to that of the magnesium compound. Calcium, however, did not form this type of structure; x-ray diffraction patterns of a fired mixture containing 2 moles of KF per mole of CaF_2 showed only the lines of KF and $KCaF_3$.

Spectral-Energy Emission Characteristics

The perfect and near-perfect coincidence of cathodoluminescent spectral-energy emission characteristic of these perovskites, illustrated in Fig. 1, 2, and 3, and Table I, is of major interest. The spectral energy emission curves of $NaF \cdot ZnF_2$, $KF \cdot ZnF_2$, and MgF_2 are identical within experimental error; each mixture in the pairs $NaF \cdot MgF_2$ — $KF \cdot MgF_2$, $KF \cdot CaF_2$ — $KF \cdot CdF_2$, and $2KF \cdot ZnF_2$ — $2KF \cdot MgF_2$ differs from the other mixture in the pair by less than 50 Å. Within the group of compounds formed in the system NaF — KF — ZnF_2 — MgF_2 , the maximum difference in peak of emission is only

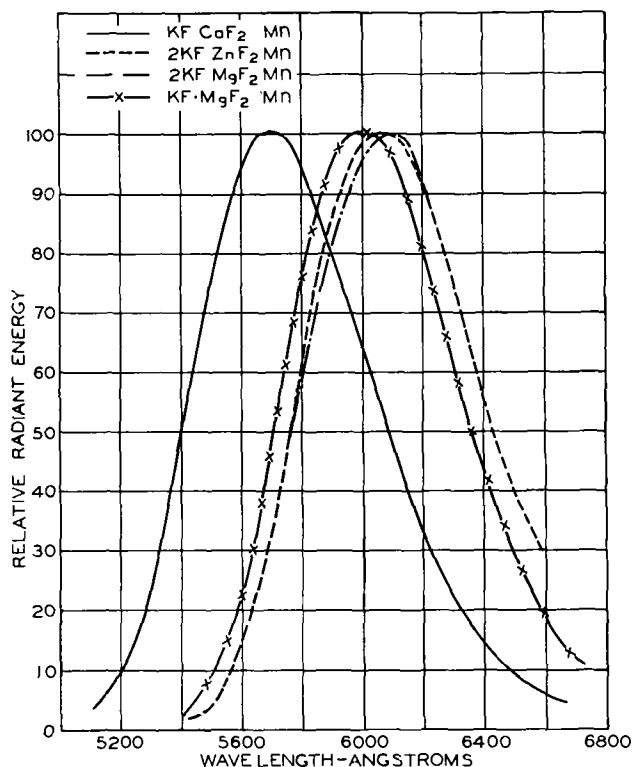


FIG 2 Potassium-magnesium-fluoride:Mn spectral energy distribution compared with those of potassium-calcium-fluoride:Mn $2KF \cdot ZnF_2$:Mn and $2KF \cdot MgF_2$:Mn

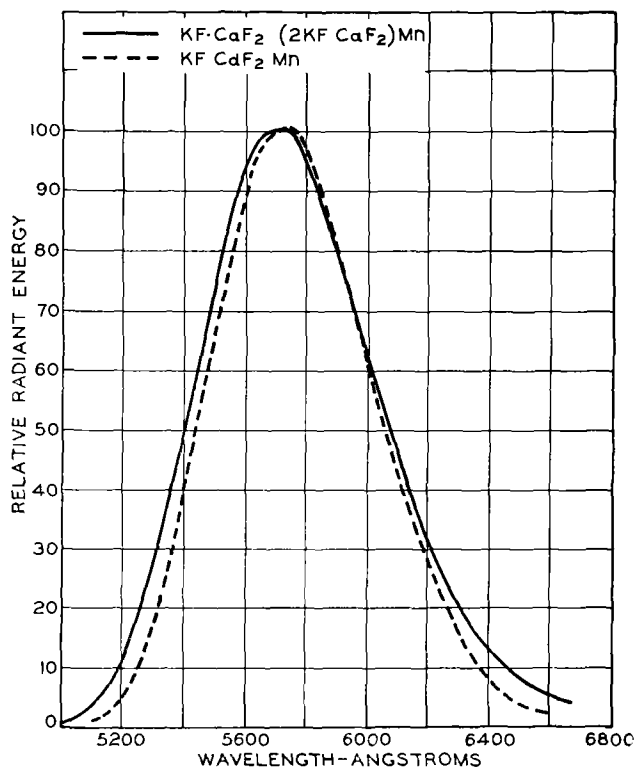


FIG 3 Spectral energy distribution curves for the manganese-activated potassium-fluoperovskites of calcium and cadmium showing the almost coincident spectra

TABLE I Wave lengths (Å) of peak spectral emission of phosphors formed from compounds shown in left vertical column in combination with compounds shown in top horizontal line

		NaF	KF	2KF	AlF_3
MgF_2	5920	6080	6000	6100	5920
ZnF_2	5870	5920	5920	6070	5870
CaF_2	4950	5020	5710	5710	5250
CdF_2	4950	—	5720	5720	—

230 Å, with zinc fluoride at one extreme at 5870 Å and $2KF \cdot MgF_2$ at the other extreme at 6100 Å.²

The difference of 750 Å in the spectral energy peak between CaF_2 or CdF_2 (4950 Å) and $KF \cdot CaF_2$ or $KF \cdot CdF_2$ (5710 Å) is also important. It is in sharp contrast to the much smaller shifts in the perovskite complexes of ZnF_2 and MgF_2 . The shift caused by the addition of sodium fluoride to calcium fluoride is less than 100 Å, as shown in Fig. 4. This

² One of the reviewers has called attention to the work of J. T. Randall, [*Proc Roy Soc London*, **170A**, 272 (1939)] on the low temperature cathodoluminescent spectra of manganese halides. At 90°K, the peak emission occurred at 6285 Å for the fluoride, 6360 Å for the chloride, and 6330 Å for the bromide. Randall concluded that the red fluorescence is a property of all the manganese ions in the crystal, with the transitions of the forbidden type ($2E \rightarrow 4F$) characteristic of the divalent manganese ion. In all cases manganese occurs in sixfold coordination.

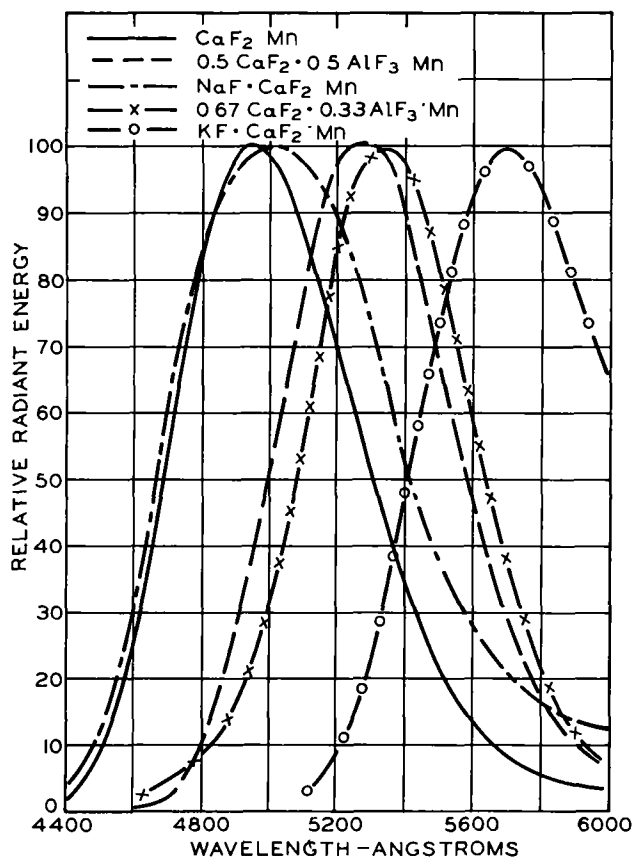


FIG 4 Spectral energy distribution curves of a number of manganese-activated complex fluoride phosphors containing calcium compared with that of calcium fluoride:Mn itself

relatively small shift confirms the observation that sodium fluoride forms no definite perovskite structure such as that formed with potassium fluoride. As shown in Fig. 3, the spectral energy emission characteristics of $\text{KF} \cdot \text{CaF}_2$ and $\text{KF} \cdot \text{CdF}_2$ do not differ by more than 25 Å. This small change indicates that precisely the same mechanism caused the shift for both the calcium and cadmium compounds.

Efficiencies

Table II gives the relative peak efficiencies of the various fluorides. The peak efficiency of zinc fluoride, the highest of all the fluoride efficiencies, has been used as the standard to which all the others are related. Most of the phosphors containing alkali

TABLE II. Relative peak spectral emission efficiencies (%) of phosphors formed

		NaF	KF	2KF	AlF ₃
MgF ₂	54	24	41	20	40
ZnF ₂	100	61	100	53	20
CaF ₂	30	3	20	4	50
CdF ₂	1	0	45	6	1

TABLE III Emission color and relative peak efficiencies of inefficient phosphors containing alkali fluorides

Compound	Color	Relative peak efficiency (ZnF ₂ = 100)
LiF · AlF ₃	Orange-yellow	1
3LiF · AlF ₃	Yellow-green	1
NaF · AlF ₃	Blue-green	1
3NaF · AlF ₃	Blue-green	2
NaF · 2AlF ₃	Yellow-orange	1
5NaF · 3AlF ₃	Yellow-green	5
KF · 2AlF ₃	Orange-red	1
LiF · CaF ₂	Green	2
LiF · CdF ₂	Blue-green	1

fluorides are less efficient than those free from alkali fluoride, with two exceptions. The compound $\text{KF} \cdot \text{ZnF}_2$ is as efficient as ZnF_2 itself, and $\text{KF} \cdot \text{CdF}_2$ shows a considerable improvement in efficiency over CdF_2 . The probable reason for the difference in these two mixtures is treated later.

FLUORIDE PHOSPHORS CONTAINING ALUMINUM

There is a considerable number of compounds which contain alkali metals, aluminum, and fluorine, as shown in Table III. None of these produced efficient phosphors when manganese was used as an activator. The disparity in size and charge between manganese ions and alkali or aluminum ions is probably the reason why manganese could not effectively substitute in these structures. There was, however, enough weak but definite luminescence to indicate that some manganese was incorporated, and that the nature and concentration of the alkali ion were the main factors in the color of the emission.

Fluorides of zinc and magnesium form only limited solid solutions with aluminum fluoride, but form definite compounds with alkali fluorides. Addition of aluminum fluoride to zinc or magnesium fluorides merely decreases the efficiencies of the simple fluoride phosphors without causing any shift of peak emission. The effect of aluminum fluoride is less drastic on the magnesium fluoride phosphor than on zinc fluoride. In a 50-50 mole % mixture, the reduction of efficiency is only 20% for magnesium fluoride, but 80% for zinc fluoride, as shown in Table II. X-ray diffraction analyses of $\text{ZnF}_2 \cdot \text{AlF}_3$ and $\text{MgF}_2 \cdot \text{AlF}_3$ show the presence of both original components. There is some distortion of the AlF_3 structure, but little or no distortion of the magnesium or zinc fluoride lattice. Results differ only slightly for variations about the 50-50 mole % composition.

Addition of aluminum fluoride to calcium fluoride produces different results, as shown in Table IV and Fig. 4. Within this system at least three compounds, or phases, are found, as well as solid solu-

TABLE IV Emission color and relative peak efficiencies of a series of calcium-aluminum-fluorides

Molar composition	Peak emission (approx) (Å)	Relative peak efficiency (ZnF ₂ = 100)
CaF ₂	4950	30
0.9 CaF ₂ —0.1 AlF ₃	4950 and 5250 (two bands)	30/30
0.8 CaF ₂ —0.2 AlF ₃	4950 and 5380 (two bands)	15/32
0.7 CaF ₂ —0.3 AlF ₃	5380	35
0.6 CaF ₂ —0.4 AlF ₃	5380	45
0.5 CaF ₂ —0.5 AlF ₃	5250	50
0.3 CaF ₂ —0.7 AlF ₃	5250	35
0.2 CaF ₂ —0.8 AlF ₃	5250	20

tions. It is not yet possible to assign unambiguous stoichiometric ratios to the various phases, but a reasonable approximation can be made. Correlation of the spectral distribution data with x-ray diffraction data indicates that three compounds are present in the system, having the following spectral distribution characteristics and identifying lattice spacings:

Compound	Peak emission (Å)	Lattice spacing (<i>d</i> values in Å)
2CaF ₂ ·AlF ₃	5380	(3.5), 2.90, 2.75, 1.87, 1.83, 1.74, 1.76
CaF ₂ ·AlF ₃	5250	(3.5), 3.25, 2.80, 2.00, 1.82
CaF ₂ ·2AlF ₃	5250	(3.5), 3.20, 2.80, 1.98, 1.81

Interpretation of these data is difficult because of the probability that some lines are common to more than one phase, and because one line at 3.5 is common to all phases as well as to AlF₃ itself. There is no doubt, however, that the phase which emits at 5380 Å can be distinguished by the unique lines at *d* values of 2.90, 1.87, and 1.83, and that the 5250 Å emission is associated with a phase uniquely determined by *d* values of 3.25, 2.80, and 2.00. The third phase has lines very similar to those of the previous phase (*d* = 3.20, 2.80, 1.98) and also emits at 5250 Å. It is possible, therefore, that this compound is not a unique phase but a solid solution of CaF₂·AlF₃ with AlF₃. However, the lack of gradation of this slight, but very definite, shift, and the existence of the shift even in very large discernible excesses of AlF₃ make it probable that a definite phase does exist having a crystal configuration very similar to the CaF₂·AlF₃ compound.

The freezing point diagram of CaF₂—AlF₃—NaF (15) is in rough agreement with these findings. A eutectic was reported at 62.5 CaF₂—37.5 AlF₃. Here, a compound formation was hypothesized at 66.7 CaF₂—33.3 AlF₃ (2CaF₂·AlF₃). Between this eutectic point and the composition 42.5 CaF₂—

57.5 AlF₃, the curve for CaF₂—AlF₃—NaF shows two very minor peaks at 52.5 CaF₂—47.5 AlF₃ and 47.5 AlF₃ and 47.5 CaF₂—52.2 AlF₃.

In this region, a new "phase" called CaF₂·AlF₃ was found. Fedotieff and Iljinsky (15) did not investigate concentrations beyond 57.5 mole % AlF₃; they said such concentrations were in an "unrealizable" or "indeterminate" region. At a concentration of 80 mole % CaF₂ and 20% AlF₃, they were also unable to determine a freezing point. Laboratory analysis of this concentration indicated that there were two phases coexistent—CaF₂ and the "2CaF₂·AlF₃" phase. It is hoped that a careful study may be made in the future of the melting point, x-ray diffraction pattern, and spectral energy emission characteristics of this binary so that the system may be positively defined.

DISCUSSION

The crystal structure of all simple fluorides has been determined previously and may be found summarized in various publications (11b, 16). Both calcium fluoride and cadmium fluoride are of the fluorite (CaF₂) structure, in which each cation is surrounded by six fluoride ions. The fluorides of zinc, magnesium, and manganese are classed in the rutile (TiO₂) structure, in which each cation is surrounded by six fluoride ions. Aluminum fluoride crystallizes with a symmetry close to that of the rutile type, each aluminum ion occupying octahedral holes formed by close-packed fluoride ions. The perovskite-type structure has been described previously; the divalent cation in this type is surrounded by six fluoride ions.

The coordination number of the divalent cations may explain the almost negligible influence of the alkali ions on the spectral energy emission characteristics of zinc and magnesium fluorides and the pronounced shift of emission characteristics produced with calcium and cadmium fluorides. Zinc and magnesium are in sixfold coordination in both their simple fluorides and in perovskite complexes. Calcium and cadmium, on the other hand, are in eightfold coordination in their simple fluorides, but in sixfold coordination in their potassium perovskite complexes. It appears that in fluoride structures, therefore, substitution of manganese into a sixfold coordination structure produces a spectral energy emission in the orange region, and substitution in an eightfold coordinated structure produces emission in the green region. This hypothesis is analogous to that of Linwood and Weyl (17) for oxygen-dominated structures, in which green emission is attributed to fourfold coordination and red emission to sixfold or higher coordination. All the spectral energy emissions in the orange region of fluorides

occur in sixfold coordinated structures, while the two in the green region are in eightfold coordinated structures. When the coordination structure of calcium is changed from eightfold to sixfold, the emission shifts 750 Å toward the orange region. Cadmium shows a similar shift, and also produces an efficient perovskite phosphor, although its simple fluoride is poorly efficient. Reduction in size of the holes in which manganese can substitute probably permits a more efficient energy transfer.

Addition of sodium fluoride to calcium fluoride does not produce new compounds, but only solid solutions. The spectral energy emission curve is broadened and the peak shifted slightly by about 100 Å. Efficiency is decreased by 90%.

Little can be said about the $\text{CaF}_2\text{—AlF}_3$ compounds, because nothing is known about their crystal structure. From conclusions reached on a hole-size-and-coordination theory (8), it can be hypothesized, however, that in these new compounds calcium remains in eightfold coordination, but its ionic radius is decreased.

ACKNOWLEDGMENTS

The assistance of the following associates is gratefully acknowledged: L. E. Whitmer for the preparation of samples, A. E. Hardy and staff for optical measurements, and A. D. Power and S. B. Deal for x-ray diffraction measurements.

Any discussion of this paper will appear in a Discussion Section to be published in the December 1954 issue of the JOURNAL.

REFERENCES

- 1 H W LEVERENZ, "Research and Development Leading to New and Improved Radar Indicators," NDRC Publication, PB25481
- 2 H W LEVERENZ, "An Introduction to Luminescence of Solids," J. Wiley & Sons, Inc, New York (1950).
- 3 F. E WILLIAMS, *J. Opt Soc Amer*, **37**, 302 (1947)
- 4 J H CRAWFORD, JR, AND F. E WILLIAMS, *J Chem Phys*, **18**, 775 (1950).
- 5 W W. PARKINSON, JR, AND F E. WILLIAMS, *ibid*, **18**, 534 (1950).
- 6 P D JOHNSON AND F E WILLIAMS, *ibid*, **18**, 323 (1950)
- 7 F WICK, *J Opt Soc Amer*, **27**, 275 (1937)
8. A. L SMITH, Electrochem Society 103rd Meeting, April 1953, Abstract #20
- 9 A E HARDY, *Trans Electrochem Soc*, **91**, 127 (1947)
- 10 R J GINTHER, *This Journal*, to be published.
- 11a A F WELLS, "Structural Inorganic Chemistry," p 330, Oxford University Press, London (1945)
- 11b *Ibid*, p 275
- 12 "Alphabetical and Grouped Numerical Index of X-Ray Diffraction Data," Special Technical Publication 48-B, American Society for Testing Materials, Philadelphia (1950)
- 13 A G BERGMAN AND E P. DERGUNOV, *C A.*, **37**, 823 (1943); *Compt rend. Acad U.R.S.S*, **31**, 7534 (1941)
- 14 H REMY AND W. SEEMANN, *Rec Trav Chem*, **59**, 516 (1940).
- 15 P P. FEDOTIEFF AND W. P ILJINSKY, *Z anorg u allgem Chem*, **129**, 93 (1923)
- 16 R W G. WYCKOFF, "Crystal Structures," Vol I, Interscience Publishers, Inc, New York (1951)
- 17 S H LINWOOD AND W A WEYL, *J Opt Soc Amer*, **32**, 443 (1942)

Effect of Chain Branching on Electrochemical Carbon-Halogen Bond Fission. Possible Mechanism for the Process^{1,2}

PHILIP J. ELVING AND JOSEPH M. MARKOWITZ

University of Michigan, Ann Arbor, Michigan

AND

ISADORE ROSENTHAL³

The Pennsylvania State College, State College, Pennsylvania

ABSTRACT

As part of a continuing study of the electrochemical reduction of carbon-halogen bonds, a group of branched-chain α -bromoalkanoic acids with several of their ethyl esters and straight-chain isomers were investigated polarographically. The relation between half-wave potential, $E_{1/2}$, and pH for the acids follows an S-shaped pattern having pH -invariant regions in the alkaline and acidic ranges, $E_{1/2}$ in the latter region being considerably more negative. The $E_{1/2}$ values for the esters are pH -independent, being slightly more positive than those of the corresponding acids in the acidic region. Polarographic waves all involve a diffusion-controlled two-electron reduction. In the acidic region, the branched-chain acids are more easily reducible than their straight-chain isomers by 0.20 to 0.13 volt, the larger differences being observed for the lower molecular weight acids. In the alkaline region the situation is more complicated, all acids in the series having ethyl groups or larger in the α -position have their $E_{1/2}$ shifted to more negative values.

The trend of the variation of $E_{1/2}$ with chain length is treated as the operation of three effects: (a) electrostatic effects which are important in the lower acids and esters, (b) steric effects related to ring-formation, which become important in the higher acids and make reduction more difficult, (c) bulk effects which are responsible for the over-all trend of reducibility in the higher acids. Variation of $E_{1/2}$ with pH is discussed briefly. Two hypothetical mechanisms, ionic and free-radical, are compared on the basis of the structural influences developed by the data.

INTRODUCTION

Previous polarographic work on electrochemical carbon-halogen bond fission in α -halogenated alkanolic acids is reviewed in a study (1) of the straight chain acids. At all pH values, as chain length increases, observed $E_{1/2}$ decreases, there being one exception, bromobutanoic, in the alkaline region. The bond fission involves a two-electron reduction with conversion to the corresponding saturated acid. The effect of ethanol on $E_{1/2}$ and diffusion current, i_d , is also discussed, as are the influences of structure and inductive effect on the ease of reduction.

For several reasons, it seemed logical to inquire next into the effect of branching of the carbon chain and of chain lengths on the ease of reduction. In the first place, one objective of the systematic study of electrochemical carbon-halogen bond fission is the

possibility of defining a correlation between organic chemical reactivity of such bonds and polarographic half-wave potentials. Since both the chemical and electrochemical processes are usually irreversible, analogy between chemical reactivity and half-wave potential would be expected if both processes involved the same essential reaction pattern. Obviously, in any attempt to ascertain whether the electrochemical process is a displacement reaction or a free radical process, the structural factor of branching is important.

The behavior of 2-bromobutanoic acid in the previous study (1) was considered anomalous. The authors felt, however, that an attempt should be made to determine whether this anomaly was more general, and if so, whether some pattern underlay its occurrence. This represents a further reason for extending the study to the branched acids.

Another matter which required further investigation is the consistently observed and repeatedly verified result (1-8) that, for α -haloalkanoic acids, $E_{1/2}$ varies with pH in an S-shaped pattern. This behavior has never been satisfactorily explained on a quantitative basis, although related phenomena

¹ Manuscript received June 18, 1953. This paper was prepared for delivery before the New York Meeting, April 12 to 16, 1953.

² No. XVI in a series on the polarographic behavior of organic compounds.

³ Present address: Rohm and Haas Company, Research Laboratories, Philadelphia, Pennsylvania.

TABLE I. Polarographic data for straight and branched chain 2-bromoalkanoic acids, C₂ to C₈

Temp, 0°C, mercury head, 50 cm. Diffusion coefficients were calculated from the Stokes-Einstein equation. *n*-Value from Ilkovic equation is 2 in all cases. Concentration of bromoacid ran from 0.1 to 0.7 mM, lower values were used to eliminate maxima.

Acid D × 10 ⁶	MM		ME		EE		BE		HH		HM		HE	
	2.02		1.97		1.92				2.15		2.08		2.02	
	-E _{1/2}	I	-E _{1/2}	I	-E _{1/2}	I	-E _{1/2}	I	-E _{1/2}	I	-E _{1/2}	I	-E _{1/2}	I
1.1	0.29	2.1	0.25	2.3	0.22	1.6	0.14	1.7	0.67*	2.3	0.52*	2.1	0.47*	1.8
1.4							0.16	1.9						
1.8	0.28	2.1	0.26	2.1	0.22	1.8	0.16	1.9	0.67*	2.2	0.56*	2.0	0.50*	1.9
4.0	0.47	1.5	0.40	1.4	0.39	1.2								
4.8	0.58	1.7	0.49	1.6	0.48	1.2								
5.6	0.80	1.8	0.69	1.5	0.71	1.4	0.45	1.3						
7.8	1.06	1.9	1.03	1.6	1.10	1.5								
8.2							0.82	1.2	1.24	2.2	1.20	2.2	1.22	1.8
8.6							0.78	1.3						
8.9	1.06	1.7	1.03	1.7	1.07	1.4			1.23	2.2	1.20	2.0	1.22	1.8
9.0							0.79	1.4						

* 0.01% gelatine was used in this solution to eliminate maxima

in other groups of compounds, e.g., the double wave in pyruvic acid, have been more or less successfully treated (9, 10). It is not clear at present whether the S-shaped curve requires merely a modification of some of these treatments or whether entirely new concepts are required. An attempt by Saito (11) to use a modification of Brdicka and Wiesner's (9) approach to the problem is quite unsatisfactory. No completely satisfactory treatment of this matter can be formulated at present. Accordingly, the phenomenon of the S-shaped curve is given only brief attention in the present paper.

Consequently, the polarographic behavior of bromoethanoic (HH), 2-bromopropanoic (MH), 2-bromobutanoic (EH), 2-bromo-2-methylpropanoic (MM), 2-bromo-2-methylbutanoic (ME), 2-bromo-2-ethylbutanoic (EE), and 2-bromo-2-ethyl hexanoic (BE) acids was investigated, the first three for comparison with the previous study (1).⁴ In order to complete the work, the ethyl esters of five of these acids were also investigated.

EXPERIMENTAL

Experimental conditions differ somewhat from those of previous work (1-3). The following buffer systems, adjusted to an ionic strength of 0.5M, were used: HCl-KCl (pH 1 to 2), HC₂H₃O₂-NaC₂H₃O₂ (pH 4 to 6), and NH₃-NH₄Cl (pH 8 to 9). The operating temperature was 0° ± 0.1°C; the test solution contained 9.5% ethanol by volume;

⁴ For brevity and clarity, the various acids will be subsequently referred to through the use of the abbreviations indicated. These consist of the initial letters of the substituents, other than bromine, on the *alpha* carbon atom, i.e., H is hydrogen, M is methyl, E is ethyl, etc.; in the case of the ethyl esters, Et will be prefixed, e.g., EtMH is ethyl-2-bromopropionate.

the mercury head was 50 cm. To determine the nature of the current-controlling processes, temperature coefficients for *i*_a were found by making supplementary measurements at 25°C. Likewise, supplementary measurements at 75 cm mercury head allowed computation of current ratios for different values of drop-time. The capillary (Corning marine barometer tubing) had a drop-time of 5.94 sec and an *m*-value of 1.071 mg/sec at open circuit in distilled water (50 cm, 0°C). A Sargent Model XXI Polarograph was used in connection with a Leeds and Northrup student-type potentiometer. All potentials given are corrected for *IR* drops and are referred to the S.C.E. Beckman Model G and H pH meters were used to measure pH. In view of the 9.5% ethanol content of the test solutions, strict interpretation of the pH values is unwarranted; accordingly, pH values are given to only one decimal place in the summary table (Table I) even though measured to ±0.02 pH units and so reported in the primary data tables which are available from the authors.

MM, EE, EtBe, EtEE, and EtMM were obtained from Sapon Laboratories. EtEH, EtMH, HH, MH, and EH were Eastman Kodak white label grade chemicals. ME and BE were synthesized. No special attempt was made to purify these compounds, except for ME and BE which were purified in the course of their synthesis. The former distilled at 104°-107°C/8 mm; the latter at 100°-101°C/2 mm. All compounds were found to be polarographically pure.

Test solutions were prepared by diluting a 5-ml portion of stock solution, containing a known concentration of the compound in 95% ethanol, to 50 ml with buffer solution. All stock solutions were

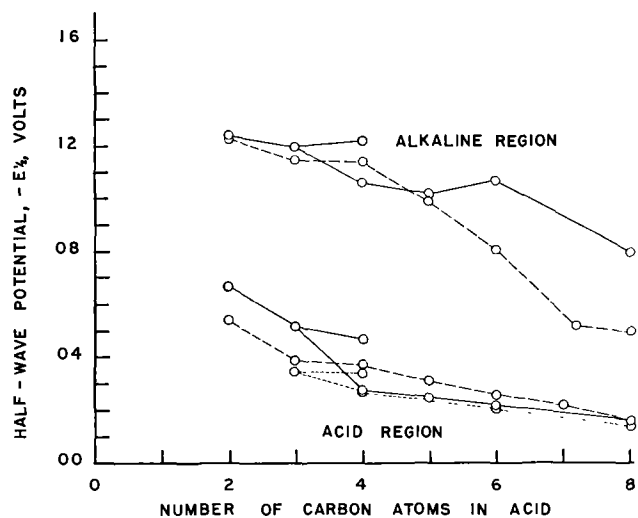


FIG. 1. Relation of $E_{1/2}$ to chain length of the acid for α bromo acids and their ethyl esters. Solid lines acids, dotted lines, esters, dashed lines data for acids in Reference (1)

prepared at 0° ; stock and buffer solutions were stored at 0° . Concentration and pH values subsequently given are those of the final test solutions. Solutions were deoxygenated with nitrogen, purified as described (2). Base solution (obtained by mixing 95% ethanol with buffer) curves were used in every case to correct the test solution curves.

Choice of operating conditions was governed by the following factors: poor solubility of some of the compounds in water indicated the necessity for a mixed solvent; use of ethanol and the proportion of 9.5% by volume were somewhat arbitrary, being selected on the basis of solubility improvement and minimum $E_{1/2}$ effect. At $25^\circ C$, the rapid hydrolysis of some compounds, particularly in alkaline media, even during the relatively short period of deoxygenation and electrolysis, resulted in curves worthless for calculation; this difficulty was effectively eliminated at 0° .

TABLE II Effect of structure on half-wave potential for acids and esters

Acid	Structure	$-E_{1/2}$		Ester	Structure	$-E_{1/2}$
		Acidic region	Alkaline region			
HH	$\begin{array}{c} \text{Br} \\ \\ \text{C}-\text{COOH} \end{array}$	0.67	1.24			
MH	$\begin{array}{c} \text{Br} \\ \\ \text{C}-\text{C}-\text{COOH} \end{array}$	0.54	1.20	EtMH	$\begin{array}{c} \text{Br} \\ \\ \text{C}-\text{C}-\text{COOEt} \end{array}$	0.35
EH	$\begin{array}{c} \text{Br} \\ \\ \text{C}_2-\text{C}-\text{COOH} \end{array}$	0.48	1.22	EtEH	$\begin{array}{c} \text{Br} \\ \\ \text{C}_2-\text{C}-\text{COOEt} \end{array}$	0.34
MM	$\begin{array}{c} \text{Br} \\ \\ \text{C}-\text{C}-\text{COOH} \\ \\ \text{C} \end{array}$	0.28	1.06	EtMM	$\begin{array}{c} \text{Br} \\ \\ \text{C}-\text{C}-\text{COOEt} \\ \\ \text{C} \end{array}$	0.25
ME	$\begin{array}{c} \text{Br} \\ \\ \text{C}-\text{C}-\text{COOH} \\ \\ \text{C}_2 \end{array}$	0.26	1.03			
EE	$\begin{array}{c} \text{Br} \\ \\ \text{C}_2-\text{C}-\text{COOH} \\ \\ \text{C}_2 \end{array}$	0.22	1.08	EtEE	$\begin{array}{c} \text{Br} \\ \\ \text{C}_2-\text{C}-\text{COOEt} \\ \\ \text{C}_2 \end{array}$	0.21
BE	$\begin{array}{c} \text{Br} \\ \\ \text{C}_4-\text{C}-\text{COOH} \\ \\ \text{C}_2 \end{array}$	0.15	0.80	EtBE	$\begin{array}{c} \text{Br} \\ \\ \text{C}_4-\text{C}-\text{COOEt} \\ \\ \text{C}_2 \end{array}$	0.14

TABLE III Polarographic data for the esters of the 2-bromo acids
(Temp 0°C, mercury height 50 cm)

Ester	pH	Ester conc	$-E_{1/2}$	<i>I</i>
			mM	
EtMH	1 07	0 108	0 348	1 82
	1 41	0 169	0 353	1 85
	8 60	0 169	0 368	1 70
EtEH	1 07	0.112	0 336	1 83
	1 41	0.156	0 335	1 63
	8 60	0.156	0 340	1 85
EtMM	1 41	0 546	0 243	1 34
	9 00	0 109	0 268	1 46*
	9 00	0 109	0 269	1 39*
	9 00	0 109	0.268	1 43*
EtEE	1 41	0 509	0.212	1 48
	1 41	0 102	0 205	2 05†
EtBE	1 41	0 116	0 143	1 48

* Maxima present even at this low concentration. Distortion of wave makes these data less accurate

† The current values here are inexplicably high

OBSERVED BEHAVIOR

All the acids exhibited a sigmoidal variation of $E_{1/2}$ with pH, the curve having flat portions in the acid region below pH 2 and in the alkaline region above pH 8; values of $E_{1/2}$ in these invariant regions are given in Table II and are plotted in Fig. 1 against the number of carbon atoms. Complete data for the acids are available from the authors and are summarized in Table I. Fig. 1 includes a similar plot for the straight chain 2-bromoalkanoic acids (1). Since the latter data were obtained under somewhat different experimental conditions (temperature difference and alcohol absence), the curve is displaced along the ordinate. However, the similarity in the trends of those acids covered by both sets of data (HH, HM, and EH) is such that a qualitative extrapolation may be made for purposes of comparison. This plot and its interpretation constitute the basis of much of the subsequent discussion.

In the acid region, the acids exhibit a continuous decrease in (negative) $E_{1/2}$ with chain length, i.e., they become more easily reducible. However, the difference in $E_{1/2}$ between MH and EH is very much less than that between other neighboring pairs of acids. There is a sharp break between straight chain acids and their branched chain isomers, the latter being more easily reducible. Following this break, the trend is almost the same for both series.

In the alkaline region, the situation is more complicated. In general, $E_{1/2}$ again decreases continuously with increasing molecular weight in both series of acids. The pattern of the decrease is not,

however, perfectly consistent. EH, ME, and EE seem out of line, the latter, in particular, actually has an $E_{1/2}$ value larger than both its neighbors. This is responsible for a crossover in the curves for branched and straight-chain acids (even when allowance is made for the effect of differing experimental conditions used in assembling data for each curve). This crossover is not expected to be reversed, since the complexity of these curves has a straightforward explanation, which is subsequently discussed; in this regard, it should be noted that the onset of the complexity occurs at the point in the series at which there is an ethyl substituent in the α position.

Temperature coefficients of i_d and current ratios upon variation of the drop-time (mercury head) agree closely with theoretical values consequent to diffusion-controlled current-producing processes. Values of α [the empirical constant in the equation for $E_{1/2}$ (12)] vary from 0.6 or 0.7 in the acidic region to 0.3 or 0.4 in the alkaline region. Diffusion current constants, I , are lower in the alkaline region than in the acidic region, passing through a minimum in the intermediate region.

The $E_{1/2}$ values for the esters (Table III) are invariant with pH. Such slight variations as do occur can be attributed to the specific effect of the buffer systems used. Variation of ester $E_{1/2}$ with number of carbon atoms in the parent acid is shown in Fig. 1. The ester $E_{1/2}$ is in each case very close to $E_{1/2}$ of the corresponding acid in the acidic region, being slightly less negative. These results agree with previous observation (4, 5). The activating influence of the carbonyl group on the carbon-halogen bond fission is emphasized by the fact that the β -bromoalkanoic acids and esters do not show reduction within the observable potential range. It is interesting that the slight difference between EtMH and EtEH appears to reflect the situation for the corresponding acids.

DISCUSSION

Variations of $E_{1/2}$ with pH and with chain length indicate that at least three effects are operative, i.e., data obtained can be explained only by the action of all three and, in that sense, are evidence for them. These effects are: (a) short range, electrostatic effects, (b) steric effects involving those molecules which have an α ethyl or larger substituent; and (c) bulk effects (adsorption, orientation). In addition, there exists the important question of mechanism.

Dependency of $E_{1/2}$ on pH

Although a detailed analysis of the sigmoid relation between $E_{1/2}$ and pH cannot now be presented,

certain aspects of the phenomena involved will be discussed.

The appearance of only one diffusion-controlled polarographic wave in the fission of the carbon-halogen bond in α -halo acids and esters indicates that the kinetic process of acid-anion equilibration is not directly rate-controlling. Consequently, one or another of the following processes probably prevails. (A) Only one of the equilibrium forms is reducible over the potential span used; its $E_{1/2}$ is pH -dependent. (B) Both forms are reducible, and the form reducible at the less negative potential is reduced preferentially over the whole pH range, its $E_{1/2}$ is pH -dependent. (C) Both forms are reducible and one or both of the forms have $E_{1/2}$ pH -dependent, the separate curves of $E_{1/2}$ vs. pH cross, i.e., one form is preferentially reduced over one end of the pH range, and the other form over the other end. (D) Both forms are reducible with pH -independent $E_{1/2}$; the rising portion of the curve is due to some as yet undetermined feature of the electrode process kinetics.

It is highly probable that the more readily reducible form is the undissociated acid. Brdicka and Wiesner (9) made this assumption in the case of pyruvic acid; their mathematical treatment produced calculated results in good agreement with the data. Secondly, the ethyl esters of the haloacids, which are more closely related to the undissociated acid form than to the anion of the parent acid, have pH -invariant $E_{1/2}$ values very close to those of the acids in the acid region [Fig 1, Table III (4, 5)]. It is important in this connection to emphasize that the data on the esters indicate the fundamental phenomenon of carbon-halogen bond fission to be itself pH -independent; thus, the pH -dependence of $E_{1/2}$ for the acids must be ascribed to other phenomena.

Electrostatic Effects

Without entering into mechanism at this point, it appears that the initial decrease in $E_{1/2}$ in going from HH to MH and the sharp drop in going to MM (and similarly with the esters) are best explained by the electron drift from the alkyl substituents, i.e., by a permanent polarization effect. Such an hypothesis requires a tapering off of this effect after one or two carbon atoms (13); this expectation is contradicted by the data. Consequently, other effects must enter into the situation when the α alkyl substituent is ethyl or larger.

Using the data reported in this paper for the α -bromoalkanoic acids (with the exception of BE) at pH 1.1, Taft (14) has been able to correlate $E_{1/2}$ values with polar substituent σ -values similar to those developed by Hammett (15). The calculated

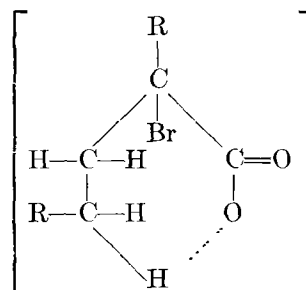
ρ -value for this correlation is 0.397 ± 0.012 . However, BE does not fit this correlation. Furthermore, the straight chain acids (1) do not correlate at all beyond the first three members, the deviations of the higher members being of such a trend as to indicate that $E_{1/2}$ is becoming positive at too great a rate as the chain length increases. This and other attempts at similar correlation indicate that, if Taft's parameters are indeed reflections of the polar character of the substituents, a polar effect cannot be used to explain the continuing trend of $E_{1/2}$ as the substituent size increases above that of ethyl.

Branching has a very pronounced effect on $E_{1/2}$ (Fig. 1). In the acidic region, the difference in reducibility between corresponding isomers in the straight and branched series varies from 0.20 to 0.13 volt in going from the C_4 to C_8 isomers. The difference appears to converge gently, indicating that higher branched acids would be more difficult to reduce; this is in accord with steric effects discussed in the following section. In the alkaline region, the effect of branching is not so clearly delineated, although the effect is evidently present.

The pronounced effect of branching in the acidic region is explicable on the basis of permanent polarization. The combined effects of two alkyl substituents on the same carbon atom will be much greater than the effect of one substituent alone. There is ample evidence to support this in the known lability of tertiary carbon atoms as compared with the secondary or primary carbon atoms. Elving and Westover (16) found the polarographic behavior of the butyl bromides to be in accord with the effects observed here, although the differences were not so striking. They find $E_{1/2}$ values of -2.47 , -2.44 , and -2.35 volts for *n*-butylbromide, *iso*-butylbromide, and *sec*-butylbromide, respectively.

Steric Effects

It is proposed that the complexity of behavior encountered in the alkaline region has its source in the tendency toward stable ring formation found in compounds having chains of at least six members with terminal atoms differing in electronegativity. In each of the acids having α substituents at least as large as ethyl, there is a possibility of forming at least one ring of the form:



Such rings, if closed by a loose, nonbonding interaction, would possess an augmented steric resistance to reaction, thus, the carbon-bromine bond would gain an increased stability toward fission.

The trend of data supports this hypothesis. It is very obvious (Fig. 1) that EH, for example, possesses an augmented stability. Further, if one compares the $E_{1/2}$ values for MH and PH, it is seen that the difference is much less than that between PH and BH. Thus, the extra stability of EH must also be possessed by larger acids, or else all points after EH should have a more positive $E_{1/2}$ value. It can therefore be concluded from the data that all acids having ethyl substituents or larger have their $E_{1/2}$ shifted to larger negative values.

The concept of *6-number*, devised by Newman (17) in elucidating rules for predicting the rates of certain acid-catalyzed esterifications, fits in well with this behavior. The *6-number* is the number of atoms in the six-position on the acid chain if counting is begun at the carbonyl oxygen. Newman's prediction, that the larger the *6-number*, the larger the steric hindrance to reaction, is borne out by present data. In the straight chain series, the largest *6-number* possible is 3, and the lowest molecular weight acid to possess it is EH. Consequently, it should be expected that EH, PH, BH, and higher acids would be relatively more stable than HH and MH; this is precisely the conclusion reached in the preceding paragraph. In the branched series, the *6-number* values are: MM, 0; ME, 3; EE and BE, 6. Actually, ME is only slightly less stable than MM (Fig. 1), while EE, for which the *6-number* doubles, has a greater (negative) $E_{1/2}$.

Smith (18, 19), Berliner (20, 21), Dippy (22), and Evans (23, 24) have described similar behavior. Dippy's work is of particular interest because of the close association of the compounds studied with those of the present work; he presents ionization constant values for saturated straight chain aliphatic acids out to octanoic, and for certain of their branched chain isomers. There is a consistent decrease in K_i among the straight chain acids except for the striking anomaly of *n*-butanoic acid, whose K_i is greatly in excess of the values for its neighbors in the series. The *n*-butanoic and the succeeding acids lie on a curve which is shifted to higher values of K_i than expected, based on the first two acids of the series. In the branched series, diethylacetic and ethylmethylacetic show a similar shift. These are the parent acids of the very compounds found to show anomalies in the present work.

To explain these phenomena, the authors cited have suggested formation of a cyclic six-member structure whose angles conform more closely than any other ring structure to the normal tetrahedral

bond angle for carbon. Stabilization of this structure is supposed to be effected by a loose chemical connection which is discussed in terms of hydrogen bonding (Dippy), hyperconjugation (Berliner), and resonance (Evans). Hunter (25), in a review on hydrogen bonding, states that C—H—O bonds are very weak, and are probably manifested only under some directing influence; such bonds are very difficult to detect. Nevertheless, even such a weak influence might exert sufficient stabilization on the structure to produce the effects observed. Thus, in the data on the straight-chain acids (1), the increment of potential associated with the $E_{1/2}$ shift cited (EH) is, as a guess, about 0.1 volt, corresponding to an energy increment for a two-electron process of about 5 kcal/mole; this is of the commonly accepted magnitude for many hydrogen bonds. EE, as can be demonstrated with models, can so dispose itself that the two possibilities for C—H—O bonds can be simultaneously realized, thus accounting for its increased stability.

Thus far, only the alkaline region has been discussed. The reason that EE, for example, does not show as marked an interaction in the acidic region as in the alkaline region is that in the anion carboxylate group there are two oxygen atoms possessing a negative charge, this is not so for the acid carboxyl group, where only one uncharged oxygen is available for closure. In general, the deviation from Newman's rule of six in the acid region must be due to a near "saturation" of this one carboxyl oxygen.

A final proof of this interpretation of the shift of $E_{1/2}$ to more negative values would be the fulfillment of the prediction in the case of the C_8 acids, that di-*n*-*P* (α -bromodi-*n*-propylacetic acid; *6-number* = 6, where 4 of the *6-atoms* are hydrogens) would have an $E_{1/2}$ less than, but close to, that of BE (*6-number* = 6, where 5 of the *6-atoms* are hydrogens). Certainly the $E_{1/2}$ would be greater than that of 2-bromo-octanoic acid. Furthermore, di-*iso*-*P* (*6-number* = 12) should have a value of $E_{1/2}$ more negative than that of BE, with *iso*-*P*-*n*-*P* somewhere in between.

In concluding the discussion of steric effects, it must be noted that B-strain (26, 27) may contribute to the effect of branching on $E_{1/2}$, which has been discussed in a previous paragraph in terms of electrostatic effects.

Bulk Effects

It has been shown how electrostatic effects can cause an initial decline in $E_{1/2}$ with chain length, and how the ring formation effect shifts the whole $E_{1/2}$ vs. chain length relation to more negative values. To explain the further decline of $E_{1/2}$ when the chain length has reached a point beyond which

electrostatic factors can cause no significant variation, it is necessary to recognize other factors.

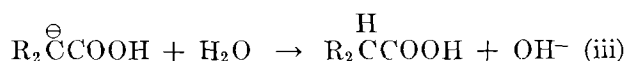
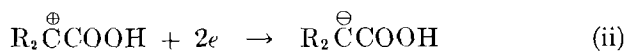
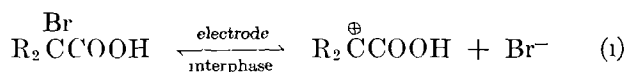
In discussing the straight chain acids, Rosenthal, Albright, and Elving (1) indicate that the apparent conflict with the concept of permanent polarization is due to the operation of such factors as ease of approach to, orientation to, and adsorption on the electrode surface. In particular, they consider that adsorption may be the principal factor in causing the steady decrease in $E_{1/2}$ with chain length. Adsorption on mercury of the normal primary alcohols from the vapor phase shows a regular increase in free energy as chain length increases (28). Further confirmation is found in the fact that the ease of adsorption of long chain acids, esters, and alcohols from hydrocarbon solution onto metals increases with chain length (29). If a similar situation exists in the case of adsorption of the acids on mercury from aqueous solution, and if the adsorption is fast enough so that it is not the rate-determining step, the electrode reaction could take place within the adsorbed film, and still reveal itself as diffusion-controlled. Thus, differences in the energy of adsorption would contribute to the potential, as well as differences in bond strength, in the acids; the factors may be related. It must be emphasized, in this connection, that data are consistent in indicating diffusion control

Mechanism

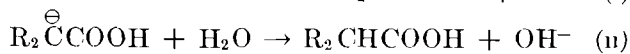
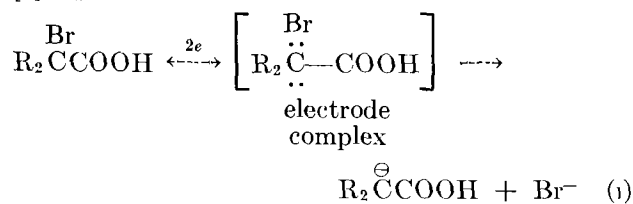
Elucidation of reaction mechanism in a polarographic process is extremely difficult. To be perfectly satisfactory, it must assign, unambiguously, a potential-determining step and a rate-controlling step to the proper chemical processes; these steps are generally masked by the current-limiting process, e.g., diffusion, as in the present case. The nature of the polarographic process makes rate studies impossible. It is often a matter of great difficulty even to determine the nature of the products with certitude. One can only assign steps according to various hypotheses and compare consequences with the data. The authors present the following discussion in full awareness of the limitations of this method; the basis for and value of such treatment has been discussed (8).

Three hypothetical reaction schemes can be described:

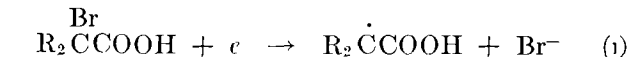
[1] S_N1 :



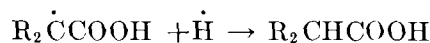
[2] S_N2 :



[3] Free radical:



or



There is actually little difference between the S_N1 and S_N2 mechanisms in this case, as the following considerations will show. In the description given of the S_N1 reaction, the electron-transfer step (ii) ought to be potential-determining, leaving aside for a moment the possibility of a contribution from adsorption energy. But if this were the case, it would be hard to justify, for example, the effect of branching; entry of reduction electrons would be made more difficult in the branched compound by the augmented electron drift to the carbon center. To restore agreement with the data, it seems necessary to assume that (i) is potential-controlling, which is unreasonable unless the electrons enter simultaneously. But such a situation is exactly the transition state described for the S_N2 mechanism. Thus, it is justifiable to speak of "the" ionic mechanism.

The ionic mechanism accommodates the data in the following respects. The slow step involves attack by electrons, so that it is potential-determining, moreover, there is simultaneous dissociation of the bromide entity, so that the carbon-bromine bond strength must be involved in the potential required for reaction. According to the electron-releasing properties of alkyl groups, bond strengths in the acids ought to decrease in the order $\text{HH} > \text{MH} > \text{EH} > \text{MM} > \text{ME}$, this is the order shown by the data, after allowance is made for the magnitude of the β -effect. For the longer range decrease of $E_{1/2}$ with chain length, it is necessary to include the concept of a contribution from adsorption energy, discussed in a previous paragraph. The β -effect itself is clarified by this mechanism with its pronounced susceptibility to steric influences.

The free radical hypothesis is even more satisfactory, and is considerably more popular (30, 31).

The isolation of dimer products (30, 32-35) is powerful evidence for this mechanism. The potential-determining step in this mechanism may be assigned to the introduction of the first electron, i.e., to step (i). This is reasonable because this step involves bond fission, and, as has been shown, the $E_{1/2}$ values reflect the influence of carbon-bromine bond strengths. Further confirmation can be found in the work of Gardner (36) who studied the reduction of benzophenone. Two diffusion-controlled waves appear in the acid region, each involving a one-electron reduction, the first wave is pH -dependent and the second is pH -independent, so that the waves merge as the pH increases. Gardner postulates a two-step free-radical mechanism for carbonyl group reduction, a radical being produced at the potential of the first wave and reduced at the potential of the second wave. This is completely analogous to the present case, except that the possibility for resonance stabilization in Gardner's postulated intermediate, diphenylhydroxymethyl, is of a much higher order than in the case of the dialkyl-carboxymethyl. Consequently, radical destruction in Gardner's case occurs in the acid region at a higher potential than radical formation. In the present case, step (ii α) occurs immediately after step (i), the radical having poor stability at potentials requisite for its formation; consequently, there is only one wave. To explain the continuing decline of $E_{1/2}$ at longer chain lengths, the same adsorption phenomenon must be postulated as for the ionic mechanism.

ACKNOWLEDGMENT

The authors wish to thank the Atomic Energy Commission, the Office of Naval Research, and the Research Corporation for grants-in-aid which supported the work described.

Any discussion of this paper will appear in a Discussion Section to be published in the December 1954 issue of the JOURNAL

REFERENCES

- 1 I ROSENTHAL, C H ALBRIGHT, AND P J ELVING, *This Journal*, **99**, 227 (1952)
- 2 P J ELVING, I ROSENTHAL, AND M K KRAMER, *J Am Chem Soc*, **73**, 1717 (1951)
- 3 I ROSENTHAL AND P J ELVING, *ibid*, **73**, 1880 (1951).
- 4 P J ELVING AND C-S TANG, *ibid*, **74**, 6109 (1952)
- 5 I ROSENTHAL, C-S TANG, AND P J ELVING, *ibid*, **74**, 6112 (1952)
- 6 P J ELVING, J C KOMYATHY, R E VAN ATTA, C-S TANG, AND I ROSENTHAL, *Anal Chem*, **23**, 1218 (1951)
- 7 E GERGELY AND T. IREDALE, *J Chem Soc*, **1951**, 3502
- 8 P J ELVING, *Record Chem Progr*, **14**, 99 (1953)
- 9 R BRDICKA AND K WIESNER, *Collection Czechoslov Chem. Communs*, **12**, 138 (1947)
- 10 J. LOUTECKY AND R BRDICKA, *ibid*, **12**, 337 (1947)
- 11 E SAITO, *Bull soc chim France*, **1951**, 957
- 12 I M KOLTHOFF AND J J LINGANE, "Polarography," 2nd ed., Vol. I, Interscience Publishers, New York (1952).
- 13 E R ALEXANDER, "Principles of Ionic Organic Reactions," John Wiley & Sons, Inc., New York (1950)
- 14 R W TAFT, JR, *J Am Chem Soc*, **75**, 4231 (1953)
- 15 L P HAMMETT, "Physical Organic Chemistry," McGraw-Hill Book Co., New York (1940)
- 16 P J ELVING AND L C WESTOVER, unpublished work
- 17 M S NEWMAN, *J Am Chem Soc*, **72**, 4783 (1950).
- 18 H J SMITH, *ibid*, **61**, 254 (1939)
- 19 H J SMITH AND J P MCREYNOLDS, *ibid*, **61**, 1963 (1939)
- 20 E BERLINER AND F BERLINER, *ibid*, **71**, 1195 (1949)
- 21 E BERLINER AND F BERLINER, *ibid*, **72**, 222 (1950)
- 22 J DIPPY, *Chem Revs*, **25**, 189 (1939)
- 23 D EVANS, *J Chem Soc*, **1936**, 785
- 24 D EVANS AND J GORDON, *ibid*, **1938**, 1434
- 25 L HUNTER, *Ann Repts. on Progress Chem. (Chem Soc London)*, **43**, 141 (1946)
- 26 H C BROWN, H BARTHOLOMAY, AND M D TAYLOR, *J Am Chem Soc*, **66**, 435 (1944)
- 27 H C BROWN AND R S FLETCHER, *ibid*, **71**, 1845 (1949)
- 28 C KEMBALL, *Proc Roy Soc London*, **A190**, 117 (1947)
- 29 S G DANIEL, *Trans Faraday Soc*, **47**, 1345 (1951)
- 30 C L WILSON, *Record Chem Progr*, **10**, 25 (1949)
- 31 W A WATERS, "The Chemistry of Free Radicals," Oxford University Press, New York (1946)
- 32 C J HAGGERTY, *Trans Am Electrochem Soc*, **56**, 421 (1929)
- 33 G W WHELAND, "Advanced Organic Chemistry," 2nd ed., John Wiley & Sons, Inc., New York (1949)
- 34 P J ELVING AND C E BENNETT, unpublished work
- 35 P J ELVING AND J T LEONE, unpublished work
- 36 H J GARDNER, *Chemistry & Industry*, **1951**, 819

Cation Exchange Process for the Preparation of Potassium Cyanide¹

C. H. LEMKE

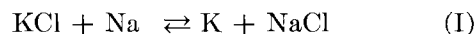
Research Division, Electrochemicals Department, E. I. du Pont de Nemours & Co., Inc., Niagara Falls, New York

ABSTRACT

Equilibrium data are presented for the reactions of Na + KCN, KCl + NaCN, and KOH + NaCN in the fused state. The latter two reactions were effected by a new "alloy bridge" technique which does not require direct contact of reactant salts. In this manner, potassium cyanide was obtained substantially free of anions other than CN⁻. Reaction rate data are presented for reaction of KCl + NaCN by the "alloy bridge" method, and other possible applications of the method are suggested.

INTRODUCTION

Chemical equilibria between fused alkali metals and their salts have been extensively studied by Rinck (1) who established equilibria for the systems:



Reactions (I) and (II) have been used for production of sodium-potassium alloys and metallic potassium.

In such systems, fused metals form layers which float on top of fused salts. It is thus possible to have an alloy layer simultaneously in contact with two separate salt melts. For example, a vessel divided into two compartments by a vertical partition may be used as a reactor to produce KCN from KCl and NaCN. Fused KCl is charged to one compartment, and fused NaCN to the other. Fused sodium metal, which floats on the fused salts, is added until it rises to a level above the top of the partition to form a "bridge" between the two fused salts (Fig. 1). On the chloride side of the reactor, potassium metal is extracted from KCl and replaced by equivalent sodium. Potassium rapidly diffuses through the metallic layer to the cyanide side, where it displaces equivalent Na from NaCN to form KCN. This process of exchanging K and Na between the two salt fusions continues until chemical equilibrium is reached. The resulting melt of KCN—NaCN may in like manner be reacted with a fresh batch of KCl in a second stage of the process, and a further exchange of K and Na will occur with resultant increase in KCN content of the cyanide melt. Similarly, chloride melt from the first stage may be reacted with fresh NaCN to achieve a greater utilization of KCl.

This may be regarded as a double countercurrent

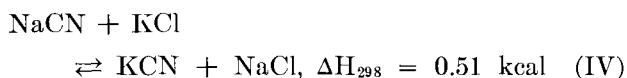
extraction in which the fused alloy replaces K with Na on the chloride side and simultaneously replaces Na with K on the cyanide side. Compositions of the alloy bridges in the several stages remain unchanged after the system has been brought to steady operation, and no metallic Na or K is consumed by the process except for mechanical losses. Composition of the cyanide melt and chloride melt at their respective discharge ends can be controlled by varying the number of stages or the ratio of KCl to NaCN fed to the apparatus.

It is evident that this technique is not limited to the application described, but could be used for exchange of alkali cations between hydroxides, bromides, iodides, chlorides, cyanides, or other suitable salts (2). Only salts which melt below the boiling points of the alkali metals and anions which are not readily reduced by alkali metals can be used.

DISCUSSION

Equilibrium Studies

Having Rinck's data for the equilibria represented by reactions (I) and (II) above, it was only necessary to determine the equilibrium in the fused state for reaction (III) to be able to calculate the equilibria for reactions (IV) and (V).



Assuming the law of mass action to hold, Rinck's values for the equilibrium constants for reactions (I) and (II) may be expressed as:

$$\frac{(\text{NaCl})(\text{K})}{(\text{KCl})(\text{Na})} = 0.087 \text{ at } 900^\circ\text{C} \quad (\text{VI})$$

¹ Manuscript received May 5, 1953. This paper was prepared for delivery before the New York Meeting, April 12 to 16, 1953.

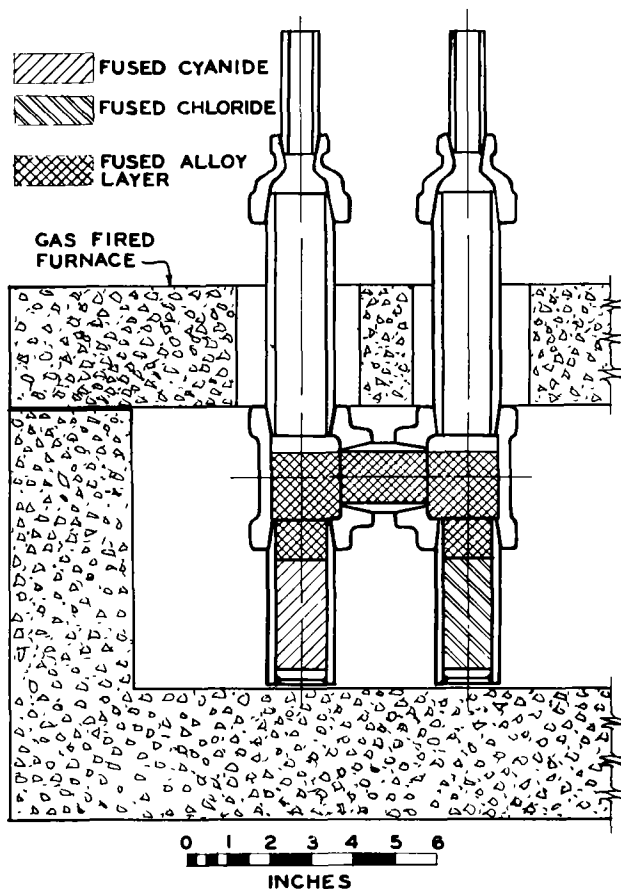


FIG 1 Apparatus

and

$$\frac{(\text{NaOH})(\text{K})}{(\text{KOH})(\text{Na})} = 2 \text{ at } 700^\circ\text{C} \quad (\text{VII})$$

where the quantities in parentheses represent mole percentages of the respective salts in the salt phase and respective metals in the metal phase.

Experimental value for the equilibrium constant for reaction (III) (Table I and Fig. 2) is:

$$\frac{(\text{Na})(\text{KCN})}{(\text{K})(\text{NaCN})} = 8.7^2 \text{ at ca. } 680^\circ\text{C.} \quad (\text{VIII})$$

This value was obtained statistically, and the 90% confidence interval for the average constant for reaction (III) is 6.0–11.7. From this result and the values given by Rinck, constants for reactions (IV) and (V) may be calculated as follows:

$$\frac{(\text{Na})}{(\text{K})} = 8.7 \frac{(\text{NaCN})}{(\text{KCN})} \quad (\text{IX})$$

$$\frac{(\text{Na})}{(\text{K})} = \frac{1}{0.087} \frac{(\text{NaCl})}{(\text{KCl})} \quad (\text{X})$$

² A logarithmic transformation of individually calculated values of the constant for reaction (III) gives an approximately normal distribution of "log C" values. The antilog of the average "log C" value then gives a measure of "C" which is least affected by extreme determinations.

Equating (IX) and (X):

$$\frac{(\text{NaCl})(\text{KCN})}{(\text{KCl})(\text{NaCN})} = 8.7 \times 0.087 = 0.76 \quad (\text{XI})$$

Thus, the calculated constant for reaction (IV) is approximately 0.76. A similar calculation gives a constant for reaction (V) of 17.4.

These calculated constants indicate that reactions (IV) and (V) are favorable for the production of KCN, using NaCN and either KCl or KOH, respectively, as raw materials.

The equilibrium constant for reaction (IV) was checked experimentally and found to be 14 as compared with the calculated value of 0.76. Equilibrium was approached in all cases from the NaCN + KCl side. Experimental data are presented in Table II. These data were analyzed statistically, and the 90% confidence interval for the true value of the equilibrium constant is 0.9–2.0.

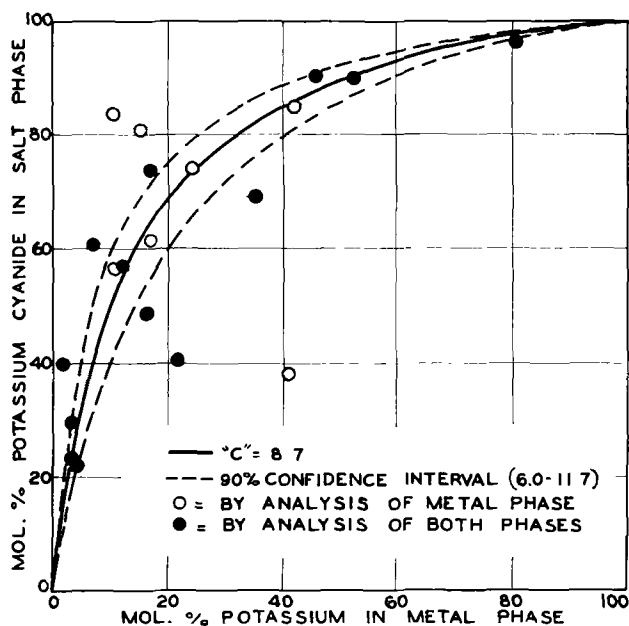
Fig. 3 shows a plot of experimental data and the spread covered by the 90% confidence interval.

The equilibrium constant for reaction (V) was checked at three points, starting in all cases from the NaCN + KOH side. Reactions of K and KOH

TABLE I Experimentally determined equilibrium for the reaction $\text{K} + \text{NaCN} \rightleftharpoons \text{KCN} + \text{Na}$

Mole % K in alloy	Mole % KCN in cyanide	°C	Calculated log C*
<i>Part 1: Points determined by analysis of alloy and stoichiometric calculation of cyanide composition</i>			
24.2	74.0	650–690	0.949
15.7	81.0	650	1.360
17.0	61.5	580–620	0.892
10.8	83.5	650–700	1.621
42.0	85.0	680–690	0.892
41.0	38.0	650–670	–0.046
10.8	56.2	520	1.025
<i>Part 2: Points determined by analysis of both phases</i>			
2.0	39.8	600	1.511
17.2	73.3	680	1.121
7.8	60.9	660–675	1.265
46.0	90.6	640–660	1.053
52.3	90.5	650–680	0.940
3.5	23.2	740–770	0.919
12.5	57.0	760–780	0.969
3.6	29.4	780–820	1.045
16.4	48.5	730–820	0.681
35.1	69.5	740–760	0.623
4.4	21.9	620–640	0.785
21.8	40.2	550–650	0.380
80.2	96.3	620–660	0.806
Average C*			0.940
			8.7

$$* C = \frac{(\text{Na})(\text{KCN})}{(\text{K})(\text{NaCN})}$$

FIG 2 Equilibrium data, $K + NaCN \rightleftharpoons KCN + Na$

such as $2K + KOH \rightleftharpoons K_2O + KH$ are known to occur, but such side reactions were neglected in this study. The experimental value of the constant, 7.5, compares with the calculated value of 17.4. Experimental data are given in Table III and are plotted on Fig. 4, which also shows reaction curves corresponding to the equilibrium constants 7.5 and 17.4. It has been estimated that the difference in the two curves corresponds to about one stage in a countercurrent process for KCN from KOH and NaCN.

Effect of Temperature on Equilibria

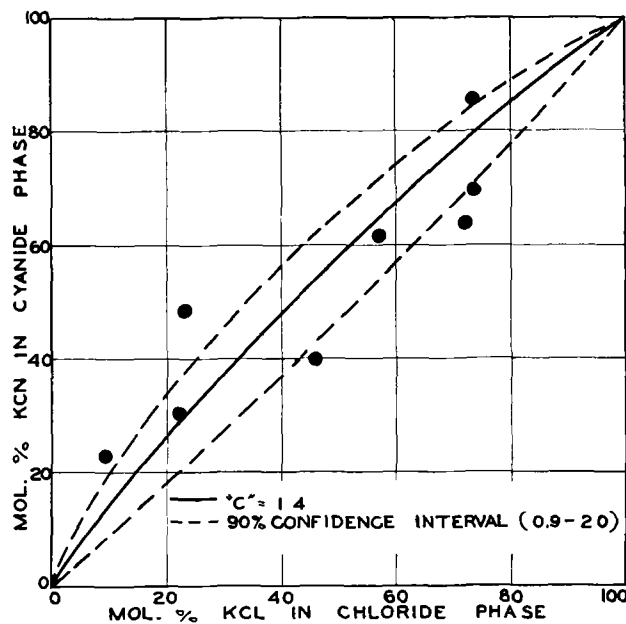
Heats of reaction for (IV) and (V) are small. From the van't Hoff equation (3) it may be ex-

TABLE II Experimentally determined equilibrium for the reaction $KCl + NaCN \rightleftharpoons KCN + NaCl$

Mole % KCN in cyanides	Mole % KCl in chlorides	°C	Calculated log C†
39.8	46.4	800	-0.097
23.2	9.8	740-770	0.447
29.4	22.5	780-820	0.146
48.5	23.6	730-740	0.477
69.5	74.4	750-770	-0.097
61.6	57.2*	710-760	0.079
63.6	72.3*	740	-0.155
85.5	73.5	680-720	0.322
Average			0.140
C			1.4

* 3-5% cyanide was found in the chloride melts from these runs, all others were cyanide free

$$\dagger C = \frac{(NaCl)(KCN)}{(KCl)(NaCN)}$$

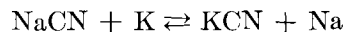
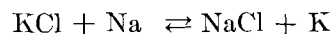
FIG 3 Equilibrium data, $KCl + NaCN \rightleftharpoons KCN + NaCl$

pected that the effect of temperature on the equilibrium constant will be small, and no attempt was made to determine this effect. Equilibrium studies were all made at temperatures which would be required for operation of a commercial process.

Reaction Rate

A limited amount of work was done to obtain order-of-magnitude rate data for the reaction: $KCl + NaCN \rightleftharpoons KCN + NaCl$ when carried out by the alloy bridge method.

The mechanism of this reaction is complex. Two reactions are involved:



These are linked to each other by the layer of fused K—Na alloy in contact on one end with the fused KCl—NaCl melt, and on the other end with the

TABLE III. Experimentally determined equilibrium for the reaction $KOH + NaCN \rightleftharpoons KCN + NaOH$

Mole % KCN in cyanides	Mole % KOH in hydroxides	°C	Calculated log C*
61.5	9.7	580-620	1.173
21.9	5.0	620-660	0.724
96.3	83.0	620-660	0.724
Average			0.874
C			7.5

$$* C = \frac{(NaOH)(KCN)}{(KOH)(NaCN)}$$

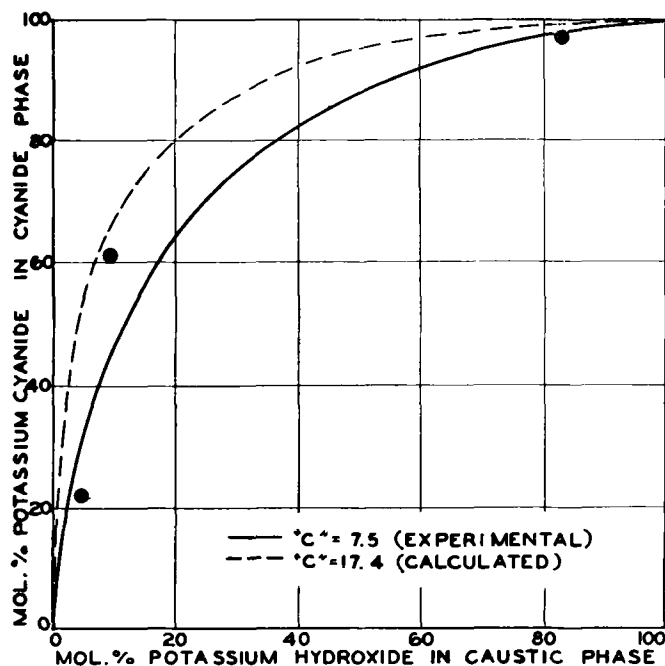


FIG 4 Equilibrium data, $\text{KOH} + \text{NaCN} \rightleftharpoons \text{KCN} + \text{NaOH}$

fused KCN—NaCN melt. The rate of reaction may be limited for any given set of conditions by rate of either of the above reactions or rate of transport of K and Na to opposite ends of the bridge.

No effort has been made to measure these quantities independently. It was not practical in the laboratory to operate a continuous countercurrent system. Therefore, all measurements were made on a batch basis. Based on earlier studies involving the above reactions, it was probable that the rate of reaction would not be the limiting factor. This supposition is substantiated by data which show that the over-all reaction does not slow down as equilibrium is approached.

Results of the rate experiments are summarized in Table IV and plotted in Fig. 5. Rates of the order of 0.2 kg KCN/hr/dm² (4 lb/hr/ft²) were obtained, based on total contact area.

TABLE IV Results of the rate experiments for the reaction $\text{KCl} + \text{NaCN} \rightleftharpoons \text{KCN} + \text{NaCl}$

	Both salt chambers of 3.25 cm ID	KCl chamber 7.62 cm ID, NaCN chamber 3.25 cm ID
Kg KCN made/hr/dm ² , based on		
Cyanide—alloy contact area	0.23	0.88
Chloride—alloy contact area	0.23	0.16
Combined contact area	0.11	0.14
Average temperature, °C	725	730

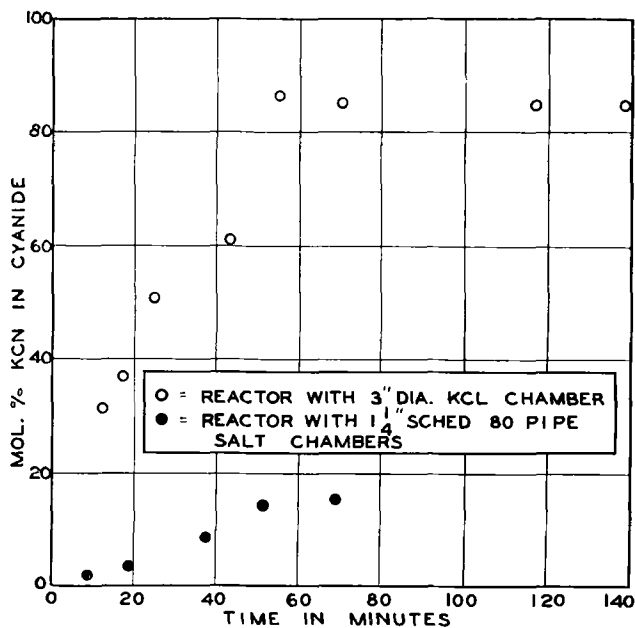


FIG 5. Reaction rate data; $\text{KCl} + \text{NaCN} \rightleftharpoons \text{KCN} + \text{NaCl}$.

EXPERIMENTAL

Apparatus

Steel pipes 1.9 cm ID and 25 cm long were used to study the reaction $\text{K} + \text{NaCN} \rightleftharpoons \text{KCN} + \text{Na}$. These pipes were closed by welding a plate in the bottom, and a rapid stream of purified nitrogen was fed to the open upper end to prevent oxidation. The pipes were heated by immersion to a depth of about 15 cm in a fused NaCl—CaCl₂ bath.

The apparatus used for the bridge reaction studies was an H-tube as shown in Fig. 1. This was made of steel pipe approximately 3.25 cm ID (A.S.A. Standards B-36, 10-1939 1 1/4 in schedule 80 steel pipe) connected with pipe fittings. Bottom ends of the legs were closed with steel plate welded in place. Top ends were threaded and fitted with connections for purified nitrogen, thermocouple wells, and openings for removal of samples.

A special apparatus was constructed for part of the rate study. This was essentially an H-tube as shown in Fig. 1, except that one leg was made of 7.62-cm (3-in.) ID tubing. The H-tubes were heated in a gas-fired furnace controllable to $\pm 50^\circ\text{C}$.

Procedure

Weighed quantities of the dry salts, KCl, KOH, NaCN, etc., as desired, were charged to the salt compartments and melted. The apparatus was blanketed with nitrogen, and weighed amounts of sodium and/or potassium were charged to the reactor.

Obtaining clean, representative samples presented many difficulties. Ultimately, samples of the fused

salts and alloys were taken by steel pipettes at temperatures of 650°–800°C. Salt samples were cast on a slab of cold iron, and alloy samples were quenched in cold white mineral oil. In nearly all cases there were small globules of alkali metal present in the salt samples. So far as possible, these were removed by hand sorting. Oil quenching of alloy samples did not entirely prevent oxidation. Under such circumstances it is known that potassium is selectively oxidized.

Potassium was determined by the perchlorate method. Potassium content of alloy samples was checked by freezing point determination (4). Sodium components were calculated by difference. Results

were not corrected for the small amounts of iron which were determined in some samples.

Any discussion of this paper will appear in a Discussion Section to be published in the December 1954 issue of the *JOURNAL*.

REFERENCES

1. E. RINCK, *Ann chim (Paris)*, **18**, 395 (1932)
2. C. H. LEMKE (to E. I. du Pont de Nemours & Co., Inc.) U. S. Pat. 2,533,593, December 12, 1950
3. S. GLASSTONE, "Textbook of Physical Chemistry," 2nd ed., p. 828, D. Van Nostrand Co., Inc., New York (1946)
4. G. VAN BLEISWIJK, *Z. anorg. u. allgem. Chem.*, **74**, 152 (1912)



Semiconductors as Solid Electrolytes in Electrochemical Systems¹

KURT LEHOVEC² AND JACOB BRODER

Signal Corps Engineering Laboratories, Fort Monmouth, New Jersey

INTRODUCTION

There are many applications of batteries where weight and space are of concern. Considerable progress in the miniaturization of batteries would be achieved if the liquid electrolyte, conventionally used in present batteries, could be replaced by a solid ionic conductor.

At the end of 1951, the authors started the development of "solid state batteries," which was directed toward two types of batteries: (a) a high current density "single-shot" battery; (b) a low current density long-life battery for use in connection with the transistor device. This note describes the initial phase of the program until the summer of 1952, when one of the authors (K. L.) left this laboratory.

THEORY

Consider a compound, AB , sandwiched between two phases A and B , to which electrodes are applied. If at least one of the phases A or B can migrate through the reaction product, AB , the reaction $A + B = AB$ can proceed. Under favorable conditions, to be discussed later, the free energy of the reaction gives rise to an emf between the phases A and B . Such a system is the prototype of a solid state battery.

In ionic compounds AB , the migration of A or B takes place in the form of ions. Usually only one of the components is mobile, say A^+ . If the ions A^+ were the only charges to move from A to B , then phase B would acquire a positive charge and the reaction would stop soon because of repulsion of further ions A^+ , approaching B . However, a continuous reaction is possible if migration of ions A to B is accompanied by a transfer of electrons from A to B . Transfer of electrons from A to B can occur in a twofold manner: (a) externally through a metal connection between A and B (external load), or (b) internally by means of partial electronic conduction³

of AB . In the absence of an external connection, the partial electronic conduction of AB , even if very small as compared to the ionic conduction, becomes rate-determining for the progress of reaction AB and determines, therefore, the life of the battery under open circuit condition (shelf life). It is well to emphasize that the partial electronic conductivity of ionic compounds is not a constant of the material, but depends on impurities and on deviations from stoichiometry. There is no basic difference between the progress of the reaction in a solid state battery under open circuit conditions and tarnishing reactions. The importance of the electronic partial conductivity for tarnishing reactions (1) and the role of minute amounts of impurities (2) are well known.

For compound AB to be a suitable electrolyte for a solid state battery, the following requirements have to be fulfilled:

[1] Large free energy decrease, $-\Delta F$, of the reaction $A + B = AB$.

[2] Electronic transference number negligible: $\sigma_e \ll \sigma_i$.

[3] Ionic conductivity σ_i of high absolute value.

[4] Electronic conductivity σ_e of low absolute value. Conditions [1] and [2] are necessary for a high emf, since the emf at zero load is (1): $(\Delta F/e) \cdot \sigma_i / (\sigma_i + \sigma_e)$.⁴ Condition [3] is necessary for a high short circuit current; condition [4] is necessary for a long shelf life.

Conditions for a good solid electrolyte have been formulated above in terms of its bulk properties only. There are further conditions which deal with ease of transfer of ions and electrons over the inter-phase boundaries A/AB and AB/B (3). Ions A^+ must be able to cross these boundaries easily in order to avoid polarization phenomena, when drawing current from the battery, i.e., the concentration of A^+ in AB at the boundaries A/AB and AB/B should not be modified by the current flow. On the

¹ Manuscript received August 27, 1952.

² Present address Sprague Electric Company, North Adams, Massachusetts.

³ Both the movement of electrons in the "empty energy

band" and the movement of holes in the "filled energy band" may contribute to the electronic conduction

⁴ In the case that σ_i and σ_e are space dependent, average values are to be used

other hand, harmful internal electron conduction can be decreased by presence of barrier layer effects at the electrode interfaces (4, 5).

HIGH CURRENT DENSITY "SINGLE-SHOT" BATTERY

For a solid state battery capable of delivering a high current density, a compound of high ionic conductance has to be used as electrolyte. Ionic conductivity of the order of $1 \text{ ohm}^{-1}\text{cm}^{-1}$ is found in the high temperature modifications of AgI, Ag_2S , and of Ag_2HgI_4 , among others. Their ionic conductivity compares favorably with that of strong liquid electrolytes. High ionic conductivity results from the peculiar lattice structure of these compounds: only the anion is bound to fixed lattice positions whereas the cations are distributed at random over a number of equivalent lattice positions, exceeding the number of cations available (6-8).

The authors experimented with systems involving the high temperature modification of AgI and Ag_2S . Tubandt and Lorenz (9) measured the conductivity of AgI both above and below the transition point (145°C) and found $1.31 \text{ ohm}^{-1}\text{cm}^{-1}$ above 145°C , and $3.4 \times 10^{-1} \text{ ohm}^{-1}\text{cm}^{-1}$ just below 145°C . Conductivity is almost completely ionic. The emf of the combination Ag, AgI, I_2 has been reported as 0.7 volt (10). However, because of immediate difficulties associated with operation of an I_2 electrode at or above 145°C (the transition point above which AgI has a high ionic conductivity) this work was directed to an examination of the reaction $2\text{Ag} + \text{S} = \text{Ag}_2\text{S}$. The reaction product, Ag_2S , is a relatively good conductor above 179°C , but at this temperature a large portion of the conductivity is electronic. Thus, although the free energy change corresponds to an emf of 0.2 volt, Wagner (11) found that an Ag- Ag_2S -S cell above 179°C gave an emf of only 2-10 millivolts. In order to obtain the full 0.2 volt corresponding to the ΔF of formation of Ag_2S , it is necessary to suppress the electronic conduction. This is possible by inserting a layer of AgI (10), which is nearly a purely ionic conductor above 145°C .

A cell of composition Ag, AgI, Ag_2S , S was constructed as follows: an AgI-film of about 25 microns thickness was prepared on an Ag-sheet by tarnishing in iodine vapor. The sulfur electrode consisted of a sulfur-carbon mixture of composition 15%S-85%C by weight compressed into a pellet at 7000 atmospheres. The Ag_2S -layer was formed upon contact of

the sulfur electrode with the AgI/Ag. The open circuit voltage of the cell at about 200°C was 0.2 volt, confirming Reinhold's value (10). Short circuit currents of 0.18 amp/cm^2 were obtained. Shelf life of the cell at operating temperature (200°C) was about 100 min.

Comparison of (a) the observed current density with ionic conductance of AgI (9) and of Ag_2S (12), and (b) of the shelf life of the cell with rate of tarnishing of AgI (13) suggests that there was considerable interface resistance present in these cells.

For a cell of high current density, which is useful at lower temperatures (and possibly at room temperature), other compounds, e.g., Ag_2HgI_4 and $\text{Ag}_x\text{Cu}_{1-x}\text{I}_4$, appear to be promising.⁵

LOW CURRENT DENSITY LONG LIFE CELLS

The authors have constructed cells of the composition Ag-AgI-I(+C) operating at room temperature with current densities of several hundred microamps/cm². The emf of this combination is 0.7 volt (10). Cells did not change during the period of this study.

ACKNOWLEDGMENT

The authors wish to express their gratitude to Dr. J. N. Mrgudich for his helpful discussion of and interest in this topic.

Any discussion of this paper will appear in a Discussion Section to be published in the December 1954 issue of the JOURNAL.

REFERENCES

1. C. WAGNER, *Z. physik. Chem.*, **B21**, 25 (1933).
2. K. HAUFFE, *Ann. Physik*, **18**, 201 (1950).
3. W. SCHOTTKY, *Wiss. Veroff. Siemens-werken*, **14**, 19 (1935), see for detailed treatment.
4. K. HAUFFE AND W. PFEIFFER, *Z. Elektrochem.*, **56**, 390 (1952).
5. H. J. ENGBELL AND K. HAUFFE, *Metall*, **6**, 285 (1952).
6. L. W. STROCK, *Z. physik. Chem.*, **B25**, 441 (1934).
7. J. A. A. KETELAER, *Z. physik. Chem.*, **B26**, 327 (1934).
8. J. A. A. KETELAER, *Trans. Faraday Soc.*, **34**, 875 (1938).
9. C. TUBANDT AND F. LORENZ, *Z. physik. Chem.*, **B7**, 513, 560 (1914).
10. H. REINHOLD, *Z. Elektrochem.*, **40**, 361 (1934).
11. C. WAGNER, *Z. physik. Chem.*, **B21**, 42 (1933).
12. H. REINHOLD AND K. SCHMITT, *Z. physik. Chem.*, **B44**, 75 (1939).
13. C. WAGNER, *Z. Elektrochem.*, **40**, 364 (1934), footnote 4.

⁵A paper on the preparation and properties of this compound will be published in the near future by Dr. L. Suchow of the Signal Corps Engineering Laboratory.

Kinetics of the Reaction of Hydrogen with Zirconium¹

JACK BELLE, B. B. CLELAND, AND M. W. MALLETT

Battelle Memorial Institute, Columbus, Ohio

ABSTRACT

The rate of reaction of hydrogen with high purity zirconium was determined for the temperature range of 250° to 425°C at 1 atm pressure. The reaction was found to follow a parabolic law, and the parabolic rate constant in (ml/cm²)² per second was calculated to be $k = 2.3 \times 10^5 e^{-17,200/RT}$ where 17,200 ± 200 cal/mole is the activation energy for the reaction.

INTRODUCTION

Kinetics of surface reactions of zirconium with nitrogen and oxygen have been discussed in previous papers from this laboratory (1, 2). The present paper concerns the kinetics of the zirconium-hydrogen reaction. Very little on this subject was found in the literature. Gulbransen and Andrew (3) investigated the reaction in the temperature range 235° to 300°C at pressures from 0.6 to 2.6 cm, using thin zirconium foil, 0.005 in. thick. Their conclusions can be summarized as follows: (a) a surface film is not formed as a product of the reaction; (b) the rate of the reaction deviates from a linear law; and (c) the rate of the reaction is directly proportional to the square root of the pressure.

The present study was made in the temperature range 250° to 425°C at a hydrogen pressure of 1 atm, using low-hafnium zirconium (0.01 weight % hafnium) in the form of solid cylinders.

EXPERIMENTAL

Method.—The method for measuring the rate of the reaction between zirconium and hydrogen was essentially that previously described for other zirconium-gas reactions (1, 2). A schematic diagram of the apparatus used is shown in Fig. 1. Vacuum-ground stopcocks greased with Apiezon N grease were used throughout except for the air inlets to the McLeod gauge and to the mechanical pumps. The system was evacuated by a 2-stage glass mercury-diffusion pump backed by a mechanical pump. The cold trap between the diffusion pump and the reaction system was cooled with liquid nitrogen. It was found necessary to place an additional trap, cooled with dry ice-acetone, adjacent to the reaction tube to remove contaminating grease and mercury vapors.

A modified White gas buret (4) was used to store the hydrogen and to measure the rate of con-

sumption of gas. The buret consisted of 10 bulbs, each of approximately 25 ml, and of a connected open-end full-length manometer, one arm of which was a graduated 25-ml buret. The entire assembly was maintained at constant temperature (±0.5°C) with running water.

The Vycor reaction tube was sealed to the system with Apiezon W wax, and its dead volume was decreased by a bundle of fused Vycor rods. The reaction tube was heated by a resistance-wound furnace which was controlled by a Brown Pyro-Vane controller with a V20 Variac in the input line. Temperature was controlled to ±5°C.

Prior to specimen preparation, machined zirconium cylinders about 2 cm long and 0.6 cm in diameter were degassed to about 1 to 2 ppm hydrogen by heating in vacuum at 900°C for 24 hr. Specimens were abraded with kerosene-soaked 240-, 400-, and 600-grit silicon carbide papers and washed in successive baths of naphtha, ether, and acetone. Care was taken to keep specimens under acetone until they were placed in the reaction tube.

The reaction tube was sealed to the system which, then, was evacuated to about 10⁻⁵ mm Hg as measured by the ion gauge. The specimen was annealed under vacuum for 1 hr at 800°C, after which the furnace was removed and its temperature adjusted to that of the rate run. The furnace was again placed around the reaction tube. The temperature was permitted to stabilize while hydrogen was being generated and stored.

With the specimen at the desired temperature, hydrogen was admitted from the buret and maintained at atmospheric pressure in the reaction tube by manual manipulations of the buret leveling bulb, except when the gas was expanded into the buret from storage bulbs. Short-time pressure fluctuations did not affect reaction rates. Readings, taken as the buret manometer arms were precisely leveled, were made as often as possible for rapid reaction rates and every 2 to 10 min for slower rates. The quantity of gas consumed by the specimen was the volume

¹ Manuscript received October 15, 1953. Work performed under AEC Contract W-7405-eng-92.

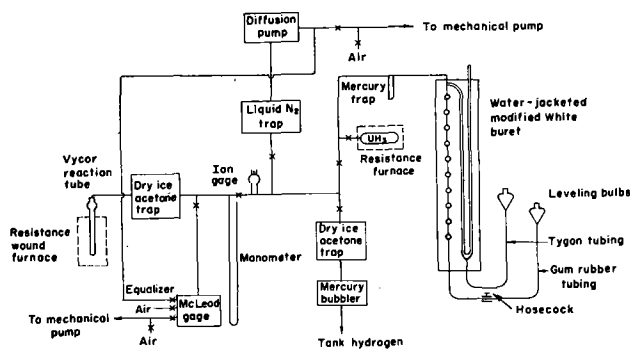


Fig. 1. Schematic diagram of modified hydrogen Sieverts apparatus.

added from the buret minus that remaining in the gas phase in the calibrated dead space. Geometric dimensions of specimens were used in calculating the quantity of hydrogen reacted per unit area.

Materials.—The pure zirconium used in these experiments was iodide crystal bar produced by the de Boer process, arc-melted, forged to $1\frac{1}{8}$ in.² at 1450°F, hot rolled at 1450°F, and cold drawn to $\frac{3}{8}$ -in. diameter rod. Test specimens were machined from this rod. Impurities in zirconium were determined by spectrographic, chemical, and vacuum-fusion analyses. Weight percentages of principal impurities detected were: silicon, 0.03; iron, 0.02; hafnium, 0.01; oxygen, 0.04; nitrogen, 0.002; and hydrogen, 0.003 (before degassing).

Pure hydrogen was obtained from the thermal decomposition of uranium hydride. The hydride was prepared by reacting tank hydrogen, dried in a dry ice-acetone cold trap, with degreased high purity uranium chips.

RESULTS AND DISCUSSION

Initial deviations are often observed for gas-metal reactions which follow the parabolic law, $w^2 = kt$. Gulbransen (5) has enumerated a number of complex factors which contribute to the breakdown of the law during early stages of the reaction. In addition to these phenomena, there may be interface effects. As was discussed by Jost (6) and Kubaschewski and Hopkins (7), these interface reactions may become rate-determining in initial stages of the reaction. The empirical equation which combines both reaction at an interface and diffusion through the film can be written in the form, $w^2 + \frac{k_p}{k_1} w = k_p t$. Here, k_1 represents the contribution of any linear interface reaction and k_p is the parabolic rate constant determined by diffusion through the growing film. If w is plotted as a function of t/w , the slope of the straight line is the parabolic rate constant, k_p . Such a plot is often more convenient to use than the quadratic plot, particularly for

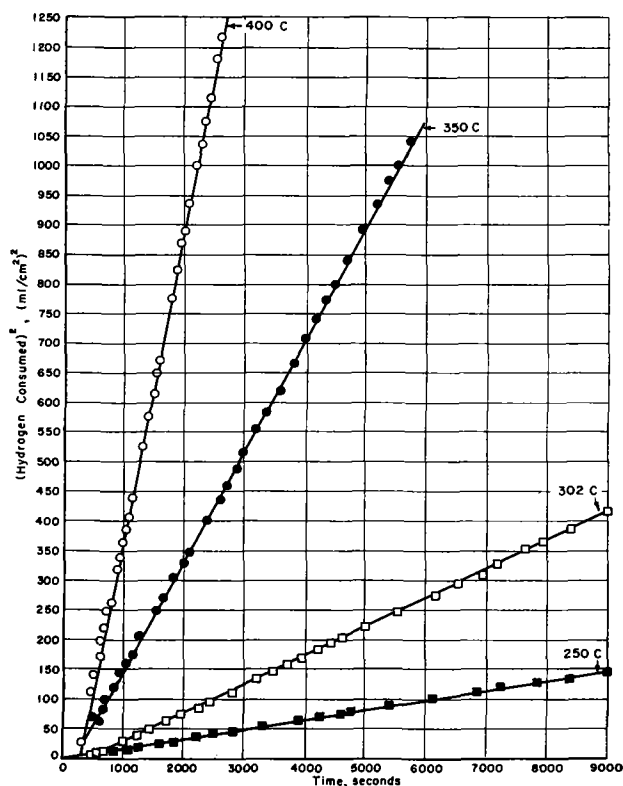


Fig. 2. Reaction of zirconium with hydrogen (ml H₂, STP, consumed per cm² metal surface)² vs. time.

those reactions where an induction period is present or initial stages of the reaction are uncertain.

The rate of the surface reaction of zirconium with hydrogen was measured in the range 250° to 425°C at 1 atm pressure. Results of several measurements are shown in Fig. 2 and 3. In Fig. 2, the square of the quantity (ml STP) of hydrogen consumed per unit surface area of the metal is plotted against time for four temperatures. Fig. 3 is a plot of w vs. t/w for two temperatures. It was found that, in all cases, the reaction conformed to the parabolic rate law with initial deviations in the direction of a slower initial rate. The duration of the induction period was usually less than five minutes and was independent of the annealing time, provided the system was evacuated to about 10^{-4} to 10^{-5} mm Hg.

In addition to the short induction period, there were also some deviations from the parabolic law after considerable hydrogen had been reacted. (The film thickness produced by the parabolic reaction ranged from 150μ at 300°C to 300μ at 425°C.) Deviations, which were always in the direction of a faster rate, did not occur below 300°C, and were not always present above that temperature. It is suspected that this breakdown of the parabolic nature of the reaction may be due to cracking of the film. It is not known why this effect was not reproducible.

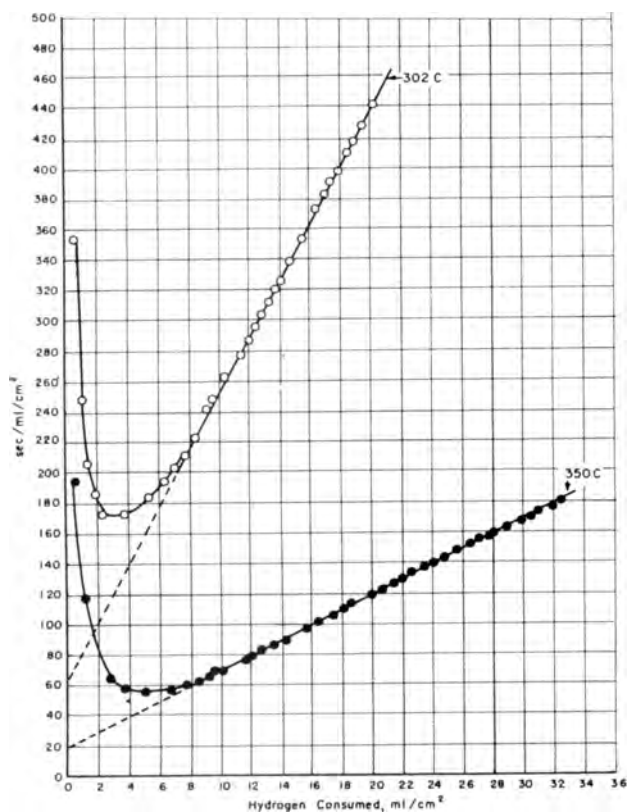


FIG. 3. Reaction of zirconium with hydrogen

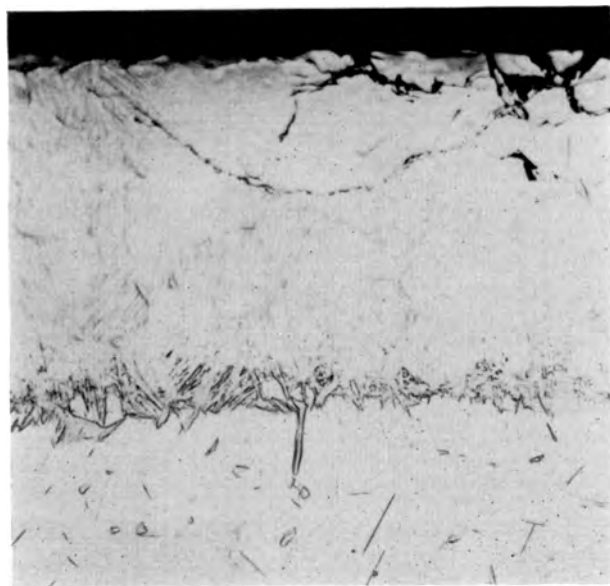


FIG. 4. Hydrogen reacted with iodide zirconium at 302°C for 2½ hr at 743 mm Hg absolute pressure. 250X

A reaction product was formed on the surface of all specimens, in contrast with the findings of Gulbransen and Andrew (3) who reported the absence of a surface film. Metallographic examination of the surface film indicated it to be an apparently single-phase layer, as can be seen from the photomicrograph shown in Fig. 4. On the other

TABLE I. Parabolic rate constants for the reaction of zirconium with hydrogen

Temp., C ± 5°	Rate constant, k_p , (ml/cm ²) ² /sec	Slope of log-log plot
249	0.015	0.47
250	0.017	0.50
276	0.032	0.47
277	0.035	0.49
302	0.056	0.56
304	0.074	0.52
323	0.11	0.50
323	0.12	0.53
323	0.11	0.50
350	0.20	0.57
351	0.19	0.57
353	0.22	0.49
373	0.33	0.57
378	0.38	0.49
397	0.61	0.61
400	0.70	0.64
421	0.88	0.47
424	0.88	0.57
424	1.05	0.58

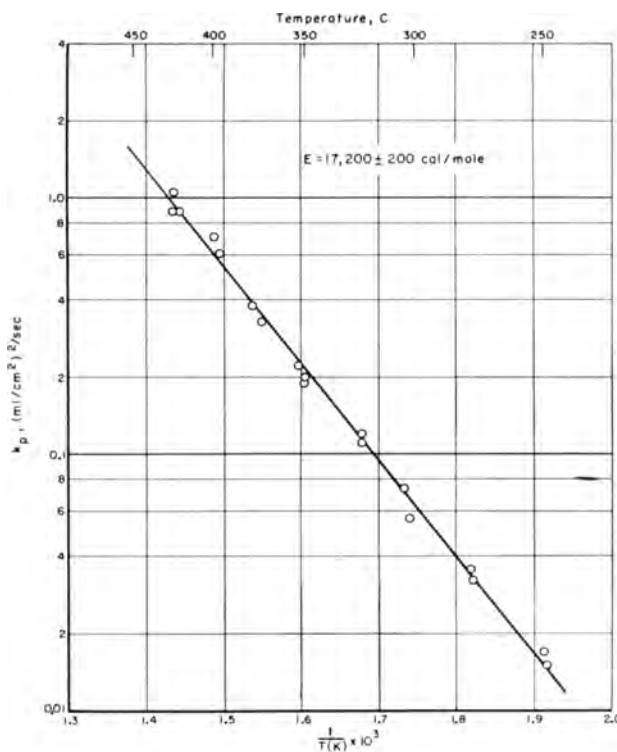


FIG. 5. Zirconium-hydrogen reaction, variation of reaction-rate constant with temperature.

hand, x-ray diffraction examination of the surfaces of several specimens revealed the presence of three phases: (a) an outer layer of tetragonal ZrH₂; (b) an intermediate layer of Hägg's (8) ZrH; and (c) an inner layer of a second tetragonal hydride phase. When the outer ZrH₂ was removed by light abrasion of the surface, the pattern of ZrH was obtained. Upon further abrasion, another hydride phase

appeared, adjacent to the metal. As discussed by Schwartz and Mallett (9), this latter hydride phase may be similar to the tetragonal phase of lowest hydrogen content reported for the hafnium-hydrogen system by Sidhu and McGuire (10). What effect these multiple hydride phases have on the kinetics of the zirconium-hydrogen reaction is not known.

If the parabolic law is obeyed, a plot of the logarithm of the amount of hydrogen consumed per unit surface area vs. the logarithm of time should give a straight line with a slope equal to 0.5. This was observed, as can be seen from Table I, where the parabolic rate constants, k_p 's, calculated from the w vs. t/w plots are also given.

Fig. 5 is a plot of $\log k_p$ vs. $1/T$. The equation of the best straight line through the points from 250° to 425°C was determined by the method of least squares. The experimental energy of activation and the frequency factor were calculated from the Arrhenius-type equation, $k = Ae^{-Q/RT}$. Energy of activation was calculated to be $17,200 \pm 200$ cal/

mole. The parabolic rate constant in $(\text{ml}/\text{cm}^2)^2/\text{sec}$ is $k = 2.3 \times 10^5 e^{-17,200/RT}$.

Any discussion of this paper will appear in a Discussion Section to be published in the December 1954 issue of the JOURNAL.

REFERENCES

1. M. W. MALLET, J. BELLE, AND B. B. CLELAND, *This Journal*, **101**, 1 (1954).
2. J. BELLE AND M. W. MALLET, To be published.
3. E. A. GULBRANSEN AND K. F. ANDREW, *J. Metals*, **185**, 515 (1949).
4. A. H. WHITE, *J. Am. Chem. Soc.*, **22**, 343 (1900).
5. E. A. GULBRANSEN AND K. F. ANDREW, *This Journal*, **98**, 241 (1951).
6. W. JOST, "Diffusion in Solids, Liquids, Gases," p. 353, Academic Press, New York (1952).
7. O. KUBASCHEWSKI AND B. E. HOPKINS, "Oxidation of Metals and Alloys," p. 41, Academic Press, New York (1953).
8. G. HÄGG, *Z. Phys. Chem.*, **B11**, 433 (1930).
9. C. M. SCHWARTZ AND M. W. MALLET, American Society for Metals Preprint No. 14 (1953).
10. S. S. SIDHU AND J. C. MCGUIRE, *J. Applied Phys.*, **23**, 1257 (1952).

Potentials of Iron, 18-8, and Titanium in Passivating Solutions¹

HERBERT H. UHLIG AND ARTHUR GEARY

Corrosion Laboratory, Department of Metallurgy, Massachusetts Institute of Technology, Cambridge, Massachusetts

ABSTRACT

Potentials of iron in chromates show a linear relation for $C/\Delta E$ vs. C , where C is concentration and ΔE is change of potential, suggesting that they follow the Langmuir adsorption isotherm. Maximum potential change corresponding to an adsorbed monolayer of chromate ions occurs at 0.0025 molar K_2CrO_4 , which approximates the minimum concentration for passivity reported by Robertson. The evidence agrees with a primary mechanism of passivity based on adsorption rather than on oxide film formation. For example, potentials of iron exposed to several organic inhibitors, where the mechanism is undoubtedly one of adsorption, also follow the adsorption isotherm as shown by Hackerman and coworkers. Passivity of 18-8 stainless steel and titanium in sulfuric acid containing cupric or ferric salts appears similarly to be accompanied by adsorption of Cu^{++} or Fe^{+++} . The irreversible nature of the potentials is in accord with the view that the adsorbate, in part, is chemisorbed.

Hydroxyl ions in 4% NaCl produce more active potentials in passive 18-8 or titanium presumably by displacing adsorbed oxygen. Potentials of 18-8 in alkaline NaCl as a function of partial pressure of oxygen follow the adsorption isotherm, which adds confirming evidence that an adsorbed oxygen film is responsible for passivity. The decreased potentials between active and passive areas plus precipitation of passivity-destroying metal chlorides as hydrous oxides at incipient anodes accounts for inhibition of pitting in chloride solutions by alkalis.

Calculated Langmuir isotherm constants, taking into account competitive chemisorption processes, agree qualitatively with expected relative values based on chemical properties of metals and adsorbates.

INTRODUCTION

Chromates are in the class of inhibitors called passivators because the potential of iron immersed in a chromate solution is several tenths volt more noble than in water, and iron no longer corrodes visibly. Two points of view have been proposed regarding the mechanism of passivation by these and similar compounds. Hoar and Evans (1) proposed that chromates react with soluble ferrous salts throwing down a protective film of hydrated ferric and chromic oxides. Accordingly, a film of ferric oxide on air-exposed iron will, if introduced into chromates, be made more protective because the chromate "repairs" the film discontinuities. Since then, this view has been restated by several investigators (2-4). Mayne and Pryor (3) modified the picture somewhat, based on their electron diffraction studies, proposing initial adsorption of chromates followed by direct reaction with iron to form an unhydrated γ Fe_2O_3 film which they suggested was a better diffusion barrier layer than a film of hydrated oxides.

A second view attributes passivity to adsorption of chromate ions on the metal surface (5-8). Formation of an oxide film is considered unnecessary, although such a film may form eventually and aid in the over-all protection. The primary protection, however, is considered to result from satisfaction of valence forces of the surface metal atoms by chemical bonding with chromate ions, and without the metal atoms leaving their respective lattices. A similar mechanism has been proposed for specific organic inhibitors (9).

Passivators, in accord with this view, are substances having high affinity for the metal and accompanying high activation energy for any reaction which results in a new lattice belonging to a surface stoichiometric compound. These are the essential conditions for chemisorption. Consequently, an iron-chromium oxide or iron oxide, whichever forms ultimately when iron is exposed to chromate solutions, accumulates only slowly. Chlorine, for example, is not a passivator because, despite high affinity for the metal, its activation energy for reaction is low, resulting in rapid production of iron chlorides rather than a chemisorbed film of chlorine atoms. Oxygen, by way of contrast, readily

¹ Manuscript received September 1, 1953. This paper was prepared for delivery before the Wrightsville Beach Meeting, September 12 to 16, 1953.

chemisorbs on many metals and is a good passivator. Halide ions break down passivity by competing with oxygen or other passivators for a place on the metal surface; but once they succeed, metal corrodes at such areas until additional passivator adsorbs.

Evans (10) and others (1, 3, 11) isolated oxide films on iron exposed to chromates and supposed these to be the primary source of protection. Circumstantial evidence of this kind is not conclusive, however, in view of the primary process of adsorption which, if it occurs at all, always precedes the formation of oxides or other compounds, and continues in effect even after the usually permeable, although relatively thick, oxide films are formed. In specific instances, some chemical reagents used for stripping of surface films may actually produce an oxide reaction product (12, 13). When this is the case, the stripping reagent may hasten reaction of adsorbed films, if not of other substances, with the metal, resulting in a surface compound where none existed before.

McKinney and Warner (14) in discussing a paper by Evans expressed doubt that chromates could act merely by precipitation of ferric-chromic oxides on the metal surface, in view of the fact that chromic salts are relatively poor inhibitors compared with chromates. Evans (15) replied that, when chromic salts precipitate a film of hydrated chromic oxide on cathodic areas, attack is not hindered; whereas with chromates, mixed hydroxides are precipitated locally at places where anodic attack would otherwise set in and prevents it from developing. This explanation, however, is less convincing in light of Robertson's (8) subsequent data which showed that molybdates and tungstates, analogous to chromates structurally, and inhibiting at the same minimum concentration, fail to oxidize ferrous salts [or do so extremely slowly (4)] and, hence, are quite unlike chromates in their capacity to precipitate a supposed protective anodic coating.²

² Criticism of Robertson's conclusions has been made on the basis that the otherwise weak oxidizing capacity of molybdate and tungstate in acid solution might be greater in neutral solutions (16) corresponding to actual conditions of pH at the surface of iron. However, the oxidizing tendency of these salts is less in neutral or alkaline media as compared with acid solutions (as can be demonstrated thermodynamically). This, in fact, was demonstrated for molybdates and tungstates by Pryor and Cohen by titrations in neutral media. They found only 11% of 0.0072*N* ferrous sulfate to be oxidized by 0.1*N* sodium tungstate after as long a period as three days, although they interpret this slow rate as sufficient to form the supposed protective film. Actually, molybdates and tungstates are less effective oxidizers than is dissolved oxygen.

This is not to say that iron does not reduce molybdates and tungstates in solution and become oxidized in the process. However, the minimum concentration of these substances for passivity or inhibition, identical with the

Rozenfel'd and Akimov leaned to the possibility that anodic polarization of iron by chromates was due to adsorption of the chromate ion (17). Indelli (18) also interpreted potential behavior of iron and 18-8 in chromates in terms of adsorption of the inhibiting ion.

Simnad (19), using radioactive chromium, concluded that the view of Hoar and Evans was corroborated by the almost similar pickup of radioactive chromium whether iron was immersed in chromic chloride or in chromates, and by the spotty deposition of radio-chromium salts on an iron surface exposed to chromates, presumably revealing anode areas. However, his conclusions do not take into account reaction of chromic chloride with iron to form hydrated oxides which adhere to the metal surface in the same manner as hydrous FeO, but which are not protective in the same sense as chromates. Similarly, chromates may be reduced at preferential metal areas, particularly if chlorides or sulfates are present in solution which accelerate consumption of the passivator (20). Impurities in the metal may also accelerate reduction of chromates.

Brasher and Stove (21) report that the amount of radioactive chromium picked up by abraded mild steel after three days' immersion as a function of chromate concentration follows the form of a typical adsorption isotherm. They find a maximum of 5.5×10^{15} chromium atoms/cm² geometric surface. Considering a probable value of the roughness factor for an abraded surface equal to 3 (22), and a diameter of CrO₄²⁻ equal to 5.4 Å (23), their value corresponds to the equivalent of 4.5 layers of close-packed chromate ions. The number of layers would be less if correction were made for any chromate adsorbed on the air-formed surface oxide or reduced to chromic oxide during the three days' exposure.

Powers and Hackerman (24), also using abraded steel, found, in agreement with Brasher and Stove, that after two days' immersion in 10⁻³*M* radio-chromate at pH 7.5 there were 5.2×10^{15} chromium atoms remaining per cm² of surface, uniformly distributed.

Potential measurements of iron exposed to chromate solutions add to the pertinent evidence concerning the mechanism of passivation. Data of this kind are presented herewith, together with parallel data for 18-8 stainless steel and titanium in other passivating electrolytes.

PROCEDURE

Potentials were measured using a precision potentiometer and vacuum-tube galvanometer in conjunction with a silver chloride reference electrode

minimum concentration of chromates, despite differing oxidizing tendencies, suggests that the mechanism of protection does not depend on an oxidation-reduction reaction.

in 0.1N KCl. The potential of the latter on the hydrogen scale omitting liquid junction potentials is 0.288 volt at 25°C. All measurements were conducted in an air thermostat maintained within 0.2° of 25°C. Final values are for steady state where the net change within 12 hr was less than 5 mv. This often required successive measurements over several days. The maximum change, however, within a few centivolts was obtained usually during the first 24 hr.

Iron electrodes were prepared from high purity 0.030-in. diameter wire obtained by courtesy of the National Bureau of Standards (C < 0.001%, total impurities about 0.008%). Six-inch lengths were mounted in glass tubing and sealed, using polystyrene cement with about 1 cm of wire projecting. The surface was prepared by pickling in 10% H₂SO₄, followed by washing and immediate transfer to the test solution.

Electrodes of 18-8 were prepared from Type 304 0.028-in. diameter wire. The wire was first annealed by heating electrically to 1000°C and quenching in air, then was pickled in 15 vol % HNO₃, 2 vol % HF at 70°–80°C, and washed. It was immersed directly into the electrolyte to a depth of about 1 cm.

Titanium electrodes were made by cutting thin strips of Bureau of Mines cold rolled titanium, followed by pickling in HNO₃-HF at 70°–80°C. No heat treatment was employed.

Ferric ion concentration in sulfuric acid was determined by reduction first with stannous chloride, the excess of which was eliminated by adding HgCl₂, followed by titration with permanganate. Cupric ion concentration was determined by titration using thiocyanate. Dichromate or chromate solutions were made up by weighing out the required amount of salt. Low carbonate NaOH was prepared by cooling hot saturated NaOH and decanting into wax-lined bottles.

The cell used for potential determinations consisted of a 4-oz bottle fitted with a rubber stopper. A salt bridge containing the same solution as the electrolyte made contact with 0.1N KCl in which the silver chloride electrode was immersed. The latter electrode was mounted in a glass tube, the bottom of which was constricted to provide a liquid junction by means of a sealed-in asbestos fiber.

Air, first bubbled through caustic soda and water, was used to aerate and stir most of the solutions. When nitrogen was used, it was purified by passing over 4 ft of copper turnings maintained at 400°C.

In tests for reversibility,³ the same metal electrode

³ Reversibility not in the thermodynamic sense, but referring to reproducibility of potentials as approached from either more concentrated or more dilute solutions.

was used throughout, but for measurements of potentials as a function of concentration, different electrodes in separate cells were set up. In view of the considerable time to reach steady state, the latter arrangement was the only practical procedure. This produced a greater scatter of the data, but also made the observed correlation of potential with concentration more convincing.

POTENTIAL DATA

Iron in Chromates

Iron in contact with distilled water attains noble values of potential as K₂CrO₄ is added. At a concentration of 0.0025 molar, the potential change is about 0.5 volt (Fig. 1). Further change at higher concentrations is not pronounced. The maximum potential change agrees with data presented by Burns (25) for iron in 0.01N K₂Cr₂O₇ solution.

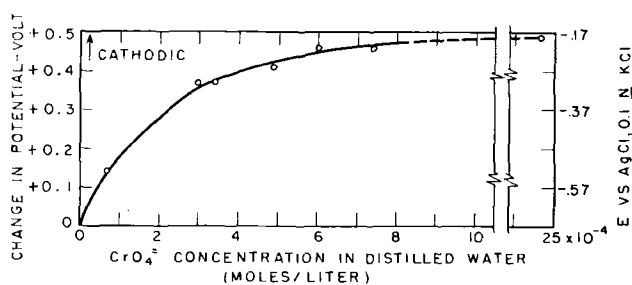


FIG. 1. Effect of CrO₄²⁻ additions on the electrode potential of electrolytic iron in distilled water; (25.0 ± 0.2°C); aerated solutions.

On first immersing the electrodes in a dilute solution of chromate, potentials are relatively active, changing to more noble values within about 2 to 4 hr. The time required is less as the concentration of chromate increases. Steady-state values in all cases were reached in less than 24 hr.

When the electrodes at steady state in 0.0025M chromate are transferred to progressively more dilute solutions, it is found that a maximum of half the ennobling effect of the chromate is lost. This is true even after exposure to distilled water for 41 hr.

18-8 Stainless Steel and Titanium

18-8 stainless steel corrodes in dilute sulfuric acid, but corrosion is effectively inhibited (26) on addition of small amounts of ferric or cupric salts. Similar inhibition is observed to hold for titanium (27, 28), but with the difference that the beneficial effects extend to hydrochloric acid, unlike the situation for 18-8. It is of interest, therefore, to determine the parallel potential behavior of 18-8 and titanium in sulfuric acid as these inhibitors are added. Potentials in 0.2N H₂SO₄ containing up to 0.191M ferric sulfate are summarized in Fig. 2, and for similar additions of cupric sulfate up to 0.70M

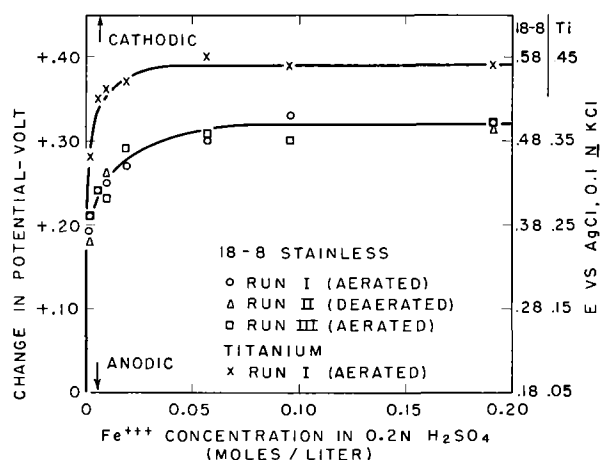


FIG. 2. Effect of Fe^{+++} additions on the electrode potentials of 18-8 stainless steel and titanium in $0.2N \text{H}_2\text{SO}_4$; ($25.0 \pm 0.2^\circ\text{C}$).

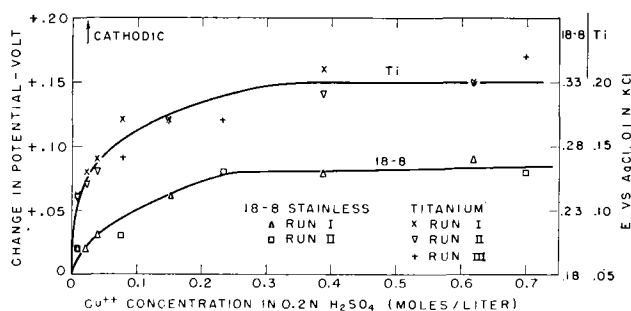


FIG. 3. Effect of Cu^{++} on the electrode potentials of 18-8 stainless steel and titanium in $0.2N \text{H}_2\text{SO}_4$; ($25.0 \pm 0.2^\circ\text{C}$); aerated solutions.

in Fig. 3. Potentials of 18-8 in ferric sulfate solution, followed for several days, are found to become more noble by a maximum of 0.32 volt, whereas titanium similarly is ennobled to a maximum of 0.39 volt. Since 18-8 is initially more noble than titanium by 0.13 volt, final potentials are not far different. The general reproducibility of measurements can be gauged by a comparison of two separate runs for 18-8 in aerated solutions. In addition, one run in nitrogen-saturated solution showed that oxygen exerts no effect on the potential behavior.

Potentials of 18-8 and titanium are not reversible, as shown by data of Table I. On immersing 18-8, previously at steady state in $0.19M \text{Fe}^{+++}$, into $0.002M \text{Fe}^{+++}$ (referring to $0.2N \text{H}_2\text{SO}_4$), the second steady-state potential remained more noble by 0.07 volt after 27 hr of exposure than the original steady-state value of 0.18 volt. However, on re-immersing the electrode into $0.19M \text{Fe}^{+++}$, the potential of 0.35 volt at the end of 20 hr was only 0.04 volt more noble than the original value.

With cupric sulfate additions, potential changes are less than for ferric sulfate, even though the final concentration of cupric ion is higher. Maximum ΔE averaged 0.08 volt for 18-8 and 0.15 volt for titanium.

TABLE I. Test of reversibility

Electrolyte	Initial ΔE (volt)	Change of concentration in moles/liter	Final ΔE (volt)
<i>18-8</i>			
$0.19M \text{Fe}^{+++}$ in $0.2N \text{H}_2\text{SO}_4$	0.31		
	0.26	Decrease to 0.010	0.27 (4 hr)
	0.18	Decrease to 0.002	0.25 (27 hr)
	0.31	Increase to 0.191	0.35 (20 hr)
<i>Titanium</i>			
$0.70M \text{Cu}^{++}$ in $0.2N \text{H}_2\text{SO}_4$	0.17		
	0.12	Decrease to 0.23	0.16 (1 hr)
	0.09	Decrease to 0.078	0.14 (1 hr)
	0.00	Decrease to 0.0	0.12 (1 hr)
	0.09	Increase to 0.078	0.13 (1 hr)
	0.12	Increase to 0.23	0.17 (1 hr)
	0.17	Increase to 0.70	0.19 (1 hr)
<i>Iron</i>			
$2.5 \times 10^{-3}M \text{K}_2\text{CrO}_4$	0.49	Decrease to 0.0	0.25 (41 hr)
$0.35M \text{NaOH}$ in 4% NaCl	0.45		
	0.18	Decrease to 0.04	0.20 (1 hr)
	0.15	Decrease to 0.025	0.17 (1 hr)
	0.00	Decrease to 0.0	0.10 (1 hr)
	0.15	Increase to 0.025	0.17 (1 hr)
	0.18	Increase to 0.04	0.18 (1 hr)
	0.45	Increase to 0.35	0.35 (1 hr)

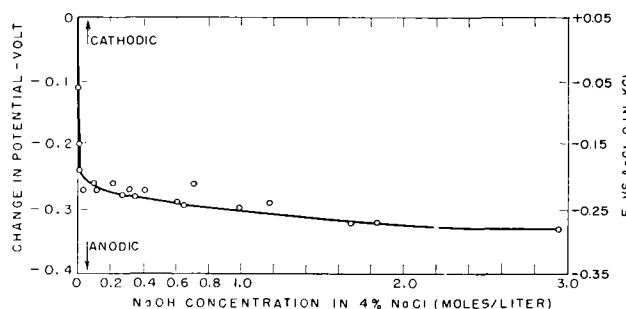


FIG. 4. Effect of NaOH additions on the electrode potential of 18-8 stainless steel in aerated 4% NaCl; ($25.0 \pm 0.2^\circ\text{C}$).

In aerated NaCl, 18-8 stainless steels in time corrode by pitting. Addition of alkali inhibits this type of attack (29). Titanium, on the other hand, is relatively resistant to pitting in chloride solutions without alkali additions, including sea water. The potential behavior of 18-8 in 4% NaCl upon addition of NaOH up to 2.9 molar is shown in Fig. 4, and similarly in Fig. 5 for titanium with addition of NaOH up to 0.2 molar. Potentials were followed for a total period of about 120 hr. The remarkable difference in behavior of the metals in this electrolyte compared with previous electrolytes is that NaOH additions produce more active potentials, or decrease passivity as measured by potential. Effects are most pronounced with first additions of NaOH below

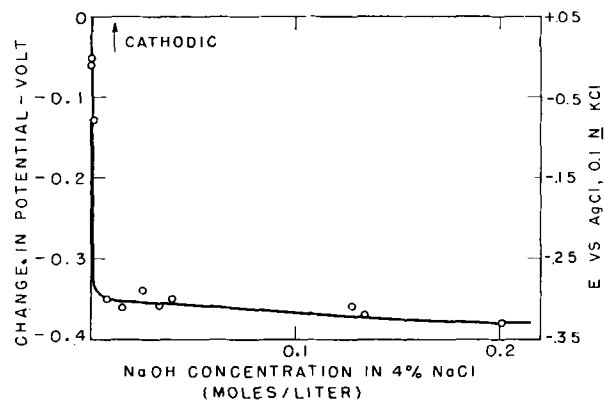


FIG. 5. Effect of NaOH additions on the electrode potential of titanium in aerated 4% NaCl; ($25.0 \pm 0.2^\circ\text{C}$).

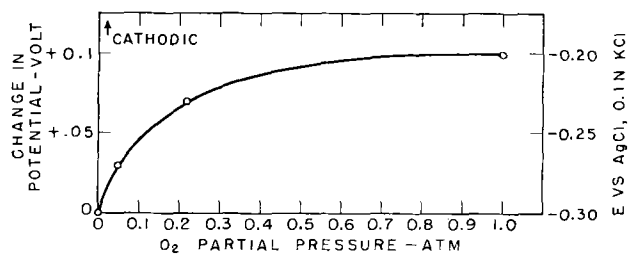


FIG. 6. Effect of varying O_2 partial pressure on the electrode potential of 18-8 stainless steel in 4% NaCl; 0.3M NaOH; ($25.0 \pm 0.2^\circ\text{C}$).

about 0.01 molar, subsequent additions producing only slight change. The maximum change of potential for 18-8 was -0.33 volt and for titanium -0.38 volt, indicating again similar behavior of both metals.

It was also of interest to learn the effect of oxygen on the potentials of 18-8 in this system, because of the importance oxygen has with respect to passivity of stainless steels exposed to the atmosphere. Potential measurements were carried out in 4% NaCl containing 0.3M NaOH through which nitrogen, oxygen, or air was bubbled. Also, one gas mixture was prepared, containing 0.05 atm partial pressure oxygen, by compressing air and nitrogen to appropriate pressures in a single gas cylinder and using this mixture to aerate and stir the electrolyte. Results are given in Fig. 6 showing that oxygen, as expected, ennobles the potential of 18-8 as the partial pressure increases.

Potentials were also determined for iron in 4% NaCl as a function of NaOH additions. Here the potential becomes *more noble*, opposite to the trend for 18-8 or titanium (Fig. 7). About 24 hr or less were required for steady state. The values, on immersing the electrodes in several more dilute NaOH solutions after reaching steady state in 0.35M NaOH, were the same as previously determined within 0.02 volt (after one hour) and on returning the electrode to 0.35M NaOH, the potential was less noble by 0.1 volt (Table I). It is especially

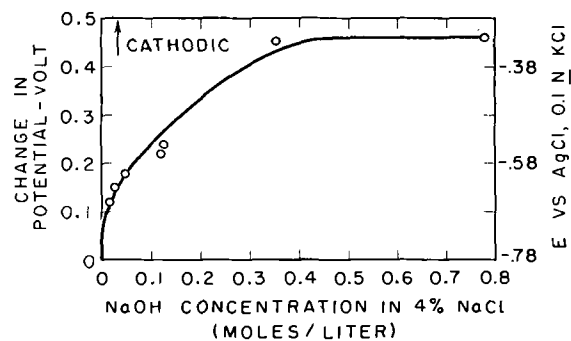


FIG. 7. Effect of NaOH additions on the electrode potential of electrolytic iron in 4% NaCl; ($25.0 \pm 0.2^\circ\text{C}$); aerated solutions.

significant that the potential of iron, initially active in 4% NaCl, and the potential of 18-8 initially noble, approach the same value on additions of NaOH. This suggests that the final surface states of iron and 18-8 (which contains 74% iron) in alkaline NaCl are comparable, despite large initial differences in neutral NaCl. Perhaps it is not surprising, therefore, that corrosion rates in alkaline NaCl are comparably low for both metals, but are quite different in neutral or near neutral NaCl solutions.

DISCUSSION

For each metal studied, the potential behavior as a function of passivator or inhibitor concentration resembles a typical adsorption isotherm. This relation is expected if inhibitors function by adsorbing on the metal surface, but would not be predicted, presumably, by any mechanism involving diffusion-barrier oxide or other type reaction-product films. Interpretation of the data, therefore, in terms of an adsorption process appears worthwhile.

Adsorption Isotherm and Potentials

The adsorption isotherm proposed by Langmuir (30) is expressed as follows:

$$x = \frac{abp}{1 + ap}$$

where x is the amount of gas adsorbed per unit area at pressure p , and a and b are constants. The constant b is equal to maximum adsorbate x_m at high values of p , and a is related to heat of adsorption (31). Assuming that Henry's law applies, this can be converted to a similar expression for adsorption from liquids where concentration of solute C substitutes for gas pressure p .

Furthermore, if the ions adsorbing on a metal surface form dipoles each of electric moment μ , electrostatic theory leads to the expression $4\pi n\mu$ for the total change of potential ΔE produced by n

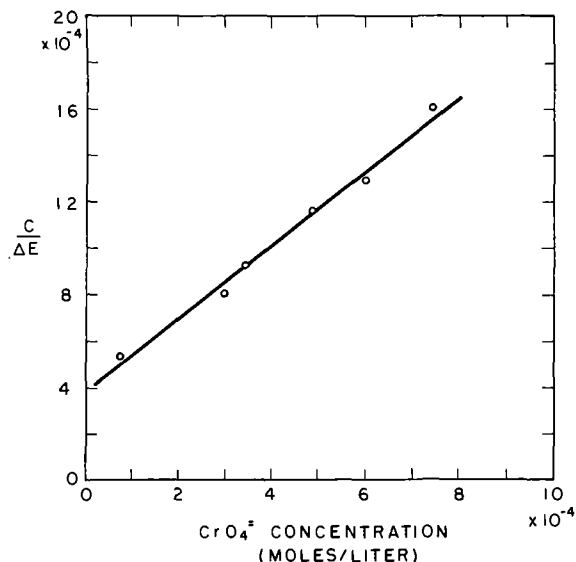


FIG. 8. Langmuir adsorption plot for electrolytic iron in distilled water containing CrO_4^{2-} inhibitor.

dipoles adsorbing per unit area of metal surface.⁴ Therefore, ΔE is proportional to x , and maximum ΔE_m is similarly proportional to x_m .

$$\text{Therefore, } \frac{C}{\Delta E} = \frac{C}{\Delta E_m} + \frac{1}{a'\Delta E_m}$$

If the Langmuir isotherm applies, therefore, a linear relation should exist between $C/\Delta E$ plotted with C , the slope of which is equal to $1/\Delta E_m$, and the intercept is equal to $1/a'\Delta E_m$ at $C = 0$. Data for various inhibitor concentrations satisfactorily conform to this relation as shown by Fig. 8 to 13. Potentials for 18-8 and titanium in 0.2N H_2SO_4 containing Cu^{++} show a degree of scattering, caused probably by the small measured potential differences in these solutions compared with experimental variations, the maximum ΔE being only 0.08 to 0.15 volt. $C/\Delta E$ vs. C was not reproduced for Ti and 18-8 in 4% $\text{NaCl} + \text{NaOH}$, even though linearity is obtained for all but the lowest NaOH concentrations. The test of linearity, however, loses significance when values of ΔE are essentially

⁴ If one considers a supplementary diffuse double layer in accord with Gouy and Chapman, the additional potential change equals $4\pi\sigma/D\kappa$ (32) where σ is the total electric charge per unit area, D is the dielectric constant, and κ is equal to $(4\pi e^2/DkT [\sum n_i z_i^2])^{1/2}$ having the same significance as in the Debye-Hückel theory of electrolytes. Since κ has the dimensions of reciprocal length and may be identified with the effective separation of charges in the dipole layer, this expression, if $D = 1$, achieves the same form as the expression for a fixed dipole layer.

Adsorption of ions can be looked upon as forming new cathodic areas, the extent of which reaches a maximum at completion of a monolayer. Anodic areas are simultaneously restricted to a minimum corresponding to maximum anodic polarization by corrosion currents and a shift of potential to more noble values.

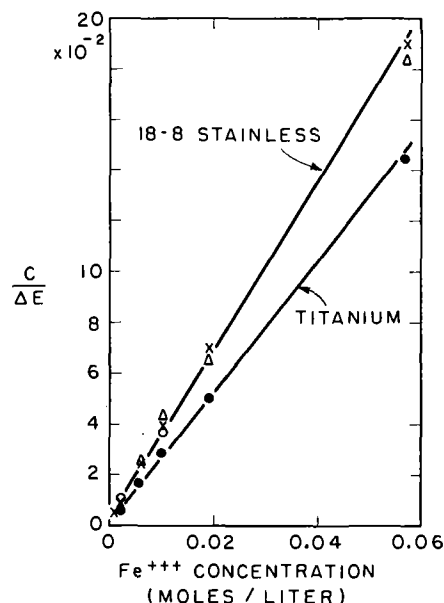


FIG. 9. Langmuir adsorption plot for 18-8 stainless steel and titanium in 0.2N H_2SO_4 containing Fe^{+++} inhibitor.

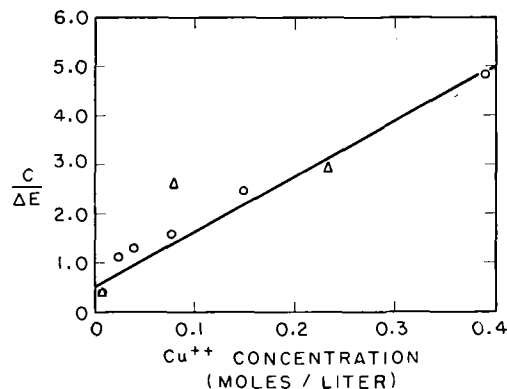


FIG. 10. Langmuir adsorption plot for 18-8 stainless steel in 0.2N H_2SO_4 containing Cu^{++} inhibitor.

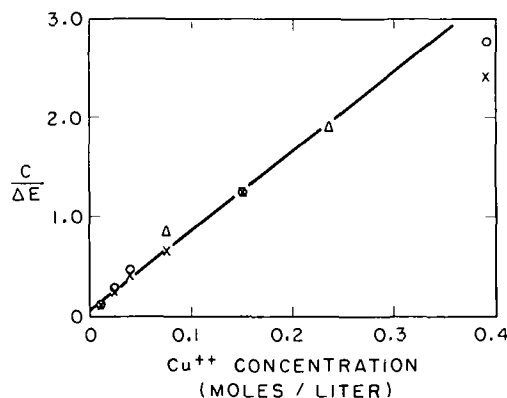


FIG. 11. Langmuir adsorption plot for titanium in 0.2N H_2SO_4 containing Cu^{++} inhibitor.

constant with change of inhibitor concentration, as is true in this instance.

Correspondence, by and large, of potential data to the Langmuir type isotherm points strongly to

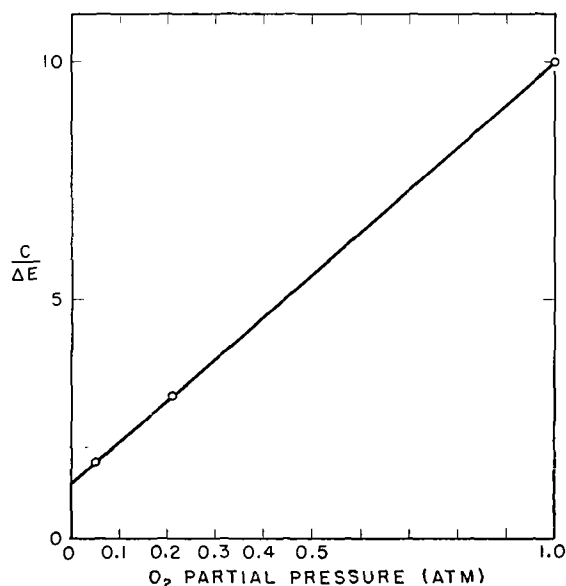


FIG. 12. Langmuir adsorption plot for 18-8 stainless steel in 4% NaCl with 0.3M NaOH, varying O₂ partial pressure.

the view that the inhibitors considered at present function by adsorbing on the metal surface. Furthermore, the observed correspondence suggests adsorption of the monolayer type, as was pointed out by Langmuir in the derivation of his isotherm equation. These conclusions are strengthened by measurements of Hackerman and Sudbury (33), showing that potentials of steel in contact with organic amine inhibitors also follow the Langmuir adsorption isotherm. The linearity of $C/\Delta E$ vs. C reported by them is especially significant, since it is generally conceded that organic inhibitors function by adsorbing on the metal surface (34, 35).

Maximum potential change, in accord with present considerations, occurs with formation of a complete monolayer of chemisorbed ions, any additional adsorption being accompanied by relatively small potential changes and lesser effects on the corrosion rate. It is important to note, therefore, that maximum change of ΔE in Fig. 1 for iron in chromates occurring at 2.5×10^{-3} molar, corresponds approximately to the minimum concentration of chromates (1×10^{-3} molar) found necessary by Robertson (8) for inhibition and passivity. It is probably reasonable to conclude, therefore, that optimum passivity is associated with a monolayer film of adsorbed chromate ions.

Part of the adsorbed chromate is chemisorbed and part is reversibly adsorbed, as is pointed out by the time necessary to achieve steady-state potentials, indicative of the usually longer times required for chemisorption, and by the partially irreversible nature of the potentials. Even after thorough washing in distilled water, iron passivated in radio-

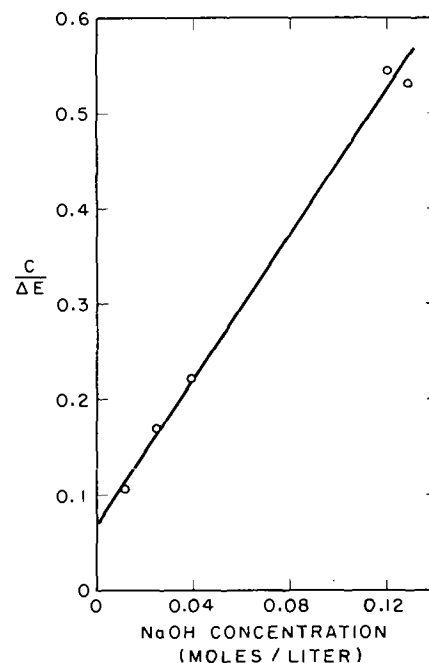


FIG. 13. Langmuir adsorption plot for electrolytic iron in aerated 4% NaCl with NaOH additions.

active chromates shows residual radioactivity (19, 21, 24), and the potential is more noble than initially. The final irreversible or chemisorbed portion exerts about half the total effect on the potential. This result is in agreement with a similar observation of Gatos (36) who found that, on first immersing iron in chromate solutions, the amount of metal reacting initially when iron is made passive in concentrated nitric acid is less than in absence of chromate exposure, and that half this effect of chromate, but no more, could be removed by washing in water.

Powers and Hackerman (24) suggested adsorption of chromate ions on a surface oxide rather than on the metal. Although such adsorption presumably may occur, any mechanism of corrosion protection accompanying a film of this kind is not yet clear. An air-formed film, at least, is not necessary to adsorption. Preliminary measurements in this laboratory using radiochromate showed that the usual radioactivity is picked up by oxide-free Armco iron sheet (0.024% C). Iron specimens were heated in dried pure H₂ at 1000°C, cooled in this gas, transferred to deaerated $10^{-3}M$ Cr⁵¹O₄, pH 1.9, out of contact with air, and after 2 to 17.5 hr, washed successively in three 200-ml portions of distilled water. Somewhat greater residual chromium (3×10^{16} atoms/cm²) was found than that reported by Brasher and Stove and by Hackerman and Powers for abraded iron. No residual radioactivity was found on similar specimens immersed directly into deaerated radioactive chromic perchlorate of pH 1.9.

Adsorption of Oxygen and Ferric, Cupric, and Hydroxyl Ions

Presumably, ferric and cupric ions also adsorb on 18-8 and titanium, producing passivity as gauged by reduced corrosion rates or noble potentials. Ions have a certain electron affinity and when adsorbed receive a certain amount of negative charge from the metal. The net effect, including the effect of negative ions in solution, is an over-all negatively charged ion layer near the surface and an equal positive image charge in the metal, similar to the situation for chromates. This accounts for increasingly noble potentials as more ferric and cupric ions adsorb, trivalent ferric ion being more effective in this respect than divalent cupric ion, corresponding also to the order of inhibition in dilute sulfuric acid (27).

The more active potentials of titanium and 18-8 in sodium chloride solution on addition of sodium hydroxide can be interpreted as competition between hydroxyl ion and oxygen for a place on the metal surface, the adsorbed hydroxyl ion producing a lower order dipole moment than adsorbed oxygen. Chemisorbed oxygen, according to one viewpoint, is primarily responsible for passivity (5, 37, 38) in these metals. If the partial pressure of oxygen is increased, the potential becomes more noble (Fig. 6) in agreement with this view. The potential change from 0 to 1 atmosphere oxygen amounts to only 0.1 volt, suggesting that the fundamental passive layer of chemisorbed oxygen in alkaline NaCl is only slightly disturbed by hydroxyl ions. This concurs with the observation that apparent equilibrium in this instance is effected between dissolved gas and molecularly adsorbed oxygen and not atomically adsorbed oxygen, as shown by the linearity of $p/\Delta E$ plotted with p but lack of linearity plotting $\sqrt{p}/\Delta E$ vs. \sqrt{p} , where p refers to partial pressure of oxygen. Previous quantitative adsorption data obtained for oxygen on 18-8 (39) provided evidence, in fact, that the alloy exposed two days to aerated water is covered by a close packed atomic oxygen layer over which a molecular oxygen layer is adsorbed. Were the chemisorbed atomic oxygen on 18-8 entirely displaced by OH^- , the potential change would be in the order of 0.5 volt, corresponding to complete breakdown of passivity, but a potential change of 0.4 volt occurs only in concentrated alkalis, e.g., 20% NaOH (40).

When iron, on the other hand, is immersed in alkaline NaCl, competition includes not only adsorbed OH^- and oxygen, but also adsorbed H. Iron exposed to an aqueous solution has a definite tendency to react, liberating hydrogen and hydrous ferrous oxide, the free energy for the reaction being negative (41) and independent of pH, so long as

these corrosion products form and no other. Hydrogen so produced adsorbs on the iron surface and, in neutral or alkaline solutions, escapes reluctantly as H_2 impeding corrosion reaction. With presence of dissolved oxygen, adsorbed hydrogen reacts to form water as rapidly as oxygen reaches the metal surface. If, however, rate of consumption falls below the diffusion rate to the surface, excess oxygen, in turn, can adsorb on the metal. This adsorption, when it occurs, is accompanied by a lowered corrosion rate and a more noble potential (passivity). Therefore, as hydroxyl ions are added to the solution, adsorbed H is increasingly displaced by OH^- and reaction of the former with dissolved oxygen slows down. Consequently, oxygen is in excess at the surface, and conditions are favored for its adsorption. Support of this state of affairs is provided by the observation that, in absence of oxygen, the potential of iron in water is more active when alkalis (42, 43) are added, as is expected from the reduced solubility of $\text{Fe}(\text{OH})_2$ under these conditions. Only in presence of oxygen does the potential become more noble, the measured potential being a compromise between the iron and oxygen electrode values. In acid media, on the other hand, the iron electrode covered with adsorbed hydrogen behaves approximately as a reversible hydrogen electrode (44, 45). Since iron and 18-8 have about the same potential in aerated alkaline NaCl, the inference is that if oxygen is chemisorbed on 18-8, it is also, under these conditions, chemisorbed on iron and is responsible for observed passivity in both metals. The energy of bonding of oxygen to the metal need not be the same in both cases, however, and, therefore, the degree of passivity may differ.

Powers and Hackerman showed that competitive adsorption of CrO_4^{--} and OH^- takes place on Cr (46) and iron (24) surfaces, similar to competitive adsorption of H, O_2 , and OH^- described above.

Pitting Tendencies of 18-8 and Titanium

Inhibition of pitting in 18-8 by hydroxyl ion can be accounted for by the reduced difference of potential between active and passive areas in the galvanic cells that account for pitting (47), since the passive areas are no longer so noble as before. In addition, metal chlorides at incipient pits react with hydroxyl ions which migrate rapidly to anodic areas to form metal hydroxides. Hydroxides, unlike soluble chlorides, do not continuously destroy passivity or, what is the same, do not maintain activity at the site of chemical disturbance; hence, the pit never gets started. With titanium, pitting tendency is decreased by the pronounced tendency of titanium chloride to hydrolyze to hydroxide or hydrous oxide even in absence of hydroxyl ions.

Hence, titanium, better than 18-8, resists pitting in sea water, and potential data indicate that in alkaline salt solutions, the tendency would be still less.

Separation of Charge in Dipole Layer

Values of ΔE in combination with the equation $\Delta E = 4\pi n\mu$ make it possible to calculate the average separation of negative charge in the adsorbed chromate layer from the iron surface. Assuming a diameter of chromate ion equal to 5.4 \AA , there will be 4.0×10^{14} ions/cm² adsorbed in a close packed monolayer. A layer based on true surface rather than apparent area would still be equivalent in projected dipole moment to this number of ions. Since the change of potential produced by a monolayer is 0.5 volt (Fig. 1), the calculated value of d , where μ is equal to de (d = separation of negative and positive charge, and e = electronic charge), is $0.5/(300 \times 4\pi \times 4 \times 10^{14} \times 4.8 \times 10^{-10})$ or 0.07×10^{-8} cm. Hence, the excess electrons, according to this calculation, are, on the average, only 0.035×10^{-8} cm from the metal surface, since the positive image charge within the metal is at a similar distance from the surface. In other words, a relatively slight asymmetry of electron density at the metal surface suffices to explain the observed adsorption potentials.

Values of Langmuir Constants

Values of the Langmuir constants ΔE_m and a' are summarized in Table II. In general, ΔE_m calculated from the slope of $C/\Delta E$ vs. C agrees reasonably well with the observed maximum ΔE_m . For iron in alkaline NaCl, the difference in values suggests that potential relations are more complex than the simple adsorption of oxygen alone, in accord with the discussion of iron potentials above.

Values of a' are equal to the reciprocal of the concentration at which half the maximum potential shift is obtained. According to the Langmuir derivation, these values are larger as the heat of adsorption increases. Hence, O₂ on 18-8 and chromates on iron show appreciable affinity of adsorbate for metal. Similarly, ferric ions have greater affinity for 18-8 and titanium than cupric ions. The low value of a' for iron in alkaline NaCl supports the point of view that competitive chemisorption takes place between several species, e.g., H, OH⁻, and O₂, heats of adsorption for one species tending to cancel out heats of desorption for the species it displaces. Competition between possible adsorbates very likely accounts for the partial reversibility of potentials involving chemisorbed films. In general, it should be emphasized that values of a' reflect a resultant heat effect of one or more

TABLE II. Values for constants of Langmuir adsorption isotherm

Electrode	Electrolyte	E vs. AgCl, 0.0 <i>N</i> inhib., volt	ΔE_m (volt)		Intercept a'^{-1} ΔE_m^{-1}	a' (liters/mole)
			(calc)	(obs)		
18-8	Fe ⁺⁺⁺ in 0.2 <i>N</i> H ₂ SO ₄	0.18	0.30	0.33	0.001	3300
	Cu ⁺⁺ in 0.2 <i>N</i> H ₂ SO ₄	0.18	0.09	0.08	0.5	22
	O ₂ in 0.3 <i>N</i> NaOH in 4% NaCl	-0.30	0.11	0.1	0.0011	8400
Ti	Fe ⁺⁺⁺ in 0.2 <i>N</i> H ₂ SO ₄	0.05	0.37	0.38	0.001	2700
	Cu ⁺⁺ in 0.2 <i>N</i> H ₂ SO ₄	0.05	0.13	0.15	0.15	50
	OH ⁻ in aerated 4% NaClCrO ₄ ⁻⁻ in H ₂ O	-0.78	0.26	0.46	0.065	59
Fe		-0.67	0.63	0.5	0.00039	4000

competitive adsorption processes, even if the substance displaced is nothing more than physically adsorbed H₂O. The primary process, of course, has the largest effect. By and large, relative values of a' are in accord with the expected trend based on chemical properties of the metals and adsorbates.

ACKNOWLEDGMENT

This research was supported by the Office of Naval Research under Contract N5ori-07815 to whom the authors express their appreciation.

Any discussion of this paper will appear in a Discussion Section to be published in the December 1954 issue of the JOURNAL.

REFERENCES

1. T. P. HOAR AND U. R. EVANS, *J. Chem. Soc.*, **1932**, 2476.
2. T. P. HOAR, *Trans. Faraday Soc.*, **45**, 683 (1949).
3. J. MAYNE AND M. PRYOR, *J. Chem. Soc.*, **1949**, 1831.
4. M. J. PRYOR AND M. COHEN, *This Journal*, **100**, 203 (1953).
5. H. H. UHLIG, *Chem. Eng. News*, **24**, 3154 (1946).
6. H. H. UHLIG, *Metaux et Corrosion*, **22**, 204 (1947).
7. "CORROSION Handbook," (H. H. Uhlig, Editor) p. 31, John Wiley & Sons, Inc., New York (1948).
8. W. D. ROBERTSON, *This Journal*, **98**, 94 (1951).
9. N. HACKERMAN AND H. SCHMIDT, *Corrosion*, **5**, 237 (1949).
10. U. R. EVANS, *J. Chem. Soc.*, **1927**, 1020.
11. U. R. EVANS AND J. STOCKDALE, *ibid.*, **1929**, 2651.
12. W. VERNON, F. WORMWELL, AND T. NURSE, *J. Iron Steel Inst. (London)*, **150**, 81P (1944).
13. M. FONTANA, *Trans. Electrochem. Soc.*, **93**, 335 (1948).
14. D. MCKINNEY AND J. C. WARNER, *Ind. Eng. Chem.*, **37**, 705 (1945).
15. U. R. EVANS, *ibid.*, p. 706.
16. M. PRYOR AND M. COHEN, *This Journal*, **98**, 513 (1951).
17. I. ROZENFEL'D AND G. AKIMOV, *Doklady Akad. Nauk. S.S.S.R.*, **67**, 879 (1949); *C. A.*, **44**, 459 (1950).
18. A. INDELLI, *Ann. Chim. (Rome)*, **40**, 189 (1950); *C. A.*, **45**, 10177 (1951).
19. M. SIMNAD, *J. Inst. Metals Monograph No. 13*, p. 23, London (1953).

20. M. DARRIN, *Ind. Eng. Chem.*, **38**, 368 (1946).
21. D. BRASHER AND E. STOVE, *Chem. and Ind.*, No. 8, 171 (1952).
22. T. L. O'CONNOR, Corrosion Lab., M.I.T., Unpublished measurements.
23. B. E. WARREN, Private communication.
24. R. POWERS AND N. HACKERMAN, *This Journal*, **100**, 314 (1953).
25. R. M. BURNS, *J. Applied Phys.*, **8**, 398 (1937).
26. J. MONYPENNY, "Stainless Iron and Steel," 3rd ed., p. 302, Chapman and Hall, London (1951).
27. J. COBB AND H. H. UHLIG, *This Journal*, **99**, 13 (1952).
28. D. SCHLAIN AND J. SMATKO, *ibid.*, 417.
29. H. H. UHLIG AND J. W. MATTHEWS, *Corrosion*, **7**, 419 (1951).
30. I. LANGMUIR, *J. Am. Chem. Soc.*, **40**, 1361 (1918).
31. I. LANGMUIR, *ibid.*, **54**, 2798 (1932).
32. S. GLASTONE, "Introduction to Electrochemistry," p. 524, D. Van Nostrand Co., Inc., New York (1942).
33. N. HACKERMAN AND J. SUDBURY, *This Journal*, **97**, 109 (1950).
34. U. R. EVANS, "Metallic Corrosion, Passivity and Protection," p. 537, Ed. Arnold and Co., London (1946).
35. T. P. HOAR, "Pittsburgh International Conference on Surface Reactions," p. 127, Corrosion Publishing Co., Pittsburgh (1948).
36. H. C. GATOS AND H. H. UHLIG, *This Journal*, **99**, 250 (1952).
37. Ref. 7, p. 24
38. H. H. UHLIG, *This Journal*, **97**, 215C (1950).
39. H. H. UHLIG AND S. S. LORD, JR., *ibid.*, **100**, 216 (1953).
40. H. H. UHLIG, *Trans. Am. Inst. Mining Met. Engrs.*, **140**, 387 (1940).
41. J. C. WARNER, *Trans. Electrochem. Soc.*, **83**, 319 (1943).
42. A. TRAVERS AND J. AUBERT, *Compt. rend.*, **194**, 2308 (1932).
43. E. MEUNIER AND O. L. BIHET, *Congres. Chem. Ind.*, p. 444 (1933).
44. J. D'ANS AND U. BRECKHEIMER, *Z. Elektrochem.*, **56**, 585 (1952).
45. O. GATTY AND E. SPOONER, "The Electrode Potential Behavior of Corroding Metals in Aqueous Solutions," p. 310, Oxford Press, New York (1938).
46. N. HACKERMAN AND R. POWERS, *J. Phys. Chem.*, **57**, 139 (1953).
47. Ref. 7, p. 165.

Contribution to the Theory of Electropolishing¹

CARL WAGNER

Department of Metallurgy, Massachusetts Institute of Technology, Cambridge, Massachusetts

ABSTRACT

An ideal electropolishing process is characterized by a plateau of the current density-potential curve corresponding to the maximum diffusion rate of an acceptor for metal ions toward the anode. Such a process is amenable to a quantitative theoretical analysis. Formulas are derived for decrease of surface roughness as a function of the recess of the average surface, amount of metal dissolved per unit surface area, and product of current density and time.

INTRODUCTION

Jacquet (1) and others have shown that a plot of current density J vs. cell voltage or anode potential E gives a horizontal plateau for many solutions used in electropolishing processes. Such a curve is found whenever the diffusion of one reactant consumed by an electrode process is the controlling factor, i.e., the concentration of the reactant at the surface of the electrode is much less than its bulk concentration, and the effective thickness of the hydrodynamic boundary layer has a definite value determined by forced or natural convection. In particular, a limiting current density is observed for the electrodeposition of metals at a cathode. Kolthoff and Miller (2) have also observed a limiting current density for the anodic dissolution of mercury if the diffusion of complexing ions such as $S_2O_3^{2-}$, SO_3^{2-} , CN^- , and SCN^- is the limiting factor.

Elmore (3) has interpreted the occurrence of a limiting current density for the anodic dissolution of a metal by assuming that the solution at the surface of the anode is saturated with respect to a salt of the dissolving metal, and the current density is determined by the diffusion rate of metal ions from the surface of the electrode into the bulk solution. This interpretation, however, is contradictory to the fact that the potential of the anode can be varied within rather wide limits, e.g., between 0.25 and 1.5 volt for copper in 86% H_3PO_4 according to Walton (4), whereas a constant concentration of metal ions at the anode and a constant current density are compatible only with a constant electrode potential.

According to Edwards (5, 6), the plateau of the current density-potential curve is due to diffusion of an "acceptor" for metal ions toward the anode. When silver is electropolished in a cyanide bath (7), cyanide ions are the acceptor forming $Ag(CN)_2^-$. In highly concentrated phosphoric or perchloric

acid, the acceptor may be water whose significance has been discussed particularly by Darmois, Epelboin, and Amine (8). Water is needed for the formation of hydrated cations such as $Cu(OH_2)_4^{++}$. A limiting value of the current density corresponds to a maximum concentration gradient when practically all the acceptor approaching the anode readily reacts with metal ions, and thus the acceptor concentration at the anode is much lower than the bulk concentration. This interpretation of the plateau of the current density-potential curve implies that either the standard free energy of nonhydrated cations is much higher than that of hydrated cations, or the activation energy for the formation of nonhydrated cations is considerably greater than the activation energy for the formation of hydrated cations. A process satisfying these conditions will be called an "ideal electropolishing process."

MATHEMATICAL ANALYSIS OF AN IDEAL ELECTROPOLISHING PROCESS

Consider a sine-wave profile surface shown in Fig. 1 with a wave length, a , and an amplitude, b . At the surface of the electrode the concentration, c , of the acceptor determining the dissolution rate is supposed to vanish. Thus

$$c = 0 \text{ at } y = b \sin(2\pi x/a) \quad (I)$$

where y is the distance from the "average surface plane" of the anode indicated by the dotted line in Fig. 1, and x is the coordinate parallel to the average surface plane.

If the dimensions a and b are much smaller than the effective thickness of the hydrodynamic boundary layer, only the innermost part of the boundary layer has to be considered, and thus flow of the liquid in the x or y direction may be neglected, since the velocity components at the surface of the electrode vanish. Then Fick's second law applies.

¹ Manuscript received October 15, 1953.

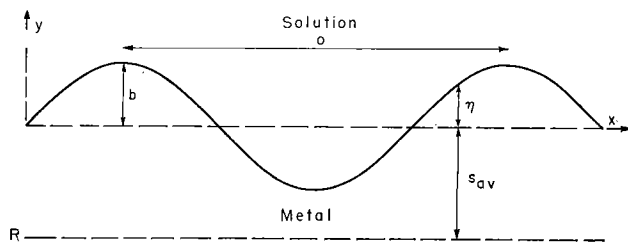


FIG. 1. Sine-wave profile electrode

For steady-state conditions it follows that

$$\frac{\partial c}{\partial t} = D \left(\frac{\partial^2 c}{\partial x^2} + \frac{\partial^2 c}{\partial y^2} \right) = 0 \quad (\text{II})$$

where D is the diffusion coefficient of the acceptor.

Edwards (5, 6) has already obtained solutions of equation (II) by determining experimentally the distribution of the electrical potential in a trough, involving a large scale model of the electrode, filled with tap water, and using the similarity between differential equations and boundary conditions for the concentration and the potential field. To arrive at general conclusions, it seems profitable to consider an analytical solution of equation (II). A particular solution reads

$$c(x, y) = B[y - b \exp(-2\pi y/a) \sin(2\pi x/a)] \quad (\text{III})$$

where B is a constant. If $b \ll a$, equation (III) virtually satisfies the boundary condition in equation (I) as is verified by substituting $y = b \sin(2\pi x/a)$ in equation (III) and letting the exponential function be unity as a close approximation since the exponent tends to zero for $b/a \rightarrow 0$.

Differentiation of equation (III) with respect to y yields

$$\frac{\partial c}{\partial y} = B[1 + (2\pi b/a) \exp(-2\pi y/a) \sin(2\pi x/a)]. \quad (\text{IV})$$

From equation (IV) it follows that the concentration gradient becomes virtually independent of x and y at some distance from the electrode, i.e., if $y \gg a$. Furthermore, the constant B is found to be equal to the average value of the concentration gradient at the anode, $(\partial c/\partial y)_{\text{avg}}$. A linear dependence of concentration on distance y will be found only in the innermost part of the boundary layer where flow of liquid can be neglected. A schematic concentration distribution for the entire boundary layer is shown schematically in Fig. 2. The effective thickness of the boundary layer, δ , may be defined as the distance of the intersection of the tangent line on the c vs. y curve at $y = 0, x = 0$ and the extrapolated plateau of the bulk concentration c_0 . Since equations (III) and (IV) presuppose a virtually constant concentration gradient at $y \gg a$, e.g., $y > 4a$, and thus the region $y < 4a$ must belong to the innermost

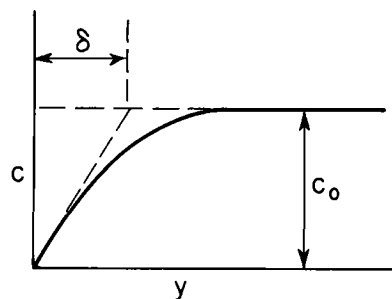


FIG. 2. Schematic graph of acceptor concentration as a function of distance from the electrode.

boundary layer, the effective thickness must be much greater than the wave length of the electrode profile. This is a necessary condition for the validity of equation (III) and subsequent equations derived therefrom.

Upon substituting $y = b \sin(2\pi x/a)$, expanding the exponential function, and neglecting terms involving higher powers of (b/a) except for the first power, the concentration gradient at the surface in the y direction is found to be

$$\left(\frac{\partial c}{\partial y} \right)_{y=b \sin(2\pi x/a)} \cong \left(\frac{\partial c}{\partial y} \right)_{\text{avg}} \left[1 + \frac{2\pi b}{a} \sin(2\pi x/a) \right] \quad (\text{V})$$

if $b \ll a, \quad a \ll \delta$

In view of the condition $b \ll a$, we may disregard the difference between the concentration gradient normal to the average surface plane and that normal to the local surface, e.g., at $x = 0$ and $x = \frac{1}{2}a$.

Next, consider the change in the shape of the surface profile as a function of time, t . Let η be the distance of a point at the surface from the average surface plane, and s_{avg} the distance of the average surface plane from the reference plane, R , inside the electrode (see Fig. 1). Then the distance of a point at the surface of the electrode from the reference plane, R , equals

$$s = s_{\text{avg}} + \eta \quad (\text{VI})$$

where

$$\eta = b \sin(2\pi x/a). \quad (\text{VII})$$

Decrease of distances s and s_{avg} per unit time is proportional to the local and to the average dissolution rate, i.e., proportional to the local and the average concentration gradient of the acceptor, respectively. Thus, in view of equation (V)

$$-ds/dt = C[1 + (2\pi b/a) \sin(2\pi x/a)] \quad (\text{VIII})$$

$$-ds_{\text{avg}}/dt = C \quad (\text{IX})$$

where C is a constant, which is equal to the product of the average concentration gradient, the diffusion

coefficient, and the volume of the metal reacting with one mole of the acceptor. Upon substituting equation (VI) in equation (VIII) and subtracting corresponding sides of equations (VIII) and (IX), it follows that

$$-d\eta/dt = C(2\pi b/a) \sin(2\pi x/a). \quad (\text{X})$$

Decrease of the distance s_{avg} of the average surface plane from the reference plane, R , is equal to the displacement, u , of the average surface plane with respect to its position at time $t = 0$. Thus

$$-ds_{\text{avg}} = du. \quad (\text{XI})$$

Dividing corresponding sides of equations (X) and (IX) and substituting equations (VII) and (XI), one obtains

$$-db/du = 2\pi b/a. \quad (\text{XII})$$

Upon integration, it follows that

$$b = b_0 e^{-2\pi u/a} \quad \text{if } b \ll a, a \ll \delta \quad (\text{XIII})$$

where b_0 is the amplitude of the sine-wave surface profile at zero time and b is the amplitude at time, t , corresponding to the displacement, u , of the average surface plane.

From equation (XIII) we readily recognize that percentagewise the amplitude of short sine waves will decrease far more rapidly than the amplitude of long sine waves. In other words, "microroughness" will disappear more rapidly than "macroroughness" in accordance with many observations.

A triangular wave profile or any other periodic profile may be represented by a superposition of sine waves of different wave lengths and amplitudes as a Fourier series. During electropolishing the contributions of the shorter waves disappear more rapidly, and thus the profile approaches a sine wave profile involving the greatest wave length of the original pattern. This is in accord with results reported by Edwards (5, 6).

From equation (XIII) it follows that the displacement, u , for a decrease of the amplitude from b_0 to b is

$$u = a[\ln(b_0/b)]/2\pi. \quad (\text{XIV})$$

The corresponding loss of metal per unit area, $\Delta m/A$, is found to be

$$\Delta m/A = u\rho = a\rho[\ln(b_0/b)]/2\pi \quad (\text{XV})$$

where ρ is the density of the metal.

From a copper electrode having a sine-wave profile with a wave length of 0.0134 cm, which was investigated by Edwards (5, 6), one has therefore to remove 0.013 gram/cm² in order to obtain a

decrease of the amplitude to half the initial value. This value is in accord with results reported by Edwards for the later stages of experiments when his samples had a nearly sine-wave profile.

The corresponding number of coulombs per unit area, equal to the product of current density, J , and time, t , is found to be

$$J(\text{amp/cm}^2)t(\text{sec}) = \frac{96,500 a(\text{cm})\rho(\text{g/cm}^3)}{EqW} \ln \frac{b_0}{b} \quad (\text{XVI})$$

where 96,500 is the numerical value of the Faraday constant in coulomb/equivalent and EqW is the equivalent weight of the metal. For copper, e.g., 96 coulombs are required in order to decrease the amplitude by a factor of 10 if the wave length is 0.01 cm.

The foregoing analysis is that of an ideal electropolishing process. The following complications may occur.

1. If the amplitude, b , is not much smaller than the wave length, a , equation (III) does not satisfy equation (I). Qualitatively, the foregoing conclusions remain valid, but a rigorous mathematical analysis would require the replacement of the one-term expression in equation (III) by a Fourier series.

2. If the wave length, a , is not much smaller than the thickness of the boundary layer, the decrease in amplitude will be less than calculated from equation (XIII). This can be readily recognized from a consideration of the extreme case that the thickness of the wave length of the profile is much greater than the effective thickness of the boundary layer. In this case no differences in the local diffusion rate of the acceptor can be expected. Since according to equation (XIII) electropolishing removes microroughness more rapidly than macroroughness if $a \ll \delta$, the case $a \gtrsim \delta$ is not of great interest, especially when the viscosity of the solution is rather high and, therefore, δ is fairly large, e.g., 0.1 cm.

3. In solutions consisting mainly of perchloric or phosphoric acid, enrichment of salt and depletion of water increase viscosity. Accordingly, the diffusion coefficient may not be constant. Under these conditions, equation (II) has to be replaced by a more involved expression and the foregoing analysis has only qualitative significance.

4. Further complications may be caused by the evolution of gas bubbles and, eventually, local variations of the reactivity of the dissolving metal, especially in the case of heterogeneous alloys so that equation (I) is not satisfied at all points of the surface of the electrode.

INTERPRETATION OF ETCHING

For a comparison, consider the behavior of an anode at which polarization is supposed to be negligible. Then the electrical potential φ along the surface is constant and may be set equal to zero as the reference potential. Using the notation introduced in Fig. 1 and equation (I), we have for a sine-wave profile anode

$$\varphi = 0 \text{ at } y = b \sin(2\pi x/a). \quad (\text{XVII})$$

Inside the electrolyte, the Laplace equation

$$\partial^2\varphi/\partial x^2 + \partial^2\varphi/\partial y^2 = 0 \quad (\text{XVIII})$$

holds. Consequently, we obtain the potential gradient at the surface of the anode in a form analogous to that for the concentration gradient indicated in equation (V),

$$\left(\frac{\partial\varphi}{\partial y}\right)_{y=b \sin(2\pi x/a)} \cong \left(\frac{\partial\varphi}{\partial y}\right)_{\text{avg}} \left[1 + \frac{2\pi b}{a} \sin(2\pi x/a)\right] \quad (\text{XIX})$$

if $b \ll a$, $a \ll \delta$.

The local current density, J , is proportional to the local potential gradient according to Ohm's law. In view of the similarity between equations (V) and (XIX), equations (XIII) to (XVI) will hold if polarization is negligible. Consequently, the amplitude of a given roughness will decrease in the same manner as in the case of diffusion of an acceptor as the factor determining the local dissolution rate. Actually, however, polarization is not negligible. If the wave length a is small in comparison to the parameter k defined as the product of electrical conductivity and the absolute slope of the potential-current density curve, the current density

is far more uniform than according to equation (XVIII) for vanishing polarization (9).

For $a < 0.01$ cm and a current density J lower than the plateau of the J vs. E curve, we have $a \ll k$ and thus we have to expect a practically uniform current density if k is uniform, i.e., the slope of the current density-potential curve is the same at all points of the anode. At different crystallographic faces, however, the magnitude of activation polarization for the anodic dissolution of a metal is different, as is known from investigations involving single crystals (10). This corresponds to local variations of the slope of the current density-potential curve and the parameter k . Thus, different crystallographic faces dissolve at different rates, i.e., we observe electrolytic etching.

Any discussion of this paper will appear in a Discussion Section to be published in the December 1954 issue of the JOURNAL.

REFERENCES

1. P. A. JACQUET, *Bull. soc. chim. France*, (5) **3**, 705 (1936); *Trans. Electrochem. Soc.*, **69**, 629 (1936).
2. I. M. KOLTHOFF AND C. S. MILLER, *J. Am. Chem. Soc.*, **63**, 1405 (1941).
3. W. C. ELMORE, *J. Appl. Phys.*, **10**, 724 (1939); **11**, 797 (1940).
4. H. F. WALTON, *This Journal*, **97**, 219 (1950).
5. J. EDWARDS, *J. Electrodepositors' Tech. Soc.*, **28**, 137 (1952).
6. J. EDWARDS, *This Journal*, **100**, 189C, 223C (1953).
7. L. I. GILBERTSON AND O. M. FORTNER, *Trans. Electrochem. Soc.*, **81**, 199 (1942); D. G. GRAY, *Proc. Am. Electroplaters' Soc.*, **35**, 241 (1948); *Metal Finishing*, **47**, 55 (1949); E. RAUB AND B. WALLHORST, *Die Metalloberflaeche*, **4**, A92 (1949).
8. E. DARMOIS, I. EPELBOIN, AND D. AMINE, *Compt. rend.*, **230**, 386 (1950); **231**, 1222 (1950); I. EPELBOIN, *J. Chim. Phys.*, **49**, C214 (1952).
9. C. WAGNER, *This Journal*, **98**, 116 (1951).
10. A. T. GWATHMEY AND A. F. BENTON, *Trans. Electrochem. Soc.*, **77**, 211 (1940); H. LEIDHEISER AND A. T. GWATHMEY, *Trans. Electrochem. Soc.*, **91**, 95 (1947).

Potentiometric Titration of Simple Salts with Potassium in Liquid Ammonia^{1,2}

GEORGE W. WATT, GREGORY R. CHOPPIN,³ AND JAMES L. HALL⁴

Department of Chemistry, The University of Texas, Austin, Texas

ABSTRACT

By means of potentiometric titration of solutions of salts with solutions of potassium in liquid ammonia at -38° , it has been shown that bismuth(III) iodide is reduced to Bi^0 , K_3Bi_3 , and K_3Bi_5 without intermediation of either the +2 or +1 oxidation state of bismuth. Reduction of iron(II) bromide is very complex and apparently does not involve the intermediate formation of Fe^{+1} . Reduction of potassium nitrate involves only reduction of nitrate ion to nitrite ion, followed by precipitation of potassium hydronitrite. Data relative to reduction of cobalt(II) nitrate have permitted a choice between two possible reduction mechanisms previously proposed. Data presented in this paper clearly demonstrate the usefulness of the potentiometric titration technique in the study of the mechanism of inorganic reduction reactions in ammonia.

INTRODUCTION

In an earlier report (1), equipment and procedures useful in carrying out potentiometric titrations involving solutions of metals in liquid ammonia were described. Subsequently, these techniques have been applied to detection of intermediate oxidation states of Group III nontransitional elements with particular emphasis on aluminum (2-4).

Experiments described in this paper were carried out for the purpose of determining whether the potentiometric titration method might be useful in elucidating the mechanism of reduction of simple inorganic salts with solutions of metals in ammonia. For this purpose, halides and nitrates of two transitional and two nontransitional elements were employed, and the specific cases selected were deliberately ones studied previously by less exacting methods.

EXPERIMENTAL

Materials.—With the exceptions noted below, all materials employed in this work were reagent grade chemicals that were used without further treatment.

Bismuth(III) iodide was prepared in 72% yield by a method described elsewhere (5). Analysis calculated for BiI_3 : Bi, 35.4. Found: Bi, 35.4. X-ray diffraction data for this product are listed in Table I.

¹ Manuscript received July 3, 1953.

² This work was supported in part by the Office of Naval Research, Contract N6onr-26610.

³ E. I. du Pont de Nemours and Company Fellow, 1952-53; present address: Radiation Laboratory, University of California, Berkeley, California.

⁴ Magnolia Petroleum Company Fellow, 1952-53; present address: Department of Chemistry, Michigan State College, East Lansing, Michigan.

Iron(II) bromide (as the 6-ammonate) was prepared as described by Watt and Jenkins (7).

Reagent grade potassium nitrate was recrystallized from water and dried to constant weight at 110°C .

Ammonated cobalt(II) nitrate was prepared by displacement of water of hydration with ammonia by recrystallization from liquid ammonia as follows. Cobalt(II) nitrate 6-hydrate was converted to the corresponding 2-hydrate by drying *in vacuo* over concentrated sulfuric acid. A 1-gram sample of the very finely divided 2-hydrate was placed on the fritted glass disk of a filter tube⁵ and that end of the tube was sealed about 3 in. from the disk. The tube was cooled, inverted, air in the tube was displaced with ammonia gas, the end of the tube containing the salt was immersed in a dry ice-isopropanol bath at -70°C , and 3 to 4 ml of ammonia was condensed on the salt. The open end of the tube was then sealed, also about 3 in. from the filter disk. The tube was removed from the bath and allowed to warm to and remain at room temperature for three days. The saturated solution was then transferred by inverting the tube and immersing the empty end in a refrigerant bath at -70°C . When the temperature of this solution was allowed to return to *ca.* 25° , a small crop of well-defined pink crystals separated. In this manner, transfer of the solution and removal of crystals was repeated until a major portion of the salt had been crystallized from the ammonia solution. In the final transfer, the ammonated salt was retained on the filter disk and the solution was contained in the end containing the original sample. The tube was opened, the ammonia was allowed to

⁵ Ace Glass Company filter tube, porosity B, 10 mm ID.

TABLE I. X-ray diffraction data for bismuth (III) iodide

This work*		Literature†	
d, A	I/I ₁	d, A	I/I ₁
7.03	<0.1	3.25	0.7
5.97	<0.1	3.00	1.0
5.17	0.1	2.53	0.7
3.85	0.2	2.27	0.7
3.32	1.0	2.15	1.0
2.57	0.3	2.07	0.9
2.19	0.4	1.96	0.9
1.98	0.1	1.87	1.0
1.83	0.1	1.81	1.0
1.66	<0.1	1.29	0.7
1.40	0.1	1.25	0.7
1.36	0.1	1.10	0.7
1.32	0.1	1.09	0.7
1.07	<0.1	1.03	0.7
		1.02	0.7‡

* Data obtained using Cu K_α radiation, Ni filter, 30-kv tube voltage, 15-ma filament current, and 4-hr exposure.

† These data are taken from the ASTM Index of X-ray Diffraction Patterns and are attributed to Caglioti (6). Lack of agreement between our data and those of Caglioti is obvious and it is concluded that his data are in error since both interplanar spacing and relative intensity data for several different samples prepared in connection with the present work were in excellent agreement. More recently, in entirely independent experiments, these data have been confirmed by Phillip S. Gentile of this laboratory.

‡ Spacings corresponding to relative intensities <0.7 are not included.

evaporate, residual ammonia was displaced with dry, oxygen-free nitrogen, and the tube was transferred to a dry box wherein all subsequent sampling of the ammoniated salt was done in an atmosphere of nitrogen. Analysis: calculated for Co(NO₃)₂·6NH₃: Co, 20.6; NH₃, 35.8; calculated for Co(NO₃)₂·5NH₃: Co, 22.0; NH₃, 31.7. Found: Co, 20.0; NH₃, 33.0. The composition indicated by these data is Co(NO₃)₂·5.7NH₃.

Experimental methods.—With but one exception, equipment and methods used in this work were substantially the same as those described earlier (1). In a typical case, the solution to be titrated consisted of the salt in question dissolved in anhydrous liquid ammonia. Into this solution was immersed a platinum reference electrode and a differential electrode comprising a platinum wire immersed in a solution having the same composition as the solution to be titrated, and connected to the main body of this solution by means of a capillary tube. The differential electrode was connected to the positive terminal of the potentiometer.

The exception referred to above was concerned with titrations involving nitrate solutions. For these, a reference electrode comprising the half-cell: Cu; Cu(NO₃)₂0.1N, KNO₃ (satd.), of the type used by Pleskov and Monosohn (8) was employed. This

change was incorporated when use of the usual platinum reference electrode gave anomalous results that are currently being further investigated.

The alkali metal used was potassium in all cases, and the titrations were carried out at $-38 \pm 1^\circ\text{C}$. *Bismuth(III) iodide.*—In a typical experiment, a solution of 0.2298 gram of bismuth(III) iodide in 40 ml of liquid ammonia was titrated with a 0.0975N potassium solution. A black precipitate formed upon the first addition of potassium solution, and the reaction mixture assumed a purple color after addition of 17 ml of potassium solution. Total time required for this particular titration was 12 hr; data are shown in Fig. 1. In other titrations that differed only with respect to concentrations of reactants used, somewhat different results were obtained. For example, titration of 0.3485 gram of bismuth(III) iodide in 46 ml of ammonia with 0.0773N potassium solution over a period of 7 hr gave the data shown in Fig. 2. Results of the type shown in Fig. 1 and 2 were confirmed both with and without the use of potassium iodide as a supporting electrolyte.

In a related case, 0.0410 gram of potassium dissolved in 50 ml of liquid ammonia was titrated with a saturated solution of bismuth(III) iodide in liquid ammonia (0.2574 gram BiI₃ in 51.0 ml NH₃). Use of these conditions was dictated by limitations imposed by the capacity of available equipment and by solubility relationships; as a consequence, results

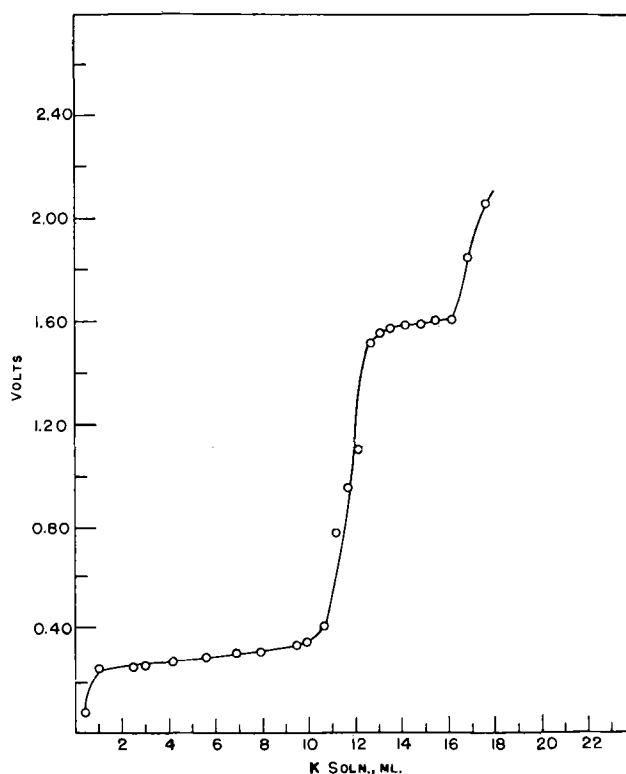


FIG. 1. Potentiometric titration: bismuth(III) iodide with potassium.

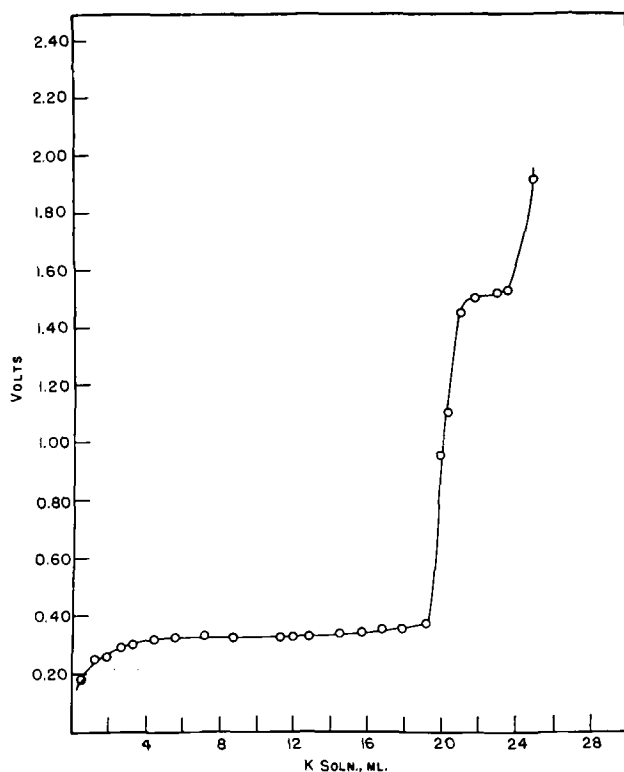


FIG. 2. Potentiometric titration: bismuth(III) iodide with potassium.

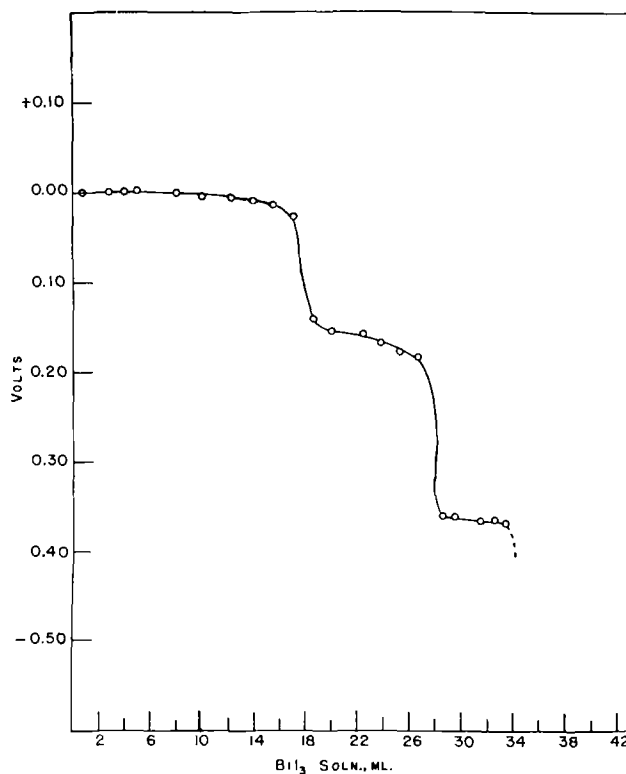


FIG. 3. Potentiometric titration: potassium with bismuth(III) iodide.

must be interpreted on the basis of internal agreement rather than on an absolute basis. Complete titration required 7 hr; data are given in Fig. 3. The characteristic blue color of potassium solution was replaced by a distinct purple color after addition of 18.3 ml of saturated bismuth(III) iodide solution. After 33 ml had been added, the purple color decreased in intensity and the presence of a black precipitate was observed.

Iron(II) bromide.—Iron(II) bromide 6-ammonate (0.0917 gram) in 50 ml of liquid ammonia was titrated with 0.0449*N* potassium solution over a period of 6 hr. Early stages of the titration were characterized by erratic emf values; after 8.3 ml of potassium solution had been added, a progressive, but at no time abrupt, increase in potential began and amounted to a total change of 700 mv by the time 15.9 ml of potassium solution had been added. The characteristic blue color of potassium solution was not observed, even though an excess of almost two gram-atoms of potassium/mole of bromide was added.

Potassium nitrate.—A solution of 0.0332 gram of potassium nitrate in 45 ml of liquid ammonia was titrated with 0.0969*N* potassium solution. As titration proceeded over a period of 29 hr, the solution became yellowish-green in color, then intensely green, and finally a yellow precipitate formed. The titration curve is shown in Fig. 4.

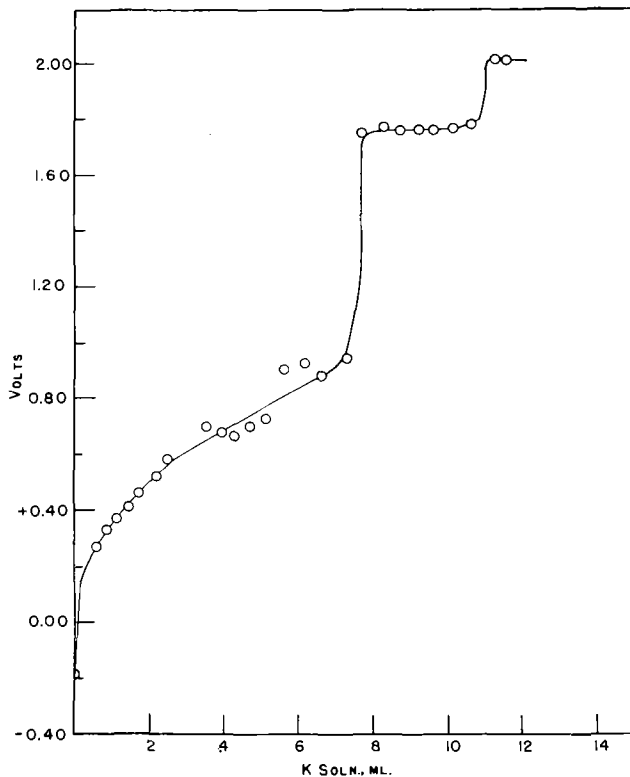


FIG. 4. Potentiometric titration: potassium nitrate with potassium.

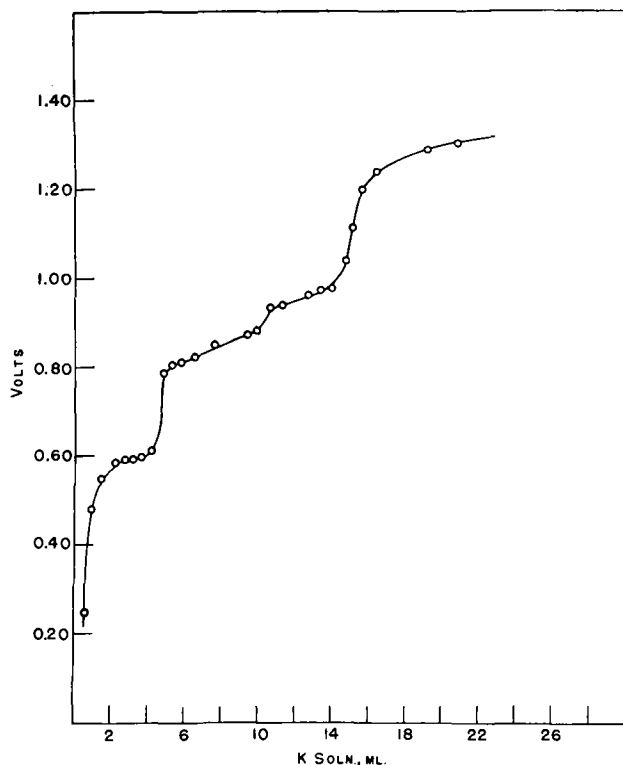


FIG. 5. Potentiometric titration: cobalt(II) nitrate with potassium.

Cobalt(II) nitrate.—An ammonate (0.0602 gram) corresponding to the composition $\text{Co}(\text{NO}_3)_2 \cdot 5.4\text{NH}_3$ dissolved in 46 ml of liquid ammonia was titrated with 0.0868*N* potassium solution. The initially pink solution became green in color and a black precipitate formed concurrently. A total of 21 ml of potassium solution was added over a period of 13 hr; the final reaction mixture consisted of a black precipitate and a greenish-yellow supernatant solution. Data are given in Fig. 5.

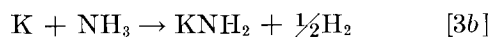
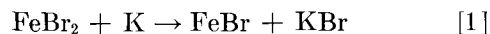
DISCUSSION

Titration involving bismuth(III) iodide and potassium were carried out for the twofold purpose of attempting to detect the formation of Bi^{2+} and/or Bi^+ and to clear up uncertainties in the results reported by Zintl and coworkers (9). In the reaction corresponding to Fig. 1, changes in potential occurred only upon addition of 12.0 and 16.5 ml of potassium solution; these values are to be compared with 12.0 and 16.0 ml calculated on the assumption of formation of Bi^0 and K_3Bi_3 , respectively. Thus, the first reaction observed is the three-electron change resulting in precipitation of elemental bismuth, and there is no indication of intermediation of the +2 and +1 oxidation states of bismuth. Fig. 1 shows clearly the formation of the polybismuthide K_3Bi_3 , but not the intermediate species K_3Bi_5 . In

contrast, data of Fig. 2 show formation of Bi^0 and K_3Bi_5 upon addition of 20.4 and 24.6 ml of potassium solution. The corresponding calculated values are 20.4 and 24.5 ml. Zintl and coworkers (9) titrated bismuth(III) iodide with sodium solutions at -60° and reported evidence for the formation of Na_3Bi , Na_3Bi_3 , and Na_3Bi_5 , although their evidence for the latter was admittedly inconclusive. While results of the present study are in reasonable agreement with those of Zintl and coworkers, it has been demonstrated that K_3Bi_3 may be formed without intermediation of K_3Bi_5 which exhibits an intense brown color in liquid ammonia solution; this color was not observed during the course of titration represented by Fig. 1. While the present work provides much more conclusive evidence for the existence of bismuthides of the type M_3Bi_5 (where M is an alkali metal), it is still not clear why these species are not formed in all cases. Zintl and coworkers suggested that the course of these reactions may be strongly dependent upon concentration, but the range of concentrations employed in the present work appears to rule out this explanation.

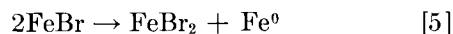
When potassium in liquid ammonia was titrated with saturated bismuth(III) iodide solution, the results obtained were in good agreement with comparable data for corresponding reactions with sodium (9). Marked changes in potential occurred after addition of 17.8, 28.2, and 34.0 ml of bismuth(III) iodide solution as compared with calculated values of 17.8, 26.7, and 35.6 ml corresponding to the formation of K_3Bi , K_3Bi_3 , and Bi^0 , respectively. For reasons indicated previously, the latter values were calculated on the basis of the volume of iodide solution required for formation of K_3Bi ; this end point is visually detectable. Titrations of this type gave no evidence for the formation of K_3Bi_5 .

Study of the reduction of iron(II) bromide was prompted by the desire to obtain evidence for the existence of Fe^+ in liquid ammonia solution. It has been shown previously (10) that principal products of this reaction are elemental iron and iron(I) nitride. The latter may arise from the following sequence of reactions.



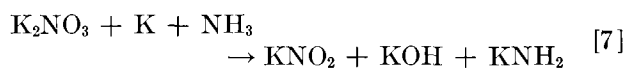
Iron(I) nitride most probably is formed by the deammonation of iron(I) amide which as indicated above may result from either ammonolysis of iron(I) bromide or from reaction between iron(I) bromide and potassium amide. In either case, the reduction of Fe^{+2} to Fe^{+1} must be postulated, and it was therefore considered worthwhile to attempt to obtain evidence for the existence of Fe^{+1} under these conditions.

In view of the immediate precipitation of elemental iron and the concurrent evolution of hydrogen (10), it follows that if iron(I) amide arises via reactions [1], [2], and [3a], competitive reactions with subsequently added potassium would involve reactions [1], [2], [3b], and the interaction of potassium with the ammonium bromide formed in [3a]. Of these, the latter and [3b] would probably proceed at the greatest rate. It is not surprising, therefore, that erratic potentials were observed in the early states of the titration. Although Fe^0 may, of course, result from the direct two-electron reaction with Fe^{+2} , there is an alternative mechanism that provides for both the precipitation of Fe^0 and at least the transitory existence of Fe^{+1} , i.e., reaction [1] followed by disproportionation,

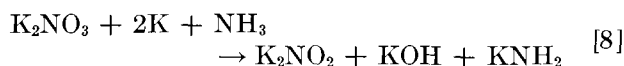


Thus, after formation of sufficient Fe^0 to catalyze [3b], the latter reaction would compete with the probably slow reaction [5].

Reduction of both alkali metal nitrates and nitrites to "hydronitrites" of the type M_2NO_2 has been observed previously (11-13) but only in terms of the identity of the initial and final substances. Formation of K_2NO_2 from KNO_3 , for example, may follow the course,

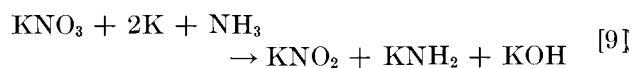


or,

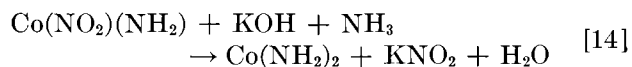
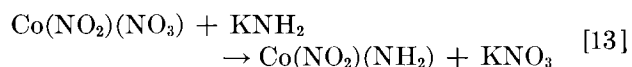
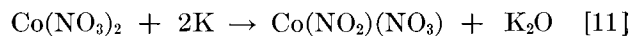


As shown in Fig. 4, however, changes in potential corresponding only to two- and three-electron changes were observed, i.e., upon addition of 7.4 and 10.9 ml of potassium solution, as compared with calculated values of 7.5 and 11.2 ml. Hence, it appears that the formation of K_2NO_3 as an intermediate does

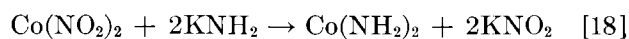
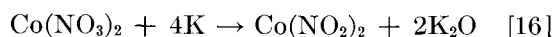
not occur and that the only reactions that take place are,



Watt and Keenan (14) suggested that reduction of cobalt(II) nitrate with potassium in ammonia may follow the course,



or alternatively,



Both mechanisms were compatible with their experimental data, but the methods employed did not lead to data that would permit a choice between the two.

From the data of Fig. 5 it is evident that significant changes in potential occur after addition of volumes of potassium solution corresponding to 2, 4, and 6 gram-atoms of potassium/mole of cobalt(II) nitrate. That the reaction must follow the path suggested by equations [11] to [15] rather than [16] is strongly indicated by the occurrence of a marked change in potential after addition of two equivalents of potassium. Further evidence in favor of the first mechanism is found in the fact that the plateau at 0.8 volt (Fig. 5) is in agreement with that for the reduction of nitrate ion to nitrite ion found in the reduction of potassium nitrate (Fig. 4). The last of the three observed changes in potential [i.e., that which corresponds to 6 gram-atoms of potassium/mole of cobalt(II) nitrate] is attributable to the previously observed (14) and relatively slow reduction of cobalt(II) amide to elemental cobalt.

Any discussion of this paper will appear in a Discussion Section, to be published in the December 1954 issue of the JOURNAL.

REFERENCES

1. G. W. WATT AND J. B. OTTO, JR., *This Journal*, **98**, 1 (1951).

2. G. W. WATT, J. L. HALL, AND G. R. CHOPPIN, *J. Am. Chem. Soc.*, **73**, 5920 (1951).
3. G. W. WATT, J. L. HALL, AND G. R. CHOPPIN, *J. Phys. Chem.*, **57**, 567 (1953).
4. G. W. WATT AND J. L. HALL, Unpublished work.
5. G. W. WATT, W. W. HAKKI, AND G. R. CHOPPIN, "Inorganic Syntheses," Vol. IV, McGraw-Hill Book Co., Inc., New York, In press.
6. V. CAGLIOTI, *Gazz. chim. ital.*, **60**, 935 (1930).
7. G. W. WATT AND W. A. JENKINS, JR., "Inorganic Syntheses," Vol. IV, McGraw-Hill Book Co., Inc., New York, In press.
8. V. A. PLESKOV AND A. M. MONOSSOHN, *Acta Physicochim. U.R.S.S.*, **1**, 871 (1935).
9. E. ZINTL, J. GOUBEAU, AND W. DULLENKOPF, *Z. physik. Chem.*, **A154**, 1 (1931).
10. G. W. WATT AND W. A. JENKINS, JR., *J. Am. Chem. Soc.*, **73**, 3275 (1951).
11. E. B. MAXTED, *J. Chem. Soc.*, **111**, 1016 (1917).
12. E. ZINTL AND O. KOHN, *Ber.*, **61B**, 189, 2063 (1928).
13. W. M. BURGESS AND F. R. HOLDEN, *J. Am. Chem. Soc.*, **59**, 459 (1937).
14. G. W. WATT AND C. W. KEENAN, *ibid.*, **74**, 2048 (1952).

FUTURE MEETINGS OF The Electrochemical Society



Chicago, May 2, 3, 4, 5, and 6, 1954

Sessions on

Electric Insulation, Electronics, Electro-Organic
Chemistry, Industrial Electrolytics, Theoretical
Electrochemistry

Headquarters at the La Salle Hotel

★ ★ ★

Boston, October 3, 4, 5, 6, and 7, 1954

Headquarters at the Statler Hotel

★ ★ ★

Cincinnati, May 2, 3, 4, and 5, 1955

Headquarters at the Sheraton-Gibson Hotel

★ ★ ★

Pittsburgh, October 9, 10, 11, 12, and 13, 1955

Headquarters at the William Penn Hotel

Papers are now being accepted for the meeting to be held in Boston. Five copies of each abstract (not exceeding 75 words in length) are due at the Secretary's Office, 216 West 102nd Street, New York 25, N. Y., *not later than July 15, 1954*. Complete manuscripts should be sent in triplicate to the Managing Editor of the JOURNAL at the same address.

an important

Since its earliest days the fluorescent lamp industry has made astounding progress in both commercial production and technology. In about 1938, the first commercial fluorescent lamp was marketed. Production in 1945 was 37 million lamps, in 1951 — 110 million and has averaged about 90 million per year over the last three years.

When the industry was very young the average life rating of a fluorescent lamp was only 100 hours, and efficiency was extremely low. By 1948 life rating had been increased to approximately 3000 hours, but the efficiency drop was as much as 40% after only 1000 hours. Furthermore, some of the early phosphors were undesirably toxic.

Faced with the problems of increasing lamp life and efficiency, and eliminating the hazards of toxic phosphors, scientists and engineers in the industry came up with a phosphor which was both safe and remained 90% efficient after a 3000 hour life test—a halo-phosphate phosphor.

Manufacturing a halo-phosphate phosphor, however, was a problem. The pure calcium phosphate needed to make it was not commercially available. This phase of the problem was brought to Mallinckrodt because of its outstanding record and experience in producing high purity chemicals. Mallinckrodt has supplied the industry with chemicals, some with impurity tolerances as low as one part per million.

Could Mallinckrodt produce a calcium phosphate of exceptional purity and uniformity — in a hurry?

Mallinckrodt's versatile and experienced technical staff went to work and successful



MALLINCKRODT CHEMICAL WORKS

Mallinckrodt Street, St. Louis 7, Mo .

72 Gold Street, New York 8, N. Y.

Chicago • Cincinnati • Cleveland • Los Angeles

Philadelphia • San Francisco • Montreal • Toronto

American industry

... and the role  played
in its growth

laboratory samples were produced in a matter of days. Dependable delivery of substantial quantities began *within a month* after the laboratory samples were approved. Once again Mallinckrodt proved its ability to provide the electronics industry with *enough* of the right chemical, precision processed to the exact consistent degree of purity and proper physical form — *at the right time*.

Since the industry's inception constant progress has been made. The efficiency of fluorescent lamps has been steadily improved. Lamp life of more than 5000 hours is now commonplace.

Through these years Mallinckrodt has worked closely with the electronics industry. Many carloads of dibasic calcium phosphate and other Mallinckrodt electronic chemicals have been produced, and Mallinckrodt has progressively widened its service to the electronics industry.

This experience and ability to produce precision chemicals so essential in the electronics industry are important facts to remember. *The next time you have a question, a problem, or a need for the purest chemicals available, write or talk to Mallinckrodt.*

Millions of pounds of
Mallinckrodt Standard Luminescent Chemicals
have been manufactured
to the exacting specifications of the
Electronics Industry.

A few of the many

**Mallinckrodt
Chemicals** for the
**Electronics
Industry . . .**

Acid Silicic
Barium Acetate
Barium Carbonate
Barium Nitrate
Cadmium Chloride
Cadmium Sulfate
Calcium Carbonate
Calcium Fluoride
Calcium Nitrate
Calcium Phosphate Dibasic
Ether Anhydrous
Magnesium Carbonate
Manganese Carbonate
Strontium Nitrate
Zinc Oxide

Divisions of the Society

Battery

EUGENE WILLIHNGANZ, Chairman
N. C. CAHOON, Vice-Chairman
E. J. RITCHIE, Sec.-Treas.
The Eagle-Picher Company
Joplin, Mo.

Corrosion

W. D. ROBERTSON, Chairman
J. V. PETROCELLI, Vice-Chairman
C. V. KING, Sec.-Treas.
Dept. of Chemistry
New York University
New York, N. Y.

Electric Insulation

R. A. RUSCETTA, Chairman
A. GUNZENHAUSER, Vice-Chairman
L. L. DEER, Sec.-Treas.
U. S. Naval Ordnance Plant
Indianapolis, Ind.

Electrodeposition

M. L. HOLT, Chairman
C. A. SNAVELY, Vice-Chairman
SIDNEY BARNARTT, Sec.-Treas.
Westinghouse Research Labs.
East Pittsburgh, Pa.

Electronics

R. H. CHERRY, Chairman
J. H. SCHULMAN, Vice-Chairman
A. U. SEYBOLT, Vice-Chairman
A. E. HARDY, Vice-Chairman
C. W. JEROME, Sec.-Treas.
Sylvania Electric Products Inc.
Salem, Mass.

Electro-Organic

C. L. WILSON, Chairman
H. M. SCHOLBERG, Vice-Chairman
STANLEY WAWZONEK, Sec.-Treas.
State University of Iowa
Iowa City, Iowa

Electrothermic

I. E. CAMPBELL, Chairman
J. S. DEWAR, Vice-Chairman
A. C. HASKELL, JR., Sec.-Treas.
Battelle Memorial Institute
Columbus, Ohio

Industrial Electrolytic

F. W. KOERKER, Chairman
A. R. ORBAN, Vice-Chairman
MILTON JAMES, Sec.-Treas.
National Carbon Company
Cleveland, Ohio

Theoretical Electrochemistry

J. P. FUGASSI, Chairman
E. B. YEAGER, Vice-Chairman
P. DELAHAY, Sec.-Treas.
Dept. of Chemistry
Louisiana State University
Baton Rouge, La.

Local Sections of the Society

Chicago

SIMON P. GARY, Chairman
HOWARD T. FRANCIS, Vice-Chairman
WERNER JACOBSON, Treasurer
A. ROEBUCK, Secretary
Argonne National Laboratories
Lemont, Illinois

Cleveland

N. C. CAHOON, Chairman
ERNEST B. YEAGER, Vice-Chairman
W. H. STOLL, Treasurer
MERLE E. SIBERT, Secretary
Horizons, Inc.
2891 East 79th Street
Cleveland, Ohio

Detroit

GLENN COLEY, Chairman
DAN TRIVICH, 1st Vice-Chairman
WRIGHT WILSON, 2nd Vice-Chairman
GERALD V. KINGSLEY, Sec.-Treas.
12083 Ward Avenue
Detroit, Mich.

Midland

W. R. PERRY, Chairman
F. N. ALQUIST, Vice-Chairman
M. P. NEIPERT, Sec.-Treas.
The Dow Chemical Company
Midland, Mich.

New York Metropolitan

HERBERT BANDES, Chairman
MARTIN F. QUAELEY, Vice-Chairman
KENNETH B. McCAIN, Sec.-Treas.
Wilbur B. Driver Company
150 Riverside Ave.
Newark, N. J.

Niagara Falls

HARRY R. OSWALD, Chairman
WARREN D. SHERROW, Vice-Chairman
JOHN E. CURREY, Sec.-Treas.
Hooker Electrochemical Company
Niagara Falls, N. Y.

Pacific Northwest

GLEN C. WARE, Chairman
JOSEPH B. HEITMAN, Vice-Chairman
G. H. KISSIN, Sec.-Treas.
Kaiser Aluminum and Chemical Corp.
Spokane, Wash.

Philadelphia

J. FRED HAZEL, Chairman
EDGAR L. ECKFELDT, Vice-Chairman
G. FRANKLIN TEMPLE, Treasurer
GEORGE W. BODAMER, Secretary
Rohm & Haas Company
Philadelphia, Pa.

Pittsburgh

M. T. SIMNAD, Chairman
R. D. WILLIAMS, Vice-Chairman
ROBERT A. WOOFER, Sec.-Treas.
Jones & Laughlin Steel Corp.
Pittsburgh, Pa.

San Francisco

R. F. BECHTOLD, Chairman
C. W. TOBIAS, Vice-Chairman
H. F. MYERS, Sec.-Treas.
Columbia Steel Company
Pittsburg, Calif.

Washington-Baltimore

SAMUEL EIDENSOHN, Chairman
D. T. FERRELL, JR., Vice-Chairman
FIELDING OGBURN, Sec.-Treas.
9607 Riley Place
Silver Spring, Md.

India

M. S. THACKER, Chairman
V. M. DOKRAS, Vice-Chairman
S. RAMASWAMY, 2nd Vice-Chairman
J. BALACHANDRA, Sec.-Treas.
Indian Institute of Science
Bangalore, India

Potentiometric Titration of Ammines of Rhodium, Iridium, and Platinum with Solutions of Potassium and Potassium Amide in Liquid Ammonia^{1,2}

GEORGE W. WATT, GREGORY R. CHOPPIN,³ AND JAMES L. HALL⁴

Department of Chemistry, The University of Texas, Austin, Texas

ABSTRACT

Potentiometric titration of tetrammineplatinum(II) bromide with potassium in liquid ammonia at -38°C shows that reduction of this salt to an ammine of platinum(0) is exactly a two-electron change and that the +1 oxidation state of platinum is not an intermediate. Similar reduction of bromopentammineiridium(III) bromide is apparently more complex and leads to observed changes in potential that do not correspond to any reasonable or probable reactions. Titration of this same iridium salt with potassium amide solution, however, provides evidence for stepwise replacement of bromine by amido groups followed by conversion of the resultant iridium(III) amide to (probably) a potassium amidoiridate(III). Bromopentamminerhodium(III) bromide and potassium amide react similarly, but only to and including the formation of rhodium(III) amide.

INTRODUCTION

In previous papers from this laboratory, development of a method for carrying out potentiometric titrations in liquid ammonia and use of this method in the study of unusual oxidation states and reduction reaction mechanisms have been described (1). This paper is concerned with similar studies involving reduction of ammines of certain transitional metal bromides with solutions of potassium in ammonia. In addition, two reactions in which liquid ammonia solutions of potassium amide were used as titrant are described; the course of reactions of this type has not previously been followed potentiometrically.

EXPERIMENTAL

Experimental details were in all respects analogous to those described earlier (1). In all cases reported in this paper, anhydrous liquid ammonia solutions that were titrated with either standard potassium or standard potassium amide solutions contained not only the ammine bromide of interest but also a suitable supporting electrolyte. The two electrodes consisted of a platinum reference electrode and a differential electrode of the type used previously (1, 5).

¹ Manuscript received July 8, 1953.

² This work was supported in part by the Office of Naval Research, Contract N6onr-26610.

³ E. I. du Pont de Nemours and Company Fellow, 1952-53; present address: Radiation Laboratory, University of California, Berkeley, California.

⁴ Magnolia Petroleum Company Fellow, 1952-53; present address: Department of Chemistry, Michigan State College, East Lansing, Michigan.

The differential electrode, which was connected to the positive terminal of the potentiometer, consisted of a platinum wire immersed in a solution having a composition the same as that of the solution to be titrated, and was connected to the main body of the latter solution via a fine capillary tube.

Appropriate ammine bromides of rhodium (2), iridium (3), and platinum (4) were prepared and characterized by methods described elsewhere.

Titration of tetrammineplatinum(II) bromide with potassium.—Preliminary experiments showed that adequately sensitive potentiometer readings could be obtained only through use of a supporting electrolyte. Accordingly, 0.1217 gram of $[\text{Pt}(\text{NH}_3)_4]\text{Br}_2$ and 0.10 gram of potassium bromide, both dissolved in 40 ml of liquid ammonia, were titrated with 0.0506*N* potassium solution over a period of 9 hr. The initially clear solution became progressively darker in color until near the end of titration, whereupon intensity of the color decreased relatively rapidly and the presence of a pale yellow precipitate was observed. Addition of a considerable excess of potassium failed to produce either the blue color characteristic of solutions of alkali metals in ammonia or the potential anticipated for an ammonia solution of potassium amide. The data are shown in Fig. 1.

Titration of trans-diammineplatinum(II) bromide with potassium.—Potentiometric titrations involving these two reactants gave results substantially identical with those in Fig. 1.

Titration of bromopentammineiridium(III) bromide with potassium.—In a typical case, 0.1114 gram of $[\text{Ir}(\text{NH}_3)_5\text{Br}]\text{Br}_2$ and 0.15 gram of potassium bromide in 70 ml of liquid ammonia was titrated with

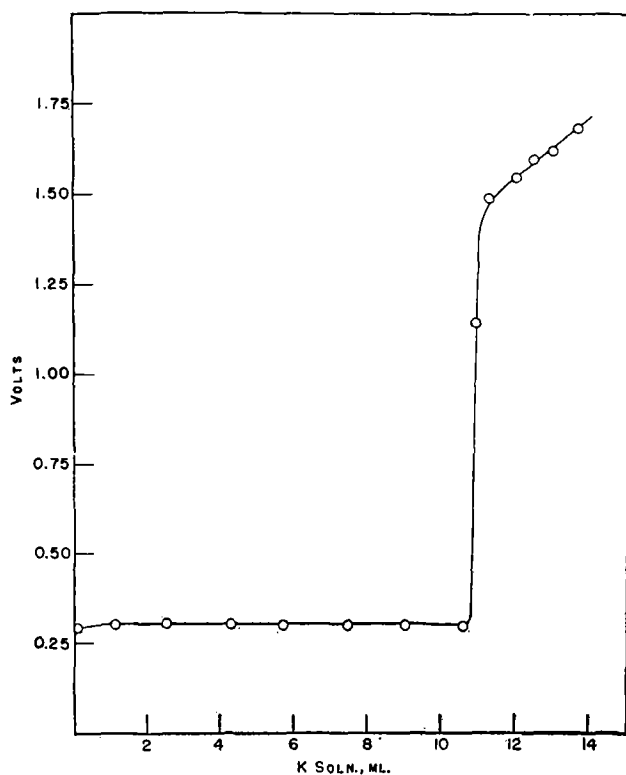


FIG. 1. Potentiometric titration: tetrammineplatinum(II) bromide with potassium.

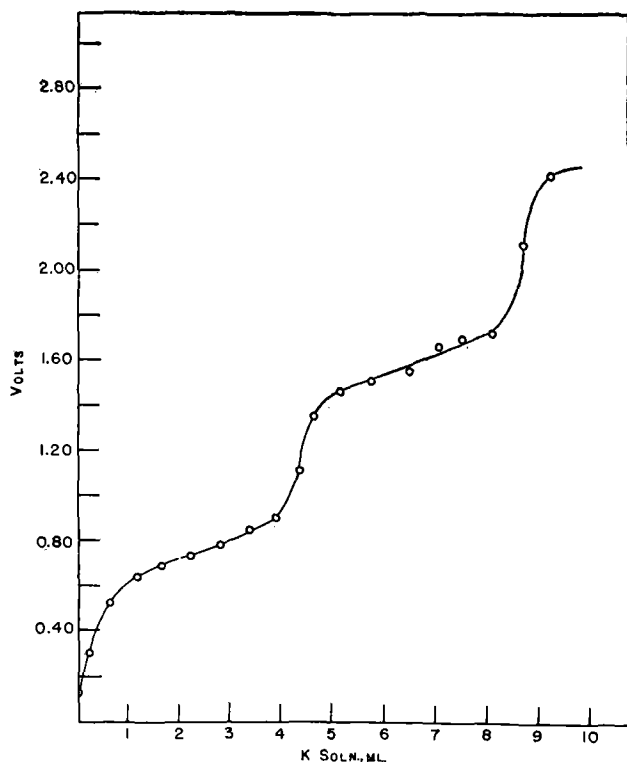


FIG. 2. Potentiometric titration: bromopentammineiridium(III) bromide with potassium.

0.0663*N* potassium solution (time, 14 hr). A precipitate formed slowly, and the blue color of the potassium solution was discharged rapidly during approximately the first half of the titration. Thereafter, rate

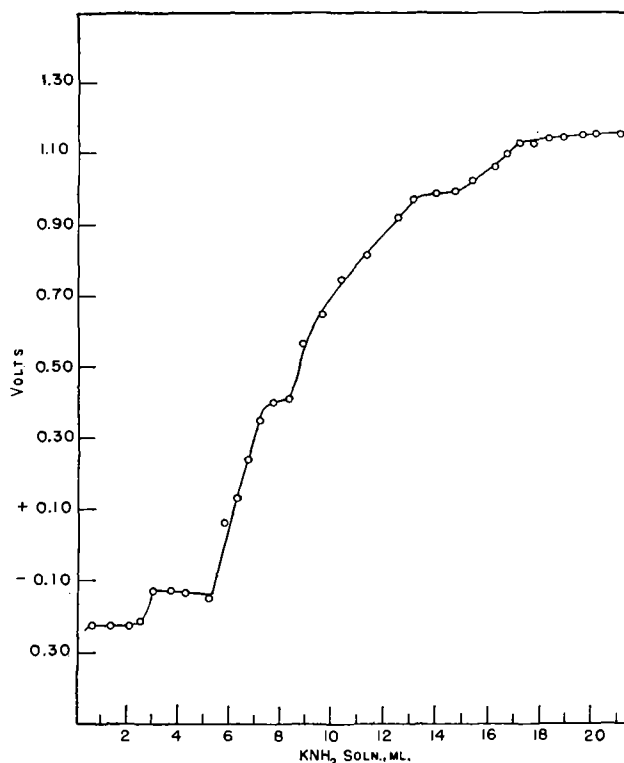


FIG. 3. Potentiometric titration: bromopentammineiridium(III) bromide with potassium amide.

of reaction decreased markedly, the presence of a cream colored precipitate was observed, and equilibrium was re-established relatively slowly after each addition of potassium solution. The blue color of the potassium solution persisted after addition of a total of 9.4 ml. The data are shown in Fig. 2.

Titration of bromopentammineiridium(III) bromide with potassium amide.—A solution of 0.125 gram of potassium bromide and 0.0931 gram of $[\text{Ir}(\text{NH}_3)_5\text{Br}]\text{Br}_2$ in 50 ml of liquid ammonia was titrated with 0.0605*N* potassium amide solution over a period of 20 hr (Fig. 3). The amide solution was prepared by interaction of potassium and liquid ammonia in the presence of an iron wire catalyst in the vessel ordinarily used for preparation of standard alkali metal solutions (5). A white finely divided precipitate was observed after addition of 4.2 ml of potassium amide solution, and the following solution colors were observed upon addition of the indicated volumes of titrant: 0, colorless; 7.0, yellow; 14, orange; 16.7, bronze.

Titration of bromopentammineiridium(III) bromide with potassium amide.—In an experiment of the type described above, a solution of 0.91 gram of potassium bromide and 0.0433 gram of $[\text{Rh}(\text{NH}_3)_5\text{Br}]\text{Br}_2$ in 70 ml of liquid ammonia was titrated with 0.0266*N* potassium amide solution (time, 8 hr). Resulting data are given in Fig. 4. The intensity of color of the initially pale yellow solution decreased during addition of 6.5 ml of the amide solution, whereupon there appeared a turbidity that persisted until 10.0 ml had

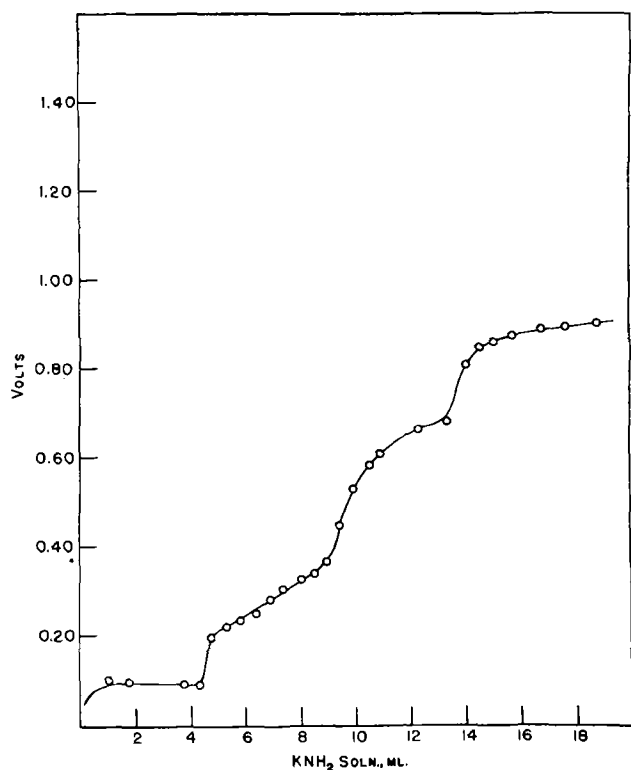


FIG. 4. Potentiometric titration: bromopentamminerhodium(III) bromide with potassium amide.

been added. Thereafter, the solution became progressively more intensely green in color until 14 ml had been added and the solution color began to change from green to yellow-green.

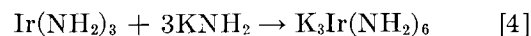
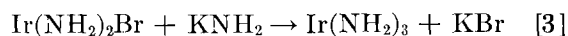
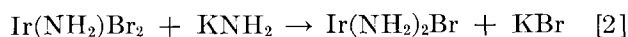
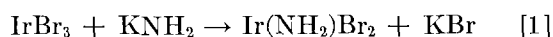
DISCUSSION

In studies leading to the conclusion that reduction of tetrammineplatinum(II) bromide with potassium in ammonia produces an ammine of platinum in the zero oxidation state (4), it became necessary to establish exactly the reaction ratio involved. Titrations of the type shown in Fig. 1 were carried out for this purpose and also with a view to determining whether this reaction proceeds via a single two-electron reaction or two consecutive one-electron changes. It is evident from Fig. 1 that intermediation of the +1 oxidation state is not involved and that reduction of one mole of the bromide requires exactly two gram-atoms of potassium. An increase in potential of the order of 1.3 volts occurred sharply upon addition of 11.0 ml of potassium solution; the volume calculated on the assumption of a two-electron change is 11.3 ml. That substantially identical results were obtained in titrations involving transdiammineplatinum(II) bromide is consistent with the fact that the trans-isomer is slowly converted to the tetrammine in liquid ammonia at its boiling temperature (4).

In several titrations of bromopentammineiridium-

(III) bromide with potassium, changes in potential that apparently may not be correlated with any anticipated stoichiometry were observed. With reference to Fig. 2, for example, the increases in potential that occurred upon addition of 4.5 and 8.5 ml of potassium solution are to be compared with 6.5 and 9.7 ml calculated on the assumption of reduction of Ir^{+3} to Ir^{+1} and its subsequent reduction to Ir^0 . Similarly, change in potential (and appearance of a permanent blue color) corresponding to complete reduction of Ir^{+3} to Ir^0 was also premature in all cases, and since different and authentic samples of the bromide were employed, these results cannot be attributed to impure starting materials. It is possible to postulate a mechanism in which it is assumed that Ir^{+3} is reduced to Ir^{+1} which in turn reduces Ir^{+3} to Ir^{+2} and the latter is reduced to Ir^0 upon further addition of potassium solution. If it is further assumed that (owing to competitive rates that may be involved) one-third of the Ir^{+1} is ammonolyzed to iridium(I) amide, then it may be shown that the observed changes in potential are almost exactly those to be anticipated under such conditions. This requires, however, that iridium(I) amide be stable in the presence of subsequently added potassium solution and that it constitute one of the final products. This is clearly incompatible with other data relative to the identification of pentammineiridium-(0) as the end product (3).

Changes in potential that are shown in Fig. 3 and that result from addition of 2.8, 5.8, 8.6, and 17.2 ml of potassium amide solution (calculated: 3.0, 6.0, 8.9, and 17.8 ml) apparently correspond to the reactions (coordinated ammonia omitted),



or,



This interpretation is further supported by the fact that iridium(III) amide has been isolated (in the form of the 1-ammonate) as the only ammonia-insoluble product of the interaction of the bromide and potassium amide in a $\frac{1}{3}$ mole ratio (3). Neither the present nor previous work (3) permits a choice between alternatives suggested by equations [4] and [4a].

From data shown in Fig. 4, it is apparent that reactions between bromopentammineiridium(III) bromide and potassium amide are strictly analogous to those with the corresponding iridium compound,

i.e., equations [1] to [3], inclusive, except for the fact that rhodium(III) amide is not converted to a soluble species by action of excess potassium amide, i.e., rhodium(III) amide is less amphoteric than iridium(III) amide. Rhodium(III) amide has been independently isolated and characterized (2). Attention should be called to the fact that the volumes of potassium amide solution corresponding to the changes in potential shown in Fig. 4, i.e., 4.6, 9.5, and 14.0 ml, are higher than calculated volumes based on concentration of the potassium amide solution used, i.e., 3.8, 7.6, and 11.4 ml. However, if the final increase in potential is taken as evidence for the formation of rhodium(III) amide, which is reasonable in the light of other available evidence (2), then the

two preceding changes in potential should occur upon addition of 4.7 and 9.3 ml.

Any discussion of this paper will appear in a Discussion Section, to be published in the December 1954 issue of the JOURNAL.

REFERENCES

1. G. W. WATT, G. R. CHOPPIN, AND J. L. HALL, *This Journal*, **101**, 229 (1954).
2. G. W. WATT, W. A. JENKINS, JR., AND A. BROODO, To be published.
3. G. W. WATT AND P. I. MAYFIELD, *J. Am. Chem. Soc.*, **75**, 6178 (1953).
4. G. W. WATT, M. T. WALLING, JR., AND P. I. MAYFIELD, *ibid.*, **75**, 6175 (1953).
5. G. W. WATT AND J. B. OTTO, JR., *This Journal*, **98**, 1 (1951).

Adherence of Electrodeposited Zinc to Aluminum Cathodes¹

F. H. C. KELLY

University of Tasmania, Hobart, Tasmania, Australia

ABSTRACT

An apparatus for measuring the adherence of zinc electrodeposited from acid zinc sulfate solutions on aluminum cathodes is described. Adherence was recognized as "sheet" or "spot" behavior. Chloride favored increase in sheet adherence and fluoride ion favored spot adherence. Mechanical, thermal, and electrolytic treatments of cathode surface as well as chemical composition of electrolyte were investigated. There was no correlation between surface roughness and adherence. Smaller aluminum crystals in the cathode surface favored stronger adherence.

The first stage of deposition was development of ovoid particles 8 x 5 microns, increasing in number until a complete sheet was obtained. Such particles preferred to develop at sharp points and crystal boundaries. Rupture of interface was observed microscopically in the aluminum surface. Zinc diffused into cathode with time, but aluminum on the surface of the zinc electrodeposit was attributed to fracture in aluminum during stripping. Mechanism of adherence was explained as an attachment at a varying number of active spots rather than by mechanical anchoring.

INTRODUCTION

In the commercial production of zinc by electrolysis, low adherence to an aluminum cathode is desirable. Separation of the zinc sheet from the cathode is effected manually, and the process of plating and stripping may be repeated up to 1000 times or more on a single cathode sheet before the aluminum is rejected from service, usually for reasons other than a damaged surface. Whereas electroplaters for ornamental or protective work require adherence values of probably 1000 or more kg/cm², production of electrolytic zinc commercially is best served if the adherence is between one and two kg/cm². In this paper, the measurement of adherence of zinc electrodeposits is described, and the mechanism of adherence is discussed by considering these results in relation to information obtained from the following investigations: (a) an examination of the microroughness of surfaces with "Talysurf" instrument (see later); (b) metallographic examination; (c) microscopic examination of first stages of electrodeposition; (d) examination of interface between cathode and electrodeposit; (e) chemical analysis of thin layers from the surface of metals at the interface after separation of the electrodeposit.

EXPERIMENTAL

Measurement of Adherence

The apparatus used for this purpose is illustrated in Fig. 1. It is a modification of the "Burgess" method described by Schlötter (1) giving results in absolute values, i.e., kg/cm². Schlötter soldered a

metallic loop to the surface before pulling off the electrodeposit, but as this is undesirable for zinc electrodeposited on aluminum, a glue bond between the electrodeposit and the pulling bar was used.

For these measurements, cathodes 5 cm x 5 cm x 0.6 cm (thick) were cut from rolled aluminum sheet of a high grade of commercial purity. A single cathode was plated at a time in a beaker carrying electrolyte of the required composition. Anodes cut from pure lead sheet were used, one on each side of the cathode. Zinc was plated for three hours to a thickness of approximately 0.15 mm. These deposits were strong enough to be pulled off without breaking. A suitable area for the adherence test was 2.5 cm x 1.25 cm and this was outlined by grooving the face of the cathode sheet with a sharp pointed tool. The plated zinc sheet was cut along these lines with a very sharp knife and stripped from areas other than those required. For adherence values up to approximately 7 kg/cm² this proved satisfactory, but for greater adherence a smaller area of zinc was used.

Two test rectangles were marked on one face of the cathode sheet. One end of a steel bar 18 cm long and 2.5 cm x 1.25 cm cross section was glued to the back of one of the rectangles of zinc. The most satisfactory method for attaching the bar to the zinc sheet was to insert a piece of linen between the two metal surfaces and glue to each with a liquid glue, the whole being dried at 18°C for 15 hr.

A current density of 32 ma/cm² was used as a standard procedure in plating. The cell temperature was maintained at 35°C. The electrolyte was a solution of zinc sulfate (70 g/l zinc) in dilute

¹ Manuscript received May 4, 1953.

sulfuric acid (100 g/l of H_2SO_4). To this electrolyte was added one or more of the common impurities experienced in commercial zinc electrolysis. With only zinc sulfate-sulfuric acid solutions, no "addition" agent was necessary, but when additional ions were added, 24 mg/l of glue was used. When arsenic and/or antimony was present, then 10 mg/l of beta-naphthol was also added. The addition agent was put in before electrolysis and the initial amount was sufficient for the three-hour plating period. Before each plate was deposited, the test cathode was immersed in the particular electrolyte for 16 hr at 18°C. Some exceptions to these standard procedures were also investigated.

Adherence values were difficult to reproduce with a high degree of accuracy, but it was possible to arrange results in groups according to certain ranges of adherence. The standard deviation of a determination from a single test area was $\pm 50\%$. It was

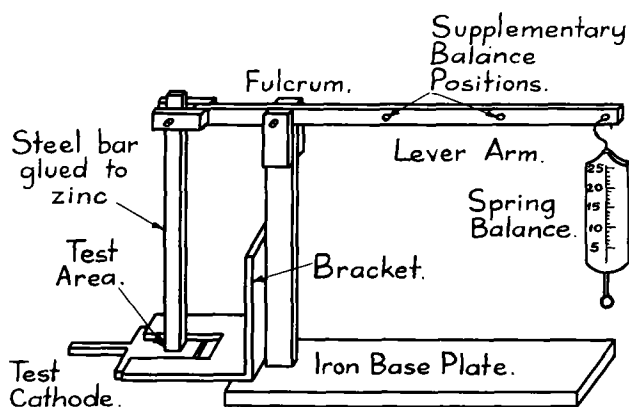


Fig. 1. Laboratory adherence tester

found that results from one side of the rolled aluminum sheet differed from those on the reverse side, so that for comparative purposes only one side of the sheet was used. The difference was related to crystal structure in the surface. Higher adherence was obtained on the surfaces with smaller crystals of aluminum.

Values for adherence from less than 0.1 to as high as 57 kg/cm² were observed. For this investigation, the important range of values was 1 to 2.5 kg/cm² and there was not much point in attempting to measure adherence in excess of 7 kg/cm². This was related to the requirements for manually stripping a zinc sheet from the aluminum cathode during the course of the commercial manufacture of electrolytic zinc. Sheets deposited under conditions giving adherence values in excess of this figure were far too difficult to remove.

In commercial plant practice it had been observed that on some occasions the electrodeposit adhered with reasonable uniformity over the whole cathode

surface, whereas, in other cases, adherence was experienced in smaller patches. Two types of adherence conditions were therefore specified and referred to descriptively as "sheet" adherence and "spot" adherence. In order to differentiate between these conditions in the test cathodes the following method was adopted for interpretation of results. A quantitative estimate of adherence was determined, using values from two adjacent test areas of the experimental cathodes. Spot adherence was identified from the ratio of the higher value to the lower value of adherence from two adjacent areas. On the other hand, the average value from adjacent test areas has been used as a measure of sheet adherence.

Values for spot adherence estimations varied over the range 1 to 13, whereas for sheet adherence values from 0.1 to 57 kg/cm² were recorded, as has already been indicated.

Tests giving spot adherence ratio values lower than 3 were considered satisfactory, whereas values in excess of 6 were considered to be high, and those in excess of 9 to be very high and unsatisfactory.

Tests were conducted under 53 sets of conditions and the most significant of these are given in Table I.

From these tests it was concluded that mechanical roughening of the aluminum surface did not necessarily result in increased adherence of the zinc deposit. Of the chemical factors tested in the electrolyte only chloride ion showed increase in sheet adherence of statistical significance. Spot

TABLE I

Test No.	Electrolyte composition (rolled surface of Al as cathode)	Adherence—kg/cm ²		Ratio of adherence of adjacent areas
		Individual values	Average values	
1	Pure ZnSO ₄ at 70 g/l Zn and 100 g/l H ₂ SO ₄	1.1 & 1.3	1.2	1.2
2	Same as above, with addition of 16 g/l Mn as MnSO ₄	1.9 & 1.8	1.85	1.1
3	Same as for test 2, plus 80 mg/l Cl as HCl	3.2 & 3.9	3.55	1.2
4	Same as for test 2, plus 200 mg/l Cl as HCl	6.0 & 5.3	5.65	1.1
5	Same as for test 2, plus 40 mg/l F as HF	0.85 & 0.85	0.85	1.0
6	Same as for test 2, plus 80 mg/l Cl as HCl and 100 mg/l F as HF	2.25 & 1.4	1.82	1.6
7	Same as for test 2, plus 80 mg/l Cl as HCl and 40 mg/l F as HF	2.25 & 2.55	2.4	1.1
8	Same as for test 7, but with 64-hr pickle	5.3 & 0.4	2.8	13.0
9	Same as for test 7, plus 0.5 mg/l Cu as CuSO ₄	1.3 & 0.85	1.08	1.5
10	Same as for test 7, plus 10 mg/l Cu as CuSO ₄	1.0 & 0.4	0.7	2.5

adherence was experienced when electrolysis was conducted in an electrolyte containing fluoride ion. This type of adherence was also experienced if the cathode had been pickled in acid electrolyte for a long period before electrodepositing. The effect after long pickling was the same, whether fluoride ion was present or not.

Surface Roughness Measurements

Through the services of the Defence Research Laboratories (one time Munitions Supply Laboratories), Maribyrnong, Victoria, Australia, measurements were obtained of the surface roughness of 31 specimens of aluminum and 6 of zinc using a "Talysurf" indicator-recorder. The description and use of this instrument has been published elsewhere by the D.R.L. (then called M.S.L.) (2).

Some of these results are given in Table II. No correlation was found between surface roughness so measured and the degree of adherence.

Metallographic Examination of Crystal Structure

Metallographic examination had limitations because the observation of crystal structure involved destruction of the surface used for electrodeposition.

For microscopic examination, specimens of aluminum were prepared by polishing selected areas of a cathode surface with fine abrasive cloth, followed by a buffing with alunite powder. The final finish was obtained by polishing with "Brasso,"² and using freshly prepared etchant of the following composition: 50% hydrochloric acid; 47% fuming nitric acid; and 3% pure hydrofluoric acid.

With a 30-sec etch, the orientation and size of crystals were clearly seen at a magnification of 900 \times . Surface scratches were widely enough spaced to enable clear fields to be observed at this magnification.

In all cases examined, the crystals were smaller in the specimens which had given higher values for the adherence of the electrodeposit (other factors remaining unchanged).

Microscopic Observation of Electrodeposition

Specimens of aluminum were examined microscopically after deposition of zinc had proceeded for periods such as 30, 60, 90, and 120 sec.

Zinc did not deposit as a uniform sheet but as small ovoid particles, each with its long axis normal to the plane of the aluminum surface. Size of these particles was remarkably uniform and with axis lengths of approximately 8 and 5 μ . The number of particles rather than the size of individual particles

²"Brasso" is a product of Reckett and Colman Ltd., Hull, England, and is recommended for polishing soft metals.

TABLE II

Specimen examined	Talysurf meter readings		Adherence kg/cm ²
	Max. & min.	Mean of six readings	
New aluminum, pickled 16 hr at 18°C; plated and stripped (electrolyte = pure zinc sulfate, 70 g/l Zn & 100 g/l H ₂ SO ₄)	0.38-0.51	0.46	1.27
	0.38-0.51	0.43	1.15
	0.43-0.66	0.53	
	0.46-1.08	0.66	
Specimen as above, but electrolyte contained 16 g/l Mn and 200 mg/l Cl in addition	0.38-0.46	0.41	5.28
	0.43-0.81	0.53	6.05
Specimen as above, but electrolyte contained 16 g/l Mn and 4 mg/l F in addition to ZnSO ₄ and H ₂ SO ₄	0.41-0.53	0.51	0.84
	0.48-0.71	0.53	0.84
Specimen as above, but pickled 64 hr at 18°C in electrolyte with 40 mg/l F	0.81-1.02	0.91	7.75
	0.58-0.74	0.63	1.27
Specimen brushed by hand with steel wire brush. Pickled, plated, and stripped, electrolyte from commercial plant cells	1.78-2.59	2.16	1.69
	1.35-1.58	1.50	2.32
New aluminum, different sheet	0.28-0.30	0.28	—
	0.36-0.41	0.38	—
Same as above, but brushed by hand with steel wire brush	0.70-1.98	1.86	—
	1.60-2.29	2.03	—

increased as plating progressed. Also, by changing the surface treatment or electrolyte characteristics the rate at which these particles appeared could be varied. It would appear that these primary particles deposit at points where the aluminum oxide film is cracked or particularly thin. Where surface irregularities were conspicuous it was noted that particles developed preferentially at sharp peaks or ridges or at the lips of surface depressions. These, no doubt, were points of higher current density.

On a specimen prepared for examination of crystal structure, it was noted that particles preferred to form at crystal boundaries. This was in agreement with work reported by Kyropoulos (3) who studied the manner in which electrodeposits form on aluminum crystals.

Conditions which favored rapid development of primary zinc particles also favored strong adherence of the zinc electrodeposit, and vice versa. Conditions for strong adherence showed 20 to 30 times as many primary particles in 90 sec of plating as conditions for weak adherence.

It was found possible to obtain an estimate of the relative adherence of primary zinc particles by

manipulating a thin steel wire under the objective of the microscope when examining prepared specimens. Adherence of these particles was found to vary appreciably; those which were earliest to appear were generally more firmly attached than those appearing after a longer plating period.

Dependence of points of deposition on the oxide film was demonstrated by anodizing an aluminum cathode in a chromic acid bath. Using this as a cathode in acid zinc sulfate electrolyte, a continuous sheet of zinc was obtained, but it was attached to the cathode at only a very few points.

A film type of deposit was obtained following the technique of Bullough and Gardam (4), designed to remove the oxide film completely and limit its re-appearance before deposition commences. The aluminum surface was prepared in a nitric-hydrofluoric acid bath, and then transferred to a sodium zincate bath, through water washes, without allowing the face to dry. A thin, but continuous, immersion deposit of zinc, very firmly adherent to the aluminum, was obtained in this manner. Attachment was virtually at an infinite number of points and adherence values of the order of the tensile strength of aluminum were recorded by Bullough and Gardam (4).

Film type deposits were also obtained in the current experiments when copper and lead were used as cathodes instead of aluminum.

Microscopic Examination of the Interface

Plated specimens, cut on the taper using the technique described by Nelson (5), were prepared but were not suitable for microscopic examination owing to the softness of the aluminum. A specimen cut normal to the plane of plating allowed zinc or aluminum to be etched individually, but at magnifications high enough to reveal the structure of the interface it was not possible to obtain both surfaces in focus simultaneously.

Specimens of smooth rolled aluminum which had been plated and stripped were examined microscopically. Small craters appeared in the surface after removal of the electrodeposit. In subsequent short periods of plating, primary particles of zinc preferred to form at the lips of these craters rather than in the depressions. These crater-like pits apparently had been foci of attachment for the original zinc deposit, and rupture had taken place in the aluminum surface. These craters were of the order of 1.5μ deep and several microns across; frequently several craters were joined to give trough-like indentations.

Bullough and Gardam (4) when examining the adherence of nickel deposits to aluminum and its

alloys, using zinc as an intermediate layer, also observed fracturing in the aluminum.

A Brinell indenter was used to examine the hardness of specimens of aluminum and zinc. Nothing unusual was noted in specimens of aluminum for which values of the order of 40 were obtained. Values for the zinc were, however, appreciably higher. Over the surface of stripped zinc electrodeposited sheets, values varying between 150 and 225 were obtained, the average being approximately 200. On the other hand, with sections cut through the zinc sheet, normal to the face, values of the order of 70 were obtained. While all these values for zinc may have been unexpectedly high, nevertheless they are consistent with the microscopic observation of fracture in the aluminum surface, indicating greater softness of this metal.

Hanley and Clayton (6) investigated the adherence of zinc electrodeposits to aluminum cathodes. These authors explain the mechanism of adherence in terms of physical anchorage. Generally results obtained by the present author were in line with the findings of Hanley and Clayton, but it is not possible to agree on the mechanism of adherence. On the other hand, there are no results quoted by Hanley and Clayton which could not be explained by a theory of attachment at electrochemically active points.

ANALYSIS OF INTERFACIAL LAYERS

Some tests were made in which a thin layer of aluminum was scraped from the surface of a cathode after having been in service for some time in the commercial zinc plating plant. These scrapings were analyzed for copper and zinc. Of ten cathodes tested, five had been associated with a zinc electrodeposit which stripped easily, and five had been difficult to strip.

The thickness of the layer scraped averaged between 40 and 50μ . The analysis of the easily stripped cathodes averaged 0.071% copper and 3.44% zinc. Zinc content was remarkably uniform, but copper varied widely from sample to sample, from a maxi-

TABLE III

Depth of layer examined, microns	% Aluminum	Remarks
8.3	0.15	Commercial plant cathode, stripped easily
4.35	0.035	Commercial plant cathode, stripped with difficulty
4.2	0.015	Commercial plant cathode, stripped with difficulty
Not determined	0.0026	Pilot plant cathode, stripped easily

mum of 0.191 % to a minimum of 0.023 %. In the case of the cathodes which were difficult to strip, both copper and zinc concentrations were reasonably uniform, averaging 0.022 % and 2.43 %, respectively.

Hanley and Clayton (6) drew attention to the influence of copper in the electrolyte increasing the adherence of the electrodeposit, but this effect was not obtained in the present series of tests (see tests 9 and 10 in Table I). It is believed that the initial distribution of copper in the aluminum sheet exercises a controlling influence on the adherence, but the tests were not carried far enough to produce conclusive evidence on this point. The solid solubility of copper in aluminum is usually reported as 0.25–0.30 % at room temperature. Some workers, however, consider that the solubility is nearer 0.08–0.12 %. Copper concentration of the aluminum sheet used for cathodes covers this range, and presence of CuAl_2 as a solid phase may have some bearing on the problem.

The effect of pickling in spent electrolyte on the removal of zinc from the aluminum surface was examined. Large lumps of zinc left after stripping were removed quite effectively in this manner. Whether they fell off as the result of aluminum in the immediate vicinity being dissolved, or whether they dissolved preferentially in spite of the relative positions of zinc and aluminum in the electrochemical series was not examined critically. There was, however, obvious liberation of hydrogen from large lumps of zinc still attached to the cathode surface. The zinc of more particular interest for this investigation was that which had apparently diffused into the surface of the aluminum. It was observed that during the pickling process zinc was certainly not removed any faster than aluminum, but tests were not extended to determine whether the converse may have been the case, although such was not conspicuous.

Full sections of aluminum sheets were also analyzed for copper, and the following results were obtained from nine sheets of aluminum: 0.051, 0.27, 0.04, 0.05, 0.07, 0.153, 0.04, 0.04, and 0.006 % Cu. The heterogeneity with respect to copper was thus a property of the sheet as a whole, not confined to the surface, and not a result of electrolysis. The new aluminum sheet was free from zinc. There was no evidence that the zinc referred to in these

analyses had been left in the aluminum as the result of fracturing of a bond during the stripping process, but it seemed quite logical to conclude that, with long periods of interfacial contact, diffusion could take place.

Four surfaces of zinc electrodeposit were scraped on the adhering side and analyzed for aluminum. Results are summarized in Table III.

While commercial plant cathodes appeared to leave more aluminum on the zinc face when stripping was relatively easy, this was not confirmed by pilot plant tests. It is believed that the presence of aluminum on the surface of the zinc can be attributed to the fracture of the bond in the aluminum sheet as observed in microscopic examinations reported above. It is unlikely that very much diffusion would have taken place during the plating period which was 72 hr in the case of sheets sampled for analysis of surface. More extensive sampling and analysis is required to provide a rational explanation on the basis of chemical analysis.

CONCLUSION

The mechanism of adherence of a zinc electrodeposit to an aluminum cathode is more plausibly explained in terms of attachment at a varying number of electrochemically active spots than by a concept of mechanical anchoring under ledges and crevices.

ACKNOWLEDGMENT

Acknowledgment is gratefully made to the Electrolytic Zinc Company of Australasia Limited, Risdon, Tasmania, where the author was employed as an investigator in the research department when these experiments were conducted.

Any discussion of this paper will appear in a Discussion Section to be published in the December 1954 issue of the JOURNAL.

REFERENCES

1. F. SCHLÖTTER, *Z. Metallkunde*, **10**, 242 (1910).
2. *Commonwealth Engineer*, **34**, 130 (1946).
3. S. KYROPOULOS, *Z. anorg. allgem. Chem.*, **119**, 299 (1922).
4. W. BULLOUGH AND G. E. GARDAM, *J. Electrodepositors' Tech. Soc.*, **22**, 169 (1947).
5. H. R. NELSON, Special Summer Conf., Proc. Mass. Inst. Tech., 217 (1940).
6. H. R. HANLEY AND C. Y. CLAYTON, *Am. Inst. Mining Met. Engrs.*, **159**, 210 (1944).

Luminescence of the System β $\text{Zn}_3(\text{PO}_4)_2$ - $\text{Cd}_3(\text{PO}_4)_2$: Mn^1

A. L. SMITH

Tube Department, Radio Corporation of America, Lancaster, Pennsylvania

AND

A. D. POWER

Tube Department, Radio Corporation of America, Harrison, New Jersey

ABSTRACT

When zinc orthophosphate and cadmium orthophosphate mixtures are activated by manganese and fired at 850°C, phosphors are obtained whose luminescence is not a linear function of the mole proportions of the initial ingredients. The peak emission vs. composition curve shows several abrupt breaks which correspond to abrupt phase changes as determined by x-ray diffraction analysis.

INTRODUCTION

Luminescence of end members of the system β $\text{Zn}_3(\text{PO}_4)_2$ - $\text{Cd}_3(\text{PO}_4)_2$ has been described by Smith (1), Andrews (2), and Kroeger (3). Color of the luminescence of zinc orthophosphate:manganese may vary from green to red, depending on manganese content and firing temperature (1). Cadmium orthophosphate:manganese was erroneously reported by Andrews (2) to have a red emission, but Kroeger (3) correctly described its emission as yellow. Although double activation of the cadmium salt by lead and manganese causes greater phosphorescence than that obtained by simple manganese activation, the yellow emission remains unaltered (4). McKeag (5) and McKeag and Randall (6) found that when halides in almost any form are added to cadmium orthophosphate, new compound formation occurs and structures of the type $\text{Cd}_3(\text{PO}_4)_2$: MX_2 result; halide fluxes cannot be used, therefore, without altering internal composition to some extent.

Andrews (2) prepared a zinc-cadmium orthophosphate containing equal weights of zinc and cadmium orthophosphates. If the possible use of hydrates is neglected, this mixture corresponds to approximately 40 mole % zinc orthophosphate. The mixture was fused "at full red heat for 15-20 min and poured onto a cold soapstone. The fluorescence under the iron spark is a light pink, and its phosphorescence is a deep red, resembling hot coals, and fairly persistent" (2).

PREPARATION

Zinc orthophosphate dihydrate was prepared as previously described (1). Cadmium orthophosphate

was prepared in a similar manner: disodium hydrogen phosphate was added to a cadmium sulfate solution; the precipitate was filtered, then dried at 160°C. The material thus obtained was a tetrahydrate, $\text{Cd}_3(\text{PO}_4)_2 \cdot 4\text{H}_2\text{O}$, the x-ray diffraction pattern of which agreed with the A.S.T.M. card index labeled " $\text{Cd}_3(\text{PO}_4)_2$ " (7). Firing the hydrate at 650°C converts it to the anhydrous form, the x-ray diffraction pattern of which is given in Table I. A step-by-step dehydration occurs and some intermediate hydrate is formed; composition and stability range of this hydrate, however, were not determined.

In preparation of the phosphors, a water slurry of individual phosphates in proper molar ratio was ball-milled together with the requisite proportion of manganous sulfate for about 14 hr, then evaporated to dryness at 160°C. Equivalent results were obtained by coprecipitation of zinc-cadmium-manganese phosphates, but preparation of various zinc-to-cadmium ratios by ball-milling techniques was more convenient. After evaporation, samples were placed in quartz vessels and fired either at 650° or 875°C in air for two 1-hr periods. Samples were lightly ground between firings to promote homogeneity.

TESTING OF PHOSPHORS

X-ray diffraction analyses were made with nickel-filtered radiation from a copper target tube operated at 40 kv and 15 ma. Samples were rotated within a circular camera 14.32 cm in diameter.

Cathodoluminescent efficiencies and emission spectra were determined by use of a defocused electron beam having a current density of $1.5\mu\text{a}/\text{cm}^2$ and an accelerating potential of 8000 volts. Peak efficiencies and spectral distributions of energy were measured by means of the spectroradiometer and the method described by Hardy (8).

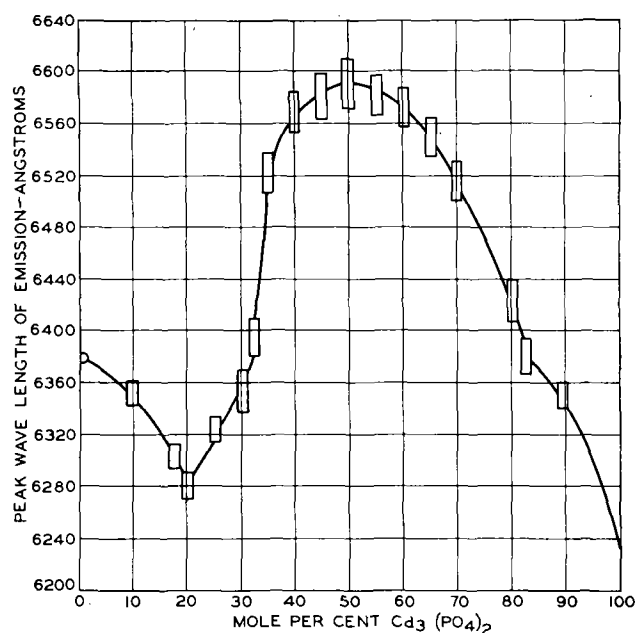
¹ Manuscript received July 6, 1953. This paper was prepared for delivery before the New York Meeting, April 12 to 16, 1953.

TABLE I. Diffraction data for anhydrous $\text{Cd}_3(\text{PO}_4)_2$

Lattice spacing (d -) Å	Estimated relative intensity
4.3	0.80
4.0	0.40
3.8	0.40
3.42	1.00
3.35	0.80
3.29	1.00
3.15	0.30
3.06	0.35
2.95	1.00
2.89	0.20
2.82	0.30
2.65	0.90
2.59	0.70
2.50	0.30
2.43	0.90
2.30	0.10
2.15	0.20
2.10	0.20
2.02	0.20
1.97	0.35
1.92	0.35
1.87	0.20
1.84	0.20
1.77	0.20
1.70	0.25
1.65	0.15
1.59	0.25
1.57	0.15
1.54	0.10
1.51	0.20
1.47	0.10
1.435	0.30
1.402	0.10
1.390	0.20
1.360	0.20
1.265	0.20
1.235	0.20
1.220	0.20
1.210	0.20
1.140	0.30
0.990	0.30

RESULTS AND DISCUSSION

A number of binary phosphor systems are known in which the peak wave length of emission shifts in a regular manner with change in composition. Before this study was undertaken, it was assumed that the zinc-cadmium orthophosphate:manganese system would also exhibit a simple shift of color from the light red of zinc orthophosphate to the deep yellow of cadmium orthophosphate. Such a simple shift does not occur, however, as can be seen in Fig. 1, in which the peak wave length of emission is plotted vs. the mole per cent concentration of cadmium phosphate. Each rectangular box shown on the graph indicates relative variance obtained from a particular composition. Included within the rectangles are values obtained from manganese-concentration tests, firing-temperature studies, and

FIG. 1. Peak wave length, in Å, of emission as a function of composition in the system β $\text{Zn}_3(\text{PO}_4)_2\text{-Cd}_3(\text{PO}_4)_2\text{:Mn}$.

repetitive runs. Variances between repetitive runs were as great as those from processing variables, hence all values are grouped as a single unit.

Effect of manganese concentration.—As in zinc orthophosphate (1), concentrations of manganese between 2 and 5% did not change the position of the peak of emission. Since this investigation was concerned primarily with β $\text{Zn}_3(\text{PO}_4)_2$, concentrations below 2 mole % manganese were not tested systematically. This procedure was followed to insure the presence of only β $\text{Zn}_3(\text{PO}_4)_2$, for it has been established that lower manganese content gives rise to α $\text{Zn}_3(\text{PO}_4)_2$ (1). Only one spot check of 0.5 mole % manganese was made at the 50–50 composition. Although the efficiency of this sample was low, all other properties were similar to those of samples of higher manganese content. It was also found that x-ray diffraction patterns of pure cadmium orthophosphate containing as much as 5 mole % manganese were identical with those without added manganese. This result indicates that cadmium orthophosphate does not display a phase change upon addition of manganese as does the zinc analogue.

Effect of firing temperature.—Although the majority of tests were conducted at 875°C, several runs were made at 650°C to determine whether phase changes due to temperature would occur. Except in the 100 to 90 mole % zinc region, where the expected α to β shift occurred, no other phase change was found which was due solely to temperature. A possible trend toward shorter wave lengths was found at the 650° firing temperature and toward longer wave

lengths for the 875°C firing temperature, but it was quite indefinite. Efficiencies were about 20% better, however, at the 875° value, and it was for this reason that the majority of tests were made at that temperature.

Since results involving activator concentration and firing temperature showed no greater variances than did those between repetitive runs, they were included in the make-up of Fig. 1. The 650° values at high zinc concentrations were omitted, however, because it was obvious that the α form of zinc phosphate was present. Each series tended to give a slightly different curve, but the over-all shape of the curve and position of the breaks were substantially unchanged, the only difference being one of slight magnitude. The plot is a very sensitive one, so that small errors in measurement or preparation appear magnified.

Fig. 2 shows spectral energy distribution curves for β $Zn_3(PO_4)_2:Mn$, $Cd_3(PO_4)_2:Mn$, and a 50-50 mole ratio of the two substances. The curve of the 50-50 composition is symmetrical, without the hint of a double peak. This symmetry is evident in all other ratios as well. As the cadmium content is increased, the curve remains relatively narrow until a content of 20 mole % is reached. The curve broadens rather abruptly at about the same concentration at which emission starts to shift toward deep red, and remains relatively unchanged for all concentrations up to pure $Cd_3(PO_4)_2$. This fact is

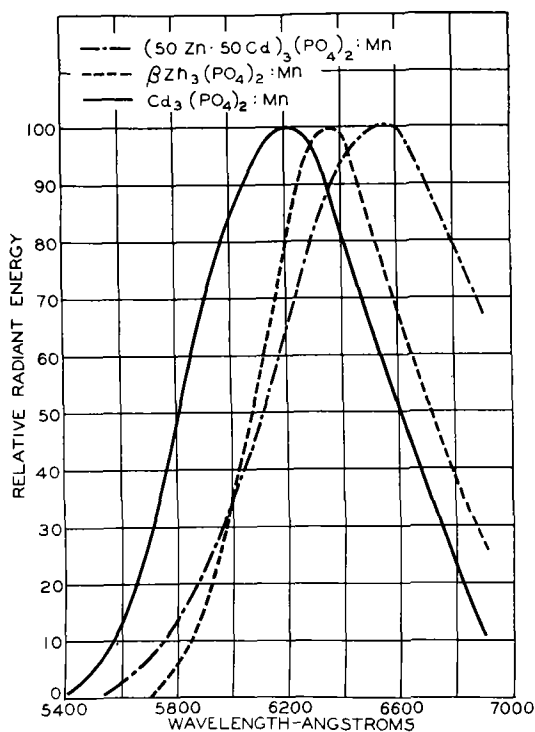


FIG. 2. Spectral energy distribution curves of the phosphors $[Zn_3(PO_4)_2:Cd_3(PO_4)_2]:0.05 Mn$, $\beta Zn_3(PO_4)_2:Mn$, and $Cd_3(PO_4)_2:Mn$.

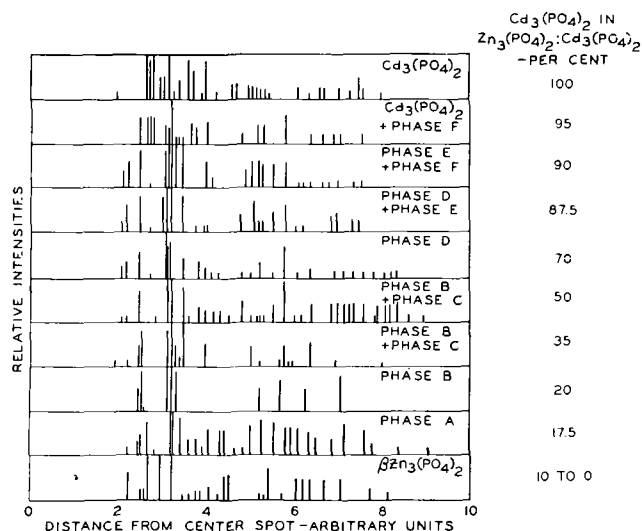


FIG. 3. Schematic representation of typical x-ray diffraction patterns obtained for various compositions in the $\beta Zn_3(PO_4)_2-Cd_3(PO_4)_2:Mn$ system.

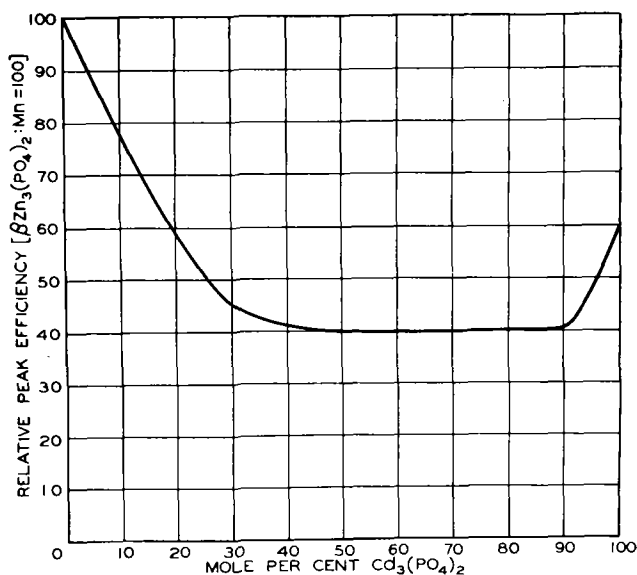


FIG. 4. Plot showing the variation in efficiency as a function of composition for the system $\beta Zn_3(PO_4)_2-Cd_3(PO_4)_2:Mn$ fired at 875°C.

especially interesting because x-ray diffraction patterns indicate that pure phases are present at only a few points, all other points showing mixed phases (see Fig. 3). It might be assumed that each phase would have its own peak of emission and, with two phases present, either a double peak would be seen or the curve would be quite broad. Why this does not occur is not known.

Fig. 4 shows rather rapid decrease in peak efficiency as cadmium content is increased (preparation at 875°). At concentrations of about 40 or 50 mole % cadmium orthophosphate, the efficiency curve flattens to a value of about 40% of that of $\beta Zn_3(PO_4)_2$. The efficiency remains at that value until

90% $\text{Cd}_3(\text{PO}_4)_2$ is reached, at which point it rises to 60% of $\text{Cd}_3(\text{PO}_4)_2$ itself.

From pure zinc orthophosphate to compositions with up to 17.5 mole % cadmium orthophosphate, the structure is essentially that of β $\text{Zn}_3(\text{PO}_4)_2\text{:Mn}$ (see Fig. 3). At about the latter value a very abrupt phase change occurs which corresponds quite closely to the abrupt shift in peak of the emission curve (Fig. 1). The first phase, *A*, is of very narrow composition. At concentrations of 20 mole % cadmium orthophosphate another apparently pure phase, *B*, appears; this phase persists through concentrations having 50 mole % cadmium orthophosphate. Somewhere in the 50 mole % region a *C* phase is also found, but it could not be isolated. The *D* phase begins at concentrations of about 70 mole % cadmium orthophosphate and continues to concentrations of about 90 mole %; the *D* phase is contaminated in small portion by the *E* phase at concentrations of about 85 mole %. The *D* phase disappears at concentrations of 90 mole %, but another phase, *F*, is then found with the *E* phase. The *E* form could not be isolated; the appearance of the *E* form is coincident with another sharp break in the peak of the emission curve. At concentrations of 95 mole % cadmium orthophosphate, the *F* form is found together with normal cadmium orthophosphate. No pure cadmium orthophosphate phase is present in the composition made with as much as 90 mole % cadmium phosphate.

Chloro-complexes of some of these phases are of interest. At and above 87.5 mole % cadmium composition, chloro-complexes were formed having emission and x-ray diffraction patterns essentially identical with those published by McKeag and Randall (6). At and below 20 mole % cadmium composition, emissions and patterns were distorted γ $\text{Zn}_3(\text{PO}_4)_2$ (1). Between these limits, however, no complexes were formed; the added chloride acted only as a "mineralizer" promoting crystal growth and did not affect emission or x-ray diffraction patterns.

CONCLUSIONS

When β zinc orthophosphate and cadmium orthophosphate mixtures are activated by man-

ganese and fired at 875°C, phosphors are obtained whose luminescence is not a linear function of the mole proportions of the initial ingredients. The peak emission vs. composition curve shows several abrupt breaks, which correspond to abrupt phase changes as determined by x-ray diffraction analysis. There are probably six phases present in the β zinc orthophosphate-cadmium orthophosphate system, some of which are partially intersoluble. Three of these phases could be isolated, but the other three could not, even though only fractional percentage changes were made in regions where these compositions were thought to lie. Only two of the abrupt phase changes manifested themselves as abrupt changes in luminescence; the other variations showed only what would be expected from simple solid solutions. The unusual feature of these mixtures is that more abrupt changes in emission were not observed in the light of complex phase changes indicated by x-ray analyses. Lack of abrupt emission changes implies that the activator center was not altered radically by these phase changes, but rather was influenced in a very gradual manner.

ACKNOWLEDGMENTS

Thanks are due to L. E. Whitmer for preparation of most of the samples, and to A. E. Hardy and R. F. Jefferies for optical measurements.

Any discussion of this paper will appear in a Discussion Section, to be published in the December 1954 issue of the JOURNAL.

REFERENCES

1. A. L. SMITH, *This Journal*, **98**, 363 (1951).
2. W. S. ANDREWS, *Am. Mineral.*, **7**, 19 (1922).
3. F. A. KROEGER, "Some Aspects of the Luminescence of Solids," Elsevier Publishing Co., New York (1948).
4. A. H. McKEAG AND P. W. RANBY, U. S. Pat. 2,476,676, July 19, 1949.
5. A. H. McKEAG, U. S. Pat. 2,201,698, May 21, 1940; 2,214,643, Sept. 10, 1940; 2,226,407, Dec. 24, 1940.
6. A. H. McKEAG AND J. T. RANDALL, U. S. Pat. 2,191,351, Feb. 20, 1940.
7. "Alphabetical and Grouped Numerical Index of X-ray Diffraction Data," Special Technical Publication 48-B, American Society for Testing Materials, Philadelphia (1950).
8. A. E. HARDY, *Trans. Electrochem. Soc.*, **91**, 127 (1947).

Sensitized Luminescence of $\text{CaF}_2:(\text{Ce} + \text{Mn})^1$

R. J. GINTHER

Chemistry Branch, Metallurgy Division, Naval Research Laboratory, Washington, D. C.

ABSTRACT

Calcium fluoride activated by cerium and manganese is shown to be a sensitized phosphor of high quantum efficiency. Studies of its reflection and excitation spectrum reveal that both cerium singlets and aggregates of cerium ions serve as sensitizers for manganese. The range of interaction (K) over which energy may be transferred from sensitizer to activator was found to be from 30 to 80 lattice sites. Variation in K with increasing sensitizer and constant manganese concentration is interpreted as being due to the competition of two types of sensitizing centers rather than to an energy transfer between sensitizer ions.

INTRODUCTION

The sensitized luminescence of manganese-activated phosphors has been the subject of numerous investigations. While a number of sensitized systems of simple structure, principally alkali halides (1) and calcite (2), are known, the most recent investigations have been concerned with compounds of more complicated structure such as $\text{CaSiO}_3:(\text{Pb} + \text{Mn})$ (3), $\text{Sr}_3(\text{PO}_4)_2:(\text{Sn} + \text{Mn})$, $\text{Ca}_3(\text{PO}_4)_2:(\text{Ce} + \text{Mn})$ (4), and $3\text{Ca}_3(\text{PO}_4)_2\text{CaFCl}:(\text{Sb} + \text{Mn})$ (5). Although the interest in the more complicated systems originated largely in their practical application, it is from these phosphors that the most recent information concerning the mechanism of energy transfer and the range of sensitizer-activator interaction has been derived (6, 7, 8). Alkali halides and calcite, either for reasons of low activator or sensitizer solubility or because of poor luminescence efficiency, are not well adapted to the detailed investigation of the transfer mechanism and range.

Calcium fluoride is a compound of simple structure which has high solubility for both sensitizer and activator permitting preparation of efficient phosphor samples over a wide range of concentrations. It therefore appears to be ideally suited for the investigation of sensitized luminescence.

EXPERIMENTAL METHODS AND RESULTS

Preparation and Identification of Samples

No commercially available raw materials were found satisfactory for preparation of the phosphors studied. Although calcium and manganous fluorides sufficiently free of heavy metals were available, all samples of these materials were partially hydrolyzed, leading to oxidation of the manganese activator upon

firing. Some samples of calcium fluoride contained sufficient calcium hydroxide to produce a separate manganese-activated calcium oxide phase upon firing phosphor samples prepared from them.

A satisfactory calcium fluoride raw material can be prepared from calcium carbonate and hydrofluoric acid. When 25.0 grams of CaCO_3 are added to a solution of 25.0 ml of 48% HF in 250 ml of water, the calcium fluoride produced settles rapidly and may be washed by decantation. When dried at low temperature, preferably *in vacuo*, it suffers little or no hydrolysis, and samples will nearly completely disappear in a liquid of refractive index 1.434. The effect of using more concentrated acid is to produce finer particles of calcium fluoride which do not settle well, are more difficult to wash, and apparently are more susceptible to hydrolysis. Samples prepared from concentrated acid will not disappear in the refractive index medium mentioned above presumably because of the presence of an extra hydrolyzed phase. Of commercially available calcium fluoride, only optical quality crystals, either natural or synthetic, would meet the above described immersion test.

Cerous fluoride was prepared by a rather complicated procedure. Cerous nitrate solution was purified first with H_2S , then with ammonium sulfide in an alkaline solution of ammonium tartrate. Next, cerous oxalate was precipitated and washed. The oxalate was then dissolved in nitric acid; the solution was reduced with hydrogen peroxide, then the fluoride was precipitated with hydrofluoric acid. No attempt was made to separate other rare earths from cerium.

The most satisfactory source of manganese proved to be an ammonium manganous fluoride which is easily precipitated from manganous chloride solution with ammonium fluoride. The manganese content of this complex fluoride is somewhat variable; samples

¹ Manuscript received October 2, 1953. This paper was prepared for delivery before the New York Meeting, April 12 to 16, 1953.

of it prepared in this laboratory averaged about 70.0% MnF_2 .

While luminescent preparations can be made simply by coprecipitation of the mixed fluorides and drying under an infrared lamp, the most efficient phosphors were prepared by dry mixing the component fluorides and firing at 1000°–1200°C in an inert atmosphere. Most of the samples prepared in this investigation were fired in platinum containers in helium or nitrogen at 1100°C. Inert gas was purified by passage over hot copper and calcium hydride. This firing technique produced samples with as much as 20% Mn which were perfectly white by reflected light and free of any observable effects of manganese oxidation. No "skinning" of any sample was necessary.

Representative samples were examined by x-ray diffraction. All samples had the fluorite structure. Manganese produced a contraction, and cerium an expansion of the crystal lattice, as one would expect. Only in samples containing 20% cerium was an extra unidentified line observed in the x-ray pattern. This line could not be correlated with any of the reported lines of any fluoride or oxide of calcium, cerium, or manganese.

Calcium Manganous Fluoride Phosphors

Many references to natural luminescent fluorite containing manganese have been made. Emission colors are variously reported as green to yellow. Synthetic manganese-activated fluorite was prepared by Wick (9), but no details of its emission spectrum were reported. Fig. 1 shows the cathode ray excited emission spectra of typical members of a series prepared in this laboratory and containing from 0.05 to 10.0 mole % Mn. Samples of from 0.05% to 1.0% Mn have an emission peak at 4900 Å.² With increasing manganese concentration, the emission peak shifts to longer wave lengths. At 5.0% Mn the peak is at 5000 Å, while the peak of a 10.0% Mn sample is at 5100 Å. A sample containing 20.0% Mn was luminescent only at low temperature under cathode rays. None of the above described samples was appreciably excited by ultraviolet in the wave length range from 2200–4000, although a weak excitation band at 4000 Å exists in these phosphors as will be shown in a later section.

$\text{CaF}_2(\text{Ce})$ Phosphors

Kroger and Bakker (10) have briefly investigated calcium fluoride activated by cerium. They report

² In concurrent work, Dr. Arthur L. Smith, of Radio Corporation of America, located the emission peak of synthetic fluorite containing 1.0% Mn at 4950 Å. The reason for the minor discrepancy between his and the present work is not known, but may possibly be due to differences in either raw materials or preparation technique employed.

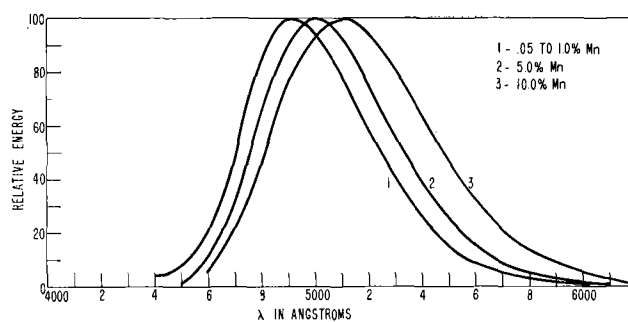


FIG. 1. Emission spectra of $\text{CaF}_2:(\text{Mn})$ under cathode ray excitation.

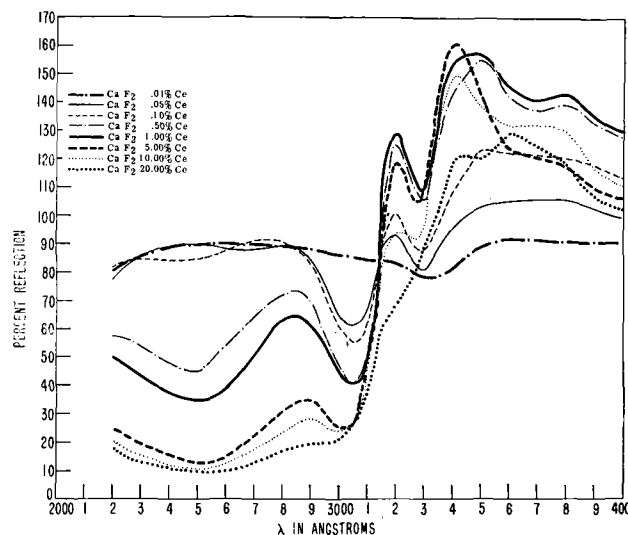


FIG. 2. Reflection spectra of $\text{CaF}_2:(\text{Ce})$

an absorption edge at 3000 Å and an emission consisting of two peaks at 3100 Å and 3300 Å in a sample containing 1.0% Ce. In a sample containing 10% Ce, a third emission peak between 3500 Å and 4000 Å was observed.

In the present work, samples of from 0.01 to 20.0 mole % cerium were prepared. Absorption spectra of this series, as shown by the reflection curves of Fig. 2, are much more complicated than the simple edge described by Kroger and Bakker. At a concentration of only 0.01% Ce, a single reflection minimum corresponding to an absorption band at 3300 Å is observed. With concentrations of from 0.05% to 0.10%, only one additional minimum at 3050 Å is obtained. With concentrations of 0.50% Ce and higher, a band at about 2500 Å appears. While the absorption band at 3050 Å grows continuously with increasing cerium content, the band at 2500 Å grows much more rapidly at the higher cerium concentrations. At 1.0% Ce the 2500 Å and 3050 Å reflection minima are about equal, while the 2500 Å minimum is predominant at all higher cerium concentrations.

Reflections of more than 100% are obtained at

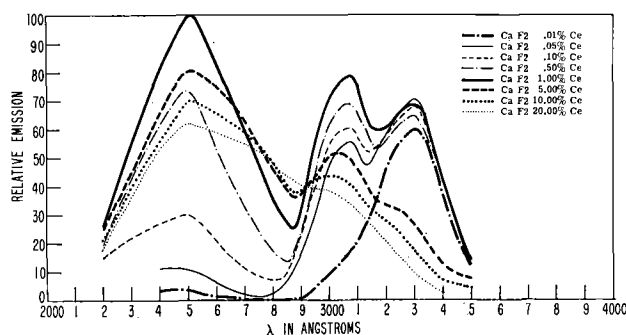


FIG. 3. Excitation spectra of $\text{CaF}_2:(\text{Ce})$ for 3850 Å emission band.

3200 Å and in two peaks between 3400 Å and 4000 Å. Apparent reflections of over 100%, due to luminescent emission, are obtained whenever the reflection spectrum of a phosphor is measured with the sample exposed to the total spectrum of the hydrogen lamp at the monochromator entrance slit, as was done in the present work.

Growth of the 3300 absorption band as a function of cerium concentration is obscured by the presence of the 3200 Å and 3400 Å emission peaks, while the growth of the 3050 Å absorption band is accentuated by its superposition upon the tail of the 2500 Å band. However, the presence of both the 3050 Å and 3300 Å bands in the sample containing only 0.05% Ce indicates that both of these bands are due to cerium singlets. The appearance of the 2500 Å band at only high concentrations of cerium and the rapid growth of this band relative to the singlet bands as a function of cerium concentration demonstrates that the shortest wave length absorption is due to cerium aggregates. For the present purpose, a cerium aggregate may be defined as consisting of at least two cerium ions whose proximity provides sufficient interaction to modify the absorption properties of the cerium center. The question of actual maximum separation of ions of an aggregate is left open.

Excitation spectra of $\text{CaF}_2:(\text{Ce})$ phosphors cannot be completely determined by the usual excitation measurement. The close proximity of the 3050 Å absorption and the 3200 Å emission bands as well as the proximity of the 3300 Å absorption to the emission at about 3400 Å prohibits the measurement of the excitation of the two short-wave emission bands by conventional methods. The technique of interposing filters between the phosphor sample and the phototube detector in order to separate the phosphor emission from light of the exciting wave length reflected from the sample surface could not be applied, since no filters could be found to effect the separation. The excitation spectrum for the 3800 Å emission was obtained in the usual manner by employing a Corning #5113 filter.

Fig. 3 represents the excitation spectra for the 3800 Å emission band. At the lowest cerium concentration a single sharp excitation peak at 3300 Å is obtained. As the cerium concentration is increased, a second excitation peak at about 3070 Å is observed. This latter peak grows relative to the 3300 Å peak with increasing cerium concentration. At a concentration of 0.10% Ce, an excitation peak at 2500 Å is well defined, and this peak is the most prominent at all higher concentrations. The latter excitation peak grows relative to the longer wave length excitation peaks with increasing cerium concentration, and its rapid growth at high cerium content is consistent with the interpretation that this peak is due to cerium aggregates. The growth of the 3070 Å peak relative to the 3300 Å peak is not obviously in agreement with the assumption that both these absorption bands are due to cerium singlets. However, it will be shown in the next section that the emission produced upon excitation in these two bands is not identical. Therefore, an identical behavior in the growth of the two excitation bands for only the 3800 Å emission should not necessarily be expected. It may be observed that the 2500 Å and 3070 Å excitation bands overlap considerably for all cerium concentrations except the lowest three, and that the amount of overlap increases with increasing cerium content.

Correction to equal energy of excitation was made only in the wave length range 2500–4000 Å; consequently, decrease in excitation shown at wave lengths shorter than 2500 Å is an exaggeration of the true decrease. However, since the excitation peak at 2500 Å coincides exactly with the absorption peak at this wave length, there can be little doubt that the peak is correctly located.

In the behavior of aggregate cerium ions as absorbers for 2500 Å radiation may lie the explanation why relatively high cerium concentrations are necessary for efficient excitation of other cerium-activated phosphors by 2537 Å radiation.

Since excitation spectra for all three emission bands could not be determined, information concerning the emission associated with the individual absorption bands was obtained by measuring the emission spectra of the phosphors with monochromatic exciting radiation in each of the three absorption bands. Exciting light was rendered monochromatic by passage through two quartz monochromators in series. Emission spectra were then recorded with a spectroradiometer in the conventional manner. For excitation in the 2500 Å band, 2537 Å radiation was employed, while for excitation in the 3070 Å band, the 2967 Å mercury line was used. The source of these mercury lines was an H-4 type mercury burner enclosed in a quartz envelope. For

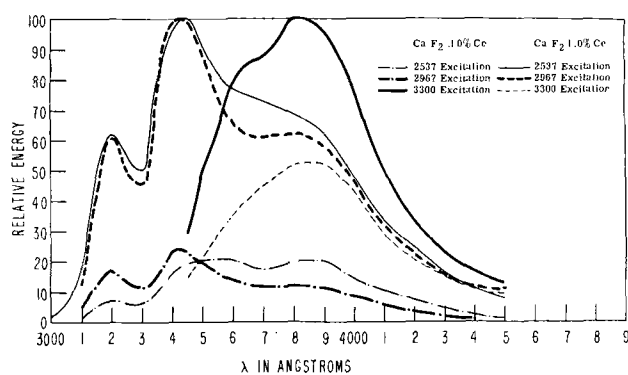


FIG. 4. Emission spectra of $\text{CaF}_2:(\text{Ce})$

3300 Å excitation, a band about 100 Å wide centered at the desired wave length was selected from the spectrum of either an AH-6 water-cooled mercury lamp or from a Xenon arc lamp. Emission spectra of all samples of the series were similar under any particular type of excitation. The emission of samples containing 0.10% Ce and 1.0% Ce are shown in Fig. 4. Under 3300 Å excitation, an emission consisting of a single peak at 3850 Å is obtained from the 1.0% Ce sample, while the emission of the 0.10% Ce sample shows resolution with a second peak at about 3650 Å. With both 2537 Å and 2967 Å excitation, emission peaks at 3200 Å and 3450 Å, as well as the 3850 Å peak, are observed. Minor variations in both peak positions and in their relative intensities were obtained as a function of cerium concentration, but emission spectra shown are typical for all members of the series. It can be observed with reference to Fig. 3 that excitation with 2967 Å radiation will result in absorption in both singlet and in aggregate cerium centers because of the overlap of the absorption bands of these centers at high cerium concentration. However, for cerium concentrations of 0.50% and lower, the overlap at 2967 Å is insignificant so that it can be stated with certainty that absorption in both the 3050 Å and 2500 Å bands produces all three emission peaks.

$\text{CaF}_2:(\text{Ce} + \text{Mn})$ Phosphors

While calcium fluoride activated separately by cerium and by manganese has been previously prepared, no sensitized combination of these two activators in fluorite seems to have been reported. In the present investigation, sensitized luminescence was observed in samples containing from 0.01% to 20.0% Ce and 0.05% to 20.0% Mn. Optimum concentration for 2537 Å excitation was found to be in the region of 1.0% to 10.0% of both cerium and manganese.

Reflection Spectra

Reflection spectra of sensitized phosphors are similar to those of phosphors containing only

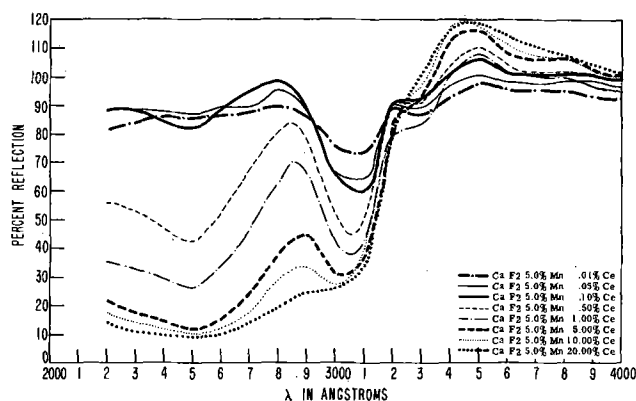


FIG. 5. Reflection spectra of $\text{CaF}_2:(5.0\% \text{ Mn, varying Ce})$.

cerium. Fig. 5 shows the reflection spectra of a series of samples of 5.0% Mn and of varying cerium concentration. The three absorption bands found are located at the same wave lengths as in phosphors activated by cerium alone. The only distinguishing difference between the data of Fig. 5 and the reflection spectra of $\text{CaF}_2:(\text{Ce})$ phosphors is the smaller amount of ultraviolet emission obtained from phosphors containing manganese. Ultraviolet emission of these phosphors is depressed by transfer of energy to manganese, resulting in visible emission.

Reflection spectra of another series of phosphors of the same cerium contents but of 0.50% Mn were found to be identical with those of the 5.0% Mn phosphors except for the magnitude of the ultraviolet emission. The reflection spectra of two series of samples of constant cerium concentration but of varying manganese content from 0.05% to 20.0% were also determined. For samples of both 0.10% Ce and 1.0% Ce, reflection spectra were independent of manganese concentration, except in regard to the magnitude of the ultraviolet emission. It may, therefore, be concluded that no new absorption bands are introduced by the presence of cerium + manganese pairs. In this respect, the sensitized calcium fluoride phosphor resembles most sensitized phosphors whose absorption spectra have been investigated. Notably, it differs from $\text{CaSiO}_3:(\text{Pb} + \text{Mn})$ in which Pb + Mn pairs appear to have a discrete absorption (7).

Excitation of Ce Emission

Excitation spectra for the 3850 Å-peaked ultraviolet emission of the $\text{CaF}_2:5\% \text{ Mn, Ce}$ phosphors are shown in Fig. 6. Again, correction to equal energy of excitation was made only to 2500 Å. For all samples, the excitation peak in the region of 3300 Å is predominant. Poor sensitization of manganese should, therefore, be obtained at this wave length. The rapid growth of a 2500 Å excitation band due to cerium aggregates is not demon-

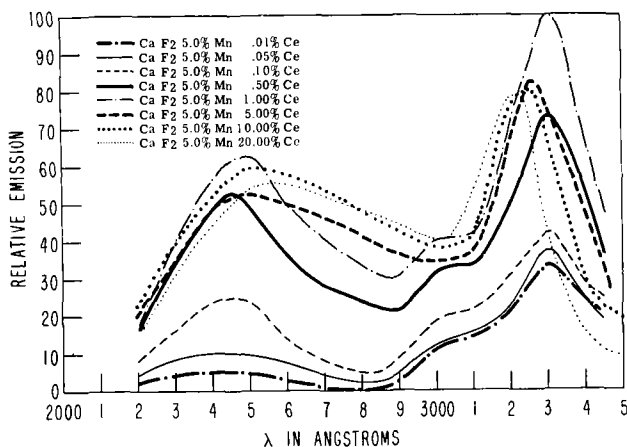


FIG. 6. Excitation spectra for 3850 Å emission band of CaF_2 :(5.0% Mn, varying Ce).

strated in these curves. This growth should not be expected if good sensitization of manganese occurs in this band. In none of the samples is the 3050 Å excitation band well resolved, indicating that good sensitization should occur at this wave length.

Excitation spectra for ultraviolet emission obtained with other phosphor series were in agreement with the data for the series illustrated. A series containing constant 0.50% Mn and varying cerium concentrations showed the 2500 Å and 3050 Å bands in greater intensity relative to the 3000 Å band than was obtained with the 5.0% Mn series. Since at lower manganese concentration the opportunity for energy transfer and emission from manganese is lower than in the phosphors of 5.0% Mn, excitation spectra should more nearly resemble the data obtained for CaF_2 :(Ce) phosphors. Measurements on phosphors of constant cerium but of varying manganese concentrations gave results also in agreement with data reported above. With 0.10% Ce and low manganese concentration, strong ultraviolet excitation peaks at 3050 Å and 3300 Å are obtained. As manganese is increased, the 3050 Å peak is suppressed. With 1.0% Ce present, excitation peaks at 2500 Å, 3050 Å, and 3300 Å are obtained with low manganese content. As the manganese concentration of this series is increased, the two short wave length peaks are reduced relative to the 3300 Å peak, indicating efficient sensitization of manganese in both the short wave length absorption bands.

Ultraviolet Emission Spectra

Ultraviolet emission spectra of Mn-activated CaF_2 :Ce phosphors varied very little as a function of cerium concentration. As in the case of the phosphors activated with cerium alone, three emission peaks were obtained with either 2537 Å or 2967 Å excitation, but only a single peak at about 3800 Å was obtained with excitation at 3300 Å.

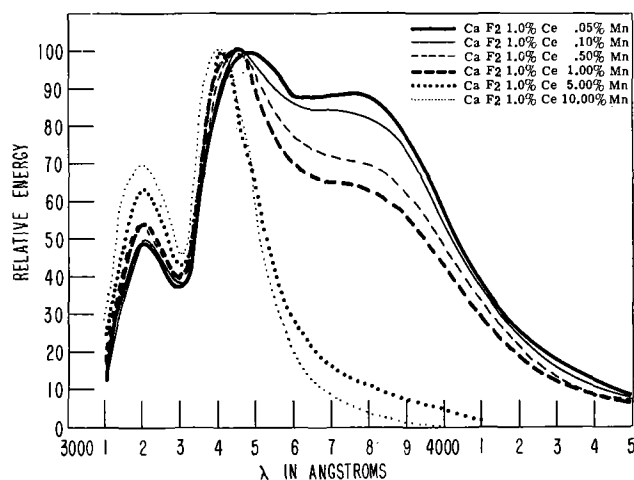


FIG. 7. Ultraviolet emission spectra of CaF_2 :(1.0% Ce, varying Mn).

Minor differences occurred in the relative heights of the three emission bands of some samples, but no regular variation of peak intensities was found as a function of cerium concentration.

A more significant variation of ultraviolet emission spectra of phosphors of constant cerium but varying manganese concentration was obtained. As shown in Fig. 7 the 3800 Å emission of samples of 1.0% Ce is depressed relative to two short-wave emission bands with increasing manganese concentration. At a concentration of 5.0% Mn, the 3800 Å band is no longer distinguishable. Emission spectra shown were obtained with 2967 Å excitation. Results with 2537 Å excitation were similar.

Excitation Spectra of Manganese Emission

Excitation spectra of the manganese emission of a series of samples with 5.0% Mn are shown in Fig. 8. As expected, poor excitation occurs in the 3300 Å band. All samples have a strong excitation at 3050 Å, while the 2500 Å band grows relative to the 3050 Å band with increasing cerium content in agreement with the assumption that it is due to aggregated cerium ions. While aggregates of activators are recognized as luminescent centers in

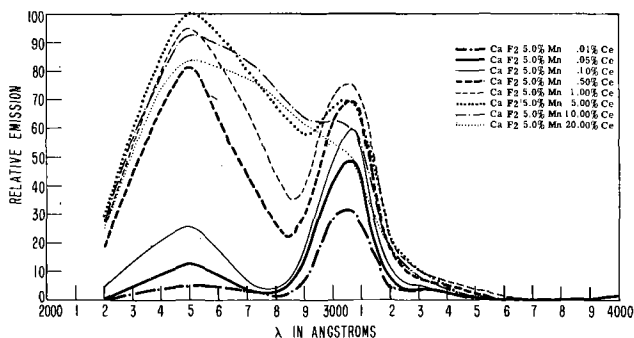


FIG. 8. Excitation spectra for manganese emission of CaF_2 :(5.0% Mn, varying Ce).

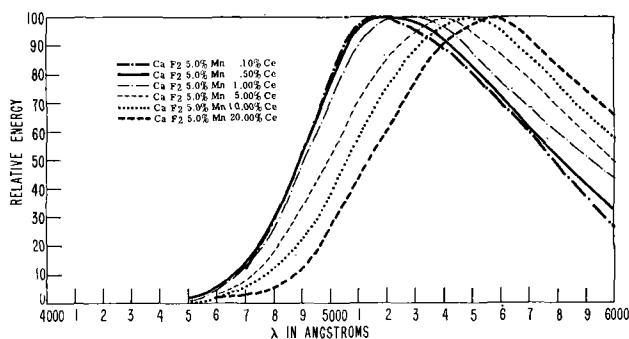


FIG. 9. Manganese emission spectra of $\text{CaF}_2:(5.0\% \text{ Mn}, \text{ varying Ce})$ under monochromatic 2537 \AA excitation.

many systems, no previous evidence for the behavior of aggregated ions as sensitizers for manganese appears to have been reported. The very slight rise in excitation at 4000 \AA is real. From measurements on samples of varying manganese content it was found that this band peaks at about 4000 \AA and is dependent on manganese, not upon cerium, concentration. It is apparently due to a weak manganese absorption band.

Manganese Emission Spectra

Manganese emission spectra under optical excitation were obtained with monochromatic excitation from the double monochromator arrangement mentioned earlier. Since the excitation energy available at 2537 \AA is very low with this arrangement, a 1P21 photomultiplier tube was used as the detector in the spectroradiometer. Use of this tube prevented reliable calibration of the system at wave lengths longer than 6000 \AA .

Emission spectra of a series of samples of $5.0\% \text{ Mn}$ and of varying Ce concentration obtained with 2537 \AA excitation is shown in Fig. 9. Increasing cerium content shifts the emission to longer wave lengths. A shift from 5150 \AA to 5550 \AA in the emission peak is obtained upon a cerium concentration increase from 0.10% to 20.0% . Emission spectra of samples containing less than 0.10% Ce could not be obtained with 2537 \AA excitation because of the low concentration of cerium aggregates in these samples.

TABLE I. $\text{CaF}_2:5.0\% \text{ Mn}-2537 \text{ \AA}$ excitation

1 % Ce	2 QE Ce	3 QE Mn	4 Total QE	5 $B = \frac{\text{QEMn}}{\text{QECe}}$	6 K
0.01	0.44	5.1	5.5	11.6	49.3
0.05	1.8	20.9	22.7	11.6	49.3
0.10	3.0	32.7	35.7	10.9	48.2
0.50	7.5	87.7	95.2	11.7	49.5
1.0	7.4	75.9	83.3	10.2	47.0
5.0	6.8	82.6	89.4	12.1	50.1
10.0	7.0	87.7	94.7	12.5	50.7
20.0	7.1	76.7	83.8	10.8	48.1

TABLE II. $\text{CaF}_2:5.0\% \text{ Mn}-2967 \text{ \AA}$ excitation

1 % Ce	2 QE Ce	3 QE Mn	4 Total QE	5 $B = \frac{\text{QEMn}}{\text{QECe}}$	6 K
0.01	9.0	39.6	48.6	4.4	32.8
0.05	12.5	58.8	71.3	4.7	33.9
0.10	14.5	68.3	82.8	4.7	33.9
0.50	10.4	62.0	72.4	6.0	
1.0	9.2	60.7	69.9	6.6	
5.0	7.0	66.6	73.6	9.4	
10.0	7.1	72.8	79.9	10.2	
20.0	6.3	62.2	68.5	9.8	

Only manganese ions coupled to aggregated cerium absorbing centers are excited by 2537 \AA . Different emission spectra were obtained upon excitation in the 3050 \AA absorption band of cerium singlets and upon excitation with cathode rays. Further details of the emission spectra of these phosphors will be reported in a separate publication.

Quantum Efficiency

Quantum efficiencies of two series of phosphors were measured by a method similar to that described by Kroger (11). Separation of the cerium and manganese emissions was made with filters. Corning #5970 was employed for the ultraviolet measurement and Corning #3387 was used for the visible emission. Details of the method of measurement will be reported separately.

Quantum efficiencies of samples containing either $5.0\% \text{ Mn}$ or $0.50\% \text{ Mn}$ and 0.01% to 20.0% Ce are shown in columns 2, 3, and 4 of Tables I, II, III, and IV. Samples of lower manganese content could not be measured with any accuracy. Total quantum efficiencies as high as 95% were obtained with some samples of $5.0\% \text{ Mn}$, while the maximum total quantum efficiency obtained with samples of $0.50\% \text{ Mn}$ was about 82% . The tables indicate that high transfer efficiency, evidenced by high quantum efficiency for manganese emission, is obtained when the $5.0\% \text{ Mn}$ phosphors are excited in either the absorption band of cerium singlets or in the aggregated cerium absorption band.

TABLE III. $\text{CaF}_2:0.50\% \text{ Mn}-2537 \text{ \AA}$ excitation

1 % Ce	2 QE Ce	3 QE Mn	4 Total QE	5 $B = \frac{\text{QEMn}}{\text{QECe}}$	6 K
0.05	1.8	0.63	2.4	0.35	59.2
0.10	8.6	3.6	12.2	0.42	69.2
0.50	58.0	19.5	77.5	0.34	57.8
1.0	62.8	19.6	82.4	0.31	53.3
5.0	41.4	18.7	60.1	0.45	73.4
10.0	38.2	20.0	58.2	0.52	82.6
20.0	47.8	19.0	66.8	0.40	66.4

TABLE IV. $\text{CaF}_2:0.50\% \text{ Mn}-2967 \text{ \AA}$ excitation

¹ % Ce	² QE Ce	³ QE Mn	⁴ Total QE	⁵ $B = \frac{\text{QEMn}}{\text{QECe}}$	⁶ K
0.05	40.2	6.8	47.0	0.17	31.0
0.10	59.5	11.9	71.4	0.20	36.0
0.50	61.7	15.8	77.5	0.26	
1.0	61.9	18.1	80.0	0.29	
5.0	38.2	18.2	56.4	0.48	
10.0	36.0	16.4	52.4	0.46	
20.0	41.8	15.0	56.8	0.36	

DISCUSSION

Several explanations of the phenomenon of sensitized luminescence have been proposed. These explanations have been reviewed by Botden (8). Since some of the mechanisms had been disproved on the basis of experimental evidence, Botden was concerned with the evaluation of three theories.

The first theory attributes transport of energy from sensitizer to activator to a so-called long wave exciton of the base lattice. The optical absorption of this exciton is assumed to be forbidden so that its existence is not normally recognized. This mechanism was suggested but not indorsed by Botden and Kroger (6).

A second theory proposed by Botden and Kroger ascribes excitation of the manganese activator to a direct transfer of energy between neighboring sensitizer and activator. Transfer between only nearest neighbor "pairs" of activators and sensitizers is assumed possible. To account for the high transfer efficiency existing in efficient phosphors, Botden and Kroger assumed that there is a preferential production of activator-sensitizer pairs in the phosphor synthesis. These authors also suggest that an excited sensitizer ion may transfer its energy to a neighboring sensitizer ion and hence to an activator, in order to account for the high transfer efficiency observed.

The third theory is that of Schulman (7) who proposed that energy is transferred from sensitizer to activator over distances greater than those separating only nearest neighbor pairs. From measurements of the absorption spectra of $\text{CaSiO}_3:(\text{Pb} + \text{Mn})$, Schulman concluded that transfer from an excited lead ion could take place to about the nearest 28 manganese ions.

Botden's critical evaluation of the three theories was based upon their predictions of the dependence of the ratio

$$B = \frac{\text{quantum efficiency of manganese emission}}{\text{quantum efficiency of sensitizer emission}}$$

upon the sensitizer concentration at constant manganese concentration. He demonstrated that

the first two theories predicted a decrease in B with increasing sensitizer concentration, whereas the third theory predicted no dependence of B upon sensitizer content. Botden found experimentally that in the systems $\text{Ca}_3(\text{PO}_4)_2:(\text{Ce} + \text{Mn})$, $\text{Sr}_3(\text{PO}_4)_2:(\text{Sn} + \text{Mn})$, $\text{Ca}_2\text{P}_2\text{O}_7:(\text{Sn} + \text{Mn})$, $\text{Mg}_2\text{P}_2\text{O}_7:(\text{Ce} + \text{Th} + \text{Mn})$ (12), and $3\text{Ca}_3(\text{PO}_4)_2 \cdot \text{CaF}_2:(\text{Sb} + \text{Mn})$ that B increased with increasing sensitizer concentration in disagreement with all three theories. Therefore, he concluded that all three were either incorrect or incomplete. He further demonstrated that an extension of Schulman's explanation which included the transfer of energy from sensitizer to activator via other sensitizer ions would account for the dependence of B upon sensitizer concentration. His calculation of K (the number of cation sites surrounding an excited sensitizer to any one of which energy may be transferred if it is occupied by an activator) gave values from 26 to 50 in agreement with the value obtained by Schulman.

Values of B , the ratio of manganese to cerium quantum efficiencies, for both 2537 Å and 2967 Å excitation are shown in column 5, Tables I, II, III, and IV. Under 2537 Å excitation, there is no increase of B with increasing cerium concentration. This is obviously apparent from data of the series of samples containing 5.0% Mn. While data of the samples containing 0.50% Mn show some scatter because of poorer precision in the measurement of these less efficient samples, nothing resembling a real increase in B with cerium content can be observed. With 2967 Å excitation, a constant B is obtained up to a concentration of 0.10% Ce in the 5.0% Mn phosphors. Less data at low cerium concentration are available for the 0.50% Mn concentration, but, for this manganese concentration as well, B can be interpreted as constant up to 0.10% Ce. At concentrations of 0.50% Ce and greater, B increases with increasing Ce concentration under 2967 Å in agreement with the results of Botden.

The behavior of $\text{CaF}_2:(\text{Ce} + \text{Mn})$ suggests an explanation of the dependence of B upon cerium concentration which does not involve transfer of energy between sensitizers.

A dependence of B upon sensitizer concentration in the absence of any sensitizer to sensitizer transfer can be expected in a system in which: (a) two species of sensitizers with different transfer ranges (K) exist; (b) the species of sensitizer with the greater transfer range is favored by an increase in sensitizer concentration; (c) the excitation energy is shared by the two sensitizer species. As the sensitizer concentration is increased, more of the excitation energy is absorbed by sensitizing centers with the greater transfer range. The increased transfer range of the system makes manganese emission more probable

with respect to sensitizer emission since the excited sensitizers have an opportunity to transfer energy to activator centers situated at greater distances from the sensitizer. Therefore, the ratio B will increase with increasing sensitizer content.

Sensitized System

In order to conclude that the foregoing mechanism takes place in a sensitized system it is necessary to demonstrate that:

1. Two species of sensitizer centers exist in the system with one type favored at higher sensitizer concentrations.

2. No sensitizer-to-sensitizer transfer takes place when each type of center is excited separately. Evidence for this must be no dependence of B upon sensitizer concentration when the centers are separately excited.

3. The sensitizer species favored at high sensitizer concentration must have a greater transfer range (K).

4. An increase of B is obtained with increasing sensitizer content when the excitation energy is shared by the two types of absorbing centers.

An examination of the data obtained from $\text{CaF}_2:(\text{Ce} + \text{Mn})$ reveals that this system meets all four specifications listed.

1. Both reflection and excitation data demonstrate that two types of sensitizer species exist with different absorption and excitation bands. The 3050 Å and 3300 Å bands appear at low cerium concentrations, while the 2500 Å band is created only at higher cerium contents and grows relative to the long wave length bands with increasing cerium concentration. The assignment of the long wave length bands to cerium singlets and the 2500 Å bands to aggregated cerium ions is an obvious designation.

2. No increase in B is observed from the data of Tables I and III under 2537 Å. This indicates that no sensitizer-to-sensitizer transfer occurs upon excitation in the aggregated cerium absorption band. B increases with cerium content under 2967 Å only in samples containing more than 0.10% Ce. From the excitation spectra of Fig. 6 and 8 it may be seen that considerable overlap of the singlet and aggregate cerium excitation bands exists at 2967 Å in samples with concentrations of cerium higher than 0.10%. It is therefore only in the samples of 0.10% and lower cerium concentration that 2967 Å radiation excites only singlet cerium absorbers. Within this concentration range no dependence of B upon cerium content is observed under 2967 Å as well. It can therefore be concluded that no evidence for a transfer of energy from sensitizer to sensitizer exists.

3. The transfer range of aggregated cerium ions is

greater than the range of cerium singlets. The transfer range K may be determined from the ratio B according to the relationship

$$B = \frac{1 - (1 - X\text{Mn})^K}{(1 - X\text{Mn})^K} \quad (\text{I})$$

in which $X \text{ Mn}$ is the mole fraction of manganese. The formula represents the ratio of the number of sensitizers having at least one manganous ion within the nearest K cation sites to the number of sensitizers not having a manganous ion within this range of lattice positions. No specification to denote either the presence or absence of sensitizer aggregates is needed in the formula since this specification would appear in both the numerator and denominator of the expression. In this relationship, radiationless transitions are neglected. The derivation of this ratio was made by Schulman (7) who related it to the ratio of $\text{Pb} + \text{Mn}$ pair absorption to Pb singlet absorption in $\text{CaSiO}_3:(\text{Pb} + \text{Mn})$. The relation of the same expression to B , the ratio of the quantum efficiencies of activator to sensitizer emission, was made by Botden (8), who concluded that its use is not justified for systems in which an energy transfer between sensitizers takes place. However, the demonstration that no sensitizer-to-sensitizer energy transfer takes place in calcium fluoride justifies the use of the formula with this system. Values of K calculated from the above formula are tabulated in column 6 of Tables I, II, III, and IV. The transfer range of singlet cerium sensitizers is found to be about 35, and good agreement is found in the data for both manganese concentrations. The value of K found for aggregate cerium sensitizers in the case of the 5.0% Mn samples is about 50, whereas in the case of 0.50% Mn the average value of K was found to be 66.

4. An increase of B as a function of cerium concentration is obtained when both the aggregate and singlet cerium sensitizers are simultaneously excited. It may be observed with reference to Fig. 6 and 8 that because of the overlap of the aggregate and singlet cerium excitation bands at 2967 Å, excitation energy of this wave length is shared by the two species of sensitizer ions. As the cerium concentration is increased, an increased number of sensitizer aggregates are formed, and the ratio of aggregates to singlets increases. Since aggregates have a greater transfer range than singlets, an increase in B is observed as a function of cerium concentration under 2967 Å excitation. From excitation data, it appears that significant overlap of excitation bands occurs only at concentration of 0.50% Ce and greater. An increase in B as a function of cerium should be observed, therefore, only within this concentration range. The latter con-

clusion is corroborated by the data of Tables II and IV.

No variation in K as a function of either manganese or cerium content is predicted by the derivation of equation (I). No variation of K for singlet cerium sensitizers is obtained, nor is any variation of K for aggregate cerium sensitizers observed in the 5.0% Mn series. In the samples of 0.50% Mn, the value of K for cerium aggregates shows a spread from 53.3 to 82.6. Since this spread is simply a scatter, not a regular function of the cerium content, it must be within the limits of experimental error for these samples. Better precision in the determination of K at higher manganese concentrations is to be expected. Not only are samples of higher manganese concentration more easily reproducible since small errors in manganese content are less significant, but the value of K is a less sensitive function of B at the higher manganese content. At a value of $K = 50$, the slope of the curve of K vs. B has a value of about 150 for 0.50% Mn, whereas the slope of the curve for 5.0% Mn at the same value of K is only about 1.5. The values of the slope were calculated from

$$\frac{dK}{dB} = \frac{-(1 - XMn)^K}{\ln(1 - XMn)}$$

Therefore, although it appears more desirable to calculate K from data obtained at high manganese content in order to obtain better precision, it is necessary to demonstrate that no sensitizer-to-sensitizer transfer exists at low manganese contents as well, for at high manganese contents, sensitizer-to-sensitizer transfer should not be expected since the probability that at least one of the K sites around a sensitizer ion is occupied by an activator is so great that energy transfer between sensitizers is improbable. The probability that at least one of the K sites is occupied by an activator in a sample containing 5.0% Mn with $K = 50$ is 0.92. However, at a concentration of 0.50% Mn with the same values of K , the probability is only 0.22. Therefore, if sensitizer-to-sensitizer transfer existed in the calcium fluoride system, it would have appeared at the lower manganese concentration.

From the determination of K it may be concluded that the transfer range of aggregate cerium sensitizers is about 50% greater than that of cerium singlet centers. This is based on the value of K for cerium aggregates obtained at high manganese concentration, where the determination is made with better precision.

Interpretations of Difference in K

The simplest explanation of the higher value of K for cerium aggregates might be based on the geometry of the phosphor system. A cerium aggregate could be

considered as consisting of a pair of singlet cerium sensitizers whose fields of possible transfer sites (K) overlap. Sensitization of a manganese ion situated at any lattice site included in the overlapping fields could occur following absorption in either of the cerium ions of the aggregate. Transfer from the more remote sensitizer to the activator could take place via the intermediate sensitizer. This process would involve a limited type of sensitizer-to-sensitizer transfer which is restricted to cerium ions constituting an aggregate. While this explanation cannot be completely excluded, it is not particularly attractive. In regarding a cerium aggregate as a pair of singlet sensitizers, absorption and excitation properties which distinguish the aggregate center from the singlet center are overlooked. Moreover, further evidence against this explanation may be derived from manganese emission spectra. Excitation of cerium singlets produces a manganese emission situated at shorter wave lengths than the manganese emission observed upon excitation of cerium aggregates. According to the intermediate transfer scheme, the manganese emission spectrum should be affected only by the cerium ion from which it receives the transferred energy directly. This would be particularly true if the separation between cerium ions constituting an aggregate is greater than the distance between nearest cation neighbors.

A second interpretation of the difference in K for singlet and aggregate sensitizers is more plausible. From the excitation data of Fig. 2 and 6, it may be observed that the 3050 Å and 3300 Å excitation bands overlap at all cerium concentrations. It has been demonstrated that poor excitation of manganese occurs upon excitation in the 3300 Å band while efficient excitation takes place upon irradiation at 3050 Å. Obviously at all cerium contents the excitation energy is shared by the two excited states of the cerium singlet ion upon excitation at 2967 Å, while it is only from the higher of these two states that efficient transfer can proceed. In the determination of B it is assumed that energy transfer is governed only by the consideration that a manganese ion is situated sufficiently near to a sensitizer ion. The probability that a sensitizer ion is in an excited state from which transfer can proceed is assumed to be unity. In the case of 2967 Å excitation, this probability is less than unity since the absorbed quantum can produce excitation of the sensitizer to either of two states. If an expression which incorporates this probability could be used to define B , a higher value of K than that reported here for cerium singlets would be necessary in order to account for the measured value of B . Since no way of approximating a value of this probability is at hand, the determination of K for cerium singlets cannot be further refined at the present time.

Although this interpretation invalidates the value of K obtained for cerium singlets, it does not affect the value determined for cerium aggregates. It does not concern the demonstration that no sensitizer-to-sensitizer transfer occurs in this system and that the observed variation in B under 2967 Å excitation at high sensitizer concentrations is due to the competition of two types of sensitizing centers.

Although the absence of sensitizer-to-sensitizer transfer has been shown in the $\text{CaF}_2:(\text{Ce} + \text{Mn})$ system, its existence in other systems as proposed by Botden may be quite correct. However, it should be pointed out that in the systems discussed by Botden the existence of two types of sensitizer species with different transfer ranges was not considered, although aggregates of sensitizers existed in the concentration range he studied. For none of these systems is sufficient absorption and excitation data available to determine whether aggregated sensitizers constitute a distinct species of sensitizer center.

ACKNOWLEDGMENTS

The author wishes to express his indebtedness to Dr. David L. Dexter, who has made a general theoretical analysis of the sensitized luminescence of inorganic solids (13), and to Dr. C. C. Klick for many discussions and to Mrs. E. W. Claffy for the x-ray diffraction data and for the preparation of some of the samples.

Any discussion of this paper will appear in a Discussion Section to be published in the December 1954 issue of the JOURNAL.

REFERENCES

1. K. J. MURATA AND R. L. SMITH, *Am. Mineral.*, **31**, 527 (1946); J. H. SCHULMAN, E. BURSTEIN, L. W. EVANS, R. J. GINTHER, AND M. WHITE, *Bull. Am. Phys. Soc.*, **24**, 25 (1949); R. J. GINTHER, *This Journal*, **93**, 874 (1951).
2. J. H. SCHULMAN, L. W. EVANS, R. J. GINTHER, AND K. J. MURATA, *J. Applied Phys.*, **18**, 732 (1947).
3. J. B. MERRILL AND J. H. SCHULMAN, *J. Optical Soc. Am.*, **38**, 471 (1948); H. C. FROELICH, *This Journal*, **93**, 101 (1948).
4. M. HUNIGER AND H. PANKE, U. S. Pat. 2,241,950 and 2,241,951 (1941).
5. H. G. JENKINS, A. H. MCKEAG, AND P. W. RANBY, *This Journal*, **96**, 1 (1949); R. NAGY, R. W. WOLLENTIN, AND C. K. LUI, *ibid.*, **95**, 183 (1949).
6. TH. P. J. BOTDEN AND F. A. KROGER, *Physica*, **14**, 553 (1948).
7. J. H. SCHULMAN, R. J. GINTHER, AND C. C. KLICK, *This Journal*, **97**, 123 (1950).
8. TH. P. J. BOTDEN, *Philips Research Repts.* **7**, 197 (1952).
9. F. WICK, *J. Optical Soc. Am.*, **27**, 275 (1937).
10. F. A. KROGER AND J. BAKKER, *Physica*, **8**, 628 (1941).
11. F. A. KROGER, "Some Aspects of The Luminescence of Solids," p. 257, Elsevier Publishing Co., Inc., Houston (1948).
12. H. C. FROELICH, *This Journal*, **95**, 254 (1949).
13. D. L. DEXTER, *J. Chem. Phys.*, **21**, 836 (1953).

Effect of Solvents and Electrolytes on Polarograms of Carbon Tetrachloride¹

JOHAN J. LOTHE² AND L. B. ROGERS

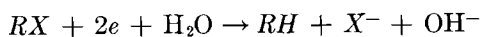
Department of Chemistry and Laboratory for Nuclear Science, Massachusetts Institute of Technology, Cambridge, Massachusetts

ABSTRACT

Polarographic reduction of carbon tetrachloride has been studied in different mixtures of organic solvents with water, using a number of alkali halides and tetraalkylammonium halides as supporting electrolytes. On the positive side of the electrocapillary maximum of mercury, a marked effect of the nature of the anion of the supporting electrolyte on the half-wave potential was observed. On the negative side of the electrocapillary maximum, the cation effected a similar change. It was further observed that reduction became more difficult with increasing concentration of organic solvent. The last can be interpreted in terms of a change in activation energy of the electron transfer process. An equation has been derived which gives the effect of drop-time on the observed half-wave potential for irreversible reactions where the rate of the electron transfer process is the limiting factor. This has been verified experimentally with carbon tetrachloride. Finally, factors governing the occurrence of maxima on the polarographic wave in predominantly aqueous solutions have been investigated.

INTRODUCTION

During recent years a steadily increasing amount of work has been done on the polarographic reduction of organic halides (1-6). Von Stackelberg and Stracke (2) found that the half-wave potentials of halogenated hydrocarbons are independent of the pH of the medium, and that iodides are reduced more easily than bromides, and these, in turn, more easily than chlorides. By controlled-potential, large-scale electrolysis of some halogenated hydrocarbons showed that in most cases waves represented conversion of a carbon-halogen bond to a carbon-hydrogen bond according to the following all-over scheme:



For halogenated organic acids, the polarographic wave is pH-dependent and is shifted to more negative values with increasing pH (3-5). Elving and coworkers (5), studying the polarographic wave of α -bromo-*n*-butyric acid, found that an increase in ionic strength in the alkaline region displaced the half-wave potential to more positive values, whereas the effect was opposite in the low pH region and much less pronounced. In some cases, they observed that the half-wave potential, at constant pH and ionic strength, depended on the kind of buffer used.

Shreve and Markham (7) reported on the effect of organic solvent on the polarographic reduction of *p*-nitroaniline. A marked shift of the half-wave

potential to more negative values occurred with increasing ethanol concentration.

Only scattered remarks can be found in the literature about the effect of organic solvents on polarographic reduction of organic halogen compounds. It has been reported that half-wave potentials for halogenated acetones are shifted to more negative values by the addition of alcohol (8). Von Stackelberg and Stracke (2), working in a 90% butanol-water solution, found half-wave potentials up to 0.10 volt more negative than corresponding potentials in a 75% dioxane-water solution. Gergely and Iredale (6) mentioned, without data, that the half-wave potential for some aromatic iodo compounds was a function of the ionic strength, the alcohol content of the solution, and the nature of the cation of the supporting electrolyte. Rosenthal, Albright, and Elving (9) found that increasing ethanol concentration in the alkaline region shifted the half-wave potential of 2-bromo-*n*-alkanoic acids to more negative values, whereas, in the acid region, evidence of a shift was inconclusive.

A stepwise removal of the halogen atoms has been reported for carbon tetrachloride (2, 10). In 75% dioxane and 0.05*M* tetraethylammonium bromide, two waves were observed (2) with half-wave potentials of -0.78 volt and -1.71 volts. The latter corresponds well to the wave at -1.67 volts for the reduction of chloroform. In a (2:1) methanol-water mixture containing 0.10*M* tetramethylammonium bromide (10), waves for carbon tetrachloride were found at -0.75 volt and -1.70 volts and, for chloroform, at -1.70 volts. In this laboratory (11)

¹ Manuscript received July 9, 1953.

² Visiting Fellow. Present address: Central Institute for Industrial Research, Blindern, Oslo, Norway.

carbon tetrachloride gave a wave at -1.01 volts in 75% dioxane and $0.10M$ lithium chloride. It is obvious that the medium has a profound effect upon reduction, and that a more systematic investigation of the influence of the medium on the half-wave potential is needed. With more data on polarographic reduction of organic halogen compounds it should eventually be possible to formulate the reaction mechanism.

The present investigation deals with polarographic reduction of carbon tetrachloride in mixtures of methanol and water, *n*-propanol and water, acetone and water, and a (1:1) mixture of benzene and methanol, using various inorganic salts and tetraalkylammonium halides as the supporting electrolyte. In a few instances, the effect of ionic strength on the half-wave potential and the influence of concentration of carbon tetrachloride on the wave-shape are also reported. Polarographic reduction of chloroform was investigated briefly in methanol-water mixtures to allow comparisons to be made with the second wave of carbon tetrachloride.

EXPERIMENTAL

Chemicals.—Mallinckrodt's "analytical reagent" grade of carbon tetrachloride, chloroform, methanol, acetone, and benzene was used without further purification. The *n*-propanol was Eastman white label. All the salts used were polarographically pure.

Apparatus.—Measurements of polarographic waves were made manually with a Sargent Model XII Polarograph. In some cases a Sargent Model XXI Recording Polarograph was used to study wave-shapes. Applied potentials were measured at each setting against a potentiometer. All potential measurements were made against an external saturated calomel electrode (S.C.E.) at 27°C . The S.C.E. was connected to the sample cell by means of an agar bridge. Potassium chloride was used as the salt in the bridge for runs with an inorganic salt as supporting electrolyte. When using a tetraalkylammonium halide as electrolyte, the last part of the bridge was made of tetraethylammonium bromide. Resistance of the circuit was measured with a Serfass Conductance Bridge, Model RC M 15. The capillary used had a value for m of $1.46 \text{ mg}^{2/3}/\text{sec}^{1/6}$ at open circuit in $0.1M$ potassium chloride.

Preparation of the solutions.—The supporting electrolyte was dissolved in 25 ml of a mixture of the organic solvent and water. Carbon tetrachloride was added in form of 0.50 ml of a $6.9 \times 10^{-2} M$ solution in the pure organic solvent. Since this investigation was primarily concerned with the effect of the medium on the half-wave potential, no

measurements were taken to determine exact concentrations of organic halide in solutions.

Procedure.—Nitrogen was passed through a portion of the supporting electrolyte before going through the solution in the polarographic cell. Deaeration of 30 min for predominantly organic solutions and 15 min for predominantly aqueous solutions was found to be sufficient to remove oxygen. Then, 0.50 ml of the stock solution of the alkyl halide was added and the mixture flushed for an additional period. In the pure organic solvents one could flush for several minutes without a significant decrease of concentration of the alkyl halide, whereas in water only a few seconds of degassing was possible, owing to the high volatility of the alkyl halide in this medium.

All the data were corrected for residual current as obtained from a blank (prepared in a similar way by adding 0.50 ml of pure organic solvent) and for IR-drop. Unless otherwise stated, experiments were run at a head of mercury of 78 cm, and the solutions were $0.05M$ in supporting electrolyte.

RESULTS

Effect of Organic Solvents on Half-Wave Potentials of Carbon Tetrachloride

Table I gives the half-wave potential for the first wave of carbon tetrachloride in a series of methanol-water mixtures. With all salts studied, changing from water to 20% methanol had little or no effect on the half-wave potential. Beyond 20% the half-wave potential rapidly became more negative and then more or less leveled off, depending on the supporting electrolyte, at very high concentrations of organic solvent.

The second half-wave potential (Table II) was also shifted to more negative values by addition of methanol; the effect was, however, less pronounced. In all mixtures investigated, the second half-wave potential of carbon tetrachloride was practically

TABLE I. *Effect of the concentration of methanol and the nature of the 0.05M supporting electrolyte on half-wave potentials vs. S. C. E. of the first wave of carbon tetrachloride. Values are for $-E_{1/2}$*

Vol. ratio methanol/ water	LiNO_3	LiCl	LiBr	KI	$(\text{CH}_3)_4\text{NBr}$	$(\text{C}_2\text{H}_5)_4\text{NBr}$	$(\text{CH}_3)_4\text{NI}$	$(\text{C}_2\text{H}_5)_4\text{NI}$	$(\text{C}_4\text{H}_9)_4\text{NI}$
Meth- anol	1.09	1.10	1.08	1.08	0.89	0.82	0.92 ^a	0.87	0.88
5:1	0.95	0.95	0.95	0.95	0.82	0.74	0.81		0.74
2:1	0.78	0.80	0.78	0.79	0.70	0.62	0.70	0.65	0.64
1:1		0.59	0.60	0.64	0.58	0.50	0.61		0.59
2:3	0.46	0.47	0.48	0.59	0.46	0.44	0.57	0.57	0.57
1:4	0.35	0.35	0.40	0.54	0.40	0.37	0.53		0.53
Water	0.35	0.35	0.40	0.53	0.40	0.37	0.53		0.53

^a A saturated solution, less than $0.05M$, was used.

TABLE II. A comparison of half-wave potentials (vs. S.C.E.) for chloroform with that for the second-wave of carbon tetrachloride in methanol-water mixtures containing 0.05M electrolytes. Values are for $-E_{1/2}$

Vol ratio CH ₃ OH/H ₂ O	(CH ₃) ₄ NBr		(C ₂ H ₅) ₄ NBr		(CH ₃) ₄ NI		(C ₂ H ₅) ₄ NI		(C ₄ H ₉) ₄ NI		(CH ₃) ₄ NCl CCl ₄	LiCl CCl ₄	KJ CCl ₄
	CCl ₄	CHCl ₃	CCl ₄	CHCl ₃	CCl ₄	CHCl ₃	CCl ₄	CHCl ₃	CCl ₄	CHCl ₃			
CH ₃ OH	1.64	1.62	1.73	1.72	1.66 ^a					1.90			
5:1	1.65	1.65	1.72	1.72	1.64	1.65				1.89	1.91		
2:1	1.64	1.64	1.68	1.68	1.63	1.63	1.75	1.76	1.84	1.84			
1:1	1.60	1.60	1.62	1.63	1.60	1.60			1.77				
2:3	1.57	1.57	1.59	1.59	1.57	1.58	1.65	1.66	1.73	1.72			
1:4	1.54	1.54	1.53	1.54	1.55	1.55			1.68	1.68	1.54	1.71	1.72
H ₂ O	1.53	1.54	1.50	1.51	1.53	1.53			1.65	1.65			

^a A saturated solution, less than 0.05M, was used.

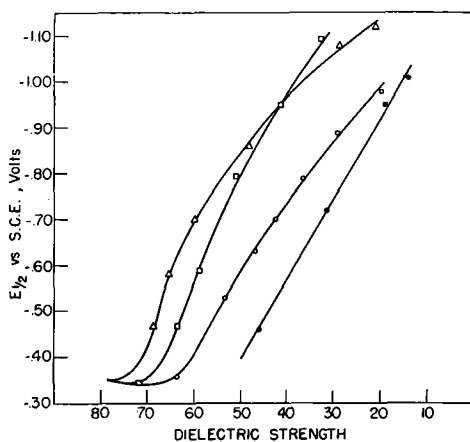


FIG. 1. Half-wave potential of the first wave of carbon tetrachloride as a function of the dielectric strength of mixtures of organic solvents with water. Electrolyte 0.05M lithium chloride. □—methanol-water; △—*n*-propanol-water; ○—acetone-water; ●—dioxane-water [data for dioxane solutions are taken from reference (11)].

identical with the first half-wave potential of chloroform, in agreement with previous observations (2, 10).

The very large shift with change in solvent for the first half-wave potential made it desirable to investigate the reduction in other media. Therefore, studies were made on *n*-propanol-water mixtures and on acetone-water mixtures; Fig. 1 shows the observed half-wave potential vs. the dielectric strength (12) of the solvents (without added electrolyte). As with methanol-water mixtures, reduction became more difficult at higher concentrations of organic solvent. One might have expected methanol and propanol solutions of the same dielectric strength to give the same half-wave potential,³ but this was not the case. It is difficult to state what effect, if any, the capillary activity of the alcohols has on the half-wave potential.

The apparent numbers of electrons involved in the reaction, α , were calculated from the equation of the waves.

³ Strictly speaking, solvents should only be compared at zero ionic strength, but the effect of ionic strength appears to be the same in both solutions.

$$E = E_{1/2} + \frac{0.06}{\alpha} \log \frac{i_a - i}{i}$$

In general, α -values of the first wave of carbon tetrachloride (Fig. 2) decreased markedly with increasing methanol concentration up to about 60% methanol, while at concentrations above 60% α increased slightly. Only with tetrabutylammonium iodide as electrolyte did α decrease throughout the region. Fig. 3 gives α of the second wave of carbon tetrachloride as a function of methanol concentration.

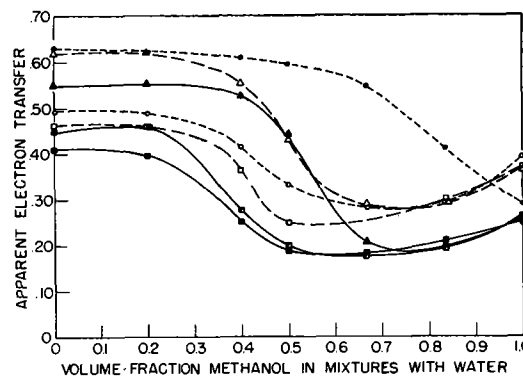


FIG. 2. α -values for the first wave of carbon tetrachloride as a function of methanol concentration and nature of the 0.05M electrolyte. ■—LiCl; ■—LiBr; ▲—KI; □—(CH₃)₄NBr; △—(CH₃)₄NI; ○—(C₂H₅)₄NBr; ●—(C₄H₉)₄NI.

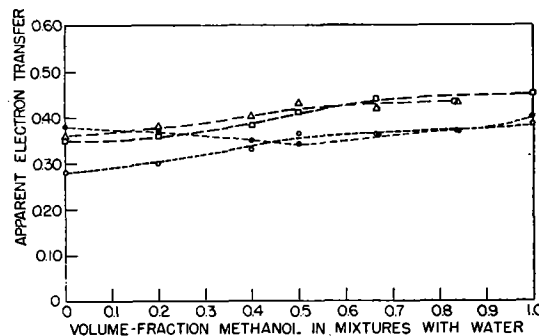


FIG. 3. α -values for the second wave of carbon tetrachloride as a function of methanol concentration and nature of the 0.05M electrolyte. □—(CH₃)₄NBr; △—(CH₃)₄NI; ○—(C₂H₅)₄NBr; ●—(C₄H₉)₄NI.

TABLE III. Half-wave potentials vs. S.C.E. of the first wave of carbon tetrachloride in (1:4) methanol-water mixtures containing 0.05M electrolytes

Electrolyte	$-E_{1/2}$	Electrolyte	$-E_{1/2}$
LiCl	0.35	LiBr	0.40
KCl	0.35	$(\text{CH}_3)_4\text{NBr}$	0.40
NH_4Cl	0.35	$(\text{C}_2\text{H}_5)_4\text{NBr}$	0.37
$(\text{CH}_3)_4\text{NCl}$	0.34	KSCN	0.44
HCl	0.34	KI	0.54
LiOH	0.35	$(\text{CH}_3)_4\text{NI}$	0.53
LiNO_3	0.35	$(\text{C}_4\text{H}_9)_4\text{NI}$	0.53

Effect of Nature of Supporting Electrolyte and Ionic Strength on Half-Wave Potential

The most extensive investigation of the effect of supporting electrolyte on the half-wave potential of carbon tetrachloride was carried out in methanol-water mixtures where eight different electrolytes were studied. Data in Table I show clearly that in predominantly aqueous solutions the first half-wave potential is a function only of the anion of the supporting electrolyte. The same anion effect on the first half-wave potential in predominantly aqueous solutions was found with *n*-propanol-water mixtures and acetone-water mixtures. In high concentrations of methanol, the first half-wave potential of carbon tetrachloride does not depend upon which alkali salt is used as supporting electrolyte, but does depend upon the cation of the supporting alkylammonium halide. On the other hand, only a cation effect was observed for the second half-wave potential throughout the whole range of solvent mixtures (Table II).

In order to get further insight into the observed anion effect on the first half-wave potential in predominantly aqueous solutions, six additional electrolytes were investigated in the (1:4) methanol-water mixture (Table III). The pH had little or no effect, as shown by the constancy of the half-wave potential in going from a lithium hydroxide to a hydrochloric acid solution. Different chlorides, nitrates, and hydroxides gave the same half-wave potential, -0.35 volt, while other anions shifted the potential to more negative values. Iodides shifted it more than thiocyanates,⁴ and these, in turn, more than bromides. Wave shape was also affected by anions, steepness increasing upon going from chlorides to bromides to iodides (Fig. 2).

As shown in Fig. 4, increasing the ionic strength of an alkali halide shifted the first half-wave potential to more negative values in predominantly aqueous solutions, and to more positive values in predominantly organic solutions. Different tetraalkylammonium halides produced a similar shift.

⁴ It was difficult to get maximum-free waves in the thiocyanate solutions.

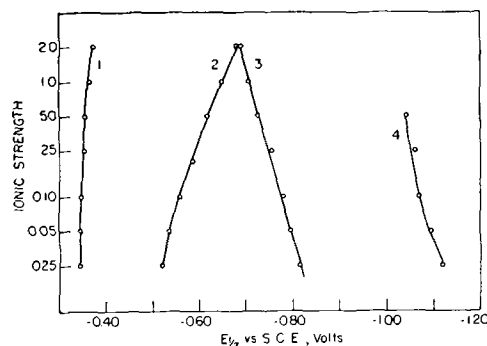


FIG. 4. Effect of ionic strength on the first half-wave potential of carbon tetrachloride. Curve 1—LiCl in a (1:4) methanol-water mixture; curve 2—KI in a (1:4) methanol-water mixture; curve 3—LiCl in a (2:1) methanol-water mixture; curve 4—LiCl in methanol.

The large iodide effect in the (1:4) methanol-water mixture is obvious from these curves. In pure methanol, however, increasing concentrations of iodide and chloride produced the same shift. For the second half-wave potential a shift to more positive values throughout the whole region from water to methanol was found with increasing ionic strength of different tetraalkylammonium halides.

Effect on Shape of Polarographic Wave of Concentration of Carbon Tetrachloride, Temperature, and Head of Mercury

Maxima often occurred on the first polarographic wave of carbon tetrachloride in predominantly aqueous solutions and thereby complicated the waves. Therefore, a series of experiments were carried out to get an idea of the factors governing occurrence of maxima. It was found that formation of maxima was favored at higher concentration of carbon tetrachloride, at longer drop times, and at higher temperatures.

Curves in Fig. 5 showing the effect of concentration of carbon tetrachloride and head of mercury, the latter used as a measure of the drop time, on the polarographic wave in a (1:4) methanol-water mixture, were obtained on the same sample. For one particular concentration of carbon tetrachloride, currents were measured at each potential setting with the mercury reservoir at different levels. After finishing one set of curves in this way, the solution was flushed for a few seconds to decrease the concentration of carbon tetrachloride, and a new set of curves obtained. Fig. 5 shows that in the region of the maxima, the current increased upon lowering the head of mercury, the reverse of the relationship for a diffusion-controlled process. When the concentration of carbon tetrachloride was very high, this rule was apparently not obeyed because curves for lower heads of mercury lay below curves for higher heads. However, polarograms obtained with a

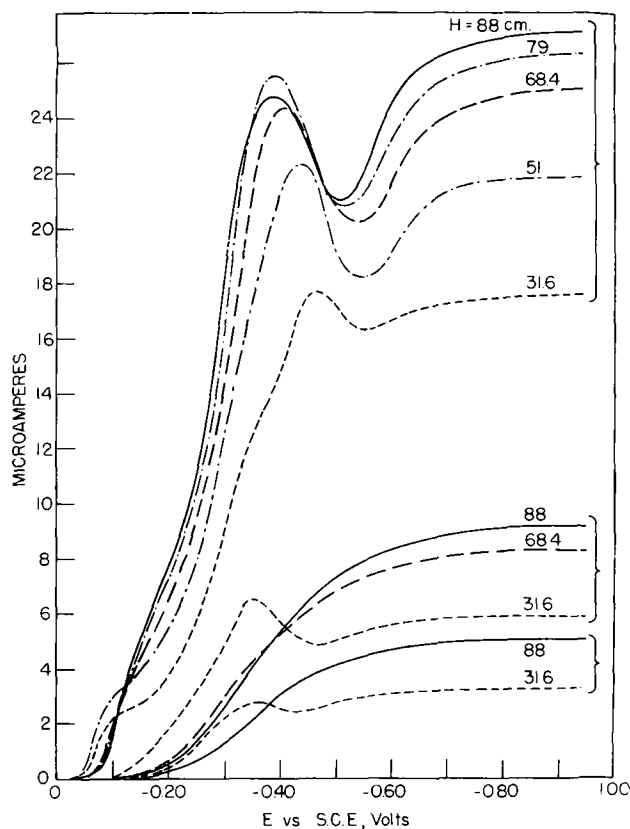


FIG. 5. Effect of concentration of carbon tetrachloride and the head of mercury on the polarographic wave in a (1:4) methanol-water mixture containing 0.05M lithium chloride. All curves within a given bracket were obtained at one particular concentration of carbon tetrachloride.

Sargent Model XXI Recording Polarograph on solutions of very high concentration of carbon tetrachloride showed that, in the region where the maxima occurred, the current-time curves for individual drops also had irregular shapes and went through one or two maxima. This "discharge," shown in Fig. 6, obviously prevented the current from attaining higher values.

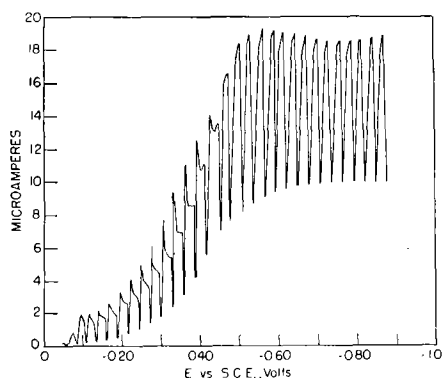


FIG. 6. First wave of carbon tetrachloride, at approximately five times the usual concentration, in a (1:4) methanol-water mixture containing 0.05M lithium chloride.

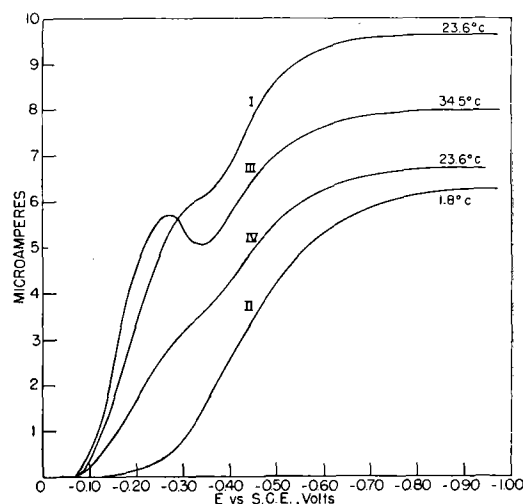


FIG. 7. Effect of temperature on the first wave of carbon tetrachloride in a (1:4) methanol-water mixture containing 0.05M lithium chloride. Numbers attached to the curves give the order in which the runs were made.

In an effort to determine whether or not an adsorption wave was involved, the temperature dependence of the maximum was investigated. A number of runs were carried out on the same sample in the order indicated by numbers attached to each curve in Fig. 7. In these runs, three times the usual concentration of carbon tetrachloride was used to accentuate changes in wave shape that accompany a change in temperature. Some carbon tetrachloride was lost when heating the sample for the high-temperature run as seen from a comparison of the values for the limiting current in the two runs at 23.6°C. In spite of this fact, it is clear that the size of the maximum increased with temperature. It is also interesting to note that no maximum occurred on the polarographic wave at 1.8°C. The possibility of suppressing the maximum with gelatin was also tried, but, in the usual concentration of 0.005% gelatin there was no effect.

In spite of these irregularities, the limiting current for the first wave showed normal diffusion-controlled behavior, i.e., limiting current was proportional to the square root of the height of the mercury reservoir, and had a temperature coefficient of 1.3% per degree.

Influence of Temperature and Head of Mercury on Half-Wave Potential

The temperature-coefficient of the first half-wave potential of carbon tetrachloride was unusually high. In a (2:1) methanol-water mixture, in a (2:1) acetone-water mixture, and in a (1:1) benzene-methanol mixture using potassium iodide, lithium chloride, and tetraalkylammonium halides as supporting electrolytes, the half-wave potential shifted about +3.7 mv/°C. In a (1:4) methanol-water

mixture with lithium chloride and potassium iodide as electrolyte the temperature-coefficient was 3.1 mv/°C. The slightly lower temperature-coefficient in aqueous solutions may indicate a lowering of the activation energy of the electrode process, but the difference is small and may not be significant.

Drop time was another factor of importance for the half-wave potential of carbon tetrachloride. A small shift of the half-wave potential with changing drop time has been predicted by Strehlow and von Stackelberg (13) from a consideration of a modified Ilkovic equation. The shift was predicted, and found to be slightly negative with increasing drop time for thallos and cadmium ions. For carbon tetrachloride, increasing the drop time from 5.5 sec to 16 sec shifted the half-wave potential +0.08 volt in a (2:1) methanol-water mixture which was 0.10M in tetramethylammonium bromide. This shift was opposite in sign and of larger magnitude than the shift predicted by Strehlow and von Stackelberg. This behavior of the half-wave potential may account for the discrepancy between the half-wave potential of the present study and that found by Kolthoff and coworkers (10) using the same solution.

An inspection of the waves revealed that the shift of half-wave potential with increasing drop time was due to the fact that the first part of the wave was nearly independent of the head of mercury, whereas the latter part was not (Fig. 8). It was necessary to determine whether this behavior was a general phenomenon, or whether it applied only in this case because the first part of the wave was located on the positive side of the electrocapillary maximum. A run was made with 0.10M potassium chloride in a (5:1) methanol-water mixture, where nearly the whole wave was located on the negative side of the electrocapillary maximum. The same relationship between the half-wave potential and the height of the mercury reservoir was found.

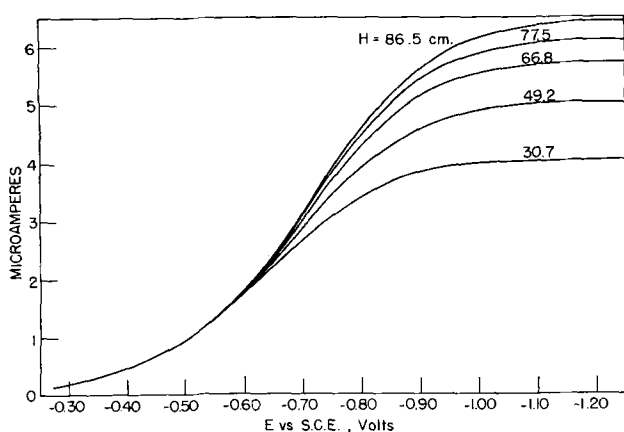


FIG. 8. Effect of the head of mercury on the first wave of carbon tetrachloride in a (2:1) methanol-water mixture containing 0.1M tetramethylammonium bromide.

DISCUSSION

Effect of Added Electrolytes on Half-Wave Potential

A large anion effect on the first half-wave potential was observed in predominantly aqueous solutions and a cation effect in predominantly organic solutions. For the second wave only a cation effect was observed. This behavior leads one to suppose that the difference may be explained by the fact that the two waves in aqueous solutions are located on different sides of the electrocapillary maximum of mercury.

A study of Table III reveals that there exists a relationship between the effect of different anions on the half-wave potential and on the electrocapillary curve of mercury. Anions shifted the half-wave potential in the following order: $\text{Cl}^- < \text{Br}^- < \text{SCN}^- < \text{I}^-$, which is in the same order as their capillary activity (14). The less capillary active anions OH^- , NO_3^- , and Cl^- gave the same half-wave potential. A relationship between half-wave potential and electrocapillary activity is further substantiated by observing the effect of different iodide concentrations on half-wave potential. Using the shift of the electrocapillary maximum as a measure of the capillary activity, Fig. 9 gives curves for the observed half-wave potential and of the potential of the electrocapillary maximum (14) as a function of the iodide concentration. The shift of the half-wave potential with increasing iodide concentration is of

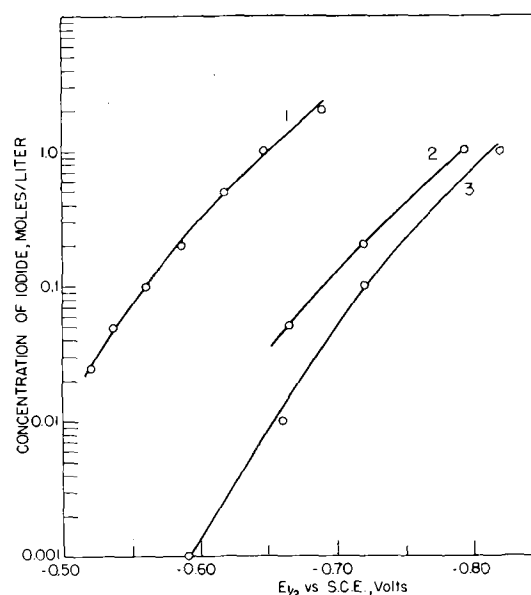


FIG. 9. Effect of iodide concentration on the first half-wave potential of carbon tetrachloride and on the electrocapillary curve of mercury. Curve 1—half-wave potential in (1:4) methanol-water mixtures containing potassium iodide; curve 2—electrocapillary maximum of mercury in (1:4) methanol-water mixtures containing potassium iodide; curve 3—electrocapillary maximum of mercury in water containing sodium iodide (14).

the same magnitude as the shift of the electrocapillary maximum.

This electrocapillary effect on the half-wave potential may be explained by the properties of the electrical double layer which exists between the solution and the mercury drop. Capillary active anions are strongly adsorbed to the mercury surface and form, at potentials more positive than that of the electrocapillary maximum, a sheath of negative ions very close to the mercury drop (the inner Helmholtz plane) (15). Consequently, the electrical potential is much more negative in the inner Helmholtz plane than at the mercury drop, and electrons need more energy to overcome this electrical potential barrier before effecting reduction of the carbon tetrachloride molecule in the inner Helmholtz plane or just outside it. Introduction of more strongly adsorbed anions or higher concentrations of a particular adsorbable anion produces a greater barrier, which in turn requires higher energy of electrons, i.e., a more negative potential to effect reduction. Thus, a change from chloride to iodide of the same concentration results in shifting a half-wave potential on the positive side of the electrocapillary maximum to more negative values.

The fact that waves in the predominantly aqueous solutions are steeper with iodides as electrolyte than with chlorides can be accounted for also. The adsorbed anions are more rapidly desorbed in the case of iodides for a given change toward a more negative potential (16). Thus, the more rapid decrease of this opposing potential in the iodide solutions should favor a steeper polarographic wave.

Similar reasoning can be used to explain the positive shift of the half-wave potential by capillary active cations on the negative side of the electrocapillary maximum. Here, a sheath of adsorbed positive ions produces a potential drop which facilitates reduction. Unfortunately, sufficient data are not available on the capillary activity of tetraalkylammonium salts to allow the effects to be compared. It is, therefore, difficult to say whether or not the shift of the half-wave potential can be explained completely by a capillary activity effect. It is interesting to note that a similar shift of the half-wave potential has been observed by Ashworth (17) in a study of the reduction of benzophenone and fluorenone.

Mechanism of Electrode Reaction

A high temperature coefficient of the half-wave potential is usually associated with an irreversible reaction. The temperature coefficient of the first half-wave potential of carbon tetrachloride, about +3.4 mv/°C, is one of the highest values observed for a polarographic reduction. For comparison, a

coefficient of 3 mv/°C was found in the reduction of hydrogen ions (18).

Further indication of the irreversibility of a polarographic reduction can be found in the behavior of the polarographic wave with respect to the height of the mercury reservoir. If the electron-transfer reaction is very slow, the current in the beginning of the wave is limited not by diffusion, but by the drop time-independent electron-transfer reaction rate. This can be shown by making use of the following equation based on the absolute reaction-rate theory for electrode processes (19):

$$\frac{i}{nFA} = [Ox] \cdot k_1 \cdot e^{(-\alpha' E n F) / (RT)} - [Red] \cdot k_2 \cdot e^{(1-\alpha') E n F / (RT)} \quad (I)$$

Where A is the area of the electrode; α' is the fraction of the applied potential acting in the direction of reduction; and k_1 and k_2 are the rate constants for the forward and backward electron-transfer reactions in the absence of applied potential. k_1 and k_2 depend on the free energy of activation, ΔF^* , and the standard reduction potential, E^0 , of the reaction in the following way:

$$k_1 = \frac{kT}{h} \cdot e^{(-\Delta F_1^*) / (RT)} \quad (II)$$

$$\frac{k_2}{k_1} = e^{-(nFE^0) / (RT)} \quad (III)$$

where k and h are the Boltzmann and Planck constants, respectively. Concentrations of oxidant and reductant at the interface are given by the Ilkovic equation:

$$i_d - i = \text{const. } nFD_{Ox}^{1/2} m^{2/3} t^{1/6} [Ox] \quad (IV)$$

$$i = \text{const. } nFD_{Red}^{1/2} m^{2/3} t^{1/6} [Red] \quad (V)$$

Introducing these expressions into equation (I) and remembering that the area of the mercury drop is proportional to $m^{2/3} t^{2/3}$,

$$i = \frac{i_d}{1 + \frac{D_{Ox}^{1/2}}{D_{Red}^{1/2}} \cdot e^{(E-E^0)nF / (RT)} + \text{const. } \frac{D_{Ox}^{1/2}}{k_1 \cdot t^{1/2}} \cdot e^{(\alpha' E n F) / (RT)}} \quad (VI)$$

For present purposes, this is considered as:

$$i = \frac{i_d}{1 + A + B} \quad (VII)$$

We shall now use this equation to consider the shape of the polarographic wave in three cases:

1. $A \gg B$. When the electron-transfer is rapid, the last exponential in the denominator of equation (VI) can be neglected and the equation becomes

the regular equation for "reversible" polarographic waves where the current is proportional to $m^{2/3} t^{1/6}$, and the half-wave potential is essentially independent of drop time.

2. $A \ll B$. This is a highly irreversible reduction, where the electron-transfer process is very slow and, hence, k_1 is small. The first exponential in the denominator of equation (VI) may be neglected so that the current is given by:

$$i = i_d \left[1 + \text{const.} \frac{D_{ox}^{1/2}}{k_1 \cdot t^{1/2}} \cdot e^{(\alpha' E_{nF}) / (RT)} \right]^{-1} \quad (\text{VIII})$$

At the beginning of the wave, the term 1 may be neglected and the current is independent of the height of the mercury reservoir. At more negative potentials (near the middle of the wave) the term with the exponential is of the same order of magnitude as 1, and the current depends on the drop time, though it is not proportional to $m^{2/3} t^{1/6}$. At still more negative values, where the exponential in equation (VIII) may be neglected, limiting current is proportional to $m^{2/3} t^{1/6}$ and shows the normal diffusion-controlled behavior.

In this case, the coefficient of the logarithmic term in the equation for the polarographic wave at 30°C is given by:

$$\frac{dE}{d \left(\log \frac{id - i}{i} \right)} = \frac{0.06}{\alpha'n} \quad (\text{IX})$$

The half-wave potential, more negative than the reversible value in case 1, depends on the drop time in the following way:

$$\frac{dE_{1/2}}{d(\log t^{1/2})} = \frac{0.06}{\alpha'n} \quad (\text{X})$$

That is, the half-wave potential should be shifted to more positive values with longer drop times, and the magnitude of the shift should be given by the coefficient of the logarithmic term. A plot of the half-wave potential vs. the logarithm of the square root of the drop time should yield a straight line.

3. $A \approx B$. This case is for an intermediate degree of "irreversibility." The current near the beginning of the wave should be only slightly affected by drop time, whereas the limiting current should show normal diffusion-controlled behavior. The half-wave potential should be found in a region intermediate between the values found in cases 1 and 2, and should depend on the drop time in some complicated manner.

Data for carbon tetrachloride fall into case 2 since the limiting current showed normal diffusion-controlled behavior, whereas the current at the beginning of the wave was independent of drop time. Furthermore, the half-wave potential shifted

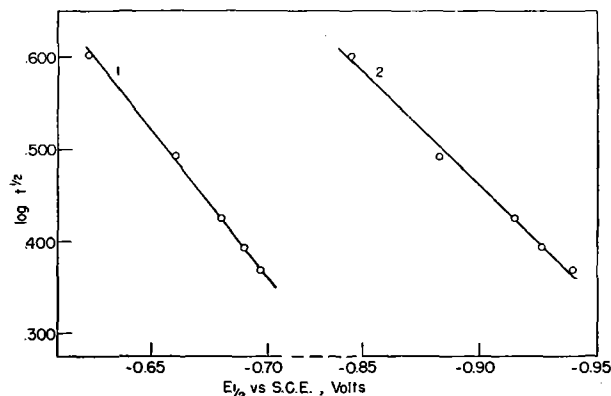
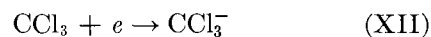
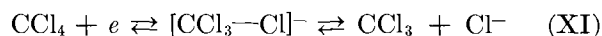


FIG. 10. Half-wave potential of carbon tetrachloride as a function of drop time. Curve 1— $0.1M$ $(\text{CH}_3)_4\text{NBr}$ in a (2:1) methanol-water mixture; curve 2— $0.1M$ KCl in a (5:1) methanol-water mixture.

to positive values with increasing drop times. Curves in Fig. 10 show that there is a linear relationship between the half-wave potential and the logarithm of the square root of drop time which should be found if the reduction at the beginning of the wave is limited by the rate of the electron-transfer reaction. For a $0.10M$ potassium chloride—(5:1) methanol-water solution, equation (X) gave 0.15 for $\alpha'n$ and the slope of the polarographic wave gave 0.20 . Agreement between the two is reasonably good and indicates that the rate of the electron-transfer reaction is the limiting factor at the beginning of the wave.

The different observed effects of solvents and electrolytes on the polarographic wave of carbon tetrachloride can be represented by the following reaction scheme:



There is a slow addition of one electron to carbon tetrachloride to form an unstable transition state complex of the form $[\text{CCl}_3\text{—Cl}]^-$, which at once dissociates to a free radical and a chloride ion. At potentials necessary for this first reduction step, the free radical is immediately reduced further to a negative ion which, in turn, reacts with water to give chloroform. Any factor that contributes to stabilizing the transition state complex, and thereby lowers the activation energy of the first step (k_1 becomes higher), would displace the half-wave potential to more positive values. This is in accord with the observation that reduction is more easily accomplished in water than in organic solvents. Recalling the observed effect of capillary active electrolytes on the half-wave potential, it is obvious that an inactive salt should be used as the support-

ing electrolyte when comparing the effect of solvents on the wave.

Equation (XI), which gives the first step in the reduction of carbon tetrachloride, might indicate a specific chloride effect on the half-wave potential. This is not observed. The reason for this seemingly contradictory behavior is that the chloride effect enters equation (VI) only in the factor before the last exponential in the denominator. It has just been shown that when the polarographic reaction is highly irreversible owing to a slow electron-transfer process, this exponential may be neglected, i.e., equation (VIII) is operating.

Maxima on the Polarographic Wave

Behavior of the maximum for carbon tetrachloride is difficult to reconcile with currently accepted theories of maximum formation. The observation that current-time curves for individual drops in the region of maximum formation had irregular shapes and went through one or two maxima (Fig. 6) might indicate adsorption phenomena, where each maximum on the current-time curve corresponds to a different adsorption process. However, the effect of temperature makes an explanation based upon adsorption less likely. The electrokinetic theory set forth by Antweiler (20), where a difference in potential at different parts of the drop causes streaming of the solution around the drop, might help to explain the phenomena. One would expect capacity currents to be smaller than observed currents. It is possible that a new reaction mechanism favored by higher temperatures occurs in the predominantly aqueous solutions.⁵

ACKNOWLEDGMENT

Discussions with Mr. Hugh Keily as well as criticism of the manuscript by Professor David C.

⁵ After the present manuscript had been submitted for publication, the authors found an abstract of the work of Frumkin and Florianovitch (21) in which the shift toward positive potentials of the reduction waves for nitrates, bromates, and iodates by the addition of cations was explained by a theory very similar to the one proposed here for carbon tetrachloride. Likewise, a paper by Kivalo, Oldham, and Laitinen (22) has just been published in which the hexaaquonickel (II) ion was employed to show experimentally dependence of half-wave potential on drop time and of the current on head of mercury in much the same way that carbon tetrachloride was used in the present study.

Grahame and Professor Philip J. Elving are gratefully acknowledged.

One of the authors (J.J.L.) is indebted to Royal Norwegian Council for Scientific and Industrial Research for a fellowship; the other (L.B.R.) wishes to thank the Atomic Energy Commission for partial support.

Any discussion of this paper will appear in a Discussion Section to be published in the December 1954 issue of the JOURNAL.

REFERENCES

1. R. BRDICKA, *J. Gen. Physiol.*, **19**, 843 (1936); R. PASTERNAK AND H. V. HALBAN, *Helv. Chim. Acta*, **29**, 190 (1946); H. KELLER, M. HOCHWEBER, AND H. V. HALBAN, *ibid.*, **29**, 761 (1946).
2. M. VON STACKELBERG AND W. STRACKE, *Z. Elektrochem.*, **53**, 118 (1949).
3. E. SAITO, *Bull. soc. chim. France*, **1948**, 404; *ibid.*, **1950**, 1185.
4. P. J. ELVING AND C.-S. TANG, *J. Am. Chem. Soc.*, **72**, 3244 (1950); P. J. ELVING, I. ROSENTHAL, AND M. K. KRAMER, *ibid.*, **73**, 1717 (1951).
5. P. J. ELVING, J. C. KOMYATHY, R. E. VAN ATTA, C.-S. TANG, AND I. ROSENTHAL, *Anal. Chem.*, **23**, 1218 (1951).
6. E. GERGELY AND T. IREDALE, *J. Chem. Soc.*, **1951**, 13.
7. O. D. SHREVE AND E. C. MARKHAM, *J. Am. Chem. Soc.*, **71**, 2993 (1949).
8. A. WINKEL AND G. PROSKE, *Ber.*, **69**, 693 (1936).
9. I. ROSENTHAL, C. H. ALBRIGHT, AND P. J. ELVING, *This Journal*, **99**, 227 (1952).
10. I. M. KOLTHOFF, T. S. LEE, D. STOCESOYA, AND E. P. PARRY, *Anal. Chem.*, **22**, 521 (1950).
11. E. B. MIKRUT, B. S. Thesis, Massachusetts Institute of Technology, May 1950.
12. P. DEBYE AND H. SACK, "Constantes Dielectriques, Moments Electriques. Tables Annuelles de Constantes et Donnees Numeriques," Vol. XI, Chap. 22, p. 29-30.
13. E. STREHLOW AND M. VON STACKELBERG, *Z. Elektrochem.*, **54**, 51 (1950).
14. D. C. GRAHAME, *Chem. Revs.*, **41** (1947), Table I, p. 451.
15. Ref. 14, p. 467.
16. Ref. 14, Fig. 3, p. 456; Fig. 5 and 6, pp. 462-463.
17. M. ASHWORTH, *Collection Czechoslov. Chem. Commun.*, **13**, 229 (1948).
18. V. NEJEDLY, *ibid.*, **1**, 319 (1929).
19. H. EYRING, L. MARKER, AND T. C. KWON, *J. Phys. & Colloid Chem.*, **53**, 1453 (1949).
20. H. J. ANTWEILER, *Z. Elektrochem.*, **43**, 596 (1937); *ibid.*, **44**, 719, 831, 888 (1938).
21. A. N. FRUMKIN AND G. N. FLORIANOVICH, *Doklady Akad. Nauk. S.S.S.R.*, **80**, 907 (1951); through *C. A.*, **46**, 1371 (1952).
22. P. KIVALO, K. B. OLDHAM, AND H. A. LAITINEN, *J. Am. Chem. Soc.*, **75**, 4148 (1953).

Preparation of High Purity Lead^{1,2}

RAY C. HUGHES

Philips Laboratories, Inc., Irvington-on-Hudson, New York

ABSTRACT

Previously published methods for the preparation of high purity lead are critically reviewed. The presumably more effective of these methods were subjected to trial and analytical evaluation. Based on these analytical results, a combination of procedures is described which produces lead of extremely high purity. The method employed involves electrolytic displacement of bismuth and other elements from lead salt in solution by treatment with lead metal, coprecipitation of numerous impurities on lead sulfide, conversion to metal, and final vacuum distillation.

INTRODUCTION

Efforts to prepare pure samples of lead and its compounds date back to the work of Stas (1) in 1860. Pure samples have been required for atomic weight determinations, study of the properties of the element and its compounds, and as an analytical aid, especially in assays for gold and in standards for spectrographic analysis. Numerous publications and several reviews on the subject have appeared. However, none of the original publications has presented adequate analytical evidence as to the purity attained. Consequently, the reviews do not clearly establish relative efficacy of the various methods described and, in addition, all are incomplete to a greater or lesser extent.

The purpose of this paper is to present an analytical evaluation of previously described methods and to describe in detail a combination of methods for preparation of pure lead.

Review of Previous Methods

Mellor (2) and Vanino (3) described a method employed by Stas (1) for preparing high purity lead. It comprises purification of a lead acetate solution and several subsequent precipitations and resolutions to obtain a pure lead carbonate which is reduced to metal with potassium cyanide. No adequate analytical data are available for the metal made by this method.

Mellor also refers to the use of vacuum distillation by Lambert and Cullis (4) to purify further lead produced by the Stas method. Baxter and Grover (5) and Richards and Wadsworth (6) purified lead by recrystallization from nitrate solution; the yield from such a method is quite low, and quality of the product questionable. Archibald (7)

¹ Manuscript received December 17, 1951. This paper was prepared for delivery before the Montreal Meeting, October 26-30, 1952.

² This work was supported in part under Contract W33-038 AC-15141 with the Air Materiel Command.

reviews early work in preparing samples for atomic weight determinations; Schopper (8) presents a rather comprehensive review of work done to 1939 on preparation of high purity lead. He considers the method of Haber and Jaenicke (9) to be superior; this method depends on coprecipitation of impurities with lead sulfide. Russell (10) developed an electrolytic method using a perchlorate solution.

Lead of high purity (99.998+ %), with the only impurities being iron and copper,³ has been reported (11). McLellan (12) generously supplied the following details:

1. A new storage battery box with three anodes and two cathodes makes a good cell. Anodes about $\frac{3}{4}$ in. thick with supporting lugs are cast from bismuth-free lead.⁴ Cathodes, made from pure lead deposited on rolled lead⁴ starting sheets equal in area to the anodes, are supported by heavy Pyrex rods.

2. Ideally, the electrolyte, which does not require stirring, has a specific gravity of 1.21; it is composed of 67 g/l Pb as PbSiF_6 and 95 g/l H_2SiF_6 .⁵ Lead should be introduced in the form of bismuth-free PbCO_3 .⁴ Pure glue in a minimum of hot water is added daily. A reasonable current density is 0.5 amp/in.²

3. Wash cathodes thoroughly in distilled water then melt in a spun iron crucible and cast. Remelt in a glass or pure iron container. Gradually add pure red phosphorus while stirring constantly. Keeping the temperature around 350°C, tap off from the bottom most of the decopperized lead. Melt in a spun iron crucible and add reagent grade NaOH and NaNO_3 . Stir 15 min at 400°C and cool. Dissolve caustic skin in distilled water, remelt lead, and granulate in distilled water. Remelt in a beaker, using reagent sodium acetate and NaOH as slag

³ Prepared in Research Department, American Smelting and Refining Company, Barber, New Jersey.

⁴ St. Joe brand.

⁵ Merck reagent grade.

cover. Introduce clean air or oxygen to the lead through a Pyrex tube; skim slag and repeat with fresh slag materials.

Details of a method for preparation of rather pure lead, and a sample of lead so produced, have been supplied by G. K. Williams (13) and associates.⁶ The method has been described by Green (14).

Vacuum distillation has been investigated by Lambert and Cullis (4) and Tamman and Dreyer (15). Kroll (16), Leitgeb (17), and Dushman (18) present reviews on vacuum evaporation of metals and considerations involving purification of lead by such methods. A study of all available data on vacuum distillation of lead indicates that, except for bismuth and possibly antimony, impurities should remain in the initial and final distillate of such a process.

Haber and Jaenicke (9) use a method which appears to have considerable merit for the preparation of pure lead. It is essentially a coprecipitation of contaminants with a small amount of lead (from a solution of lead salt) according to principles which have been elucidated by Hahn (19). Experimental work (see later) shows that not all impurities are adequately removed by this method.

EXPERIMENTAL INVESTIGATION OF METHODS

An experimental investigation was made of the more promising methods selected from those just reviewed. In general, the methods were applied to small samples of lead (or a compound) of low impurity content. Starting materials, purified samples, and concentrates obtained during sample purification were all examined and compared by spectrographic methods developed to give maximum sensitivity. Details of the method have been published elsewhere (20). The following sensitivities of detection (in ppm) were obtained in the direct analysis of a lead sample: Ag, 0.01; Cu, 0.03; Bi, 0.3; Fe, 0.1; Cd, 0.03; Sn, 0.3; Zn, 0.05. Additional sensitivity of at least one order of magnitude was obtainable in specific cases by use of fractions separated from the sample.

As, Se, and Te were not included in the analytical investigation due to the known low sensitivity of spectrographic detection of these elements. The behavior of antimony has not been adequately determined because of its relatively low sensitivity of detection.

Throughout the experimental work extensive precautions were taken to avoid contamination of samples. Water and acids were redistilled from a fused quartz still. Dust-proof fused quartz, high purity alumina, and platinum containers were

used. All vessels were cleaned thoroughly in hot dilute nitric acid and rinsed with redistilled water. When these precautions were not observed, contamination from dust and containers (such as Pyrex glass and porcelain) was detected.

Sulfide Coprecipitation

Experimental work was initiated with a study of the sulfide coprecipitation method of Haber and Jaenicke (9). It was found that Ag, Fe, Mo, and Cu are strongly concentrated in the precipitate and efficiently removed. Bi, Cd, Sb, Sn, and Zn either preferentially remain in solution, or are about equally distributed between the two phases; thus they are not effectively eliminated.

Vacuum Distillation

In view of the foregoing, other methods were tested, one of which was high vacuum distillation. A sample of lead containing approximately 1 ppm each of Ag and Bi, 2 ppm each of Cu and Fe, and 0.1 and 0.5 ppm, respectively, of Cd and Zn was employed. A single distillation in fused quartz at 700°–800°C and 10⁻⁶ mm resulted in lowering the Fe, Cu, and Ag content below the limit of spectrographic detectability. Reheating the distillate at approximately 500°C caused volatilization of a small amount of material which condensed in the pump leads and gave strong spectra of cadmium and zinc. Residual lead gave no spectroscopic evidence of cadmium or zinc. Bismuth was distributed about equally between distillate and residue. Therefore, except for bismuth and possibly antimony for which no data were obtained, high vacuum distillation is an effective and convenient method for removal of impurities from lead. A combination of the Haber and Jaenicke process and vacuum distillation leaves only bismuth and antimony.

Electrolytic Displacement

At this stage it became evident that bismuth is by far the most persistent impurity, and that for which no proved effective method of removal is available. According to the method employed by Stas (1), Sb, Bi, Cu, Ag, Au, and the platinum metals should be displaced from solution by the action of metallic lead. However, no quantitative data exist as to its efficacy.

The method was studied by use of lead acetate filtrate from a prior trial of the sulfide coprecipitation method. To a neutral solution containing 500 grams lead acetate and 500 ml redistilled water, 1 gram finely chipped, high purity lead was added, and the solution heated overnight at the boiling point. The lead was separated and portions of it and the solution analyzed spectrographically. Treat-

⁶ Broken Hill Associated Smelter's Proprietary Limited, Port Pirie, South Australia.

ment with 1-gram portions of lead was repeated several times.

In a single treatment, bismuth was removed from the solution to an extent such that it no longer gave spectrographic evidence of its presence. The metal, of course, gave strong lines of bismuth. Several successive treatments resulted in removal of progressively smaller quantities of bismuth, although after the first treatment the solution must have contained less than 0.3 ppm bismuth based on lead content. Copper and silver were also efficiently removed. Cadmium, zinc, and antimony are not removed by this treatment.

PROCEDURE FOR THE PREPARATION OF HIGH PURITY LEAD AND ITS COMPOUNDS

Due to failure of any single procedure to remove all impurities from lead, a combination of procedures was selected as most suitable for the production of a pure sample. These procedures are applied in proper sequence to avoid reintroduction of contaminants previously removed.

Lead acetate is the most convenient and suitable starting material; however, the metal, nitrate, or other compound may be employed, provided it is eventually converted to the acetate. Technical acetate is of acceptable purity for the starting material.

Preparation of pure lead consists of three processes: (a) treatment of lead acetate or lead nitrate with lead metal, primarily for elimination of bismuth. This may be the first or second step, or it is eliminated if removal of bismuth is not required; (b) lead sulfide coprecipitation specifically for removal of copper, silver, gold, selenium, and tellurium;⁷ (c) high vacuum distillation is required for elimination of cadmium and zinc. It is also effective for removal of practically all metallic elements except bismuth and possibly antimony. Further, this reduces the gas content to a low level.

For step (a) the solution should be highly concentrated, e.g., about 100 ml water to each 200 grams acetate, and contained in a fused quartz or silica flask. Finely divided lead is added in the proportion 1 g/100 g Pb in solution. For 12–24 hr the solution is heated in contact with the lead. The solution is decanted, a fresh quantity of lead is added, and the procedure repeated for a total of five treatments, or until spectrographic analysis of residual lead shows that further treatment removes

⁷ Conversion to metal by ignition of the purified acetate probably aids in elimination of alkalis, alkaline earths, silica, and other soluble impurities which escape precipitation as sulfides, and which are not readily reduced to the elemental condition. However, this is not relied upon for separation of any impurity.

no more impurities. Lead employed for each treatment must be prepared from acetate solution by ignition, unless pure lead is available from a previous preparation. Considerable care must be exercised to avoid copper contamination from vessels or water during this treatment. Addition of water during the last several treatments should be avoided.

To the solution obtained from the above treatment, 1 gram thiourea/100 grams lead in solution is added. The solution, again contained in fused silica or quartz, is heated at the boiling point on a hot plate until it darkens and begins to deposit lead sulfide. Heating is continued 1–2 hr. The solution is then filtered through a fritted silica filter. (Pyrex may be substituted since the exposure is brief.) The solution is again heated for a similar period and filtered. Under these conditions it should be possible to obtain four small precipitates of lead sulfide. Finally, the solution is heated for 12–24 hr, to ensure complete decomposition of thiourea, and filtered. Spectrographic analysis of the precipitates should show that, after the third, there is no further concentration of impurities in the precipitate.

The purified solution is now transferred to a dense, high purity, aluminum oxide crucible, which initially should be no more than $\frac{1}{2}$ full. The solution is cautiously evaporated at gradually increasing temperature until a solid residue of lead acetate is obtained. The crucible is transferred to a pot-type crucible furnace and the temperature of the crucible gradually increased to approximately 700°C. (Close control of temperature is not required.) During heating, the acetate melts, becomes viscous, foams, and finally decomposes to a mixture of metal, oxide, and carbon. Fresh lead acetate solution is dropped onto the lead-lead oxide mixture while heating is continued. The previously formed oxide is now largely reduced. Contact of cold solution with the hot crucible wall should be avoided. Crucible contents should have free access to air in order to oxidize the carbon residue. It is convenient to stir the residue and keep it compacted with a rod of aluminum oxide or spectroscopically pure graphite. Ignition should be conducted in a hood. At some stages, fumes may burn above the crucible. When prepared in this manner, a large proportion of lead is formed with relatively little oxide. The lead may be separated from the oxide by pouring off into a clean silica or Pyrex container; remelting and mechanical separation by pouring into a clean container three or four times results in elimination of all visible oxide.⁸

⁸ If oxide or other compound of lead is desired, the ignition may be carried out at 300°C in fused quartz without subsequent addition of fresh quantities of acetate. Under these conditions, pure lead oxide is formed. However, it should be noted that zinc and cadmium may still be present.

For the final step in purification, lead prepared as described above is transferred to a fused quartz still and redistilled under high vacuum at 700°-800°C. Head and end fractions (1-2% of total) should be discarded.

Lead produced by the procedure described here contains no spectrographically detectable impurities within the sensitivity limits given earlier. Traces of Si, Ca, Mg, Cu, and Fe which are occasionally detected spectrographically are believed to originate from even the best obtainable graphite electrodes. All available evidence would indicate that this lead is probably of the highest purity which has been attained. The methods employed are relatively convenient, rapid, and allow high recovery.

ACKNOWLEDGMENT

It is a pleasure to acknowledge the encouragement of O. S. Duffendack, President and Director of Research of this Laboratory, throughout this work; the assistance of J. S. Schulz with all phases of the experimental work; and the kindness of R. D. McLellan and G. K. Williams, for permission to publish details of methods supplied by them.

Any discussion of this paper will appear in a Discussion Section, to be published in the December 1954 issue of the JOURNAL.

REFERENCES

1. J. S. STAS, *Bull. acad. roy. sci. Belg.*, (2), **10**, 295 (1860).
2. J. W. MELLOR, "A Comprehensive Treatise on Inorganic and Theoretical Chemistry," Vol. VII, p. 508, Longmans, Green and Co. Ltd., London (1947).
3. L. VANINO, "Handbuch der Preparativen Chemie," Band 1, pp. 610-2, Ferdinand Enke, Stuttgart (1925).
4. B. LAMBERT AND H. E. CULLIS, *J. Chem. Soc.*, **107**, 210 (1915).
5. G. P. BAXTER AND F. L. GROVER, *J. Am. Chem. Soc.*, **37**, 1027 (1915).
6. T. W. RICHARDS AND C. WADSWORTH, *J. Am. Chem. Soc.*, **38**, 221 (1916).
7. E. H. ARCHIBALD, "The Preparation of Pure Inorganic Substances," pp. 219-23, John Wiley and Sons, Inc., New York (1932).
8. W. SCHOPPER, in "Reine Metalle," (A. E. van Arkel, Editor), pp. 501-15, Julius Springer, Berlin (1939).
9. F. HABER AND J. JAENICKE, *Z. anorg. u. allgem. Chem.*, **147**, 156 (1925).
10. R. S. RUSSELL, *Proc. Australasian Inst. Mining and Met.*, N.S., No. 95, 125 (1934).
11. T. A. WRIGHT, "Spectroscopy in Science and Industry," pp. 47-50, John Wiley and Sons, Inc., New York (1938).
12. R. D. McLELLAN, Private communications.
13. G. K. WILLIAMS, J. MURRIE, F. A. GREEN, AND N. G. READ, Private communications.
14. F. A. GREEN, Symposium on Refining Non-Ferrous Metals 1949, Inst. Mining and Met. (London), 281-36 (1950).
15. G. TAMMAN AND K. L. DREYER, *Z. anorg. u. allgem. Chem.*, **190**, 53 (1930).
16. W. J. KROLL, *Trans. Electrochem. Soc.*, **87**, 571 (1945).
17. LEITGEBEL, *Z. anorg. u. allgem. Chem.*, **202**, 317 (1931); *Metall U. Erz*, **32**, 206 (1935).
18. S. DUSHMAN, "Scientific Foundations of Vacuum Technique," pp. 740-78, John Wiley & Sons, New York (1949).
19. O. HAHN, "Applied Radiochemistry," The Collegiate Press, Menasha, Wisconsin (1936).
20. R. C. HUGHES, *Spectrochim. Acta*, **5**, 210 (1952).

Mathematical Studies on Galvanic Corrosion

I. Coplanar Electrodes with Negligible Polarization¹

J. T. WABER

Los Alamos Scientific Laboratory of the University of California, Los Alamos, New Mexico

ABSTRACT

Distribution of potential within an electrolyte produced by a coplanar arrangement of electrodes has been determined mathematically. Only the limiting case of negligible anodic and cathodic polarization is considered. Distribution of corrosion attack on the anode has been derived from this potential distribution.

INTRODUCTION

A mathematical study of a typical case of galvanic corrosion is presented in this discussion. Two coplanar electrodes placed in juxtaposition are considered. The arrangement is characteristic of local cells that occur frequently in corrosion. Pertinent galvanic cells may consist either of many tiny electrodes imbedded in a metal or, in some cases, of large pieces of different metals connected electrically. It is possible to distinguish more satisfactorily, in a qualitative way, between microscopic and macroscopic galvanic cells on the basis of current density distribution. In microscopic cells, current density is relatively uniform over each electrode, whereas in macroscopic cells it varies significantly.

In a given environment, and irrespective of its physical size, a galvanic cell may behave as though it were "macroscopic" or "microscopic," depending on whether its critical dimension is much larger or much smaller than a polarization parameter, ϱ . This critical dimension is that which affects distribution of current density most strongly and thus depends upon the geometry of the cell. In certain cases, it may be the separation of electrodes and, in others, the smallest dimension of one electrode. This parameter² has the dimension of length and is defined by Wagner (1) as

$$\varrho_i = K \left| \frac{d\Delta E_i}{dJ_i} \right| \quad [1]$$

where K is the specific conductivity of the corrodent, ΔE_i is the overvoltage of the i th metal or electrode, and J_i is the current density. The vertical bars denote the absolute value of the derivative.

¹ Manuscript received February 23, 1953. This paper was prepared for delivery before the Detroit Meeting, October 9 to 12, 1951.

² The symbol ϱ is used to emphasize the dimensional character of this parameter and to remove any possible confusion with K which is commonly used to denote conductivity.

DERIVATION OF RESULTS

Only the limiting case in which polarization can be neglected is considered. It is equivalent to assuming that ϱ is negligibly small. Such would be the case if the electrolyte resistance were very high, or if the smallest critical dimension, λ , of the galvanic cell were large in comparison with ϱ . Hence, because λ/ϱ is large, such galvanic cells behave as though they were macroscopic, irrespective of their physical size. If the electrolyte resistance is very large, almost all electrodes behave macroscopically. On the contrary, under corrosive conditions that permit strong polarization of the electrodes (ϱ large), arrays of macroscopic elements may behave as though they were of microscopic dimensions. Solutions of high conductivity can also produce the same effect.

Distribution of Potential

Distribution of potential throughout the electrolyte is given by Laplace's equation because space charges and sources or sinks for ions are not present in bulk corrosive media. The exact potential distribution depends on the geometry of electrodes as well as their voltages. Electrodes are considered to be part of the boundary of the electrolyte. In order to calculate the distribution of the potential, one must solve a boundary-value problem for which the values of potential imposed on the boundary of the electrolyte, as well as the geometry of the boundary, are specified.

Fourier series and conformal mapping are two methods which may be used for solving such problems. Fourier series and conformal mapping are discussed by Churchill (2) among others, while a less mathematical approach to various boundary value problems is given by Jakob (3) on heat transfer.

One may calculate the local corrosion intensity by evaluating the normal gradient of the potential at one electrode. The numerical evaluation may be difficult and tedious in some cases.

Boundary Conditions

For corrosion by local cells, a coplanar arrangement of electrodes is pertinent and illustrates the principal features needed for an analysis. The primary interest lies in the effects due to the anode-cathode junctions. In order to eliminate other edge effects it is assumed: (a) that long, narrow strips of each electrode are juxtaposed to form an infinite, alternating array, (b) that the array has even symmetry, and (c) that the length in the Z direction is so large as to have no effect on the current distribution. Such an arrangement is shown in Fig. 1a. At the center of each anode (or cathode) one can see intuitively that there must be no net current flow since the flow of ions changes direction to either side of the center. We shall choose the origin in the center of one of the anodes. Since there is no variation in potential in the Z direction, and

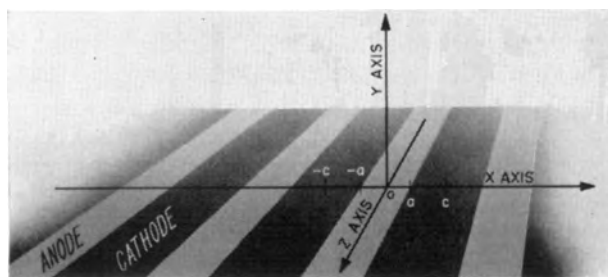


FIG. 1a. Perspective view illustrating relative orientation and shape of the electrodes.

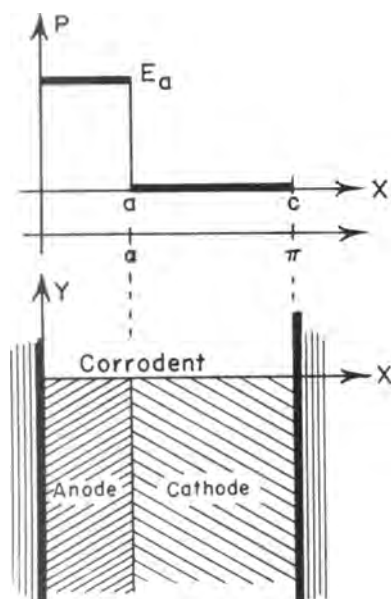


FIG. 1b. Distribution of potential assumed as the boundary conditions is shown in the upper drawing. In the lower drawing the anode and cathode arrangement is illustrated. At the remote edges of the electrodes, boundary conditions are equivalent to assuming insulation.

consequently none in the current density, we may restrict our attention to the two-dimensional flow problem. Because of the highly symmetrical arrangement, only a semi-infinite strip of liquid lying in the first quadrant of the XY plane above the array needs to be considered. The width of this strip is equal to half of the sum of the anode and cathode widths. Geometric relations are illustrated in Fig. 1b.

There can be no flow of electrons across the boundary formed by the Y axis, and on this boundary the gradient of the potential in the X direction is zero. This statement is mathematically equivalent to assuming insulation of the boundary. A similar argument shows that the horizontal gradient in Fig. 1b is zero at the boundary, $x = c$.

The potential is measured with respect to the unpolarized cathode. The anodic potential in excess of the cathodic potential, i.e., the potential difference, is designated as E_a and the potential in the solution as $P(x, y)$.

The pertinent boundary conditions are:

$$\lim_{y \rightarrow \infty} P(x, y) < \text{const.} \quad [2]$$

$$\left. \frac{\partial P}{\partial x} \right|_{x=0} = \left. \frac{\partial P}{\partial x} \right|_{x=c} = 0 \quad [3]$$

$$P(x, 0) = \begin{cases} E_a & 0 \leq x \leq a \\ 0 & a \leq x \leq c \end{cases} \quad [4]$$

Solution by Fourier Series

A Fourier series, which satisfies Laplace's equation and conditions [2] and [3], is

$$P(x, y) = A_0 + \sum_{n=1}^{\infty} A_n \exp(-nhy) \cos(nhx) \quad [5]$$

where the constants A_0 and A_n are determined by boundary condition [4]. In [5], n is an integer and h is a reciprocal length equal to

$$h = \pi/c \quad [6]$$

One may employ the orthogonal properties of a cosine series to obtain the coefficient A_n . That is, both sides of [5] are multiplied by $\cos mhx$ and then integrated termwise with respect to x over the range $x = 0$ to $x = c$. Thus

$$A_m = \frac{2h}{\pi} \int_0^c P(x, 0) \cos(mhx) dx = \left(\frac{2E_a}{\pi^m} \right) \sin(mha) \quad [7]$$

$$A_0 = \frac{1}{c} \int_0^c P(x, 0) dx = E_a(a/c) \quad [8]$$

After substitution, the potential at any point is given by

$$P(x, y) = \frac{E_a a}{c} + \frac{2E_a}{\pi} \sum_{n=1}^{\infty} \exp(-nhy) \frac{\sin(nha)}{n} \cos(nhx) \quad [9]$$

The equations can be simplified slightly by defining the dimensionless variables.

$$\begin{aligned} \xi &= hx \\ \eta &= hy \\ \alpha &= ha \end{aligned} \quad [10]$$

Hence,

$$P(\xi, \eta) = E_a \alpha + \frac{2E_a}{\pi} \sum_{n=1}^{\infty} \frac{1}{n} \exp(-n\eta) \sin(n\alpha) \cos(n\xi) \quad [11]$$

The normal gradient is the η -derivative of P . Therefore the local anodic corrosion rate, $r(\xi)$, at any point on the electrode surface is

$$r(\xi) = - \left(\frac{\pi R_o}{2} \right) \frac{\partial P}{\partial \eta} \Big|_{\eta=0} \quad [12]$$

where the constant R_o is defined as

$$R_o = \frac{2KM}{\pi Fv} \quad [13]$$

In [13], M is the atomic weight of the anodic metal ion, v is its charge, and F is Faraday's number. Substitution of [11] into [12] leads to

$$r(\xi) = R_o E_a \sum_{n=1}^{\infty} \sin(n\alpha) \cos(n\xi) \quad [14]$$

Series [14] does not converge and hence it cannot be used for evaluating the corrosion current. Substitution of a small nonzero value of η_o into the derivative of [12] leads to small bounded values of a series similar to [14]. However, it is preferable to evaluate the derivative at zero by a different method, and not to depend upon a limiting value as η_o approaches zero.

Solution by Conformal Mapping

A closed analytic expression which is bounded over most of the anodic region may be obtained for the η -derivative by conformal mapping. Wagner (4) has applied this technique to the solution of similar problems in cathodic protection.

The semi-infinite strip of corrodent in Fig. 1b may be regarded as the complex Z plane by letting

$$z = x + iy$$

where i is the imaginary square root of minus one. Mathematical transformations are used to rearrange the electrode positions into one for which the potential distribution is well known. The four steps necessary to transform the arrangement of electrodes shown in Fig. 2a into that shown in Fig. 2b are defined below. The effect of each transformation is shown in Fig. 3. The quantity

$$\gamma = \sin \left(\frac{\pi}{2} \cdot \frac{2a - c}{c} \right) \quad [15]$$

is used in the following equations for convenience. The first transformation is an expansion which changes the scale,

$$z^i = \frac{\pi}{2} \left(\frac{2z - c}{c} \right) \quad [16]$$

The second transforms the strip into a semi-infinite plane,

$$z^{ii} = \sin z^i \quad [17]$$

The third shifts the origin by γ units,

$$z^{iii} = z^{ii} - \gamma \quad [18]$$

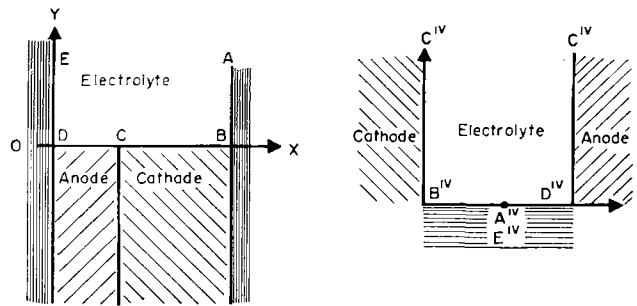


FIG. 2. Net change in relative anode and cathode positions brought about by the series of transformations. Fig. 2a (left) shows the initial location and Fig. 2b (right) shows the final location.

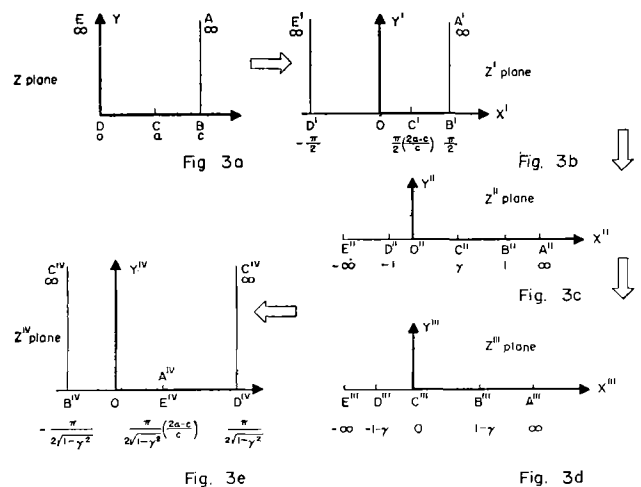


FIG. 3. Detailed effects of each transformation from the Z plane in Fig. 3a to the Z^{IV} plane in Fig. 3e.

The fourth transforms the semi-infinite plane back into a strip, but with a relocation of the vertices, i.e., corners. It is a special type of Schwartz-Christoffel transformation.

$$z^{iv} = \int \frac{dz^{iii}}{z^{iii}(z^{iii} - 1 + \gamma)^{\frac{1}{2}}(z^{iii} + 1 + \gamma)^{\frac{1}{2}}} \quad [19]$$

Integration of [19] gives

$$z^{iv} = \frac{1}{\sqrt{1-\gamma^2}} \arcsin \left(\gamma - \frac{1-\gamma^2}{z^{iii}} \right) \quad [20]$$

It can be shown that boundary condition [4] transforms to

$$P = 0 \text{ for } x^{iv} = \frac{-\pi}{2\sqrt{1-\gamma^2}} \quad [21]$$

$$P = E_a \text{ for } x^{iv} = \frac{\pi}{2\sqrt{1-\gamma^2}}$$

as long as Y^{iv} is positive and finite. The solution of the problem in the Z^{iv} plane is well known and gives isopotential lines parallel to the Y^{iv} axis.

The boundary conditions are satisfied by

$$P = E_a \operatorname{Re} \left(\frac{1}{2} + \frac{z^{iv} \sqrt{1-\gamma^2}}{\pi} \right) \quad [22]$$

where **Re** stands for the real part of the enclosed expression. By reversing the sequence of transformations one can show that

$$P = E_a \operatorname{Re}$$

$$\left\{ \frac{1}{2} + \frac{\arcsin \left[\gamma - \frac{1-\gamma^2}{\sin \frac{\pi}{2} \left(\frac{2z-c}{c} \right) - \gamma} \right]}{\pi} \right\} \quad [23]$$

Equation [23] has an advantage in permitting direct calculation of the Y derivative; whereas the equivalent Fourier representation [14] does not converge at $y = 0$. The derivative can be shown to be

$$\frac{\partial P}{\partial y} \Big|_{y=0} = \frac{E_a}{c} \left\{ \frac{\cos \left(\frac{\pi}{2} \cdot \frac{2a-c}{c} \right)}{\sin \left(\frac{\pi}{2} \cdot \frac{2x-c}{c} \right) - \sin \left(\frac{\pi}{2} \cdot \frac{2a-c}{c} \right)} \right\} \quad [24]$$

if one notes that

$$\frac{\partial P}{\partial y} = \left(\frac{dP}{dz} \cdot \frac{\partial z}{\partial y} \right) = \operatorname{Re} \left(i \frac{dP}{dz} \right) \quad [25]$$

It may be seen that this derivative goes to infinity at $x = a$. Practically, current density remains finite because of polarization, but this factor has been ignored in the idealized analysis presented here.

Potential of a Composite Electrode

The potential in solution of a galvanic cell with respect to an infinitely remote reference electrode can be derived from equation [9]. The potential at infinite y and any value of x is:

$$P(x, \infty) = E_a(a/c) = E_a(\alpha/\pi) \quad [26]$$

Under such conditions, the potential of a composite metal or of a galvanic cell depends on the percentage of anodic material or phase present. This highly important result may also be derived from [23].

NUMERICAL EVALUATION

Potential fields have been calculated for the α -value of $\pi/2$, $\pi/4$, and $\pi/8$; that is, for values of the ratios of the anodic to the cathodic width of 1, $\frac{1}{3}$, and $\frac{1}{4}$.

Expression [11] or [23] may be used and, in a number of cases, tabulated values of $P(x, y)$ have been checked with both expressions.

Evaluation of Equation [23]

The real and imaginary parts of the arcsin must be separated in order to facilitate direct calculation. For a slightly simpler calculation procedure, the reader is referred to Hawelka's tables (5) of the sines and cosines of complex numbers. However, the following equations are evaluated easily and depend only upon the usual trigonometric functions of a real variable. Two variables, s and t , are defined such that

$$P(x, y) = E_a \left\{ \frac{1}{2} + \frac{1}{\pi} \operatorname{Re} \sin^{-1} \left(\gamma - \frac{1-\gamma^2}{t+is} \right) \right\} \quad [27]$$

Hence,

$$s = \cos \left(\xi - \frac{\pi}{2} \right) \sinh \eta \quad [28]$$

$$t = -\gamma + \sin \left(\xi - \frac{\pi}{2} \right) \cosh \eta \quad [29]$$

It may then be shown that

$$P(x, y) = E_a \left\{ \frac{1}{2} + \frac{1}{\pi} \operatorname{Re} \sin^{-1} (\mu - i\nu) \right\} \quad [30]$$

where the quantities μ and ν are

$$\mu = \frac{\gamma(t^2 + s^2) - t(1-\gamma^2)}{t^2 + s^2} \quad [31]$$

$$\nu = \frac{s(1-\gamma^2)}{t^2 + s^2} \quad [32]$$

The real part of the arcsin is

$$\operatorname{Re} \sin^{-1} (\mu - i\nu) = \sin^{-1} \left\{ \frac{2\mu}{\sqrt{(1+\mu)^2 + \nu^2} + \sqrt{(1-\mu)^2 + \nu^2}} \right\} \quad [33]$$

Although the expression for the potential in terms of s and t is cumbersome to write, only 40 arithmetic operations are involved in calculating the potential at a given point.

Potential Fields

Waber has tabulated elsewhere (6) values of the dimensionless parameter representing potential, $P(x, y)/E_a$, for the values of α equal to $\pi/2$, $\pi/4$, and $\pi/8$.

The potential fields are presented as perspective drawings in Fig. 4, 5, and 6. Regard that portion of these fields which has a potential in excess of $E_a/2$ as "anodic" and the remainder as "cathodic." The equipotential line, $P = E_a/2$, is concave toward the anode if $\alpha < \pi/2$. Thus, considerable portions of the corrodent are left at potentials near that of the cathode. Shrinkage of the anodic portion toward the anode, as α decreases, is illustrated in these figures. Daniel-Bek's (7) and Copson's (8) experi-

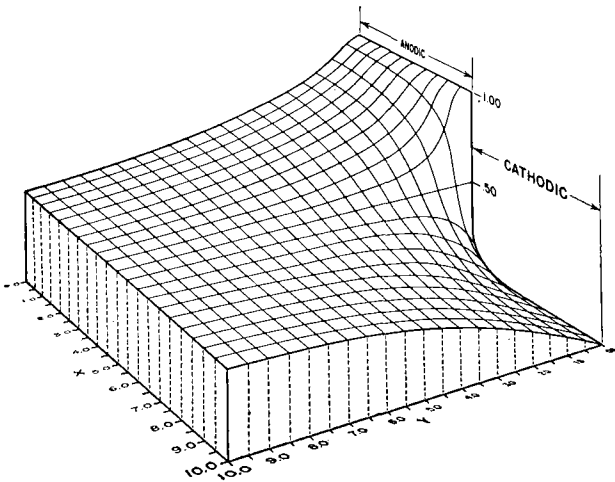


FIG. 4. Perspective drawing of the distribution of potential for equal relative anode and cathode areas.

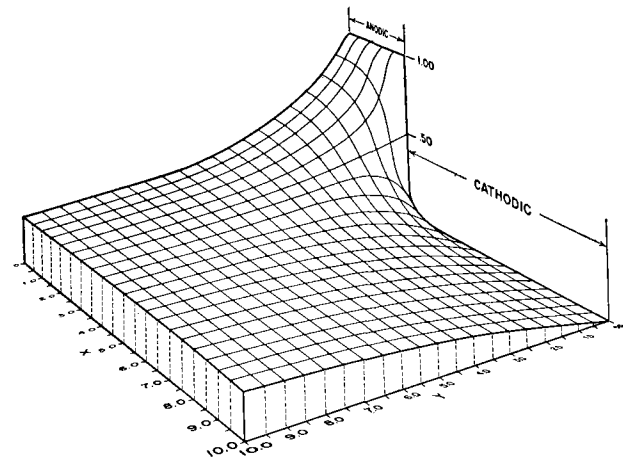


FIG. 5. Perspective drawing of the distribution of potential where $\alpha = \pi/4$, that is, where the anode is one third the width of the cathode.

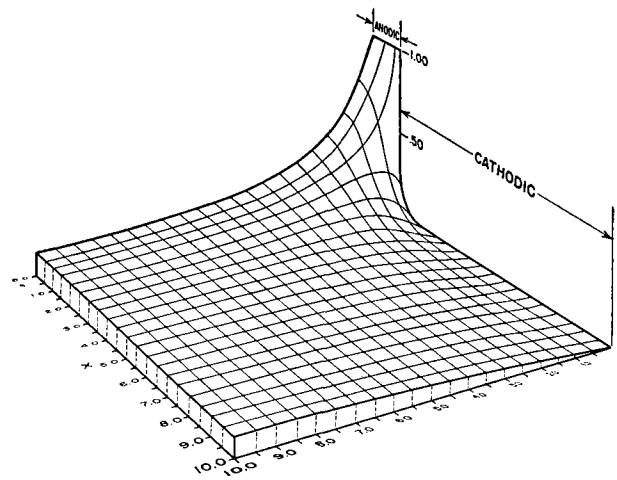


FIG. 6. Perspective drawing of the distribution of potential where $\alpha = \pi/8$, that is, where the anode is one seventh the width of the cathode.

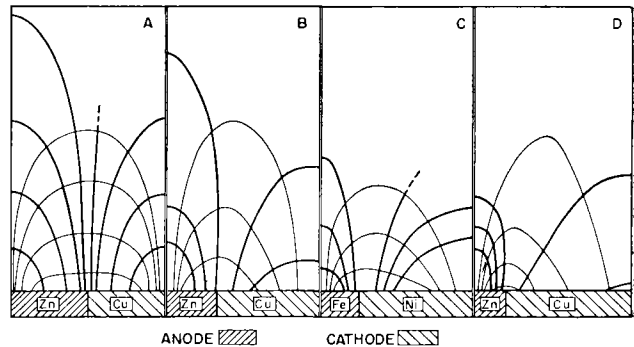


FIG. 7. A diagrammatic summary of measurements by Daniel-Bek and by Copson illustrating the effect of relative anodic size on potential distribution in a corrodent. (A) Equal anode and cathode areas for Cu-Zn couple in NaCl; (B) relative anode area $\alpha = \pi/3$ for Cu-Zn couple in NaCl; (C) relative anode area $\alpha = \pi/4$ for Fe-Ni couple in Bayonne tap water; (D) relative anode area $\alpha = \pi/5$ for Cu-Zn couple in NaCl. Horizontal dimensions of various test specimens have been replaced by a common scale. The ordinate in the graph is the relative distance perpendicular to the metallic surface. Heavy lines are the equipotential lines and the others are the flow lines of the ions.

TABLE I. Relative corrosion current density $r(x)/E_a R_a h$

x	$\alpha = \pi/2$	$\alpha = \pi/4$	$\alpha = \pi/8$
0*	0.5000	1.207	2.515
0.5	0.5098	1.227	2.554
1.0	0.5411	1.292	2.684
1.5	0.6013	1.415	2.930
2.0	0.7074	1.631	3.363
2.5	0.9003	2.023	4.150
3.0	1.3068	2.789	5.799
3.5	2.5628	5.365	11.372
3.75	5.0968	10.429	21.026
4.00	∞	∞	∞

* Anodic region assumed to be 4 units wide.

mental data which are summarized on a common relative scale in Fig. 7, qualitatively show this shrinkage of the anodic field. In slightly different terms the equipotential line that corresponds to $E_a(a/c)$ and goes to infinity is straight where $\alpha = \pi/2$. However, this line becomes concave toward the anode if α is less than $\pi/2$. Daniel-Bek (7) made this conclusion on the basis of his experimental studies.

Evaluation of the Current Density

The local corrosion rate is given by equation [12]. The constant, R_o , includes the effect of conductivity of the corroding medium as well as the valence type and atomic weight of the anodic metal. It is desirable to work with dimensionless parameters so that the tabulated values may be applied to all similar problems. To this end, $r(\xi)$ is divided by $E_a R_o$. Use of simple algebra results in

$$\frac{r(\xi)}{E_a R_o} = \frac{r(x)}{E_a R_o h} = \left(\frac{c}{2E_a} \right) \frac{\partial P}{\partial y} \Big|_{y=0} \quad [34]$$

Values for the right hand side of [34] are given in Table I for three percentages of anodic material. For application to a specific experimental problem to be discussed in a subsequent report, the anodic region was assumed to be four units wide. The width of the cathode was adjusted so that the three values of α were $\pi/2$, $\pi/4$, and $\pi/8$.

As α decreases (for fixed a), the relative corrosion current density increases somewhat faster than does the sum of the half widths c .

SUMMARY

An expression has been derived for the distribution of potential within a solution brought about by the

immersion of a coplanar galvanic couple in the solution, and numerical values have been obtained. Only the limiting case of negligible polarization is discussed. The local corrosion rate was calculated from the normal derivative of the potential evaluated at the electrodes.

ACKNOWLEDGMENTS

The fruitful suggestions and kind advice of Carl Wagner are gratefully acknowledged. Also appreciated are the help of S. F. Waber and the assistance of several members of the Computing Group in the Theoretical Physics Division of the Los Alamos Scientific Laboratory in certain phases of the calculations. This work was initiated at Illinois Institute of Technology and the author would like to thank most heartily Hugh J. McDonald for his continuing encouragement.

Any discussion of this paper will appear in a Discussion Section to be published in the December 1954 issue of the JOURNAL.

REFERENCES

1. C. WAGNER, *This Journal*, **98**, 116 (1951).
2. R. CHURCHILL, "Fourier Series and Boundary Value Problems," p. 94, McGraw-Hill Book Co., New York (1941).
3. M. JAKOB, "Heat Transfer," Vol. I, John Wiley & Sons, Inc., New York (1949).
4. C. WAGNER, *This Journal*, **99**, 1 (1952).
5. R. HAWELKA, "Vierstellige Tafeln der Kreis- and Hyperbelfunktionen sowie ihrer Umkehrfunktionen," F. Vieweg Braunschweig (1931).
6. J. T. WABER, AEC Document LA 1488, Jan. 26, 1953.
7. V. S. DANIEL-BEK, *Zhur. Fiz. Khim.*, **18**, 250 (1944).
8. H. R. COPSON, *Trans. Electrochem. Soc.*, **84**, 71 (1943).

Intensity Anomalies in Electron Diffraction Patterns of CuO¹

J. M. COWLEY

Chemical Physics Section, Division of Industrial Chemistry, Commonwealth Scientific and Industrial Research Organization, Melbourne, Australia

ABSTRACT

The oxide layer, giving the so-called CuO' electron diffraction pattern and formed by heating copper in air at 600°C, has been examined by high-resolution electron diffraction and electron microscopy. It is shown that the intensity anomalies which differentiate the CuO' pattern from the normal CuO pattern are not due to impurities as has been suggested. The oxide grows in the form of long needle-like spines approximately perpendicular to the copper surface, with one or more screw dislocations along the axis of each spine. Each spine is a single crystal of CuO, about 1000 Å in diameter, elongated along the (110) zone axis. Intensity anomalies of the CuO' pattern result from this particular morphology.

INTRODUCTION

Since Murison (1) first reported that the electron diffraction pattern obtained from copper surfaces heated in air at 300°–600°C is often not that of normal CuO, but, instead, a "three-ring" pattern, a number of authors have repeated his observations and offered various explanations for the anomaly. The three-ring pattern, or "CuO' pattern," as it has been called, has the same dimensions as the normal CuO ring pattern and so appears to be given by a similar monoclinic crystal lattice with unit cell dimensions of the normal CuO, $a = 4.65$, $b = 3.41$, $c = 5.11$ Å, and $\beta = 99^\circ 29'$. The relative intensities of the rings are, however, markedly different. In particular, the innermost ring, the (110) with $d = 2.73$ Å, is strong instead of weak, and the (11 $\bar{2}$) ring with $d = 1.95$ Å is also stronger than normal.

Murison concluded that the pattern is given by another crystal form of CuO. Other suggestions have been that it is given by an oxide with the CuO structure, but with an excess of oxygen or copper, or, more specifically, by an oxide intermediate between CuO and Cu₂O. Honjo (2) showed that the rings of the CuO' pattern are usually arced and suggested that anomalous intensities result from a preferred orientation of crystallites of normal CuO, due to the preferential development of certain crystal faces in the growing oxide layer.

Recently, Gulbransen and McMillan (3) studied the oxidation of pure copper and examined conditions under which the CuO' pattern appeared. They found a dependence on the purity of the copper used, in that intensity anomalies were less pronounced for high purity copper than for less pure copper. They concluded that the high intensities of the rings at $d = 2.73$ and 1.95 Å result from the

superposition of strong rings from oxides of other metals present as impurities in the copper.

A series of observations made in this laboratory during the early part of 1951 provides ample evidence that, at least in the case of the oxides studied by the author, the explanation given by Gulbransen and McMillan cannot be correct, and that, in fact, abnormally intense rings are given by the same material as the other rings. The author used an electron diffraction camera of high resolving power (4) and obtained arc patterns and single-crystal patterns from the oxide formed on a fine copper gauze by heating it in air. Some of the specimens were examined in the RCA Model EMU electron microscope.

Abnormal intensities of the rings may be explained in terms of the particular morphology of crystals of normal CuO growing in the form of thin spines around screw dislocations. This has become evident in the course of an investigation on the influence of screw dislocations on crystal morphology and electron diffraction intensities, with special reference to CuO and ZnO smoke crystals (5).

EXPERIMENTAL OBSERVATIONS

Electrolytic copper grids, with 200 meshes to the inch, such as are sometimes used to support electron microscope specimens, were heated in air at 600°C for periods of up to 25 hr. The grids then appeared jet black in color, with an obvious decrease in the size of the holes, indicating a thick oxide layer. When the electron beam was limited to a small region along the edge of a hole in the mesh, an arc pattern, such as that shown in Fig. 1*a*, was obtained by transmission of the beam through projecting oxide crystals. From the positions of the arcs it can be deduced that crystals of CuO are preferentially oriented with the (110) zone axis perpendicular to

¹ Manuscript received August 18, 1953.

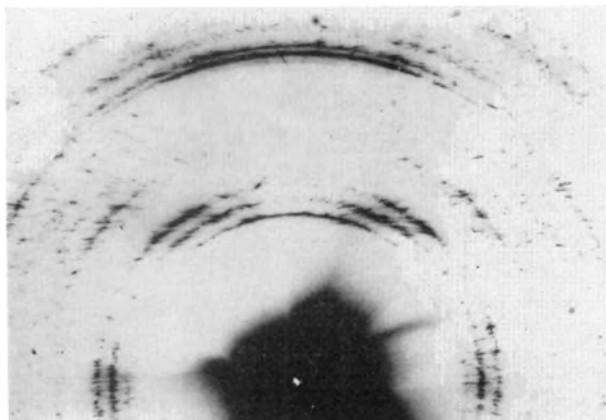


FIG. 1a. Part of an arc pattern from CuO crystals grown on a copper mesh.

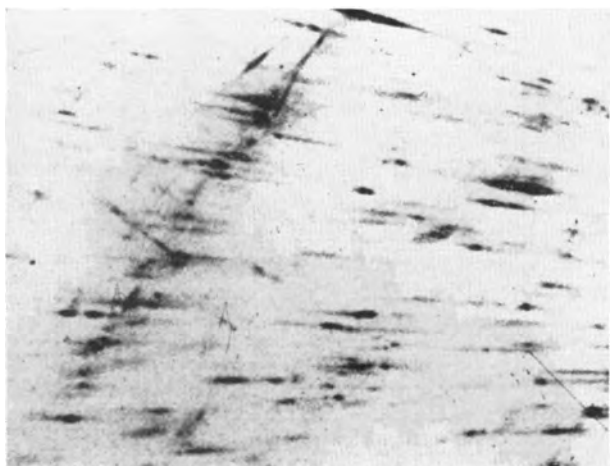


FIG. 1b. Enlargement of single-crystal spots from an arc pattern such as Fig. 1a.

the copper surface. Individual arcs are resolved into a large number of single-crystal spots, each of which is elongated in a direction perpendicular to the (110) zone axis. An examination of individual elongated spots under very high resolution conditions (Fig. 1b) shows that elongation is due to extended "shape transforms" similar to those previously described in patterns of ZnO smoke (6). It may therefore be concluded that the oxide grows in the form of long thin needles perpendicular to the copper surface, with the long axis of the needles parallel to the (110) zone axis.

Electron micrographs of similar regions, Fig. 2, confirm that the oxide is in the form of long thin needles growing approximately perpendicular to the surface. Average diameter of the needles is a little over 1000 \AA ; lengths are very much greater. In some cases, a spine was observed to extend right across one of the grid apertures.

Some single-crystal diffraction patterns were obtained by using a very fine electron probe to pick

out individual needles. Fig. 3 shows such a pattern obtained with the beam in the $(\bar{1}10)$ direction. The $(00l)$ reflections give the closely spaced line of spots through the central spot. Of these, the reflections with l odd are "forbidden" in that the intensity calculated for them from the known structure of CuO is zero. The fact that they appear with appreciable intensity implies that considerable secondary scattering or "dynamic interaction" has taken place. This is to be expected for CuO crystals more than 100 \AA thick. Weak, continuous lines running between the spots of the pattern indicate that there is a considerable amount of disorder in the crystal. The lines are stronger near the spots of the pattern. Lines running near to the central spot are less pronounced than those further out. The direction of the lines is perpendicular to the axis of the needle. These observations suggest that the disorder in the crystal may take the form of screw dislocations along the axes of the needle-like CuO crystals. Wilson (7) has examined diffraction effects given by a screw dislocation along the axis of a cylindrical crystal. The apparent crystal size is, in effect, decreased in directions perpendicular to the axis. This effect is zero for reflections from planes parallel to the dislocation axis, and the more marked, the greater is the angle between the reflecting plane and this axis. In a single-crystal pattern, such as Fig. 3, this would result in an elongation of the spots in a direction perpendicular to the long crystal axis, as observed. Each needle-like crystal of CuO may therefore be considered to contain one or more screw dislocations along its axis. The rapid growth of the crystals in the (110) direction may then be attributed to growth about screw dislocations.

Observations were also made by "reflection" from the surface of a copper block which had been heated in the same way as the copper mesh. The patterns

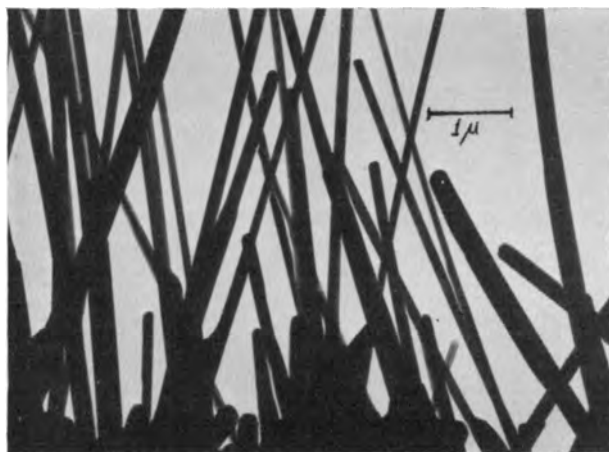


FIG. 2. Electron micrograph of CuO crystals growing from the side of an aperture of a fine copper mesh.

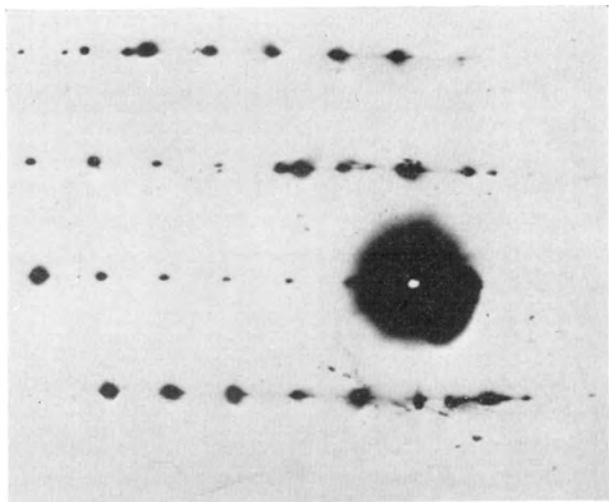


FIG. 3. Single crystal pattern obtained from a needle-like CuO crystal. A background of spots given by other crystals has been removed by masking.

obtained are similar to that of Fig. 1 except that more than half of the pattern is obscured by the shadow of the block, and the arcing of the rings is not quite so pronounced. The individual spots are elongated in the same way, indicating that the same acicular crystal habit is present. The general appearance is exactly that of the CuO' patterns previously obtained by reflection methods. The two broad (110) arcs form an almost-continuous inner ring which is of about the same strength as the next two rings. These rings are actually composite, the first being made up of (002) and $(\bar{1}11)$ arcs, the second being a combination of (200) and (111) arcs. The merging of the several arcs on these strong rings gives the appearance of continuous rings even in the presence of a considerable degree of orientation. As Honjo has pointed out, this fortuitous circumstance has prevented many authors from realizing that a preferred orientation is present.

Relative intensities of the arcs in the patterns obtained from the heated copper grids are the same as in these CuO' reflection patterns. It is therefore clear that, in the present case at least, the three-ring pattern is given by thin needle-like crystals of CuO growing approximately perpendicular to the copper surface.

DISCUSSION

The evidence from which it may be concluded that the intensity anomalies are not due to impurities may be summarized as follows:

1. The arcing of the (110) and $(11\bar{2})$ rings is consistent with that of the other rings of the pattern. It is unlikely that an impurity would give arcs in the same positions even if the crystals of the impurity had a similar preferred orientation.

2. The fine structure of single crystal spots which make up the (110) and $(11\bar{2})$ arcs is similar to that of spots in other arcs, indicating that these arcs are given by crystals of the same size, shape, and degree of imperfection.

3. Intensities of the (110) and $(11\bar{2})$ arcs are high enough to account for the appearance of abnormally intense rings in a reflection pattern from crystals with a concealed preferred orientation.

Differences between the normal CuO and the CuO patterns are, therefore, differences which occur in single-crystal patterns, and it is unnecessary to postulate the presence of an impurity. The observation of Gulbransen and McMillan that the intensities of the (110) and $(11\bar{2})$ rings are dependent on the purity of the copper used may perhaps be explained if the purity is considered to affect the habit, degree of orientation, or degree of imperfection of the crystals.

The idea that the anomalous intensities are the result of a defect or excess of copper atoms in the lattice need not be considered in detail. Such a high concentration of defects or excess atoms would be required to give the observed modification of the intensities that either the lattice symmetry or the unit cell dimensions, and hence the ring diameters, would be appreciably changed.

Honjo suggested that the intensity anomalies follow from preferred orientation of the crystallites, but orientation by itself cannot give rise to the observed intensities. This is apparent from the diagrammatic representation of the arc patterns, Fig. 4. On the first layer line, the intensity of the (110) arc should be much less than that of the neighboring arcs for a normal CuO lattice, whereas in Fig. 1, the (110) arc is almost as strong as its neighbors. The abnormal intensity of the (110) arc must, therefore, be a result of the previously unsuspected spine-like habit of the oxide.

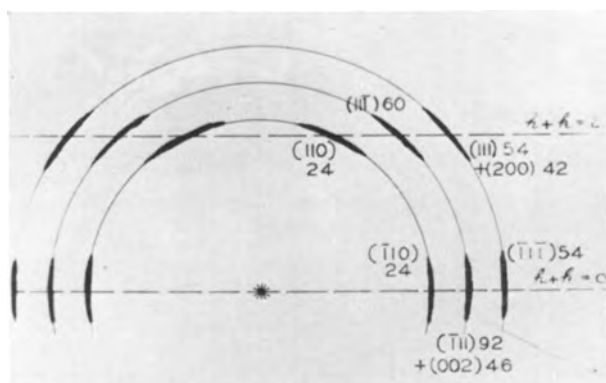


FIG. 4. Diagram showing the indices (in brackets) and structure factors for the normal CuO structure, for the arcs on the inner three rings of Fig. 1a (not to scale).

The average thickness of the spines is about 1000 Å. A perfect single crystal of this thickness would not give diffraction intensities according to the simple kinematic theory. Dynamic effects would be strong. Intensities would be proportional to the first power, rather than the square of the structure factors, and dynamic interaction effects would be expected to even out the intensities, making strong reflections weaker and weak reflections stronger. Thus the (110) arc would not be as weak, compared to its neighbors, as would be expected from the kinematic theory.

Because of the spine-like habit of the crystals, the average thickness of crystal traversed will vary appreciably for reflections from different planes. The spines vary widely in orientation. Planes perpendicular to the spine axis can reflect only when the spine is perpendicular to the electron beam. Planes parallel to the spine axis can reflect for any orientation of the spine. For planes perpendicular to the spine axis the average thickness will be least. The greater the thickness of crystal traversed, the more the intensity of a reflection will be reduced by extinction, absorption (inelastic scattering), and dynamic interaction. The intensities of the (110) arcs on the first layer line, which are given by planes nearly perpendicular to the spine axis, should therefore be reduced less than the intensities of other arcs. The arcs on the zero layer line should be weakened most, since they are given by reflections from planes parallel to the spine axis.

Imperfections of the crystal lattice, presumably taking the form of screw dislocations parallel to the axes of the spines, will modify the intensities in much the same way. Wilson's analysis of the case of a screw dislocation along the axis of a cylinder, showed that, in effect, the apparent crystal size is smaller for reflections from planes more nearly

perpendicular to the axis of the dislocation. Thus, extinction effects will reduce intensities much more for reflections from planes nearly parallel to the axis than for reflections from planes nearly perpendicular to the axis.

The relative intensities of the various arcs on the innermost ring in the pattern, Fig. 1a, give a clear indication that some such modification of the intensities has occurred. The (110) arc (planes parallel to the spine axis) is very much weaker than the (110) arc (planes almost perpendicular to the spine axis), although the two reflections have the same structure factor. Similar differences are evident on other rings. Therefore, it seems probable that a complete explanation of the intensity anomalies of the CuO' pattern may be possible in terms of the particular morphology of normal CuO crystals, resulting from growth about screw dislocations.

ACKNOWLEDGMENTS

The writer wishes to thank Mr. J. L. Farrant for taking the electron micrographs and Mr. J. A. Spink who took a number of the electron diffraction patterns.

Any discussion of this paper will appear in a Discussion Section to be published in the December 1954 issue of the JOURNAL.

REFERENCES

1. C. A. MURISON, *Phil. Mag.*, **17**, 96 (1934).
2. G. HONJO, *J. Phys. Soc. Japan*, **4**, 330 (1949).
3. E. A. GULBRANSEN AND W. R. McMILLAN, *This Journal*, **99**, 393 (1952).
4. J. M. COWLEY AND A. L. G. REES, *J. Sci. Instr.*, **30**, 33 (1953).
5. A. L. G. REES, J. L. FARRANT, AND J. M. COWLEY, To be published.
6. A. L. G. REES AND J. A. SPINK, *Acta Cryst.*, **3**, 316 (1950); *Nature*, **165**, 645 (1950).
7. A. J. C. WILSON, *Acta Cryst.*, **5**, 318 (1952).

Reduction of Oxidation-Ions in Hydrocarbons¹

ANDREW GEMANT

Engineering Laboratory and Research Department, The Detroit Edison Company, Detroit, Michigan

ABSTRACT

The formation of oxidation-ions, resulting from oxidation of aromatic ortho dihydroxyl compounds in hydrocarbons, is shown to be either completely or partially reversed upon reduction. Compounds studied were catechol, butylcatechol, and 1,2-naphthalenediol. Among the oxidizing agents, ozone was studied in detail. Reduction was by hydrogen at atmospheric pressure and room temperature.

From the easy reduction of ions it appears that a large fraction of them are relatively simple molecules; their possible structures are indicated. Ortho derivatives of aromatics containing additional side chains are likely to be parents of oxidation-ions.

SCOPE OF STUDY

A preceding study (1) attempted to identify the ions causing increase in electrical conductivity of hydrocarbons upon oxidation. An attempt was made to find a group of easily oxidizable compounds which possess known oxidation products and show increased conductivity upon oxidation. Such a group was considered to be chemically representative of what can be termed a parent of oxidation-ions.

Compounds of these characteristics were found among the hydroquinones, particularly in the ortho position. In concentrations of a few millimoles per liter of hydrocarbon solvent and on mild oxidation, a marked increase in conductivity takes place. It is not yet possible to assign with certainty a structure to the oxidation-ions formed. They were tentatively identified as originating from semiquinone radicals as oxidation intermediates, stabilized by addition or loss of an electron. It is realized, however, that this explanation might be modified by future work.

If this explanation is correct, it should be possible to reverse by suitable means, at least partly, the observed increase in electrical conductivity. It was this question to which the present investigation was devoted. Since the ions are formed by oxidation, it was concluded that subsequent reduction should eliminate the ionic species formed and cause conductivity to decrease. It is known that *o*-quinone is readily reduced by agents like potassium iodide (2, 3). The same probably holds for intermediate products which form the ions.

In addition to the process of reduction, the present study was also concerned with ion generation by means of oxidation with ozone. Results obtained by this method throw added light on the nature of oxidation-ions.

¹ Manuscript received November 16, 1953. This paper was prepared for delivery before the Chicago Meeting, May 2 to 6, 1954.

REDUCTION OF OXIDATION-IONS FROM CATECHOL

Reduction was carried out with hydrogen at room temperature and atmospheric pressure on a platinum black catalyst. A small glass container was used for the reduction; it contained 10 cc of solution into which were lowered platinum plates which were electrolytically coated with platinum black and a glass tube with fritted glass at the lower end. Hydrogen was bubbled through the solution via this tube. Reduction was under rather mild conditions.

A typical result is presented in Fig. 1. Catechol, 5 millimole/l in dioxane, was oxidized by silver oxide for 2 hr. The increase in conductivity (corrected for change in dielectric constant) is drawn as a dotted line, since only initial and end values were measured, the general trend of the curve being known from previous data (1). The solution, which had a reddish-brown coloration due to *o*-quinone, was decanted from solid silver oxide and subjected to reduction. After 2 hr the conductivity level was about the same as before oxidation; the color at the same time faded markedly. The quinone was, therefore, reduced to a considerable extent. After 18 hr the conductivity was nearly the same as before, 2.0×10^{-12} mho/cm. According to later experiments, dioxane is not very suitable as a solvent involving reduction; the peroxide content of some batches apparently interferes with the reduction process.

Further results along similar lines are assembled in Fig. 2, referring to 3 millimole/l *p*-*tert*-butylcatechol (recrystallized from the Eastman product). In curves 1 and 2 oxidation time was 10 min, and in curve 3 it was 20 min. Immediately after oxidation, which utilized KMnO_4 , reduction was achieved using a hydrogen stream. Oxidation, accompanied by green coloration, increased conductivity; reduction, accompanied by decoloration, reduced conductivity. The final level in the case of benzene and octane

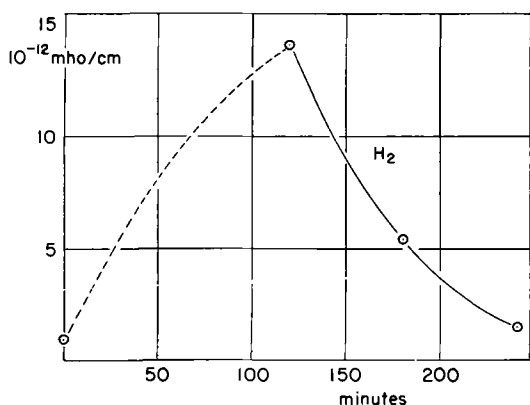


FIG. 1. Electrical conductivity vs. time of oxidation and reduction of 5 millimole/l catechol in dioxane.

was close to the initial one, but somewhat higher for xylene. No correction was applied to these data because of the small change in dielectric constant.

It has been pointed out (1) that intermediate oxidation products, which form ions, are not always stable; conductivity may change with time. It was of interest, therefore, to compare oxidized samples that were undergoing reduction with samples of the same batch that were allowed to stand after oxidation. Two results of this kind are shown in Fig. 3. Group 1 shows an oxidation curve for 20 min, followed by a branching of the curve. The bottom branch refers to reduction, and the top branch to a sample that was allowed to stand after initial oxidation. Group 2 shows a curve for an oxidation time of 135 min, followed by two branches analogous to those in the first group. While the top branches show only little change, the reduction curves exhibit sharp drops. These drops are, therefore, not caused by inherent instability of oxidation-ions.

It was also of interest to ascertain whether reversals could be effected by repeating oxidation and reduction processes. One of the tests carried out for

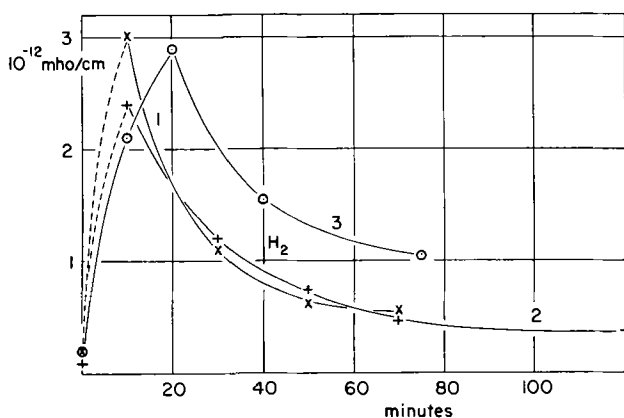


FIG. 2. Conductivity vs. time of oxidation and reduction of 3 millimole/l butylcatechol in benzene (curve 1), *n*-octane (curve 2), and xylene (curve 3).

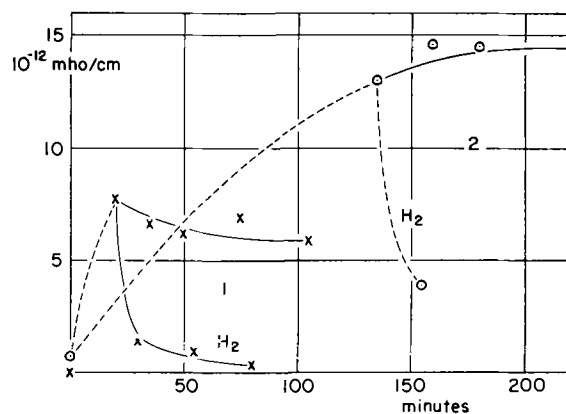


FIG. 3. Conductivity vs. time for oxidation, reduction, and standing after oxidation. Group 1: butylcatechol in benzene; group 2: catechol in dioxane.

this purpose, using the benzene-butylcatechol system, is reproduced in Fig. 4. It shows four oxidation peaks and four corresponding reduction drops, indicating that the initial condition was restored after each reduction. The peaks are of different magnitude because no effort was made to keep conditions of oxidation constant (amount and particle size of KMnO_4 crystals, conditions of stirring, and the like). At each oxidation the greenish color of the quinone appeared, disappearing at each reduction.

REDUCTION OF OXIDATION-IONS FROM *o*-NAPHTHALENEDIOL

All work up to this point was carried out with dihydroxyl derivatives of benzene. The following was an attempt to extend the work to a naphthalene derivative. Ortho naphthalenediol is not readily available, so 1,2-(or β -) naphthoquinone (Eastman product) was used. The compound was dissolved in benzene and the clear filtered red solution used; in some tests it was previously recrystallized from ether. In order to obtain the corresponding ortho diol, the quinone solution was reduced in the apparatus described above. The color faded to a faint pink hue.

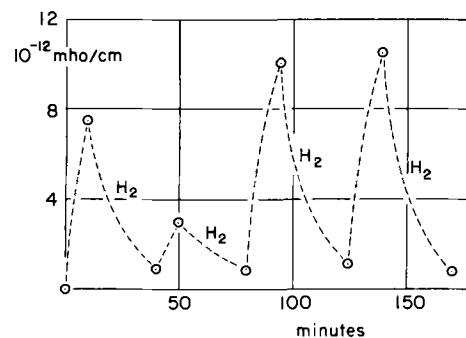


FIG. 4. Repeated oxidations and reductions in a 4 millimole/l butylcatechol solution in benzene.

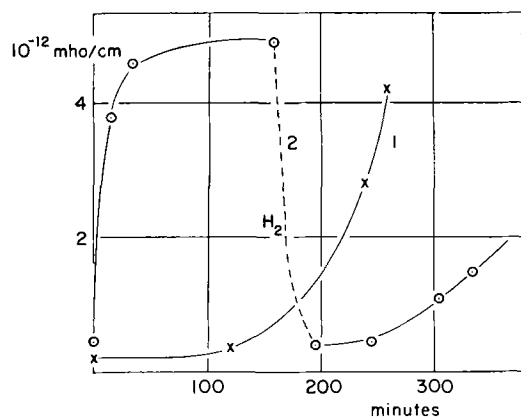
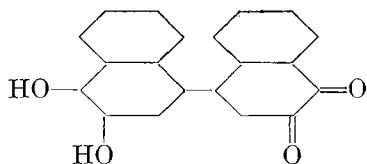


FIG. 5. Oxidation and reduction of β -naphthoquinone. Curve 1: 2.5 millimole/l 1,2-naphthalenediol in benzene-dioxane; curve 2: 5 millimole/l β -naphthoquinone in benzene.

When such a solution was diluted by an equal part of dioxane (final concentration of the diol being 2.5 millimole/l) and oxidized with silver oxide, curve 1 of Fig. 5 was obtained. In contrast to previous curves it shows an induction period of about 2 hr, after which a rapid increase of conductivity takes place, the solution assuming a reddish color.

A somewhat unexpected observation was made with β -naphthoquinone. If no reduction precedes oxidation, but the original benzene solution (concentration 5 millimole/l) is used and oxidized with Ag_2O , an immediate increase in conductivity takes place, as shown in the first part of curve 2. This solution was next subjected to reduction, showing a rapid drop of conductivity. Repeated oxidation with Ag_2O produces the same type of oxidation curve as in curve 1, as expected.

The chemical nature of intermediate ions in this case is probably similar to that postulated for the case of *o*-benzoquinone (1). It is known (4) that *o*-naphthoquinone upon standing forms a quinhydrone type compound, (3,4-dioxynaphthyl-1)-naphthoquinone-1,2, of the following probable constitution:



The compound, a dimer of *o*-naphthoquinone, is a dark powder, moderately soluble in benzene. When this is oxidized, the hydroxylated benzene ring acts as a catechol molecule, leading to semiquinone radicals. This is the probable cause of ion formation, as shown in the first part of curve 2, when the quinone, and not its reduced form, was used.

OXIDATION BY OZONE

A further group of experiments was concerned with ozone as oxidizing agent, and subsequent reduction. The results are instructive in providing further support for the hypothesis that ions are intermediate chemical forms between the fully reduced and fully oxidized form.

Referring to the reduction arrangement described earlier, for oxidation the tube could be connected to a cylindrical glass ozonizer, the outer electrode of which consisted of aluminum foil, and the inner of water. High voltage to the ozonizer was supplied by a transformer using a primary voltage regulator, and oxygen was fed from a tank.

Results on oxidation by ozone are presented in Fig. 6, curve 1, which refers to a 6 millimole/l butyl-catechol solution in xylene. Ozone has an advantage over solid oxidants in that its concentration can be easily varied. This is done by varying the electric field across the gap (4 mm) between the two glass cylinders of the ozonizer. Curve 1 consists of various sections, each referring to periods of 30 min in which the field was increased in steps as indicated; the figures give effective kilovolts per centimeter. Concentration of ozone in the oxygen stream increases with increasing electric field, as was ascertained by the intensity of darkening of KI-starch paper. Hence, it may be seen that the conductivity effect depends upon the concentration of O_3 , going through a maximum at about 26 kv_{eff}/cm. The increasing part of the curve seems obvious, but the decreasing part is unexpected. A possible explanation is that oxidation of catechol then proceeds too vigorously; the relatively unstable intermediate ionic stages are then further oxidized to the end product.

Curve 2 of Fig. 6 is a control test with xylene, without butylcatechol, carried out at the same field intensities as the previous test. Increase in con-

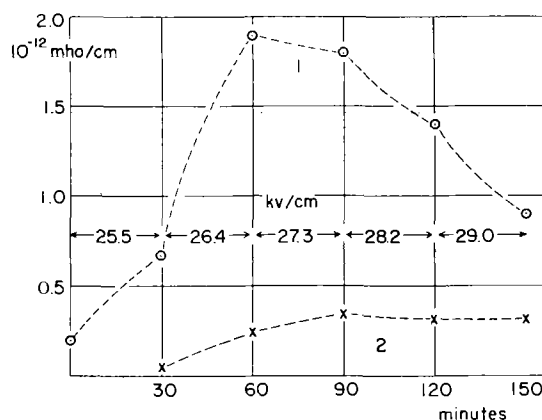


FIG. 6. Oxidation by means of ozone at various field intensities in the ozonizer. Curve 1: 6 millimole/l butyl-catechol in xylene; curve 2: xylene only.

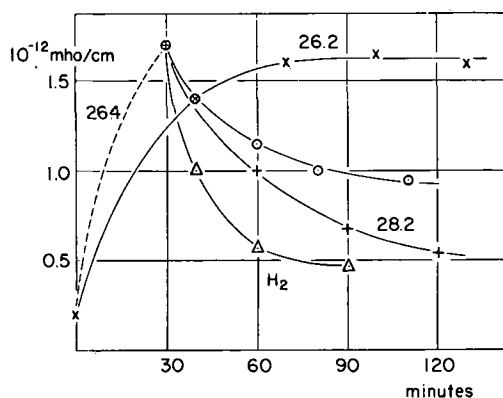


FIG. 7. Conductivity changes upon oxidation by ozone at various field intensities, upon standing, and upon reduction by hydrogen after oxidation; 6 millimole/l butylcatechol in xylene.

ductivity is small, hence the major portion of the effect shown in curve 1 is due to the presence of catechol, i.e., conductivity is due to ions formed from catechol.

Further results, using ozone as oxidant, are presented in Fig. 7. All data refer to a 6 millimole/l butylcatechol solution in xylene. The curve marked 26.2 refers to an oxidation test at the optimum field intensity. After the maximum conductivity of 1.6×10^{-12} mho/cm is reached, it remains constant with continued oxidation, indicating a dynamic equilibrium between ion generation and annihilation.

The other group of curves has a 30-min oxidation section at the optimum field. From this point on, three branches are shown. The top branch refers to standing of the solution, showing a decrease of conductivity due to inherent instability of the ionic species. The next branch gives further oxidation data at a higher than optimum field intensity, showing a more rapid drop than on standing. The third branch refers to reduction by hydrogen; this drop is the steepest, indicating rapid annihilation of ions.

CONCLUSIONS CONCERNING STRUCTURE OF IONS

Before discussing some conclusions that may be drawn from the results on reduction, two pertinent points are mentioned.

One is that only ortho compounds exhibit the effect of prompt conductivity changes on oxidation. This was shown by previous work (1) and also in Fig. 8, comparing butylcatechol (curve 1) with butylhydroquinone (curve 2). The absence of any increase of conductivity in curve 2 proves the point in question. A possible explanation is given later.

The second point is whether or not ions are formed in thermodynamic equilibrium with the fully reduced and oxidized parent compounds. From experimental material available it appears that such an equilibrium could at best account for a small

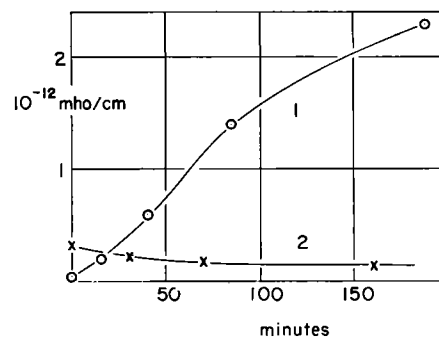


FIG. 8. Comparison of butylcatechol (curve 1) and butylhydroquinone (curve 2) in benzene, oxidized by KMnO_4 .

fraction of ions present and that the major fraction are intermediates of relative stability. It is realized that this conclusion is not final and may be subject to revision. Michaelis (5) found equilibrium between quinones and semiquinones, but conditions in hydrocarbons are certainly different from those in aqueous solutions. An experimental indication of the absence of an equilibrium in the present case is presented in Fig. 9.

Curves 1 and 2 refer to phenanthrenequinone solutions in xylene and xylene-dioxane 1:1. The left parts of the curves reproduce data during reduction of the yellow quinone solution, in the course of which the colorless 9,10-phenanthrenediol was formed. The right parts refer to oxidation by KMnO_4 , converting the colorless diol back into yellow quinone. The diol in solution is known to be unstable (6), oxidizing very rapidly to quinone. Such rapid oxidation precludes the presence at any moment of a noticeable concentration of intermediate ionic species, as mentioned above, and accordingly there is no increase of conductivity observable in the course of oxidation. The absence of such increase during the entire course of curves 1 and 2 seems to indicate, moreover, that the mere presence of the reduced and oxidized forms, even if they are present simultaneously, does not lead by

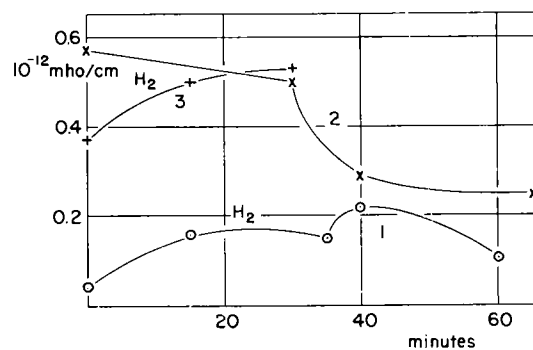


FIG. 9. Reduction and oxidation of phenanthrenequinone in xylene (curve 1) and dioxane-xylene (curve 2). Reduction of butyl-*o*-quinone (curve 3).

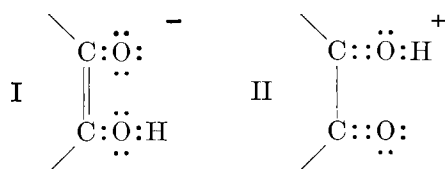
means of an equilibrium to a marked concentration of ionic species.

Curve 3 refers to reduction of red butyl-*o*-quinone, prepared from the corresponding catechol (7). No significant increase in conductivity occurs, in spite of the fact that in the course of the reduction both quinone and catechol were present. From the standpoint of the explanation based on ionic intermediates, the result shown in curve 3 seems surprising. One would expect ions to form also during reduction. If the observation is confirmed in further studies, then it shows that reduction follows a path different from that of the oxidation. Considering the many different ways in which a net reaction can and does occur, this is not improbable.

The observed effect of reduction on conductivity shows that oxidation-ions are reduced to nonionic molecules. The observed effect is in many cases complete, in others partial. It is perhaps safe to assume that the ions that are promptly reduced by hydrogen at atmospheric pressure and room temperature are chemically simple compounds, whereas those that are more resistant to reduction are secondary molecules of more complicated structure or higher molecular weight. The ionic species generated from aromatic dihydroxyl compounds appear, therefore, to be simple molecules. In a subsequent paper on this study, cases will be presented that exhibit a partial effect upon reduction, indicating that only part of the ions are primary products.

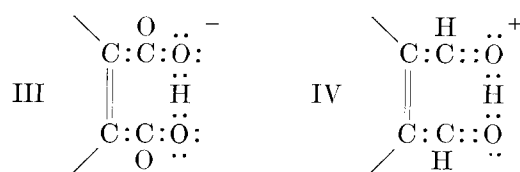
Sticher and Piper (8) subjected the reaction product of electron-bombarded decalin to hydrogenation with nickel as catalyst at about 240°C and 200 atm; a decrease of conductivity in a ratio 1:7 was observed. Since reduction in their work was carried out under severe conditions, a direct comparison with the present work is not possible. However, the two results appear to be in agreement, and it may be that the conductivity in their work was of a kind described here.

The chemical nature of the ions can only be tentatively inferred from the various observations. If the ions are intermediate compounds, they are of the nature of semiquinone radicals. The group with two ortho carbon atoms thus has the formula C_2O_2H . The molecule must exist in two forms, an anion and a cation; since both are relatively stable, the oxygen atoms must have completed electronic octets. The probable structure of the ortho groups in question is then the following:



The remainder of the molecule depends, of course, on the original compound present, and may, in addition, have the structure of a dimer, tetramer, and the like, if such were formed in the course of oxidation. Continued oxidation of the radicals and the ions leads to quinones; reduction, to ortho diols. As may be seen, the assumed structures are a diol anion and an oxonium type cation. The kinetics of their formation cannot be derived with certainty from experimental results of this study.

The ionic group does not need to be always the same. There can be longer side chains than those shown above. Since only ortho diols lead to ion formation, there is a likelihood that the hydrogen is situated between the two oxygen atoms, in other words, there may be a hydrogen bond in such ions. Such an anion, derived from phthalic acid, is shown in III, and a cation, as an oxonium ion of phthalic aldehyde, in IV.



The anion structure shown by III is similar to the chelate structure of anions of dicarboxylic acids in aqueous solution, discussed by McDaniel and Brown (9).

When the starting compound is not a diol, hydroxyl groups might form as the first step of oxidation, and ion formation is then a secondary process. Side chains in the ortho position, like in *o*-xylene, substantially facilitate such a process. A single hydroxyl group, as in phenol, favors formation of a second hydroxyl in the ortho position. Experimental results along these lines will be given in a subsequent paper.

It is quite likely that not all oxidation ions in hydrocarbons have the assumed structures of a diol anion and an oxonium cation. Other possibilities, such as formation of ion-radicals, should be kept in mind.

Presence of ortho substituents in the benzene ring is not the only criterion for a substance to be an ion parent. In order to be stable, ions need solvating action on the part of solvent molecules. This action is partly nonspecific, dependent on the dielectric constant of the solvent, partly specific, dependent on the chemical constitution of both solvent and solute. This latter action on the ions is analogous to the solvent action on the parent molecule which causes its greater or lesser solubility. The more soluble a compound in a solvent, the more likely it will

form ions. Hence a reasonably good solubility is a second essential criterion.

This is illustrated by catechol, which does not give an effect in benzene, but does so in dioxane. Butylcatechol, the solubility of which in benzene is considerably greater than that of catechol, gives a positive effect in benzene. Since side chains generally increase the solubility of hydroxyl compounds in hydrocarbons, alkyl substituted compounds in hydrocarbon mixtures facilitate the formation of oxidation-ions.

Any discussion of this paper will appear in a Discussion Section to be published in the December 1954 issue of the JOURNAL.

REFERENCES

1. A. GEMANT, *This Journal*, **100**, 320 (1953); *Z. Elektrochem.*, **57**, 277 (1953).
2. R. WILLSTÄTTER AND F. MÜLLER, *Ber.*, **41**, 2580 (1908).
3. J. SCHMIDLIN, J. WOHL, AND H. THOMMEN, *Ber.*, **43**, 1302 (1910).
4. W. SIEGMUND, *Monatsh. Chem.*, **29**, 1096 (1908).
5. L. MICHAELIS AND M. P. SCHUBERT, *Chem. Rev.*, **22**, 437 (1938).
6. "Beilstein Handbook of Organic Chemistry," Springer (Berlin) **6**, 1036 (1923).
7. E. DYER AND O. BAUDISCH, *J. Biol. Chem.*, **95**, 483 (1932).
8. J. STICHER AND J. D. PIPER, *Ind. Eng. Chem.*, **33**, 1567 (1941).
9. D. H. MCDANIEL AND H. C. BROWN, *Science*, **118**, 370 (1953).

High Purity Silicon¹

FELIX B. LITTON AND HOLGER C. ANDERSEN

Footo Mineral Company, Research and Development Laboratories, Berwyn, Pennsylvania

ABSTRACT

Thermal decomposition of silicon tetraiodide was investigated in both standard iodide (de Boer) and intermittent flow systems for potential use as a method for preparing high purity silicon metal.

Purity of metal obtained from operation of a standard iodide process cell appeared to be a function of impurities in crude silicon source material. Iodide metal having resistivities from 0.5–3 ohm-cm in the single crystal form was produced from Electro-Metallurgical high purity silicon. When iodide metal was used as silicon source material, the resistivity of single crystals of doubly refined metal varied from 3–8 ohm-cm.

Silicon of higher purity was obtained through thermal decomposition of fractionally distilled silicon tetraiodide in an intermittent flow system. After preparation of tetraiodide by reaction of resublimed iodine and Electro-Metallurgical high purity silicon, it was subjected to a 16 step distillation at 200 mm pressure in a packed quartz column. The modified iodide process silicon was *p*-type, and the resistivity varied in seven preparations from 30–200 ohm-cm.

INTRODUCTION

Becket (1) and Tucker (2) are credited with the first successful attempt to produce high purity silicon in commercial quantities. Using metal prepared by their process, Scaff (3) observed that different impurities segregated at various rates in directionally solidified metal, and that this procedure could be used for controlling distribution of impurities and, consequently, electrical properties of the metal. In 1949, Lyon, Olson, and Lewis (4) reported preparation of "hyper-pure" silicon by vapor-phase reduction of silicon tetrachloride with zinc.

Other methods have been investigated for the preparation of silicon in small quantities. Van Arkel (5) and Hölbling (6) studied hydrogen reduction of the tetrachloride. Silicon was prepared by reduction of potassium fluosilicate with potassium (7) and electrolysis of fused potassium fluosilicate (8). Von Wartenberg (8) thermally decomposed silicon tetraiodide on a graphite rod, while Stock (9) investigated thermal decomposition of silanes.

The objective of this research was to prepare silicon of the highest possible purity by the iodide process (10–12).

EXPERIMENTAL WORK

General Consideration

It is known that extremely small amounts of impurity elements decrease resistivity of silicon metal (13). Elements in groups III and V have a pronounced effect on electrical properties. The

¹ Manuscript received June 12, 1953. This paper was prepared for delivery before the Chicago Meeting, May 2 to 6, 1954.

effect of impurity elements from other groups is not as clearly defined.

During this investigation, thermodynamic calculations were made in order to estimate the order of thermal stability of groups III and V metal iodides relative to silicon tetraiodide. Brewer's data (14) were used for reference purposes. A filament temperature of 982°C and an iodide cell pressure of 10 μ were assumed to represent normal iodide process cell operation.

Calculations indicated that iodides of P, As, and Sb were less stable, and that those of Al, In, Ga, B, and Bi were more stable, than silicon tetraiodide. Therefore, it was anticipated that the concentration of the latter elements would decrease and that the former elements would not decrease in concentration in iodide metal relative to the concentration of those elements in the source silicon.

Factors Influencing Rate of Silicon Formation in the Iodide Process Cell

Rate of silicon deposition through thermal decomposition of silicon tetraiodide on a heated wire in a standard de Boer type iodide cell was studied as a function of three operating variables: (a) amount of iodine introduced in the cell, (b) cell temperature, and (c) filament (hot-wire) temperature.

Initial experiments were carried out in an Inconel cell, 4 in. in diameter by 12 in. long, similar to that previously described (12). Low-aluminum grade silicon metal² was used as crude source material and was supported at the cell wall by means of a molybdenum screen. A U-shaped molybdenum wire, 0.060 in. in diameter by 10 in. long, attached to

² Obtained from Electro-Metallurgical Division, Union Carbide and Carbon Corporation.

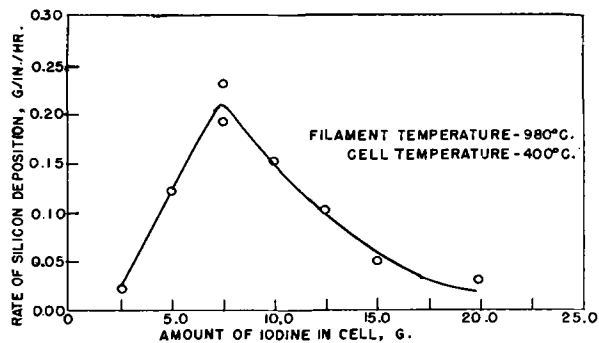


Fig. 1. Effect of iodine on rate of silicon deposition. Filament temperature, 980°C; cell temperature, 400°C.

the head of the cell through suitable electrode connections, served as the surface for thermally decomposing tetraiodide. The head was also fitted with a 1/2-in. diameter evacuation tube, a sight glass for optically determining filament temperature, and a thermocouple well for measuring the temperature of the source material.

After crude silicon was placed in the annular space between the molybdenum screen and cell wall, the filament was attached and the head bolted in position. The cell was leak-tested at 40 psi internal pressure, after which it was evacuated at 500°C to 0.05 μ . When the cell had cooled to room temperature, a weighed amount of iodine was admitted and the evacuation tube sealed off. Before adjustment of the filament and cell temperatures to desired operating values, the cell was reheated to 400°C for one hour to form silicon tetraiodide. When the experiment was completed, the filament was weighed and the rate of decomposition calculated. The crude silicon charge was washed with dilute nitric and hydrofluoric acids before it was reused for subsequent experiments.

The influence of iodine addition on rate of silicon formation at constant filament and cell temperatures is shown in Fig. 1. In the iodine weight range of 2.5–7.5 grams, the rate increased with increased

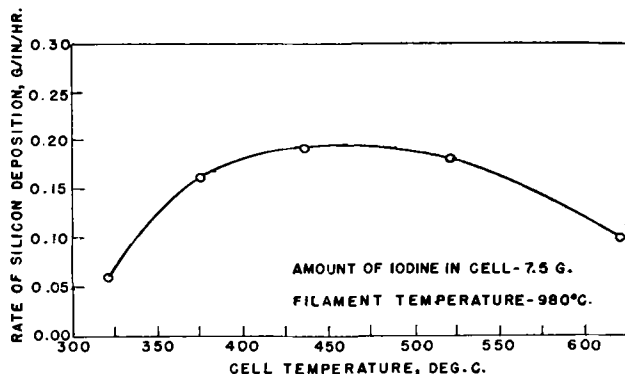


Fig. 2. Influence of cell temperature on rate of silicon deposition. Amount of iodine in cell, 7.5 grams; filament temperature, 980°C.

iodine addition, then decreased with further iodine addition.

The effect of varying the cell temperature using constant iodine addition and filament temperature is shown in Fig. 2. Data indicated that maximum rate of silicon formation occurred at 460°C. Even though an optimum cell temperature was observed, its influence on rate of silicon formation was not as critical as the amount of iodine added to the cell for the deposition process.

The influence of filament temperature on the rate of silicon formation, using 7.5 grams iodine addition and cell temperature of 460°C, is shown in Fig. 3. Data showed that 770°C was the minimum temperature at which measurable decomposition of the tetraiodide occurred, and that the rate increased with increasing temperature to the highest value studied (1040°C).

Standard Iodide Process Silicon

Apparatus.—An Inconel iodide process cell, 18 in. in diameter by 12 in. deep, was fabricated as the initial step in preparing silicon in approximately one-pound quantities for test purpose. The cell was designed to operate with a flat spiral filament of 0.10-in. diameter tantalum wire, 240 in. in length, suspended above the crude silicon starting material, which was distributed at the bottom of the cell. Vacuum seal and head arrangement similar to those used for the smaller cell were incorporated in the larger unit. Operating temperature was manually controlled by means of strip heaters in contact with the cell.

Cell operation.—Prior to operating this cell, filaments were prepared from molybdenum, tungsten, tantalum, and carbon for silicon formation experiments. When molybdenum was used, a continuous alloy zone 0.070 mm thick formed between the filament wire and silicon deposit. Metal droplets, assumed to be silicon-tungsten alloy, formed during the initial stage of deposition on a tungsten filament.

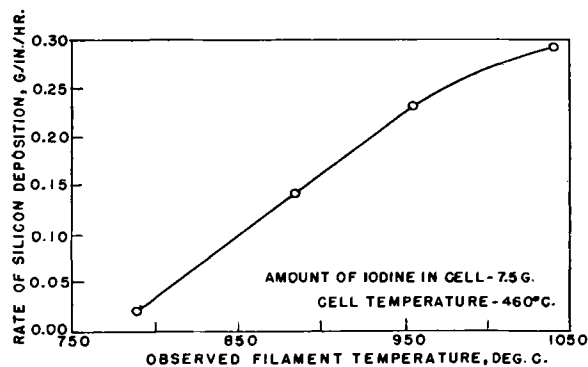


Fig. 3. Effect of filament temperature on rate of silicon deposition. Amount of iodine in cell, 7.5 grams; cell temperature, 460°C.



FIG. 4. View of a typical iodide process silicon, actual size.

A discontinuous alloy layer 0.017 mm thick formed between the silicon deposit and tantalum wire, showing that tantalum was to be preferred over either molybdenum or tungsten for filament material. In the case of carbon, a reaction zone 0.70 mm thick was formed.

The cell was operated on a charge of 5 lb of high purity grade silicon² and 50 grams of resublimed iodine. The following operational data were obtained from a typical preparation: tantalum wire temperature, 982°C; filament length, 170 in.; cell temperature, 450°C; preparation time, 74.5 hr; silicon obtained, 472 grams.

The "as deposited" iodide metal was polycrystalline, and vitreous in appearance. A view of a typical preparation is shown in Fig. 4.

Spectrochemical analysis.—Total impurities as reported from spectrochemical analyses on 16 deposits produced from high purity silicon showed that the metal contained 1–120 ppm detectable impurities which were one or more of the following elements: Fe, Al, Ca, Mg, Mn, Cu, and Na.

Electrical properties.—Resistivity and type rectification of iodide process silicon prepared from three different source materials are shown in Table I. Results are average values obtained on at least four preparations from measurements on "as deposited" and single crystal specimens.

Specific resistance was determined by measuring the voltage drop across 0.10 in. of the specimen with a L&N Type 7651 potentiometer. Rectification type was indicated by direction of current flow in a simple thermoelectric circuit.

These data indicated that silicon purification was

² Obtained from Electro-Metallurgical Division, Union Carbide and Carbon Corporation.

TABLE I. Resistivity and type rectification of iodide process silicon

Source material	Form	Resistivity, ohm-cm	Type rectification
High Purity (Electro-Metallurgical)	As deposited	0.5–3.0	<i>p</i> and <i>n</i>
High Purity (Electro-Metallurgical)	Single crystal*	0.1–3.0	<i>p</i> and <i>n</i>
Iodide process silicon	As deposited	5.0–8.0	<i>n</i>
Iodide process silicon	Single crystal*	3.0–8.0	<i>p</i>
High Purity (Sylvania Electric)†	As deposited	3.0–7.0	<i>n</i>
High Purity (Sylvania Electric)	Single crystal*	0.2–6.0	<i>n</i>

* Drawn from quartz crucibles.

† Metal prepared from zinc reduction of silicon tetrachloride; 99.85% minimum Si content.

obtained, but that both donor and acceptor elements were transferred in the standard iodide process cell from a given source material. It was not possible to obtain either the degree of purification desired, or to determine which elements transferred in this work, due to unreliability of chemical procedure in the analytical range of interest.

Preparation of Silicon from Fractionally Distilled Silicon Tetraiodide in an Intermittent Flow System

Preparation and properties of silicon tetraiodide.—Silicon tetraiodide was prepared by allowing iodine to react with silicon at 700°–850°C in quartz apparatus, similar to that employed by Schwarz and Pflugmacher (15). Resublimed iodine was vaporized from a heated flask and carried by tank argon through a 1-in. reaction tube containing high purity silicon. Silicon tetraiodide, a clear yellow liquid (mp 122°C), condensed in the downstream portion of the apparatus and was retained in a receiving flask.

The yield of tetraiodide was essentially quantitative with respect to iodine in the presence of excess silicon. However, only 45–65% of the silicon charge was utilized in a given iodination experiment.

Tetraiodide is strongly hygroscopic and corrosive, and gradually assumes a red color on exposure to air.

Vapor pressure of fractionally distilled silicon tetraiodide measured in a static isoteniscope as reported elsewhere (16) was expressed by the equation

$$\log P_{\text{mm}} = 23.3809 - \frac{3,862.7}{T} - 4.9934 \log T$$

where T is in degrees Kelvin. The normal boiling point was calculated to be 301.5°C , compared with 290°C reported by Friedel (17). The liquid density, measured in a small, sealed pycnometer over the range $128^{\circ}\text{--}243^{\circ}\text{C}$ was expressed by the equation: $\rho = 3.40 - 2.5 \times 10^{-3} (t-120) \text{ g/cc}$, $t = ^{\circ}\text{C}$ (16).

Fractional distillation of silicon tetraiodide.—After exploratory work on fractionation of silicon tetraiodide in a 3.7 step distillation, a column containing 16 theoretical plates was assembled to obtain metal more efficiently in 50-gram quantities for test and melting purposes.

The transparent fused quartz column, 6 ft in length by $1\frac{5}{8}$ in. in diameter, was randomly packed with $\frac{3}{16}$ in. diameter by $\frac{3}{16}$ in. long quartz Raschig rings, and during operation kept adiabatic by conventional means. Reflux was controlled and fractions obtained with a quartz du Pont type swinging funnel reflux splitter (18), the former actuated by an adjustable electric timer. A 9:1 reflux ratio was used in distillation experiments. Pressure in the column was controlled by a manostat in combination with a vacuum pump and tank argon bleed.

The column was calibrated by fractionally distilling a 20 mole % carbon tetrachloride-benzene mixture, and analyzing simultaneously collected distillate and residue samples with an Abbé refractometer. The number of theoretical steps was determined by the McCabe-Thiele (19) method, and, for comparison, calculated by the Fenske equation (20), using an average relative volatility of 1.134. It was observed that the number of theoretical steps increased with increased throughput, and varied from 16–42 at throughputs of 23 and 72 ml/min, respectively. Inasmuch as the turbulence noted at lower throughput approximated that in silicon tetraiodide distillation, the more conservative number of steps was selected to describe the performance of this column.

A pressure of 200 mm Hg was chosen for column operation, corresponding to a boiling temperature of 238.1°C for silicon tetraiodide. Referring to Table II, showing the boiling point and vapor pressure of

TABLE II. Boiling point at 200 mm and vapor pressure at 238°C of groups III and V metal iodides

Compound	Boiling point at 200 mm pressure, $^{\circ}\text{C}$	Vapor pressure at 238°C , mm Hg	Relative volatility	Reference
BI_3	157	1360	6.8	(16)
PI_3	169	910	4.6	(21)
GaI_3	299	36	0.18	(21)
Al_2I_6	324	24	0.12	(21)
AsI_3	336	24	0.12	(21)
SbI_3	369	11	0.06	(21)
InI_3	414	1.1	0.006	(21)

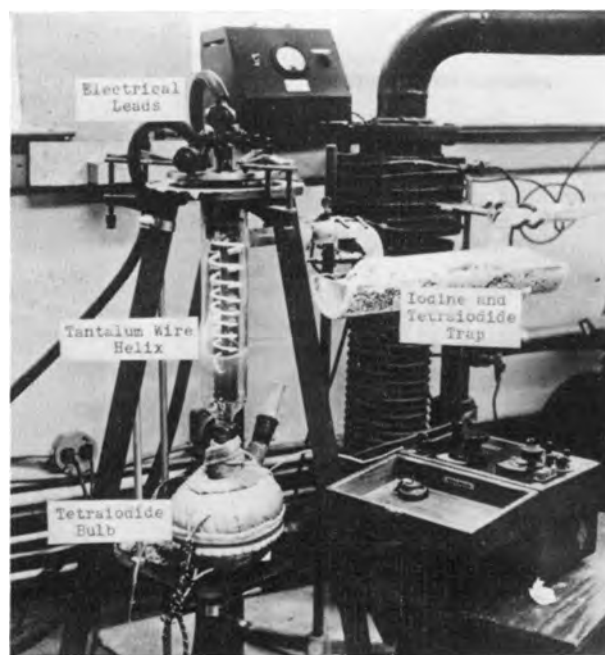


FIG. 5. View of apparatus for decomposing silicon tetraiodide.

groups III and V metal iodides, the relative volatility, α , of these iodides in comparison to silicon tetraiodide indicated that, based on the assumption of Raoult's law, boron and phosphorus would segregate in the first distillate, while gallium, aluminum, arsenic, antimony, and indium would tend to remain in the still-pot residue. An enrichment of 4.6 and a depletion of 5.5 per equivalent plate was anticipated in the vapor respectively for phosphorus and gallium, the iodides having vapor pressures nearest to silicon tetraiodide.

Thermal decomposition of fractionally distilled silicon tetraiodide.—Thermal decomposition of fractionally distilled silicon tetraiodide was carried out in the apparatus shown in Fig. 5. A tantalum wire, 0.10 in. in diameter by 3 ft long, formed into a helix, which represented the most efficient form, was used

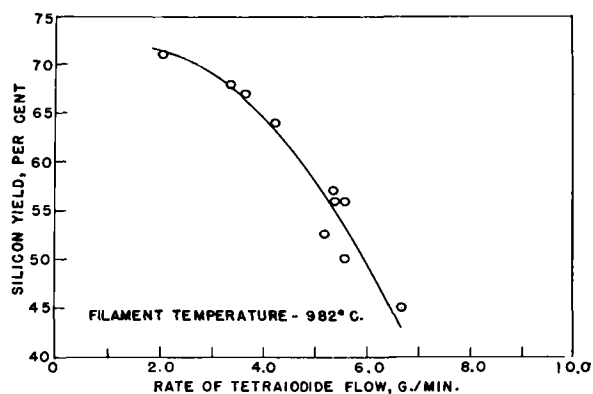


FIG. 6. Yield of silicon metal vs. flow rate of silicon tetraiodide. Filament temperature, 982°C .

for filament. Electrical connections were made to the filament through a flanged Inconel head and molybdenum electrodes. Neoprene gaskets were used for electrode insulation, and for sealing the head to the flanged quartz decomposition cell, which measured $2\frac{3}{4}$ in. in diameter by 12 in. long.

The cell was attached to the vacuum system and the tetraiodide flask through 20 mm ground quartz joints. During cell operation, undecomposed tetraiodide and free iodine were collected at 28° and 0°C and returned to the decomposition cell and iodinator, respectively, for reuse.

Yield of silicon from a given quantity of tetraiodide varied with the flow rate of silicon tetraiodide through the decomposition cell at constant filament temperature. At a flow rate of 6.9 g/min tetraiodide, 45% was decomposed; by decreasing the flow rate to 2.15 g/min, 71% was decomposed. The efficiency of tetraiodide decomposition at various flow rates is shown in Fig. 6. Dependence of decomposition efficiency on flow rate could result either from increased pressure or decreased contact efficiency.

Electrical properties.—Resistivity and type rectification of silicon prepared from center distillates of fractionally distilled tetraiodide are shown in Table III. In each distillation, approximately 50% of the still charge was obtained as center distillate, with the balance equally distributed between first distillate and residue.

Resistivity and type rectification were also determined on silicon prepared from the first distillate and

residue tetraiodide obtained during processing silicon No. 1226 and 1234 (refer to Table III). The first distillate yielded metal having 8 ohm-cm and type-*p* rectification; 0.2 ohm-cm and type-*n* rectification were obtained on metal from the residue from silicon No. 1226. Similar values from processing silicon No. 1234 were 10 and 7 ohm-cm resistivity and type-*p* rectification, respectively, from first fraction and residue tetraiodides.

CONCLUSIONS

1. Rate of silicon formation in a standard iodide cell was observed to depend on the variables studied as follows: the rate reached a maximum with respect to amount of iodine used, then decreased with further iodine addition; the rate also reached a maximum with respect to cell temperature and rose continuously with filament temperature up to the highest value employed (1040°C).

2. Resistivity and type rectification of silicon prepared in a standard type iodide process cell showed that groups III and V elements were transferred in the iodide process.

3. Silicon prepared from fractionally distilled tetraiodide had resistivities of a higher order than standard process metal, indicating that the tetraiodide was purified through fractional distillational procedure. As work is in progress at the present time to determine the degree to which contaminating elements are removed and where they are segregated, no conclusion could be drawn relative to ultimate purification obtainable by this procedure.

ACKNOWLEDGMENT

The work described is part of a research project carried out by Foote Mineral Company on the preparation of high purity silicon under Contracts DA 36-039-sc-5550 and DA-36-039-sc-56693 for the Signal Corps Engineering Laboratories. The authors acknowledge permission to publish these data.

The authors gratefully acknowledge the assistance of Messrs. H. C. Daly, L. H. Belz, and Dr. R. J. Brumbaugh for the enthusiastic manner in which they performed separate phases of the work described.

Any discussion of this paper will appear in a Discussion Section, to be published in the December 1954 issue of the JOURNAL.

REFERENCES

1. F. M. BECKET (To Electro-Metallurgical Division, Union Carbide and Carbon Corp.), U. S. Pat. 1,386,227, August 2, 1951.
2. N. P. TUCKER, *J. Iron Steel Inst. (London)*, **15**, 412 (1927).
3. J. H. SCAFF (To Bell Telephone Laboratories, Inc.), U. S. Pat. 2,402,582, June 25, 1946.

TABLE III. Resistivity and type rectification of silicon prepared from center distillates of fractionally distilled silicon tetraiodide

Silicon No.	Resistivity, ohm-cm	Type rectification	Remarks
1226 ^a	18	<i>p</i>	SC ^c
1234 ^b	30	<i>p</i>	SC ^c
1420 ^c	30-200	<i>p</i>	SF ^f
1422 ^c	100	<i>p</i>	SC ^g
1464 ^c	35-95	<i>p</i>	PF ^f
1477 ^c	40-80	<i>p</i>	SF ^f
1479 ^c	37-98	<i>p</i>	PF ^f
1481 ^c	40-80	<i>p</i>	PF ^f
1486 ^c	44-51	<i>p</i>	PF ^f

^a SiI₄ distilled in 3.7 step column.

^b SiI₄ doubly distilled in 3.7 step column.

^c SiI₄ distilled in 16 step column.

S—Single crystal.

P—Polycrystalline, with large faces.

F—Floating-zone technique.

C—Czoehrlski technique.

^e Prepared by Dr. F. H. Horn, General Electric Research Laboratory.

^f Prepared by Dr. P. H. Keck, Squier Signal Laboratory.

^g Prepared by Dr. A. C. Sheckler, General Electric Company, Syracuse, N. Y.

4. D. W. LYON, C. M. OLSON, AND E. D. LEWIS, *This Journal*, **96**, 359 (1949).
5. A. E. VAN ARKEL, *Metallwirtschaft*, **13**, 405, 511 (1934).
6. R. HÖLBLING, *Z. angew. Chem.*, **40**, 655 (1927).
7. J. J. BERZELIUS, *Ann. Phys.*, Ser. II, **1**, 169 (1824).
8. H. VON WARTENBERG, *Z. anorg. u. allgem. Chem.*, **265**, 186 (1951).
9. A. STOCK AND C. SOMIESKI, *Ber.*, **49**, 111 (1916).
10. A. E. VAN ARKEL AND J. H. DE BOER, *Z. anorg. u. allgem. Chem.*, **141**, 289 (1924).
11. I. E. CAMPBELL, R. I. JAFFEE, J. M. BLOCHER, JR., JOSEPH GURLAND, AND B. W. GONSER, *This Journal*, **93**, 271 (1948).
12. F. B. LITTON, *ibid.*, **98**, 488 (1951).
13. H. C. TORREY AND C. A. WHITMER, "Crystal Rectifiers," pp. 64-67, (Radiation Laboratory Series 15) McGraw-Hill Book Co., Inc., New York (1948).
14. L. L. QUILL (Editor), "The Chemistry and Metallurgy of Miscellaneous Materials," Paper 6, p. 76, McGraw-Hill Book Co., Inc., New York (1950).
15. R. SCHWARZ AND A. PFLUGMACHER, *Ber.*, **75B**, 1062 (1942).
16. H. C. ANDERSEN AND L. H. BELZ, *J. Am. Chem. Soc.*, **75**, 4828 (1953).
17. C. FRIEDEL, *Liebigs Ann. Chem.*, **149**, 96 (1868).
18. A. S. CARTER AND F. W. JOHNSON (To E. I. du Pont de Nemours & Co.), U. S. Pat. 2,251,185, July 29, 1941.
19. J. H. PERRY, "Chemical Engineer's Handbook," McGraw-Hill Book Co., Inc., New York (1950).
20. M. P. FENSKE, *Ind. Eng. Chem.*, **24**, 482 (1932).
21. F. D. ROSSINI, D. D. WAGMAN, W. H. EVANS, S. LEVINE, AND I. JAFFE, Cir. No. 500, National Bureau of Standards, U. S. Government Printing Office, Washington, D. C. (1952).

Phenomena Observed in the Melting and Solidification of Germanium¹

S. E. BRADSHAW

Research Laboratories of the General Electric Co. Ltd., Wembley, Middlesex, England

ABSTRACT

Small spheres of molten germanium, weighing around 10 mg, form pear-shaped solids on freezing, and a solidification mechanism is advanced to explain the shape and impurity distribution which occurs. Solids are shown to be substantially single crystal germanium.

The shape of a germanium ingot is shown to involve the ratio of the densities of liquid and solid germanium, d_L/d_S , at the melting point, and from the value of 1.13 obtained for d_L/d_S , it is deduced that the melting point of germanium is lowered by an increase of pressure. It is suggested that germanium may undergo an allotropic modification under pressure.

INTRODUCTION

The melting and solidification of germanium are somewhat unusual processes. It is possible to arrange external conditions so that the solidification-front progresses uniformly through the mass of molten material, and the solid which results has the shape predicted by an analysis based on simple ideas. This can be illustrated by some practical methods employed in the preparation of germanium for use in semiconductor devices.

Globule Melting

Small spheres of molten germanium, weighing around 10 mg, form pear-shaped solids, "globules," when allowed to solidify on a graphite support. The shape of a fraction of these globules closely approximates a right-circular cone standing on a hemispherical base, and the remainder possess shapes intermediate between this and a sphere; the germanium solidifies in such a way that the globule's cone-axis is roughly vertical.

It has been shown (1) that small spheres of molten germanium, solidifying in contact with a flat support, form slender right-circular cones due to uniform progress of a planar solidification front. It has also been shown (2) that small spheres of molten germanium can supercool by as much as 235°C. If it is assumed that the supercooled material nucleates at the graphite contact surface, rapid advance of the solidification front may be postulated as freezing-in the original spherical shape, but since the solidification process liberates some 8 kcal/g-atom, the temperature of the remaining liquid rises; consequently the rate of solidification becomes smaller.

¹ Manuscript received May 20, 1953. This paper was prepared for delivery before the New York Meeting, April 12 to 16, 1953.

When the solidification front has slowed down sufficiently, the coning phenomenon results.

Thus, solidification of a small molten sphere of germanium to the shape formed by mounting a cone on a hemisphere requires a somewhat restricted set of conditions, and when these conditions are not satisfied, intermediate shapes of globules result.

Normal Freezing

Progressive solidification of molten germanium in a horizontal direction results in an ingot whose cross section varies uniformly along its length, and for a horizontal crucible of constant cross section, the cross section of the ingot is smaller at the end first to solidify and larger at the end last to solidify.

If the effect due to surface tension is neglected and the phenomenon regarded as being due solely to the difference in density between solid and liquid germanium, the height, Y , of the ingot produced by a horizontal crucible of constant cross section is given by

$$(1 - x)^{(d_S/d_L)-1} = f(Y) \quad (\text{I})$$

where x = fractional distance along the ingot from the end first to solidify, d_S = density of solid germanium at solidification temperature, and d_L = density of liquid germanium at solidification temperature. The function $f(Y)$ depends on the cross section of the crucible employed and, for a rectangular cross section, is equal to Y/Y_0 where Y_0 is the height at $x = 0$.

If the crucible is tilted at an angle to the horizontal, the equation describing the shape of the ingot is too involved to be of direct value, but it can be shown that for certain angles of tilt the variation in cross section of ingots is a minimum. It is found in practice that tilting the crucible against the



FIG. 1. Shapes of typical germanium globules

direction of solidification by about 5° gives optimum uniformity of ingot cross section.

Zone Melting

The shape of ingot which results from passage of a molten zone (3) along a charge-ingot contained in a horizontal crucible of constant cross section depends on shape of the charge ingot. When this is of constant cross section, passage of a single zone results in an ingot whose height is given by:

$$(d_L/d_S) - [(d_L/d_S) - 1] \exp(-d_S x/d_L c) = f(Y) \quad (\text{II})$$

where c is the zone length expressed as a fraction of the length of the ingot, and the previous notation is retained.

Now, if further zones are passed along this ingot, a limiting shape will be reached at which the shape of the ingot is unaltered by passage of a molten zone. The height of this ingot is given, to a close approximation, by

$$\exp 2[(d_L/d_S) - 1]x/c = f(Y) \quad (\text{III})$$

with the notation used in equation (II).

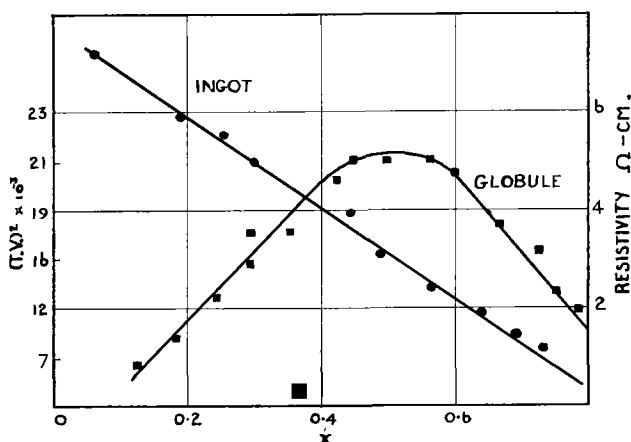


FIG. 2. The fraction of germanium solidified, x , at a point in a germanium globule vs. the mean value of (turn-over voltage)² occurring at this point.



FIG. 3. Shape of the solid obtained by partial dissolution of a germanium globule.

Neither equation (II) nor (III) will hold for the last portion of the ingot to solidify. This will solidify normally with a height given by equation (I). Equation (III) indicates that the smaller the zone length the greater is the variation in the cross section of the ingot. For the length of zone commonly employed, however, tilting the crucible by about $5-10^\circ$ against the motion of the zone gives optimum uniformity.

EXPERIMENTAL

A shallow depression in a graphite bar was filled with germanium in the form of a fine black powder and heated at 1000°C in an atmosphere of N_2 for 15 min. At the end of this period, the bar was rapidly cooled by being brought into the cold part of the furnace; subsequently the globule, weighing about 10 mg, was removed from the depression. A prepared surface in which the axis of the cone lay was explored for turn-over voltage (t.v.), using a micro-manipulator and tungsten whiskers. In Fig. 1, the

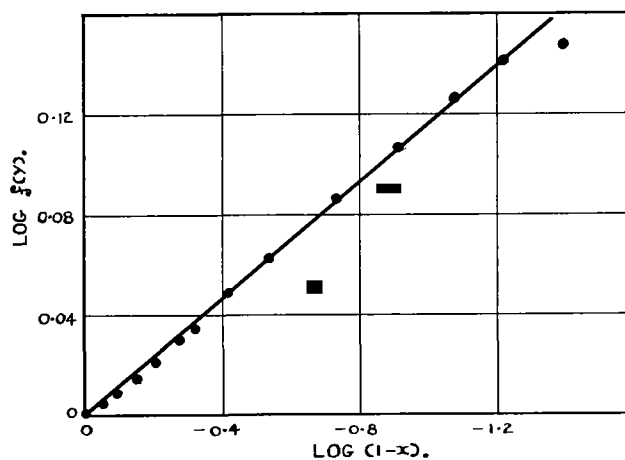


FIG. 4. $\text{Log } f(Y)$ vs. $\text{log } (1 - x)$ for a normally-frozen germanium ingot.

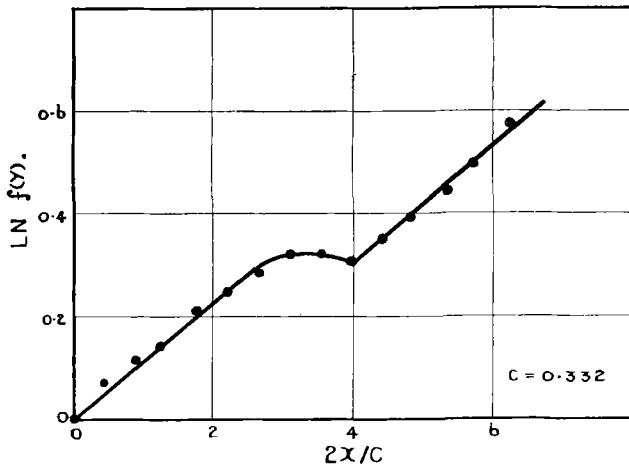


FIG. 5. $\ln f(Y)$ vs. $2x/c$ for a zone-melted germanium ingot, where c is 0.332.

shapes of typical surfaces are illustrated, and in Fig. 2 the fraction of germanium solidified at a certain distance along this axis is plotted against the mean value of $(t.v.)^2$ occurring at this distance. Fig. 3 illustrates the shape obtained from a globule by partial dissolution in a solvent consisting of equal volumes of 4*N* sodium hydroxide solution and 4*N* sodium hypochlorite solution, the temperature being held at 80°C with vigorous stirring.

An ingot was produced from a horizontal graphite crucible of constant cross section by normal freezing, and its height, Y , measured for different values of x . A plot of $\log f(Y)$ vs. $\log (1 - x)$ is given in Fig. 4.

A similar procedure was employed with the zone-melting technique, and a plot of $\ln f(Y)$ vs. $2x/C$ is given in Fig. 5. The zone length, C , was taken as being the average distance between the two solid-liquid interfaces of the 24 zones passed along the ingot.

DISCUSSION

The mechanism of solidification of the globules results in a segregation of impurity analogous to that which occurs in an ingot (4) and varying rates of solidification are reflected in distribution of impurities obtained. For the initial rapid solidification, segregation is low and impurity concentration in the solid is high. As the solidification rate becomes smaller, and segregation becomes more effective, the impurity concentration in the solidifying germanium becomes smaller. Since, however, the concentration in the liquid fraction is now increasing, the concentration in the solid begins to increase at some point and continues to do so until all the germanium is solid.

An approximate theory of semiconductors indicates that $(t.v.)^2$ is roughly inversely proportional to impurity concentration. For comparison, the result for a typical ingot is included in Fig. 2; the two

ordinate scales have been adjusted until they are approximately equivalent. It would appear that both shape of the globule and distribution of impurity within it are consistent with the solidification mechanism advanced.

Absence of a surrounding crucible for the solidifying germanium and presence of a planar solidification front are common to both the globule technique and the Czochralski pulling method used in the preparation of germanium single crystals (5). Cubes with truncated corners which are produced from the globules by preferential etching technique indicate that they are, in fact, substantially single crystals, and this was confirmed by an x-ray examination which showed the presence of some mosaic structure. The result illustrated in Fig. 3 is in harmony with the concept of a reciprocity between growth and dissolution (6) since it is known that the preferred direction of growth in germanium is [100].

Values of d_L/d_S calculated from Fig. 4 and 5 are 1.13 and 1.11, respectively, but uncertainty in the value of C probably makes the latter estimate less reliable. The value of 1.13 is intermediate between the value of 1.22 reported by Hall (7) and 1.05 found by Mokrovskii and Regel (8). The abrupt change in height of the zone-melted ingot, apparent in Fig. 5, is inherent in the process and occurs when the volume of liquid in the zone reaches the point where the balance of hydrostatic and surface-tension forces becomes unstable. Molten germanium then flows back over the trailing edge of the zone for a short distance, and the balance of forces is restored. From equation (III) it can be seen that if a limiting shape is rapidly regained, the slopes of the straight-line portions of the graph of $2x/C$ vs. $\ln f(Y)$ will be the same.

Among the elements, a value of d_L/d_S greater than one is the exception rather than the rule, and it is confined to those cases where bonding mechanism is substantially covalent. These strongly directive bonds result in a relatively open structure, and during melting the complete or partial collapse of the covalent bonds leads to an increase in density, the coordination number for germanium increasing from 4 to 8 during melting (9).

The Clausius-Clapeyron equation for phase changes,

$$\Delta S/\Delta V = dp/dT \quad (\text{IV})$$

relates dp/dT , rate of increase of pressure with melting point, with ΔS , entropy of fusion, and ΔV , increase of volume on melting. At the melting point, the free-energy of fusion is zero and $\Delta H = T\Delta S$ where ΔH is the heat of fusion. Employing Greiner's values (10) ($\Delta H = 8100$ cal/g-atom and $T = 1209^\circ\text{K}$) gives $\Delta S = 6.7$ cal/°C. $\Delta V = -1.6$ cc is obtained by substituting $(d_S/d_L - 1) = -0.115$,

$A = 72.6$, and $d_s = 5.25$ in $\Delta V = A(d_s/d_L - 1)/d_s$.² Substituting these values in equation (IV) gives

$$\frac{dp}{dT} = -4.2 \text{ cal/}^\circ\text{C/cc} = -1.8 \times 10^8 \text{ dynes/cm}^2/^\circ\text{C}.$$

The negative value for this differential coefficient implies that an increase of pressure lowers the melting point of germanium initially, but calculation of the melting point corresponding to any given pressure requires a knowledge of the dependence of this coefficient on pressure. For bismuth and gallium, Bridgman (11) found that d^2p/dT^2 was negative and suggested that this indicated some sort of instability in structure. With bismuth, gallium, and antimony, which have $d_L/d_s > 1$, polymorphic transitions were found to occur under very high pressure. In the case of gallium a new solid phase appeared around 10^{10} dynes/cm², which was denser than the liquid (11). In the cases of carbon and tin, it is well known that the diamond structure is the thermodynamically unstable allotrope at normal temperatures and pressures, and a graphitic silicon has been reported (12). It would seem reasonable to suggest, therefore, that the diamond structure of germanium may not be stable under pressure, particularly for elevated temperatures.

Pressure exerted locally by the whisker of a point-contact diode is very high—of the order of 10^{10} dynes/cm² for a 10-gram load on an apparent whisker area of 10^{-6} cm²—and its effect upon structure or melting point of germanium may be of importance during such processes as the "forming" treatment, where it is known that temperatures in excess of 500°C may be attained. Whisker pressure alone may be sufficient to cause a small region of the germanium to undergo allotropic modification, and it is significant that Jordan (13) has reported that localized pressures of the order of 10^{10} dynes/cm² can modify conduction characteristics of very restricted areas from *n*-type to *p*-type. This modification is permanent.

APPENDIX

DERIVATION OF EQUATION (I)

For a horizontal crucible of unit length and constant cross section, the cross section of the ingot at any point, x , is a function of the height of the ingot, Y , and some constants. Call this function $g(Y)$. If, during normal freezing, the charge is solid from $x = 0$ to $x = x$, and liquid from

² After this paper was written, a letter by R. G. Schulman and D. N. Van Winkle ["Pressure Welded *P-N* Junctions in Germanium," *J. Applied Phys.*, **24**, 224 (1953)] was published in which a volume change of 5% and a melting point of 935°C were quoted as having been obtained experimentally. Using these values and 110 cal/gram for the heat of fusion, they obtain $dT/dP = -2.4 \times 10^{-3}$ degrees/kg/cm².

$x = x$ to $x = 1$, then, neglecting the effect of surface tension, the weight of liquid, W_L , is

$$W_L = d_L(1 - x)g(Y) \quad (\text{V})$$

In this equation, d_L is the density of liquid germanium at solidification temperature, and it is assumed that the germanium is at this temperature everywhere. Differentiating equation (V) with respect to x gives

$$\frac{-dW_L}{dx} = -d_L[(1 - x)g'(Y) - g(Y)] \quad (\text{VI})$$

where $g'(Y)$ denotes the differential coefficient of $g(Y)$ with respect to x . But if W_S is the weight of the solid,

$$\frac{-dW_L}{dx} = \frac{dW_S}{dx} = d_S g(Y) \quad (\text{VII})$$

where d_S is the density of solid germanium at solidification temperature. On combining (VI) and (VII),

$$\frac{-\left(\frac{d_S}{d_L} - 1\right)}{(1 - x)} = \frac{g'(Y)}{g(Y)} \quad (\text{VIII})$$

and integration of (VIII) gives

$$(1 - x)^{(d_S/d_L)-1} = g(Y)/g(Y_0) \quad (\text{IX})$$

where Y_0 is the height of the ingot at $x = 0$. Replacing $g(Y)/g(Y_0)$ by $f(Y)$ gives equation (I). For a crucible of rectangular cross section $g(Y) = bY$, where b is the breadth of the crucible; hence $f(Y) = Y/Y_0$.

DERIVATION OF EQUATION (II)

If, during zone-melting, the charge has been zoned from 0 to x , is liquid in the zone x to $x + c$, and solid in the portion still to be zoned from $x + c$ to 1, then

$$W_R = d_L c g(Y) + d_S(1 - x - c)g(\bar{Y})$$

and hence

$$\frac{-dW_R}{dx} = -d_L c g'(Y) + d_S g(\bar{Y}) \quad (\text{X})$$

Where $g(\bar{Y})$ is uniform cross section of the charge ingot, W_R is weight of material to be zoned and in process of being zoned, and c is length of the molten zone, which is constant. The same assumptions are made as in the previous case. As before,

$$\frac{-dW_R}{dx} = \frac{dW_S}{dx} d_S g(Y) \quad (\text{XI})$$

where W_S is the weight of germanium which has been zoned. Combining (XI) and (X) gives

$$\frac{d_S [g(Y) - g(\bar{Y})]}{d_L c} = g'(Y) \quad (\text{XII})$$

The weight of liquid in the first zone to be formed is $d_L c g(Y_0)$, and this zone was formed by melting a weight of the charge ingot $d_S c g(\bar{Y})$, hence

$$g(\bar{Y}) = \frac{d_L}{d_S} g(Y_0) \quad (\text{XIII})$$

Substituting (XIII) in (XII) gives

$$\frac{g(Y_0) - \frac{d_S}{d_L} g(Y)}{c} = g'(Y) \quad (\text{XIV})$$

and integration gives

$$(d_L/d_S) - [(d_L/d_S) - 1] \exp(-d_S x/d_L c) = g(Y)/g(Y_o) \quad (\text{XV})$$

Replacing $g(Y)/g(Y_o)$ by $f(Y)$ gives equation (II).

DERIVATION OF EQUATION (III)

Let the relationship between $g(Y)$ and x for an ingot treated with a large number of zones be

$$g(Y) = \phi(x) \quad (\text{XVI})$$

Then the condition that this relationship will be unaltered by the passage of further zones is

$$\int_x^{x+c} \phi(x) dx = \frac{d_L}{d_S} c g(Y) \quad (\text{XVII})$$

An approximate solution of this equation is

$$\exp 2[(d_L/d_S) - 1]x/c = g(Y)/g(Y_o) \quad (\text{XVIII})$$

Substituting $g(Y)/g(Y_o)$ by $f(Y)$ gives equation (III).

Any discussion of this paper will appear in a Discussion Section, to be published in the December 1954 issue of the JOURNAL.

REFERENCES

1. J. W. RYDE AND B. S. COOPER, *Engineering*, **173**, 690 (1952).
2. D. TURNBULL AND R. E. CECH, *J. Applied Phys.*, **21**, 804 (1950).
3. W. G. PFANN, *J. Metals*, **4**, 747 (1952).
4. G. L. PEARSON, J. D. STRUTHERS, AND H. C. THEURER, *Phys. Rev.*, **77**, 809 (1950).
5. G. K. TEAL AND J. B. LITTLE, *Phys. Rev.*, **78**, 647 (1950).
6. H. E. BUCKLEY, "Crystal Growth," p. 304, John Wiley & Sons, Inc., New York (1951).
7. R. N. HALL, *Science*, **112**, 419 (1950).
8. N. MOKROVSKII AND A. REGEL, *J. Tech. Phys. (U.S.S.R.)*, **22**, 1281 (1952).
9. H. HENDUS, *Z. Naturforsch.*, **2a**, 505 (1947).
10. E. S. GREINER, *J. Metals*, **4**, 1044 (1952).
11. P. W. BRIDGMAN, "The Physics of High Pressure," G. Bell & Sons, Ltd., London (1949).
12. F. HEYD, F. KOHL, AND A. KOCHANOVSKA, *Collection Czechoslov. Chem. Commun.*, **12**, 502 (1947).
13. J. P. JORDAN, *Elec. Eng.*, **71**, 619 (1952).

Preparation and Examination of Beryllium Carbide¹

M. W. MALLETT, E. A. DURBIN, M. C. UDY, D. A. VAUGHAN, AND E. J. CENTER

Battelle Memorial Institute, Columbus, Ohio

ABSTRACT

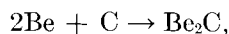
Properties of beryllium carbide were studied to determine its suitability as a high-temperature refractory. Various methods of preparing it were tried and a number of the physical and chemical properties of the resulting products were determined. Lots containing 85 weight % of useful product were prepared by the beryllium metal-carbon reaction. Because the material was to be fabricated into refractory bodies, particular attention was paid to the chemical analysis for unreacted BeO, beryllium metal, and free carbon; x-ray diffraction identification of the various phases present; and microscopical examination for mineral composition, crystal size, and crystal habit.

As a refractory, beryllium carbide has several disadvantages. It tends to hydrolyze in atmospheric moisture and to react with both oxygen and nitrogen, when heated.

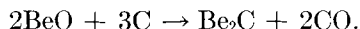
INTRODUCTION

Because of recent interest in the use of unconventional refractories such as carbides, nitrides, and sulfides, an investigation was made of the suitability of beryllium carbide as a high-temperature refractory.

The earliest work on beryllium carbide appears to be that of Lebeau (1) in 1895. He prepared the carbide by two methods: (a) heating a mixture of beryllium and sugar charcoal in an electric furnace,



and (b) heating beryllium oxide with sugar charcoal in an electric furnace (40 kw) for about 10 min,



Lebeau gave it the formula Be_4C_3 , but, after Henry (2) pointed out an error in the atomic weight and the valency of beryllium had been proven, he adopted the formula Be_2C . No other carbides seem to exist. This compound was described (3) as consisting of yellowish-brown transparent crystals with properties quite similar to those of aluminum carbide. It is so hard it scratches quartz easily.

The crystal structure of Be_2C was studied by Stackelberg and Quatram (4). X-ray investigation showed that Be_2C has an antiferite (CaF_2) lattice like Mg_2Si . The following constants were determined: $a_o = 4.33 \text{ \AA}$; x-ray density, $d = 2.44$; Be - C distance = 1.87 \AA ; and C - C distance = 3.06 \AA .

Work described in the present paper was completed in 1948. Subsequently, Geller (5) summarized previously known data on physical and chemical properties of Be_2C , and Coobs and Koshuba (6) discussed fabrication of this compound. Procedures

for determination of the principal constituents and contaminants of Be_2C were recently described by Gallagher (7).

PREPARATION

The Be_2C prepared for this investigation was made by the two basic methods used by Lebeau, that is, by heating an intimate mixture of BeO and carbon and by reacting beryllium metal and carbon.²

Apparatus

A typical furnace setup is shown in Fig. 1. A semi-permanent graphite heater crucible was packed in the induction coil with Norblack powder insulation. Vent holes were formed by pushing twelve $\frac{1}{8}$ -in.-diameter wires into the Norblack packing. The top of the packing was then sealed with Alundum cement before the wires were removed. Care was taken not to form the vent holes after applying the Alundum cement, because any oxide carried into the packing forms gas when heated and forces the Norblack out, sometimes explosively. A second graphite crucible containing the charge was slipped into the heater crucible. Holes were provided near the top of the inner crucible, into which a heavy iron wire bail could be placed for lifting the hot crucible from the assembly upon completion of a heat. Another crucible and charge could then be placed in the hot furnace and reacted without delay. A solid graphite cover rested on the charge, leaving about $1\frac{1}{2}$ in. of space between this cover and a clay-graphite cover which rested on the top edge of the crucible. Into this space was flowed a continuous stream of argon through a fused-silica tube. This provided a

² A proposed method, which appears feasible but has not been tried, is a vapor-deposition method in which a mixture of a beryllium halide and a hydrocarbon gas, carried in a stream of hydrogen, would be reacted on contact with a hot filament depositing Be_2C on the filament.

¹ Manuscript received July 1, 1953. This paper was prepared for delivery before the Wrightsville Beach Meeting, September 13 to 16, 1953.

blanket of inert gas over the charge during heating. A second hole in the outer lid was used for making optical pyrometer readings on the inner lid. Occasional setups contained a graphite-tube sight-well ($\frac{3}{4}$ in. ID x 1 in. OD) centrally located in the charge and extending downward through both covers to within one inch of the bottom of the charge. Lid temperatures were compared with "true" temperatures throughout the range of temperatures used. Lid temperatures varied from 300°C low at 1700°C to about 600°C low at 2200°C .

Experimental Procedure

In a small exploratory heat, a mixture of stoichiometric quantities of BeO^3 (-200 mesh) and graphite powder (-60 mesh) was placed in a graphite crucible and heated in a vacuum furnace ($<10^{-4}$ mm Hg). As the temperature was raised, the first indication of reaction occurred at 1500°C , when rapid gas evolution began. The reaction had not reached completion after two hours' heating at 1650°C . X-ray diffraction analysis indicated that considerable BeO and unreacted carbon still remained. Subsequent larger heats (600-gram charge) were made using a similar mixture except that fluorescent-grade BeO^4 was substituted for the more refractory H. F.-grade BeO . Oxide and graphite were intimately mixed by ball milling together. This mixture was heated in an argon atmosphere to a minimum temperature of 1900°C . Even though a temperature of about 2800°C was reached in the hottest part of the charge, some unreacted BeO and carbon remained after four hours' heating. About 60% yield of material containing about 90% Be_2C , with the balance BeO and free carbon, was obtained.

The useful product of each heat or lot (described above or below) tended to form a sintered or semi-sintered mass which could be distinguished by color (metallic or red-brown) from the relatively loose unreacted charge. The unreacted material was usually confined to the upper part of the charge. The amount to be discarded was determined by visual inspection and was readily separated from the selected product. Percentage of yield was based on the weight of selected product and the theoretical weight of Be_2C to be expected from the beryllium content of the charge.

Several lots of Be_2C were prepared by heating a mixture of beryllium metal flake (Clifton Products, Inc.) and minus 60-mesh graphite powder. In some cases, carbon black (Norblack) was used in place of graphite. It was impossible to get uniform mixing because of the nature of the flakes which were about one inch in diameter and foil-like in thickness. How-

³ Brush Beryllium Company H. F. grade.

⁴ Clifton Products, Inc.

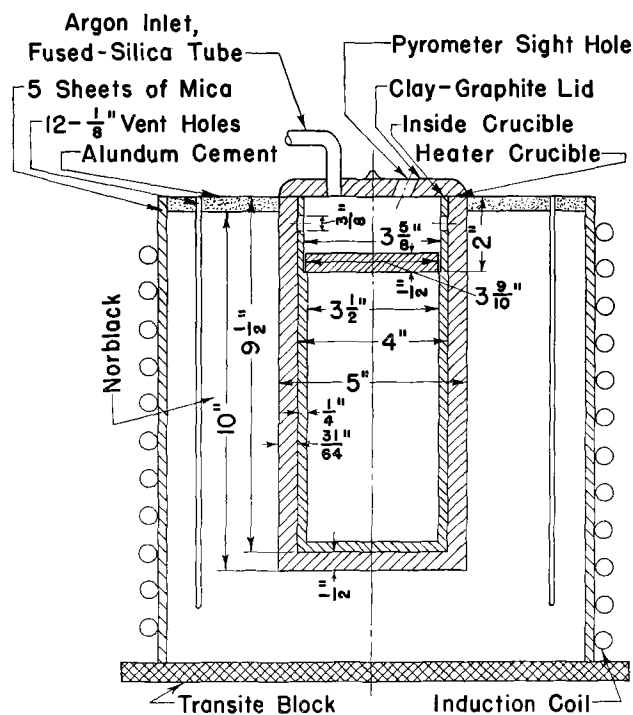


FIG. 1. Furnace setup for metal-carbon reaction

ever, this was inconsequential because the beryllium apparently vaporized during heating so that the end product consisted of a cylindrical mass, approximately $3\frac{1}{2}$ in. in diameter by 8 in. in length, of loosely sintered Be_2C grains of about 30-mesh grain size. The product ranged from red, through tan, bronze, brown, or black according to the free-carbon content.

Later, a rather large supply of finely divided beryllium metal in the form of saw chips and turnings was available; this material was substituted for beryllium flake with similar results. Some advantage was gained in using the saw chips because about 650 grams of charge could be packed in a crucible which would hold only 500 grams using the bulkier flake.

Twenty to thirty minutes at 1700°C was found sufficient to complete the metal-carbon reaction. This was much more rapid than the BeO -carbon reaction and a greater percentage (85 weight %) of useful product was obtained. Therefore, this method was used to the exclusion of other methods and about 40 lots of beryllium carbide were prepared.

An Alternative Method

In addition to the above methods of producing Be_2C , several others were tried. Experience gained during the pouring of beryllium into hot graphite molds showed that beryllium reacts exothermically with graphite to form Be_2C . The reaction seemed to start about 50°C above the melting point of beryllium. Similar reactions were noted when beryllium melts in graphite crucibles were superheated. The

reaction could not always be brought about, apparently because, in some cases, a thin adherent layer of carbide formed on the inner surface of the crucible preventing further reaction.

When the reaction did occur, the melt solidified in spite of increasing temperature. This thickening or freezing of the melt was caused by the formation of many individual grains of Be_2C in the metal matrix. In many cases, 80–90% of the volume was comprised of these carbide crystals (see Fig. 2). Average particle size ran from about 0.5μ to about 100μ , depending, among other things, on the temperature of formation and time at temperature. Although grain size varied greatly from heat to heat, grains of an individual heat were all of the same approximate order of magnitude. Upon exposure of a polished section of this material to air for several days, carbide particles took on a pink color. Air etch was the result of hydrolysis of the carbide by the moisture of the atmos-

phere. Highlights in the large grains (Fig. 2A) are reflections from within the translucent Be_2C grains. Be_2C grains were separated by dissolving the beryllium metal matrix in dilute hydrochloric acid. Although smaller grains were greatly hydrolyzed, large well-formed crystals showed little attack. This method appears well suited for producing relatively pure Be_2C , although it has been used only on a small scale to date.

Sloman (8) found similar grains of Be_2C formed by the action of graphite on the metal during electrolysis. Remelting allowed carbide particles to segregate in the bottom of the beryllium ingot. Upon solution of the metal with very dilute HCl, pink crystals were obtained which were identified as Be_2C by chemical and x-ray analysis. Sloman states that, in metal containing segregated carbide, the carbides appear grayish-brown under ordinary vertical illumination. Using a wide-angle lens, an intense pink coloration was noted. He thought this pink color was caused by a trace of iron carbide. This is unlikely and, in view of observations made on many Be_2C materials, the pink color in reflected light is evidently due to the hydrolysis product on the surface of the carbide.

ANALYSIS AND PROPERTIES OF Be_2C

Various lots of Be_2C were examined and analyzed as they were made or processed. In addition to visual examination, the principal analyses made included: (a) chemical analysis for total and free carbon, water, and Be_2C ; (b) x-ray diffraction identification of phases; and (c) microscopic observations which included measurement of crystal size, identification of crystal types, identification of phases and estimation of percentage by area measurement, and adjusted mineral composition after correction for relative apparent densities of the constituents. In addition, observations were made on hardness, density, and melting point of Be_2C . Also, a technique was worked out for recording in natural color the appearance of the carbide under the microscope.

Types of Beryllium Carbide

Casual examination of the product of the usual oxide-carbon or metal-carbon reaction has led to varied descriptions of the carbide. It has been described as pink, red, yellow, orange, tan, bronze, brown, black, metallic, or gray. These designations taken alone are quite deceptive. As seen under the microscope, in either transmitted or reflected light, Be_2C appears as translucent amber grains. The masking power of black free-carbon particles is great. As little as 10% by area, as measured under the microscope, causes the product to look black to the naked eye.

The types of Be_2C observed in the investigation

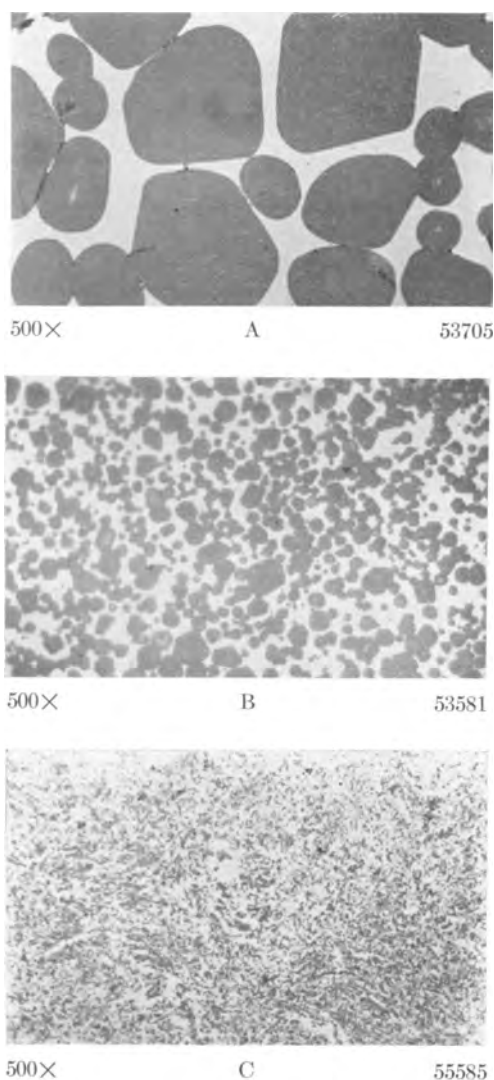


FIG. 2. Be_2C crystals in a beryllium metal matrix, illustrating differences in particle size.

may be described as: (a) coarsely crystalline, (b) microcrystalline (nodular), and (c) vermiculate (defined below). The coarsely crystalline Be₂C was obtained in several ways. One product containing 100% of this type of crystal was extracted from beryllium metal (see Fig. 2A) which had reacted with a graphite crucible. This was the purest carbide produced, containing only traces of opaque material (free carbon or metal) and a small amount of hydrolysis product resulting from the acid-extraction process. In lots of Be₂C made by the metal-carbon reaction at about 2000°C for 1 hr, 95–99% of the crystals were coarse and well formed (see Table I). In addition, this material usually contained 5–10% unreacted carbon. However, the Be₂C grains contained no internal free carbon (graphite flakes).

Microcrystalline Be₂C of the nodular or "grape cluster" type was produced by reacting beryllium metal and carbon at lower temperatures (1700°C) or for short times (20–30 min) at 2000°C. A few lots were made in which 98–99% of the Be₂C phase was microcrystalline (see Table I). This material, when crushed and pressed, showed better sintering characteristics than the more coarsely crystalline material. Nodular Be₂C is readily made by the metal-carbon reaction; whereas, in the oxide-carbon method, where a long time at temperature is required to complete the reaction, only coarse crystals are produced.

The term "vermiculate" applies primarily to the mass of wormlike tubes often produced when beryllium carbide heats are taken above 2200°C (see Fig. 3). These tubes appear to be formed from drippings of a viscous fluid. Although they intermingle, they do not adhere to each other. The interior of the hollow structure is an aggregate of angular reddish



FIG. 3. Vermiculate Be₂C. Top—core of high-temperature heat; bottom—individual tubes showing hollowness.

TABLE I. Preparation and crystal properties of beryllium carbide

Lot* No.	Preparation of material		Crystal sizes (microns)			Crystal habit	
	Time, min	Temp, °C	variation		Avg size	% "grape-cluster" finely crystalline nodules in calcined powder	% individual crystal grains plus crystals in calcined powder
			min.	max.			
1	30	1700	0.5	32	5	98–99	<2
2	30	2200	3.0	95	42	5	95
3	30	2020	0.5	50	13	90–95	5–10
4	30	2020	0.5	33	9	98–99	<2
5	30	2020	0.5	47	12	93–95	5–7
6	50	2020	1.0	249	82	5	95
7	15	2020	—	—	—	—	—
	+30	2200	4.0	230	83	Traces only	98–99
8	15	2020	—	—	—	—	—
	+30	2200	1.0	154	58	2–5	95–98

* These products were made by the metal-carbon reaction using the stoichiometric ratio for Be₂C.

crystals, while the exterior is smooth and metallic in appearance. The metallic color is caused by a thin layer of highly oriented carbon crystals. Because of the similarity of the individual crystals of this and clinker-like porous material which exhibits the vermiform structure to a lesser degree, all high-temperature products with the metallic-appearing surface have been termed vermiculate.

Vermiculate Be₂C is evidently a decomposition product, formed by loss of beryllium through vaporization. This leaves an excess of carbon which precipitates as graphite flakes in a Be₂C matrix (see Fig. 4). In one case, graphite flakes were formed by heating "pure" Be₂C (no free carbon) to 2200°C. The vermiculate structure appears to have been formed by pressure (possibly CO) from within. The



250×

FIG. 4. Graphite flakes in a Be_2C matrix. Left, unetched, right, air etched.

fact that the tubes distort and conform to the contour of the crucible wall is evidence that incipient melting has occurred. However, this is not a useful melting point as the material cannot be cast at atmospheric pressure.

Samples of Be_2C powder contained in graphite capsules and heated in argon for 30 min at 2400°C formed a clinker-like product. Incipient fusion appeared to have taken place. At 2300°C , some sintering occurred, but no fusion. When similar samples were heated in closed graphite capsules in a vacuum at $>2100^\circ\text{C}$, Be_2C sublimed and condensed as red crystals on the lid (2100°C) of the capsule which was slightly cooler than the bottom of the capsule. This sublimation seems to take place through dissociation of the carbide to its elements and recombination at a favorable temperature. A similar experiment at slightly higher temperature (2120°C on the lid) yielded metallic appearing crystals. The metallic appearance was caused by a thin layer of vaporized carbon on the surface of the carbide crystals. It is apparent that, if Be_2C is to be melted, it must be done at high pressures in an inert atmosphere.

Chemical Analysis

Various lots of Be_2C were analyzed for total and free carbon and soluble beryllium. The percentage of Be_2C was calculated from these figures. A list of the typical chemical analyses appears in Table II. Usually, a mineral balance (free carbon plus Be_2C) of about 98% was obtained. The rest may be accounted for as BeO , as evidenced by the x-ray diffraction analysis and $\text{Be}(\text{OH})_2$, small amounts of which form by hydrolysis of Be_2C with atmospheric moisture. Total carbon was determined by combustion of a sample of Be_2C in O_2 at 2500°F for 15 min.

Ingot iron was added as a flux for the BeO , combustion product, which otherwise tends to protect the carbide from complete oxidation. Carbon was collected as CO_2 and weighed. The total carbon figure was not always reliable because, even with the precautions taken, the analyses appear low and often did not agree with the calculated Be_2C .

Soluble beryllium was determined by hydrolyzing Be_2C in 2.5N HCl near the boiling point until hydrocarbon evolution, as evidenced by bubble formation, ceased. Free carbon was filtered off and determined by combustion as above.

The free-carbon analyses appear reliable. Microscopic estimates of carbon are sometimes low. This is probably caused in part by the presence of colloidal carbon within the Be_2C crystals. This is measured by chemical means, but not by the microscope. For the soluble-beryllium analysis, it was assumed that the BeO , which was highly fired during production of the Be_2C , was insoluble. The presence of unreacted beryllium was ruled out because of the high vapor pressure (about 0.4 cm Hg) at the minimum reaction temperature, 1700°C . The only other soluble beryllium compound likely to be present was $\text{Be}(\text{OH})_2$. In our early work, no analysis was made for H_2O

TABLE II. Analytical data on beryllium carbide

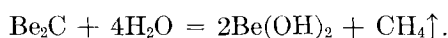
Lot No.	Petrographic Analysis*				Chemical analysis				X-ray diffraction analysis		
	Adjusted wt, % mineral composition after applying ratio factors				Total carbon (C), %	Free, uncombined carbon (C), %	Soluble beryllium compound (Be), %	Calculated beryllium carbide Be_2C , %			
	Beryllium carbide (Be_2C)	Carbon (C)	Beryllium oxide (BeO)	Beryllium hydroxide [$\text{Be}(\text{OH})_2$]					(Be_2C)	(BeO)	(C)
1	91.5	7.5	Trace†	None	44.8	9.6	53.1	88.5	S	VVF	MF
2	92.4	5.6	None	Trace†	45.3	10.2	53.6	89.4	VS	VVF	M
3	—	14.1	—	—	41.0	11.5	51.7	86.1	S	VF	MS
4	73.4	21.9	1.2	3.8	50.4	23.2	43.8	72.7	S	VF	VS
5	88.0	9.7	0.6	1.8	37.5	5.0	56.0	93.4	VVS	MF	S
6	—	9.1	—	—	39.2	9.0	52.8	87.9	VS	—	M
7	—	7.8	—	—	39.0	11.6	51.5	85.8	M	—	M
8	—	4.9	—	—	39.6	7.5	55.1	91.8	VS	MF	M

* Two lots analyzed for beryllium silicate ($2\text{BeO}\cdot\text{SiO}_2$) showed none in one case and a trace to $<1\%$ in the other instance.

† Less than 1%, but visible.

and all soluble beryllium was assumed to be Be₂C. Later it was found that about 1% H₂O was picked up during handling even though the material was stored in tightly sealed containers immediately after being produced. Assuming that 1% H₂O is present as BeO·H₂O (2.389%), then the Be₂C value is 0.833% high and the total assay 1.556% low. Thus, the BeO shown to be present by x-ray diffraction and the small amount of Be(OH)₂ which is probably present in all samples account for the difference between the total of the free carbon and Be₂C and 100%.

As indicated above, Be₂C has a strong tendency to hydrolyze. This reaction takes place according to the following reaction:



Hydrolysis has been particularly noticeable in connection with vermiculate (high temperature) carbide. Hard clinker-like lumps of this material, which were very difficult to break when first made, crumbled into small grains after exposure to air for one or two weeks. Samples of the clinker mounted in Bakelite hydrolyzed after several days in air and swelled to such an extent that the plastic was cracked into several pieces. Typical lots of -30 mesh Be₂C, as made and stored in covered fruit jars for several days, analyzed 1.0 weight % H₂O. A sample of Be₂C crystals (Fig. 2A), when extracted from Be metal with dilute HCl, washed with H₂O, and dried with ether, analyzed 6.5% H₂O. Hydrolysis appears unavoidable in this process. A sample of vermiculate material, which had hydrolyzed in air, was analyzed in the hydrolyzed condition and after drying at various temperatures. Before drying, it contained 4.2% H₂O; drying at 100°C for 1 hr reduced this but slightly to 3.7%. Even drying at 400°C for 1 hr left appreciable H₂O, 0.71%. When the 400°C treatment was followed by an hour at 650°C, the H₂O fell to 0.20%. An additional hour at 800°C practically completed the drying, leaving only 0.09% H₂O. The H₂O analysis was made by collecting the H₂O evolved when Be₂C was heated at 1000°C for 15 min in a slow stream of dry oxygen.

It appears that certain porosity of beryllium castings, made in previously used graphite molds, may be attributed to hydrogen from hydrolysis products of Be₂C. Be₂C formed on the surface of the mold by previous castings may hydrolyze and, in spite of preheating to 600°F (316°C), may retain sufficient moisture to cause porosity. Preheating to at least 1000°C is recommended. After drying, the mold may, of course, be cooled to a lower temperature for use.

Chemical analysis of pressed bodies of Be₂C heated

in nitrogen at 1100°C showed an increase of nitrogen content (x-ray diffraction analysis showed the presence of Be₃N₄). At lower temperatures, no nitrogen pickup was noted. Other compacts tended to oxidize when heated in air at 800°C.

X-Ray Diffraction Analysis

In general, the x-ray diffraction analyses of the major phases agreed with chemical analyses and with observations made using the microscope. Constituents present in quantities less than 5-10% are often not detectable by x-ray methods. However, in this series of analyses, BeO as low as 1% was detected. Be(OH)₂ was found in nearly all the samples examined by x-ray diffraction. This is probably, in part, the result of hydrolysis of the Be₂C during preparation of samples for x-ray analysis. The density of Be₂C determined from lattice parameter measurements agrees with the value $d = 2.44$, as reported by Stackelberg (4).

MICROSCOPY OF BERYLLIUM CARBIDE

The various phases present in the usual "as made" material were identified under a petrographic microscope and percentage estimates made by area measurement. An attempt was made to convert area measurements to weight percentages by use of conversion factors based on the apparent density of the constituents. The minimum, maximum, and average size of the carbide crystals were determined, and the physical nature of crystals of typical lots were assigned on the basis of crystal-size measurement. Results of microscopical examination, chemical analyses, and x-ray diffraction analysis are summarized in Table II. The agreement of the results by the three methods is self-evident.

Identification of Phases

Beryllium carbide does not occur in nature because of its strong tendency to hydrolyze. No optical data on beryllium carbide were found in the literature. It was found to crystallize in the isometric system and to exhibit an amber color in either reflected or transmitted light. The color in reflected light tends to be somewhat more red; whereas, in transmitted light the color is slightly more brown. Examined in plane polarized, transmitted light, the crystals are translucent. They are isotropic and so appear dark in polarized light between crossed nicols. A typical lot of coarsely crystalline Be₂C, produced from the metal-carbon reaction, is readily crumbled to minus 30-mesh grain size in the hand. The individual particles thus produced are, in certain cases to a large extent, single crystals.

Because Be₂C crystallizes in the isometric system,

it has only one index of refraction value. Through use of fused solid melts containing mixtures of selenium and sulfur, the average index of refraction of crystalline Be_2C was found to be $N = 2.64_{\text{Li}} \pm 0.01_{\text{Li}}$. White light was employed for making index of refraction measurements because monochromatic yellow, sodium vapor light was absorbed within the dark-red embedding medium. Therefore, the refractive index measurements were made by means of the red wave band portion of the transmitted white light.

In addition to the carbide phase, the usual lot of "as made" beryllium carbide may contain free carbon, free beryllium metal, BeO , and $\text{Be}(\text{OH})_2$. It was not found possible to distinguish between beryllium metal and the black, opaque carbon particles. It may be possible that this could be done by some technique, such as mounting the material in clear plastic and examining polished sections under reflected light. However, if free metal occurred in the usual product, it must have been very minor compared to free carbon, as evidenced by x-ray examination data.

Area measurements of free carbon, including graphite flakes in the Be_2C matrix, were made. In order to convert these measurements to weight percentages for comparison purposes, a conversion factor for carbon was first determined. Comparison of microscopical area measurements and chemical free-carbon analyses of 30 samples of the product of the metal-carbon reaction indicated that, if the percentage of carbon by area measurement were divided by 1.6 to convert area percentage to weight percentage, satisfactory agreement between microscopical and chemical methods would be obtained. Having assigned a weight percentage value to carbon by this means, the area measurements of Be_2C and $\text{Be}(\text{OH})_2$ were converted to weight percentage on the basis of their relative densities. Carbon could not be corrected on the basis of density alone because it is evidently present as porous, bulky particles of low apparent density. The carbon of materials from the high-temperature BeO -carbon reaction was even bulkier than that of the metal-carbon reaction and required use of a conversion factor of 3.0. A possible explanation of the difference is that the carbon of the metal-carbon reaction product is unreacted and may be considered as rough spheres comparable to the shape of the Be_2C particles, while the carbon in the BeO -carbon reaction product, which is present principally in the form of thin graphite flakes within the Be_2C matrix, retains some of its flaky nature even when ground to $<10 \mu$ and so covers a greater area than an equal weight of spherical particles.

BeO was occasionally present as prismatic crystals that were birefringent in polarized light between

crossed nicols. It apparently formed in the cooler regions of the charge because of incomplete shielding by the argon atmosphere.

Some carbide products appeared more subject to hydrolysis than others. In the typical hydrolyzed material, $\text{Be}(\text{OH})_2$ completely enveloped the Be_2C crystals. The hydroxide appeared to possess a cryptocrystalline, fibrous structure that was birefringent in polarized light between crossed nicols.

Crystallography of Beryllium Carbide

Crystallographic properties of Be_2C appear to resemble closely those of fluorite (CaF_2). Euhedral (Be_2C) occurs as octahedrons, dodecahedrons, tetrahedrons, or as truncated octahedrons containing the usual 8 octahedral faces plus 6 "cubic" pinacoid faces, adding up to 14 faces in the completed form. Twinning of the truncated octahedrons can occur parallel to the cubic pinacoid face to form "accordion-like" structures. The crystalline phase of Be_2C exhibited perfect octahedral cleavage along four directions. Twinning of Be_2C occurred only in high-temperature, coarsely crystalline products. Threelings were the highest order of twinning observed to date, although fourlings are possible if all conditions for stable crystal twinning symmetry were satisfied. The threelings were joined together through two 45° -angle bends. Simple, contact-twin crystals of the Carlsbad or Siamese twin type were observed, as well as twolings composed of two crystals joined together at a 45° angle. Crystals also tended to form an open link-chain-type of structure composed of from 5–25 euhedral or subhedral crystals that adhere together in a continuous, irregular chain. Also, a closed-chain type of structure occasionally occurred in which individual crystals formed densely packed, parallel rows, having the appearance of a beaded fabric. Both porous and very dense nonporous chain-type structures were observed.

Other crystal structures include the individual euhedral and subhedral crystals mentioned previously and coarsely crystalline intergranular aggregates of these crystals. In addition, there is the microcrystalline "grape cluster" or nodular type of crystal aggregate that predominates in beryllium carbide produced by the metal-carbon reaction at relatively low reaction temperatures (1700°C). The grape clusters are composed of anhedral and subhedral crystals which form dense and nonporous aggregates.

Colored Photographs of Beryllium Carbide

Because of the difficulty of accurately describing in words the colors of beryllium carbide particles, a technique was worked out by which the appearance of several representative lots of Be_2C were recorded

in natural color on Ektochrome transparencies. A sample of the material was suspended in a cyanthien red Y dye solution in nitrobenzene on a glass slide. Limited transmitted light produced a light brown background. Peripheral lighting from small fluorescent tubes illuminated the translucent Be₂C grains. Exposures were made with a Bausch & Lomb research metallograph, each exposure requiring approximately 45 min. In the colored transparencies, one can distinguish among translucent, amber Be₂C, the black opaque unreacted carbon, and precipitated flakes of graphite occurring within the Be₂C crystals. Occasional grains of Be₂C exhibited an olive green color, possibly caused by the presence of precipitated colloidal carbon. In other Be₂C grains, the greenish color may be caused by the thinness of section.

HARDNESS MEASUREMENTS

Coarse crystals of Be₂C were mounted in Lucite and polished. Knoop hardness numbers were then taken by means of a Tukon hardness tester. When a 100-gram load was used, crystals shattered or chipped away at the impression. Satisfactory readings were taken with lighter loads. Readings of 2678, 2520, and 2613 were obtained with a 50-gram load, and 2740 with a 25-gram load. It appears that the hardness of Be₂C is greater than that of silicon carbide and approaches the hardness of boron carbide.

CONCLUSIONS

Be₂C may be made by several methods, principal of which are the BeO-carbon and the Be-metal-carbon reactions. The metal-carbon reaction appears better when controlled crystal size is desired. The

true translucent amber color of Be₂C is revealed only under the microscope. As a refractory, it has several disadvantages. It tends to hydrolyze even in atmospheric moisture. In heating, Be₂C must be protected against both oxygen and nitrogen. It decomposes at about 2150°C with vaporization of the beryllium which reunites with carbon in cooler regions, or with oxygen or nitrogen, if present. Be₂C has no useful melting point at atmospheric pressure.

ACKNOWLEDGMENT

This work was performed at Battelle Memorial Institute under the sponsorship of the Nepa Division of the Fairchild Engine and Airplane Corporation.

Any discussion of this paper will appear in a Discussion Section to be published in the December 1954 issue of the JOURNAL.

REFERENCES

1. P. LEBEAU, *Compt. rend.*, **121**, 496 (1895); *J. Soc. Chem. Ind.*, **15**, 141 (1895); *J. Chem. Soc.*, **70**, 169 (1895).
2. L. HENRY, *J. Chem. Soc.*, **70**, 169 (1895).
3. P. LEBEAU, *J. Phys. Chem.*, **4**, 222 (1899); *J. Chem. Soc.*, **76**, 554 (1899); *Z. Kryst.*, **34**, 629 (1899); also see: C. L. PARSONS, "Chemistry and Literature of Beryllium," The Chemical Publishing Co., New York (1909); J. N. FRIEND, "Textbook of Inorganic Chemistry," Vol. III, Pt. II, pp. 27-28, Charles Griffin & Co., Ltd., London (1926); J. W. MELLOR, "Treatise of Inorganic and Theoretical Chemistry," Vol. 5, p. 866, Longmans, Green and Company, London (1924).
4. M. V. STACKELBERG AND F. QUATRAM, *Z. physik. Chem.*, **27**, 50 (1934).
5. R. F. GELLER, *Nucleonics*, **7** (1950).
6. J. H. COOBS AND W. J. KOSHUBA, *This Journal*, **99**, 115 (1952).
7. M. GALLAGHER, *J. Southern Research*, **3**, No. 4, 14 (1951).
8. H. A. SLOMAN, *J. Inst. Metals*, **49**, No. 2, 365 (1932).

Ionic Mass Transfer and Concentration Polarization at Rotating Electrodes¹

M. EISENBERG,² C. W. TOBIAS, AND C. R. WILKE

Department of Chemistry and Chemical Engineering, University of California, Berkeley, California

ABSTRACT

Rates of ionic mass transfer at nickel electrodes rotating about their axes in the center of stationary electrodes were studied using the ferri-ferrocyanide couple in alkaline solutions. A general mass transfer correlation was found to apply equally well to dissolution rates of rotating solids and to rates of ionic mass transfer at rotating electrodes. This correlation takes into account physical properties of the system as well as geometric and hydrodynamic factors. The correlation allows prediction of limiting currents and concentration polarization at rotating electrodes under a wide range of conditions.

The nature of polarization involved in reduction of $\text{Fe}(\text{CN})_6^{-3}$ and oxidation of $\text{Fe}(\text{CN})_6^{-4}$ was also investigated. Polarization was found to depend strongly on the presence of electrode poisons. With freshly prepared solutions, under exclusion of light, and with cathodically treated nickel electrodes, relatively small chemical polarizations were determined. For rotational speeds not exceeding Reynolds number 11,000, chemical polarization was found to be negligible in comparison with concentration polarization. Under such conditions, the ferro-ferricyanide couple can be conveniently used to obtain mass transfer rates for various hydrodynamic conditions, or conversely, to verify the validity of mass transfer equations by a comparison of experimental and calculated values of limiting currents and concentration polarization.

The rotating electrode model was found to be most suitable for studying the nature of electrolytic polarization phenomena because of uniformity of the current distribution and the hydrodynamic diffusion layer at the electrode surface.

INTRODUCTION

Study of mass transfer at working electrodes is of fundamental importance (1, 2) in analysis of electrode phenomena and in consideration of concentration polarization, limiting currents, and rates of electrode reactions. Several typical cases have been analyzed by the methods of hydrodynamics and boundary layer theory, and for a few models, experimental results were successfully correlated (1, 2). The effect of natural convection in electrolysis was quantitatively evaluated by Wagner (3) and Wilke and coworkers (4) among others. Rotating disk electrodes were treated mathematically by Levich (5). This theory applies if the diffusion boundary layer at the disk is laminar. Along the lines suggested by Agar (6), Lin and coworkers (7) correlated limiting current densities for the inner electrode of an annular cell with streamline and turbulent longitudinal flow. An extension of this study for laminar and turbulent flow along flat plate electrodes was recently reported (8).

The present investigation is concerned with cylindrical central electrodes rotating in concentric

cylindrical cells. Among many possible methods of stirring, the case of a rotating electrode is noteworthy, not only because it affords experimental reproducibility, but also because it permits application of methods of hydrodynamics and mass momentum transfer analogy in interpretation and correlation of data (9–11). Theoretical analysis of this problem for electrodes is further facilitated by uniformity of current distribution resulting from the geometry of concentric cylindrical electrodes and uniform thickness of the diffusion layer formed on the rotating electrode.

Recently, rotated electrode surfaces have been used in chemical analysis and in corrosion studies in parallel with polarographic methods (12, 13). Industrial applications of this forced convection model are known, and further important uses are anticipated.

The effect of speed of rotation upon rate of mass transfer was first studied by Brunner (14, 15). He found that the diffusion layer thickness, δ ,³ decreases with the $\frac{2}{3}$ power of the speed. However, he considered neither the effect of rotor diameter nor the dependence on physical properties of the electrolyte. Therefore, only qualitative conclusions can be drawn from these experimental results.

³ A table of nomenclature is collected at the end of this paper.

¹ Manuscript received December 16, 1953. This paper was prepared for delivery at the Chicago Meeting, May 2 to 6, 1954.

² Present address: Stanford Research Institute, Stanford, California.

Eucken (16) analyzed the effect of laminar flow forced convection upon rate of mass transfer at an electrode. In his experiments the external vessel containing the solution was rotated, and laminar flow past the fixed inner flat plate electrode resulted. Eucken's mathematical analysis is valid only for this particular condition. Kambara and coworkers (17) adapted Eucken's treatment to a 0.5-mm diameter platinum wire electrode projecting perpendicularly 6 mm from the axis of a rotating glass rod. In the derivation, it is assumed that the velocity gradient at the electrode surface is proportional to rpm. This is valid for Eucken's model, where laminar flow exists in the entire region of flow, but is inadmissible for the turbulent flow case, where laminar flow is restricted to the boundary layer adjacent to the electrode surface.

For the sake of clarity, the term "rotating electrode" is used henceforth only in reference to cylindrical electrodes rotating about their axes in the center of stationary, circular, cylindrical electrodes. Recently, Roald and Beck (18) used such rotating electrodes in a study of dissolution rates of magnesium and its alloys in hydrochloric acid solutions. They found that rates of dissolution increase in low acid concentrations with the 0.71 power of the speed of rotation. At higher acid concentrations (1.4M and higher), the reaction rates become entirely independent of rotational speeds, as the stirring effect produced by hydrogen bubbles evolving at the metal interface becomes predominant. This stirring effect, however, should not be ignored even at low acid concentrations because of turbulence caused by hydrogen bubbles moving in the boundary layer adjacent to the dissolving magnesium rod. For this reason the work of Roald and Beck represents a rather special case of forced convection mass transfer.

In studies of dissolution and corrosion rates of rotated metal rods, King and coworkers (19-22) estimated the mass transfer coefficients employing King and Shack's earlier experimental finding (23), according to which "normal diffusion (or transport) control requires that rates be linear with peripheral speed above about 5000 cm/min" (22). King and Cathcart (24) indicated that the mass transfer coefficient is directly proportional to the 0.7 power of the diffusion coefficient of the reacting ionic species.

The effect of cylinder diameter, speed of rotation, diffusion coefficient, and viscosity on mass transfer rates has not been successfully incorporated into a single correlation, although the usefulness of the Chilton-Colburn analogy for correlating the pertinent variables was realized by King and coworkers in 1937 (25).

The present work was undertaken with the follow-

ing aims in mind: (a) to establish correlations between physical properties of a system, geometrical and hydrodynamic conditions, and rates at which a solute (ion) is transferred to or from a rotating electrode; (b) to determine whether such general mass transfer correlations enable prediction of concentration polarization and limiting currents in steady state electrolysis.

EXPERIMENTAL

To assure the latter objective it was important to choose an electrode reaction which occurs with negligible chemical polarization. For such an electrode process the total measured polarization (ΔE_T)³ would represent concentration polarization (ΔE_{conc}) only, and would make a comparison between theoretical prediction and experiment possible. However, most of the known electrode reactions take place with considerable chemical polarization (ΔE_{chem}) when finite currents are passed. Some oxidation-reduction reactions have long been suggested by investigators (26-28) to occur with negligible chemical polarization. Recently, Moll (29) found no measurable chemical polarization for the ferrous-ferrocyanide couple at gold and platinum electrodes freshly treated by hydrogen and oxygen discharge. Essin and coworkers (30) made similar studies on the ferrocyanide-ferricyanide couple at platinum and nickel electrodes and concluded that there is no appreciable chemical polarization "when the metal is free of all film that may form on the surface." In contrast, Carmody and Rohan (31) reported a measurable chemical polarization for this latter system on platinum. A similar conclusion was arrived at by Petrocelli and Paolucci (32) who studied this couple up to current densities of 25 ma/cm². They found, however, that "cathodic activation," i.e., a hydrogen discharge treatment of the electrode, tends to decrease chemical polarization.

For the purposes of this study, smoothness of the electrode surface was important because of hydrodynamic considerations. In a redox electrolysis, unlike in a metal deposition process, the electrode surface remains physically unaltered. Another advantage of the redox reaction is that steady-state electrode potentials are attained in much shorter time than in a deposition reaction.

These findings, in addition to stability considerations of several contemplated couples, resulted in selection of the ferricyanide-ferrocyanide couple and nickel electrodes for the present studies. A large excess of sodium hydroxide was used in order to eliminate the contribution of ionic migration to mass transfer (1).

Solutions of potassium ferri- and ferrocyanide,

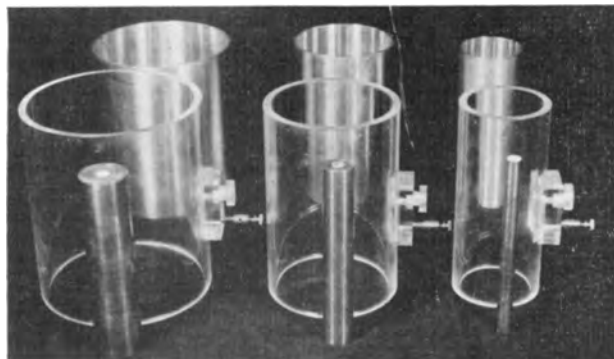
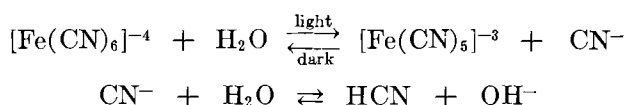


FIG. 1. Lucite cylinders, outer and inner nickel electrodes.

and particularly the ferrocyanide, are known to decompose slowly in light, resulting in formation of cyanide and hydroxide ions according to the following equations (33, 34):



In alkaline solutions kept in darkness, decomposition of these cyanide complexes is practically eliminated (35). Solutions used in these studies were freshly prepared for each series of runs in black Jena glass bottles.

Apparatus and Procedure

A concentric cylindrical cell, 6.16 in. high, built from acrylic plastic (Lucite), was equipped with grooved endplates which could hold as desired one of three cylindrical plastic tubes of 2.48, 4.00, 5.47 in. ID (Fig. 1 and 2). A $\frac{1}{2}$ -in. diameter stainless steel driving shaft passing through a teflon packing gland in the top plate was equipped with a $\frac{1}{4}$ -in. standard thread allowing nickel electrodes of 1.273, 2.48, and 5.024 cm diameter to be screwed onto it. The rotated electrode was supported from below by a guide pin and teflon lining in order to eliminate eccentric motion. Concentric outer cylindrical nickel electrodes of 6.07, 9.87, and 13.69 cm ID, all

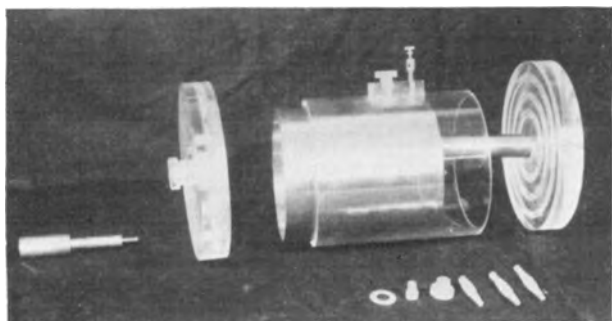


FIG. 2. Components of the cell

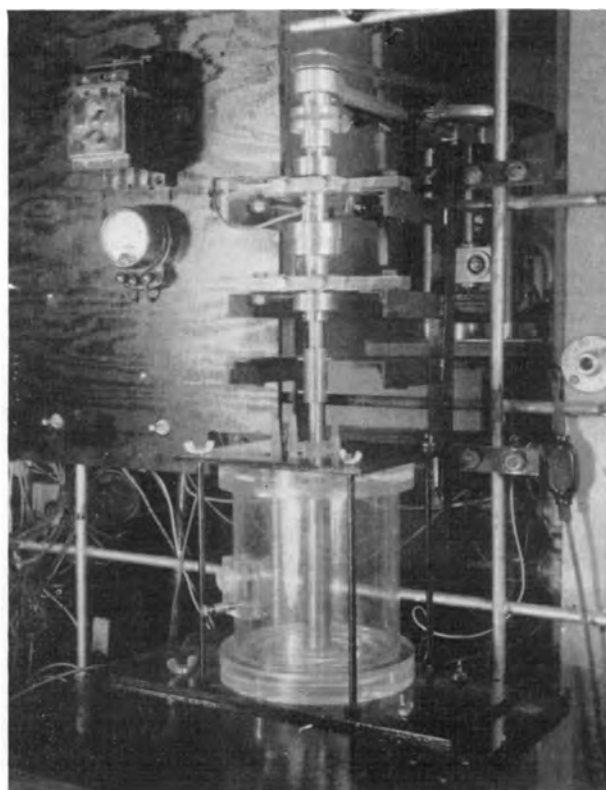


FIG. 3. Cell with supporting structure. (Outer electrode removed.)

15.11 cm long, were fitted tightly into corresponding Lucite tubes (Fig. 1 and 2). The cell was made liquid tight with neoprene rubber gaskets placed in the grooves. A ground glass joint thermometer fitted into the top plate with its bulb reaching about $\frac{3}{4}$ in. into the cell. The assembled cell with supporting structure designed to eliminate vibrations is shown in Fig. 3.

Electrodes permitted a variation of the ratio of gap to the diameter of the inner electrode ranging from 0.104 to 4.88. A Lucite nipple on the top

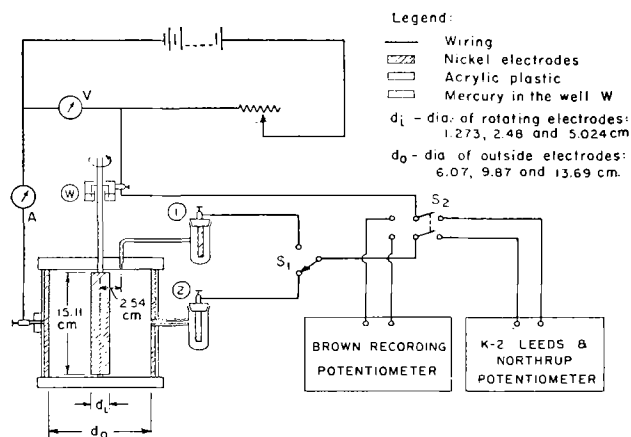


FIG. 4. Schematic diagram of the electrolyzing and measuring circuits used with the cell for rotating electrodes.

plate of the assembled cell was screwed into a small tapered hole which ended with a $\frac{1}{4}$ mm diameter on the inside of the plate and was located 2.541 cm from the cell axis (Fig. 4). Through this hole and a piece of polyethylene tubing, a continuous liquid junction led to reference cell No. 1 equipped with a nickel electrode and filled with the same solution as that in the electrolytic cell. Reference cell No. 2 was connected with the cell by means of a teflon nipple ($\frac{1}{4}$ -in. OD) leading through the center of the Lucite cylinder and ending flush with the inner surface of the outside electrode. Such arrangements of the liquid junction leading to reference electrodes are preferable for two reasons: (a) the flow pattern in the cell remains undisturbed, and (b) a distortion of current distribution over the electrode surface is avoided.

As can be seen from the diagram in Fig. 4, a potential measurement of the rotating electrode by means of reference electrode No. 1 involved an ohmic potential drop over the annular solution space between the radius of the rotating electrode and the distance of 2.54 cm at which the small opening leading to that reference cell was located. For a total current, i , this ohmic drop was therefore

$$iR_{(1)} = \frac{i}{2\pi\kappa h'} \ln \frac{2.54}{r_i} \quad (1a)$$

where $R_{(1)}$ = resistance, ohms; r_i = radius of rotated inner electrode, cm; h' = height of cell, here 15.11 cm; κ = conductivity of solution, $\text{ohm}^{-1} \text{cm}^{-1}$.

Similarly a potential measurement of the rotated electrode by means of reference No. 2 involved an ohmic drop given by:

$$iR_{(2)} = \frac{i}{2\pi\kappa h'} \ln \frac{r_o}{r_i} \quad (1b)$$

Since r_o , internal radius of the outer electrode, was either 6.84, 4.94, or 3.035 cm, respectively, for series of runs I, II, and III, the ohmic drop could be computed more reliably by equation (1b), i.e., using reference No. 2. This is particularly true since a small geometrical misalignment will cause a lesser relative error in the ratio r_o/r_i of equation (1b).

In all runs, potential measurements of the rotating electrode were taken by means of both reference junctions selected one at a time with switch S-1 (Fig. 4). Net values obtained after subtracting $iR_{(1)}$ and $iR_{(2)}$ drops, respectively, rarely differed by more than 1%. However, for reasons stated above, in most cases measurements with reference electrode No. 2 were preferred over an arithmetic average of the two measurements.

Electrical connection to the rotating electrode

was accomplished by means of a mercury well (W in Fig. 4). A copper contact screw provided the connection to the outer stationary electrode. Current was measured with a d-c milliammeter⁴ or a d-c ammeter.⁵ All ammeters were carefully calibrated by means of standard resistors. Selector switch S-2 (Fig. 4) permitted measurements of potential by either (a) recording potentiometer⁶ with five ranges, the largest being up to 500 mv, or a (b) manual potentiometer,⁷ using a high sensitivity galvanometer as zero instrument.⁸ The recorder was used first to ascertain whether steady-state polarization was achieved, then the final value was measured accurately by means of the manual potentiometer.

Sodium hydroxide, 2*N*, was used as neutral electrolyte in preparing five approximately equimolar potassium ferricyanide and potassium ferrocyanide solutions in the concentration range of 0.009 to 0.204 mole/l. C.P. reagents⁹ were used throughout. Slight changes in concentrations of ferri- and ferrocyanide ions, caused by use of a solution up to limiting current densities, were followed up by strict analytical control. Ferricyanide was determined by the iodometric procedure (36) and ferrocyanide by permanganate titration (37).

Before introduction into the cell, each solution was alternately deaerated in a glass column by means of vacuum, and saturated with nitrogen several times to remove dissolved oxygen. Presence of a considerable amount of dissolved oxygen in the cell would have interfered with electrode reactions of ferricyanide and ferrocyanide, particularly at low concentrations. Furthermore, it was felt that, in absence of oxygen, nickel electrodes would remain in an "active" state longer.

Prior to each assembling of the cell, smooth electrodes were polished with rouge paper, washed with CCl_4 , and treated cathodically in a 5% NaOH solution at a current density of 20 ma/cm² for 12–15 min.

The assembled cell was filled with a given solution at approximately 25°C, the inner electrode set into rotation at a selected speed. Value of the electrode potential at no current flow (*ZCP*) was measured with both references. These were later subtracted (with proper sign) from the "at current" values. Thus any "static" potential differences due to variations in surface structure of the electrodes could be accounted for. A relatively small current was applied, and the potential of the rotating elec-

⁴ Weston (Model 45).

⁵ Cenco (Model 6935).

⁶ Minneapolis Honeywell Company (Model Y-153-X-12).

⁷ Leeds and Northrup, Type K-2 (Model No. 7552).

⁸ Leeds and Northrup (No. 2430).

⁹ Merck and Company.

trode followed with a reference electrode and recording potentiometer until steady state was achieved. Final values were then measured with the manual potentiometer, using both reference electrodes consecutively. Steady-state polarization was obtained in a few seconds at high speeds and within 2–3 min at low speeds. Achievement of the steady state, while not essential for determination of limiting currents, was important for subsequent calculations of chemical polarization. A reliable comparison of concentration and chemical polarization can be made only under steady-state conditions. Current was increased in small increments until the limiting current, noted by a sudden rise in potential, was attained. At a given speed each run was first completed with the rotor as cathode. Then polarity was reversed and a run was carried out with the rotor as anode. When a series of runs with speeds ranging from 30 to 1650 rpm was complete, the cell was taken apart, the electrodes treated as described previously, and reassembled with another electrode diameter but with the same inner electrode. Thus the effect of the gap between concentric cylindrical electrodes was studied for a given solution, given diameter of rotating electrode, and given angular velocity. The temperature of $25^{\circ}\text{C} \pm 0.3$ was maintained by blowing preheated or precooled air on the cell exterior. Physical properties required for correlative study were determined for each solution within the range 20° – 30°C .

Conductivities were measured in a conventional conductivity cell, calibrated with 0.9996*M* KCl solution, using an audiooscillator¹⁰ as power source for 1000 cycle A.C., a Wheatstone bridge, and an oscilloscope¹¹ as zero instrument.

Viscosities of solutions relative to water were measured at several temperatures in a thermostat with an Ubbelohde pipette, and absolute viscosities calculated using densities obtained by pycnometer determinations.

Diffusion coefficients for ferri-ferrocyanide ions were measured by the capillary method (38).

Methods of Calculation

Ionic mass transfer.—Potential values obtained for each run were first corrected by subtracting (with proper sign) the *ZCP* differences and the corresponding *iR* drops calculated by means of equation (I). These net resulting values represented ΔE_T . From the known areas of rotating electrodes, current densities were calculated, and plots of current density, *I* (ma/cm²) vs. ΔE_T (mv) were prepared. Limiting current densities were then determined for each run at the plateau of the curve. At this

point, in case of cathodic ferricyanide reduction runs, the consecutive electrode process was hydrogen evolution. This, however, did not take place before the potentials exceeded 600–700 mv. For anodic oxidation of ferrocyanide the plateau was shorter as the consecutive reaction (oxygen evolution) took place at ΔE_T values of 200–250 mv. As illustrations, Fig. 5 and 6 show sets of cathodic and corresponding anodic runs for solution No. 9 at speeds up to 1650 rpm. The limiting cathodic current densities (*I_c*) and the limiting anodic current densities (*I_a*) are given in the corresponding figures.

At limiting current when interfacial concentration of reacting species becomes zero, the rate of ionic mass transfer of ferricyanide ion to the cathode or of ferrocyanide ion to the anode can be expressed as (1):

$$N = \frac{I_L}{nF} (1 - t_i) = k_L c_o \quad (\text{II})$$

where *I_L* = cathodic (*I_c*) or anodic (*I_a*) limiting current densities, amp/cm²; *n* = valence change of reacting ion; *F* = the Faraday constant; *c_o* = bulk concentration of reacting ion, moles/cc; *t_i* = transference number of the reacting ion; *k_L* = average mass transfer coefficient, cm/sec. Since the estimated transference numbers of ferri- and ferrocyanide ions did not exceed 0.03 (and was usually much lower) due to excess NaOH used as the indifferent electrolyte, equation (II) can be rewritten as:

$$N = \frac{I_L}{nF} = k_L c_o \quad (\text{IIa})$$

Thus by means of equation (IIa) the average mass transfer coefficient, *k_c* for the ferricyanide reduction and *k_a* for ferrocyanide oxidation, was calculated for each run.

From the measured values of viscosity, *μ*, density, *ρ*, and diffusion coefficients, *D*, of ferrous and ferric cyanide, corrected to the temperature of given runs, the corresponding Schmidt groups *Sc* = *μ/ρD* were computed for anodic and cathodic experiments.

The Reynolds number, characterizing flow produced in the cell, was found to involve the rotating electrode diameter as the characteristic length dimension and not the gap between cylindrical electrodes (39). Accordingly, the Reynolds number was computed as:

$$R_d = \frac{V \cdot d_i}{\nu} \quad (\text{III})$$

where *V* = peripheral velocity, cm/sec; and *ν* = kinematic viscosity, cm²/sec.

Concentration polarization and chemical polariza-

¹⁰ Hewlett-Packard Model 200 C.

¹¹ RCA No. 155 A.

tion.—It is clear that as far as mass transfer studies are concerned, it is not necessary for the electrode reaction to take place with negligible chemical polarization. The mass transfer coefficient, k_L , could be calculated for any current density if in addition to the bulk concentration, c_o , the interfacial concentration, c_i , were known. Since an accurate experimental determination of c_i is extremely difficult, mass transfer coefficients are most conveniently obtained from limiting current measurements, as outlined above.

However, an electrode reaction with negligible chemical polarization was desirable in these studies in order to ascertain experimentally whether correct predictions of limiting currents and concentration polarization can be made from a general mass transfer correlation for rotating cylinders.

The ferri-ferrocyanide couple was therefore investigated as to the nature of polarization associated with both cathodic reduction of ferricyanide and anodic oxidation of ferrocyanide on nickel electrodes. This was done as follows.

(A) From graphs of I vs. ΔE_T (of the type shown in Fig. 6 and 7), values of I and ΔE_T were read off at equal current density increments and tabulated

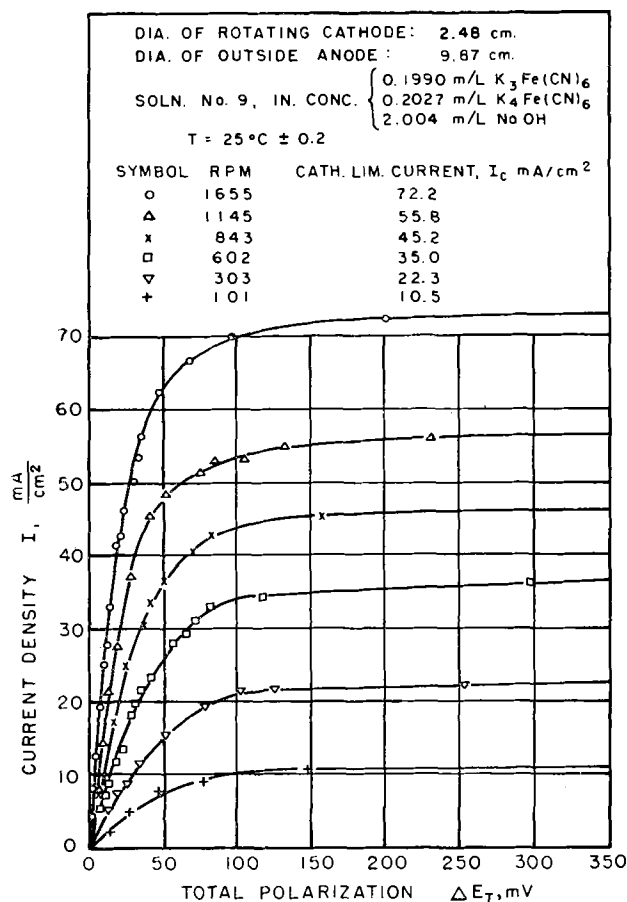


Fig. 5. Cathodic polarization curves of ferricyanide ion reduction.

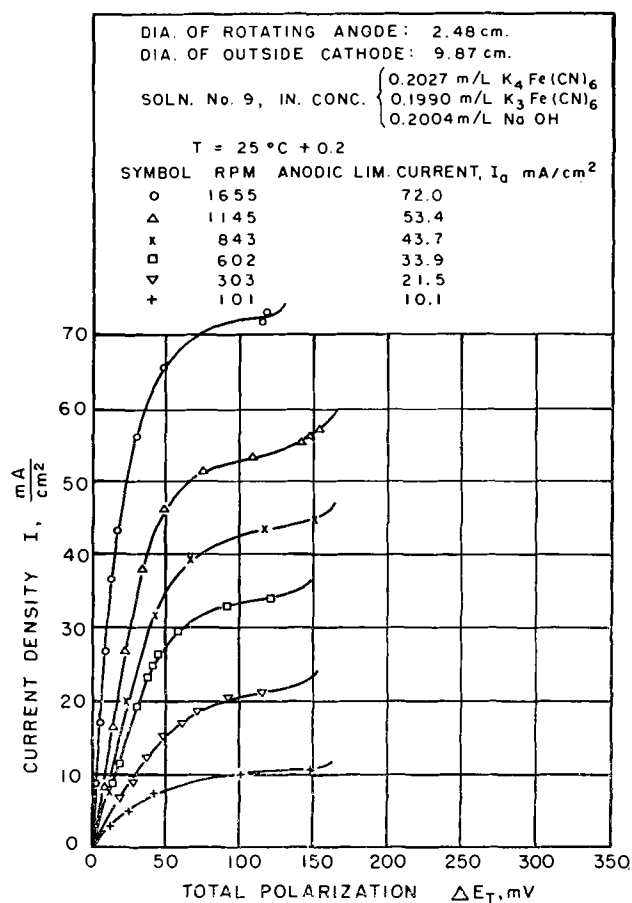


Fig. 6. Anodic polarization curves of ferrocyanide ion oxidation.

up to current densities equal to 70–75% of limiting current density.

(B) Using I_c , and I_a (both obtained for the same solution, cell geometry and speed), ΔE_{conc} for this redox couple was calculated (30, 40) for each current density by the following equations¹²:

$$\Delta E_{conc} = \frac{RT}{nF} \ln \frac{1 - I/I_c}{1 + I/I_a} \quad (\text{for cathodic case}) \quad (IVa)$$

$$\Delta E_{conc} = \frac{RT}{nF} \ln \frac{1 + I/I_c}{1 - I/I_a} \quad (\text{for anodic case}) \quad (IVb)$$

(C) ΔE_{chem} at each of the applied current densities was calculated by subtracting the calculated ΔE_{conc} from the experimentally obtained ΔE_T :

$$\Delta E_{chem} = \Delta E_T - \Delta E_{conc} \quad (V)$$

It is interesting to note that, from equations (IV) and (V) for the case of a redox electrode reaction with negligible chemical polarization, a plot of

¹² Actually the derivation of equation (IVa) assumes that the mass transfer coefficient is independent of current density. In forced convection such an assumption is well justified.

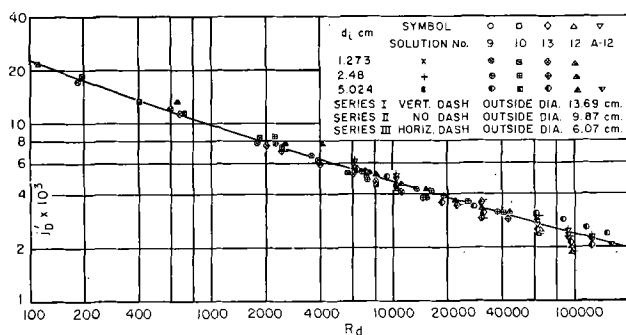


FIG. 7. Cathodic reduction of ferricyanide. Mass transfer at rotating electrodes.

$$j'_D = \frac{k_c}{V} (Sc)^{0.644} \text{ vs. } R_d$$

experimental values of ΔE_T versus $\log Q$, where

$$Q = \frac{1 \mp I/I_c}{1 \pm I/I_a} \quad (\text{VI})$$

(upper sign for cathodic, lower for anodic case) should yield a straight line with slope $2.303 RT/nF$. For the ferri-ferrocyanide couple $n = 1$, and expressing potentials in millivolts, the slope for experiments performed at 25°C should be 59.1.

RESULTS AND DISCUSSION

Correlation of Mass Transfer Rates

Ionic mass transfer results presented here were part of a broader study involving dissolution of rotating cylinders cast from benzoic and cinnamic acid into water and aqueous glycerol solutions (39). A general type of correlation based on methods of momentum-mass transfer analogy was obtained using the following parameter:

$$j'_D = \frac{k_L}{V} (Sc)^{0.644} \quad (\text{VII})$$

in which $Sc = \nu/D$ accounts for the physical properties of the system and k_L is given by equation (IIa).

Fig. 7 and 8 show logarithmic j'_D vs. R_d plots of mass transfer data for reduction of ferricyanide and oxidation of ferrocyanide, respectively. Table I gives a typical set of data,¹³ including physical properties, for one of five solutions studied. Average deviations of points in Fig. 7 and 8 from the best line are $\pm 7\%$ and $\pm 6.6\%$ for the two electrode reactions. These experiments involved a Schmidt number variation of 2230 to 3650 and a Reynolds number range of 112.0–162,000 (peripheral velocities 1.17 to 426 cm/sec). Limiting current densities varied from 0.43 to 113 ma/cm².

¹³ Complete data are given in Reference (39).

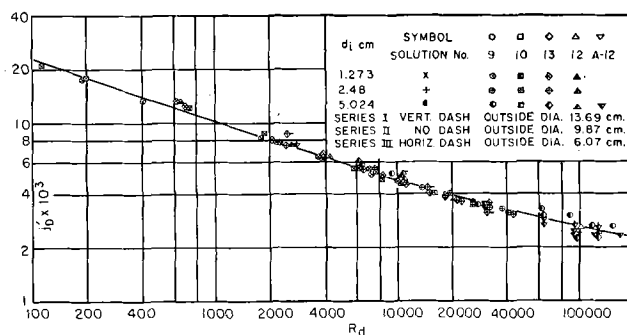


FIG. 8. Anodic oxidation of ferrocyanide. Mass transfer at rotating electrodes.

$$j'_D = \frac{k_a}{V} (Sc)^{0.644} \text{ vs. } R_d$$

In Fig. 9, lines correlating electrolytic data are compared with results obtained by solid dissolution studies. Results for the various systems agree with each other within 7% and all lie within experimental error involved in determination of frictional drag coefficient, $f/2$, obtained by Theodorsen and Regier (11).

Such an agreement is very encouraging in view of the Chilton-Colburn analogy (41) which suggests that

$$j_D = \frac{k_L}{V} \phi(Sc) = f/2 \quad (\text{VIII})$$

where $\phi(Sc)$ represents a function of the Schmidt number. [For a detailed discussion see Reference (39).]

In Fig. 10, all mass transfer data for three solid dissolution systems and the two electrolytic redox reactions were plotted together. The best curve (within $\pm 8.3\%$) through all points is represented by coordinates given in Table II.

In the Reynolds number range 1000–100,000 data are best represented by a straight line (dashed in Fig. 10) given by

$$j'_D = \frac{k_L}{V} Sc^{0.644} = 0.0791 R_d^{-0.30} \quad (\text{IX})$$

From equation (IX) a number of interesting practical relations may be derived.

Recalling that the mass transfer coefficient $k_L = I_L/nFc_o$, the following relations for limiting current density may be obtained:

$$\begin{aligned} I_L &= 0.0791 nFc_o V \left(\frac{Vd_i}{\nu} \right)^{-0.30} \left(\frac{\nu}{D} \right)^{-0.644} \\ &= 0.0791 nFc_o V^{0.70} d_i^{-0.30} \nu^{-0.344} D^{0.644} \quad (\text{X}) \\ &= nF \frac{Dc_o}{\delta} \text{ (amp/cm}^2\text{)} \end{aligned}$$

TABLE I. Mass transfer at rotating electrodes, ferri-ferrocyanide couple. (Sample data).^{*} Solution No. 9 (2.004*N* NaOH)

Run No.	<i>V</i> cm/sec	<i>T</i> °C	$\nu \times 10^2$ cm ² /sec	<i>R</i> _d	Cathodic reduction of ferricyanide						Anodic oxidation of ferrocyanide					
					$C_{\text{ferri}} \times 10^3$ mole/cc	<i>I</i> _c ma/cm ²	$k_c \times 10^5$ cm/sec	$D \times 10^5$ cm ² /sec	<i>S</i> _c	$j_b \times 10^3$	$C_{\text{ferro}} \times 10^3$ mole/cc	<i>I</i> _a ma/cm ²	$k_a \times 10^5$ cm/sec	$D \times 10^5$ cm ² /sec	<i>S</i> _a	$j_b \times 10^3$
13a. <i>d</i> _i = 1.273 cm <i>A</i> = 61.2 cm ² Ser. II (<i>d</i> _o = 9.87 cm)																
—, 276A	114.9	25	1.423	10,280	—	—	—	—	—	—	0.2030	52.0	265.5	0.390	3,649	4.55
277C, 278A	81.5	25	1.423	7,291	0.1988	42.2	219.8	0.454	3,134	4.82	0.2029	42.0	214.4	0.390	3,649	5.18
280C, 281A	40.4	25	1.423	3,614	0.1982	28.2	147.3	0.454	3,134	6.51	0.2028	26.0	132.6	0.390	3,649	6.46
284C, 285A	20.0	25	1.423	1,789	0.1976	16.6	87.0	0.454	3,134	7.76	0.2027	16.4	83.9	0.390	3,649	8.27
286C, 287A	6.8	25	1.423	608	0.1971	8.8	46.2	0.454	3,134	12.1	0.2026	8.9	45.4	0.390	3,649	13.1
290C, 291A	2.07	25	1.423	185	0.1961	3.75	19.9	0.454	3,134	17.1	0.2024	3.55	18.2	0.390	3,649	17.3
13b. <i>d</i> _i = 2.48 cm <i>A</i> = 117.6 cm ² Ser. II (<i>d</i> _o = 9.87 cm)																
133C, 134A	214.9	25	1.423	37,460	0.1990	72.2	376	0.454	3,134	3.12	0.2027	72.0	368	0.390	3,649	3.37
135C, 136A	148.7	25	1.423	25,920	0.1970	55.8	294	0.454	3,134	3.53	0.2026	53.4	273	0.390	3,649	3.62
137C, 138A	109.5	25	1.423	19,080	0.1960	45.2	239	0.454	3,134	3.89	0.2025	43.7	224	0.390	3,649	4.03
139C, 140A	78.2	25	1.423	13,630	0.1945	35.0	186	0.454	3,134	4.25	0.2024	33.9	174	0.390	3,649	4.37
141C, 142A	39.3	25	1.423	6,850	0.1935	22.3	119	0.454	3,134	5.41	0.2023	21.5	110.1	0.390	3,649	5.51
143C, 144A	13.1	25	1.423	2,283	0.1925	10.5	57	0.454	3,134	7.76	0.2023	10.1	51.8	0.390	3,649	7.77
13c. <i>d</i> _i = 5.024 cm <i>A</i> = 236.4 cm ² Ser. II (<i>d</i> _o = 9.87 cm)																
484C, 485A	26.6	25	1.423	9,391	0.1891	13.60	74.5	0.454	3,134	5.00	0.2030	13.80	70.4	0.390	3,649	5.22
486C, 487A	79.7	25	1.423	28,140	0.1904	27.8	151.3	0.454	3,134	3.39	0.2037	27.40	139.4	0.390	3,649	3.44
488C, 489A	172.8	25	1.423	61,010	0.1918	55.6	300.3	0.454	3,134	3.11	0.2044	55.6	281.9	0.390	3,649	3.21
490C, 491A	246.8	25	1.423	87,130	0.1930	73.3	393.8	0.454	3,134	2.84	0.2050	75.0	379.1	0.390	3,649	3.03
492C, 493A	332.8	25	1.423	117,500	0.1969	90.4	475.9	0.454	3,134	2.55	0.2024	87.0	445.4	0.390	3,649	2.64
494C, 495A	426.2	25.7	1.405	152,400	0.1963	109.0	575.6	0.461	3,048	2.37	0.2024	113.0	578.6	0.396	3,548	2.63

$$R_d = \frac{Vd_i}{\nu} \quad j'_D = \frac{k_L}{\nu} (Sc)^{0.644}$$

δ (cm) is then given by:

$$\begin{aligned} \delta &= \frac{1}{0.0791 V^{0.70} d_i^{-0.30} \nu^{-0.344} D^{-0.356}} \\ &= 12.64 \times \frac{d_i^{0.30} \nu^{0.344} D^{0.356}}{V^{0.70}} \quad (\text{XI}) \\ &= 99.62 \frac{d_i^{-0.40} \nu^{0.344} D^{0.356}}{S^{0.70}} \end{aligned}$$

where *D* = diffusion coefficient, cm²/sec; and *S* = rotational speed, rpm.

Thus, δ depends not only on rotational speed, but also on rotor diameter as well as on viscosity and diffusivity. The latter three variables were not considered by Brunner (14).

Assuming δ independent of rate (i.e., of the current density), as was suggested by Agar (6), one can write:

$$\frac{I}{nF} = \frac{D}{\delta} (c_o - c_i) \quad (\text{XIIa})$$

^{*} See footnote (15), p. 315.

Hence for a given applied C.D., *c*_i may be calculated by:

$$c_i = c_o - \frac{I}{nFD} \delta \quad (\text{XIIb})$$

δ is obtained for a given geometry, speed and physical properties of the electrolyte by equation (XI).

Previous studies relating to mass transfer at rotating electrodes were limited in scope and can be compared to the present work only in respect to functional dependence on rotational speed. Rold and Beck (18) found for rotating magnesium electrodes:

$$k_L = \text{const } V^{0.7} \quad (\text{XIII})$$

This is in agreement with results of the present study since equation (XIII) can be shown to follow from equation (IX) for a given system (constant ν and *S*_c) and given rotor diameter. Brunner (14) used rather impractical geometries and poorly defined experimental conditions; his results may be expressed in the form:

$$k_L = \text{const } (\text{rpm})^{2/3} \quad (\text{XIV})$$

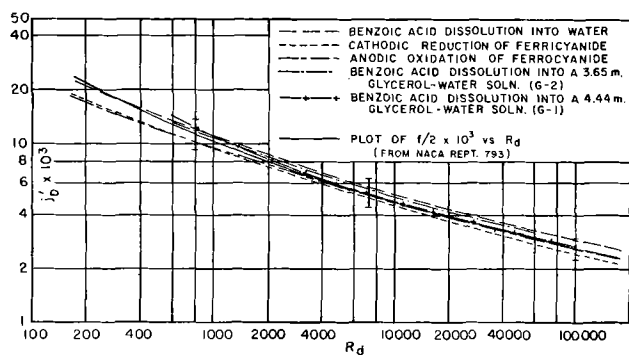


FIG. 9. Mass transfer correlation for inner rotating cylinder. Comparison of five systems studies with friction coefficients $f/2$.

For a given rotor diameter and given set of physical properties of the system, this relation is in approximate agreement with results of the present study.

A linear dependence of dissolution rates, or limiting currents on velocity of rotation as proposed by King and Shack (22, 23) is not substantiated by the present study.

Limiting Currents and Concentration Polarization

The nature of polarization of a redox electrode.—For ΔE_T of a redox electrode Petrocelli (40) obtained a general equation¹⁴ which in a somewhat modified form may be written as:

$$\Delta E_T = \frac{RT}{nF} \ln \left[\frac{1 - I/I_c}{1 + I/I_a} - \frac{I \frac{I_a}{i_0}}{(I_a + I) \exp\left(-\alpha E_T \frac{nF}{RT}\right)} \right] \quad (\text{XV})$$

where $\alpha =$ a constant between 0 and 1 (usually close to 0.5) representing the portion of the electrical potential difference across the activation energy barrier, which acts in the cathodic direction; $i_0 =$ exchange current density, representing the rate of forward (cathodic) and also backward (anodic) reaction at the reversible, or open circuit potential.

Using concepts of the absolute reaction rate theory (44) it is possible to show (40) that

$$i_0 = \frac{nF kT}{N h} c_o \cdot e^{-\Delta F^*/RT} \quad (\text{XVI})$$

where $\Delta F^* =$ standard free energy change of the activation process (at open circuit), ergs/mole; $N =$ Avogadro number, 6.023×10^{23} , molecules/mole; $h =$ Planck constant, 6.624×10^{-27} , erg-sec/mole-

¹⁴ Analogous relations have recently been obtained by a number of investigators (42, 43).

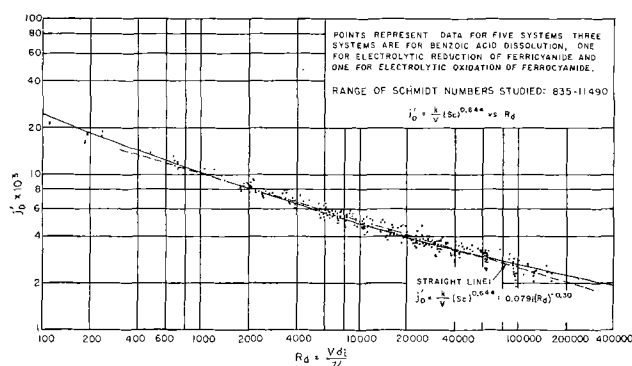


FIG. 10. General correlation for mass transfer at rotating cylinders.

cule; $k =$ Boltzmann constant, 1.3805×10^{-6} , erg/ $^{\circ}$ K-molecule.

Thus, at constant T , i_0 depends only on ΔF^* and c_o , of reacting ions. For a given electrode reaction the activation energy can be assumed to be constant provided electrode poisons are absent (29, 42). Under such conditions i_0 depends only on c_o .

In equation (XV) the first term in the bracket represents the contribution of concentration polarization, and the second represents chemical polarization. Relative magnitude of this second term depends primarily on I_a/i_0 .

For a given electrode system I_a increases with the 0.70 power of the rotational velocity, according to equation (X); i_0 , however, remains unaffected. Hence at high rotational speeds, i.e., large values of I_a/i_0 , chemical polarization should become significant in comparison with concentration polarization. It is obvious, therefore, that in order to ascertain experimentally whether a given electrolytic redox reaction comes close to thermodynamic reversibility, i.e., takes place with a comparatively small chemical polarization, ΔE_T vs. I curves must be obtained at high rotational speeds. From such curves (see, for example, Fig. 5 and 6) plots of ΔE_T against $\log \frac{1 \mp I/I_c}{1 \pm I/I_a}$ can be prepared

TABLE II. Coordinates of the general mass transfer correlation curve for rotating cylinders (see Fig. 10)

R_d	$j_D' \times 10^3$
200	18.4
500	13.0
1,000	10.2
4,000	6.53
10,000	4.88
30,000	3.54
60,000	2.96
100,000	2.61
200,000	2.24
300,000	2.05

as described previously. A comparison of equations (IV) and (XV) shows that if chemical polarization is negligible, i.e., $\Delta E_T \approx \Delta E_{\text{conc}}$, experimental points in such plots should fall close to a straight line with a slope of 59.1 (at 25°C, expressing polarization in mv). This type of plot is very convenient, as the distance of a given point from the straight line with slope 59.1 gives directly the value of chemical polarization and demonstrates its importance relative to concentration polarization (see for instance in Fig. 13).

Table III¹⁵ gives typical results for a given concentration, inner and outer diameter. Values of ΔE_{conc} and ΔE_{chem} were calculated according to equations (IV) and (V). Data for three experimental series were plotted in Fig. 11. Solutions used were only 0.05M and 0.01M in ferri- or ferrocyanide, hence, according to equations (XV) and (XVI) some chemical polarization may be expected. However, as Fig. 11 shows, even up to peripheral velocities of 157.3 cm/sec, ΔE_T consists almost entirely, within limits of experimental accuracy, of concentration polarization.

The predominant importance of the stirring rate as represented by V is interestingly demonstrated in Fig. 13 for a solution of a relatively high concentration [number 9, approximately 0.20N of $\text{Fe}(\text{CN})_6^{-3}$ and $\text{Fe}(\text{CN})_6^{-4}$]. For runs up to a velocity of 115 cm/sec, data fall close to the straight line with a slope 59.1, the value for the so-called reversible electrode. At higher speeds, i.e., when the ratio I_a/i_o increases, chemical polarization becomes relatively significant. For instance at $V = 333$ cm/sec, when the concentration polarization is 59.1 mv, the corresponding chemical polarization has already reached 19.4 mv (Fig. 13). Hence, in case of a reaction where I_a/i_o is not very small, it is possible to increase this ratio by increasing I_a with stirring (rotational speed). In this way a reaction in which polarization is predominantly controlled by mass transfer (i.e., concentration polarization) may be converted to one which is under activation control, involving large chemical polarization.

As shown previously, i_o depends greatly on the activation energy necessary for the reaction to proceed. The latter has been found by many investigators to increase in the presence of electrolytic poisons (29, 42). Thus, according to equation (XVI),

¹⁵ An extended version of these tables has been deposited as Document 4212 with the ADI Auxiliary Publications Project, Photoduplication Service, Library of Congress, Washington 5, D. C. A copy may be secured by citing the Document number and by remitting \$1.25 for photoprints, or \$1.25 for 35-mm microfilm. Advance payment is required. Make checks or money orders payable to: Chief, Photoduplication Service, Library of Congress.

TABLE III. Concentration and chemical polarizations at various rotational speeds and current densities [Sample data]¹⁵

Solution No. 13, Series II
Initial composition: (0.04996 m/l $\text{K}_3\text{Fe}(\text{CN})_6$
(0.05052 m/l $\text{K}_4\text{Fe}(\text{CN})_6$
(1.923 m/l NaOH
T = 25.0°C
Rotor diameter (d_i) = 5.024 cm
Outer cylinder diameter (d_o) = 9.87 cm

Run No.	I ma/cm ²	Cathodic reduction of $\text{Fe}(\text{CN})_6^{-3}$			Anodic oxidation of $\text{Fe}(\text{CN})_6^{-4}$		
		ΔE_{conc}^* (calc) mv	ΔE_T (meas) mv	$\Delta E_{\text{chem}} = \Delta E_T - \Delta E_{\text{conc}}$ mv	ΔE_{conc}^* (calc) mv	ΔE_T (meas) mv	$\Delta E_{\text{chem}} = \Delta E_T - \Delta E_{\text{conc}}$ mv
1208 rpm; $V = 318$ cm/sec; $I_c = 22.00$ ma/cm ² ; $I_a = 21.00$ ma/cm ²							
15a	2	-4.5	-4.0	0.5	4.8	4.0	-0.8
	4	-9.6	-9.1	0.5	9.7	8.1	-1.6
	6	-14.6	-12.4	2.2	14.8	12.4	-2.4
	8	-19.9	-17.2	2.7	20.3	17.2	-3.1
	10	-25.6	-21.6	4.0	26.3	21.6	-4.7
	12	-31.9	-26.7	5.2	33.0	27.8	-5.2
	14	-39.1	-34.1	5.0	40.8	36.3	-4.5
	16	-47.9	-43.0	4.9	50.9	50.0	-0.9
	18	-59.8	-56.7	3.1	65.5	67.2	1.7
	18.5	-63.6	-61.6	2.0	70.5	72.8	2.3
302 rpm; $V = 79.4$ cm/sec; $I_c = 8.20$ ma/cm ² ; $I_a = 8.10$ ma/cm ²							
15b	1	-6.3	-6.4	-0.1	6.3	6.4	0.1
	2	-12.8	-13.0	-0.2	12.9	13.0	0.1
	3	-19.7	-20.3	-0.6	19.8	20.3	0.5
	4	-27.5	-28.9	-1.4	27.7	28.9	1.2
	5	-36.5	-39.7	-3.2	36.9	39.7	2.8
	6	-48.1	-53.9	-5.8	48.8	53.9	5.1
102 rpm; $V = 26.8$ cm/sec; $I_c = 3.96$ ma/cm ² ; $I_a = 3.80$ ma/cm ²							
15c	0.3	-4.0	-4.0	0.0	4.0	4.0	0.0
	0.6	-8.0	-7.9	0.1	8.0	7.9	-0.1
	0.9	-12.1	-12.1	0.0	12.2	12.1	-0.1
	1.2	-16.3	-16.7	-0.4	16.6	16.7	0.1
	1.5	-20.8	-20.9	-0.1	21.1	20.9	-0.2
	1.8	-25.5	-26.0	-0.5	26.1	26.0	-0.1
	2.1	-30.7	-31.2	-0.5	31.6	31.2	-0.4
	2.4	-36.6	-37.1	-0.5	37.9	37.1	-0.8
	2.7	-43.3	-44.2	-0.9	45.2	44.2	-1.0
	3.0	-51.4	-54.2	-2.8	54.5	54.2	-0.3
	3.3	-62.1	-68.0	-5.9	67.7	68.0	0.3
	3.36	-64.8	-71.0	-6.2	71.3	71.0	-0.3
25 rpm; $V = 6.58$ cm/sec; $I_c = 1.81$ ma/cm ² ; $I_a = 1.74$ ma/cm ²							
15d	0.2	-5.8	-6.2	-0.4	5.8	6.2	0.4
	0.4	-11.7	-12.1	-0.4	11.8	12.1	0.3
	0.6	-17.8	-18.5	-0.7	17.8	18.5	0.7
	0.8	-24.7	-25.3	-0.6	25.2	25.3	0.1
	1.0	-32.3	-33.0	-0.7	33.3	33.0	-0.3
	1.2	-41.4	-42.6	-1.2	43.1	42.6	-0.5
	1.4	-53.3	-55.2	-1.9	56.7	57.0	-0.3
	1.5	-61.2	-64.7	-3.5	66.3	68.7	2.4

* $\Delta E_{\text{conc}}(\text{mv}) = 59.1 \log \frac{1 \mp I/I_c}{1 \pm I/I_a}$. (Upper sign for cathodic case, lower for anodic.)

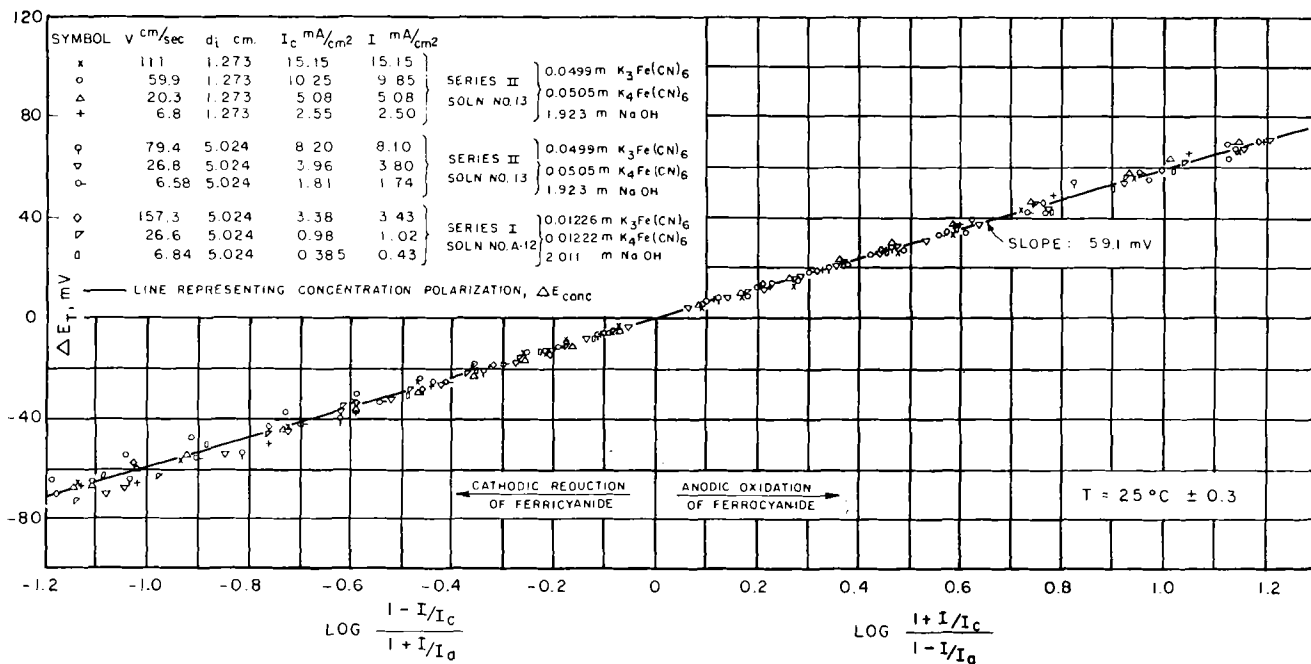


FIG. 11. Total polarization ΔE_T vs. $\log Q$

i_0 may be expected to decrease significantly under such conditions. In a special study on effects of better known electrode poisons, Gerischer (42) found that at platinum electrodes treated with a $2 \times 10^{-5}M$ H₂S solution for 1 min and 60 min, respectively, i_0 for the Fe⁺³/Fe⁺² couple dropped to 10.8% and 1.7% of the original (active state) value, respectively. The highly alkaline solutions used in the present studies, when exposed to air, could dissolve an amount of H₂S sufficient to decrease i_0 and consequently increase chemical polarization. Effects of other electrode poisons should, of course, be taken into account also. For instance, HCN formed through photochemical decomposition of ferrocyanide may exercise a powerful effect. Several investigators (45, 28) have also concluded that even electrodes made of "noble" metals such as gold, silver, and nickel become gradually covered with oxide films (when used in air-saturated solutions) causing a large increase in polarization.

In a special study designed to demonstrate the effect of electrode poisons, $\Delta E_T - I$ data were obtained for an alkaline ferro- ferricyanide solution, which was exposed to air and light for several days. Nickel electrodes used in this study were cleaned in the same manner as described previously, but were not given any cathodic hydrogen discharge treatment. Fig. 12 shows the results for solution No. 1 in the form of ΔE_T vs. $\log Q$ plot. Large chemical polarizations (demonstrated by deviations from the ΔE_{conc} line) were obtained in spite of relatively low rotational speeds (up to 56.6 cm/sec). Values of $\Delta E_{conc} = -59.1$ mv and $\Delta E_{chem} = -47.9$ mv (hence $\Delta E_T = -107$ mv) indicated in Fig. 12 (cathodic case) are for an applied C.D. of 12.1 ma/cm² and a peripheral speed of 24.6 cm/sec. It is interesting to compare these with a freshly prepared solution (number 9) at about the same C.D.

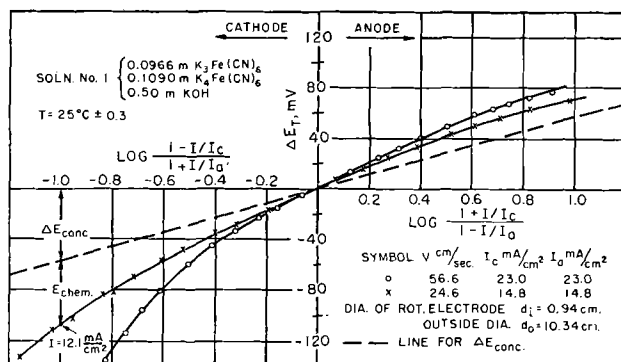


FIG. 12. Total polarization ΔE_T vs. $\log Q$ in case of "inactive electrodes" and presence of air-oxygen.

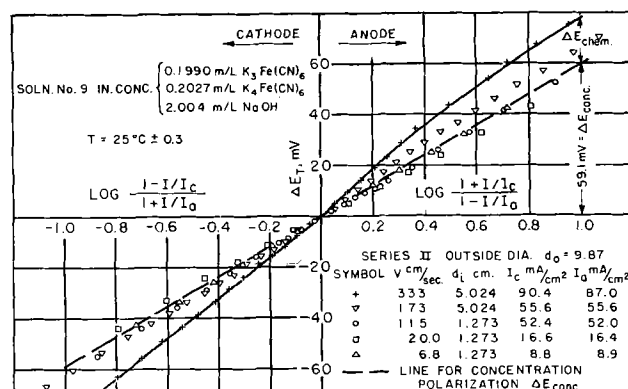


FIG. 13. Total polarization ΔE_T vs. $\log Q$ for high current density electrolysis.

and rotational speed.¹⁶ Thus at a $I = 12 \text{ ma/cm}^2$ and $V = 20 \text{ cm/sec}$, a total cathodic polarization (ΔE_T) of only -43.5 mv was measured for solution number 9.¹⁷ The corresponding concentration polarization was calculated to be -47.1 mv .¹⁸ Hence no measurable chemical polarization was determined in this case, while at the same C.D. in the case of the poisoned electrode, ΔE_{chem} represented about 45% of total electrode polarization.

With regard to the ferro-ferrocyanide couple the following conclusions may be drawn on the basis of the present study.

(A) Only freshly prepared and deaerated alkaline potassium ferri- and ferrocyanide solutions should be used with a maximum possible exclusion of light. The electrode (platinum or nickel) should be given a cathodic hydrogen treatment prior to each experiment.

(B) With the above precaution a reasonably small ΔE_{chem} is associated with the electrolytic redox reaction. The amount of ΔE_{chem} involved depends on the magnitude of the I_a/i_o ratio, i.e., on the rate of stirring (on which I_a depends). For rotating electrodes up to a peripheral velocity of 115 cm/sec , the electrode reaction is predominantly mass transfer controlled and the chemical polarization is negligibly small. The above peripheral velocity corresponds to a Reynolds number of 11,000. It should be reasonable to assume that in many other types of flow up to $R_d = 11,000$ a negligible ΔE_{chem} may be expected for the ferri-ferrocyanide couple.

(C) Under conditions (see above) at which the total electrode polarization is almost entirely represented by concentration polarization, the general mass transfer correlation for rotating cylinders (equation VII) can be used to predict δ , I_c , or I_a , and ΔE_{conc} (see equations X, XI, and IV). Conversely, from a given measured polarization, c_i of the reacting ion may be calculated at an applied current density.

To illustrate the latter point, calculations of δ , I_c , I_a , and ΔE_{conc} have been carried out below for a rotating electrode in an alkaline potassium ferro-ferrocyanide solution. To facilitate comparison with

¹⁶ The difference in concentrations of the reacting ions between solutions number 1 and 9 (a factor of 2) does not significantly affect this comparison, primarily because the ratio I_a/i_o is independent of the bulk concentration of the reacting ion.

¹⁷ See footnote (15).

¹⁸ Actually the absolute value of ΔE_T cannot be smaller than that of ΔE_{conc} . Whenever this seems to be the case, it must be attributed not only to experimental inaccuracies, but also to the possibility that achievement of a steady state polarization of the electrode was not quite complete. Fortunately in no case were these deviations very serious.

experimental measurements the physical data for one of the systems studied were used.

Illustrative example. Assumed solution: (Equivalent to solution No. 9) $0.1976M \text{ K}_3\text{Fe}(\text{CN})_6$, $0.2027M \text{ K}_4\text{Fe}(\text{CN})_6$, $2.004M \text{ NaOH}$.

Data: $d_i = 1.273 \text{ cm}$; $S = 300 \text{ rpm}$; $V = \frac{S}{60} \pi d_i = \frac{300}{60} \times 3.1416 \times 1.273 = 20.0 \text{ cm/sec}$; $R_d = 1,789$; temperature, 25°C ; $\nu = 1.423 \times 10^{-2} \text{ cm}^2/\text{sec}$; $D_{\text{ferri}} = 0.454 \times 10^{-5} \text{ cm}^2/\text{sec}$; $D_{\text{ferro}} = 0.390 \times 10^{-5} \text{ cm}^2/\text{sec}$; $c_{\text{ferri}} = 0.1976 \times 10^{-3} \text{ moles/cc}$; $c_{\text{ferro}} = 0.2027 \times 10^{-3} \text{ moles/cc}$.

Diffusion Layer Thickness, δ : From equation (XI):

$$\delta_{(\text{cm})} = 12.64 d_i^{0.30} V^{-0.70} \nu^{0.344} D^{0.356}$$

Hence for the cathodic case:

$$\begin{aligned} \delta_{\text{ferri}} &= 12.64 (1.273)^{0.30} (20.0)^{-0.70} \\ &\quad (1.423 \times 10^{-2})^{0.344} (0.454 \times 10^{-5})^{0.356} \\ &= 4.840 \times 10^{-3} \text{ cm} \\ \delta_{\text{ferro}} &= 12.64 (1.273)^{0.30} (20.0)^{-0.70} \\ &\quad (1.423 \times 10^{-2})^{0.344} (0.390 \times 10^{-5})^{0.356} \\ &= 4.585 \times 10^{-3} \text{ cm} \end{aligned}$$

Limiting Current Densities: Cathodic limiting C.D.,

$$\begin{aligned} I_c &= \frac{nFD}{\delta} c_{\text{ferri}} \\ &= \frac{1 \times 96,500 \times (0.453 \times 10^{-5})}{4.840 \times 10^{-3}} \times (0.1976 \times 10^{-3}) \\ &= 17.89 \times 10^{-3} \text{ amp/cm}^2 = 17.89 \text{ ma/cm}^2 \end{aligned}$$

as compared to experimentally determined

$$I_c = 16.6 \text{ ma/cm}^2$$

$$\text{Deviation} = 7.6\%$$

Anodic limiting C.D.,

$$\begin{aligned} I_a &= \frac{nFD}{\delta_{\text{ferro}}} c_{\text{ferro}} \\ &= \frac{1 \times 96,500 \times (0.390 \times 10^{-5})}{4.585 \times 10^{-3}} \times (0.2027 \times 10^{-3}) \\ &= 16.64 \times 10^{-3} \text{ amp/cm}^2 = 16.64 \text{ ma/cm}^2 \end{aligned}$$

as compared to experimentally determined

$$I_a = 16.4 \text{ ma/cm}^2$$

$$\text{Deviation} = 1.5\%$$

Concentration Polarization at Applied C.D. of 10 ma/cm^2 :

$$\begin{aligned} \text{Cathodic } \Delta E_{\text{conc}} &= 59.1 \log \frac{1 - I/I_c}{1 + I/I_a} \\ &= 59.1 \log \frac{1 - 10/17.89}{1 + 10/16.64} \\ &= -33.1 \text{ mv} \end{aligned}$$

as compared to the experimentally measured total cathodic polarization

$$\Delta E_T = -33.0 \text{ mv}$$

$$\begin{aligned} \text{Anodic } \Delta E_{\text{conc}} &= 59.1 \log \frac{1 + I/I_c}{1 - I/I_a} \\ &= 59.1 \log \frac{1 + 10/17.89}{1 - 10/16.64} \\ &= +34.9 \text{ mv} \end{aligned}$$

as compared to the experimentally measured total anodic polarization

$$\Delta E_T = 32.8 \text{ mv}$$

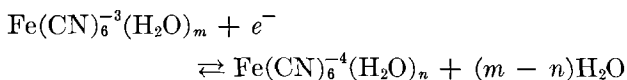
Hence chemical polarization is negligible for these cathodic and anodic runs, and prediction of ΔE_T is possible. It should be noted that the general mass transfer correlation enables prediction of limiting currents and concentration polarization even when chemical polarization is large; however, then the total electrode polarization could not be calculated.

The ferro-ferricyanide couple can thus be used conveniently to study mass transfer in liquids for various types of geometries and hydrodynamic conditions. The advantages of using an electrolytic redox reaction over solid dissolution for purposes of studying rates of mass transfer are: (a) achievement of steady state in a relatively short time; (b) direct control of rates, i.e., applied current (This is not possible in case of solids.); (c) preservation of smooth interfacial surface throughout the experiment; (d) higher accuracy and convenience in determination of rates of mass transfer.

The present study has proved that, when properly carried out, the ferro-ferricyanide electrode reactions may be considered to remain predominantly under mass transfer control up to stirring rates corresponding to $R_d = 11,000$. However, chemical polarization is essentially present whenever finite currents are passed, and becomes significant at high stirring rates. The reason Essin and coworkers (30) could claim that electrolytic reactions of the ferri-ferrocyanide couple involve only concentration polarization is that their experiments were carried out at low stirring rates.

Under proper experimental conditions, when concentration polarization is accounted for, the ferri-ferrocyanide couple is not far from thermodynamic equilibrium, i.e., ΔF^* is not very large. For the electrochemical reaction which takes place at the electrode interface itself, Lewartowicz (43) discussed two rate-determining steps. One step involves electron transfer at the interface of the electrode, the other the change in hydration of the ion under-

going recharge. For the ferri-ferrocyanide couple this may be expressed as:



Numerous investigators (46-48) have found that an ion is more hydrated the larger its charge and the smaller its radius. Hence, activation energy of the total process is composed of energy necessary for electron passage between ion and electrode and of hydration energy. The latter depends only on the state of hydration of oxidized and reduced ions, but the former is probably the one which is affected by presence of electrolytic poisons adsorbed at the electrode surface. Lewartowicz's experiments (43) on $\text{Fe}^{+3}/\text{Fe}^{+2}$, $\text{Ce}^{+4}/\text{Ce}^{+3}$ and quinone/hydroquinone couples have shown a small chemical polarization to be involved in each case. His results support in a general sense the above discussed mechanism of the electrolytic redox reaction.

It seems reasonable that electrode reactions involving only electron transfer and change in degree of ion hydration would involve small activation energies, compared to reactions involving breaking or formation of chemical bonds.

ACKNOWLEDGMENT

The authors wish to acknowledge the support of the Office of Naval Research. Appreciation is due to Mr. Lawrence Wolf and Mr. James Worley for assistance with experimental measurements.

Any discussion of this paper will appear in a Discussion Section to be published in the December 1954 issue of the JOURNAL.

REFERENCES

1. M. EISENBERG, "Studies on the Role of Ionic Diffusion and Mass Transfer in Electrode Processes," M.S. Thesis, University of California, Berkeley (1951).
2. C. W. TOBIAS, M. EISENBERG, AND C. R. WILKE, *This Journal*, **99**, 359C (1952).
3. C. WAGNER, *ibid.*, **95**, 161 (1949).
4. C. R. WILKE, M. EISENBERG, AND C. W. TOBIAS, *ibid.*, **100**, 513 (1953).
5. B. LEVICH, *Acta Physicochim. U.R.S.S.*, **17**, 257 (1942).
6. J. N. AGAR, *Disc. Faraday Soc.*, **1**, 26 (1947).
7. C. S. LIN, E. B. DENTON, N. S. GASKILL, AND G. L. PUTNAM, *Ind. Eng. Chem.*, **45**, 2136 (1951).
8. C. S. LIN, R. W. MOULTON, AND G. L. PUTNAM, *Ind. Eng. Chem.*, **45**, 636 (1953).
9. G. I. TAYLOR, *Phil. Trans. Roy. Soc. London*, **223**, 289 (1923); *Proc. Roy. Soc. London*, **A151**, 494 (1935).
10. SHIH-I PAI, NACA Tech. Note 892 (1943).
11. T. THEODORSEN AND A. REGIER, NACA Report 793 (1945).
12. I. M. KOLTHOFF AND J. J. LINGANE, "Polarography," 2nd ed., Interscience Publishing Co., New York (1952).
13. T. TSUKAMOTO, T. KAMBARA, AND I. TACHI, *J. Electrochem. Assoc. Japan*, **18**, 386 (1950).

14. E. BRUNNER, *Z. physik. Chem.*, **47**, 56 (1904).
15. W. NERNST AND E. S. MERRIAM, *Z. physik. Chem.*, **53**, 235 (1905).
16. A. EUCKEN, *Z. Elektrochem.*, **38**, 341 (1932).
17. T. KAMBARA AND T. TSUKAMOTO, *J. Electrochem. Assoc. Japan*, **18**, 356 (1950).
18. B. ROALD AND W. BECK, *This Journal*, **98**, 277 (1951).
19. H. SALZBERG AND C. V. KING, *ibid.*, **97**, 290 (1950).
20. C. V. KING AND F. S. LANG, *ibid.*, **99**, 295 (1952).
21. C. V. KING AND N. MAYER, *ibid.*, **100**, 473 (1953).
22. R. GLICKSMAN, H. MOUQUIN, AND C. V. KING, *ibid.*, **100**, 580 (1953).
23. C. V. KING AND M. SHACK, *J. Am. Chem. Soc.*, **57**, 1212 (1935).
24. C. V. KING AND W. H. CATHCART, *ibid.*, **59**, 63 (1937).
25. C. V. KING AND P. L. HOWARD, *Ind. Eng. Chem.*, **29**, 75 (1937).
26. C. FREDENHAGEN, *Z. anorg. Chem.*, **29**, 396 (1902).
27. G. JUST, *Z. physik. Chem.*, **63**, 513 (1908).
28. G. GRUBE, *Z. Elektrochem.*, **18**, 189 (1912); **20**, 334 (1914).
29. W. L. H. MOLL, *Z. physik. Chem.*, **A175**, 353 (1936).
30. O. ESSIN, S. DERENDIAYER, AND N. LADYGIN, *J. Appl. Chem. (U. R. S. S.)*, **13**, 971 (1940).
31. W. R. CARMODY AND J. J. ROHAN, *Trans. Electrochem. Soc.*, **83**, 241 (1943).
32. J. V. PETROCELLI AND A. A. PAOLUCCI, *This Journal*, **98**, 291 (1951).
33. J. MATUSCHEK, *Chem. Ztg.*, **25**, 601 (1901).
34. S. IIMORI, *Z. anorg. u. allgem. Chem.*, **167**, 145 (1927).
35. I. M. KOLTHOFF AND E. A. PEARSON, *Ind. Eng. Chem., Anal. Ed.*, **3**, 381 (1931).
36. I. M. KOLTHOFF AND N. H. FURMAN, "Volumetric Analysis," Vol. II, p. 427, J. Wiley and Sons, New York (1929).
37. F. SUTTON, "Volumetric Analysis," 12th ed., p. 235, Blakiston and Co., Philadelphia (1935).
38. J. S. ANDERSON AND K. SADDINGTON, *J. Chem. Soc.*, **1949**, S381.
39. M. EISENBERG, C. W. TOBIAS, AND C. R. WILKE, Technical Report No. 2, Nonr 222 (06). To be published in *Chem. Eng. Progr.* in 1954.
40. J. V. PETROCELLI, *This Journal*, **98**, 187 (1951).
41. T. H. CHILTON AND A. P. COLBURN, *Ind. Eng. Chem.*, **26**, 1183 (1934).
42. H. GERISCHER, *Z. Elektrochem.*, **54**, 362 (1950); **55**, 98 (1951).
43. E. LEWARTOWICZ, *J. chim. phys.*, **49**, 557, 564, 573 (1952).
44. H. EYRING, S. GLASSTONE, AND K. J. LAIDLER, *J. Chem. Phys.*, **7**, 1053 (1939).
45. M. LE BLANC, *Abhandl. Bunsen Ges.*, No. 3 (1910).
46. H. BRINTZINGER AND CH. RATANARAT, *Z. anorg. u. allgem. Chem.*, **222**, 113 (1935).
47. H. SACHSSE, *Z. Elektrochem.*, **40**, 531 (1934).
48. G. SUTRA, *J. chim. phys.*, **43**, 189 (1946).

NOMENCLATURE

Symbol	Definition	Units
c_o	Concentration of reacting ions in the bulk of the solution	mole/cc
c_i	Concentration of reacting ions at the electrode interface	mole/cc
c_{ferri}	Bulk concentration of ferricyanide ions	mole/cc
c_{ferro}	Bulk concentration of ferrocyanide ions	mole/cc
d_i	Diameter of the inner rotating electrode	cm
D	Diffusion coefficient of species k	cm ² /sec
ΔE_T	Total polarization	mv
ΔE_{conc}	Concentration polarization	mv
ΔE_{chem}	Chemical polarization	mv
f	Friction factor	dimensionless
F	Faraday equivalent	96,500 coulomb/equiv
ΔF^*	Standard free energy change of activation	ergs/mole
h	Planck constant	6.624×10^{-27} erg-sec/molecule
h'	Height of cell	cm
i	Total current	amp
i_o	Exchange current density	amp/cm ²
I	Current density	ma/cm ²
I_a	Anodic limiting current density	ma/cm ²
I_c	Cathodic limiting current density	ma/cm ²
I_L	Limiting current density, generally	amp/cm ²
j_D'	Modified Chilton-Colburn j-number	dimensionless
k	Boltzmann constant, 1.3805×10^{-6}	erg/°K molecule
k_a	Mass transfer coefficient at the anode	cm/sec
k_c	Mass transfer coefficient at the cathode	cm/sec
k_L	Mass transfer coefficient, generally	cm/sec
n	Number of electrons exchanged in electrode reaction	

NOMENCLATURE—Continued

Symbol	Definition	Units
N	Rate of mass transfer	mole/cm ² -sec
r_i	Radius of rotated inner electrode	cm
r_o	Internal radius of outer electrode	cm
$R_{(1)}, R_{(2)}$	Resistance	ohms
R	Universal gas constant	8.313×10^7 erg/°K-mole
t_i	Transference number of the reacting ion	
T	Temperature	°K
V	Peripheral velocity at the rotating cylinder	cm/sec
ZCP	Zero current potential (static potential difference between an investigated electrode and the reference cell)	mv

Greek symbols

α, β	Fractions of electrical potential difference across the activation energy barrier acting in the cathodic and anodic direction respectively	
δ	Thickness of diffusion layer	cm
κ	Electrical conductivity of a solution	ohm ⁻¹ cm ⁻¹
μ	Dynamic viscosity	g/cm-sec
ν	Kinematic viscosity	cm ² /sec
ρ	Density	g/cm ³

Dimensionless groups

$Q = \frac{1 \mp I/I_c}{1 \pm I/I_a}$	Ratio used in ΔE_{conc} calculations (upper sign for cathodic case, lower for anodic)	
$Re_d = \frac{Vd_i}{\nu}$	Reynolds number based on diameter of rotating inner cylinder	
$Sc = \frac{\nu}{D_k}$	Schmidt number for mass transfer of species k	

Electrochemical Polarization of Titanium in Aqueous Solutions of Sodium Chloride¹

NORMAN HACKERMAN AND COLBY D. HALL, JR.²

Department of Chemistry, The University of Texas, Austin, Texas

ABSTRACT

Cathodic and anodic polarization curves for titanium in neutral NaCl solutions were determined over the range $0.02 \mu\text{a}/\text{cm}^2$ to $0.01 \text{ amp}/\text{cm}^2$. These were derived from steady-state values of time-potential curves measured by the direct method using a thermionic amplifier to limit current in the potential measuring circuit to 10^{-12} amp.

On open circuit the potential increased from -0.25 volt (saturated calomel scale) to about $+0.2$ volt. As little as $0.1 \mu\text{a}/\text{cm}^2$ cathodic considerably decreased rate and extent of change, while anodic treatment of the same intensity increased these effects. At $1 \text{ ma}/\text{cm}^2$ hydrogen overvoltage was 0.84 volt and oxygen overvoltage was 0.96 volt. Tafel slopes were 0.15 and 0.14 , respectively. In aerated solution the effect of salt concentration between 0.5 and $2M$ was almost wholly that caused by change in oxygen solubility.

The anodic time-potential curves can be divided into three parts: (a) E increases linearly with time at a rate proportional to current density; (b) E is constant with time, and oxygen is evolved continuously; (c) E increases rapidly to about $+10$ volts after some hours for current densities in excess of $1 \text{ ma}/\text{cm}^2$; a visible surface film forms and a few deep pits appear, but there is no oxygen evolution. Results are considered on the basis of oxide formation and of chemisorbed oxygen atoms.

INTRODUCTION

Titanium is being studied here as part of a general investigation into characteristics of passive metals. This metal does not fit fully either the category typified by aluminum or by chromium. A careful study of its properties as a working electrode was indicated and resulted in the work reported here as well as in an analysis of the anodic charging process (1).

Although considerable work has been done on polarization of some of the newly available uncommon metals, much of it appears in reports and relatively little in the open literature.³

EXPERIMENTAL METHOD

Polarization measurements were made by the direct method. Apparatus used provided for concurrent measurements in six polarization cells, which were contained in a thermostat bath held at 30°C .

Polarization cells.—Each cell consisted of an open-top glass jar 16×21 cm, 32 cm deep, containing 5.0 liters NaCl solution, and an electrode assembly consisting of the metal, an input electrode, and a saturated calomel electrode. The 2.52 cm diameter titanium

coupon was cast in a plastic wafer, polished by hand on 2 to $2/0$ metallographic emery paper, rubber with filter paper moistened with 95% ethyl alcohol, and wiped carefully with clean, dry lens tissue. The wafer was inserted into a machined plastic holder provided with an electrical connection to the back of the coupon. The holder was sealed water-tight by application of melted ceresin wax. The platinum auxiliary electrode, consisting of 6 turns of platinum wire around a 6 -mm glass tube, was located 7 cm in front of the center of the face of the coupon. The calomel half-cell vessel was a 2 -cm glass tube with a bent side arm drawn out to a capillary tip and filled with 2% agar-saturated KCl gel. The three electrodes were mounted on a plastic support. The calomel electrode vessel could be rotated to vary the distance of the capillary tip from the face of the coupon. The electrode support was itself supported by a brass rod passing through a bracket which was clamped to the horizontal beam of a modified circular path apparatus (2). This rotated electrode assemblies in a circle 2.54 cm in diameter, in the plane of the coupon face at 26.5 rpm, and gave the coupons a linear velocity of 3.5 cm/sec.

Electrical circuits.—Six polarization cells were connected in parallel to a 4 - 12 -volt battery source for cathodic measurements, or 4 - 50 volts for anodic measurements. Current for each cell was controlled by a series resistance made up of combinations of $1/2$ -watt composition type resistors, some being provided with shorting switches, and one or two variable

¹ Manuscript received March 20, 1953. This paper was prepared for delivery before the Philadelphia Meeting, May 4 to 8, 1952.

² Present address: Dowell, Incorporated, Tulsa, Oklahoma.

³ For example, in a series of progress reports to the U. S. Atomic Energy Commission by D. S. McKinney and J. C. Warner of Carnegie Institute of Technology.

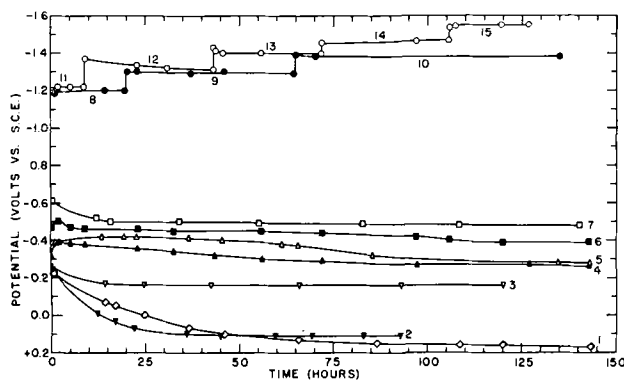


FIG. 1. Time-potential curves for cathodic polarization of titanium in aerated 0.5M NaCl at 30°C. Curve-current density in amp/cm²: 1—0.0; 2— 2×10^{-8} ; 3— 6×10^{-8} ; 4— 1×10^{-6} ; 5— 2×10^{-6} ; 6— 4×10^{-6} ; 7— 4×10^{-5} ; 8— 2×10^{-4} ; 9— 4×10^{-4} ; 10— 1×10^{-3} ; 11— 2×10^{-3} ; 12— 6×10^{-4} ; 13— 2×10^{-3} ; 14— 4×10^{-3} ; 15— 1×10^{-2} .

2-watt resistors. Current was read by measuring IR drop across a calibrated wire-wound resistor in series with the cell, and was held constant within less than 1% of the nominal value.

Potential of the titanium coupon with respect to the saturated calomel electrode was measured by an L & N thermionic amplifier and Type K-2 potentiometer. The former limited current drawn in the potential-measuring circuit to 10^{-12} amp or less, even when the potentiometer was not balanced, and thus prevented disturbance of the measured polarizing current during measurements at very low current densities. For measuring potentials in excess of the maximum range of the potentiometer, dry cells, calibrated to ± 1 mv, were connected in series with the potentiometer. All potentials are given on the saturated calomel electrode scale.

Materials.—Coupons were cut from Remington titanium sheet, 1.6 mm thick. Spectrographic analysis⁴ showed over 99% titanium, with 0.725% carbon, 0.25% iron, and 0.005% other elements.

Surface areas were determined by krypton adsorption at 78°K, and from this the coupons as prepared were found to have a roughness factor of 2.2 ± 0.2 .⁵ All current densities are given in terms of apparent or projected area.

Solutions were made with analytical reagent grade NaCl and distilled water. They were unbuffered, and had a pH of 6–7. The NaCl contained 3 ppm iron, which was essentially completely precipitated during a run, giving about 1 mg of $\text{Fe}(\text{OH})_3$ in 5 liters 0.5M solution. The colloidal precipitate trav-

⁴ National Spectrographic Laboratories, Inc., Cleveland, Ohio.

⁵ Surface areas were also determined by polarization capacity measurements (3) and led to a roughness factor of 10 ± 3 . The gas adsorption area is considered to be more reliable at present.

elled by electrophoresis to the anode, and therefore caused no interference on a cathodically polarized coupon. Solutions used in anodic runs were made iron-free by dissolving NaCl in the minimum volume of water, aerating for 12 hr, filtering through fritted glass, and diluting to desired concentration.

All anodic polarization measurements and most cathodic measurements were made in solutions which were kept saturated with air by means of a fritted glass gas dispenser. A glass chimney prevented air bubbles from coming in direct contact with the electrodes. Some measurements of cathodic polarization were made in solutions designated as "air-free." For these runs, one of the jars was fitted with a flexible plastic film cover, sealed on with masking tape. The solution was boiled, cooled under nitrogen, and forced into the polarization cell by nitrogen pressure. During the run, purified nitrogen (4) was bubbled through the solution. A porous alundum cup around the platinum anode prevented oxygen from getting into the main part of the solution around the cathodic coupon. A more rigorous exclusion of oxygen was not required in these measurements for reasons stated in the Discussion.

Correction for IR drop in the solution.—In order to prevent errors due to blocking of part of the coupon surface by the tip of the reference electrode, the capillary tip was kept 2.0 cm from the face of the coupon. The potential at that point differs from that at the coupon surface only by the IR drop for the polarizing current passing through the 2 cm of solution. This IR drop was negligible except at high current densities, for which corrections were made. Potentials were measured in 0.5M NaCl at several distances from 2.0 cm to the surface, the latter measurement being taken immediately after touching the electrode tip to the surface. These points were found to lie on a smooth curve. The effective value of R was found by dividing the potential difference from 2.0 cm to the surface by the polarizing current. This was used in calculating the correction for other current densities in 0.5M NaCl, and corresponding values of R for 0.1M and 2.0M NaCl were calculated from ratios of specific resistances of solutions.

Cathodic Polarizations

Typical time-potential curves at several current densities for cathodically polarized titanium are shown in Fig. 1. Points marked with the same symbol represent measurements on the same coupon in a continuous run. In describing the curves a potential becoming more positive, i.e., moving down, is said to be increasing.

On open circuit and up to $0.06 \mu\text{a}/\text{cm}^2$ the initial potential is -0.25 volt and increases slowly to a constant value after a day or more (6 days at zero

current). Generally, at low cathodic current densities, the initial increase in potential is more rapid the lower the current density.

The most noticeable characteristic in the range 1–4 $\mu\text{a}/\text{cm}^2$ is the long time needed for constant potential—more than 6 days. Initial potentials are more negative the higher the current density, and decrease during the first few hours. Between 10 and 60 $\mu\text{a}/\text{cm}^2$, after a comparatively rapid increase for several hours, a slow increase takes place for as long as 10 days.

In the range 0.1 to 0.16 ma/cm^2 potentials do not become sufficiently steady to plot, varying from average values at first by as much as ± 0.1 volt in less than a minute and, at the end, by ± 0.03 volt. Average initial and final values (48 hr) were as follows:

ma/cm^2	volt	volt
0.1	-0.6	-0.6
0.12	-0.5	-1.10
0.14	-0.65	-1.15
0.16	-1.06	-1.17

Curves 8, 9, and 10 were obtained in a single run on the same coupon, as were curves 11–15. The length of time for which the current was held at each value was arbitrary, being at least long enough for the potential to become constant. At these high current densities, the potential does not change greatly from its initial value and becomes constant in a short time. When current is increased to a new constant value, the potential immediately decreases to a more negative value. Usually it then increases slightly but becomes essentially constant in a few hours.

At 0.2 ma/cm^2 the rapid variation of potential has an amplitude of ± 0.02 volt. The amplitude of the swings decreases, at higher current densities, to about ± 0.001 volt at 10 ma/cm^2 .

Time-potential curves for 0.1 and 2.0M NaCl show the same general features as those of Fig. 1. At about the same current densities, curves for the three concentrations show no greater dissimilarities than do curves of duplicate runs at the same concentration.

Effect of NaCl concentration.—Cathodic polarization curves for titanium in aerated 0.1, 0.5, and 2.0M NaCl solutions are shown in Fig. 2. Each solid point represents the constant potential finally attained by a coupon held at the same current density from the start of the run. Each open point represents a constant potential attained by a coupon at the designated current density after previous polarization at one or more other current densities.

The polarization curve for 0.5M NaCl was established with especial care. Enough points were

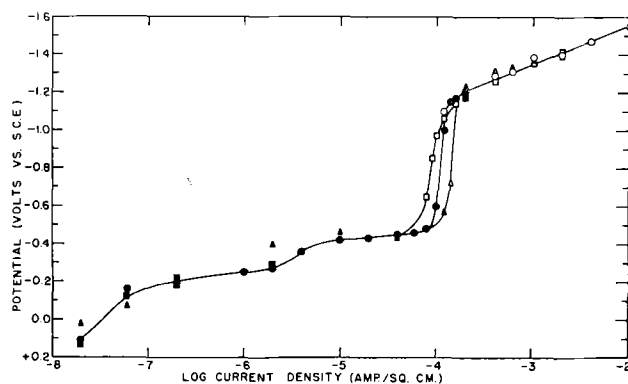


FIG. 2. Cathodic polarization curves for titanium in aerated NaCl solutions at 30°C. (Solid points give potential at original current density and open points at altered current density.) \blacktriangle \triangle —0.1 M; \bullet \circ —0.5M; \blacksquare \square —2.0M.

determined to establish that curves for the three concentrations were essentially the same. They are drawn as identical except near 0.1 ma/cm^2 . The open circuit potentials cannot be shown in Fig. 2 because the current density scale is logarithmic. These potentials for 0.1, 0.5, and 2.0M solutions are +0.18, +0.17, and +0.2 volt, respectively.

At the three lowest current densities, the curve is drawn through weighted average values of the potentials for the three different concentrations. Deviations of individual points average less than 0.03 volt. From 1–40 $\mu\text{a}/\text{cm}^2$ the curve is drawn through the points for 0.5M solution. Reality of the wave drawn in the curve in this region is considered later.

Near 0.1 ma/cm^2 a rapid decrease in potential occurs, but at a lower current density for more concentrated solutions. At higher current densities, the logarithmic polarization curve is linear. The slope, corresponding to the constant b in the Tafel equation, is 0.204 volt/log unit.

Most points above 80 $\mu\text{a}/\text{cm}^2$ were measured on a coupon which was polarized successively to several different current densities. One coupon was polarized in 0.1M NaCl for 157 hr at 0.12 ma/cm^2 , for 28 hr at 0.14 ma/cm^2 , and then for about 20 min each at decreasing current densities from 2–0.4 ma/cm^2 . A coupon in 2.0M solution was started at 0.2 ma/cm^2 which was increased successively through the other values to the maximum, 2 ma/cm^2 . It was returned to the initial current, where it then had the same potential as before. The remaining points were determined at decreasing current densities. For 0.5M solution, points from 0.2 ma/cm^2 upward were determined in two runs. It may be noted that points at 0.4 and 1 ma/cm^2 , which are from the same run, are slightly off the straight line, but would lie on a line parallel to it. The remaining points, all from the other run, fall very closely on the line.

At 0.2 ma/cm^2 , hydrogen is evolved slowly on ti-

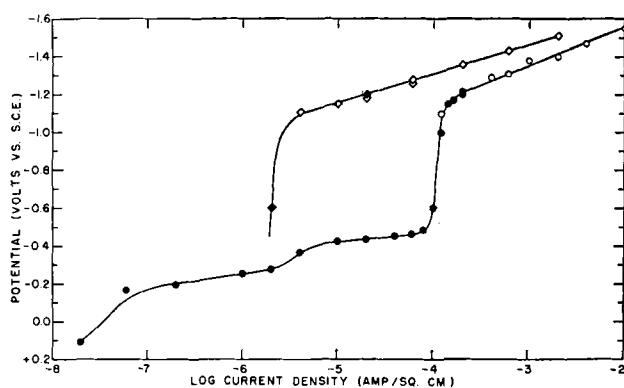


FIG. 3. Cathodic polarization curves for titanium in 0.5M NaCl at 30°C. (Solid points give potential at original current density and open points at altered current density.)
 ◆ ◇—air-free solution; ● ○—aerated solution.

tanium. Visible bubbles do not form on the surface, but large bubbles gather on the wax coating around the edge of the coupon. At higher current densities small bubbles are evolved continuously from the entire coupon surface. After long polarization at high current density, the titanium surface becomes darkened and very hard.

Effect of oxygen concentration.—Cathodic polarization curves for titanium in aerated and in air-free 0.5M NaCl solutions are shown in Fig. 3. The curve for the aerated solution is that for 0.5M NaCl in Fig. 2. The other was determined in two separate runs, one from 2 to 60 $\mu\text{a}/\text{cm}^2$ and the other from 20 $\mu\text{a}/\text{cm}^2$ on up. Agreement of the overlap data is very good. The slope of the linear portion is 0.154 volt/log unit.

The experimental arrangement in the air-free runs prevented observation of hydrogen evolution, but coupons were darkened and surfaces hardened just as in corresponding aerated runs.

Anodic Polarization

All anodic polarization measurements were made in aerated 0.5M NaCl solution. Time-potential curves were measured at constant current densities from 0.02 $\mu\text{a}/\text{cm}^2$ to 6.0 ma/cm^2 . Corresponding charging curves have been given previously (1). The curves show that potential increases linearly with time, at a rate proportional to current density, until a constant potential is reached at which oxygen is evolved. The charge required to reach the oxygen evolution potential is approximately the same for all current densities from 0.06 to 20 $\mu\text{a}/\text{cm}^2$, the average being 0.0145 coulomb/ cm^2 . At current densities above 1 ma/cm^2 , after several hours at the oxygen evolution potential, a second increase of potential begins. Visible oxygen evolution ceases, and the potential rises at an increasing rate to about +10 volts, where it becomes erratic but generally constant, and a visible oxide film develops.

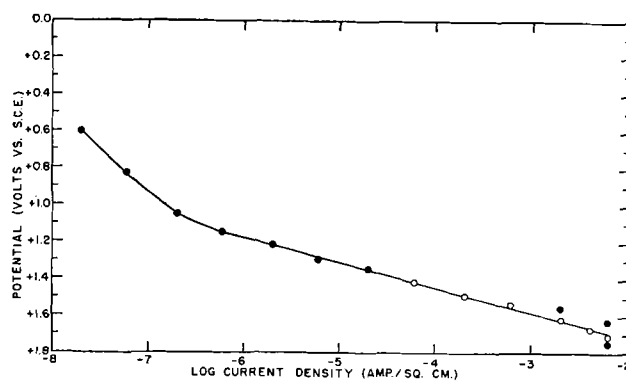


FIG. 4. Anodic polarization curve for titanium in aerated 0.5M NaCl at 30°C. (Solid points give first constant potential reached at original current density. Open points give constant potential at altered current density.)

The anodic polarization curve for titanium in aerated 0.5M NaCl solution is shown in Fig. 4. Each solid point represents the first constant potential reached by a coupon polarized at a constant current density. Each open point represents the constant potential attained by a coupon at the indicated current density after previous polarization to a constant potential at a lower current density. For the latter points, the time of polarization was not long enough for the second increase of potential to have begun when the reading was made.

All experimental points touch the straight line except for the solid points at the two highest current densities. Of these, the one at the less positive potential represents the coupon mounted in the recessed holder.

Below 0.6 $\mu\text{a}/\text{cm}^2$ the curve bends toward less positive potentials. Because of the logarithmic current density scale, the zero-current or open-circuit potential cannot be plotted. This value is +0.17 volt.

Polarization decay on open circuit and the charging process on repolarization are discussed elsewhere (1).

DISCUSSION

Cathodic polarization.—The usual cathodic reactions in aqueous solutions containing no other reducible material are reduction of dissolved O_2 to OH^- , possibly in steps involving H_2O_2 , and reduction of H^+ to H_2 . The former reaction occurs at a less negative potential, and therefore precedes hydrogen evolution as current density is increased. Results indicate that a titanium cathode in neutral NaCl solution follows this expected behavior at current densities above 0.1 $\mu\text{a}/\text{cm}^2$. Below this the effects are related to those produced by anodic polarization. In the current density range 0.1 to 100 $\mu\text{a}/\text{cm}^2$ the electrode reaction apparently is reduction of O_2 . The sharp break in the curves near 100 $\mu\text{a}/\text{cm}^2$ represents the limiting diffusion current (i.e., current density)

for oxygen under the particular conditions of the experiment. At higher current densities, and more negative potentials, hydrogen is evolved.

In order to establish that the diffusion wave represents the limiting diffusion current of oxygen, rather than that of some other substance, a portion of the polarization curve was measured in an air-free solution. For this purpose it was not necessary to use elaborate measures for rigid exclusion of oxygen. It was sufficient to reduce oxygen concentration of the solution considerably below that of an air-saturated solution. Curves in Fig. 3 show that the limiting diffusion current, I_d , was lowered from 100 $\mu\text{a}/\text{cm}^2$ in the aerated solution to 2 $\mu\text{a}/\text{cm}^2$ in the air-free solution.

The only apparent effect of variation of NaCl concentration is a small change in the limiting diffusion current of O_2 . Since the limiting diffusion current of a substance is proportional to its concentration, I_d for O_2 should be proportional to the solubility of oxygen from air in various concentrations of salt solutions. The following table gives concentrations of O_2 under conditions of the experiment, calculated from data for oxygen solubility (5):

NaCl conc	0.1	0.5	2.0M
O_2 conc	2.23	1.93	$1.18 \times 10^{-4}M$
I_d (obs)	1.3	1.0	0.8×10^{-4} amp/cm ²
I_d (calc)	1.15	1.00	0.61×10^{-4} amp/cm ²

The values of I_d (calc) are proportional to the O_2 solubilities, taking the value for 0.5M NaCl as the standard. Agreement for 0.1M and 2.0M solutions is fairly good, considering that points for these concentrations were determined by a somewhat different procedure from those for 0.5M solution.

From the ratio of diffusion currents in aerated and in air-free solutions, and the solubility of oxygen in 0.5M NaCl, the concentration of oxygen in air-free solutions was $4 \times 10^{-6}M$, corresponding to an oxygen partial pressure of 3 mm.

At current densities larger than the oxygen limiting diffusion current, the potential follows the Tafel equation for hydrogen overvoltage. In aerated solutions at all three concentrations of NaCl, the potential is given by the equation

$$E = -1.97 - 0.204 \log I, \quad (\text{I})$$

where I is current density in amp/cm². In the air-free solution, the equation is

$$E = -1.93 - 0.154 \log I. \quad (\text{II})$$

Since hydrogen overvoltage depends on current actually involved in hydrogen evolution rather than on total current, the relation of $I - I_d$ to E for aerated solutions would better represent the hydrogen

overvoltage. A plot (not shown) of E vs. $\log(I - I_d)$ is linear from 0.01–1 ma/cm² and lies parallel to the line for air-free solution, at potentials 0.11 volt more positive. With this correction, the slope for hydrogen overvoltage in aerated solution agrees with that in the air-free solution. The difference between this slope, 0.15, and the usual Tafel slope of 0.12 may be attributed to the presence of concentration polarization effects in the unbuffered NaCl solution.

Hickling and Salt (6) state that for current densities greater than ten times I_d the presence of dissolved oxygen has no effect on hydrogen overvoltage. In the present work, both the $\log I$ and the $\log(I - I_d)$ curves for aerated solutions, which coincide above 10 I_d , differ by about 0.1 volt from the curve for air-free solution. There is no apparent explanation for this lack of agreement. The air-free curve, however, probably is a good representation of hydrogen overvoltage on titanium. The reversible hydrogen potential here is -0.63 volt and the hydrogen overvoltage on titanium thus is given by

$$\omega = 1.30 + 0.154 \log I. \quad (\text{III})$$

At 1 ma/cm² the overvoltage is 0.84 volt, placing titanium with lead and mercury with respect to its very high overvoltage.

After prolonged rapid evolution of hydrogen on titanium, the surface of the metal was darkened and became very hard. Polishing by hand on No. 2 emery paper removed the tarnish and left a bright surface, which in some instances contained numerous very small pits. However, it was necessary to use a motor-driven metallographic polishing wheel and fresh emery paper in order to remove the hardened surface layer and expose unaltered metal. It appears that hydrogen evolution on titanium produces some sort of hydride, either a compound or a solid solution, to an appreciable depth. The solubility of hydrogen in titanium is high; according to Bornelius (7) it is higher than in palladium, and hydride formation is not unexpected.

At current densities below the oxygen limiting diffusion current, the cathode reaction is reduction of O_2 to OH^- . Under conditions of the experiment, the reversible potential of this reaction is $+0.60$ volt, so that the overvoltage for oxygen reduction is 0.85 volt at 1 $\mu\text{a}/\text{cm}^2$. If the polarization curve were drawn as a straight line from 0.1 to 100 $\mu\text{a}/\text{cm}^2$, the slope would be 0.11 volt/log unit. Thus, it may be that reduction of oxygen follows an overvoltage law similar to that for hydrogen or oxygen evolution, and with about the same value for the constant b in the Tafel equation.

The small wave shown in Fig. 3 near 4 $\mu\text{a}/\text{cm}^2$ seems to be real. Points shown represent the steady potentials reached after prolonged polarization. A

similar wave would be present at about the same current density if either the initial potentials or the most negative potentials attained at each current density were plotted. After coupons polarized at 1 and 4 $\mu\text{a}/\text{cm}^2$ reached their steady potentials (167 hr), both were changed to 2 $\mu\text{a}/\text{cm}^2$, and in 48 hr both reached potentials within 0.01 volt of the value obtained at the same current density in a previous run. Points at 10 and 40 $\mu\text{a}/\text{cm}^2$ are for 250 hr runs, and gave no indication of becoming appreciably more positive.

Time-potential curves of points on the wave are shown in Fig. 1, curves 4, 5, and 6. The increase of potential begins sooner, the lower the current density. If the wave represented the limiting diffusion current of some depolarizer being formed by electrolysis, the increase of potential would occur sooner at a higher current, since the concentration of this substance would increase more rapidly at the higher current. This eliminates both hydrogen peroxide and chlorine as possible depolarizers. Chlorine is also ruled out by the fact that the cathode potential at the wave is about -0.3 volt. For a limiting diffusion current of 4 $\mu\text{a}/\text{cm}^2$, the concentration of the depolarizer must be about $7 \times 10^{-6}M$. For this concentration of Cl_2 (or HClO) in $0.5M$ chloride, the reversible potential is $+0.9$ volt, and the chlorine electrode does not usually show large overvoltages. It is possible that the wave is in some way associated with a change from the two-electron reaction for reduction of O_2 to H_2O_2 to the four-electron reaction for reduction of O_2 to H_2O as the potential is made more negative. It is not clear in what manner this change of reaction would be expected to affect time-potential behavior.

The polarization curve in Fig. 2 is probably typical of the behavior of titanium in many other aerated salt solutions not containing reducible ions. Since electrode processes which control potential do not involve ions of the dissolved salt, the only effects of using a different salt or changing concentration should be those resulting from differences in $p\text{H}$ or oxygen solubility. The entire curve should be shifted to potentials 0.06 volt more negative for each increase of one $p\text{H}$ unit, and vice versa. This would not hold true, however, in strongly acidic solutions. Titanium is corroded in fairly concentrated acids, and its polarization behavior under such conditions would be expected to differ considerably from that in neutral solutions. The general form of cathodic curves for many other noncorroding metals in aerated salt solutions probably is similar to that for titanium. Curves would be shifted in potential by different overvoltages for reduction of oxygen or for evolution of hydrogen.

Anodic polarization.—Oxygen overvoltage follows the Tafel equation from 0.2 $\mu\text{a}/\text{cm}^2$ to 6 ma/cm^2 , the

highest current density measured. The potential, for solutions of $p\text{H} = 6.2$, is given by

$$E = 1.98 + 0.134 \log I, \quad (\text{IV})$$

where I is in amp/cm^2 of projected area. The reversible oxygen potential at $p\text{H} = 6.2$ is $+0.63$ volt, so that oxygen evolution overvoltage is given by

$$\omega = 1.35 + 0.134 \log I. \quad (\text{V})$$

The overvoltage is 0.95 volt at 1 ma/cm^2 , and 0.55 volt at 1 $\mu\text{a}/\text{cm}^2$. The Tafel slope of 0.134 is close to 0.12, which is the theoretical value for oxygen overvoltage as well as for hydrogen overvoltage.

Anodic polarization of metals has been studied largely with respect to oxygen overvoltage and mechanism of oxygen evolution. Adam (8) says that a complete film of oxygen is present on an electrode from which oxygen is being evolved. However, the form of oxygen on the metal surface is in question; it may be chemisorbed, or a metal oxide film may be formed. The situation is not necessarily the same for all metals.

A rather full analysis of this anodic process has already been given (1). The potential reached on open circuit ($+0.2$ v) is essentially the same as that found when the metal polarized to the oxygen evolution potential is permitted to decay on breaking the circuit. From the charging curves and the true area ($r.f. = 2.2$) it is found that the equivalent of three layers of oxygen atoms will have been deposited before oxygen evolution occurs. If the oxygen is not discharged but remains as either OH^- or O^- , this amounts to about 9 equivalent layers. The calculations assume hexagonal close packing and use 0.74 \AA as the covalent radius of oxygen or 1.4 \AA as the radius of either ion. The hydroxyl ion is highly polarizable and conceivably could pack so as to give fewer layers.

It is not likely that charged particles can be packed in so closely, so in the case of the oxide ion it would necessarily be assumed that a very thin metal oxide layer formed ($<50 \text{ \AA}$) before oxygen evolution started. However, it is then not clear why the open circuit potential after polarization should be about $+0.2$ volt since the Ti , TiO_2 potential under these conditions would be about -1.6 volts. However, it is not reasonable to postulate three layers of chemisorbed oxygen atoms.⁶

Hence, these data still do not permit an unequivocal choice between chemisorption or oxide formation as the first step prior to oxygen evolution (and incidentally, as the primary reason for the passivity of titanium). There is the possibility that the charge goes into forming a double layer involving a mono-

⁶ Chemisorbed because on repolarization only a minute fraction of the original charge is needed to bring the metal back to the oxygen evolution potential (1).

layer of any one of the three particles, with the excess leaking off continuously into the metal or into the solution. Clearly, experimental evidence of the form of the attached particle is needed in order to resolve the question.

ACKNOWLEDGMENT

The authors are pleased to take this opportunity to thank Mr. N. Komodromos of these laboratories for the gas adsorption area measurements.

Any discussion of this paper will appear in a Discussion Section to be published in the December 1954 issue of the JOURNAL.

REFERENCES


1. C. D. HALL, JR., AND N. HACKERMAN, *J. Phys. Chem.*, **57**, 262 (1953).
2. O. B. J. FRASER, D. E. ACKERMAN, AND J. W. SANDS, *Ind. Eng. Chem.*, **19**, 337 (1927).
3. C. WAGNER, *This Journal*, **97**, 71 (1950).
4. L. MEITES AND T. MEITES, *Anal. Chem.*, **20**, 984 (1948).
5. "The Corrosion Handbook," (H. H. Uhlig, Editor), p. 1147, John Wiley & Sons, Inc., New York (1948).
6. A. HICKLING AND F. W. SALT, *Trans. Faraday Soc.*, **37**, 319 (1941).
7. G. BORELIUS, *Metallwirtschaft*, **8**, 105 (1929).
8. N. K. ADAM, "The Physics and Chemistry of Surfaces," 3rd ed., p. 326, Oxford University Press, London (1941).

The Nature of the Zinc-Containing Ion in Strongly Alkaline Solutions¹

THEDFORD P. DIRKSE

Calvin College, Grand Rapids, Michigan

ABSTRACT

The nature of the zinc-containing ion in strongly alkaline solutions was determined by measuring electrode potentials of zinc in such solutions under equilibrium conditions. Galvanic cells were used in which junction potentials were practically eliminated. Results indicate that in the concentration range of approximately 1-7*M* potassium hydroxide all the zinc is in the form of a zincate ion, $\text{Zn}(\text{OH})_4^{--}$. The standard free energy of formation of this ion is -206.2 kcal. 

INTRODUCTION

The question as to whether zinc, when dissolved in strong alkalis, is present as a zincate ion, (ZnO_2^{--}) or as a hydrogen zincate ion (HZnO_2^-) has received a fair share of attention. An attempt to answer this question has been made by many investigators, and a variety of techniques have been used. Hildebrand and Bowers (1) studied weakly alkaline solutions using a potentiometric titration technique. They found justification for presence of the hydrogen zincate ion only. However, Britton (2), using the same technique, was unable to confirm the presence of either ion. Bodländer (3) measured electrical potentials of cells containing solutions of zinc in aqueous sodium hydroxide. He interpreted the behavior of the zinc electrode to indicate presence of the hydrogen zincate ion at all concentrations. Later Kunschert (4) used a similar method and concluded that zinc existed as the zincate ion in the more strongly alkaline solutions. Bodländer concurred in this interpretation and retracted his earlier conclusions.

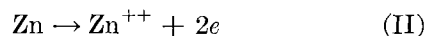
The work reported here was undertaken in an attempt to shed some light on this problem by means of a potentiometric study similar to that of Kunschert (4), but using cells in which junction potentials are negligible. The potential of the zinc electrode in alkaline solutions containing zinc will be dependent on activities of zinc-containing ions, hydroxyl ions, and water in the solution. The generalized equation for this reaction may be written as



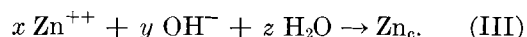
where Zn_c represents the complex ion formed. It is possible, however, that the water in this reaction is a product rather than a reactant. But, as is shown later, evidence favors the equation as given.

Manuscript received February 9, 1953.

This reaction may be considered as taking place in stages



followed by



At equilibrium, the potential of reaction (II) is

$$E_{\text{Zn}} = E_{\text{Zn-Zn}^{++}}^0 - (RT/nF) \ln (\text{Zn}^{++})/(\text{Zn}) \quad (\text{IV})$$

(The terms in parentheses refer to activities of the species indicated.) Assuming that activity of metallic zinc is unity, this becomes

$$E_{\text{Zn}} = E_{\text{Zn-Zn}^{++}}^0 - 0.0295 \log (\text{Zn}^{++}) \quad (\text{V})$$

at 25°C. The equilibrium constant for reaction (III) is

$$K = \frac{(\text{Zn}_c)}{(\text{Zn}^{++})^x (\text{OH}^-)^y (\text{H}_2\text{O})^z} \quad (\text{VI})$$

Solving for (Zn^{++}) and substituting in (V),

$$E_{\text{Zn}} = E_{\text{Zn-Zn}^{++}}^0 - (0.0295/x) \log (\text{Zn}_c) \\ + (0.0295/x) \log K + (0.0295y/x) \log (\text{OH}^-) \\ + (0.0295z/x) \log (\text{H}_2\text{O}) \quad (\text{VII})$$

The object now is to evaluate x and y . No attempt is made to evaluate z because it is doubtful whether degree of hydration can be expressed exactly.

If the activities of hydroxyl ions and water are held constant while the activity of the zinc complex ion is varied and the temperature is held at 25°C, equation (VII) assumes the form

$$E_{\text{Zn}} = K' - (0.0295/x) \log (\text{Zn}_c) \quad (\text{VIII})$$

where K' includes all the constant terms. This is an equation for a straight line having a slope of $-0.0295/x$, from which the value of x can be determined.

EXPERIMENTAL

From a stock solution of zinc oxide in aqueous potassium hydroxide, a given amount was pipetted into each of several volumetric flasks. Each sample was then diluted to the mark with a potassium hydroxide solution, a different concentration being used in each flask. This gave a series of solutions in which zinc molarity was the same but hydroxyl ion concentration varied. Several such series were prepared.

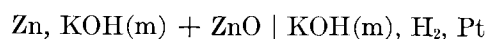
Analysis of these solutions for hydroxyl ion concentration was carried out as follows. A known excess of hydrochloric acid was added, and solutions were back-titrated with a standard sodium hydroxide solution. Alkalinity of solutions so determined includes both the free hydroxyl ion concentration and hydroxyl ion content of the zinc complex. The latter must be known to evaluate the former. Since the nature of the zinc complex was not known, several possibilities were considered, e.g., $\text{Zn}(\text{OH})_2$, $\text{Zn}(\text{OH})_3^-$, and $\text{Zn}(\text{OH})_4^{2-}$. The value for free hydroxyl ion concentration depends on which of these zinc complexes is assumed to be present. All three possibilities were considered, but these had only a slight effect on the evaluation of x , as shown below. The mean activity of the hydroxyl ion was determined by applying the data of Akerlof and Bender (5). The assumption is made that the presence of dissolved zinc does not appreciably affect the activity of free hydroxyl ions. All solutions were fairly concentrated with respect to potassium hydroxide so that the zinc complex ion contributed little to the total ionic strength.

A clean zinc electrode and the bridge of a reference electrode consisting of mercury, mercuric oxide, and a 20% potassium hydroxide solution were placed in each solution. The zinc potential was measured against this reference electrode at $25 \pm 0.2^\circ\text{C}$. A large scale plot was made of E_{Zn} vs. $\log (\text{OH}^-)$ for each series of solutions. Then a given value of $\log (\text{OH}^-)$ was chosen, and E_{Zn} in each series was read from the graph for this value of $\log (\text{OH}^-)$. This gave E_{Zn} with varying zinc concentration but constant hydroxyl ion activity. Activity coefficients of the zinc complex were assumed to be the same in all such selected solutions since the ionic strength of these solutions is almost wholly due to free potassium hydroxide. The activity of water was also assumed to be constant in such a case since it is related to hydroxyl ion activity (5). No correction was made for the junction potential between the reference electrode and the solution. This potential depends on hydroxyl ion activity in the solution, and since in plotting E_{Zn} vs. zinc ion concentration the hydroxyl ion activity was held constant, all values on such a plot would have been affected by the same amount,

and the slope would have remained unchanged. The varying amounts of zinc ion may have changed hydroxyl ion activity slightly, but for present purposes this effect is assumed to be negligible.

Several values of $\log (\text{OH}^-)$ were chosen and the results are shown on Fig. 1. Lines for the various series are approximately parallel, the average slope varying from -0.031 to -0.029 , depending on which species of zinc complex is assumed to be present in solution. This gives a value of 1 for x .

Determination of y proved to be more difficult. The method finally adopted was as follows. An H-type cell with a sintered glass disk in the cross piece was used. An aqueous solution of potassium hydroxide was placed in one compartment, and a hydrogen electrode was inserted in this solution. In the other compartment was placed a sample of the same potassium hydroxide solution to which some zinc oxide was added, and a clean zinc electrode was inserted. This cell was of the type



and $E_{\text{cell}} = E_{\text{Zn}} - E_{\text{H}_2}$, when both electrode reactions are written as oxidation processes. Since zinc oxide concentration was not large in any case, it was assumed that it did not significantly affect the mean hydroxyl ion activity, and thus did not bring about an appreciable junction potential. EMF values for this cell were measured at $25^\circ \pm 0.2^\circ\text{C}$. Hydrogen was purified in the usual way, and fresh electrodes were used for each run. Zinc electrodes appeared to behave reversibly since constant and reproducible values were obtained within a few minutes after the zinc electrode was inserted.

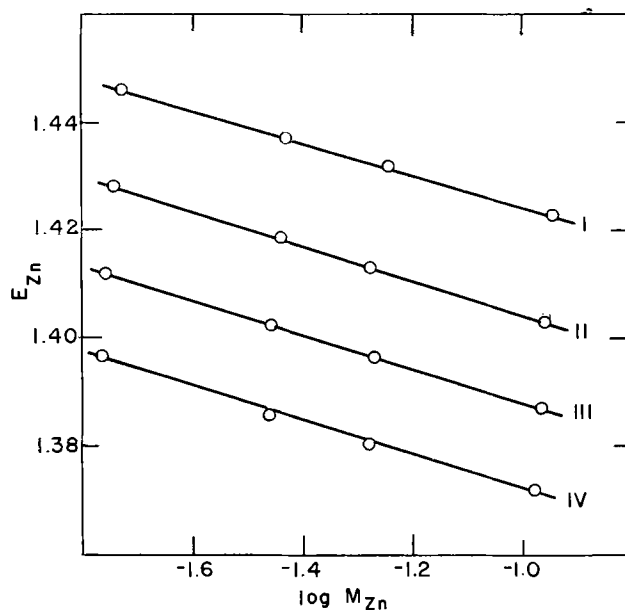


FIG. 1. Variation of E_{Zn} with $\log M_{\text{Zn}}$ at constant hydroxyl ion activity. $\log a_{\text{OH}^-}$ for curve I is 1.75; curve II, 1.40; curve III, 1.10; curve IV, 0.80.

EMF of the hydrogen electrode was calculated from the mean activity of hydroxyl ion using data of Akerlof and Bender (5); emf of the cell was measured, and E_{Zn} was calculated from these two values. Several different concentrations of potassium hydroxide were used, and for each concentration a large scale plot was made of E_{Zn} vs. molarity of the zinc. Then a given molarity of zinc was chosen and E_{Zn} values for this concentration were read from the plot for various concentrations of potassium hydroxide. Small concentrations of zinc were chosen so that the mean hydroxyl ion activity would not be affected to a large extent. For a constant value of zinc concentration, equation (VII) becomes

$$E_{Zn} = K'' + 0.0295y \log (\text{OH}^-) + 0.0295z \log (\text{H}_2\text{O}) \quad (\text{IX})$$

where

$$K'' = E_{Zn-Zn^{++}}^0 + 0.0295 \log K - 0.0295 \log (\text{Zn}_c) \quad (\text{X})$$

Equation (IX) has three unknowns in it: K'' , y , and z .

To evaluate these, certain values were assumed for z and inserted in equation (IX). The most reasonable values for z seemed to be 2, 3, or 4. Upon substituting these in equation (IX), the term $[E_{Zn} - 0.0295z \log (\text{H}_2\text{O})]$ was plotted against $\log (\text{OH}^-)$. According to equation (IX) this should give a straight line having a slope of $0.0295y$, from which y can be evaluated. In order to obtain this straight line, however, it is necessary that K'' be constant over the concentration range studied. The only term that might vary with changing hydroxyl

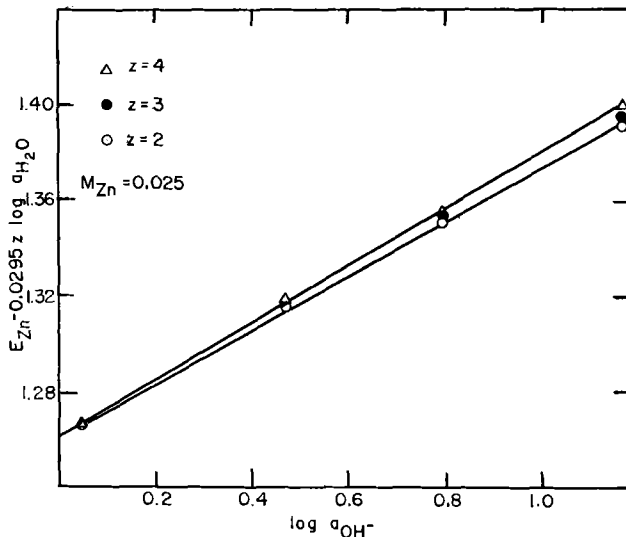


FIG. 2. Variation of $E_{Zn} - 0.0295z \log (\text{H}_2\text{O})$ with $\log a_{\text{OH}^-}$. The mean activity of the OH^- ion in KOH solutions is used.

ion concentration is the term $\log (\text{Zn}_c)$. It is possible that the activity coefficient of this species of ion may not be constant over this range of ionic strengths, even though the molarity of the species is a constant. However, when the term

$$[E_{Zn} - 0.0295z \log (\text{H}_2\text{O})]$$

is plotted against $\log (\text{OH}^-)$, reasonably straight lines are obtained (see Fig. 2). Using the slopes of these lines to evaluate y , one obtains values varying from 3.86 to 4.06. This means that the zinc-containing ion is a divalent zincate ion, and it substantiates the work of Kunschert (4).

Some idea as to the role of water in the formation of this zinc complex may also be determined by the use of equation (IX). As far as water is concerned there are three possibilities: (a) it is a reactant, and equation (IX) is correct; (b) it is a product, and the last term in equation (IX) becomes

$$[-0.0295z \log (\text{H}_2\text{O})];$$

(c) it is neither product nor reactant, and the last term in equation (IX) drops out. The correct possibility can be determined by choosing several E_{Zn} values at constant $\log (\text{Zn}_c)$. In plotting E_{Zn} vs. $\log (\text{OH}^-)$ the lines obtained will bend toward the $\log (\text{OH}^-)$ axis at higher values of $\log (\text{OH}^-)$ if the water is a reactant. These lines will bend toward the E_{Zn} axis if water is a product, and the lines will be straight if water is neither product nor reactant. Several such lines are shown on Fig. 3. These all bend toward the $\log (\text{OH}^-)$ axis indicating that water is a reactant rather than a product in the formation of the zinc complex.

At lower hydroxyl ion activities, the activity of water is high and is approaching a constant value. From equation (IX) then, it is evident that as the activity of the hydroxyl ion approaches zero, the slope of the lines in Fig. 3 should become straight

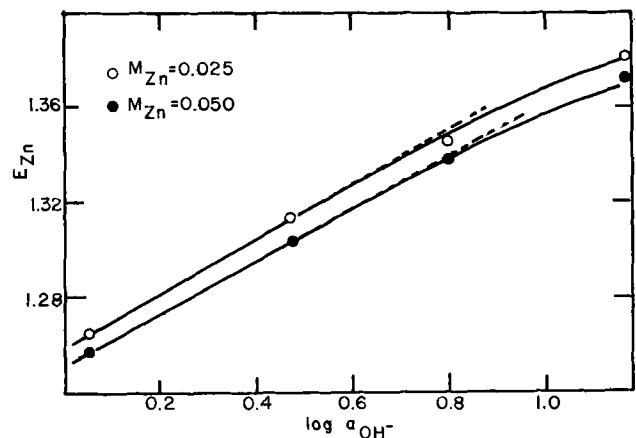


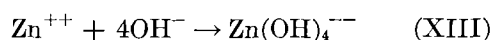
FIG. 3. Variation of E_{Zn} with $\log a_{\text{OH}^-}$. The mean activity of the OH^- ion in KOH solutions is used.

and should be a multiple of 0.0295. These limiting slopes are about 0.116, which approaches 0.118, the value the slope should have if y has a value of 4. This is a check on the value of y as determined above.

Having thus determined the values of x and y , equation (I) becomes



Making an appropriate plot, the value of E^0 for this reaction is found to be 1.211 volts. From this, ΔF_{298}^0 for this reaction is -55.85 kcal. Using the accepted free energy values for the hydroxyl ion, ΔF_{298}^0 for the zinc complex ion is -206.2 kcal. Substituting this value and other standard free energy values, ΔF_{298}^0 for reaction (XIII) is -20.7 kcal and the formation constant



of the zinc complex from Zn^{++} is 1.4×10^{15} . This is about half the value given by Latimer (6). However,

he makes the assumption that water is a product of the reaction rather than a reactant.

ACKNOWLEDGMENT

The author wishes to acknowledge with thanks the help of Mr. S. Schuldiner and Drs. J. J. Lander and Carl Wagner in the preparation of this paper, and the generosity of the Office of Naval Research in giving financial support to this work.

Any discussion of this paper will appear in a Discussion Section, to be published in the December 1954 issue of the JOURNAL.

REFERENCES

1. J. H. HILDEBRAND AND W. G. BOWERS, *J. Am. Chem. Soc.*, **38**, 785 (1916).
2. H. T. S. BRITTON, *J. Chem. Soc.*, **127**, 2120 (1925).
3. G. BODLÄNDER, *Ber.*, **36**, 3933 (1903).
4. F. KUNSCHERT, *Z. anorg. Chem.*, **41**, 337 (1904).
5. G. C. AKERLOF AND P. BENDER, *J. Am. Chem. Soc.*, **70**, 2366 (1948).
6. W. M. LATIMER, "Oxidation Potentials," p. 156, Prentice-Hall, Inc., New York (1938).



SURFACE REACTIONS OF STEEL IN DILUTE Cr⁶⁺O₄ SOLUTIONS: APPLICATIONS TO PASSIVITY

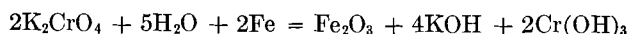
R. A. Powers and Norman Hackerman (pp. 314-319)

M. J. PRYOR¹: The adsorption theory of inhibition by chromate has undergone several modifications since it was first suggested. Originally² it was supposed that inhibition was simply due to adsorption of a monolayer of chromate ions, "in such a manner that they satisfied the secondary valency forces of the iron ions but did not disrupt the metal lattice." Even in the earlier work of Uhlig³ it was admitted that films thicker than a monomolecular layer were formed during passivation, but no protective action was ascribed to them. In view of the fact that the authors are now postulating adsorption of chromate ions on top of an incomplete oxide layer as well as adsorption on bare and presumably anodic areas, it would appear pertinent to determine what sound experimental evidence there is to support the adsorption theory of inhibition. The crux of any argument between an adsorption theory and a film theory of inhibition can be stated as follows. If inhibition is due to a monolayer of adsorbed chromate ions, then passivation of an originally film-free iron surface should yield only a "film" of monomolecular thickness. If, however, it can be demonstrated that an appreciably thicker film is formed, then it is clear that an adsorbed monolayer is not preventing corrosion since thickening of the film can only occur if the monolayer is not protective; if this is the case, inhibition must be ascribed to causes other than absorption. With this in mind, it is apparent that the authors could have performed more critical experiments by starting with film-free iron surfaces instead of iron surfaces already carrying an air formed oxide film.

It has been shown by means of electron diffraction³ that passivation of initially film-free iron specimens by solutions of potassium chromate resulted in the formation of thin films composed mainly of γ -Fe₂O₃; the thickness of the films appeared to increase with increasing time of exposure of the specimens to the passivating solution and, after two days' immersion, achieved an estimated thickness of 150 Å–200 Å, based on the apparent surface area of the specimens. The thickness of passivity films calculated on the real surface area of the specimens was undoubtedly less, probably around 50 Å–70 Å, but there is absolutely no doubt that they were considerably thicker than a monolayer. For instance, films could be detached from the metal by a suitable film stripping reagent and were then visible to the naked eye. They could be handled relatively easily and could be mounted on small grids and identified by electron diffraction. Identification of

stripped films was supported by electron diffraction identification of the films while still attached to the metal³ and has later been confirmed, using a stripping technique which permits isolation of passivity films without bringing specimens into contact with air after passivation.⁴ Since the isolation of films was carried out in air-free nonaqueous solutions there was no chance of film formation during the stripping process.

Films formed by chromate, on examination by normal electron diffraction methods, show no constituent other than oxide.³ This means that any second phase is present in amounts less than approximately 10%. Other work⁵ has shown that chromium, either as chromic compounds or as chromate, is undoubtedly present but in smaller amounts than the stoichiometric quantity expected from a reaction such as:



Evidently the major portion of the passivity film is formed by the heterogeneous interaction of dissolved oxygen and the iron surface, despite the fact that the rate of interaction of chromate ions with ferrous ions in neutral solutions is greater than that of dissolved oxygen and ferrous ions. It has been suggested⁶ that the function of the chromate is largely confined to repairing those areas where the oxide film is discontinuous. It is agreed that the first step in this localized film repairing is the absorption of chromate ions into the steel surface. It is believed, however, that the reaction does not stop at this point but is followed by oxidation of the iron and reduction of the chromate ion.

Distribution of chromium in passivity films has not been previously determined; consequently, the work of the authors is timely. However, distribution of ferric phosphate in passivity films formed in sodium orthophosphate^{7, 8} and of lepidocrocite in films formed in sodium hydroxide⁹ has been investigated. Both of these are anodic inhibitors and, although they are nonoxidizing anions with respect to iron, it has been suggested that the mechanism of inhibition is not dissimilar to that of chromate.⁶ The size of the inclusions of ferric phosphate and lepidocrocite is of the order of 1–2 μ in diameter

³ J. E. O. MAYNE AND M. J. PRYOR, *J. Chem. Soc.*, **1949**, 1831.

⁴ M. J. PRYOR, Unpublished work.

⁵ D. M. BRASHER AND E. R. STOVE, *Chemistry & Industry*, **1952**, 171.

⁶ M. J. PRYOR AND M. COHEN, *This Journal*, **100**, 203 (1953).

⁷ M. J. PRYOR, F. BROWN, AND M. COHEN, *This Journal*, **99**, 452 (1952).

⁸ J. W. MENTER, *Compt. rend. du Premier Congrès International de Microscopie Electronique Paris (1950)*; Editions de la *Rev. opt. Paris* (1952).

⁹ J. E. O. MAYNE, J. W. MENTER, AND M. J. PRYOR, *J. Chem. Soc.*, **1950**, 3229.

¹ Kaiser Aluminum & Chemical Corporation, Spokane, Wash.

² H. H. UHLIG, *Offic. Dig. Federation of Paint & Varnish Production Clubs*, **313**, 660 (1952).

and they were present in amounts of between 2–10% of the passivity film (excluding a few results on acid washed surfaces in solutions on the borderline between passivity and inhibition where the phosphate contents were higher). The distance separating the inclusions was, on the average, between 5–7 μ . Whereas it cannot be assumed arbitrarily that distribution of chromium compounds would be on a similar scale, convincing evidence concerning the distribution of these compounds in passivity films will not be obtained unless experiments, sensitive enough to pick up heterogeneity on this scale, are carried out. This is not easy to do by radioautographic means, since heterogeneity of the nature indicated above would be equivalent to a large number of point sources separated by very small distances (5–7 μ).

Therefore, there are two questions that I would like to ask the authors on their radioautographs. These are:

1. What was the magnification of the radioautograph of the passive surface?
2. What was the emulsion thickness and approximate grain size of the plate used for the radioautograph of the passive surface?

The exclusion of these details from the experimental section makes it difficult to determine the value of the radioautograph of passive surfaces. To prove conclusively that the distribution of activity is homogeneous, the grain size of the emulsion would have to be of the order of 2–3 μ and the emulsion thickness of the same order. To the best of my knowledge, characteristics of this nature can only be obtained by painted emulsions which, I believe, are not produced commercially. Plates of highest resolving power available commercially have a resolving power of the order of 1000 lines/mm. These plates might be just sensitive enough to detect heterogeneity of the nature indicated above when examined under high magnification.

It may be that the radioautographic techniques used by the authors were carried out in this manner; if they were, their conclusions are valid; if such was not the case, the arguments advanced in the discussion are unconvincing.

Two other points in this paper require some qualification. Firstly, the reference to the work of Robertson¹⁰ on tungstate and molybdate is misleading. It was pointed out in the discussion to this paper^{11, 12} that tungstate and molybdate had been proved to be nonoxidizing anions only in 1N sulfuric acid which has a considerable stabilizing influence on ferrous ions. Experiments reported in this discussion¹¹ and later published in the JOURNAL⁶ show that tungstate and molybdate have mild oxidizing properties toward ferrous ions in neutral solutions where they are effective as anodic inhibitors. Unlike chromate, however, they are not sufficiently powerful oxidizing agents to inhibit corrosion in deaerated solutions.

Secondly, I would like to ask the authors why they measured contact potentials instead of solution potentials. It is granted that the interpretation of either measure-

ment is not easy, but the interpretation of contact potentials would seem to suffer from the additional disadvantage that specimens have to be removed from the passivating solution and exposed to the atmosphere before a measurement can be made. Is there, therefore, some special advantage to contact potential measurement which outweighs this disadvantage?

To sum up these comments, it is evident that during the last ten years a considerable volume of experimental work on anodic inhibitors has been carried out. To explain these observations in a satisfactory manner requires, of necessity, a relatively comprehensive theory; to say inhibition is due to adsorption, or to precipitation, or to film-formation is not enough. It must be shown how a particular theory best explains the available data. It appears that the adsorption theory is not consistent with a large volume of data published by many other corrosion investigators. Few will disagree that adsorption of chromate ions at anodic areas is one step in the inhibitive process. However, the writer disagrees that the reaction stops at this point, but believes that adsorption of chromate takes place only at small anodic areas and is followed by oxidation of the iron and reduction of the inhibitor anion.

R. A. POWERS AND NORMAN HACKERMAN: In answer to Dr. Pryor's specific questions, the radioautographs shown were actual size, and were taken at various times during the investigation on both Kodak nuclear track plates and Kodak No-Screen X-ray film. The particular radioautograph shown for a passive surface was obtained using x-ray film, and was specified as showing only the apparent uniform distribution of Cr⁵¹. There was no pretense of having shown uniformity on an absolute scale, nor would one expect it in view of the heterogeneous nature of surfaces and surface reactions. One should not confuse the term "monolayer" with absolute uniformity, since "layers" exist primarily as the result of calculations based on values of absolute surface area and mass of reactant retained on the surface. We refer rather to "equivalent monolayers" which implies no predetermined distribution. Note also that the distribution of activity was not one of the seven factors on which our conclusions were based.

The measurement of contact potential has the inherent advantage that it measures irreversible changes in the electrical properties of a surface independently of the media or conditions producing the change. They can thus be more directly related to the structure or composition of the surface than can solution potentials. Contact potential measurements also permit comparison of surface conditions before and after exposure to passivating or other environments, which solution potentials do not. They may also be applied to gaseous and nonaqueous systems. It is true that transfer of specimens from passivating solution to air for measurement produces secondary changes in potential. In fact, measurement of contact potentials in dry, oxygen-free nitrogen, shows that secondary changes such as these can be minimized.¹³ However, in the case of steel from chromate solutions,

¹³ L. L. ANTES AND N. HACKERMAN, *J. Appl. Phys.*, **22**, 1395 (1951).

¹⁰ W. D. ROBERTSON, *This Journal*, **98**, 94 (1951).

¹¹ M. J. PRYOR AND M. COHEN, *This Journal*, **98**, 513 (1951).

¹² P. DELAHAY, *This Journal*, **98**, 514 (1951).

these changes were slow enough to follow with ease and were always constant in magnitude, so that there is no valid reason to question the significance of the values used.

The reported work on the passivation of iron and steel by chromates is primarily limited to experiments of three types: (a) oxide-free surfaces and solutions containing dissolved air; (b) air oxidized surfaces and de-aerated solutions; or (c) air oxidized surfaces and solutions containing dissolved air. In the references cited by Dr. Pryor, and in his discussion of the subject paper, there are no explicit statements or descriptions of film stripping and electron diffraction work with both oxide-free surfaces and de-aerated solutions.

Hackerman and Hurd¹⁴ have reported on the reaction between steel and de-aerated dichromate-acetic acid solutions. In these solutions, up to 60% of the original dichromate (300–450 ppm) was reduced before the rate of reduction leveled off after 90–100 hr. In the presence of air, however, there was no measurable change in dichromate concentration and no apparent change in appearance of the steel in contrast to the dark reddish-brown film formed in air-free solutions.

These data illustrate the point that there is no necessity, and perhaps no valid reason, to postulate a universal mechanism for the passivation of steel by hexavalent chromium. The authors have advanced a mechanism which is derived from, and self-consistent with, the behavior of oxide-bearing steel and chromium in dilute chromium-VI solutions containing dissolved oxygen—the most common condition under which passivity is observed. If one admits the possibility that the heterogeneous reaction between iron and dissolved oxygen takes precedent over any reaction between iron and chromium-VI,^{14, 15} then the concept of inhibitor adsorption onto an oxidized surface applies to the cases cited by Dr. Pryor for oxide-free surfaces and aerated chromate solutions.¹⁶

The amounts of chromium found firmly fixed to a passive steel or chromium surface were such that one would not expect them to be detected by normal electron diffraction examination of stripped oxides, so that in this sense we agree with the experiments of Mayne and Pryor.¹⁶ The 48×10^{-8} gram of chromium retained per cm^2 of oxide-bearing steel surface passivated in $1 \times 10^{-3}M$ sodium chromate of pH 7.5 corresponds to approximately 8% of the weight of a $\gamma\text{-Fe}_2\text{O}_3$ film 200 Å in thickness. In this connection, it is worth pointing out that the amount of chromium retained by an oxide-bearing steel surface passivated in chromium-VI solutions is a sensitive function of solution pH , and possibly other variables. Hence, one is not justified in making inclusive statements regarding the amount of chromium that should or should not be associated with such surfaces. For example, little

¹⁴ N. HACKERMAN AND R. M. HURD, *This Journal*, **98**, 51 (1951).

¹⁵ M. J. PRYOR AND M. COHEN, *This Journal*, **100**, 203 (1953).

¹⁶ J. E. O. MAYNE AND M. J. PRYOR, *J. Chem. Soc.*, **1949**, 1831.

or no firmly fixed chromium is associated with steel surfaces passivated in $10^{-3}M$ chromate solution of pH 11, while approximately 100×10^{-8} g/cm² are retained at pH 4. In the case of chromium surfaces in $10^{-4}M$ solution, retention of chromium from solution is limited not only by pH , but by the ratio of surface to solution volume, and the concentration of anions such as sulfate and chloride.¹⁷ Data like these call attention to the fact that, in order to have meaning, any statement made concerning the character of a passive surface should be carefully modified by the conditions under which passivation was produced, e.g., state of the initial surface, solution concentration, pH , oxygen content, etc.

ANODIC FORMATION OF COATINGS ON MAGNESIUM, ZINC, AND CADMIUM

Kurt Huber (pp. 376–382)

H. J. WRIGHT¹⁸: What are the compositions of some of the anodically formed coatings on magnesium?

How are these affected by traces of chlorides, phosphates, sulfides?

We need to know if the metal oxides on magnesium are resistant to polyphosphates, etc., under anodic conditions.

KURT HUBER: The experiments described in my paper dealing with the anodic behavior of magnesium were performed in solutions prepared with purest NaOH. Therefore, no predictions can be made at present concerning the effect of traces of chlorides, phosphates, and sulfides on these anodically formed coatings.

However, Flückiger in his doctoral research work [Reference (2) of my paper] investigated the anodic formation of coatings on magnesium in aqueous solutions of Na_3PO_4 and NH_4F as well as in various polishing baths. After isolation, the composition of these coatings was determined by x-ray and electron diffraction methods.

In $4N$ Na_3PO_4 , coatings were formed in which MgO , $\text{Mg}(\text{OH})_2$, and occasionally $\text{Mg}_3(\text{PO}_4)_2 \cdot 4\text{H}_2\text{O}$ could be detected. MgO predominated, particularly with short formation periods (1 min at 10–40 volts), while $\text{Mg}(\text{OH})_2$ became the principal component after longer formation periods. In an analogous manner, MgO , $\text{Mg}(\text{OH})_2$, and MgF_2 were formed in $2N$ NH_4F solution.

The change in composition of the coatings with increasing periods of anodic treatment seems to indicate in these cases as well that MgO is produced as the primary product, and that then in a subsequent reaction it is hydrated or converted to an insoluble salt. In a polishing bath containing 375 ml H_3PO_4 ($d = 1.71$) and 625 ml absolute alcohol, coatings containing MgO and $\text{Mg}(\text{OH})_2$ were formed. At higher voltages corresponding to those employed for anodic polishing, magnesium phosphate was also occasionally formed. However, MgO was always the predominant component.

¹⁷ N. HACKERMAN AND R. A. POWERS, *J. Phys. Chem.*, **57**, 139 (1953).

¹⁸ Socony-Vacuum Oil Company, 26 Broadway, New York, N. Y.

FACTORS AFFECTING THE TRANSFORMATION TO GRAY TIN AT LOW TEMPERATURES

R. R. Rogers and J. F. Fydell (pp. 383-387)

F. A. LOWENHEIM¹⁹: The authors are to be complimented on a most interesting study of a question which appears to be again attracting considerable attention. I question, however, whether the grade of tin which they used for their experiments should be called "commercial." I have no criticism of using for research work the purest materials which can be found but, considering that rather small amounts of impurities appear to have large effects on the phenomenon the authors are studying, it may be well to point out that grades of tin available commercially may behave quite differently from that which the authors designate as commercial. For example, the authors' tin contained 0.0005% antimony; commercial tin may contain up to 80 times this amount and still be designated Grade A. Similarly, the authors' tin contained 0.0005% lead; the maximum specification for Grade A is 100 times this amount. Similar remarks would hold for the other impurities cited by the authors. Details of the specification for Grade A tin and for typical analyses of all the leading brands may be found in "Metal Statistics 1952" published by the American Metal Market, page 451. It would be interesting if the authors could fit into their program a study of more typical commercially available tin.

The effect of zinc is of particular interest in view of commercial possibilities of the tin-zinc alloy deposit. It may be pointed out that, although the very small amounts of zinc the authors have studied appear to accelerate the phase transformation, some work which is in progress in the United States shows that zinc in considerably larger amounts acts as an inhibitor. In fact, electrodeposits of the 80% tin-20% zinc alloy show little or no tendency to transform, even when inoculated, after a testing period of six months. I recognize, of course, that 20% zinc is no longer an impurity, but the reversal of the trend should be noted, and it might be interesting to investigate the range of tin-zinc alloy compositions to find at what percentage of zinc this reversal occurs.

R. R. ROGERS AND J. F. FYDELL: In describing the tin used in these experiments we stated that two of the three types were obtained from ordinary commercial sources. It was left to the reader to decide whether or not such tin should be called "commercial."

We agree with Dr. Lowenheim that the composition of commercial tin varies over a comparatively wide range, and the tendency to form gray tin is very different in different parts of this range. This was demonstrated clearly in the present investigation. As stated in our paper, when a small amount of copper was added to Type I tin, containing 0.0005% antimony and 0.0005% lead, the average m value of the resulting material was 0.342 at -29°C . On the other hand, when a similar amount of copper was added to Type II tin, containing 0.015% antimony and 0.009% lead, the average m value was only 0.006 at the same temperature.

¹⁹ Metal & Thermit Corporation, Rahway, N. J.

We agree also with Dr. Lowenheim's statement that, although a small amount of zinc tends to accelerate the transformation to gray tin, a larger amount of zinc actually acts as an inhibitor. This is brought out clearly by the following data taken from Table IV of our paper:

Composition of tin	m Value
Type I tin + 0.019% zinc.....	0.130
Type I tin + 0.037% zinc.....	0.115
Type I tin.....	0.07
Type I tin + 0.05% zinc.....	0.020

It would appear that the m value of Type I tin with the addition of approximately 0.040% of zinc would be the same as that of Type I tin alone. When smaller zinc additions (as 0.019 or 0.037%) are made to the tin, the m value tends to be greater than that figure, but when larger zinc additions (as 0.05%) are made, the m value tends to be less.

ATTEMPTS AT THE ELECTROLYTIC INITIATION OF POLYMERIZATION

H. Z. Friedlander, Sherlock Swann, Jr., and C. S. Marvel (pp. 408-410)

GARRETT W. THIESSEN²⁰: Relative to reluctance of "free radicals" $\text{R}\cdot\text{COO}$, to leave the anode in the Kolbe aqueous electrolysis, work is in progress at Monmouth College, doing the acetate electrolysis between Pt plates at variable frequency. At 60 cycles, only very small amounts of H_2 only are found; even at 1 cycle, the yield of Kolbe gas is highly inhibited. We infer that the $\text{CH}_3\cdot\text{COO}$ radical coheres within itself, and adheres to the electrode, for times of the order of one second.

No comment from the authors.

STRUCTURAL FEATURES OF OXIDE COATINGS ON ALUMINUM

F. Keller, M. S. Hunter, and D. L. Robinson (pp. 411-419)

CHARLES L. FAUST²¹: This is a very interesting discussion to one interested in anodic processes. The electron microscope pictures are certainly excellent.

The quality in eye appeal of an electrobrightened-, anodized-, and dyed-aluminum surface is better than that of abrasively finished and buffed aluminum that is anodized and dyed. This situation suggests that the nature of the starting surface is influential in determining the characteristics of the oxide formed in anodizing. The authors' comments on this point would be of interest.

How does surface distortion, strain, and cold work influence the character of oxide coating vs. that of oxide coating over the nonworked, nonstrained, and undistorted electrobrightened surface?

²⁰ Monmouth College, Monmouth, Ill.

²¹ Battelle Memorial Institute, Columbus, Ohio.

The authors state that the ideal electrobrightening treatment would be one in which the oxide layer was dissolved as fast as it was formed. Morize, Lacombe, and Chandron²² report that aluminum electropolished in perchloric-acetic acid bath has no oxide coating. As evidence of this, the electrode potentials are cited. Assuming that this claim of no oxide is correct, would such an electrobrightened aluminum surface anodize to different oxide-cell size, pore dimensions, etc., than a surface electrobrightened, but containing a thin oxide film or "smudge?" The thin oxide is mentioned on page 418, left column, of the Keller, Hunter, and Robinson paper.

F. KELLER, M. A. HUNTER, AND D. L. ROBINSON: While the appearance of anodically coated and dyed aluminum surfaces is dependent on the nature and characteristics of the starting surface, we believe that such differences in appearance are not related to the cell and pore dimensions of the oxide coating. In the case of surfaces which are abrasively finished and buffed, the dull appearance is generally attributed to particles of abrasive or buffing compound which have been incorporated into the surface layer of metal. It is doubtful that surface distortion, strain, or cold work influence the dimensions of the oxide cells because no differences in oxide structure have been observed between coatings applied to annealed aluminum and those applied to hard rolled aluminum.

We would expect a thin oxide film or "smudge" remaining after an electrobrightening treatment to have little or no effect on the dimensions of an anodic oxide film applied subsequently, particularly if the anodic film was of appreciable thickness. When an anodic coating is applied to an aluminum surface which already has an anodic coating applied in a different electrolyte and under different conditions, there is a relatively rapid transition from the cell structure characteristic of the initial coating to that characteristic of the final coating. The time required for this transition is a function of current density and is apparently only slightly longer than that required to establish the cell and pore pattern initially. Thus, the presence of a thin oxide layer remaining from an electropolishing treatment would have no significant effect on the pore and cell dimensions of the major portion of the anodic coating. Inasmuch as such a layer would remain on the outer surface of the anodic layer, however, some difference in appearance might result.

DETERMINATION OF CURRENT EFFICIENCY OF DIAPHRAGM ALKALI-CHLORINE CELLS BY GAS ANALYSIS

M. S. Kircher, H. R. Engle, B. H. Ritter, and
A. H. Bartlett (pp. 448-451)

RALPH M. HUNTER²³: I am wondering if you have ever compared the quantities of the three products collected, i.e., measure the collected chlorine and correct for chlorate, chlorine losses in the brine, and other undesired reactions; collect the caustic soda, making corrections for impurities; and collect the hydrogen. Under these conditions, you should account for 35.5 grams of Cl₂, 40 grams of NaOH,

²² P. MORIZE, P. LACOMBE, AND G. CHANDRON, *Compt. rend des J. des Etats de Surface*, **34**, 242 (1945).

²³ The Dow Chemical Company, Midland, Mich.

and 1 gram of H₂. It occurs to me that this might be an excellent method for studying cell operation.

M. S. KIRCHER: In normal plant operation, the quantities of chlorine, caustic soda, and hydrogen produced are measured. It is because of the inaccuracies of these measurements as carried out on a plant scale that the gas analysis measurement of current efficiency was devised.

It would be relatively simple to conduct the measurements which Dr. Hunter suggests on a single cell. We have not done this, but consider that it should be done if a further investigation, such as that done earlier,²⁴ were undertaken.

THE ELECTROCHEMISTRY OF THE FIRST LAYERS OF ELECTRODEPOSITED METALS

T. Mills and G. M. Willis (pp. 452-458)

J. O'M. BOCKRIS²⁵: Values obtained by Mills and Willis for the capacity on silver electrodes seem very high indeed.²⁶ It would be of the utmost interest to learn if these authors could obtain any solid evidence with regard to hydrogen atom adsorption from their charging curves; the position in this respect is particularly ambiguous with respect to silver.

T. MILLS AND G. M. WILLIS: Our capacities are comparable with those found by Veselovsky for etched silver (350-400 $\mu\text{F}/\text{cm}^2$). We also find similar variations in capacity with the state of the surface, which may be attributed to changes in surface area. We agree with Dr. Bockris that the capacities, even after allowing for a high ratio of real to apparent surface, seem high. This appears to be generally true of the double layer capacities of solid metals when compared with that of mercury. Measurement of true surface area would be of assistance in interpreting results. It is possible that reduction of surface oxide or deposition of adsorbed hydrogen contributes to the high measured capacity.

We have no definite evidence for hydrogen adsorption on silver. The second arrest in alkaline solutions which was found by Veselovsky (and which we have confirmed) was ascribed by him to a strongly bound oxide film. From changing curves *alone* it is not possible to distinguish an oxide film which can only be reduced at highly cathodic potentials from an adsorbed hydrogen film. Removal of oxygen with simultaneous deposition of adsorbed hydrogen is another possibility which cannot be excluded from consideration.

SOME PROPERTIES OF TIN-II SULFATE SOLUTIONS AND THEIR ROLE IN ELECTRODEPOSITION OF TIN

II. Solutions with Tin-II Sulfate and Sulfuric Acid Present

C. A. Discher (pp. 480-484)

A. H. DU ROSE²⁷: Dr. Graham has suggested the use of fluoride in the sulfate bath to prevent sludging. It has

²⁴ R. L. MURRAY AND M. S. KIRCHER, *Trans. Electrochem. Soc.*, **86**, 83 (1944).

²⁵ John Harrison Laboratory, University of Pennsylvania, Philadelphia, Pa.

²⁶ Cf. Y. VESELOVSKY, *Acta Physicochim.*, **11**, 815 (1939).

²⁷ The Harshaw Chemical Company, Cleveland, Ohio.

been our experience that, while fluoride will prevent sludging for a time, dependent on the fluoride concentration, it does so by holding the Sn-IV in solution, and the rate of formation of Sn-IV is faster in the presence of fluoride. The effect of Rochelle salts is similar. Copper and iron in the solution accelerate the formation of Sn-IV.

C. A. DISCHER: During my work with Dr. Mathers, we conducted a series of experiments with the sulfate bath in which hydrofluoric acid was substituted for sulfuric acid.²⁸ Under the conditions used, sludging was not a problem even over relatively long periods of time. However, this approach was discontinued since its merit was not considered sufficient to overcome certain disadvantages inherent in the fluoride type of bath.

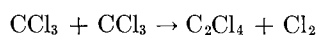
MECHANISM OF REACTION OF ALUMINUM AND ALUMINUM ALLOYS WITH CARBON TETRACHLORIDE

Milton Stern and Herbert H. Uhlig (pp. 543-552)

H. G. OSWIN²⁹: It would seem that further investigation should be carried out before any reaction mechanisms can be proposed for this system.

While the presence of certain "inhibitors" appears to prevent the initiation of the reaction, this only indicates that the initial steps involve free-radical mechanisms; it does not preclude the possibility of a chemical reaction in later stages. This could, of course, be checked by addition of inhibitors to the system at suitable time intervals.

Presence of C₂Cl₆ as the sole organic end product is surprising, since other authors,³⁰ working with systems likely to contain CCl₃ radicals, have failed to detect any hexachloroethane. It seems more likely from this other evidence that C₂Cl₄ is usually formed,³¹ possibly with the formation of chlorine, in some such disproportionation as:



Bowen and Rohatgi,³² working in the liquid phase, also do not report the formation of any C₂Cl₆.

I should also like to know the ratio of the end products C₂Cl₆/AlCl₃. This would probably provide a very good indication of the mechanism.

Presumably, in the proposed mechanism the chain-propagating process is AlCl₃ + CCl₄ → AlCl₃⁺ [CCl₃]⁻ + Cl. The induction period of the reaction is then affected by the concentration [AlCl₃]. It would be interesting to observe how the addition of AlCl₃ to the system would affect the induction period.

Finally, it would be worthwhile investigating the reaction from a photochemical viewpoint to see whether it could be initiated by a direct photolysis or a photosensitized method.

²⁸ F. C. MATHERS AND C. A. DISCHER, *Proc. Indiana Acad. Sci.*, **56**, 141 (1946).

²⁹ National Research Council, Ottawa, Ontario, Canada.

³⁰ H. SCHUMACHER AND K. WOLFF, *Z. physik. Chem.*, **B25**, 161 (1934).

³¹ H. F. SMYSER AND H. M. SMALLWOOD, *J. Am. Chem. Soc.*, **55**, 3499 (1933).

³² E. J. BOWEN AND K. K. ROHATGI, *Disc. Faraday Soc.*, **14**, 146 (1953).

MILTON STERN AND H. H. UHLIG: Many of the questions raised by Mr. Oswin are answered directly in the text of the paper. For example, compounds effective as inhibitors were found also effective after the reaction had started, as is described on page 550. Also, detailed discussion of the effect of aluminum chloride on the induction period is found on page 541 and in reference (1). There is, of course, no difference between the reaction mechanism we propose and that of a chemical reaction, and we feel that sufficient data have now been assembled to establish that the reaction depends on a chain sequence in which free radical species participate.

We did not state in our paper that C₂Cl₆ is the sole organic reaction product, but only that our work, confirming other investigators, proves it to be the major product. However, as we have indicated in the abstract and also in the text beginning page 550, it would be quite unusual, if not exceptional, to find a free radical reaction which produces no side products. Accordingly, a complex residue of by-products was found, but no measurable quantities of chlorine were evolved during the reaction. It should be emphasized that where reactions with lower activation energy are possible, trichloromethyl radicals may be consumed by processes other than dimerization (formation of C₂Cl₆). This is generally the case in the systems which Oswin has quoted. On the other hand, Melville, Robb, and Tutton³³ have shown that trichloromethyl radicals may be involved in dimerization as the predominant termination reaction, or they may react with other available species, depending on the concentrations and substances present. For the aluminum-carbon tetrachloride reaction, where no third organic material is available for combination with trichloromethyl radicals, it is readily understood why hexachloroethane is the major end product.

We agree that the reaction should prove fruitful from the standpoint of the photochemist, and hope that sometime this phase of the problem will be investigated by those familiar with photochemistry.

W. W. SMELTZER³⁴: Stern and Uhlig suggest that vacuum treatment at 400°C for 7 hr does not damage the oxide film on aluminum and, thus, will not account for the shorter delay in the aluminum-carbon tetrachloride reaction. It has not been established whether the crystalline structure of the oxide may have an effect on the duration of this induction period. Heating at 400°C may cause crystallization of the amorphous oxide to gamma-alumina, as the diffraction studies of Brouckère³⁵ show that this crystalline form of alumina occurs in the oxide film after 6 hr of heating in air at 400°C. Also, Hass³⁶ found that gamma-alumina crystals form at temperatures less than 400°C on the (III) face of evaporated oriented aluminum films, although a temperature of 450°C was required to

³³ H. MELVILLE, A. ROBB, AND R. TUTTON, *Disc. Faraday Soc.*, **14**, 150 (1953).

³⁴ Aluminium Laboratories Limited, Kingston, Ontario, Canada.

³⁵ L. DE BROUCKÈRE, *J. Inst. Metals*, **71**, 131 (1945).

³⁶ G. HASS, *Optik*, **1**, 134 (1946).

initiate crystallization of the amorphous oxide on polycrystalline aluminum films.

It has been suggested by Hass³⁷ that this crystallization of the oxide may produce cracks in the oxide film. If this is valid, then the decrease in induction time for specimens heated at 400°C in vacuum may be partially caused by formation of a less protective film by crystallization of the amorphous oxide.

The conclusion of Stern and Uhlig that water and, perhaps, oxygen in the oxide are probably responsible for the induction period, would be strengthened if it is proven that crystallization of the amorphous oxide does not occur with heating of specimens at 400°C in vacuum for 7 hr, or if specimens with either an amorphous or crystalline thin oxide film exhibit the same characteristic behavior.

MILTON STERN AND H. H. UHLIG: In answer to W. W. Smeltzer, heating the oxide film on aluminum undoubtedly causes some structural changes, including recrystallization and perhaps the production of cracks. However, these changes do not explain decrease of the induction period after vacuum treatment. For example, similar oxides heated in air would be expected to undergo a similar structural change; yet, for specimens so treated, the induction period is either the same or somewhat greater than for the untreated specimens. Increase in thickness of oxide films on heating does not balance any supposed loss of protection through structural change, because anodized films equal to or thicker than the oxide films produced by heating are also not very effective in extending the induction period. On the other hand, our experiments show clearly the marked effect of water and oxygen on delaying the reaction. Since natural oxide films on aluminum contain water and perhaps oxygen as well, both of which are removed by vacuum treatment, it is more likely that these factors account for the observations rather than a mechanism based on cracking of the film.

M. J. PRYOR³⁸: The authors have presented an interesting interpretation of their data on the corrosion of aluminum alloys in carbon tetrachloride by suggesting that the reaction is initiated by the formation of $\cdot\text{CCl}_3$ free radicals. The $\cdot\text{CCl}_3$ free radical is one that has been generated with relative ease in carbon tetrachloride solutions by photolysis. If the interaction of aluminum and carbon tetrachloride proceeds by a free radical mechanism, then it should be possible to initiate the reaction by photolysis. Have any experiments of this nature been carried out by the authors?

MILTON STERN AND H. H. UHLIG: We agree with M. J. Pryor that there should be considerable effect of radiation on the reaction, and that studies of this kind would be both interesting and valuable. Although we excluded light from the reaction vessels in which our experiments were carried out, we made no systematic effort to determine the magnitude of the effect.

³⁷ G. HASS, *Verhandl. deut. physik. Ges.*, **22**, 1 (1941).

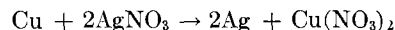
³⁸ Kaiser Aluminum and Chemical Corporation, Spokane, Wash.

RATE OF DISPLACEMENT OF SILVER FROM AQUEOUS SILVER NITRATE BY ZINC AND COPPER

Richard Glicksman, H. Mouquin, and Cecil V. King (pp. 580-585)

H. J. AXON AND P. A. CARTWRIGHT³⁹: We were particularly interested in this paper since we have recently studied the reaction between solid copper and aqueous AgNO_3 solution under static conditions, and have also done a few experiments with rotating specimens of the type described by King and his coworkers. In the "rotating specimen" experiments, using a copper cylinder with peripheral speed 4500 cm min^{-1} (900 rpm) and 0.1M AgNO_3 , we found that silver tended to adhere to randomly distributed areas of the rotating copper, thus producing erratic values of k . When the rotating specimen was continuously scraped with a light glass scraper, a consistent value of 0.78 was obtained for the rate constant k . Considering the different concentration and geometry in the two investigations, this value is in reasonable agreement with Fig. 4 of the paper.

We would also like to relate the results of our experiments with "stationary" specimens to some of the gaps in the literature which have been pointed out in the paper. For stationary conditions we have found that the replacement process in the $\text{Cu}/0.1\text{M AgNO}_3$ system may be described by the equation



to an accuracy better than 1%, in general, the actual loss of weight of solid copper being 1% greater than that calculated from an analysis of the silver ions remaining in solution. We are convinced that most of this discrepancy is due to the mechanical loss of small particles of copper from the corroded specimen, but have detected the simultaneous evolution of hydrogen during the reaction. Special care is required to detect this hydrogen, since in our experiments we estimate that the deposition of 1 gram of metallic Ag is associated with the evolution of only ~ 2 ml H_2 at N.T.P.

A further possible, but again small, contribution to the 1% discrepancy noted above is associated with the redeposition of copper onto previously deposited silver. We suspect that this redeposition of copper takes place at cathode areas of differential aeration cells, the anode process of which would be the solution of copper from the main specimen. It is certain that artificially accentuated differential aeration increases the amount of redeposited copper. Spectrographic tests of the silver crystals before and after washing with dilute HNO_3 show that the copper deposit is superficial, and microscopic examination of the silver crystals suggests that the copper is deposited onto actively growing surfaces of the depositing silver, and, having deposited, prevents further growth of silver on that particular surface.

RICHARD GLICKSMAN, H. MOUQUIN, AND CECIL V. KING: We are very much pleased with the information supplied by H. J. Axon and P. A. Cartwright, which adds materially to the available knowledge about these displacement reactions.

³⁹ Metallurgy Department, University of Manchester, Manchester, U. K.

Kinetics of the High Temperature Oxidation of Zirconium¹

JACK BELLE AND M. W. MALLETT

Battelle Memorial Institute, Columbus, Ohio

ABSTRACT

The rate of oxidation of high purity zirconium was determined for the temperature range of 575° to 950°C at 1 atm pressure. Data can be fitted to a cubic law and the rate constant in (ml/cm²)³/sec has been calculated to be $k = 3.9 \times 10^6 e^{-47,200/RT}$, where 47,200 ± 1,000 cal/mole is the activation energy for the reaction.

INTRODUCTION

The early work on the oxidation of zirconium has been reviewed by Gulbransen and Andrew (1) who studied the reaction. Cubicciotti (2) also investigated the oxidation of zirconium recently. Each study involved the use of thin zirconium foil, approximately 0.005 in. thick, for specimens. Hafnium content of the zirconium was approximately 3% in both cases. Gulbransen and Andrew worked in the temperature range of 200°–425°C at an oxygen pressure of 7.6 cm, while Cubicciotti investigated the reaction at 600°–920°C at pressures ranging from 0.1 mm to 20.2 cm. Gulbransen and Andrew stated that the oxidation reaction could not be fitted to any simple rate law over a wide temperature range, but assumed the reaction to follow the parabolic law with initial deviations. Cubicciotti reported that oxidation curves were parabolic at all temperatures except 920°C, where a small deviation toward a linear rate was observed. Energies of activation found by these investigations were 18,000 cal/mole by Gulbransen and Andrew and 32,000 cal/mole by Cubicciotti.

To supplement previous work done largely at lower temperatures and pressures, this study was made in the temperature range 575°–950°C at an oxygen pressure of 1 atm, using low-hafnium zirconium (0.01 weight %).

EXPERIMENTAL

Method.—Rate of reaction between zirconium and oxygen was determined by measurement of the rate of consumption of the gas by the metal at high temperature. The apparatus used was similar to that described in an earlier paper (3) with a few modifications. A 4-kw tungsten-gap-type Lepel converter was used to heat the metal. The zirconium specimen was supported at the bottom by a Vycor stand in the reaction tube, and a platinum-platinum + 10% rhodium thermocouple was welded to the top of the sample. The thermocouple was calibrated against an

optical pyrometer in the same manner as for some previous work reported from this laboratory (3).

Zirconium specimens were machined cylinders of two sizes, about 4 cm long by 0.7 cm in diameter and about 5 cm long by 1.4 cm in diameter. Specimens were abraded with kerosene-soaked 240-, 400-, and 600-grit silicon carbide papers and washed in successive baths of naphtha, ether, and acetone.

After placement in the reaction tube, a specimen was degassed by heating to 800°C or higher for 1 hr in a vacuum in order to remove hydrogen prior to the addition of oxygen. Oxygen was added to the reaction tube to atmospheric pressure in measured amounts from a 50-ml glass buret. Pressure measurements were made every 2 min at the start of each run and at longer time intervals as the reaction rate decreased. Oxygen, present in the apparatus as a gas phase, was determined from pressure measurements on a full-length open-end mercury manometer and the calibrated dead space of the system. After the reaction had been followed for the desired time, the system was evacuated and the specimen was cooled to room temperature in vacuum.

The difference between the quantity of oxygen added and that remaining in the gas phase was the quantity reacted with the specimen. The original geometrical dimensions of the specimen were used to compute the quantity of gas reacted per unit surface area.

Materials.—The pure zirconium used in these experiments was de Boer-process iodide crystal bar which had been double arc melted, forged to 1½ in.² at 1450°F, hot rolled at 1450°F, and cold rolled into ¾-in. and 5/8-in. diameter rods. Test specimens were machined from these rods. Impurities in the zirconium were determined by spectrographic, chemical, and vacuum-fusion analyses. Weight percentages of the principal impurities detected were: silicon, 0.03; iron, 0.020; hafnium, 0.010; oxygen, 0.01; nitrogen, 0.001; and hydrogen, 0.003.

Oxygen used in this study was prepared from degassed potassium permanganate by the method

¹ Manuscript received October 22, 1953. Work performed under AEC Contract W-7405-eng-92.

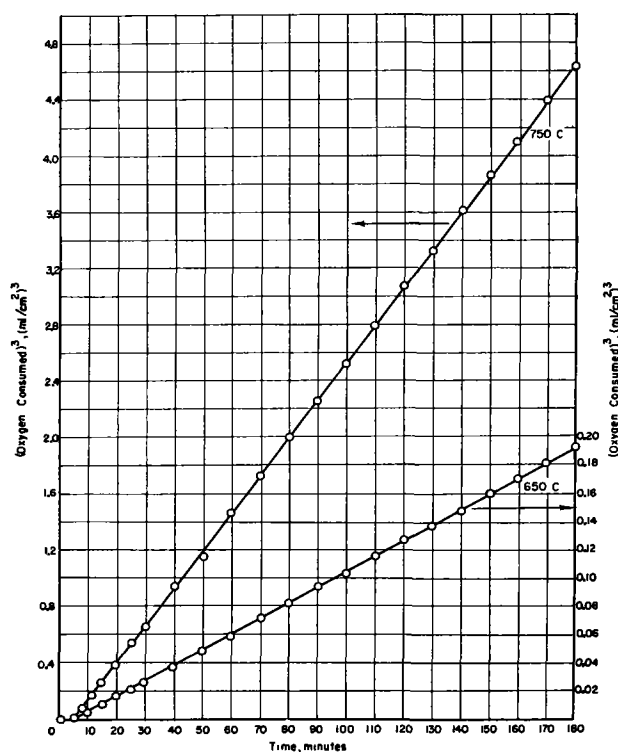


FIG. 1. Reaction of zirconium with oxygen (ml O_2 , STP, consumed/ cm^2 metal surface) 3 vs. time.

described by Hoge (4). The gas was dried by passing through a dry ice-acetone cold trap.

RESULTS

Measurements of rates of consumption of oxygen by zirconium were made from 575°–950°C at 1 atm

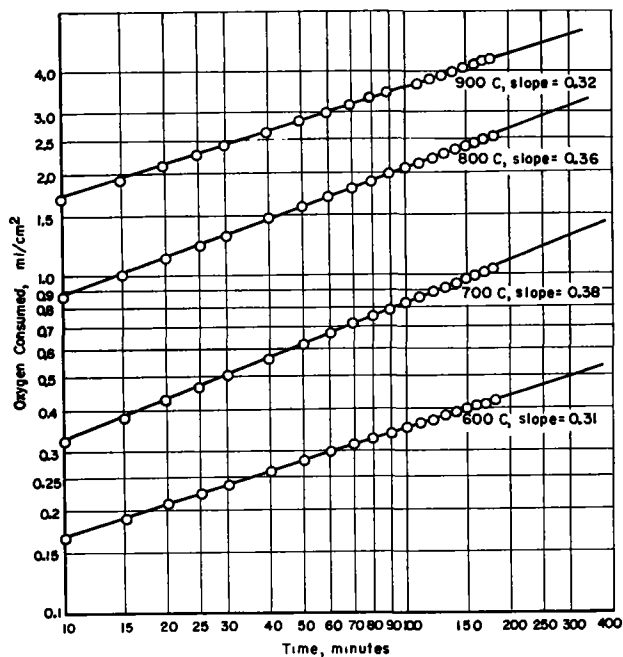


FIG. 2. Log of oxygen consumed in ml/cm^2 vs. log of time in minutes for 600°, 700°, 800°, and 900°C.

TABLE I. Rate constants for the reaction of zirconium with oxygen

Temp, °C $\pm 5^\circ$	Rate constant (k) (ml/cm^2) $^{1/3}$ /sec	Slope of log-log plot
575	2.1×10^{-6}	0.32
600	7.1×10^{-6}	0.31
625	1.4×10^{-5}	0.39
650	1.8×10^{-5}	0.38
675	5.8×10^{-6}	0.39
700	1.0×10^{-4}	0.38
725	1.9×10^{-4}	0.38
750	4.4×10^{-4}	0.36
775	5.5×10^{-4}	0.33
800	1.6×10^{-3}	0.36
825	7.9×10^{-4}	0.33
850	1.6×10^{-3}	0.34
875	3.0×10^{-3}	0.32
900	7.7×10^{-3}	0.32
920	7.6×10^{-3}	0.35
950	2.1×10^{-2}	0.32

pressure. Data below 575°C could not be obtained with the apparatus because of the slowness of the reaction. Above 950°C, the rapidity of the reaction made it difficult to control and often resulted in cracking of the oxide film. Fig. 1 shows typical results of measurements for two temperatures. It was found that the data could not be fitted to the parabolic law, but, except for slight initial deviations, could be represented by a cubic law, $w^3 = kt$, where $w = \text{ml (STP) of oxygen consumed per unit surface area}$. Thus, Fig. 1 is a plot of the cube of the quantity of oxygen consumed per unit surface area against time, and it is seen that the data fall on straight lines. Also, for a cubic oxidation, a graph of $\log w$ vs. $\log t$ should be a straight line with slope equal to 0.33. Fig. 2 shows such plots for several other

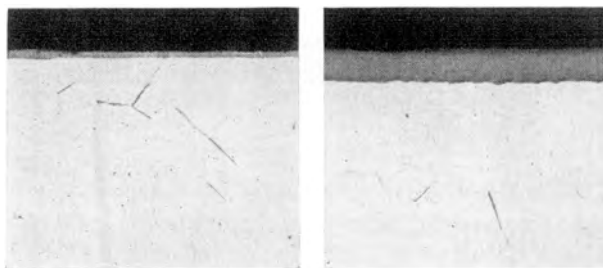


FIG. 3. Structure at surface of zirconium reacted with oxygen. (Note single surface-oxide layers. Needle-like inclusions probably are hydride.) Left, zirconium reacted with oxygen at 575°C for 3 hr. Surface layer about 0.0002 cm thick. Note absence of region of solid solution of oxygen in zirconium. Polished with Linde "B" suspended in chromic acid, then chemically polished in acid solution (45HNO_3 , $45\text{H}_2\text{O}$, and 10HF); right, zirconium reacted with oxygen at 825°C for 3 hr. Surface oxide layer about 0.0015 cm thick. Polished with Linde "B" suspended in chromic acid and then etched (etchant: 49 lactic acid, 49 nitric acid, and 2HF). The narrow gray band is ZrO_2 , below it is solid solution of oxygen in zirconium. Both 500 \times .

temperatures, and it is seen that good agreement is obtained with the cubic-law expression. Values of the rate constant, k , calculated from various plots and slopes of the log-log plots, are given in Table I.

At the end of a reaction run, the specimen was cooled in vacuum and examined. In all cases throughout the temperature range investigated, reacted specimens were covered with a shiny gray-black coating which adhered very strongly to the metal. Metallographic examination showed that a single oxide layer was present on the surface. This can be seen from the two photomicrographs in Fig. 3. X-ray patterns taken at room temperature indicated that the film was the monoclinic form of ZrO_2 . In agreement with the observation of Cubicciotti (2), it was noticed that white spots appeared on the black coating. The white spots, however, did not show up, even at the higher temperatures, within the 3-hr reaction period generally used in the present investigation. However, they did form after long-time runs at all temperatures. Above $1000^\circ C$, where the results were erratic, a flaky white coating sometimes formed on top of the gray-black oxide film.

The microstructure of the high temperature specimens, such as that for $825^\circ C$ shown in Fig. 3, gave evidence of a region of solid solution of oxygen underlying the surface oxide. Ordinarily, this could

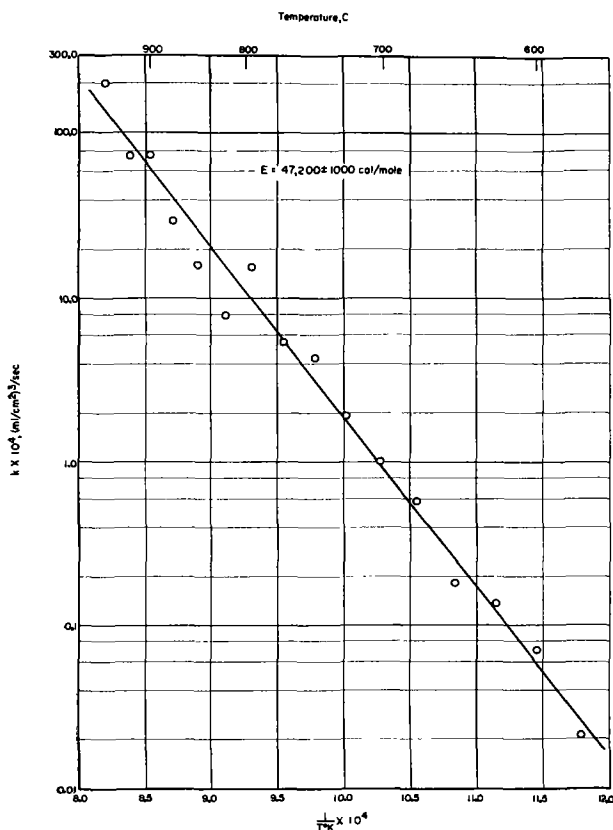


FIG. 4. Zirconium-oxygen reaction—variation of reaction rate constant with temperature.

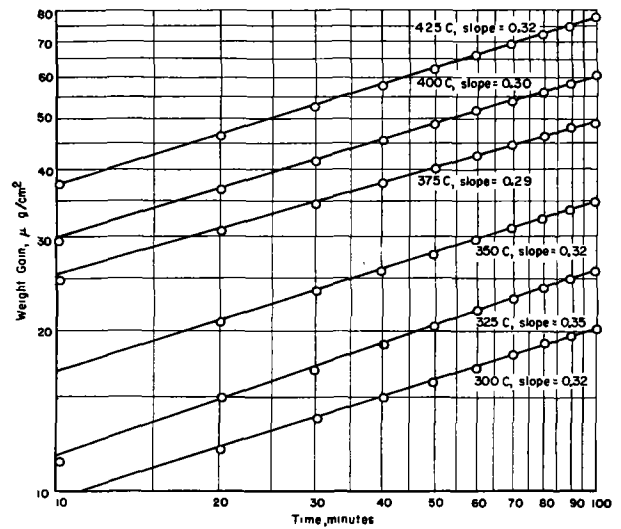


FIG. 5. Log of weight gain in $\mu g/cm^2$ vs. log of time in minutes. Data read from plot (Fig. 3) in paper by Gulbransen and Andrew (1).

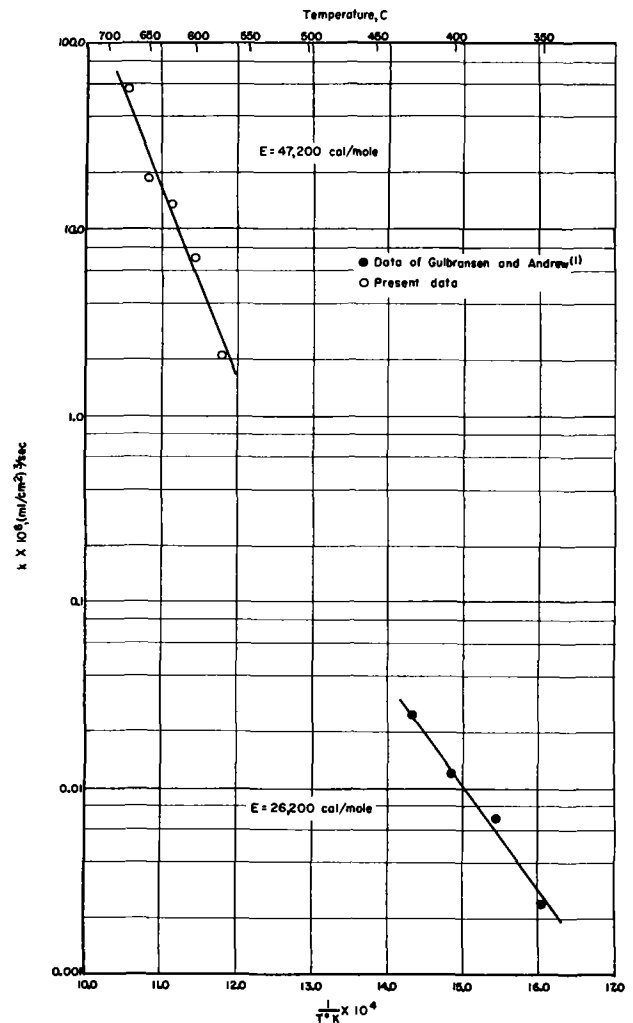


FIG. 6. Zirconium-oxygen reaction—comparison of present data with those of Gulbransen and Andrew.

not be observed metallographically. However, zirconium almost inevitably contains a trace of hydrogen which is manifested as a precipitate within the grains or at grain boundaries. The solution of considerable oxygen appears to displace hydrogen with the result that the solid-solution region is seen as a structureless zone under the microscope.

The effect of temperature on the rate of oxidation can be seen from Table I and Fig. 4. In Fig. 4, the logarithm of the cubic rate constant is plotted as a function of the reciprocal of the absolute temperature. The equation of the best straight line through the points from 575°–950°C was determined by the method of least squares. The experimental energy of activation and the frequency factor were calculated from the Arrhenius-type equation, $k = Ae^{-Q/RT}$. The energy of activation was calculated to be $47,200 \pm 1,000$ cal/mole. The rate constant in $(\text{ml}/\text{cm}^2)^3/\text{sec}$ is $k = 3.9 \times 10^6 e^{-47,200/RT}$.

DISCUSSION

Gulbransen and Andrew (1) reported that the zirconium oxidation reaction was not initially parabolic, but tended toward parabolic as the reaction proceeded. Limiting slopes at long times were used to calculate rate constants. Although arbitrary, this procedure does have merit if the initial deviations are slight and oxidation times long. However, if the oxidation data of Gulbransen and Andrew (1) (Fig. 3 of their paper) are plotted on a log-log basis, conformity with a cubic law is suggested. This is shown in Fig. 5 where the logarithm of weight gain in $\mu\text{g}/\text{cm}^2$ is plotted against the logarithm of time. Slopes very close to the theoretical 0.33 are obtained. Rate constants were calculated from straight-line plots of the cube of the weight gain vs. time. These rate constants are compared with the present data in Fig. 6.² Straight lines drawn through the separate points are of markedly different slope. The activation energy for the reaction from the data of Gulbransen and Andrew was calculated from the slope of the line in Fig. 6. The value obtained is 26,200 cal/mole as compared with the value of 47,200 cal/mole calcu-

² Units of the calculated rate constants from the data of Gulbransen and Andrew were converted to $(\text{ml}/\text{cm}^2)^3/\text{sec}$ for comparison with the present data.

lated from the present data. The data of Cubicciotti (2) could not be interpreted in terms of the cubic law. Therefore, no comparison can be made with the present data.

According to the Mott and Cabrera (5) theory of the oxidation of metals, rate of formation of thin oxide films can be expressed by a cubic law for those metals whose oxides are *P*-type semiconductors. (ZrO_2 is probably an *N*-type semiconductor.) The same mechanism, of course, cannot be used to explain the present rate data for formation of thick films during the high temperature oxidation of zirconium. Recent work by Charlesby (6) on the formation of thin oxide films formed electrolytically on metals indicated that a cubic law of oxidation can prevail over a short range of temperatures. No correlation can be made, however, with the present data for the high temperature oxidation of zirconium and the data of Charlesby (7) for the thin anodized oxide films on zirconium.

Waber (8), citing some oxidation data of titanium and tantalum, suggested that the cubic law of oxidation may have a greater range of applicability than has hitherto been expected. The present work appears to be the first experimental evidence to date that this growth law can prevail over a wide temperature range.

ACKNOWLEDGMENT

The authors gratefully acknowledge the assistance of Mr. B. G. Koehl in making the experimental runs.

Any discussion of this paper will appear in a Discussion Section to be published in the June 1955 issue of the JOURNAL.

REFERENCES

1. E. A. GULBRANSEN AND K. F. ANDREW, *J. Metals*, **185**, 515 (1949).
2. D. CUBICCIOTTI, *J. Am. Chem. Soc.*, **72**, 4138 (1950).
3. M. W. MALLETT, J. BELLE, AND B. B. CLELAND, *This Journal*, **101**, 1 (1954).
4. H. J. HOGE, *J. Research Natl. Bur. Standards*, **44**, 321 (1950).
5. N. CABRERA AND N. F. MOTT, *Repts. Progr. Phys.*, **12**, 163 (1949).
6. A. CHARLESBY, *Proc. Phys. Soc. London*, **B66**, 317 (1953).
7. A. CHARLESBY, *Acta Met.*, **1**, 340, 348 (1953).
8. J. T. WABER, *J. Chem. Phys.*, **20**, 734 (1952).

Electrodeposition of Bismuth¹

KELSO B. MORRIS, DOLORES Z. DOUGLASS,² AND CLARENCE B. VAUGHN

Department of Chemistry, Howard University, Washington, D. C.

ABSTRACT

Bismuth metal of high purity has been electrodeposited from molten mixtures of bismuth trioxide (10% and 25%) and the eutectic mixture of sodium and calcium chlorides. The rate of metal recovery (g/hr) is good. Energy consumption, based solely on the electrolysis and not on the furnace requirements, is approximately 1 kwhr/lb of bismuth.

INTRODUCTION

Bismuth metal occurs chiefly in nature as bismite, largely Bi_2O_3 , and as bismuthinite or bismuth glance, largely Bi_2S_3 . The National Production Authority regards bismuth as a "critical" metal chiefly because (a) it is important to the defense program of the federal government, and (b) high grade ores of the metal are not abundant. However, the total yearly production, according to Leighou (1), is only 2000 tons. In spite of such low tonnage, the metal finds extensive use in the preparation of matrix metal for holding dies and in the preparation of fusible alloys which are employed in making safety plugs in boilers, automatic sprinkling devices, electric fuses, etc. The fact that the metal is able to confer upon alloys its property of expanding on solidification has been responsible for the use of some of its fusible alloys as casting material for statuettes and in dental work.

Several investigators (2) have studied the electrodeposition of bismuth from aqueous solutions on a small scale. Some baths from which the metal has been obtained in reasonably good yields employed nitric acid, hydrochloric acid, or perchloric acid as solvent. Very few studies have been concerned with the electrodeposition of bismuth from molten materials. Drosbach (3) used graphite electrodes and electrolyzed molten BiCl_3 in a U-tube type cell of clear glass for 16 hr at a temperature at 340°C and at a current strength of 2 amp. The cathode, 8 mm in diameter, was immersed in the melt to a depth of about 40 mm. Cathode current efficiency was 49.3%. The phase diagram for the system, $\text{BiCl}_3\text{-Bi}$, is such

that the metal is obtained only after prolonged electrolysis. As the metal electrodeposits at the cathode, it dissolves in the molten BiCl_3 . Eventually, the monochloride (BiCl) forms and, at 320°C , there result two layers. After prolonged electrolysis and subsequent cooling of the melt, bismuth metal is isolated by remelting the metal-rich layer under NaCl .

Industrially, the metal is obtained chiefly by reduction of oxide ores with carbon or iron in crucibles (4) or in small reverberatory furnaces, in the presence of a suitable flux, and by an aqueous electrolysis process (5) that makes use of the anode slimes at electrolytic lead and tin refineries.

The present research was undertaken in order to study the electrodeposition of bismuth from mixtures of Bi_2O_3 and the NaCl-CaCl_2 eutectic and to estimate whether electrometallurgy of this sort would be superior to and/or more economical than existing methods for producing the metal. A choice of the eutectic mixture as solvent was based on the following, viz., (a) the molten material is an excellent conductor (6) of the electric current; (b) the component salts are extremely cheap; (c) the metal of each salt is considerably more active than bismuth; and (d) the melting point (505°C) of the eutectic mixture (51.8 mole % NaCl ; 48.5 mole % CaCl_2) is relatively low by comparison with the melting points of the components (NaCl , mp is 798°C ; CaCl_2 , mp is 770°C).

EXPERIMENTAL

Preliminary Studies

Some phase studies were made first since it was important to determine the solubility of Bi_2O_3 in the NaCl-CaCl_2 eutectic mixture. Also, it was necessary to know the influence of the oxide upon the electrical conductivity of the eutectic mixture.

Solubility studies.—Mixtures, of Bi_2O_3 and the NaCl-CaCl_2 eutectic or of Bi_2O_3 and NaCl , of known composition were placed in 250 ml porcelain crucibles and heated to 950°C in a pyrometer-controlled electric crucible furnace (chamber diameter, 8 in.;

¹ Manuscript received August 17, 1953. This paper is based on a part of the thesis submitted by Clarence B. Vaughn to the Graduate School, Howard University, in partial fulfillment of the requirements for the degree, Master of Science. The research was performed under Contract No. DA-36-034-ORD-853-RD between Office of Ordnance Research (Philadelphia Ordnance District) and Howard University.

² Present address: Pharmacy, Freedmen's Hospital, Washington, D. C.

chamber depth, 18 in.). Mixtures containing from 25–30% Bi_2O_3 formed pastes which did not liquefy at temperatures 200° higher than the melting point of the solvent. In the early stages of the work, melts containing up to about 25% Bi_2O_3 in either NaCl or eutectic appeared homogeneous. Stirring was not employed. Each fusion was allowed to cool slowly. When the temperature had dropped to about 100° above the solidification point expected for the mixture, temperature readings were taken every three minutes until solidification of the material was complete. Temperature readings (millivolt readings of the potentiometer converted to Centigrade degrees) were made by means of a platinum-platinum (10) rhodium thermocouple which had been calibrated according to the recommendations of Roeser and Wensel (7). The mullite or silica protection tube for the thermocouple dipped into the melt to a depth of about 2 in. From the data, cooling curves of both the direct type (temperature vs. time) and of the inverse rate type (temperature vs. time required for the melt to fall through a definite temperature interval) were plotted.

Cooling curves could not be duplicated exactly for either the same sample or for separate samples of the same composition. This caused us to suspect a change in composition because of (a) interaction of the components and subsequent loss of a volatile reaction product, and (b) volatilization of unreacted material. A series of weight-loss-on-heating experiments on the single compounds were carried out and it was found that volatilization for each was of the order 0.5% for a 3-hr heating period. However, the weight loss due to volatilization was appreciable (as high as 4% for a mixture consisting of 25% Bi_2O_3 and 75% eutectic) for mixtures of the components. It was found later that, except for the pastes, all other mixtures of Table I consisted of two liquid layers which could be observed easily through the sides of Vycor crucibles. Analysis of the layers, after cooling of the melts, varied even for mixtures of the same composition and regardless of whether the melts were quenched (by transferring the Vycor crucibles immediately to a cold air environment) or were allowed to cool slowly. The amount of Bi_2O_3 in all solvent-rich (large top layer) layers was less than 5%. The authors concluded, on the basis of the following facts, that chemical change had occurred in the melts: (a) variability of analytical data; (b) occasional escape of gas bubbles slowly from the melts at higher temperatures; and (c) the authors' observation that the molten mixtures (particularly those containing the eutectic) yielded larger quantities of smoke than the single components when molten. An indication of the nature of the reaction(s) will be given later in the discussion section of this paper. In spite of the fact

that phase rule studies were terminated early because of the conclusion that chemical change had occurred in the molten mixtures, the authors now possessed some useful knowledge, in advance of the electrolysis studies, about the behavior of the mixtures at temperatures up to 950°C.

Electrical conductivity studies.—A dip-type cell designed by the authors of Vycor glass was used in measuring the electrical conductivity (at 1000 cycles only) of the mixtures. Briefly, the cell consisted of two vertical arms (of Vycor tubing 1.9 cm diameter and 10 cm long) which were joined horizontally by a 5-cm length of Vycor capillary tubing. The underside of the capillary, at the center, was slotted to permit entry of melt into the cell. A length of 8-mm Vycor tubing, extending vertically from the center of the upper side of the capillary, served as a handle for the cell. Platinum disk electrodes, welded to platinum leads, dipped into the vertical arms of the cell. The cell constant was determined by measuring the specific resistance of fused sodium chloride in this cell and then using that value together with the specific conductance values available in the literature (8).

It was observed that the conductances of the molten mixtures were never lower than $1.5 \text{ ohm}^{-1} \text{ cm}^{-1}$ [NaCl (8) is $4.05 \text{ ohm}^{-1} \text{ cm}^{-1}$ at 950°C]. The conductivity was observed to be independent of the depth of immersion of the platinum disk electrodes in the melt as long as the time interval between measurements was of the order 2 or 3 min. One can attribute this fact to the extremely small change in resistance. For time intervals longer than 2 or 3 min, fluctuations in conductivity were observed for the same mixture because of composition changes and not because of encountering two liquid layers. Aside from the fact that the studies furnished additional evidence for changes in composition, it was of interest to know that the melts were good conductors of the current.

Electrodeposition

In the electrolysis studies, mixtures containing 10% and 25% by weight of Bi_2O_3 in the NaCl-CaCl₂ eutectic or in NaCl or in CaCl₂ were employed. Various combinations of platinum, tungsten, graphite, and copper were used as electrodes. The cathode always rested on the bottom of the crucible containing the fusion, while the anode dipped sufficiently far enough into the fusion to make electrical contact. The distance between the electrodes was 4 cm. A copper coulometer placed in series with the electrolysis cell made it possible to calculate approximately the average current which passed through the cell during the period of electrolysis. Porcelain crucibles of 250-ml capacity proved to be more satisfactory than either clay, graphite, or Vycor crucibles as containers

TABLE I. *Electrodeposition of bismuth*
 Solvent: NaCl-CaCl₂ eutectic mixture (mp, 505°C) 51.5 mole % NaCl and 48.5 mole % CaCl₂

Expt.	Wt of charge (g)	Bi ₂ O ₃ (%)	Temp °C	Electrodes		Cell voltage	Ammeter (amp)	Cathode current density (amp/dm ²)	Elapsed time (hr)	Metal recovered (g)	Rate of metal recovery (g/hr)	Product purity (% Bi)	Cathode current efficiency (%)
				Cathode	Anode								
1	258	25	800	W	Pt	5.7	5.1	204	1.50	12.1	8.1	88 ^a	35 ^a
2	346	25	800	W	Pt	4.5	5.0	198	1.23	15.3	12.4	98	95
3	345	25	800	W	Pt	7.5	4.7	184	1.40	8.9	6.4	99	52
4	269	10	600	C	Pt	8.5	5.0	46	1.62	Powder	—	—	—
5	269	10	600	W	C	7.5	2.5	22	2.06	Powder	—	—	—
6	368	10	600	W	C	5.5	4.0	39	1.65	Powder	—	—	—
7	345	10	600	W	C	6.3	4.0	39	2.12	11.2	5.3	94	51
8	359	10	600	W	C	8.2	4.0	39	1.55	4.5	2.9	98	28
9	334	10	600	W	C	9.1	4.5	44	2.00	2.3	1.2	98	10
10	294	0	600	W	C	7.4	4.0	40	1.92	Ca, CaC ₂ traces	—	—	—
11	410	25	800	W	C	5.5	4.0	40	1.27	10.0	7.9	98	75
11a	375	25	800	W	C	2.7	4.0	39	1.20	9.6	8.0	97	76
12	392	25	800	Cu	C	6.9	4.0	160	1.38	10.2	7.4	89 ^b	63 ^b
13	383	25	800	Cu	C	2.0	4.0	160	1.48	18.4	12.4	75 ^b	88 ^b
14	397	25	800	W	C	4.8	2.1	21	2.10	13.1	6.2	98	113
15	347	25	800	W	C	9.1	2.0	21	2.10	12.6	6.0	96	115
16 ^c	344	25	950	W	C	4.0	4.5	44	0.80	14.4	18.0	98	152
17 ^c	361	25	950	W	C	3.9	2.3	19	0.58	6.0	10.3	97	172
18 ^d	465	25	950	W	C	4.7	4.8	46	1.71	18.6	10.9	96	87
19 ^d	479	25	950	W	C	4.6	5.0	49	0.92	49.1	53.0	98	410

^a Based on actual Bi content; 11% Pt as impurity.

^b Based on actual Bi content; copper impurity.

^c CaCl₂ as solvent.

^d NaCl as solvent.

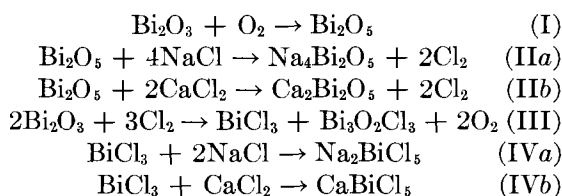
for the mixtures. For a particular mixture, the heating time necessary to secure a two-layer melt (10% Bi₂O₃, small orange-red liquid layer on the bottom and a large yellow liquid layer on the top) or an apparently homogeneous paste (25% Bi₂O₃, yellow throughout) averaged approximately 50 min. At the end of that period, electrodes were inserted into the mixture and the electrolysis begun. The temperature of the furnace was maintained constant during the entire period of electrolysis. At the end of the electrolysis and after the crucible and contents were cool, the metal slug or button found on the bottom of the crucible was crushed until fine granules and powder resulted. The crushed material was then digested with a large volume of hot water for about 15 min, filtered, and dried at 100°C. Samples of the dried material were then analyzed for bismuth.

The bismuth was determined (9) by precipitating it as the phosphate, by means of 10% diammonium phosphate, from dilute nitric acid solution and finally igniting at 800°C. Tungsten, carbon, and platinum were present in very small amount as impurities

largely because of the sparking which occurred occasionally around the electrodes during electrolysis. The "anode effect," generally observable in the electrolysis of molten materials, was present in most experiments of our research. However, in spite of the anode effect, current efficiencies were reasonably good. Electrolysis data appear in Table I.

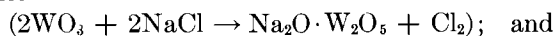
DISCUSSION

Interaction of the components.—There appear to be at least four reactions which involve the components even when a melt is not being electrolyzed. They are the following:



It is generally known that bismuth (V) oxide is formed when oxygen is passed over hot bismuth

(III) oxide. When bismuth trioxide was added to molten NaCl and/or CaCl₂ contained in a porcelain crucible in some of the authors' preliminary studies, a scarlet to reddish brown substance was formed on the surface of the melt. This substance sank slowly through the melt and the color persisted only until the mass had reached the bottom of the crucible. At the same time, there was the expulsion of a quantity of gas greater than that observable initially from the melt. The scarlet color, which is definitely characteristic of the higher oxide, led us to believe that bismuth (V) oxide had been formed. Thus, the first reaction is a logical one. Three facts support reaction (II), viz., (A) the gas which escaped from the mixture did contain chlorine; (B) the Kahlenbergs (10) have demonstrated quantitatively that tungsten oxide, a substance similar in some respects to bismuth (V) oxide, reacts with molten sodium chloride in the manner



(C) Belladen (11) has shown the existence of lead pyrobismuthite, $2\text{PbO} \cdot \text{Bi}_2\text{O}_3$ or $\text{Pb}_2\text{Bi}_2\text{O}_5$, melting at 625°C. Reaction (III) is in keeping with the observation of others (12) that the trichloride, together with smaller amounts of an oxychloride ($\text{Bi}_3\text{O}_2\text{Cl}_3$), is formed by the action of chlorine on heated Bi_2O_3 or Bi_2O_5 . The double chloride of reaction (IV) is quite analogous to the potassium pentachlorobismuthite, K_2BiCl_5 , an amber-yellow solid which Aloy and Frébault (13) prepared by passing a current of chlorine and bismuth trichloride vapor over potassium chloride at red heat. Thus, the evidence cited lends considerable support to the four series of reactions which appear to be involved in the interaction of the components.

The electrolysis.—The data of Table I reveal that bismuth metal can be obtained easily by the electrolysis of mixtures of Bi_2O_3 and either the NaCl-CaCl₂ eutectic or the single salts. Platinum anodes were attacked severely because of a combination of conditions which were present during the electrolysis, such as the sparking which accompanied the anode effect together with the evolution of both oxygen and chlorine at the anode; consequently, the large-scale use of the metal in this particular electrolysis is economically unsound.

A tungsten cathode and carbon anode represent the best electrode combination employed in this work. Abnormally high current efficiencies, that is, values greater than 100% in some experiments, are attributable definitely to chemical reduction of bismuth compounds by fairly large pieces of graphite which became detached from the anode as a result of unusually severe sparking which accompanied the anode effect in those experiments. However, it is

reasonable to assume that all current efficiencies would have run a little higher if there had not been partial short-circuiting of the electrodes through the walls of the porcelain crucible. Others (10) found this to have been true in their work.

From an academic point of view, it would be more desirable if the data showed definite relationships among the following variables: electrode combinations, cathode current density, cathode current efficiency, purity of deposit, and recoverable metal deposited in unit time. Such definite relationships do not exist for the cathode current densities which were employed in these studies. Despite the absence of such relationships in this work, the data are of preliminary interest from an industrial or commercial point of view. Conditions for obtaining bismuth metal electrolytically from melts, such as employed in this work, are not critical! All deposits were satisfactory except in experiments 12 and 13 where copper was used as cathode material. In those experiments, there was serious contamination by copper. However, if one were interested in obtaining an alloy of bismuth and copper, use of a copper cathode in melts of the type used in this work might be of value. Wide differences in cell voltages were perhaps due to the anode effect and to electrode polarizations and resistance changes of the electrolyte. Energy consumption values, based solely on the electrolysis and not on the furnace requirements, calculated for experiments 11 and 11a are, respectively, 1.275 and 0.614 kwhr/lb of bismuth. The rating of the crucible furnace used in this work was 6 kw at 63 volts. The authors believe that energy consumption values calculated for the two experiments would compare favorably with industrial electrolytic processes for many different metals. Work, now in progress, is being carried out with a view toward ascertaining more completely the applicability of the process to the large-scale production of bismuth metal. Ores will be studied. It is very likely that some impurities from the ores may codeposit with the bismuth metal; however, it should be possible to remove such impurities easily by an electrorefining process.

What can one say concerning the reaction(s) by which bismuth metal was formed in the research? Actually, both chemical and electrochemical processes were involved. Consider the following processes: (a) cathodic discharge of trivalent bismuth ion present in the melts; (b) cathodic discharge of sodium or calcium as the metal and subsequent interaction of the metal and bismuth (III) oxide to yield metallic bismuth; and (c) anodic oxidation of $\text{Bi}_2\text{O}_5^{-4}$ ion [cf. equations (IIa) and (IIb)] to bismuth (V) oxide and reduction of the latter by fragments of the carbon anode to metallic bismuth.

The sources of trivalent bismuth ions in the melt would be both BiCl_3 [cf. equation (III)] and unreacted Bi_2O_3 . According to Mellor (14), electrolysis of the oxide has been detected at 200° even though the oxide melts in the vicinity of 800°C . If such is the case, then the oxide in the melts should contain the trivalent bismuth ion. Discharge of bismuth ion, Bi^{+3} , [process (a)] should, under normal conditions, be easy in view of the fact that the metal is still considerably more noble than either sodium or calcium in melts, just as is true for aqueous solutions. Process (b) cannot be excluded as a possibility when one considers the fact that the electrolyzing voltages were, in all experiments except one, higher by at least one volt than the decomposition voltages which have been obtained by others for both salts from a study of their current-potential curves. Kortüm and Bockris (15) give the following decomposition voltages: NaCl , 3.06 volts at 800°C and CaCl_2 , 3.23 volts at 852°C . Another consideration in support of the process as a possible one is that cathodic discharge of either sodium or calcium would involve the decomposition voltage(s) of the original salt(s) and/or the pyrobismuthite and pentachlorobismuthite formed by interaction of the components. For any one of the salts, the decomposition voltage might conceivably be less than 2.7 volts if its measurement involved using a carbon anode and tungsten cathode. It has been reported [Reference (15), p. 477] that decomposition potentials of cryolite-alumina melts, at low current densities, are 2.10 volts with a platinum anode and 0.98 volt with carbon. However, complete justification for process (b) would require a determination of decomposition voltages for the pure salts under the conditions of this work and cathode potentials for the electrodeposition of bismuth under the same conditions. Evidence for process (c) is not readily available.

Thermodynamic calculation of decomposition voltages for the melts and for various electrode combinations would require the making of an extensive number of fundamental assumptions. However, the number of such assumptions could be reduced considerably if one were to make a kinetic study of the slight interaction which takes place between the components of the mixtures.

SUMMARY

1. Bismuth metal of high purity can be obtained by the electrolysis of molten mixtures of Bi_2O_3 (10% and 25%) and either the NaCl-CaCl_2 eutectic mixture or the single salts.

2. Conditions for electrodeposition of bismuth from such melts are not critical in spite of the fact that

slight interaction does occur between the components of the melts.

3. A tungsten cathode and carbon anode appear to be the best electrode combination employed in the work.

4. A discussion is given of the nature of the interaction between the components of the mixtures and the reactions by which the bismuth metal was formed.

5. Results reported herein are sufficiently encouraging to warrant research now in progress to ascertain more completely the applicability of the process to the large-scale production of bismuth metal from ores.

Any discussion of this paper will appear in a Discussion Section to be published in the June 1955 issue of the JOURNAL.

REFERENCES

1. R. B. LEIGHOU, "Chemistry of Engineering Materials," 4th ed., p. 195, McGraw-Hill Book Co., New York (1942).
2. E. F. KERN AND T. R. JONES, *Trans. Am. Electrochem. Soc.*, **57**, 255 (1930); V. BAGERLE, *Rec. trav. chim.*, **44**, 514 (1925); J. LUKAS AND A. JILEK, *Chem. Listy*, **21**, 541 (1927); M. HARBAUGH AND F. C. MATHERS, *Trans. Am. Electrochem. Soc.*, **64**, 293 (1933); A. MOHN, *Electrochem. Met. Ind.*, **5**, 314 (1907)
3. P. DROSBACH, *Z. Elektrochem.*, **44**, 124 (1938); *ibid.*, **43**, 897 (1937)
4. R. B. LEIGHOU, *ibid.*, p. 195.
5. C. I. MANTELL, "Industrial Electrochemistry," 3rd ed., p. 323, McGraw-Hill Book Co., New York (1950); H. J. CREIGHTON AND W. A. KOEHLER, "Principles and Applications of Electrochemistry," 2nd ed., Vol. II, p. 191, John Wiley & Sons, Inc., New York (1944).
6. C. SANDONNINI, *Gazz. chim. ital.*, **50**(I), 289 (1920), V. P. BARZALOVSKII, *J. Applied Chem (U.S.S.R.)*, **13**, 1117 (1940).
7. W. F. ROESER AND H. T. WENSEL, *J. Research Natl. Bur. Standards*, **10**, 275 (1933), RP-530.
8. J. D. EDWARDS, C. S. TAYLOR, A. S. RUSSELL, AND L. F. MARANVILLE, *This Journal*, **99**, 527 (1952); C. SANDONNINI, *op. cit.*
9. W. F. HILLEBRAND, G. E. F. LUNDELL, H. A. BRIGHT, AND J. I. HOFFMAN, "Applied Inorganic Analysis," 2nd ed., p. 238, John Wiley & Sons, Inc., New York (1953).
10. L. KAHLENBERG AND H. H. KAHLENBERG, *Trans. Am. Electrochem. Soc.*, **46**, 183 (1924).
11. L. BELLADEN, *Gazz. chim. ital.*, **52**(I), 160 (1922).
12. M. M. P. MUIR, G. B. HOFFMEISTER, AND C. E. ROBBS, *J. Chem. Soc.*, **39**, 32 (1881).
13. J. ALOY AND A. FRÉBAULT, *Bull. Soc. Chim.*, (3), **35**, 397 (1906).
14. J. W. MELLOR, "A Comprehensive Treatise on Inorganic and Theoretical Chemistry" Vol. IX, p. 647, Longmans, Green and Co., New York (1929).
15. G. KORTÜM AND J. O'M. BOCKRIS, "Textbook of Electrochemistry," Vol. II, p. 476, Elsevier Publishing Co., New York (1951).

Mechanism of the Reaction of Hydrogen with Zirconium

I. Role of Oxide Films, Pretreatments, and Occluded Gases¹

E. A. GULBRANSEN AND K. F. ANDREW

Westinghouse Research Laboratories, East Pittsburgh, Pennsylvania

ABSTRACT

Previous studies have shown the reaction of zirconium with hydrogen to be sensitive to surface preparation, surface films, heat treating cycles, cold working of the metal, and nonmetallic impurities.

Experiments were made on the rate of reaction of high purity zirconium with pure hydrogen using a sensitive microbalance method, and an all glass and ceramic vacuum system to minimize contamination.

The effect of a preliminary vacuum heating cycle on rate of reaction with hydrogen at 150°C was studied by varying the temperature of the vacuum heating cycle from 150° to 700°C. Samples having the room temperature oxide present showed only a slow rate of reaction, while samples heated to 700°C for one hour showed a rate of reaction 7700 times as great. Results also showed that the oxide film was effectively removed by heating in a vacuum for one hour at 500°C.

A study was made of the thickness and nature of the oxide film. Thus, the film formed in air at room temperature was more resistant to hydrogen attack than thicker oxides formed at higher temperatures. Studies on the effect of small quantities of oxygen and nitrogen in solid solution indicate only minor effects. Results suggest that considerable revision is necessary in concepts of the mechanism of the hydrogen reaction on metals.

INTRODUCTION

Occlusion of hydrogen by metals has been the subject of a large number of scientific studies (1); however, comparatively minor attention has been given to the question of rate of reaction. Unfortunately, many experimental studies on exothermic occluders such as zirconium appear to have been made under poorly defined experimental conditions and conclusions drawn from inadequate data. Therefore, the mechanism of occlusion has been found to be complicated, and the influence of surface preparation, cold working of the metal, occluded gases, hydrogen pretreatment, oxide films, and composition of the gas atmosphere is not understood.

A simple physical chemical analysis of the rate of occlusion would show that a number of separate processes are involved for metals such as zirconium. These are: first, preliminary processes at the surface, including chemisorption of the molecule and subsequent splitting apart of the molecule into atoms or ions; second, diffusion of hydrogen atoms, ions, or molecules through the oxide or other surface film; third, transfer at the metal-oxide interface of the hydrogen molecule, atom, or ion from the oxide into the metal; fourth, diffusion of hydrogen along grain boundaries or through the metal lattice; fifth, formation and growth of one or more hydride phases.

From an experimental point of view, it is difficult to separate the rate-controlling process from the other rate processes. This is especially true for zirconium where two phases may exist. In addition, stable oxide films and other contaminating films form readily on the metal surface, and these may retard reaction with hydrogen. These films may dissolve in the metal at higher temperatures under vacuum or inert gas atmospheres and reappear if the rate of film formation is greater than the rate of solution of the oxide into the metal. Therefore, it has been difficult to study the relative influence of oxide films and the physical structure of the metal, and many unusual physical effects have been noticed for this reaction.

Occlusion of hydrogen by zirconium has been reviewed by Smith (1). De Boer and Fast (2) and Hägg (3) have studied the solubility of hydrogen and find that at room temperature the solubility corresponds to $ZrH_{1.95}$. Desorption occurred on lowering the pressure. Hydrogen was stated to be more soluble in the β -form, and the transition between α and β forms occurs at 865°C. Hall, Martin, and Rees (4) have studied the solubility of hydrogen in zirconium and zirconium-oxygen solid solutions at temperatures up to 1000°C and at pressures of 1–760 mm of Hg. Special care was used to remove the contaminating influence of oxide and other films. These authors suggested that much of the disagreement on the temperature at which hydrogen reacts with zirconium was due to poor experimental techniques and the

¹ Manuscript received August 20, 1953. This paper was prepared for delivery before the New York Meeting, April 12 to 16, 1953.

presence of surface films. The effect of oxygen on occlusion capacity showed that oxygen diminishes the quantity of hydrogen taken up by a volume equivalent to the oxygen solution.

Crystal structures of the hydrogen-zirconium system have been studied by Hägg (3). Four hydride phases were observed. Hydrogen was adsorbed up to 5 atom % in the hexagonal close-packed lattice without an appreciable change in lattice parameters. An expansion of 15.4% occurs in zirconium for a hydrogen pickup corresponding to $H/Zr = 1.92$ (5).

Gulbransen and Andrew have studied the rate of reaction of hydrogen with zirconium specimens containing room temperature oxide film (6). Very little reaction occurred at 200°C while a more rapid reaction was found at 300°C. The effect of pressure on rate of reaction followed a square root relationship. The reaction was found to be very sensitive to pretreatment and surface films. A similar square root of pressure relationship was found for the rate of flow of hydrogen through Zr at temperatures between 375° and 920°C by Bernstein and Cubicciotti (7).

In this work the role of oxide films, pretreatments, and occluded gases on the rate of reaction of hydrogen with zirconium was studied.

Interpretation of the nature of the Occlusion Process

Theories on the variable rate of reaction.—An analysis of literature on the occlusion process for exothermic occluders such as zirconium indicates that two theories exist for the variable rate of reaction observed when zirconium is exposed to hydrogen. The first is the "rift theory" of occlusion developed by Smith (1). In this theory an expanding and contracting series of rifts are used to explain active and passive states of the metal. The second is the oxide film theory in which a coherent thin oxide film prevents access of hydrogen to the metal. However, this oxide dissolves in the metal at high temperature under high vacuo conditions. Clean metal is then exposed for reaction. The most recent work supporting this point of view is that of Hall, Martin, and Rees (4).

Before presenting the authors' work, it is of interest to indicate the main experimental characteristics of the occlusion process upon which Smith has developed the rift theory of occlusion. It should be noted that much of the work was made on specimens probably contaminated with oxide and other films.

Smith's characteristics of the occlusion process.—

(A) Metal is inert to gaseous hydrogen at room temperature and normal pressure in its ordinary form. (B) If gradually heated the metal begins to react at an indefinite opening temperature. (C) The rate of reaction is self-accelerating in its early stages. (D) At high pressures the metal in its ordinary state reacts and is permeable at lower pressures. (E) Metal

in its ordinary state reacts with hydrogen liberated upon it by chemical displacement or by electrolysis.

(F) Permeability of metal to hydrogen may be increased or decreased by repeated absorption and evolution of hydrogen, apparently depending upon the rate with which the gas is expelled. (G) Metal heated to high temperatures in vacuo is inert to gaseous hydrogen and may be impervious to cathodic hydrogen. (H) Permeability is increased by plastic deformation, in some cases manyfold. This increase is accompanied by an increase in occlusive capacity.

In addition to these general characteristics Smith gives five additional characteristics of exothermic occluders such as zirconium. (I) After a metal is heated to an activation temperature above that described in (B), the metal possesses for some time an induced high permeability at ordinary temperatures and pressures. This is known as thermal activation. (J) This high permeability declines gradually at a rate which differs from one lot of metal to another. (K) Metal having high permeability and charged with hydrogen loses its permeability slower than if uncharged. (L) If heated and cooled while charged with hydrogen, the metal shows decreased permeability and does not give up its hydrogen to vacuum until heated to above its opening temperature. (M) In the composition range of two solid phases, exothermic occluders show smaller permeability and occlusion capacity during absorption than during evolution of hydrogen. This phenomena is called hysteresis.

It is, of course, impossible to test all of these characteristics in one paper. However, results obtained in this work should be related in each case to the characteristics given by Smith and checked with the two theories of occlusion.

EXPERIMENTAL

A vacuum microbalance was used for all measurements (8). The 0.0127 cm thick specimens had surface areas of about 10 cm² and weighed 0.500 gram. Sensitivity of the balance was 1 division (0.001 cm) per microgram, and weight change was estimated to 1/4 of a division (0.25×10^{-6} gram). A mullite furnace tube was used to contain the specimen and was sealed directly to the Pyrex apparatus. The vacuum system, behavior of which has been studied previously (9), was of all glass construction and could be evacuated readily to pressures considerably lower than 10^{-6} mm of Hg.

Pure hydrogen was prepared by diffusing purified electrolytic hydrogen through a palladium tube (10). A special gas train was used for preparing pure oxygen. Reagent grade nitrogen was used for preparing zirconium specimens with given nitrogen contents.

Two sources of high purity iodide zirconium were

TABLE I. Analyses of zirconium samples

	(W) APD Zr		Footo Zr
	Spec. %	Chem. %	Typical
Si	0.002-0.007		0.01
Fe	0.037-0.049	.01	0.04
Al	0.0027-0.0037		0.01
Cu	(0.0005-0.0030)		<0.01
Ti	0.002-0.003		0.03
Mn	0.005		<0.001
Ca			0.01
Mg	(0.001)		<0.003
Pb	(0.0025)		<0.001
Mo	(0.001)		<0.001
Ni	0.0025-0.004		0.01
Cr	0.001-0.0018	.003	0.001
Sn	<(0.001)		0.001
W	0.010		<0.001
N		.001-.0025	<0.01
O		(.020)	<0.01
H		(.002)	<0.02
C		(.010)	<0.001
Hf			2.40

() Outside limits or isolated values.

used. The first² contained 2.4% hafnium, and the second³ was a hafnium-free zirconium. Spectrographic and chemical analyses are given in Table I.

All specimens used had previously been abraded starting with 0 and finishing with 4/0 emery paper. The last two papers were used under purified kerosene. Samples were then cleaned successively with soap and water, distilled water, petroleum ether, and absolute alcohol. After a preliminary weighing, specimens were placed in a desiccator until ready for use. Chemically polished specimens were dipped in a solution of 40 cc nitric acid, 40 cc water, and 10 cc hydrofluoric acid.

RESULTS AND DISCUSSION

To study the rate of hydriding of zirconium it was necessary to devise a test procedure which gave a reaction rate characteristic of an oxide-free metal and a reaction rate which was reproducible. Since the oxide film normally present on the surface cannot be reduced in the case of zirconium oxides, it was necessary to remove the oxide by heating in high vacuo. It was found that heating the specimen to 700°C in a vacuum of 10^{-6} mm or less for one hour gave a reproducible reaction rate with hydrogen. For convenience the conditions of 150°C and a pressure of 2.4 cm of Hg were chosen. The reaction showed no evidence of an induction period.

Results are given in terms of weight gain in micro-

² Prepared by the Footo Mineral Company.

³ Made by the Westinghouse Atomic Power Division and secured through the courtesy of the Atomic Energy Commission.

grams/cm² and plots are made of weight vs. time in minutes.

Effect of temperature of vacuum heating.—To show the effect of vacuum heating procedures on rate of hydriding at test conditions, specimens were heated for 1 hr at a series of temperatures in high vacuo before cooling to 150°C to determine the rate of hydriding. If it is assumed that the rate of reaction with hydrogen at low temperatures was limited by the presence of oxide films, vacuum heating at higher temperatures, which tends to dissolve the oxide, should increase the rate of reaction. In experiments presented here vacuum heating was made in the same apparatus as the rate study and without intermediate exposure to a gas atmosphere of any kind.

Fig. 1 and 2 show the results. A new specimen was used for each experiment. Curve A in Fig. 1 was the reaction of a specimen having the room temperature equilibrium film, while curve B shows the rate of attack after a preheat of one hour at 150°C. Curves A, B, and C of Fig. 2 show the rate of attack with hydrogen after preheats of one hour at 300°, 500°, and 700°C. It was found that the 500° and 700° experiments gave similar rates of attack. Curves B and C were typical of many tests for these conditions of

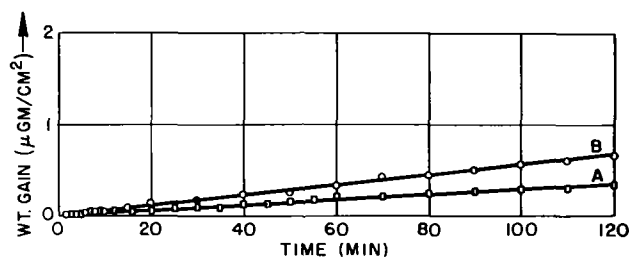


FIG. 1. Effect of time and temperature of heating on hydriding of Zr at 150°C, 2.4 cm of Hg of H₂. Curve A—room temperature equilibrium film; curve B—preheated 150°C, 1 hr.

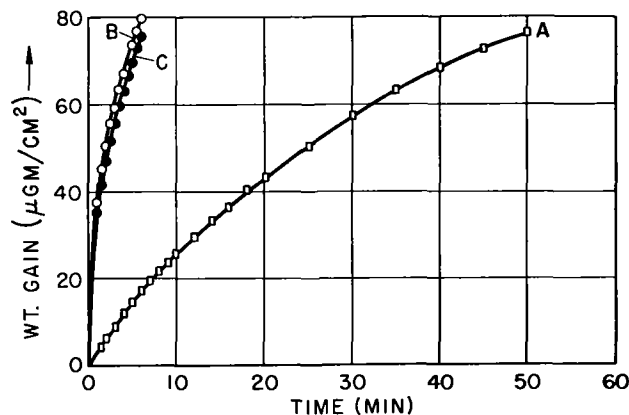


FIG. 2. Effect of temperature of heating on hydriding of Zr at 150°C, 2.4 cm of Hg of H₂. Curve A—preheated 300°C, 1 hr; curve B—preheated 500°C, 1 hr; curve C—preheated 700°C, 1 hr.

pressure and temperature. Results were reproducible within the limits of experimental error.

The rate of reaction for curve A of Fig. 1 was zero for the first 5 min and averages 0.473×10^{-4} $\mu\text{g}/\text{cm}^2/\text{sec}$ for the first 2 hr. Curve C of Fig. 2 shows a rate of reaction of $0.365 \mu\text{g}/\text{cm}^2/\text{sec}$ for the first 2 min. The ratio of the rate of reaction of specimens having the room temperature oxide present to the specimen annealed at 700°C was 1/7700. An even greater ratio would be found if the rates were calculated for the one-minute time interval.

Results can be interpreted readily by the oxide film theory. Thus, the inert character of the metal in its ordinary state can be attributed to the normal room temperature oxide film having a thickness of the order of 10 to 50 \AA . This film is transparent and is an effective barrier to diffusion of gaseous hydrogen. It dissolved gradually into the zirconium as the temperature of heating was raised and the rate of reaction, therefore, was greatly increased. There appears to be no evidence that high heating of a metal such as zirconium renders it inert as interpreted by Smith (1).

Effect of thickness and character of oxide films on rate of reaction.—Fig. 3 shows weight gain vs. time curves for a series of oxide pretreatments in which the thickness and character of the oxide was studied. Curve A shows the weight gain curve for the specimen containing the room temperature equilibrium oxide. Curve B shows the rate of reaction for a specimen having been preheated under high vacuo to 700°C for one hour and then exposed to 0.1 atm pressure of oxygen at 25°C for 20 hr. Curve C shows the rate of reaction for a specimen which had been annealed at 700°C and then oxidized at 150°C at an oxygen pressure of 7.6 cm Hg for 5 min to form an oxide film 63 \AA thick. Curves D and E show the effect

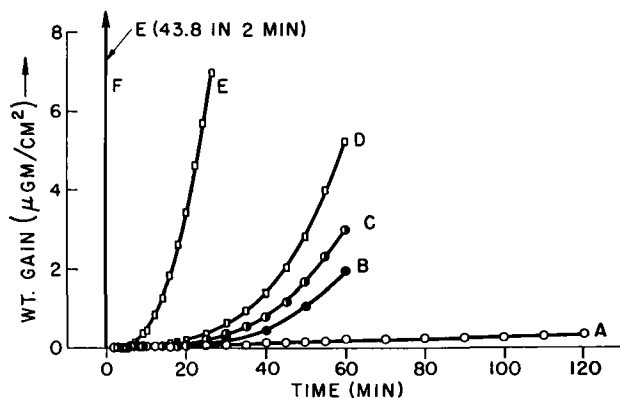


FIG. 3. Effect of oxide on hydriding of Zr, 150°C , 2.4 cm H_2 . Curve A—room temperature equilibrium film; curve B—preheated +20-hr exposure to O_2 at room temperature; curve C—preheated +63 \AA film at 150°C ; curve D—preheated +500 \AA film at 250°C ; curve E—preheated +500 \AA film at 275°C ; curve F—preheated, no film.

of oxide films of 500 \AA thickness formed at 250° and 275°C , while curve F shows the rate of reaction of a film-free specimen.

These results again may be explained on the basis of a coherent oxide film which dissolves slowly in the metal at temperatures of 250°C and higher. In general, oxides formed at room temperature have the greatest effects on rate of hydriding. The thicker films formed at temperatures of 250° and 275°C are less resistant to hydriding for two reasons. First, solution of the film occurs which diminishes the film thickness. Second, the oxides formed at higher temperatures have a larger crystallite size. Thus, the fitting of the grains of oxide may be less perfect, and a greater porosity would be noted.

The fact that rate of reaction increases with time can be attributed to gradual breakdown of the oxide film physically by passage of hydrogen as well as to the gradual solution of the oxide into the metal.

Again the oxide film theory appears to explain observed facts better than the rift theory.

Comparison of source of zirconium.—Fig. 4 and 5 show a comparison of reaction rates for two sources of zirconium.^{2,3} Fig. 4 shows comparison of the rate of reaction of the two specimens having the room

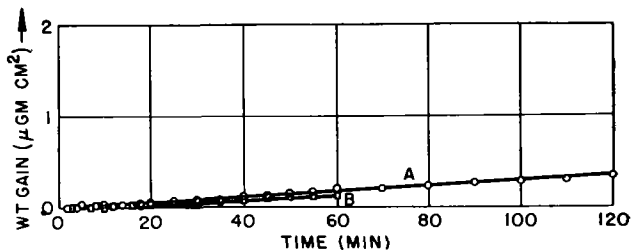


FIG. 4. Comparison of source of Zr. Curve A—room temperature equilibrium film, Foote Zr, hydriding 150°C , 2.4 cm of Hg of H_2 ; curve B—room temperature equilibrium film, A.P.D. Zr, hydriding 150°C , 2.4 cm of Hg of H_2 .

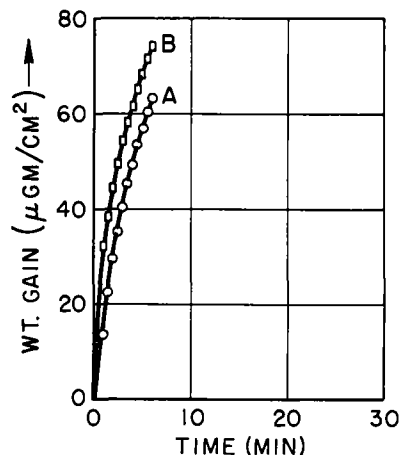


FIG. 5. Comparison of source of Zr. Curve A—Foote Zr, preheated 1 hr, 700°C , hydriding 150°C , 2.4 cm of Hg of H_2 ; curve B—A.P.D. Zr, preheated 1 hr, 700°C , hydriding 150°C , 2.4 cm of Hg of H_2 .

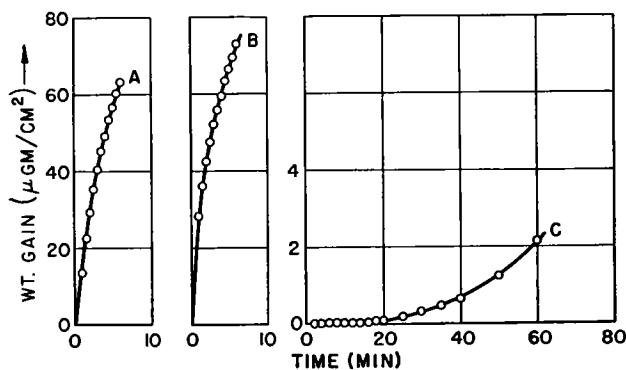


FIG. 6. Effect of pretreatment on hydriding Zr 150°C, 2.4 cm of Hg of H₂. Curve A—preheated 700°C, 1 hr; curve B—preheated-hydrided 150°C, heat up 700°C; curve C—preheated-hydrided 150°C, heat up 700°C, room temperature oxidation.

temperature equilibrium oxide film present, while Fig. 5 shows a similar comparison for the 700°C annealed specimens. Agreement between results for the two sources of zirconium was good.

Effect of successive hydrogen treatments and exposure to O₂.—Smith (1) has stated that successive hydrogen treatments affect permeability and occlusive capacity of the metal. In early stages of the reaction up to a H/Zr ratio of 0.2, no such evidence was observed providing one is working with an oxide-free zirconium surface.

Three rates of hydriding experiments were compared in Fig. 6. Curve A shows the control experiment with the rate of hydriding determined after the 700°C vacuum anneal. Curve B shows a rate of hydriding experiment for a sample which was given a high vacuo anneal at 700°C, hydrided at 150°C to 100 μg/cm² or to ZrH_{0.2}, the hydrogen removed by heating to 700°C then cooled to 150°C for the second hydriding. Curve A shows a total reaction of 57 μg/cm² for 5 min while Curve B shows a total reaction of 66.5 μg/cm² for 5 min. A small change appears in the rate of reaction due to previous adsorption and desorption of hydrogen in the lattice. However, the effect is a minor one when compared to the effect of oxide films. This is shown in curve C of Fig. 6. In this experiment the sample was heated, hydrided at 150°C, heated to 700°C, exposed to room temperature oxygen, then hydrided at 150°C. The effect of room temperature oxidation was great.

More experiments will have to be made to determine effect of the reaction of large quantities of hydrogen and subsequent removal on the rate of hydriding. Small quantities adsorbed and removed have only minor effects on the rate of hydriding.

Effect of oxygen in solid solution.—Samples of zirconium were heated to 700°C to dissolve the oxide film, then dosed with oxygen to give samples having 0.16, 0.027, 0.064, and 0.068 weight per cents

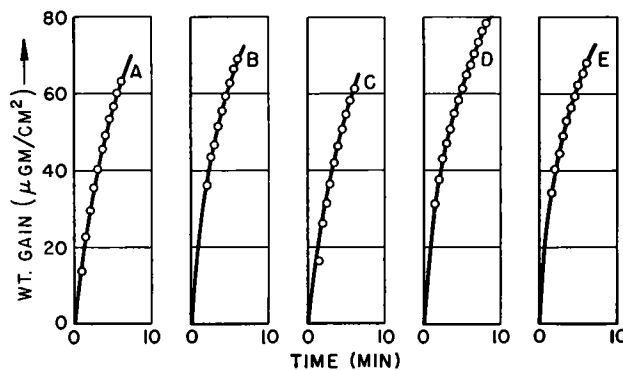


FIG. 7. Effect of dissolved oxygen on hydriding of Zr 150°C, 2.4 cm of Hg of H₂. Curve A—700°C preheated 1 hr; curve B—0.016% O₂ added, preheated 1 hr; curve C—0.027% O₂ added, preheated 1 hr; curve D—0.064% O₂, preheated 1 hr; curve E—0.0679% O₂ added, preheated 1 hr.

of oxygen above the oxygen content of the original metal. Specimens were then heated in vacuo for 1 hr at 700°C to homogenize the oxygen before cooling to 150°C where further reaction with hydrogen occurred. Rapid homogenization was assumed to occur in the one-hour vacuum anneal at 700°C for the following reasons: (a) thickness of the specimens was only 0.0127 cm with both sides of the specimen exposed to the original oxygen treatment; (b) the small amounts of oxygen that had to be homogenized; (c) the high rate of attack of zirconium with oxygen at 700°C.

Results are shown in Fig. 7. The curves show total weight gain values varying from 55 μg/cm² to 63 μg/cm² after 5 min of reaction. Within experimental error, oxygen in solid solution in small amounts exerts only minor effects on the rate of hydriding at 150°C.

Effect of nitrogen in solid solution.—Samples of zirconium were prepared as described above except that reagent grade nitrogen gas was used to dose the

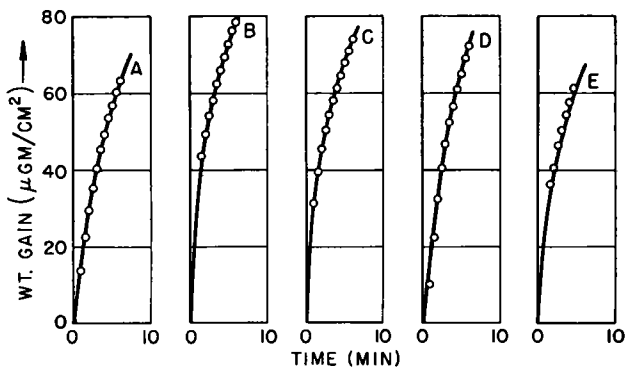


FIG. 8. Effect of dissolved nitrogen on hydriding of Zr 150°C, 2.4 cm of Hg of H₂. Curve A—700°C, preheated 1 hr; curve B—0.0095% N₂ added, preheated 1 hr; curve C—0.0196% N₂ added, preheated 1 hr; curve D—0.0491% N₂ added, preheated 1 hr; curve E—0.096% N₂ added, preheated 1 hr.

samples with given amounts of nitrogen. Thus, samples having 0.0095, 0.0196, 0.0491, and 0.096 weight per cent of nitrogen above the original nitrogen content were prepared. Again homogenization was assumed to occur in a one-hour vacuum treatment at 700°C for reasons given above. Results are shown in Fig. 8. As in the case of oxygen in solid solution, the curves show that small amounts of nitrogen have only minor effects on the rate of reaction.

SUMMARY AND CONCLUSIONS

High purity zirconium containing the room temperature equilibrium oxide film reacts very slowly with hydrogen at 150°C and 2.4 cm of Hg pressure, and in a self-accelerating manner. Similar specimens preheated in high vacuo at temperatures above 500°C for one hour react very rapidly with hydrogen at 150°C and 2.4 cm of Hg pressure without an induction period. The ratio of the rate of reaction for the preheated specimens relative to those not preheated was 7700 or greater.

Results were interpreted in terms of an oxide film limiting the rate of reaction, this film dissolving in the metal as the temperature of annealing was raised. Thus the oxide film present on the unannealed specimen limits the rate of reaction and imposes an induction period on the reaction.

Previous work summarized by Smith, showing that vacuum heating the metal decreases the rate of reaction of hydrogen, may be interpreted now as due to formation of an oxide or other contaminating film.

Further experiments show that the nature of the oxide film was very important in its resistance to hydrogen. Thus, room temperature equilibrium

oxide films were more resistant to hydrogen than thicker oxide films formed at higher temperatures. This was explained in part by a partial solution of the oxide and to the presence of larger oxide crystallites in the films formed at higher temperatures.

Small amounts of dissolved oxygen and nitrogen up to 0.1 weight per cent have only a minor effect on the rate of hydriding at 150°C.

Successive hydrogen treatments show only minor effects on the rate of hydriding for hydrogen adsorptions up to 0.2 atom of H per atom of Zr.

Many of the unusual occlusive characteristics given by Smith may be interpreted on the basis of the oxide film theory which offers an effective resistance to the reaction with hydrogen at low temperatures.

Any discussion of this paper will appear in a Discussion Section, to be published in the June 1955 issue of the JOURNAL.

REFERENCES

1. D. P. SMITH, "Hydrogen in Metals," University of Chicago Press, Chicago (1948).
2. J. H. DE BOER AND J. D. FAST, *Rec. trav. chim.*, **55**, 459 (1936).
3. G. HÄGG, *Ztsch. Phys. Chem.*, **B11**, 433 (1931).
4. M. N. A. HALL, S. L. H. MARTIN, AND A. L. G. REES, *Trans. Faraday Soc.*, **41**, 306 (1945).
5. A. SIEVERTS, A. GOTTA, AND S. HALBERSTADT, *Z. anorg. u. allgem. Chem.*, **187**, 156 (1930).
6. E. A. GULBRANSEN AND K. F. ANDREW, *Trans. Am. Inst. Mining Met. Engrs.*, **185**, 515 (1949).
7. R. B. BERNSTEIN AND D. CUBICCIOTTI, *J. Phys. and Colloid Chem.*, **55**, 238 (1951).
8. E. A. GULBRANSEN, *Rev. Sci. Instr.*, **15**, 201 (1944).
9. E. A. GULBRANSEN AND K. F. ANDREW, *Ind. Eng. Chem.*, **41**, 2762 (1949).
10. E. A. GULBRANSEN, *Trans. Electrochem. Soc.*, **81**, 187 (1942).

Electrical Properties of Semiconducting AlSb¹

R. K. WILLARDSON, A. C. BEER, AND A. E. MIDDLETON²

Battelle Memorial Institute, Columbus, Ohio

ABSTRACT

Measurements of some of the electrical properties of the compound AlSb indicate semiconducting characteristics comparable with those reported for silicon. Data were taken on the electrical resistivity, thermoelectric power, and Hall voltage as a function of temperature over the range from 80° to 1200°K. The energy band separation, as determined from the temperature dependence of the conductivity, is 1.5 to 1.6 ev. Mobilities of electrons and holes are approximately equal and are greater than 100 cm²/volt-sec at room temperature. Rectification characteristics are given for both *P*- and *N*-type samples of various resistivities. Both photovoltaic and photodiode effects were observed.

INTRODUCTION

During the past decade, much effort has been applied to the preparation and investigation of semiconducting properties of such elements as silicon, germanium, selenium, and tellurium. The object of this research has been not only to develop useful devices such as transistors and rectifiers, but also to interpret the properties of these elements in terms of modern theories of solids. Such extension of our knowledge concerning these fundamental processes is obviously of value whether one is interested in improving the characteristics of existing components, in developing new devices, or in the discovery and evaluation of new semiconducting materials. Electronic-device development has, in fact, proceeded to such a stage that a great variety of materials having special semiconducting characteristics are desired. To be more specific, in certain applications a high mobility of the charge carriers is of prime importance. Of the elements in common use at the present time, germanium exhibits the highest mobility. On the other hand, many applications require concentrations of minority carriers to be small over the temperature range of operation. Hence, the energy separation between filled and conduction bands must be sufficiently large so that the intrinsic contribution to the conductivity is negligible. Since this energy gap in silicon is approximately 1.1 ev as compared to 0.72 ev in germanium, it is understandable why extensive work is now being done on silicon for use in high temperature rectifiers and transistors.

In addition to elements such as those discussed above, a number of compounds have semiconducting properties. Several well-known examples of these are lead sulfide, cadmium sulfide, and cuprous oxide.

¹ Manuscript received April 13, 1953. This paper was prepared for delivery before the New York Meeting, April 12 to 16, 1953.

² Present address: P. R. Mallory and Company, Inc., Indianapolis, Indiana.

Many other binary compounds which are semiconductors are known. In particular, it has been noticed that a large number of elements combine with antimony to form useful semiconducting materials. For example, with elements in Column I of the periodic table, such as Cs, Rb, and K, antimony combines to give compounds, such as Cs₃Sb, which find extensive use in photoemissive cells. From Column II, one obtains Mg₃Sb₂, whose semiconducting properties have been studied in detail by Boltaks (1), Zhuse (2), and others. The other series of elements in Column II yield materials of lower intrinsic resistivity, such as ZnSb and CdSb. The properties of these compounds have been studied by Telkes (3), and by Justi and Lautz (4). Elements of Column VI, when combined to form the compounds Sb₂S₃ (5), Sb₂Se₃ (6), and Sb₂Te₃, are also known to exhibit semiconducting properties.

Antimony also forms compounds with elements of the third column of the periodic table, that is, with aluminum, gallium, and indium. These compounds are especially interesting since they possess the zincblende crystal structure. At the initiation of the present investigations, there was no information available on the electrical properties of these compounds. Recently, however, a publication by Welker has appeared (7). Welker contrasts the structural and electrical characteristics known for the elements diamond, silicon, germanium, and gray tin of the fourth column of the periodic table with those expected for the general series of compounds composed of elements from the third and fifth columns. Specifically, these compounds are AlSb, InSb, GaSb, AlAs, InAs, GaAs, AlP, InP, and GaP.

PHASE DIAGRAM AND CRYSTAL STRUCTURE

Equilibrium studies of the aluminum-antimony system were carried out by Gautier (8) over fifty years ago. He noted that a high melting point was associated with the composition in which an equal

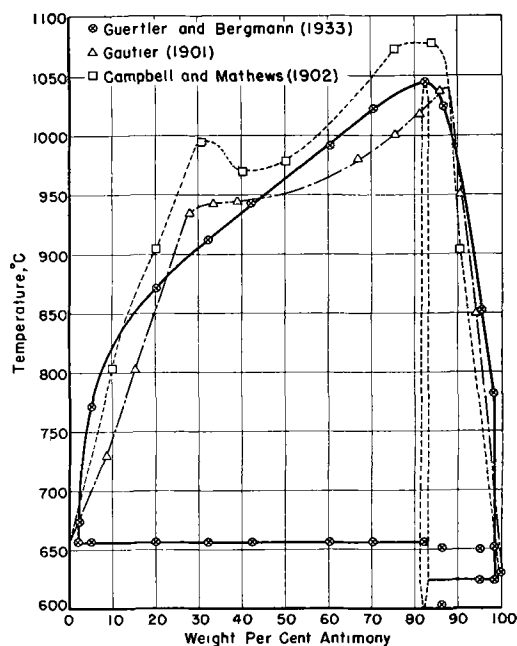


FIG. 1. Phase diagram of the aluminum-antimony system.

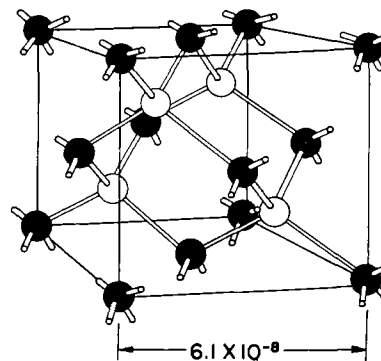
number of aluminum and antimony atoms are present. Subsequent investigations were carried out by Campbell and Mathews (9), and by Tammann (10). It was not until 1933, however, that the currently accepted phase diagram was published by Guertler and Bergmann (11). Results of these investigations are summarized in Fig. 1.

It will be noted that the compound AlSb has a melting point of 1050°C as compared with melting points of 660° and 630°C for aluminum and antimony, respectively.

X-ray studies by Owen and Preston (12) in 1924 indicated that the intermetallic compound AlSb had the zincblende structure with a lattice constant of 6.126 Å. Recent x-ray studies at Battelle confirm the structure type and are in agreement with the reported lattice constant. These measurements indicate a lattice constant of $6.1361 \pm 0.0003 \times 10^{-8}$ cm as compared with the Owen and Preston value which, when converted from kx units, is 6.138×10^{-8} cm.

The structure of a unit cell of AlSb is shown in Fig. 2. Atoms of one element may be pictured as defining a face-centered cubic arrangement, while those of the second element define a similar configuration which interpenetrates the first. Hence, a total of 8 atoms—4 Al and 4 Sb—are contained in the unit cell. Each antimony atom has 4 aluminum atoms as nearest neighbors, at a distance of 2.657×10^{-8} cm. They are connected by a two-electron homopolar bond.

It is to be noted that the AlSb structure and bonding are similar to those of germanium and silicon. These semiconducting elements possess the diamond structure, a crystal form to which that of AlSb would



**Face-Centered Cubic
Diamond Structure**

Diamond
Silicon
Germanium
AlSb

Lattice Constant

3.5597×10^{-8} cm
5.431
5.657
 6.1361 ± 0.0003

FIG. 2. Crystal structure of the compound AlSb

reduce if both atoms were identical. The lattice constants of diamond, silicon, germanium, and AlSb are also given in Fig. 2.

RESISTIVITY AND ASSOCIATED PROPERTIES

Electrical resistivity, thermoelectric power, and Hall measurements were made over a temperature range from 80°K to 1200°K on a number of samples of aluminum antimonide containing different extrinsic carrier concentrations. The specimens, which were polycrystalline, were carefully annealed in order to reduce inhomogeneities in the samples, such as grain-boundary effects.

Specimens were measured, which showed resistivities ranging from 1×10^{-2} ohm-cm to 32 ohm-cm, at room temperature. These specimens had charge-carrier concentrations, determined from the Hall measurements, which ranged from 4×10^{19} to 1.5×10^{15} per cm^3 . The specimen containing 1.5×10^{15} carriers/ cm^3 has a resistivity of 32 ohm-cm at 25°C. Germanium with the same *P*-type carrier concentration would have a resistivity of around 2 ohm-cm.

Resistivity data are shown in Fig. 3. It was noted that the general shapes of the AlSb resistivity curves were remarkably similar to those of polycrystalline silicon containing boron impurities, except for the higher intrinsic slope in the case of AlSb. Resistivity data for silicon, as reported by Pearson and Bardeen (13), are consequently indicated by the dashed curves in Fig. 3. Carrier concentrations at room temperature as determined from the Hall measurements are shown for both AlSb and silicon specimens. Measurements presented in Fig. 3 were taken on *P*-type material, and mobilities of positive holes were computed from the resistivity and Hall data. The Hall coefficient as function of temperature for these specimens is shown in Fig. 4. Again, silicon curves from the data of

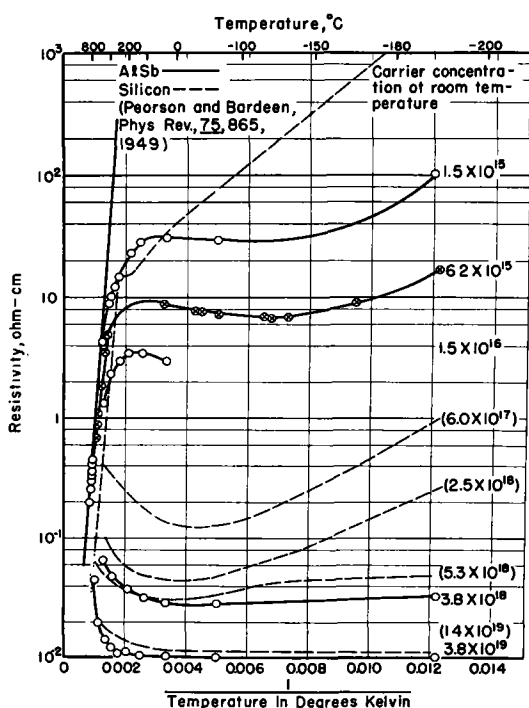


Fig. 3. Resistivity of AlSb as a function of temperature

Pearson and Bardeen are shown for comparison. Especially interesting is the fact that the Hall coefficient for AlSb begins to decrease at temperatures lower than those at which it decreases for silicon. This decrease is due primarily to the increase in the number of the minority *N*-type carriers from the filled band. Also, the sign of the Hall constant does not reverse in the intrinsic region. Both of these facts

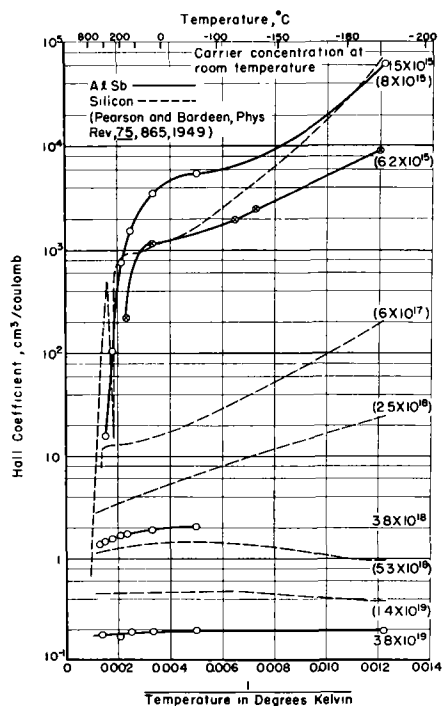


Fig. 4. Hall coefficient of AlSb as a function of temperature.

indicate that the ratio of the electron mobility to hole mobility in AlSb is nearly unity. Hence, the ratio of the effective mass of the electrons to that of the holes is also about one. In this respect, AlSb is different from silicon and germanium, where the effective mass of the electron is significantly less than that of the holes. For samples containing less than 10^{16} impurities/cm³, lattice scattering predominates even at temperatures as low as 80°K, and the temperature dependence of the mobility approximates quite closely the $T^{-3/2}$ relationship. Magnitudes are very close to those reported for polycrystalline *P*-type silicon. In particular, room temperature mobility for the positive holes in AlSb was observed to be 100 cm²/volt-sec. As was found in the case of silicon, it is to be expected that the crystallite boundaries might give a significant contribution to the resistivities measured on the polycrystalline specimens. Hence, the value given above can be considered only as a lower boundary. Values obtained for single crystals may be much larger. For ionized impurity concentrations greater than 10^{17} /cm³, impurity scattering causes a reduction in the mobility at low temperatures. In fact, in the specimen containing 3.8×10^{19} carriers/cm³, the mobility has been reduced, even at room temperature, to about 15 cm²/volt-sec.

Another observation on an AlSb sample containing 1.5×10^{15} carriers/cm³ was that the thermoelectric power changed from positive to negative at 275°C. In the sample with 6.2×10^{15} *P*-type carriers, the crossover temperature increased to approximately 500°C.

An approximate value of the energy-band separation in a semiconductor can be obtained from the slope of the $\log \rho$ vs. $1/T$ curve in the intrinsic region. Such a calculation gives a value of approximately 1.5 to 1.6 eV for AlSb.³ This is somewhat larger than that of silicon, which is approximately 1.1 eV. A very important practical consideration is connected with the width of this forbidden band. This factor is important in determining the upper limit to the temperature at which a semiconductor device can be operated. For example, with germanium, having a band separation of 0.72 eV, the present upper limits of operation are 70°–80°C for most operations. With silicon, on the other hand, *P-N* junction diodes have been reported to operate at temperatures as high as 300°C.

RECTIFICATION AND PHOTOEFFECTS

When a metallic point contact is made with an impurity semiconductor as shown in Fig. 6 (lower

³ Note added in proof: Since the presentation of this paper, there has appeared a publication by H. WELKER in *Z. Naturforsch.*, **8a**, 248 (1953). His value of 1.65 eV for the energy-band separation in AlSb is in good agreement with the above result.

right corner), an asymmetric nonlinear current-voltage relationship is observed. If the semiconductor is *P*-type and the metal point is negative, a low resistance to the current is obtained, while for reversed polarities, a high resistance occurs. Such a device is called a *P*-type point-contact rectifier.

A number of specimens of AlSb were investigated for rectification and photoelectric phenomena. Rectification was found at point contacts of several different metals with polycrystalline AlSb specimens of various resistivities. Current-voltage characteristics for several such rectifiers are shown in Fig. 5. It will be noted that both *P*- and *N*-types of rectification were obtained. Although a number of different metals of widely varying work functions were used for the point contact, it was not possible to correlate observed rectification characteristics with differences in work functions. A somewhat similar situation has been reported by Meyerhof (14) in connection with silicon point-contact rectifiers.

Some rectifiers made from specimens containing *P-N* junctions exhibited saturation regions in their forward characteristics. In these cases, when the contact was moderately illuminated with white light, photoelectric effects were observed. Changes in forward current in the saturation region by as much as 100% were observed. The same contacts exhibited photo-emf's up to 25 mv. Similar observations have been reported for germanium by Benzer and others (15).

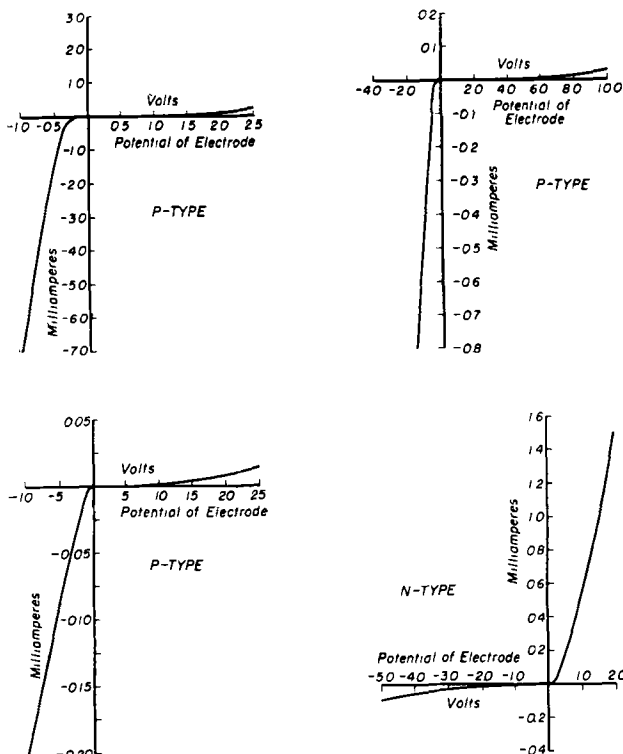


FIG. 5. D-C current vs. voltage characteristics for AlSb rectifiers.

Characteristics of AlSb point-contact rectifiers are compared in some detail with those of silicon rectifiers in Fig. 6 and 7. For this purpose, a more informative presentation of the current-voltage characteristics of semiconductor rectifiers is used. Fig. 6 shows the reverse and forward current variations with applied voltage of a *P*-type AlSb point-contact rectifier compared with those for Si rectifiers made from polycrystalline Si reported by Scaff and Ohl (16) in 1947. In addition to the similarity between the rectifiers, it will be noted that the rectification ratio at one volt for the AlSb rectifier, although slightly less than that for the Si, is about 800.

Fig. 7 shows characteristics for *N*-type AlSb point-contact rectifiers. These have been compared with the characteristics for improved point-contact silicon rectifiers reported by Ohl (17) in 1952. Improvement was obtained through bombardment by helium ions. It will be noted that the *N*-type AlSb rectifiers compare favorably with these silicon rectifiers. Rectification ratios as high as 10,000 at 4 volts are apparent. Although peak inverse voltages are low in the AlSb and the silicon rectifiers shown in the figure, higher peak inverse voltages can be obtained. For example, in other experiments, for which data are not presented in the figures, voltages

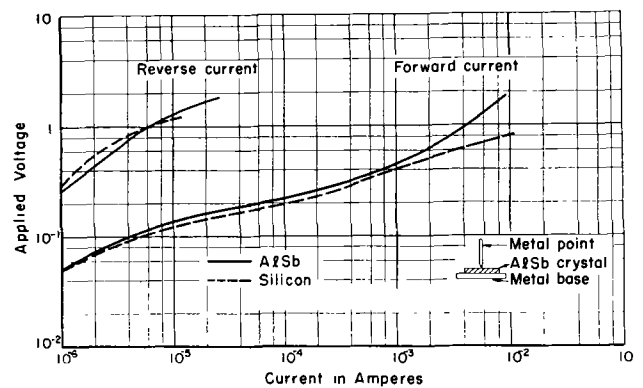


FIG. 6. Logarithmic plot of the d-c current vs. voltage characteristics for *P*-type AlSb and silicon.

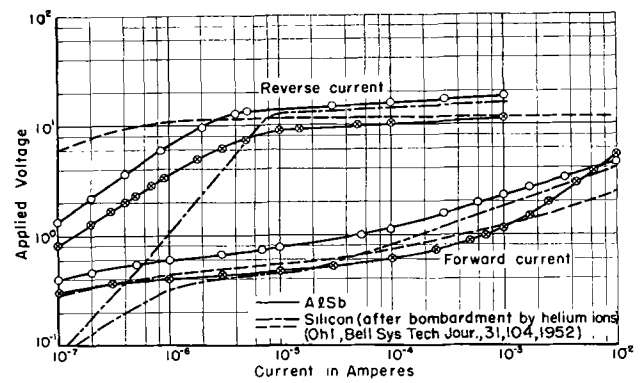


FIG. 7. Logarithmic plot of the d-c current vs. voltage characteristics for *N*-type AlSb and silicon.

as high as 90 volts were applied in the reverse direction without damage to the AlSb rectifiers.

CONCLUSIONS

In summary, this work has revealed that the compound AlSb can be considered as a new addition to the germanium and silicon family of semiconductors. Its structure is the diamond structure; its electrical properties vary with changes in amount of atomic imperfections in a manner strikingly similar to that of silicon. A wide range of electrical resistivities varying from 1×10^{-2} to greater than 30 ohm-cm has been achieved in homogeneous polycrystalline materials, and both *P*- and *N*-type electrical conductions were obtained. Outstanding differences between electrical properties of AlSb and Si appear to be the equivalence of electron and hole mobilities and the energy gap of 1.5 to 1.6 eV in AlSb as compared, respectively, with the 4 to 1 ratio and 1.1 eV gap for Si.

Also like Si, AlSb will make rectifying contacts with many different types of metal points. These rectifying contacts are characterized by low peak inverse voltages in the case of material with large carrier concentration, and higher peak inverse voltages in material with smaller charge-carrier concentrations. Further, preliminary evidence has been obtained to show that AlSb point-contact devices can be produced to act as electrical switches on exposure to light as well as used to convert light to electrical energy.

Appraisal of collected data on AlSb suggests that it may have advantages over Ge and perhaps Si for high temperature electronic-device applications of interest to the military. Its melting point being only 1050°C, whereas that of Si is 1420°C, indicates that procedures for processing AlSb may be more easily evolved than for Si.

Besides these advantages, the cost of high purity Al and Sb comparable in purity to the Ge and Si used as starting materials in rectifier and transistor manufacture is markedly smaller; for example, high purity Al and Sb cost less than \$5/lb as compared to \$300/lb for Ge and Si.

Based on these findings, it is apparent that further

efforts to develop AlSb for use in place of Ge and Si in solid-state electronic devices should be rewarding.

ACKNOWLEDGMENTS

The authors are indebted to H. Goering, S. Miller, and R. Heiks for the preparation of specimens, to O. Huber and C. Schwartz for precision lattice-constant determinations, and to C. Meyer for assistance with electrical measurements. Consultations with C. Peet concerning the contact phenomena were appreciated. The research on AlSb presented herein was carried out under sponsorship of the Bradley Mining Company, to whom the authors wish to express their thanks for permission to publish these results.

Any discussion of this paper will appear in a Discussion Section to be published in the June 1955 issue of the JOURNAL.

REFERENCES

1. B. I. BOLTAKS AND V. P. ZHUSE, *J. Tech. Phys., U.S.S.R.*, **18**, 1459 (1948).
2. V. P. ZHUSE, I. V. MOCHAN, AND S. M. RYOKEN, *ibid.*, **18**, 1494 (1948).
3. M. TELKES, *J. Appl. Phys.*, **18**, 1116 (1947).
4. E. JUSTI AND G. LAUTZ, *Wissenschaftl. Abhandl.*, **4**, 107 (1952).
5. G. FREY, *Arkiv Kem. Mineral. Geol.*, **11A**, No. 4, 1 (1932).
6. B. D. CULLITY, M. TELKERS, AND J. T. NORTON, *Trans. Am. Inst. Mining Met. Engrs.*, **188**, 47 (1950).
7. H. WELKER, *Z. Naturforsch.*, **7a**, 744 (1952).
8. H. GAUTIER, *Contrib. à l'Étude d'alliages*, **112** (1901).
9. W. CAMPBELL AND J. MATHEWS, *J. Am. Chem. Soc.*, **24**, 259 (1902).
10. G. TAMMANN, *Z. anorg. Chem.*, **48**, 54 (1906).
11. W. GUERTLER AND A. BERGMANN, *Z. Metallkunde*, **25**, 81 (1933).
12. E. Z. OWEN AND G. D. PRESTON, *Proc. Phys. Soc., London*, **36**, 341 (1924).
13. G. I. PEARSON AND J. BARDEEN, *Phys. Rev.*, **75**, 865 (1949).
14. W. E. MEYERHOF, *ibid.*, **71**, 727 (1947).
15. H. C. TORREY AND C. A. WHITMER, "Crystal Rectifiers," p. 394, McGraw-Hill Book Co., New York (1948).
16. R. S. OHL AND J. H. SCAFF, *Bell Sys. Tech. Jour.*, **26**, 1 (1947).
17. R. S. OHL, *ibid.*, **31**, 104 (1952).

Surface States of Cadmium Sulfide¹

S. H. LIEBSON

Electricity Division, Naval Research Laboratory, Washington, D. C.

ABSTRACT

Photoconductive and phosphorescent properties of cadmium sulfide are modified by adsorbed molecules. Change in spectral response of photoconductivity and the phosphorescence efficiency when crystals are exposed to vapors suggest that surface states due to adsorbed molecules aid in recombination. Photovoltaic behavior of rectifying contacts lends credence to the hypothesis that infrared releases otherwise immobile holes.

INTRODUCTION

Electron traps play an important role in conduction processes in photoconductors, affecting such properties as spectral sensitivity of photoconductivity and time for rise or decay of photoconductivity due to intermittent irradiation (1). For highly photoconductive hexagonal cadmium sulfide, surface localization of a considerable portion of the traps has been reported (2). The extent to which these surface states modify electrical behavior of this crystal must be evaluated for proper application of photoconductivity theories based on isotropic bulk properties. Experiments are performed in which effects due to adsorbed vapors predominate in the measurements.

Since it is difficult to grow photoconductive cadmium sulfide with any degree of quantitative reproducibility of electrical and photoconductive properties, particular attention must be paid to results which indicate a consistency independent of the magnitude of observed effects. The crystals for which data are presented (3) were grown by a modified form of Frerichs' method (4). Cadmium vapor with argon as vehicular agent is fed into a spherical quartz oven to react with H₂S. Crystals grow from vapor produced by the reaction and phosphorescence observations are made on them; their red phosphorescence has been attributed to excess cadmium (5). For photoconductive measurements those crystals are chosen which show little or no red phosphorescence under ultraviolet excitation.

QUENCHING OF PHOSPHORESCENCE BY VAPORS

Red phosphorescence of these crystals is measured by means of an RCA Type 6217 photomultiplier with a red filter, such as Corning Type 2-62, covering the photosensitive surface. Crystals are placed on the filter and irradiated with a mercury vapor lamp

used in conjunction with a Corning Type 7-60 ultraviolet filter. Observations are made of the photomultiplier current when vapors of iodine, hydrogen chloride, or water are introduced into the atmosphere near the crystal. A reduction in photomultiplier current is usually observed, taking place in less than one second. For a particular batch of crystals, current reduction due to iodine vapor is a factor of about 1000, the lowest measurable current being determined by ultraviolet excitation of the red filter and photomultiplier combination. With the removal of vapors from the crystal atmosphere, the photomultiplier current usually returns to its original value.

QUENCHING OF PHOTOCONDUCTIVITY BY VAPORS

Bube (6, 7), and Caspary and Müser (8) observed changes in photoconductivity of cadmium sulfide in vacuum. Caspary and Müser observed an increase of up to 20% and Bube reported an increase of more than 60%. Bube found atmospheric moisture to be responsible for decrease in sensitivity and increase in rate of current decay when the exciting light was removed.

To determine spectral photosensitivity of the crystals, they are mounted with nonrectifying indium electrodes (9) and inserted into a brass cylindrical container which can be evacuated to a pressure of about 10⁻⁶ mm Hg. A cylindrical heater is mounted externally. At a rate of 25°C/hr, the crystal is heated to 100°C in an atmosphere of a few microns pressure of helium to effect thermal conductivity between the brass container and the crystal, temperature being measured by a thermocouple adjacent to the crystal. The crystal is cooled to room temperature in vacuum. Measurements are made with the crystal connected in series with a direct current voltage source, of the order of 100 volts, and a current meter. Light from a 100-watt tungsten lamp is focused on the entrance slit of a Gaertner monochromator. Light from the exit slit is reflected by a concave mirror through a quartz

¹ Manuscript received October 12, 1953. This paper was prepared for delivery before the Chicago Meeting, May 2 to 6, 1954.

window onto the crystal in the container. The monochromator slits are kept fixed at 10μ .

Fig. 1 shows results of photosensitivity measurements for the same crystal in vacuum and after exposure to air at 45% relative humidity, room temperature. A current correction is applied so that current plotted in the figure corresponds to equal intensities at each wave length. It is seen that the effect of admitting air is depression of spectral sensitivity over the entire photoconductive spectrum, with a proportionately greater decrease in sensitivity toward the blue end. Fig. 2 illustrates measurements on another crystal. The coincidence in vacuum and in air of photoconductive response beyond the absorption edge at about 5200 \AA (4) may be evidence that, for this crystal, the long wave length sensitivity is primarily determined by its bulk properties. Bube (7) varied the relative humidity and found that the effect of water vapor was current depression for wave lengths shorter than about $5,000 \text{ \AA}$ indicating that internal properties determined the long wave length response of his crystal.

Admission of iodine vapor to the evacuated container reduces current sensitivity of the crystal,

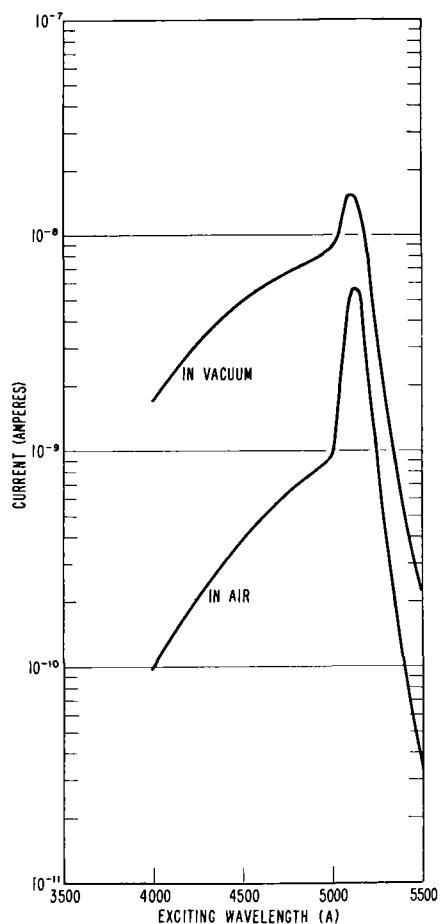


FIG. 1. Spectral sensitivity of a photoconductor before and after exposure to air.

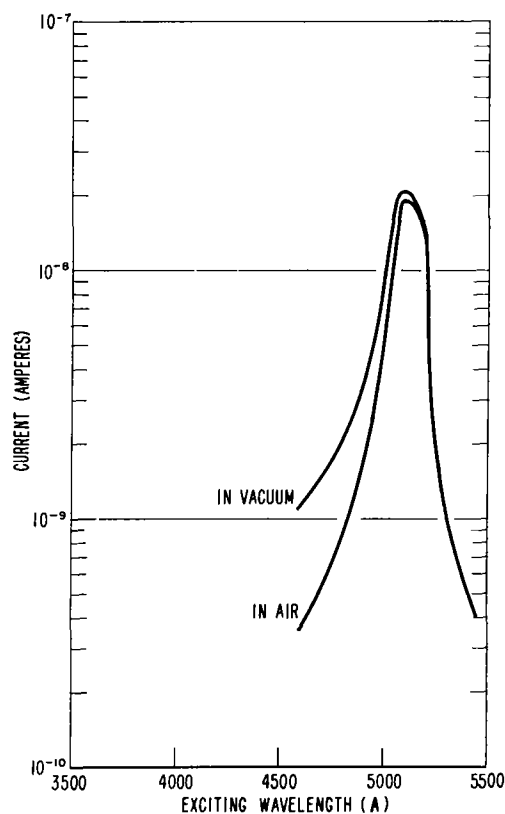


FIG. 2. Spectral sensitivity of a photoconductor with bulk effects dominating long wave length response.

with factors of 100 to 1000 being not uncommon for wave lengths shorter than 5200 \AA .

RECTIFICATION

Other investigators (10-13) have reported that a potential drop usually occurred at the negative electrode on a cadmium sulfide crystal used as a photoconductor, with accompanying rectification. In repeating their experiments, it is found that rectification at broad area colloidal graphite electrodes may be enhanced by exposing the contact to hydrogen chloride for a few seconds, then washing with water. This phenomenon is apparently due to an increased capability of the crystal to take on adsorbed water vapor at the contact, since rectification is greatly diminished when the crystal is in vacuum, and is re-established when moist air is admitted. Crystals are chosen for rectification investigations by probing with a well-defined beam of light to insure that one contact is the major seat of photoconductivity.

Crystals with one predominantly rectifying contact are mounted so that two beams of light can be superimposed on the crystal. An infrared source is provided by the monochromator and lamp described earlier. The other source of light is a 100-watt tungsten lamp with a green filter. Photogenerated

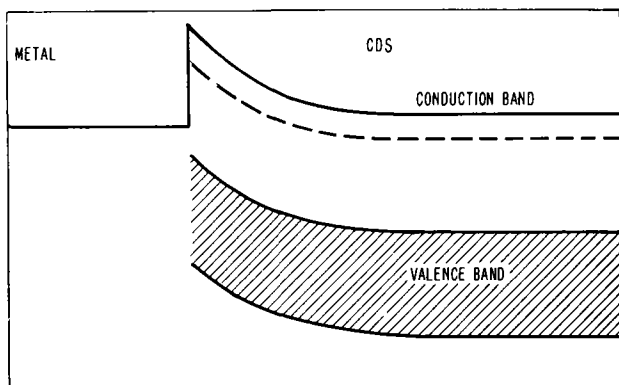


FIG. 3. Energy band diagram of rectifying contact

current at the contact is measured with a Perkin-Elmer breaker type amplifier, whose internal impedance is small compared to that of the contact, while the photogenerated voltage at the contact is measured by a Rubicon potentiometer connected so that its output voltage opposes that generated at the contact. Photogenerated voltage is given by that value of opposing voltage which nullifies current detected by the amplifier.

The effectiveness of infrared in quenching photoconductivity due to green light (2, 4, 14) is proportionately greater with the voltage applied to the crystal in the high impedance direction (electrode at rectifying contact is negative). For many crystals almost no infrared quenching is observed in the forward direction, and for some crystals there is a slight increase in current. The spectrum of infrared quenching centers at about 9000 Å and 14,000 Å identify it as the same phenomenon observed by Taft and Hebb (2).

The sign of the photogenerated voltage due to green light implies the shape of the potential barrier at the contact to be similar to that shown in Fig. 3 (15).

With green light incident at the contact, and with intensity such that photogenerated voltage is not saturated, superposed infrared light increases the generated voltage. Infrared alone produces no measurable photovoltage. Green light generates current at the contact flowing in the high impedance direction. Infrared superposed on green light increases the generated current by an amount considerably greater than is generated by infrared itself, e.g., for one crystal, infrared generated less than 10^{-11} amp, green light generated 3×10^{-11} amp, and green and infrared light combined generated 6×10^{-11} amp.

DISCUSSION

If one assumes that the effect of water vapor at the contact is similar to the effect of water vapor on

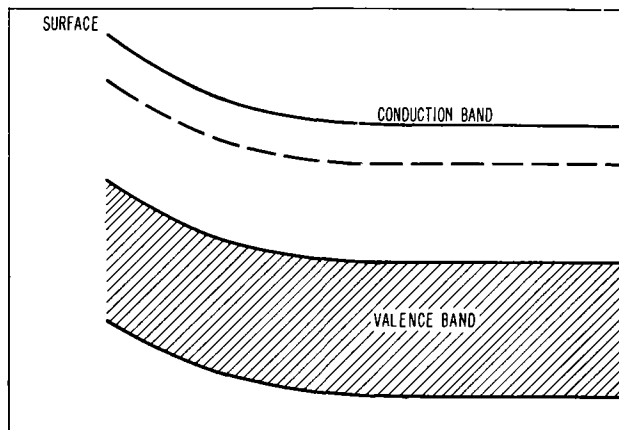


FIG. 4. Energy band diagram for surface with adsorbed vapor.

the crystal surface, these observations suggest an interpretation similar to that discussed by Bardeen (16) in connection with surface states of germanium. The increase in rectification at a contact due to water vapor may be interpreted as being due to an increased number of surface states for electrons made possible by the adsorbed vapor, creating a potential barrier at the contact. The decrease in phosphorescence and photoconductivity due to vapors is explained as being due to increased recombination at the surface, a conclusion previously arrived at by Bube (7) based on photoconductivity and time constant measurements. The infrared effects at the rectifying contact may be explained by the hypothesis of Rose (1) and Taft and Hebb, (2) that infrared frees holes within the crystal. Release of positive holes in the potential barrier at the contact may heighten the barrier and increase its thickness, increasing generated voltage and current. Bube (7) attributed surface effects to a surface conductivity increased by the presence of water vapor, and implied the existence of occupied surface states on "dry" crystals due to an essential difference in the nature of the surface and volume. If the interpretation given here is valid, based on increased rectification due to water vapor at the contact and recombination enhanced by electro-negative or dipolar vapors, the surface states are due to adsorbed molecules. Fig. 4 depicts the energy band diagram for a surface with adsorbed vapors.

Any discussion of this paper will appear in a Discussion Section to be published in the June 1955 issue of the JOURNAL.

REFERENCES

1. A. ROSE, *RCA Rev.*, **12**, 362 (1951).
2. E. A. TAFT AND M. H. HEBB, *J. Opt. Soc. Amer.*, **42**, 249 (1952).

3. M. E. BISHOP AND S. H. LIEBSON, *J. Appl. Phys.*, **24**, 660, 963 (1953)
4. R. FRERICHS, *Phys. Rev.*, **72**, 594 (1947).
5. H. W. LEVERENZ, "An Introduction to Luminescence of Solids," p. 174, John Wiley & Sons, Inc., New York (1950).
6. R. H. BUBE, *Phys. Rev.*, **83**, 393 (1951).
7. R. H. BUBE, *J. Chem. Phys.*, **21**, 1409 (1953).
8. R. CASPARY AND H. MUSER, *Z. Physik*, **134**, 101 (1952).
9. R. W. SMITH AND A. ROSE, *Phys. Rev.*, **92**, 857A (1953).
10. R. W. SMITH, *RCA Rev.*, **12**, 350 (1951).
11. R. FRERICHS, *Phys. Rev.*, **76**, 1869 (1949).
12. H. KALLMANN AND R. WARMINSKY, *Ann. Physik*, **4**, 69 (1948).
13. A. ROSE, P. I. WEIMER, AND S. V. FORGUE, *Phys. Rev.*, **76**, 179 (1949).
14. A. E. HARDY, *Trans. Electrochem. Soc.*, **87**, 355 (1945).
15. N. F. MOTT, *Proc. Roy. Soc. London*, **171A**, 281 (1939).
16. J. BARDEEN, *Phys. Rev.*, **71**, 717 (1947).

Electronic Configuration in Electrodeposition from Aqueous Solutions

I. The Effect of Ionic Structures¹

ERNEST H. LYONS, JR.²

Department of Chemistry, University of Illinois, Urbana, Illinois

ABSTRACT

Consideration of electronic structures of metal ions in aqueous solutions indicates that metals are electrodeposited from ions in which coordinate linkages involve only orbitals of the outermost electronic shell. When coordination involves the penultimate shell also, that is, with Taube's "inner orbital" complexes, the metal is not electrodeposited. Apparently the energy required to break such hybridization exceeds that required for cathodic discharge of hydrogen from these solutions. Platinum metals are exceptions, probably because of extraordinary stability of the metallic state for these elements; deposition, however, requires high activation, as shown by overpotentials and low current efficiencies. Between different oxidation states, electrolytic oxidation or reduction is irreversible if the electronic configuration must be changed significantly. Irreversible deposition is observed for transition metals or when the ion is bound in a hydrolyzed aggregate. Since inner orbital hybridization is associated with a lack of substitutional lability of the coordinated groups, whereas lability of outer orbital complexes probably results from formation of a dissociation intermediate, it is likely that such an intermediate is also important in the cathode process. These considerations are used to account for and extend the Piontelli electrolytic classification of metals. In considering the effects of anions, it is shown that aquo complexes are reduced with highest irreversibility, which is attributed to high activity of water; the influence of halide ions may be labilization by the trans effect.

INTRODUCTION

Metals which have been electrodeposited from aqueous solution lie to the right of the vanadium group in the extended form of the periodic table (1). Near this boundary, deposition occurs with poor cathode efficiencies, high activation overpotentials,³ and close dependence on conditions of electrodeposition. These circumstances suggest that the electrodeposition mechanism is seriously limited in rate, that the hydrogen discharge reaction can easily

become competitive, or that both of these factors may operate. It should be noted, however, that hindered mechanisms of deposition often lead to fine-grained or even bright deposits so that deposition may be relatively simple in its technical applications.

Left of the deposition boundary line discharge of hydrogen becomes easier than that of the metal ion, while far right of the boundary, metal discharge is so easy that little or no hydrogen is produced, overpotentials are low, and ease of deposition is such that coarse, crystalline deposits are common. It is hoped, in the present discussion, to indicate reasons for these differences.

ELECTRODE POTENTIALS

Ordinarily, concentration of metal ions is sufficiently large relative to rate of deposition that concentration overpotentials do not affect the possibility of deposition. Activation overpotentials influence only rate and current efficiency. The equilibrium potential, which is decisive, expresses relative free energies of ionic and metallic states of the metal. In other words, electrode potential is determined by difference between free energy of interaction of a metal ion with whatever groups are coordinated with it in solution, and that of ion interaction with electrons of the metallic phase of the electrode.

¹Manuscript received May 12, 1952. This paper, prepared for delivery before the Montreal Meeting, October 26 to 30, 1952, is taken from a thesis presented to the Graduate College, University of Illinois, in partial fulfillment of the requirements for the degree of Doctor of Philosophy.

²Present address: Department of Chemistry, The Principia College, Elsah, Illinois.

³Overpotential is used here in the ordinary sense, namely, the difference between equilibrium potential with no current flowing and the actual potential observed experimentally when metal (or hydrogen) is being deposited. For a discussion of experimental methods and interpretations, see Reference (2). When overpotentials due to ohmic resistance and concentration effects are removed either experimentally or by calculation, the remaining overpotential is regarded as due to activation requirements for the cathode process. It will be clear that overpotentials refer to kinetic effects, while equilibrium potentials refer to thermodynamic relationships.

According to Butler (3), the difference Ω in free energy between these states is measured by the sublimation energy, χ , equivalent to the lattice energy of the metallic crystals, the sum of the appropriate ionization energies, ΣI , and the coordination energy, W (which is usually simply hydration energy of the ion):⁴

$$\Omega = \frac{1}{z}(\chi + \Sigma I - W) \quad (I)$$

where z is the number of electrons involved in the electrode reaction. The applicability of equation (I) has recently been corroborated (5, 2).

For ions of alkali and alkaline earth metals, hydration energies (4) are very nearly equal to ionization energies. This has been regarded (6-8) as indicating that hydration in effect restores electrons removed in ionization. For these metals, therefore, electrode potential depends mainly on lattice or sublimation energy.

For transition metals, however, hydration energies are not as large as ionization energies; that is, coordination with water does not stabilize these ions as fully as those of alkali metals. Moreover, sublimation energies are high. Accordingly, electrode potentials are more positive than those of alkalis, so that in many cases electrodeposition of metal is favored over that of hydrogen. With zinc, sublimation energy is low, and the electrode potential is quite negative, even though the ionic state is relatively unstable. Hydrogen would be discharged preferentially were it not for its exceptionally high overvoltage on zinc.

ELECTRON CONFIGURATION AND STABILITY⁵ OF COMPLEX IONS

Considering only "simple," aquated ions, energies of hydration, W , change but little through the transition series. Sublimation energies, χ , do not vary significantly. However, because ionization potentials increase, relative instabilities, $\Sigma I - W$, rise. Consequently, electrode potentials become more

⁴ This equation evidently suffers from two difficulties. It neglects entropy effects, which are certainly important. Furthermore, Ω is obtained as a relatively small difference between two large quantities, one of which, W , can only be determined indirectly (4) and with uncertainties which are often as large as Ω . In view of this, the agreement of Ω with electrode potentials as indicated by Piontelli (2) is surprisingly good. For purposes of this discussion, the point to be observed is the importance of coordination energy, W , in determining electrode potentials.

⁵ *Stability* is used to indicate an energy relationship relative to the metallic state. Stability is often taken to refer to tendency to be transformed to the aquated or "simple" ion. As is shown shortly, such thermodynamic stability is not necessarily directly related to the stability considered here.

positive, until with chromium, metal deposition competes with hydrogen discharge. Metal deposition is increasingly favored on through the series until at copper cathode current efficiency reaches 100%.

With cyano complexes, the same trend is seen. Great stability of these complexes is expressed by high values for W . Consequently, electrode potentials are more negative than with aquo complexes, and not until copper is reached do they become sufficiently positive for metal deposition.

Thus, iron, which is deposited with some ease from hexaquo ion in sulfate baths, is not deposited from hexacyano ion. A study of a number of such series indicates that there is a shift in bond type when deposition becomes possible. In the case of iron, bonds in the cyano complex involve stable octahedral d^2sp^3 hybridized orbitals (9), while those of the aquo complex involve much less stable sp^3d^2 orbitals (10).

Since the cuprous ion has a full complement of $3d$ electrons, d orbitals can be made available for hybridization only by unpairing and promotion of electrons. As energy is not available for this process, only less stable orbitals are employed. Consequently, coordination energy is low, the electrode potential is more positive than that of preceding metals, and electrodeposition of copper occurs from cyano ion.

Likewise with aquo complexes, electrodeposition occurs only from ions not involving hybridized $3d$ orbitals.

Taube (10) designates such complexes as "outer orbital," while those in which d orbitals are hybridized with s and p orbitals of the next higher principal quantum number group are termed "inner orbital." Thus, iron is deposited readily from aquo and chloro complexes, which have outer orbital configurations, but not from cyano or *o*-phenanthroline ions, which are of the inner type. Cadmium, which does not form inner orbital complexes because $4d$ orbitals are full, is deposited readily from cyano and *o*-phenanthroline (11) complexes as well as from aquo and chloro ions.

From Table I it is evident that distinction between inner and outer orbital complexes is of fundamental importance in determining whether a metal can be electrodeposited from aqueous solution. Since inner orbitals represent lower energy levels than outer orbitals, inner orbital hybridization represents a configuration of greater energy of coordination, resulting in a metal complex which is more difficult to discharge than hydrogen ion (12).

According to Taube (10), a similar distinction is seen in lability of complex ions toward substitution of coordinated groups by new groups. With outer orbital complexes, substitution is ordinarily complete within a few minutes; with many inner orbital

TABLE I. Classification of metal complex ions according to electronic structure and character of electrodeposition from aqueous solutions.

Inner Orbital Complexes
<i>No deposits obtained:</i> All complexes of Ti, Zr, Hf, V, Nb, Ta; most complexes of Cr, Mo, W; cyano complexes of Mn, Fe, Co, Ni, Ru, Rh, Pd, Os, Ir, Pt; <i>o</i> -phenanthroline complexes of Fe, Co, Ni, Cu, Rh, Ir, and other platinum metals; α, α' -bipyridine complexes of Fe, Co, Ni, Rh, Ir, and other platinum metals.
<i>Deposits obtained only as amalgams:</i> Tetracyano nickelate.
<i>Deposits obtained at low current efficiencies and high activation overpotentials:</i> Many complexes of the platinum metals.
<i>Deposits obtained at high current efficiencies and low activation overpotentials:</i> None
Outer Orbital Complexes
<i>No deposits obtained:</i> Al, Be, Mg.
<i>Deposits obtained as amalgams only:</i> Alkali metals, Ca, Sr, Ba, probably Sc, Y, lanthanide metals.
<i>Deposits obtained only at low current efficiencies and high activation overpotentials:</i> None
<i>Deposits obtained at high current efficiencies and low activation overpotentials:</i> Aquo and chloro complexes of Mn, Fe (II), Co (II), Ni, Cu (II), Zn, Cd, Hg, Ga, In, Tl, Pb, Sn, pyrophosphate complexes of Cu, Zn, Cd, Sn; amino complexes of Ni, Cu, Ag, Zn, Cd; <i>o</i> -phenanthroline complexes of Zn and Cd; thiosulfate complexes of Cu and Ag; iodo complexes of Ag, Cd, and Hg; thiostannate; cyano complexes of Cu, Ag, Au, Zn, Cd, Hg, Tl, and In; hydroxo complexes of Zn and Sn; and others.

Notes

1. Current efficiencies are considered high, for the purposes of this table, if they exceed about 50%.

2. Activation overpotentials are considered low, for the purposes of this table, if they are markedly less than those commonly observed (2) with the transition metals and the platinum group in general, if they are less than about 0.05 volt.

3. Certain entries in the table are based on experimental work by the author to be described in a later paper.

4. Deposition from certain ions, such as Cr(III) and Co(III), although it may appear to occur from an inner orbital complex, actually takes place from a lower valence state. Details of such cases are discussed below.

complexes, substitution requires several hours. However, inner orbital complexes are labile in substitution reactions if unoccupied inner *d* orbitals remain after d^2sp^3 hybridization. Taube attributes this last type of lability to the possibility of using vacant *d* orbitals to form activated addition complexes with coordination number of seven as intermediates in the substitution process [cf. (13)]. Since reduction to metal requires removal of coordinated groups, such an addition mechanism is unlikely to facilitate deposition; accordingly, this type of substitutionally labile complex is unsuitable for electrodeposition.

In contrast, lower stability of outer orbital hy-

bridization favors dissociation, an essential step in electrodeposition. With such complexes, Taube supposes that substitution proceeds by a dissociation mechanism. Similarly, it is likely that dissociation of one or more coordinated groups is the first step in electrodeposition.

DEPOSITION FROM LOWER COORDINATE IONS

Metals of the copper and zinc groups, which are deposited with current efficiencies of 100% under suitable conditions, have coordination numbers usually not exceeding four. For tetrahedral ions, such as zinc, cadmium, and mercuric, hybridization is outer orbital sp^3 . Taube considers substitution in these ions to occur by an addition mechanism, using outer *d* orbitals. However, since metal deposition proceeds readily, it is likely that dissociation requires little energy, in accordance with the type of hybridization.

Furthermore, existence of dicyano and tricyano ions in equilibrium with tetracyano ions (14) suggests that dissociation is very easy.⁶ The tricyano cuprate(I) ion is present in solutions of tetracyano cuprate (14), and copper is deposited at 100% current efficiency if the formal cyanide concentration is so limited that a substantial fraction of copper must be in tricyano form. With silver, only dicyano and tricyano complexes are known; and with gold(I), only the dicyano. As these ions are outer orbital hybrids, dissociation to a species of lower coordination number would require little energy.

Although relatively high activation overpotentials have been reported for deposition from these ions, these potentials are in reality due to concentration effects (18), for they are very highly dependent on the ratio of metal ion concentration to total cyanide concentration. Glasstone (18) found the activation overpotentials too low to be measured, and postulates such ions as $[Cu_2CN]^+$, $[Cu_3CN]^{++}$, $[Ag_2CN]^+$, and $[Ag_3CN]^{++}$ as intermediates in deposition. Evidence for such ions is found in the high solubility of silver cyanide in solutions of silver nitrate, existence of solid $2AgNO_3 \cdot AgCN$, and transport evidence for $[Ag_2I]^+$ and $[Ag_3I]^{++}$ (19). Moreover, such ions would not be repelled by negative cathode charge.

Exceptionally low thermodynamic dissociation constants of cyano complexes of copper, silver, and gold reflect high stability relative to formation of

⁶ The ions might be partially hydrated so as to retain the coordination number of four. However, the thermodynamic dissociation constant of tetracyano ion into tetraquo ion and four cyanide ions is 2×10^{-27} (15). This exceedingly low value indicates that water does not compete effectively with cyanide ion for positions in the coordination sphere. Furthermore, solid salts of the di- and tricyano ions have been obtained, with lower coordination numbers (16, 17). For these reasons, partial aquation does not seem probable.

aquo complexes, even though dissociation in the sense of loss of a cyano group with consequent lowering of coordination number evidently demands little energy. Low thermodynamic dissociation constants do not always correspond to low substitutional lability (10, 13). However, inner orbital complexes, which are so stable that the equilibrium concentration of "free" metal ion or aquo complex is experimentally inappreciable, do not undergo rapid substitutions.

According to Taube (10), the dsp^2 structure of coplanar tetravalent ions suggests that substitution reactions will be rapid because a relatively stable p orbital is available to form an addition intermediate. This, however, would not facilitate electrodeposition, and since an inner d orbital is involved, the stability is too high to favor dissociation. Accordingly, although the tetracyano nickelate ion is particularly labile in substitution reactions, it furnishes only thin "flash" deposits in electroplating (20, 21).

However, deposition proceeds at high efficiencies and low activation overpotentials from aquo and cyano complexes of zinc and cadmium. This is to be expected from their outer orbital configurations. Platinum and palladium are deposited, though with difficulty, from square coplanar ions; yet it is clear that tetrahedral structure is far more favorable for electrodeposition than square configuration, on account of lesser stability of outer orbital hybridization.

CHANGE OF OXIDATION STATE

The ferrocyanide ion is not electrolytically reduced to metal in aqueous solutions, yet the ferrocyanide-ferricyanide couple is reversible (22). Hence activation for oxidation and reduction is low. Even though the ions have inner orbital configurations, little activation is needed for reaction (23), for no essential change in configuration occurs. Similar reversibility is observed for iron complexes of *o*-phenanthroline and α, α' -bipyridine (22), which also have inner orbital structures, and others (24-33). Besides these, there are many reversible couples of outer orbital complexes for which no important change in configuration appears probable, as ferric-ferrous, thallic-thallicous, ceric-cerous (34), copper complexes of ammonia and of citrate (35), and chromic-chromous (36).

But, because the ions in each pair differ in structure, change of configuration is necessary with the following irreversible couples (37): stannic-stannous, plumbate-plumbite, arsenate-arsenite (acid solution), tetracyano nickelate(II)-tricyano nickelate(I), chromate-chromic, vanadyl-vanadate, and others (38).

Evidently transfer of electrons between ion and electrode requires little activation (even where two

electrons are involved, as with thallium), unless change of configuration occurs (23).

ELECTRODEPOSITION OF METALS

Chromium.—Although its hexaquo(III) ion has an inner orbital configuration, chromium is deposited from chromic sulfate baths (39). Low cathode efficiencies, often less than 50%, and high oxygen content of the deposit (1-4% as chromic oxide) indicate that reduction is difficult.

The presence of chromous ions is vital (40). Reduction to the chromous state is reversible or nearly so (36). At the dropping mercury electrode, reduction to metal proceeds through this state (41). Electrodeposition from the chromic bath is very similar to that from the chromous bath (40). It appears, therefore, that configuration of the chromous complex is decisive.

As with other complexes having four inner d orbitals occupied by single electrons, the configuration is uncertain and even the coordination number is unknown (10). Magnetic moment measurements indicate four unpaired electrons. In view of reversibility of the chromic-chromous couple (36), it may be supposed that d^2sp^3 hybridization is preserved, with the fourth electron in a $4d$ orbital. This corresponds to susceptibility of chromous ion to oxidation, but offers no explanation of deposition. It may be that the equilibrium concentration of a more favorable configuration of nearly equal energy is sufficient to facilitate electrodeposition.

Furthermore, chromic complexes show somewhat greater substitutional lability than is predicted by Taube's classification, indicating that the ion is near the arbitrary border line. This fact likewise suggests the presence of a less stable configuration.

Chromium is also deposited from the hexavalent state in chromic acid baths in presence of a critical concentration of an anion such as sulfate or fluosulfate, usually regarded as a catalyst. At best, the range of temperature and current density for deposition is sharply restricted. The cathode efficiency is generally less than 15%, and the deposit contains large amounts of hydrogen (42) and oxygen (43). Chromic ion is produced during deposition. Moreover, chromate ion is reduced to chromic both electrolytically (44) and by cathodic hydrogen (42). It has been shown that radioactive chromic ion added to the bath is not reduced to metal, suggesting that it does not participate in the electrode process (45). It is possible that access to the cathode may be denied by a barrier film (46). Both chromic and chromous states are probably involved in reduction, just as at the dropping mercury cathode (47).

Molybdenum and tungsten.—From molybdate and tungstate ions, which are of inner orbital type, the

metals have been deposited as alloys with iron and other metals. The difficulty in depositing pure metals is attributed to hydrogen overvoltage effects (48). Metal deposition with cathode efficiencies of about 2% has been reported (49, 50), but deposition ceases after thin films are obtained, and the purity apparently was not examined; reduction was considered to be effected by cathodic hydrogen rather than electrolytically. Tungsten (51), but not molybdenum (52), is deposited at the dropping mercury cathode.

Cobalt.—Aquo cobalt(II) complexes are readily reduced to metal at the cathode, although with considerable activation overpotential. Reduction is also irreversible at the dropping mercury electrode. The chemical resemblance of cobalt(III) to chromium(III) complexes extends to electrodeposition (53). Cathode efficiencies are generally below 5% and many deposits are powdery. Such deposits contain considerable quantities of hydrogen and oxygen, supposedly as basic material,⁷ and this indicates irreversible reduction.

Electronic configurations of cobaltic complexes, which have a special resemblance to their chromic counterparts (9), are of the inner orbital type. It is probable that deposition proceeds through the cobaltous state as at the dropping mercury electrode (54), with a change to outer orbital sp^3d^2 hybridization. Reduction of hexammino cobalt(III) ion involves aquation of the cobalt(II) ion, since the ammino cobalt(II) ion is unstable (54); pronounced irreversibility of reduction is therefore to be expected.⁸

According to Taube (10), the hexaquo cobalt(III) ion is more labile in substitution reactions than the corresponding ammino ion. Both are diamagnetic, but the paramagnetic state with sp^3d^2 hybridization is only slightly above the ground state in energy. The hexafluoro ion is paramagnetic (9, 55). As water is intermediate in polarizability between fluoride ion and ammonia, the diamagnetic state is not stabilized as much in these ions as in the ammine; Taube considers that there is a sufficient amount in the paramagnetic state to account for lability.

This circumstance would be expected to favor electroreduction of the hexaquo cobalt(III) ion, but observation of this effect would be difficult because the ion is rapidly reduced by water. In deposition from hexammino ion, cobaltous ions doubtless are

reduced to metal about as rapidly as they are produced from the stable cobaltic state. Relatively high pH of the bath favors production of powdery deposits through partial precipitation of hydroxide or basic salts. When ethylenediamine is present these deposits are not powdery, but smooth and metallic because of stability of the chelate (53).

Nickel.—In 6-covalent nickel complexes, hybridization is either sp^3d^2 , with two unpaired electrons in 3d orbitals, as indicated by magnetic studies, or alternatively, d^2sp^3 , with the single electrons in 4d orbitals (10). On the basis of substitutional lability, Taube indicates that the first, or outer orbital configuration, represents hexammino and tris(ethylenediamino) ions. From both, satisfactory electrodeposits are obtained at current efficiencies of around 90% and with high activation overpotentials.⁹ The bipyridine complex is of the inner orbital type, and deposits are not obtained from it. Analogous to the ammine, the hexaquo complex is of the outer orbital type, and accounts for deposition from ordinary sulfate baths.

The cyano complex of nickel has a square, coplanar configuration, and hybridization is inner orbital dsp^2 (10). At a solid cathode, deposition is limited to a flash plate (21). As soon as the cathode is covered with nickel, the complex is reduced only to tricyano nickelate(I) ion (20). The change in configuration accounts for irreversibility of this reduction. Due to high hydrogen overvoltage of mercury, compared with that of nickel, cyano complex is reduced to the amalgam at the dropping mercury cathode, but reduction is highly irreversible (56). 4-Covalent nickel complexes are both diamagnetic and paramagnetic (57). The latter should permit electrodeposition.¹⁰ While there is no direct evidence that paramagnetic complexes are tetrahedral, such configuration is very likely (58). The alternative explanation, that bonds are largely ionic with square configuration (59), also suggests that electrodeposition is possible.

Iron and manganese.—Iron and manganese (60) are deposited from aquo complexes with outer orbital configurations. Activation overpotentials are high. In aqueous solutions, complexes with inner orbital coordination, such as cyano compounds, are not reduced to metals. An exception is manganese, which is deposited at the dropping mercury cathode from hexacyano ion because of higher hydrogen overvoltage of mercury (61). Since iron is nearly

⁷ Considerations to be presented later suggest that this is probably water.

⁸ M. W. Grieb of the University of Illinois has found that reduction is reversible in the presence of excess ethylene diamine which stabilizes cobalt(II) against aquation. The significance of this observation will be discussed in a later paper.

⁹ When the current efficiency drops below 100%, the activation overpotential is high. Low overpotentials have not been observed for nickel, even when current efficiency was 100%, within experimental error.

¹⁰ Experimental studies of electrodeposition from these complexes will be reported later.

insoluble in mercury, it is not deposited from cyano complex.

Technetium (62) and rhenium (63) have been deposited, but the character of the processes has not been reported.

Platinum metals.—In ions of platinum metals, inner orbitals are available without electron promotion, and all complexes are presumably of inner orbital type, with configurations which are either square planar dsp^2 or octahedral d^2sp^3 (64). Nevertheless, deposits of all the metals are obtained, although with low cathode efficiencies, often less than 10%.

The metals are of exceptional stability, as is evidenced by high densities and melting points. Heats of sublimation must be very high; for platinum an estimate of 4.86 eV is given (65). On this account, Ω is more positive than would be expected from stability of the complexes alone, thereby making electrodeposition possible.

In conformity with their inner orbital configurations, the octahedral complexes are not labile in substitution reactions (10). In no other instance is electrodeposition possible with substitutionally inert ions unless they pass through a labile lower oxidation state. With platinum metals, high sublimation energy appears to be decisive.

Oxidation potentials of various ion-metal couples are generally more positive than that of hydrogen by an amount sufficient to make deposition possible even if hydrogen overvoltages are ignored (66). As a direct result of inner orbital stabilities, dissociation and subsequent reductions are slow and take place at low current efficiencies and high overpotentials.

Even high sublimation energies are not enough to make deposition possible from the very stable cyano complexes, with the possible exception of those of palladium (67, 68) for which the cathode efficiency is less than 1%. However, reduction of cyano complexes to lower oxidation states is reported for all platinum metals.

Platinum is deposited from divalent chloro, nitro, amino, phosphato, and hydroxo complexes. Deposition from platinum(IV) complexes proceeds through the divalent state. Calculations indicating high efficiencies are probably in error because of the presence of lower oxidation states (69). At the dropping mercury electrode, platinum catalyzes hydrogen evolution (70) and is not deposited under usual circumstances (68, 71).

The platinum black used in potentiometry is a typical powdery deposit. It is obtained from inner orbital hexachloroplatinate(IV) ion through the tetrachloroplatinate(II) state (72). The latter ion is also inner orbital type, like all platinum complexes, but it is thermodynamically unstable, disproportionating to give the metal and platinum (IV) ion

(73), which sometimes produces colloidal metal in the bath (74), and accounts for the powdery form of the deposit. This disproportionation of an inner orbital complex reflects exceptional stability of the metallic state. However, electrolysis is apparently predominant in deposition (71).

Electrodeposition of palladium is closely similar. The tetrachloropalladate(II) ion, although somewhat more stable than the corresponding platinum complex, is rapidly reduced in the cold by hydrogen (75). It is reported that palladium is deposited at the dropping mercury electrode (68).

In electrodeposition, ruthenium, osmium, and iridium are similar to platinum. However, the actual oxidation state from which deposition occurs is uncertain, and configurations are octahedral rather than square. The metals are not deposited at the dropping mercury cathode (68).

Rhodium is deposited with comparably low current efficiencies, from trivalent complexes similar to those suitable for platinum. It is also deposited from phosphato and oxalato complexes, and from the aquo complex in sulfate, fluoroborate, and perchlorate solutions with somewhat higher current efficiencies (76). Moreover, rhodium is deposited at the dropping mercury electrode (77).

Titanium and vanadium group metals.—As ions of the titanium and vanadium groups have several unoccupied d orbitals, their complexes are inner orbital. Consequently, deposition of the metals from aqueous solution is not to be expected. The "simple" ions are hexaquo complexes which are too stable to undergo reduction before hydrogen is discharged. Efforts to deposit the metals on solid or mercury cathodes have been unsuccessful (78).

Alkali and alkaline earth metals.—As already discussed, the negative potentials of alkali and alkaline earth metals result from low stability of the metallic state. Accordingly, the metals are not deposited except as alloys, particularly as the amalgams. In obtaining Ω , sublimation energy χ must be replaced by energy of amalgamation. This makes the electrode potential sufficiently positive to permit deposition (79). There is, of course, no possibility of inner orbital complexes; consequently deposition proceeds with very low activation overpotentials (80).

Scandium, yttrium, and the lanthanides.—Like the alkali and alkaline earth metals, lanthanides are deposited from aqueous solutions as amalgams (81), although the process is unsatisfactory on account of heavy precipitation of basic salts on mercury surface. Better results are obtained with alcohol solutions, owing partly to lower stabilities of the alcoholates. Aquo complexes have outer orbital configurations. Although yttrium is especially difficult to deposit, it

is reported that scandium is reduced at the dropping mercury electrode (82). With these metals, polarographic reduction is irreversible (83) and may represent only hydrogen evolution (84). Hydrolysis accounts both for irreversibility and poor current efficiencies.

Oxidation and reduction between valences of two and three for europium and ytterbium are reversible processes (85), no change in configuration being involved.

Copper and zinc group metals.—Metals of the copper and zinc groups contrast sharply with platinum metals in depositing readily at high current efficiencies and low activation overpotentials. The contrast is somewhat less marked with iron, cobalt, and nickel. This difference is explained by filling of the *d* orbitals, so that only outer orbital complexes are formed. Furthermore, hydrogen overvoltage is high for these metals, and the complexes dissociate readily, offering little kinetic resistance to deposition.

Electrodeposition from cyano complexes has already been discussed. Because the coordination of water is weaker than that of cyanide, deposition from aquo complexes proceeds at high efficiencies and low activation overpotentials even at very high current densities.

Complexes of zinc, cadmium, and mercury(II) are tetrahedral. Deposition from the aquo, ammino, cyano, hydroxo (zincate), and pyrophosphato complexes of zinc is essentially the same process and can occur at 100% current efficiency under suitable conditions.

Metal is deposited from divalent aquo and ammino complexes of silver at substantially 100% current efficiencies. Similar results are obtained with complex iodides and thiosulfates.

The tetrachloroaurate(III) ion is square planar with inner orbital dsp^2 hybridization. At the cathode it is reduced to the unstable dichloroaurate(I) ion (86) which may decompose spontaneously to gold (87), although deposition appears to be largely electrolytic. The reduction to gold, therefore, occurs from an outer orbital state.

Copper is deposited at approximately 100% current efficiencies from tetraquo and tetrammino copper(II) complexes, which are square planar and therefore have been presumed to be of inner orbital dsp^2 configuration. With the ammino ion, reduction proceeds through the cuprous state (88), which is necessarily of outer orbital type. A two-stage reduction is also observed with chloro, thiocyanato, and pyridino ions. With the aquo complex, however, there is no indication of cuprous state at the dropping mercury cathode (88), yet reduction occurs with low activation overpotentials and at substantially 100% current efficiency. This is not in accord with inner

orbital hybridization. Furthermore, the cupric ion forms a series of complexes containing from one to five ammino groups (89), with at least two species coexisting in considerable amounts in solution. Although equilibria indicate that the 4-coordinate ion is the most stable of the series, it does not show the exceptional stability expected for dsp^2 hybridization. Moreover, the 5-coordinate form could not have inner orbital configuration.

Magnetic moment studies (90) suggest that aquo, ammino, and certain other cupric complexes do not have inner orbital hybridization. Thus, chelate diammino complexes, which are reduced to metal in one step at the dropping mercury cathode (91), appear to have outer spd^2 hybridization.¹¹

Furthermore, reversibility of the first stage of reduction of the ammino ion (88) indicates that no fundamental change in configuration occurs. Since the cuprous complex is not inner orbital, and since it is diamagnetic and has no vacant *d* orbital for hybridization, it follows that the cupric complex also is outer orbital. Thus, reversible two-electron reduction of diammines is accounted for, and since the aquo complex is similar except for weaker coordination of water, single step reduction of the aquo complex is also explained. Two steps in reduction are observed only in the presence of a coordinated group which will sufficiently stabilize the cuprous state (38).

As there is no direct evidence for the exact value of the coordination number of aquo complexes in solution, it is customary to assume that it is the same as is observed in the crystalline state. Usually this agrees with the number for the most stable ammino ion and for other typical complexes in solution (92). For inner orbital complexes, this is very probably correct, considering the special stability of this configuration. For outer orbital ions, it is required only that dissociation occur with sufficient ease to allow electrodeposition. It is, therefore, the type of bonding rather than the coordination number which is decisive.

Gallium, indium, and thallium.—The deposition of thallium (93, 94) proceeds with little activation overpotential in accordance with the outer orbital configuration. Gallium, however, is reduced irreversibly at the dropping mercury cathode (95). This irreversibility is due to binding of the ions, to greater or less degree, in colloidal sol formation by hydrolysis (96). It is therefore expected that current efficiencies at solid cathodes will be less than 100% (97).

Indium is deposited at low efficiencies from both cyanide and sulfate solutions (98). Moreover, the

¹¹ An experimental study of electrodeposition from copper complexes will be reported later.

aquo complex is reduced irreversibly at the dropping mercury cathode (99). Hydrolysis (100) evidently prevents reversible reduction. In the presence of chloride ion, reduction becomes reversible at the mercury cathode (101), probably because the stable chloro complex is less readily hydrolyzed than the aquated ion. It is likely that deposition at a solid cathode will show high efficiencies from chloride baths.

Germanium, tin, and lead.—From acidified stannous sulfate baths, tin is deposited at high current efficiencies and low overpotentials which suggest reversibility. However, reduction is irreversible at the dropping mercury electrode unless chloride is present (101). The irreversibility is ascribed to hydrolysis of the aquo ion in less acid solutions, just as with gallium and indium.

Reduction of aquated stannic ion is too irreversible to be effected at the dropping mercury cathode (102). The hexachloro ion is reduced irreversibly to the tetrachloro tin(II) complex, from which reduction to the amalgam is reversible. Irreversibility of the first step is accounted for by change from octahedral to tetrahedral configuration, while reversibility of the second step is in accord with outer orbital configuration of the ion.

Tin is deposited at high efficiencies from stannite ion (103), but as this ion disproportionates spontaneously into tin and stannate (104), the deposits are usually powdery. Better deposits are obtained from the hexahydroxo stannate(IV) ion in stannate bath. Deposition proceeds through the tin(II) state, and the attendant change in configuration accounts for low cathode efficiency. The first step is irreversible, the second reversible. Stannite ions are reduced as fast as they are formed and do not accumulate in the bath sufficiently to produce a powdery deposit. At the dropping mercury electrode, reduction follows the same course through the stannous state (102).

Irreversibility of reduction from tartrate solutions (105) is probably the result of hydrolysis; irreversibility of oxidation to the stannic state is associated with change in configuration.

Lead is deposited from fluoroborate, perchlorate, sulfamate, and other baths with high current efficiencies and low activation overpotentials. Reduction is reversible also at the dropping mercury cathode (106). Biplumbite ion is reduced reversibly.

Germanium is deposited from sulfate and also from germanate baths (107). Although current efficiencies were not reported, reduction is probably highly irreversible on account of hydrolysis.

Arsenic, antimony, and bismuth.—Arsenic is deposited from solutions of sodium arsenite or thioarsenite (108), but current efficiencies are not

reported. At the dropping mercury electrode, arsenious acid in the presence of hydrochloric acid is reduced to the metal and arsine (109), but apparently not when other acids (110) or neutral solutions are used. Reduction is irreversible because of hydrolysis. Arsenate ion is not reduced at the dropping mercury cathode.

Antimony is deposited from a number of baths, of which the fluoride is said to be best (111). Activation overpotentials are high except in halide baths (112), because the metal is bound in hydrolysis products. "Explosive antimony" containing 10 to 15% halide (113) is produced at current densities too high for reversible deposition.

Bismuth is readily deposited (114) at very low activation overpotentials from chloride baths, but with somewhat higher polarization from sulfate solutions (115). It should be mentioned that good deposits are obtained from perchlorate baths.

Irreversible deposition from most salts of these metals suggests that oxo or hydroxo complexes are polymerized, just as with gallium (96). It has been found that bismuth exists as tetrabismuthyl ion, $(\text{Bi}_4\text{O}_4)^{4+}$, in all but highly acid solutions (55). Since arsenic and antimony are more strongly hydrolyzed, the tendency to polymerize is greater. Thus, irreversible deposition is to be expected, even though electronic configurations are outer orbital in type. The chloro complexes are more stable and hydrolyze less extensively. It has been stated that appreciable concentrations of "free" unhydrolyzed ions exist because metal can be deposited from the solutions (116). This conclusion is unjustified, for deposition probably proceeds directly from the chloro complex.

DISCUSSION

From the foregoing, it appears that metals cannot be electrodeposited from aqueous solutions if equilibrium of the deposition reaction lies so far on the ionic side that electrode potential is more negative than hydrogen discharge potential. This occurs if: (a) stability of the metallic state is low, as with alkalis; or (b) the ionic state is especially stabilized by inner orbital hybridization (unless this is counterbalanced by exceptional stability of the metallic state).

Iron, cobalt, and nickel, although their aquo complexes are of outer orbital configuration (10), are deposited with pronounced activation overpotentials, and with lower current efficiencies than copper and zinc. Furthermore, they are reduced irreversibly at the dropping mercury cathode. In general, electrodeposition from hexaquo ions appears to be irreversible. Since 4-coordinated complexes are also well known for those metals, it might be postulated that electrodeposition proceeds through the tetraquo ion and the attendant change in configuration accounts

for irreversibility. This point is to be discussed further in a future paper.

Accordingly, irreversibility of electrode reactions is explained by: (a) alteration of electronic configuration in change of oxidation state; (b) limited availability of the metal ion because it is bound in hydrolyzed polymeric aggregates; or (c) kinetic hindrances associated with deposition from complexes of the transition metals.

Electrolytic Classification of Metals

On the basis of behavior in electrode systems, Piontelli (6) divides metals into three classes.

Normal metals are those which: (a) quickly establish stable potentials when immersed in solutions of their salts, with little influence by previous treatment of the electrode metal; (b) are electrodeposited with low activation overpotentials, which are roughly equal at anode and cathode; (c) give cathode deposits with well-developed, relatively large crystals, not readily affected by addition agents in the bath (117); (d) are deposited with high current efficiencies, often close to 100%; (e) show good correlation between position in the electromotive series and behavior in displacement reactions; (f) are deposited reversibly at the dropping mercury cathode; and (g) have high hydrogen overvoltages.

Inert metals are those which: (a) show potentials which fluctuate widely in solutions of their salts, and are determined in part or entirely by reactions other than ionization of the metal; (b) are deposited with high activation overpotentials for the cathode reaction, and usually for the anode reaction as well; (c) are deposited as fine crystals, readily modified by action of addition agents in the bath, so that it is relatively easy to produce a "bright" deposit in technical electroplating; (d) are deposited with current efficiencies appreciably less than 100%; (e) in displacement reactions, show more nobility in the metallic state, and less in the ionic state, than is expected from their position in the electromotive series; (f) are deposited irreversibly at the dropping mercury cathode; and (g) have low hydrogen overvoltages.

Intermediate metals are those which show characteristics of both groups.

Metals with incompletely filled *d* orbitals are inert, as is to be expected since they may form inner orbital ions. Metals with filled *d* orbitals are either normal or intermediate. The behavior of copper, silver, gold, and zinc is so close to normal that they may be considered to belong to the normal class. The intermediate behavior of arsenic, antimony, and bismuth appears to be a consequence of hydrolysis of the ions.

When the behavior of amalgam electrodes is considered, alkali and alkaline earth metals are assigned to the normal class, in accordance with their electronic structures. Thus the complete classification of Table II is obtained. Normal metals come after inert gases and again after platinum metals, which have inert gas-like structures. Gallium is termed normal on the basis of stable potential of the gallium electrode. Germanium is probably intermediate due to its tendency to hydrolyze.

Effects of Anions

Electrode potentials become more negative when the concentration of coordinating species in solution increases beyond that needed to form the complex. Thus, excess (or "free") cyanide ions lower the copper potential. This shift is often incorrectly interpreted in terms of repression of dissociation of the complex into the "simple" metal ion (actually the aquo complex). The latter is often so exceedingly low in concentration that the electrode must be considered to respond to the predominant complex.

If loss of one of the coordinated groups is a controlling step in the cathode reaction, the presence of uncombined groups will shift the equilibrium toward the undissociated complex; the complex is made more stable, and the electrode potential is therefore more negative. In some instances, new complexes of higher coordination number will be formed. Moreover, there may also be a kinetic effect.

As the electrode potential becomes more negative, there is increased competition of the hydrogen discharge reaction with the deposition process. This

TABLE II. *Electrolytic classification of elements*

	H																		
He	Li	Be	No deposits										No deposits		B	C	N	O	F
Ne	Na	Mg													Al	Si	P	S	Cl
A	K	Ca	Sc	Ti	V	Cr	Mn	Fe	Co	Ni	Cu	Zn	Ga	Ge	As	Se	Br		
Kr	Rb	Sr	Y	Zr	Nb	Mo	Tc	Ru	Rh	Pd	Ag	Cd	In	Sn	Sb	Te	I		
Xe	Cs	Ba	La*	Hf	Ta	W	Re	Os	Ir	Pt	Au	Hg	Tl	Pb	Bi	Po	At		
Rn	Fr	Ra	Ac†	Inert—no deposits			Inert					Normal				Inter- medi- atc			

* Lanthanides † Actinides.

TABLE III. Polarographic Half-Wave Potentials
 [From Reference (94)]

Substance	Supporting electrolyte	$E_{1/2}$ vs S.C.E. volt	Difference volt
Bismuth	1N HNO ₃	-0.01	
	1N HCl	-0.08	-0.07
Cadmium	1N KNO ₂ , HNO ₃ , or H ₂ SO ₄	-0.586	
	1N KCl or HCl	-0.642	-0.056
	1N KI	-0.74	-0.15
Lead	1N KNO ₂ or HNO ₃	-0.405	
	1N KCl or HCl	-0.435	-0.035
Zinc	1N KNO ₂	-1.012	
	1N KCl	-1.022	-0.010
Cobalt	None (CoCl ₂ only)	Irreversible	
	0.1N KCl or NaCl	-1.20	More positive
Indium	0.1N HClO ₄	-0.95	
	0.1N KCl or HCl	-0.561	0.39
	0.1N KI	-0.53	0.52
Iron (II)	1N NH ₄ ClO ₄	-1.45	
	1N KCl or HCl	-1.3	0.15
Nickel	NH ₄ ClO ₄ or KNO ₃	Irreversible	
	1N KCl	-1.1	More positive
Tin	2N HClO ₄	Not reduced	
	2N HClO ₄ 0.5N NaCl	-0.35	Large positive shift

accounts for the decreased current efficiencies often observed. There may be an effect on hydrogen overvoltage also.

Furthermore, halide ions appear to facilitate deposition of almost every metal (2, 118). At the dropping mercury cathode, irreversibility of deposition of tin, cobalt, nickel, iron, and indium is either greatly lowered or eliminated by the presence of halide ions. For a number of metals, the lowest activation overpotentials, both anodic and cathodic, are observed in chloride and iodide solutions (2). Moreover, in technical electroplating, the nickel chloride bath operates at higher current densities and higher current efficiencies than the sulfate or Watts baths (119), and the character of the deposit under favorable conditions suggests that reduction is more nearly reversible.

The effect of chloride ion is attributed to formation of a chloro or chloro-aquo complex ion. Such coordinate bonds are more stable than those of the

aquo ion; otherwise, of course, the chloro complex would not be formed. Increased stability raises the value of W in the expression for Ω , and the electrode potential becomes more negative.

Measurements of equilibrium potentials to test this deduction are lacking, but related polarographic half-wave potentials are given in Table III (94). The predicted negative shift is seen for bismuth, cadmium, lead, and zinc. As these are normal metals, or nearly so, activation overpotentials are small and do not mask the shift due to chloride. For the highly irreversible reductions of iron, cobalt, and nickel, large decreases in activation overpotentials evidently outweigh the effect on equilibrium potentials. With tin and indium, the shift is probably due to stabilization of the complex with respect to hydrolysis.

Activation overpotentials are generally influenced by anions. In solutions of simple salts, overpotentials usually increase in the order: iodide, chloride, sulfate, fluoroborate, sulfamate, nitrate, perchlorate (2). Activation is lower with anions showing stronger tendencies to coordinate. Furthermore, when several anions are present, activation overpotential is determined largely by the anion with the strongest coordination tendency. Thus, addition of chloride ions to the solution of a metal sulfate lowers the activation overpotential to approximately that of a simple chloride solution, whereas addition of sulfate to a chloride solution has little effect. Adding cyanide ions lowers activation potentials still further, if the cyano complex is outer orbital. Similar effects of anions are observed in exchange reactions between metals and their solvated ions (120, 121).

For electrodeposition from aqueous solutions, aquo complexes generally require greater activation energies than do other types, although the former must be the least stable or else the others would not be formed in aqueous solutions. This circumstance results, of course, from the fact that overpotentials are kinetic, not equilibrium, phenomena. It may be supposed that in the dissociation step the exceedingly high activity of water in aqueous solutions affects such rapid reassociation that high activation is needed to produce sufficient quantities of the intermediate dissociated complex to allow reduction to proceed. Other complexes require less activation because the activity of uncoordinated species, such as chloride or cyanide ions, is relatively low.

It is unknown whether chloride ions form a proportion of fully chlorinated ions, or whether the aquo complexes are partly chlorinated, as $[M(H_2O)_5Cl]^-$ or $[M(H_2O)_4Cl_2]$, etc. (122). Chloro-aquo complexes are probably present in many solutions. They may require less activation for dissociation and electroreduction because of the labilizing effect of chloride ion on the aquo group in trans position according to

the well-known trans effect (123). Reducibility of complex ions by molecular and atomic hydrogen is increased by this effect (124). According to Heyrovsky (125), polarization of the chloride ion facilitates electron transfer.

The deposition process may continue by discharge of the dissociated complex (71). More likely, the dissociated intermediate may be first adsorbed on the cathode surface by interaction of unsatisfied bond functions on the metal surface with orbitals of the ion vacated in dissociation. Then, with acquisition of the requisite number of electrons from the cathode, the metal ion assumes the metallic state structure and releases remaining coordinated groups (126). Effects of addition agents can then be explained by their influence on adsorption. These points will be elaborated in a later paper.

SUMMARY

In the foregoing, major characteristics of electrode systems in electrodeposition are explained on structural considerations. Inasmuch as deposition characteristics at solid and mercury cathodes are generally parallel, activation needed to build up crystal lattices of deposited metals (127) appears to be of relatively small magnitude. The sharp decrease in activation overpotential as temperature of the solution is raised suggests that the rate-controlling step is chemical, rather than electrolytic in character. Dissociation of the metal complex therefore appears to be decisive.

Hydrogen overvoltage (128) exerts a secondary influence, but it is striking that inert metals are also those with low hydrogen overvoltage. From their densities, tensile strengths, interatomic distances, melting points, etc., it is seen that inert metals form very strong bonds in both the metallic and ionic states. Accordingly hydrogen atoms should be strongly adsorbed, and equilibrium in the reaction: $M + H^+ (aq) + e^- = M \cdot H$, should lie well to the right, corresponding to low overvoltage. On the other hand, with the weaker bonds of normal metals, equilibrium lies to the left. This is in accord with conclusions of Bockris and Potter (129) that the rate determining reaction on platinum is the combination of atomic hydrogen. For silver and mercury, the relatively weak bonds do not interfere with this combination, and the discharge reaction becomes controlling. However, results with nickel are not in accord with this explanation.

Furthermore, the strength of bonds formed by inert metals in both states suggests that the potential barrier to be surmounted in passing from one state to another is high, whereas it is low for normal metals. This is in agreement with the magnitudes of activation overpotentials, and explains the rough symmetry in anodic and cathodic overpotentials (2).

Finally, standard electrode potentials for various complex ions afford estimates of relative energies of coordination through the expression for Ω . Although experimentally this can be realized only for normal metals, and should be modified by entropy changes, it provides a comparison of strengths of coordinate bonds.

ACKNOWLEDGMENTS

Invaluable criticism and suggestions have been received from Professors John C. Bailar, Jr., H. A. Laitinen, and Sherlock Swann, Jr. The author is grateful for support of this work through a Fellowship awarded by the Atomic Energy Commission.

Any discussion of this paper will appear in a Discussion Section to be published in the June 1955 issue of the JOURNAL.

REFERENCE

1. H. J. T. ELLINGHAM, *J. Electrodepositors' Tech. Soc.*, **10**, 109 (1935); W. BLUM, *Monthly Rev. Am. Electroplaters' Soc.*, **27**, 923 (1940); G. DUBPERNELL, *Proc. Am. Electroplaters' Soc.*, **1946**, 244; F. A. LOWENHEIM, *ibid.*, **1948**, 187.
2. R. PIONTELLI, *J. chim. phys.*, **45**, 288 (1949); *J. Inst. Metals*, **19**, 99 (1951); *Compt. rend. 2me. Reunion Com. Internat. Thermodynamique Cinetique Electrochim.*, **1950**, pp. 79, 185, 369, E. Tamburini, Milan (1951); *ibid.*, (3me. Reunion) Berne (1952); *Z. Elektrochem.*, **55**, 128 (1951).
3. J. A. V. BUTLER, "Electrocapillarity," Methuen and Co., London (1939).
4. J. A. V. BUTLER, *loc. cit.*, p. 36; W. M. LATIMER, K. S. PITZER, AND C. M. SLANSKY, *J. Chem. Phys.*, **7**, 108 (1939); cf. *Chem. Rev.*, **18**, 349 (1936).
5. See also, E. N. GAPON, *J. Phys. Chem. U.S.S.R.*, **20**, 1025, 1209 (1946); E. A. KANEVSKII, *ibid.*, **22**, 1397 (1948).
6. J. D. BERNAL AND R. H. FOWLER, *J. Chem. Phys.*, **1**, 515 (1933).
7. M. CALVIN AND N. C. MELCHIOR, *J. Am. Chem. Soc.*, **70**, 3270 (1948).
8. K. B. YATSIMIRSKII, *Zhur. Obschei Khim.*, **20**, 1404 (1950).
9. L. PAULING, "Vol. Commemorative Victor Henri, Liege," p. 1 (1948); see also, *Phys. Rev.*, **54**, 899 (1930); *J. Am. Chem. Soc.*, **69**, 542 (1947).
10. H. TAUBE, *Chem. Revs.*, **50**, 69 (1952).
11. B. E. DOUGLAS, H. A. LAITINEN, AND J. C. BAILAR, JR., *J. Am. Chem. Soc.*, **72**, 2484 (1950).
12. R. DAUDEL, P. DAUDEL, AND M. MARTIN, *Compt. rend.*, **219**, 129 (1944).
13. A. W. ADAMSON, J. P. WELKER, AND M. VOLPE, *J. Am. Chem. Soc.*, **99**, 169 (1952).
14. N. V. SIDGWICK, "The Chemical Elements and Their Compounds," p. 156, Oxford Press, Oxford (1950); P. SOUCHAY AND J. FAUCHERRE, *Bull. Soc. chim. France*, **1947**, 529.
15. F. KUNSCHERT, *Z. anorg. Chem.*, **41**, 359 (1904).
16. H. GROSSMAN AND P. V. D. FORST, *ibid.*, **43**, 94 (1905).
17. J. BRIGANDO, *Compt. rend.*, **214**, 908 (1942).
18. S. GLASSTONE, *J. Chem. Soc.*, **1929**, 690, 702.
19. K. HELLWIG, *Z. anorg. Chem.*, **25**, 157 (1900).

20. G. GRUBE AND H. LIEDER, *Z. Elektrochem.*, **32**, 561 (1926).
21. C. L. FAUST, Private communication; G. B. HOGABOOM, Private communication; also experimental studies by the author; see also C. W. BENNETT, C. C. ROSE, AND L. G. TINKLER, *Trans. Electrochem. Soc.*, **28**, 339 (1915); O. P. WATTS, *ibid.*, **27**, 141 (1915).
22. G. H. WALDEN, L. P. HAMMETT, AND R. P. CHAPMAN, *J. Am. Chem. Soc.*, **55**, 2649 (1933); D. N. HUME AND I. M. KOLTHOFF, *ibid.*, **71**, 867 (1949).
23. W. F. LIBBY, *J. Phys. Chem.*, **56**, 39 (1952); Abstracts, Phys. and Inorganic Section, 115th Meeting American Chemical Society, San Francisco, March 27-April 1, 1949; cf. also E. J. B. WILLEY, "Collisions of the Second Kind," E. Arnold and Co., London (1937); K. J. LAIDLER AND K. K. SHULER, *Chem. Revs.*, **48**, 153 (1951).
24. F. P. DWYER, J. E. HUMPOLETZ, AND R. S. NYHOLM, *J. Proc. Roy. Soc. N. S. Wales*, **80**, 212 (1947).
25. T. STEIGMAN, N. BIRNBAUM, AND S. M. EDMONDS, *Ind. Eng. Chem., Anal. Ed.*, **14**, 30 (1942).
26. G. A. BARBIERI, *Atti accad. nazl. Lincei, Classe sci. fis., mat. e. nat.*, **4**, 561 (1948).
27. F. H. BURSTALL, F. P. DWYER, AND E. C. GYARFAS, *J. Chem. Soc.*, **1950**, 953.
28. G. GRUBE AND W. BRAUSE, *Ber.*, **60**, 2273 (1927).
29. H. LIEDER AND P. SCHACTERLE, *Z. Elektrochem.*, **32**, 565 (1926); D. N. HUME AND I. M. KOLTHOFF, *J. Am. Chem. Soc.*, **71**, 867 (1949).
30. D. N. HUME AND I. M. KOLTHOFF, *ibid.*, **65**, 1897 (1943).
31. O. COLLENBERG, *Z. physik. Chem.*, **146**, 81, 177 (1930); I. M. KOLTHOFF AND W. J. TOMSICEK, *J. Phys. Chem.*, **40**, 247 (1936).
32. O. COLLENBERG, *Z. physik. Chem.*, **109**, 353 (1924).
33. H. TERRY, *J. Chem. Soc.*, **1928**, 202.
34. A. A. NOYES AND C. S. GARNER, *J. Am. Chem. Soc.*, **58**, 1265 (1936); G. C. WALTERS AND T. DEVRIES, *ibid.*, **65**, 119 (1943); M. S. SHERRILL, C. B. KING, AND R. C. SPOONER, *ibid.*, **65**, 170 (1943).
35. M. KALOUFEK, *Collection Czechoslov. Chem. Commun.*, **11**, 592 (1939).
36. G. GRUBE AND L. SCHLECT, *Z. Elektrochem.*, **32**, 178 (1926); G. GRUBE AND G. BREITINGER, *ibid.*, **33**, 112 (1927).
37. H. GLASSTONE AND A. HICKLING, "Electrolytic Oxidation and Reduction," Chapman and Hall, Ltd., London (1935); W. M. LATIMER, "Oxidation States of the Elements," Prentice-Hall, Inc., New York (1938).
38. E. I. ONSTOTT AND H. A. LAITINEN, *J. Am. Chem. Soc.*, **72**, 4724 (1950); M. CALVIN AND R. H. BAILES, *ibid.*, **68**, 949 (1946).
39. R. R. LLOYD, W. T. RAWLES, AND R. G. FEENEY, *Trans. Electrochem. Soc.*, **89**, 443 (1946).
40. R. W. PARRY, S. SWANN, JR., AND J. C. BAILAR, JR., *Trans. Electrochem. Soc.*, **92**, 507 (1947).
41. R. L. PECSOK AND J. J. LINGANE, *J. Am. Chem. Soc.*, **72**, 189 (1950).
42. A. SNAVELY, *Trans. Electrochem. Soc.*, **92**, 537 (1947).
43. A. BRENNER, P. BURKHEAD, AND C. W. JENNINGS, *J. Research Natl. Bur. Standards*, **40**, 31 (1947).
44. S. A. DURBAN AND D. J. BROWN, *J. Phys. Chem.*, **43**, 491 (1939).
45. F. OGBURN AND A. BRENNER, *Trans. Electrochem. Soc.*, **96**, 347 (1949).
46. E. MULLER, *Z. Elektrochem.*, **49**, 16 (1943).
47. J. J. LINGANE AND I. M. KOLTHOFF, *J. Am. Chem. Soc.*, **62**, 852 (1940).
48. M. L. HOLT, *Trans. Electrochem. Soc.*, **66**, 453 (1934); **71**, 301 (1937).
49. M. J. KSYCKI AND L. F. YNTEMA, *ibid.*, **96**, 48 (1949).
50. Y. P. HOKHSHEIN, *J. Gen. Chem. U.S.S.R.*, **10**, 1752 (1940); R. HOLTJE AND R. GEYER, *Z. anorg. u. allgem. Chem.*, **246**, 258 (1941).
51. I. M. KOLTHOFF AND J. J. LINGANE, "Polarography," p. 296, Interscience Publishers, Inc., New York (1946).
52. A. GLAZUNOV AND V. JOLKIN, *Atti Congr. intern. chem., 10th Cong., Rome 1938*, **4**, 355 (1939).
53. M. KRAMER, S. SWANN, JR., AND J. C. BAILAR, JR., *Trans. Electrochem. Soc.*, **90**, 27 (1946).
54. I. M. KOLTHOFF AND J. J. LINGANE, *op. cit.*, p. 285, J. B. WILLIS, J. A. FRIEND, AND D. P. MELLOR, *J. Am. Chem. Soc.*, **67**, 1680 (1945); H. A. LAITINEN, J. C. BAILAR, JR., H. F. HOLTZCLAW, JR., AND J. V. QUAGLIANO, *ibid.*, **70**, 2999 (1948).
55. P. SOUCHAY AND D. PESCHANSKI, *Bull. soc. chim. France*, **1948**, 439.
56. Y. P. HOKHSHEIN, *J. Gen. Chem. U.S.S.R.*, **7**, 2486 (1937).
57. D. P. MELLOR AND D. P. CRAIG, *J. Proc. Roy. Soc. N. S. Wales*, **74**, 475 (1940).
58. A. R. BURKIN, *Quart. Revs. London*, **5**, 1 (1951).
59. M. CALVIN AND N. C. MELCHIOR, *J. Am. Chem. Soc.*, **70**, 3270 (1948).
60. W. E. BRADT AND L. R. TAYLOR, *Trans. Electrochem. Soc.*, **73**, 327 (1938).
61. I. M. KOLTHOFF AND J. J. LINGANE, *op. cit.*, p. 257.
62. J. F. FLAGG AND W. E. BLEIDNER, *J. Chem. Phys.*, **13**, 269 (1945).
63. C. G. FINK AND P. DEREN, *Trans. Electrochem. Soc.*, **66**, 471 (1934); C. B. F. YOUNG, *Metal Ind. New York*, **34**, 176 (1936).
64. R. S. NYHOLM, *Quart. Revs. London*, **3**, 321 (1949).
65. K. K. KELLEY, "Heats of Fusion of Inorganic Compounds," U. S. Bureau of Mines Bull. 393 (1936).
66. W. M. LATIMER, "Oxidation Potentials," Prentice-Hall, Inc., New York (1938).
67. G. GRUBE AND D. BEISCHER, *Z. Elektrochem.*, **39**, 44, 131 (1933).
68. J. B. WILLIS, *J. Am. Chem. Soc.*, **67**, 547 (1945).
69. L. P. HAMMETT AND A. E. LORCH, *ibid.*, **55**, 71 (1933).
70. I. M. KOLTHOFF AND J. J. LINGANE, *op. cit.*, p. 200.
71. H. A. LAITINEN AND E. I. ONSTOTT, *J. Am. Chem. Soc.*, **72**, 4565 (1950).
72. G. GRUBE AND H. REINHARDT, *Z. Elektrochem.*, **37**, 316 (1931).
73. N. V. SIDGWICK, *op. cit.*, p. 1582.
74. W. J. McCaughey, *Trans. Electrochem. Soc.*, **15**, 523 (1909); W. J. McCaughey and H. E. PATTON, *ibid.*, **17**, 278 (1910).
75. V. V. IPATIEV AND V. G. TRONER, *J. Gen. Chem. U.S.S.R.*, **5**, 643 (1935).
76. G. GRUBE AND E. KESTING, *Z. Elektrochem.*, **39**, 951 (1933); C. G. FINK AND G. C. LAMBROS, *Trans. Electrochem. Soc.*, **63**, 181 (1933).
77. J. B. WILLIS, *J. Am. Chem. Soc.*, **66**, 1067 (1944).
78. Vanadium: H. FISCHER, *Trans. Electrochem. Soc.*, **30**, 175 (1916); G. TAMMAN AND J. HINNUBER, *Z. anorg. Chem.*, **160**, 256 (1927); J. J. LINGANE, *J. Am. Chem. Soc.*, **67**, 182 (1945). Niobium: N. IZGUARISHEV AND A. F. PREDE, *Z. Elektrochem.*, **39**, 283 (1933); N. IZGUARISHEV AND G. E. KAPLAN, *ibid.*, **40**, 33 (1934);

- A. G. STROMBERG AND L. M. REINUS, *J. Phys. Chem. U.S.S.R.*, **20**, 693 (1946). Tantalum: N. IZGUARISHEV AND A. F. PREDE, *Z. Elektrochem.*, **40**, 295 (1934); H. J. SEIM AND M. L. HOLT, *Trans. Electrochem. Soc.*, **96**, 43 (1949). Zirconium: A. W. LAUBENGAYER AND R. B. EATON, *J. Am. Chem. Soc.*, **62**, 2704 (1940).
79. I. M. KOLTHOFF AND J. J. LINGANE, *op. cit.*, p. 150.
80. J. HEYROVSKY, *Disc Faraday Soc.*, **1**, 86 (1947).
81. L. F. AUDRIETH, E. E. JUUKOLA, R. E. MEINTS, AND B. S. HOPKINS, *J. Am. Chem. Soc.*, **53**, 1805 (1931); **56**, 303 (1934); *Trans. Electrochem. Soc.*, **66**, 135 (1934); H. N. MCCOY, *J. Am. Chem. Soc.*, **63**, 1622 (1941), see also W. KETTEMBEIL, *Z. anorg. Chem.*, **38**, 213 (1904); L. HOLLECK, *Z. Elektrochem.*, **45**, 249 (1939); G. C. WALTERS AND T. DEVRIES, *J. Am. Chem. Soc.*, **65**, 119 (1943).
82. R. H. LEACH AND H. TERREY, *Trans. Faraday Soc.*, **33**, 480 (1937).
83. W. NODDACK AND A. BRUKL, *Angew. Chem.*, **50**, 362 (1937); H. A. LAITINEN AND W. A. TAEBEL, *Ind. Eng. Chem., Anal. Ed.*, **13**, 825 (1941); C. R. ESTEE AND G. GLOCKLER, *J. Am. Chem. Soc.*, **70**, 1344 (1948); A. TIMNICK AND G. GLOCKLER, *ibid.*, 1347; S. W. RABIDEAU AND G. GLOCKLER, *ibid.*, 1342.
84. H. A. LAITINEN, Private communication.
85. H. A. LAITINEN, *J. Am. Chem. Soc.*, **64**, 1133 (1942).
86. J. BJERRUM, *Bull. soc. chim. Belges*, **57**, 432 (1948).
87. N. V. SIDGWICK, *op. cit.*, p. 147.
88. I. M. KOLTHOFF AND J. J. LINGANE, *op. cit.*, p. 176, 279.
89. J. BJERRUM, "Complex Ammine Formation in Solution," P. Haase & Son, Copenhagen (1941).
90. P. RAY AND D. N. SEN, *J. Indian Chem. Soc.*, **25**, 473 (1948).
91. H. A. LAITINEN, E. I. ONSTOTT, J. C. BAILAR, JR., AND S. SWANN, JR., *J. Am. Chem. Soc.*, **71**, 1550 (1949).
92. A. R. BURKIN, *Quart. Revs London*, **5**, 1 (1951); J. P. HUNT AND H. TAUBE, *J. Chem. Phys.*, **18**, 757 (1950).
93. O. W. BROWN AND A. MCGLYNN, *Trans. Electrochem. Soc.*, **53**, 351 (1928).
94. I. M. KOLTHOFF AND J. J. LINGANE, *op. cit.*, p. 266.
95. S. ZELTZER, *Collection Czechoslov Chem. Commun.*, **4**, 319 (1932).
96. T. MOELLOR AND G. I. KING, *J. Am. Chem. Soc.*, **74**, 1355 (1952).
97. H. C. FOGG, *Trans. Electrochem. Soc.*, **66**, 107 (1934).
98. H. B. LINFORD, *Trans. Electrochem. Soc.*, **79**, 443 (1941); M. A. WHITEHEAD, *Metal Finishing*, **42**, 405 (1944).
99. I. M. KOLTHOFF AND J. J. LINGANE, *op. cit.*, p. 274.
100. S. TAKAGI, *J. Chem. Soc.*, **1928**, 301; E. M. HATTOX AND T. DEVRIES, *J. Am. Chem. Soc.*, **58**, 2126 (1936).
101. I. M. KOLTHOFF AND J. J. LINGANE, *op. cit.*, p. 263.
102. J. J. LINGANE, *J. Am. Chem. Soc.*, **67**, 919 (1945).
103. E. H. LYONS, JR., Unpublished experiments.
104. N. V. SIDGWICK, *op. cit.*, p. 621.
105. J. J. LINGANE, *J. Am. Chem. Soc.*, **65**, 866 (1943).
106. I. M. KOLTHOFF AND J. J. LINGANE, *op. cit.*, p. 267.
107. J. I. HALL AND A. E. KOENIG, *Trans. Electrochem. Soc.*, **65**, 215 (1934); I. P. ALIMARIN AND B. N. IVANOV-EMIN, *J. Appl. Chem. U.S.S.R.*, **17**, 204 (1944); C. G. FINK AND V. N. DOKRAS, *Trans. Electrochem. Soc.*, **93**, 80 (1949).
108. W. BLUM AND G. B. HOGABOOM, "Principles of Electroplating and Electroforming," 3rd ed., p. 333, McGraw-Hill Book Co., New York (1949).
109. I. M. KOLTHOFF AND J. J. LINGANE, *op. cit.*, p. 261.
110. I. N. Y. KHLOPIN, *Zhur. Obscheih Kim.*, **18**, 364 (1948).
111. F. C. MATHERS, K. S. MEANS, AND B. F. RICHARDS, *Trans. Electrochem. Soc.*, **31**, 293 (1917).
112. O. ESIN, *J. Appl. Chem. U.S.S.R.*, **17**, 114 (1944).
113. N. V. SIDGWICK, *op. cit.*, p. 759.
114. M. HARBAUGH AND F. C. MATHERS, *Trans. Electrochem. Soc.*, **64**, 293 (1933).
115. O. ESIN, M. LOSHKAREV, Z. LIVITINA, AND K. RUSANOVA, *J. Appl. Chem. U.S.S.R.*, **13**, 56 (1940).
116. N. V. SIDGWICK, *op. cit.*, p. 793.
117. H. FISCHER, *Z. Elektrochem.*, **49**, 342, 376 (1943).
118. E. MULLER AND H. BARCHMANN, *ibid.*, **39**, 341 (1933).
119. W. A. WESLEY AND J. W. CAREY, *Trans. Electrochem. Soc.*, **75**, 209 (1939).
120. J. SILVERMAN AND R. W. DODSON, *J. Phys. Chem.*, **56**, 21 (1952), A. W. ADAMSON, *ibid.*, **33**, W. F. LIBBY, *ibid.*, 69.
121. M. HAISSINSKY, M. COTTIN, AND B. VERJABEDIAN, *J. chim. phys.*, **45**, 212 (1948).
122. N. V. SIDGWICK, *op. cit.*, pp. 1390-1.
123. Y. K. SYRKIN, *Bull. acad. sci. U R S S, Classe sci. chim.*, **1948**, 69.
124. V. G. TRONEV AND V. N. CHULKOV, *Doklady Akad. Nauk. S.S.S.R.*, **63**, 545 (1948).
125. J. HEYROVSKY, *Disc. Faraday Soc.*, **1**, 331 (1947).
126. A. GLAZUNOV, *Rev. met.*, **43**, 214 (1946).
127. T. ERDEY-GRUZ AND M. VOLMER, *Z. phys. Chem.*, **157**, 182 (1931).
128. J. O'M. BOCKRIS, *This Journal*, **98**, 153C (1951).
129. J. O'M. BOCKRIS AND E. C. POTTER, *ibid.*, **99**, 169 (1952).

Electronic Configuration in Electrodeposition from Aqueous Solutions

II. The Deposition Process¹

ERNEST H. LYONS, JR.²

Department of Chemistry, University of Illinois, Urbana, Illinois

ABSTRACT

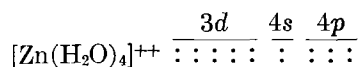
It is proposed that electrodeposition proceeds through an intermediate complex ion adsorbed on the cathode by a coordinated bridge. Subsequently, the bridge is eliminated and a metallic bond established. By applying Pauling's theory of the metallic state, reversible deposition of post-transition metals and irreversible deposition of transition metals are explained. A close correlation with electron-transfer reactions is shown. Inclusions in deposits represent residual coordinated groups, in agreement with results of recent studies.

INTRODUCTION

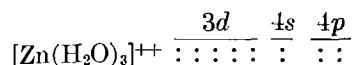
Recently, reasons were given for regarding electrodeposition as closely related to the possibility of dissociation of a coordinated group from the metal ion (1). The resulting ion, which may be regarded as an activated intermediate, accordingly has a coordination number which is one less than usual. This ion may, of course, reunite with another coordination group and return to its original state. At the electrode surface, however, coordination unsaturation may be satisfied by forming a covalent bond with an electron pair of one of the surface atoms of the metal. Whether this surface compound will then be reduced to the metallic state will depend on availability of necessary electrons in the cathode metal.

DEPOSITION OF NORMAL METALS

Consider reduction of the normal³ metal ion $[\text{Zn}(\text{H}_2\text{O})_4]^{++}$. Its outer electronic structure may be represented by:

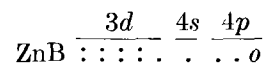


Accordingly, the structure of the activated intermediate is:

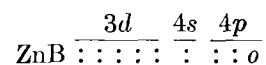


Pauling (3) considers the predominant electronic structure contributing to the resonance hybrid rep-

resenting metallic zinc to be:



where single dots represent single bonding electrons, and "o" indicates the so-called metallic orbital, empty except for resonating electrons. Pauling regards the metallic orbital as giving rise to special resonance which explains characteristic metallic properties. In the metal lattice, where bonding electrons are paired with electrons from neighboring atoms, the structure may be written:



This structure is substantially identical with that of the activated intermediate, $[\text{Zn}(\text{H}_2\text{O})_3]^{++}$. In this ion, three electron pairs, $4s4p^2$, are shared with coordinated water molecules. However, in ZnB, four electron pairs, $3d4s4p^2$, are shared with adjacent zinc atoms.

Dissociation of the complex ion by loss of a coordinated group therefore amounts to opening of the metallic orbital. Loss of another coordinated group would result in two open metallic orbitals, and the ion would correspond to Pauling's ZnC configuration.

It is now proposed that opening the metallic orbital permits the intermediate complex ion to participate in metallic resonance of the cathode lattice, so that a bond which is at least partially metallic in character is established, and the ion is bound to the cathode surface. Remaining pairs of bonding electrons then have the alternatives of continuing in coordination hybridization with the remaining coordinated water molecules, or of participating in metallic resonance with neighboring metal atoms. Hybridiza-

¹ Manuscript received August 20, 1952. This paper was prepared for delivery before the Montreal Meeting, October 26 to 30, 1952.

² Present address: Principia College, Elmhurst, Illinois.

³ The word "normal" is used in the sense that electrode reactions are substantially reversible, after Piontelli (2).

tion of fewer orbitals than the preferred number represents a state of less stability than that of the normal complex ion, but metallic resonance confers special stability. Consequently the latter will be preferred, if the necessary number of electrons is available to fill appropriate orbitals.

To ascertain the number of electrons required for conversion to the metallic state, it is noted that loss of the three remaining coordinated water molecules will remove all six electrons in the $4s$ and $4p$ orbitals. The ZnB structure calls for four single bonding electrons in the $3d4s4p^2$ orbitals. After loss of the water molecules, only two electrons are available, namely, those in the last $3d$ orbital. Thus, two additional electrons are needed, and if they are available in the lattice structure of the cathode, in excess of the normal quota, they will migrate to the ion, completing conversion to the metal atom.

This explanation implies that actual transfer of electrons to the ion undergoing discharge will not be much more difficult than transfer of electrons in metallic conduction. The processes are essentially similar, if not identical. This inference is in agreement with the observation that electron transfer in reduction of such ions as ferricyanide requires negligible activation (4).

The mechanism described accords more closely with the hypothesis that processes of discharge and deposition are simultaneous (5, 6) than with the view that deposition follows discharge (7). It requires interaction between ion and metal lattice as a prerequisite to neutralization of the ionic charge.

Since configurations of $[\text{Zn}(\text{H}_2\text{O})_3]^{++}$ and ZnB are so nearly identical, it is to be expected from previous considerations (1) that the zinc electrode will be reversible⁴ both anodically and cathodically. This, of course, is in agreement with facts.

Ionic and metallic structures of copper(I), sil-

⁴ A number of oscillographic studies (8) have shown that many electrode reactions ordinarily considered reversible are in fact irreversible. Few if any reactions are strictly reversible, just as no machines are totally frictionless. In the absence of a quantitative measure of irreversibility, the following criteria have been adopted for the present purposes.

A reaction is considered to be reversible if the activation in ordinary electrodeposition (2) amounts to no more than a few hundredths volt overpotential; or if a polarogram made under usual conditions with customary apparatus (9) gives, in plotting E vs. $\log i/(i_a - i)$, a straight line with a slope within five per cent of the theoretical value (10). In this, E represents impressed voltage, i the current, and i_a the diffusion current.

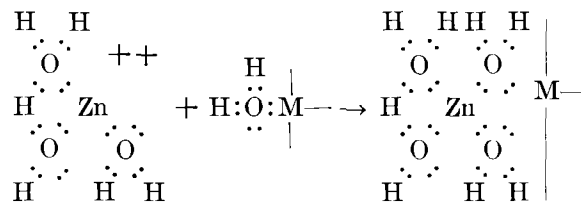
Normally, reversible electrodeposition processes take place at theoretical current efficiencies, but this is not always a reliable criterion. Nickel, for example, is often deposited at theoretical efficiencies within experimental error, although it is well known to be reduced irreversibly in all cases (11).

ver(I), gold(I), cadmium, mercury(II), gallium, indium, and thallium(III) are essentially similar (3) to those of zinc. Ions are reduced reversibly, and presumably by similar mechanisms, except when they are bound in hydrolysis products (4).

BONDING OF METAL ION TO CATHODE SURFACE

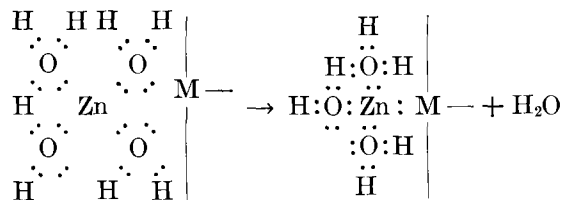
In the preceding section, it was tacitly assumed that electron pairs are available at the cathode surface for bonding with the intermediate ion, $[\text{Zn}(\text{H}_2\text{O})_3]^{++}$. The metal surface is probably hydrated, for, in terms of the mechanism just suggested, surface atoms on deposition do not find enough adjacent metal atoms to convert all of their bonding electrons to shared electron pair bonds. Consequently, a certain number will remain in coordination hybridization with water molecules.

Therefore, it is probable that electron pairs available for bonding at the cathode surface are largely those of coordinated water molecules. It may be imagined that binding of the 3-coordinate metal ion occurs first through a water bridge:



where M—represents the metal atoms (in this case, zinc) in the cathode lattice structure. The activation and adsorption process is equivalent to replacement of a water molecule originally located within the coordination sphere of the undissociated ion by a water molecule which is coordinated to the metal surface; or, what is essentially the same thing, adsorption on the surface of a coordinated water molecule of the undissociated ion.

Next occurs replacement of the water bridge by a metallic resonating bond between the ion and metal atom, with simultaneous or subsequent neutralization of the ionic charge:



The process is facilitated by the geometry of the bridging water molecule which, by virtue of the angularity of its bonds, brings ion and metal atom fairly close together. The change is facilitated also by relatively great extension of $4p$ orbitals of the ion

3*d* orbitals. As soon as two electrons have entered the 3*d* orbital, the resulting configuration is substantially identical with that of the metallic state. Subsequently, the state of remaining bonding electron pairs will be transformed from coordination hybridization to more stable metallic resonance, just as it was in the case of zinc. Electrons needed to neutralize the ionic charge are, of course, already present.

It may seem surprising that transfer of two electrons from the 4*p* to 3*d* level requires an appreciable activation, since stability is increased. However, the entering electrons were not originally in the 4*p* orbital, but rather in a resonance state somewhat more stable than this orbital. Apparently activation serves to lift resonating electrons to the 4*p* state momentarily, before transition to the 3*d* orbital can occur. Thus, activation represents energy needed to compensate for resonance stabilization.

This type of activation is not needed for zinc, because electrons continue to resonate in 4*p* orbitals after the ion is transformed to the metallic state, just as before transition. That is, there is no transfer from the *N* shell to the *M* shell, such as occurs with nickel.

These considerations can, of course, readily be applied to anodic processes. They can also be extended to other metals, such as iron and manganese, and to other coordinating groups, such as ammonia, chloride, or cyanide ions, as long as the complex ions do not have configurations designated "inner orbital" by Taube (14).

Platinum metals may have different electrode mechanisms, for they are deposited from inner orbital complexes. Until resonance structures contributing to the metallic state are suggested, it is difficult to propose a mechanism. Breaking of inner orbital hybridization will certainly require considerable activation. Further activation may be needed if there are other substantial differences in configuration between the two states. The highly irreversible character of electrode processes is therefore to be expected.

INCLUSIONS IN DEPOSITS

It has long been known that electrodeposits contain small amounts of oxygen and hydrogen. Frequently there are also present other substances which originate from anions or "nondepositing" cations. The presence of such impurities has often been ascribed to mechanical inclusion of adsorbed material. It is more likely that they represent coordinated groups remaining in the deposit because electron systems of a few ions were not fully converted from coordination hybridization to metallic resonating bonds.

Such incomplete conversion may occur at discontinuities in the cathode microstructure. Again, co-

ordinated groups may not always be released if local rate of deposition becomes so high that the available time is too short for conversion of bond type and subsequent diffusion of released groups out from the cathode surface.

For every solution there is a limiting current density above which deposits become spongy (16) and contain relatively high amounts of hydrogen and oxygen. Unfortunately, no systematic study of the nature and composition of these inclusions has been reported.

It is well established that electrodeposits from chloride baths contain chlorides. It has also been claimed that sulfur is found in deposits from sulfate baths (17), but more recent studies failed to confirm this statement (18). Since chloride ion has a stronger tendency to coordinate than the sulfate, this difference is to be expected. In sulfate baths, the predominating complexes are aquated ions, and therefore it would be expected that water would be included in the deposits. In chloride baths, mixed complexes are probably present, and both water and chlorides would likely be included.

For many years it has been assumed that oxygen in nickel deposits represents basic material precipitated in the cathode film, where *pH* was presumed to be high. The precipitate was considered to be adsorbed or mechanically included in the electrodeposit (19). However, observations of the cathode film by various methods (20) fail to show the high *pH* values which would be required by this theory, although presence of a very thin film of the required *pH* is not excluded.

Recent studies (18, 21) show that the average weight ratio of oxygen to hydrogen in a large number of nickel and chromium deposits is 8.0 ± 2.6 . This indicates that inclusions are water, not basic material, as predicted by the theory set forth above. Much more water is included in chromium than in nickel deposits, in accordance with comparative oxygen coordinating abilities of the two metals. Water is coordinated so firmly that it is not driven off or decomposed except at relatively high temperatures (18).

If inclusions originate from basic precipitates, deposits made at low current efficiencies will contain greater amounts of oxygen because the *pH* of cathode film will be higher. Data (18) indicate that there is no trend of this sort, although the study was not sufficiently extensive to be regarded as conclusive. Furthermore, observations of the cathode film by the drainage method (22) do not show the expected dependency of *pH* upon current efficiency. Evidence therefore indicates that inclusions are not primarily dependent upon cathode efficiency, as is required by the basic precipitate theory. However, residual coor-

dination does not depend on either current efficiency or pH of the cathode film.

Nevertheless, it is possible to suggest a mechanism leading to conversion of coordinated water to basic substances which does not require an unusually high pH at the cathode. Upon transfer of two electrons to $3d$ orbitals of the nickel ion, a new intermediate, $[\text{Ni}(\text{H}_2\text{O})_3]^\ominus$, is produced, which has a transient existence on the cathode surface. This intermediate has an excessive number of electrons for stability. Ordinarily electrons are released along with water molecules during transition to metallic resonance. However, electrons might also be eliminated by release of hydrogen atoms from coordinated water. If two hydrogen atoms are expelled, the product would be $\text{NiO} \cdot 2\text{H}_2\text{O}$, which might be included in the deposit as hydrous nickel oxide. The net effect would be reduction of hydrogen rather than nickel from the nickel complex.

The average oxygen content observed in nickel deposits (18) indicates that this mechanism can account for only about 0.0005% of current flow, even if all the oxygen is present as $\text{NiO} \cdot 2\text{H}_2\text{O}$. Observed cathode efficiencies in nickel deposition frequently depart from the theoretical by more than 0.1% and occasionally by as much as 1–5%. At least in these cases, most of the hydrogen evolved must come ultimately from water or hydrogen ion not coordinated with nickel ion. The composition of inclusions confirms this deduction, since basic material does not seem to be prominent. Evidently activation required for metal deposition allows effective competition of the hydrogen discharge mechanism, at least in some instances.⁵

It is possible that precipitation and inclusion of basic material may become important when the bath pH is quite high, about 5.5 in the case of nickel sulfate. Available data (18) do not permit conclusions on this point. But at lower pH , inclusions from nickel sulfate baths appear to consist largely, if not entirely, of coordinated water incorporated in deposits. This observation lends support to the deposition mechanism proposed above.

COMPARISONS WITH ELECTRON TRANSFER STUDIES

Electrode processes are but a special case of electron transfer reactions, in which one reactant is a separate phase, that is, the solid or liquid electrode. Similarities between electrode reactions and electron transfer processes in general are therefore to be expected.

A summary of rates of electron transfer reactions thus far reported (23) shows that transfer is very slow whenever it necessitates a change from inner to outer

orbital configuration, or vice versa. Where no shift in configuration occurs, reaction is generally complete in less than about two minutes. This is sufficiently close to the arbitrary limit of one minute selected by Taube (14) for indicating lability in substitution reactions of metal complex ions.

For example, cobalt(III) complexes are inner orbital; consequently, electron transfer from outer orbital cobalt(II) amines is very slow (24). However, with tetraphenylporphino complex, which is very probably inner orbital in both valence states, exchange is very rapid (25). The correlation is good in a number of other instances.

From considerations based on the Franck-Condon principle (26), Libby (27) deduced a "symmetry principle," which applies to electron transfer between different valence states of the same ion in solution. It appears to be equivalent to the principle that electrolytic oxidation or reduction is reversible if no substantial change in electronic configuration is required (1). Libby predicted that the symmetry principle would be applicable at electrodes.

In iron (28), europium (29), and thallium (30) systems, it is found that electron transfer is much more rapid in the presence of chloride ions. Several investigators (4) have reported that chloride ions decrease activation overpotentials and diminish polarographic irreversibility in electrodeposition. It was previously suggested that the effect results from formation of mixed complexes such as $[\text{Ni}(\text{Cl})(\text{H}_2\text{O})_3]^\oplus$. Labilization of a water group by the trans effect, according to the present theory, facilitates formation of the activated intermediate, $[\text{Ni}(\text{Cl})(\text{H}_2\text{O})_2]^\oplus$, or more precisely, a bridge-complex in which the water bridge is labilized by the chloride ion. Concentration of the mixed complex will be proportional to the first power of chloride ion concentration. This accounts for dependence of the rate of electron transfer reaction on this quantity.

Libby considers the catalytic effect of chloride ion dependent on electrostatic forces as well as on specific complexing properties of the ions in some instances. However, it is difficult to see how such electrostatic effects can be important in the electric field at the cathode unless complexes are formed. Still, structures described by Libby resemble, to some extent, bridge-complexes in which the chloride ion functions as the bridge.⁶

⁶ Note added in press: H. Taube and H. Myers [*J. Am. Chem. Soc.*, **76**, 2103 (1954)] present strong evidence for the role of an "activated bridge complex" involving chloride or sulfate bridges in electron transfer reactions. Structures proposed are strikingly similar to those here suggested for electrode reactions. Lowering of activation energy by Cl^- ions probably results, at least in part, from the formation of bridge complexes. Furthermore, the importance of bridging atoms in the electron transfer in crystalline solids has been emphasized by C. Zener [*Phys. Rev.*, **82**, 493 (1951)].

⁵ There is evidence that intermediates of the type described here are vital in hydrogen overvoltage phenomena.

ACTIVATION STEP

Rates of exchange of cyanide ion with complex cyanides (31) show that outer orbital cyano complexes exchange rapidly, whereas inner orbital ions exchange hardly at all. This observation supports the dissociation mechanism advanced by Taube (14) to explain substitution reactions, and employed with some modifications in the present paper to account for electrode reactions. In all three classes of reactions, thermodynamic dissociation constants are misleading as to rate of reaction. This circumstance results from the difference that in rate studies, dissociation refers to actual separation of a coordinated group, while familiar dissociation constants are concerned with conversion to aquo complexes. This has been explained previously (1).

These observations, together with excellent correlation between substitution reactions and electron transfer processes, indicate that the activation process is not a result of the electric field at the cathode, nor of surface effects (8). It is therefore ascribed to thermal effects (cf. 32). This is in accord with marked reduction in activation overpotential, and consequent increase in reversibility, with rise in temperature.

ACKNOWLEDGMENTS

Valuable criticisms and suggestions have been received from Professors John C. Bailar, Jr., H. A. Laitinen, and P. E. Yankwich. The work was supported by a Pre-doctoral Fellowship awarded by the Atomic Energy Commission.

Any discussion of this paper will appear in a Discussion Section, to be published in the June 1955 issue of the JOURNAL.

REFERENCES

1. E. H. LYONS, JR., *This Journal*, **101**, 363 (1954).
2. R. PIONTELLI, *J. Chim. phys.*, **45**, 288 (1949); *J. Inst. Metals*, **19**, 99 (1951); *Compt. rend. 2me. Reunion Com. Internat. Thermodynamique Cinetique Electrochim.*, **1950**, pp. 79, 185, 369, E. Tamburini, Milan (1951); *ibid.*, *3me. Reunion*, Berne (1952); *Z. Elektrochem.*, **55**, 123 (1951).
3. L. PAULING, *Proc. Roy. Soc. London*, **A196**, 343 (1949).
4. See Reference (1).
5. W. BLUM AND H. S. RAWDON, *Trans. Electrochem. Soc.*, **44**, 397 (1923).
6. P. K. FROHLICH AND G. L. CLARK, *Z. Elektrochem.*, **31**, 649 (1925).
7. See for example, L. B. HUNT, *Trans. Electrochem. Soc.*, **65**, 413 (1934); T. ERDEY-GRUZ AND M. VOLMER, *Z. phys. Chem.*, **157**, 165, 182 (1931).
8. See for example, J. HEYROVSKY, *Disc. Faraday Soc.*, **1**, 221 (1947).
9. I. M. KOLTHOFF AND J. J. LINGANE, "Polarography," Interscience Publishers, Inc., New York (1946).
10. J. J. LINGANE, *Chem. Revs.*, **29**, 1 (1941).
11. See Reference (9), p. 281.
12. E. H. LYONS, JR., *Trans. Electrochem. Soc.*, **88**, 281 (1945).
13. A. R. BURKIN, *Quart. Reviews, London*, **5**, 1 (1951); J. P. HUNT AND H. TAUBE, *J. Chem. Phys.*, **18**, 757 (1950).
14. H. TAUBE, *Chem. Revs.*, **50**, 69 (1952).
15. J. BJERRUM, "Complex Ammine Formation in Solution," P. Haase and Son, Copenhagen (1941).
16. O. KUDRA AND E. GITMAN, *Zhur. Priklad. Khim.*, **20**, 605 (1947); **21**, 284, 352 (1948).
17. H. N. HUNTZICKER AND L. KAHLBERG, *Trans. Electrochem. Soc.*, **63**, 349 (1933).
18. A. BRENNER, V. ZENTNER, AND C. W. JENNINGS, *Plating*, **39**, 879 (1952).
19. K. M. OSTERLE, *Z. Elektrochem.*, **35**, 505 (1929); J. B. O'SULLIVAN, *Trans. Faraday Soc.*, **26**, 89 (1930); *J. Electrodepositors' Tech. Soc.*, **5**, 37 (1930); G. E. GARDAM AND D. J. MACNAUGHTAN, *Trans. Faraday Soc.*, **29**, 755 (1933); *J. Electrodepositors' Tech. Soc.*, **9**, 26 (1933).
20. H. E. HARING, *Trans. Electrochem. Soc.*, **41**, 351 (1922); A. K. GRAHAM, S. HEIMAN, AND H. J. READ, *Proc. Am. Electroplaters' Soc.*, **1939**, 95; H. J. READ AND A. K. GRAHAM, *Trans. Electrochem. Soc.*, **78**, 279 (1940); A. BRENNER, *Proc. Am. Electroplaters' Soc.*, **1940**, 95.
21. A. BRENNER, P. BURKHEAD, AND C. JENNINGS, *J. Research Natl. Bur. Standards*, **40**, 31 (1948).
22. A. BRENNER AND G. WRANGLER, Unpublished paper.
23. A. W. ADAMSON, *J. Phys. Chem.*, **56**, 33 (1952).
24. W. B. LEWIS, C. D. CORYELL, AND J. W. IRVINE, JR., *J. Chem. Soc.*, **1949**, Supplement No. 2, 5386.
25. G. D. DARRAUGH AND R. W. DODSON, *Quarterly Progress Report*, Brookhaven Nat. Lab., July-Sept. 1951.
26. W. F. LIBBY, *Abstracts, Phys. and Inorg. Section*, 115th Meeting American Chemical Society, San Francisco, March 27-Apr. 1, 1949; cf. E. J. B. WILLEY, "Collisions of the Second Kind," E. Arnold and Co., London (1937); E. J. LAIDLER AND K. E. SHULER, *Chem. Revs.*, **48**, 153 (1951).
27. W. F. LIBBY, *J. Phys. Chem.*, **56**, 39 (1952).
28. J. SILVERMAN AND R. W. DODSON, Brookhaven Quarterly Report, BNL-93, p. 65, Oct.-Dec. 1950.
29. D. J. MEIER AND C. S. GARNER, *J. Am. Chem. Soc.*, **73**, 1894 (1951).
30. J. W. GRYDER, *Trans. N. Y. Acad. Sci.*, [II], **12**, 18 (1949).
31. A. W. ADAMSON, J. P. WELKER, AND M. VOLPE, *J. Am. Chem. Soc.*, **72**, 4030 (1950).
32. G. EMSCHWILLER, *J. chim. phys.*, **74**, 184 (1950).

Depolarization Effects after Current Reversal at Silver Anodes and Cathodes¹

A. L. FERGUSON AND D. R. TURNER²

University of Michigan, Ann Arbor, Michigan

ABSTRACT

Anode and cathode reactions at silver electrodes in hydrogen saturated 2*N* sulfuric acid following a current reversal were studied by recording potential-time curves. Three anodic processes and three cathodic processes are indicated when the current is reversed from cathode to anode and anode to cathode, respectively. The final anode reaction is silver dissolution. Silver sulfate forms on the electrode at a critical silver ion concentration.

INTRODUCTION

Most of the work to date on electrochemical polarization phenomena has sought in one way or another to determine the nature of anode and cathode reactions. Three types of experiments have been used: (a) measurement of single electrode potentials at various current densities; (b) polarization growth and decay curves, plotting electrode potential against time; and (c) depolarization effects at anodes and cathodes upon current reversal. The third method is probably the most effective for electrode reaction studies and is the one used in the work described here.

The meaning of the term depolarization effect is illustrated in Fig. 1. The potential of an electrode that has been cathodically polarized is represented by the line *a-b*. At *b* the current is reversed. If the potential changes immediately to the final anodic process producing anodic polarization as along the line *bcd*, then there is no depolarization effect. If, however, there exists some kind of potential arrest, or delay in reaching the final polarization potential as *e-f* in curve *abefgd*, then there is a depolarization effect. The material producing this depolarization may be the oxidation of some material cathodically produced previous to current reversal or the formation of some anodic product prior to the final anodic process. The potentials at which depolarization effects occur are characteristic of the electrochemical reaction involved, while the coulombs of electricity consumed by the process is a measure of the amount

of the material reacting at the electrode-solution interface.

Many electrode processes have been studied in recent years by means of depolarization effects at anodes and cathodes. Butler and co-workers (1-3) observed the depolarization effects of hydrogen and oxygen at bright platinum electrodes in hydrogen saturated solutions. Ferguson and Towns (4) studied anodic and cathodic depolarization curves for platinized platinum in hydrogen- and nitrogen-saturated acid solutions.

In addition to platinum, Piontelli and Poli (5) studied the cathodic depolarization processes on copper, lead, and cadmium by measuring the cathode potential at various current densities after an anodic prepolarization in acid and alkaline solutions which were saturated with air, oxygen, nitrogen, or hydrogen. In every case, a single stage of depolarization was observed and attributed to dissolved oxygen in the solution.

Luther and Pokorny (6) anodically polarized a silver electrode at a small constant current in alkaline solutions, and observed two definite arrests prior to oxygen evolution. Silver was assumed to be oxidized, quantitatively and reversibly, first to Ag₂O and then to Ag₂O₂. The cathodic reduction of the same silver oxides, formed anodically, was studied by Rollet (7). The oxidized silver electrode, with a nonpolarizing auxiliary electrode, was made the source of current which was measured as a function of time. Three level stretches of current were observed, the first was attributed to the peroxide, Ag₂O₂, the second to Ag₂O, and the last to the reduction to free silver.

The thickness of tarnish films on copper and silver were determined by Campbell and Thomas (8) from quantitative measurements on the depolarizing effects of these films while the metals were cathode in an appropriate electrolyte.

Recently, Hickling and co-workers studied the

¹ Manuscript received December 17, 1951. This paper was prepared for delivery before the Cleveland Meeting, April 19 to 22, 1950. This paper is based on part of a thesis submitted by D. R. Turner in partial fulfillment of the requirements for the Ph.D. degree to the Graduate School of the University of Michigan.

² Present address Bell Telephone Laboratories, Murray Hill, New Jersey.

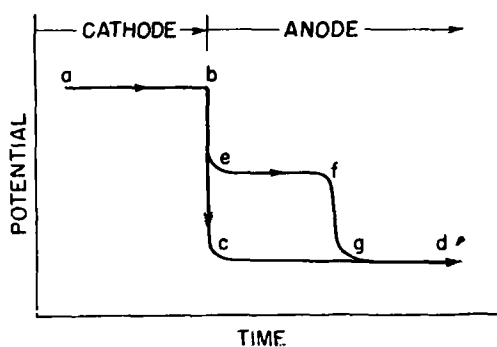


FIG. 1. Typical potential-time curves upon current reversal. (A) No depolarization effect, curve *a b c d*; (B) with depolarization effect, curve *a b e f g d*.

anodic behavior of several metals: platinum (9), gold (10), nickel (11), silver (12), and copper (13). Employing the automatic electronic system devised by Hickling (14), recurrent anode potential-time curves were obtained by means of a cathode-ray oscillograph in acid, neutral, and alkaline solutions. Breaks in the curves, in many cases, were shown to correspond to potentials of certain metal oxide electrodes prepared and measured by the authors.

In the present work, reactions at silver anodes and cathodes were studied in 2*N* sulfuric acid solutions. The experimental method employed was to record the change in the potential of a silver electrode with time following a current reversal. These potential-time curves are interpreted then in terms of specific anode and cathode reactions.

APPARATUS

The electrolytic cell used is described elsewhere (15). All potentials were measured relative to a mercury-mercurous sulfate reference electrode. Its potential against a normal hydrogen electrode at 25°C was +0.673 volt. Silver electrodes were prepared by electroplating about 0.001 in. (0.0025 cm) of silver on copper disks 1.13 cm in diameter. A cyanide silver plating solution of standard composition was used. The back side was coated with an insulating wax³ leaving an exposed silver area of 1.00 cm². After plating, the electrodes were rinsed first in distilled water and then in 2*N* sulfuric acid before being placed in the cell.

Tank hydrogen was used after removing oxygen traces by bubbling through a concentrated chromous sulfate solution. The gas was then bubbled through 20% sodium hydroxide and finally through 2*N* sulfuric acid before entering the electrolytic cell.

A constant current power supply was used consisting of a 90-volt dry battery with a variable high resistance in series. Switching the current was done automatically by a specially designed photocell cir-

³ United Chromium Stop-off Compound 311.

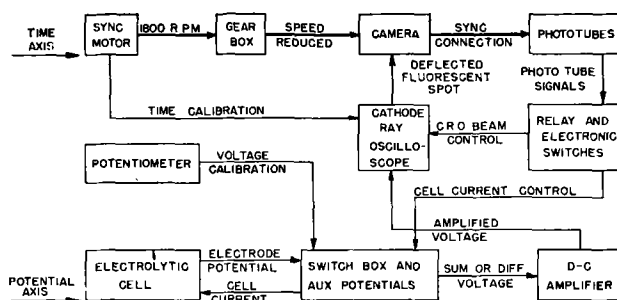


FIG. 2. Block diagram of cathode ray recording apparatus.

cuit which was synchronized to the film position of the recording drum-type camera. A block diagram of the recording and switching apparatus is shown in Fig 2. Calibration voltages and times were placed on each oscillograph record. All potential values referred to in this paper are on the hydrogen scale.

EXPERIMENTAL

The open-circuit potential of a silver electrode in a hydrogen saturated 2*N* sulfuric acid solution is +0.29 volt. When this electrode is made cathode at about 1.00 ma/cm², the electrode potential changes rapidly to that of hydrogen gas evolution. Silver ions enter the solution when the electrode is made anode. These may be removed by prolonged cathodic treatment (24 hr). The white silver surface becomes black with a finely divided, loosely adherent coating of silver. It was more convenient to use fresh solution frequently rather than electrolyze out the dissolved silver. A fresh solution was electrolyzed for about 2 hr prior to use to remove traces of metal impurities.

Anodic Depolarization Effects

In all experiments the current density, usually 1.00 ma/cm², was unchanged before and after current reversal. When the current is reversed making the silver electrode anode, the potential-time curve passes through several potential arrests before reaching a relatively stable anode polarization potential (Fig. 3 from *a* to *f*). After a rapid initial potential change *a-b*, a linear stage of depolarization occurs between -0.19 and +0.28 volt. This is followed by an almost horizontal potential arrest *c-d* and then a transition section *d-e*. The final anodic process begins at *e* and continues to a maximum potential of +0.70 volt. The meaning of *f* is discussed later. The amount of anodic depolarization is a function of cathodic pretreatment time. A freshly plated silver electrode usually requires several hours of cathodic pretreatment, however, before an appreciable anodic depolarization effect can be obtained. Cathodically formed anode depolarizer is always destroyed after a few minutes of anodic treatment.

Cathodic Depolarization Effects

The typical cathodic depolarization curve obtained following an anodic pretreatment is shown in Fig. 3 from *g* to *l*. Note that there are two arrest stages of depolarization, *g-h* and *j-k*. If the current is reversed before the anode potential reaches +0.65 volt, then only one cathodic depolarization stage results, *j-k*. This indicates that the stage *g-h* is the reduction of an anodic product which begins to form at +0.65 volt. While several hours of cathodic pretreatment were required to generate an appreciable amount of anode depolarization, only a few seconds anode time before switching to cathode produced a large amount of cathodic depolarization.

Freshly plated silver electrodes were made anode at a constant current of 1.00 ma/cm² for various times up to 15 sec and then the current was reversed. The amount of cathodic depolarization resulting was measured on the oscillograph record from *g* to *l* (see Fig. 3). The relation between the coulombs used in the anodic pretreatment and coulombs of cathodic depolarization is given in Fig. 4. About two millicoulombs of anodic pretreatment are required to produce one millicoulomb of cathodic depolarization. Although quantitative measurements were not made on depolarization obtained with anodic pretreatments longer than 15 sec, it was observed that cathodic depolarization reached a maximum after about 1 min of anodic pretreatment at 1.00 ma/cm².

Electropolishing the silver electrode appeared to have no effect on anodic or cathodic depolarization curves. Freshly plated silver electrodes were electropolished in a water solution containing 100 g/l KCN and 50 g/l KOH by passing 2 amp of 60 cycle alternating current for a few seconds between the plated electrode and a coiled silver wire.

A fruitful type of experiment in this method of studying electrode reactions is to dissect polarization curves into parts (*a*) by permitting the anode or cathode prepolarization to decay briefly before current reversal, and (*b*) by reversing the current at various stages of the depolarization stage. The first type of experiment indicates what part of the initial potential change is due to a gas overvoltage since these potentials are usually large in magnitude and

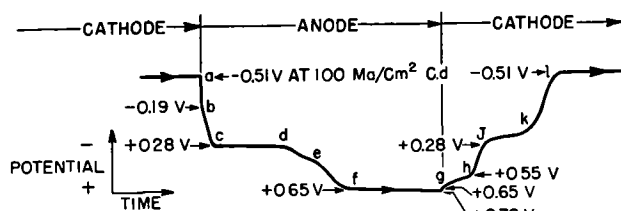


FIG. 3. Typical anodic and cathodic depolarization curves of a silver electrode in 2N sulfuric acid.

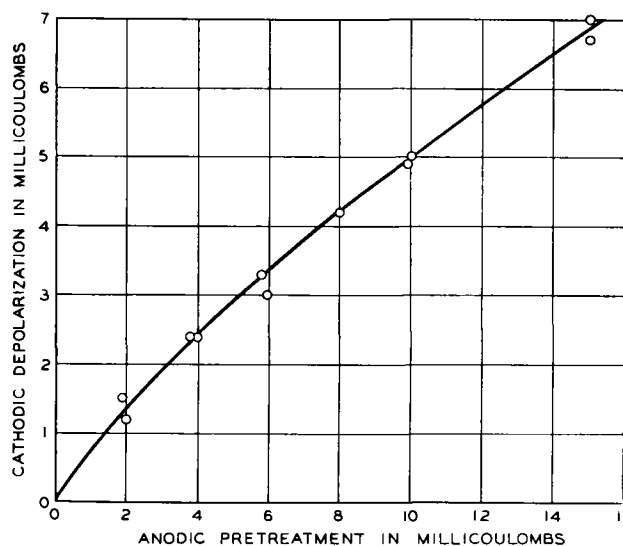
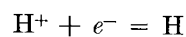


FIG. 4. Effect of anodic pretreatment on cathodic depolarization.

rapid in decay. The decay period also gives the experimenter some idea of the stability or solubility of any electrochemically formed depolarizing material in the electrolyte used. By reversing the current at various stages of the depolarization, it is possible to define clearly the individual electrode processes and determine the reversibility of each electrochemical reaction. The results of these observations are included in the discussion which follows.

DISCUSSION OF RESULTS

The anode and cathode potential-time curves of silver electrodes in 2N sulfuric acid consist of several depolarization stages. Each stage corresponds to a definite electrode reaction. A symbolic description of these phases of depolarization is given in Fig. 5. Prior to *a* the silver electrode is cathode, the potential being a function of current density. At 1.00 ma/cm² it was -0.51 ± 0.02 volt. The electrochemical reaction occurring is



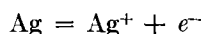
The cathode potential did not change appreciably during prolonged electrolysis. A part, at least, of the cathode polarization is due to an equilibrium concentration between atomic hydrogen and hydrogen ions at the metal-solution interface.

At *a* the direction of current through the cell was reversed and the potential changed suddenly to *b*. This is the rapid portion of the cathode polarization decay which would occur regardless of whether the current was reversed or the cathode polarization simply allowed to decay on open circuit. From *b* to *c* the potential changes in a linear manner with time. This stage of depolarization is attributed to the reionization of the surface absorbed hydrogen. It

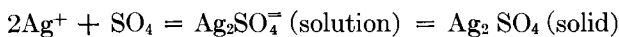
can be compared to the initial anodic depolarization stage obtained with platinized platinum (4).

Beginning at *c*, the electrode passes through a region where its potential remains essentially constant. A similar arrest is observed when bright platinum electrodes are used (1-3, 16) and at approximately the same potential, +0.28 volt. Butler and Armstrong (16) explained the effect as due to the ionization of absorbed hydrogen. The actual form of hydrogen in the metal was not considered by them. Since the potential remains essentially constant in this region at both platinum and silver electrodes, it seems probable that this stage of depolarization is due to oxidation of a definite compound, in this case a hydride (17). With both metals, this stage of anodic depolarization increased with longer cathodic pre-polarizations. The cathode efficiency for hydride formation appears to be very low, about 0.01% for silver. This suggests that atomic hydrogen diffuses into platinum and silver only very slowly. The stable potential of a silver electrode in a hydrogen saturated 2*N* sulfuric acid solution without any current flow was +0.29 volt. This may represent the steady condition for molecular, atomic, and ionic hydrogen at the metal-solution interface.

The amount of hydrogen available for ionization begins to decrease at *d* in Fig. 3 and the potential changes to the start of silver dissolution which begins at *e*, about +0.4 volt.



The potential continues to change toward more positive values as the silver ion concentration increases. Finally at *f*, +0.65 volt, the concentration of both silver and sulfate ions exceeds the solubility product for the precipitation of silver sulfate.



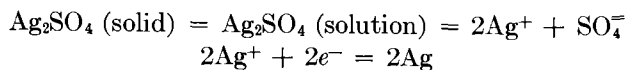
and the potential again assumes a relatively stable value due to the Ag_2SO_4 on the surface maintaining a constant concentration of Ag^+ ions. The dark, finely divided silver deposit which can be produced by plating out dissolved silver turns white soon after the electrode is made anode. This is consistent with the assumption that the compound formed is silver sulfate, since Ag_2SO_4 is white.

Experimental results indicated that no silver sulfate is produced on a silver anode in 2*N* sulfuric acid if the electrode potential does not become more positive than about +0.65 volt. Latimer (18) gives an E^0 value of +0.653 volt for the formation of silver sulfate which is precisely the value observed for the start of silver sulfate formation.

The maximum anode potential reached under all circumstances at 1.00 ma/cm² was +0.70 volt. This

increase above +0.65 volt probably resulted from an excess concentration of silver ions collecting at the electrode-solution interface. In a few experiments at 1.00 ma/cm², the anode potential did not become more positive than about +0.55 volt after about 10 sec anode time. This is believed to be due to an unusual condition where atomic hydrogen was able to diffuse continuously from the metal interior to maintain the electrolysis current at the metal-solution interface, thus preventing a sufficient concentration of silver ions from building up to the point of precipitation of silver sulfate.

When the electrode polarity was reversed from anode to cathode, the material first formed anodically was reduced. The initial rapid potential rise to *g* is due to the decay of a concentration polarization produced by the slight excess of silver ions that had accumulated at the electrode surface just prior to the reversal. The cathodic depolarization stage from *g* to *h* resulted from the discharge of silver ions formed from the dissolved Ag_2SO_4 precipitate. The slope in the curve is attributed to silver ions being removed from the metal-solution interface faster than they are formed.



As all the silver sulfate is dissolved and the silver ions are discharged, the cathode potential changes

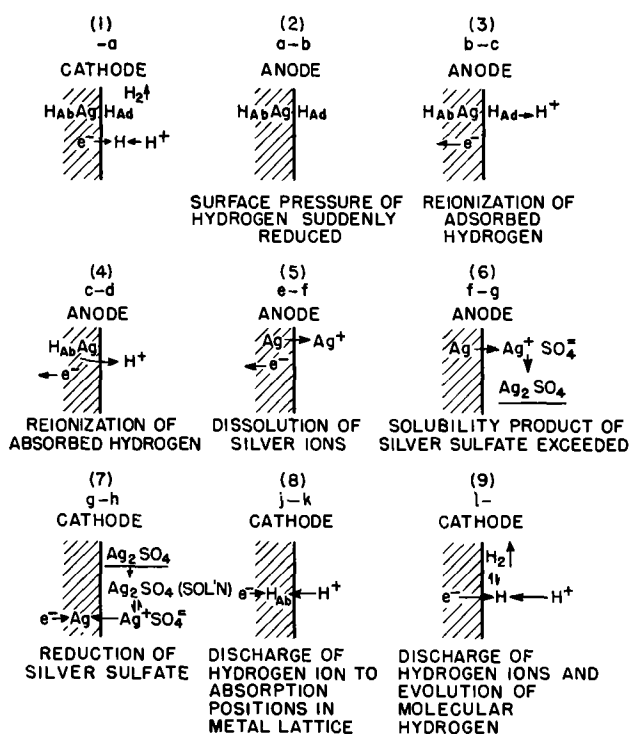


FIG. 5. Suggested reactions and conditions at the metal-solution interface at various places in the anodic and cathodic depolarization curves.

from h to where the next cathodic process begins at j . The stage of depolarization from j to k is interpreted as the discharge of hydrogen ions and subsequent absorption of the atomic hydrogen into the silver lattice, perhaps forming a silver hydride. The physical condition of the surface apparently determines how much atomic hydrogen is absorbed and thus, the length of the second cathodic depolarization stage. The length of both cathode depolarization stages is a function of the anodic pretreatment. Between k and l there is a transition from the hydrogen absorption stage to the formation and evolution of molecular hydrogen which begins at l . The potential at l corresponds to that at a and is a function of the current density used; at 1.00 ma/cm² it is -0.51 volt.

An interesting relation was observed between the coulombs used in anodically pretreating a silver electrode and the coulombs of cathodic depolarization which followed. This is shown in Fig. 4. Within the range studied, from 0 to 15 millicoulombs anode pretreatment, the total amount of cathodic depolarization observed was approximately one-half the coulombs used for the anodic pretreatment. This cannot be considered significant since some of the anodically formed silver sulfate is lost through the dissolving action of the 2*N* sulfuric acid before complete cathodic reduction of the silver ions can take place. In distilled water, silver sulfate is cathodically reduced to silver and sulfuric acid at 100% efficiency (19). While silver sulfate is essentially insoluble during the course of an experiment in distilled water, it is readily dissolved in 2*N* sulfuric acid. Results of anode polarization decay experiments show that a 10-sec anodic deposit of silver sulfate is wholly dissolved in about 5 sec decay time. The potential changes in the decay curves during the dissolving period of the silver sulfate correspond exactly to those occurring when the electrode is cathodic. This means that the potential of the electrode in the region $g-h$ is controlled by the silver ion concentration at the metal-solution interface regardless of whether the silver ions are removed by cathodic electrodeposition or by diffusion and convection away from the surface. As expected, stirring shortened the cathodic depolarization stage $g-h$.

SUMMARY AND CONCLUSIONS

Three anodic processes occur at silver electrodes in 2*N* sulfuric acid when the current is reversed from cathode to anode: (a) ionization of adsorbed hydrogen atoms; (b) oxidation of adsorbed hydrogen (silver hydride); and (c) dissolution of silver. When the silver ion concentration exceeds a critical value, silver sulfate is formed on the electrode. This film of silver sulfate is readily dissolved in the 2*N* sulfuric acid electrolyte.

Upon current reversal from anode to cathode, three cathode reactions take place: (a) reduction of the silver sulfate film; (b) discharge of hydrogen ions into absorption and adsorption positions in the silver electrode; and (c) discharge of hydrogen ions and formation of molecular hydrogen.

Any discussion of this paper will appear in a Discussion Section to be published in the June 1955 issue of the JOURNAL.

REFERENCES

1. G. ARMSTRONG, F. R. HIMSWORTH, AND J. A. V. BUTLER, *Proc. Roy. Soc. London*, **A137**, 694 (1932).
2. G. ARMSTRONG, F. R. HIMSWORTH, AND J. A. V. BUTLER, *ibid.*, **A143**, 89 (1933).
3. J. D. PEARSON AND J. A. V. BUTLER, *Trans. Faraday Soc.*, **34**, 1163 (1938).
4. A. L. FERGUSON AND M. B. TOWNS, *Trans. Electrochem. Soc.*, **83**, 271, 285 (1943).
5. R. PIONTELLI AND G. POLI, *Atti reale accad. Italia*, **13**, 903 (1942).
6. R. LUTHER AND F. POKORNY, *Z. anorg. u. allgem. Chem.*, **57**, 290 (1908).
7. A. P. ROLLET, *Compt. rend.*, **186**, 748 (1928).
8. W. E. CAMPBELL AND U. B. THOMAS, *Trans. Electrochem. Soc.*, **76**, 303 (1939).
9. A. HICKLING, *Trans. Faraday Soc.*, **41**, 333 (1945).
10. A. HICKLING, *ibid.*, **42**, 518 (1946).
11. A. HICKLING AND J. E. SPICE, *ibid.*, **43**, 762 (1947).
12. A. HICKLING AND D. TAYLOR, *Discussions Faraday Soc.*, **1**, 277 (1947).
13. A. HICKLING AND D. TAYLOR, *Trans. Faraday Soc.*, **44**, 262 (1948).
14. A. HICKLING, *ibid.*, **33**, 1540 (1937).
15. D. R. TURNER, *This Journal*, **98**, 434 (1951).
16. J. A. V. BUTLER AND G. ARMSTRONG, *J. Chem. Soc. London*, **1934**, 743.
17. D. T. HURD, "Chemistry of the Hydrides," p. 195, John Wiley & Sons, Inc., New York (1952).
18. W. M. LATIMER, "Oxidation Potentials," p. 180, Prentice-Hall Inc., New York (1938).
19. P. JOLIBOIS AND V. SPRETER, *Compt. rend.*, **229**, 167 (1949).



Continuous and Uniform Generation of Stibine

An Electrolytic Apparatus and Method¹

ARNOLD REISMAN², MELVIN BERKENBLIT², E. C. HAAS, AND ALLISON GAINES, JR.

Material Laboratory, New York Naval Shipyard, Brooklyn, New York

During the course of an investigation it was necessary to subject an instrument to an atmosphere containing a mixture of 3–4% hydrogen and $\frac{1}{60}$ this amount of stibine. This volume ratio had to be maintained for 24 hr. Stibine is not available commercially because it is unstable; consequently, a method was sought which would supply the gas in the desired concentration throughout the test period. A survey of available literature indicated that no reported methods would meet this requirement.

Electrolytic methods for generation of stibine using antimony electrodes have been previously reported (1, 2). These methods proved unsuitable because the production of stibine was either too low or too irregular. It was found that if the antimony electrode were replaced by a 40 gauge, platinum-iridium electrode (90:10) in conjunction with an antimony solution, stibine output at the cathode was fairly uniform and of the desired order of magnitude.

Apparatus.—The generator unit consists of a 250 ml wide-mouth Erlenmeyer flask into which is inserted an arrangement for preventing intermixing of gases liberated at the cathode with oxygen liberated at the anode. The cathode consists of a 5 mm diameter glass tube with 40 gauge platinum-iridium wire fused into one end. The anode is a 16 gauge platinum wire. A variable d-c source supplied power.

The assembly used in calibrating the generator was made up of a series of three traps followed by a conventional wet test meter, thermal conductivity bridge for measurement of hydrogen, and a regulated vacuum pump for drawing gases through the system. In order to permit uninterrupted running, two of these trap series were connected in parallel. At given time intervals the series through which the gas had been passing was removed for analysis, and the second series was brought into the circuit by means

of a three-way stopcock. The first two units of each trap series contained 200 ml 0.01N iodine and 32 ml concentrated hydrochloric acid. The third unit of the series contained 300 ml 0.01N sodium thiosulfate to prevent loss of iodine by mechanical carry over.

Generating solutions.—(A) (4N in H₂SO₄)³—Dissolve 8 grams purified Sb metal in 100 ml boiling H₂SO₄, cool slightly (a white gel forms), pour with vigorous stirring into 700 ml water containing 80 grams tartaric acid, dilute to 900 ml with water.

(B) (1N in H₂SO₄)—Dissolve 5.3 grams Sb₂O₃ in 400 ml of solution containing 75 grams tartaric acid and 14 ml H₂SO₄, dilute to 500 ml with water.

(C) (0.5N in H₂SO₄)—Dissolve 7.5 grams Sb₂O₃ in 600 ml of a solution containing 77 grams tartaric acid and 10 ml H₂SO₄, dilute to 700 ml with water.

(D) (No H₂SO₄)—Dissolve 10.6 grams Sb₂O₃ in 900 ml of a solution containing 110 grams tartaric acid, dilute to 1 liter with water.

Analysis of stibine and hydrogen.—Stibine output at the cathode was determined using a modification of the iodimetric method of Haring and Compton (3). Periodically contents of the traps were mixed and back titrated with sodium thiosulfate. The quantity of stibine was then calculated using the stoichiometry given in reference (3). To determine the validity of the method, stibine triiodide resulting from the titration was converted to antimony trioxide. This was titrated with iodine to the pentavalent state (4). Results obtained from both methods checked to within 0.01 mg. Table I shows quantities of stibine as determined by the above method.

Effluent gases from the traps were drawn through a hydrogen measuring thermal conductivity bridge. Spot checks of this gas, using the conventional Orsat combustion method, were made periodically and agreed with the thermal conductivity bridge to within 0.1%.

¹ Manuscript received August 13, 1953. This paper was prepared for delivery before the Chicago Meeting, May 2 to 6, 1954.

² Present address: International Business Machines Corporation, Watson Scientific Computing Laboratory at Columbia University, New York, N. Y.

³ Sulfuric acid was used exclusively because of its low vapor pressure. Hydrochloric acid or other acids with relatively high vapor pressure would evolve sufficient vapors to damage the instrument under test and the thermal conductivity bridge.

CONCLUSIONS

As time did not permit complete evaluation of varying conditions, a comprehensive discussion cannot be presented here. However, certain inferences can be drawn from Table I.

It was found that if any two of the three variables (acid normality, impressed amperage, and electrode length) were held constant while the third was changed, an optimum value for the variable was found to exist. Below or above this optimum value, either the hydrogen-to-stibine ratio was too great or evolution of stibine was not constant over an extended period. It is apparent, therefore, that for a given set of conditions certain combinations of the variables must be employed. These conditions, in addition to being affected by already described variables, will to a lesser extent be a function of the given stibine generator. Thus, variation in electrical com-

TABLE I

Run No.	Generating solution	Electrode length (mm)	Amp	Time elapsed (min)	Stibine (mg/min)	Hydrogen (%)
1	I	13	1.0	60	0.24	4.4
				90	0.24	4.4
				120	0.28	4.4
				150	0.28	4.4
				180	0.27	4.4
				210	0.26	4.4
				270	0.27	4.4
				330	0.25	4.4
				390	0.26	4.4
				450	0.26	4.4
				510	0.27	4.4
				570	0.27	4.4
				630	0.25	4.4
2	I	8	1.0	30	0.50	5.3
				60	0.47	5.3
				90	0.47	5.3
				120	0.48	5.3
				150	0.41	5.3
				180	0.38	5.3
				240	0.35	5.3
				300	0.34	5.3
360	0.32	5.3				
420	0.23	5.3				

TABLE I—Continued

Run No	Generating solution	Electrode length (mm)	Amp	Time elapsed (min)	Stibine (mg/min)	Hydrogen (%)		
3	I	3	0.75	60	0.50	3.6		
				120	0.48	3.6		
				180	0.48	3.6		
				240	0.49	3.6		
				300	0.48	3.6		
				360	0.49	3.6		
				420	0.48	3.6		
				480	0.50	3.6		
				540	0.48	3.6		
				600	0.48	3.6		
				660	0.49	3.6		
				720	0.48	3.6		
				780	0.49	3.6		
840	0.48	3.6						
4	II	10	1.0	30	0.39	4.0		
				60	0.29	4.0		
				90	0.25	4.0		
				120	0.25	4.0		
				150	0.23	4.0		
				180	0.21	4.0		
5	III	10	0.7	30	0.19	4.2		
				60	0.07	4.2		
	IV			10	0.3	30	0.08	4.4
						210	0.02	4.4

Flow was held at 0.16 l/min.

ponents of the d-c source would require compensations and individual calibration for a given unit. The system gave the desired 60/1 ratio of hydrogen to stibine when the variables were held as shown in Table I, run 3.

Any discussion of the paper will appear in a Discussion Section, to be published in the June 1955 issue of the JOURNAL.

REFERENCES

1. H. J. S. SAND, E. J. WEEKS, AND S. W. WORREL, *J. Chem. Soc.*, **123**, 456 (1923).
2. M. HLASKO AND M. MASLOWSKI, *Roczniki Chem.*, **10**, 240 (1937).
3. H. E. HARING AND K. G. COMPTON, *This Journal*, **68**, 283 (1935).
4. W. W. SCOTT, "Standard Methods of Chemical Analysis," 5th ed., p. 76, D. Van Nostrand Co., New York (1925).

Formation of Anodic Oxide Films on Cathodes¹

D. A. VERMILYEA

General Electric Research Laboratory, Schenectady, New York

ABSTRACT

The total voltage applied across an anodic film during its formation consists of the voltage applied to the cell minus any polarization voltage at the cathode and resistive drop in the electrolyte, plus the potential of the electrochemical reaction. It is shown that, because of the latter potential, it is possible to form an oxide film on tantalum even when the tantalum is considerably negative with respect to a hydrogen electrode.

INTRODUCTION

In a previous paper (1) the calibration of an optical step gauge for estimating the thickness of anodic Ta_2O_5 films was described. The step gauge was made by anodizing specimens of tantalum to a series of voltages, the temperature and current density being held constant. Under these conditions it was found from weight change measurements that the thickness of the oxide film was directly proportional to the applied voltage. It was also found that the plot of thickness against applied voltage had a small positive intercept on the thickness axis. Since specimens used for the calibration were probably covered initially with a thin air-formed oxide film, no additional oxide would be formed upon anodization until the voltage equivalent to the thickness of the initial film was exceeded. It was expected, therefore, that no weight increase would be observed below a certain voltage and that the thickness vs. voltage plot would have a small negative intercept on the thickness axis. It was suggested that the positive intercept was the result of the voltage of the electrochemical reaction occurring in the cell. Since there was a considerable amount of experimental uncertainty in the intercept obtained from the weight measurements, it was decided to make a further study of the formation of anodic films in the region of zero voltage.

EXPERIMENTAL

The material used in these experiments was 0.004 in. rolled tantalum sheet obtained from Fansteel Metallurgical Company. All specimens were chemically polished in a mixture of 5 parts by volume 95% H_2SO_4 , 2 parts 70% HNO_3 , and $1\frac{1}{2}$ parts 48% HF before use. The solutions used for anodizing were 2% HNO_3 and 2% NaOH.

Fig. 1 shows a wiring diagram of the apparatus, which consisted of a type 650A General Radio impedance bridge, an ammeter, and a potentiometer, of low resistance in series with the reaction cell.

The potentiometer, shunting a storage battery, provided a means of varying the voltage applied across the cell.

At the start of an experiment, a specimen of tantalum was attached to the specimen holder ready to be placed into the electrolyte, and the potentiometer was adjusted so that the tantalum was at a potential of -2 to -3 volts with respect to a platinum electrode in the electrolyte. The specimen was then dipped in 48% HF for a few seconds to remove any existing oxide film, and then immediately immersed in the electrolyte without removing the HF which clung to the specimen. The capacity was then measured as a function of voltage, starting with negative voltages and measuring the voltages between the tantalum and a calomel reference electrode, using a vacuum tube voltmeter.

The oxide film thickness calculated from the reciprocal of the capacity may be in error for several reasons. In the first place, the measured capacity is that of the tantalum oxide film in series with the double layers in the electrolyte near the anode and cathode. The cathode used was platinum with an area of about 100 cm^2 . The capacity of the double layer near platinum was found by direct measurement to be about $20\ \mu\text{f}/\text{cm}^2$, so that the total capacity of the cathode double layer was about $2000\ \mu\text{f}$. The largest capacity measured in the experiments was about $100\ \mu\text{f}$, so that a maximum error of 5% in the reciprocal of the capacity was introduced by the cathode double layer. The capacity of the anode double layer cannot be measured directly since it is in contact with the oxide film whose capacity is not precisely known. The reciprocal of the measured capacity is, therefore, larger than the reciprocal of the capacity of the tantalum oxide film by an unknown amount.

The second difficulty in estimating thickness from capacity measurements is that the dielectric constant of the film has been found to be a function of the field present in the oxide film during formation and also of the field applied during the capacity measurement. Temperature of measurement also introduces

¹ Manuscript received February 23, 1954

some variation in the capacity of a cell, but these experiments were all conducted at room temperature. The maximum variation in capacity observed from these causes is approximately 5%.

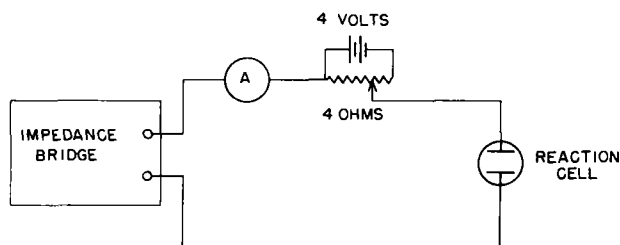


FIG. 1. Schematic wiring diagram

Because of the errors involved, therefore, no attempt was made to calculate the actual film thickness, and only the reciprocals of the measured capacities are reported. For a rough estimate, however, the thickness may be calculated from the formula

$$X = 236C^{-1}$$

where X is the thickness in angstrom units and C is the capacity in microfarads. This formula is calculated using a dielectric constant of 25 (2), an average value obtained from many measurements of capacity and optical thickness of anodic films formed at different temperatures with different applied fields. The area of the specimens used was approximately 1 cm^2 .

RESULTS AND DISCUSSION

Fig. 2 and 3 show plots of the reciprocal of the capacity against voltage for formation in 2% HNO_3 and 2% NaOH , respectively. In these figures, voltage refers to the voltage which would have existed between the tantalum and a standard hydrogen electrode. Voltage values were obtained by adding 0.28 volt (the potential of the normal calomel electrode on the hydrogen scale) to observed voltages. Also indicated in each figure is the direction of current flow, "negative" indicating that the current flow would liberate hydrogen at the tantalum electrode, "positive" indicating that hydrogen would be liberated at the platinum electrode.

It may be seen from the figures that the reciprocal of the capacity is a linear function of voltage even in the region where the tantalum potential was considerably negative on the hydrogen scale, and even though the current was in the direction to liberate hydrogen at the tantalum. The fact that an oxide film has actually been formed at these negative potentials was established by decreasing the potential at several points and again measuring the capacity. Values obtained in this manner are also shown in the figures. It may be seen that some de-

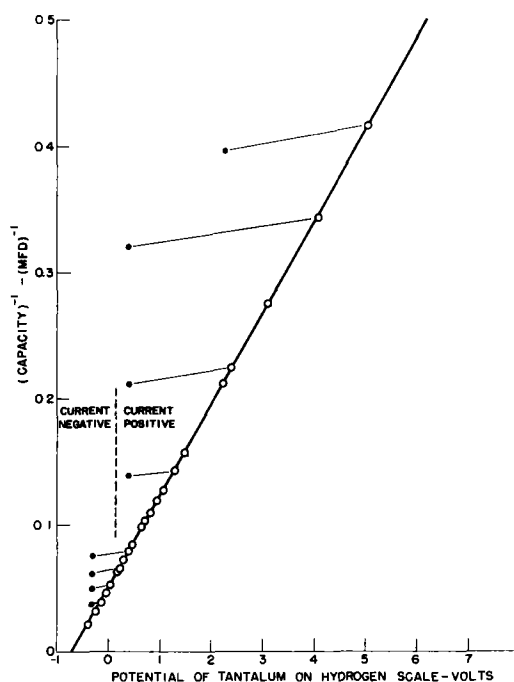


FIG. 2. Reciprocal of capacity vs. voltage for formation in 2% HNO_3 . O—capacity measured with forming voltage applied; ●—capacity measured at a voltage less than the forming voltage indicated.

crease in the reciprocal of the capacity occurs on lowering the potential, perhaps caused partly by changes in the double layer capacities and partly by changes in the dielectric constant of the oxide film.

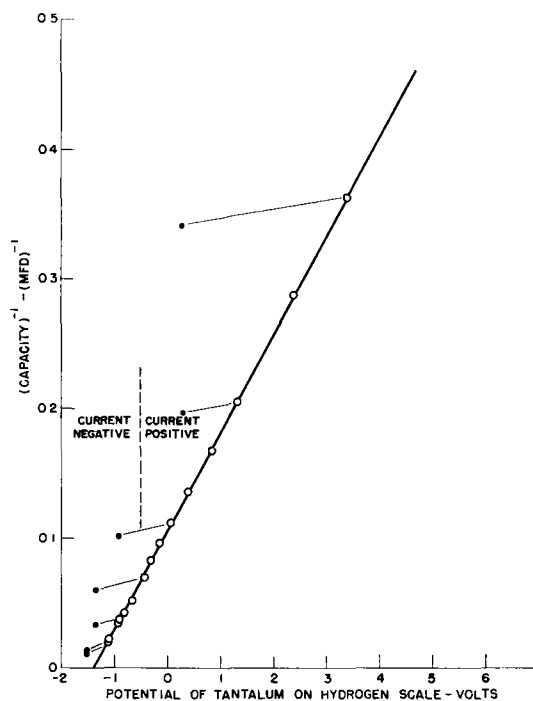
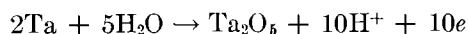


FIG. 3. Reciprocal of capacity vs. voltage for formation in 2% NaOH . O—capacity measured with forming voltage applied; ●—capacity measured at a voltage less than the forming voltage indicated.

For a given voltage decrease the reciprocal of the capacity decreases by roughly the same amount at all thicknesses, however, and does not follow the original curve of C^{-1} vs. V . Since the increase in reciprocal capacity at negative voltages is not reversible, therefore, and since the values obtained lie on the same straight line as do those obtained at positive voltages, it is concluded that an oxide film has been formed.

These results may be explained as follows. When the tantalum electrode is made negative with respect to the platinum in the electrolyte, distribution of potential is presumed to be as shown schematically in Fig. 4. A large drop in potential occurs due to oxygen overvoltage at the platinum and a much smaller one (negligible at the current densities employed here) as IR drop in the electrolyte. At the tantalum electrode two reactions are possible, evolution of hydrogen and formation of tantalum oxide. The equation for the latter may be written



$$E_o = -0.81 \text{ volt}$$

When the tantalum is covered with an oxide film, as it is in these experiments, activity of the tantalum is probably very small, so that the potential for the reaction will be less negative than 0.81 volt, and is designated in Fig. 4 by V_R . It is supposed that this potential difference occurs across a very thin double layer in the solution next to the tantalum oxide film. It may be seen from the figure that, although the tantalum is negative with respect to the bulk of the solution, it is positive with respect to the solution immediately in contact with the tantalum oxide film, so that the field in the oxide film is in a direction to cause tantalum ions to move out through it to react with the water and form tantalum oxide. When the voltage applied to the tantalum is increased (made more positive or less negative), the potential of the tantalum with respect to the solution also increases, so that the field across the oxide film increases. On raising the voltage, therefore, the oxide film will increase in thickness at a rapidly decreasing rate, and will practically stop growing when the field has been reduced to about 0.05 volt per angstrom unit, which takes only a few seconds when the total thickness is very small. At the same time, since the oxide film is so very thin (0.5 volt would correspond to approximately 10 \AA), it is possible for electrons to tunnel from the tantalum to hydrogen ions in the solution through the oxide film and the potential barrier in the solution and thus form hydrogen gas. As the voltage is increased, it would be expected that the negative current, that is, the current flowing in the direction to liberate hydrogen at the tantalum, would decrease and that

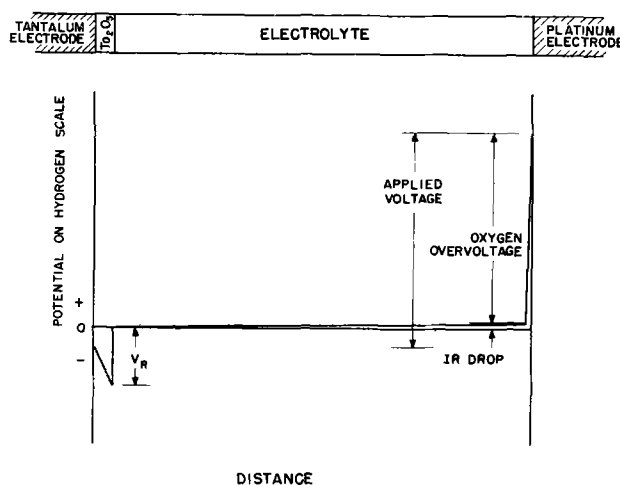


FIG. 4. Postulated distribution of potential during anodic oxidation of tantalum.

there would be a positive current (to form oxide) until the oxide film grows to the thickness corresponding to the new voltage. Total current should therefore decrease sharply, then increase as the positive current dies away. The current does actually behave in this manner when the voltage is increased, the transient occurring in a few seconds. (The circuit time constant is less than 0.1 sec.) Also, as the voltage is increased so that the oxide film grows, the capacity should decrease rapidly at first, reaching a stable value in a few seconds; this, too, is actually observed.

The intercepts on the voltage axis of the plots of the reciprocal of the capacity vs. voltage are -0.72 and -1.38 volts for the 2% HNO_3 and 2% NaOH solutions, respectively. This change in intercept is due to the change in pH from 0.6 to 13.5, which should produce a change of 0.76 volt. The theoretical value is in reasonable agreement with the observed shift of 0.66 volt. The reaction voltage for the tantalum electrode with unit tantalum activity in the acid solution would be -0.85 volt. The actual reaction voltage cannot be more negative than the intercept of the C^{-1} vs. V plot, or -0.72 volt. Also, the observed intercept is probably more negative than it should be, since the reciprocals of the double layer capacities should be subtracted from each measured value of C^{-1} . However, the reaction voltage must be at least -0.41 volt, the lowest voltage at which capacity measurements were made. Thus, the actual reaction voltage is between -0.41 and -0.72 , considerably smaller than the potential for unit activity of tantalum. In the basic solution, actual reaction voltage is between -1.12 and -1.38 , in comparison with the potential for unit activity of tantalum, -1.61 volts. If the entire decrease in reaction voltage below the value for unit activity of tantalum must be ascribed to a low tantalum concentration, the re-

quired activity would be less than 10^{-12} , probably by several orders of magnitude. It seems unlikely that the concentration of excess tantalum in the oxide film is really that low, and an alternative explanation is that there is some small overvoltage accompanying the reaction.

SUMMARY

Tantalum oxide may be formed on tantalum when the potential of the tantalum on the hydrogen scale is considerably negative, and even though the total current is in the direction to liberate hydrogen at the tantalum. It seems probable that the reason for this behavior is that the voltage of the electrochemical reaction to form tantalum oxide must be added to the applied voltage. When this is done it is found that there is a field in the oxide film in the direction to form more oxide even when the tantalum potential is negative. Because the oxide film is very thin, however, electrons can tunnel from the tan-

talum to hydrogen ions in the solution through the oxide and any potential barriers in the solution, so that hydrogen gas is liberated. The magnitude of the voltage of the electrochemical reaction to form tantalum oxide is much less than the theoretical value for unit tantalum activity, and it may be that some overvoltage accompanies the reaction.

ACKNOWLEDGMENTS

The author acknowledges with pleasure the benefit of discussions of this work with D. Trumbull and C. P. Bean.

Any discussion of this paper will appear in a Discussion Section to be published in the June 1955 issue of the JOURNAL.

REFERENCES

1. D. A. VERMILYEA, *Acta Metallurgica*, **1**, 282 (1953).
2. L. YOUNG, *Trans. Faraday Soc.*, **50**, 153 (1954).

Corrosion of Aluminum in Potassium Chloride Solutions

I. Effects of Concentrations of KCl and Dissolved Oxygen¹

W. BECK,² F. G. KEIHN,³ AND R. G. GOLD⁴

Lehigh University, Bethlehem, Pennsylvania

ABSTRACT

The corrosion of aluminum was studied by weight loss measurements in 0.0001*N* to 1*N* neutral electrolyte solutions at constant temperature. Oxygen concentration in these solutions was varied over a wide range either by bubbling the gas through the solution or by increasing the partial pressure above the solutions.

Weight loss increased with time and increasing oxygen concentration, but decreased with increasing electrolyte concentration. The electrode potential increased in anodic direction with time and increasing electrolyte concentration. Chloride solutions were more aggressive than any other solutions used. Hydrogen peroxide, which might have been a corrosion accelerator in experiments under high oxygen pressure, was found absent in all cases.

Results are discussed in the light of the electrochemical theory of corrosion. The relation of oxygen solubility in potassium chloride solutions to corrosion is also discussed.

INTRODUCTION

The questions of how and to what extent the corrosion of aluminum and its alloys in neutral electrolyte solutions is affected by increasing the concentration of dissolved oxygen are of considerable theoretical and practical significance. It is understandable, therefore, that a number of investigators have contributed to the study of this problem. The results of these investigations have been summarized as follows (1). In most aqueous solutions Al base alloys are relatively insensitive to the concentration of dissolved oxygen. In general, high concentrations of dissolved oxygen tend to stimulate attack somewhat, especially in acid solutions. . . . Some authors have reported that they succeeded in arresting the corrosion of Al and Al base alloys almost completely by deaerating such aggressive solutions as sea water, KCl and NaCl solutions (2). It has been shown further that the weight loss of an Al-Cu alloy was increased by raising the partial pressure of oxygen above a dilute NaCl solution (3).

The experiments just mentioned indicate that the corrosion of Al and Al alloys in solutions containing certain alkali chlorides can be stimulated by increasing the concentration of dissolved oxygen. However, experimental results secured up to now

are not sufficient to disclose the mechanism which controls the accelerated corrosion rate brought about by increased oxygen concentration.

Moreover, the aforementioned investigations were carried out in sea water or in NaCl and KCl solutions of various concentrations, but no attempt was made to separate the corrosive effect of the electrolytic concentration from that of the oxygen concentration. Most of the studies were made on Al base alloys with a complex structure, which makes the interpretation of corrosion data rather difficult.

Since many questions have arisen from the previous investigations, the following corrosion experiments were undertaken to add to the knowledge of the corrosion of Al.

EXPERIMENTAL METHODS

Commercially pure Al (Al 2SO), 0.8% Fe, 0.01% Cu, and 0.14% Si, and high purity Al from two lots with 0.12% and 0.03% impurities (predominantly Fe) were used in these experiments.

All test samples were punched from sheet material 0.33 mm thick in the form of disks with a total area of 40.50 cm². The disks were degreased, etched in 0.3*N* NaOH, wiped with a rubber policeman under running water (4), rinsed in distilled water, and dried at 110°C.

Specimens were kept in a desiccator until they were weighed, which was immediately before immersion in the electrolytic solution. Every specimen was pretreated in exactly the same manner.

After the desired time of immersion, the corrosion products were removed by cleaning the specimens at 90°C in a solution which consisted (5) of 170 g

¹ Manuscript received August 4, 1953.

² Present address: Department of Metallurgy, Syracuse University, Syracuse, New York

³ Present address: General Electric Company, Electronics Park, Syracuse, New York

⁴ Present address: Bethlehem Steel Corporation, Bethlehem, Pennsylvania.

H_3PO_4 and 80 g Cr_2O_3 dissolved in 300 g distilled water, and diluted with water in a ratio of 1:5. After this treatment, the specimens were washed in distilled water, dried in an oven at 110°C , and cooled in a desiccator before weighing. Uncorroded specimens lost less than 1 mg in the cleaning solution. All experiments were conducted in a water bath with the temperature controlled at $35^\circ \pm 0.5^\circ\text{C}$.

Chemicals used in the preparation of the solutions were of C.P. grade. Electrolytic oxygen was employed. The nitrogen contained traces of oxygen as an impurity.

Oxygen concentration in the solutions was controlled in two ways. In the first, oxygen was bubbled into the solution through a fritted Pyrex glass crucible, with a flow rate of 0.075 l/min, to saturate the solution. In these experiments, the Al disks were suspended vertically at the same depth in a 4-liter beaker in such a way that no gas bubbles could come in contact with the specimens.

In the second method, the partial pressure of oxygen above the solutions was increased by placing specimens suspended in 375 ml of electrolytic solution within an autoclave. The autoclave was flushed

several times with oxygen and the pressure was raised to the desired value for that experiment. The flushing operation took 10 min. The pressure for each run was held constant at its original value. Gauge pressures up to 325 psi were obtained in this manner for exposures of 5–200 hr.

The electrode potentials of the corroding specimens were obtained with a 0.1N Hg_2Cl_2 reference electrode and a Leeds and Northrop Type K potentiometer. The reference electrode was connected to the corroding solution by a salt bridge filled with a stiff agar jelly to avoid diffusion of electrolyte. Details for the potential measurements under high oxygen pressure are shown in Fig. 1.

The potential of the 0.1N Hg_2Cl_2 electrode was measured against another standard electrode before starting and after completion of a run to see if it was pressure sensitive or underwent irreversible change. The change of the relative potential of the Hg_2Cl_2 electrode was very slight and could be neglected.

The concentration of oxygen dissolved in the solutions when this gas was bubbled into them was determined by the Winkler (6) method. The resistivity of solutions, with several concentrations of electrolyte before and after corrosion experiments, was measured by means of a commercial dip cell and an electronic device.

RESULTS

The weight loss measured throughout an initial period of about 5 hr was very small and not sufficiently reproducible. Reproducibility improved after this period, but it remained poor in experiments made in 0.0001N and 0.001N solutions. Reproducibility improved with increasing electrolyte concentration. The maximum deviation from the arithmetic mean value of measurements for 0.01, 0.1, and 1N solutions, when made after 5 hr had elapsed,

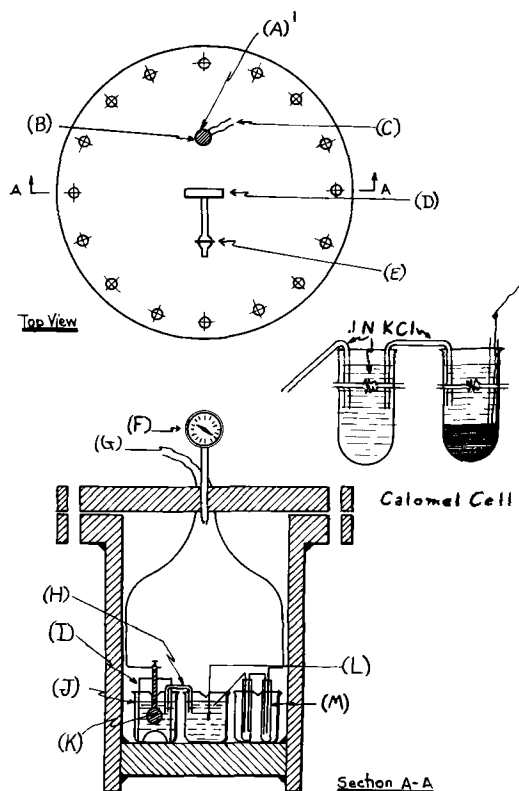


FIG. 1. Setup for recording electrode potentials under high oxygen pressure. (A)¹, insulating material; (B), bushing; (C), to potentiometer, (D), gauge, (E), valve; (F), pressure gauge, (C and G), to potentiometer; (H), 0.001N KCl + agar; (I), plastic sheet for mounting specimen; (J), 400 ml beaker filled with corroding KCl solution; (K), Al sample; (L), 0.1N KCl, (M), calomel cell (0.1N).

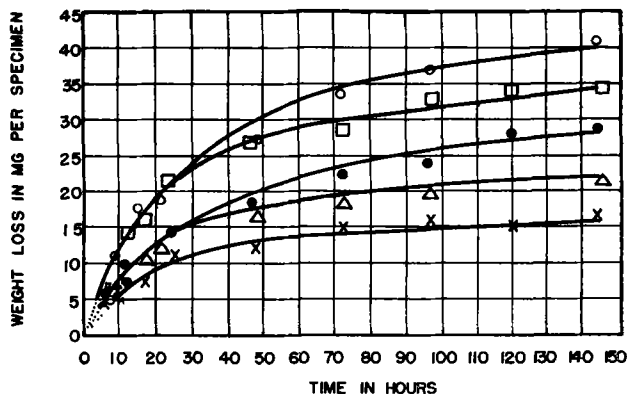


FIG. 2. Effect of time on weight loss of commercially pure Al. Partial pressure of oxygen, 150 psi; temperature, $35^\circ \pm 0.5^\circ\text{C}$; \circ , 0.0001N KCl; \square , 0.001N KCl; \bullet , 0.01N KCl; \triangle , 0.1N KCl; \times , 1N KCl.

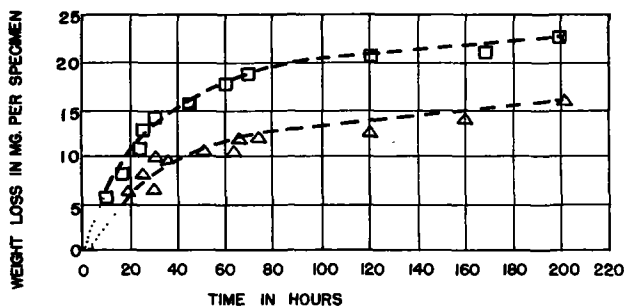


FIG. 3. Effect of time on weight loss of commercially pure Al. Solutions saturated at $35^{\circ} \pm 0.5^{\circ}\text{C}$ by bubbling 0.075 l of oxygen per minute through solution. \square , 0.001N KCl; Δ , 0.1N KCl.

remained below 10%. Weight loss values for 0.0001 and 0.001N solutions, plotted in curves reproduced below, were averaged over at least 6 measurements; for less dilute solutions they were averaged over at least 3 measurements. The reproducibility obtained in runs made under high oxygen pressure was slightly superior to that in the experiments with bubbling oxygen.

The dependency of the weight loss on time found on specimens of commercially pure Al, corroded under a partial pressure of 150 psi oxygen above KCl solutions of various concentrations, is shown in Fig. 2. With increasing time the rate of increase in weight loss became progressively slower and finally approached a constant value. The rise of the weight loss-time curves was less rapid in 0.01 and 0.1N solutions than in 0.0001 and 0.001N solutions, and the rise was least marked in the 1N solution.

The almost steady values of weight loss dropped continually with higher electrolytic concentration (7). Up to about 25 hr the same weight loss was

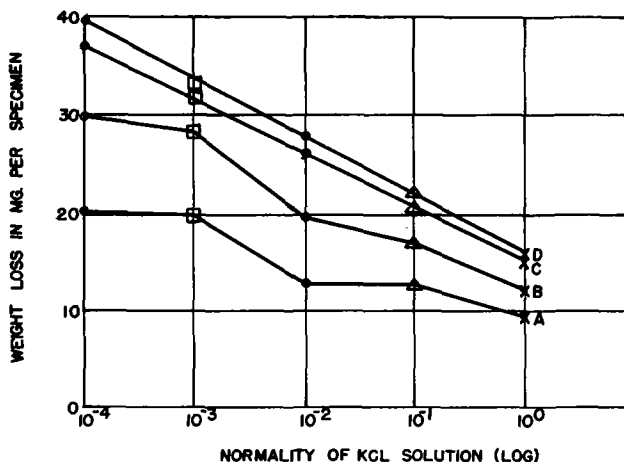


FIG. 4. Effect of concentration of KCl on weight loss of commercially pure Al. Partial pressure of oxygen, 150 psi; temperature, $35^{\circ} \pm 0.5^{\circ}\text{C}$. Curve A, exposure 20 hr; curve B, exposure 50 hr; curve C, exposure 100 hr; curve D, exposure 140 hr

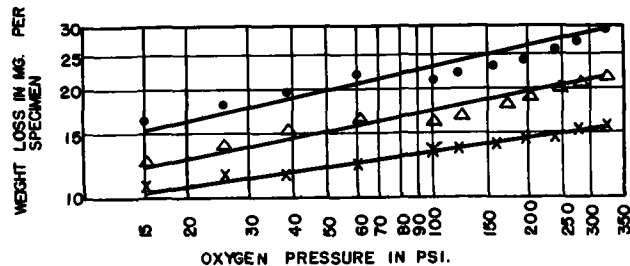


FIG. 5. Change of weight loss of commercially pure Al with increasing partial pressure of oxygen. Exposure, 72 hr; temperature, $35^{\circ} \pm 0.5^{\circ}\text{C}$. \bullet , 0.01N KCl; Δ , 0.1N KCl; \times , 1N KCl

found in 0.0001 and 0.001N solutions; the same held true for 0.01 and 0.1N solutions.

Effect of time on weight loss of specimens immersed in KCl solutions with bubbling oxygen is depicted in Fig. 3.

The trends of the curves reproduced in Fig. 3 are similar to those shown in Fig. 2. With bubbling oxygen a lower weight loss was obtained in higher KCl concentration, but this was smaller than that under 150 psi oxygen. Fig. 4 shows the decrease in weight loss with increasing KCl concentrations for various exposure periods.

Corrosion products formed in KCl under high oxygen pressure or with bubbling oxygen were either distributed colloiddally or were present as a white fluffy precipitate. They were completely dispersed colloiddally in 0.0001 and 0.001N KCl solutions, while in the 0.01N solution they were partly distributed colloiddally and partly precipitated. The 0.1 and 1N solutions were water clear with a precipitate present. The dispersed phase precipitated on addition of KCl when the concentration reached 0.05N KCl. The coagulation rate was slow but after a number of hours the originally turbid solution became water clear. A colloidal solution or precipitate formed at a very early stage of the corrosion process.

The surface of specimens corroded in 0.0001 and 0.001N solutions appeared dark and brownish. Such a dark layer was formed at a very early stage of the corrosion process. In contrast to this, the surface of the specimens corroded in 0.1 and 1N solutions appeared very light.

Pitting was found on all corroded surfaces. However, specimens exposed in 0.1 and 1N solutions appeared more pitted than those immersed in 0.0001 and 0.001N solutions (8).

The effect of the partial pressure of oxygen is shown in Fig. 5.

Exposure was 72 hr because in the runs with 150 psi oxygen (Fig. 2) it was found that at this time the weight loss had reached a steady or almost steady state. Weight loss at a pressure of about 14.7 psi was determined in solutions saturated by

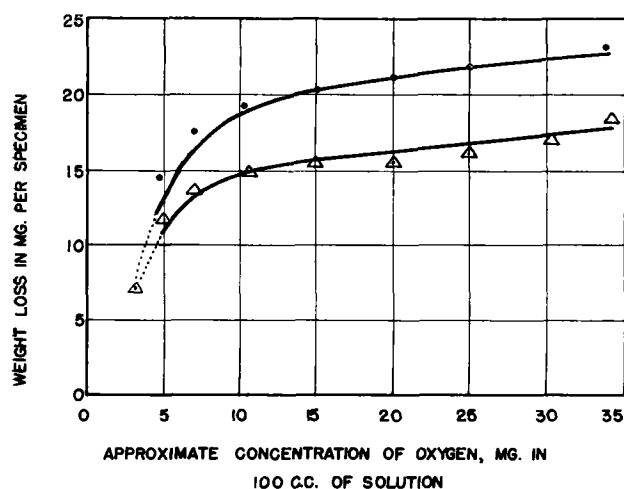


Fig. 6. Effect of concentration of dissolved oxygen on weight loss of commercially pure Al. Exposure, 72 hr; temperature, $35^{\circ} \pm 0.5^{\circ}\text{C}$.; ●, 0.01N KCl; Δ, 0.1N KCl.

bubbling oxygen through the solution at a constant rate.

Note that in all cases the weight loss increased with rising oxygen pressure but it decreased with increasing electrolytic concentration. The lines illustrating the dependency of the weight loss on the oxygen pressure became less steep with higher KCl concentration.

The concentration of oxygen dissolved in water, in equilibrium with a given partial pressure of this gas above the liquid phase, can be found in the literature (9, 10). The saturated concentration of oxygen in KCl solutions up to a concentration of 0.1N is almost entirely independent of the electrolyte concentration. Due to that, the weight loss measured in a 0.1N or in more dilute KCl solutions can be plotted against the equilibrium concentration of oxygen (Fig. 6). The curves rose noticeably when the oxygen concentration was increased from 3.3 mg in 100 cc solution to approximately 7 mg. The former concentration is the concentration of oxygen in water of 35°C under a partial pressure of this gas of 14.7 psi (11). The latter was produced in water of 25.9°C by a partial pressure of 27.2 psi oxygen.⁵ The weight loss plotted for 3.3 mg oxygen in 100 cc solution, was determined for specimens exposed in 0.01 and 0.1N KCl solutions at 35°C under normal atmospheric conditions. The weight loss rose noticeably when the concentration was raised up to approximately 12 mg oxygen in 100 cc solution (being in equilibrium with 46 psi oxygen at 25.9°C). Increasing the oxygen concentration above this value brought

⁵ Values for the equilibrium concentrations of oxygen in the corrosion experiments were in reality something lower than those given in Fig. 5. The temperature at which these concentrations were determined was 25.9°C , while the corrosion experiments were conducted at 35°C (9).

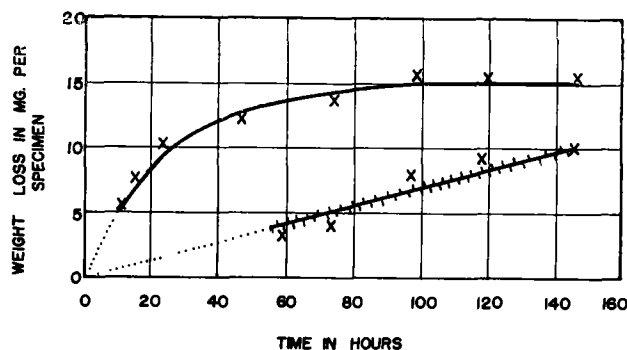


Fig. 7. Effect of time on weight loss of commercially pure Al. Temperature, $35^{\circ} \pm 0.5^{\circ}\text{C}$; —, partial pressure of oxygen, 150 psi; +, partial pressure of nitrogen, 150 psi; ×, 1N KCl.

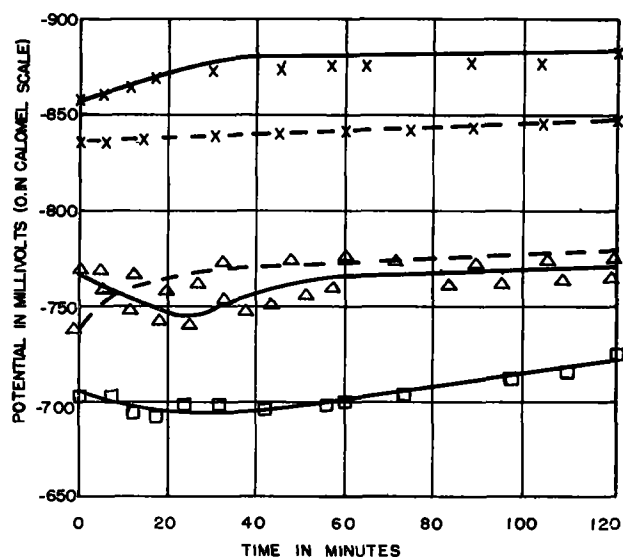


Fig. 8. Effect of time on the potential of commercially pure Al recorded at $35^{\circ} \pm 0.5^{\circ}\text{C}$. —, partial pressure of oxygen, 150 psi; ---, solution saturated by bubbling oxygen. □, 0.001N KCl; Δ, 0.1N KCl, ×, 1N KCl.

about only a comparatively slight increase of weight loss.

Numerous measurements were made on specimens corroded under identical conditions, but in a number of runs the specimens were exposed in a horizontal and in a vertical position. Differences in weight loss found in these runs were within the limits of the experimental error.

Experiments with nitrogen under a pressure of 150 psi were made in a 1N KCl solution. Fig. 7 shows that up to 145 hr the weight loss in the experiments with oxygen was higher than in those with nitrogen. However, it increased continuously in nitrogen.

Potential measurements.—The reproducibility of electrode potential measurements was within ± 15 mv when made in 0.01, 0.1, and 1N solutions, but was less in 0.0001 and 0.001N solutions. The potentials are the averages from 4 measurements taken

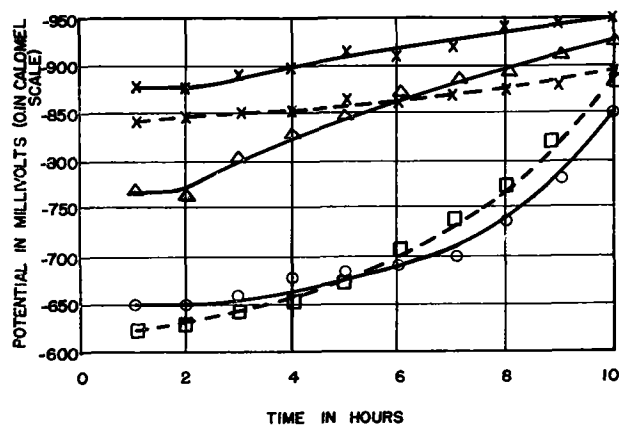


FIG. 9. Effect of time on the potential of commercially pure Al, recorded at $35^\circ \pm 0.5^\circ\text{C}$. —, partial pressure of oxygen, 150 psi; ---, solution saturated by bubbling oxygen; ○, 0.0001N KCl; □, 0.001N KCl; Δ, 0.1N KCl; ×, 1N KCl.

from 4 separate potential records. Fig. 8 gives time-potential curves for less than 120 min. Zero time is the commencement of potential measurements after the flushing operation was completed. The curves reveal a marked shift of potentials in anodic direction with higher electrolytic concentration and a very slow rise of the potential-time curves in the same direction. The potential is plotted against time up to 10 hr in Fig. 9.

Fig. 9 discloses again that with increasing time and KCl concentration the potentials became more anodic. The increase of the potentials in anodic direction in the solutions 0.1N or less was more rapid than that in the 1N solution. Trends of the potential-time curves based on measurements made under the condition of bubbling oxygen are very similar to those derived from measurements under high oxygen pressure. The potential-time curves resulting after a 10-hr period had very irregular trends and, therefore, were not reproduced in Fig. 9.

Other factors.—The oxygen pressure, concentration of KCl, and time were varied over a wide range, and the solutions were analyzed for H_2O_2 . This substance could not be detected by the titanium sulfate or prussian blue tests in any of the solutions (12). In order to determine if H_2O_2 was decomposed by high oxygen pressure, a number of beakers filled with a 1N KCl solution containing 0.1 and 1% H_2O_2 were put in the autoclave. Runs were made under oxygen pressures of 150 and 325 psi for 72 hr. Solutions of the same KCl and H_2O_2 concentrations were kept under the same conditions of time and temperature in the atmosphere. The concentration of H_2O_2 decreased considerably in the atmospheric runs but did not diminish in the solutions under high oxygen pressure.

Weight loss in NaCl solutions was the same as in

TABLE I. Weight loss of commercially pure and high purity Al in a 0.01N KCl solution
Exposure: 72 hr; temp: $35^\circ \pm 0.5^\circ\text{C}$

Al content of specimen, %	Weight loss in mg/specimen:	
	Normal atmospheric conditions	Partial pressure of oxygen, 300 psi
approx. 99.1*	8	31
99.88	approx. 5	6
99.97	0	0

* Commercially pure Al.

TABLE II. Effect of corrosion of commercially pure Al on resistivity

Partial pressure of oxygen: 150 psi; temp: $35^\circ \pm 0.5^\circ\text{C}$

Normality of KCl solutions	Specific resistivity, ohms:	
	Before immersion	After immersion period of 48 hr
0.0001	6.3×10^4	5.8×10^4
0.001	6.5×10^3	6.2×10^3
0.01	7.0×10^2	6.7×10^2
0.1	1.5×10^2	1.4×10^2

KCl solutions. A change of the anion from Cl^- to SO_4^{--} had a very strong effect on the metal loss. The weight loss in a 0.001N K_2SO_4 solution (150 psi oxygen, 72-hr exposure) was 70% lower than that in a KCl solution of the same normality; in 0.01 and 1N K_2SO_4 solutions it was too small to give reproducible values.

The weight loss of commercially pure Al and of high purity Al, immersed in a 0.01N KCl solution under normal atmospheric conditions and under an oxygen pressure of 300 psi, is listed in Table I.

The table shows that an effective amplification of the weight loss, accomplished by increasing the concentration of dissolved oxygen, was only feasible on commercially pure Al, but not on an Al of 99.88% purity. The weight loss was almost zero on an Al of 99.97% purity, even when the partial pressure of oxygen was raised from atmospheric to 300 psi.

Resistivities of a number of KCl solutions of various concentrations are compiled in Table II.

Resistivity was slightly decreased during a period of 48 hr and similar values were found after 100 hr under high oxygen pressure or bubbling oxygen. The pH was measured along with the resistivity. In all cases it increased slightly, from approximately 5.5 to 6.5. However, the fact has to be stressed that pH measurements even with the glass electrode, when made in unbuffered solutions in the neighborhood of the neutral point, are not very reliable.

DISCUSSION

More comprehensive studies are required for establishing the mechanism which controls the

TABLE III. Corrosion rate and electrode potential of commercially pure Al (partial pressure of oxygen 150 psi)

Temp: 35° ± 0.5°C; exposed area: 40.50 cm²

Exposure, hr	Normality of KCl solution	Corrosion rate in mg/hr/spec	Electrode potential in mv, 0.1N Hg ₂ Cl ₂ scale	Normality of KCl solution	Corrosion rate in mg/hr/spec	Electrode potential in mv, 0.1N Hg ₂ Cl ₂ scale
2	0.0001	1.25	-650	0.1	0.80	-760
4	0.0001	1.16	-670	0.1	0.60	-830
6	0.0001	1.12	-690	0.1	0.56	-870
10	0.0001	0.92	-850	0.1	0.53	-930
40	0.0001	0.29	—	0.1	0.07	—
80	0.0001	0.20	—	0.1	0.01	—

increase of the weight loss with increasing concentration of dissolved oxygen, increasing time (13) and decreasing concentration of electrolyte. However, it appears feasible to draw some qualitative conclusions, which might serve as a base for a future, more comprehensive interpretation.

The plot of log of weight loss vs. log of oxygen partial pressure gave straight lines (Fig. 5). Apparently the relationship between weight loss and concentration of dissolved oxygen as determined by the partial pressure of this gas is an exponential one.

It is of great interest that an effective amplification of the weight loss requires the presence of a certain amount of impurity in Al, which in this case was predominantly Fe.

Herzog and Chaudron (3, 14) have shown that the weight loss of an Al-Cu alloy of the type 24S, immersed in a 3% NaCl (0.5N) solution, was increased by raising the oxygen pressure above the solution. These authors attributed amplification of the metal loss to the action of H₂O₂, which, according to Herzog and Chaudron, was formed when the Al alloy was corroded under high oxygen pressure. It is a well-known fact (15) that even small quantities of H₂O₂, when added to dilute NaCl or KCl solutions, greatly amplify the corrosion of Al and Al-Cu alloys. If H₂O₂ was formed in these experiments and if its concentration increased with increased oxygen pressure, amplification of the weight loss can easily be due to H₂O₂. However, H₂O₂ could not be detected in the corroding solutions. It may be that the quantity of H₂O₂ formed was below the limit of the detectability with the tests used. Nevertheless, it was found in this laboratory⁶ that a measurable increase of the weight loss of commercially pure Al above that resulting in an agitated 3% KCl solution could only be achieved when the concentration of H₂O₂ was in the order of magnitude of 0.01%. The fact that the tests used indicate much lower concentrations than 0.01% H₂O₂ justifies the assumption

⁶ Unpublished measurements made in this laboratory by George P. Condon.

that there was no connection between a possible formation of this substance and the amplification of corrosion, at least not in the case of commercially pure Al corroded in KCl solutions with concentrations between 0.0001 and 1N under a partial pressure of oxygen up to 325 psi.

It is easier to discuss the effects of time and KCl concentration on the weight loss when the corrosion rate is taken into consideration. If the weight loss is expressed by a power function, $w = at^n$ (4), then the instantaneous rate of corrosion at a constant temperature may be computed from the weight loss

and the time by the simple expression $\frac{w}{t}n$, where

t is the time in hours, w is the weight loss in mg per specimen, and n is a proportionality factor. A plot of $\log w$ against $\log t$ showed straight lines which consisted in every case of 3 sections with 3 different slopes. The slope belonging to an initial period was greater than that belonging to an adjacent period, while the third section was almost parallel to the time axis. By inserting the values for the 3 different slopes for n in the above given expression, the rate of corrosion can be calculated. The rate for an interval between 0 and 5 hr, when the weight loss was not sufficiently reproducible, may be computed from values taken from the sections in the curves (dotted lines in Fig. 3) extrapolated from 5 hr to zero time.

Rates of corrosion for different times, together with (16) the corresponding electrode potentials, recorded over a period of 10 hr are compiled in Table III.

This shows that regardless of the concentrations of the KCl solutions the rate decreased with time, while the potentials increased in anodic direction. Probably, the decrease of the corrosion rate was the result of a protective coating formed during the corrosion process, which gradually increased on the metal surface. It might be inferred from the increase of the potential in the anodic direction that the local cathodes (Fe impurity) were preferentially polarized.

The potentials were considerably more cathodic in the 0.0001N solution than in the 0.1N solution (17). It may be assumed, therefore, that the acceleration of the corrosion rate in the 0.0001N solution as compared with the rate computed for the 0.1N solution was controlled by cathodic processes (of unknown nature).

It is not known if there is a relationship between the formation of the dark coating or of colloiddally dispersed corrosion products in 0.0001 and 0.001N solutions and the relatively high corrosion rate resulting in these solutions. Formation of a colloidal phase and its precipitation may be explained as follows. In solutions with high oxygen concentra-

tions, anodically formed Al ions were rapidly converted into Al (OH)₃. Very low concentrations of electrolytes (much below that necessary for coagulation, about 0.05N KCl for colloidal Al (OH)₃) favor the formation of colloidal dispersions and stabilize such systems effectively. Higher electrolytic concentrations (in the order of magnitude of the coagulation value and above) discharge and precipitate the colloidal phase. This explains why a colloidally dispersed phase would not be observed in 0.1 and 1N KCl solutions.

As was shown above a tentative, qualitative discussion of the dependency of the corrosion rate on time and KCl concentration could be based on the electrochemical theory of corrosion. It does not seem justified therefore to argue that increasing corrosion with decreasing conductivity of the solutions is not compatible with the electrochemical theory. Corrosion reactions proceed actually in a very thin layer of electrolyte in the solid-liquid interface. It is rather questionable if the conductivity measured in the bulk of the solution is also representative for the conductivity in the boundary layer. It seems to be particularly improbable that these conductivities are identical in experiments made under stagnant conditions.

The corrosion behavior of Al in K₂SO₄ solutions revealed that the increase in weight loss with decreasing concentration of electrolyte is not limited to the Cl⁻ anion alone.

It is of great interest that the specific effect on the weight loss of the concentrations of a KCl or NaCl solution and of the concentration of dissolved oxygen (19-21) is not limited to Al. Bengough and Wormwell (20) obtained similar results on mild steel. These authors, who corroded their specimens in 0.1N and 0.5N KCl and NaCl solutions under high oxygen pressures, state that there is a greater difference between the corrosion rate, computed for specimens immersed in solutions of the above concentrations, than corresponds to the respective oxygen solubility.

The authors' corrosion studies of Al in 0.0001 to 0.1N KCl solutions have shown that a decreasing oxygen concentration with increasing electrolytic

concentration cannot be the explanation for the retardation of the corrosion rate.

ACKNOWLEDGMENT

The authors are pleased to acknowledge support of this research by the Signal Corps Engineering Laboratories, Fort Monmouth, New Jersey.

Any discussion of this paper will appear in a Discussion Section to be published in the June 1955 issue of the JOURNAL.

REFERENCES

1. R. B. MEARS, "Corrosion Handbook," (H. H. Uhlig, Editor), p. 41 John Wiley & Sons, Inc., New York (1948).
2. J. M. BRYAN, "Aluminum and Aluminum Alloys in the Food Industry," pp. 43, 55, His Majesty's Stationary Office, London (1948).
3. E. HERZOG AND G. CHAUDRON, *Compt. rend.*, **190**, 1189 (1930).
4. M. A. STREICHER, *J. (and Trans.) Electrochem. Soc.*, **93**, 285 (1948).
5. W. WIEDERHOLT, R. DUFFEK, AND E. VOLLMER, *Korrosion u. Metallschutz*, **18**, 38 (1942).
6. J. C. THRESH, J. F. BEALE, AND E. V. SUCKLING, "The Examination of Waters and Water Supplies," p. 271, P. Blackiston's Son and Co., Inc., Philadelphia (1953).
7. G. MASING, *Z. Metallkunde*, **37**, 107 (1946).
8. R. B. MEARS AND R. H. BROWN, *Ind. Eng. Chem.*, **29**, 1090 (1937).
9. L. CASSUTO, *Physik. Z.*, **5**, 233 (1904).
10. H. A. PRAY, C. E. SCHWEICKERT, AND B. H. MINNICK, *Ind. Eng. Chem.*, **44**, 1147 (1952).
11. LANDOLT-BORNSTEIN, "Physico-Chemical Tables," Vol. I, p. 765 (1923).
12. W. MACHU, "Wasserstoffperoxyd," p. 361, Springer Verlag, Wein (1951).
13. F. A. CHAMPION, *Trans. Faraday Soc.*, **41**, 593 (1945).
14. G. CHAUDRON, *Helv. Chim. Acta*, **31**, 1560 (1948); *J. Inst. Metals*, **76**, 11 (1949).
15. E. RACKWITZ AND E. K. O. SCHMIDT, *Korrosion u. Metallschutz*, **2**, 57, (1926); *ibid.*, **3**, 5 (1927); *ibid.*, **5**, 9, 131 (1929).
16. T. P. HOAR AND D. HAVENHAND, *J. Iron Steel Inst. (London)*, **133**, 248 (1936).
17. R. ERGANG AND G. MASING, *Z. Metallkunde*, **40**, 314 (1949).
18. H. FREUNDLICH, "Kapillarchemie," Vol. II, p. 96 ff, Akademische Verlagsgesellschaft, Leipzig (1932).
19. A. R. LEE, *Trans. Faraday Soc.*, **28**, 709 (1932).
20. G. D. BENGOUGH AND F. WORMWELL, Fourth Report of the Corrosion Committee, Iron & Steel Institute (London), p. 213 (1936).
21. W. J. WHITTON, *Trans. Faraday Soc.*, **46**, 932 (1950).

Studies on the Anodic Polarization of Zirconium and Zirconium Alloys¹

MARIO MARAGHINI,² GEORGE B. ADAMS, JR., AND PIERRE VAN RYSSELBERGHE

Department of Chemistry, University of Oregon, Eugene, Oregon

ABSTRACT

The anodic polarization of zirconium and of some of its alloys was studied in several different aqueous electrolytes. In chloride solutions corrosion potentials below that of oxygen evolution were established, but the addition of nitrate ion in the ratio of 3:5 to chloride ion brings the potential above that of oxygen evolution. Formation of the oxide film along the three portions of the potential-time curve (initial rapid increase, evolution of oxygen at practically constant potential, final rapid increase) was studied in detail and quantitative information about local currents and the efficiency of the film building process was obtained.

INTRODUCTION

Hackerman and Cecil (1) have made cathodic and anodic polarization and potential-time studies on zirconium in aerated and in air-free sodium chloride solutions. In their anodization studies they obtained the same type of constant current potential-time curves that are reported in this work.

Rothman, McKinney, and Warner (2) have reported anodic potential-time curves for zirconium in sulfuric acid solutions which show the same characteristic linear portions as those reported above by Hackerman and those obtained in the present work, using other electrolytes.

Charlesby (3) studied the growth of the oxide film formed in the anodization of zirconium and aluminum at formation voltages in excess of 4 volts. His work can be interpreted quite satisfactorily in terms of the equation proposed on theoretical grounds by Mott (4) for the ionic currents involved in the growth of thin oxide films on metals.

In the present work, the anodic polarization of zirconium and of some of its alloys was studied at 25°C over a range of current densities from 0.5 to 2000 $\mu\text{a}/\text{cm}^2$. Potential-time measurements were also carried out in the absence of external current. Solutions of HCl, KCl, Na_2CO_3 , Na_2SO_3 , and other salts were used.

Two types of potential-time curves were observed according to whether chloride ion was present in the solution or not.

In the latter the potential difference between the

zirconium anode and a saturated calomel electrode (S.C.E.) changes with time toward nobler potentials at a constant rate after a brief initial period. When it reaches about 1.1–1.3 volts the rate of increase decreases considerably and remains at these lower values for intervals of time varying with the current density. When the voltage reaches 1.9–2.1 volts the rate of increase again becomes larger and attains a value of the same order of magnitude as below 1.1 volt. This behavior is shown in curve 1 of Fig. 1.

Above 4 volts thin films of oxide which had gradually been forming become visible by the display of strong interference colors, the color depending upon the formation voltage. The film building process was observed at varying formation voltages up to 100 volts, but the polarization can be pushed well above this value (3).

In solutions containing chloride ion as the only anion the potential-time curve follows the same course as in the absence of chloride ion until a definite limiting value of the potential difference is reached, which then remains constant with time. This limiting value depends upon the chloride ion concentration. This behavior is shown in curve 2 of Fig. 1.

After the limiting corrosion potential has been reached the coupons show a very pronounced pitting, and zirconium can easily be detected in the solution.

If the solution contains chloride ion plus another anion, the behavior may be of either of the types mentioned, according to the nature of this second anion and to the ratio of its concentration to that of chloride ion.

Experimental studies were carried out on: (a) the steep branch of the potential-time curve below 1.1 volt; (b) the constant corrosion potential obtained in the presence of chloride ion; (c) the nearly horizontal branch between 1.1 and 2 volts; and (d) the steep branch over 2 volts.

¹ Manuscript received December 28, 1953. This paper was prepared for delivery at the Wrightsville Beach Meeting, September 13 to 16, 1953. Work carried out under a contract between the University of Oregon and the U. S. Atomic Energy Commission.

² Present address: Institute of Applied Chemistry, University of Rome, Rome, Italy.

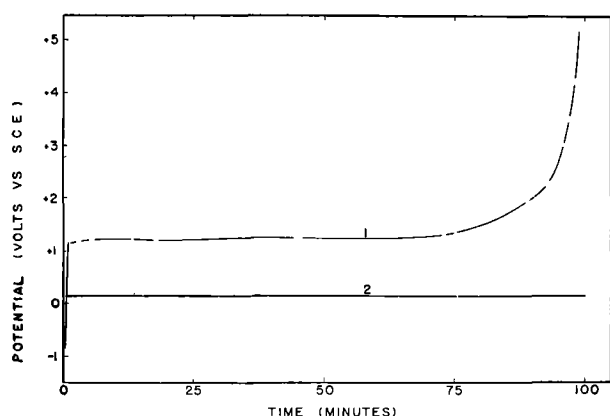


FIG. 1. Time-potential curves for anodization of zirconium at $250 \mu\text{a}/\text{cm}^2$ in: curve 1, $1.0M \text{Na}_2\text{CO}_3$; curve 2, $1.0M \text{KCl}$, both aerated.

EXPERIMENTAL PROCEDURE

Coupons of zirconium alloys and of the unalloyed metal were cut out of 0.070-in. sheet³ in the shape of square electrodes with extensions for electrical connections. They were completely covered with an impervious baked coating of Valdura rubber base enamel which was then ground away from one face of the electrode. Prior to each test the exposed face of the coupon was abraded on 0, 2/0, and 3/0 emery, and a known apparent exposed area was obtained by coating part of the freshly abraded surface with a rosin-beeswax mixture. The coupon was immersed in the electrolyte (with external current, if any, already on) of a cell containing a stirring device, a bubbling tube, an agar bridge to the auxiliary electrode, and a Haber-Luggin capillary. The other end of the capillary was placed in a vessel (containing the same solution as that in the cell) in which an agar salt bridge was also immersed. This led to saturated KCl in another vessel which contained the reference electrode also. Current was supplied by a very high resistance circuit fed by 100-volt storage batteries or by a 300-volt tube rectifier to minimize the variations of current due to polarization of the electrode. Current was measured with a calibrated resistor and a potentiometer. The voltage between anode and reference electrode was measured with an electronic voltmeter in series with a wire potentiometer. The accuracy was about 2 mv in the range 0–2 volts. Cell, salt bridges, and reference electrode were all immersed in a thermostatically controlled bath at $25.0^\circ \pm 0.1^\circ\text{C}$. Generally air was bubbled during the run. Measurements were begun 6 sec after immersion of the prepared coupons and carried on for as much as several hours.

³ Specimens were either in the annealed or less than 20% cold worked state with a hardness of the order of Rockwell B 68–81.

The work reported in the present paper included experiments on the eight zirconium samples listed in Table I, with metals No. 1, 2, and 8 receiving special attention. These were selected from a total of fifteen alloys.⁴

STEEP BRANCH OF THE POTENTIAL-TIME CURVE BELOW 1.1 VOLT OR BELOW THE CORROSION POTENTIAL IN SOLUTIONS CONTAINING CHLORIDE ION

The general form of the potential-time curve for various applied current densities is shown by the charging curves in Fig. 2, obtained in $1.0M \text{Na}_2\text{CO}_3$ solution. Three characteristics of these curves should be noted. Initially, there is a rapid, nonlinear potential-time dependence which then merges into a linear dependence. Although not included in the figure, this linear dependence continues until oxygen evolution begins. The slope of the linear portion of the curve shows a small, but definite, increase with increasing current density. The time interval over which the curve is nonlinear decreases with increasing current density.

The variation in the slopes of these charging curves with time is shown in Fig. 3. The points were obtained from the differences in potential measured at intervals from the immersion time, corresponding to constant increases of the logarithms of these time intervals. The points were plotted directly without smoothing. In Fig. 4, 5, and 6 the log rate-log time curves are given for other aqueous salt solutions. Data used to construct Fig. 1 through 8 were obtained using an electrode made from sample No. 2 (WA-3983). Experimental points are given in Fig. 3 and 4 to indicate the type of precision obtained in this work. Most of the curves are the result of duplicate or triplicate runs on the same specimen electrode. The same degree of reproducibility was obtained with the data used to draw Fig. 5 and 6. Complete data for all of this work appear in a recent report (5).

The following features of these curves are apparent:

(A) With no applied current:

The logarithm of the rate of increase of potential, $\log(\Delta E/\Delta t)$, decreases linearly with the logarithm of the immersion time, $\log t$, from 6 sec after immersion to 20 min. With some media there is then a break followed by a segment of greater slope.

(B) With applied current:

Curves obtained with external polarization current are initially nearly coincident with, or parallel to, the corresponding zero external current curve. Their slopes then begin to deviate in the direction of

⁴ Kindly supplied by Dr. E. T. Hayes of the Bureau of Mines, Albany, Oregon.

TABLE I. Partial analyses of the zirconium samples

Sample No.	1	2	3	4	5	6	7	8
Code No.	W-3992	WA-3983	WA-3941	WA-3949	SA-3247	SA-3248	SA-3230	SA-3249
Al	30	20	60	—	30	20	50	20
B	0.3	0.3	0.5	—	0.2	0.2	0.7	0.2
C	—	370	—	—	—	250	370	190
Cd	<0.5	0.5	0.5	—	0.5	<0.5	<0.5	<0.5
Co	<10	10	<10	—	<10	<10	<10	<10
Cr	30	<5	30	—	<5	<5	<5	<5
Cu	30	50	100	—	20	20	30	20
Fe	200*	600	2000*	9900	600	900	1000	1100
Mg	20	10	30	—	10	10	10	10
Mn	10	10	20	—	20	10	10	10
Mo	<10	<10	<10	—	<10	<10	<10	<10
N ₂	360	70	60	50	80	30	40	60
Ni	50	20	20	—	<5	20	<5	10
O ₂	—	1650	1950	1100	800	750	2000	900
Pb	30	30	30	—	50	30	50	50
Si	50	100	100	—	30	50	20	40
Sn	<5*	500	<5*	—	11000	21900	25300	32400
Ti	<50	50	50	—	<50	50	<50	50
V	<20	50	20	—	<20	20	<20	20
Zn	<50	<50	<50	—	<50	<50	<50	<50

C, Fe, N, O₂, Sn by chemical analysis (exceptions: values with asterisks are spectroscopic), others by spectroscopic analysis. All values are in parts per million. WA-3949, incompletely analyzed, is similar to W-3992 and W-3941. All analyses kindly furnished by Dr. E. T. Hayes and collaborators at the Bureau of Mines, Albany, Oregon.

higher values of $\Delta E/\Delta t$. Finally, these rates become constant. When applied current density is increased, the initial period of coincidence or parallelism with the zero-current curve is shorter and the final constant value is higher. The degree of initial noncoincidence is seen to increase with increasing current density.

By plotting the logarithm of the constant rate against the logarithm of the applied current density with which this constant rate was obtained, a precise linear dependence is found for the whole range

of current densities investigated. From these plots one obtains the two constants A and B in the relationship:

$$\log(\Delta E/\Delta t) = \log A + B \log I \text{ or } \Delta E/\Delta t = A I^B \quad (1)$$

where I is the current density and A is the rate for unit current density.

These facts are interpreted by assuming that the increase in potential between coupon and reference electrode is due to a film building process,⁵ and that, in the case of zero applied current, local current controls the rate of the film building process and, consequently, the rate of change of the potential. The local current decreases rapidly with time as shown by the decreasing rates in the initial portions of the log rate-log time curves. If an external current of constant value is superimposed upon the local current, the same process of corrosion goes on practically unaltered as long as the external current is small compared with the local current and the two curves in the log rate-log time plot remain merged or parallel. When the local current, which is steadily decreasing, becomes comparable with the external applied current, the two curves begin to diverge.

⁵ That the film building process under these conditions is actually the formation of ZrO₂ is shown by electron diffraction studies of the films formed upon anodizing zirconium in various aqueous solutions. In dilute HNO₃ a cubic modification is formed ($a_0 = 5.103 \text{ \AA}$) while in dilute H₂SO₄, ammonium borate, and other solutions, the film has a more amorphous structure but with crystallites of this cubic modification present (3).

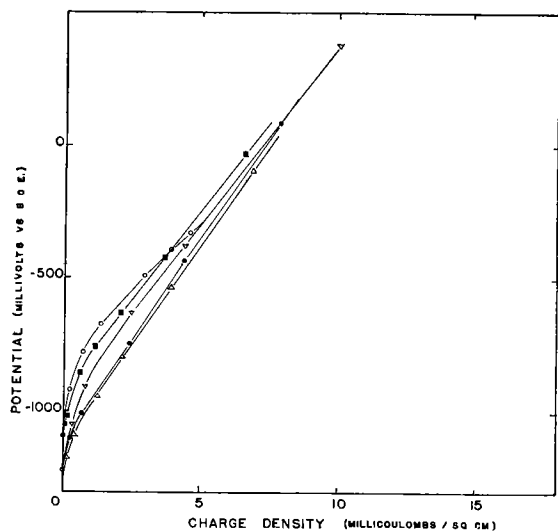


FIG. 2. Anodic charging curves for zirconium in aerated 1.0M Na₂CO₃ (current densities in $\mu\text{a}/\text{cm}^2$). \circ , 0.39; \blacksquare , 1.95; ∇ , 4.14; \triangle , 20.5; \bullet , 41.4.

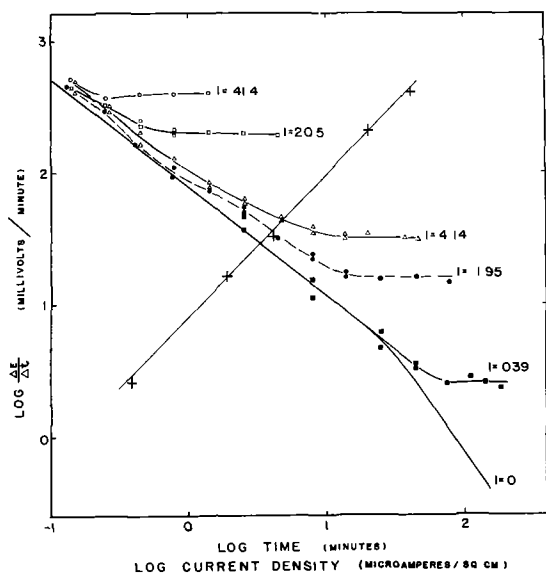


FIG. 3. Logarithm of the rate of increase of potential vs. logarithm of immersion time, and vs. logarithm of current density (+) in aerated 1.0M Na₂CO₃.

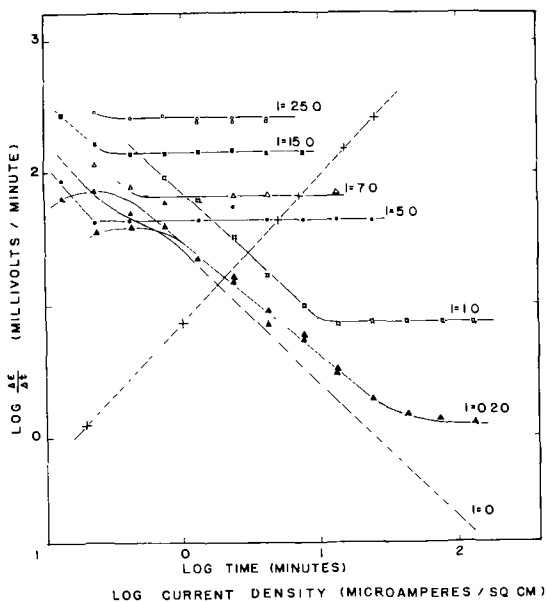


FIG. 4. Logarithm of the rate of increase of potential vs. logarithm of immersion time, and vs. logarithm of current density (+) in 1.0M Na₂SO₃.

Finally, when the local current has become negligible compared with the external current, a constant rate is attained with a value depending only on the magnitude of the external current.

Since the same film building process occurs, whether the current responsible for it is constant or decreasing with time, one can calculate the local current at a given time from equation (I) and from the value of $\log(\Delta E/\Delta t)$ on the log rate-log time curve for zero external current. These local current values should be valid over the range of external current densities for which the constants in (I) were eval-

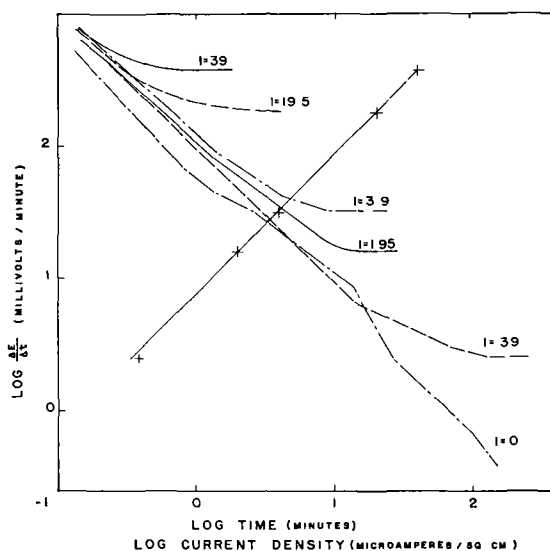


FIG. 5. Logarithm of the rate of increase of potential vs. logarithm of immersion time, and vs. logarithm of current density (+) in aerated 0.1M KCl.

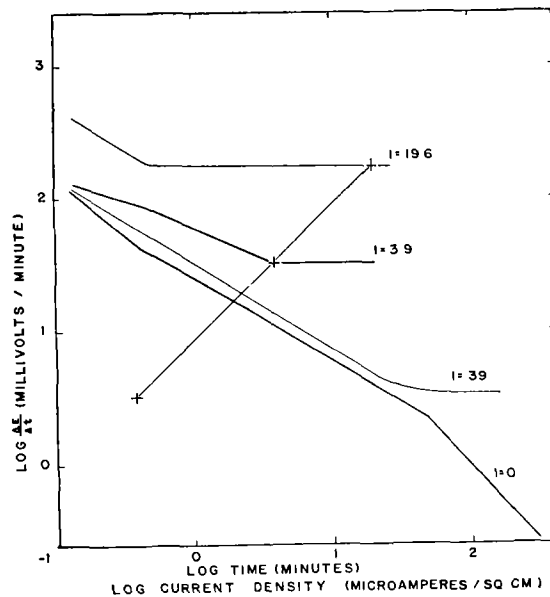


FIG. 6. Logarithm of the rate of increase of potential vs. logarithm of immersion time, and vs. logarithm of current density (+) in aerated 1.5M HCl.

uated. In Table II the values of the constants A and B of equation (I) are reported, together with the calculated values of the local cell current at logarithmic time intervals for zirconium sample No. 2 (WA-3983). Values of A and B should be accurate to within $\pm 2\%$, and the deviation of B from unity is significant within these limits.

From an inspection of Table II it is seen that three of the A values are identical at 7.4 ± 0.2 mv/min.

The small local current in the 1.0M Na₂SO₃ solution is probably due to the complete absence of dissolved oxygen in the solution, resulting in a relatively low value for the local cathodic current. The runs in

TABLE II

Solution	A (mv/min)	B	Local current ($\mu\text{a}/\text{cm}^2$) at time (min)				
			0.56	1.8	5.6	18	56
1.0M Na_2CO_3	7.4	1.08	13	5.3	2.2	0.98	0.27
1.0M Na_2SO_3	7.4	1.12	5.3	1.8	0.64	0.22	0.08
0.1M KCl	7.6	1.07	12	4.6	2.1	0.68	0.19
1.5M HCl	8.3	1.01	4.1	2.1	1.0	0.48	0.22

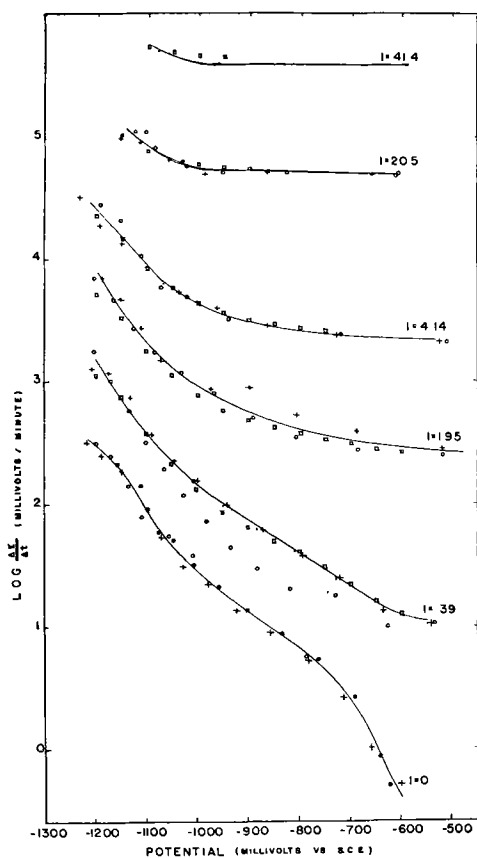


Fig. 7. Logarithm of the rate of increase of potential vs. potential in aerated 1.0M Na_2CO_3 .

the three other solutions were carried out with air saturated solutions. However, the rate at unit current density is the same in the absence of dissolved oxygen as in its presence, and this is evidence that for zirconium the primary process responsible for the increase in potential with time is the formation of the oxide film and not the adsorption of dissolved oxygen. The role of dissolved oxygen is limited to its effect on the local cathodic polarization curve for this process.

At this point it might be mentioned that the method of determining local currents described above is still valid if the oxide film dissolves in the electrolyte at a rate proportional to its rate of formation. This is equivalent to saying that, of the external current I_E , only a fraction, ηI_E , is actually film building, because the film produced by the remain-

ing $(1 - \eta)I_E$ is dissolved. So, the relation $\Delta E/\Delta t = A I_E^B$ becomes $\Delta E/\Delta t = A \eta^B I_E^B$. If the fraction is the same for the dissolution in the case of the local current (and this is the basic assumption upon which the whole method is based, namely, that the effects and consequences of the anodic external current and of the local anodic current are the same), dissolution of the film should not invalidate the calculated value of the local current, because in both cases the value of the constant A has been changed to $A' = \eta^B A$.

If the rate of dissolution of the oxide were to be proportional to the total amount of film present at a given time, the above reasoning would not hold, but in such an event the value of $\Delta E/\Delta t$ resulting from a constant external current would not be constant. In effect the rate of dissolution should increase continuously, so that the difference of the two rates, (constant rate of formation) - (increasing rate of dissolution), corresponding to the observed rate $\Delta E/\Delta t$, should decrease.

The following is given as evidence that the local currents calculated by this method are real.

Fig. 7 and 8 show how the complete log rate-log time curve can be calculated from equation (I) and the zero current curve. The assumption is made that, in the runs with external current, the local current, at a given potential E , is equal to the local

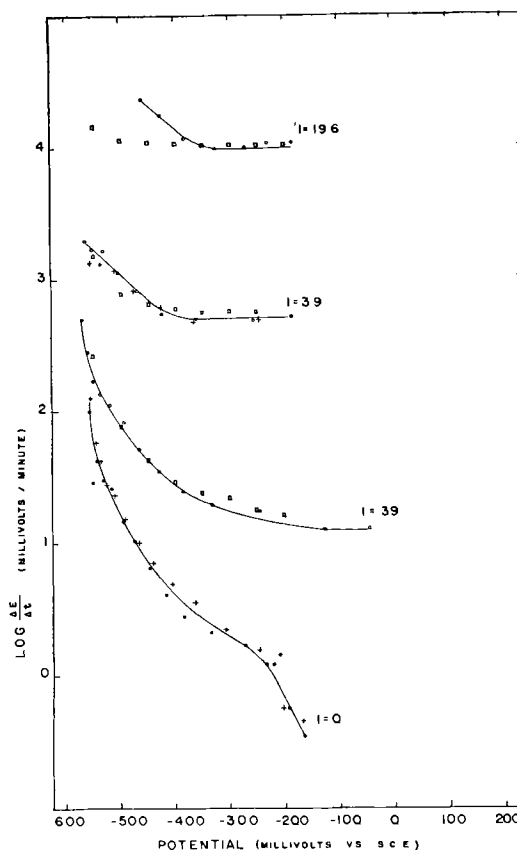


Fig. 8. Logarithm of the rate of increase of potential vs. potential in aerated 0.1M KCl.

current in the runs with zero external current, at the same potential E . This assumption appears reasonable, because the net current is flowing toward the external cathode, but the local anodic current must flow toward internal cathodes, and its value is determined by the value of E on the cathodic polarization curve. The foregoing assumption is based on the hypothesis of a sufficiently stable local cathodic curve (corresponding to the reduction of oxygen and hydrogen ion, or water, on the electrode). Thus, by plotting log rate-potential curves for each log rate-log time curve one can, at a given potential E , read off the corresponding $\log \Delta E/\Delta t$ value for the $I = 0$ curve and calculate a local current by substitution in equation (I). Then, by adding the value of the constant external current, I , to the local current so obtained and substituting this total current in equation (I), a value of $\log \Delta E/\Delta t$ for this external current I can be calculated. This value is now plotted at the same potential E for which the local current was calculated. In this way the log rate-potential curve is constructed for each external current density. In Fig. 7 and 8 the calculated values are shown as open squares. The curves represent experimental log rate values at different potentials. (All points, other than those indicated by open squares, are experimental values.) The origin of ordinates has been shifted upward by 0.6 unit for each consecutive line. The agreement is good, and lends support to the assumptions made.

Another indication of the probable validity of this method of obtaining local currents is obtained by comparing the local cathodic polarization curve, as calculated from the local currents indirectly derived above from anodic measurements, with the corresponding portion of the net cathodic polarization curve obtained experimentally for the same solution. In Fig. 9 the experimental curve is shown for 0.1M KCl. The points shown in the figure are the local anodic currents calculated from equation (I) and the zero-current log rate values corresponding to given values of the observed potential. The best agreement is to be expected at the high current end of the curve where the anodic contribution to the experimental net cathodic curve is small. At the low current end the deviation of the experimental curve from the calculated local polarization curve is seen to be in the direction expected, and the experimental values change with time toward the calculated curve as the local anodic contribution becomes gradually smaller.

It may seem surprising to find any agreement at all, since in one case a cathodic curve is used, and in the other the points are calculated from anodic polarization measurements only, and by a rather indirect method. This agreement, however, should be expected if it is assumed that the local cathodic

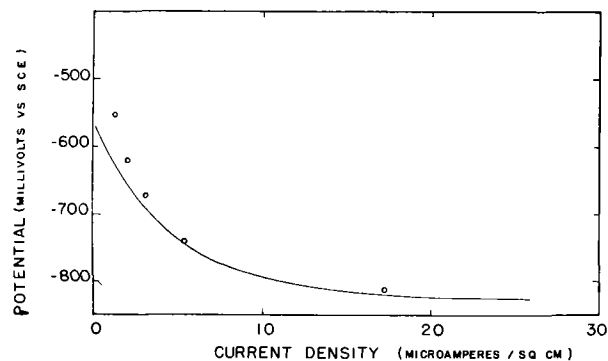


FIG. 9. Comparison between the calculated local cathodic polarization curve (solid line) and the experimental cathodic curve (open circles) in aerated 0.1M KCl.

polarization curve is more or less stable, and invariable during the run, so that the potential (mixed potential) is always given by the intersection of the local cathodic and local anodic curves. With time the local anodic curve tends to stick more and more to the potential axis on account of the growth of the oxide film. Therefore, if the anodic local current is plotted vs. the corresponding potential the local cathodic curve is obtained (neglecting IR drops).

If the local cathodic polarization curve, as obtained by the above method, is the true curve, it should follow that a point on the local anodic polarization curve for a given time, t , could be obtained by taking the difference between a point on the calculated local cathodic curve and a point on the net cathodic curve for time t and for the same potential. Thus, potential-time curves for both anodic and cathodic polarization would provide sufficient information to obtain the local cathodic polarization curve and the local anodic curve and their change with time. The potential range for these curves is limited to the range of potentials observed for the zero current anodic potential-time curve.

Referring to Table II again, a comparison between the A and B values for KCl and Na_2CO_3 solutions shows that the presence of chloride ion has no effect on the film building process at potentials lower than the corrosion potential. The anomalous action of chloride ion manifests itself only when a given potential is reached.

CORROSION POTENTIAL IN PRESENCE OF CHLORIDE ION

Solutions Containing Chloride Ion As the Only Anion

For a solution containing a chloride or HCl, anodizing at constant current density leads eventually to a constant potential. The time required to reach this corrosion potential decreases with increasing chloride ion concentration and with increasing current density. For chloride ion concentrations less

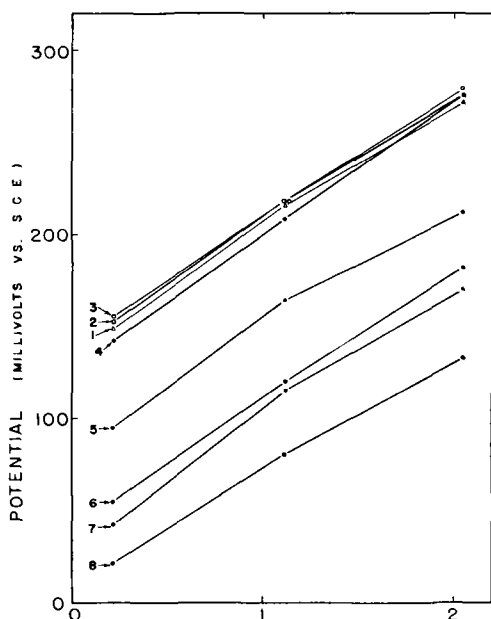


FIG. 10. Corrosion potential of different zirconium alloys vs. pCl^- in aerated KCl solutions.

than $10^{-3}N$, slow oscillations occur in the potential. An increase in current density has very little effect on the constancy of the corrosion potential. For example, in $1.0N$ KCl there is an increase of about 10 mv in the corrosion potential when the current density is increased from 10 to 2000 ma/cm^2 . Visible pitting is invariably observed with coupons submitted to this treatment. At high chloride ion concentrations many pits are formed, while at the lowest chloride ion concentration ($10^{-3}N$) only two or three pits occur per square centimeter, but these are much deeper.

Plotting the constant corrosion potential against the negative logarithm of the chloride ion activity, one obtains approximate straight lines with the same slope for all the alloys that were tested. This plot is shown in Fig. 10.

In Table III the corrosion potential in millivolts, obtained with a current density of $3.9 \mu a/cm^2$, is tabulated for the various alloys at three different chloride activities.

Zirconium and these alloys are readily corroded and pitted in the presence of chloride ion, even when only small anodic currents of the order of $1 \mu a/cm^2$ are impressed. For titanium the same pitting is observed, but at potentials of the order of 9–10 volts (6). Furthermore, while alloys of the WA series have about the same corrosion potentials, alloys of the SA series, containing percentages of tin increasing from 1–3%, exhibit increasingly less noble potentials as the percentage of tin increases. The greater permeability to anions (here chloride ion) of the film formed on the tin-alloyed metal at low current

densities before the corrosion potential is attained presents other aspects which are discussed below.

Solutions Containing Chloride Ion and an Additional Anion

After the corrosion potential had been attained in a cell containing a solution of NaCl of given concentration, increasing amounts of a solution of the sodium salt of the anion to be tested and containing NaCl also, at the same concentration as the original solution, were added to the cell. After addition of a measured volume of the second solution, the change in the corrosion potential was recorded and the additions continued. Generally the corrosion potential changed in the direction of greater nobility as the concentration of added anion increased. Results of these measurements are shown graphically in Fig. 11, 12, 13, and 14.

The anions tested can be divided into three groups according to their effects.

(A) With additions of nitrate ion the following observations were made: When the ratio $C_{NO_3^-}/C_{Cl^-}$ reaches values of about 3, the increase in the corrosion potential becomes very abrupt and large oscillations set in. When this ratio reaches a value of 5 the potential is between 1.5 and 1.6 volts, and oscillations cease, oxygen evolution begins, and pitting apparently stops or is reduced to a marked degree. Measurements were made at chloride ion concentrations of 0.1, 0.01, and 0.004*N*.

(B) Sulfate, chromate, and phosphate ions produce abrupt increases in the corrosion potential when their concentration ratios to chloride ion are around 20–30. In 0.004*N* chloride ion solutions, sulfate and chromate ions bring the potential above that of oxygen evolution when their concentration ratios to that of chloride ion are about 40 to 50.

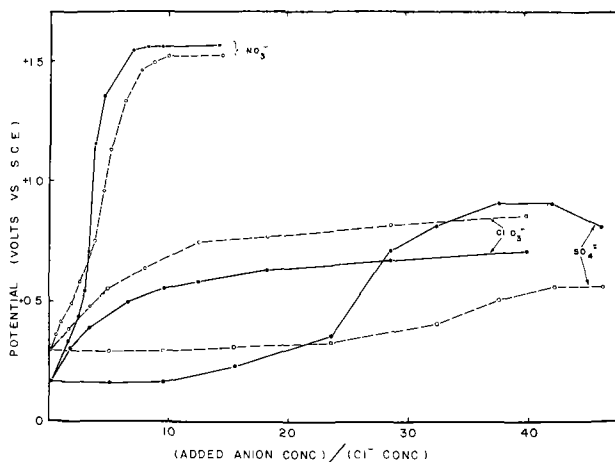


FIG. 11. Corrosion potential in presence of chloride and of another anion for aerated 0.1*M* NaCl. —○—○—, alloy No. 1; —●—●—, alloy No. 8.

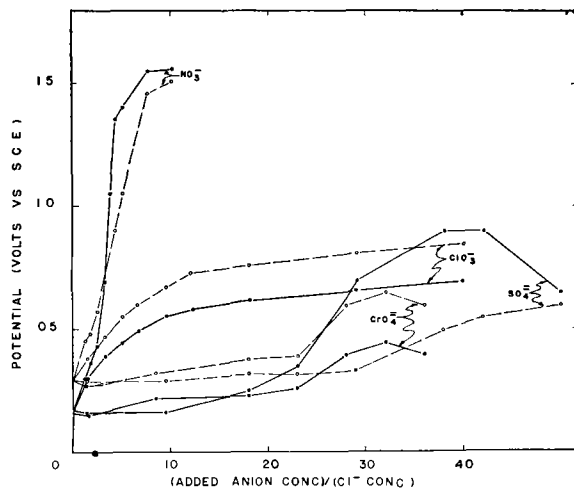


FIG. 12. Corrosion potential in presence of chloride ion and of another anion for aerated 0.01M NaCl. - ○ - - - ○ -, alloy No. 1; - ● - - - ● -, alloy No. 8.

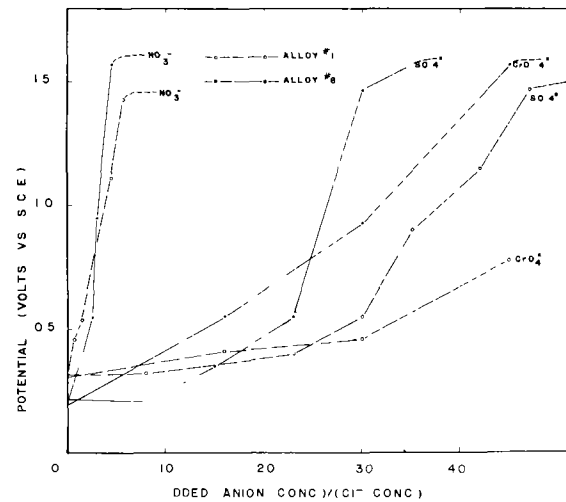


FIG. 14. Corrosion potential in presence of chloride ion and of another anion for aerated 0.004M NaCl. - ○ - - - ○ -, alloy No. 1; - ● - - - ● -, alloy No. 8.

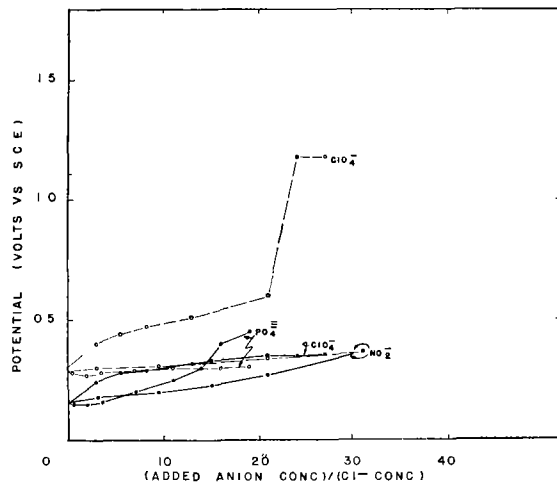


FIG. 13. Corrosion potential in presence of chloride ion and of another anion for aerated 0.01M NaCl. - ○ - - - ○ -, alloy No. 1; - ● - - - ● -, alloy No. 8.

(C) Chlorate, perchlorate, and nitrate ions (this last ion belonging perhaps as well to group B) produce a rather abrupt increase in the potential at low ratios to chloride ion, and a leveling off at high ratios. The potential always remains below that for oxygen evolution in the range of concentration ratios investigated.

These measurements were all carried out using two types of zirconium specimens: sample No. 1, (WA-3992) and sample No. 8, (SA-3249). A common feature of the various cases is that, when the added anion concentration becomes high enough to raise the potential above that of oxygen evolution, the curve of potential vs. added anion ratio for the tin alloy intersects that for the pure metal and reaches the oxygen evolution potential at a lower ratio of added anion.

TABLE III

Alloy	1.0N KCl (log aCl ⁻ = -0.21)	0.1N KCl (log aCl ⁻ = 1.11)	0.01N KCl (log aCl ⁻ = -2.04)
1 WA-3992	149 ± 5	216 ± 3	272 ± 2
2 WA-3983	153 3	218 3	265 2
3 WA-3941	154 4	218 3	279 3
4 WA-3949	142 3	208 2	265 3
5 SA-3247	95 4	164 3	212 4
6 SA-3248	55 5	120 2	182 2
7 SA-3230	42 5	115 2	170 3
8 SA-3249	11 3	80 4	133 3

The peculiar action of nitrate ion in repairing the film and preventing pitting by the action of chloride ion correlates with the results of other investigators (7), who proposed that anodization in nitric acid promotes nucleation of oxide grains on zirconium. The character of the oxide film structure on the tin alloys which allows a greater permeability to chloride ion than does the oxide film on the pure metal (see Table III) also renders the fixation of nitrate ion in the film easier and this ion can thus catalyze the formation of additional oxide at the very points where the film is most permeable. This property would account for the intersection of the curves for the tin alloy with those of the purer metals.

It is interesting to note that nitrite, chromate, and phosphate ions, which are generally good corrosion inhibitors, exhibit a much less marked effect here than does nitrate ion.

NEARLY HORIZONTAL BRANCH OF THE POTENTIAL-TIME CURVE BETWEEN 1.1 AND 2 VOLTS

Runs were taken in 1.0M Na₂CO₃ solution with electrodes made up from samples No. 1 (WA-3992)

TABLE IV

Current density $\mu\text{a}/\text{cm}^2$	Coulombs/cm ² to increase the potential from 1.25 to 2.00 volts	
	WA-3992 (sample 1)	SA-3249 (sample 8)
200	0.26	—
300	0.16	0.47
500	—	0.16
1000	0.089	0.14
1500	0.066	0.076
2000	0.052	0.040

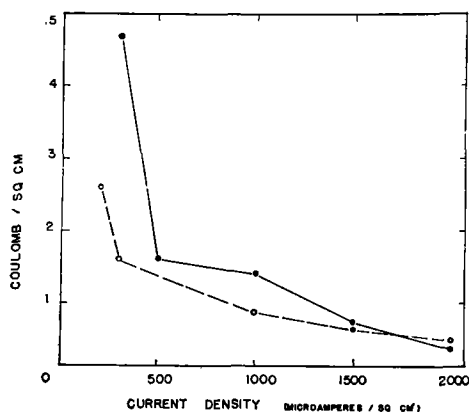


FIG. 15. Coulombs/cm² required to pass from 1.25-2.00 volts, vs. current density, in aerated 1.0M Na₂CO₃. ○ — ○ — ○, alloy No. 1; ● — ● — ●, alloy No. 8.

and No. 2 (SA-3249). The time required to reach 1.25 and 2.00 volts, corresponding approximately to the beginning and to the end of the nearly horizontal branch of the curve, was determined for different constant current densities. The corresponding number of coulombs per square centimeter was calculated. Individual results show an appreciable scattering due to the highly localized nature of the oxygen evolution process. Results reported in Table IV are the mean values of five single measurements.

In Fig. 15 data in Table IV are shown graphically. It is apparent that the film building efficiency increases with increasing current density, and that it drops off very rapidly for formation current densities less than 500 $\mu\text{a}/\text{cm}^2$. This efficiency is the ratio of the current carried by the ions (probably oxide ions) involved in the film building process to the total current. The difference between total current and ionic current is the electron current, which does not contribute to oxide film growth. The electron current might also be termed the oxygen evolution current in this case. The tin alloy has a lower film building efficiency during oxygen evolution than the pure metal except at the highest current densities.

Along the flat on the time-potential curve the oxygen evolution, which is mainly localized, takes a large share of the total current and the film build-

TABLE V

Current density $\mu\text{a}/\text{cm}^2$	Efficiency of the film building process	
	Range 15-25 volts	Range 25-35 volts
SA-3249: 117	0.37	0.39
234	0.40	0.44
351	0.42	—
WA-3992: 200	0.47	0.50
2000	0.62	0.70

ing process proceeds at a reduced rate. As the localized pores⁶ where oxygen evolution can readily occur are gradually closed over by the thickening oxide film, the effective current density for the localized oxygen evolution increases and, for oxygen evolution to continue, the potential must rise. (In Fig. 1 the gradual rise in potential all along the flat is not apparent, but it is evident in a diagram where the potential scale is expanded.) Finally, as localized pores are eliminated, the potential climbs rapidly because a much larger fraction of the current is then available for oxide film formation. The slope of the curve then becomes comparable to the slope below oxygen evolution, but it is never as great.

For the mixed electrode reaction occurring during the localized oxygen evolution one would expect that an increase in current density would increase the overvoltage for oxygen evolution and thus, for a given potential, the fraction of current used in evolving oxygen should decrease with increasing current density, allowing a more rapid film formation at the higher current densities. This is what is observed.

The fact that the tin alloy requires more time to complete the oxide film than does the purer metal would indicate the presence of a greater density of localized pores. This idea is consistent with the fact that chloride ions appear to penetrate the oxide film on the tin alloy more readily than the oxide film formed on the purer metal, and that the fixation of nitrate ions within the film occurs more readily with the tin alloy than with the pure metal.

STEEP BRANCH OF THE POTENTIAL-TIME CURVE ABOVE 2 VOLTS

In the absence of any information as to how great a variation occurs in the roughness factor in the transition from invisible films to the visible films formed above 4 volts, Charlesby's value of the maximum formation rate at zero electron current, namely, 17 volt cm²/ma min, was used to calculate

⁶ By the term localized pore, as used here, is meant any path through the oxide film that offers a considerably lower resistance to the passage of electrons from the oxide film surface to the metal than does the bulk of the oxide structure which surrounds it.

the efficiency of the film building process above 2 volts. This value was derived by Charlesby from measurements taken above 10 volts using ammonium borate at 18°C. The present measurements were made in 1.0M Na₂CO₃ at 25°C, but due to the similar nature of the two electrolytes there should be no great error in using his value.

The efficiencies calculated in this manner are given in Table V, and are the mean values of two or more separate measurements of the formation rate over the voltage range indicated.

These results are in good agreement with those given by Charlesby. The tin alloy does not exhibit any unusual behavior.

Additional details and complete tables of data are available in a Technical Report to the Atomic Energy Commission (5).

Any discussion of this paper will appear in a Discussion

Section to be published in the June 1955 issue of the JOURNAL.

REFERENCES

1. N. HACKERMAN AND O. B. CECIL, Technical Report to the Office of Naval Research, December 1952.
2. A. ROTHMAN, D. S. MCKINNEY, AND J. C. WARNER, Progress Reports to the U. S. Atomic Energy Commission NYO 548, June 1951, and NYO 549, January 1952.
3. A. CHARLESBY, *Acta Met.*, **1**, 340 (1953); also Atomic Energy Research Establishment, Harwell, Report M/R 1014 (1952).
4. E. N. MOTT, *Trans. Faraday Soc.*, **43**, 429 (1947).
5. M. MARAGHINI, G. B. ADAMS, AND P. VAN RYSSELBERGHE, Technical Report to the U. S. Atomic Energy Commission, AECU-2797, September 1953.
6. C. D. HALL AND N. HACKERMAN, *J. Phys. Chem.*, **57**, 262 (1953).
7. R. D. MISCH AND W. E. RUTHER, Argonne National Laboratory Report, October 1952; also, *This Journal*, **100**, 531 (1953).

Electronic Configuration in Electrodeposition from Aqueous Solution

III. Metal Deposition from Certain Complex Ions¹

ERNEST H. LYONS, JR.,² JOHN C. BAILAR, JR., AND H. A. LAITINEN

University of Illinois, Urbana, Illinois

ABSTRACT

The cathodic behavior of cobalt, nickel, copper, and zinc complexes of 8-hydroxyquinoline-5-sulfonic acid, 1,10-phenanthroline, glycine, 1,2- and 1,8-naphthalenediamines, tetramethylethylenediamine, and dimethylglyoxime was investigated by determining cathode current efficiencies and polarograms. Deposition was not obtained from ions believed to have hybridized orbitals which involve the penultimate electron shell, that is, from the "inner orbital" complexes of Taube. Deposits were obtained from "outer orbital" ions, thus confirming the rule previously proposed. Evidence is given that copper, as well as cobalt and nickel, forms both types of ions.

INTRODUCTION

In the first paper of this series (1), it was pointed out that, in aqueous solutions, the electrodeposition of metals appears to be impossible from ions having hybridized orbitals which involve the penultimate electron shell, that is, from the "inner orbital" complexes of Taube (2). On the other hand, deposition is generally possible when hybridization involves only the outermost shell, that is, from "outer orbital" complexes. To test the validity of this rule, the cathodic behavior of cobalt, nickel, copper, and zinc complexes of 8-hydroxyquinoline-5-sulfonic acid, of 1,10-phenanthroline, and of glycine was investigated. In addition, the nickel complexes of naphthalene-1,2-diamine, naphthalene-1,8-diamine, tetramethylethylenediamine, and the copper complexes of dimethylglyoxime were examined.

For this purpose, cathode current efficiencies were determined. However, these quantities may not be significant where solubility of the complex salt is very low. Accordingly, polarograms were also obtained. With many of these, interpretation is obscured by reduction of the coordinating agent or by catalytic hydrogen waves. Together, however, the results seem to indicate fairly clearly whether deposition of metal occurs.

EXPERIMENTAL

Cathode efficiency determinations.—These were made in the conventional manner on copper cathodes in

¹ Manuscript received June 30, 1953. This paper was prepared for delivery before the Wrightsville Beach Meeting, September 12-16, 1953, and is taken from a thesis submitted by E. H. Lyons, Jr., to the Graduate College of the University of Illinois in partial fulfillment of the requirements for the Ph.D. degree.

² Present address: The Principia College, Elmhurst, Illinois.

solutions usually 0.01*M* in metal, and 0.1*M* in sodium acetate. The solutions were vigorously agitated with a glass stirrer. Electrolysis was continued for 60 min at 1 amp/dm², for 20 min at 3 amp/dm², and for 10 min at 5 amp/dm². Bath temperature was between 30° and 36°C. The *pH* usually increased 0.2 to 0.3 units. Although some deposits were so fragile that bits of the material were lost on drying, enough metal remained to indicate a substantial current efficiency. The cells were operated in series with the conventional copper coulometer. Duplicate determinations agreed to within about 10%, except for very low efficiencies, where it was clear that significant deposition was not obtained. Since at 100% efficiency about half the metal in the cell would be deposited, higher efficiencies are not necessarily representative of the initial bath composition; but this is not of consequence since it was only required to show that deposition is possible. In many experiments the anodes, which always consisted of the metal to be deposited, were visibly corroded, and the increase in *pH* suggested that the efficiency is higher at the anode than at the cathode.

Polarographic studies.—These were made using standard techniques with both a dropping mercury cathode and a rotating platinum cathode (3). With the latter, purified hydrogen was bubbled through the solution in the open arm of an H-cell (4) during the runs. Preliminary experiments indicated that under these conditions the reduction of oxygen was not observed on the polarograms. The solutions were generally 0.1*N* in KNO₃, and 0.001*M* in metal. Polarograms with the rotating cathode were reproducible as to general form, but not as to precise values. Those with the mercury electrode showed the usual reproducibility. The temperature was close to 30°C.

Chemicals.—C.P. or reagent grade chemicals were used. *o*-Phenanthroline was purchased from G. F. Smith Chemical Co. 8-Hydroxyquinoline-5-sulfonic acid, referred to as "sulfonated oxine," was prepared by sulfonating Eastman 8-hydroxyquinoline. Commercial dioxane was purified by diluting it with an equal volume of 20:1 hydrochloric acid, and refluxing the solution with magnesium powder for about 8 hr. Polarograms indicated that no reducible substances remained, and residual magnesium chloride did not affect the results.

EXPERIMENTAL RESULTS

Complexes with o-phenanthroline.—Weighed portions of *o*-phenanthroline were added to solutions of sulfates or acetates of the metals, in ratios of 3.5 moles of the amine to 1 mole of cobalt or nickel, 2.5:1 for copper, and 2.2:1 for zinc. The *pH* was adjusted by adding hydrochloric acid and sodium hydroxide; runs were made at *pH* 3, 5, and 10, each within 0.5 unit.

With cobalt, the solution became dark in a few minutes at *pH* 10, in a few hours at *pH* 5, and not at all at *pH* 3. When the dark solution was acidified, the color faded in a few minutes. This is attributed to a cobalt (III) complex, unstable in acid solutions.

With cobalt, nickel, and copper, cathode current efficiencies were less than 1%. According to the criterion previously adopted (1), these compounds are considered to be nondepositing. A dark, tarry film, which was removed before weighing, remained on the cathode. When the tarry material was dissolved in nitric acid, neutralized with ammonia, and treated with sodium sulfide, no precipitate resulted. Cathodes showed no visible metal deposit, and those from the nickel bath did not give colors with dimethylglyoxime (after treatment with acid and neutralization).

With zinc, however, efficiencies ranging from 2.1 to 21% were obtained. The deposit was dark, spongy, and resembled the so-called "burned" deposit. It evolved gas vigorously when dipped in hydrochloric acid, and the resulting solution on neutralization with ammonia, and treatment with sodium sulfide, gave a dirty white precipitate. A thin, dark coating remained on the cathode even after the zinc had been dissolved.

It appears, therefore, that zinc, but not cobalt, nickel, or copper, is deposited from these complexes.

For nickel, cobalt, and copper, the polarograms show catalytic hydrogen waves at potentials less negative than in the corresponding solutions without the metals (5). The zinc solutions, however, show distinct waves indicating metal deposition at about -1.4 volts vs. S.C.E., except at *pH* 2.7, where hydrogen evolution is indicated. This is in agreement

with the work of Kruse and Brandt (5). The polarograms therefore agree that zinc, but not the other metals, may be deposited.

The *o*-phenanthroline complex of iron is known to be of the inner orbital type (2). Since the coordinating ability of amines for metals increases through the transition series from iron to copper (6), it may be assumed that the cobalt, nickel, and iron complexes also have this configuration, as is suggested by their colors. The data indicate that electrodeposition is not obtained.

The electronic structure of zinc precludes inner orbital configuration, and correspondingly the metal is deposited. The low efficiencies and polarographic irreversibility of the reduction suggest that the coordination is very strong. Deposits are also obtained from the cadmium *o*-phenanthroline complex, which doubtless has a similar structure (7). The ability of these strong complexes to undergo reduction to metal parallels that of the corresponding cyanide complexes, except that no cyanocuprate (II) ion is known.

Complexes with glycine.—Glycine complexes are unusually stable even though they are of the outer orbital type (2). Cathode efficiencies, obtained with baths 0.01*M* in metal (0.02*M* in the case of zinc), 0.1*M* in sodium acetate, and with glycine-metal ratios of 3.5:1 for cobalt and nickel, 2.5:1 for copper, and 5:1 for zinc, range from 22–94%. No consistent trends were observed. All of the deposits were spongy, probably because of the great firmness of coordination as previously explained (1).

Polarograms were obtained with solutions 0.001*M* in metal, 0.1*M* in KNO_3 and 0.2*M* in glycine. In addition, a copper solution 0.002*M* in glycine was also examined, but the wave did not differ significantly from that with the greater concentration. To suppress maxima, 0.02% gelatin was added to the nickel and copper solutions. All of the reductions were irreversible, except that of copper at *pH* 4.1, for which the slope of the plot of E vs. $\log i/(i_a - i)$ was 0.031. The manner of variation of current observed as each mercury drop grew and fell indicated that the cathode was covered by an adsorbed film during the deposition. It is not possible, of course, to determine half-wave potentials. The approximate mid-points of waves observed with the dropping mercury electrode are given in Table I.

With the rotating platinum cathode, polarograms indicated that metal was deposited. After each run, the platinum was coated with a black deposit; with copper, the red luster could be faintly seen.

From glycine complexes, deposition of copper is well known (8–11), and polarograms indicate that iron, nickel, and cobalt are deposited from complexes with other amino acids (12, 13). It is clear, there-

TABLE I. Reduction potentials of glycine complexes (vs. S.C.E.)

Cobalt		Nickel		Copper		Zinc	
pH	volts	pH	volts	pH	volts	pH	volts
3.0	-1.1	3.0	-1.2	3.0	-1.1	2.4	-1.0
5.0	-1.2	6.0	-0.9	4.1	-1.2	5.0	-1.0
10.0	-1.3	8.7	-1.2	8.8	-1.4	9.0	-1.3

TABLE II Reduction potentials of sulfonated oxine complexes (vs. S.C.E.)

No metal		Cobalt		Nickel		Copper		Zinc	
pH	volts	pH	volts	pH	volts	pH	volts	pH	volts
3.0	-1.0	3.0	-1.1	3.0	-0.7	2.4	-0.1	2.6	-0.9
6.4	-1.2	5.0	-1.0	5.0	-0.8	5.4	-1.5	5.9	-1.2
9.8	-1.4	10.0	-1.3	8.0	-1.2	9.1	-1.5	9.8	-1.5

fore, that deposition is obtained from all of these outer orbital complexes.

Complexes with sulfonated oxine.—Zinc and copper complexes with sulfonated oxine are relatively insoluble, although supersaturated solutions are readily prepared. However, by using a 1 to 1 dioxane-water mixture as solvent, the copper bath was made 0.005*M* in metal, 0.035*M* in oxine, and 0.1*M* in sodium acetate. The zinc solution was 0.007*M* in metal, 0.018*M* in oxine, and 0.1*M* in acetate. The nickel and copper baths were 0.01*M* in metal, 0.035*M* in oxine, and 0.1*M* in acetate.

With cobalt, cathode efficiencies ranged from 1–18%. The highest values were obtained at pH 10, where the deposits were spongy. At lower pH, the deposits were black, or bright with black streaks. With nickel, the efficiencies lay between 1–13%, and the deposits were dark, dull gray, or spongy. At pH 9.1, the efficiency was 3%. Although similar in appearance, the copper deposits showed efficiencies greater than 40% at pH 2.3, and about 0.4% at pH 5.5. At pH 9.1, the cathode was so heavily filmed that current did not flow appreciably even with 100 volts potential. The zinc baths gave gray, matte deposits with efficiencies from 18–76%.

These data show that the metals are deposited, except copper in the "neutral" and alkaline baths.

Polarograms obtained with these complexes are difficult to interpret. Oxine itself is reduced at the dropping mercury electrode (14), as is sulfonated oxine (15). Moreover, it is well known that metals may sometimes be deposited at a mercury cathode although they cannot be deposited on solid cathodes.

The polarograms indicate that reduction occurs at the approximate potentials shown in Table II, but it is not clear what is being reduced. With cobalt and nickel, reduction occurs at potentials less negative than for the aquo complexes or for the sul-

fonated oxine alone. With copper and zinc, the reverse is true except at low pH. The ease of reduction in the copper solution at pH 2.4 suggests that the metal is being deposited; the current readings were very erratic, and the wave height suggests that both oxine and copper are reduced. This might be attributed to a shift to some other form of the complex, as by conversion of the oxygen-copper bond to an oxygen-proton bond (16), followed by more ready reduction of the metal, with reduction of the oxine facilitating the process. Yet the oxine complex is completely extracted by chloroform at pH 2.5 or higher (17). Although interpretation of these results must await further study, they appear to be parallel to the cathode efficiency determinations, in indicating that copper is deposited only at low pH, but the other metals probably at all pH values tested. Results with the rotating platinum electrode are similar.

As nickel oxinate is paramagnetic (18), it has outer orbital configuration. This is probably true for cobalt also, especially since it is not readily oxidized. The zinc complex, of course, can only be outer orbital. Since the presence of the sulfonic acid group would not be expected to alter the configuration, deposition of these metals is in accord with the ionic structures.

According to Ray and Sen (19), copper-oxine bonds are strongly covalent, which indicates inner orbital configuration. Since the coordinating tendency of the transition metals for amines reaches a maximum at copper (6), the inner orbital configuration of the copper complex alone in the series is plausible. The data indicate that, at least at solid cathodes, copper deposits are not obtained except at pH 2.4. Deposition at this pH may be the result of mobile equilibrium between the inner orbital ion and an outer orbital form, which may be protonated.

Nickel complexes of naphthalenediamines.—It has been reported that the naphthalene-1,8-diamine complex of nickel is diamagnetic (18), while the 1,2 complex is paramagnetic. The difference is striking in view of the similarities in the formulas.

The complexes are very slightly soluble; with the 1,8 compound, a solution 0.0006*M* in metal was obtained in 1:1 alcohol-water, and 0.0009*M* in 1:1 dioxane-water. With the 1,2 compound, a 0.0009*M* solution was obtained in the alcohol-water, and 0.0016 with dioxane-water. The difference in solubilities is in accord with the difference in structures. The solutions were provided with a slight excess of amine (0.0002*M*), and were 0.1*M* in KNO₃.

With the 1,8 compound, thin black films with occasional bright spots were obtained on the cathode, but the weight increase was less than 0.2 mg. On cathodes which had been previously nickel-plated, no change in appearance or weight was detected. With the 1,2 complex, bright, brittle coatings were

obtained at efficiencies ranging from 0.8–4.2%, which is surprisingly high in view of the low metal concentrations. "Burning" occurred at the higher current densities. The best deposits were obtained with the dioxane solutions, no doubt on account of the greater metal content.

With the dropping mercury electrode, polarograms showed a well-defined diffusion current at a potential of about -0.7 volt at pH 6.0 and 10.0. This appears to indicate nickel deposition; as in solutions containing pyridine or thiocyanate, the reduction potential is less negative than that of the aquated nickel ion (20). At pH 3.0, a catalytic hydrogen wave is obtained, as with the cyanide complex (21, 22).

With the rotating platinum electrode, results were identical with those from a similar solution from which nickel was omitted. It appears, therefore, that nickel is deposited at the mercury cathode, but not at the solid cathodes.

With the 1,2-diamine, polarograms indicate reduction of nickel at -0.9 volt at pH 2.6, and -1.2 volts at pH 6.1 and 10.2. Deposition is also observed at the rotating platinum cathode. Thus the results of cathode efficiency tests were confirmed, that deposition occurs from the outer orbital complex, but not from the inner.

The tetramethylethylenediamine complex of nickel is diamagnetic³ and has a yellow color, indicating inner orbital configuration. Results were similar to those with the 1,8 diamine, indicating deposition at the mercury cathode, but not at copper or platinum cathodes (except as "flash" deposits).

Copper complexes of dimethylglyoxime.—In hydrochloric acid solutions, a complex $[Cu(DH_2)Cl_2]$ is formed ($DH_2 =$ unionized dimethylglyoxime) (23). In neutral solutions, the complex is $[Cu(DH)_2]$, and in alkaline solutions $[Cu(D)_2]^-$. According to Ray and Sen (19), the coordinate bonds of the neutral complex are strongly covalent. The electronic configuration is therefore probably inner orbital. On the other hand, in the acid complex, the bonds are weakly covalent and correspond to outer orbital configuration.

Current efficiencies were determined in 3:1 alcohol-water, which has been recommended as the best solvent (24). The solutions were $0.01M$ in copper, $0.03M$ in dimethylglyoxime, and $0.1M$ in sodium acetate. At pH 2, the efficiencies were about 20%, and the deposit was a rough, matte coating. At pH 4, the efficiency was about 3%, and above pH 5, it was 0.4%, the cathode remained substantially bare. At pH 10.5, the efficiency was still less than 1% but at pH 11.1 the efficiency was greater than

11%, and a rough, dark coating was obtained. On nickel-plated cathodes, a powdery brown coating was obtained at pH 6.5, but the current efficiency was less than 1%; this is therefore a "flash" deposit, and deposition quickly ceased. However, with fresh solutions, efficiencies higher than 5% were sometimes obtained, although after the solutions stood for several hours, the efficiency dropped to less than 1%. This may be due to slowness of formation of the neutral complex.

A 1:1 alcohol-water solution saturated with the complex was $0.00049M$ in metal. It was made $0.02M$ in dimethylglyoxime and $0.1M$ in potassium nitrate, and was examined polarographically. The polarograms indicate that copper is deposited at all pH values, and the slope of the plot of E vs. $\log i/(i_a - i)$ is 0.03 at pH 11. There are a number of peculiarities in the polarograms.

Apparently only flash deposits are obtained from the inner orbital ion, but deposition proceeds readily from the outer orbital ion in acid solutions, and also in alkaline solutions. At the mercury electrode, however, deposition occurs from both ions. Deposition at the mercury cathode has previously been reported for a number of inner orbital ions such as the acetylacetonate (25, 26).

Structure determinations of copper (II) ions so far show only planar configurations. This has been taken as evidence for inner orbital dsp^2 hybridization, and accounts for failure to obtain deposits thicker than flash coatings from sulfonated oxine, *o*-phenanthroline, and dimethylglyoxime complexes. Heavier deposits are obtained from the pyridine, ethylenediamine, ammonia, and chloro complexes, and according to the present work, from the acid dimethylglyoxime ion. All of the latter ions, according to Ray and Sen (9), have relatively weak covalent bonds, and are presumably outer orbital. Deposits are also obtained from the glycine complex and, of course, from the aquated ion. It seems probable that, notwithstanding their planar configurations, these complexes are of the outer orbital type, and the bonds are predominantly ionic. Ray and Sen suggest that the hybridization is sp^2d .

CONCLUSIONS

It has been shown that metal is not deposited in thicknesses greater than flash coatings, from aqueous solutions of the following: cobalt, nickel, and copper complexes of *o*-phenanthroline; nickel complexes of naphthalene-1,8-diamine or tetramethylethylenediamine; and copper complexes with sulfonated oxine and dimethylglyoxime. These substances are either known to be, or reasonably presumed to be, inner orbital complexes.

On the other hand, deposition is obtained from the

³ Supplied by F. Basolo and R. K. Murman, Northwestern University, Evanston, Illinois; magnetic determination by S. Adler.

glycine complexes of cobalt, nickel, and copper, from the sulfonated oxine complexes of cobalt and nickel, and from the acid dimethylglyoxime complexes of copper. These complexes are either known to be of outer orbital configuration, or may be reasonably presumed to have this configuration, even though some of them have superficial resemblances to the inner orbital ions. Furthermore, zinc, which can form only outer orbital complexes, gives deposits from all of the compounds tested.

Results, therefore, are in accord with the rule previously proposed (1). Certain inner orbital ions, however, give deposits with mercury cathodes, or flash deposits on copper cathodes, but deposition quickly ceases and thick deposits are not built up. Together with the results obtained previously (1), present data lend strong support to the rule that deposition is obtained only from outer orbital complexes.

Some copper complexes are inner orbital, as is commonly assumed, but others appear to be outer orbital, as Ray and Sen have postulated.

ACKNOWLEDGMENTS

This work was supported in part by a fellowship granted to E. H. Lyons by the Atomic Energy Commission, for which he is most grateful. He is also indebted to the Research Corporation for a grant to The Principia College, which supplied apparatus for certain of the experiments.

Any discussion of this paper will appear in a Discussion Section to be published in the June 1955 issue of the JOURNAL.

REFERENCES

1. E. H. LYONS, JR., *This Journal*, **101**, 363 (1954).
2. H. TAUBE, *Chem. Rev.*, **50**, 69 (1952).
3. H. A. LAITINEN AND I. M. KOLTHOFF, *J. Phys. Chem.*, **45**, 1079 (1941).
4. J. J. LINGANE AND H. A. LAITINEN, *Ind. Eng. Chem., Anal. Ed.*, **11**, 504 (1939).
5. J. M. KRUSE AND W. W. BRANDT, *Anal. Chem.*, **24**, 1306 (1952).
6. M. L. COPLEY, L. S. FOSTER, AND J. C. BAILAR, JR., *Chem. Rev.*, **30**, 227 (1942); D. P. MELLOR AND L. MALEY, *Nature*, **159**, 370 (1947); D. P. MELLOR, *Chem. Rev.*, **33**, 178 (1943); B. E. DOUGLAS, *J. Chem. Educ.*, **119** (1952); H. IRVING AND R. J. P. WILLIAMS, *Nature*, **162**, 746 (1948).
7. B. E. DOUGLAS, H. A. LAITINEN, AND J. C. BAILAR, JR., *J. Am. Chem. Soc.*, **72**, 2484 (1950).
8. E. R. ROBERTS, *Trans. Faraday Soc.*, **37**, 353 (1941).
9. R. M. KEEFER, *J. Am. Chem. Soc.*, **68**, 2329 (1946).
10. T. S. G. JONES, *Biochem. J.*, **42**, No. 3 (1948).
11. N. C. LI AND H. DOODY, *J. Am. Chem. Soc.*, **74**, 4194 (1952).
12. See, for example, R. PLETICHA, *Collec. Czech. Chem. Commun.*, **15**, 807 (1950).
13. H. A. LAITINEN, E. I. ONSTOTT, J. C. BAILAR, JR., AND S. SWANN, JR., *J. Am. Chem. Soc.* **71**, 1550 (1949).
14. J. T. STOCK, *J. Chem. Soc.*, **1949**, 586.
15. J. P. PHILLIPS AND C. FERNANDO, *J. Am. Chem. Soc.*, **74**, 4459 (1952).
16. H. GOTO, *J. Chem. Soc. Japan*, **54**, 725 (1933).
17. T. MOELLER, *Ind. Eng. Chem., Anal. Ed.*, **15**, 270, 346 (1943).
18. D. P. MELLOR AND D. P. CRAIG, *J. Proc. Roy. Soc. N. S. Wales*, **74**, 475 (1940).
19. P. RAY AND D. N. SEN, *J. Indian Chem. Soc.*, **25**, 473 (1948).
20. J. J. LINGANE AND H. KERLINGER, *Ind. Eng. Chem., Anal. Ed.*, **13**, 77 (1941).
21. G. GRUBE AND H. LIEDER, *Z. Elektrochem.*, **32**, 561 (1926).
22. J. M. KRUSE AND W. W. BRANDT, *Anal. Chem.*, **24**, 1306 (1952).
22. D. N. HUME AND I. M. KOLTHOFF, *J. Am. Chem. Soc.*, **72**, 4423 (1950).
23. E. THILO, "Die Valenz der Metalle, Fe, Co, Ni, Cu und ihre Verbindungen mit Dioximen," Ferdinand Euhe, Stuttgart (1932).
24. U. PERINELLI, *Boll. soc. ital. biol. sper.*, **16**, 575 (1941).
25. M. CALVIN AND R. H. BAILES, *J. Am. Chem. Soc.*, **68**, 949 (1946).
26. H. F. HOLTZCLAW, JR., K. W. P. JOHNSON, AND F. W. HENGEVELD, *ibid.*, **74**, 3776 (1952).

Lanthanum Oxychloride Phosphors¹

FRANK E. SWINDELLS

Photo Products Department, E. I. du Pont de Nemours, Parlin, New Jersey

ABSTRACT

Lanthanum oxychloride can be activated to show strong fluorescence under excitation by cathode rays. Bismuth as an activator gives a blue emission extending into the ultraviolet with the peak at 3580 Å; antimony a greenish white with the peak at 4960 Å, and samarium a reddish orange emission composed of a series of lines or narrow bands, the strongest of which are at 5640 Å, 5770 Å, 6060 Å, and 6510 Å. The phosphor activated with antimony has a blue emission when excited by 2537 Å.

INTRODUCTION

Various lanthanum compounds have been shown to function as host crystals in phosphor systems. Thus it is reported that lanthanum oxide can be activated with bismuth (1) or various rare earth elements (2); lanthanum phosphate with silver, tin, thallium (3), or bismuth (1); lanthanum borate, chloride, fluoride, or carbonate with cerium (4); lanthanum sulfate with cerium or samarium (5). Also, it has been shown that doubly activated lanthanum oxysulfide is stimulable by infrared (6).

In this paper phosphors having lanthanum oxychloride as the host crystal will be described. These phosphors are quite stable, and with activation by antimony, bismuth, or samarium, are remarkably efficient when excited by cathode rays. While not as bright as the best sulfide phosphors, they are comparable in efficiency with the best oxide type phosphors, such as titanium-activated silicates and manganese-activated zinc and cadmium phosphates. Neodymium and praseodymium are less efficient activators.

PREPARATION AND GENERAL PROPERTIES

The method chosen as most suitable for laboratory preparation of phosphors was heating of hydrated lanthanum chloride in air for a fairly extended time. In practice the heating was conducted in two or three stages. First a solution of lanthanum chloride containing the activator was evaporated to dryness, baked, and thoroughly pulverized. A partial conversion to the oxychloride by hydrolysis occurred. A further conversion took place slowly by heating in air at 600°C, partly by further hydrolysis and partly by direct displacement of chlorine by oxygen. The odor of chlorine was detected in the effluent gases. Complete conversion was found to be rather slow. After two hours, 35% of the product was still soluble

in water, but when heating was extended to 16 hr at 600° an insoluble product was obtained which contained 18.3% chlorine compared with 18.6% calculated for LaOCl. Further heating for one hour at 1000°C in air had no effect on composition as indicated by the chlorine content of 18.4%, but in some cases it improved luminescent properties. Quite frequently nonuniform fluorescent response throughout the preparation was observed, in which case the phosphor was ground and refired at 1000° or 1100°C.

Lanthanum oxide from which the chloride was prepared was stated by the manufacturer² to contain about 0.05% rare earth oxides, so phosphors to be described are far from pure.

Lanthanum oxychloride is a white crystalline material of definite chemical composition. It can be heated for long periods at 900° and for shorter periods at higher temperatures without decomposition. It is insoluble in water or dilute acids, but prolonged contact with water causes some decomposition with impairment of fluorescent properties. It crystallizes in the tetragonal system and has a characteristic layer structure similar to oxychlorides of antimony, bismuth, and the rare earths (7).

LUMINESCENT PROPERTIES

Table I summarizes visual observations of the luminescence of a number of preparations excited by different sources of energy. The column headed CR indicates response to cathode rays produced in an evacuated chamber by a Tesla coil leak tester; XR to x-rays from a tungsten target at 60 kv; 2537 Å to the filtered output of a low pressure mercury arc and 3650 Å to the filtered output of a high pressure mercury lamp. Intensity and color of response are indicated by symbols listed at the end of the table.

Preparations to which no activator had been added showed a weak luminescence possibly due to activation by contaminants. The results do show definite activation of lanthanum oxychloride by antimony,

¹ Manuscript received August 10, 1953. This paper was prepared for delivery before the Chicago Meeting, May 2 to 6, 1954.

² Lindsay Light and Chemical Company.

TABLE I. List of typical preparations

Composition	Firing conditions	CR	XR	2537 Å	3650 Å
LaOCl	1 hr 1000°	F:GW	I	VF	I
LaOCl:0.05 Bi	1 hr 1000°	S:B	F:B	F:B	I
LaOCl:0.05 Sb	1 hr 1000°	S:GW	M:GW	M.B	I
LaOCl:0.05 As	1 hr 800°	M:GW	F:GW	VF.B	I
LaOCl:0.001 Sm	1 hr 1100°	S:OR	M:OR	VF	I
LaOCl:0.01 Sm	1 hr 1000°	S:OR	M:OR	M·OR	F.R
LaOCl:0.1 Sm	1 hr 1100°	M.O	M O	M:O	F:R
LaOCl:0.01 Pr	16 hr 600°	M:Pk	VF	I	I
LaOCl:0.01 Nd	16 hr 600°	M:Lt.B	VF	I	I
La ₂ O ₃	1 hr 1000°	F.O	VF:O	VF	I
La ₂ O ₃ :0.02 Bi	2 hr 600°	M:B	VF	M·B	VF
La ₂ O ₃ :0.02 Sb	2 hr 600°	VF	I	I	I
La ₂ O ₃ :0.002 Sm	30 min 1100°	M O	VF	VF	VF
La ₂ O ₃ :0.002 Pr	30 min 1100°	F	VF	F:O	I
La ₂ O ₃ :0.002 Nd	30 min 1100°	F	VF	I	I
LaCl ₃	1 hr 500°—HCl gas	I	F:BW	I	I
LaCl ₃ :0.01 Bi	1 hr 500°—HCl gas	I	VF	I	I
LaCl ₃ :0.01 Sb	1 hr 500°—HCl gas	I	VF	I	I

Key to Symbols: I—inert; VF—very faint; F—faint; M—medium; S—strong; Lt.B—light blue; B—blue; G—green; GW—greenish white; O—orange; Pk—pink; and R—red.

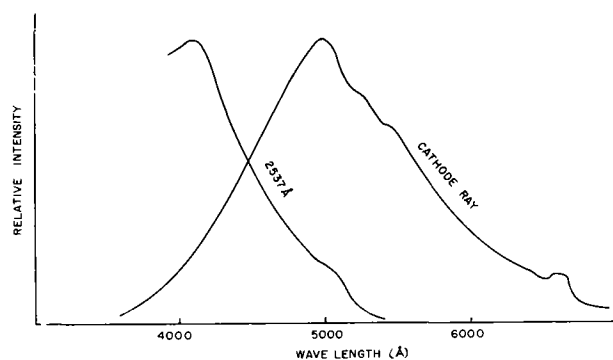


FIG. 1. Spectral emission of LaOCl:0.05 Sb

bismuth, and the three rare earth metals. For purposes of comparison, some observations on lanthanum oxide and lanthanum chloride are included. Oxide phosphors, although capable of activation by bismuth or samarium, have different luminescent properties from oxychloride phosphors. Lanthanum chloride is responsive only to x-ray excitation. Response is not dependent on the added activator, but appears to be a property of the matrix or a common activating impurity.

No activation by Ag, Au, Ce, Cr, Cu, Mn, Pb, Sn, Ti, Tl, or U was proved. Some of these elements, especially chromium, were strong poisons both in the "unactivated" phosphors and in those containing added activators.

Activation by antimony and bismuth.—The optimum concentration of antimony was found to be of the order of 0.05 gram atom Sb per mole of LaOCl. Excited by cathode rays, the emission is a strong greenish white, composed of a wide emission band with a peak at 4960 Å, with indication of unresolved bands at 5200 Å and 5400 Å, and a weak band at 6600 as shown in Fig. 1. These curves were obtained with a G. E. Spectroradiometer and "normalized"

by replotting, so that maximum intensity is the same for this and succeeding emission curves.

When excited by 2537 Å, the above bands are suppressed and a new band appears in the blue, with a peak at about 4100 Å. Course of the curve below 4000 Å was obscured by reflected mercury radiation from the exciting source. There is no indication of the presence of this blue band in the emission excited by cathode rays, but the green band excited by cathode rays appears weakly with 2537 Å. When the phosphor is warmed on a hot plate during irradiation by 2537 Å, the emission color changes to a paler blue, possibly indicating a broadening of the blue band, or more likely that the green band is more stable at the elevated temperature.

Bismuth was also found to be a strong activator, but the emission excited by 2537 Å is a deeper blue and visibly weaker than the emission of the antimony-activated phosphor. A spectral distribution curve of the emission excited by 2537 Å could not be obtained because of interference of reflected mercury radiation not removed by a Corning 9863 filter. The emission excited by cathode rays is also a deep blue, having in this case a fairly strong visible component. However, Fig. 2 shows that most of the emission is in the near ultraviolet with a peak at 3580 Å. While there is some indication of the narrow band of unactivated LaOCl at 5020 Å, the longer wave length bands are completely suppressed.

A few preparations to which arsenic had been added showed a weak fluorescence with both bismuth and antimony bands present. Activation by arsenic appears doubtful because of its volatility, and the weak luminescence is more likely to be attributed to traces of antimony and bismuth either in added arsenic or in lanthanum oxychloride.

With cathode ray excitation LaOCl:Sb has a strong and persistent phosphorescence, but LaOCl:Bi decays so rapidly that visual detection is difficult. A few measurements showed the antimony-activated phosphor to decay to about $\frac{1}{10}$ of its initial intensity in the first millisecond, after which it followed a

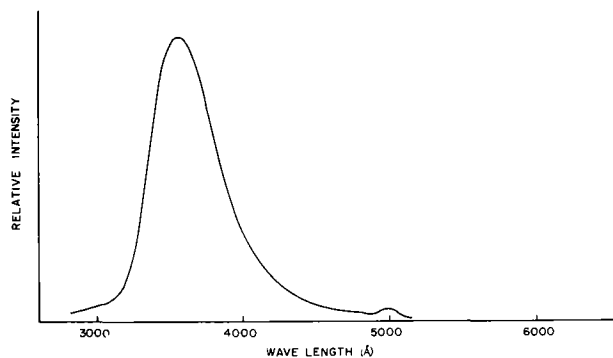


FIG. 2. Spectral emission of LaOCl:0.05 Bi, cathode ray excitation.

power law with a constant of 1.4 up to about 30 sec. The fast initial decay was also shown by the bismuth-activated phosphor but proceeded to a much lower intensity before the power law tail appeared.

Activation by samarium, praseodymium, and neodymium.—When unactivated lanthanum oxychloride was prepared it showed a rather weak greenish fluorescence with cathode ray excitation. The emission shown in Fig. 3 consisted of a number of lines or narrow bands of the type usually associated with rare earth activation. However, inclusion of samarium in the preparations increased brightness considerably and shifted the color to a bright orange. Strongest cathodoluminescence was obtained from preparations containing about 1 gram atom Sm per 1000 moles LaOCl. Higher concentrations of Sm diminish the response to cathode rays and cause the phosphor to respond to 2537 Å, and to a lesser degree to 3650 Å. It will be seen from Fig. 4 that the strongest emission lines are at 5640 Å, 5770 Å, 6060 Å, and 6510 Å. A comparison of solid and dashed lines of Fig. 4 shows that there is a close resemblance but nonidentity of spectra of the oxide and oxychloride phosphors activated with samarium.

Phosphors containing praseodymium and neodymium also showed characteristic cathodolumines-

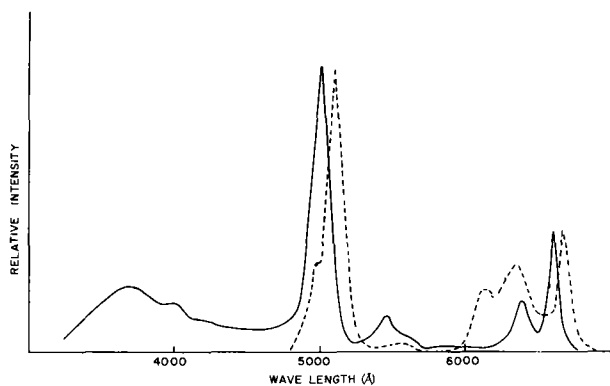


FIG. 3. Spectral emission of LaOCl (solid line) and La_2O_3 (dotted line) with no activator added, cathode ray excitation.

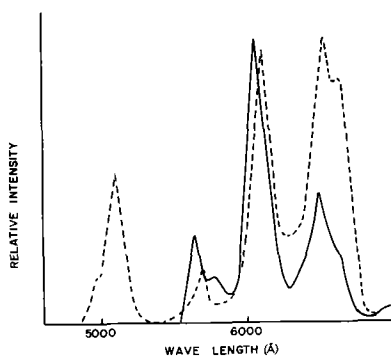


FIG. 4. Spectral emission of LaOCl:0.01 Sm (solid line) and La_2O_3 :0.002 Sm (dotted line), cathode ray excitation.

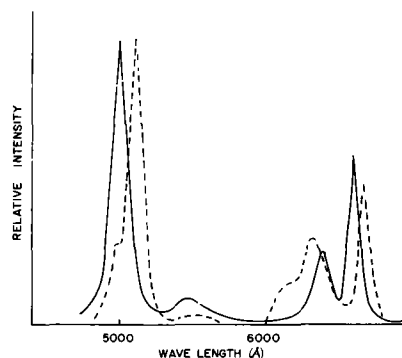


FIG. 5. Spectral emission of LaOCl:0.01 Pr (solid line) and La_2O_3 :0.002 Pr (dotted line), cathode ray excitation.

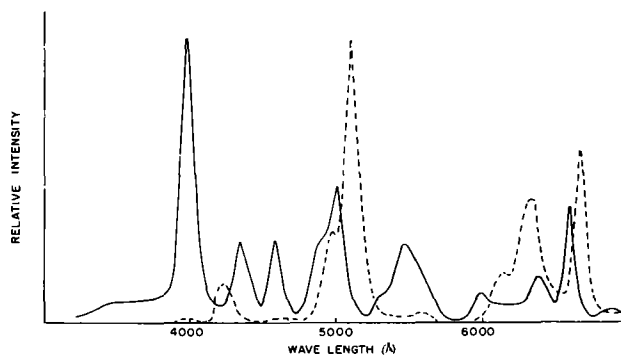


FIG. 6. Spectral emission of LaOCl:0.01 Nd (solid line) and La_2O_3 :0.002 Nd (dotted line), cathode ray excitation.

cence, but much weaker than in the samarium preparations. Emission curves of these phosphors are shown in Fig. 5 and 6. Comparing these curves with the corresponding curves in Fig. 3, it appears that "unactivated" LaOCl contained Pr as an impurity since the emission spectra of the two oxychloride phosphors are identical, as are the two oxide phosphors, addition of Pr serving only to increase intensity of emission. Ultraviolet emission of unactivated oxychloride corresponding to the bismuth band of Fig. 2 was either quenched by the added quantity of praseodymium, or, more likely, the lower excitation intensity used in obtaining Fig. 5 failed to bring the ultraviolet band up to a recordable intensity.

The neodymium-activated phosphor is interesting. In the oxychloride a number of new bands appear, the strongest being at 4000 Å, 4350 Å, 4590 Å, 4900 Å, 5450 Å, and 6000 Å. The visual effect is a pale blue luminescence of moderate intensity. The oxide to which neodymium had been added had an emission quite similar to La_2O_3 :Pr except that a new band at 4230 Å appeared.

DISCUSSION

It is of some significance that only the trivalent elements Bi, Sb, Sm, Pr, and Nd were found to function as activators. These elements all form relatively

stable oxychlorides having crystal structures similar to that of LaOCl , and radii of the trivalent ions are in no case appreciably larger than that of La^{3+} . It would thus appear that activator atoms replace some lanthanum atoms with a minimum of lattice distortion. Samarium, for example, functions efficiently as an activator in concentrations as high as 30 mole %.

No satisfactory explanation can be offered for change in emission color of the antimony-activated phosphor from blue with ultraviolet excitation to green with cathode rays, and particularly for the absence of the blue band with the latter form of excitation. Either two types of centers or two energy levels in the same center are involved, only one of which can be excited to luminescence by cathode rays. It is most probable that two types of centers or transitions exist in a common matrix, since there is no evidence known to the writer of the existence of more than one crystal form of lanthanum oxychloride. It has been suggested (8) that the SbO_4Cl_4 group as a whole might be excited by the radiation. With one type of excitation, electrons from oxide ions are excited and with the other type of excitation, electrons from chloride ions are excited. In any event, the process producing green emission must involve deep traps as evidenced by persistent phosphorescence.

It is also interesting to note that the higher energy blue band is excited by photons, while the lower energy green emission is excited by electrons. In other phosphors having emission colors dependent on type of excitation, such as magnesium arsenate activated with manganese, the emission band having the higher energy change in the transition is also produced by the higher energy exciting source. The reason for the reverse being true with lanthanum oxychloride is not known.

Any discussion of this paper will appear in a Discussion Section to be published in the June 1955 issue of the *JOURNAL*.

REFERENCES

1. F. A. KROEGER, J. TH. G. OVERBEEK, J. GOORISSEN, AND J. VAN DEN BOOMGAARD, *J. (and Trans.) Electrochem. Soc.*, **96**, 132 (1949).
2. H. GOBRECHT AND R. TOMASCHEK, *Ann. Phys.*, **29**, 324 (1937).
3. M. HUENIGER AND H. PANKE, U. S. Pat. 2,270,124, Jan. 13, 1942.
4. F. A. KROEGER AND J. BAKKER, *Physica*, **8**, 628 (1941).
5. R. TOMASCHEK, *Ann. Phys.*, **84**, 329 (1927).
6. J. J. PITHA AND R. WARD, U. S. Pat. 2,462,547, Feb. 22, 1949.
7. A. F. WELLS, "Structural Inorganic Chemistry", 2nd ed. p. 308, Oxford University Press, Oxford (1950).
8. R. WARD, Private communication.

The Electrochemical Polarization of Zirconium in Neutral Salt Solutions¹

NORMAN HACKERMAN AND OLIN B. CECIL²

Department of Chemistry, University of Texas, Austin, Texas

ABSTRACT

Cathodic and anodic polarization curves of zirconium in neutral sodium chloride solution were determined at constant current densities between 3.5×10^{-8} and 3.5×10^{-3} amp/cm².

In aerated 0.5M NaCl, the cathode reaction occurring below the oxygen limiting diffusion current of 2×10^{-4} amp/cm² was reduction of O₂ to OH⁻. At current densities above the diffusion wave, hydrogen was evolved. Change in salt concentration resulted in a slight shift of diffusion current due to change in oxygen solubility. In de-aerated 0.5M chloride solution, the oxygen diffusion current decreased with decrease in oxygen concentration. The slope of the Tafel line obtained is 0.12, and the hydrogen overvoltage for this system is 0.83 volt at 1 ma/cm². Another wave occurred at 2×10^{-6} amp/cm² and is explained as the reduction of a surface oxide layer on the metal.

Anodically, zirconium dissolved in 0.5M NaCl. The dissolution potential, 0.15 volt, did not vary with current density. Commercial zirconium and pure hafnium also dissolved under similar conditions.

In neutral sulfate solutions, zirconium was passive under anodic treatment. At current densities above 1×10^{-3} amp/cm² the potential reached an apparently constant value in about ten minutes. After a period depending on current density, this was followed by a sudden increase in potential to 28.5 volts. This potential is a result of an *IR* drop across a surface layer of oxide.

INTRODUCTION

This is a study with zirconium paralleling earlier work with titanium (1, 2). The methods and procedures used here are essentially the same as those used previously and details may be obtained there. Interest in these metals lies not only in their electrochemical properties, but also in the fact that they exhibit characteristics of passivity. A small amount of metallic hafnium was available and some results with this metal are also reported.

METHODS AND MATERIALS

The direct method of measurement was used, and potentials obtained this way include any *IR* contributions in the cell. Foremost are those across the solution between the metal and reference electrode, and those resulting from films on the metal surface. The former were measured and corrections made, whereas the latter are included in the reported polarization values.

The polarizing system consisted of several external dropping resistors in series with the metal electrode and a platinum auxiliary polarizing electrode. With this arrangement the bulk of the voltage

drop was across the external resistors, thus minimizing any current change across the cell itself.

All potentials were measured with respect to a saturated calomel half cell. A vacuum tube amplifier was used in conjunction with the potentiometer to reduce the current drawn by the measuring system. In this way not more than 10^{-12} amp was drawn from the cell even when the system was out of balance (1).

Measurements in aerated solutions were made in an apparatus permitting simultaneous operation of six cells. The electrode assembly of each cell consisted of the metal, a platinum auxiliary polarizing electrode, and a saturated calomel reference electrode. The three electrodes were mounted in one holder such that the platinum electrode was 7 cm from the coupon face, and the assembly was supported from a beam which was connected to the circular stirring mechanism, enabling all three electrodes to maintain the same relationship with each other at all times. The metal specimens were mounted in Lucite by a pressure molding process, and these wafers were placed in phenolic plastic holders.

Hafnium-free zirconium³ was 98.6% pure with 1.34% oxygen, the remainder being mostly carbon. The metal was furnished in the form of punched coupons, 1.9 cm in diameter and 0.25 cm thick. Com-

¹ Manuscript received April 24, 1953. This paper was prepared for delivery before the New York Meeting, April 12 to 16, 1953.

² Present address: Monsanto Chemical Company, St. Louis, Missouri.

³ All metal samples used were supplied by the Argonne National Laboratory, Lemont, Illinois.

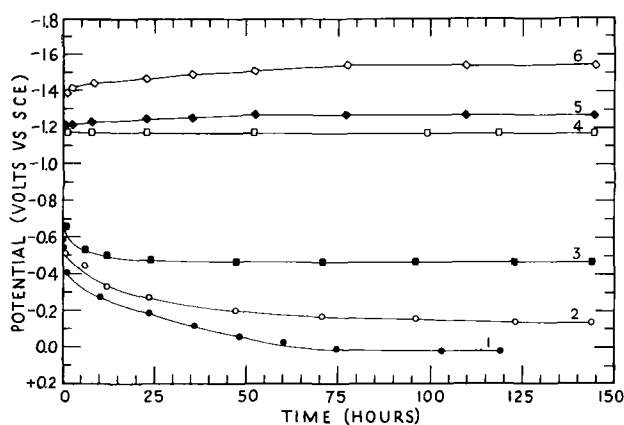


FIG. 1. Cathodic time-potential curves in aerated 0.5M NaCl at 30°C. In increasing curve number: 0, 3.5×10^{-6} , 1.8×10^{-5} , 1.8×10^{-4} , 3.5×10^{-4} , 1.8×10^{-3} amp/cm².

mercial zirconium and pure hafnium samples were machined coupons of the same dimensions.

Scrubbed air was passed through fritted gas bubblers into the cells. Temperature was maintained at about 30°C; stirring was by a circular, vertical path mechanism.

The effect of oxygen concentration was studied in a similar apparatus⁴ which was smaller and was contained in an air-tight box. For this work oxygen was not excluded rigorously but was reduced substantially below the partial pressure of oxygen in the aerated system. Because of the small size of this apparatus, only the zirconium electrode was rotated. This resulted in mechanical blocking of varying amounts of the polarizing current during each revolution of the zirconium electrode, so results from this system, while internally consistent, cannot be quantitatively translated to the other.

Before use, all solutions for the aerated studies were either aerated and filtered or pre-electrolyzed between carbon electrodes. Solutions prepared in either way gave the same results. Only pre-electrolyzed solutions were used in the de-aeration studies. Evaporation losses during a run were replaced with distilled water. No attempt was made to buffer the solutions since buffering ions would interfere with the electrode process in an unknown fashion. Fortunately, this offered no difficulty since the observed pH changes during a run were less than one unit. The close proximity of the anode and cathode, the stirring, and the large volumes used account for this buffering action.

Coupons were prepared by hand polishing on No. 2 emery paper followed by 150 strokes on No. 2/0 paper. They were then wiped with lens tissue and cleaned with 95% ethyl alcohol.⁵

⁴ Referred to as de-aerated systems.

⁵ Just as a matter of interest, coupons prepared in this manner had a roughness factor of 2.6 ± 0.4 as determined with krypton at -195.8°C .

All values of current density are stated in terms of amperes per square centimeter of projected or measured area. Unless otherwise noted, all potentials are steady-state values, which means here a constant value for at least four hours.

CATHODIC POLARIZATION

Typical time-potential curves are shown in Fig. 1; cathodic polarization curves for zirconium in aerated 0.5 and 1.0M NaCl solutions are given in Fig. 2. Although each point on the 0.5M curve represents a separate determination, two or more runs at many current densities were in good agreement. Measurements in 1.0M NaCl were made to determine the effect of change in salt concentration. These points represent constant potentials obtained from one coupon run successively at several current densities.

Since the current density scale is logarithmic, the open circuit potential cannot be shown. For 0.5M NaCl it is 0.018 volt.

Two waves appear in the Fig. 2 curves. For the 0.5M solution, one is at about 2×10^{-6} amp/cm² and the other is near 2×10^{-4} amp/cm². For 1.0M chloride the steeper break comes at a lower current density. At 2×10^{-4} amp/cm² gas begins to evolve slowly on the zirconium. Although visible bubbles do not form on the surface, large bubbles gather on the wax coating around the edge of the coupon. At higher current densities, visible bubbles evolve continuously from the coupon surface. After an extended period of polarization in this current density region, the zirconium surface darkens considerably. If the period of polarization is extended to one or two days, the surface becomes coated with a layer of fine black powder. The slope of the straight line for this region is 0.15 volt per log unit.

In many instances it was desirable to determine the effect of such variables as salt concentration by determining only sections of the polarization curve. This could most readily be accomplished by running

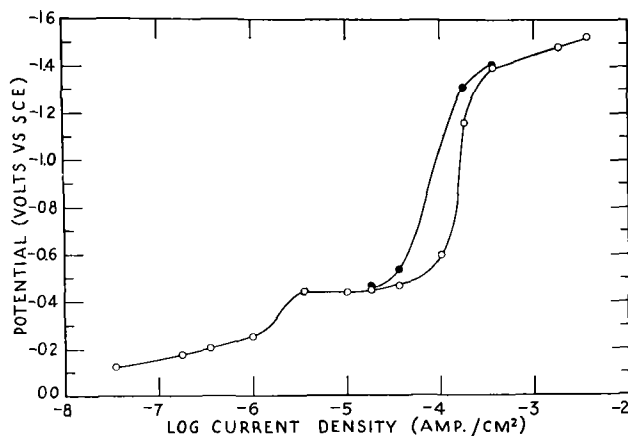


FIG. 2. Cathodic polarization in aerated NaCl solutions at 30°C. O, 0.5M; ●, 1.0M.

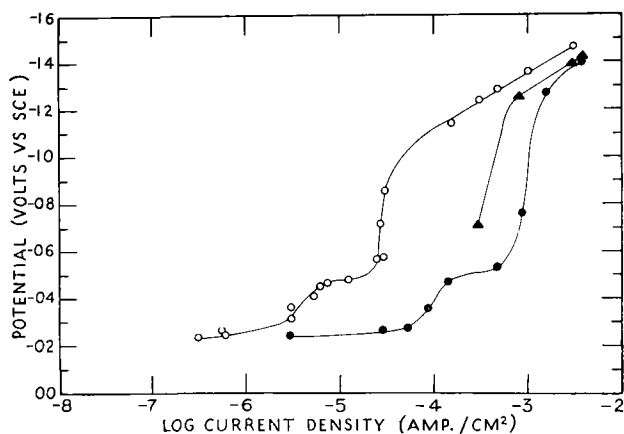


FIG. 3. Cathodic polarization in 0.5M NaCl at 30°C. O, de-aerated; ●, aerated; ▲, open to atmosphere.

one coupon at the several current densities. To investigate the validity of potentials obtained in this manner, a complete polarization curve was obtained with one coupon. The curves were essentially the same except in the lowest current density region. Here a slight amount of hysteresis was observed.

One coupon was etched in 5.0% aqueous hydrogen fluoride just prior to use to determine the effect of this pretreatment. The resulting polarization curve was not different from the equivalent one in Fig. 2.

Cathodic polarization curves for zirconium in aerated and de-aerated 0.5M NaCl solutions, all obtained in the apparatus designed to permit running at lower oxygen concentration, are given in Fig. 3. Since these studies were performed only to determine the effect of changes in oxygen concentration, it was not considered necessary to exclude oxygen rigorously. The top curve was obtained with oxygen excluded as completely as possible; the next was obtained after completion of the previous determinations by opening cells to the atmosphere and aerating them for an hour; and the bottom curve was obtained with cells open to the atmosphere and undergoing continuous aeration.

The aerated and de-aerated curves are essentially the same, the only difference being a displacement along the current density axis. Because of the difference in geometry and stirring rates between the systems used to obtain the curves of Fig. 2 and those for Fig. 3, no attempt was made to correlate the results of the two.

ANODIC POLARIZATION

Typical time potential curves on anodically polarizing in NaCl to constant potential are shown in Fig. 4a and 4b. (Note different time scales.) Contrary to the experience with titanium (1), the charging curves for zirconium even at lowest current densities consisted of two essentially linear portions,

the horizontal one being a dissolution potential in NaCl solutions.

The anodic polarization curve for zirconium in aerated 0.5M NaCl solution is shown in Fig. 5, curve 2. The most important observation is that the potential is independent of current density. At the lowest current density, 3.5×10^{-7} amp/cm², the surface of the coupon became slightly duller. Coupons run at progressively higher current densities exhibited increasing amounts of surface attack. One coupon, run anodically at 3.5×10^{-2} amp/cm² for less than 36 hr, dissolved almost completely. During the course of the run, a large amount of a white gelatinous precipitate collected on the bottom of the polarization cell. When washed and dried, this precipitate turned dark blue. The front surface of the undissolved portion of the coupon was black and flaky; whereas the back was unchanged and showed no signs of attack. An electron diffraction pattern of the unwashed coupon surface gave lines corresponding mainly to the spacings of NaCl. The remaining lines could not be indexed as belonging to

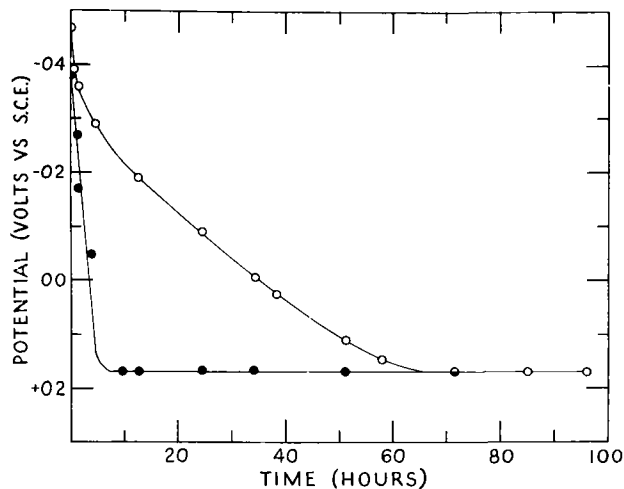


FIG. 4a. Anodic time-potential curves in aerated 0.5M NaCl at 30°C. O, 3.5×10^{-8} ; ●, 3.5×10^{-7} amp/cm².

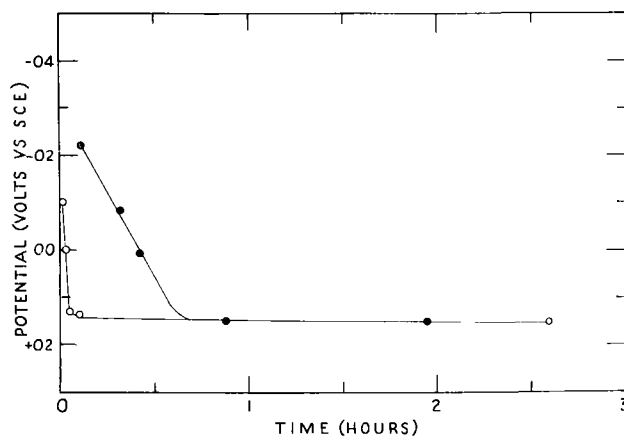


FIG. 4b. Anodic time-potential curves in aerated 0.5M NaCl at 30°C. ●, 3.5×10^{-6} ; O, 1.8×10^{-5} amp/cm².

any compound of zirconium whose spacings have been reported.

During one of the anodic runs in aerated 0.5M solutions, chlorine gas was bubbled directly over one coupon. Although no change in potential was observed, a comparison of the coupon surface with one from an earlier determination at the same current density showed that the degree of attack was considerably increased by the presence of chlorine.

Curves 1 and 4 of Fig. 5 demonstrate the effect of NaCl concentration on anodic polarization potentials of zirconium. The potentials still showed no dependency on current density but were slightly more positive in more dilute solutions. These coupons also showed signs of attack, the degree being dependent on current density.

Cessation of aeration during the runs carried out in NaCl solutions caused no change in electrode potentials.

A study of the effect of hafnium on the anodic polarization of zirconium was carried out to determine if its presence was an important factor in anodic dissolution of zirconium in NaCl solutions. Anodic polarization curves were obtained with commercial zirconium and zirconium-free hafnium coupons (curves 3 and 5, respectively, of Fig. 5). These show little deviation from those obtained with hafnium-free zirconium. In all cases there is evidence of attack on the surface of the metal in question.

Curve 6 of Fig. 5 gives results of an anodic polarization study of zirconium in aerated 0.5M Na₂SO₄

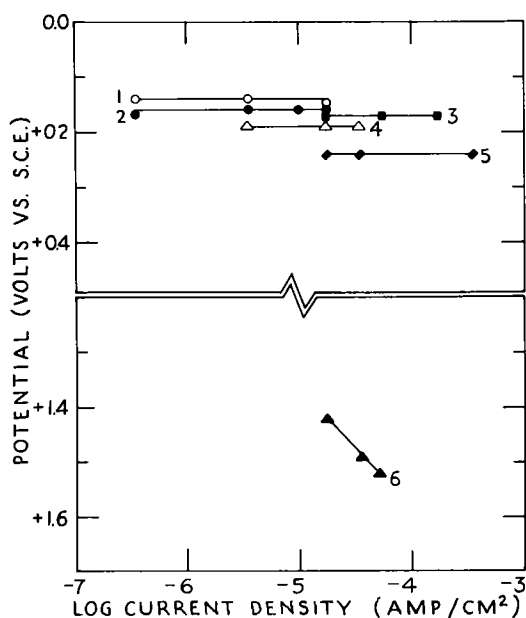


FIG. 5. Anodic polarization in aerated solutions at 30°C. In increasing curve number: Zr in 0.7M NaCl; Zr in 0.5M NaCl; Hf-containing Zr in 0.5M NaCl; Zr in 0.2M NaCl; Hf in 0.5M NaCl; Zr in 0.5M Na₂SO₄.

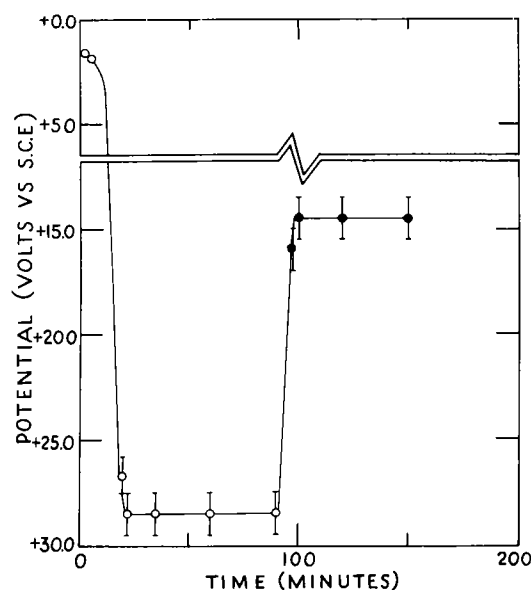


FIG. 6. Anodic time-potential curves in aerated 0.5M Na₂SO₄ at 30°C. ○, 1.8×10^{-3} ; ●, 7.0×10^{-4} amp/cm².

solution. Only a small segment was determined since results of the few points obtained clearly demonstrated that the metal was passive in the sulfate solution. At all three current densities, oxygen was evolved. After four days, the coupon was removed from solution just long enough to observe the surface. No change in appearance was evident. When the coupon was returned to the sulfate solution, the potential immediately went to the constant value it showed before the coupon was removed.

Enough NaCl was added to the sulfate solution to make it approximately 0.5M with respect to chloride. The electrode potential decreased rapidly from 1.5 to 0.18 volts, a value approaching that obtained with the 0.5M NaCl solution alone.

Higher current density runs were made, in part to compare with similar work on titanium (1), and in part to gain some information on rectifying properties of a zirconium anode. The results are given in Fig. 6 in the form of a time-potential plot. During the first few minutes of the run when the potential had apparently leveled off, gas could be seen evolving from the metal surface. However, when the sudden increase in potential occurred, gas evolution ceased. The surface of this coupon was darkened considerably; the entire surface was etched slightly, and there were a few deep pits around the edge.

DISCUSSION

Cathodic Polarization

The usual cathodic reactions in aerated aqueous solutions containing no foreign reducible materials are reduction of dissolved O₂ to OH⁻ and reduction of H⁺ to H₂. The complexity of the former is not

completely known; however, it occurs at a less negative potential than the latter and thus precedes hydrogen evolution as the current density is increased. This study shows that a zirconium cathode in neutral chloride solutions follows this pattern. Up to about 2×10^{-4} amp/cm² the electrode reaction is reduction of O₂ except perhaps near 2×10^{-6} amp/cm². (This step is discussed later.) The step occurring at 2×10^{-4} amp/cm² represents the limiting diffusion current density for oxygen under these experimental conditions.⁶ At current densities above this value, hydrogen is evolved. The de-aeration experiments supported the validity of the assumption that the break represented the limiting diffusion current of oxygen.

The only effect of changing salt concentration was to change the limiting diffusion current of O₂. This is proportional to the concentration of the reducible substance, in this case to the solubility of oxygen in the salt solutions used. The observed ratio of $I_d(1.0M)/I_d(0.5M)$ of 0.7 is in reasonable agreement with 0.86 as calculated using known oxygen solubilities (4).

From the ratios of the limiting diffusion currents, the concentration of dissolved oxygen in the de-aerated solution is calculated to have been $3.1 \times 10^{-6}M$, or 0.1 ppm. Similarly, oxygen concentration in the partially aerated run was 2.3 ppm.

At current densities larger than the oxygen limiting diffusion current, hydrogen is evolved and potentials follow a Tafel relationship for hydrogen overvoltage. In the aerated systems the electrode potential is given by

$$E = -1.47 - 0.15 \log i \quad (\text{I})$$

where i is current density in ma/cm².

The pH of the solution was 6.5, from which the reversible hydrogen potential on the saturated calomel scale is -0.63 volt. The hydrogen overvoltage (always given as positive) on zirconium in this case is

$$\eta = 0.84 + 0.15 \log i. \quad (\text{II})$$

At 1×10^{-3} amp/cm² the overvoltage is 0.84 volt.

Calculation based on equating rate of hydroxyl production with rate of diffusion would show a steady-state pH in excess of 6.5, the actual value depending on conditions assumed. The constants of equation (II) would change accordingly. For instance, if the pH of the liquid film adjacent to the electrode were as much as 10 to 11, the value of η

at 1 ma/cm² would be between 0.5 and 0.6, and the slope of the line about 0.14. However, stirring plus neutralization by hydrogen ion produced at the anode should combine to keep the pH lower than that estimated above. Experimentally, the pH of the solution (in the bulk and between electrodes) never rose above 7. Attempts were made to measure pH within a millimeter of the cathode, and although they were not notably successful, such indications as were obtained suggest that the pH remained around, and certainly did not exceed, 8. In any event, evidence here points to zirconium as one of the high hydrogen overvoltage metals.

Values for b in the Tafel equation usually fall between 0.09 and 0.13. However, the value obtained for zirconium is not unique since high values have been reported for such metals as titanium, mercury, and lead, among others.

Hydrogen overvoltage depends on current actually involved in hydrogen evolution rather than on total current. Consequently, it is better to represent the hydrogen overvoltage as the relationship between E and $\log(I - I_d)$, i.e., total current minus the oxygen limiting diffusion current. Such a relationship results in a line having a slightly less positive slope. For the aerated run, the slope at 1 ma/cm² is 0.12 and the overvoltage is 0.85 volt.

As mentioned earlier, after hydrogen evolution for extended periods of time, the surface of the zirconium coupon became black and hard. If periods of evolution were very long and evolution was rapid, the surface became covered with a thin layer of black powder. Apparently in this region either a hydride or a solid solution of the metal with hydrogen is produced. Both have been reported for zirconium (5, 6). Presence of a hydride produced by cathodic treatment of zirconium has been previously reported (7).

The current density region below the oxygen limiting diffusion wave is attributed to cathodic reduction of O₂ to OH⁻. If the polarization curve were drawn as the best straight line from the lowest current density to the break occurring at 2×10^{-4} amp/cm², the slope would be nearly the same as that for the hydrogen evolution portion of the curve. This indicates that reduction of O₂ to OH⁻ followed an overvoltage equation similar to that for hydrogen. However, the step occurring at 2×10^{-6} amp/cm² is definitely present under the existing experimental conditions. Several possible explanations⁷ for such a break present themselves: (a) changing from

⁶ In an unstirred aerated solution the calculated limiting current density is approximately equal to 10^{-4} amp/cm². Assuming a decrease in diffusion layer thickness from 0.01 cm to 0.005 gives an i_d about the same as that obtained experimentally. The thickness assumed is reasonable (3).

⁷ It has been suggested that chlorine evolution or platinum dissolution at the anode might contribute to this wave. However, calculations show that unless there is a peculiar overvoltage involved, neither of these reactions should occur at this potential.

the two-electron reduction of O_2 to H_2O_2 to the four-electron reaction for the reduction to OH^- ; (b) reduction of some impurity in the solution; (c) production of a depolarizer by electrolysis; (d) reduction of some metallic component of the system, e.g., a surface oxide.

Experimental evidence for the break indicates that it is oxygen-dependent, analogous to the break occurring at 2×10^{-4} amp/cm². This suggests that the explanation is one involving a step in the reduction of O_2 to OH^- as in (a). However, the two breaks occur at current densities differing by a factor of 100. Such a difference would mean that if the break occurring at the higher current density were for the four-electron reduction, the lower break must be for a process involving a fractional electron change. Thus, this explanation is hardly acceptable. For the two breaks to be an indication of a stepwise reduction would involve a mechanism probably very complex. It is not clear in what manner such a reduction would operate.

Explanation (b) is hardly likely since the solutions were pre-electrolyzed with no resulting change in the curve.

If the wave represented the limiting diffusion of some depolarizer formed by electrolysis, the time potential curves for low current density values (Fig. 1, curves 1, 2, and 3) would have increased sooner the higher the current density, since the concentration of the depolarizer being formed would increase more rapidly at these higher current densities. Instead, the reverse is observed. This eliminates possibilities (a) and (c).

Thermodynamically, a surface film of ZrO_2 or some other oxide could exist at the potentials observed. The existence of such a film at low cathodic current densities has been postulated (7). Such an oxide film should not be able to withstand cathodic reduction at higher current densities, especially in the hydrogen evolution portion. Although etching in hydrofluoric acid would strip the oxide film from the metal, the film could re-form on exposure to a solution saturated with oxygen.

If reduction of a surface film is the explanation of the break in the polarization curve occurring at the lower current density, film formation must involve direct surface oxidation by dissolved oxygen to explain the data. This is in contrast with the work of Moore, McKinney, and Warner (7) who postulated reaction of the metal with water to form the oxide.

Hysteresis observed in this region is best explained as the result of a surface change of the metal caused by hydrogen evolution.

The cathodic polarization curve for zirconium (Fig. 2) is probably typical for zirconium in other

aerated salt solutions, unless a specific reaction occurs. Thus, any change in type of salt or salt concentration should result only in effects arising from pH changes or changes in oxygen solubility. The general shape of the curve should be typical for other noncorroding metals in similar solutions.

Anodic Polarization

When zirconium is treated anodically in neutral sodium chloride solutions, the metal dissolves. No definite indication of weight loss would be detected at lower current densities studied, since the total amount of electricity passed would cause loss of less than a milligram of metal. At higher current densities metal loss was quite evident since one coupon dissolved almost completely in less than 36 hr.

No real difference is observed between pure zirconium, commercial zirconium, and hafnium on anodic treatment in neutral chloride solutions. All dissolve at a characteristic potential which remains constant with change in current density. Hafnium would be expected to dissolve at a potential somewhat different from that of zirconium. Since the potential for hafnium dissolution is more positive than for zirconium, commercial zirconium should dissolve at essentially the same potential as the pure metal.

Under similar anodic treatment in neutral sodium chloride solutions, titanium was observed to be passive (2). Because of similarity between the metals, any mechanism for dissolution of zirconium in chloride solutions should be expected to apply equally well to titanium. Conversely, any mechanism for passivity of titanium in chloride solutions should be expected to apply as well to zirconium. No explanation for this anomaly can be given.

Anodic treatment of the metal in neutral sulfate solution resulted in passivation with accompanying oxygen evolution. If sodium chloride is added to the sulfate solution, the metal again becomes active, as indicated by the observed sudden decrease in potential. When such a decrease occurred, the metal dissolved.

The passivity of zirconium in sulfate solutions may be explained by formation of a protective layer of an insoluble, or only sparingly soluble, oxide film on the metal surface.⁸ Actually, at higher current densities a visible layer does appear after a time. The presence of reducing agents or cathodic treatment destroys this oxide layer, resulting in loss of passivity.

Since chlorine gas bubbled over the zirconium coupon had no effect on the electrode potentials,

⁸ Passivity of zirconium by virtue of adsorbed oxygen is also possible, but the evidence here provides less support for that postulate than for the oxidation mechanism.

no mechanism dependent on the presence of Cl_2 would be applicable. This eliminates discharge of Cl^- to Cl_2 at the anode. The mechanism of the dissolution involves a transfer of metal, in the form of zirconium or zirconyl ion, across the metal-solution interface. These ions can form soluble chlorides. As more positive metal ions are transferred, more salt is formed. The salt can hydrolyze at the solution pH to form ZrO_2 , probably in the hydrated form which is rather stable.

Large positive potentials observed at high anodic current densities in 0.5M sulfate solutions are apparently caused by a surface oxide layer acting as an ohmic resistance. Thus, as current is decreased, the potential should decrease proportionally. Observed potential values would correspond to an ohmic resistance of 5.7×10^3 ohms for the higher value of current and 7.2×10^3 ohms for the lower value. These values are in fair agreement, considering the fact that there were voltage oscillations of the order of 0.5 volt in the data plotted in the latter portions of the curve of Fig. 6.

ACKNOWLEDGMENT

This work was carried out as part of Contract Nonr 375(02) with the Office of Naval Research. The authors take this opportunity to express their appreciation for this aid.

Any discussion of this paper will appear in a Discussion Section to be published in the June 1955 issue of the JOURNAL.

REFERENCES

1. N. HACKERMAN AND C. D. HALL, JR., *This Journal*, **101**, 321 (1954).
2. C. D. HALL, JR. AND N. HACKERMAN, *J. Phys. Chem.*, **57**, 262 (1953).
3. G. KORTUM AND J. O'M. BOCKRIS, "Textbook of Electrochemistry," Vol. II, p. 404, Elsevier, Amsterdam (1951).
4. H. H. UHLIG, Editor, "Corrosion Handbook," p. 1147, John Wiley and Sons, Inc., New York (1948).
5. M. N. A. HALL, S. L. H. MARTIN, AND A. L. G. REES, *Trans. Faraday Soc.*, **41**, 306 (1945).
6. T. P. GIBBS, *This Journal*, **93**, 198 (1948).
7. C. G. MOORE, O. S. MCKINNEY, AND J. C. WARNER, U. S. Atomic Energy Commission Progress Report, March 1950, NYO-544.

Hydrogen Overvoltage on Bright Platinum¹

II. pH and Salt Effects in Acid, Neutral, and Alkaline Solutions

SIGMUND SCHULDINER

Naval Research Laboratory, Washington, D. C.

ABSTRACT

Hydrogen overvoltage on bright platinum was measured over the pH range 0.5–12.1. The effects of pH and of added sodium and ammonium ions were determined. Relative rates of over-all hydrogen producing reactions at low current densities were determined for solutions studied. Mechanisms of hydrogen overvoltage in these solutions are discussed.

INTRODUCTION

Part I reported work regarding hydrogen overvoltage on bright platinum (1). In this paper pH and salt effects are investigated in greater detail and over a wide range in pH.

Overvoltage-current density relationships at $25 \pm 1^\circ\text{C}$ were measured in vigorously agitated solutions to minimize concentration overvoltage, and the potential drop caused by solution resistance was corrected (1). Since use of pseudocapacitance measurements to determine surface cleanliness of the cathode (1) are effective only in acid solutions, it was necessary to modify the experimental technique so that cleanliness of the platinum cathode would be rigorously maintained during overvoltage measurements in all solutions. This was done by making all measurements in a Teflon cell and by accepting only those measurements that met requirements which were obtainable only with an unpoisoned platinum surface.

EXPERIMENTAL METHOD

General experimental requirements were essentially the same as described in Part I. Only modifications in technique are described here.

Glass cells introduce impurities into the electrolyte, so the electrolytic cell (Fig. 1) was constructed of Teflon. The platinum (99.99%) cathode was a small sphere at the end of a short length of wire. Apparent area of this cathode was 0.01324 cm^2 . The true area was determined to be 0.0273 cm^2 by double layer capacitance measurements, which gave a correction factor of 2.06. The anode, a large platinum grid made of several layers of fine mesh platinum gauze, was a cylindrical cone with about the dimensions of the main compartment of the cell. It fitted against the inside wall as shown in Fig. 1. Hydrogen

was bubbled constantly over this surface, the area of which was so large that at the maximum currents used for overvoltage measurements, there was negligible polarization (less than 1 mv). This easily avoided introduction of oxygen to the electrolyte by the anode reaction. Since the anode is essentially an unpolarized electrode, the potential required for formation of oxygen or oxide at this surface is never reached. The oxidation reaction is the ionization of molecular hydrogen. Similar techniques using such an unpolarized anode have been used by Hammett (2) and others.

Although the anode could have been used as a reference electrode also, a square of platinum 0.5 cm in edge was used. It served a double purpose: (A) the distance between reference electrode and cathode was reduced by about one half, which was advantageous for interrupter measurements; (B) a two-way check on the potential of the anode and cathode could be made on open circuit. The "pre-polarization" electrode was a strip of platinum placed in a remote compartment which could be isolated from the main cell by closing a stopcock.

Capacity of the electrolytic cell was about 15 ml. After the solution had been introduced into the cell, a platinum strip was repeatedly heated white hot and plunged into the solution to remove traces of organic matter which may have been present in the solution. The cell compartment was then sealed off at the top with molten polyethylene so that there was only one vent (Fig. 1). The solution was further purified by pre-electrolyzing at 5–10 ma using the anode (Fig. 1) and the pre-electrolysis cathode with the connecting stopcock opened. After pre-electrolysis this stopcock was closed. The period of pre-electrolysis varied greatly among solutions. In acid solutions an overnight treatment was usually sufficient; in neutral solutions the period varied from one to several days, and in alkaline solutions some cases required a pre-electrolysis as long as a week.

¹ Manuscript received September 25, 1953. This paper was prepared for delivery before the Chicago Meeting, May 2 to 6, 1954.

An attempt to determine the overvoltage in strongly alkaline solutions (above pH 12.1) was tried using highly purified sodium amalgam to prepare the solutions; however, it was not possible to obtain consistent results even after pre-electrolysis periods as long as several weeks and increasing the pre-electrolysis current as high as 50 ma. Data in the pH range 2.7 to 7.1 were also inconsistent; therefore these data are not reported.

Since the solution capacity of the cell was small, and pre-electrolysis caused water decomposition and increase in hydrogen ion concentration in the main compartment (because of the remote pre-electrolysis cathode), each solution was analyzed at the end of a run. Before the solution was removed from the main compartment of the cell for analysis, a saturated calomel electrode was introduced, and the open circuit potential between it and the platinum anode (H_2 electrode) was taken. This potential was converted to pH units by the relationship

$$pH = (E - 0.246)/0.059$$

where E was the measured open circuit potential between the hydrogen and saturated calomel electrodes.

The solution was agitated by a rapid stream of purified hydrogen. During overvoltage measurements the hydrogen rate of flow was increased to the point where a further increase did not alter potential readings. Temperature was maintained at $25 \pm 1^\circ C$.

Since the pseudocapacitance test for surface cleanliness was effective for acid solutions only, the following three requirements were established:

1. A zero potential (± 0.5 mv) was maintained on open circuit between the platinum cathode and both the anode and reference electrodes. This potential

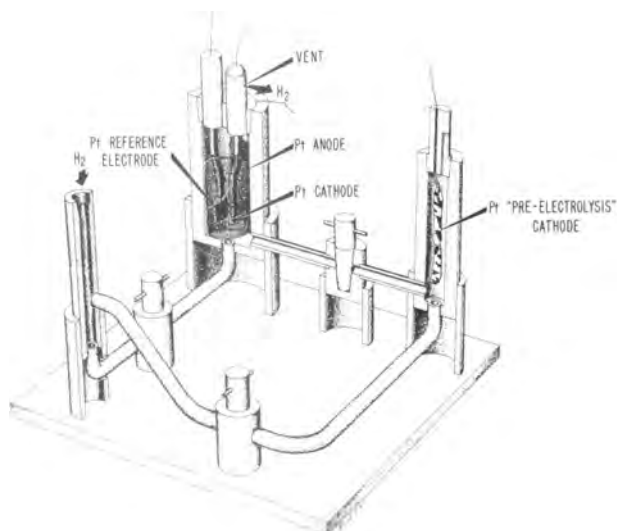


FIG. 1. Electrolytic cell

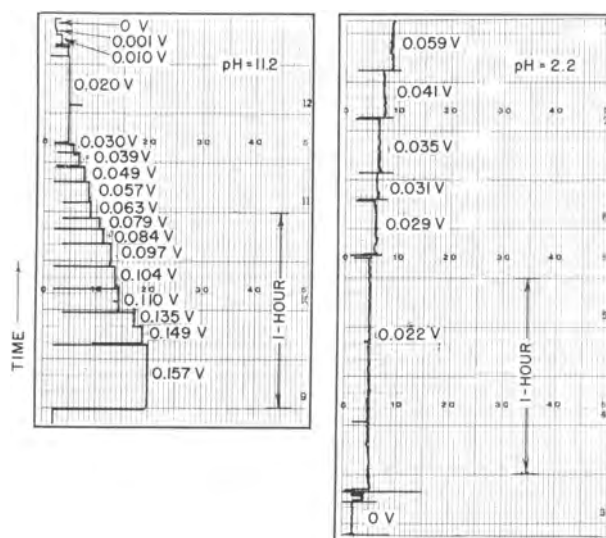


FIG. 2. Effect of time on hydrogen overvoltage measurements. (Voltages represent steady-state readings at different current densities.)

was repeatedly checked during a run. For a properly prepared solution it was found that this condition held for a day. For test purposes, this condition was actually met for periods as long as several days.

2. On application or change of current density through the cell, a constant potential between the cathode and reference electrode was quickly reached and maintained for a reasonable length of time. Fig. 2 shows two typical examples of how this condition was met in properly prepared solutions (the short time fluctuations shown for pH 2.2 were due to a noisy tube in the recorder). This constancy of potential at a given current density was actually maintained in many cases for as long as three or four hours.

3. On determination of the overvoltage-current density relationship by starting at the maximum current density and reducing the current density by steps to zero current and then increasing the current density by the same steps to the maximum current density, essentially the same overvoltage-current density values were obtained. This taking of measurements when increasing or decreasing the current density was usually done for several such cycles.

pH and Salt Effects in Acid Solutions

The overvoltage-log current density relationship for a series of acid solutions, with all but one containing sodium or ammonium sulfate, are shown in Fig. 3. These results are consistent with data given in Part I. (Individual points are not shown in Fig. 3, 4, and 5 since it was felt that there would be some confusion in following each curve; the spread of points was the same as shown in the curves in Part I).

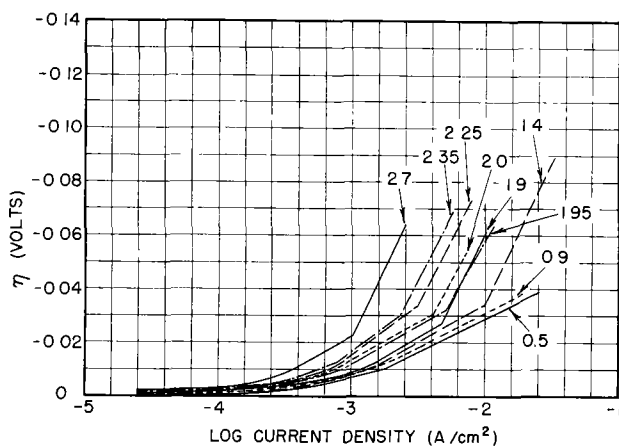


FIG. 3. Effect of pH on hydrogen overvoltage in acid solutions.

pH	Solution	b Values	
		0.029 range	0.12 range
0.5	0.205M H ₂ SO ₄	0.026	—
0.9	0.23M Na ₂ SO ₄ 0.16M H ₂ SO ₄	0.026	—
1.4	0.25M Na ₂ SO ₄ 0.035M H ₂ SO ₄	0.030	0.106
1.9	0.30M (NH ₄) ₂ SO ₄ 0.03M H ₂ SO ₄	0.030	0.113
1.95	0.27M Na ₂ SO ₄ 0.025M H ₂ SO ₄	0.030	0.092
2.0	0.265M (NH ₄) ₂ SO ₄ 0.0225M H ₂ SO ₄	0.030	0.096
2.25	0.315M Na ₂ SO ₄ 0.02M H ₂ SO ₄	0.035	0.102
2.35	0.34M Na ₂ SO ₄ 0.015M H ₂ SO ₄	0.035	0.100
2.7	0.28M (NH ₄) ₂ SO ₄ 0.005M H ₂ SO ₄	0.029	0.107

Starting from different assumptions, both de B ethune (3) and Frumkin (4) derived the following relationship on the effects of added monovalent cations and hydrogen ion concentration on the overvoltage:

$$\Delta\eta = \frac{1 - \alpha}{\alpha} \frac{RT}{F} \ln \frac{c}{[H_3O^+]} \quad (I)$$

where α is a coefficient between 0 and 1, c is the over-all concentration of electrolytes in solution, and the other symbols have their usual meanings.

Assuming $\alpha = 0.5$ at 25°C, and using activities, the following relationship results:

$$\Delta\eta = 0.059 \log \left(\frac{a_{S^\pm} + a_{H^+}}{a_{H^+}} \right) \quad (II)$$

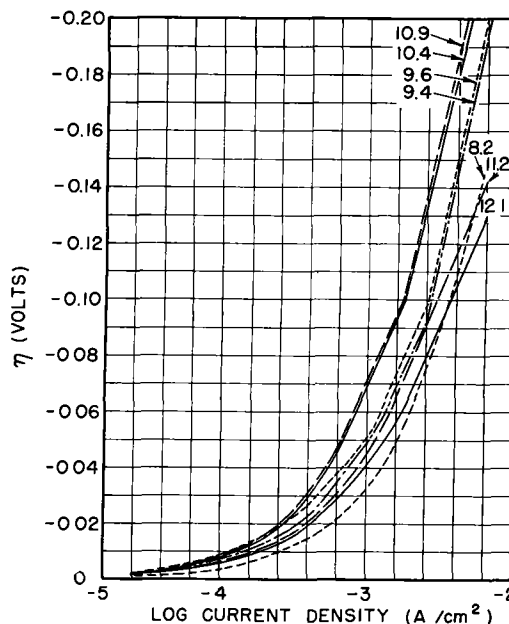


FIG. 4. Effect of pH on hydrogen overvoltage in neutral and alkaline solutions. Sodium ion series

pH	Solution	b Values	
		0.12 range	0.24 range
8.2	0.125M Na ₂ SO ₄ 0.04M Na ₂ CO ₃ 0.03M NaHCO ₃	0.138	0.220
9.4	0.19M Na ₂ CO ₃ 0.26M NaHCO ₃	0.116	0.252
9.6	0.15M Na ₂ CO ₃ 0.12M NaHCO ₃	0.126	0.252
10.4	0.23M Na ₂ CO ₃ 0.03M NaHCO ₃	0.125	0.238
10.9	0.5M Na ₂ CO ₃ 0.03M NaHCO ₃	0.127	0.235
11.2	0.345M Na ₂ SO ₄ 0.015M Na ₂ CO ₃	0.128	—
12.1	0.22M Na ₂ SO ₄ 0.05M NaOH	0.126	—

where a_{S^\pm} is the mean activity² of the added salt and a_{H^+} is the hydrogen ion activity.

² In the calculation of $\Delta\eta$, the mean activity, a_{S^\pm} , of the added salt was used. The correct quantity to use is a_+ , which is unknown. However, since in this investigation the mean activities of the added salt are about the same, and $\Delta\eta_{calc}$ includes the difference in these quantities, the effect of the formal hydrogen ion activity far outweighs that of added cation activity. If, for example, it is assumed that the added salt cation activity is ten times that of the salt anion activity, then using the relationship $a_{S^\pm} = a_+^2 a_-$, $a_+ = 2.15 a_{S^\pm}$. By substituting this value of a_+ for a_{S^\pm} in the fourth column of Table I, the values of $\Delta\eta_{calc}$ are increased by 2 mv for the lower pH values and 3 mv for the higher pH values. Such an increase improves the agreement with $\Delta\eta_{exp}$.

TABLE I. Comparisons of calculated with experimental changes in overvoltage caused by hydrogen ion and added salt activities

pH	Solution	Mean activity coefficient of added salt γ^{\pm} *	Mean activity of added salt $a_{S^{\pm}} = 1.59M \gamma^{\pm}$	$\frac{\Delta\eta = 0.059 \log \left[\frac{a_{S^{\pm}} + a_{H^+}}{a_{H^+}} \right]}$	$\Delta\eta_{calc}$ in $b = 0.12$ range pH 1.4 as base	$\Delta\eta_{exp}$ in $b = 0.12$ range pH 1.4 as base ($i = 10^{-2}$ amp/cm ²)
0.5	0.205M H ₂ SO ₄	—	—	0	—	—
0.9	0.23M Na ₂ SO ₄ 0.16M H ₂ SO ₄	0.342	0.125	0.0177	—	—
1.4	0.25M Na ₂ SO ₄ 0.035M H ₂ SO ₄	0.335	0.133	0.0376	0	0
1.9	0.30M (NH ₄) ₂ SO ₄ 0.03M H ₂ SO ₄	0.273	0.130	0.0623	0.025	0.027
1.95	0.27M Na ₂ SO ₄ 0.025M H ₂ SO ₄	0.328	0.141	0.0668	0.029	0.025
2.0	0.265M (NH ₄) ₂ SO ₄ 0.0225M H ₂ SO ₄	0.289	0.122	0.0661	0.029	0.033
2.25	0.315M Na ₂ SO ₄ 0.02M H ₂ SO ₄	0.310	0.155	0.0860	0.048	0.050
2.35	0.34M Na ₂ SO ₄ 0.015M H ₂ SO ₄	0.304	0.164	0.0930	0.055	0.057
2.7	0.28M (NH ₄) ₂ SO ₄ 0.005M H ₂ SO ₄	0.282	0.126	0.1066	0.069	0.091

* See reference (5) Sodium sulfate values at 25°C from Pearce and Eckstein; ammonium sulfate values at 0°C from Seatchard and Prentiss. It was assumed that the presence of the relatively small amounts of sulfuric acid (pH 1.4–2.7) would not materially change these values. Conversion of salt concentration from molar to molal units was not done since this correction would have negligible effect on the results. For example, the ratio (M/m) (where M = moles/liter and m = molality) would be about 1.0025 for sodium sulfate solutions.

It was concluded in Part I that the salt and pH effects would be felt where the Tafel slope $b \approx 0.12$, since the current density at which the change from slope 0.029 to slope 0.12 would be determined by hydronium ion activity in the double layer. Table I shows a reasonable agreement between the calculated change in η in the 0.12 range and the experimental results. The actual agreement between $\Delta\eta_{calc}$ and $\Delta\eta_{exp}$ would be even better except for two reasons. The first of these is explained in footnote 2. The second is that values of the mean activity coefficients for ammonium sulfate solutions are at 0° rather than 25°C, hence the correct γ^{\pm} for these solutions should be a little higher. This, in turn, would slightly increase values of $\Delta\eta_{calc}$ for the ammonium ion series.

In Part I the data indicated that in acid solutions there was no significant pH effect in the $b = 0.029$ range. This work shows that in weaker acid solutions containing added salts there is such an effect in this range; however, it is small. It amounts to 20 mv over a pH range from 0.5–2.7, or less than 10 mv per pH unit.

pH and Salt Effects in Neutral and Alkaline Solutions

Fig. 4 and 5 show the data for η vs. log current density curves in neutral and alkaline solutions containing sodium and ammonium ions, respectively. Whereas in the case of acid solutions there is a direct relationship between pH, salt effect, and overvoltage (for either sodium or ammonium ion addition), in neutral and alkaline solutions there is a complex pH and salt effect which is dependent on whether the added cation is sodium or ammonium. Another complicating factor in these solutions is that in the sodium ion series from pH 8.2–10.9 and in the ammonium ion series at pH 7.1 there is a change in b from 0.12 to 0.24. At pH values above those indicated there is no such transition in the investigated current density range.

The range at low current density in which there is not a linear relation between overvoltage and log current density consists of two parts. In the first section at the lowest current densities there is a linear relation between overvoltage and current density. (In acid solutions this linear relationship holds to the overvoltage value at which the $b = 0.029$ slope begins.) This straight line portion holds

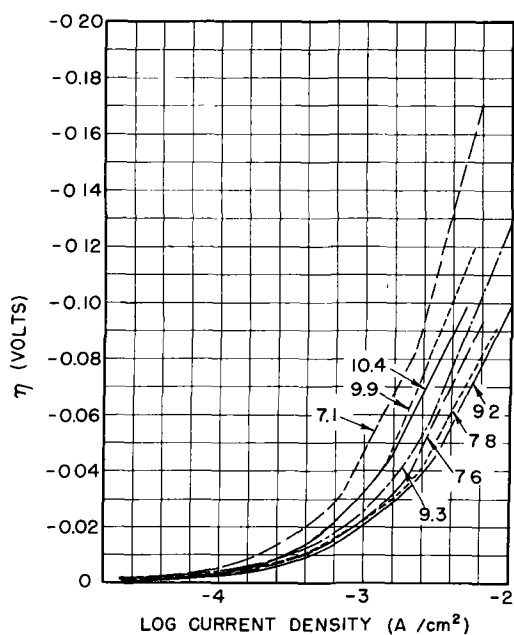


FIG. 5. Effect of pH on hydrogen overvoltage in neutral and alkaline solutions. Ammonium ion series.

pH	Solution	b Values	
		0.12 range	0.24 range
7.1	0.395M $(NH_4)_2SO_4$ 0.01M NH_4HCO_3	0.107	0.20
7.6	0.325M $(NH_4)_2SO_4$ 0.01M NH_4HCO_3	0.114	—
7.8	0.31M $(NH_4)_2SO_4$ 0.02M NH_4OH	0.102	—
9.2	0.30M $(NH_4)_2SO_4$ 0.24M NH_4OH	0.109	—
9.3	0.3M $(NH_4)_2SO_4$ 0.42M NH_4OH	0.128	—
9.9	0.7M NH_4OH 0.1M $(NH_4)_2CO_3$	0.132	—
10.4	0.75M NH_4OH	0.114	—

for about $\frac{1}{2}$ – $\frac{1}{3}$ of this overvoltage region. The second portion of this region, η , is not linear with respect to either current density or log current density.

The relationship between pH and overvoltage for all solutions can be seen in Fig. 6. The higher overvoltage values for the sodium ion series can be easily explained on the basis of the initial reversible reactions which take place at low current densities. This is discussed below.

DISCUSSION

Much information concerning the mechanism of hydrogen overvoltage on smooth platinum can be obtained from a study of overvoltage-current density relationships in the range in which overvoltage is

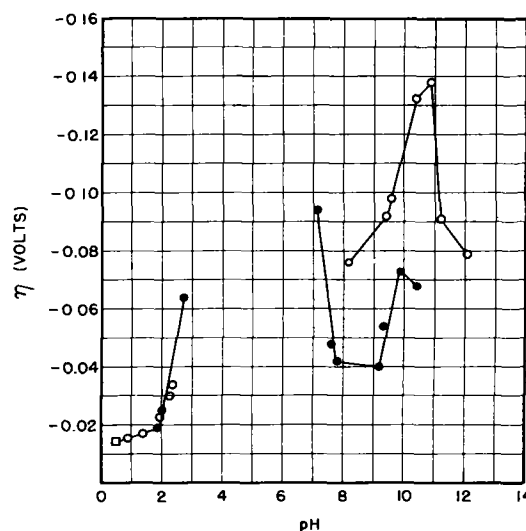


FIG. 6. Relationship between hydrogen overvoltage and pH . $i = 0.0025$ amp/cm². □, no added salt; ○, Na^+ ; ●, NH_4^+ .

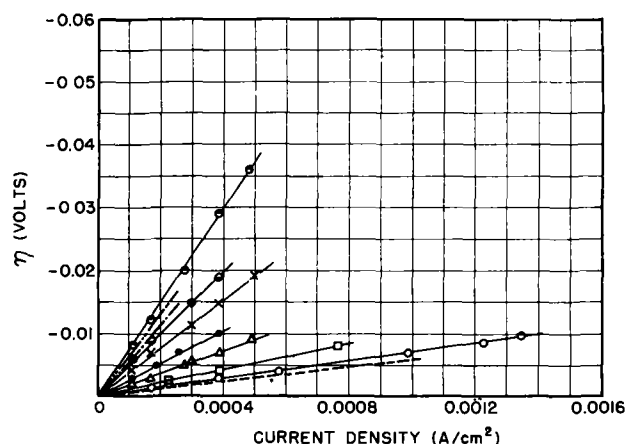


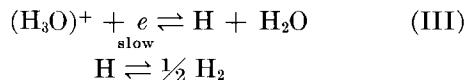
FIG. 7. Hydrogen overvoltage in the range in which η is linearly dependent on current density. - - - - -, Hammett (2); Dolin, Ershler, and Frumkin (6) in NH_4Cl , - - - - -, Dolin, Ershler, and Frumkin in 1N $NaOH$ (6); - - - - -, Dolin, Ershler, and Frumkin in 1N N_2S_4 + 0.05N $NaOH$ (6). ○, $pH = 0.5$; □, $pH = 1.9$ (NH_4^+); △, $pH = 1.95$ (Na^+); ●, $pH = 7.6$ (NH_4^+); ×, $pH = 8.2$ (Na^+); ⊙, $pH = 10.4$ (Na^+); ⊖, $pH = 12.1$ (Na^+).

linearly dependent on current density. This occurs at low current densities, and it is generally believed that this linear range is the net result of the reversible reaction at the electrode surface.

Fig. 7 shows some typical curves in this linear range. Also included are several curves from a study by Dolin, Ershler, and Frumkin (6) who verified the results of Hammett (2) for acid solutions. They pointed out that in this linear range i/η (where i is the current density) is characteristic of the rate of the over-all electrode process.

The plot of i/η vs. pH (Fig. 8) in the linear range shows that in acid solutions where the principal

hydrogen-producing reaction is



that,

$$(i/\eta)_{p\text{H}0.5-2.7} = 0.165 - 0.052 \text{ pH}. \quad \text{(IV)}$$

This relationship is unaffected by the choice of either sodium or ammonium ion as the added salt cation.

In neutral and alkaline solutions the change in the rate of the over-all reaction where η vs. i is linear can be considered as virtually independent of $p\text{H}$. This is expected since the hydronium ion concentration is then so low that its rate of reduction is negligible. Here the principal hydrogen-producing reaction would probably be

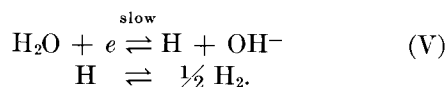


Fig. 8 shows that in the presence of sodium ion the relative rate of the above over-all reaction in neutral and alkaline solution is about 0.016, whereas in the presence of ammonium ion the value is about 0.033 or roughly twice the rate found for sodium ion solutions. This can be explained on the basis of retardation of the reverse reaction shown in (V). With ammonium ion, weakly ionized ammonium hydroxide is formed, reducing hydroxyl ion activity and thereby causing an increase in the over-all rate of hydrogen production for a given value of overvoltage. Sodium ion does not alter the OH^- activity.

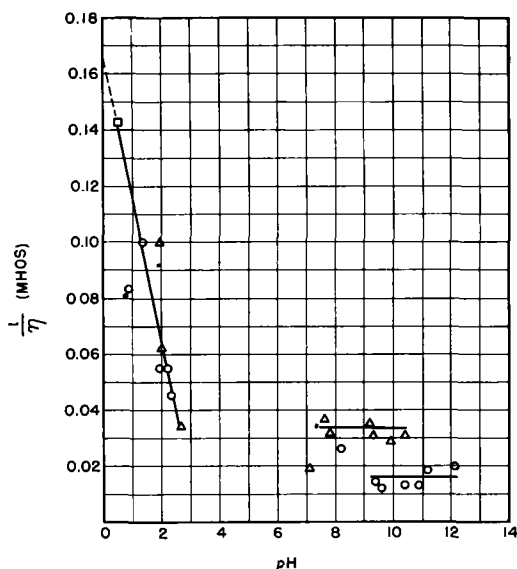


Fig. 8 Effect of $p\text{H}$ on the rate of the over-all hydrogen producing reaction in the range in which η is linearly dependent on current density. \square , no added salt, \circ , Na^+ ; Δ , NH_4^+ .

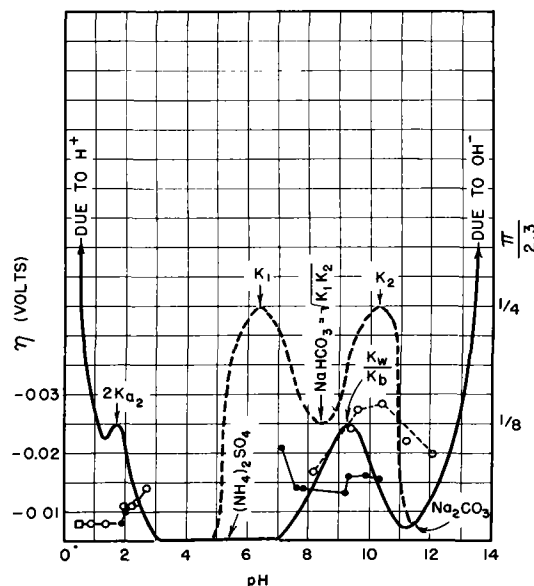


Fig. 9. Relationships between buffer capacity, $p\text{H}$, and hydrogen overvoltage. \bullet , η vs. $p\text{H}$, NH_4^+ , \circ , η vs. $p\text{H}$, Na^+ , \square , η vs. $p\text{H}$, H^+ only; in all three of which $i = 0.00032$ amp/cm²; —, π vs. $p\text{H}$, $\text{H}_2\text{SO}_4/\text{NH}_4\text{OH}$ system [see Reference (7), pp. 237 and 249]; ---, π vs. $p\text{H}$, $\text{H}_2\text{CO}_3/\text{NaOH}$ system [see Reference (7), pp. 237 and 249]. K_w = ion-product constant of water = 10^{-14} ; K_b = dissociation constant $\text{NH}_4\text{OH} = 1.8 \times 10^{-5}$; K_1 = 1st dissociation constant $\text{H}_2\text{CO}_3 = 4 \times 10^{-7}$; K_2 = 2nd dissociation constant $\text{H}_2\text{CO}_3 = 5 \times 10^{-11}$; K_{a2} = 2nd dissociation constant $\text{H}_2\text{SO}_4 = 10^{-2}$, $\pi/2.3$ is in terms of unit concentration.

In Part I it was hypothesized that there were two parallel hydrogen-producing reactions which could take place at all current densities on a platinum surface. These are given as mechanism (III) and (V) above. In acid solutions at low current densities the concentration of hydronium ions at the interface is high enough to maintain the current without discharge of water; therefore, mechanism (III) would be rate-controlling. When the current density is increased so that depletion of hydronium ions reduces the over-all rate of (III), the over-all rate of (V) becomes controlling. The overvoltage at which this shift in rate-controlling mechanisms takes place can be determined experimentally from a shift in Tafel slope from 0.029 to 0.12.

Data in Fig. 8 confirm this hypothesis since they show that at $a_{\text{H}^+} = 10^{-2.7}$, the rate of mechanism (III) is of the same magnitude as mechanism (V). Fig. 3 shows that the change in Tafel slope from 0.029 to 0.12 takes place at metal-solution interface hydrogen ion activities of 10^{-2} – 10^{-3} . It is also significant that the overvoltage at which this break in the curve occurs is lower for solutions containing ammonium ion than for those of about the same $p\text{H}$ containing sodium ion. Another interesting conclusion from Fig. 8 is that the reaction rate of the over-all reaction in the most acid solution is only

5-10 times higher than the rates in neutral and alkaline solutions.

The difference in the comparative over-all reaction rates of solutions containing ammonium and sodium ions is also reflected in comparative overvoltage values at higher current densities. This is borne out by Fig. 6, which shows that in neutral and alkaline solutions at constant current density and at the same pH, overvoltage values for the sodium ion solutions do run considerably higher than for ammonium ion solutions.

The Tafel a is determined in the overvoltage range before b reaches 0.12. This displacement in overvoltage is then fixed by activities of the reactants at the cathode surface at low current densities. For the reversible hydrogen electrode the potential at low current densities is determined by the hydrogen ion activity at the electrode surface. For this reversible range the Nernst relation between pH and the electrode potential holds.

Use of the concept of buffer capacity can be of some help in understanding the effects of pH on overvoltage. The buffer capacity of a solution with respect to a particular solute is discussed in detail by Ricci (7) and is defined by him as the change in concentration of that solute required for a unit change in pH of the solution. Or,

$$\pi = \left| \frac{db}{d \text{pH}} \right|$$

where π is the buffer capacity and b is the concentration of added acid or base.

The buffer capacity is equal to the reciprocal of the slope of the acid-base titration curve. For example, at an active cathode hydroxyl ion is formed at a rate dependent on current density. At very low current densities the effective activity of the hydroxyl ion, which is formed at the solution interface, depends on the buffer capacity of the solution. The measured overvoltage is in turn a function of the effective change in hydroxyl ion activity from that of a cathode-solution interface at zero current.

In this investigation, solutions of the ammonium and sodium ion series were used. Comparative relationships between buffer capacity, π , and pH for these two systems, and plots of overvoltage vs. pH are shown in Fig. 9. These curves represent a low current density (0.00032 amp/cm²) so that the pH at the active electrode surface would not be far removed from open circuit values. In this way a

fair comparison between pH, η , and π can be made. The data show that an inverse relationship between buffer capacity and overvoltage holds for acid and neutral solutions, whereas a direct relationship exists between these factors in alkaline solutions.

In acid solutions, at a given current density and at a given concentration of added ammonium or sodium ion, three cases are possible. In the first two cases there is either a linear η vs. i or η vs. $\log i$ relationship with $b = 0.029$. The first case is for solutions with high buffer capacity where $\Delta\eta$ is independent of pH; the second case is for solutions with no buffer capacity, where $\Delta\eta$ is dependent on pH with $\Delta\eta < 0.059$ pH. The third case occurs for $b = 0.12$, where $\Delta\eta = 0.059$ pH. Here, η is independent of buffer capacity because the current density at which there is a change to the 0.12 slope is relatively high, and any initial buffer capacity at the interface of the electrode and solution is depleted.

In the neutral and alkaline range when there is no buffer capacity, $\Delta\eta$ is dependent on pH. If there is a high buffer capacity there evidently will be only a slight dependence of $\Delta\eta$ on pH.

ACKNOWLEDGMENTS

The author is indebted to Drs. J. C. White, J. J. Lander, and H. W. Salzberg of the Chemistry Division, Naval Research Laboratory. He is also grateful to Mr. E. Boone of the Plastics Laboratory for construction of the Teflon cell used in this study, to D. D. Williams of the Physical and Inorganic Branch for the preparation of high purity sodium amalgam, and to T. F. Ruffy of Graphic Arts for illustrations.

Any discussion of this paper will appear in a Discussion Section to be published in the June 1955 issue of the JOURNAL.

REFERENCES

1. S. SCHULDINER, *This Journal*, **99**, 488 (1952).
2. L. P. HAMMETT, *J. Am. Chem. Soc.*, **46**, 7 (1924).
3. A. J. DE BÉTHUNE, *ibid.*, **71**, 1556 (1949).
4. A. N. FRUMKIN, *Z. Fiz. Khim.*, *U.S.S.R.*, **24**, 244 (1950).
5. J. N. PEARCE AND H. C. ECKSTEIN, *J. Am. Chem. Soc.*, **59**, 2689 (1937); G. SCATCHARD AND S. S. PRENTISS, *ibid.*, **54**, 2696 (1932).
6. P. DOLIN, B. ERSHLER, AND A. FRUMKIN, *Acta Physicochim. U.S.S.R.*, **13**, 782 (1940).
7. J. E. RICCI, "Hydrogen Ion Concentration," Princeton University Press, Princeton (1952).

Corrosion Inhibitors and Polarographic Maxima¹

HARRY C. GATOS

*Engineering Research Laboratory, Engineering Department, E. I. du Pont de Nemours and Company, Inc.,
Wilmington, Delaware*

ABSTRACT

Electrical polarization phenomena occurring in corrosion and polarographic processes are compared, and certain similarities are pointed out. On this basis, results of polarographic studies of a number of corrosion inhibitors are presented, particularly for the iron-sulfuric acid system. It is found that these inhibitors considerably suppress one or more of the oxygen, lead, or nickel polarographic maxima. The maxima-suppressing effectiveness of compounds known to inhibit corrosion by adsorption is a function of concentration resembling gas adsorption isotherms. Furthermore, certain inhibitors which function by either anodic or cathodic polarization are also effective in suppressing either anodic or cathodic maxima. Some general inhibitors are general maxima suppressors as well.

Polarography is suggested as a valuable tool in corrosion inhibitor studies.

INTRODUCTION

Chemical and physical changes responsible for metallic corrosion in liquid media take place mostly on metal surfaces and at metal-liquid interfaces. A thorough understanding of the function of metal surfaces and metal-liquid interfaces, so critical in corrosion, is limited by the facts that (a) metal surfaces are very difficult to obtain and maintain chemically pure and physically reproducible, and (b) metal-liquid interfaces, due to their extreme thinness and intricate structure, are beyond the sensitivity range of conventional experimental techniques.

Among metals, mercury is unique in that it can be obtained in highly pure chemical form, and its surface-physical characteristics can be easily reproduced, mainly because of its liquid state. These outstanding characteristics of mercury have been primarily responsible for the development of polarography.

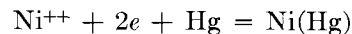
Although mercury as a material of construction is of no practical significance, it has been extensively used in obtaining information about metal-liquid interface phenomena, which have been of importance in understanding metal-liquid interfaces in general.

It is the purpose of this paper to point out how some characteristic phenomena occurring at the interface of a mercury microelectrode in contact with electrolyte solutions can be employed for corrosion inhibitor studies.

Polarographic Maxima

By applying an increasing potential between a dropping mercury microelectrode (cathode) and a

reference electrode (nonpolarizable anode) in the presence of electroreducible materials, a typical "polarographic wave" (1) is obtained as in Fig. 1 (curve IV).² In the presence of NiCl₂, the cathode reaction is:



The limiting current is proportional to the concentration of the reacting substance, a relationship which is employed in quantitative analysis.

The potential corresponding to one-half the limiting current value is called the "half-wave potential." In contrast to the "decomposition potential," the half-wave potential is a well definable quantity, and it is usually independent of concentration of the reacting material. Hence, it is employed for qualitative analysis.

The dropping mercury electrode is under virtually complete concentration polarization when the limiting current is reached. Thus, the amount of current flowing through the cell is primarily controlled by the diffusion rate of the reacting material to the polarized electrode (diffusion current) and within certain limits is independent of the applied emf. The electrical migration of the reducible ions is minimized by employing a nonreducible electrolyte (supporting electrolyte) such as KCl in the electrolysis solution. The supporting electrolyte is present at considerably higher concentrations than the reducible ions, and thus the transference number of the latter is reduced practically to zero. Under these conditions the limiting current becomes entirely a diffusion current.

The current-voltage curves with the dropping mercury electrode quite often exhibit more or less

¹ Manuscript received January 8, 1954. This paper was prepared for delivery before the Boston Meeting, October 3 to 7, 1954.

² Methyl amine (see figure caption) does not participate in the electrode reaction. Its role is discussed later.

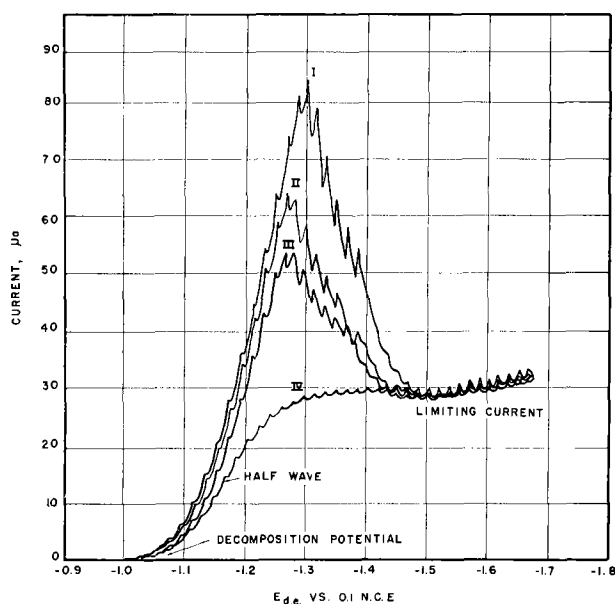


FIG. 1. Polarograms of NiCl_2 in 0.1M KCl . $E_{d.e.}$ —potential of dropping electrode. Curve I—Ni maximum; curve II—maximum partially suppressed 0.03% methylamine; curve III—maximum further suppressed with 0.06% methylamine; curve IV—Ni “polarographic wave,” 0.30% methylamine.

pronounced current maxima (polarographic maxima) before the limiting value for the current is reached (Fig. 1, curve I). These maxima are fairly reproducible, and their shapes are independent of the direction in which the applied voltage is changed. They interfere with determination of the half-wave potential and the limiting current. They are suppressed, however, in the presence of certain substances, e.g., methylamine, which usually do not affect the limiting current.

The origin and suppression of polarographic maxima have been the subject of extensive investigations (2). It has been shown that the dropping mercury electrode remains depolarized until the peak of the maximum is reached. Beyond this point, concentration polarization sets in and the current reaches its limiting value.

According to Heyrovsky (3), the maxima can be distinguished as positive or negative depending upon the charge of the mercury with respect to the solution at the potential at which the maxima occur. Mercury, when immersed in solutions of capillary-inactive electrolytes, such as potassium chloride, is positively charged. If a cathodic potential is applied to mercury, its charge decreases as the cathodic potential increases to about -0.52 volt vs. the saturated calomel electrode. At this point (electrocapillary zero) mercury is electrically uncharged with respect to the solution, as indicated by its maximum surface tension (Fig. 2). At more cathodic potentials mercury becomes negatively charged, and its surface

tension decreases again. Positive maxima appear at potentials below, and the negative above, -0.52 volt.

A considerable amount of work has been reported in connection with the suppression of polarographic maxima (4), and a number of mechanisms have been proposed. Whatever the exact mechanism may be, it appears that, in the presence of the maxima suppressors, the microelectrode becomes polarized at emf values at which it is ordinarily depolarized, as indicated by the appearance of polarographic maxima.

Corrosion and Polarographic Processes

It is widely accepted that metallic corrosion in liquid media is under electrochemical control with local electrolytic cells operating during the corrosion process. Anodic, cathodic, or mixed polarization of local cells leads to a decrease or elimination of corrosion, depending on the degree of polarization (5, 6). On the other hand, depolarization of local cells results in promotion of corrosion. It is thus apparent that polarization-depolarization phenomena on metal surfaces in contact with liquids are of paramount importance in corrosion processes. It is believed that a number of substances (in particular organic compounds) inhibit metallic corrosion by adsorbing on the metal surfaces and thus inducing polarization of the active local galvanic cells (7–9).

As mentioned previously, polarography is based on electrode polarization phenomena. Complete polarization of the dropping mercury microelectrode is necessary for the appearance of typical polarographic waves (Fig. 1, curve IV). Lack of complete polarization of the same electrode at certain emf values results in the appearance of polarographic maxima. Substances suppressing these maxima are

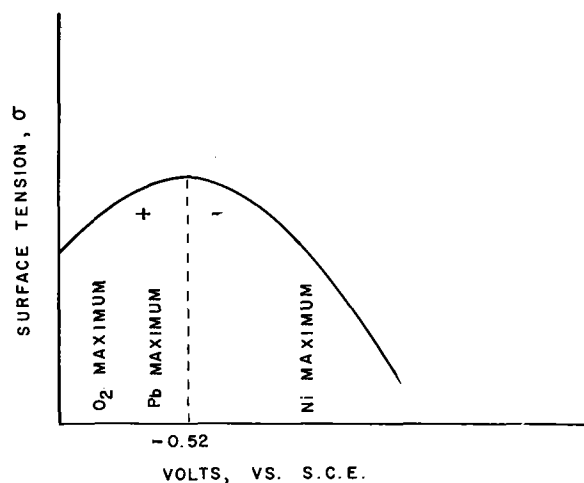


FIG. 2. Electrocapillary curve

believed to polarize microelectrodes at the above emf values. Most probably, this polarization is brought about mainly by adsorption of maxima suppressors on the metal surface (10).

Thus, it becomes apparent that both corrosion and polarographic processes are electrical-polarization dependent. Electrical polarization, therefore, results in corrosion protection and in typical polarographic waves. Lack of polarization usually promotes corrosion and causes polarographic maxima.

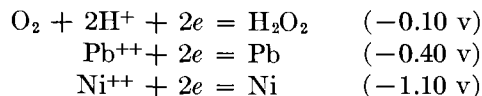
At this point, a comparison between polarographic maxima suppressors and corrosion inhibitors becomes of considerable interest. To begin with, a number of polarographic maxima suppressors (11), e.g., organic sulfur derivatives, amines, gelatine, etc., are also well known for their corrosion inhibiting properties. Furthermore, capillary active anions and negative colloids in general preferentially suppress maxima appearing on the positive side of the electrocapillary zero (positive maxima), whereas capillary-active cations and positive colloids are effective with the negative maxima. High molecular weight substances like gelatine suppress maxima of various metal ions on both sides of the electrocapillary zero. This behavior of maxima suppressors appears comparable to that of corrosion inhibitors, since corrosion inhibitors also, according to their nature, are known to act preferentially on anodic or cathodic areas (anodic and cathodic inhibitors, respectively) as well as indiscriminately over the metal surfaces (general inhibitors) (12).

On the basis of the above comparison between polarographic maxima suppressors and corrosion inhibitors, it was felt worth while to investigate their common characteristics and thus better understand similarities between phenomena occurring in polarographic and in corrosion processes. The present broad knowledge of polarographic processes could prove quite useful to corrosion in general and to corrosion inhibitors in particular.

EXPERIMENTAL

In order to investigate any existing similarities between corrosion inhibition and polarographic processes, the behavior of a number of substances toward various polarographic maxima was studied over a large range of emf values. These substances were reported as possessing corrosion-inhibiting properties. Preference was given to inhibitors for which comparative data in specific environments were available.

Polarographic maxima.—Three polarographic maxima were chosen for this investigation corresponding to the following reduction reactions. (The half-wave potential, referred to a saturated calomel electrode, for each reduction is shown in parentheses.)



All maxima were obtained in 0.1 molar KCl supporting electrolyte containing the reducible ions. A dropping mercury microelectrode served as the cathode.

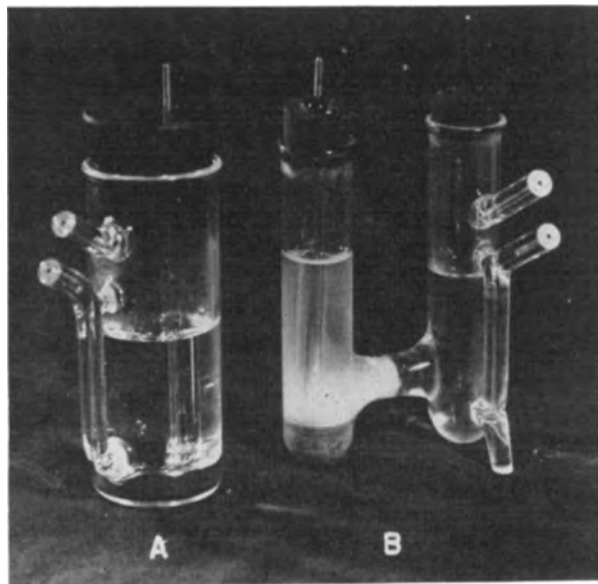


FIG. 3. Electrolytic cells employed with the dropping mercury electrode.

The oxygen maximum was obtained by saturating the 0.1M KCl solution in the electrolytic cell with oxygen immediately before the polarographic run. The lead maximum was obtained from a $4.05 \times 10^{-3}\text{M}$ solution of $\text{Pb}(\text{NO}_3)_2$ in 0.1M KCl. Immediately before each run, nitrogen was bubbled through this solution for about 15 min to remove any oxygen present in the solution. Traces of oxygen suppress the lead as well as the nickel maximum. The nickel maximum was obtained from a $3.22 \times 10^{-3}\text{M}$ NiCl_2 solution under conditions described for the lead maximum.

Electrolytic cell.—A single-compartment electrolytic cell was used with a pool of mercury as the nonpolarizable electrode (Fig. 3A). A gas inlet and outlet allowed bubbling of gases through the solution, thus maintaining the desirable gas atmosphere over the solution during polarographic runs. The cell was kept at constant temperature (25°C) by means of a constant temperature bath.

Polarograph.—Throughout this investigation an automatic recording polarograph³ was used. Characteristics of the dropping mercury electrode, e.g.,

³ "Electro-Chemograph, Type E, Leeds and Northrup Philadelphia, Pa.

dropping time (5.55 sec/drop at zero applied potential) and mercury flow rate (1.240 mg/sec at zero applied potential) were maintained constant through the investigation.

Inhibitors for Steel in Sulfuric Acid

A number of inhibitors for steel in sulfuric acid (13) were polarographically tested with the oxygen, lead, and nickel polarographic maxima. For each test, one of the three maxima was obtained by using 15 cc of solution containing the corresponding reducible substance as described previously (blank run). Thereafter, 0.2 cc of a 0.2% aqueous solution of inhibitor was added to the electrolytic cell to determine its effect upon the maximum. The final arbitrarily chosen inhibitor concentration was approximately 27 ppm. In cases of slightly soluble inhibitors, small amounts were added directly to the cell. It was found necessary to run a blank with each test in order to make sure that the maximum was not affected by accidental causes prior to addition of the inhibitors.

Effectiveness of various inhibitors in suppressing polarographic maxima was expressed as "per cent suppression" and was calculated as follows:

$$\begin{aligned} \text{\% suppression} &= \frac{(M_1 - i_d) - (M_2 - i_d)}{(M_1 - i_d)} \times 100 \\ &= \frac{M_1 - M_2}{M_1 - i_d} \times 100 \end{aligned}$$

TABLE I. *Inhibitors for steel in sulfuric acid in the approximate order of decreasing effectiveness**

Inhibitor	% Suppression of maxima		
	O ₂	Pb	Ni
1. Butyl disulfide	100	100	7
2. Phenyl thiourea	100	100	23
3. Thiourea	100	53	22
4. Butyl mercaptan	100	100	52
5. Triamylamine	100	100	100
6. Aldol	100	100	100
7. Phenyl morpholine	100	100	100
8. <i>p</i> -Tolualdehyde	94	100	38
9. Phorone	89	100	100
10. Diamylamine	100	100	100
11. Dicyclohexylamine	100	100	100
12. Ethanol morpholine	8	26	18
13. α -Naphthylamine	100	100	100
14. Phenyl hydrazine	94	100	100
15. Benzaldehyde	64	100	32
16. Morpholine	29	37	66
17. Cyclohexanone	66	100	100
18. Dimethylamine	37	100	100
19. Diethylaniline	65	100	21
20. Acridine	100	100	100
21. Ethylenediamine	4	34	100
22. Dimethylaniline	100	100	21
23. Pyridine	41	60	35

* The tests (13) were run in 4.9% H₂SO₄ for 48 hr at 25°C.

TABLE II. *Substances found less effective as inhibitors compared with those in Table I under similar conditions**

Inhibitor	% Suppression of maxima		
	O ₂	Pb	Ni
Diethylamine	0	16	35
Butylamine	5	49	51
<i>n</i> -Amyl alcohol	12	18	15
Ethylamine	12	34	49
Isopropylamine	13	2	30
Methylamine	20	13	24
Aniline	66	100	13

* See reference (13).

where M_1 = polarographic maxima in μ a, M_2 = polarographic maxima in μ a after addition of inhibitor, and i_d = diffusion current.

As a rule, diffusion current was not affected by addition of inhibitors at the concentration mentioned above. When it was decreased, the corresponding maximum was totally suppressed. Results obtained with the three maxima are shown in Table I. It can be seen that practically all inhibitors tested suppress considerably one or more of the employed polarographic maxima. Of 23 inhibitors, 18 suppress the lead maximum 100%. The oxygen maximum is suppressed either to the same or lesser extent than the lead maximum, except for thiourea. Since the lead maximum is less anodic than the oxygen, it is perhaps more effectively suppressed under conditions favoring anodic polarization.

In the case of the nickel maximum, which appears at the cathodic side of the electrocapillary zero, it is of interest to notice that the suppressing effectiveness of a large number of inhibitors changes considerably, e.g., it decreases for sulfur derivatives. In other cases it increases. This is consistent with the fact that certain substances are specific in induc-

TABLE III. *Inhibitors for aluminum**

Inhibitor	% Suppression of maxima	
	O ₂	Ni
α -Naphthoquinoline	100	100
Acridine	100	100
Thiourea	100	22
Iodine	80	14
Pyridine	41	35
Dimethylamine	37	100
Nicotinic acid	20	60
Methylamine	20	24
Hexamethylenetetramine	18	20
Sodium chromate	8	100
Phenol formaldehyde	7	86
Butylamine	5	51
Ethylamine	12	49
Diethylamine	0	35

* See reference (14).

TABLE IV. *Inhibitors for copper*

Inhibitor	% Suppression of maxima	
	O ₂	Ni
Benzanilide.....	100	100
Butyl mercaptan.....	100	52
Rosin.....	100	71
Aniline.....	66	13
Sodium benzoate.....	50	21
Lauryl mercaptan.....	49	9
Morpholine.....	29	66
Sodium nitrite.....	11	13
Potassium dichromate.....	9	100
Sodium silicate.....	6	100
Ethylenediamine.....	4	100

ing polarization at either anodic or cathodic metal surfaces.

Some inhibitors reported to be less effective than those of Table I, under similar experimental conditions, were also observed, as a whole, to be relatively less effective maxima suppressors (Table II).

Other inhibitors.—A group of inhibitors for aluminum (14) were tested for their effectiveness in suppressing oxygen and nickel polarographic maxima. These experiments were carried out under conditions identical to those described for iron inhibitors. Results are shown in Table III. It can be seen that all inhibitors tested suppressed one or both maxima by at least 20%. Here again the suppressing effectiveness of some of these inhibitors changes sharply from the oxygen to the nickel maximum.

Some compounds relatively ineffective in inhibiting corrosion of iron and at the same time not very effective maxima suppressors (Table II) are, nevertheless, listed among inhibitors for aluminum. Polarographic conditions employed in testing inhibitors for either metal were identical, and no attempt was made at this point to characterize polarographic behavior of inhibitors under varying conditions with reference to specific corrosion systems.

A number of representative inhibitors for copper selected from the literature were tested like the inhibitors for iron and aluminum. Results for oxygen and nickel maxima are shown in Table IV. In addition to the general maxima-suppressing ability of these inhibitors, it is of interest to notice that some of those least effective in suppressing the oxygen maximum are most effective in suppressing the nickel maximum.

Effect of Noninhibitors on Polarographic Maxima

It is difficult to find compounds which are not corrosion inhibitors to some extent under some experimental conditions. However, a few substances were selected which are not commonly reported as

TABLE V. *Effect of noninhibitors on polarographic maxima*

Name of substance	% Suppression of maxima		
	O ₂	Pb	Ni
Methyl alcohol.....	5	18	27
Ethyl alcohol.....	0	15	30
Propyl alcohol.....	6	13	13
Butyl alcohol.....	7	8	10
Isoamyl alcohol.....	1	13	13
<i>tert</i> -Amyl alcohol.....	6	12	8
Ethyl ether.....	0	13	10
Propyl ether.....	14	8	7
Cane sugar.....	0	11	16
Formic acid.....	20	27	67
Acetic acid.....	0	6	44
Propionic acid.....	0	5	43
Butyric acid.....	0	7	33

effective corrosion inhibitors. Their influence on the polarographic maxima is shown in Table V. It is apparent that these compounds are as a whole considerably poorer maxima suppressors than those reported in Tables I, III, and IV.

From results reported to this point it appears that in general the polarizing ability of corrosion inhibitors can be demonstrated polarographically. The conclusiveness of these findings is limited by the fact that inhibitors were tested at a single concentration. Furthermore, corrosion test data for all these inhibitors under identical conditions are not available.

Quantitative Approach

On the basis of the above qualitative experiments, it was felt worth while to extend these studies on a quantitative basis in order to shed some light on common characteristics of polarographic and corrosion inhibition processes.

In the following experiments, the single-compartment polarizing cell was replaced with an H-type cell shown in Fig. 3B. A 0.1*N* calomel electrode was employed as the reference electrode instead of the mercury pool. Electrical contact between the calomel electrode and electrolysis compartment was established through a fritted glass disk and an agar plug. The main advantage of the H-type cell over the single compartment cell is that the potential of the calomel reference electrode is not susceptible to variations.

Effect of pH on Polarographic Maxima

Determining the effect of pH on polarographic maxima was considered essential since pH of solutions from which the maxima were obtained could change to a different extent by addition of various inhibitors. For this purpose, solutions containing the reducible substances were prepared over a wide pH range. Since conventional buffered solutions in

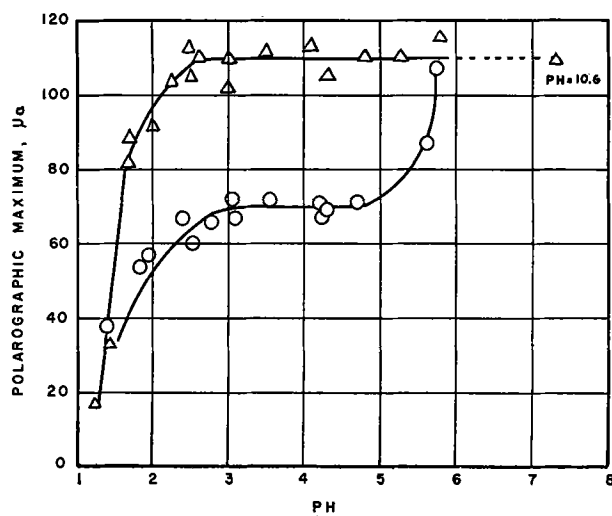


FIG. 4. Effect of pH upon the oxygen and nickel maximum. Δ —oxygen maximum; limiting current $17 \mu a$; \circ —nickel maximum; limiting current $25 \mu a$.

general affect polarographic maxima, small amounts of hydrochloric acid and potassium hydroxide solution were employed for pH adjustments. Polarographic maxima were then obtained from these solutions. The pH was measured with a Beckman pH meter. Results obtained for the oxygen and nickel maxima are shown in Fig. 4. Values of the maxima include the corresponding limiting current which remained constant over the employed pH range. It is apparent that the oxygen maximum is completely eliminated at about pH 1; it increases with increasing pH up to pH 2.5, and it remains constant for higher pH values. The nickel maximum is also considerably suppressed at pH 1, and it increases with increasing pH. It remains constant, however, only for pH values of 3–5 and increases rapidly beyond this range.

Suppression of maxima in high H^+ concentrations indicates that the microcathode becomes polarized at the potentials of the maxima. As mentioned previously, the microcathode is not polarized when the maxima appear. This polarization is perhaps brought about by adsorption of H^+ on the mercury surface. In this respect, it is of interest to notice that the oxygen maximum occurring at an emf value at which the dropping electrode is positively charged with respect to the solution is somewhat less affected by H^+ concentration than the negative nickel maximum. Similar H^+ adsorption probably occurs at cathodes of metals corroding in strong acids. This adsorption of H^+ on cathodic areas very likely hinders corrosion inhibitors from acting upon local cathodes. Thus, anodic inhibitors would be expected to act more effectively than cathodic ones in low pH solutions, a fact widely accepted.

Amines as Corrosion Inhibitors and Polarographic Maxima Suppressors

A number of amines, both aliphatic and aromatic, were employed for a basic comparison of polarization phenomena occurring in polarographic and corrosion inhibition processes. Amines chosen have been extensively studied by Mann and his coworkers (7–9) as corrosion inhibitors for mild steel in $1N H_2SO_4$ at room temperature. Among the various maxima, that of nickel was found most responsive and, in general, more suitable for the study of the above amines.

Aliphatic amines.—The following aliphatic amines were studied in connection with maxima suppression: methyl-, ethyl-, propyl-, butyl-, and amylamine. According to Mann (Fig. 5), the effectiveness of these amines in inhibiting corrosion of mild steel in $1N H_2O_4$ at room temperature ($25^\circ C$) increases with increasing molecular weight for any given amine concentration expressed in per cent nitrogen. The effectiveness of each amine increases with its concentration and eventually levels off. Effectiveness at the leveling-off point is again higher, the higher the molecular weight of the amine. Since the covering power and the ability of normal aliphatic amines to adsorb on metal surfaces increase with increasing chain length, these corrosion inhibition results are in agreement with the widely accepted theory that amines inhibit corrosion by adsorbing on metals.

Effectiveness of the above amines in suppressing the nickel polarographic maximum was studied as a function of concentration. The nickel maximum was obtained from $6.25 \times 10^{-3}M NiCl_2$ solution in $0.1M KCl$ supporting electrolyte. A blank run

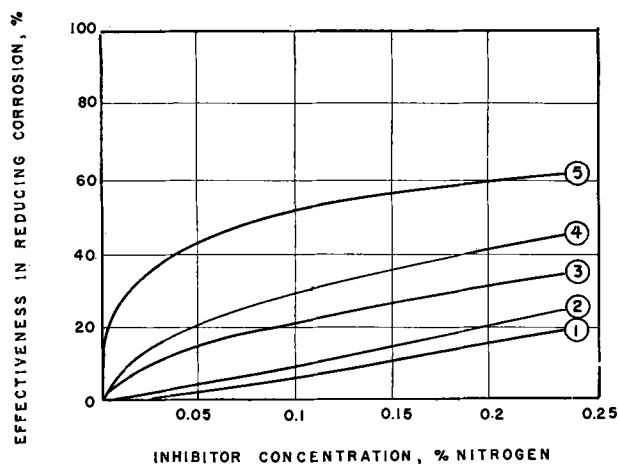


FIG. 5. Inhibition by aliphatic amines of mild steel corrosion in $1N H_2SO_4$ at $25^\circ C$ (7). Curve 1—methylamine; curve 2—ethylamine; curve 3—propylamine; curve 4—butylamine; curve 5—amylamine.

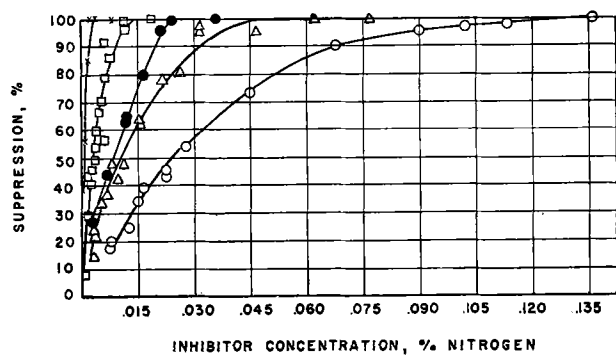


FIG. 6. Suppression of the nickel maximum as a function of concentration of aliphatic amines. \circ —methylamine; \triangle —ethylamine; \bullet —propylamine; \square —butylamine; \times —amylamine.

preceded every test. Specific amounts of amine solutions of known concentration were added to the polarizing cell containing the nickel chloride-potassium chloride solution. The amine solutions were also at the same concentration in respect to nickel chloride and potassium chloride as the solution from which the maximum was obtained. In this way, changes in Ni^{++} concentration during testing were avoided. Individual runs were performed for all concentrations of the amines tested. The pH of all solutions was adjusted to a value of about 3.0 by means of small amounts of HCl. All experiments were performed at $25^\circ \pm 0.1^\circ\text{C}$.

The effectiveness of the tested aliphatic amines in suppressing the nickel maximum is shown as a function of nitrogen concentration in Fig. 6. There is a striking similarity between the behavior of these amines as corrosion inhibitors and as nickel maximum suppressors. The suppression of the nickel maximum increases with amine concentration and becomes complete above a critical amine concentration. For a given concentration of amine, expressed in per cent nitrogen, the maximum suppression increases with molecular weight of the amines. Inhibitor concentrations in the polarographic and corrosion experiments are not the same since different metals and electrolytes are involved in the two cases.

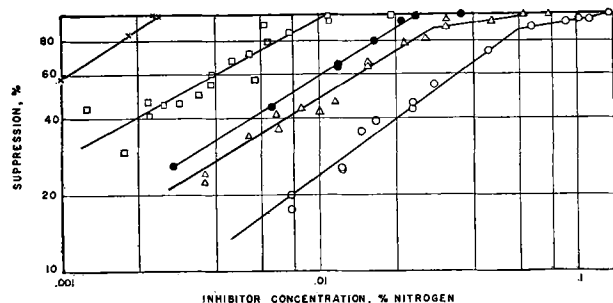


FIG. 7. Logarithmic plot of Fig. 6

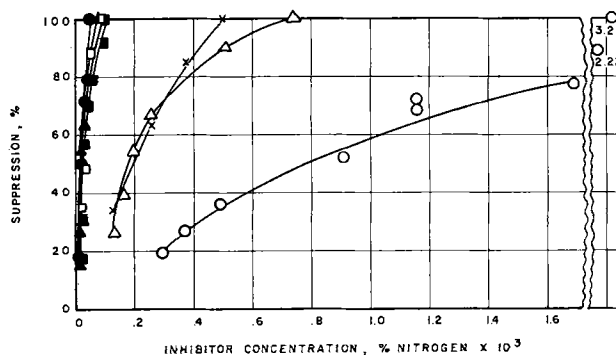


FIG. 8. Suppression of the nickel maximum as a function of concentration of aromatic amines. \circ —aniline; \triangle —*p*-toluidine; \times —*o*-toluidine; \blacksquare —3,5-xylidine; \square —dimethylaniline; \blacktriangle —2,3-xylidine; \bullet —2,6-xylidine.

By plotting the logarithm of the per cent suppression vs. the logarithm of the amine concentration, straight lines result (Fig. 7). Similar curves are obtained from Mann's data for these amines by plotting the logarithm of corrosion inhibiting effectiveness vs. the logarithm of their concentration in per cent nitrogen. In some cases, the slope of the lines changes at certain amine concentrations, suggesting a change in adsorption rates of these compounds at certain concentrations.

Aromatic amines.—Seven aromatic amines were selected to study further the polarographic behavior of corrosion inhibitors: aniline, dimethylaniline, *o*-toluidine, *p*-toluidine, 2,6-xylidine, 3,5-xylidine, and 2,3-xylidine. The procedure described for studies of aliphatic amines was employed for aromatic amines also. Polarographic results are shown in Fig. 8, and corresponding corrosion data (7) in Fig. 9. In the case of these amines also, the function

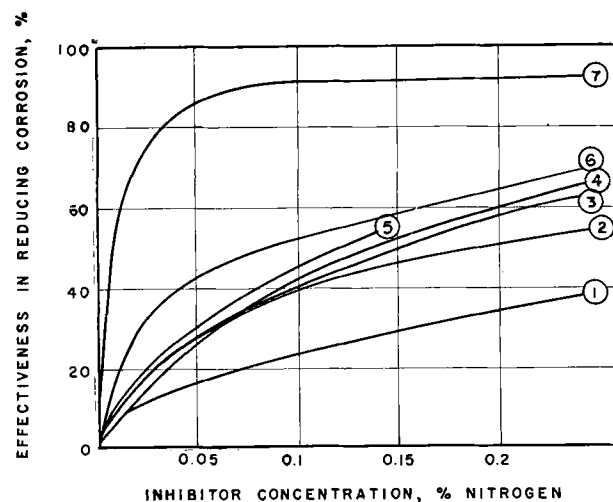


FIG. 9. Inhibition by aromatic amines of mild steel corrosion in $1N \text{H}_2\text{SO}_4$ at 25°C (7). Curve 1—aniline; curve 2—2,6-xylidine; curve 3—*p*-toluidine; curve 4—*o*-toluidine; curve 5—3,5-xylidine; curve 6—*N,N*-dimethylaniline; curve 7—2,3-xylidine.

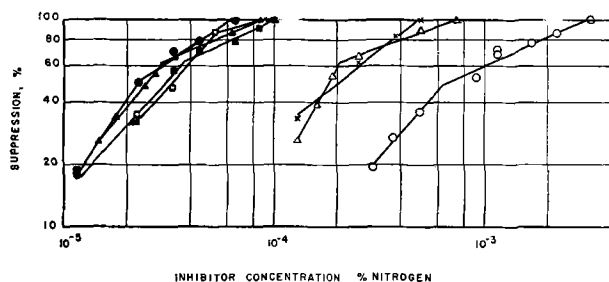


FIG. 10. Logarithmic plot of Fig. 8

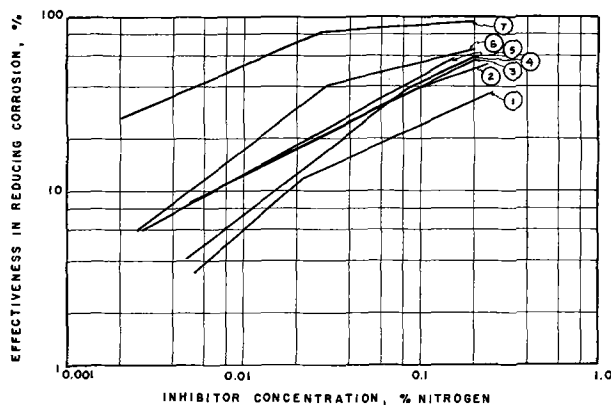


FIG. 11. Logarithmic plot of Fig. 9

of their polarographic maximum suppression effectiveness vs. their concentration resembles gas adsorption isotherms. Corresponding logarithmic plots are shown in Fig. 10. Here again the slope of all but one of the lines changes as it does in five of the corresponding corrosion plots (Fig. 11). Thus, polarographic behavior of the above aromatic amines resembles their behavior as corrosion inhibitors, which in turn is comparable to that of aliphatic amines. The order of maximum polarographic effectiveness, with the exception of 2,6-xylydine, is the same with that of maximum corrosion effectiveness. In both cases, however, differences in effectiveness of some aromatic amines are small and overlap as the concentration changes.

DISCUSSION

The appearance of polarographic maxima is associated with the fact that at certain emf values of current-voltage curves there is a higher concentration of reactive material in the immediate vicinity of the dropping microelectrode than at the emf range corresponding to the limiting current.

Although a satisfactory interpretation of all the phenomena associated with polarographic maxima is not available, it seems that polarization of the mercury microelectrode at the maxima is not established because an excess supply of reactive material is available at the microelectrode as a result of some specific electrochemical phenomenon. It has been

established, however, that surface-active or highly adsorbable substances suppress or eliminate polarographic maxima. It is believed that such an action is brought about by a "hindering" effect caused by maxima suppressors, which prevent reducible substances from reaching the mercury surface. Adsorption of suppressors on the metal surface is very probably the most predominant factor associated with the electrode polarization. In fact, suppressive action of various substances has been employed as an indicator of their adsorbability (15). In some cases the degree of suppression of the maxima has been suggested as a means of quantitative analysis of various substances (16), surface-active ones in particular (17).

With regard to mechanisms of corrosion and corrosion inhibition, electrical polarization and adsorption are of paramount importance according to current theories. It becomes thus apparent that significant similarities exist between the processes involved in polarographic maxima and their suppression on one hand, and in metallic corrosion and its inhibition on the other. On this basis, it is reasonable to believe that polarography constitutes a valuable tool for corrosion and corrosion inhibition studies.

In the present study, it is shown that the behavior of a number of inhibitors in the mild steel-sulfuric acid system is reflected in their action on some polarographic maxima obtained in 0.1M KCl solutions as supporting electrolyte. Particularly for the amines studied, it was demonstrated that their order of relative inhibiting effectiveness is the same as that of their suppressing effectiveness. It was further demonstrated that the inhibiting as well as the suppressing effectiveness is a function of concentration of the adsorption isotherm type. This is in agreement with the proposed (7) thesis that amines inhibiting corrosion adsorb on metal surfaces by means of the active amino-group. Their effectiveness increases with their covering power and concentration. The former increases, within limits, with molecular weight and molecular polarity. The latter affects inhibiting effectiveness according to the gas adsorption isotherm function. Polarographically, the degree of maximum suppression is an indicator of the adsorbability of certain substances, and the amines studied fall into this category.

According to Mann and his coworkers (7) the above amines act as cathodic inhibitors in acid solutions. They form positively charged ammonium-

type ions $\left[\begin{array}{c} X \\ | \\ X-N-X \\ | \\ X \end{array} \right]^+$ (where X stands for organic radicals or hydrogen atoms) and thus are

attracted by negative poles (cathodes) of the local cells. The present data are in agreement with these views, since amines are generally more effective with the nickel maximum at an emf such that the microelectrode is negatively charged with respect to the solution.

It should be pointed out, however, that, although electrostatic attraction constitutes the main driving force for adsorption in the case of ions or charged colloids, additional factors are probably associated with the adsorption process. Thus, ions in general are preferentially effective with either the negative or positive maxima; in many cases, however, they suppress both types of maxima to a small or great extent. It appears plausible that the nature of various inhibitors, insofar as being anodic, cathodic, or both is concerned, is very probably revealed by their effectiveness in suppressing positive or negative maxima. This correlation does not hold if local cathodes and anodes of a corroding system are either both negatively charged or both positively charged with respect to the corrosive medium. Further systematic studies in that direction should prove of considerable interest.

In comparing processes of corrosion inhibition and maxima suppression, it should be kept in mind that no single mechanism can explain all the phenomena involved in these processes, nor is this necessary. Furthermore, considerably different mechanisms may lead to similar results depending on the substances and experimental conditions involved. Thus, in connection with maxima suppression, Heyrovsky (3) suggested that the suppressing ability of various substances increases with their ability to coagulate colloidal solutions. This holds true in a number of cases, although not in all. In corrosion studies, it has also been suggested (18, 19) that colloidal phenomena are of importance in corrosion protection, especially where corrosion products easily acquire the colloidal state. In such cases, the action of corrosion inhibitors may be due primarily to coagulation of corrosion products to a protective film. The above views on the importance of coagulating properties of some substances in maxima suppression and corrosion inhibition expressed independently could serve as an additional indication of similarities between the two processes.

In this respect, it is of interest to mention the

fact that gelatine, a so-called "general inhibitor," has been used for many years as a "general suppressor" over a wide range of anodic and cathodic maxima.

On a practical basis, it is suggested that a polarograph properly used could provide a convenient tool for screening promising candidate corrosion inhibitors, e.g., for the iron-sulfuric acid system.

ACKNOWLEDGMENT

The author wishes to acknowledge the skillful assistance of C. T. Cinaglia.

Any discussion of this paper will be published in a Discussion Section which will appear in the June 1955 issue of the JOURNAL.

REFERENCES

1. For an extensive treatment see I. M. KOLTHOFF AND J. J. LINGANE, "Polarography," Interscience Publishers, New York (1952).
2. M. VON STACKELBERG, *Fortschr. chem. Forsch.*, **2**, 229 (1951).
3. J. HEYROVSKY, "A Polarographic Study of the Electrokinetic Phenomena of Adsorption, Electroreduction and Overpotential Displayed at the Dropping Mercury Cathode," *Actualités Scientifiques et Industriels*, No. 90, Hermann et Cie, Paris (1934).
4. For comprehensive reviews, see reference (1), p. 160, Vol. 1 and reference (2).
5. U. R. EVANS, "Metallic Corrosion, Passivity, and Protection," p. 350, Edward Arnold & Co., London (1948).
6. R. B. MEARS, *This Journal*, **95**, 1 (1949).
7. C. A. MANN, *ibid.*, **69**, 115 (1936).
8. C. A. MANN, B. E. LAUER, AND C. T. HULTIN, *Ind. Eng. Chem.*, **28**, 159, 1948 (1936).
9. S. CH'IAO AND C. A. MANN, *ibid.*, **39**, 910 (1947).
10. E. J. W. VERWEY, *Chem. Revs.*, **16**, 374 (1937).
11. Reference (1), p. 160, Vol. 1.
12. Reference (5), p. 534.
13. G. G. ELDREDGE AND J. C. WARNER, "Corrosion Handbook," (H. H. Uhlig, Editor) p. 905, John Wiley & Sons, Inc., New York (1948).
14. G. G. ELDREDGE AND R. B. MEARS, *Ind. Eng. Chem.*, **37**, 736 (1945).
15. O. H. MÜLLER, "The Polarographic Method of Analysis," p. 58, Chemical Education Publishing Co., Easton, Pa. (1951).
16. G. SEMERANO, *Arch. sci. biol. (Italy)*, **20**, 329 (1934).
17. M. VON STACKELBERG AND H. SCHÜTZ, *Koll. Z.*, **105**, 20 (1943).
18. J. N. FRIEND, *Trans. Am. Electrochem. Soc.*, **40**, 63 (1921).
19. S. YAMAGUCHI, *Koll. Z.*, **126**, 155 (1952).

Corrosion Properties of Titanium in Marine Environments¹

H. B. BOMBERGER, P. J. CAMBOURELIS, AND G. E. HUTCHINSON

Rem-Cru Titanium, Inc., Midland, Pennsylvania

ABSTRACT

Data are presented on the behavior of commercially pure titanium and several common structural metals exposed up to five years at Kure Beach, North Carolina. Tests include exposures to the atmosphere, quiet and flowing sea water, jet impingement, stress corrosion, and galvanic couples. These tests indicate that titanium is unaffected by marine environments.

INTRODUCTION

Commercially pure titanium has, in addition to a high strength-to-weight ratio, the desirable property of outstanding corrosion resistance to a number of chemicals. It has excellent resistance to nitric acid solutions (1-5), although violent reaction of a titanium-manganese alloy with red fuming nitric acid (12) suggests that work with any titanium-base material in fuming nitric should be conducted with caution. Especially interesting is the metal's resistance to moist chlorine gas (1), sodium and calcium hypochlorites, chloride salt solutions including cupric and ferric chlorides, and some mixed acids (1, 2). Titanium also has a high resistance to many organic acids and compounds (1, 6), but the metal is attacked by hydrochloric, hydrofluoric, sulfuric, oxalic, trichloroacetic, and unaerated formic acid solutions.

Hutchinson and Permar (1) reported on the apparent immunity of titanium to sea water by atmospheric, jet impingement, and sea water immersion tests.

These results were confirmed by Williams (7) along with additional information. Exposures up to eight months in the atmosphere, in quiescent and rapidly moving sea water, and on jet impingement had a negligible effect. No evidence of stress corrosion was observed after six months on titanium stressed to nearly the yield strength for 0.1% offset.

LaQue (8) reported similar results for titanium subjected to marine environments for extended periods of time under many test conditions. No significant effect was observed under any test condition. Excellent resistance to erosion, corrosion fatigue, stress corrosion, crevice corrosion, and pitting was reported. The galvanic effect of titanium in contact with other materials was found to be about the same as that of the 18-8 stainless steels.

This paper reports additional information on titanium and a number of controls exposed to marine environments at Kure Beach since midsummer of 1948.

EXPERIMENTAL

Commercially pure, cold-rolled titanium² was tested along with the controls listed in Table I. Titanium sheet had a nominal composition of more than 99% titanium, 0.3% carbon, and a few tenths to a few hundredths of 1% oxygen, nitrogen, and iron.

Except in jet impingement and galvanic tests, materials were tested as 6 in. x 1½ in. x ⅛ in. to ⅜ in. strips. After testing, aluminum alloys, stainless steels, Inconel, and titanium were cleaned by swabbing in 65% nitric acid for three minutes. The copper and Monel were swabbed in 20% hydrochloric acid for 10 seconds. Cleaning techniques had negligible effect on the base material.

Atmospheric Tests

Unlike the control specimens, titanium showed no significant weight loss or change in appearance on being exposed to sea air 80 and 800 ft from the ocean for five years, as indicated by Fig. 1. Aluminum alloys acquired a mottled limestone gray appearance, stainless steels became rusty brown, Monel turned dark green, and Inconel became speckled with brown spots. Control specimens from the shore rack were more discolored and corroded more rapidly than those in the main lot 800 ft from the ocean.

Materials exposed to the industrial atmosphere of Bridgeport, Connecticut, for four years and eleven months were similar in appearance to those removed from the main lot at Kure Beach, but the average corrosion rates, given in Table II, were a little higher. The same materials exposed five years to the rural atmosphere north of Wilmington, Delaware, appear by visual examination to be completely un-

¹ Manuscript received November 12, 1953. This paper was prepared for delivery before the Wrightsville Beach Meeting, September 13 to 16, 1953.

² Produced by Rem-Cru Titanium, Inc.

TABLE I. Control alloys tested at Kure Beach, N. C.
Aluminum alloys

Alloy	Surface condition	Cu	Fe	Si	Mn	Mg	Cr	Zn	Ti	Al
24S-T3	Bright	4.54	0.30	0.15	0.58	1.46	—	—	—	Bal.
Alclad 24S-T3	Bright									
coating		0.27	0.13	0.07	0.01	0.13	—	—	—	Bal.
core		4.19	0.28	0.11	0.56	1.39	—	—	—	Bal.
52S-1/2H	Bright	0.02	0.15	0.12	0.05	2.53	0.21	—	—	Bal.
Alclad 75S-T6	Bright									
coating		0.09	0.36	0.07	0.01	0.15	—	1.31	—	Bal.
core		1.58	0.15	0.08	0.12	2.61	0.24	5.90	0.05	Bal.

Stainless steels

Alloy	Surface condition	Cr	Ni	Mn	P	S	Si	C	Mo	Cb	Fe
Type 302	Bright, cold rolled	18.37	8.71	0.93	0.019	0.009	0.600	0.099	—	—	Bal.
Type 316	Hot rolled & pickled	17.36	12.68	1.60	0.024	0.023	0.44	0.053	1.89	—	Bal.
Type 347	Hot rolled & pickled	18.58	11.27	1.76	0.026	0.020	0.58	0.058	—	0.87	Bal.

Nickel alloys

Alloy	Surface condition	Cu	Cr	Ni	Mn	P	S	Si	C	Fe
Monel	Cold rolled & annealed	29.75	—	67.85	1.04	0.029	0.008	0.127	0.072	0.98
Inconel	Hot rolled	—	14.79	77.63	0.20	0.010	0.008	0.183	0.056	6.96

affected, except Monel which had a green tarnish film and the aluminum alloys which had weathered to a limestone gray. Exposures at these three test sites are being continued indefinitely for future examination.

Immersion Tests

The titanium specimens immersed in sea water flowing at 3 ft/sec had, after cleaning, essentially the same weight and bright surface that they had when installed 4.5 years earlier. Although all materials were fouled by marine organisms, corrosion was observed only on the control specimens as indicated in Fig. 2 and 3. Inconel, Monel, 24S-T3 aluminum alloy, and Type 347 stainless steel suffered rather heavy localized attack. Corrosion rates and maximum pit depths for these materials are given in Table III. Corrosion rates for control specimens after 483 days were of the same order as those obtained after 618 days and 4.5 years, except for

TABLE II. Corrosion rates of materials exposed to the atmosphere

Materials*	5 Years at Kure Beach, N. C.		4 Years, 11 months in Bridgeport, Conn.
	Shore rack 80 ft from breakers	Main lot 800 ft from breakers	
Titanium	Nil	Nil	0.00008
24S-T3	0.0256	0.0028	0.0154
Alclad 24S-T3	0.0197	0.0034	0.0122
52S-1/2H	0.0139	0.0026	0.0135
Alclad 75S-T6	0.0278	0.0034	0.0140
302 Stainless	0.0009	Nil	0.0001
316 Stainless	0.0013	Nil	0.0003
347 Stainless	0.0011	Nil	0.0003
Monel	0.0175	0.0107	0.0349
Inconel	0.0014	0.0003	0.0094

* Average corrosion rates from three specimens in mils per year.

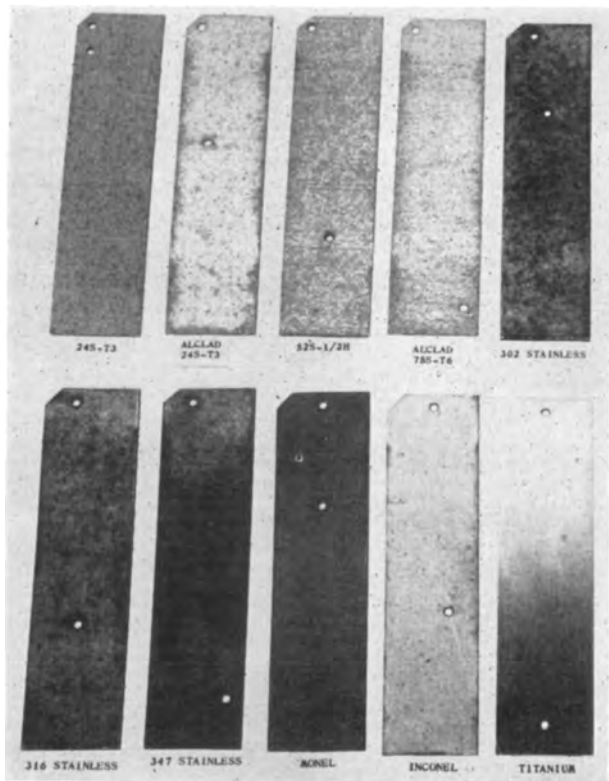


FIG. 1. Materials exposed 80 ft from the ocean for five years

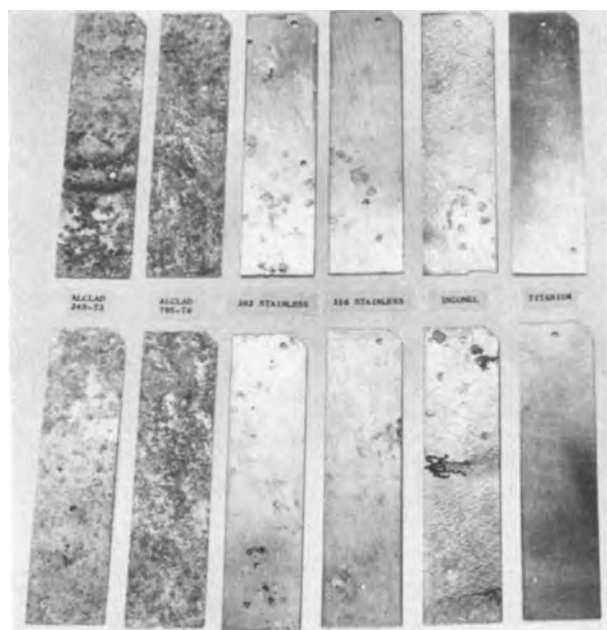


FIG. 2. Materials exposed to flowing sea water for 4½ years

Monel and Type 347 stainless steel where a slight increase was noted. Slightly higher rates were reported for these controls by Hutchinson and Permar for 120-day exposure tests in a trough (1).

Similar results were observed for materials exposed for 480 days in quiet sea water in the basin at Kure Beach as illustrated in Fig. 4. Some materials were heavily attacked by pitting and crevice corrosion. No noticeable change or measurable weight loss could be detected on the six titanium test specimens. Corrosion rates, given in Table IV, are essentially the same as those reported by Hutchinson and Permar for 120-day exposures in the basin.

Galvanic Couple Tests

Although titanium is an inherently reactive metal, it is found at the noble end of the galvanic series

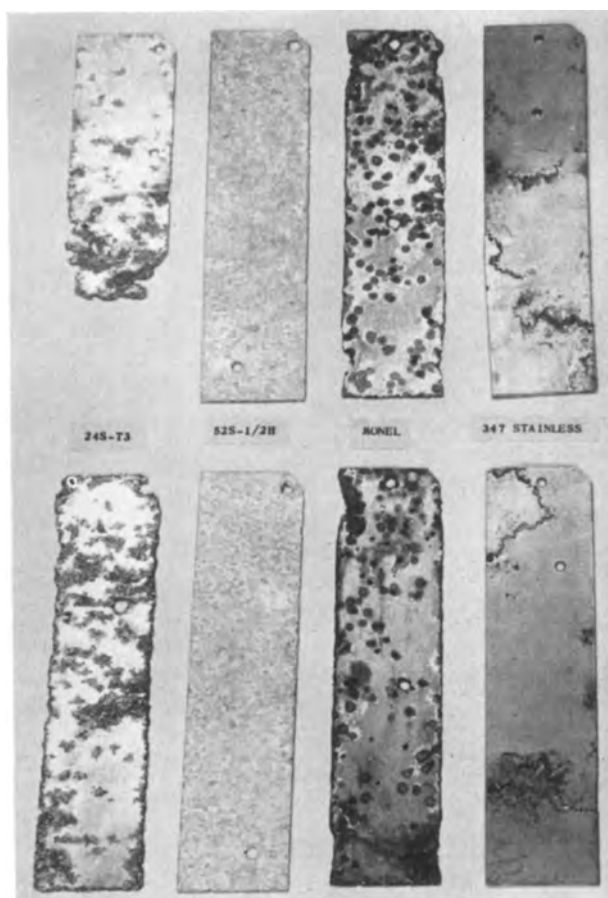


FIG. 3. Materials exposed to flowing sea water one year and 253 days.

for metals in sea water along with silver, Monel, and passive Type 316 stainless steel, and has a steady-state potential of -0.15 volt, vs. saturated calomel, at 25°C . The metal is even more noble at lower temperatures.

Additional potential studies at Kure Beach show that titanium has the property of polarizing readily to the potential of more anodic materials, such as

TABLE III. Materials immersed in sea water flowing at 3 ft/sec in trough at Kure Beach, N. C.

Material*	483 Days			618 Days			4½ Years		
	Corr. rate mpy	Max. face pitting, in.	Max. edge pitting, in.	Corr. rate mpy	Max. face pitting, in.	Max. edge pitting, in.	Corr. rate mpy	Max. face pitting, in.	Max. edge pitting, in.
Titanium.....	Nil	None	None	—	—	—	0.00003	None	None
24S-T3.....	4.80	0.054†	0.14	5.08	0.054†	0.15	—	—	—
Alclad 24S-T3.....	1.10	None	None	—	—	—	1.17	0.035†	0.050
52S-1/2H.....	1.52	0.046	0.10	1.47	0.035	0.040	—	—	—
Alclad 75S-T6.....	1.21	None	None	—	—	—	0.781	0.035†	0.20
302 Stainless.....	0.08	0.031	0.060	—	—	—	0.088	0.060	0.20
316 Stainless.....	0.16	0.020	0.10	—	—	—	0.061	0.050	0.10
347 Stainless.....	0.28	0.068†	1.5‡	3.57	0.068†	1.5‡	—	—	—
Monel.....	0.144	0.020	0.12	1.27	0.045†	0.050	—	—	—
Inconel.....	Nil	0.008	None	—	—	—	0.094	0.035†	0.10

* Three specimens of each.

† Specimens perforate with pits.

‡ Maximum depth of crevice corrosion.

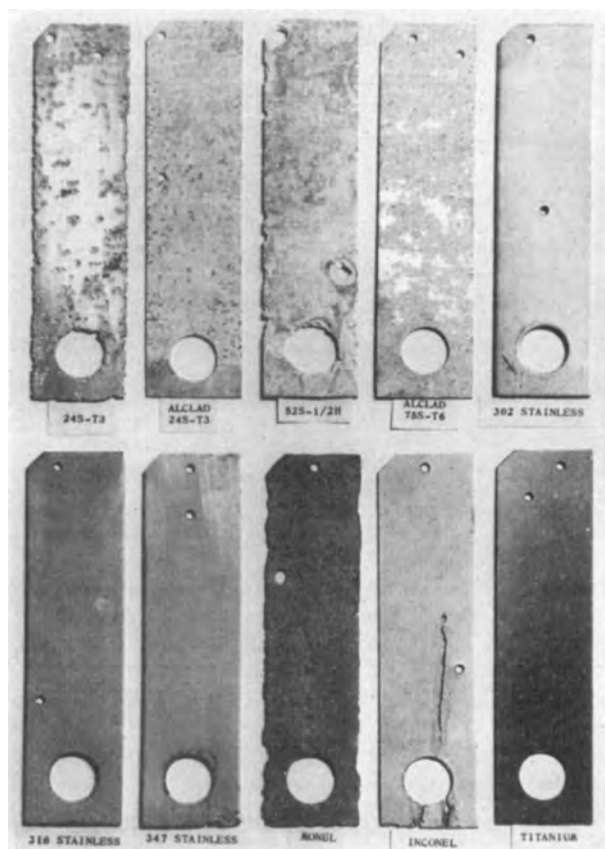


Fig. 4. Materials immersed in quiet sea water 480 days

plain carbon steel, with which it may be in contact (8, 9). The effect of this characteristic was investigated by experiments in which panels of one material were riveted to another with different area relationships. According to LaQue (8), the galvanic contribution of titanium in a couple is about the

TABLE IV. Materials immersed 480 days in quiet sea water in the basin at Kure Beach, N. C.

Material*	Average corrosion rate, mpy	Max. face pitting, in.	Max. edge pitting, in.
Titanium.....	Nil	None	None
24S-T3.....	2.24	0.054†	0.37
Alclad 24S-T3.....	0.612	0.001	0.001
52S-1/2H.....	0.96	0.065†	0.21
Alclad 75S-T6.....	0.60	0.001	0.001
302 Stainless.....	0.146	0.060	0.050
316 Stainless.....	0.24	0.060	1.50‡
347 Stainless.....	1.43	0.067†	2.50‡
Monel.....	1.38	0.039	0.20
Inconel.....	0.49	0.034	4.75‡

* Six specimens of each.
 † Specimens perforated.
 ‡ Maximum depth of crevice corrosion.

same as an 18-8 stainless steel, and experiences with this material can be used as a safe guide on replacing stainless steel with titanium.

In marine atmosphere and sea water tests there were no indications that titanium suffered in any way as a result of being in contact with the common metals and alloys. Corrosion rates for the materials in contact with titanium in the basin at half tide are given in Table V. Titanium coupled with Inconel, silver, and Types 302 and 316 stainless steels appeared to have a negligible effect on these materials. However, a noticeable increase in corrosion occurred with the remaining specimens coupled to titanium. This was especially true for magnesium. In general, rates obtained after 360 days' exposure are similar to or slightly less than those observed after 193 days.

Schlain (10), and Paige and Ketcham (11) re-

TABLE V. Sea water galvanic couple tests in basin at half tide at Kure Beach

Materials	193-Day exposures			369-Day exposures		
	Uncoupled corr. rates, mpy*	Coupled corr. rates, mpy		Uncoupled corr. rate, mpy*	Coupled corr. rate, mpy	
		Metal area 7 × Ti area**	Metal area 1/2 × Ti area†		Metal area 7 × Ti area**	Metal area 1/2 × Ti area†
FS-1 Magnesium.....	65.06‡	920.7§	Lost	—	—	—
Alclad 24S-T3.....	0.55	1.20	1.70	0.233	0.89	Lost
52S-1/2H.....	0.457	0.91	7.42	Lost	0.75	4.60
Alclad 75S-T6.....	1.21	1.38	6.12	0.633	0.83	Lost
Copper.....	0.511	0.92	1.015	0.577	0.94	2.00
Steel (low carbon).....	6.10	12.32	17.24	8.60	12.20	12.90
Monel.....	0.071	0.060	0.130	0.073	0.06	0.130
Inconel.....	0.002	Nil	0.002	Nil	Nil	Nil
302 Stainless.....	0.058	0.010	0.120	0.004	0.008	0.096
316 Stainless.....	Nil	Nil	Nil	Nil	Nil	Nil
Silver.....	—	—	—	0.70	1.10	1.22

* Average of one 6 in. x 1.5 in. specimen and two 1.5 in. x 0.75 in. specimens.
 ** One 6 in. x 1.5 in. specimen.
 † Average of two 0.75 in. x 1.5 in. specimens.
 ‡ 44-day exposure.
 § Two-day exposure.

TABLE VI. Atmospheric galvanic-couple tests on shore rack, Kure Beach

Material	360-Day exposure			4 Years & 8 months exposure		
	Uncoupled corr. rates,* mpy	Coupled corr. rate, mpy		Uncoupled corr. rates,* mpy	Coupled corr. rate, mpy	
		Metal area 7 × Ti area**	Metal area 1/7 × Ti area†		Metal area 7 × Ti area**	Metal area 1/7 × Ti area**
FS-1 Magnesium.....	1.26	2.50	5.5	0.88‡	1.17‡	3.52‡
Alclad 24S-T3.....	0.06	0.277	0.86	0.0549	0.2130	0.291
52S-1/2H.....	0.05	0.056	0.199	0.0845	0.0362	0.0813
Alclad 75S-T6.....	0.10	0.460	0.99	0.0525	0.0786	0.393
Copper.....	0.12	0.022	0.42	0.0852	0.1350	0.241
Steel (low carbon).....	6.13	9.82	Lost	—	—	—
Monel.....	Nil	0.020	0.032	0.0152	0.0197	0.0320
Inconel.....	0.011	0.006	0.003	0.0025	0.0029	0.0032
302 Stainless.....	Nil	0.009	0.023	0.0083	0.0091	0.0015
316 Stainless.....	0.004	0.004	0.003	0.0035	0.0029	0.0058

* Average of one 6 in. x 1.5 in. specimen and two 0.75 in. x 1.5 in. specimens.

** One 6 in. x 1.5 in. specimen.

† Average of two 0.75 in. x 1.5 in. specimens.

‡ Three years and 160 days' exposure.

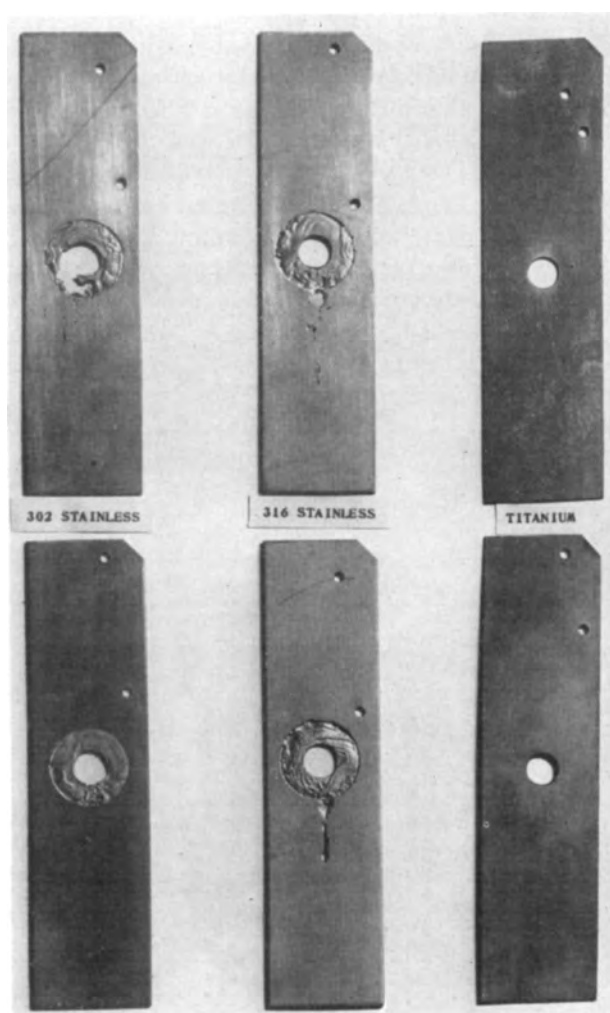


FIG. 5. Materials tested for crevice corrosion in quiet sea water.

ported higher corrosion rates than these for copper, iron, magnesium, aluminum alloys coupled with titanium of the same area in two to three liters of aerated sodium chloride solutions for relatively short times (24–48 hr). These higher rates may be due in part to short test periods and probable changes in solution composition, since rate-controlling phenomena such as film growth and polarization are a function of time and environment. Paige and Ketcham also noted that stainless steel and titanium are similar in their electrochemical behavior.

The galvanic couples tested on the 80-ft shore rack gave similar results, although in this case, as indicated in Table VI, all corrosion rates are significantly less. Again, Inconel and Types 302 and 316 stainless steels appeared to be unaffected by the titanium, and corrosion rates of these materials varied little with time. However, the corrosion of copper, magnesium, and the aluminum alloys was increased by titanium and the rates of these materials decreased with time.

Erosion Tests

Titanium subjected to the action of a submerged jet of sea water for 30 days containing 2.4% by volume of entrained air at a velocity of 12 ft/sec and an average temperature of 23.5°C resulted in no significant weight loss. There was no change in the surface appearance. Titanium specimens whirled through sea water at 30 ft/sec for 60 days suffered negligible attack. Titanium also has an unusually high resistance to cavitation erosion. The metal is said to be superior to conventional propeller alloys and almost as good as stainless steel designed especially for cavitation resistance (8).

Crevice Corrosion Tests

Special tests were designed to determine the susceptibility of titanium to crevice corrosion. In these experiments, fiber, and zinc and cadmium-plated steel washers were bolted to 6 in. x 1.5 in. test strips. After 360 days' immersion in sea water in the basin and four years and eight months exposure on the shore rack no evidence of pitting, crevice corrosion, or any other form of attack could be found on the titanium. However, the nontitanium control specimens suffered from localized attack as illustrated by Fig. 5.

Stress Corrosion Tests

Titanium containing high residual stresses or under static tensile loads does not appear to be susceptible to stress corrosion or corrosion fatigue in sea air and water. Erichsen cup test specimens, stressed as highly as possible without causing failure, were exposed in the basin for 360 days and in the salt air for four years and eight months. In this time there was no evidence of stress corrosion cracking. Titanium tensile specimens with a yield strength of 105,000 psi have been under static loads up to 80,000 psi for over five years in the main lot at Kure Beach without a sign of failure.

There appears to be no difference between the endurance limit of titanium in sea water and in air. The value for titanium in sea water is 60,000 psi. This is well above the values for materials regularly used for pump and propeller shafts (8).

SUMMARY

Commercially pure titanium exposed to sea, industrial, and rural atmospheres for approximately five years and to sea water up to four and a half years appeared to be completely unaffected. Long-time tests designed to show susceptibility to sea

water erosion, crevice corrosion, galvanic corrosion, pitting, stress corrosion, and corrosion fatigue had no noticeable effect on the metal. Titanium coupled to Inconel, silver, and Types 302 and 316 stainless steels had a negligible effect on the corrosion rates of these materials, but the rates of Monel, copper, low-carbon steel, and aluminum alloys were in some cases more than doubled.

ACKNOWLEDGMENTS

The authors are grateful to Mr. F. L. LaQue and the staff of the International Nickel Company, Inc., at the Kure Beach and Harbor Island Test Stations for their advice and assistance in carrying out this work.

Any discussion of this paper will appear in a Discussion Section to be published in the June 1955 issue of the JOURNAL.

REFERENCES

1. G. E. HUTCHINSON AND P. H. PERMAR, *Corrosion*, **5**, 319 (1949).
2. L. B. GOLDEN, I. R. LANE, JR., AND W. L. ACHERMAN, *Ind. Eng. Chem.*, **44**, 1930 (1952).
3. E. A. GEE, L. B. GOLDEN, AND W. E. LUSBY, JR., *ibid.*, **41**, 1668 (1949).
4. G. C. KIEFER AND W. W. HARPLE, *Metal Progr.*, **63**, 74 (1953).
5. F. H. BECK AND M. G. FONTANA, *Corrosion*, **9**, 287 (1953).
6. I. R. LANE, JR., L. B. GOLDEN, AND W. L. ACHERMAN, *Ind. Eng. Chem.*, **45**, 1067 (1953).
7. W. L. WILLIAMS, U. S. Engineering Experimental Station Report C-3395, C-3501B.
8. F. L. LAQUE, Engineering Research and Development Laboratory Symposia, Fort Belvoir, Virginia, 55, August (1952).
9. F. L. LAQUE, *Am. Soc. Testing Materials, Proc.*, **51**, 545 (1951).
10. D. SCHLAIN, Bureau of Mines Report of Investigation 4965, April (1953).
11. H. PAIGE AND S. J. KETCHAM, *Corrosion*, **8**, 413 (1952).
12. J. F. SCHEER, *Metal Progr.*, **64**, 110 (1953).

Jet Impingement Tests¹

P. T. GILBERT

British Non-Ferrous Metals Research Association, London, England

AND

F. L. LAQUE

International Nickel Company, Inc., New York, New York

ABSTRACT

This paper describes the operation of jet impingement test apparatus in the laboratories of The British Non-Ferrous Metals Research Association in London and at International Nickel Company's Marine Corrosion Test Station at Harbor Island, N. C. Certain differences in results obtained on the same materials in the two laboratories are discussed with relation to differences in testing conditions. Particular attention is given a comparison between results secured with water that is recirculated and used over and over again, as is the practice in the B.N.F.M.R.A. laboratories, with results obtained with water that is passed through the apparatus only once, as has been the regular practice at Harbor Island. Effects of air bubbles, jet velocity, and other incidental factors are also discussed. The relationship between test results and service experience is considered. It is concluded that test conditions established for use in the B.N.F.M.R.A. laboratory, using recirculated water, are too drastic when applied at Harbor Island, using water that is not recirculated, to permit proper comparisons of materials. The testing conditions at Harbor Island can be modified to yield results in harmony with the B.N.F.M.R.A. results either by reducing the jet velocity or by recirculating the water.

INTRODUCTION

Failure of certain condenser tube alloys as a result of corrosion-erosion produced by salt water moving at moderately high velocity stimulated research on this subject, which has been carried on more or less continuously since the pioneer work of Bengough and May (1). They found that the type of attack encountered in service could be reproduced in the laboratory by subjecting specimens to jets of sea water containing air bubbles of a particular size. Apparatus used and other details of the test procedure have been described (2, 3).

A 24-unit jet impingement apparatus was used with recirculated water in the B.N.F.M.R.A. Laboratory in London, and a similar apparatus was installed at the Harbor Island Test Station for use with sea water that passed through only once. A duplicate apparatus at Harbor Island was arranged so that water could be recirculated as in the B.N.F.M.R.A. Laboratory.

Prior to installation of the B.N.F.M.R.A. type of apparatus at Harbor Island, jet tests were conducted there with apparatus in which air was drawn into the water by aspirating action of a venturi-type nozzle (4, 5). This device produced damage not unlike that observed with the British apparatus, but in comparing results with specimens of several

alloys which were exchanged for parallel tests in the two laboratories, considerable difference in behavior was observed. It was thought that this might be due to some peculiar characteristics of the two types of apparatus. Therefore, arrangements were made to operate a duplicate of the British apparatus at Harbor Island.

This paper presents an account of some of the tests made in England and at Harbor Island which illustrate differences in behavior that have been observed with the same apparatus and which show effects of some important variable factors.

RESULTS OF TESTS IN TWO LABORATORIES

Lack of agreement between results in the two laboratories is illustrated conveniently by comparing relative behavior of Admiralty Brass and Aluminum Brass and by observation of the effects of air bubbles on the extent of impingement attack of Admiralty Brass.

Table I presents data on the average performance of Aluminum Brass and Admiralty Brass under nominally the same testing conditions (except for recirculation of water in the British tests) in the two laboratories. The approximately 8:1 superiority of Aluminum Brass over Admiralty Brass, shown by British tests with air bubbles admitted, was reduced to about 2:1 in Harbor Island tests. This was due to much more severe attack of Aluminum Brass at Harbor Island, since Admiralty Brass

¹ Manuscript received November 4, 1953. This paper was prepared for delivery before the Wrightsville Beach Meeting, September 13 to 16, 1953.

TABLE I. Results of Jet impingement tests with B.N.F.M.R.A. apparatus at Harbor Island, N. C.

Velocity of jet: 15 ft/sec
Duration: 28 days

Water system	% Air added	Temp, °C	Depth of impingement attack (mm)	
			Arsenical	
			Admiralty Brass	Aluminum Brass
Once through.....	3	18	0.37	No test
		20	0.36 ^a	0.15 ^b
		24	0.22	0.16
Once through.....	0	15	0.15	No test
		25	0.33	No test
Recirculated.....	3	20 ^c	0.34 ^{c, d}	0.04 ^{c, e}
		30	0.25	0.01
Recirculated.....	0	25	0.27	0.00

^a Range 0.20 to 0.61.
^b Range 0.08 to 0.23.
^c Test made in England, 30-day run.
^d Range 0.14 to 0.51.
^e Range 0 to 0.66 (one specimen out of 20 pitted to depth of 0.66 mm. No impingement attack greater than 0.02 mm.)

was affected to about the same extent at both locations.

Similarity in nature and extent of attack of Admiralty Brass and Aluminum Brass in the apparatus as used at Harbor Island is illustrated by Fig. 1.

Another major difference between the British and the Harbor Island results was the failure of the latter to show any important or consistent effect of air bubbles in aggravating impingement attack on Admiralty Brass under conditions which regularly showed no impingement attack unless air bubbles were present in the British Laboratory. This is illustrated by results of tests on Admiralty Brass as shown in Table I. Fig. 2 shows Admiralty Brass specimens after test with and without air bubbles.

TESTS WITH RECIRCULATED WATER AT HARBOR ISLAND

Since the principal difference between testing conditions was recirculation of water in the British Laboratory as compared with passing it through the jets only once at Harbor Island, it was decided to modify a test unit at Harbor Island to permit recirculation of water. This change in testing conditions sufficed to bring results more in line with those regularly observed in the B.N.F.M.R.A. Laboratory. A typical comparison of results on Admiralty Brass and Aluminum Brass with once-through and recirculated sea water at Harbor Island is provided by Table I.

It will be seen that when sea water at Harbor Island was recirculated as in the B.N.F.M.R.A. Laboratory, the relative behavior of Aluminum Brass and Admiralty Brass came into line with that ordinarily observed in British tests.

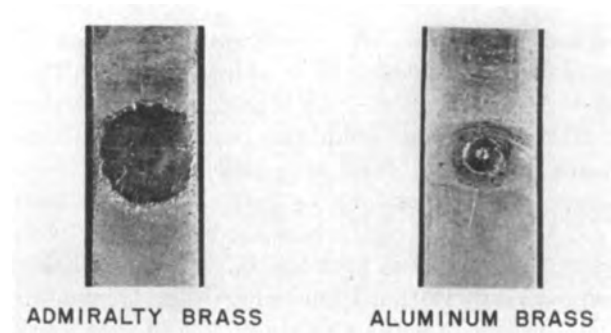


FIG. 1. Admiralty Brass and Aluminum Brass specimens after impingement test with once-through water at 15 ft/sec at Harbor Island.

However, even with recirculated water at Harbor Island, it was not possible to show any strong effect of air bubbles on the extent of impingement attack. Typical results of tests at Harbor Island with and without the admission of air bubbles are shown in Table I.

Without further reference to effects of air bubbles, it became evident that, at least regarding comparison between Admiralty Brass and Aluminum Brass, both the B.N.F.M.R.A. Laboratory and Harbor Island tests with recirculated water rated these alloys more in line with their behavior under many conditions of use than did the more drastic tests at Harbor Island with water that was not recirculated. Apparently what was involved was some sort of trigger effect of erosive conditions created by the jet test. This trigger effect seemed to be a breakdown of protective film. Once this occurred, there would be an abrupt increase in extent of impingement attack to a level which would not be increased much further by greater intensification of erosive forces. In this connection, it has been observed in

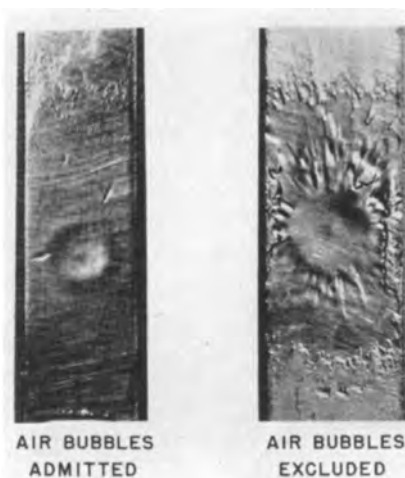


FIG. 2. Tests at Harbor Island with once-through water at 15 ft/sec. Impingement attack of Admiralty Brass with and without air bubbles in the jet.

the B.N.F.M.R.A. Laboratory that materials attacked at a certain jet velocity without air are no more deeply attacked if air is added at this or higher jet velocities.

Normal testing conditions with once-through water at Harbor Island were sufficiently drastic to promote film breakdown on both Aluminum Brass and Admiralty Brass, while conditions used with recirculated water in both the B.N.F.M.R.A. Laboratory and at Harbor Island caused film breakdown and consequent serious damage only to Admiralty Brass.

Under these circumstances, it would be easy to understand why the possible mechanical effects of air bubbles might be masked in tests with once-through water at Harbor Island. However, a question remains as to why the effects of air bubbles observed with recirculated water in the B.N.F.M.R.A. Laboratory were not observed also with recirculated water at Harbor Island.

TESTS WITH ONCE-THROUGH WATER IN ENGLAND

A jet test was operated with once-through sea water in England with the cooperation of Imperial Chemical Industries, Ltd. Results so far obtained are summarized in Table II. The amount of attack produced was in general less than that in once-through tests at Harbor Island, but results were

TABLE II. Results of tests in England using once-through water

Run No.	BA/53	BB/53	BC/53	BD/53
Water speed (ft/sec)	15	15	15	30
% Air by volume	3	0	3	3
Average water temp, °C	7.5	9	13	16
Material	Depth of impingement attack (mm)			
70:30 Cu Ni, 0.04% Fe	0.05	0.03	0.09	0.10
	0.06	0.04	0.07	0.08
70:30 Cu Ni, 0.8% Fe	0.10	0.01	0.07	0.18
	0.11	0.01	0.10	0.14
90:10 Cu Ni, 1% Fe	0.08	0.05	0.09	0.07
	0.07	0.05	0.09	0.05
90:10 Cu Ni, 2% Fe	0.09	0.0	0.09	0.16
	0.09	0.0	0.10	0.15
95:5 Cu Ni, 0.6% Fe	0.07	0.06	0.11	0.10
	0.09	0.03	0.09	0.12
95:5 Cu Ni, 1.3% Fe	0.08	0.07	0.12	0.23
	0.07	0.06	0.13	0.25
Arsenical copper	0.06	0.06	0.11	0.17
	0.07	0.06	0.11	0.15
Admiralty Brass (70:29:1)	0.09	0.05	0.11	0.11
	0.08	0.07	0.11	0.08
Aluminum Brass (76:22:2)	0.06	0.07	0.07	0.08
	0.05	0.07	0.07	0.09

similar in most respects. Thus, Aluminum Brass was attacked only slightly less than Admiralty Brass, and the differences among all materials were slight. There appeared to be some effect of adding air

TABLE III. Effect of variation of water speed in recirculating jet impingement test without added air bubbles in B.N.F.M.R.A. laboratory

Run No.	AD/52	AG/52	Z/49	AB/49	B/53	AE/52	AA/49	D/53	A/53
Water speed (ft/sec)	10	15	15	15	22.5	30	30	15*	15**
% Air	0	0	0	0	0	0	0	0	0
Material	Depth of impingement attack								
70:30 Cu Ni, 0.04% Fe	0	0	—	0	0.73	0.50	0.47	0	0.35
	0	0	—	0	0.55	0.23	0.52	0	0.23
70:30 Cu Ni, 0.4% Fe	—	0	—	—	—	—	—	0	—
	—	0	—	—	—	—	—	0	—
70:30 Cu Ni, 0.8% Fe	—	0	—	—	—	—	—	0	—
	—	0	—	—	—	—	—	0	—
65:30 Cu Ni, 2% Fe	0	0	0	0	0	0	0	0	0
	0	0	0	0	0	0	0	0	0
90:10 Cu Ni, 1% Fe	—	0	—	—	—	—	—	0	—
	—	0	—	—	—	—	—	0	—
90:10 Cu Ni, 2% Fe	0	0	0	0	0	0	0	0	0
	0	0	0	0	0	0	0	0	0
95:5 Cu Ni, 0.6% Fe	—	0	—	—	—	—	—	0	—
	—	0	—	—	—	—	—	0	—
95:5 Cu Ni, 1.3% Fe	—	0	0	0	—	—	0	0	—
	—	0	0	0	—	—	0	0	—
Arsenical copper	0	0.23	—	0.38	0.16	0.18	0.89	0.41	0.11
	0	0.17	—	0.39	0.16	0.15	0.73	0.38	0.13
70:30 Brass	0	0.02	—	0.27	0.44	0.43	0.70	0.32	0.32
	0	0.03	—	0.35	0.39	0.56	0.70	0.32	0.31
Admiralty (70:29:1) Brass	0	0	0	—	0.61	0.67	—	0	0.38
	0	0	0.01	—	0.64	0.68	—	0	0.36
Aluminum Brass (76:22:2)	—	0.01	—	<0.01	—	—	0	0	—
	—	0.03	—	<0.01	—	—	0	0	—

* Air bubbled into the bath instead of passing through the jets.

** Air bubbled into the bath and nitrogen (3%) passed through jets; depth of attack in mm.

bubbles with some of the cupro-nickels, but not with the brasses, and, in general, addition of air had much less effect than in tests made at B.N.F.M.R.A. with recirculated water. Tests made in the B.N.F.M.R.A. laboratories with recirculated sea water taken from the site of the once-through test equipment gave results similar to other recirculating tests and quite different from once-through tests.

Sea water in once-through tests was filtered through nylon cloth before passing through the jets. The first two runs in Table II were carried out in winter, and it was observed that appreciable quantities of fine silt came through the filter. During the runs carried out in spring and summer much less silt passed, but considerable quantities of small marine organisms came through the jets and grew on the sides of the containing basin, specimen holders, etc.

EFFECTS OF AIR BUBBLES IN TESTS WITH RECIRCULATED WATER

B.N.F.M.R.A. investigators developed data to indicate the severity of erosive forces with respect to the jet velocity above which air bubbles were not required to produce impingement attack. Several alloys were tested with recirculated water, giving the data summarized in Table III.

Referring to data on Admiralty Brass, B.N.F.M.R.A. tests indicate that air bubbles are not essential for impingement attack when jet velocity is 22.5 ft/sec or greater. However, a similar critical velocity must be below 15 ft/sec with recirculated water at Harbor Island since, as shown by Table I, as much attack occurs with this jet velocity without air bubbles as with them. Up to now, sufficient tests have not been made under those circumstances to establish whether there is a jet test velocity with recirculated water at Harbor Island such that air bubbles exert a controlling effect. One run without air bubbles at a jet velocity of 7.5 ft/sec developed attack of Admiralty Brass to a depth of 0.19 mm. This was less attack than the 0.27 mm depth in a companion test without air bubbles at a jet velocity of 15 ft/sec. However, it appears that the jet test velocity at which zero attack of Admiralty Brass would occur in the absence of air bubbles in recirculated water at Harbor Island would be under 7.5

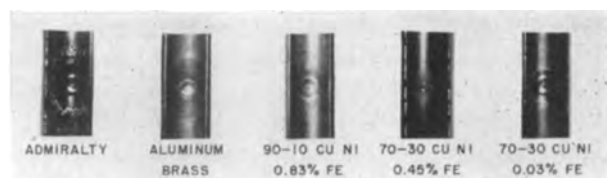


FIG. 3. Jet impingement attack of condenser tube alloys with once-through water at 15 ft/sec at Harbor Island.

ft/sec and, therefore, well under the 22.5 ft/sec critical velocity indicated by British results.

Data in the last two columns of Table III are particularly significant in showing that the effect of air bubbles observed in British tests is mechanical rather than chemical, since saturation of water with air outside the jets did not promote impingement attack, whereas admission of nitrogen through the jets did do this.

TESTS OF COMMON CONDENSER TUBE ALLOYS

As indicated by data for Admiralty Brass and Aluminum Brass in Table I, standard testing conditions with once-through water at Harbor Island may be so severe as to cause film breakdown on most of the common condenser tube alloys and thus tend to mask differences that show up under less drastic testing conditions and in common practical service. The appearance of specimens after test with once-through water at Harbor Island is shown in Fig. 3. Similar, but less severe effects occurred in once-through tests in England as shown in Table II.

Results of tests at 15 ft/sec velocity with recirculated water in the B.N.F.M.R.A. Laboratories and in once-through water at Harbor Island involving a number of common condenser tube alloys are summarized in Table IV.

While tests with once-through water at Harbor Island placed alloys in roughly the same order of merit as did the British tests, attack on the more resistant materials was much greater than in the British tests. Additional data are given in Tables V and VI. This was further evidence that Harbor

TABLE IV. Comparison of results of tests of condenser tube alloys in the B.N.F.M.R.A. laboratories and at Harbor Island

Material	Average depth of attack (mm)	
	B.N.F.M.R.A.	Harbor Island Run 12
	Testing conditions	
	Velocity of jet, 15 ft/sec	
	Air added, 3% by volume	
	Duration, 28 days	
	Water recirculated at B.N.F.M.R.A.	
	Not recirculated at Harbor Island	
Arsenical Admiralty Brass	0.34	0.28
Arsenical 70:30 brass	0.31	0.43
Arsenical copper	0.30	—
70:30 Cupro nickel, 0.04% Fe	0.11	0.23
Aluminum Brass	0.04*	0.20
70:30 Cupro nickel, 0.8% Fe	0.02	0.10**
90:10 Cupro nickel, 2% Fe	0.00	0.15

* One specimen out of 20 pitted to a depth of 0.66 mm. No other specimen greater than 0.02 mm.

** Iron content, 0.45%.

TABLE V. Typical results in recirculating jet impingement test with added air bubbles in B.N.F.M.R.A. laboratory

Run No.	N/53	Y/50	J/50	W/53	M/50	B/50
Water speed (ft/sec)	10	15	15	15	30	30
% Air by volume	3	1.5	3	3	3	5
Material	Depth of impingement attack					
70:30 Cu Ni, 0.04% Fe	0	0.11	0.06	0.04	0.56	0.46
	0.01	0.11	0.06	0.05	0.47	0.45
65:30 Cu Ni, 2% Fe	—	0	0	0	0	0.02
		0	0	0	0	0.07
70:30 Cu Ni, 0.8% Fe	0			0		
	0	—	—	0	—	—
90:10 Cu Ni, 2% Fe	0	0	0	0	0	0
	0	0	0	0	0	0
95:5 Cu Ni, 0.6% Fe	0			0		
	0	—	—	0	—	—
95:5 Cu Ni, 1.5% Fe	0	0	0.02	0	0.03	0.06
	0	0.08	0.04	0	0.01	0.06
Arsenical copper	0	0.25	0.10	0.50	0.62	—
	0	0.20	0.10	0.50	0.67	—
70:30 Brass, 0.03% As	0.59	0.22	0.28	0.49	0.61	0.61
	0.74	0.20	0.26	0.49	0.62	0.67
70:29:1 Brass, 0.03% As	0.42			0.44		
	0.05	—	—	0.45	—	—
Aluminum Brass (76:22:2 + 0.03% As)	0	0	0	0.01	0	0.34
	0	0	0	0.01	0	0

TABLE VI. Summary of a number of results with the recirculating jet impingement test at 15 and 30 ft/sec with 1.5–5% added air in B.N.F.M.R.A. laboratory

Material	15 ft/sec			30 ft/sec		
	Range of Depths mm	Average Depth mm	No. of Runs*	Range of Depths mm	Average Depth mm	No. of Runs*
70:30 Cu Ni, 0.04% Fe	0.03–0.31	0.11	11	0.11–0.73	0.40	7
70:30 Cu Ni, 0.8% Fe	0.00–0.07	0.02	9	0.00–0.14	0.02	9
65:30 Cu Ni, 2% Fe	0	0	11	0.00–0.07	<0.01	7
90:10 Cu Ni, 2% Fe	0	0	11	0.00–0.57	0.05	7
95:5 Cu Ni, 1.5% Fe	0.00–0.09	0.03	11	0.00–0.23	0.05	7
95:5 Cu Ni, 1.5% Fe Aged 600°C/30 min.	0.01–0.30	0.14	8	0.07–0.71	0.29	4
Arsenical Copper	0.08–0.61	0.30	7	0.17–0.67	0.50	3
70:30 Brass (0.03% As)	0.20–0.44	0.31	10	0.50–1.16	0.66	6
70:29:1 Brass (0.03% As)	0.14–0.51	0.34	6	0.04–0.55	0.31	6
76:22:2 Aluminum Brass (0.03% As)	0.00–0.66**	0.04**	10	0.00–0.34	~0.05	7

* Normally two specimens in each run.

** One specimen out of 20 pitted to a depth of 0.66 mm. No other specimen greater than 0.02 mm.

TABLE VII. Effect of jet velocity on impingement attack of Admiralty Brass and 90:10 cupro nickel alloy with once-through water in B.N.F.M.R.A. apparatus at Harbor Island

Testing conditions

Air added, 3% by volume

Temperature, 20°C

Duration, 28 days

Jet Velocity (ft/sec)	Depth of Impingement Attack (mm)	
	Admiralty Brass	90:10 Cupro Nickel, 2% Fe
15	0.28	0.15
12	0.35	0.13
9	0.26	0.13
7.5	0.18	0.06
6	0.25	0.05
4	0.15	0.03

Island tests were much more drastic—perhaps too drastic to permit ready evaluation of difference in resistance to impingement attack among compositions that performed well in British tests.

TESTS AT REDUCED WATER VELOCITY

An effort was made to discover whether, by reducing jet velocity, the extent of damage to the more resistant alloys by once-through water at Harbor Island could be brought into line with results secured with recirculated water in the B.N.F.M.R.A. Laboratory. Data obtained with Admiralty Brass and an iron-modified 90/10 cupro-nickel alloy as shown in Table VII illustrate results of this series of experiments.

It was evident from these results that tests with

TABLE VIII. Impingement attack of condenser tube alloys as tested in several ways

Material	15 ft/sec B.N.F.M.R.A. Lab.	15 ft/sec Once-through water in England	Depth of Impingement Attack (mm)		
			15 ft/sec Once-through water at Harbor Island	15 ft/sec Recirculated water at Harbor Island	4 ft/sec Once-through water at Harbor Island
Arsenical Admiralty	0.34	0.11	0.28	0.28	0.15
70:30 Cupro Nickel, 0.04% Fe	0.11	0.08	0.23	0.14	—
Arsenical Aluminum Brass	0.04	0.07	0.20	0.01	—
90:10 Cupro Nickel, 1.5% Fe	0.00*	0.10*	0.15	0.02	0.01
70:30 Cupro Nickel, 0.45% Fe	0.02**	0.09**	0.10	0.01	0.01

* 2% Iron.
** 0.8% Iron.

once-through water at Harbor Island might be brought into line with those obtained with recirculated water in the B.N.F.M.R.A. Laboratory if the jet velocity at Harbor Island were reduced sufficiently, e.g., to 4 ft/sec. That such was the case is shown by data for some common condenser tube alloys tested with once-through water at Harbor Island at 4 ft/sec jet velocity (Table VIII). Included in this table for convenient comparison are results for the same alloys as tested in once-through water in England and in recirculated water at both Harbor Island and the B.N.F.M.R.A. Laboratory. Appearance of specimens after these tests at Harbor Island is shown in Fig. 4 which should be compared with Fig. 3.

RELATION OF TEST RESULTS TO PERFORMANCE IN SERVICE

Results of jet impingement tests made in the laboratory of B.N.F.M.R.A. have provided a satisfactorily reliable guide in establishing relative merits of condenser tube alloys under practical conditions in marine and power plant condensers. For example, they were the basis for commercial development of Aluminum Brass as a condenser tube alloy having

resistance to impingement attack superior to that of Admiralty Brass. They also demonstrated the advantage of iron additions to cupro-nickel alloys as summarized in a recent paper (6). Therefore, since the relative performance of materials in practical service seems to be reflected better by jet impingement tests at the level of severity obtained in B.N.F.M.R.A. tests with recirculated sea water than by more drastic tests with once-through sea water at the same jet velocity (15 ft/sec) at Harbor Island, it is in order to lessen the severity of the latter testing conditions either by reducing jet velocity of once-through water to about 4 ft/sec or by recirculating water at 15 ft/sec. Of the two possibilities, use of once-through water at the lower velocity might be preferable since, in ordinary practice, sea water used for cooling passes through heat exchanger tubes only once. However, the final choice will be influenced by additional data to be accumulated at Harbor Island.

While use of a 15 ft/sec jet velocity with once-through water at Harbor Island may be too drastic to rate materials for normal service conditions, it could be of value for qualifying them for exceptionally severe conditions. For example, Fig. 5 shows specimens of three alloys that remained free from impingement when tested with once-through water at 15 ft/sec at Harbor Island. Presumably these alloys will perform well where service conditions are too severe for ordinary condenser tube compositions.

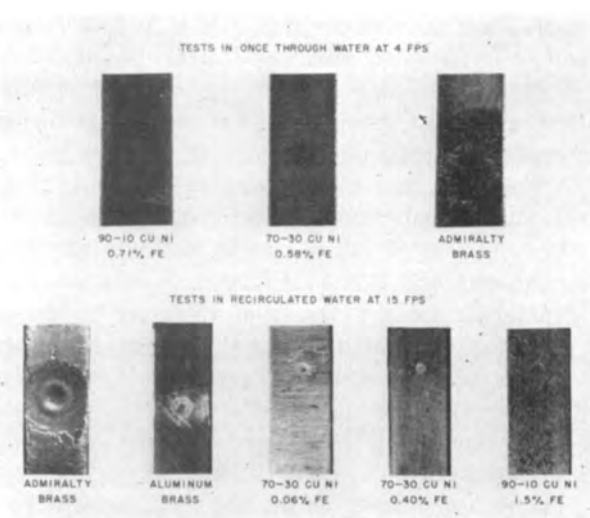


FIG. 4. Tests at Harbor Island

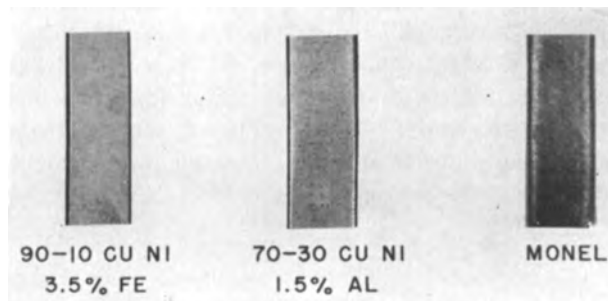


FIG. 5. Alloys resistant to jet impingement attack with once-through water at 15 ft/sec at Harbor Island.



FIG. 6. Pitting of Aluminum Brass around supports in recirculated water to which silt was added at Harbor Island.

CAUSES OF DIFFERENCE BETWEEN ONCE-THROUGH AND RECIRCULATED WATER AT HARBOR ISLAND

In view of difference in behavior of certain alloys in once-through and recirculated water as illustrated by Table VIII, there have been many speculations as to the underlying cause or causes. Measurements of *pH* and the Copper Corrosion Index² in once-through and recirculated water showed no variations in these factors that would account for the difference in results. However, there was a strong feeling that the critical factor was in some way affected by biological influence. This would be based on the abundance of plankton in the once-through water and its scarcity in recirculated water from which it settled out in the tests at Harbor Island or was filtered out in tests in the B.N.F.M.R.A. Laboratory. These organisms could exert both chemical and mechanical effects, the latter through abrasive action of the animals or their hard skeletons, e.g., the silicious material in diatoms. At present, there has been insufficient opportunity to settle the matter, but experiments at Harbor Island introducing silt that had settled from flowing water indicated that organic material in suspension may be important. A method for increasing and controlling the amount of suspended matter in recirculated water has not yet given reproducible results. However, there have been strong indications that the presence of suspended organisms or their skeletons may make recirculated water as aggressive toward some materials as is once-through water. This has been observed especially with iron-modified 90/10 cupro-nickel alloys. Intensity of attack on Admiralty Brass has not been increased by silt additions, and high-iron 70/30 cupro-nickel alloy has resisted impingement attack equally well in the presence or absence of added silt.

² The Copper Corrosion Index was developed by Rogers (7) as a means of comparing corrosivity of different samples of sea water, particularly as it might be influenced by contaminants resulting from biological activity.

Presumably the principal effect of suspended matter is to promote removal of protective films under action of the jet. In addition, there appear to be some chemical effects, principally in the form of severe corrosion of Aluminum Brass specimens in crevices that exist where they are attached to their specimen holders (Fig. 6).

The reason for the anomalous situation that tests with recirculated water give better correlation with practical experience than once-through tests may be connected with the fact that ships normally steam at full power for long periods only in the open sea where there is little suspended matter. Occurrence of fine silt and small marine organisms capable of causing abnormal corrosive effects may be confined mainly to coastal waters.

Results of all tests given in this paper were obtained using clean or relatively clean sea water. Very different effects and much more severe attack have been obtained from time to time in the B.N.F.M.R.A. Laboratory using naturally polluted sea water samples.

CONCLUSIONS

Severity of jet impingement tests with once-through sea water at Harbor Island was much greater than with recirculated sea water under otherwise similar testing conditions in laboratories of the British Non-Ferrous Metals Research Association. Materials that were badly attacked in recirculated water were, however, no more severely attacked in once-through water.

Tests with once-through water in England gave less severe attack than those with once-through water at Harbor Island, but results otherwise were very similar.

Under severe impingement test conditions it was not necessary to have air bubbles in the water for attack to occur. Air bubbles had more effect in recirculated water in the B.N.F.M.R.A. Laboratory than in recirculated water at Harbor Island.

Relative behavior of common condenser tube alloys when tested at the level of severity provided by tests with recirculated water at 15 ft/sec in the B.N.F.M.R.A. Laboratory was in line with their performance under many conditions of practical use.

Tests at Harbor Island can be made to duplicate results from the B.N.F.M.R.A. Laboratory either by reducing jet velocity from 15 ft/sec to about 4 ft/sec, or by recirculating the water at 15 ft/sec.

The presence of suspended plankton in the water at Harbor Island is suspected as being the principal factor in increasing the severity of tests with once-through water.

The greater severity of the test with once-through water at Harbor Island should provide a means for

qualifying materials to resist exceptionally severe conditions of impingement attack in practical service.

ACKNOWLEDGMENT

Several past and present staff members of The British Non-Ferrous Metals Research Association assisted in carrying out part of the work reported in this paper, and their help is gratefully acknowledged. Thanks are also due the Director and Council of the Association for permission to publish results.

The authors wish to acknowledge the help of the staff at International Nickel Company's Harbor Island Test Station in performing tests that were undertaken there.

Any discussion of this paper will appear in a Discussion Section to be published in the June 1955 issue of the JOURNAL.

REFERENCES

1. G. D. BENGOUGH AND R. MAY, *J. Inst. Metals*, **32**, 81 (1924).
2. R. MAY, *ibid.*, **40**, 141 (1928).
3. R. MAY AND R. W. DEVERE STACPOOLE, *ibid.*, **77**, 331 (1950).
4. F. L. LAQUE AND W. C. STEWART, *Metaux & corrosion*, **23** [274], 147 (1948).
5. F. L. LAQUE AND J. F. MASON, JR., Paper presented before Corrosion Session, American Petroleum Institute, Division of Refining, May 1950.
6. G. L. BAILEY, *J. Inst. Metals*, **79**, 243 (1951).
7. T. H. ROGERS, *ibid.*, **76**, 597 (1950).

Effect of Rapid Cathode Rotation and Magnetic Fields on Crystal Orientation in Electrodeposited Metals¹

LING YANG

Metals Research Laboratory, Carnegie Institute of Technology, Pittsburgh, Pennsylvania

ABSTRACT

Crystal orientations in metals electrodeposited on a cathode rotating at 3000 rpm were studied by electron diffraction; results were compared with those on a stationary cathode. It was found that orientation could (a) be destroyed, (b) be changed to another type, or (c) remain unchanged. These observations were satisfactorily explained by considering the effect of the forced convection of rotation on the nature of the diffusion layer surrounding the cathode and, thus, on the amount of hydrogen codeposited, the latter being known as an important factor controlling the crystal orientation in electrodeposited metals. Under bath conditions used in this work, presence of a magnetic field of 5400 gauss strength, either perpendicular or parallel to the cathode, had no effect on the types of crystal orientation in iron, nickel, and cobalt deposits. However, when the field was perpendicular to the cathode, the surface of these deposits became very rough and covered with projections protruding in the direction of the field. A possible explanation of this observation was given.

INTRODUCTION

In previous investigations (1-12) of how various factors affect the crystal orientation in electrodeposited metals, attention has chiefly been paid to factors normally present during electrodeposition, such as bath temperature, bath composition, and current density. It seems to be of interest to extend the study to factors which are not always present but which are imposed purposely. Attempts have been made to study the effect of two of these factors—high speed rotation of the cathode and the presence of a magnetic field.

EFFECT OF HIGH SPEED ROTATION OF CATHODE

Experimental

The cathode was a brass disk 1 mm thick and 2 cm in diameter. A small brass nut was soldered to the center of one face of the disk, through which the disk could be screwed to the axis of the driving motor, while the other side of the disk (the working side) was polished and degreased. All the metal parts in contact with the electrolytic solution, except the working side of the disk, were covered with a thin layer of polythene to prevent deposition. The driving motor was held vertical and the disk cathode was screwed to its axis with the polished working side downward facing a horizontally disposed stationary anode (5 cm x 5 cm x 1 mm) about 3 cm away. The bath container was a one-liter beaker about three-fourths filled with the desired electrolyte and the cathode was about 5 cm below the liquid level. During deposition, the electric connec-

tion to the rotating cathode was made through a slip ring. Motor speed was 3000 rpm, as measured with a Hasler tachometer. For comparison, each experiment was run twice, one on a rotating cathode and the other on a stationary cathode under the same bath conditions.

Crystal orientation in the deposited metal was studied by electron diffraction for two reasons. Firstly, owing to the low penetration of electron beam, the structures of the deposit could be studied without interference from the substrate. Secondly, because of the high intensity of the diffraction pattern shown on the fluorescent screen, different regions of the deposit surface could readily be examined by moving the focused beam across it.

Electrolytic baths were all prepared from chemically pure reagents and further purified by electrolysis. Anodes were all electrolytic metals. Compositions of the baths in grams per liter are: (a) nickel, $\text{NiSO}_4 \cdot 7\text{H}_2\text{O}$ 240, H_3BO_3 30, $\text{pH} = 2.9$; (b) iron, $\text{FeSO}_4 \cdot (\text{NH}_4)_2\text{SO}_4 \cdot 6\text{H}_2\text{O}$ 350, H_2SO_4 2.5; (c) silver, AgCN 35, KCN 37, K_2CO_3 38; (d) copper₁, $\text{CuAc}_2 \cdot 2\text{H}_2\text{O}$ 25, $\text{Na}_2\text{SO}_3 \cdot \text{H}_2\text{O}$ 50, KCN 35, Na_2CO_3 10; (e) copper₂, $\text{CuSO}_4 \cdot 5\text{H}_2\text{O}$ 200, H_2SO_4 30; (f) antimony, SbCl_3 200, HCl (conc) 300 cc.

Results and Discussions

In all cases studied (see Table I and Fig. 1 and 2), orientations of crystals deposited on the rotating cathode, as compared with those on stationary cathode, fall into three categories according to whether (a) crystal orientation was destroyed, (b) crystal orientation was changed to the type in which the most densely packed lattice plane was parallel to

¹ Manuscript received July 23, 1953.

TABLE I. Influence of rotation of cathode (3000 rpm) on the crystal orientation of electrodeposited metals

Deposit	Bath temp (°C)	Current density (amp/dm ²)	Current efficiency (%)	Orientation
Ni*	20	1.25	90	(110)
Ni†	20	1.25	45	Random
Ni*	52	1.25	95	(100)
Ni†	52	1.25	55	Random
Fe*	20	3.75	90	(111)
Fe†	20	3.75	25	Random
Fe†	20	7.50	85	(111)
Ag*	20	3.00	80	Weak (110)
Ag†	20	3.00	100	Weak (111)
Cu ₁ *	80	0.75	75	(110)
Cu ₁ †	80	0.75	90	(111)
Cu ₂ *	20	1.25	98	(110)
Cu ₂ †	20	1.25	98	(110)
Sb*	20	0.10	100	Amorphous
Sb†	20	0.10	100	Amorphous
Sb*	75	0.65	92	(100)
Sb†	75	0.65	93	(100)

Note: Deposit thickness, 2.5–5 μ .

* Deposit on stationary cathode.

† Deposit on rotating cathode.

the substrate, or (c) crystal orientation was unaffected.

For all three cases, the type and the degree of the orientation persisted over the whole cathode surface. This indicates that at 3000 rpm the influence of rotation of the cathode on the crystal orientation of the deposited crystals could not be due to the centrifugal forces produced by the rotation. If this were the case, observed changes in crystal orientation in (a) and (b) would vary with the radial position of the crystals on the disk cathode. These changes, however, were found to be accompanied always by a pronounced change in current efficiency, suggesting a modification of the nature of the diffusion layer contiguous to the cathode surface by the forced convection introduced by rotation. This is discussed below in the light of examples under headings of the three above-mentioned cases.

Crystal Orientation Destroyed

Data for nickel and iron indicate that, where rotation of the cathode decreases current efficiency, crystal orientation may be destroyed by rotation. Loss of crystal orientation in these cases is, therefore, probably due to disturbances caused by the excessive amount of codeposited hydrogen on the rotating cathode.

The relation between current efficiency and rotation of the cathode can be explained as follows. It

was first postulated by Nernst and later proved experimentally by many investigators that a thin layer of liquid surrounds the surface of the cathode and that ionic concentrations there differ from those in the bulk of the solution. Replenishment of the ions used up at the cathode surface must be made by diffusion and transport through this layer. Although this theory has been criticized by Eucken (13), Levich (14), and Agar (15), the idea is still useful for the present qualitative explanation of results. Based on this theory, actual concentrations of the deposited ions at the cathode surface are therefore determined, on the one hand, by the rate of removing them by deposition and, on the other hand, by the rate of replenishment through the diffusion layer. The latter is usually less than the former at the beginning of the deposition, and they do not

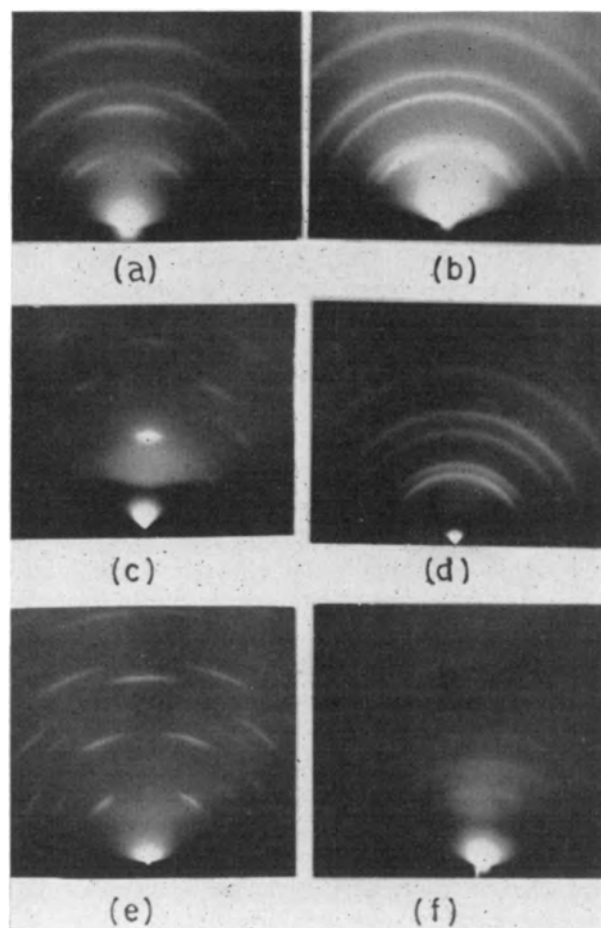


FIG. 1. Examples of crystal orientation destroyed by rotation of cathode. Left hand column, stationary cathode; right hand column, rotating cathode, 3000 rpm. Top, nickel: sulfate bath, 20°C, 1.25 amp/dm², 5 x 10⁴ Å thick; (a) (110) current efficiency 90%; (b) random, current efficiency 45%. Center, nickel:sulfate bath, 52°C, 1.25 amp/dm², 4 x 10⁴ Å thick; (c) (100) current efficiency 95%; (d) random, current efficiency 55%. Bottom, iron:sulfate bath, 20°C, 3.75 amp/dm², 5 x 10⁴ Å thick; (e) (111) current efficiency 90%; (f) random, current efficiency 25%.

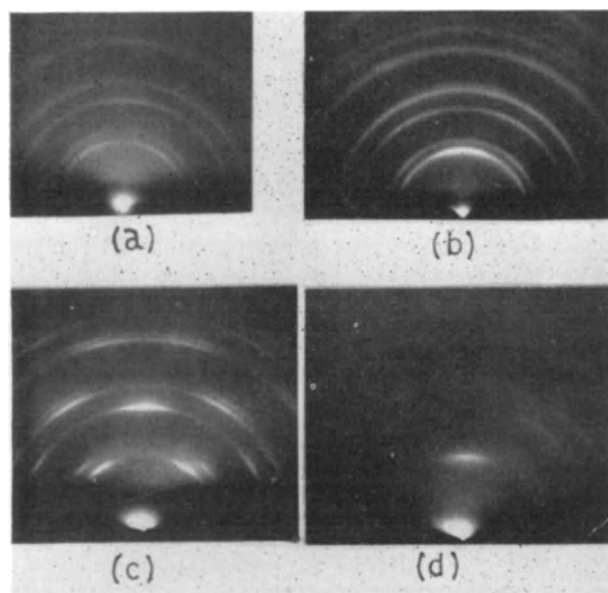


FIG. 2. Examples of crystal orientation changed by rotation of cathode. Left hand column, stationary cathode; right hand column, rotating cathode, 3000 rpm. Top, silver: cyanide bath, 20°C, 3 amp/dm², 3.5×10^4 Å thick; (a) weak (110), current efficiency 80%; (b) weak (111), current efficiency 100%. Bottom, copper:cyanide bath, 80°C, 0.75 amp/dm², 2.5×10^4 Å thick; (c) (110), current efficiency 75%; (d) (111), current efficiency 90%.

become equal until a steady state has been reached in which concentrations of the depositable ions at the cathode surface are more or less impoverished and give rise to concentration polarization.

Under conditions such that hydrogen ions can codeposit with metal ions, both types of ions are impoverished at the cathode surface, but the extent of their impoverishment may not be equal. For the nickel and iron baths used here, the hydrogen ion is apparently more susceptible to depletion than metal ions, as indicated by the facts that the amount of codeposited hydrogen is decreased by increasing the current density, and that the pH value of the solution at the cathode surface is so high that basic metal hydroxides are precipitated and included in the deposit (16, 17). This low hydrogen ion concentration at the cathode surface lessens the amount of codeposited hydrogen and hence the disturbances to the growth of metal crystals. The deposit is, therefore, highly oriented.

However, if the cathode is rotated at high speed, forced convection produced by rotation decreases the thickness of the diffusion layer. For a circular disk rotating about an axis passing through its center, Levich (18) has shown that the thickness of the diffusion layer is inversely proportional to the square root of the speed of rotation. This decrease of thickness of the diffusion layer increases the rate of ion supply, particularly hydrogen ion,

to the cathode surface. As a result, hydrogen ion concentration at the cathode surface and the amount of codeposited hydrogen increase. Thus, there is increasing disturbance to the growth of deposited crystals. When the disturbance is severe enough, deposited crystals become randomly disposed.

If this explanation is true, a higher current density would outweigh the increased rate of diffusion of hydrogen ions to the cathode surface because of cathode rotation. In other words, increased current efficiency may give oriented deposits even when the cathode is rotated. This was the case. Iron deposited from the sulfate bath at 20°C and 3.75 amp/dm² on a cathode rotating at 3000 rpm in randomly arranged crystals, the current density being 25%; by increasing current density to 7.50 amp/dm², current efficiency increased to 85% and the deposited crystals showed (111) orientation.

Crystal Orientation Changed

If rotation of the cathode causes a marked increase in current efficiency, deposited crystals may change from the type of orientation characteristic of prevailing bath conditions on a stationary cathode to the type in which the most densely packed lattice plane is parallel to the substrate. This is illustrated in Table I by the cases of silver and copper deposited from their cyanide baths.

This change of orientation can be explained in the same way as that in the previous section. In these cyanide baths, it is the metal ions which are more susceptible to depletion than the hydrogen ion, as shown by the fact that current efficiency decreases rapidly when current density is increased. Since the forced convection caused by rotation of the cathode decreases the thickness of the diffusion layer on the cathode surface, the metal ion concentration near the cathode surface is increased, and so is the current efficiency. Decrease in codeposited hydrogen diminishes the disturbance to the growth of the deposited crystals and, consequently, these crystals show a preferred orientation with the most densely packed lattice plane parallel to the substrate. The latter is the type of orientation developed in most metals deposited under bath conditions involving little or no disturbance to the growth of crystals.

Crystal Orientation Unaffected

If rotation of the cathode causes little or no change in the current efficiency of the deposition, then the crystal orientation of the deposit likewise remains unchanged, no matter whether the cathode is rotating or stationary. This is illustrated by copper deposited from a sulfate bath and antimony deposited from a chloride bath, as shown in Table I.

EFFECT OF MAGNETIC FIELD

Various attempts to study the influence of a magnetic field on the mode of crystal growth have almost all led to negative results. For example, Bergala and Gorskii (19) found that the rates of crystallization of water, salol, and diphenylamine were unchanged by fields up to 17,000 gauss. Steacie and Stevens (20) reported that a field of 5000 gauss had no effect on the rate of crystallization of sodium thiosulfate from its supersaturated solution, but for nickel sulfate a slightly increased rate was noted. Bozorth (2) could not find any change in the amount of crystal orientation of electrodeposited nickel when deposition was carried out in a magnetic field of unspecified strength. Cobalt was electrodeposited in a magnetic field of several hundred oersted strength (21) and iron, nickel, and cobalt were electrodeposited in a magnetic field of 12,000 oersted strength (22), but the crystal orientations of the deposit were not studied. The purpose of the present work was to find out whether the presence of a magnetic field of 5400 gauss strength could modify the crystal orientation of electrodeposited iron, nickel, and cobalt.

Experimental

A horse-shoe permanent magnet having a field strength of 5400 gauss was used. The poles were

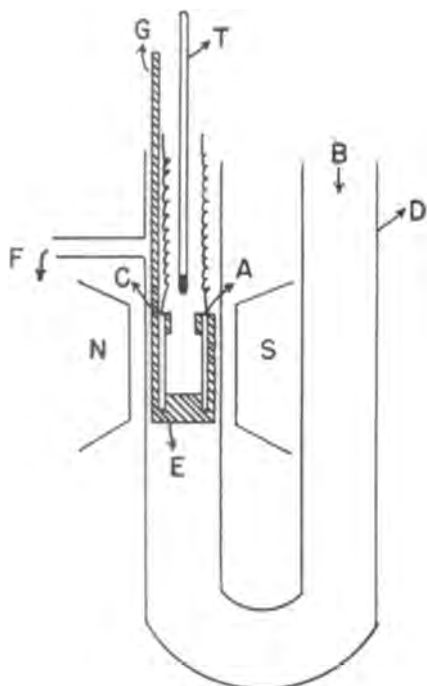


FIG. 3. Arrangements for electrodeposition in a magnetic field. A—anode; B—entrance for fresh solution; C—cathode; D—tube containing electrolytic solution; E—Bakelite frame for supporting electrodes; F—exit for used solution; G—arm of Bakelite frame; N, S—poles of magnet; T—thermometer.

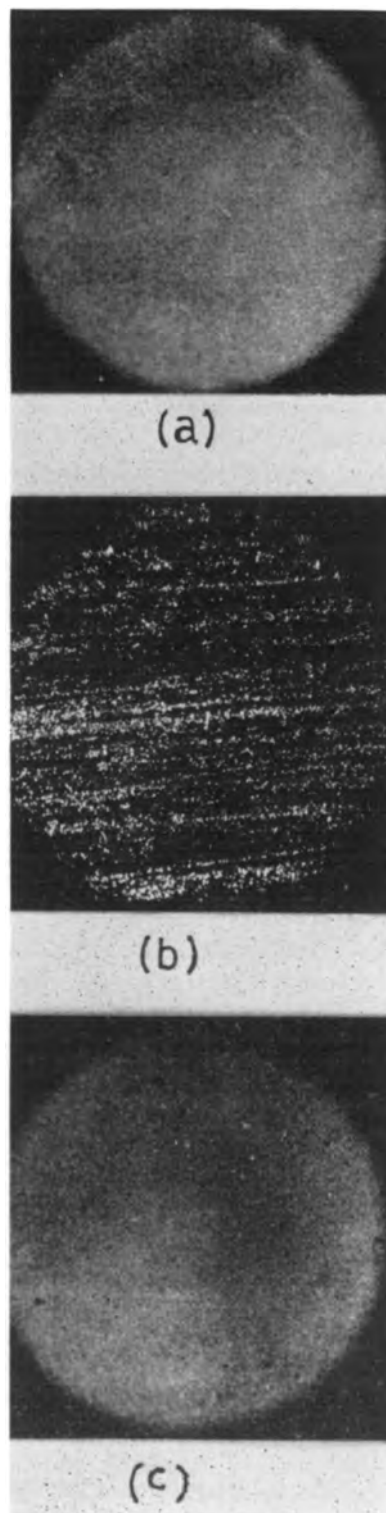


FIG. 4. Appearance of iron electrodeposited on brass from a sulfate bath at 80°C and 3.75 amp/dm^2 . (a) In the absence of magnetic field; (b) specimen surface is perpendicular to the direction of a magnetic field of 5400 gauss strength; (c) specimen surface is parallel to the direction of the magnetic field. Time of deposition, 10 min. $15\times$.

circular (diameter 2.0 cm) and the pole gap was 1.2 cm. The small size of the pole gap limited the dimensions of the solution container which was a U-tube of 1 cm diameter. One of its arms containing the electrodes was put into the pole gap of the magnet. Through the other arm, fresh solution was introduced slowly, after passing the lower part of the U-tube immersed in a constant temperature bath, to displace the solution which had been impoverished of the deposited ions (Fig. 3). The electrodes, both of which were 0.4 cm x 0.6 cm x 0.1 cm, were fixed rigidly on a Bakelite frame, at a distance of about 0.4 cm, and one arm of the frame was held by a copper clamp. The cathode was a brass plate, polished and degreased, and the anode was a piece of electrolytic metal of the kind to be deposited. Electrodes were immersed about 1 cm below the liquid level and all immersed surfaces of the electrodes, except the facing areas, were coated with collodion.

Compositions of the nickel and iron baths used were the same as described above, while the cobalt bath contained 200 g of $\text{CoSO}_4 \cdot (\text{NH}_4)_2\text{SO}_4 \cdot 6\text{H}_2\text{O}$ and 30 g of H_3BO_3 /l ($\text{pH} = 3.0$). Deposition of nickel was carried out at 1.25 amp/dm², 20° and 60°C; that of iron at 3.75 amp/dm², 20° and 80°C; and that of cobalt at 2.50 amp/dm² and 20°C.

Crystal orientations in the deposits were studied by electron diffraction, but the specimen had to be demagnetized before it was put into the camera because of the interaction between the electron beam and the magnetic field of the specimen. Each experiment was done in three ways: without magnetic field; with field parallel to the surface of the electrodes; and with field perpendicular to the surface of the electrodes.

RESULTS

No change in the types of crystal orientation of nickel, iron, and cobalt deposits was observed as a result of the presence of a magnetic field of 5400 gauss. The iron deposit showed (111) orientation at 20°C and (110) orientation at 80°C; the nickel deposit showed (110) orientation at 20°C and (100) orientation at 60°C; and the cobalt deposit was a mixture of face-centered-cubic and hexagonal-close-packed forms showing (110) and (11 $\bar{2}$ 0) orientations, respectively. However, when the field was perpendicular to the surfaces of the electrodes, the deposit surface became very rough and covered with projections protruding in the direction of the field. This is evident from Fig. 4(a), (b), and (c), showing photomicrographs of the surfaces of iron deposited from a sulfate bath at 80°C and 3.75 amp/dm² for 10 min, (a) with no field, (b) with a magnetic field normal to the deposit surface, and (c) with a magnetic field parallel to the deposit surface. The deposit seemed to grow predominantly

on the ridges resulting from the polishing of the substrate. If the deposit was made on an iron substrate instead of on a brass one, this tendency was even more pronounced. No such phenomenon was observed, however, for copper deposited from an acid sulfate bath and antimony from a chloride bath.

It is tentatively suggested that the effect is due in part to the magnetic lines of force being more concentrated near the projecting parts on the surface of the brass substrate after the latter had been coated with ferromagnetic deposits. It is possible that this uneven distribution of field along the cathode surface causes an uneven distribution of Fe^{++} , Ni^{++} , and Co^{++} concentrations there, since these ions are paramagnetic, with the result that metal ion concentration is higher near these projecting regions and thus facilitates deposition there. The fact that the crystal orientation of the deposit is not affected suggests that this outgrowth is merely a macroscopic phenomenon and that the tendency of the growth of the crystal nuclei in iron, nickel, and cobalt deposits is not affected by a magnetic field of the strength used.

Any discussion of this paper will appear in a Discussion Section to be published in the June 1955 issue of the JOURNAL.

REFERENCES

1. R. GLOCKER AND E. KAUPP, *Z. Physik*, **24**, 121 (1924).
2. R. M. BOZORTH, *Phys. Rev.*, **26**, 390 (1925).
3. G. I. FINCH AND C. H. SUN, *Trans. Faraday Soc.*, **32**, 852 (1936).
4. G. I. FINCH AND A. C. WILLIAMS, *ibid.*, **33**, 564 (1937).
5. W. HUME-ROTHERY AND M. R. J. WYLLIE, *Proc. Roy. Soc.*, **A181**, 331 (1943).
6. G. I. FINCH, H. WILMAN, AND L. YANG, *Discussion Faraday Soc.*, **1**, 144 (1947).
7. M. R. J. WYLLIE, *J. Chem. Phys.*, **16**, 52 (1948).
8. L. YANG, *This Journal*, **97**, 241 (1950).
9. W. SMITH, J. H. KEELER, AND H. J. READ, *Plating*, **36**, 355 (1949).
10. G. L. CLARK AND S. H. SIMONSEN, *This Journal*, **98**, 110 (1951).
11. H. LEIDHEISER, JR., AND A. T. GWATHMEY, *ibid.*, **98**, 225 (1951).
12. A. BRENNER, V. ZENTNER, AND C. W. JENNINGS, *Plating*, **39**, 865 (1952).
13. A. EUCKEN, *Z. Elektrochem.*, **38**, 341 (1932).
14. B. LEVICH, *Discussion Faraday Soc.*, **1**, 37 (1947).
15. J. N. AGAR, *ibid.*, **1**, 26 (1947).
16. D. J. MACNAUGHTAN, G. E. GARDAM, AND R. A. F. HAMMOND, *Trans. Faraday Soc.*, **29**, 729 (1933).
17. G. E. GARDAM AND D. J. MACNAUGHTAN, *ibid.*, **29**, 755 (1933).
18. B. LEVICH, *Acta Physicochim.*, *U. R. S. S.*, **17**, 257 (1942).
19. R. YA BERLAGA AND F. K. GORSKII, *J. Exp. Theor. Phys.*, *U. R. S. S.*, **4**, 527 (1934).
20. E. W. R. STEACIE AND C. F. B. STEVENS, *Canadian J. Res.*, **10**, 483 (1934).
21. A. PERRIER AND C. MERMOD, *Helv. Phys. Acta*, **11**, 362 (1938).
22. A. PERRIER, C. MERMOD, AND E. BESSE-WALTER, *Helv. Chim. Acta*, **26**, 1861 (1943).

Role of Sulfur in the Luminescence and Coloration of Some Aluminosilicates¹

RUSSELL D. KIRK

Dielectrics Branch, Solid State Division, Naval Research Laboratory, Washington, D. C.

ABSTRACT

Certain complex, sulfur-containing sodalite-type silicates, synthesis of which is described, exhibit under 3650 Å excitation an emission extending from 5000 Å to beyond 7000 Å, the spectrum varying with composition. The band structure of this emission at -196°C is similar to the emission structure shown by a mixture of Na₂S_x and Na₂SO₄. It is concluded that luminescence is due to the presence of Na₂S_x, which replaces part of the NaCl normally present in sodalite.

Synthetic sodalites containing both NaCl and Na₂S are tenebrescent, coloring purple on irradiation with 2537 and 3650 Å ultraviolet.

INTRODUCTION

The orange-yellow luminescence of certain forms of the mineral sodalite has long been known (1). The variety of sodalite known as hackmanite is not only luminescent, but is tenebrescent as well. It colors rapidly from white to red-purple on exposure to a short-wave ultraviolet source (2-4). Visible light causes a bleaching of the color. Medved (5) prepared sodalite which colored under 2537 Å ultraviolet by firing synthetic sodalite in hydrogen.

The purpose of this investigation was to duplicate the luminescence and tenebrescence of natural sodalite with synthetic products and to obtain more information concerning the centers involved.

Since it is known that sulfur compounds are often present in natural sodalite, it was suspected that sulfur may play a role in luminescence and tenebrescence.

Gobrecht and Hahn (6), who first reported and described the luminescence of polysulfides, prepared a large number of alkali polysulfides and partially reduced alkali sulfates by various methods. They found in many of the products a red luminescence under 3650 Å excitation and a blue emission on exciting with 2537 Å radiation. These workers ascribe the red emission to the presence of polysulfide ion and the blue to alkali metal activation of sulfate.

The present work confirms some of the results obtained by Gobrecht and Hahn and describes the preparation and properties of a group of sodalite-type compounds which, in some cases, show both luminescence and tenebrescence.

EXPERIMENTAL METHODS

Preparation

Sodalite has the composition 3(Na₂O·Al₂O₃·2SiO₂)·2NaCl, the natural sulfate analog (the mineral noselite), 3(Na₂O·Al₂O₃·2SiO₂)·Na₂SO₄. The synthetic sodalite-type compounds prepared for this work contain, in place of NaCl, combinations of NaCl, Na₂SO₄, and Na₂S_x in varying amounts such that they have the general composition 3(Na₂O·Al₂O₃·2SiO₂)·XNaCl·YNa₂S_x·ZNa₂SO₄, where X + 2(Y + Z) = 2. Thus within the parameters of this formula, one Na₂SO₄ or one Na₂S_x replaces 2NaCl.

The following reagents were used in the preparations: Linde "A" aluminum oxide, Mallinckrodt's Special Bulky grade silicic acid, and the usual C.P. grades of sodium carbonate, sodium chloride, and sodium sulfate.

Dry mixing methods were used for the sodalite products, since traces of nonvolatile residues introduced by milling in organic liquids caused some reduction of the sulfate on firing, and some of the components are water soluble. Desired quantities of the starting compounds were mixed by stirring together the dry powders, prefiring in silica dishes at 750°C in air, and grinding the resulting cake in an automatic mortar. Prefiring and grinding operations were repeated several times to insure intimate mixing and complete reaction.

When Na₂S was to be introduced into the sodalites, this was done by hydrogen reduction of the Na₂SO₄ which had been prefired into the mixture.

The final firing, whether in helium, hydrogen, or air, was for two hours at 900°C.

Several sodalite sample series were prepared with varying ratios of Na₂S/Na₂SO₄ and of (Na₂S +

¹ Manuscript received November 12, 1953. This paper was prepared for delivery before the New York Meeting, April 12 to 16, 1953.

Na_2SO_4)/NaCl within the series. Thus, end members of a particular series had the composition $3(\text{Na}_2\text{O} \cdot \text{Al}_2\text{O}_3 \cdot 2\text{SiO}_2) \cdot X\text{NaCl} \cdot Y\text{Na}_2\text{S}$ and $3(\text{Na}_2\text{O} \cdot \text{Al}_2\text{O}_3 \cdot 2\text{SiO}_2) \cdot X\text{NaCl} \cdot Z\text{Na}_2\text{SO}_4$. Intermediate members were made by grinding together the previously fired end members in the desired ratios and firing the mixtures in dried helium. Only the end member sulfide-containing sodalites fired in hydrogen are believed to contain sulfide as Na_2S . Products prepared by firing an end member containing Na_2S with one containing Na_2SO_4 are, for reasons stated in the discussion section, believed to contain Na_2S_x , where $x > 1$. Since the amount of Na_2S_x formed is not known, compositions given in the text and figures hereafter will, for simplicity, refer to the mole ratio of components used in the preparation and are not intended to represent the final chemical composition.

In this paper, the terms "sodalite compounds" and "sodalites" will be used to describe the sodalites with sodium sulfate or sodium sulfides substituting partially or completely for sodium chloride. Strictly speaking, these are not sodalite, although they are closely related crystallographically and chemically.

Sodium polysulfide-sulfate mixtures were prepared in a manner similar to that used by Gobrecht and Hahn, i.e., by heating $\text{Na}_2\text{S}_2\text{O}_3 \cdot 5\text{H}_2\text{O}$ or Na_2SO_3 in air at 900°C until most of the polysulfide sulfur first produced was oxidized. This state is reached when the solidified melt is translucent, has a very pale yellow color, and shows a yellow luminescence under a 3650 \AA source. The time necessary to reach this stage depends upon empirical conditions such as the amount of exposed surface and the degree of air circulation in the furnace.

A polysulfide mixture with a red visible emission under 3650 \AA excitation was prepared from Na_2SO_3 by the same method, except that the heating was stopped while a large proportion of polysulfide was still present in the melt. The resulting solidified mixture is opaque yellow in visible light.

$\text{Na}_2\text{S}_2\text{O}_3$ is known to decompose on heating into Na_2S_x and Na_2SO_4 . Na_2SO_3 disproportionates on heating into Na_2SO_4 and Na_2S , the latter oxidizing readily in air to polysulfide and other products, even at room temperature. Since the ratio of Na_2S_x to Na_2SO_4 in the decomposition products is not known, the mixture, for the sake of brevity, will be designated as $\text{Na}_2\text{S}_x \cdot n\text{Na}_2\text{SO}_4$.

All products made by heating $\text{Na}_2\text{S}_2\text{O}_3$ or Na_2SO_3 which luminesced either yellow or red gave a positive test for polysulfide with the reagent used by Gobrecht and Hahn. The formation of a purple color with this complex cobaltic-dimethylglyoxime-aniline reagent is claimed by the discoverers, Beato

and Brügger (7) to be a specific test for the polysulfide ion.

Physical Measurements

Luminescence of the preparations was observed under a 100-watt, high-pressure mercury lamp with red-purple Corex + Corning #5860 filters unless otherwise specified. Emission spectra were obtained with an automatically recording spectroradiometer with the above exciting source and filters.

Excitation spectra were determined in the usual manner with a Beckman hydrogen lamp and monochromator. The spectra illustrated are corrected to equal energy of excitation.

Tenebrescence was observed after exposure to various sources. $1850 \text{ \AA} + 2537 \text{ \AA}$ radiation was obtained from an unfiltered, low-pressure, silica-envelope mercury arc; 2537 \AA radiation, from the same lamp with a Corning #9863 filter. The 3650 \AA source was the above-mentioned high-pressure mercury lamp and filters; the soft x-ray irradiation used was that from a Machlett Type OEG 60 tube with a tungsten target.

Reflection spectra were obtained by means of an automatically recording apparatus described by Schulman and Klick (8).

Visual observations on the luminescence and tenebrescence of the synthetic products described in this paper are summarized in Tables I and II, respectively.

Excitation curves for sodium polysulfide-sulfate from $\text{Na}_2\text{S}_2\text{O}_3$ and all the synthetic sodalite products were identical. The relative excitation spectra extend from 2500 to 5000 \AA with a single peak at 4000 \AA as shown for a typical sample in Fig. 1.

TABLE I. Luminescence properties of synthetic sodalites

$3(\text{Na}_2\text{O} \cdot \text{Al}_2\text{O}_3 \cdot 2\text{SiO}_2)$ with:	Emission color, 3650 \AA excitation	Color in white light
NaCl.....	None	White
Na_2SO_4	None	White
Na_2S	None†	Gray
$\text{NaCl} + \text{Na}_2\text{S}$	None†	Gray
$\text{Na}_2\text{SO}_4 + \text{Na}_2\text{S}^*$	Orange-yellow	White‡
$\text{NaCl} + \text{Na}_2\text{SO}_4$	None	White
$\text{NaCl} + \text{Na}_2\text{S} + \text{Na}_2\text{SO}_4^*$...	Orange-yellow	White‡
$\text{NaCl} + \text{Na}_2\text{SO}_4$ fired in sulfur vapor.....	Orange-yellow	White

* Starting composition. As stated in the text, this composition is believed to produce Na_2S_x on firing.

† When ordinary reagent grade aluminum oxide was used in place of Linde "A" in the Na_2S -containing preparations, a weak green luminescence with afterglow was observable. This may possibly be the iron activated Na_2S luminescence described by Tiede and Reinicke (9).

‡ Samples containing both sulfate and sulfide occasionally had small amounts of blue or green ultramarine on the outside of the cake.

TABLE II. Tenebrescence properties of synthetic sodalites

3(Na ₂ O·Al ₂ O ₃ ·2SiO ₂) with:	Firing atmosphere	X-rays	Radiation			Day-light
			1850+2537 Å	2537 Å	3650 Å	
NaCl	Air	+	-	-	-	-
NaCl, Na ₂ SO ₄	Air	+	+	-	-	-
NaCl, Na ₂ S	H ₂	+	+	+	+	+
NaCl, Na ₂ S, Na ₂ SO ₄	He	+	+	+	+	-
NaCl, Na ₂ SO ₄	S vapor + He	+	+	-	-	-
Na ₂ SO ₄	Air	-	-	-	-	-
Na ₂ S	H ₂	-	-	-	-	-

+ = purple color after exposure.
 - = no color after exposure.

The sodium polysulfide-sulfate prepared from thiosulfate or sulfite exhibits, in addition to the yellow-appearing, 3650 Å-excited emission, a blue luminescence under 2537 Å irradiation. The excitation peak for the blue emission was found to be at 2450 Å, the emission maximum, at 4600 Å. These results are similar to those obtained for "alkali-metal-activated" alkali sulfates by Gobrecht and Hahn, who found an excitation band from 2400 to 2900 Å and emission from 3600 to 5150 Å, peaking at 4300 Å. This blue emission and its excitation band can be found in products prepared by heating Na₂S₂O₃ or Na₂SO₃ until the solidified melt is white and no emission is observable under 3650 Å excitation. The synthetic sodalites do not show this blue emission.

Emission spectra of the synthetic sodalites and of Na₂S₂·nNa₂SO₄ from the thiosulfate are shown in Fig. 2 and 3 for 20°C and -196°C, respectively. Although the luminescence colors are yellow and red at the two respective temperatures, the emission

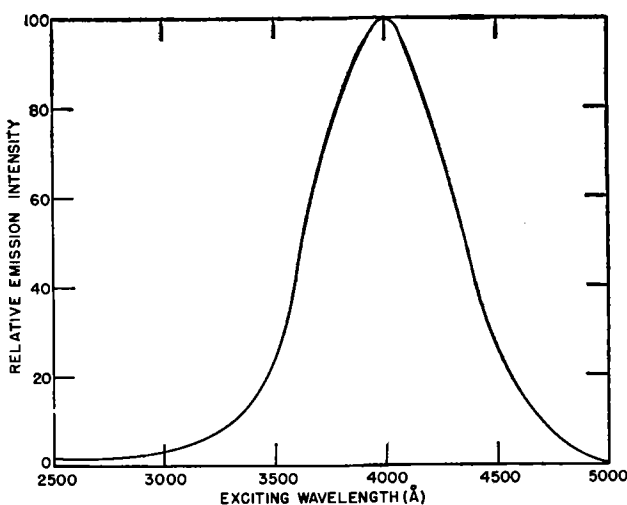


FIG. 1. Excitation spectrum of 3(Na₂O·Al₂O₃·2SiO₂) 1.0NaCl·0.25Na₂S·0.25Na₂SO₄.

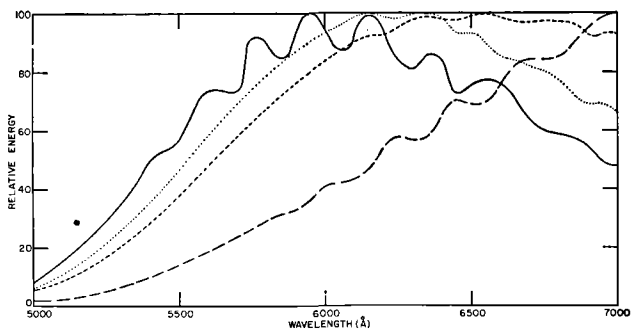


FIG. 2. Emission spectra at 20°C with 3650 Å excitation. 3(Na₂O·Al₂O₃·SiO₂) 1.8 NaCl·0.05Na₂S·0.05Na₂SO₄; - - - - 3(Na₂O·Al₂O₃·2SiO₂)1.0NaCl·0.25Na₂S·0.25Na₂SO₄; - - - - 3(Na₂O·Al₂O₃·2SiO₂) 0.5Na₂S·0.5Na₂SO₄; ——— Na₂S₂·n Na₂SO₄ from Na₂S₂O₃.

is broad in both cases, extending from about 5000 Å to beyond 7000 Å. Gobrecht and Hahn mention the yellow emission of the polysulfide-sulfate prepared from sodium thiosulfate, but give no emission spectrum of this particular material.

The small amount of structure shown by the sodalites at room temperature becomes clearly resolved at the low temperature into a series of maxima spaced about 200 Å apart; the observed emission color shifts from yellow or orange-yellow to red. At about 150°C and above the orange-yellow sodalite emission color changes to pale yellow.

It will be observed that the progressive substitution of 1(Na₂S + Na₂SO₄) for 2NaCl in the sodalite compounds shifts the emission maximum to longer wave lengths, e.g., when equimolecular concentrations of Na₂S and Na₂SO₄ are used in a chloride-free preparation, the product at room temperature shows a maximum beyond 7000 Å, as compared to peaks at 6150 and 6350 Å for the high NaCl composition.

When the NaCl remains constant, e.g., in the series 3(Na₂O·Al₂O₃·2SiO₂)1.0NaCl·0.5(Na₂S + Na₂SO₄), the emission brightness slowly increases

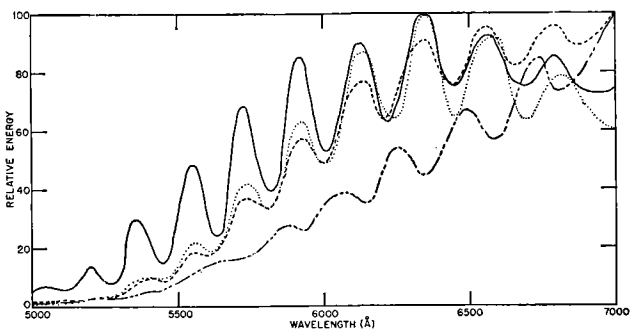


FIG. 3. Emission spectra at -196°C with 3650 Å excitation. 3(Na₂O·Al₂O₃·2SiO₂) 1.8NaCl·0.05Na₂S·0.05Na₂SO₄; - - - - 3(Na₂O·Al₂O₃·2SiO₂)1.0NaCl·0.25Na₂S·0.25Na₂SO₄; - - - - 3(Na₂O·Al₂O₃·2SiO₂) 0.5Na₂S·0.5Na₂SO₄; ——— Na₂S₂·n Na₂SO₄ from Na₂S₂O₃.

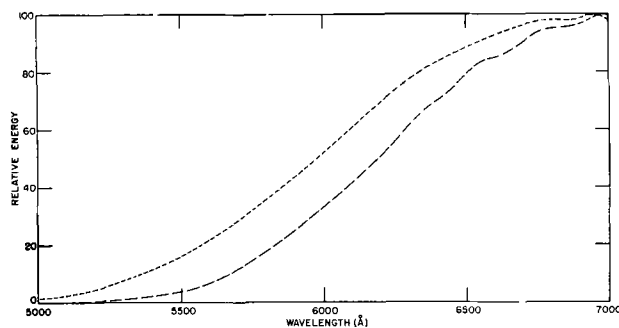


FIG. 4. Emission spectra of $\text{Na}_2\text{S}_x \cdot n \text{Na}_2\text{SO}_4$ from Na_2SO_3 (early stage of heating) with 3650 \AA excitation. - - - - 20°C ; — — — -196°C .

with increasing $\text{Na}_2\text{SO}_4/\text{Na}_2\text{S}$ ratio. Maximum brightness was obtained with a starting $\text{Na}_2\text{SO}_4/\text{Na}_2\text{S}$ mole ratio of 5.7; increase of this ratio to a value greater than 7 caused a rapid decrease in brightness.

In this series, decreasing the $\text{Na}_2\text{SO}_4/\text{Na}_2\text{S}$ ratio to less than one appeared to cause the position of the emission maximum to shift toward the red, e.g., the emission maximum of the product with $\text{Na}_2\text{SO}_4/\text{Na}_2\text{S} = 0.1$ was 500 \AA farther toward the red than that of the product with $\text{Na}_2\text{SO}_4/\text{Na}_2\text{S} = 1$. This may be only an apparent shift due to an internal filtering effect, since the high Na_2S members rapidly colored pink under the exciting source.

Spectrographic analysis of some of the early synthetic sodalite products disclosed the presence of traces of several heavy metals. Therefore, an attempt was made to determine whether the band structure emission of the sodalites was due to the presence of metal activators. Emission spectra of $3(\text{Na}_2\text{O} \cdot \text{Al}_2\text{O}_3 \cdot 2\text{SiO}_2) \cdot 0.5 \text{Na}_2\text{S} \cdot 0.5\text{Na}_2\text{SO}_4$ fired with mole ratios of 10^{-3} , 10^{-4} , and 10^{-5} of salts of each of the following metals, Mn, Pb, U, Sm, Ce, and Eu, were examined. None of these activators

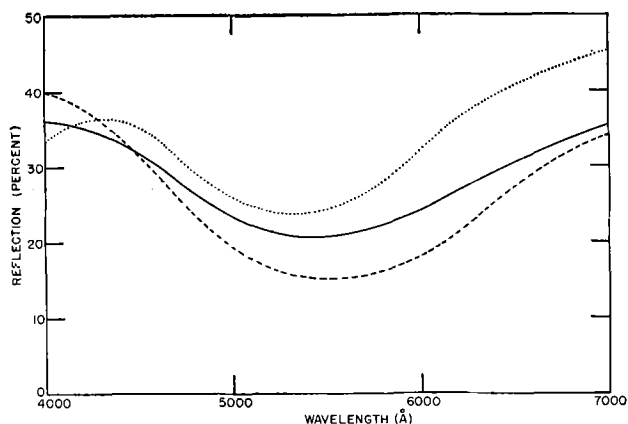


FIG. 5. Reflection spectra of natural hackmanite and synthetic products after coloring by 2537 \AA radiation. . . . Hackmanite; ——— $3(\text{Na}_2\text{O} \cdot \text{Al}_2\text{O}_3 \cdot 2\text{SiO}_2) \cdot 1.8\text{NaCl} \cdot 0.05\text{Na}_2\text{S} \cdot 0.05\text{Na}_2\text{SO}_4$; - - - - $3(\text{Na}_2\text{O} \cdot \text{Al}_2\text{O}_3 \cdot 2\text{SiO}_2) \cdot 1.0\text{NaCl} \cdot 0.25\text{Na}_2\text{S} \cdot 0.25\text{Na}_2\text{SO}_4$.

effected any change in the structure of the emission at either 20° or -196°C .

Fig. 4 illustrates the emission spectra at 20° and -196°C of the sodium polysulfide-sulfate mixture formed by heating Na_2SO_3 for only a short period so that little polysulfide oxidation occurs, as described in the preparation section. The luminescence appears red to the eye, with practically no structure discernible in the emission spectra obtained by the author; low temperatures cause a shift to longer wave lengths with only very slight resolution into band structure. This emission is similar to that recorded by Gobrecht and Hahn for pure polysulfides with the exception that they found no evidence of structure at either 20° or -180°C .

Reflection spectra for the visible range, as recorded for two typical tenebrescent synthetic products and for natural hackmanite, are shown in Fig. 5. These, after coloring by ultraviolet, show only a single reflection minimum in the range of 5300 to 5500 \AA . Medved found an absorption maximum at $5300 \pm 50 \text{ \AA}$ for natural hackmanite colored by exposure to 2537 \AA radiation.

DISCUSSION

There appear to be two distinct types of 3650 \AA -excited luminescence of sodium polysulfides: (a) a nearly structureless emission, appearing red to the eye and peaking in the infrared; this was obtained by the author from $\text{Na}_2\text{S}_x \cdot n\text{Na}_2\text{SO}_4$ from Na_2SO_3 after the early stages of heating, and also by Gobrecht and Hahn from pure polysulfides; (b) the yellow appearing emission with line structure shown by sodium polysulfide-sulfate prepared from $\text{Na}_2\text{S}_2\text{O}_3$ and from Na_2SO_3 in the final stages of heating. Reasons for this emission difference are not known but may be related to the $\text{Na}_2\text{S}_x:\text{Na}_2\text{SO}_4$ ratio or to the value of x in Na_2S_x , since only the polysulfide-sulfate mixtures which are almost completely oxidized to sulfate have the yellow emission with line structure.

From an inspection of Fig. 3 it can be seen that the peaks of the band structure of the emission of the synthetic sodalite materials and of the $\text{Na}_2\text{S}_x \cdot n\text{Na}_2\text{SO}_4$ are nearly identical in spectral position. Thus it appears likely that the luminescence centers are the same and that the sodalite luminescence is connected with the presence of sodium polysulfide. Although the exact nature of the reaction occurring when the sodium monosulfide- and the sodium sulfate-sodalites are fired together is not known, it is quite possible that a sodium polysulfide-sodalite is one of the reaction products, the Na_2SO_4 acting as an oxidizing agent for the Na_2S .

From Table II it can be seen that the ability of the synthetic sodalites to color under radiation of

2537 Å or longer wave length is apparently due to the combined presence of Na₂S and NaCl in the sodalite-type aluminosilicate lattice. Sodalites containing only one of these compounds do not color strongly under this radiation nor do sodalites containing only Na₂SO₄ or Na₂SO₄ + NaCl. The red-purple color of the Na₂S-containing sodalites bleaches rapidly under a tungsten light source.

Medved (5) reported formation of 2537 Å-sensitive products by heating NaCl-sodalite in hydrogen at 1060°C. In trials by the author, sodalite containing NaCl with no sulfur compounds added was fired in hydrogen at 900° and at 1060°C. The products were found to give an extremely weak coloration under 2537 Å radiation. It is believed by this author that these products contained traces of sulfur. Medved detected Cl⁻ in the effluent gas and attributed its presence to replacement by hydrogen of part of the chlorine in NaCl to produce NaH and HCl. Attempts by this author to duplicate Medved's work at 1060°C caused extensive loss of NaCl. Thus, a two-hour firing at 1060° in hydrogen resulted in a weight loss of 55% of the contained NaCl, 99% of which could be condensed on a water-cooled silica tube.

It is not unlikely that sodalites containing Na₂SO₄ could be reduced to sodalites with Na₂S_x by firing in sulfur vapor. Such reduction could not produce Na₂S as long as excess sulfur is present. Tables I and II illustrate that sodalites which contain both NaCl and Na₂SO₄ are neither luminescent under 3650 Å nor tenebrescent under 2537 Å. When these sodalites are fired in sulfur vapor, it can be seen that they are still nontenebrescent under 2537 but have become luminescent (now contain Na₂S_x).

Unlike the luminescence, the tenebrescence of the sodalites could not be duplicated by the simple salt system without the aluminosilicate lattice. Incorporation of the Na₂S and NaCl into the sodalite crystal structure is apparently requisite for the color formation. Mixtures of NaCl and Na₂SO₄ fired in graphite crucibles in H₂ until all the Na₂SO₄ was reduced to Na₂S were nontenebrescent under ultraviolet. X-raying of these NaCl-Na₂S mixtures

caused only the weak yellow coloration of F-centers in NaCl.

As seen from Table II, sodalites containing NaCl and Na₂SO₄ colored under x-rays and 1850 Å ultraviolet. The resulting coloration was bluer and bleached much more slowly than that of sodalites containing Na₂S.

SUMMARY

The luminescence emission of a group of sulfur-containing, synthetic sodalites exhibits at -196°C a series of bands spaced about 200 Å apart. These bands are similar in spectral position to a previously undescribed band emission from sodium polysulfide at -196°C, leading to the conclusion that the sodalite luminescence is due to the presence of sodium polysulfide.

When the synthetic sodalites contain sodium monosulfide and sodium chloride they are tenebrescent, coloring to a red-purple color under ultraviolet radiation.

ACKNOWLEDGMENTS

The author wishes to express his gratitude to Dr. James H. Schulman, Dr. Clifford C. Klick, and Mr. Robert J. Ginther of this laboratory for their helpful discussions of this work.

Any discussion of this paper will appear in a Discussion Section to be published in the June 1955 issue of the JOURNAL.

REFERENCES

1. TH. LIEBISCH, *Sitzber. deut. Akad. Wiss. Berlin*, **13**, 229 (1912).
2. L. H. BORGSTRÖM, *Geol. Fören. Stockholm Förh.*, **23**, 563 (1901).
3. E. VREDENBURG, *Records Geol. Survey India*, **31**, 43 (1904).
4. O. I. LEE, *Am. Mineralogist*, **21**, 764 (1936).
5. D. B. MEDVED, *J. Chem. Phys.*, **21**, 1309 (1953).
6. H. GOBRECHT AND D. HAHN, *Z. Physik*, **132**, 111 (1952).
7. J. BEATO AND M. D. BRÜGGER, *Anales soc. españ. fis. y quim.*, **27**, 822 (1929); *C.A.*, **24**, 1051 (1930); original work not consulted.
8. J. H. SCHULMAN AND C. C. KLICK, *J. Opt. Soc. Amer.*, **43**, 516 (1953).
9. E. TIEDE AND H. REINICKE, *Ber.*, **56**, 666 (1923).

Preparation and Properties of Lead Telluride¹

EDWARD L. BRADY

Research Laboratory, General Electric Company, Schenectady, New York

ABSTRACT

Single crystals of lead telluride, PbTe, have been prepared and their resistivity and Hall coefficients determined. Both *n*- and *p*-type lead telluride have been produced, but they were not of high resistivity. Charge carrier concentration in every case has been $1-5 \times 10^{18}/\text{cm}^3$. Hall mobility of *n*- and *p*-type carriers was found to be about 2240 and 860 $\text{cm}^2/\text{volt-sec}$, respectively.

Material of *p*-type was converted to *n*-type by allowing lead to diffuse into the crystal at 500°C. The value of the diffusion coefficient of Pb in PbTe at this temperature is estimated to lie between 5.6×10^{-8} and 9.2×10^{-8} cm^2/sec .

INTRODUCTION

In recent years, a great deal of experimental work has been done with the series of compounds PbS, PbSe, and PbTe, stimulated by the observations that these compounds are photoconductive in the infrared (1) and that they exhibit transistor action (2, 3). Preparation of these compounds as single crystals is described by Lawson (4), and some of their electrical and optical properties are reported by Smith (1), Chasmar and Putley (5), Gibson (6, 7), and Putley (8). The present work had the following purposes: (a) determination of the ease of preparation of PbTe in pure, stoichiometric form; (b) determination of methods of producing *p*- and *n*-type PbTe at will; (c) measurement of the resistivity, Hall effect, and rectification properties of *p*- and *n*-type PbTe; and (d) obtaining information about the chemical stability of PbTe.

EXPERIMENTAL

Preparation of Lead Telluride

Lead telluride was prepared following a modification of the procedure described by Lawson (4). Elementary lead and tellurium were weighed with an accuracy of about one part in 20,000 to 50,000. The lead was spectrographically standardized grade.² The analysis states that total impurities are less than $2 \times 10^{-3}\%$. The following elements were detected spectrographically: bismuth, copper, cadmium, silver, calcium, aluminum, and sodium. The bars of lead as received are covered with an oxide layer, which was removed by electrolytic etching in a mixture of perchloric and acetic acids. After removal from the acid bath, the bar was washed with distilled water, dried rapidly with lens paper, and stored

in a nitrogen atmosphere until weighed. For weighing purposes the bar was cut into pieces weighing 50–100 mg, and the final weight was adjusted by removing slivers of lead from the pieces with a scalpel. When necessary, the weight could easily be adjusted to 0.1 mg. Although the surface of the lead must have become at least partly oxidized during the weighing procedure, there was no observable change in weight of the pieces of lead while standing in air for a time comparable to that required for weighing.

Before it was used, the tellurium³ was distilled in vacuum in a three-bulb distillation train, and was finally sealed off in vacuum until used. Tellurium prepared in this way was *p*-type and had a resistivity of 0.4 ohm-cm. Intrinsic tellurium is reported to have a resistivity of 0.56 ohm-cm and 0.29 ohm-cm, depending on orientation (9), and has a carrier concentration of about $10^{16}/\text{cm}^3$. For use, the tellurium was broken into pieces weighing 20–50 mg and then weighed. Here again, there was no weighable oxidation during the weighing procedure. The approximate desired quantity of tellurium was weighed, and the weight of lead was adjusted to the required amount.

The container for the reaction was either a graphite cup or a fused quartz tube. Graphite was used to eliminate complications from traces of oxygen left in the system, since room temperature equilibrium conditions for reactions of carbon with oxides of lead and tellurium are far toward the side of the formation of carbon dioxide accompanied by reduction of lead and tellurium. Furthermore, no compounds of carbon with lead have been reported. Carbon ditelluride is reported in an electric arc reaction, but would not be expected to form under the conditions of this experiment. When quartz was used, the tube was filled with about 30–35 cm of hydrogen and heated to glowing before addition of lead and tellu-

¹ Manuscript received March 17, 1954. This paper was prepared for delivery before the New York Meeting, April 12 to 16, 1953.

² Obtained from Johnson, Mathey and Company.

³ Obtained from A. D. Mackay, Inc., 99.9% Te by company specifications.

rium. If this was not done, lead telluride stuck to the quartz tube, and, on cooling, both the tube and the lead telluride cracked badly.

The reaction of lead with tellurium proceeds rapidly with evolution of sufficient heat to maintain the reaction once it is started, if the reactants are intimately mixed. When the reaction is carried out with lumps of both reactants, pieces of lead swell as the reaction takes place and on occasion have cracked the graphite crucible. To avoid this difficulty, the tube containing the unreacted lead and tellurium was inserted into a furnace at a temperature 50°–60°C above the melting point of 905°C. All carbon cups in which the reaction was carried out were heated in a hydrogen furnace at 1100°C prior to use. The cup containing the unreacted elements was sealed into a fused quartz tube at a pressure of about 10^{-5} mm after the system had been pumped at this pressure for several hours. Sometimes the tube was sealed with a few centimeters of helium; an estimate of the rate of transmission of helium through the silica glass indicates that the pressure drops by about a factor of two per day at 900°C. The estimate also indicates that helium pressure in the tube sealed in high vacuum will increase to a pressure of about 1μ during the time of the experiment. Permeation of oxygen through the glass is not fast enough to be an important consideration.

When a carbon cup was not used, the reactants were placed initially in the Pyrex arm of a Y-tube constructed with one Pyrex arm and one silica glass arm. The Y-tube was fitted with a ball joint so that rotation about the joint would cause the reactants to drop into the silica glass tube. Hydrogen was admitted to the system at a pressure of 30–35 cm and the silica arm heated with a torch to a glowing temperature. The line was pumped out to about 5×10^{-5} mm, keeping the tube hot. After the tube had cooled, lead and tellurium were transferred to the silica arm by rotating the Y-tube about the ball joint. The tube was then sealed off about two inches above the reactants. In none of the experiments to be described was there any observable correlation between properties of lead telluride and type of container used.

Production of single crystals of PbTe was accomplished without difficulty by lowering the melt through a temperature gradient of about 20°/cm starting about 50°C above the melting point and ending about 50°C below. The lowering rate was 1 cm/hr. The equipment used is indicated in Fig. 1.

Before the crystal was grown, the tube was maintained at a temperature of 955°–965°C for three or four hours to ensure thorough mixing of the contents. During this time, the tube was agitated occasionally by moving it up and down inside the furnace. After

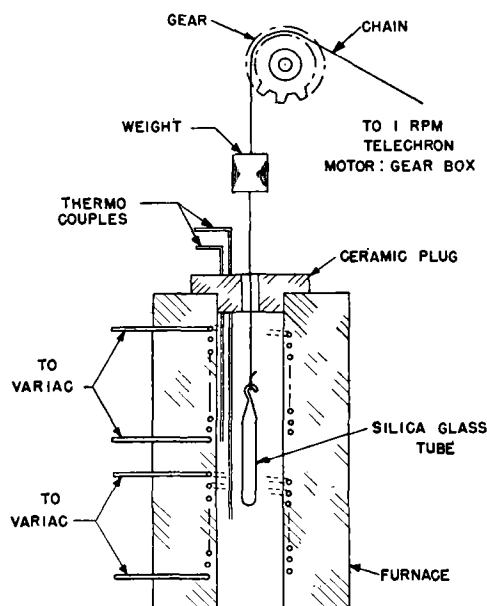


FIG. 1. Apparatus for producing single crystals of lead telluride.

the tube had been lowered about 12 cm (the crystal was usually 3–4 cm long), temperature was decreased to room temperature over a period of about eight hours to permit annealing. However, there was no apparent difference in crystals when the current was shut off and the furnace allowed to cool to room temperature at its natural rate.

The free volume in all tubes used to prepare crystals was kept as small as possible in order to minimize composition changes due to volatility and partial decomposition of lead telluride. Vapor pressure of PbTe at 950°C is claimed to be several centimeters (4), although no accurate measurements could be found in the literature. In all experiments in which a carbon cup was sealed in a silica glass tube, lead telluride condensed on the silica. Occasionally a small amount of solid was found in the bottom of the tube. Evidence for partial decomposition of PbTe is given by the characteristic yellowish color of tellurium vapor observed over lead telluride above its melting point. Thermodynamic data required for an estimate of the dissociation constant are not available in the literature.

Ingots of lead telluride have a bright, silvery appearance with a large number of small pits in the surface. In each of these pits there is usually one or more flat surfaces, and, if the ingot is a single crystal, these are all oriented in the same direction. Reflections from these surfaces provide fairly good evidence that the ingot is composed of a single crystal, but this visual indication was checked occasionally with x-rays. Lead telluride has the sodium chloride structure and cleaves fairly easily, but not controllably. For this reason the material was difficult to

saw to a shape suitable for making electrical measurements. Some of the data reported here were obtained with rather irregular samples and therefore are not of high accuracy.

In order to minimize the effect of surface conditions on electrical measurements of semiconductors, it is customary to etch the surface to produce a smooth bright finish. Various acid and base treatments were used on lead telluride without success. Hydrochloric, hydrofluoric, perchloric, and acetic acids alone or mixed with each other had no visible effect. Dilute nitric acid alone or with other acids turned the surface black, and concentrated nitric produced a much lighter gray surface and converted the black surface to gray. Presumably the black coating is elementary tellurium which is oxidized to tellurium dioxide by concentrated acid. Tellurium dioxide is soluble in a strong base solution, but a bright surface was not obtained by dipping the gray-coated solid in potassium hydroxide solution. A mixture of sodium hydroxide and sodium acetate had no visible effect on the surface. Electrolytic etching in a mixture of concentrated perchloric and glacial acetic acid produced a black coating when the lead telluride was the anode and no visible effect when the PbTe was the cathode. A bright etch can be achieved only by use of a technique which removes lead and tellurium equally rapidly from the surface. Perhaps thermal evaporation in vacuum would be successful; experiments to be described later indicate that partial volatilization in a hydrogen atmosphere produces a dull gray finish. The surface can easily be polished to a mirror finish by standard polishing techniques, but an x-ray examination of a polished surface reveals residual irregularities which a properly etched surface would not have. No difference in properties was observed between crystals with a mirror polish and those obtained with a diamond saw cut. Because of the difficulties with the etching procedure, measurements reported here were obtained with blocks which had a saw-cut surface smoothed with 2/0 emery polishing paper.

Another procedure often used to minimize the effect of surface conditions is to solder electrical contacts to the surfaces. It was found that a physically strong, nonrectifying contact could be achieved with ordinary soft solder by using a drop of concentrated hydrofluoric acid as flux. However, heating lead telluride in air changes its surface properties, and, since contacts could be obtained with no difficulty by pressure alone, all electrical measurements in this report were obtained with pressure contacts.

Resistivity and Hall coefficient data were obtained using equipment and techniques previously described by Dunlap (10).

Electrical Properties of Lead Telluride Ingots

When lead and tellurium were mixed in as nearly stoichiometric proportions as possible and a single crystal prepared as previously described, the ingot was invariably found to have the following properties. Almost all of the outside surface was *n*-type, as determined by a thermoelectric effect probe, but over most of the crystal the *n*-type character was present to a depth of only .002–.010 cm. The bulk of most of the crystal was *p*-type and only the last 5–10% of the crystal was *n*-type throughout. Typical values of electrical resistivities and Hall coefficients of *p*- and *n*-type material are presented in Table I, together with the mobilities and carrier concentrations calculated from these data.

An attempt was made to prepare high resistivity lead telluride by recrystallization of the ingots after discarding 5–10% of the crystal from each end. After the first recrystallization, the *n*-type region at the end of the crystal was very much smaller than before; the bulk of the crystal (except for the *n*-type skin) was *p*-type with about the same resistivity and Hall coefficient as before. Two more recrystallizations had very little effect on the electrical properties; resistivity and Hall coefficient were not significantly different from the values in Table I.

From an ingot prepared from fresh materials a section was cut out which was *n*-type on one face and *p*-type on the opposite, as determined by the thermoelectric probe. The resistivity of this block was 0.0147 ohm-cm and the Hall coefficient was +4.02. This resistivity is about a factor of four higher than that of the *p*-type samples, a result which is to be expected qualitatively since, in at least part of the block, *n*-type carriers should balance *p*-type. The boundary between *n*- and *p*-types was very sharp. A region of intermediate resistivity could not be detected with the thermoelectric probe when resistivity was judged qualitatively by the galvanometer response.

After each crystallization, small crystals that had deposited from the vapor were collected from the wall of the quartz tube. These crystals ranged in linear dimensions from about 0.1 mm up to 1 to 2 mm, were a few hundredths of a millimeter thick, and were always rectangular in shape, quite often square. These crystals were invariably *n*-type on

TABLE I. *Properties of typical PbTe*

	<i>p</i> -type	<i>n</i> -type
Resistivity (ohm-cm)	0.005	0.00090
Hall coef. (cm ³ /coulomb)	+4.2	−2.0
Mobility (cm ² /volt-sec)	840	2220
Concentration (cm ^{−3})	1.5 × 10 ¹⁸	3.1 × 10 ¹⁸

TABLE II. Effect of hydrogen on electrical properties of lead telluride

Sample	Temp (°C)	Time heated (hr)	Type by thermoelectric effect	Hall coef. (cm ³ /coul)	Remarks
1	—	0	<i>n</i> on one side, <i>p</i> on others	+4.02	—
1	500	6	<i>n</i> , all surfaces	+3.67; +5.26	<i>n</i> -Type layer very thin
1	845	6	—	—	Sample completely volatilized
2	—	0	<i>p</i> , all surfaces	+2.12	—
2	600	6	<i>n</i> , all surfaces	+3.11	<i>n</i> -Type layer removed by light sanding
2	695	6	<i>n</i> , all surfaces	+3.30	<i>n</i> -Type layer removed by light sanding

both sides by thermoelectric measurements. The *n*-type character is consistent with the hypothesis that the vapor is partly decomposed at the melting point and that, since tellurium is more volatile than lead, the condensate has a stoichiometric excess of lead, which furnishes electrons to the crystal, making it *n*-type. However, the solid collected from the bottom of the tube, composed of material which also had come through the vapor phase, was *p*-type on the surface in contact with the quartz tube and *n*-type on the exposed surface.

Treatment of *p*-Type Lead Telluride with Hydrogen

If *p*-type lead telluride is treated with hydrogen, the material will be converted to *n*-type if the hydrogen can react with and remove *p*-type impurities or excess tellurium, or if hydrogen can dissolve in lead telluride and provide electrons. To discover the effect of hydrogen, a number of experiments were carried out in which a block of PbTe was heated at various temperatures in a stream of hydrogen. The tank hydrogen⁴ was passed through a Deoxo unit and a Drierite tube before it came in contact with the lead telluride. Results obtained are listed in Table II. It is apparent from these results that treatment with hydrogen will convert *p*-type PbTe to *n*-type, but that the effect of the hydrogen does not penetrate more than a few mils in several hours at a temperature low enough to prevent appreciable volatilization of lead telluride. Hydrogen treatment dulled the surface of lead telluride considerably, probably indicating that some reaction with the surface had occurred rather than a dissolution of hydrogen into the solid.

Distillation of *p*-Type Lead Telluride

Since lead telluride condensed from the vapor was usually *n*-type, a vacuum distillation of the *p*-type material was carried out in order to prepare bulk *n*-type material. The *p*-type material in a carbon cup was placed in a silica tube with the end of the tube extending outside the furnace. Pumping was continued while the tube was heated to a final maximum

⁴ Produced by the General Electric Company.

temperature of 980°C, which was maintained for one-half hour. The solid which condensed on the cooler portion of the tube was almost black and was *n*-type thermoelectrically. A portion of this solid was placed in a silica tube and about 10 cm of hydrogen admitted to the system. When the tube was heated, the color of the solid changed from black to the silvery gray characteristic of the bulk ingots. The line was pumped out and the heating with hydrogen repeated. The line was again pumped out and the usual procedure for producing a single crystal followed. This crystal was *p*-type everywhere, including the surface. Hence, the sublimation procedure seems useful for producing small flat *n*-type crystals, but does not seem promising as a means of obtaining a quantity of *n*-type lead telluride which can be recrystallized to an *n*-type ingot.

Diffusion of Lead Into Lead Telluride

It is well known that lead sulfide containing excess lead is an *n*-type semiconductor, while with excess sulfur it is *p*-type (11). Similar observations have been reported for lead selenide (12) and lead telluride (4). Anderson and Richards (12) have measured the diffusion coefficient of lead in powdered, pressed lead sulfide and report that the diffusion coefficient, *D*, is given by

$$D = (1.38)(e^{-42,000/RT}) \text{ cm}^2/\text{sec}$$

At 500°C, this equation gives $D = 2.2 \times 10^{-12}$ cm²/sec. Since tellurium ions are considerably larger than sulfide ions, one would expect the activation energy of the diffusion of lead in lead telluride to be lower than in lead sulfide and the value of *D* correspondingly greater. Hence it seems feasible to convert *p*-type lead telluride to *n*-type by allowing lead to diffuse into it at a moderate temperature for a few hours.

To test this point, a disk cut from a single crystal of *p*-type lead telluride was heated in vacuum between two disks of lead for 6.5 hr at a temperature of 290°C. After this period, the three disks had not changed in weight, and the lead telluride was still *p*-type.

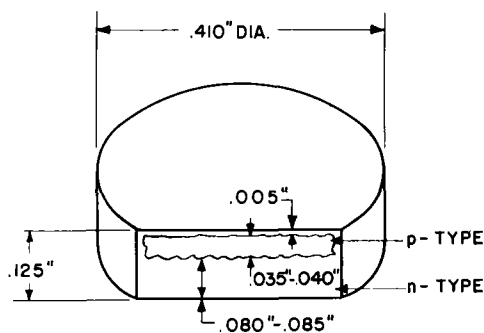


FIG. 2. Disk of lead telluride after diffusion of lead

The temperature was maintained below the melting point of lead in order to minimize solubility of lead telluride in the lead. At the melting point of lead, 327°C, the solubility of tellurium in lead is reported to be about 0.05% (13). Since no effect was observed at 290°C, a similar experiment was carried out at 500°C. In this experiment, the same disk of lead telluride was placed above a lump of spectrographic lead in a small carbon cup. Enough lead was used to ensure contact of the whole area of the flat surface of lead telluride with lead, so that diffusion through lead telluride would be uniform.

The silica glass tube containing the carbon cup with the lead telluride and lead was evacuated (to about 0.05μ) and heated to 500°C. After 40 min at this temperature, a dark deposit was observed on the cooler parts of the tube. To reduce evaporation and consequent changes in composition, the tube was filled with 35 cm of helium and the temperature maintained at $500 \pm 5^\circ\text{C}$ for a total of 7 hr (including the time in vacuum). At the conclusion of the experiment, the disk of lead telluride could not be easily removed from the lead. Separation of the two was accomplished by heating in a helium atmosphere with the lead resting on a nichrome grid. Above the melting point of the lead-tellurium solution (almost that of pure lead) the solid and liquid phases separated easily. No measure was obtained of the completeness of separation, but there was a thin fringe, apparently mostly lead, projecting from the edge of the disk, and the surface of the disk which had been in contact with the lead was shiny and irregular. The top surface was somewhat duller, but there was no major change in appearance. Several measurements of the thickness of the disk averaged to 0.326 cm, whereas the initial thickness had been 0.305–0.310 cm.

From the phase diagram, the solubility of tellurium in lead at 500°C is estimated to be 1%. Since the weight of lead taken was 7.05 g, the solubility of tellurium would be about 0.070 g, corresponding to 0.184 g of lead telluride. The original weight of the lead telluride was 2.124 g, large enough so that the amount of lead telluride dissolved would be only a

small fraction of the total. The solid phase in equilibrium with liquid at 500°C is reported to contain 25 weight % (34 atom %) tellurium, and lead should diffuse into the stoichiometric lead telluride until this composition is reached. At equilibrium, a total of 1.05 g of lead would have diffused into the lead telluride.

All exposed surfaces of the disk had changed to *n*-type, including the top, which had had no direct physical contact with the lead. The disk was sawed perpendicular to the top surface and the freshly exposed face probed with a thermoelectric-effect needle in a micromanipulator. The *n*- and *p*-type character of the exposed face is indicated in Fig. 2. It is seen that the lead had penetrated sufficiently deeply into the lead telluride to convert most of it to *n*-type. Surface diffusion or deposition of lead from the vapor phase was rapid enough to convert the whole surface to *n*-type and to penetrate about 0.01 cm into the interior.

An estimate of the diffusion coefficient of lead in lead telluride can be obtained from the data indicated in the figure. The solution of the diffusion equation for one-dimensional diffusion with the boundary conditions of the present situation is given by (14):

$$C(x, t) = C_o \left[1 - \frac{2}{\sqrt{\pi}} \int_0^{x/2\sqrt{Dt}} e^{-y^2} dy \right],$$

in which $C(x, t)$ is the concentration at the distance x and the time t , C_o is the constant concentration at $x = 0$, and D is the diffusion coefficient. In the present problem, C_o is taken to be the difference in concentration (atoms/cc) between solid lead telluride saturated with lead at 500°C and stoichiometric lead telluride. The distance x is taken to be the furthest distance from the boundary surface at which conversion to *n*-type has occurred, and t is the time of heating at 500°C. The concentration, $C(x, t)$, is more difficult to estimate. It must be at least equal to the concentration of *p*-type carriers in the original material, and may be a good deal higher. The diffusion coefficient will be calculated on the assumptions that $C(x, t)$ is roughly equal to the original hole concentration, and that it is roughly ten times greater. The correct value of the diffusion coefficient should lie between these two values.

Since no data are available for the density of lead telluride saturated with lead, it is assumed that the density is equal to that of the stoichiometric compound. With this assumption, C_o equals $3.5 \times 10^{21}/\text{cm}^3$. A reasonable value for the hole concentration is $3.5 \times 10^{18}/\text{cm}^3$. Rearranging the diffusion equation, one can obtain:

$$\frac{2}{\sqrt{\pi}} \int_0^{x/2\sqrt{Dt}} e^{-y^2} dy = 1 - \frac{C}{C_o} = 1 - \frac{1}{1000} = 0.999$$

Tables of the error function (the left side of the above equation) give a value of:

$$\frac{x}{2\sqrt{Dt}} = 2.326$$

The depth of penetration, x , equals about 0.175 cm after correction is made for the lead telluride that dissolved in the lead, and $t = 7 \text{ hr} = 2.52 \times 10^4 \text{ sec}$. When the above equation is solved for D , a value of $D = 5.61 \times 10^{-8} \text{ cm}^2/\text{sec}$ is obtained. When a ratio of $c/c_0 = 0.01$ is assumed as a reasonable upper limit, a value of $D = 9.15 \times 10^{-8} \text{ cm}^2/\text{sec}$ is obtained. This range of values for the diffusion coefficient of Pb is considered to be of a reasonable order of magnitude. It is seen that they are $2.5 \times 10^4 - 4 \times 10^4$ times greater than the value for the diffusion coefficient of lead in lead sulfide.

The foregoing discussion is all based on the assumption that the substance which diffuses into the lead telluride is excess lead. There is no proof that lead is responsible for the conversion to n -type; one of the impurities present in the spectrographic lead may have caused the change. If this were the case, the diffusion coefficient would be of the order of 10^2 to 10^3 times greater than that calculated above.

When the hot point of the thermoelectric probe rested in contact with an n -type region, the potentiometer deflection decreased in a few minutes, often changing sign. This effect was observed over almost all of the n -type surface. The region closest to the lead did not change sign but only exhibited a change in magnitude. During a period of about 1.5 hr of standing in air at room temperature, about two-thirds of the n -type surface had changed to p -type, and after about three hours only a small fraction of the surface remained n -type. The original pattern was recovered, however, by light sanding with fine emery paper. Changes in type are almost certainly associated with oxidation of the surface. When a stream of oxygen was directed on the surface, the rate of change from n - to p -type was increased considerably. With a stream of hydrogen on the surface an entirely different effect was obtained; the initial contact of the probe with the surface was p -type and remained p -type as long as the stream of hydrogen was maintained. On removal of the hydrogen, the surface reverted to n -type.

An attempt was made to observe rectification across the n - p barrier in the lead telluride. One electrical contact was made with a small aluminum vise used to hold the sample, which was in contact with both n -type flat surfaces. The other contact was established with the p -type region of a freshly sanded surface, by use of a brass probe. With the probe in very light contact and with a potential difference of 1 v, slight rectification was observed—apparently all

associated with the probe contact, since an increase in pressure caused the oscilloscope trace to become ohmic in character. Since the conductivity of the material is so high and the n - p boundary so sharp, the potential drop across the n - p boundary may exceed the Zener breakdown potential.

When an ohmic trace was obtained and the lead telluride surface illuminated with the light from a flashlight, the current through the solid increased significantly. No quantitative measurements were obtained.

Nonstoichiometric Lead Telluride

Lawson (4) has reported that lead telluride prepared from the pure elements will always be p -type even when 2–5% excess lead is used, unless the reaction tube is treated with hydrogen and the reactants melted in hydrogen before reaction. His technique leads to an indeterminate but probably small loss of tellurium before reaction. Lawson's procedure was modified somewhat in an attempt to simplify the procedure and avoid loss of tellurium. The equipment consisted of the Y-tube with one silica glass arm previously described and preparations were made as described.

After preparation of the ingot, a block was sawed from the middle portion, and resistivity and Hall coefficient measurements made. In the samples containing excess lead, it was found that the portion of the ingot that crystallized last was invariably n -type (as was the surface) and that the thickness of the n -type region was 1 to 2 mm. Samples containing excess tellurium showed no n -type regions anywhere. Results of electrical measurements are presented in Table III.

Considering the irregularities in the samples due to cleavage during sawing, results are considered to be identical within the limit of accuracy of the measurements. The bulk of each of the samples is p -type, even with 2% excess lead, just as Lawson observed.

TABLE III. *Electric properties of nonstoichiometric lead telluride*

Sample	Resistivity (ohm-cm)	Hall coefficient (cm ² /coul)	Mobility (cm ² /volt-sec)	Carrier concentration (1/cm ³) (× 10 ¹⁸)	Thermoelectric type
%					
0.5 Te	0.00493	+4.16	845	1.50	<i>p</i>
0.1 Te	0.00379	+3.46	914	1.81	<i>p</i>
0.1 Pb	0.00726	+5.93	817	1.05	<i>p</i>
0.5 Pb	0.00468	+5.47	1170	1.14	<i>p</i>
0.5 Pb*	0.00553	+4.26	773	1.47	<i>p</i>
1.0 Pb	0.00475	+3.78	795	1.65	<i>p</i>
2.0 Pb	0.00380	+2.81	740	2.22	<i>p</i>

* Sample crystallized in 20 cm helium. All others in vacuum.

Lattice spacings in the samples containing 0.5% excess tellurium and 0.5% excess lead have been determined.⁵ Results obtained were 6.4579 ± 0.0030 Å and 6.4576 ± 0.0019 Å, respectively. The difference, of course, is not significant. The literature value is 6.453 Å. It is believed that the value obtained here is more accurate than the literature value.

DISCUSSION

The study of electrical properties of lead telluride is hindered by its chemical behavior and by limitations of measuring methods; no volumetric or gravimetric measuring technique is adequate to prepare a mixture of the two components in exactly stoichiometric ratio. Furthermore, no adequate means of ensuring sufficient purity in the initial reactants is available, necessitating purification of the compound after formation. Recrystallization from the melt, a technique that produces adequate purity in elementary semiconductors, is complicated by relatively high vapor pressure and partial decomposition of the compound at its melting point, so that loss of material and change of composition must be minimized by operating in a closed system with a free volume as small as possible. With these restrictions, recrystallization as carried out in the present experiments leads either to ineffective rejection of impurities or to a nonstoichiometric compound, or to both.

The *p*-type character of most of the lead telluride (all but about the last 10% to crystallize) indicates that the solid phase of PbTe is not in equilibrium with a liquid of exactly the same composition, and, indeed, there is no reason to expect such a condition to exist. If it is assumed that the solid is in thermal equilibrium both with empty lead sites and empty tellurium sites, it seems reasonable that the concentration of empty lead sites should be greater than that of empty tellurium sites, since the energy required to create an empty lead site is undoubtedly considerably less than that required for a tellurium defect. Electrical neutrality in the crystal can be maintained, by assuming either that excess tellurium is zerovalent (or monovalent) or that excess telluride ion is balanced by the abstraction of electrons from divalent lead. Any description in terms of a purely ionic lattice, however, is certainly an oversimplification.

Therefore, in the usual case, crystallization from the melt is expected to lead to a nonstoichiometric compound, although in principle the composition of the melt could be adjusted so that the solid phase would have the desired composition. In general, this would require extremely delicate control not only of the liquid phase composition, but also of all other

⁵ By Mrs. B. F. Decker.

variables affecting the solid phase, such as crystal growth rate and thermal environment.

Since the presence of impurities cannot be distinguished from deviations from stoichiometry by experiments of the type described here, it is impossible to decide definitely at present which of these sources of donors and acceptors is responsible for the electrical properties. However, it is believed that deviations from stoichiometry are probably responsible for the electrical behavior of the ingots prepared in the present work.

Another aspect of the chemical behavior of lead telluride which contributes to the difficulties of making significant reproducible electrical measurements is its reactivity with oxygen. The change of an *n*-type surface to *p*-type when exposed to air at room temperature indicates that the compound should be handled at all times in an inert atmosphere.

Properties of the material obtained in the present research confirm results obtained with the material prepared by Lawson. In his paper on the absorption spectra of lead sulfide, selenide, and telluride, Gibson (7) reports carrier concentrations of 1×10^{18} to 2×10^{18} for *p*-type lead telluride and $1-6 \times 10^{18}$ for *n*-type, essentially identical with those obtained here. However, Gibson has worked with lead telluride containing only 5×10^{16} carriers/cm³ (6). Putley (8) reports the best values of hole mobility and electron mobility at 290°K to be 840 cm²/volt-sec and 2100 cm²/volt-sec, respectively. Values obtained for the room-temperature mobilities of holes and electrons in the present research were 860 cm²/volt-sec and 2240 cm²/volt-sec.

ACKNOWLEDGMENTS

The author wishes to acknowledge many helpful discussions with Dr. W. C. Dunlap and Dr. L. Apker. Many of the electrical measurements were made by Miss Sally Schwartz.

Any discussion of this paper will appear in a Discussion Section to be published in the June 1955 issue of the JOURNAL.

REFERENCES

1. R. A. SMITH, "Semi-Conducting Materials," (H. K. Henisch, Editor) pp. 198-207, Butterworths Scientific Publications Ltd., London (1951).
2. H. A. GEBBIE, P. C. BANBURY, AND C. A. HOGARTH, *Proc. Phys. Soc., London*, **B63**, 371 (1950).
3. C. A. HOGARTH, *ibid.*, **B64**, 822 (1951); **B65**, 958 (1952).
4. W. D. LAWSON, *J. Appl. Phys.*, **22**, 1444 (1951); **23**, 495 (1952).
5. R. P. CHASMAR AND E. H. PUTLEY, "Semi-Conducting Materials," (H. K. Henisch, Editor) pp. 208-217, Butterworths Scientific Publications Ltd., London (1951).
6. A. F. GIBSON, *Proc. Phys. Soc., London*, **B65**, 196 (1952).
7. A. F. GIBSON, *ibid.*, **B65**, 378 (1952).

8. E. H. PUTLEY, *ibid.*, **B65**, 388 (1952).
9. V. E. BOTTOM, *Science*, **115**, 570 (1952).
10. W. C. DUNLAP, *Phys. Rev.*, **79**, 286 (1950).
11. For a review of the information on PbS see K. HAUFFE, *Ergeb. exakt. Naturw.*, **25**, 243 (1951).
12. J. S. ANDERSON AND J. R. RICHARDS, *J. Chem. Soc.*, **1946**, 537.
13. W. HOFMANN, "Blei und Bleilegerungen," pp. 52-55, Julius Springer, Berlin (1941); republished by J. W. Edwards, Ann Arbor, Michigan (1944). G. O. HIERS, "Metals Handbook," (Taylor Lyman, Editor) ASM, Cleveland (1948).
14. R. M. BARRER, "Diffusion In and Through Solids," p. 12, Cambridge University Press, London (1951).

Crystal Structure and Thermodynamic Studies on the Zirconium-Hydrogen Alloys¹

EARL A. GULBRANSEN AND KENNETH F. ANDREW

Westinghouse Research Laboratories, East Pittsburgh, Pennsylvania

ABSTRACT

The phase diagram of zirconium-hydrogen alloys was studied on alloys prepared at low temperature and for alloys in the composition range of $ZrH_{0.025}$ to $ZrH_{1.965}$. Decomposition pressure studies were made over the composition range and for a series of temperatures. Results of these measurements were in complete agreement with crystal structure studies on the major phases.

Results show presence of two major hydride phases, namely, the δ - and ϵ -phases as described by Hägg. No evidence was found for either the γ - or β -phases of Hägg, although the latter phase was found only at high temperature by Hägg. The ϵ -phase was found to have a wide range of homogeneity from $ZrH_{1.965}$ to about $ZrH_{1.65}$. The δ -phase was found to have a composition near $ZrH_{1.50}$ and a range of homogeneity from $ZrH_{1.4}$ to $ZrH_{1.66}$.

A new minor transitional phase was found having the face-centered tetragonal structure and existing only in the presence of α -Zr and δ -phases. It has been designated as the γ' -phase since its composition is probably near that of Hägg's γ -phase.

The free energy of formation of the δ -phase in contact with α -Zr containing hydrogen was determined from decomposition pressure data.

INTRODUCTION

The reaction of zirconium with hydrogen has been the subject of a number of experimental studies. The literature was reviewed by Smith (1) in 1948 and more recently by Gulbransen (2) in 1953. An analysis of the literature shows some confusion concerning the phases present in the zirconium-hydrogen system and in the interpretation of the absorption isotherms.

Since hydrogen has been found to embrittle zirconium under certain conditions for concentrations as low as 10 ppm (3) and since zirconium is rapidly becoming an industrially important metal, it is of interest to reexamine the role of hydrogen in the metal.

This communication will present both thermodynamic studies on the formation of hydrogen alloys from the metal and crystal structure studies of these alloys. Studies are made for alloys prepared at temperatures below 300°C and for compositions of $ZrH_{0.025}$ to $ZrH_{1.965}$.

It has been known for a long time that zirconium can absorb considerable quantities of hydrogen and still show a metallic appearance. Winkler (4, 5) first observed the large capacity of zirconium for absorption of hydrogen and proposed that definite gaseous and solid hydrides were formed. Gaseous

hydrides were not confirmed by Wedekind (6), nor by Schwarz and Konrad (7). The formation of the hydride ZrH_2 was suggested by Weiss and Neumann (8) and Wedekind (9) from studies of the absorption of hydrogen by zirconium.

Smith (1) has designated zirconium as belonging to the class of exothermic occluders. These metals absorb hydrogen in large quantities, form alloys of greater complexity, exhibit solid solution phenomena, and form one or more secondary phases.

Absorption isotherms.—Sieverts and Roell (10) first studied absorption isotherms on samples of metal powders containing 91% zirconium at 800° and 1100°C and an absorption isobar at 760 mm of Hg hydrogen pressure. Consistent results were difficult to attain by their methods.

Hall, Martin, and Rees (11) recognized the role of surface contamination and eliminated surface oxide by heating to high temperature in vacuo before studying the absorption of hydrogen. Absorption isotherms show strong "kinks" for compositions between $ZrH_{1.0}$ and $ZrH_{1.4}$ and the shapes of the curves show a resemblance to those found for the palladium-hydrogen system where a two-phase region has been noted. Hall, Martin, and Rees (11) interpret the shape of the curves in terms of two solution processes occurring together, only one of which is rate-determining.

Crystal structure studies.—Hägg (12) has studied zirconium-hydrogen phases on specimens prepared at high temperature and cooled to room tempera-

¹ Manuscript received March 19, 1954. This paper was prepared for delivery before the Chicago Meeting, May 2 to 6, 1954.

TABLE I. Crystal structure data on Zr-H system

Atom % H	Lattice structure and dimensions kX units	Reference	
0 α -phase	h.c.p.; $a = 3.228$ $c = 5.140$	13	
Transition temp, °C	$862^\circ \pm 5^\circ\text{C}$		
0 β -phase	b.c.c.; $a = 3.61$ at 900°C	12	
0-5	α -phase; h.c.p. $a_{\text{max}} = 3.247$ $c_{\text{max}} = 5.173$		
20	β -phase; f.c.c. $a = 4.66$		
33	γ -phase; h.c.p. $a = 3.335-3.339$ $c = 5.453-5.455$		
50	δ -phase; f.c.c. (fluorite) $a = 4.765-4.768$		
66.7	ϵ -phase; f.c. tetrag. $a = 4.964$ $c = 4.440$ $c/a = 0.894$		
66.0	ϵ -phase; f.c. tetrag. $a = 4.87$ $c = 4.58$		15

ture. Although no details of his preparation procedures are given, many of the samples were prepared above the α - β transformation temperature for zirconium, the existence of which Hägg was probably unaware. Five phases were noted by Hägg (12), including the β -phase Zr_4H which is stable only at high temperatures.

Table I shows a compilation of crystal structures of the two zirconium phases and the several zirconium-hydrogen phases. Data for pure metal phases are averaged values of the published literature given by van Arkel (13). The dimensions of the unit cells are given in kX units. A value of 1.00202 has been set (14) as the conversion factor for kX units into Angstrom units. Criticism has been raised by Smith (1) concerning the existence of some of Hägg's phases on the grounds that stresses were set up in the sample on cooling through the transition temperature and that inhomogeneities might occur in the method of preparation. Hägg probably realized many of these difficulties and has not suggested that the work was complete.

EXPERIMENTAL

Vacuum microbalance.—A vacuum microbalance and associated apparatus is used for preparing all specimens and for studying decomposition pressures of these specimens. The construction and use of the microbalance has been described (16).

Specimens are sheets of zirconium 0.0125 cm thick. For convenience two sizes are used. The first size weighs 0.05 g and has an area of 1.25 cm². These specimens are used for preparing and studying

TABLE II. Analyses of zirconium samples

	Footc Zr Typical
Si	.01
Fe	.04
Al	.01
Cu	<.01
Ti	.03
Mn	<.001
Ca	.01
Mg	<.003
Pb	<.001
Mo	<.001
Ni	.01
Cr	.001
Sn	.001
W	<.001
N	<.01
O	<.01
H	<.02
C	<.001
Hf	2.40

hydrogen alloys of compositions above $\text{ZrH}_{0.10}$. The second size weighs 0.50 g and has an area of about 12 cm². They are used for preparing and studying hydrogen alloys below $\text{ZrH}_{0.10}$.

The sensitivity of the balance was 0.79 μg /division (0.001 cm) and the weight change was estimated to $\frac{1}{4}$ of a division or $(0.20 \times 10^{-6} \text{ g})$.

Vacuum system.—Vacuum and reaction systems are of critical importance in studying reactions of highly reactive metals such as zirconium. The vacuum system used in this study is of all glass construction and can be evacuated readily to pressures considerably lower than 10^{-6} mm of Hg. A mullite furnace tube (17) which contains the specimen is sealed directly to the Pyrex apparatus. Previous studies (17) have shown that pressures less than 10^{-8} mm of Hg can be achieved in this system with the furnace tube at 900°C after pumping over night.

Preparation of gases.—Pure hydrogen is prepared by diffusing purified electrolytic hydrogen through a hot palladium tube. Experience has shown that gas purity is also a critical factor in the study of the zirconium-hydrogen reaction. Reproducible results are obtained only with the purest preparations of hydrogen.

Samples and sample preparation.—High purity iodide process zirconium is used for all experiments. Spectrographic and chemical analyses are given in Table II. The largest impurity is 2.4% of hafnium.

All specimens are abraded starting with 1/0 polishing paper and finishing with 4/0. The last two papers are used with purified kerosene. Samples are then cleaned successively with soap and water,

distilled water, petroleum ether, and absolute alcohol. After a preliminary weighing, specimens are placed in a desiccator until ready for use.

X-ray diffraction apparatus.—An iron target x-ray tube was used as a source of x-rays. The x-ray beam was monochromatized to give FeK_α radiation. A 9-cm Unicam powder camera was used to record reflections. Ilford x-ray film was used in the camera.

To reduce the background the camera was evacuated to 0.01 mm of Hg pressure. An exposure time of one day was used to bring out the weak lines of minor phases present in some samples.

A pure NaCl specimen was used for calibrating the camera at a 2θ value of 90°C .

METHOD

Preparation of samples.—The vacuum microbalance was well suited for the preparation of hydrogen alloys of definite composition. The weighed sample was placed on the supporting wire and suspended from one end of the balance beam. After closing off the system, the apparatus was partially evacuated and the liquid nitrogen trap put in place. The evacuation was now completed and the system pumped for 16 hr or longer at a pressure below 10^{-6} mm of Hg.

To remove the room temperature oxide a furnace at 700°C was placed around the furnace tube for 2 hr, after which the sample was cooled to the reaction temperature in vacuo to prepare the particular hydrogen alloy. During this heating cycle some pick-up of gases from the vacuum system would be expected to occur. This was found to be of the order of 2 to 3 μg or less which was negligible for our purposes. To assure homogeneity the specimen was homogenized for 20 hr or longer at the preparation temperature. For specimens prepared above 150°C this treatment appeared to give a uniform composition throughout. Weight changes occurring during this treatment were 2 to 3 μg or less.

Decomposition pressure studies.—Zirconium reacts with hydrogen to form at least two stable hydrides in addition to the α -phase of zirconium containing hydrogen. The phase diagram of the zirconium-hydrogen system can be determined by measuring decomposition pressures at a series of temperatures over the complete composition range. Decomposition pressure was determined by closing off the sample from the vacuum pumps and reading the hydrogen pressure by means of a calibrated McLeod gauge. Readings were made on both the decomposition (heating) cycle and on the absorption (cooling) cycle. In this way true equilibrium values could be obtained. Extreme care was used to avoid contamination. If contamination occurred, readings were erratic and nonreversible.

Crystal structure studies.—Special samples were made for x-ray diffraction analyses following the method described above (Vacuum microbalance). Brittle specimens were ground to a powder and placed in a 0.3 mm glass capillary having a wall thickness of 0.01 mm. Strips were cut from the ductile specimens of $0.013 \times 0.05 \times 1.0$ cm size. X-ray diffraction patterns were made directly on these samples.

Since the absorption coefficient of the K_α iron x-ray radiation by Zr was large, the outer surface of the specimen contributes mainly to the x-ray diffraction pattern. This makes it possible to test the presence of surface contamination or inhomogeneities in the specimen by the use of etching processes. Thus, some of the specimens were etched in a mixture of 1 cc conc. HNO_3 , 10 cc of 48% HF, and 90 cc of H_2O . The etching process required 5 to 30 sec time, the 30-sec etch removing about 50% of the material.

RESULTS AND DISCUSSION

Decomposition Pressure Studies

Twenty-one compositions were prepared and studied in the range of $\text{ZrH}_{0.025}$ to $\text{ZrH}_{1.74}$. Decomposition pressures were measured in the temperature range of 325° to 550°C directly after preparation to avoid contamination.

Fig. 1 to 4 show typical results. Decomposition

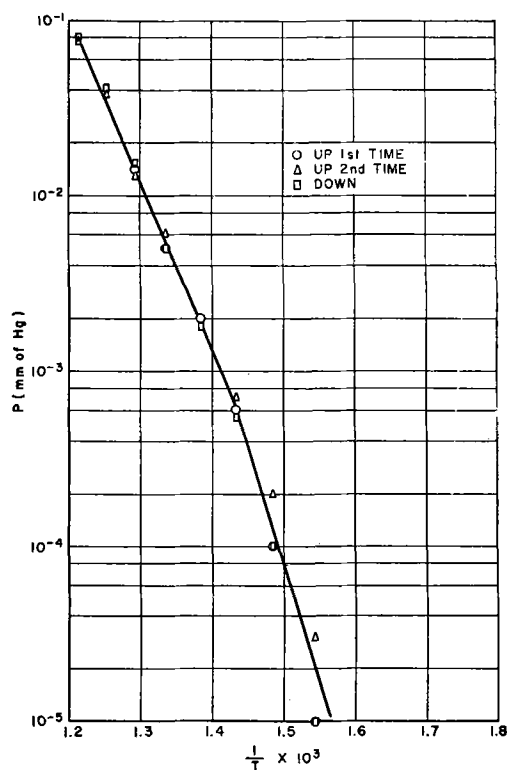


FIG. 1. Decomposition pressure of $\text{ZrH}_{0.99}$

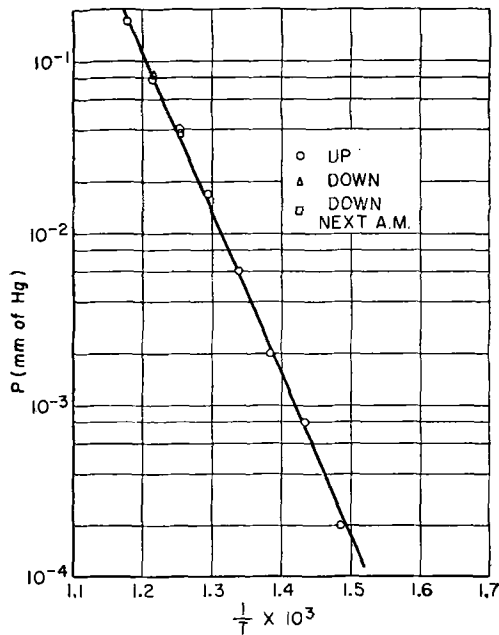


FIG. 2. Decomposition pressure of $ZrH_{1.36}$

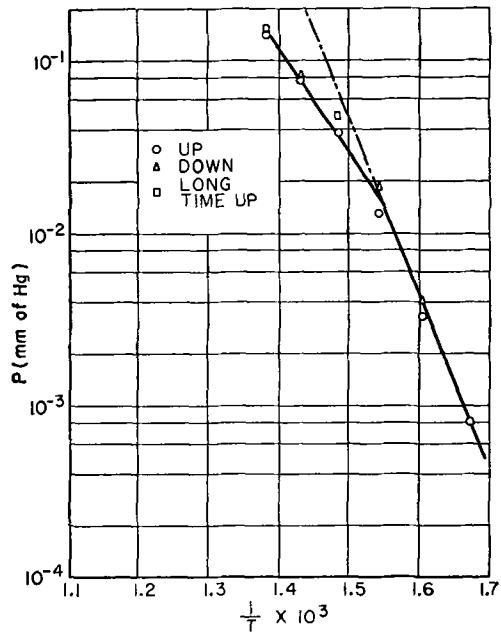


FIG. 4. Decomposition pressure of $ZrH_{1.74}$

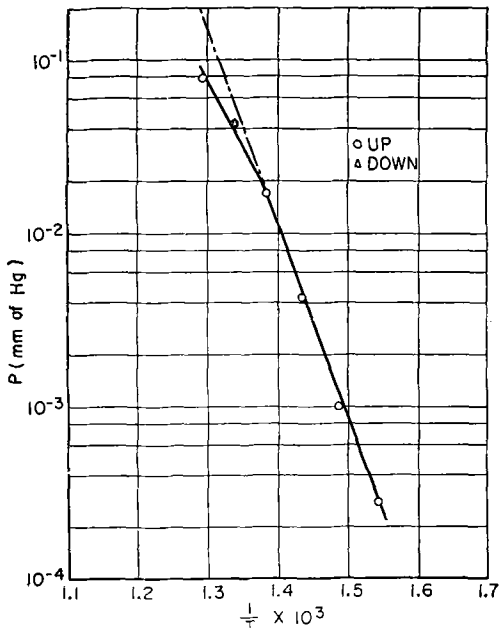


FIG. 3. Decomposition pressure of $ZrH_{1.51}$

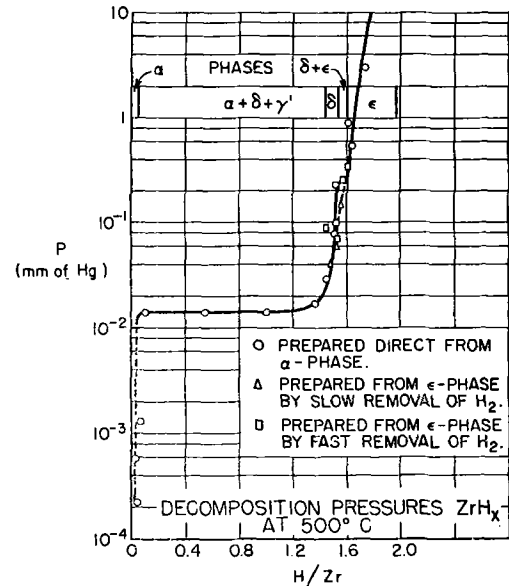


FIG. 5. Decomposition pressure ZrH_x

pressures are plotted on a logarithmic scale against $1/T$. Fig. 1 shows a plot of results for the composition $ZrH_{0.99}$. A reversible process was noted. Since the total quantity of hydrogen was small for the 0.05 g samples, the composition of the alloy changes for pressure readings above 10^{-2} mm of Hg. For Fig. 1 this change in composition has no effect on the straight line character of the plot at this point. This suggests that the composition $ZrH_{0.99}$ is in a two-phase region where the pressure is independent of composition. This can be seen in Figure 5. Fig. 2 shows a similar plot for the composition

$ZrH_{1.36}$. This plot also shows a reversible character and individual measurements are nearly identical with those for the composition $ZrH_{0.99}$. The straight line character of the curve persists above 10^{-2} mm of Hg which suggests that the composition $ZrH_{1.36}$ is also in a two-phase region.

Fig. 3 shows the plot for the composition $ZrH_{1.51}$. Here, a break occurs in the plot between 1 and 2×10^{-2} mm of Hg. Decomposition pressure is dependent upon the composition which suggests a single-phase region.

Fig. 4 shows a similar type of plot for the composition $ZrH_{1.74}$. This composition is also in a single phase region.

TABLE III. Summary of x-ray data (25°C)

Exp. No.	Temp, °C	Preparation time, min	Compn.	Treatment	Results
63-17	100	10	ZrH _{0.10}	Hom. ^a 100°C, 21 hr	$\alpha + \delta + \text{tr } \gamma'$
63-16	125	10	ZrH _{0.15}	Hom. 125°C, 20.5 hr	$\alpha + \delta + \text{tr } \gamma'$
63-15	150	12	ZrH _{0.246}	Hom. 150°C, 20 hr	$\alpha + \delta + \text{tr } \gamma'$
63-9	150	45	ZrH _{0.48}	Hom. 150°C, 20 hr	$\alpha + \delta + \text{s.a. } \gamma'$
65-11	150	81	ZrH _{0.52}	Hom. 250°C, 19 hr	$\alpha + \delta + \text{tr } \gamma'$
65-12	250	—	ZrH _{0.52}	Prep. from ϵ -phase	$\alpha + \delta + \text{s.a. } \gamma'$
65-15	150	48	ZrH _{0.53}	Direct, no hom.	$\alpha + \delta + \text{s.a. } \gamma'$
63-10	200	13	ZrH _{0.55}	Hom. 200°C, 20 hr	$\alpha + \delta + \text{tr } \gamma'$
63-14	225	8	ZrH _{0.755}	Hom. 225°C, 20 hr	$\alpha + \delta + \text{tr } \gamma'$
63-13	225	15	ZrH _{0.84}	Hom. 225°C, 20.3 hr	$\alpha + \delta + \text{tr } \gamma'$
63-6	175	165	ZrH _{1.105}	Hom. 175°C, 15.5 hr	$\alpha + \delta + \text{s.a. } \gamma'$
63-12	225	38	ZrH _{1.33}	Hom. 225°C, 20.5 hr	$\alpha + \delta + \text{tr } \gamma'$
64-45	225	51	ZrH _{1.44}	Hom. 325°C, 18 hr	$\delta + \text{tr } \gamma'$
64-41	225	65	ZrH _{1.44}	Hom. 225°C, 19 hr	$\delta + \text{tr } \gamma'$
64-17	230	1	ZrH _{1.51}	Heated to 500°C, hom. 200°C, 63 hr	δ
64-46	250	27	ZrH _{1.54}	Heated to 375°C, hom. 325°C, 19 hr	δ
64-47	250	29	ZrH _{1.56}	Prep. from ϵ -phase (fast)	$\delta + \text{tr } \epsilon$
64-34	250	48	ZrH _{1.60}	Prep. from ϵ -phase (fast)	$\delta + \epsilon$
64-35	270	51	ZrH _{1.64}	Hom. 250°C, 18 hr	ϵ
63-18	275	23	ZrH _{1.64}	H ₂ quenched	$\epsilon + \text{tr } \delta$
63-11	225	57	ZrH _{1.647}	Hom. 225°C, 19.5 hr	δ^b
63-21	225	82	ZrH _{1.77}	Hom. 225°C, 19 hr	ϵ
62-52	150	5580	ZrH _{1.84}	H ₂ cooled	ϵ
63-4	200	300	ZrH _{1.87}	Hom. 175°C, 15 hr	ϵ
63-2	225	180	ZrH _{1.965}	Hom. 200°C, 19 hr	ϵ

^a Homogenized.

^b Not in agreement with other observations.

tr—Trace.

s.a.—Small amount.

Fig. 5 shows a summary of the decomposition pressures at 500°C on a logarithmic scale, together with room temperature crystal structure studies of the phases. These studies will be discussed later. Fig. 5 suggests the following conclusions at 500°C. (A) The ϵ -phase has a range of homogeneity extending from ZrH_{1.965} to a composition near ZrH_{1.64}. (B) The δ -phase has a range of homogeneity from about ZrH_{1.4} to ZrH_{1.56}. (C) A two-phase region $\epsilon + \delta$ may exist between ZrH_{1.56} and ZrH_{1.64} although this has not been proved. (D) A two-phase region consisting of α - and δ -phases was found to exist between ZrH_{0.04} to ZrH_{1.40}. (E) Below a composition of ZrH_{0.04} a single phase region of α -Zr with hydrogen in solid solution was found to exist.

Crystal Structure Studies

A summary of the results are shown in Table III and in a graphical form in Fig. 5. Thermodynamic studies at 500°C are in essential agreement with crystal structure studies made on specimens prepared at temperatures of 300°C and lower. One exception is to be noted. This is the presence in the crystal structure studies of a minor transitional phase. The existence of this phase now designated as the γ' -phase in the zirconium-hydrogen system was first recognized by Jack (19) in a preliminary

x-ray study of our specimens. It was also suggested by Jack (19) that this phase is a transition phase between the hexagonal α -Zr phase and Hägg's face-centered cubic δ -phase. It is present only in small or trace amounts together with the α - and δ -phases.

The evidence for the existence of the γ' -phase is rather strong, as can be noted in Table III, since lines associated with this phase were found on many samples both etched and unetched. No evidence was found for this phase from the decomposition pressure studies at higher temperatures.

Fig. 6 shows a microphotometer trace of an x-ray diffraction pattern of a ZrH_{0.52} composition prepared from ϵ -phase by heating in vacuo. Three definite extra reflections are noted in the pattern. Calculations show these reflections fit a face-centered tetragonal cell with lattice parameters given in

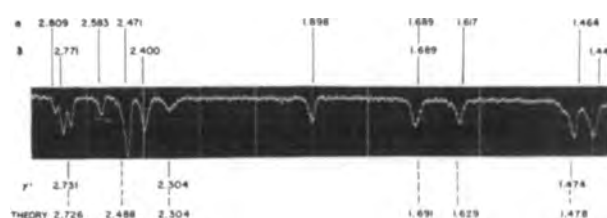


FIG. 6. Evidence for γ' phase

TABLE IV. Comparison lattice parameters zirconium hydride phases

Phase	Composition	Structure	Lattice parameters	
			Present work	Hägg
ϵ	ZrH _{1.966} - ZrH _{1.64}	Face-centered tetragonal	$a = 4.97 \pm 0.01 \text{ \AA}$ $c = 4.48 \pm 0.01 \text{ \AA}$ $a/c = 1.11 \pm 0.01$	$a = 4.974 \text{ \AA}$ $c = 4.440 \text{ \AA}$ $a/c = 1.118$
δ	ZrH _{1.44} - ZrH _{1.56}	Face-centered cubic	$a = 4.78 \pm 0.01 \text{ \AA}$	$a = 4.778 \text{ \AA}$
γ'	ZrH ₂	Face-centered tetragonal	$a = 4.61 \pm 0.01 \text{ \AA}$ $c = 4.975 \pm 0.01 \text{ \AA}$ $a/c = 0.926 \pm 0.003$	

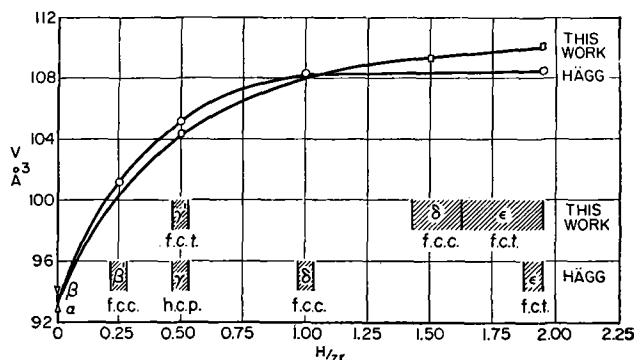
TABLE V. Calculated patterns

γ' Phase		α -Zr phase		δ -Phase	
hk	d_{hkl} (Å)	hkil	d_{hkil} (Å)	hkl	d_{hkl} (Å)
111	2.726	1 $\bar{1}$ 01	5.140	111	2.75
002	2.488	1 $\bar{1}$ 0 $\bar{1}$	2.795	200	2.384
200	2.304	10 $\bar{1}$ 1	2.455	220	1.687
202	1.691	10 $\bar{1}$ 2	1.892	311	1.438
220	1.629	1 $\bar{1}$ 03	1.715	222	1.376
113	1.478	11 $\bar{2}$ 0	1.616	400	1.192
311	1.398	11 $\bar{2}$ 1	1.541	331	1.094
222	1.363	10 $\bar{1}$ 3	1.461	420	1.066
004	1.244	20 $\bar{2}$ 0	1.398	422	.973
400	1.152	11 $\bar{2}$ 2	1.368	{333}	.921
{313}	1.095	20 $\bar{2}$ 1	1.349	{511}	
{204}					
331	1.061	1 $\bar{1}$ 04	1.286		
402	1.046	20 $\bar{2}$ 2	1.229		
420	1.031	11 $\bar{2}$ 3	1.176		
f.c.t. $a = 4.61 \text{ \AA}$ $a/c = 0.926$		h.c.p. $a = 3.229 \text{ \AA}$ $c = 5.141$		f.c.c. $a = 4.78 \text{ \AA}$	

Table IV. The theoretical pattern based on this structure is shown in Table V and compared with the calculated patterns for the α -Zr and δ -phases. With the exception of the three observed reflections, the other lines are masked by lines from the α - and δ -phases.

Thermal properties of this new phase have not been investigated. It appears to form by direct preparation in the $\alpha + \delta$ region of composition or by removal of hydrogen from the ϵ -phase. The composition of this phase has not been determined. However, a plot of the volume of the several hydride phases in Fig. 7 suggests a composition near ZrH_{0.5} or the same composition as Hägg's hexagonal γ -phase which we have not observed in this study.

Table IV shows a summary of crystal structure data on the several phases formed in the zirconium-hydrogen system with the alloys being formed at low temperatures. Averaged lattice parameters are also given in Table IV. The δ -phase was studied by direct hydriding to the given composition and

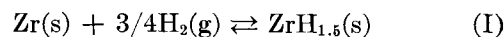
FIG. 7. Volume Zr and ZrH₂ structures

also by removal of hydrogen from ϵ -phase preparations until the proper composition was achieved. Results were in complete agreement with one possible exception noted in Table III.

Free Energy of Formation of the Delta Phase

The decomposition pressure of the δ -phase in Fig. 5 at 500°C was found to be dependent upon composition. However, in the two-phase region, the decomposition pressure of the δ -phase is the same as that for the α -phase saturated with hydrogen. Therefore, over the composition range of ZrH_{0.04} to ZrH_{1.40} a constant pressure is observed at 500°C. It is, therefore, of interest to determine the free energy equation for the δ -phase in contact with the α -phase saturated with hydrogen. For purposes of calculation a composition of ZrH_{1.5} for the δ -phase is taken.

Consider the equation



The equilibrium constant K is given by

$$K = p_{\text{H}_2}^{-3/4} \quad (\text{II})$$

The standard free energy of formation ΔF^0 is given by

$$\Delta F^0 = +3/4RT \ln p_{\text{H}_2} \quad (\text{III})$$

Here, R is the gas constant, T the temperature, and p the pressure in atmospheres.

TABLE VI. Decomposition pressure $ZrH_{1.5}$ (in contact with α -Zr)

t	T	$\ln P$	$-\Delta F^0$ avg
400	673.1	-15.84	15,820
425	698.1	-14.05	14,603
450	723.1	-12.90	13,820
475	748.1	-11.84	13,300
500	773.1	-10.80	12,600
525	798.1	-9.87	11,750
550	823.1	-9.18	11,230
575	848.1	-8.35	10,520

Table VI gives a summary of data and calculated values for the free energy of formation of $ZrH_{1.5}$ in contact with α -Zr.

The free energy as a function of temperature can be obtained from the relation:

$$\frac{\partial \frac{\Delta F^0}{T}}{\partial T} = -\frac{\Delta H^0}{T^2} \quad (\text{IV})$$

where

$$\Delta H^0 = \Delta H_0^0 + \int_0^T \Delta C_p dT \quad (\text{V})$$

Here, ΔH^0 is the standard heat of reaction at temperature T , ΔH_0^0 is the standard heat of reaction at 0°K, ΔC_p is the difference in heat capacities of products and reactants.

Unfortunately, heat capacity data are not available on $ZrH_{1.5}$ and only a semi-empirical equation can be derived. Kubaschewski and Evans (18) suggest the use of an approximate value for ΔC_p for reactions of this type of $\Delta C_p = 2.25$. Substituting in equations (IV) and (V) and integrating

$$\Delta F^0 = \Delta H_0^0 - 2.25 T \ln T + IT \quad (\text{VII})$$

Here, I is the conventional integration constant and ΔH_0^0 is determined from a conventional thermodynamic plot of Σ against $1/T$. Here,

$$\Sigma = \frac{\Delta H_0^0}{T} + I \quad (\text{VIII})$$

ΔH_0^0 is found equal to $-34,930$ cal/mole while the averaged value for $I = 43.88$.

The final semi-empirical equation for reaction (I) is

$$\Delta F^0 = -34,930 - 2.25 T \ln T + 43.88 T \quad (\text{IX})$$

ACKNOWLEDGMENT

The authors are indebted to Dr. K. H. Jack for pointing out the existence of the γ' phase and for his helpful suggestions in the early stages of this work.

Any discussion of this paper will appear in a Discussion Section to be published in the June 1955 issue of the JOURNAL.

REFERENCES

1. D. P. SMITH, "Hydrogen in Metals," The University of Chicago Press, Chicago (1948).
2. E. A. GULBRANSEN, To be published.
3. W. T. MUDGE, JR., "Zirconium and Zirconium Alloys," p. 730, American Society for Metals, Cleveland (1953).
4. A. WINKLER, *Ber.*, **23**, 2642 (1890).
5. A. WINKLER, *ibid.*, **24**, 873 (1891).
6. E. WEDEKIND, *Liebigs Ann. Chem.*, **395**, 149 (1913).
7. R. SCHWARZ AND E. KONRAD, *Ber.*, **54**, 2122 (1921).
8. L. WEISS AND C. NEUMANN, *Z. anorg. Chem.*, **65**, 248 (1910).
9. E. WEDEKIND, *Liebigs Ann. Chem.*, **371**, 378 (1910).
10. A. SIEVERTS AND E. ROELL, *Z. anorg. u. allgem. Chem.*, **153**, 289 (1926).
11. M. N. A. HALL, S. L. H. MARTIN, AND A. L. G. REES, *Trans. Faraday Soc.*, **41**, 306 (1945).
12. G. HÄGG, *Z. physik. Chem.*, **11**, 439 (1930).
13. A. E. VAN ARKEL, "Reine Metalle," J. Springer, Berlin (1939).
14. N. F. M. HENRY, H. LIPSON, AND W. A. WOOSTER, "The Interpretation of X-ray Diffraction Photographs," Macmillan & Co., Ltd., London (1951).
15. J. FITZWILLIAM, A. KAUFMAN, AND C. SQUIRE, *J. Chem. Phys.*, **9**, 678 (1941).
16. "Advances in Catalysis," p. 133, vol. V, Academic Press, Inc., New York (1953).
17. E. A. GULBRANSEN AND K. F. ANDREW, *Ind. Eng. Chem.*, **41**, 2762 (1949).
18. O. KUBASCHEWSKI AND E. L. L. EVANS, "Metallurgical Thermochemistry," p. 174, Butterworth-Springer, Ltd., London (1951).
19. K. H. JACK, To be published.

Determination of Barrier Layer Thickness of Anodic Oxide Coatings¹

M. S. HUNTER AND P. FOWLE

Aluminum Research Laboratories, Aluminum Company of America, New Kensington, Pennsylvania

ABSTRACT

A novel method is described for measuring the thickness of a barrier type anodic oxide coating or the barrier layer portion of a porous type anodic oxide coating. This method is used to follow the evolution of the barrier layer during the early stages of the formation of a porous type coating on aluminum and to establish certain dimensions of the fundamental oxide cells which comprise this type of coating.

INTRODUCTION

The virtues of the durable, protective anodic oxide coatings applied to aluminum have long been known and appreciated, but only recently have the submicroscopic features and dimensions of these coatings been established (1). Anodic coatings may be either porous or nonporous, depending on the electrolyte in which they are formed, but all have one feature in common, a zone of nonporous oxide or "barrier layer" adjacent to the metal. This paper describes a method for measuring the thickness of this barrier oxide layer, and demonstrates the manner in which this method may be applied to the investigation of the characteristics of oxide coatings on aluminum.

BARRIER LAYER

The barrier layer and forces that govern its formation and determine its behavior have been the subject of extensive research by many investigators. The primary forces governing formation of the coatings are believed to be ionic in nature, as indicated by Mott (2), Haring (3), Charlesby (4), and others. These investigators have stated that the barrier layer represents the distance through which a metal ion can penetrate a layer of its oxide under the influence of an applied potential. As such, the thickness of this layer is a function of the applied voltage, which is the driving force behind the metal ion. In the case of aluminum, Hass (5) has shown that barrier layer coatings form to a thickness of 14 Å per volt of applied potential.

When aluminum is made the anode in an electrolyte that can furnish oxygen-containing ions, combination between aluminum and oxygen occurs to form on the metal a continuous film composed principally of aluminum oxide. The nature of this film is such that it opposes the movement of ions and

electrons which is necessary for continued oxide formation and coating growth as long as the aluminum remains the anode. If the aluminum is made the cathode, however, the oxide film offers practically no resistance to the movement of electrons, and appreciable current can flow. This behavior is responsible for the rectifying action characteristic of anodically-formed oxide films on aluminum.

In the absence of solvent action by the electrolyte, the oxide layer formed anodically reaches a limiting thickness, at which point it becomes an effective barrier to further movement of ions and electrons, and current flow substantially ceases. The thickness of film required to block current flow effectively is a linear function of the applied voltage and, once the barrier layer has been completely formed, increases in thickness can be effected only by increasing the applied voltage. In this case, the entire coating constitutes the barrier layer (Fig. 1), and the thickness of the barrier layer in Angstrom units is 14 times the applied voltage. When the barrier layer has reached its limiting thickness, only a very low leakage current persists. This leakage current is substantially current flow through regions in the metal that contain constituent particles on which a complete barrier type of coating does not form and, consequently, differs for various alloy compositions.

In electrolytes that have the ability to dissolve the oxide, the effect of solvent action is superimposed on the oxide formation process, with the result that a somewhat different situation exists. The electrolytic cell continues to form oxide as long as the barrier layer corresponding to the applied voltage is not complete. Solvent action, however, prevents the barrier layer from reaching its limiting thickness. Under these conditions, current continues to flow, a porous oxide structure is created, and relatively thick oxide coatings are formed. As oxide continues to form, there remains between the metal and the base of the pores a thin layer of barrier oxide which restricts, but does not block, current flow. Although

¹ Manuscript received April 26, 1954. This paper was prepared for delivery before the Chicago Meeting, May 2 to 6, 1954.

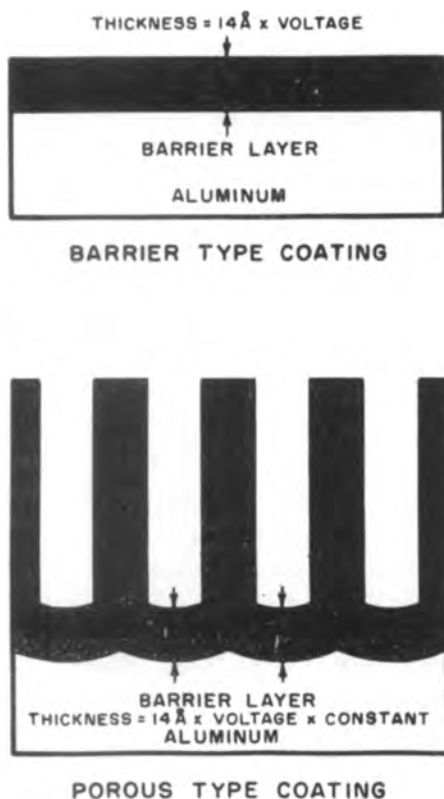


FIG. 1. Barrier layer of anodic oxide coatings

all the oxide formed was at one time in the barrier layer, this thin layer of oxide at the base of the pores is considered to be the barrier layer portion of the porous type of oxide coating (Fig. 1). The thickness of this layer in Angstrom units is 14 times the applied voltage times a factor having a value less than one. The actual value of this factor is determined by the electrolyte.

BARRIER LAYER DETERMINATION

The thickness of barrier layer coatings and the barrier layer portion of porous oxide coatings is highly significant in terms of the characteristics and behavior of the coatings. In the case of barrier type coatings, where the entire coating constitutes the barrier layer, a fairly good approximation of coating thickness can be made from the interference colors, if the coating is greater than about 300 \AA in thickness, or by microscopic examination if the coating is thicker than about 2000 \AA . With the porous type of coating, which has a layer of porous oxide above the barrier layer and has only a very thin barrier layer because of the relatively low voltages used, these methods are not practical. The electron microscope has indicated the presence of the barrier layer portion of porous coatings (6), but present replica methods are not adequate for precise measurement.

A method has been developed by which the thickness of a barrier layer coating or the barrier portion

of a porous type of coating can be determined with substantial accuracy. This method is based on oxide forming characteristics in electrolytes that do not dissolve the oxide. Here, oxide forms anodically to the 14 \AA/v value, and thickness can be increased only by increasing voltage. By the same token, if any anodic voltage less than the formation voltage is applied, only leakage current will flow. If gradually increasing voltage is applied to this nonporous barrier type of coating in an electrolyte which does not exert significant solvent action, values up to and including the forming voltage will produce only leakage current. Any value above the formation voltage will produce current flow greater than the leakage value, as the coating tends to form to the thickness corresponding to the higher voltage.

The same principles hold with the barrier layer portion of the porous type of oxide coating. With this type of coating, however, the barrier layer forms to a thickness of some value less than 14 \AA/v as indicated by the fact that current greater than leakage continues to flow. As a result, current higher than the leakage value will flow at some voltage below the formation voltage. The voltage at which current flow equals the leakage value is a measure of the thickness of the barrier layer portion of the coating.

An approximation of barrier layer thickness on an oxide coated sample may be made by observing current flow with increasing voltage in an electrolyte that forms a barrier type of coating. As voltage is increased, the leakage current rises very slowly until the voltage corresponding to the thickness of the barrier is approached. Once appreciable current starts to flow, small voltage increments produce large increases in current. The approximate thickness in Angstrom units of the barrier layer is 14 times the highest voltage that does not produce a pronounced rise in current flow. With reasonable care, it is possible to determine this voltage for coatings formed on high purity aluminum to within less than 1 v, which corresponds to a barrier thickness of about $\pm 14 \text{ \AA}$. The value determined in this manner is always low, however, because the leakage current for the particular material has not been considered.

A more accurate value for the thickness of the barrier layer may be determined by taking into account the leakage current for the material under investigation. First, the approximate barrier voltage is determined as closely as possible in the manner described above. Then, the leakage current for the material under investigation is determined at this approximate voltage. This determination is made by applying the particular voltage to a freshly cleaned sample of the material and observing the final, steady leakage current after the barrier type of coating is completely formed. Finally, the voltage re-

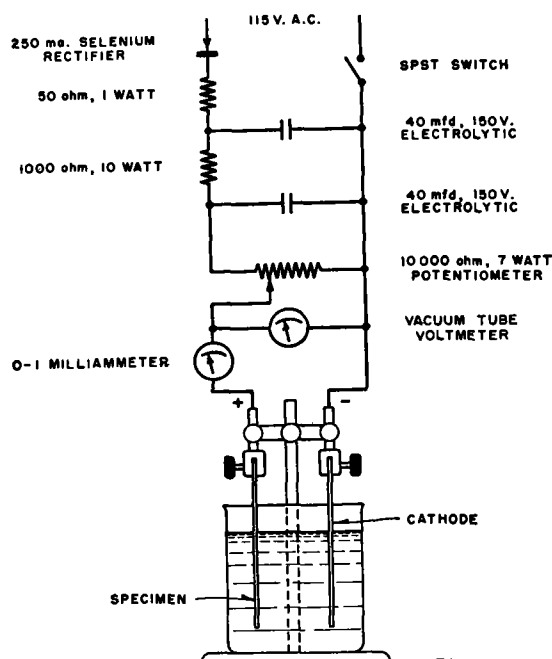


FIG. 2. Electrical arrangement for determining barrier layer thickness.

quired to produce this current flow with the unknown barrier layer is determined. This permits determination of the actual barrier layer voltage to within ± 0.1 v for coatings formed on high purity aluminum, which means that the barrier layer thickness can be found within about 3 \AA .

In the case of coatings formed on high purity aluminum, leakage current varies only slightly over a rather wide range of voltages so that further measurements of leakage current and barrier layer voltage are not necessary. In the case of aluminum alloys that have higher leakage current and show greater variations in leakage with changing voltage, such additional measurements are frequently justified.

Excellent results can be obtained with this method using the simplest of equipment. All that is required is a variable direct current source, an accurate voltmeter, and a sensitive milliammeter. The arrangement used to make the barrier measurements discussed in this paper is shown by Fig. 2. To determine the barrier layer thickness, the specimen is made anode in an electrolyte that does not exert significant solvent action on the oxide. A freshly cleaned cathode of the same material is used to avoid potential differences between the two electrodes. Current readings are then made at increasing voltages and plotted as described above. In the work described in this paper, the electrolyte used was a 3% tartaric acid solution adjusted with ammonium hydroxide to a pH of 5.5, although any other electro-

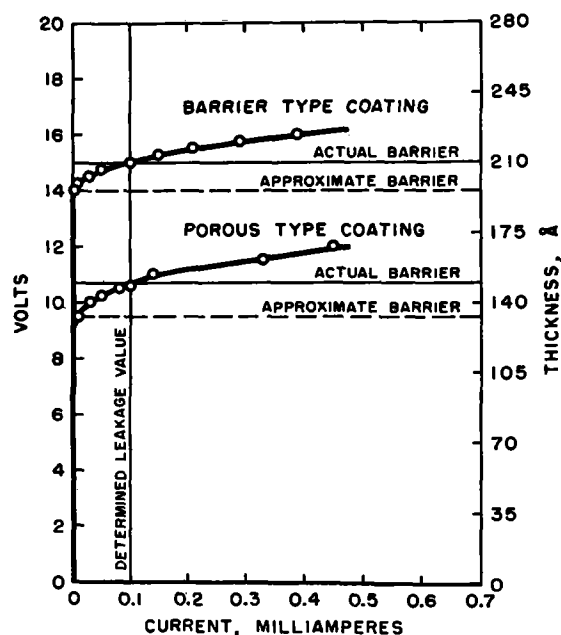


FIG. 3. Determination of barrier layer thickness

lyte having similar characteristics should be satisfactory. The electrolyte was maintained at 75°F (24°C) during the measurement.

The manner in which barrier layer thickness values are obtained is illustrated in Fig. 3. Here, the current values for increasing voltage are plotted for two 15-v anodic coatings applied to 1 in.^2 (0.065 dm^2) samples of high purity aluminum. One of these is a barrier type of coating formed in the ammonium tartrate electrolyte, and the other is a porous type of coating formed in a 15% sulfuric acid electrolyte at 70°F (21°C). Also, the steady current value representing leakage for these aluminum samples in the neighborhood of 15 volts is indicated.

In the case of the 15-v barrier type coating, the lowest voltage value to produce significant current flow was 14.0 v which gives an approximate barrier thickness value of 196 \AA . The steady leakage current measured for the high purity aluminum sheet specimens of the particular area used was 0.1 ma in the range of 10 to 15 v. The intersection of the voltage-current curve with the line representing this current value occurs at exactly 15 v. This was the voltage used to form the coating and represents a barrier layer thickness of 210 \AA , which is the maximum thickness of barrier coating that can be formed on aluminum by 15 v of applied potential.

With the porous type of coating, the barrier layer thickness must be less than the $14 \text{ \AA}/\text{v}$ value as discussed earlier. In the case of the coating formed in 15% sulfuric acid at 70°F (21°C) (Fig. 3), the approximate barrier layer thickness, as indicated by the voltage required to produce appreciable current

flow, is 133 Å. The intersection of the voltage-current curve with the leakage line occurs at 10.7 v, which shows that the actual barrier layer thickness is 150 Å. Thus, in the 15% sulfuric acid electrolyte at 70°F (21°C), the barrier layer forms at a rate of 10.0 Å/v. The term "unit barrier thickness" will be used to describe the thickness of barrier layer formed per volt of applied potential.

APPLICATIONS

The determination of barrier layer thickness may be used to establish many facts concerning the formation and behavior of anodic oxide coatings. For instance, it is possible to establish changes in barrier layer thickness which accompany current fluctuations observed during the initial stages of the formation of the porous type of oxide coating. Inasmuch as the barrier layer constitutes the principal resistance across the voltage source, a decrease in current indicates that barrier layer thickness is increasing and, conversely, an increase in current indicates a decrease in barrier layer thickness. In electrolytes that do not dissolve the oxide appreciably, current is initially high but decreases rapidly as barrier layer thickness increases. In a relatively short time, current reaches a low, steady leakage value, at which point the barrier layer has attained its limiting thickness of 14 Å/v.

In the case of electrolytes that dissolve the oxide, solvent action combined with coating formation produces a more complex situation. As in the case of the barrier type of coating, current flow is initially high and decreases with time as barrier layer thickness increases. With the porous type of coating, however, decrease in current is not as rapid because of solvent action which tends to reduce the thickness of the barrier layer. After a short time, current flow reaches a minimum value and then starts to rise as solvent action, which is increasing, first equals and then exceeds coating formation. Current flow becomes steady when formation and solution of oxide reach a balance, at which point barrier layer thickness becomes constant.

As an illustration of the evolution of the barrier layer portion of a porous type of oxide coating, changes in barrier layer thickness that occurred during the formation of a coating in a 15% sulfuric acid electrolyte at 70°F (21°C) using a potential of 15 v are presented. As shown by Fig. 4, the thickness of the barrier layer increased rapidly at first but as solvent action began to have an effect, the rate of increase of the barrier layer diminished. After about 5 sec, solvent action began to exceed the rate of oxide formation and barrier layer thickness decreased. After about 18 sec, oxide formation again exceeded solvent action and barrier layer thickness increased

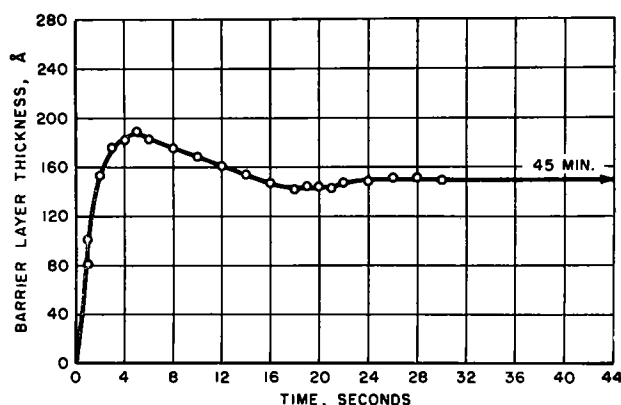


FIG. 4. Evolution of barrier layer portion of a 15-volt coating formed in 15% sulfuric acid electrolyte at 70°F.

slightly. Finally, after about 25 sec, the balance between oxide formation and solution of oxide at the base of the pores was reached and the barrier layer thickness became constant. No further change in thickness was observed up to a time of 45 min. The rapidity with which the initial fluctuations in current occur and the time required to reach equilibrium thickness are a function of the current capabilities of the voltage source. As a result, transient barrier layer thickness values shown apply only under the particular conditions of this experiment.

The method was also applied to sulfuric acid coatings sealed in boiling water to determine whether the hydrated oxide formed within the pores during sealing would interfere with the measurement of barrier voltage. If this hydrated oxide did interfere with the measurements, an apparent increase in barrier layer thickness with sealing would be noted. Measurements indicated, however, that the barrier layer thickness decreased with sealing time. Thus, the hydrated oxide produced during sealing does not interfere with this measurement. Therefore, the method can be applied to water-sealed as well as unsealed oxide coatings.

This decrease in barrier layer thickness observed on sealing in boiling water was investigated further to determine the actual effect of such sealing. It was found that barrier layer thickness was reduced by about 4 Å for each ten minutes of sealing, which indicates that prolonged sealing treatments in boiling water may be detrimental.

Determinations of unit barrier layer thickness have been made in four electrolytes used to make porous type anodic coatings inasmuch as barrier layer thickness is one of the important dimensions of the oxide cell. Electrolytes selected were those used in previous work on the dimensions of anodic oxide coatings. Unit barrier thickness was found to be practically independent of forming voltage but varied appreciably among the four electrolytes, as was the case with cell wall thickness. Also, variations in unit

barrier thickness and unit wall thickness were in the same order in the four electrolytes, although the unit barrier thickness was greater by a factor of about 1.2. The unit barrier thickness values from this work and the unit wall thickness and pore diameter values from previous work (1) are given in Table I. These values along with forming voltage establish the dimensions of oxide cells of coatings formed in these electrolytes.

TABLE I. *Basic dimensions of oxide cells*

Electrolyte	Barrier Å/volt	Wall Å/volt	Pore diameter, Å
4% Phosphoric acid, 75°F (24°C)	11.9	10.0	330
2% Oxalic acid, 75°F (24°C)	11.8	9.7	170
3% Chromic acid, 100°F (38°C)	12.5	10.9	240
15% Sulfuric acid, 50°F (10°C)	10.0	8.0	120

Barrier layer thickness determinations, in combination with determinations of oxide cell size by electron microscopic examinations of cell base patterns, may be used to obtain an approximation of the formation voltage of an unknown anodic coating made in any of these four electrolytes and the particular electrolyte in which it was formed. From previous work (1)

$$C = 2WE + P \quad (I)$$

where C is the size of the individual oxide cells, W is unit wall thickness (the thickness of oxide in the cell wall per volt of forming potential), E is forming voltage, and P is pore diameter. Also,

$$T = BE \quad (II)$$

where T is total barrier thickness, B is unit barrier thickness, and E is forming voltage. Inasmuch as unit barrier thickness is approximately 1.2 times unit wall thickness, equation (II) may be written as

$$T = 1.2 WE \quad (III)$$

Combining equations (I) and (III) gives equation (IV) which defines pore diameter in terms of cell size and total barrier thickness.

$$P = C - 1.67 T \quad (IV)$$

C can be determined from measurements of the cell base pattern of the unknown coating, and T can be found from barrier layer thickness determinations. As a result, pore diameter can be calculated and, if the electrolyte was one of the group which has been investigated, the particular electrolyte can be established. Unit barrier thickness and unit wall thickness are then known and either equation (I) or (II) may be solved to establish forming voltage.

The examples which have been presented are but a few of the many ways in which the determination of barrier layer thickness may be applied to the investigation of anodic oxide coatings. These measurements have revealed many interesting and unusual facts relating to the formation of these coatings and have been useful in establishing the electrolyte type and forming conditions used to produce coatings having certain desirable characteristics. Determination of the barrier layer thickness may be used to establish the effect of various treatments or environments on anodically formed oxide, to investigate the nature and characteristics of the natural oxide film on aluminum, and to explore other phases of anodic coating formation and behavior, the scope of which is limited only by the imagination of the investigator.

ACKNOWLEDGMENT

The authors wish to express their appreciation to F. Keller, under whose direction this work was conducted.

Any discussion of this paper will appear in a Discussion Section to be published in the June 1955 issue of the JOURNAL.

REFERENCES

1. M. S. HUNTER AND D. L. ROBINSON, *This Journal*, **100**, 411 (1953).
2. N. F. MOTT, *Trans. Faraday Soc.*, **43**, 429 (1947).
3. H. E. HARING, *This Journal*, **99**, 30 (1952).
4. A. CHARLESBY, *Proc. Phys. Soc.*, **B66**, 317 (1953).
5. G. HASS, *J. Opt. Soc. Amer.*, **39**, 532 (1949).
6. J. D. EDWARDS AND F. KELLER, *Trans. Amer. Inst. Mining Met. Engrs.*, **156**, 288 (1944).

The Söderberg Self-Baking Electrode¹

M. O. SEM

Elektrokemisk A/S, Oslo, Norway

ABSTRACT

The paper discusses the difference between electrode paste as used for prebaked electrodes and Söderberg electrodes. Baking conditions in a self-baking electrode are described. The quality depends on the calcining temperature of the dry material. New equipment giving improved baking conditions for the electrode is described.

INTRODUCTION

Consumption of Söderberg electrodes in the United States totals approximately 300,000 tons per year, while another 180,000 tons are consumed annually in Canada. Most of this is consumed in furnaces for the production of aluminum. Lately, however, a number of large carbide furnaces in the USA have been provided with Söderberg electrodes so that its use is now considerable in smelting furnaces. A discussion of conditions existing in the Söderberg electrodes is, therefore, of considerable interest.

SÖDERBERG ELECTRODE PASTE

Carbon electrode paste is made of material like calcined anthracite—alone, or with petroleum coke or pitch coke mixed with a carbonaceous binder such as a medium pitch. Exact composition of the paste depends on the product of the electric furnace, i.e., in aluminum pots the paste must be made from petroleum coke or pitch coke in order not to introduce impurities into the produced metal. In most other cases, calcined anthracite is used predominantly. When first developed, the paste for Söderberg electrodes in Norway was made as closely as possible to the paste used for prebaked carbon electrodes. The latter are pressed from a rather dry paste in heavy hydraulic presses, or by other high pressure means. This could not easily be applied to the Söderberg electrode since it is made up in place over the furnace in which it is used. It was generally believed that it would not be possible to make in this way an electrode which would compete successfully with prebaked electrodes. During the first tests it became evident that conditions prevailing in the Söderberg electrodes during baking differ radically from those of prebaked electrodes. A much softer paste is required in order to attain satisfactory operation. The production of a self-

baking electrode is an art which cannot be understood from the previous procedure.

Actually, it was found that Söderberg electrodes were highly improved in quality with increase in binder. The reason is that the baking zone in the electrode during its use is more or less horizontal, moving slowly upward as the electrode is lowered into the electric furnace to make up for electrode consumption. The soft paste in the upper part of the electrode rests with its weight on the baking zone and settles as the first volatiles are driven off during baking. Volatiles cannot rise in the electrode, but must escape downward through the pores of the already baked electrode and out the casing. This part of the electrode is incandescent (800°–900°C), and descending tar vapors passing through the carbon are cracked, leaving a considerable amount of carbon in the pores. This condition is illustrated in Fig. 1 and 2 which apply to a Söderberg electrode in a closed steel furnace and in an aluminum furnace, respectively.

Cracking of the volatiles can be studied easily in the laboratory by passing tar vapors slowly through a porous carbon electrode at temperatures between 600°–800°C. Results of such experiments (Table I) show a decided improvement in the quality of the electrode paste with higher carbon deposition. Thus, 2–3% carbon increases the crushing strength by more than 150 kg/cm².

Evidently, the quality of a Söderberg electrode depends on the amount of tar fumes forced through the porous part of the baked electrode. Actually, the content of binder in the electrode paste is made as high as practicable—under ordinary conditions, 4–10% more than in a paste used for prebaked electrodes. The actual content of binder in the paste depends on conditions and must be adjusted to the raw material of the electrode as well as to circumstances prevailing in the electrode while it is in use.

This condition may be illustrated by saying that there is no upper limit to the amount of binder that may be used in the Söderberg paste, but there

¹ Manuscript received March 12, 1954. This paper was prepared for delivery before the Chicago Meeting, May 2 to 6, 1954.

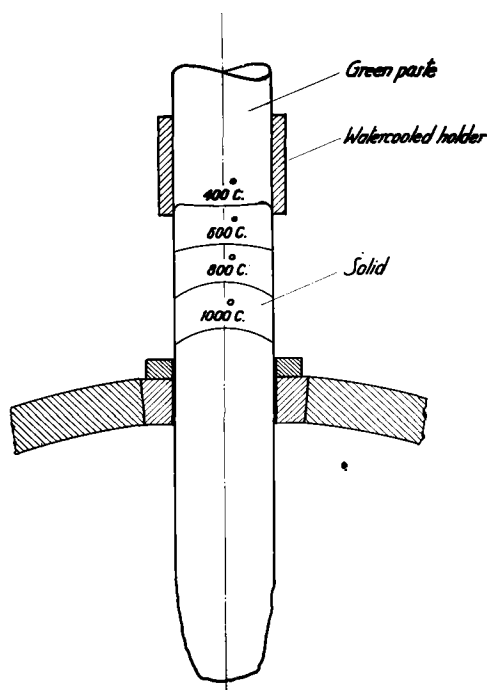


FIG. 1. Temperature zones in a Söderberg electrode in a teel furnace.

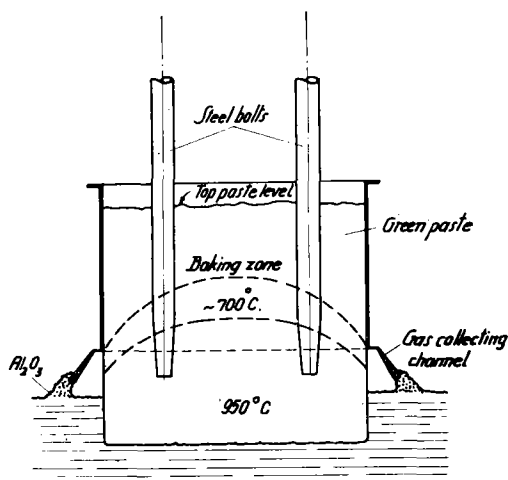


FIG. 2. Temperature zones and baking zone in a Söderberg aluminum anode.

is a decided lower limit, which is sufficiently high to render this paste useless in prebaked electrodes. Ordinarily, 18% binder is minimum.

ON CALCINING OF ANTHRACITE AND PETROLEUM COKE

These materials are calcined prior to use in the Söderberg electrode paste because volatile matter must be driven off, and shrinking of materials during calcination finished, before the binder is mixed in. If not, the electrode will crack during operation because volatiles of the binder are driven off at a lower temperature than the last fraction of

TABLE I

Temp, °C	Increase in weight	ohms/m/mm ²	Apparent density	Crushing strength kg/cm ²
No gas passed	—	128	1.38	203
700°C	1%	106	1.38	290
700°C	3.2%	94	1.42	363
800°C	2.3%	105	1.43	348

TABLE II

Anthracite		Electrode Paste		Baked Sample	
Type	El. resist. ohms/m/mm ²	Binder content %	Loss in baking %	El. resist. ohms/m/mm ²	Crushing strength kg/m/cm ²
A	810	21	14.7	102	152
B	1280	19	12	104	254

volatiles contained in the dry materials. Shrinking takes place at temperatures where volatiles have been evaporated.

For these reasons it is necessary to calcine raw materials at about 1200°C or more. The higher the calcining temperature, the more complete the shrinking and the higher the absolute density of the material. It has been found, however, that it is important not to calcine at a higher temperature than necessary. The higher the calcining temperature the more binder is needed for production of an electrode paste of a certain viscosity at operating temperatures. Many laboratory tests have been carried out showing that wetting the surface of the raw materials requires more binder, the higher the calcining temperature (Table II).

This table shows that an anthracite with higher resistance because of better wetting produces a much stronger electrode of approximately the same electrical conductivity.

These experiments show the importance of carrying out calcination under strictly controlled conditions. Actually, the best temperatures must be ascertained for each type of carbon material. Previously, calcining furnaces used for anthracite all over the world were electric shaft furnaces through which anthracite passed vertically. The material so produced has been found to be heterogeneous after calcination because electric current in the anthracite or coke concentrates in certain paths by virtue of the increase in conductivity with temperature. The calcined anthracite produced in these furnaces would therefore tend to be overheated along the center part of the furnace, while materials passing down the furnace walls would not be fully calcined. For petroleum coke, a gas- or oil-fired rotating kiln has been adopted to advantage. A higher temperature must be used for anthracite.

In order to calcine under fully controlled, even conditions an improved electric calcining furnace has been developed.² It is a rotating tube furnace, a part of which is provided with graphite electrodes. These are used to pass electric current through the anthracite, and temperature can be increased under strictly controlled conditions. Volatiles are burned and used to preheat the charge before it enters the heating zone at 600°–900°C. The power consumption of such a furnace is only 300–500 kwhr/metric ton of calcined anthracite. In comparison, the previous electric shaft furnace ordinarily consumed about 1000–1100 kwhr/metric ton. A furnace of about 50 tons of calcined anthracite per day is now operating in Norway.

SELF-BAKING OF ELECTRODES

The quality of the baked Söderberg electrode, produced from a given electrode paste, is governed by the rate of baking and the efficiency of pyrogenic cracking of volatiles in pores of the electrode during the baking process. This is considered more fully in terms of conditions prevailing in a smelting furnace such as a carbide furnace.

Descent of the electrode into the smelting furnace depends on the electrode consumption, which again is dependent on the particular process carried out in the furnace. Ordinarily, dimensions of the electrode are determined by conditions existing in the furnace. It is therefore not possible to control electrode consumption in inches per day. Consumption, however, is practically even during operation of the furnace, which is continuous. The baking process progressing through the electrode during the operation is, however, not only governed by electrode consumption per day, but also to a large extent by slipping of the electrode through the water-cooled electrode holder. The baking conditions will be very different if the electrode is slipped through the holder frequently in short lengths or seldom, but farther each time. In ordinary smelting furnaces the baking zone in the electrode is found inside the water-cooled electrode holder in such a way that the electrode is ready baked in the lower part of the holder but unbaked in the upper part of it. Thus, the electrode takes the shape of the holder, and a good electrical contact is obtained. It is easy to determine the shape and place of the baking zone by introducing a long rod through the soft green paste in the upper part of the electrode.

Ordinarily, electrode consumption in furnaces for the production of carbide and ferrolloys, as well as in steel furnaces, amounts to approximately 4–20 in./day, according to conditions. Slipping

² Through cooperation between Elektrokemisk A/S and F. L. Smidth & Co. A/S, Copenhagen.

electrodes weighing 15 tons or more through the holder has always been an awkward operation. The ordinary practice has been to slip the electrode at least 4–10 in. at a time. As seen from the baking zone, Fig. 1, every slip moves the baking zone downward in relation to the holder. After each slipping, the baking proceeds rapidly until the baking zone has again reached the starting position, where the cooling effect of the electrode holder reduces the baking rate strongly. After each electrode slip tar vapors in the baking zone are driven off very fast, and more violently the farther the electrode is slipped at each time. Since tar vapors must escape downward from the baking zone through the baked part of the electrode, such violent development of volatiles may easily result in accumulation of gas pressure in the electrode whenever the baking proceeds too fast.

At first it was the practice to make holes in the electrode casing in order to let tar vapors escape as easily as possible. This has disadvantages because the vapors condense on the electrode holder where they mix with dust and disturb the electrical contact. The most important drawback to this practice is that the tar vapor is not broken up sufficiently in the electrode pores. Thus, it has been found better to use a gas-tight electrode casing whereby the tar vapors must pass through a large part of the incandescent baked electrode. The baked electrode ordinarily has a porosity of 25% or more so that it is easy for gas to escape through this part of the electrode, provided it is developed rather evenly. If baking does not proceed slowly and evenly, gas pressure in the electrode may make it swell, and perhaps burst. (Fig. 3)

The paste swells between about 300°–400°C, depending markedly on rapidity of the temperature rise. Under ordinary conditions it does not affect the quality of the electrode. Best baking conditions are obtained if the electrode can slide continuously through the water-cooled electrode holder. For practical reasons this cannot be effected satisfactorily. It is necessary to let the electrode slide through the holder at intervals. However, baking of the electrode progresses more evenly, the shorter the slipping. Therefore, the equipment used for slipping should be remotely controlled by hydraulic, pneumatic, or similar means.

ELECTRODE HOLDER

Details of the electrode equipment must vary for different furnaces according to conditions. One of the most difficult applications is to tilting furnaces. Söderberg electrodes have been adopted in such furnaces in some important installations in Norway, Sweden, Finland, France, and Italy. How-

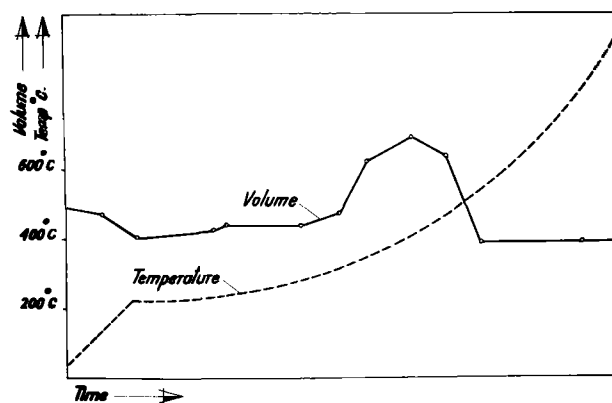


FIG. 3. Change of volume with the temperature during baking.

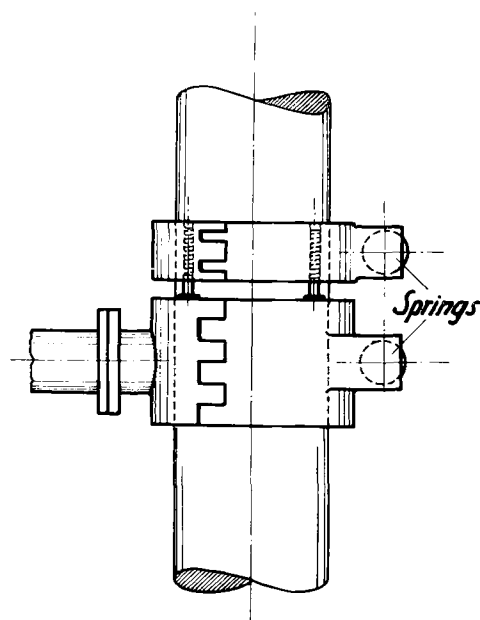


FIG. 4. Automatic slipping device

ever, conditions prevailing in these furnaces have presented particular difficulties for the following reasons:

1. Electrodes are ordinarily tilted with the furnace, which increases strain on the electrode.
2. Operation is batch type. There is little opportunity of resetting the electrode holder during heats.
3. Electrodes are ordinarily lengthened outside the furnace. Operation is therefore semicontinuous.

APPLICATION TO MELTING FURNACES

Electrode holders generally used in electric steel furnaces in Europe consist of 3 parts, one fixed and two gripped closely around the electrode like hinged jaws. The jaws are operated by means of a tangentially arranged screw. Ordinarily the holder is reset after each tapping during which the electrode is allowed to rest on the charge or on the

furnace bottom. Conditions can be improved by operating the jaws by pneumatic or hydraulic pressure. However, it is difficult to use these means during operation and to control slipping as desired unless the electrode is allowed to rest on the charge or the furnace bottom.

In order to obtain good baking conditions in the electrode, a hydraulic or pneumatic device has been developed³ which allows perfect control of slipping by simply turning a valve. The holder (1) is shown in Fig. 4. The hinged jaws have been maintained, but the tangential screw has been replaced by a spring-operated pressure device which clamps the jaws onto the electrode. The spring pressure may be released for slipping by applying compressed air or fluid pressure.

The slipping length is controlled by an automatically operated stopping device arranged on the electrode at the top of the holder. The stopping ring is like the holder except that ordinarily it has no current supply and is situated lower on the electrode. It is clamped around the electrode by fluid-operated springs exactly like those of the holder. It controls slipping by being clamped on to the electrode during the slipping. The electrode is stopped as soon as the ring hits the top of the holder. It is connected to and engages the holder with vertically arranged springs. These springs are compressed during slipping so that they automatically return the stopping ring to the initial distance above the holder as soon as the ring is released. During regular operation both holder and stopping ring clamp on to the electrode at the correct distance.

Ordinarily a slippage of 1-2 in. at a time is permitted. This insures a very smooth and safe movement under conditions which allow favorable baking of the electrode. The whole process is carried out by operating a couple of valves connected with the 3 electrode holders of the furnace.

Fig. 5 shows an electrode holder as installed in a 40-ton steel furnace of Christiania Spigerverk at Oslo. The holder has been tried out for more than 3½ years and has now been adopted for other furnaces in Norway and Sweden. It has contributed very much toward improving operating conditions in steel furnaces. In Scandinavia, where the choice is between graphite electrodes and Söderberg electrodes, consumption of the Söderberg type is somewhat less than twice that of graphite electrodes, while the cost of Söderberg electrodes is only about 1/3-1/4 the cost of a graphite electrode. This applies to electrodes of 600-700 mm diameter. Actual electrode consumption in a 25-ton furnace of Christiania Spigerverk has been about 6-7 kg/metric ton of steel (cold charge).

³ By Elektrokemisk A/S.

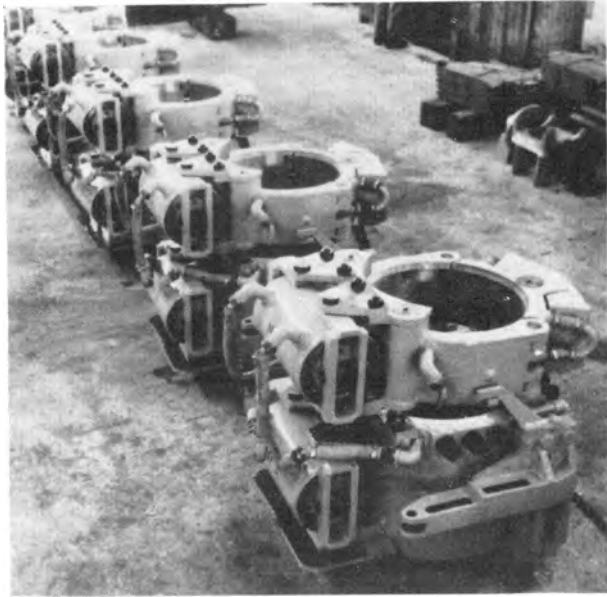


FIG. 5. Steel furnace electrode holder with automatic slipping device.



FIG. 7. Electrode with mantle as Fig. 8

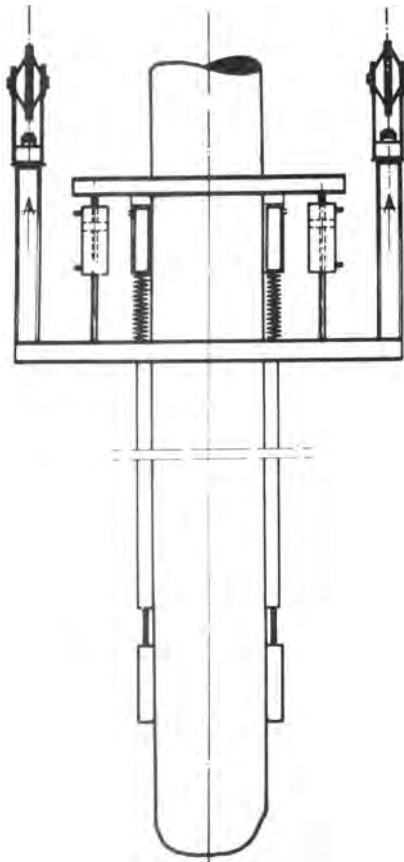


FIG. 6. Automatic slipping device for larger electrodes

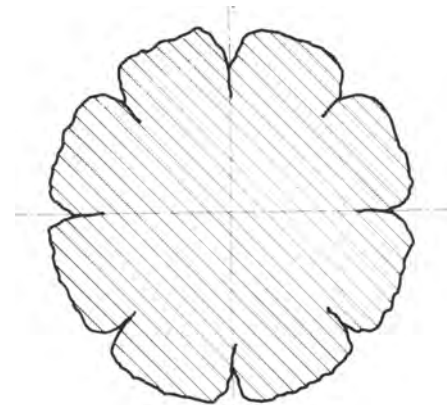


FIG. 8. Cross section of a baked Söderberg electrode under oxidizing conditions.

APPLICATION TO SMELTING FURNACES

The slipping arrangement described above has also been successfully applied to Söderberg electrodes in furnaces for calcium carbide, ferro-alloys,

and the like. Electrodes in such furnaces are ordinarily larger (up to 40-60 in. diameter). Details have been changed to meet the requirements of these big electrodes. Ordinarily, they are carried by an electrode holder which is suspended by a permanent iron casing surrounding the electrode for protection against dust and excessive heat (no baking is wanted above the electrode holder). This arrangement is shown in Fig. 6. The stopping ring is arranged at the top of the permanent iron casing and is designed for remote handling hydraulically. This makes possible a simple and perfectly controlled slipping process. Previously, slipping was controlled by applying Wisdom ribbons which were

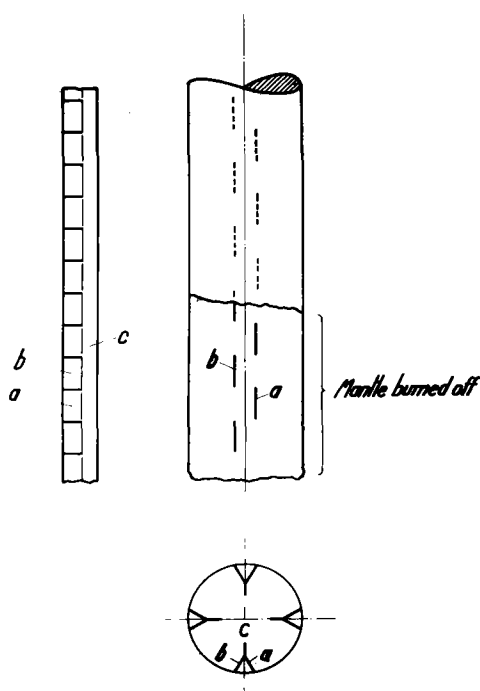


FIG. 9. New electrode mantle for steel furnace electrodes (Christiania Spigerverk).

welded to the electrode casing and consumed with the electrode.

The electrode holder has also been changed to hydraulic or pneumatic operation. This has greatly improved safety factors. At the same time, these electrode holders have been arranged inside a water-cooled, cylindrical casing which allows extension of the holder into the furnace through the furnace roof. Thereby the length of electrode from the lower end of the holder has been reduced, improving the electric conditions and simultaneously reducing strain to the electrode.

By slipping the electrode as described here, it has proved possible to simplify design of the iron casing with ribs which are filled with the electrode paste. The shape of the casing should be decided upon in each individual case. In melting furnaces a great deal of work has been done to improve the shape of the casing ribs also.

THE ELECTRODE CASING

The iron casing of the Söderberg electrode as described originally (2) is used in most furnaces all over the world. It insures good operation in most cases, but it has the drawback that the ribs form slots in the electrode periphery. This is a disadvantage if the furnace atmosphere is somewhat oxidizing, as in a steel furnace. In such a case, the lower part of the electrode may take on the shape shown in Fig. 7. Similar conditions are met in FeMn furnaces owing to O_2 development. This no

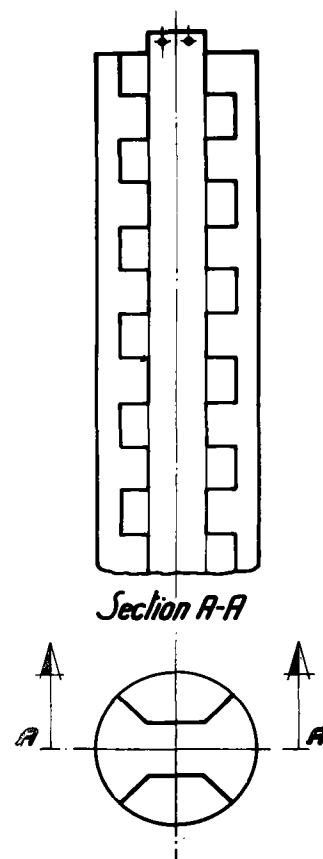


FIG. 10. Another method to avoid lengthwise slots in the baked electrode in steel furnaces (Sandviken).

doubt weakens the electrode and increases electrode consumption.

Fig. 8 shows an arrangement of ribs whereby continuous lengthwise slots have been avoided. Fig. 9 shows an electrode of this type in a steel furnace of Christiania Spigerverk.

A somewhat different arrangement has been developed by Sandvikens Jernverk in Sweden (Fig. 10). Even here the ribs form no slots in the periphery of the electrode, and they have been interconnected in such a way as to strengthen the electrode in the direction of tilting.

Both of these casing shapes are used in steel furnaces, but from operating results it has not yet been possible to decide which shape is better.

This paper has dealt mostly with electrodes in smelting and melting furnaces. Their use in aluminum furnaces is so different that it would require a separate paper. It has therefore been necessary to leave out this interesting application.

Any discussion of this paper will appear in a Discussion Section to be published in the June 1955 issue of the JOURNAL.

REFERENCES

1. K. FOYN, U. S. Pat. 2,668,183, April 2, 1923.
2. C. W. SÖDERBERG, U. S. Pat. 1,440,724, April 2, 1923.

Some Experiments with Scale Models of Electrothermic Furnaces¹

OLUF CHR. BÖCKMAN

Elektrokemisk A/S, Oslo, Norway

ABSTRACT

Reproduction of temperature distribution in furnaces of different size is shown, by dimensional analysis, to require direct proportionality between power input and linear dimensions of the furnace, if transfer of heat by conduction is a controlling factor. Experiments with scale models indicate the importance of correct temperature gradients as a criterion of similarity. A 1:5 linear scale model of an industrial furnace for calcining anthracite has been successfully run according to this criterion. The principle has been extended to electric smelting furnaces with good results.

INTRODUCTION

Several authors (1-6) have compared the size of industrial electrothermic furnaces, especially the size of the electrodes, with the power input to the furnace at normal operation. Industrial furnaces are designed and operated to give the best operating and economic conditions, which conditions are incidentally carried into the comparison. The range of furnace sizes compared is relatively narrow, as the comparison naturally is limited to existing industrial furnaces.

In this paper, a different point of view is adopted. For research and development on electrothermic processes and furnaces, it is advantageous to perform experiments on small scale apparatus. The aim, therefore, is a drastic reduction of furnace size and a method of operating the furnace as a true model of an industrial furnace.

According to the established theory of models (7-9), physical and chemical processes taking place in the industrial furnace, the prototype, must be reproduced in the model. Usually it is not possible to reproduce all processes taking place in the prototype, if processes of inherently different nature are involved. This is certainly true in the case of many electrothermic furnaces. It is then necessary to evaluate the over-all importance of the different physical and chemical processes, in order to find the rate-determining or controlling factors.

Disregarding for the moment all other factors, it seems natural to concentrate attention on the evolution of heat. Obtaining high temperatures is essential to all electrothermic processes, which usually are sensitive to even small changes in the temperatures reached. Moreover, the temperature of an industrial furnace is not uniform within the

reaction zone, but usually large temperature differences may be set up, which, in turn, impose definite conditions of the reaction zone. Thus it is necessary to reproduce not only the maximum temperature obtained in the prototype but, more significantly, the temperature distribution of the reaction zone.

Temperature differences are set up by the evolution and flow of heat. Evolution of heat may be controlled by the power input to the furnace. The flow of heat does not lend itself so readily to any control, except by deliberate design of the furnace and mode of operation.

In the reaction zone of an industrial furnace heat transfer by convection probably is insignificant. Radiant heat transfer may be important in some processes (2). It is felt, however, that heat transfer by conduction through the furnace charge and through the walls of the furnace is most important as far as temperature distribution of the reaction zone is concerned. It is assumed that reproduction of flow of heat by conduction is essential to the correct functioning of the model.

The correctness of this assumption may be tested for the simple case of a furnace where processes other than heat conduction are unimportant. Electric shaft furnaces for calcining anthracite are especially well adapted for this demonstration.

In more complex cases, e.g., electric smelting furnaces, other physical processes or even chemical reactions may to some extent become controlling factors. The over-all rate of the process may depend on diffusion of gases, e.g., diffusion of carbon monoxide for the reduction of metallic oxides. Diffusion in slag and/or metal may also be important, e.g., for reduction of metallic oxides in the slag by solid carbon, or reactions between slag and metal such as desulfurization of pig iron. Such diffusion processes usually are speeded up by any

¹ Manuscript received March 12, 1954. This paper was prepared for delivery before the Chicago Meeting, May 2 to 6, 1954.

turbulence set up by flow of the fluids, and so the pattern of gas flow or any stirring of liquid phases may be of importance. Even secondary physical processes may be important and, therefore, of a controlling nature. Thus, separation of metal and slag may be slow, or gas velocities may be high so as to nearly lift the burden. And any chemical reaction may become a controlling factor if the rate of the purely chemical reaction is low.

The importance of reproducing flow of heat by conduction even in these more complex cases may be demonstrated by the successful operation of models of smelting furnaces according to this criterion.

DIMENSIONAL ANALYSIS

The total power to a furnace is dissipated in the following three ways: (a) heating the charge to reaction temperature; (b) supplying energy to match the heats of chemical reactions; and (c) heat losses. Or

$$P = q_1 + q_2 + q_3$$

where P = power input and the q 's are heat terms.

The energy balance of a correct model must show the same distribution of the power input to the three heat absorbing items as is found in the prototype. Thus, the ratios q_1/P , q_2/P , and q_3/P must attain the same values in the model as in the prototype.

The parts of the power input q_1 required to heat up the charge, and q_2 to match the heats of chemical reactions are necessarily proportional to the rate of feed, w . Heat losses to the surroundings by conduction through the furnace charge and walls must set up in the model the same temperature differences in the reaction zone as are found in the prototype. This implies that temperature gradients in the model are larger than those in the prototype by the ratio of linear dimensions of prototype to model, since the same temperature difference shall be set up in the correspondingly shorter distance. By Fourier's equation for the conduction of heat,

$$q_{3/A} = k \frac{dT}{dD} \sim 1/D$$

the flow of heat per unit area is directly proportional to temperature gradient. D is taken as a representative linear dimension, e.g., the diameter of the furnace pot. If thermal conductivity, k , of furnace charge and walls are equal for corresponding points in model and prototype, the flow of heat per unit area is inversely proportional to linear dimensions of the furnace. The total heat losses by conduction dissipated from the surface of the furnace are then found by multiplying with area, or

$$q_3 \sim A/D \sim D$$

The model law then becomes

$$P \sim w \sim q_3 \sim D$$

The same results are obtained by a formal dimensional analysis of the problem, which shows that the dimensionless groups wc/kD (Graetz), hD/k (Nusselt), and a special dimensionless group P/kDT must attain the same values in the model as in the prototype. Here, c is the specific heat and h is the heat transfer coefficient. From the constancy of these groups is directly read

$$w \sim D$$

$$h \sim q_3/A \sim 1/D$$

$$P \sim D$$

If Ohm's law is applicable, and if electric resistivity of the furnace charge is equal for model and prototype, the ohmic furnace voltage will be equal for the two furnaces. This is seen from the constancy of the dimensionless group $P\rho/DE^2$, with E = ohmic furnace voltage and ρ electric resistivity. If the power input to the model is not made strictly proportional to the linear dimensions, or if electric resistivity of model furnace charge differs from that of the prototype, the furnace voltage will be given by

$$E^2 \sim P\rho/D$$

DISCUSSION OF MODEL LAWS

The following consequences may be deduced from these model-to-prototype relationships:

1. The linear velocity of any stream of materials is inversely proportional to linear dimensions of the furnace.
2. The time necessary for a particle to pass through the furnace is proportional to the square of linear dimensions of the furnace.
3. The electric current density (e.g., in the electrodes) is inversely proportional to the linear dimensions of the furnace.

If all extensive properties (mass, quantity of heat, electricity, etc.) are considered proportional to the cube of linear dimensions, the three points may be stated collectively by saying that the time scale is proportional to the square of linear dimensions. By heating or cooling of solids, temperature distribution is known to be a function of the Fourier number, $k\theta/\rho c D^2$, which clearly points out this relationship between time and linear scales. θ is time, and ρ is density.

If no other process than heat conduction is rate-determining, operating conditions of the prototype will be completely reproduced in the model by this

arrangement. If all parts of the system are reduced to scale, viz., lump size of the furnace charge reduced to scale, any diffusion process in the prototype will be reproduced in the model, which is seen from the formal correspondence between thermal and material diffusion. In addition, if gas velocities are low, the pattern of gas flow will be reproduced in the model, because the modified Reynolds number, based on particle size, will attain the same value in prototype and model.

Two factors of practical importance may, however, upset this simple relationship between prototype and model, viz., rapid flow of gases and slow chemical reactions or changes of physical structure within the reaction zone.

In a 1:5 linear scale model, the velocity of any gas stream is five times the velocity of the corresponding gas stream in the prototype. The ratio of velocity pressures is correspondingly 25:1. If the velocity pressure of gas flow is important in the prototype, the model will not function correctly in this respect when the operation of the model is based on the criterion of equal temperature distribution. This is the case when appreciable amounts of gases are evolved by the process. In the model, the velocity pressure of gas streams may then become exceedingly large, to the effect of lifting the burden of the furnace. It is impossible to reproduce correctly in the model both temperature distribution and velocity pressure, and a compromise must be made between the two conflicting demands.

The reduced time scale of the model requires, for the correct functioning of the model, that any chemical reaction or change of physical structure that takes place in the prototype shall occur in the model in a correspondingly shorter time. This is possible only if chemical reactions or changes of structure are sufficiently rapid to be no rate-determining step, even on the shorter time scale of the model. Fortunately, this requirement seems to be met in many cases, but in other cases the reactions obviously are too slow, and a compromise must be made between the conflicting demands.

PRACTICAL APPLICATIONS

The theory has been applied to the operation of models of electric shaft furnaces for calcining anthracite and to models of electric smelting furnaces for the production of pig iron.

Fig. 1 shows the principle of the furnace for calcining anthracite. Raw anthracite is fed to the top of the furnace; on descending it is heated to calcining temperature by passage of electric current between top and bottom electrodes, and finally discharged at the bottom.

In calcining anthracite only small volumes of

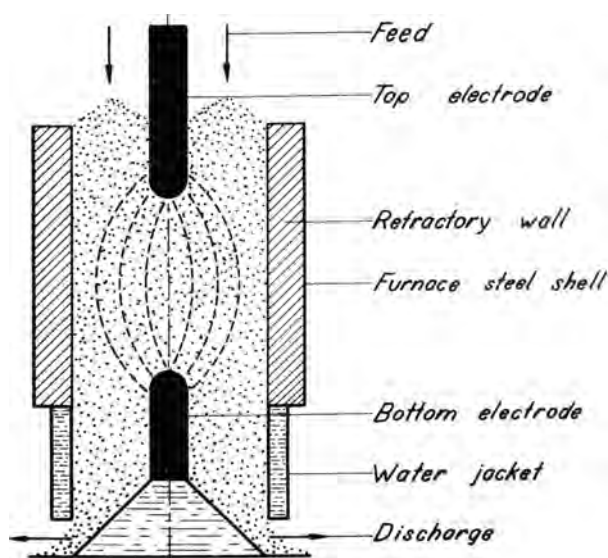


Fig. 1. Principle of the furnace for calcining anthracite

TABLE I. Operation of a 1:5 linear scale model of calcining furnace

	Prototype	Model
Power input, kw.....	735	112
Rate of feed, kg/h.....	640	94.3
Furnace voltage, v.....	54	50
Energy consumption, kw-hr/kg..	1.15	1.19
Temperature of discharge, °C....	380	325
Electrical resistivity of product Ω mm ² /m.....	450	500

gases are evolved, and the velocity pressure of gas flow is unimportant even in the model. By calcination, the anthracite is changed from an electrically nonconductive material to a conducting substance by the expulsion of volatiles and change of physical structure, reactions which are very rapid. If the theory developed is sound, it should be possible to reproduce the process correctly in a model.

A 1:5 linear scale model of a 750 kw industrial furnace was built and operated according to the theory. The correct flow of heat through the furnace lining was obtained by water-jacket cooling of the furnace steel shell.

Table I shows the corresponding figures for prototype and model. The voltage used for the operation of the model was slightly less than required by theory, because the transformer used could not give the correct voltage. Correspondingly the power input is somewhat less than required by theory. If the formula $E^2 \sim P\rho/D$ is used, observations check with theory on the assumption of 13% higher resistivity of model charge. The smaller burden weight in the model may reasonably count for this effect.

Measurements of temperature distribution of



Fig. 2. 500-kw model

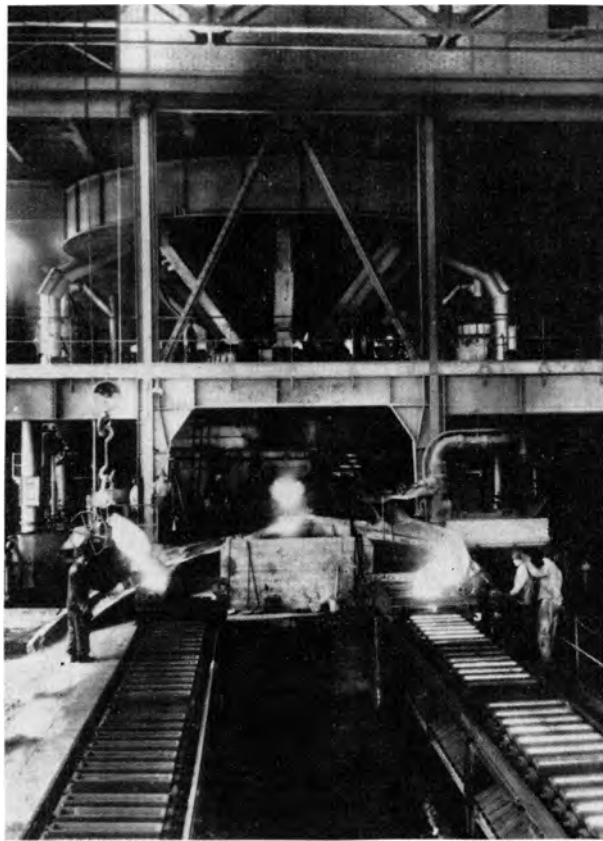


Fig. 3. 6000-kw prototype

prototype and model check well, and the quality of the product is well reproduced as indicated by the measurements of electrical resistivity.

The operation of a 1:4 linear scale model of one

TABLE II. Operation of a 1:4 linear scale model of one electrode of a three-phase 7500 kva pig iron furnace

	Prototype	Model
Power input, kw.....	6000	500
Ohmic voltage, electrode to hearth, v.....	65	60
Energy consumption, kwhr/kg..	2.5	2.51
% FeO in slag.....	1-2	2-4
% C in pig.....	3-4	3-4
% Si in pig.....	1-2	1-2

electrode of a three-phase 7500 kva pig iron furnace was undertaken to test the theory for the case of a smelting process. Table II shows that observations check reasonably well with theory even in this more complicated system. Operation of the furnace was somewhat difficult, obviously caused by the increased velocity of the gas flow. Metallurgical conditions of the prototype were, however, well reproduced, as indicated by the analyses of slag and metal produced. Reproduction of specific energy consumption is of special interest, because energy consumption of a process usually is of primary importance. Operation of this model on a variety of raw materials has shown remarkable correspondence to the operation of industrial furnaces on the same types of raw materials.

The conclusion is that it is possible to simulate operating conditions of industrial smelting furnaces by use of scale models.

Any discussion of this paper will appear in a Discussion Section to be published in the June 1955 issue of the JOURNAL.

REFERENCES

1. F. V. ANDREA, *Trans. Electrochem. Soc.*, **63**, 309 (1933).
2. P. DROSSBACH, *Z. Elektrochem.*, **46**, 643 (1940).
3. G. VOLKERT AND E. SCHWARTZ VON BERGKAMPT, *Stahl u. Eisen*, **70**, 369 (1950).
4. R. DURRER AND G. VOLKERT, (Editors), "Die Metallurgie der Ferrolegierungen," pp. 46-49; E. SCHWARTZ VON BERGKAMPT, "Modellbetrachtung des Lichtbogenofens," Springer-Verlag, Berlin (1953).
5. R. B. PEACOCK, *Chemistry & Industry*, **1952**, 888.
6. H. A. CURTIS, *This Journal*, **100**, 81C (1953).
7. P. W. BRIDGMAN, "Dimensional Analysis," Yale University Press, New Haven (1943).
8. H. L. LANGHAAR, "Dimensional Analysis and Theory of Models," John Wiley & Sons, Inc., New York (1951).
9. M. W. THRING, *Trans. Inst. Chem. Eng., (London)*, p. 8, Oct. 26 (1948).

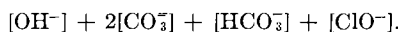
The pH in Chlorine-Caustic Electrolysis by the Mercury Cell Process¹

LARS BARR

Division of Applied Electrochemistry, Royal Institute of Technology, Stockholm, Sweden

ABSTRACT

Anolyte composition in mercury cells for chlorine-caustic electrolysis is calculated as a function of pH, and the relation between anodic current loss and the anolyte pH is derived. Reactions between anodic and cathodic by-products and dependence of the cathodic current loss upon the anolyte pH are also discussed. Finally, certain components of the feed brine which affect pH of the anolyte are examined. It is demonstrated that optimum current efficiency with respect to both chlorine and caustic cannot be reached if pH of the anolyte is greater than 3, that stirring the cathode film, e.g., by solid particles on the mercury surface, decreases current efficiency, and that alkalinity of the feed brine, which must not exceed a certain value, is made up of the following concentrations:



INTRODUCTION

Several investigations have been carried out on the influence of various process variables on current efficiency in chlorine-caustic electrolysis by both the mercury and diaphragm cell processes. Thus, in a number of laboratory experiments, Taussig (1) estimated cathodic current efficiency in the mercury cell process as a function of amalgam concentration, current density, temperature, and salt concentration, i.e., brine flow. Johnson (2) measured anodic current loss as a function of current density, temperature, and salt concentration.

However, no investigation seems to have been published concerning the influence of pH of the electrolyte.

The mercury process is run in various ways, owing to brine purification methods, material problems, etc., with good results; consequently the question of pH may seem to be of minor importance, and the allowed pH range comparatively wide.

The purpose of the following calculations is to demonstrate more exactly the pH range suitable for the mercury cell process.

ELECTROLYTE EQUILIBRIUM COMPOSITION

Besides Na^+Cl^- , H_2O , and its ions, the following substances may occur in brine because of chlorine dissolution and anodic reactions: Cl_2 , Cl_3^- , HClO , ClO^- , and ClO_3^- (3-5). In practice, the anode material is graphite; therefore, the system $\text{CO}_2 - \text{H}_2\text{O}$ is also present. Activities of these

particular substances in equilibrium will now be calculated as functions of hydrogen ion activity $\{\text{H}_3\text{O}^+\}$, at 25° and 60°C and total pressure of 1 atm.

The chlorine system is defined by the following equations, in which braces, {}, denote the activity in mole/l and "(aq)" means that the substance is dissolved in water:

$$\frac{\{\text{H}_3\text{O}^+\}\{\text{Cl}^-\}\{\text{HClO}\}}{\{\text{Cl}_2(\text{aq})\}} = K'_1\{\text{H}_2\text{O}\}^2 \simeq K_1 \quad [1]$$

and

$$\frac{\{\text{H}_3\text{O}^+\}^6\{\text{Cl}^-\}^5\{\text{ClO}_3^-\}}{\{\text{Cl}_2(\text{aq})\}^3} = K'_2\{\text{H}_2\text{O}\}^9 \simeq K_2 \quad [2]$$

both involving electron exchange, and

$$\frac{\{\text{H}_3\text{O}^+\}\{\text{ClO}^-\}}{\{\text{HClO}\}} = K'_s\{\text{H}_2\text{O}\} \simeq K_s \quad [3]$$

involving proton exchange.

The carbonic acid system is defined by the following equations, both involving proton exchange:

$$\frac{\{\text{H}_3\text{O}^+\}\{\text{HCO}_3^-\}}{\{\text{H}_2\text{CO}_3\}} = K'_{s1}\{\text{H}_2\text{O}\} \simeq K_{s1} \quad [4]$$

and

$$\frac{\{\text{H}_3\text{O}^+\}\{\text{CO}_3^{2-}\}}{\{\text{HCO}_3^-\}} = K'_{s2}\{\text{H}_2\text{O}\} \simeq K_{s2} \quad [5]$$

If the water activity is assumed to be constant, which is an approximation, the right hand sides of equations [1-5] will be constant.

From investigations of Jakowkin (3) and Sand (4, 6), equilibrium constants of the chlorine system can be calculated. Jakowkin investigated the

¹ Manuscript received August 31, 1953. This paper was prepared for delivery before the Chicago Meeting, May 2 to 6, 1954.

HClO equilibrium, equation [1], at various temperatures between 13.4° and 57.5°C, while Sand studied the chlorate equilibrium, equation [2], at 20° and 70°C, and the protolysis of HClO, equation [3], at 17° and 70°C.

If concentrations of the diluted systems studied are assumed to be identical with activities, the following values are obtained: pK_1 (25°C) = 3.35; pK_2 (25°C) = 11.24; pK_s (25°C) = 7.36; pK_1 (60°C) = 3.02; pK_2 (60°C) = 11.04; pK_s (60°C) = 7.09; where $p = -\log$.

MacInnes and Belcher (7, 8) estimated the values of K_{s1} and K_{s2} at 25° and 38°C, which give: pK_{s1} (25°C) = 6.34; pK_{s2} (25°C) = 10.25; pK_{s1} (60°C) = 6.26; pK_{s2} (60°C) = 10.12.

The following equation was used for interpolation or extrapolation which had to be carried out to 25° and 60°C.

$$\frac{d \ln K}{dT} = \frac{\Delta H^0}{RT^2} \quad [6]$$

in which T = absolute temperature, R = the gas constant, and ΔH^0 = standard enthalpy change. The latter was considered constant within the interval concerned.

As a general condition, it is now assumed that $\text{Cl}_2(\text{aq})$ and H_2CO_3 activities are constant at constant chlorine and carbon dioxide pressures, respectively, and at constant temperature. Since in this case activity is defined with reference to an infinitely dilute solution, it cannot be considered equal to the partial pressure of the gas, but only proportional to this pressure.

Provided the gas phase is ideal, the following equation concerning the chlorine system is obtained:

$$\{\text{Cl}_2(\text{aq})\} = K_{1,\text{Cl}_2} \cdot p_{\text{Cl}_2} \quad [7]$$

in which p is the pressure in atmospheres and K_1 the thermodynamic solubility constant in mole/l atm. K_{1,Cl_2} was calculated by Whitney and Vivian (9) in the temperature range 10°–25°C, the activity coefficients being assumed equal to unity.

At 25°C the value of the constant pK_{1,Cl_2} (25°C) is 1.21. If their figures at 20°–25°C are extrapolated to 60°C with pK_{1,Cl_2} as a linear function of $1/T$, the value $pK_{1,\text{Cl}_2} = 1.92$ is obtained. Since such a long extrapolation is comparatively unreliable, the 60°C figure has also been calculated from an old investigation by Gay-Lussac (10), who measured the solubility of chlorine in water at various temperatures between 0° and 100°C. After correction for the HClO formation according to equation [1] and with the activity coefficients equal to unity, the figure pK_{1,Cl_2} (60°C) = 1.82 is obtained, which value is used here.

In the same way, the CO_2 system is defined by the equation:

$$\{\text{H}_2\text{CO}_3\} = K_{1,\text{CO}_2} \cdot p_{\text{CO}_2} \quad [8]$$

pK_{1,CO_2} was calculated from the absorption coefficient of CO_2 in water at 25° and 60°C (11). After correction for HCO_3^- formation according to equation [4] and with activity coefficients equal to unity, the following values were obtained: pK_{1,CO_2} (25°C) = 1.47 and pK_{1,CO_2} (60°C) = 1.80.

A mercury cell is generally operated in the concentration range, 250–310 g/l NaCl, so the equilibrium calculation will be carried out for both 250 and 310 g/l NaCl.

If activity coefficients of the univalent ions are assumed to be 0.9 (12) at both salt concentrations and both temperatures, which is an approximation due to rapid alteration of the coefficients in this concentration range, the following chloride ion activities are obtained: $p\{\text{Cl}^-\}$ (250 g/l) = -0.58; $p\{\text{Cl}^-\}$ (310 g/l) = -0.68. Approximate mean value = -0.6.

The gas phase composition is characterized by:

$$p_{\text{Cl}_2} + p_{\text{CO}_2} + p_{\text{H}_2} + p_{\text{H}_2\text{O}} = 1 \text{ atm} \quad [9]$$

in which $p_{\text{H}_2\text{O}} = 0.025$ atm at 25°C and 0.16 at 60°C (13).

If the dried chlorine gas contains, for example, 1.0% CO_2 and 0.5% H_2 , p_{Cl_2} (25°C) = 0.96 atm, p_{Cl_2} (60°C) = 0.83 atm, p_{CO_2} (25°C) = 0.010 atm, and p_{CO_2} (60°C) = 0.0084 atm.

From equations [7] and [8] the $\text{Cl}_2(\text{aq})$ and H_2CO_3 activities are: $p\{\text{Cl}_2(\text{aq})\}$ (25°C) = 1.23; $p\{\text{H}_2\text{CO}_3\}$ (25°C) = 3.47; $p\{\text{Cl}_2(\text{aq})\}$ (60°C) = 1.90; $p\{\text{H}_2\text{CO}_3\}$ (60°C) = 3.88.

According to Sherrill and Izard (5), $\text{Cl}_2(\text{aq})$ in concentrated NaCl solutions forms Cl_3^- ions to such a great extent that they cannot be neglected. The equilibrium constant $\{\text{Cl}_3^-/\{\text{Cl}^-\}p_{\text{Cl}_2}$ is 0.01 atm⁻¹ at 25°C and hence $p\{\text{Cl}_3^-\}$ (25°C) = 1.4.

From equations [1–5] logarithms of the activities of the substances can be obtained as functions of $p\{\text{H}_3\text{O}^+\}$, i.e., of $p\text{H}$:

$$p\{\text{HClO}\} = -p\text{H} - p\{\text{Cl}^-\} + p\{\text{Cl}_2(\text{aq})\} + pK_1 \quad (\text{from [1]})$$

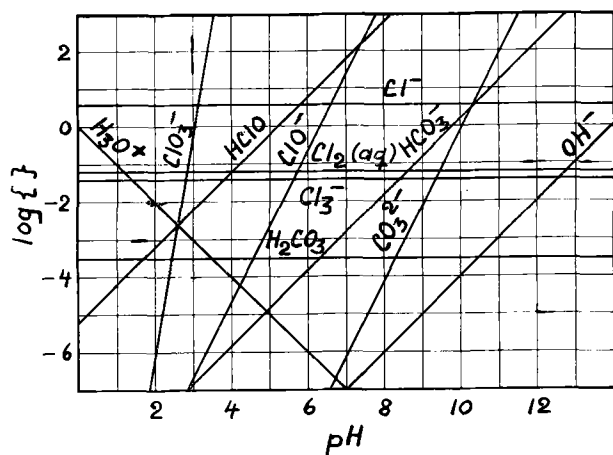
$$p\{\text{ClO}^-\} = -2p\text{H} - p\{\text{Cl}^-\} + p\{\text{Cl}_2(\text{aq})\} + pK_1 + pK_s \quad (\text{from [1] and [3]})$$

$$p\{\text{ClO}_3^-\} = -6p\text{H} - 5p\{\text{Cl}^-\} + 3p\{\text{Cl}_2(\text{aq})\} + pK_2 \quad (\text{from [2]})$$

$$p\{\text{HCO}_3^-\} = -p\text{H} + p\{\text{H}_2\text{CO}_3\} + pK_{s1} \quad (\text{from [4]})$$

TABLE I

Temp	25°C			60°C			
	NaCl conc	250 g/l	310 g/l	Mean value	250 g/l	310 g/l	Mean value
a		5.16	5.26	5.2	5.50	5.60	5.6
b		12.52	12.62	12.6	12.59	12.69	12.6
c		17.83	18.33	18.1	19.64	20.14	19.9
d		9.81	9.81	9.8	10.14	10.14	10.1
e		20.06	20.06	20.1	20.26	20.26	20.3

[FIG. 1. Logarithms of activities in mole l⁻¹ for the substances considered as a function of pH at 25°C.

$$p\{\text{CO}_3^{2-}\} = -2pH + p\{\text{H}_2\text{CO}_3\} + pK_{s1} + pK_{s2} \quad (\text{from [4] and [5]})$$

If the constant terms of modified equations [1-5] are combined, we obtain:

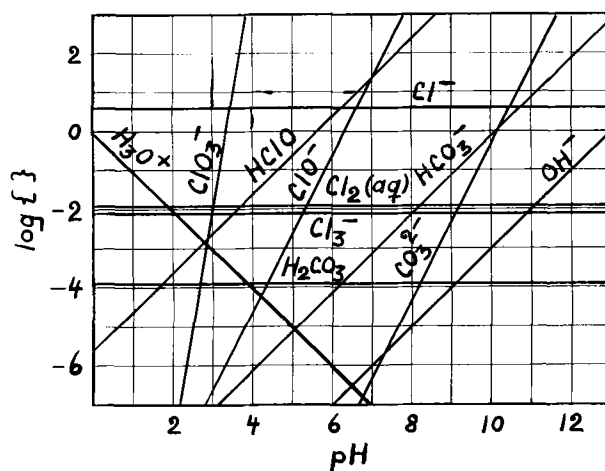
$$\begin{aligned} p\{\text{HClO}\} &= -pH + a \\ p\{\text{ClO}^-\} &= -2pH + b \\ p\{\text{ClO}_3^-\} &= -6pH + c \\ p\{\text{HCO}_3^-\} &= -pH + d \\ p\{\text{CO}_3^{2-}\} &= -2pH + e \end{aligned}$$

The values of the constants are given in Table I.

In practical operation, uncertainty of a pH measurement appears in the first decimal and, according to Table I, the influence of decreasing salt concentration during electrolysis is of the same order of magnitude as uncertainty of a measured pH value. Therefore, a mean value has also been tabulated, which will apply to the whole concentration range of a cell.

Table I shows that chlorate activity will be mostly influenced by a temperature change, and that all activities of the chlorine and carbon dioxide systems will decrease with increasing temperature at constant pH.

Fig. 1 and 2, giving the logarithm of the activity of each dissolved substance vs. pH, were drawn

FIG. 2. Logarithms of activities in mole l⁻¹ for the substances considered as a function of pH at 60°C.

using mean values of the constant terms at 25° and 60°C, respectively.

The Cl₃⁻ line of Fig. 2 is drawn with the assumption that the relation {Cl₃⁻}/ {Cl₂(aq)} is constant between 25° and 60°C. Then p{Cl₃⁻} (60°C) = 2.1.

In the figures the OH⁻ ion activity was drawn as calculated from the equation:

$$p\{\text{OH}^-\} = -pH + pK_v \quad [10]$$

in which pK_v (25°C) = 14.00 and pK_v (60°C) = 13.02 (14).

A Practical Equilibrium Diagram

The alkaline part of the Figures 1 and 2 can evidently never become actual, since [Na⁺] ≈ [Cl⁻] and the solution must be electrically neutral at a sufficient distance from the electrodes. (Square brackets indicate concentration in mole/l.)

Fig. 3 was drawn using concentrations instead of activities at 60°C. It was then assumed that activity coefficients of the ions are constant within the pH range and equal to 0.9. This figure is approximate and was extrapolated from a diagram applying at 25°C (12). According to an investigation of the solubility of chlorine in various salt solutions at room temperature (5), the activity coefficient of Cl₂(aq) is about 4 in this concentration range. This value was also used at 60°C in Fig. 3 for both Cl₂(aq) and HClO, which also constitutes an approximation.

In Fig. 3, the pH range greater than 5 and less than 1 was excluded, as well as substances whose concentrations are smaller than 1 mmole/l at pH 1-5. The water concentration was also calculated from specific gravity of the solution at 60°C, 1.150 with 280 g/l NaCl (15). The equations belonging to Fig. 3 are:

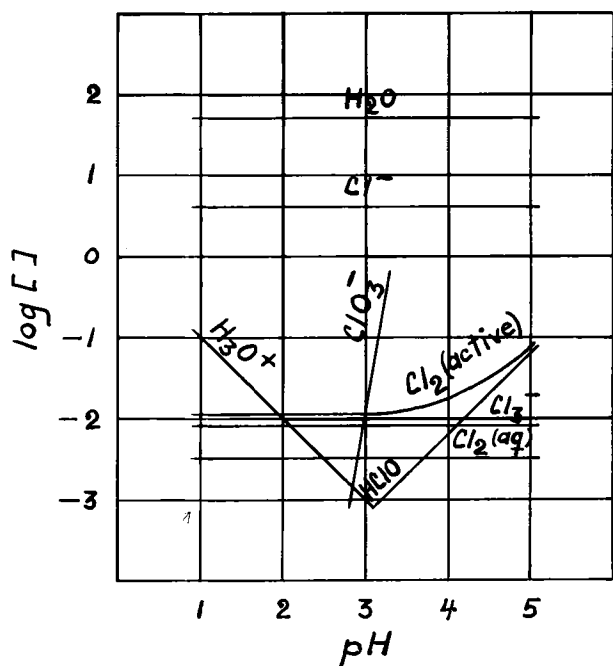


FIG. 3. Logarithms of concentrations in mole l^{-1} for the substances considered as a function of pH at $60^\circ C$.

$$p[H_3O^+] = pH + \log 0.9 \approx pH$$

$$p[Cl^-] = -0.6 + \log 0.9 \approx -0.6$$

$$p[Cl_2(aq)] = 1.9 + \log 4 \approx 2.5$$

$$p[Cl_3^-] = 2.1 + \log 0.9 \approx 2.1$$

$$p[HClO] = -pH + 5.6 + \log 4 \approx -pH + 6.2$$

$$p[ClO_3^-] = -6 pH + 19.9 + \log 0.9 \approx -6pH + 19.9$$

$$p[H_2O] = -\log \frac{1150 - 280}{18} \approx -1.7$$

Furthermore, the figure contains a curve giving the concentration of "active chlorine," defined by the expression:

$$[Cl_2(\text{active})] = [Cl_2(aq)] + [Cl_3^-] + [HClO] \quad [11]$$

The curve obtained for active chlorine agrees⁸ very well with an experimentally determined curve giving the concentration of active chlorine as a function of pH in concentrated, chlorine-saturated $NaCl$ solutions. This agreement decreases the uncertainty introduced by use of approximate activity coefficients and the $\{Cl_3^-\}/\{Cl_2(aq)\}$ relation at $60^\circ C$. Thus, Brännland (16) obtained the values shown in Table II at $65^\circ C$, 0.995 atm total pressure, and 310 g/l $NaCl$.

If sodium ion concentration is known, elec-

TABLE II

pH	1.20	4.00	4.35	4.45
$\log Cl_2$ (active)	-2.07	-1.78	-1.51	-1.49

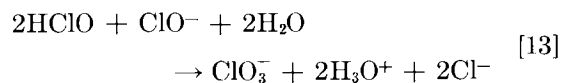
trolyte composition and pH are defined by the condition of electrical neutrality:

$$[Na^+] + [H_3O^+] = [Cl^-] + [Cl_3^-] + [ClO_3^-] \quad [12]$$

Fig. 3 shows that the chlorate equilibrium concentration increases greatly with increasing pH . At pH values greater than 3.3 this chlorate content is so great that solid phases will form (17). If, for example, the process is operated at pH 4, chlorate ions cannot be in equilibrium with other chlorine components of the brine, and chlorate will form continuously.

Chlorate Formation Rate

The rate of chlorate formation from dissolved chlorine is comparatively slow. It has been investigated by Foerster (18), and according to his results chlorate formation follows the reaction:



The chlorate formation rate is then proportional to the square of $HClO$ concentration and to the ClO^- concentration:

$$\frac{d[ClO_3^-]}{dt} = k[HClO]^2[ClO^-] \quad [14]$$

in which k is the rate constant and t the time.

Foerster gives the value of $1/t \log [ClO_3^-]_t/[ClO_3^-]_0$ \min^{-1} at 19.5° , 35° , and $49^\circ C$ and various $HClO$ concentrations. Since, after having been transformed into the natural logarithm system, this expression is equal to $k[HClO]^2$ in equation [14], the rate constant can be calculated: $k(19.5^\circ C) = 0.974$, $k(35^\circ C) = 3.72$, and $k(49^\circ C) = 13.8 \text{ l}^2/\text{min mole}^2$. By means of graphical extrapolation with $\log k$ as a function of $1/T$, the value $k(60^\circ C) = 39 \text{ l}^2/\text{min mole}^2$ is obtained.

In a mercury cell, chlorate may also be formed electrochemically at the anode and reduced at the cathode. Murray and Kircher (19) analyzed the anolyte and anode gas of American diaphragm cells and calculated various components of the anodic current loss. They reported that the electrochemical chlorate formation below pH 4 is of the same order of magnitude as the chemical one expressed in reaction [13] at the same pH . According to Foerster (20), the reaction mechanism of electrochemical chlorate formation implies ClO^- discharge and

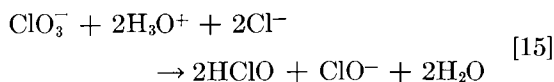
oxygen formation at the anode. This type of chlorate formation increases with increasing pH, but not so much as the chemical one (reaction [13]) which predominates at pH values greater than 4 (19).

Since anode reactions are the same in diaphragm and mercury cells, Murray and Kircher's results are applicable also to the latter.

Fig. 2 shows that $\{\text{HClO}\} = 2.5 \times 10^{-3}$ and $\{\text{ClO}^-\} = 2.5 \times 10^{-7}$ at pH 3 and 60°C. If these values are substituted for the corresponding concentrations in equation [14], the chlorate formation rate $d[\text{ClO}_3^-]/dt = 6 \times 10^{-11}$ mole/l min is obtained at pH 3. At pH 4 and pH 5 the value is 6×10^{-7} and 6×10^{-3} mole/l/min, respectively.

Thus, the chlorate formation rate is significant only at pH values above 4, because of the small content of the chlorate forming substances, HClO and ClO^- , at lower pH values.

According to Sand (4) the chlorate decomposition follows the reaction:



which is evidently the inverse reaction to that which Foerster (18) proved for chlorate formation. Sand reported the rate constant of the reaction at 70°C = $0.56 \times 10^{-3} \text{ min}^{-1}$.

If the rate constant is assumed to be increased 2.5 times by a temperature rise of 10°C, and if the values of Fig. 2 for ClO_3^- , H_3O^+ , and Cl^- at pH 3 are used, the decomposition rate of ClO_3^- , $-d[\text{ClO}_3^-]/dt$, is 4×10^{-11} mole/l min at 60°C. This decomposition rate is of the same order of magnitude as the above calculated chlorate formation rate at pH 3, i.e., the chlorate concentration is in equilibrium, which agrees with the equilibrium diagrams constructed above.

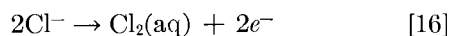
Contrary to chlorate formation, acid formation occurs instantly (4), and probably the equilibrium concentrations of HCl and HClO are reached even at the first anode which the brine touches.

The result of these calculations of electrolyte composition is verified in the investigations by Murray and Kircher (19).

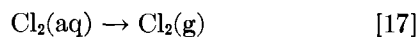
ANODE PROCESS AND pH OF THE BRINE

Only the substances included in Fig. 3 will be considered.

The desired anode reaction may be separated into an "electrochemical" part:



and a "physical" part:



in which (g) means that the substance is gaseous.

With reference to combined reactions [16] and [17], the anode potential is:

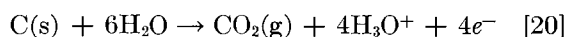
$$e_a = e_1^0 + \frac{RT}{2F} \ln \frac{\{\text{Cl}_2(\text{g})\}}{\{\text{Cl}^-\}^2} + f_1(i) \quad [18]$$

in which e_1^0 is the standard potential of reaction [16] and [17], F the Faraday constant, and $f_1(i)$ the current density dependent chlorine overvoltage.

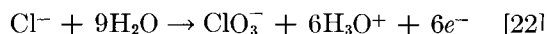
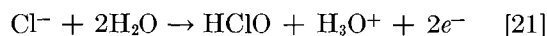
Anodic current loss is represented by a number of reactions, which may be divided into two groups: (a) "water electrolysis":



or with graphite oxidation included:



in which (s) means that the substance is solid, and (b) "chloride electrolysis":



In the first group of side reactions, irreversible reaction [20] predominates, since the anode gas generally contains about 1% CO_2 and small quantities of O_2 as well as air. This reaction causes not only current loss but also graphite loss.

The anode potential e_a is, according to reaction [19]:

$$e_a = e_2^0 + \frac{RT}{4F} \ln \frac{\{\text{O}_2(\text{g})\} \{\text{H}_3\text{O}^+\}^4}{\{\text{H}_2\text{O}\}^6} + f_2(i) \quad [23]$$

in which e_2^0 is the standard potential of reaction [19], and $f_2(i)$ represents the current density dependent polarization.

e_a is fixed by equation [18], and is evidently independent of pH of the solution. Since $\{\text{H}_2\text{O}\}$ is constant, the following equation is obtained at constant current density and temperature, provided that f_2 is independent of variations in brine composition:

$$d \log \{\text{O}_2(\text{g})\} = 4 d \text{pH} \quad [24]$$

As $\{\text{O}_2(\text{g})\}$ is proportional to p_{CO_2} in the gas phase, carbon dioxide content of the anode gas and graphite loss of the cell increase with pH according to the equation:

$$d \log p_{\text{CO}_2} = 4 d \text{pH} \quad [25]$$

In the "chloride group" current loss can be partly recovered as chlorine gas by brine dechlorination after electrolysis. Furthermore, since no graphite loss or contamination of the gas phase is caused

TABLE III

pH of anolyte	Anodic current loss, $s_a\%$	$\log (s_a - 1.5)$
3.0	1.8	-0.5
3.5	2.6	+0.1
4.0	5.1	+0.6
4.5	15.8	+1.2

by this group of reactions, it may be regarded as less harmful than the former.

By forming corresponding expressions for e_a for reactions [21] and [22], and by keeping all quantities constant except $\{\text{HClO}\}$, $\{\text{ClO}_3^-\}$, and $\{\text{H}_3\text{O}^+\}$, the following relations between these variables are obtained:

$$d \log \{\text{HClO}\} = d \text{pH} \quad [26]$$

and

$$d \log \{\text{ClO}_3^-\} = 6 d \text{pH} \quad [27]$$

These equations have already been derived in equilibrium calculations above. It has also been shown that chlorate formation will not always reach equilibrium in the cell.

If the logarithm of equation [14] is taken and $p[\text{HClO}]$ and $p[\text{ClO}_3^-]$ vs. pH inserted, the following expression is obtained:

$$\log \frac{d[\text{ClO}_3^-]}{dt} = 4\text{pH} + \text{a constant} \quad [28]$$

and after differentiating:

$$d \log \frac{d[\text{ClO}_3^-]}{dt} = 4 d \text{pH} \quad [29]$$

Evidently, the chlorate formation rate increases with pH in a similar way as equilibrium activities.

The above calculations demonstrate that anodic current efficiency increases with decreasing pH of the anolyte. Composition of the latter is given by the equilibrium diagram in Fig. 3. This result is not affected by mechanisms of the particular reactions, e.g., if hypochlorite and chlorate are formed "chemically" through internal electron change or "electrochemically" through electron delivery to the anode.

This result is also confirmed by Murray and Kircher (19). Under constant experimental conditions, they obtained the relation shown in Table III between anodic current loss, s_a , and pH of the anolyte.

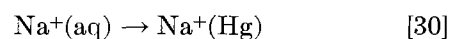
Current loss due to the anolyte content of $\text{Cl}_2(\text{aq})$ and Cl_3^- , which are entirely lost in the diaphragm process, and current loss due to sulfate content of technical brine are both independent of pH . If 1.5% is subtracted from total current loss as a correction for pH independent current losses, the logarithm of

the remaining pH dependent current loss will become a linear function of pH , which actually satisfies relations derived above between losses and pH . This is demonstrated in the last column of Table III.

In the above derivation of equilibrium composition of the electrolyte, certain constant chlorine and carbon dioxide pressures in the gas phase were assumed. Composition of the latter is, of course, changed with the current efficiency, but at a moderate change of current efficiency, change of chlorine pressure is not so great that derived equilibrium diagrams are affected. As to the carbon dioxide system, it has been shown that its presence in the electrolyte may be neglected.

CATHODE PROCESS AND pH OF THE BRINE

Since, in dilute mercury solutions, sodium is probably dissociated into sodium ions and free electrons, the desired cathode process implies merely a phase boundary passage by sodium ions:

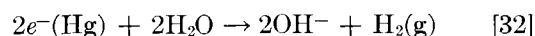


Simultaneously, the mercury cathode is supplied with electrons externally:

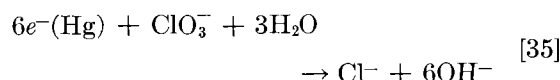
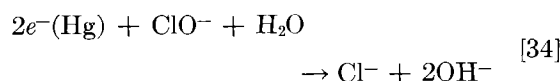
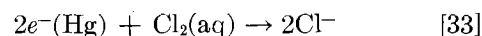


in which (Hg) means that the substance is dissolved in mercury.

According to this way of regarding the reactions, which was used by Brönsted (21) in studies of reaction mechanism for dissolution of metals in acids, sodium ions participate only in a "physical" reaction at the cathode, which is probably completely reversible. Since other current efficiency decreasing cathode reactions also take place, reaction [31] must occur a little faster than reaction [30]. The rate difference is defined by loss reactions, which may be divided into two groups as for the anodic ones, "water electrolysis":



and "chloride electrolysis":



Cathode reactions are written in alkaline form, as the liquid film near the mercury is alkaline, which may be calculated from the hydrogen overvoltage and the electrode potential electrolyte/amalgam.

The cathode potential, e_k , is -1.8 volts under conditions prevailing in a mercury cell operated with 30 amp/dm^2 (22). With reference to reaction [32] it may be written:

$$e_k = e_3^0 + \frac{RT}{2F} \ln \frac{\{\text{H}_2\text{O}\}^2}{\{\text{OH}^-\}^2 \{\text{H}_2(\text{g})\}} - f_3(i) \quad [36]$$

in which e_3^0 is the standard potential of reaction [32] and $f_3(i)$ the hydrogen overvoltage.

According to Glasstone (23), hydrogen overvoltage is independent of the pH of the solution. Tafel (24) reported that overvoltage increases with current density according to the formula $f_3(i) = a + b \ln i$, a and b being constants. If the cell gas contains, for example, 0.5% H_2 and the cell is operated with 30 amp/dm^2 of mercury surface, the current density of the hydrogen discharge is about 1.5 ma/cm^2 . With this current density the hydrogen overvoltage should be 0.9–1.0 volt at room temperature according to Knobel (25). Glasstone (23) reported that hydrogen overvoltage on mercury decreases with increasing temperature, $2.1 \text{ mv/}^\circ\text{C}$, so the lower figure is assumed to apply at 60°C . It is also assumed to apply to mercury containing a little sodium.

The standard potential e_3^0 is -0.83 volt at 25°C (26), and, after correction for temperature change of the water constant K_w (14), a value of -0.86 is obtained for 60°C .

If hydrogen is assumed to be discharged as gas bubbles on mercury, and if $\{\text{H}_2\text{O}\} = 1$, the following equation is obtained at 60°C , from equation [36]:

$$-1.8 = -0.86 + \frac{0.066}{2} \log \frac{1}{\{\text{OH}^-\}^2} - 0.9$$

which gives the result $p\{\text{OH}^-\} \simeq 0$, or at 60°C $p\text{H} \simeq 13$.

The value is, of course, very uncertain, since uncertainty in overvoltage and probably also in cathode potential amounts to some tenths of a volt.

However, it may be concluded that the cathode film of a mercury cell is more alkaline than the bulk of the electrolyte, which is represented in Fig. 3, and that pH of the film is certainly greater than 7. Moreover, the value changes along the perpendicular through the cathode film to the mercury surface, and is therefore dependent on the point of the cathode potential measurement.

In a series of kinetic studies on decomposition of sodium amalgam in various solutions, Brønsted and Ross Kane (21) found that the decomposition rate increased greatly with decreasing pH. The amalgam contained 0.055% Na, and the lowest pH was 7.5, under which value the reaction rate was too fast to be measured reliably. This agrees

Electrolyte	Na ⁺	Cl ⁻	Cl ₂ (aq)	Cl ₃ ⁻	ClO ₂ ⁻	HClO	H ₃ O ⁺	H ₂ O	acid
Cathode film	Na ⁺	Cl ⁻	Cl ₂ (aq)	Cl ₃ ⁻	ClO ₂ ⁻	ClO ⁻	H ₂ O	OH ⁻	base
Mercury	Na ⁺	e ⁻	Hg						

FIG. 4. Sketch of the composition of the bulk of the electrolyte, the cathode film, and the mercury phase.

with the above estimation of alkalinity of the cathode film.

As with the anode, the following equation is obtained by differentiating equation [36] with all variables constant, except $\{\text{OH}^-\}$ and $\{\text{H}_2(\text{g})\}$:

$$\begin{aligned} d \log \{\text{H}_2(\text{g})\} &= 2 d p \{\text{OH}^-\} \\ &= -2 d p\text{H} \end{aligned} \quad [37]$$

Reactions [34] and [35] also become faster as pH of the cathode film decreases, while reaction [33] which implies that the desired anode product is consumed at the cathode is independent of pH.

The discussion shows that cathodic current efficiency increases with increasing pH of the cathode film.

INTERACTION BETWEEN ANODIC AND CATHODIC LOSS REACTIONS

Owing to alkalinity of the cathode film and high hydrogen overvoltage on mercury, reaction [30] predominates over reaction [32], and the mercury process is rendered possible. The process may consequently be disturbed by substances which neutralize the cathode film or catalyze hydrogen discharge by decreasing hydrogen overvoltage. Among other substances, vanadium, chromium, and molybdenum belong to this latter group (27). However, such contaminated systems are outside the scope of this investigation.

It has been shown that a certain alkalinity of the film near the mercury is essential for the process. At pH values between that of the bulk of the electrolyte and that of the cathode film, HClO is protolyzed to ClO⁻. A qualitative representation of the composition of the acid electrolyte, the alkaline cathode film, and the mercury is given in Fig. 4.

Since in the electric field OH⁻ ions migrate from the cathode film, and H₃O⁺ ions migrate toward the cathode film, OH⁻ ions of the film thus lost must evidently be replaced. This is done according to reaction [32] or by chlorine reduction as in reactions [34] and [35]. The resulting current loss can never be avoided, and consequently current efficiency can never reach 100%.

With a knowledge of migration rate, the magnitude of this current loss can be estimated. If a diaphragm between the acid electrolyte and alkaline

cathode film is imagined, $[\text{OH}^-] \cdot u_- \cdot X$ mole OH^- ions/sec migrate through 1 dm^2 of the diaphragm, and in the opposite direction, $[\text{H}_3\text{O}^+] \cdot u_+ \cdot X$ mole H_3O^+ ions/ dm^2 sec, in which u is the ionic mobility in dm/sec at the field strength $1 \text{ v}/\text{cm}$ and X is the field strength in v/cm . At 60°C the mobility of OH^- ions is $33 \times 10^{-5} \text{ dm}/\text{sec v}/\text{cm}$, and that of H_3O^+ ions $52 \times 10^{-5} \text{ dm}/\text{sec v}/\text{cm}$ (28). These ionic mobilities must be corrected because viscosity of the salt solution is higher than that of pure water. According to Angel (29), the change is defined by the formula:

$$u_2 = u_1(\eta_1/\eta_2)^m \quad [38]$$

in which m is a constant = 0.614 for H_3O^+ ions and 0.718 for OH^- ions, and η the viscosity. If the viscosity of water at 60°C , 0.469 centipoise (30), is inserted for η_1 and the viscosity of a 25% NaCl solution at the same temperature, 1.11 centipoise (31), for η_2 , we obtain for OH^- , $u_- = 18 \cdot 10^{-5} \text{ dm}/\text{sec v}/\text{cm}$, and for H_3O^+ , $u_+ = 31 \times 10^{-5} \text{ dm}/\text{sec v}/\text{cm}$. The specific conductivity of the salt solution at 60°C is $0.43 \text{ ohm}^{-1} \text{ cm}^{-1}$ (15). With the current density $i \text{ amp}/\text{dm}^2$ the field strength X is $i/43 \text{ v}/\text{cm}$.

The $p\text{H}$ of the alkaline side being assumed = x , that of the acid side = y , and the current loss caused by these ion migrations = s_k , the following equation is obtained, since $i \text{ amp}/\text{dm}^2$ corresponds to $i/96500$ moles of electrons $\text{sec}^{-1}\text{dm}^{-2}$ and since $pK_w(60^\circ\text{C}) = 13$ (14) (provided that the activity coefficients = 1):

$$i \cdot s_k / 96500 = (i \cdot 18 \cdot 10^{-5} \cdot 10^{x-13} / 43) + (i \cdot 31 \cdot 10^{-5} \cdot 10^{-y} / 43) \quad [39]$$

This formula gives the minimum cathodic current loss for different $p\text{H}$ values of electrolyte and cathode film at 60°C . It is independent of current density.

For example, $p\text{H}$ 3 and $p\text{H}$ 11 inserted in equation [39] give $s_k = 0.5\%$, $p\text{H}$ 3 and $p\text{H}$ 10 give $s_k = 0.1\%$, etc.

By stirring the electrolyte, more acid than that corresponding to these electrolytic migration rates may penetrate into the cathode film. It is evidently important that the streaming state of the cathode film should be laminar. Turbulence of the cathode film decreases current efficiency since alkali neutralized thereby must be re-formed. Furthermore, chlorine diffuses more easily into the cathode film and reacts according to equations [33-35]. Solid particles floating on the mercury act as stirrers on the cathode film and thus interfere with the process.

This effect may possibly be the reason why the vertical cell built by the Germans during World

War II in order to save floor space never gave the same current efficiency as the traditional horizontal cell (32).

According to Fig. 4, the acid/base couple HClO/ClO^- is present at the boundary between electrolyte and cathode film. HClO is instantly protolyzed to ClO^- at a $p\text{H}$ between that of the electrolyte and that of the cathode film. Owing to the stirring influence of the anode gas bubbling around the anodes at only a few millimeters distance from the cathode film, HClO may easily reach the reaction zone. If the effect of H_3O^+ migration toward the cathode in the electric field is neglected, HClO should decompose the cathode film in the same manner as H_3O^+ .

Consequently, cathodic current efficiency decreases both with increasing H_3O^+ and increasing HClO concentration in the electrolyte. According to Fig. 3, concentration of $(\text{H}_3\text{O}^+ + \text{HClO})$ reaches a symmetrical minimum at $p\text{H}$ 3. Provided that a certain HClO concentration in the electrolyte has about the same neutralizing effect on the cathode film as a like concentration of H_3O^+ , which has been only argumentatively derived above, the cathodic current efficiency reaches a symmetric maximum at about $p\text{H}$ 3.

This $p\text{H}$ value, at which the acid concentration reaches its minimum, only changes by a few tenths of a unit within the generally applied temperature range, which is shown by a comparison of Fig. 1 and 2.

Since anodic current efficiency decreases with increasing $p\text{H}$, the $p\text{H}$ of the electrolyte should not exceed this value, $p\text{H}$ 3, by very much.

Unfortunately, this result cannot be illustrated by any electrolysis experiments, but it is known from practical experience that H_2 content of the gas generally increases with both exceptionally high alkalinity and acidity of the feed brine. However, the scientific basis is lacking, since these matters have been investigated very little. Probably, catalytic phenomena also have an influence.

At $p\text{H}$ 3 and 60°C the equilibrium value of $\log [\text{ClO}_3^-]$ is -1.9 , i.e., the chlorate concentration is $1.3 \text{ g}/\text{l}$ NaClO_3 . Under these conditions chlorate formation and decomposition rates are small. Above $p\text{H}$ 4 in the electrolyte, chlorate formation begins to be very strong, which has been shown in calculation of the electrolyte composition above. It is known practically that if mercury cells are supplied with alkaline brine, chlorate may accumulate in the system, unless a special device for chlorate decomposition is installed. This was the case in the so-called IG process (33). Chlorate is not harmful to the process, but, since chlorate accumulation in

the brine must be prevented, construction and operation costs of the plant are increased if the brine supplied is alkaline. Because of chlorate formation, pH of the brine should consequently not exceed pH 4, which is reconcilable with the condition that due to other current losses pH of the electrolyte should not exceed pH 3 very much.

DISCUSSION OF MOST SUITABLE COMPOSITION FOR FEED BRINE

According to the foregoing discussion, feed brine ought to have such a composition that pH of the bulk of the electrolyte, which in this case may be represented by the depleted brine, is less than pH 3. As demonstrated by the reaction formulas, anodic current loss implies acid formation, and the cathodic one alkali formation. Composition of feed brine is consequently dependent on all factors which affect current efficiency when a certain pH of the electrolyte is desired.

Experience shows that, in general, depleted brine has more than 1 g/l chlorine and pH 4 when the feed brine is "soda alkaline." In most cases it is sufficient to lower pH of the feed brine, after the precipitation of CaCO_3 and $\text{Mg}(\text{OH})_2$ in alkaline solution, to about 7 in order to obtain less than 1 g/l chlorine and pH 3 in the electrolyte.

It should be noted that not only OH^- but all the basic components of the feed brine, which consume protons during the pH decrease which occurs during the saturation with chlorine in the cell, define the alkalinity of the brine.

If, for instance, composition of the feed brine is: 0.10 g/l chlorine, 0.30 g/l Na_2CO_3 , 0.040 g/l NaOH , then at 25°C and pH 11 the molar concentrations are: $[\text{ClO}^-] = 0.0014$, $[\text{CO}_3^{2-}] = 0.0028$, $[\text{OH}^-] = 0.0010$, and the total alkalinity = $[\text{ClO}^-] + 2[\text{CO}_3^{2-}] + [\text{OH}^-] = 0.0080$ mole/l. This corresponds to a chlorine and carbon dioxide free solution with pH 12 at 25°C.

This explains why hydrogen content of the gas generally increases with increasing chlorine concentration in the feed brine, when it is alkaline. Chlorine content in the brine increases alkalinity which might previously have been near the allowable limit.

If the process is operated at pH 3 under constant experimental conditions with good results, and if the feed brine is becoming more acid, then acid formation at the anode decreases, and base formation at the cathode increases, which reactions both counteract the effect of the decreasing pH of the feed brine. If, on the other hand, the brine is getting more alkaline, acid formation at the anode increases, and also base formation at the cathode, because

then the HClO concentration of the electrolyte increases. In this case it is evidently not certain that the influence of change in brine composition is counteracted by the cell. If OH^- formation at the cathode should predominate over H_3O^+ formation at the anode, HClO content of the electrolyte would increase and loss reactions "catalyze" themselves, until the extreme case is reached, in which the cell works as a chlorate or hypochlorite cell and the gas phase contains hardly any chlorine and only hydrogen and carbon dioxide. Therefore, too alkaline brines may seem to be more hazardous than too acid ones.

In a plant with brine purification it is thus necessary to be sure that the sum $[\text{OH}^-] + 2[\text{CO}_3^{2-}] + [\text{HCO}_3^-] + [\text{ClO}^-]$ is not too great in the purified solution which is supplied to the electrolysis system.

On the other hand, in a plant which is operated with pure salt and no unit processes other than electrolysis and resaturation, Fig. 3 is applicable. It is then necessary to be sure only that chlorine and chlorate concentrations are below a certain limit. If this is exceeded, hydrochloric acid should be supplied to the system. If pH of the solution should become too low, the necessary quantity of alkali is produced in the cells.

SUMMARY

1. In chlorine-caustic electrolysis the following substances and ions, belonging to water, chlorine, and carbon dioxide systems, cannot be neglected in study of the electrolyte: H_2O , H_3O^+ , Cl^- , Cl_2 , Cl_3^- , HClO , and ClO_3^- .

2. Concentration of active chlorine in the brine is the sum of Cl_2 , Cl_3^- , and HClO concentrations. In this sum, Cl_3^- concentration predominates below pH 4, and HClO concentration above pH 4. The former is independent of pH of the electrolyte, and constant at a given temperature and chlorine pressure. The latter concentration increases with increasing pH. Equilibrium concentrations are reached instantaneously.

3. Concentration of acid in the brine is the sum of H_3O^+ and HClO concentrations. The H_3O^+ concentration predominates below pH 3, and the HClO concentration above this value. The sum of these concentrations reaches a minimum at pH 3. Equilibrium concentrations are reached instantaneously.

4. Chlorate equilibrium concentration of the brine increases greatly with increasing pH. Equilibrium concentration is *not* reached instantaneously. Above pH 3.3, it is so high that the system becomes heterogeneous at the high NaCl concentration of a mercury cell. The chlorate formation rate increases

with increasing pH but does not become noticeable until pH 4. The chlorate decomposition rate increases with decreasing pH at a given chlorate concentration, and is slight in the electrolyte.

5. Anodic current efficiency increases with decreasing pH of the electrolyte.

6. The cathode film near the mercury is alkaline, i.e., its pH is greater than 7.

7. Cathodic current efficiency increases with increasing pH of the cathode film.

8. Cathodic current efficiency cannot reach 100% owing to reactions between the acid electrolyte and alkaline cathode film.

9. Agitation of the cathode film interferes with the process.

10. Cathodic current efficiency passes a maximum at pH 3 of the electrolyte.

11. Highest possible current efficiency with respect to chlorine and caustic is not obtained if pH of the bulk of the electrolyte exceeds 3.

12. All bases in the feed brine which are protolyzed during pH decrease in the cell define proper composition of the feed brine. The sum of the concentrations of these bases (OH^- , CO_3^{2-} , HCO_3^- , and ClO^-) should not exceed a certain value.

ACKNOWLEDGMENT

The author wishes to express his deep appreciation to Dr. Ragnar Söderquist, Stora Kopparbergs Bergslags AB, for permission to publish results of the work which was carried out at this company. He is also greatly indebted to Rolf Brännland, the Royal Institute of Technology, Stockholm, for helpful criticism and discussions when writing the manuscript, and to the State Council of Technical Research for a grant making translation possible.

Any discussion of this paper will appear in a Discussion Section to be published in the June 1955 issue of the JOURNAL.

REFERENCES

1. R. TAUSSIG, *Trans. Faraday Soc.*, **5**, 258 (1909-1910).
2. N. J. JOHNSON, *Trans. Electrochem. Soc.*, **86**, 127 (1944).
3. A. A. JAKOWKIN, *Z. physik. Chem.*, **29**, 613 (1899).
4. J. SAND, *ibid.*, **50**, 465 (1904).
5. M. S. SHERRILL AND E. F. IZARD, *J. Am. Chem. Soc.*, **53**, 1667 (1931).
6. J. SAND, *Z. physik. Chem.*, **48**, 610 (1904).
7. D. A. MACINNES AND D. BELCHER, *J. Am. Chem. Soc.*, **55**, 2630 (1933).
8. D. A. MACINNES AND D. BELCHER, *ibid.*, **57**, 1683 (1935).
9. R. P. WHITNEY AND J. E. VIVIAN, *Ind. Eng. Chem.*, **33**, 741 (1941).
10. J. L. GAY-LUSSAC, *Ann. chim. phys.*, [3], **7**, 124 (1843).
11. C. D. HODGMAN, "Handbook of Chemistry and Physics," 33rd ed., p. 1480, Chemical Rubber Publishing Co., Cleveland (1951).
12. R. ROBINSON, *J. Am. Chem. Soc.*, **57**, 1163 (1935).
13. C. D. HODGMAN, *op. cit.*, p. 2033.
14. H. S. HARNED AND B. B. OWEN, "The Physical Chemistry of Electrolytic Solutions," 2nd ed., p. 485, Reinhold Publishing Corp., New York (1950).
15. L. DEMOLIS, *J. chim. phys.*, **4**, 528 (1906).
16. R. BRÄNNLAND, private communication.
17. F. WINTELER, *Z. Elektrochem.*, **7**, 360 (1900).
18. F. FOERSTER, *J. prakt. Chem.*, **63**, 141 (1901).
19. R. L. MURRAY AND M. S. KIRCHER, *Trans. Electrochem. Soc.*, **86**, 83 (1944).
20. F. FOERSTER, *Trans. Electrochem. Soc.*, **46**, 23 (1924).
21. J. N. BRÖNSTED AND N. L. ROSS KANE, *J. Am. Chem. Soc.*, **53**, 3624 (1931).
22. V. DE NORA, *This Journal*, **97**, 346 (1950).
23. S. GLASSTONE, *J. Chem. Soc.*, **125**, 2646 (1924).
24. J. TAFEL, *Z. physik. Chem.*, **50**, 641 (1904).
25. M. KNOBEL, *J. Am. Chem. Soc.*, **46**, 2613 (1924).
26. C. D. HODGMAN, *op. cit.*, p. 1500.
27. G. ANGEL AND T. LUNDÉN, *This Journal*, **99**, 435 (1952).
28. C. D. HODGMAN, *op. cit.*, p. 2153.
29. G. ANGEL, *Z. physik. Chem.*, **170**, 81 (1934).
30. C. D. HODGMAN, *op. cit.*, p. 1830.
31. J. H. PERRY, "Chemical Engineers' Handbook," 3rd ed., p. 373, McGraw-Hill Book Co., New York (1950).
32. FIAT Final Report No. 817, "Vertical Mercury Chlorine Cells," p. 34, H.M. Stationery Office, London (1946).
33. FIAT Final Report No. 816, "Horizontal Mercury Chlorine Cell," p. 62, H.M. Stationery Office, London (1946).

Some Observations on the Kroll Process for Titanium¹

F. S. WARTMAN, DON H. BAKER, J. R. NETTLE, AND V. E. HOMME

U. S. Department of the Interior, Bureau of Mines, Boulder City, Nevada

ABSTRACT

A series of small-scale Kroll process reductions, carried to varying degrees of completion, were opened and examined to obtain information concerning the mechanism of the reduction. Experiments made to determine the cause of zonal variations of hardness in the crude sponge made by the Kroll process indicate this effect is due largely to impurities in the magnesium.

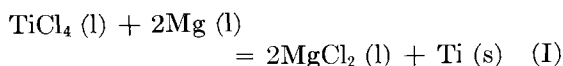
INTRODUCTION

Since the first appearance in this country of a published description (1) of the method of producing titanium by magnesium reduction, the process has been actively investigated (2-8). As a result, a number of modifications to the process as originally described have been developed or suggested. Two of these (3, 4) are: (a) elimination of the molybdenum lining for the reaction chamber, as large molybdenum-lined reactors would have been prohibitively expensive; and (b) provision for removal of the by-product magnesium chloride during and immediately after reduction to facilitate the rate of reduction, obtain up to 90% of the magnesium chloride in pure concentrated form, and simplify later purification of the product of reduction.

OUTLINE OF THE PROCESS

The technique now in use at the pilot plant operated by the Bureau of Mines is described here briefly.

The requisite quantity of magnesium ingots, previously pickled and dried, are placed in an empty reaction chamber made of mild steel; the lid is sealed in place by a weld having only slight penetration. Then the chamber is placed in the furnace, the various supply lines are attached, and the air in the reaction chamber is replaced with helium. Finally, after the temperature of the furnace has been raised to 850°C and held there long enough to melt the magnesium, a stream of liquid titanium chloride is allowed to fall on the hot magnesium until enough titanous chloride has been added to react with about 85% of the magnesium according to the equation:



¹ Manuscript received January 25, 1954. This paper was prepared for delivery before the Chicago Meeting, May 2 to 6, 1954.

The reaction is strongly exothermic and the temperature in the reaction zone is held at 900°-1050°C by suitable adjustment of the fuel input to the furnace and the rate of adding titanous chloride to the reactor. At intervals magnesium chloride is drawn off in a molten form; 85-90% of the total amount formed is removed in this manner. After reduction has been completed and the reaction chamber has been cooled to room temperature, the cover is removed by grinding off the weld, and the product is removed by mounting the open chamber in a large lathe and boring out the reaction mass. A 0.5-in. thick layer is always left on the wall and bottom of the chamber to serve as a protective lining. The opened reaction chamber must be handled in a room with a very dry atmosphere to lessen absorption of moisture by the hygroscopic MgCl_2 left in the mass. The water would react with the titanium when it was heated in later steps of the process. Chips of impure titanium, obtained by the boring, are loaded into retorts and heated at 900°C in a high vacuum to volatilize the residual magnesium and magnesium chloride, leaving the pure titanium, in the form of spongy lumps, as a residue.

OBSERVATIONS ON THE MECHANISM OF TITANIUM REDUCTION

Two interesting phenomena were observed when this operating technique was used: (a) titanium was obtained in a connected mass, with a spongelike appearance, which was attached to the walls of the reactor; and (b) the hardness of the metal in the mass of sponge produced by reduction varied according to its position in the mass.

Titanous chloride is introduced into the reaction chamber as a free-falling liquid from a pipe directed downward above the center of the bath. Observation has confirmed the probability that at least part of the liquid actually reaches the surface of the bath. Titanium has a density considerably greater than either magnesium or magnesium

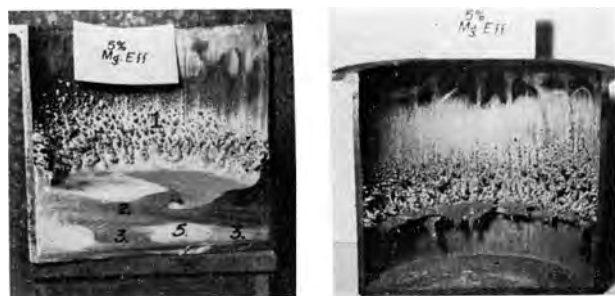


FIG. 1. Bisected chamber after 5% reduction. Left, undistilled segment; right, distilled segment.

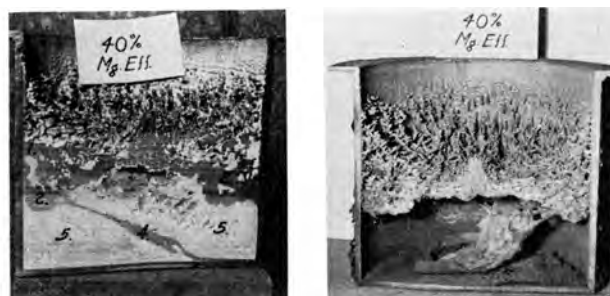


FIG. 3. Bisected chamber after 40% reduction. Left, undistilled segment; right, distilled segment.



FIG. 2. Bisected chamber after 30% reduction. Left, undistilled segment; right, distilled segment.

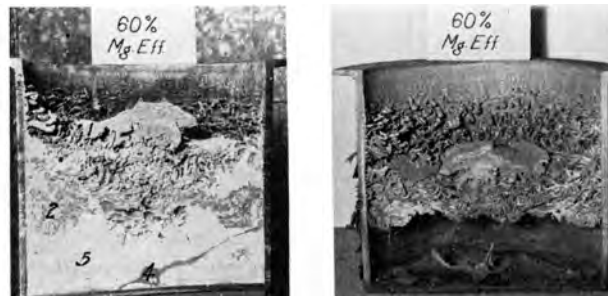


FIG. 4. Bisected chamber after 60% reduction. Left, undistilled segment; right, distilled segment.

chloride, and magnesium and titanous chloride are known to be in contact at the center of the surface of the bath. Therefore, it seems strange that they would not react to form titanium in granular or powder form which, because of its density, might be expected to sink through the bath and be found in a heap on the bottom of the reaction chamber.

A series of seven small reductions was made in an attempt to find an explanation for the apparently anomalous position of the deposit. The reaction chambers were each 25.4 cm in diameter by 25.4 cm high, with a vertical inlet pipe 5 cm in diameter by 91.4 cm long, welded into the center of the cover. They were sand-blasted and partly outgassed by heating in a vacuum for several hours at 900°C. The apparatus was quite similar to that shown in a previous paper (2).

The magnesium charge in each run was approximately 5.7 kg, the temperature at the beginning of the reduction was 800°C, and the rate of addition of titanous chloride after the initial inhibition period was 75 g/min. Thus, the apparatus, operating technique, and physical conditions were as much alike as possible in the different runs. The only variable was the total amount of titanous chloride added, which was 5, 10, 20, 30, 40, 50, and 60%, respectively, of the amount theoretically equivalent to the magnesium added to each run. After each run had been carried to its predetermined degree of completion, it was held at tempera-

ture for 1 hr and then allowed to cool. The lid was removed from the cold chamber, and the latter was divided by a vertical cut through the center, so as to expose a cross section of the contents of the chamber. After photographing the exposed face of one half, samples were taken from selected areas for chemical analysis. The locations from which the samples were taken are indicated by appropriate numerals on the photographs of the cross sections. The other halves were placed in a retort, and the volatile constituents such as magnesium and magnesium chloride were removed by vacuum distillation. The location of the residual deposit of titanium was recorded by a photograph. Some of the deposits before and after distillation are depicted in Fig. 1 to 4, and the corresponding analyses are given in Table I.

In Fig. 1, virtually all of the titanium is in the form of a ring attached to the wall of the reactor and extending upward from the point initially marking the juncture of the upper surface of the magnesium with the wall. Analyses show only a little titanium in the magnesium, and after distillation only a small amount of fine, dark powder was found on the bottom. With increasing additions of titanous chloride, the ring of deposited metal continued to extend farther up the wall and also outward toward the center. At some point between 30 and 40% utilization of magnesium, the spongy titanium formed a layer that bridged completely

TABLE I. *Composition of various portions of deposit*

% Magnesium reacted	Analyses, % by weight			Location of sample	
	Mg	Ti	MgCl ₂	Number on print	Description
5	40	38	22	1	Growths on wall above liquid level
5	94	2.0	0.8	2	Dense metal at top
5	97	1.0	0.6	3	Dense metal at bottom
5	0.2	0.08	98.0	5	MgCl ₂ phase
30	65	28	7	2	Metal just under surface
30	92	3	tr.	3	Metal at bottom
30	96	4	tr.	4	Metal surrounded by MgCl ₂
40	48	32	16	1	Metal at surface
40	60	34	7	2	Metal 2" below surface
40	67	25	66	4	Metallic vein in MgCl ₂
40	0.8	0.008	94.0	5	MgCl ₂ phase
60	17	39	40	1	Metal above surface
60	49	43	tr.	2	Metal in lower part of metallic layer
60	32	46	18	4	Metallic vein in MgCl ₂
60	—	0.03	98	5	MgCl ₂ phase

across the reactor. From this stage on, the unused magnesium was held in the pores and interstices of the sponge that had already deposited, rather than in a distinctly separate pool. Further growth of the spongy deposit was evidenced by a thickening of the whole layer, with some tendency to formation of a prominence immediately under the end of the feed pipe. In all tests, only a small amount of dark-colored, fine-grained metal was found on the bottom after distillation. The major portion of the weight of the metal produced was in the deposit attached to the walls.

To throw more light on this mode of deposition, another run was made using only 5% of the magnesium. It differed from the first in that short lengths of iron rod 1.27 cm in diameter were welded to the bottom and top of the reaction chamber so as to extend perpendicularly into the reaction space. Of the two welded to the bottom, one extended 1.27 cm above the surface of the magnesium and the other 3.82 cm above the surface. The three welded to the underside of the top terminated 1.27 cm, 2.54 cm, and 3.82 cm, respectively, above the initial level of the free surface of the magnesium. As will be seen from Fig. 5, titanium deposited on the two bars that extended up through the bath, just as it did on the walls. The three bars that extended down from the top remained clean.

If deposition of sponge on the walls had been due either to mechanical splatter or to deposition from a vapor-phase reaction, then metal should have been deposited on the bars extending down

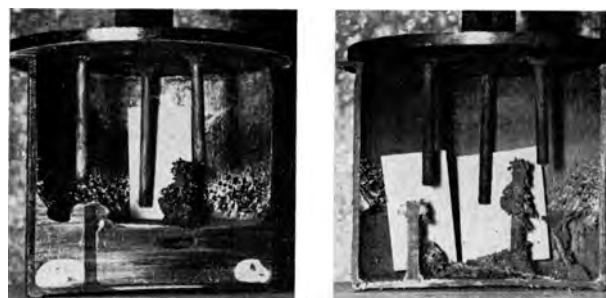


FIG. 5. Cross sections of chamber after 5% reduction. Bars were attached to bottom and top. Left, undistilled segment; right, distilled segment.

close to but not touching the surface of the magnesium. As metal was deposited only on surfaces that passed up through the magnesium, it seems likely that the deposits on the bars extending up through the bath and on the walls were due to a reaction between titanic chloride vapor and a film of magnesium formed on the vertical surfaces by wetting and capillary action. This hypothesis is supported by the known physical properties of the system. Neither magnesium nor titanic chloride is appreciably soluble in magnesium chloride. Therefore it is postulated that when the titanic chloride first comes in contact with the free surface of the magnesium some reaction occurs and some magnesium chloride is formed. This forms a film on the surface that tends to inhibit further reaction. The protective action of such salt films is known and used in the technology of melting, refining, and casting magnesium. On a vertical surface it may be supposed that gravitation causes the magnesium chloride to drain away at least partially, and thus afford better opportunity for contact between titanic chloride and magnesium. This hypothesis may serve as the basis for some interesting predictions concerning the suitability of specific techniques for conducting the reduction. For example, it may be predicted that bringing the two raw materials into contact by allowing droplets of magnesium to fall through the vapor of titanic chloride would not be satisfactory since the droplets would become inactive because of formation of an enveloping film of magnesium chloride.

The tendency to react on vertical rather than horizontal surfaces is probably fundamental, but the nature and location of the deposit formed is affected by the size of the reactor and variations in the manner of operation. For example, Fig. 6 is a view of a reaction mass, contained in a thin iron crucible and cut through the vertical axis. This small reduction run was made for several reasons, one of which was to determine the effect of adding

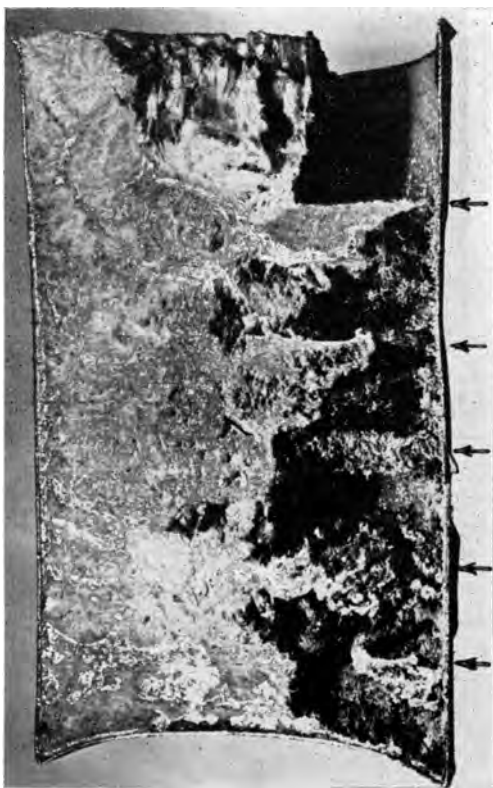


FIG. 6. Cross section of small reaction mass, made to show feasibility of thin disposable liner, multiple additions of magnesium, and tapping of molten magnesium.

the magnesium in increments during the run rather than all at once at the beginning.

About one-fifth of the magnesium was placed in the pot initially, and the rest was added in four increments during the run in the form of small pieces contained in a rubber bag attached to an opening in the top of the reactor. As indicated by the arrows at the right of Fig. 6, the five portions of magnesium resulted in the formation of five separate layers of sponge. These are exposed prominently, because this reaction chamber was removed from the furnace and laid on its side when the reduction was completed. The side at the left then became the bottom, and the still fluid magnesium chloride flowed to the position shown.

If the magnesium chloride had been drawn off so as to keep the zone of reaction at approximately the same level during the reduction, there would have been only a single, dense, thick layer of sponge.

In larger reactors making 91 kg or more of sponge per charge, there is a similar tendency to form a bridge extending upward from the level that originally marked the upper surface of the magnesium. With the greatly increased span, the mechanical strength of the spongy layer is not adequate to allow bridging, and the whole mass collapses to the bottom, particularly when the magnesium chloride is tapped off and its buoyant effect is no

longer available to support the bridge of spongy titanium. Since facilities large enough to section and distill large reaction chambers with their contents in place were not available, photographic evidence of the behavior of these large masses cannot be offered.

OBSERVATIONS ON THE SEGREGATION OF IMPURITIES DURING REDUCTION

Usual practice at the pilot plant operated by the Bureau of Mines was to mount the opened reaction chamber in a lathe and remove the mass of crude titanium sponge by turning. The chips obtained in this way were treated at 900°C in a high vacuum; as a result of this treatment, hydrogen, magnesium, and magnesium chloride were largely removed by volatilization, and purified spongy titanium remained as the residue. As previously noted, if chips from various parts of the reaction mass were kept segregated during purification, metal produced from chips that came from the center of the reaction mass was freer from impurities and softer than that made from chips that came from the outside and bottom.

Discovery of the cause and a remedy for this condition was of practical importance for several reasons. Variations in hardness and composition of sponge in the same lot introduced difficulties in sampling and testing. Compacts made from such material by powder metallurgy techniques were not uniform in composition and properties. Finally, it was considered desirable to have the best possible quality of primary metal, consistent with reasonable costs of production, in order to allow use of larger quantities of scrap, such as turnings and off-grade sponge, in making new ingots.

Two hypotheses were advanced to explain this tendency to zonal segregation of impurities in the reaction mass: (A) during reduction, gases present in the atmosphere around the reaction chamber diffused through the hot mild-steel walls of the chamber and dissolved in the titanium lying closest to the wall on the inside; (B) the first titanium formed during the reduction served as a "getter" of the impurities present in the magnesium and on the walls of the reactor and in doing so became hardened. As shown above, the first titanium made is deposited on the walls of the reactor.

The hypothesis that the zonal hardness variations were due to diffusion through the walls of the reactor was tested in two ways. Several types of empty reaction chambers were heated to operating temperature and held there while a slow stream of helium was passed through one side of an electrical thermal conductivity meter, then through the hot chamber, and finally back through the other side

of the meter. After the initial period of outgassing, no contamination of the helium was indicated. Also, small reaction chambers were packed with high grade titanium sponge, outgassed, filled with helium, and then heated for several hours at about 800°C. After the chamber had cooled, it was opened and the sponge removed. While being unloaded, the sponge was segregated into various portions according to position in the chamber during heating. Each portion of sponge was sampled and the sample melted into a small ingot on which the hardness was measured. The hardness of the sponge lying next to the walls of the reactor was not noticeably greater than that of sponge in the center. This also suggests that the zonal variations in hardness were not due to diffusion of gases through the walls of the reactor.

Evidence bearing on the "getter" theory was obtained by making three separate 90-kg Kroll reductions, runs No. 402, 403, and 404, each as nearly alike as possible except in the manner of adding the magnesium. A different reduction chamber was used for each run. Each had been used several times before and had been cleaned and wire-brushed to remove all residues from previous runs. Each pot was finally sealed and treated on the inside with moist hydrogen while at operating temperature. Before cooling, the hydrogen was replaced with helium or argon, and the inert atmosphere was maintained through all subsequent operations until the reduction had been finished and the chamber cooled to room temperature. This prevented reabsorption of nitrogen, oxygen, or water vapor on the inner walls of the chamber.

In addition to a variation in the method of adding the magnesium, the technique used in making these three reductions differed in two other ways from that previously described (4). First, the titanium tetrachloride was fed through two stationary pipes introduced into the 5.08 = cm pipes normally used for poking to break up the surface crust on the reaction mass, and the revolving feeder was not used. Second, a long thermocouple with iron protection tube was introduced through a packing gland in the top of the column cover. As the couple could be moved up and down in the packing gland, the temperature could be measured at different levels in the reaction chamber. This was done every half hour until about half of the magnesium had been used. The rate of addition of titanium tetrachloride was adjusted to hold the maximum temperature in the reaction chamber between 950° and 1050°C. The protection tube in moving up and down periodically also took over the function normally performed by the poking rods.

The magnesium used for these three reductions was standard commercial-grade electrolytic magnesium cast in cylindrical billets approximately 40.7 cm long by 10.7 cm in diameter. A typical chemical analysis in percent by weight follows:

Fe.....	0.05	Mn.....	0.06
Si.....	0.003	Al.....	trace
Ni.....	0.002	C.....	0.005-0.12
Cl.....	0.02		

The billets were cut into three or four pieces and cleaned by pickling, drying, and buffing before use.

In the first run, all the billets were put in the reaction chamber and completely melted before any titanate chloride was added. In the second run about one-fourth of the billets were introduced and melted before starting to feed the titanate chloride. The rest were added at intervals through a lock in proportion to the rate at which titanate chloride was run in. In the third run the charge of clean billets first was melted in a separate chamber under an inert atmosphere and held molten for several hours to allow the solid impurities to settle as much as possible. Then the liquid metal, protected by an inert atmosphere, was siphoned over into the reaction chamber. It was necessary to let the magnesium solidify before the chamber could be disconnected from the siphon and placed in the furnace, but the whole charge was melted again before the reduction was started.

The three reductions were completed and cooled, and the product was recovered by boring and purified by distillation, as described above. In boring, the charge was divided into four lots, approximately as indicated in Fig. 7, and during vacuum distillation each lot from each of the three runs was kept separate.

In studying the data derived from these three reductions as shown in Table II, two points are to be noted particularly. First, the product obtained from runs No. 402 and 404 in which all of the magnesium was added and melted before the reduction started shows very definitely the zonal distribution of hardness and impurities. In contrast, the product of run No. 403 to which magnesium was added in increments during the run shows little variation between the different fractions other than what might be ascribed to normal variations in testing and analysis. Second, the product of run No. 404 in which the magnesium was settled and decanted is noticeably softer than the product of run No. 402 in which the commercial billets were prepared only by cleaning the surface.

By inference, these facts lend strong support to the hypothesis that the zonal variations in hardness are due to the first titanium formed acting as a

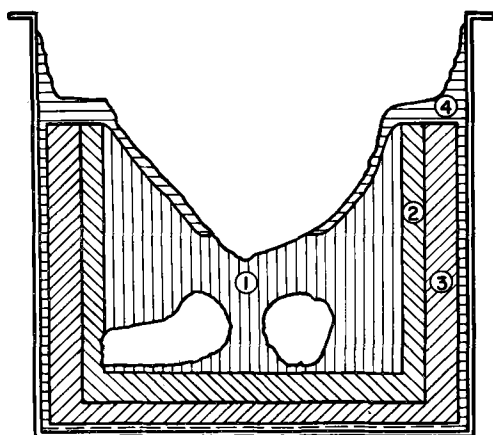


FIG. 7. Sectional diagram showing position of lots 1, 2, 3, and 4 in reaction mass.

getter, since they are to be anticipated on the basis of this hypothesis. The first titanium is deposited on the walls of the reaction chamber just above the upper surface of the magnesium, and magnesium fed by capillary action to the zone of reaction as it rises up the wall and out over the bath must pass through or over this metal. An excellent opportunity is thus afforded for removal of impurities in the magnesium. When magnesium is added during the run, it is already at the surface, is in the reaction zone, and does not have to pass through the metal previously deposited. Consequently, the purifying

action does not take place, and all the metal tends to be of about the same grade.

This same effect makes it difficult to produce alloys of titanium of uniform composition by adding the alloying element through the magnesium, if all the magnesium is placed in the reaction chamber before starting the reduction. In one test, an attempt was made to make a titanium alloy containing 1% aluminum by alloying the necessary amount of aluminum with the magnesium before commencing the reduction. Most of the aluminum went into the titanium, which had been deposited first, and only a trace was found in the metal from the center of the reaction mass.

Consideration of the data in Table II also leads to the conclusion that a considerably better grade of titanium could be produced by the Kroll process if magnesium of much higher purity were available in large ingots so as to reduce the amount of impurities both dispersed through the body of the ingot and on the surface. Fraction 1 of run No. 404 indicates the improvement to be expected by this means.

Further inspection of Table II shows that iron, manganese, and oxygen are the principal impurities which would remain after the sponge had been melted to form an ingot. To obtain some idea as to how these impurities affect the hardness of titanium, three series of alloys were made, and the relation

TABLE II. Data obtained from three special 200-lb reduction runs

Run No. and description	Lot	Kg	Analyses, % by weight										Total of determined impurities	Brinell hardness
			Fe	Mg	Si	Mn	Ti	N	O	H	Cl			
402. Magnesium in form of commercial billets, all added and melted before starting reduction.	1	36.7	0.03	0.05	0.04	0.03	99.9	0.004	0.062	0.0022	0.06	0.28	110	
	2	30.4	0.04	0.06	0.03	0.06	99.85	0.004	0.072	0.0015	0.04	0.31	133	
	3	26.7	0.19	<.04	0.03	0.20	99.5	0.003	0.112	0.0026	0.05	0.62	158	
	4	14.1	0.13	0.23	0.04	0.04	99.8	0.003	0.132	0.0034	0.11	0.69	162	
	Total	107.9												
Weighted averages			0.086	0.074	0.035	0.082	—	0.0036	0.086	0.0023	0.058	0.427	135	
403. Magnesium in form of commercial billets, one-fourth added and melted before starting reduction, rest added during run.	1	30.8	0.13	0.06	0.03	0.13	99.75	0.002	0.051	0.0016	0.09	0.49	125	
	2	28.6	0.12	0.14	0.03	0.11	99.2	0.002	0.062	0.0015	0.10	0.57	129	
	3	27.2	0.16	0.07	0.04	0.08	99.75	0.002	0.055	0.0022	0.12	0.53	123	
	4	17.2	0.19	0.25	0.03	0.02	99.5	0.002	0.074	0.0018	0.22	0.79	135	
	Total	103.8												
Weighted averages			0.145	0.116	0.033	0.093	—	0.002	0.059	0.0018	0.122	0.572	127	
404. Magnesium melted, settled, and siphoned before use to remove some of suspended impurities	1	29.5	0.04	0.08	0.03	0.04	99.9	0.002	0.039	0.0006	0.08	0.31	98	
	2	26.3	0.06	0.17	0.04	0.06	99.4	0.003	0.052	0.0008	0.09	0.48	117	
	3	26.3	0.13	0.04	0.03	0.09	99.6	0.003	0.058	0.0017	0.07	0.42	127	
	4	24.0	0.15	0.12	0.03	0.11	99.3	0.002	0.070	0.0014	0.13	0.61	153	
	Total	106.1												
Weighted averages			0.092	0.100	0.032	0.073	—	0.0025	0.054	0.0011	0.091	0.445	122	

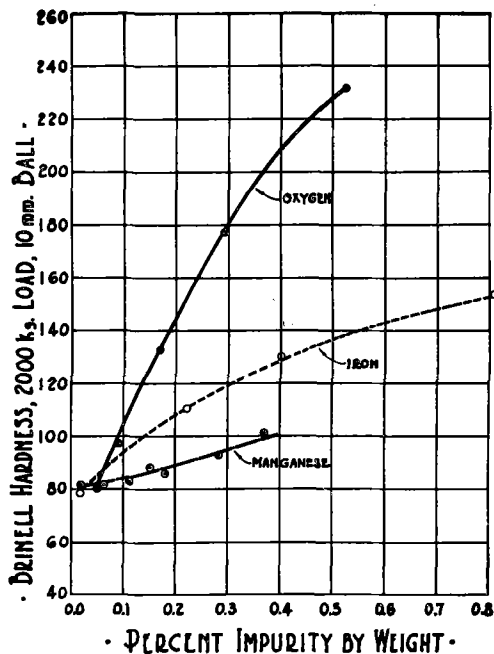


FIG. 8. Graph showing effect of oxygen, iron, and manganese on the hardness of titanium.

between amount of impurity and hardness of the as-melted ingot was determined. Electrolytic titanium² was used as the base, and the alloy additions were high grade commercial transformer iron, electrolytic manganese, and purified titanium dioxide. The alloys were made up by weight from the raw materials, but the actual composition of the melted ingot was determined by chemical analysis. Data obtained are shown in Fig. 8. The effects of all these elements as alloying additions to titanium have been studied before, but available data for iron and manganese did not indicate clearly the effect of such small amounts as are studied here. In the previous work on titanium-oxygen alloys (9-11), the oxygen content of the final alloy, on which hardness measurements were made, was not determined directly, and there was no assurance that the value taken was correct.

The curves show that the amount of manganese ordinarily present in commercial-grade sponge has little effect on the hardness, the iron content has more effect, and the oxygen most of all.

In the case of the various lots of sponge for which data are given in Table II, if separate increments of hardness due to manganese, iron, and oxygen by reference to Fig. 8 are estimated, it will be found that the sum is less than the amount the hardness of the batch exceeds that of pure titanium,

² Electrolytically purified in a small cell using a fused salt electrolyte. The purification was done in this laboratory.

about 60 BHN. This indicates, therefore, that the many other impurities present in very small amounts taken together also contribute significantly to the total hardness.

ACKNOWLEDGMENTS

This project has been conducted at the Boulder City (Nevada) Experiment Station of the Bureau of Mines, now designated as the Electrometallurgical Branch of the Metallurgical Division, Region III, under the general supervision of R. R. Lloyd, Branch Chief. The authors are also grateful to C. T. Baroch for critical review of the manuscript, and to members of the Mechanical Services Section, under the direction of C. A. Stay, and of the Chemistry and Physics Section, under the direction of P. R. Perry, for valuable assistance in their respective fields.

Any discussion of this paper will appear in a Discussion Section to be published in the June 1955 JOURNAL.

REFERENCES

1. W. J. KROLL, *Trans. Electrochem. Soc.*, **78**, 35 (1940); U. S. Pat. 2,205,854, June 25, 1940.
2. R. S. DEAN, J. R. LONG, F. S. WARTMAN, AND E. L. ANDERSON, *Trans. Am. Inst. Mining Met. Engrs.*, **166**, 369 (1946).
3. F. S. WARTMAN, J. P. WALKER, H. C. FULLER, M. A. COOK, AND E. L. ANDERSON, *U. S. Bureau of Mines Rept. of Investigations* 4519, August 1949.
4. H. C. FULLER, D. H. BAKER, AND F. S. WARTMAN, *U. S. Bureau of Mines Rept. of Investigations* 4879, June 1952.
5. M. A. COOK AND F. S. WARTMAN, *U. S. Bureau of Mines Rept. of Investigations* 4837, February 1952.
6. C. K. STODDARD AND E. PEITZ, *U. S. Bureau of Mines Rept. of Investigations* 4153, December 1947.
7. None of the operations conducted by private companies, using the Kroll process, has been described in print. Aside from a few publications by various research organizations, one must rely largely on patents to gain some insight into the trend in this work. The following list is not complete and is intended only to give an idea of the various modifications proposed for the Kroll process:
 - C. H. WINTER, JR. (assignor to E. I. du Pont de Nemours and Co.) U. S. Pat. 2,586,134, 2,607,674, 2,621,121.
 - J. GLASSER AND C. HAMPEL (assignors by Mesne assignments to Kennecott Copper Corp.) U. S. Pat. 2,618,549 and 2,618,550.
 - The British Aluminum Company, Ltd., and L. SAUNDERS, British Pat. 638,840.
 - ROBERT D. BLUE (assignor to the Dow Chemical Co.) U. S. Pat. 2,567,838.
8. P. J. MADDOX AND L. W. EASTWOOD, *J. Metals*, **188**, 634 (1950).
9. R. I. JAFFEE, *ibid.*, **1**, 646 (1949).
10. R. I. JAFFEE, H. R. OGDEN, AND D. J. MAYKUTH, *ibid.*, **188**, 1261 (1950).
11. W. L. FINLAY AND JOHN A. SNYDER, *ibid.*, **188**, 277 (1950).

Factors Affecting the Formation of Anodic Oxide Coatings¹

M. S. HUNTER AND P. FOWLE

Aluminum Company of America, New Kensington, Pennsylvania

ABSTRACT

The effect of variations in electrolyte and forming conditions on the formation of porous type anodic oxide coatings on aluminum are discussed, with particular reference to the manner in which these variables control oxide formation, pore development, and the thickness of the barrier layer. Formation and solution rate data are applied to show that, during the formation of a porous type coating, conditions at pore bases are vastly different from those existing in the main body of the electrolyte.

INTRODUCTION

It has been known for many years that characteristics of the porous type of anodic oxide coating applied to aluminum are determined by the electrolyte used in its formation and by conditions under which it is formed. As a result, the structure of these coatings and factors that control their formation have been the subject of much discussion and investigation (1-7). Recently, structural features of the cells and pores comprising these coatings have been revealed, and methods have been developed for determining their dimensions (7, 8). The present paper establishes the effect of electrolyte and forming conditions on formation of the porous type of anodic oxide coating through the use of barrier layer thickness measurements (8), and presents a new concept of conditions that may exist at the bottom of the pores during the formation process.

When anodic oxide coatings are formed on aluminum, the chemical action of the electrolyte on the oxide governs the type of coating which results. If the electrolyte has no appreciable solvent action on the oxide, a thin nonporous barrier type of coating is formed. If, however, the electrolyte has appreciable solvent action, pores develop in the oxide, and the porous type of coating is produced. This latter type of coating is characterized by a thin nonporous barrier layer of oxide next to the metal and a relatively thick porous layer of oxide situated above the barrier layer. The entire coating is at one stage barrier layer oxide; the porous layer is barrier layer oxide, which contains tubular pores developed by solvent action of the electrolyte. The barrier layer at the bottom of the pores is important, because it constitutes an effective barrier between the metal and its environment during service.

¹ Manuscript received April 26, 1954. This paper was prepared for delivery before the Chicago Meeting, May 2 to 6, 1954.

In the formation of the porous type of oxide coating, oxide production proceeds in an orderly fashion and at a relatively constant rate, once the initial fluctuations which attend the start of this process have subsided. This constancy of barrier layer thickness indicates that a balance has been attained between the rate of oxide formation and factors controlling solvent action. Inasmuch as the thickness of the barrier layer is the net result of these competing actions, a change in this balance will be reflected in a change in thickness of the barrier layer. Consequently, changes in barrier layer thickness as a result of changes in electrolyte and forming conditions are an indication of the effect of these factors on formation of anodic oxide coatings.

FACTORS AFFECTING BARRIER LAYER THICKNESS

The balance between formation and solution of oxide is of a rather complex nature, because at least six major variables are involved: electrolyte type, electrolyte concentration, bath temperature, voltage, current density, and time. Electrolyte type, concentration, and temperature, along with current density and voltage, are interdependent, with the result that no variable may be changed without effecting a change in at least one other.

Considering the effect of the six major variables on barrier layer thickness, time is not a factor because it has been shown that barrier layer thickness remains constant with time, once the balance between formation and solution of oxide has been established (8). Further simplification may be made by considering first a single concentration of a specific electrolyte. An electrolyte containing 15% by weight of sulfuric acid was arbitrarily chosen as a starting point in this investigation.

With regard to the three remaining variables, voltage, current density, and bath temperature, it is found that they also are interdependent, and that

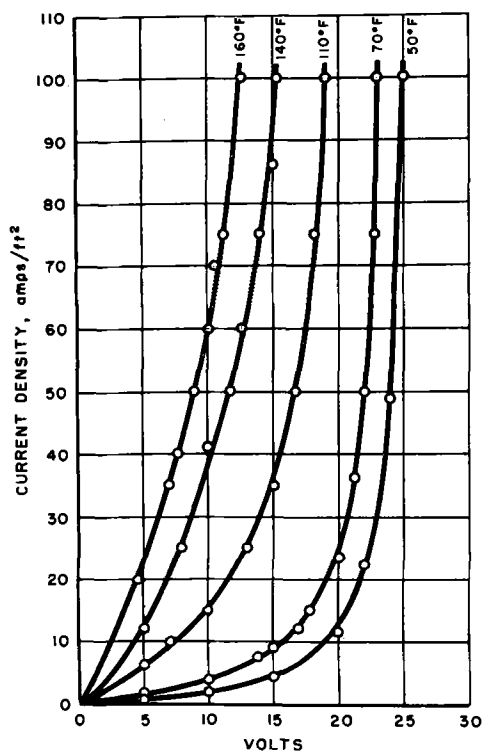


FIG. 1. Voltage, current density, and temperature relationships during coating of 99.99% aluminum in 15% sulfuric acid.

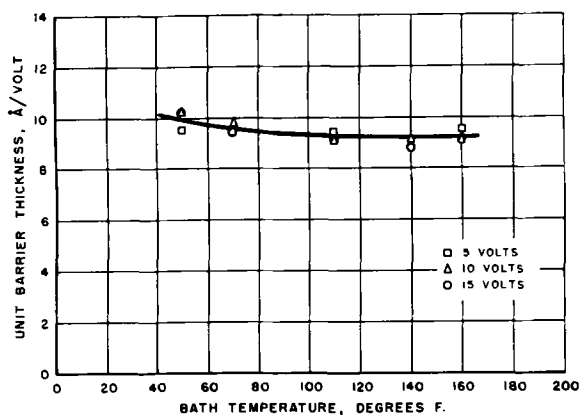


FIG. 2. Effect of voltage and temperature on unit barrier thickness for coatings on 99.99% aluminum formed in 15% sulfuric acid.

a change in one will be reflected in a change in one or both of the others (Fig. 1). Thus, if both temperature and forming voltage are chosen, current density is automatically established. Consequently, only the effects of forming voltage and bath temperature on barrier layer thickness need be considered initially.

The combined effect of these two variables on the unit barrier thickness (thickness per volt of forming potential) of coatings formed in the 15% sulfuric acid electrolyte is shown by Fig. 2. It is apparent that forming voltage in the range in-

vestigated had no effect on unit barrier thickness. Therefore, while forming voltage controls the total thickness of the barrier layer, it has no bearing on unit barrier thickness. Temperature, however, does have an effect on unit barrier thickness, and decreasing temperature results in greater unit barrier thickness. From the trend observed, it appears that at very low temperatures the unit barrier thickness will approach the 14 Å value characteristic of electrolytes that do not dissolve the oxide. This is not surprising, because solvent action of electrolytes generally decreases with temperature.

The effect of current density on unit barrier thickness may now be established by considering the interrelationship between this variable, forming voltage, and bath temperature. From Fig. 2, it is apparent that forming voltage did not affect unit barrier thickness. From Fig. 1, it is evident that for any given bath temperature the voltage range covered involved a wide range of current density values. Inasmuch as voltage had no effect on unit barrier thickness, it is apparent that current density also does not influence unit barrier thickness.

Having shown that voltage, current density, and time do not affect unit barrier thickness, it is possible to establish the effect of electrolyte concentration on unit barrier thickness by fixing bath temperature. For this part of the investigation, coatings formed at 15 volts in sulfuric acid electrolytes operated at 21°C were used. In the course of determining the relationship between barrier layer thickness and electrolyte concentration, it was observed that, at constant voltage, pronounced changes in current density occur with variations in sulfuric acid concentration (Fig. 3). The shape of the curve is similar to that of the curve for the conductivity of sulfuric acid solutions (9) (Fig. 3), although the highest current densities did not correspond to the maximum conductivities. Also, current densities were extremely low at both very low and very high acid concentrations.

Pronounced but not unexpected changes in unit barrier thickness were found to occur with variations in sulfuric acid concentration as shown by Fig. 4 and 5. As concentration was decreased to very low values (Fig. 4), the barrier approached the 14 Å/volt value characteristic of electrolytes that do not dissolve the oxide. This indicates that at very low concentrations the ability of the electrolyte to dissolve the oxide and develop pores decreases to an exceptionally low value. As concentration was increased in the range of 25–65% acid (Fig. 5), the unit barrier thickness did not vary appreciably, but at about 90% acid concentration and above, unit barrier thickness became practically zero. At these very high acid concentrations, no coating at

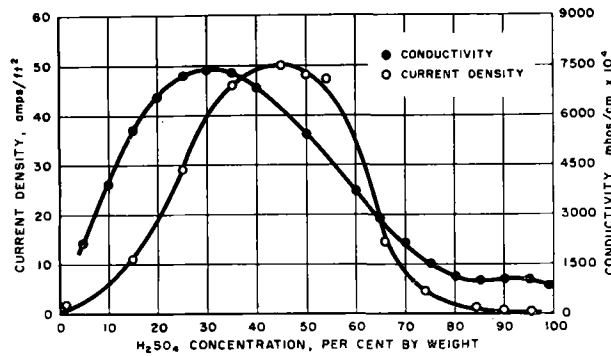


FIG. 3. Relation between concentration and conductivity of sulfuric acid solutions and between acid concentration and current density during coating of 99.99% aluminum at 15 v and 70°F.

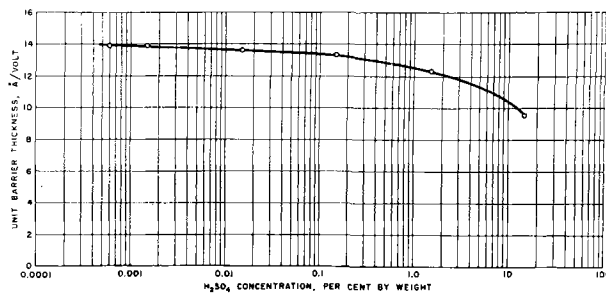


FIG. 4. Relation between concentration of dilute sulfuric acid electrolytes and unit barrier thickness of coatings formed on 99.99% aluminum at 70°F and 15 v.

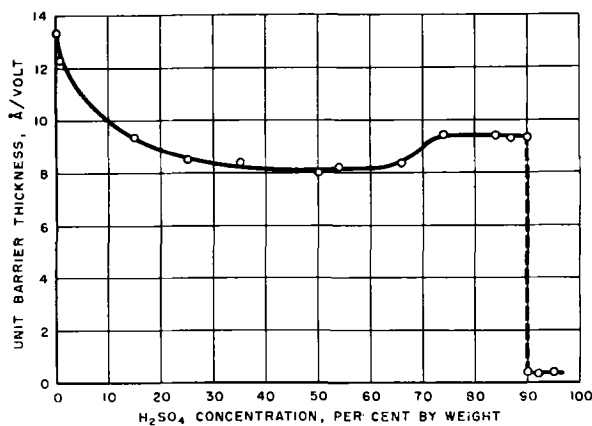


FIG. 5. Relation between sulfuric acid concentration and unit barrier thickness of coating formed on 99.99% aluminum at 70°F and 15 v.

all was formed, apparently because there was insufficient water present to ionize the electrolyte and form coating.

The effect of electrolyte type on unit barrier thickness was investigated by making barrier thickness determinations in 3% chromic acid, 4% phosphoric acid, and 2% oxalic acid electrolytes. In each of these electrolytes, unit barrier thickness changed appreciably with the bath temperature but did not change with variations in current density, voltage, and time, as was the case with the

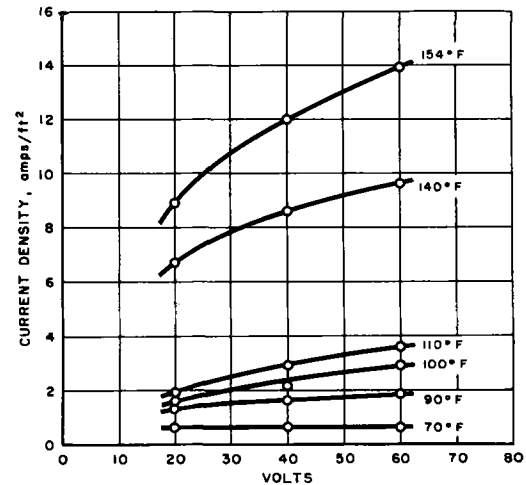


FIG. 6. Voltage, current density, and temperature relationships during coating of 99.99% aluminum in 3% chromic acid.

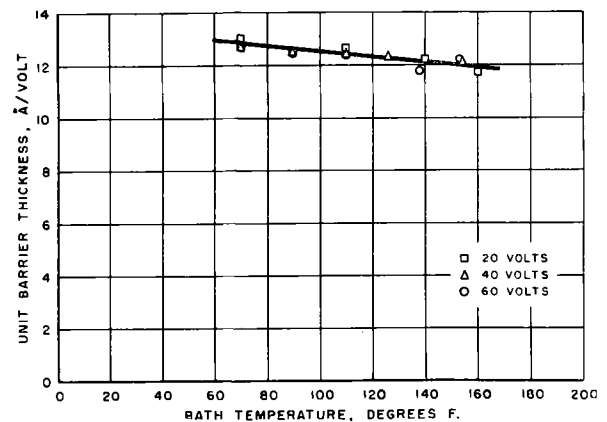


FIG. 7. Effect of voltage and temperature on unit barrier thickness for coatings on 99.99% aluminum formed in 3% chromic acid.

sulfuric acid electrolyte. Also, at any given temperature, different unit barrier thickness values were observed for the four electrolytes. The interrelationship between current density, voltage, and bath temperature, and the variation in unit barrier thickness with temperature for the 3% chromic acid electrolyte are shown by Fig. 6 and 7.

In summary, voltage, current density, and time control the amount of anodic oxide coating that forms, but these factors have no effect on unit barrier thickness. Unit barrier thickness is determined by electrolyte type, electrolyte concentration, and bath temperature.

FACTORS AFFECTING PORE FORMATION

Inasmuch as formation of the porous type of oxide coating involves a balance between oxide formation and solution, coating may form only as fast as solution occurs at the bases of the pores. In contrast to the formation of oxide which is an elec-

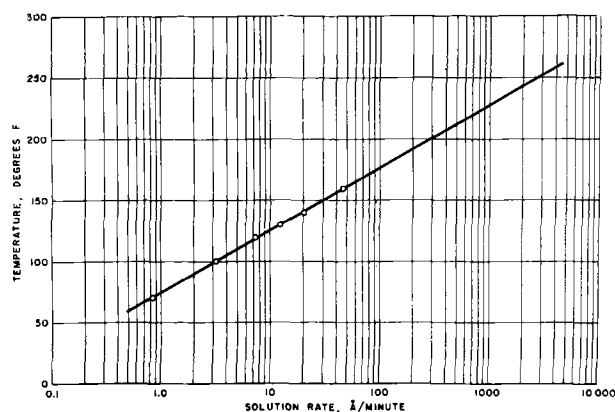


FIG. 8. Relation between solution rate and temperature in 15% sulfuric acid electrolytes.

trochemical process, solution of the oxide is primarily a chemical process. Of the six major variables under discussion, time may be eliminated by considering the rate of solution. Since the solution of oxide is a chemical process, current density will not have a direct effect but will affect solution rate only insofar as it may affect temperature. Voltage also will not affect solution rate directly but will influence the rate of solution insofar as it affects current density and temperature. Thus, the solution rate is defined in terms of electrolyte type, electrolyte concentration, and bath temperature, which are the same factors that control unit barrier thickness. In this investigation, only the effect of variations in concentration and temperature of sulfuric acid electrolytes has been investigated comprehensively, although preliminary work with other electrolytes has shown that electrolyte type has a pronounced effect on solution rate.

Solution rates were determined by immersing sulfuric acid anodic coatings in various concentrations of sulfuric acid at various temperatures without applied voltage. The reduction in thickness of the barrier layer resulting from immersion was then used to calculate linear solution rates in Angstrom units per minute.

Considering first the 15% sulfuric acid electrolyte that is used extensively in commercial applications, it is found that solution rate and temperature bear a logarithmic relationship (Fig. 8). Solution rate is doubled for every 8.6°C increase in temperature and is increased tenfold for every 28.3°C rise in temperature. These results are similar to those obtained by Hass (6) for the solution rates of barrier type oxide coatings in similar electrolytes. This relationship may be expressed more precisely by the equation

$$\log R = 0.0196T - 1.45$$

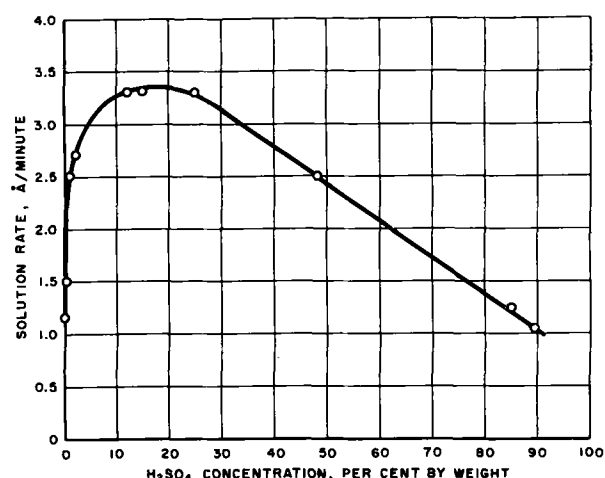


FIG. 9. Relation between solution rate and sulfuric acid concentration at 100°F.

where R is the linear rate of solution in Angstrom units per minute, and T is temperature in degrees Fahrenheit.

The specific effect of electrolyte concentration on solution rate was determined by measuring the decrease in thickness of the barrier layer portion of coatings formed in 15% electrolyte during exposure to electrolytes of other concentrations. At each concentration, the same logarithmic relationship was observed between temperature and solution rate. Thus, the plots of solution rate against temperature for various concentrations form a family of parallel lines on a semi-logarithmic plot. Solution rate varied somewhat with electrolyte concentration at all temperatures, but the effect of concentration was much less than that of temperature. Solution rate reached a peak in the range of about 12–25% acid. A typical curve showing the relation between concentration and solution rate is shown in Fig. 9. The sharp decrease in solution rate at very low concentrations is in keeping with the high unit barrier thicknesses observed at these concentrations.

From these relationships, it is apparent that temperature and electrolyte type and concentration control solution rate at the bases of the pores. Temperature is the dominant factor, and even relatively small changes in temperature result in pronounced changes in solution rate. Electrolyte concentration also affects solution rate, but rather large changes in concentration are required to produce significant changes.

CONDITIONS EXISTING AT PORE BASES

If formation rates and solution rates are considered further, an interesting hypothesis is evolved concerning the situation which may exist at the base of the pores during formation of the porous type of

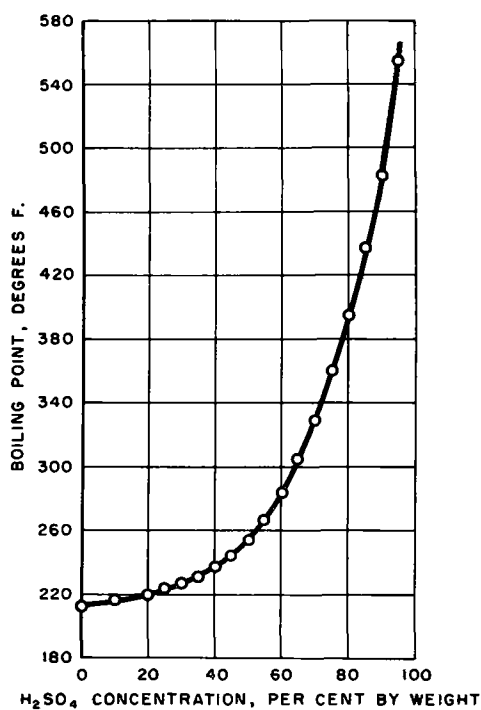


FIG. 10. Boiling points of sulfuric acid solutions

oxide coating. In the case of a coating formed in a 15% sulfuric acid electrolyte at 21°C using a current density of 12 amp/ft² (1.29 amp/dm²), oxide is formed at the rate of about 0.00088 in./hr, which amounts to 3725 Å/min. Inasmuch as the barrier thickness remains constant once the initial balance between formation and solution is established, the linear rate of solution at the base of the pores must also be 3725 Å/min. From data already presented, however, the linear rate of solution in 15% sulfuric acid at 21°C is only 0.84 Å/min. This difference in rate of over 4000:1 indicates that the electrolyte conditions at the base of the pores cannot be the same as those in the body of the electrolyte.

The conditions that probably exist at the base of the pores can be established from the solution rate data. From the solution rate formula given above, the 3725 Å/min rate which must exist to maintain constant barrier thickness corresponds to an electrolyte temperature of about 124°C for the 15% electrolyte. This is much higher than the boiling point of this electrolyte, and indicates that the electrolyte is probably of a concentration greater than 15%. Referring to the boiling points of sulfuric acid solutions (10) (Fig. 10), it is found that 124°C corresponds to the boiling point of 50% sulfuric acid. Thus, as a first approximation, the operating electrolyte at the base of the pores is boiling 50% sulfuric acid during the formation of this particular coating. Extension of this reasoning to cover the solution rate of the 50% acid instead of the 15%

acid which could not develop the required solution rate brings about only a small change. The final determination indicates that the electrolyte at pore bases is probably boiling 51% sulfuric acid.

Consideration of other relationships that apply to the formation of anodic oxide coatings can be used to estimate the temperature and concentration of sulfuric acid which is operative at pore bases under any combination of forming conditions. The amount of coating formed is a function of current density and time in accordance with Faraday's law. The rate of formation, therefore, is a function only of current density. Consequently, other variables can affect the rate of formation only insofar as they affect current density. Also, rate of solution must equal rate of formation because the barrier thickness remains constant once the initial balance is established. Therefore, rate of solution also may be treated as a function of current density. Based on known rate of formation data, solution rate may be expressed by the equation:

$$R = 310 C$$

where R is linear rate of solution in Angstrom units per minute, and C is current density in amperes per square foot.

As an example of the manner in which conditions existing at pore bases may be estimated, assume that a coating is to be applied in a 15% sulfuric acid electrolyte at 43°C using a potential of 10 volts. From Fig. 1, the current density corresponding to this voltage and temperature will be about 17 amp/ft² (1.83 amp/dm²). Rate of solution will be 310 times this value or about 4960 Å/min. From Fig. 8, a temperature of about 128°C is required to obtain this solution rate. This, in turn, corresponds to the boiling point of 53% sulfuric acid. Therefore, the electrolyte at pore bases under these conditions is approximately 53% acid at its boiling point of 128°C.

Further consideration of these various relationships reveals additional interesting information regarding the electrolyte operative at pore bases. The 15% sulfuric acid electrolyte has a solution rate of about 620 Å/min at its boiling point of about 103°C. This corresponds to a current density of about 2.0 amp/ft² (0.22 amp/dm²). At current densities below this value, the electrolyte at pore bases will be substantially 15% acid but will be at a temperature sufficient to give a solution rate corresponding to the particular current density value. At current densities above 2.0 amp/ft² (0.22 amp/dm²), the electrolyte will be at its boiling point and will be of a greater concentration and at a higher temperature to develop the solution rate required.

The existence of pronounced temperature and concentration differentials between the electrolyte at pore bases and in the body of the electrolyte emphasizes the importance of agitation in the anodic coating process. Movement of the electrolyte in and out of the pores is a very important factor in removing heat from the base of the pores where it is generated. Also, mixing of the electrolyte will tend to decrease the concentration gradient between the pore bases and the remainder of the electrolyte. Thus, agitation becomes a very important factor in the formation of the porous type of coating.

CONCLUSION

Consideration of the effects of the many variables which have been discussed emphasizes the fact that the formation of the porous type of oxide coating is a complex process and that, while formation is proceeding at a uniform rate, a delicate balance exists between formation and solution of oxide. Formation rate is primarily a function of current density and is affected by other factors only insofar as they may affect current density. Solution rate, on the other hand, is a chemical process and is determined by electrolyte type, concentration, and temperature. The barrier layer at the base of the pores, which is the net result of the balance between formation and solution, has a thickness which is apparently controlled by these same three variables—electrolyte type, electrolyte concentration, and bath temperature.

Application of the barrier layer measurement method to the anodic coating process shows that

the conditions existing at the base of the pores are vastly different from those existing in the body of the electrolyte. Conditions at pore bases are characterized by high temperatures and high electrolyte concentrations, both of which are necessary to account for the relatively rapid rates at which these coatings can be formed.

ACKNOWLEDGMENT

The authors wish to express their appreciation to F. Keller under whose direction this work was conducted.

Any discussion of this paper will appear in a Discussion Section to be published in the June 1955 issue of the JOURNAL.

REFERENCES

1. J. D. EDWARDS AND F. KELLER, *Trans. Electrochem. Soc.*, **79**, 135 (1941).
2. J. D. EDWARDS AND F. KELLER, *Trans. Am. Inst. Mining and Met. Engrs.*, **156**, 288 (1944).
3. I. RUMMEL, *Z. Phys.*, **99**, 518 (1936).
4. A. JENNY, "The Anodic Oxidation of Aluminum and Its Alloys," Charles Griffin and Company, Ltd., London (1940).
5. W. BAUMAN, *Z. Phys.*, **111**, 708 (1938).
6. G. HASS, *J. Opt. Soc. Amer.*, **39**, 532 (1949).
7. F. KELLER, M. S. HUNTER, AND D. L. ROBINSON, *This Journal*, **100**, 411 (1953).
8. M. S. HUNTER AND P. FOWLE, *ibid.*, **101**, 481 (1954).
9. "Handbook of Chemistry," N. A. LANGE, Editor, 7th ed., p. 1412, Handbook Publishers, Inc., Sandusky, Ohio (1941).
10. "Chemical Engineers' Handbook," J. H. PERRY, Editor, 2nd ed., p. 398, McGraw-Hill Book Co., Inc., New York (1941).

Polarographic and Coulometric Behavior of the Chloroacetaldehydes¹

PHILIP J. ELVING AND C. EUGENE BENNETT

University of Michigan, Ann Arbor, Michigan

and

The Pennsylvania State University, State College, Pennsylvania

ABSTRACT

Chloral hydrate gives one apparently diffusion-controlled wave ($E_{1/2}$ about -1.4 v vs. S.C.E.), dichloroacetaldehyde two kinetic-controlled waves (-1.0 and -1.7 v), and chloroacetaldehyde two kinetic-controlled waves (-1.1 and -1.7 v). The chloral hydrate wave is actually controlled by a composite of diffusion and kinetic processes. Coulometric and polarographic data show that chloral hydrate is reduced to dichloroacetaldehyde hydrate; the latter dehydrates, and the unhydrated molecule is reduced to chloroacetaldehyde, which is then reduced to acetaldehyde; finally, the latter is reduced to ethyl alcohol or 2,3-dihydroxybutane, or both. This over-all reduction process forms only one wave; the acetaldehyde, whose reduction should result in a second wave, is formed in such a small amount that the wave is clearly demarcated in ammonia buffers only. Dichloroacetaldehyde is reduced to chloroacetaldehyde, which in turn is reduced to acetaldehyde with the formation of one wave; acetaldehyde reduction accounts for the second wave. Chloroacetaldehyde's first wave is due to reduction to acetaldehyde; the second due to reduction of acetaldehyde.

INTRODUCTION

Previous work on the electrochemical reduction of polyhalogenated compounds, particularly where more than one halogen is present on the same carbon atom, has indicated a general step-wise removal of halogen atoms (1-10). With a compound such as tribromoacetic acid, the first bromine comes off more readily than the second one, which in turn comes off more readily than the third. Of the three polarographic waves produced by tribromoacetic acid, the two more negative ones correspond to the two waves of dibromoacetic acid; the most negative wave corresponds to the one wave of bromoacetic acid.

In aqueous solutions, chloral hydrate gives one wave of $E_{1/2}$ about -1.4 v (an additional wave at -1.7 v is observed in ammonia buffers), and dichloroacetaldehyde and chloroacetaldehyde each give two waves at about -1.0 and -1.7 v, and -1.1 and -1.7 v, respectively. Since these results do not show the expected pattern, a complete study of the chloroacetaldehydes was made.

Reference to chloral hydrate is made throughout this paper since chloral exists as the hydrate in aqueous solutions. A few runs made with chloral (anhydrous before dissolution) gave polarograms similar to those of chloral hydrate.

EXPERIMENTAL

Stock aldehyde solutions (10 mM) were prepared from U.S.P. chloral hydrate,² a redistilled research

sample of dichloroacetaldehyde,³ a research sample of chloroacetaldehyde⁴ [40.0% solution by weight; composition was checked by specific gravity measurement (11), sp gr 25/25°C 1.194], and acetaldehyde.⁵ Nitrogen used for deoxygenating was purified and equilibrated by bubbling through sulfuric acid, an alkaline pyrogallol solution, water, and a portion of the test solution. Buffer solutions (Table I) were prepared from C.P. chemicals.

A Sargent Model XII Polarograph in connection with an external potentiometer and a Leeds and Northrup Type E Electro-Chemograph were used. A Beckman Model G pH Meter was used for pH measurement. All items of measuring apparatus were calibrated. A thermostated H-cell (12) employing a saturated calomel reference electrode was used. All potentials are referred to the saturated calomel electrode (S.C.E.) unless otherwise stated. The dropping mercury electrodes were prepared from Corning marine barometer tubing; the m and t values (open circuit, distilled water at 25°C, 60 cm head) for the capillaries used were: (a) 1.011 mg/sec and 5.0 sec (chloral hydrate); (b) 1.249 mg/sec and 4.6 sec (dichloroacetaldehyde); (c) 1.672 mg/sec and 4.0 sec (chloroacetaldehyde); and (d) 0.916 mg/sec and 5.6 sec (all three compounds). The coulometric runs using a stirred massive mercury cathode were made

³ Westvaco Chemical Division of the Food Machinery and Chemical Corporation, b.p. 87°C at 740 mm. n_D^{25} 1.4512.

⁴ The Dow Chemical Company.

⁵ Eastman Organic Chemicals.

¹ Manuscript received April 20, 1954.

² Merck and Company, 99.5% pure.

TABLE I. Buffer solutions

Buffer	pH	Composition
1	1.4	0.5M KCl with added HCl
2	4.1-5.7	0.5M NaOAc with added HOAc
3	5.4	0.112M Na ₂ HPO ₄ ·12H ₂ O, 0.044M citric acid monohydrate, and 0.198M KCl
3	7.0	0.164M Na ₂ HPO ₄ ·12H ₂ O, 0.0176M citric acid monohydrate, and 0.073M KCl
4	8.3-9.6	0.5M NH ₄ Cl with added NH ₃
5	9.2	0.082M Na ₂ B ₄ O ₇ ·10H ₂ O and 0.32M KCl
5	9.8	0.082M Na ₂ B ₄ O ₇ ·10H ₂ O, 0.285M KCl, with added NaOH
6	10.5	0.163M Na ₂ HPO ₄ ·12H ₂ O with added NaOH
6	12.3	0.105M Na ₂ HPO ₄ ·12H ₂ O with added NaOH

in a modified Lingane (13) apparatus maintained at $25 \pm 0.1^\circ\text{C}$.

The test solutions (ionic strength of 0.45 in all cases), prepared by mixing measured volumes of the stock and buffer solutions, had essentially the same pH as the buffer used. Five minutes was used for this operation. The test solution was deoxygenated for five minutes and then electrolyzed (ten minutes); the nitrogen atmosphere was maintained throughout the electrolysis.

DISCUSSION

Using a fritted glass disk electrode, Neiman (7) reported the $E_{1/2}$ of chloral hydrate to be -0.8 v in 0.1N KCl (the reference electrode was not indicated); no interpretation of the wave was made.

After the present study was under way, Federlin (14) reported no reduction of dichloroacetaldehyde, one wave for chloral hydrate ($E_{1/2}$ of about -1.6 v) and two waves for chloroacetaldehyde (-1.1 and -1.8 v) with an additional wave appearing at -1.6 v at high pH values. He also found two waves for bromal (-1.3 and -1.8 v), two waves for dibromoacetaldehyde (-1.2 and -1.8 v), and two waves for bromoacetaldehyde (15) (-0.4 and -1.8 v), with an additional wave appearing at -1.6 v at high pH. The chloral wave was ascribed (14, 16) to a diffusion-controlled process involving reduction of the hydrated molecule to dichloroacetaldehyde, which was nonreducible; the first wave of chloroacetaldehyde was ascribed to a kinetic-controlled process involving reduction of the unhydrated molecule to acetaldehyde, and the second wave, to reduction of acetaldehyde. The additional wave which appeared only at high pH was ascribed to reduction of glycolic aldehyde (hydroxyacetaldehyde), the hydrolysis product of chloroacetaldehyde. Since reduction of dichloroacetaldehyde was not obtained, and since the explanation of the electrode process for chloral hy-

TABLE II. Variation of current with drop time and temperature

	Buffer No.	pH	Ratio of current at two heads of mercury ^{a, b}		Temperature coefficients ^c	
			Wave I	Wave II	Wave I	Wave II
Chloral hydrate	4	9.1	1.65		2.4	
	5	9.2	1.70		2.2	
Dichloroacetaldehyde	4	9.1	1.04	1.06	7.6	8.1
	5	9.8	1.0		8.1	
Chloroacetaldehyde	4	8.3	1.18	1.09	3.4	3.5
	4	8.9	1.24	1.12	3.6	3.7
	5	9.2	1.11		7.3	

^a Corrected for back pressure by use of relation, $h_{\text{back}} = 3.1/m^{1/3}t^{1/3}$.

^b With the following capillaries and the heads used, theoretical values for different current controlling processes are:

	Diffusion	Adsorption	Kinetic
(a) chloral hydrate	1.43	2.05	1.0
(b) dichloroacetaldehyde	1.23	1.51	1.0
(d) chloroacetaldehyde	1.23	1.51	1.0

^c Calculated from the compound interest formula,

$$(\tau_2)^{i_1} = (\tau_1)^{i_1} (1 + \text{temp coeff.})^{(\tau_2 - \tau_1)}$$

drate is inadequate, the work here reported was continued.

The chloroacetaldehydes were found to possess a very complex electrochemical reduction pattern. For example, variations of current with drop-time, i.e., head of mercury, and temperature (Table II) indicate that a diffusion process may control the one chloral hydrate wave, while kinetic processes control both waves of dichloroacetaldehyde and of chloroacetaldehyde.

The Ilkovic equation, when applied to chloral hydrate data (Table III), indicates that about two electrons/molecule are consumed in the reduction process. Since an over-all two-electron transfer did not seem reasonable for chloral hydrate, and since the Ilkovic equation cannot be applied to kinetic-controlled processes, coulometric electrolyses were made on all three aldehydes to aid in establishing the electrode reactions.

In order to clarify the apparently unconnected behavior observed, the following discussion of polarographic and coulometric behavior of chloroacetaldehydes utilizes some of the conclusions subsequently summarized in the section on nature of the reduction process.

Polarographic Behavior

Polarographic data for the chloroacetaldehydes are given in Tables III, IV, and V. Apparent diffusion current constant values ($I = i_d/C m^{2/3} t^{1/6}$) were calculated in the case of chloral hydrate to facilitate current comparison. Where the limiting current is not largely diffusion-controlled, it is designated as i_{L1} .

TABLE III. Effect of pH, concentration, drop time (head of mercury), and temperature on polarographic behavior of chloral hydrate

Buffer ^c No.	pH	Conc. mM	Head cm	$-E_{1/2}$ v	i_d^a μa	I^a	α	n^a	
3 ^d	7.2	0.25	40	1.42	0.86	2.60	0.35	1.4	
4 ^{d,f}	8.4	0.25	40	1.34	1.15	3.48	0.31	1.9	
4 ^{e,f}	8.9	1.0	60	1.32	4.23		0.34		
4 ^f	9.1	1.0	40	1.32	3.60	3.64	0.32	1.9	
4	9.1	1.0	80	1.36	5.94	4.98	0.32	2.6	
4 ^c	9.1	1.0	80	No wave detected					
4 ^b	9.1	1.0	80	1.45	3.33	2.79	0.29	1.4	
5	9.2	1.0	40	1.42	3.04	3.07	0.29	1.6	
5	9.2	1.0	80	1.45	5.18	4.34	0.37	2.2	
5 ^c	9.2	1.0	80	No wave detected					
5 ^b	9.2	1.0	80	1.51	3.00	2.51	0.29	1.3	
5	9.8	1.0	40	1.65	2.56	2.59	0.25	1.3	
5	9.8	1.0	80	1.67	3.84	3.22	0.32	1.7	
5 ^b	9.8	1.0	80	1.51	3.18	2.66	0.33	1.4	
6	10.5	1.0	80	Wave too small to measure					
6	12.3	1.0	80	No wave detected					

^a The i_d for chloral hydrate is pseudodiffusion-controlled and does not give true I and n values (see Discussion). The diffusion coefficient used was 1.0×10^{-5} cm²/sec [approximated from the value for trichloroacetic acid (3) since the two compounds have similar molecular weights].

^b Temperature was 0° C in these runs; it was 25° in all other runs.

^c These runs were made 24 hr after mixing chloral hydrate and buffer.

^d Capillary *c* was used for these runs.

^e Capillary *d* was used for this run; capillary *a* was used in other runs.

^f A second wave of $E_{1/2}$ about -1.66 v was observed in ammonia buffers (see Fig. 1 and Discussion).

Values of α were calculated from the slope of the wave by the relation, $\alpha = 0.056/(E_{1/4} - E_{3/4})$ at 25°. Typical polarograms of chloroacetaldehydes are shown in Fig. 1, the current vs. pH relationships in Fig. 2, and the $E_{1/2}$ vs. pH relationships in Fig. 3.

Chloral.—One cathodic wave ($E_{1/2}$ about -1.4 v) was obtained for chloral hydrate in the pH range of 7.0 to 9.1 with an additional wave appearing at -1.7 v in ammonia buffers (Fig. 1); a new wave due to reduction of chloroform (produced by the haloform reaction) appeared at -1.65 v in borate buffer at pH 9.8. The chloroform wave disappeared at higher pH as a result of its faster formation and subsequent disappearance during deoxygenating due to its volatilization and possible hydrolysis. No wave was detected in buffer 1 due to the prior hydrogen discharge wave. In buffer 2, a wave began, but the hydrogen wave appeared before its completion.

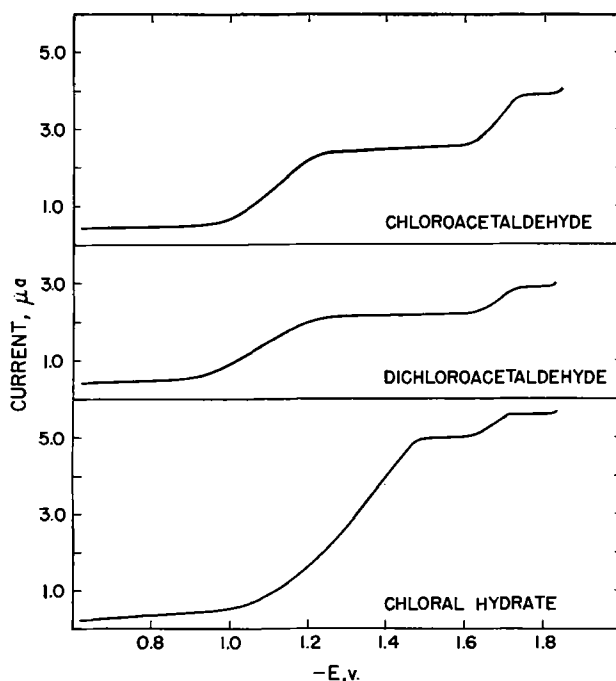


FIG. 1. Tracings (average current) of polarograms of 1.00mM solutions of chloral hydrate and chloroacetaldehyde, and a 0.99mM solution of dichloroacetaldehyde in ammonia buffer at pH 8.9 (60 cm mercury head, 25°C, capillary *d*).

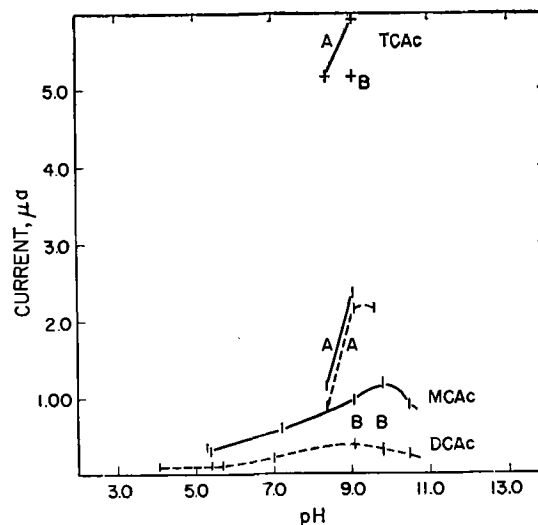


FIG. 2. Variation of the reduction current of the chloroacetaldehydes with pH. TCAC indicates chloral hydrate; DCAC and dashed lines indicate wave I of dichloroacetaldehyde; and MCAC indicates wave I of chloroacetaldehyde. A represents data in ammonia buffers and B in borate buffers. Magnitude of the currents can be compared only qualitatively since different capillaries were used.

Data are insufficient for any valid conclusions concerning the effect of pH on $E_{1/2}$. The current at pH 9.1 is greater in ammonia buffer than in borate; this is probably due, as will be shown later, to the greater currents of dichloro- and chloroacetaldehyde in

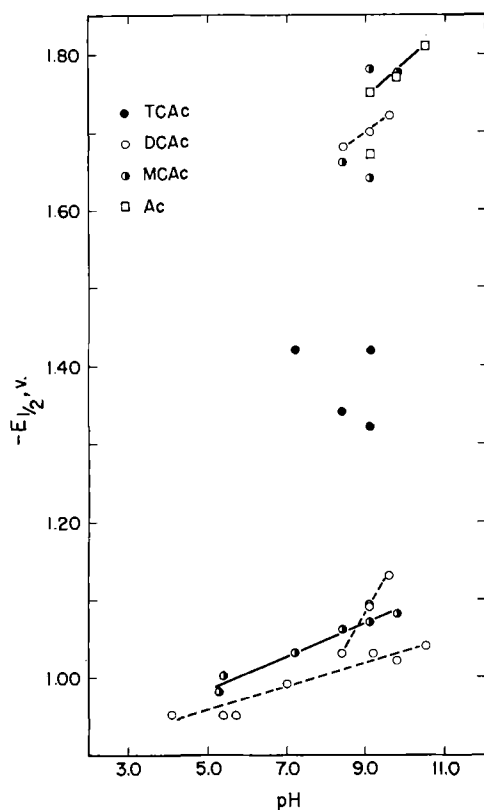


FIG. 3. Variation of $E_{1/2}$ with pH for chloral hydrate (TCAc), dichloroacetaldehyde (DCAc), chloroacetaldehyde (MCAc), and acetaldehyde (Ac). The precision of the $E_{1/2}$ values is about ± 0.02 v.

ammonia buffer which add to the over-all chloral hydrate wave.

Dichloroacetaldehyde.—In ammonia buffer two dichloroacetaldehyde waves ($E_{1/2}$ about -1.1 and -1.7 v) were obtained; the shift of the second wave to -1.54 in phosphate buffer (pH 10.4) is probably due to the reduction of glycolic aldehyde and glyoxal. Glycolic aldehyde may be formed at the electrode by hydrolysis of chloroacetaldehyde produced by dichloroacetaldehyde reduction, while glyoxal is formed by complete hydrolysis of dichloroacetaldehyde itself. The one wave at pH 12.3 evidently results from reduction of glyoxal (17). Only the first wave of dichloroacetaldehyde is observed in buffers 2 and 3 as the second wave is masked by buffer discharge.

$E_{1/2}$ for the first dichloroacetaldehyde wave increases slightly with pH except in ammonia buffers where a decided shift occurs (Fig. 3). The latter is due not only to pH change, but also to the increased formation of chloroacetaldehyde whose reduction still further enlarges the wave. Since $E_{1/2}$ of chloroacetaldehyde is slightly more negative than that of the dichloroacetaldehyde, such increase causes the midpoint of the composite wave to shift to a more negative potential.

Chloroacetaldehyde.—Two chloroacetaldehyde waves were obtained at about -1.1 and -1.7 v in buffers 4 and 5; an additional wave appeared at -1.55 v at pH values of 9.8 and greater. At pH 12.3, only the latter wave is observed; this wave is ascribed to reduction of glycolic aldehyde (14), the hydrolysis product of chloroacetaldehyde.

Acetaldehyde.—A few acetaldehyde runs were made in order to determine its $E_{1/2}$ in various buffer solutions. $E_{1/2}$ values found were -1.67 v in ammonia buffer at pH 9.1, -1.75 v in borate at pH 9.1, -1.77 v in borate at pH 9.8, and -1.81 v in phosphate at pH 10.5. An imine wave (18, 19) was observed at -1.35 v in ammonia buffer at pH 9.1.

Coulometric Behavior

Results of simple coulometric reduction of chloroacetaldehydes cannot be used as entirely conclusive evidence for the electrode process due to accompanying chemical processes; the data and their limitations will be discussed. Conclusive evidence for the nature of the electrode process was obtained by polarographically examining the solution at various stages in the coulometric reduction of chloral hydrate.

Behavior in ammonia solution.—In ammonia buffer, chloroacetaldehyde gave at -1.25 v and pH 8.4 values of 1.78 and 1.80 electrons per molecule, dichloroacetaldehyde (at -1.25 v) 3.14 (pH 8.4) and 3.16 (pH 9.1), and chloral hydrate (at -1.40 v and pH 8.4) 5.45 and 5.63 electrons per molecule. Results are difficult to interpret since carbonyl compounds generally react with ammonia to form reducible imines (18, 19); high, low, or "true" values could be obtained if such compounds were formed, e.g., (A) if the products obtained from carbon-halogen bond fission would form reducible imines, high values would be obtained; (B) if imines were formed from the original chloroacetaldehydes, in which both entities (carbon-chlorine bond and imine group) were nonreducible, low results would be obtained; (C) if the imine bond were reducible while the carbon-chlorine bonds were nonreducible in the imines formed from the original chloroacetaldehydes, low results would be obtained with chloral hydrate and dichloroacetaldehyde (polyhalogens, one imine group per molecule) while correct values would be obtained with chloroacetaldehyde.

The applied potential in chloral hydrate reduction is sufficient to reduce the imine of acetaldehyde if it were produced. The current of the first wave of dichloro- and chloroacetaldehyde is considerably higher in ammonia than other buffers; thus, imine reduction may be occurring at the potential needed for carbon-halogen bond fission.

The three chloroacetaldehydes chemically decompose to form products which are reduced only at more

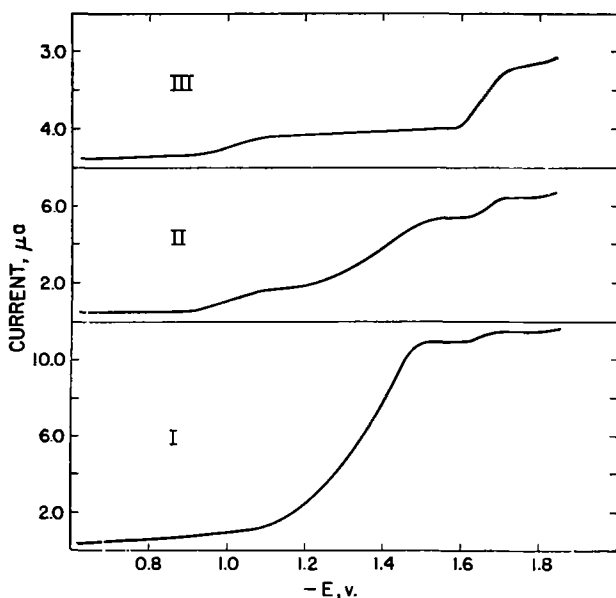


FIG. 4. Tracings of polarograms showing various stages in the coulometric reduction at -1.4 v of chloral hydrate in ammonia buffer of pH 8.4: I, before reduction; II, after a short period of reduction; III, after additional reduction.

negative values than the applied potentials used; this factor would tend to make observed coulometric values lower than true value. Decomposition is a major problem since electrolyses of these compounds generally require 10–15 hr/run because of the kinetic-controlled electrode processes; a diffusion-controlled process usually requires 1–2 hr for a two-electron reduction.

Behavior in borate and phosphate solutions.—In borate buffer (pH 9.2, -1.55 v), the value of 2.5 electrons obtained for chloral hydrate is low since, upon standing for the same length of time with no electrolysis, the concentration of chloral hydrate decreased to about one-third of the original amount. Kinetics of the processes involved are so complicated that no approximation of the true number of electrons transferred could be made by calculating the concentration actually reduced from the rate constants of the chemical and electrochemical reactions. Dichloro- and chloroacetaldehyde runs were not made in borate buffer due to the problem of chemical decomposition.

In McIlvaine buffer (pH 8.0, -1.50 v), chloral hydrate gives a value of about two electrons which is probably low due to observed chemical decomposition and to a possible interaction between chloral hydrate and the phosphate species present. Chloroethanol undergoes such a reaction (20), as apparently does trichloroethanol (21); due to its *gem*-diol structure, chloral hydrate may behave similarly.

Runs on chloroacetaldehyde (-1.20 v, McIlvaine buffer, pH 8.0) gave 1.1 and 1.2 electrons per molecule; these values are probably low due to similar

observed chemical decomposition and reaction with phosphate.

Nature of partially reduced chloral solutions.—As mentioned, conclusive evidence for the nature of the electrode process was obtained by examining chloral hydrate solutions polarographically at various stages in their coulometric reduction. The same type of behavior was observed in all three buffers used (McIlvaine, ammonia, and borate). Results obtained in ammonia buffer are illustrated in Fig. 4; waves are clearly delineated and can be compared to those of chloroacetaldehydes in ammonia buffer (Fig. 1). Before reduction began, one large wave at -1.35 v and a small wave at -1.65 v was observed; after a short period of reduction, an additional wave appeared at -1.04 v (corresponds to $E_{1/2}$ of dichloro- and chloroacetaldehyde) and the -1.65 v wave (corresponds to $E_{1/2}$ of acetaldehyde) increased in size; after additional reduction only the waves at -1.04 and -1.65 v remained. The wave at -1.65 v decreased upon standing and stirring.

It should be noted that chloroform, which may be produced by the haloform reaction, shows polarographic behavior similar to that of acetaldehyde. However, the height of this wave during and after a coulometric electrolysis is much higher than would be expected from any chloroform produced by the haloform reaction. Therefore, the major portion of the wave must be due to the electrochemical reduction product which is believed to be acetaldehyde.

Nature of the Reduction Process

Chloral.—The observed behavior of chloral hydrate is explicable by the reaction scheme shown in Fig. 5, which is based on chemical, polarographic, and coulometric characteristics of the compound. Observation of only one wave for chloral hydrate in buffers 3 and 5 is due to chloral existing only as the hydrate in aqueous solution. The latter is reduced to dichloroacetaldehyde hydrate which is in equilibrium with the unhydrated molecule. The unhydrated dichloroacetaldehyde is reduced to chloroacetaldehyde which is then further reduced to acetaldehyde; the latter, in turn, is reduced (22–24) to ethyl alcohol, 2,3-dihydroxybutane, or both. Since dichloroacetaldehyde and chloroacetaldehyde are reducible at about -1.1 v, which is more positive than $E_{1/2}$ for chloral hydrate, and since neither compound is present at the electrode until after reduction of chloral hydrate, the dichloro- and chloroacetaldehyde waves merge into the wave of chloral hydrate.

An acetaldehyde wave is not observed in chloral hydrate reduction in buffers 3 and 5, since formation and reduction of dichloro- and chloroacetaldehyde involve kinetic processes, and the concentration of

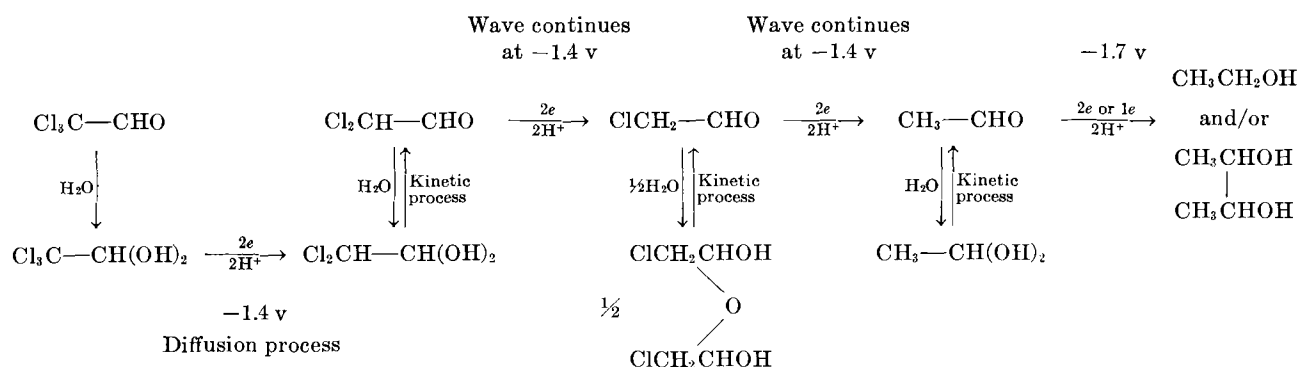


FIG. 5. Reaction scheme for the electroreduction of chloral hydrate and related compounds

TABLE IV. Effect of pH, drop time (head of mercury), and temperature on polarographic behavior of dichloroacetaldehyde^a

Buffer No.	pH	Head cm	Wave I			Wave II		
			$-E_{1/2}$ v	i_1 μA	α	$-E_{1/2}$ v	i_1 μA	α
2	4.1	60	0.95	0.08	0.36			
2	5.4	60	0.95	0.09	0.38			
2	5.7	60	0.95	0.10	0.42			
3	7.0	60	0.99	0.16	0.37			
4	8.4	60	1.03	0.85	0.49	1.68	0.29	0.86
4 ^d	8.9	60	1.08	1.58	0.46	1.68	0.55	1.1
4	9.1	60	1.09	2.18	0.42	1.70	0.49	1.1
4	9.1	90	1.10	2.33	0.41	1.70	0.51	1.1
4	9.1	60 ^b	1.08	0.35		1.70	0.07	
4	9.6	60	1.13	2.15	0.46	1.72	0.68	1.1
5	9.2	60	1.03	0.39	0.33	^c		
5	9.8	60	1.02	0.28	0.36	^c		
5	9.8	80	1.03	0.28	0.40	^c		
5	9.8	60 ^b	1.03	0.04		^c		
						Hydrolysis wave		
6	10.5	60	1.04	0.27	0.34	1.54	0.15	0.53
6	10.5	80	1.04	0.26	0.34	1.54	0.16	0.65
6	10.5	60 ^b	1.03	0.05		1.54	0.03	0.65
6	12.3	60	No first wave			1.61	0.12	

^a The concentration was 0.99 mM in all runs.^b The temperature was 0° C in these runs; its was 25° in all other runs.^c Calculations were not made since the wave was poorly defined.^d Capillary *d* was used for this run; capillary *b* for all other runs.

acetaldehyde produced is insufficient to cause an observable wave. In ammonia buffer, larger amounts of dichloro- and chloroacetaldehyde are reduced (Tables IV and V) which in turn produce acetaldehyde in sufficient amount to cause an observable wave.

The Ilkovic equation indicates a two-electron process for reduction of chloral hydrate (see Table III) since the slow kinetic processes involved maintain the concentration of the reducible species formed at such a low level that their reduction adds little to the over-all wave height. Consequently, height and temperature coefficients (Table II) indi-

cate a diffusion-controlled process, although the current is actually controlled by a combination of diffusion and kinetic processes.

Dichloro- and chloroacetaldehydes.—The reaction scheme of Fig. 5 also accounts for the observed behavior of dichloroacetaldehyde. The first wave is due to reduction to chloroacetaldehyde which, in turn, is reduced to acetaldehyde at a close enough potential so that only one wave is observed. The second wave corresponds to acetaldehyde reduction. Likewise, the first wave of chloroacetaldehyde is attributed to carbon-chlorine fission and the second wave to aldehyde reduction.

Dichloroacetaldehyde is more strongly hydrated than chloroacetaldehyde as indicated by the smaller current produced by its first wave; under diffusion-controlled conditions, the first wave of dichloroacetaldehyde (two carbon-halogen bonds are reduced) would be approximately twice the height of the first wave of chloroacetaldehyde. Since $E_{1/2}$ of dichloroacetaldehyde is much closer to $E_{1/2}$ of chloroacetaldehyde than expected, the dichloro species which is reduced in aqueous solutions is probably intermediate in structure between a hydrate and a free aldehyde.

Absence of the usually observed step-wise reduction pattern for carbon-chlorine bond fission in the chloroacetaldehydes accordingly results from the fact that different chlorinated species are being reduced. Actually, step-wise reduction does occur (Fig. 5) although only one halogen wave is observed for each of the three compounds.

Federlin's (14) failure to observe reduction of dichloroacetaldehyde may have been due to his experimental conditions. He used lithium chloride as the electrolyte, and ran in unbuffered medium and in buffered solution at pH 5.0 and 10.0. As shown in Fig. 2, the waves obtained for dichloroacetaldehyde at these pH values are quite small; therefore, at low instrument sensitivities, it is possible that a wave would not be observed.

Bromoacetaldehydes.—Federlin's interpretation of the

TABLE V. Effect of pH, drop time (head of mercury), and temperature on polarographic behavior of chloroacetaldehyde^a

Buffer No.	pH	Head cm	Wave I			Hydrolysis wave			Wave II		
			$-E_{1/2}$ v	i_1 μa	α	$-E_{1/2}$ v	i_1 μa	α	$-E_{1/2}$ v	i_1 μa	α
2	5.3	40	0.98	0.35	0.45						
2	5.3	60	0.99	0.42	0.45						
3	5.4	40	1.00	0.28	0.51						
3	5.4	60	1.01	0.29	0.48						
3	7.2	40	1.03	0.59	0.43						
3	7.2	70	1.01	0.66	0.48						
4 ^c	8.3	60	1.06	0.89	0.46				1.64	0.55	1.1
4 ^c	8.3	90	1.06	1.05	0.45				1.65	0.60	0.94
4 ^{bc}	8.3	60	1.10	0.39	0.50				1.65	0.23	1.0
4	8.4	40	1.06	1.06	0.58				1.66	0.77	1.2
4 ^c	8.9	60	1.11	1.89	0.53				1.68	1.35	1.1
4 ^c	8.9	90	1.12	2.35	0.49				1.68	1.52	1.1
4 ^{bc}	8.9	60	1.15	0.79	0.49				1.69	0.55	1.2
4	9.1	40	1.09	2.33	0.56				1.64	1.69	1.2
5	9.2	40	1.07	0.95	0.49				1.78	0.67	0.71
5 ^c	9.2	60	1.07	0.81	0.52				1.76	0.36	0.83
5 ^c	9.2	90	1.08	0.90	0.49				1.77	0.43	0.78
5 ^{bc}	9.2	60	1.05	0.14	0.40				1.74	0.10	0.68
5	9.8	40	1.08	1.17	0.52	1.55	0.10		1.77	0.77	0.63
6	10.5	40	1.13	0.91	0.37	1.59	1.26	0.96			
6	12.3	40				1.64	1.09	1.1			

^a The concentration was 1.0 mM in all runs.

^b Temperature was 0°C in these runs; it was 25° in all other runs.

^c Capillary *d* was used for these runs; capillary *c* for all other runs.

reduction mechanism of bromoacetaldehydes consists of the statement that the first wave is due to halogen reduction and the second wave to aldehyde reduction. This statement, although probably correct, does not account for the fact that only one halogen wave is obtained for each of the three compounds and does not explain the species involved in carbonyl reduction. He reported diffusion-controlled reductions of bromal and dibromoacetaldehyde which he attributed to reduction of the hydrated molecules. On the basis of the Ilkovic equation, he calculated the first wave in each compound to be a two-electron reduction process.

By reference to the present study of chloroacetaldehydes, reduction of the bromo analogs can be explained using Federlin and coworkers' data (14-16). Apparently, dibromoacetaldehyde hydrate is reduced to bromoacetaldehyde hydrate; the latter then dehydrates, and the unhydrated bromoacetaldehyde is reduced to acetaldehyde at approximately the same potential so that only one wave is observed. The second wave corresponds to acetaldehyde reduction. Insufficient data were reported for bromal hydrate to envisage precisely the reduction process; probably, however, bromal hydrate is reduced to dibromoacetaldehyde hydrate which is then reduced to bromoacetaldehyde hydrate; the latter dehydrates, and the unhydrated bromoacetaldehyde is reduced to acetaldehyde

which subsequently is reduced to ethyl alcohol, 2,3-dihydroxybutane, or both.

ACKNOWLEDGMENT

The authors wish to thank the Atomic Energy Commission which helped support the work described.

Any discussion of this paper will appear in a Discussion Section to be published in the June 1955 issue of the JOURNAL.

REFERENCES

1. P. J. ELVING, *Record Chem. Progr. (Kresge-Hooker Sci. Lib.)*, **14**, 99 (1953).
2. P. J. ELVING AND C. L. HILTON, *J. Am. Chem. Soc.*, **74**, 3368 (1952).
3. P. J. ELVING AND C.-S. TANG, *ibid.*, **72**, 3244 (1950).
4. P. J. ELVING AND C.-S. TANG, *ibid.*, **74**, 6109 (1952).
5. P. J. ELVING, I. ROSENTHAL, AND M. K. KRAMER, *ibid.*, **73**, 1717 (1951).
6. I. M. KOLTHOFF, T. S. LEE, D. STOVESOVA, AND E. P. PARRY, *Anal. Chem.*, **22**, 521 (1950).
7. M. B. NEIMAN, A. V. RYABOV, AND E. M. SHEYANOVA, *Doklady Akad. Nauk S. S. S. R.*, **68**, 1065 (1949).
8. M. v. STACKELBERG, "Polarographische Arbeitsmethoden," p. 212, Walter de Gruyter, Berlin (1950).
9. M. v. STACKELBERG AND W. STRACKE, *Z. Elektrochem.*, **53**, 118 (1949).
10. L. B. WESTOVER, M. S. Thesis, The Pennsylvania State College, State College, Pa. (1952).
11. Anon., "Chloroacetaldehyde," p. 5, The Dow Chemical Co., Technical Service and Development, Midland, Mich.

12. J. C. KOMYATHY, F. MALLOY, AND P. J. ELVING, *Anal. Chem.*, **24**, 431 (1952).
13. J. J. LINGANE, *J. Am. Chem. Soc.*, **67**, 1916 (1945).
14. P. FEDERLIN, *Compt. rend.*, **232**, 60 (1951).
15. A. KIRRMANN AND P. FEDERLIN, *Compt. rend.*, **230**, 1066 (1950).
16. A. KIRRMANN, E. SAITO, AND P. FEDERLIN, *J. chim. phys.*, **49**, C154 (1952).
17. P. J. ELVING AND C. E. BENNETT, *J. Am. Chem. Soc.*, **76**, 1412 (1954).
18. P. ZUMAN, *Sborník Mezinárod. Polarog. Sjezdu Praze, 1st Congr.*, 1951, Pt. I, Proc. 711.
19. P. ZUMAN, *Nature*, **165**, 485 (1950).
20. R. H. A. PLIMMER AND W. J. N. BURCH, *J. Chem. Soc.*, **1929**, 286.
21. P. J. ELVING AND C. E. BENNETT, *J. Am. Chem. Soc.* to be published.
22. W. DIRSCHERL AND H. U. BERGMAYER, *Chem. Ber.*, **82**, 291 (1949).
23. R. BIEBER AND G. TRUMPLER, *Helv. Chim. Acta*, **30**, 2000 (1947).
24. G. SEMERANO AND B. POLACEK, *Gazz. chim. ital.*, **68**, 292 (1938).

Evolution of Stibine at Antimony Cathodes¹

H. W. SALZBERG² AND A. J. ANDREATCH

Naval Research Laboratory, Washington, D. C.

ABSTRACT

The formation of stibine at antimony cathodes was studied by absorbing the cathode gas and analyzing the solution for antimony. The parameters studied were *pH*, salt concentration, temperature, and current density.

Results indicated that stibine was formed by the electrochemical discharge of a water molecule upon an antimony atom which was in contact with either two adsorbed hydrogen atoms or an adsorbed hydrogen molecule. Rate of the reaction was found to depend upon the voltage difference between electrode and solution. The stibine formed was inert to acid, but was readily decomposed by alkali. Stibine is probably formed by discharge of a water molecule on two adsorbed hydrogen atoms or a hydrogen molecule. Decreased rates of stibine formation in highly acid solution are thought to mean that high voltages, and, therefore, high overvoltages are not associated with hydronium ion discharge, but with water discharge.

INTRODUCTION

This is a report of an experimental investigation into the evolution of stibine at antimony cathodes. It was undertaken in continuation of work already performed in these laboratories which has indicated that water is reduced at platinum (1) and lead (2) cathodes at current densities above 10–60 ma/cm², even in fairly strong acid. Previous reports on stibine formation were contradictory (3, 4) and were felt to be unreliable.

EXPERIMENTAL TECHNIQUE

Method

This was in principle very simple. The mixture of cathode gases was swept out of the apparatus and into an absorption tube by means of a stream of finely divided hydrogen bubbles. The absorbing solution was then analyzed for antimony.

In practice there were several difficulties. Quantities of stibine were so small that a microanalysis had to be performed. The gas is so unstable that rapid flushing of the electrolytic cell was necessary, with care being taken, however, not to sweep the gas through the absorption tube. Also, *pH* changes around the cathode affected the observed rates. Finally, the reaction is voltage dependent and therefore sensitive to small amounts of impurities.

Apparatus

The cell was a large U-tube, equipped with a standard taper ground glass joint at each end, with a fritted glass gas inlet near the bottom of the

cathode limb. This fritted glass inlet served to break the incoming stream of gas into small bubbles which would stir and scour the solution more effectively.

Ground glass fittings provided suitably gas-tight connections without the use of rubber or cement.

Electrodes were mounted in glass caps sealed to ground glass joints which fitted into the ends of the U-tube. Each cap had a gas outlet. The outlet on the cathode cap was a glass tube of 7 mm inner diameter which terminated in another ground glass joint.

The anode was a strip of bright platinum approximately 6 cm² in area connected to a platinum wire sealed into the cap. The cathode was an antimony cylinder mounted on the end of an iron shaft enclosed in a Teflon sleeve. The shaft was mounted in a glass rod sealed into the glass cap. The space between the wall of the glass and the Teflon was filled with polyethylene to prevent gas leaks. The space between the antimony cylinder and the Teflon sleeve was also covered with polyethylene to prevent contact between solution and iron shaft. The flat bottom of the cylinder was covered with polyethylene, leaving as the working surface of the cathode a ring of antimony between the two polyethylene surfaces. This, it was felt, would maintain an approximately uniform current density over the electrode surface.

The absorption tube was a glass bubbler with a ground glass tip on the inlet which fitted into the joint on the outlet of the cathode cap. The absorbing solution was about 40 cm from the cathode.

Current was obtained from the power line, regulated with a Variac-rectifier and measured with a precision ammeter. Time was measured with a stopwatch.

¹ Manuscript received May 18, 1953. This paper was prepared for delivery before the Chicago Meeting, May 2 to 6, 1954.

² Present address: 171 East 90th Street, New York, N. Y.

Materials

All solutions were made from C.P. analyzed chemicals. The scouring gas was tank hydrogen passed over hot copper to remove oxygen. The absorbing solution used was 6% mercuric chloride in 6*N* HCl.

The antimony used was C.P. analyzed grade, containing no more than 0.04% of arsenic and 0.0005% of iron. The electrode was cast in glass and machined down to proper dimensions, which were, finally, 0.77 cm diameter and 1.27 cm in height. After machining, the electrode was cleaned repeatedly by etching with HCl, HNO₃, and hot fresh aqua regia. This etching process was repeated frequently during the course of these experiments and check runs were made before and after cleaning to minimize the effect of impurities depositing out during the runs.

Procedure

After introducing the electrodes and the solution into the cell, the solution was scoured with hydrogen for 5 min to remove as much dissolved oxygen as possible. The absorption tube was then inserted and current was started. Amounts of stibine obtained were linear with time and the time of current passage was therefore varied from run to run so as to obtain optimum amounts of absorbed stibine for analysis. All results have been calculated on a 5-min time interval basis.

After cutting off the current, the cell was flushed five more minutes before removing the absorption tube. This removed all stibine from the gas space over the electrode and the electrolytic solution. The cell was also flushed for 2-3 min between runs to remove any oxygen which might have diffused over from the anode limb.

No provision was made to flush out the anode compartment. The small amount of oxygen which could diffuse the 5 cm from the anode through the unstirred anolyte to the bend in the U-tube, in the short time of the experiment, would be flushed rapidly away by the hydrogen stream. Any small amount eventually reaching the surface of the cathode should have little effect at these high current densities. In retrospect, this is a potential source of error and, in future work, both limbs will be flushed or separated with a diaphragm.

The absorbing solution was about 97-98% efficient, as determined by inserting a second bubbler in series with the first. The flow rate was set at about 200 cc of gas/min and regulated with a flow meter and valve.

Analysis was made by the standard Rhodamine-B method, which is accurate and precise to less than a

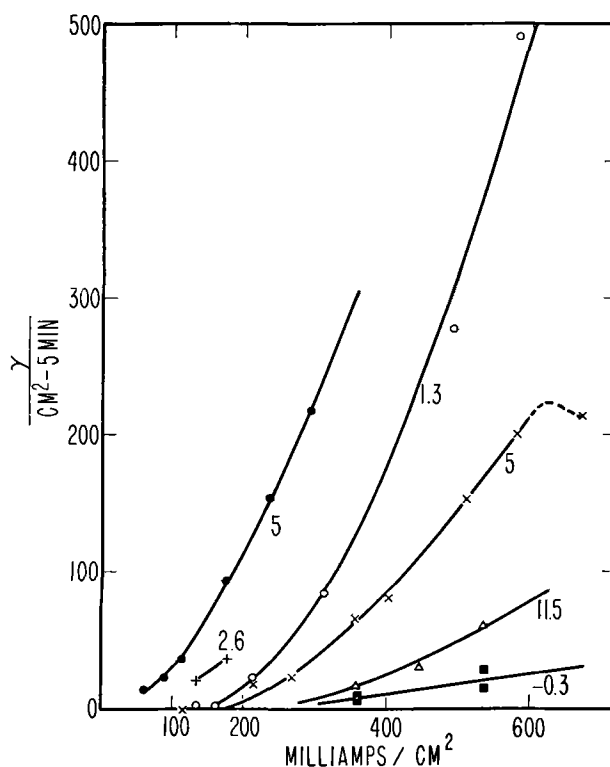


FIG. 1. pH effect, 25°C

pH	Acid and alk.	Salt
■ -0.3	2-4 <i>M</i> H ₂ SO ₄	
○ 1.3	H ₂ SO ₄	0.4 <i>M</i> Na ₂ SO ₄
+ 2.6	H ₂ SO ₄	
× 5.0		1 <i>M</i> Na ₂ SO ₄
△ 11.5	NaOH	
● 5.0		1 <i>M</i> (NH ₄) ₂ SO ₄

microgram. This precision is far greater than that of the over-all experimental results.

Some solutions were used for individual runs, others for a whole series. There were frequent checks run, some after several months, to see if the results were reproducible from day to day and solution to solution.

EXPERIMENTAL RESULTS

Results are shown in Fig. 1 to 4. These give the amounts of stibine detected as micrograms per square centimeter of cathode surface per 5-min interval, or as current passed, plotted against current density. These indicate the following:

1. Stibine evolution increases with current density at a greater than linear rate.

2. Maximum amounts of stibine detected were produced in neutral solutions buffered with ammonium ions (to minimize pH changes at the cathode). Buffered solutions show an increase in rate up to at least pH 5, while unbuffered solutions show a maximum at about pH 2.6 to 3.

3. Increasing acidity or alkalinity in the cell

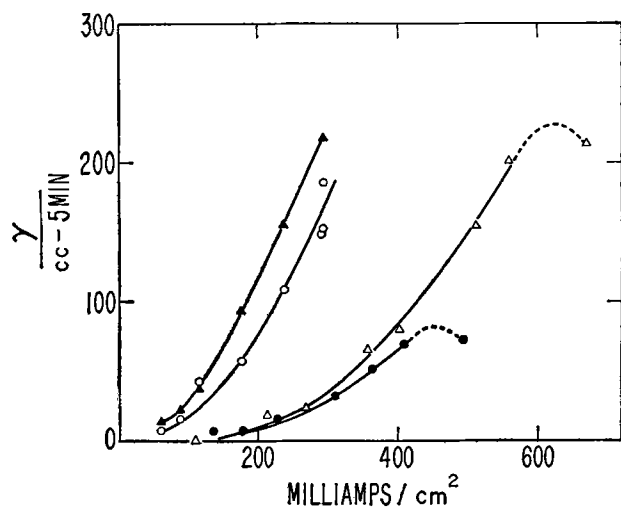


FIG. 2. Salt effect, 25°C. ▲—1M (NH₄)₂SO₄; ○—4M (NH₄)₂SO₄; △—1M Na₂SO₄; ●—1/2M Na₂SO₄.

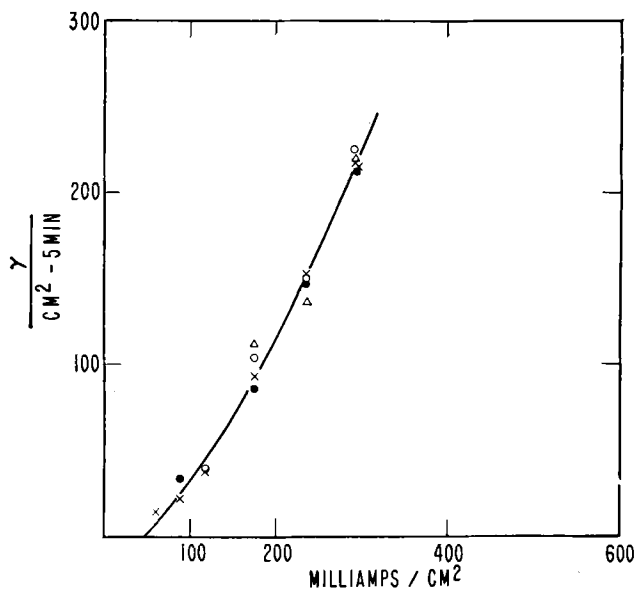


FIG. 3. Temperature effect, pH 5. ×—25°C, 1M (NH₄)₂SO₄; ○—5°C; ●—5°C; △—35°C.

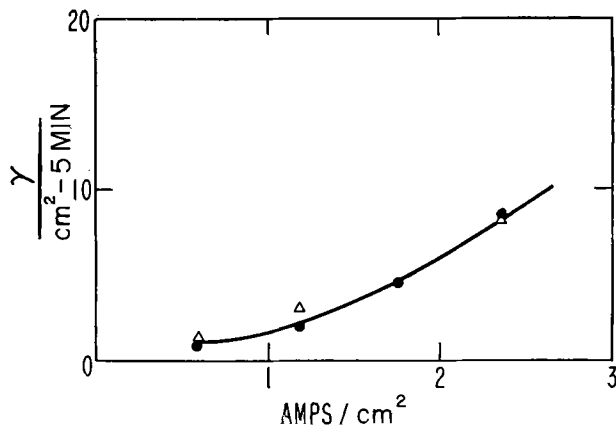


FIG. 4. Temperature effect, acid. △—5°C 2M H₂SO₄; ●—35°C 2M H₂SO₄.

lowers the amount of stibine absorbed in the bubbler, alkaline solutions showing lower amounts of stibine than acid solutions of the same concentration.

4. Higher salt concentrations in the cell gave smaller amounts of stibine in the bubbler, except for unbuffered solutions at high current densities. In this case, more concentrated solutions had lower rates than more dilute ones at low currents only and had higher rates at higher current densities. This crossover may be due to experimental error.

5. There is no appreciable temperature effect in the range from 5° to 35°C, in buffered neutral solutions and in acid solutions.

6. Amounts of stibine actually absorbed are very small, being at most about a milligram per square centimeter per five minutes of current passage.

7. At higher current densities in the unbuffered neutral solutions there is a decrease in the amounts of stibine absorbed.

Further qualitative observations which are not shown in the graphs are as follows:

8. Variations in rate of flow of the flush gas in neutral and acid solutions had no effect on the amounts of stibine absorbed in the receiver. No flow rate variations were run in alkaline solutions.

9. A black powdery antimony precipitate formed on the walls and in solutions with alkaline solutions, as reported by Sand and coworkers (3, 4), but not with acid solutions.

10. Traces of lead, added as the acetate, resulted in greatly increased stibine production.

11. Allowing metallic antimony to contact the surface of a mercury cathode which was evolving hydrogen at about 80 ma/cm² resulted in the formation of very large amounts of stibine.

12. In the absence of oxidizing agents, stibine was not absorbed when bubbled through solutions of N/10 acid, N/10 alkali, distilled water or neutral salt. Some was absorbed by 40% KOH.

DISCUSSION OF RESULTS

In the following discussion, it is necessary to remember that the graphs do not show amounts of stibine actually produced, but only amounts of stibine absorbed in the receiver, this being the difference between rates of production and of decomposition.

In the case of acid and neutral solutions, however, decomposition apparently does not take place during the short time the stibine remains in the cell. This is indicated by points 8 and 9 above. If stibine were being decomposed in the cell, a slower gas flow would lower the amounts received in the bubbler and also result in some antimony powder being

found in the cell. This does not occur in neutral or acid solutions.

Absence of an appreciable temperature coefficient also indicates that there is no decomposition in neutral or acid solutions. For the difference between production and decomposition of stibine to be independent of temperature when the rate of removal of undecomposed stibine from the cell is constant, as in this case, rate of decomposition must be equal to rate of formation, as can be shown mathematically. This means, however, that no stibine would be detected in the bubbler. Therefore, there should be no stibine decomposition in solutions in which there is no appreciable temperature coefficient of stibine detection.

Absence of a temperature effect must then be explained on the basis of the rate of production being relatively temperature independent. The likely reason is that the production rate obeys an equation similar to Tafel's equation for hydrogen overvoltages, such as:

$$d(\text{stib.})/dt = k \exp - (F^* + \alpha\eta f)/RT$$

In this equation, F^* is the activation energy required and η is the overvoltage, T is absolute temperature, f is the faraday, and α is a constant. As the temperature is increased from 25° to 35°C, the overvoltage (of hydrogen since it is being evolved) decreases by about 8%. If this decrease compensates for the temperature increase (η is negative), the rate would be temperature independent. In retrospect, it is unfortunate that temperature coefficients were not determined for alkaline solutions, where decomposition was observed to occur.

Loss of stibine in the alkaline solutions would then come about by reaction between the stibine and alkali, and not by thermal decomposition. Low rates and visible precipitate show that this attack is rapid. The fact, however, that stibine did not decompose in bubbling it through N/10 NaOH indicates that the solution immediately adjacent to the cathode would have to be very strongly alkaline. The apparent falling off in rate observed in neutral unbuffered solutions at high current densities seems to be due to increased hydroxyl ion concentrations in the vicinity of the cathode.

The mechanism of formation of stibine is not likely to be by the direct union of three hydrogen atoms and an antimony atom, but probably by electrochemical reduction of either a water molecule or a hydronium ion.

For the rate-determining step to be a combination of neutral atoms, the reaction rate would be independent of potential but dependent on current,

i.e., hydrogen atom concentration, since the amount of stibine produced is negligible in comparison to the hydrogen evolved. Neither of these conditions is fulfilled. In acid and buffered solutions, rates are not the same at equal current densities, and it has been observed that anything which increases the potential (decreased current density, high overvoltage impurities, contact with a mercury cathode) also increases the rate of stibine evolution. If the rate-determining step were combination, it could be expressed as:

$$r = k H^n \quad (\text{I})$$

where r is the rate, k is the specific rate constant, H is the concentration of hydrogen atoms, and n is an integer, either 1, 2, or more probably 3. Since stibine evolution is negligible in comparison with that of hydrogen, using Tafel's equation,

$$i = k' H^2 \quad (\text{II})$$

Combining these two gives:

$$r = k'' i^{n/2} \quad (\text{III})$$

Experimental results do not fit this type of equation.

The potential dependence of stibine formation indicates the electrochemical reduction of either water or hydronium ion. Attempts made to measure potentials to correlate with rates were, however, useless, due to indeterminate IR drops at high current densities and low concentrations.

From the decrease in rate at high acidities, coupled with the stability of stibine in acid, it appears either that hydronium ion is not discharged in the course of this reaction or that its discharge takes place at potentials too low for the formation of stibine. Consequently, it is presumed stibine is formed by water discharge, because the latter occurs at high potentials. This opinion is supported by Fig. 2, which shows higher rates at higher water activities. The rate equation for stibine is therefore probably

$$r = k H^2 \exp - \alpha\eta F/RT \quad (\text{IV})$$

or

$$r = k H_2 \exp - \alpha\eta F/RT \quad (\text{V})$$

depending on whether the reaction requires two adsorbed atoms or an adsorbed molecule. Here, α is the fraction of the overvoltage which operates between the initial and the activated states.

The results do not agree with those of Sand and coworkers (3, 4). However, the inability of Sand, Grant, and Lloyd (3) to duplicate the work of Sand, Weeks, and Worrel (4), plus their use of a porous

porcelain pot as a cell and their use of rubber and cement, suggests that both their results are incorrect, probably due to the presence of impurities. Also, the use of a gravimetric technique requiring two weighings of each of three absorption tubes, to determine quantities which were reported to be at most about 20 mg is not conducive to accuracy.

CONCLUSIONS

Stibine is formed at antimony cathodes in very small amounts increasing with increasing current densities up to at least 500 milliamp/cm². Stibine is formed from adsorbed hydrogen and water. The reaction depends upon voltage to a considerable extent. Increased acidity lowers the rate of stibine

evolution, probably through decreasing the voltage at the cathode. This indicates that water discharge is associated with higher cathode voltages and, therefore, with high hydrogen overvoltages.

Any discussion of this paper will appear in a Discussion Section to be published in the June 1955 issue of the JOURNAL.

REFERENCES

1. S. SCHULDNER, *This Journal*, **99**, 488 (1952).
2. H. SALZBERG, *ibid.*, **100**, 146 (1953).
3. H. J. S. SAND, E. J. WEEKS, AND S. W. WORRELL, *J. Chem. Soc.*, **1923**, 456.
4. H. J. S. SAND, J. GRANT, AND W. V. LLOYD, *ibid.*, **1927**, 378.

Lead-Acid Storage Batteries

Barium Sulfate as a Positive Plate Contaminant¹

J. F. DITTMANN AND H. R. HARNER

Eagle-Picher Company, Joplin, Missouri

Barium sulfate in fractional percentages is regularly used in the active material of negative plates in lead-acid storage batteries. At times, in preparing plates, some negative paste is accidentally mixed into positive paste, thus contaminating the positive paste with traces of barium sulfate. Rapid failure due to shedding has been traced to this barium sulfate contamination. Systematic tests show that as little as 0.0005% precipitated barium sulfate in positive paste markedly increases shedding on deep-cycling bench life tests. On the other hand, as much as 0.1% had no evident effect in overcharge bench tests, or in actual car service.

INTRODUCTION

The most widely used laboratory tests for storage battery durability, or life, involve successive cycles of fairly complete, or "deep", discharges followed by complete recharge. The test specified by the S.A.E. is of this type. It is widely used both as a laboratory tool for studying experimental batteries and as a procurement specification. In the latter case, batteries must yield at least a specified minimum number of cycles on the test to be considered acceptable.

Occasionally, a battery or group of batteries that should easily meet the test requirements fails prematurely due to excessive positive plate shedding. In many instances, the active material from the positive plates of these failing batteries has been subjected to spectrographic analysis. Usually, barium has been found as a contaminant in these positive plates. Since barium sulfate as precipitated *blanc fixe* is a usual constituent of paste for negative plates, finding barium in the positive active material is evidence of contamination of the positive paste with negative paste at some step in plate preparation. Since the same equipment is used alternately in many plants for manufacturing both positive and negative plates, it is surprising that such contamination is not more common.

In view of the fact that there is always this danger of contamination, it was considered most desirable to define more clearly the effect of barium sulfate as an impurity in positive paste, not only in deep cycling tests where the effect was first noted, but also in actual car service and in overcharge type tests.

¹ Manuscript received May 7, 1954. This paper was prepared for delivery before the Boston Meeting, October 3 to 7, 1954.

EXPERIMENTAL

Nine lots of positive plates were prepared from nine carefully compounded batches of positive paste. The only known variable in the nine batches was the amount of barium sulfate as precipitated *blanc fixe* that was added, and which varied from none in the control mix to 0.10% as a maximum. The positive plates used 9% antimonial lead grids 1.72 mm thick. They were assembled into 15 plate elements with stock negative plates pasted in the same type grids. This assembly is rated at 85 amp-hr at the 20-hr rate and is intentionally deficient in positive active material. Forty-five batteries were prepared, nine for each of the three bench tests and eighteen for automobile service testing. In assembling the latter eighteen, positive plate groups from three different paste batches were assembled in each battery, i.e., formulas 1, 4, 7 in one battery, formulas 2, 5, 8 in the next, etc. By this means each positive formula was tested in six cars instead of only two, exposing it to a wider range of conditions of use.

Life Tests Used

S.A.E. cycling test.—This test (1) was developed shortly after 1930 and was later adopted as standard by the Society of Automotive Engineers. It is of the deep cycling type, subjecting the batteries to 4 cycles/day, each cycle comprising 40 amp-hr of discharge and 50 amp-hr of recharge with the batteries held at $110 \pm 5^\circ\text{F}$. Each week a capacity test determines battery condition.

Emark life test.—This test (2) was developed to simulate one type of automobile service—that of a taxi or delivery car. It is of the "shallow-cycling" type in that a discharge of 300 amp for 5 sec is given, followed by 6 min 30 sec of recharge at 10 amp, then a rest of 3 min 25 sec, after which the cycle is re-

TABLE I. Effect of barium sulfate in positive plates on battery performance under various conditions of test

BaSO ₄ content, %	0.0000	0.0005	0.001	0.003	0.005	0.0075	0.010	0.050	0.100		
<i>Battery Initial Capacity</i>											
Cycle	Rate	Temp									
1	5	80°F, amp hr	84	84	84	86	86	87	86	86	87
2	300	0°F, min	4.6	4.4	4.4	4.7	4.3	4.4	4.4	4.4	4.3
3	5	80°F, amp hr	85	85	85	87	87	89	87	88	87
<i>Battery Self-Discharge on 28 Day Stand at 80° F</i>											
Initial acid gravity			1.279	1.280	1.282	1.274	1.278	1.277	1.278	1.282	1.283
Final acid gravity			1.241	1.237	1.237	1.239	1.238	1.237	1.240	1.242	1.242
decrease			0.038	0.043	0.045	0.035	0.040	0.040	0.038	0.040	0.041
<i>Life on "Deep-Cycling" S.A.E. Life Test</i>											
Yield cycle 32, amp hr			67	67	67	67	65	66	65	63	49
Yield cycle 84, amp hr			67	64	64	57	56	54	50	42	25
Yield cycle 188, amp hr			58	49	38	32	35	32	20	20	10
Estimated life, cycles			250	210	175	150	145	140	110	90	50
% Relative life			100	84	70	60	58	56	44	36	20
% Pos. shed cycle 188			5	20	30	35	40	45	55	60	75
<i>Life on "Shallow-Cycling" Emark Life Test</i>											
Yield cycle 860, amp hr			78	78	78	79	79	79	80	80	78
Yield cycle 6951, amp hr			41	40	40	43	42	40	40	43	39
Yield cycle 8468, amp hr			8	9	8	7	6	6	6	14	5
Estimated life, cycles			6960	6950	6950	7000	6975	6950	6950	7000	6900
% Pos. shed cycle 8468			Maximum estimated shedding 5%—No systematic differences.								
<i>Life on S.A.E. Overcharge Test</i>											
Yield after 1 week, min			8.0	8.2	8.2	7.5	8.4	8.3	8.5	8.1	8.0
Yield after 3 weeks, min			3.9	3.3	3.2	4.1	3.3	3.5	3.2	3.1	2.8
Yield after 4 weeks, min			0.65	0.40	0.60	0.70	0.30	0.25	0.40	0.25	0.45
% Pos. shed, 5 weeks			Maximum estimated shedding 5%—No systematic differences.								
<i>Life in Automobile Starting and Lighting Service</i>											
Yield after 18 months, amp hr			65	74	52	65	75	40	64	75	42
% Pos. shed, 18 months			6	5	14	7	5	14	8	5	13

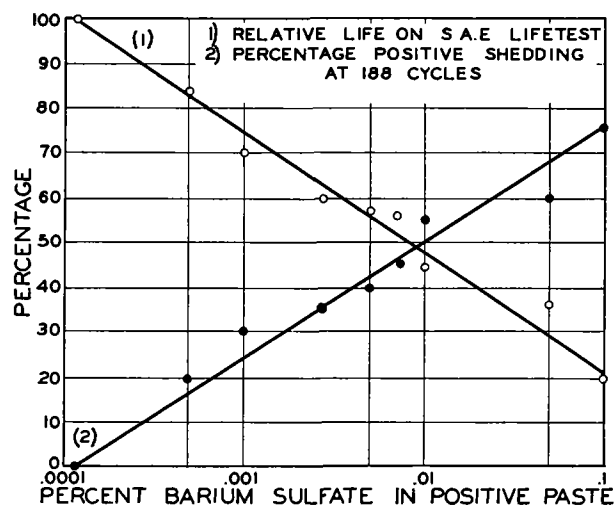


FIG. 1. Effect of barium sulfate content of positive plate active material on battery performance on S.A.E. life test.

peated. During the week the batteries are held in a water bath at $100 \pm 5^\circ\text{F}$. As in the cycling test, the capacity test is imposed once a week to determine battery condition.

Overcharge test.—This test (1) is to provide data as to the life of positive grids and of separators. Since these are major causes of failure in automobile use, this test is a useful one. The batteries on test are charged continuously for 110 hr at 9 amp, then allowed to stand for 48 hr on open circuit before receiving the weekly capacity test cycle. During the test, the batteries are held in a water-bath at $100 \pm 5^\circ\text{F}$.

Automobile service test.—Because of the great variation in the conditions of use, many thousands of batteries must be tested for definitive results. Except in a limited way it is, therefore, of little use for laboratory battery series. In the present case, many

possible auto test conditions were excluded by selecting the group of 18 test cars from among those owned by laboratory personnel. All were being used in the same kind of service and receiving similar mileage in the order of 10,000 miles/yr.

In addition to the above life tests, one set of the batteries was examined for self-discharge differences by being allowed to stand on open circuit for 28 days at 80°F.

Pertinent data have been summarized and are presented in Table I.

DISCUSSION

Barium sulfate had no detrimental effect on the initial capacity of the batteries. In fact, there is a trend to slightly higher 20-hr-rate yields with increasing barium sulfate content. Unless verified by additional testing, this cannot be considered significant since the variation is within possible experimental error.

There was no effect on self-discharge. The decrease in electrolyte specific gravity was of the same order for all cells and displays no trend.

No trend was shown on the Emark type life test, on the S.A.E. overcharge test, or in actual car service. Differences found in the batteries after car service were due to operating conditions of the car and not to formulation. The significant finding was that all batteries were still operative after 18 months in cars.

Quite a different story developed from the S.A.E. life test. The significant data are plotted in Fig. 1.

The life in cycles is an inverse function and the positive plate shedding a regular function of the logarithm of the percentage of barium sulfate in the positive plate active material.

From the above findings, the following conclusions may be drawn:

1. Barium sulfate contamination up to 0.1% of positive plate active material does not detract from the performance of batteries on noncycling tests or in average automobile use.

2. Barium sulfate contamination of positive plate active material is seriously detrimental to the life of batteries tested by a "deep-cycling" procedure and may be expected to be equally detrimental to the life of batteries used in "deep-cycling" service such as in battery propelled vehicles.

The only explanation for this harmful effect of barium sulfate is based on the theory that on "deep-cycling" the barium sulfate crystallites serve as nuclei for large lead sulfate crystals. Large lead sulfate crystals could then disrupt the bonding structure of the positive plate causing disintegration and shedding of active material.

Any discussion of this paper will appear in a Discussion Section to be published in the June 1955 issue of the JOURNAL.

REFERENCES

1. Society of Automotive Engineers, Handbook, 715-716, Business Press Inc., Lancaster, Pa. (1952).
2. J. E. HATFIELD AND H. R. HARNER, *Trans. Electrochem. Soc.*, **71**, 593 (1937).

The Role of Inverse Segregation and Redistribution of Solute Atoms in the Freezing of Hypoeutectic Lead-Antimony Alloys¹

A. C. SIMON AND E. L. JONES

Naval Research Laboratory, Washington, D.C.

ABSTRACT

Inverse segregation has been found to occur in the lead-antimony alloys of the range of concentration used for battery grids. Because of the possible harmful effects of such large concentrations of antimony at the surface of the battery grid a study has been made as to the cause of this phenomenon. The extent of the antimony dispersion in the surface layer has been found to be larger than can be explained by any one of the existing theories of inverse segregation. The effect appears to be caused by an interdendritic flow of still molten alloy of near eutectic composition into the gap left between the semisolid crust and the mold face during the solidification contraction. The difficulty of inducing the nucleation of antimony produces a condition of supersaturation for the β phase in this layer while the lead continues to crystallize out at temperatures below the normal eutectic. The continually increasing concentration of antimony added to the decrease in temperature eventually brings a limit to supersaturation, whether or not nucleation is promoted by the mold face. The antimony present in excess of the eutectic concentration then forms primary dendritic crystals which grow until the eutectic composition is again reached, at which point eutectic crystallization occurs. The result is a surface film of antimony far in excess of the distribution found within the ingot.

INTRODUCTION

When a hypoeutectic lead-antimony alloy casting is examined a great deal more antimony is found in the surface layer than would be expected from the alloy composition. As the composition of the alloy approaches that of the eutectic the surface layer becomes almost entirely antimony instead of the expected eutectic. This effect is a factor of importance in the casting process and in the subsequent use of the alloy material. In the use of lead-antimony as a battery grid material this unequal distribution of antimony at and near the surface may be a factor in the adherence of the active material, as well as an influence on the rates of corrosion and growth. The presence of large amounts of antimony in the surface layer definitely influences the structure of the initial corrosion product that is formed and contributes to the deposition of antimony at the negative plate.

The present paper deals only with the investigation of inverse segregation itself. The effect of inverse segregation on battery grid performance will be reported at a later date.

The phenomenon of inverse segregation (decreased concentration of the solute constituent toward the center of the casting, with abnormally high concentration at, or near, the surface) is well known and has been reported in many alloy systems. Excellent reviews (1-3) include most of the literature on this subject prior to 1950. These analyze the existing

theories of inverse segregation in a critical manner and contain excellent bibliographies of prior papers on inverse segregation.

Two forms of inverse segregation have been reported: (a) a gradual decrease in the low melting point constituent toward the center of the casting, detectable only by chemical analysis; and (b) exudations at the surface of high concentration of eutectoid, rich in the low melting point constituent, which may or may not be accompanied by a gradual internal change of composition. The inverse segregation observed in the lead-antimony alloys conforms to type (b), except that the surface is covered with primary crystals of antimony rather than an antimony-rich eutectic.

None of the theories of inverse segregation adequately explain the extent of antimony segregation found at the surface of the lead-antimony alloy castings nor do any of them explain the primary crystallization of the β phase in the surface layer. Further investigation of this phenomenon therefore seemed advisable.

EXPERIMENTAL PROCEDURE

Both chill and slowly cooled castings were prepared from a series of lead-antimony alloys containing 1, 3, 5, 7, 9, 11, and 13% antimony, respectively. A microscopic examination was made of the surfaces and cross sections of the ingots. Since inverse segregation appeared principally as a surface exudation of the antimony-rich material there was little of value obtained from cross-sectional examina-

¹ Manuscript received June 10, 1954. This paper was prepared for delivery before the Boston Meeting, October 3 to 7, 1954.

tion and the principal reliance was laid upon surface examination. Surfaces were examined in the as-cast condition; the castings were then etched with acetic acid-hydrogen peroxide solution (2 ml of 30% Superoxol to 48 ml of glacial acetic acid) and again inspected. This etch dissolves the lead and the lead-rich solid solution but does not appreciably attack antimony or the β phase. The antimony present in solid solution is precipitated as a very finely divided black soot-like film only upon the surface of the lead against which larger particles of antimony stand out brilliantly. There is, therefore, no difficulty experienced in differentiating between lead and antimony in the surface layer. The black film which obscures the surface of the lead-rich areas can be readily rubbed off, although it cannot be removed by washing. Rubbing, however, distorts the surface structure of the soft lead matrix. Scotch tape applied to this surface and gently pressed (but not rubbed) into contact with the surface by means of a very soft pencil eraser or other soft rubber pad was found to be very effective in removing this black deposit. If the etch is prolonged slightly, the thin surface layer of antimony is undermined and can be transferred intact to the Scotch tape. Thus, both sides of the antimony film can be examined as well as the new surface of the ingot revealed by the removal of the antimony. In one case this stripped film was subjected to x-ray analysis and identified as antimony as a check on other observations. Repeated etching and stripping in this manner revealed the structure to a considerable depth below the original surface.

On another series of castings, heavily plated with copper, taper sectioning (4) was employed to observe the structure of the very thin surface layer. Taper sectioning caused an apparent increase in the sectional thickness of the surface layers while the copper preserved the original surface contours.

Still another series of castings were made in a special mold, the two opposite sides and bottom of which were composed of aluminum while the other two sides were of transite. The top was left open to the air. Such a mold design insured very rapid chill casting at the cold aluminum faces and a progressive growth of the dendrites into the much more slowly cooled interior and provided a means of studying the effects of unequal freezing. All castings were approximately $1\frac{1}{4}$ in. high, 1 in. wide, and $\frac{1}{2}$ in. thick.

OBSERVED SURFACE STRUCTURE

Examination revealed that antimony appeared at the surface in excessive amounts under all the conditions that were investigated. The excess antimony that appeared on the surface increased as the antimony concentration in the alloy increased but to a greater proportional extent. Thus, an alloy that had

contained 10% antimony in the liquid state showed a surface after freezing that appeared to be almost entirely antimony.

For equal amounts of antimony, the alloys chill cast very suddenly showed the least amount of exudation of antimony on the surface and the surface structure agreed with the internal structure. Alloys cooled very slowly (less than $1^{\circ}\text{C}/\text{min}$) appeared to show no exudations but closer inspection revealed a high concentration of antimony at the bottom of the ingot (which was also the last portion to cool). The dendritic structure of the ingot was clearly revealed elsewhere on the surface by a withdrawal of the low freezing constituent, but at the bottom surface and a short distance up the sides the surface was smooth as if all the low freezing constituent had drained to this area. Alloys that were cast in a mold with unequal cooling of the mold faces gave the greatest evidence of exudations at the surface. Here also the greatest amount of exudation appeared at the more slowly cooled face and the surface structure was quite different from that found in the interior of the ingot.

For the alloys of low antimony content the surface antimony was concentrated at interdendritic and grain boundaries in a continuous layer that had no similarity to eutectic crystallization (Fig. 1).

As the amount of antimony in the alloy was increased the antimony-rich layer was found to cover the whole surface. This film, apparently continuous

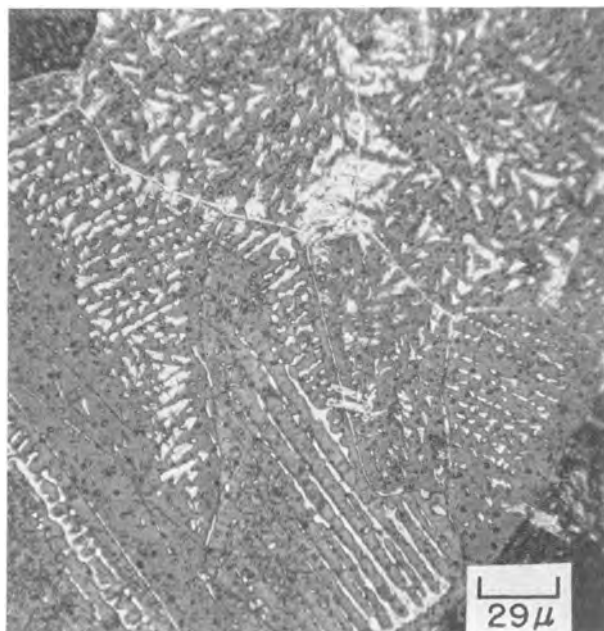


FIG. 1. Appearance of the vertical surface of chill cast lead-antimony ingot containing 2% antimony after an etch with acetic acid-hydrogen peroxide solution. Inverse segregation is indicated by excessive antimony (lightest areas) at interdendritic and intergranular extrusions. $300\times$.



FIG. 2. Appearance at vertical surface of chill cast lead-antimony ingot after etch with acetic acid-hydrogen peroxide solution. Antimony (light areas) covers almost the entire surface and shows primary crystallization although representing only 5% of the total alloy. 500X.

before etching, was found after etching to present a dendritic structure in which the antimony appeared as the primary crystallization and in amounts far in excess of the lead (Fig. 2). When this surface film was removed, a second layer was revealed which had the appearance of a true eutectic crystallization and in which the proportions of lead and antimony appeared to be normal. Beneath this second layer the true dendritic structure of the alloy was found.

For castings in which unequal cooling had occurred the still molten metal from the warmer regions was found to have flowed into the space between the frozen crust and the chill wall of the colder portion, forming a second antimony-rich film on top of that which had been formed by flow through the interdendritic channels (Fig. 3). The path of this flow was often plainly marked by the difference in crystal appearance and the fact that the frozen wave was actually visible, arrested by the freezing process before completely covering the original surface (Fig. 4).

Where the surface layer was thick, as in the case where flow had occurred from one area to another along the mold face, the surface was characteristically covered with tetrahedral crystals originating in the primary crystallization of antimony. Examination showed that while these crystals showed primary dendritic crystallization of antimony and a surface layer that was essentially antimony there appeared beneath the surface a layer of eutectic crystallization

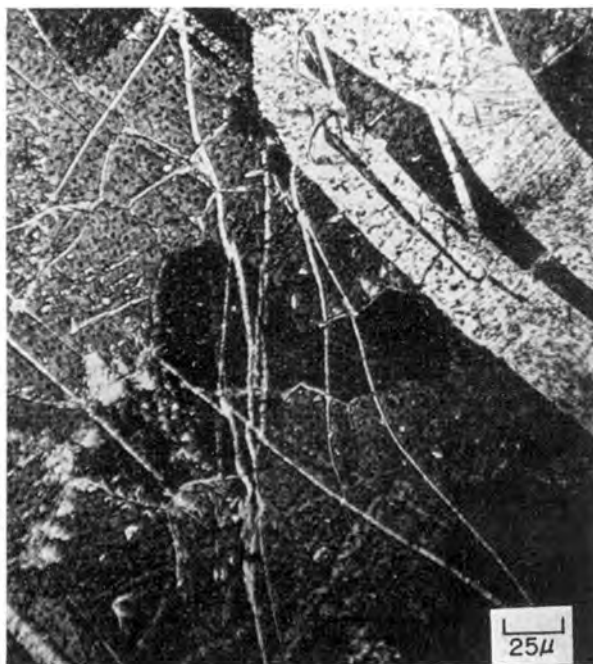


FIG. 3. Surface area from vertical wall of unequally cooled lead-antimony ingot containing 2% antimony. Original surface containing a few interdendritic and intergranular extrusions of antimony has been overrun by a molten stream of antimony-rich material originating at a mold face of lesser chill. Last formed film can be distinguished by its disregard for grain boundaries and other crystal structure. (Acetic acid-hydrogen peroxide etch.) 300X.

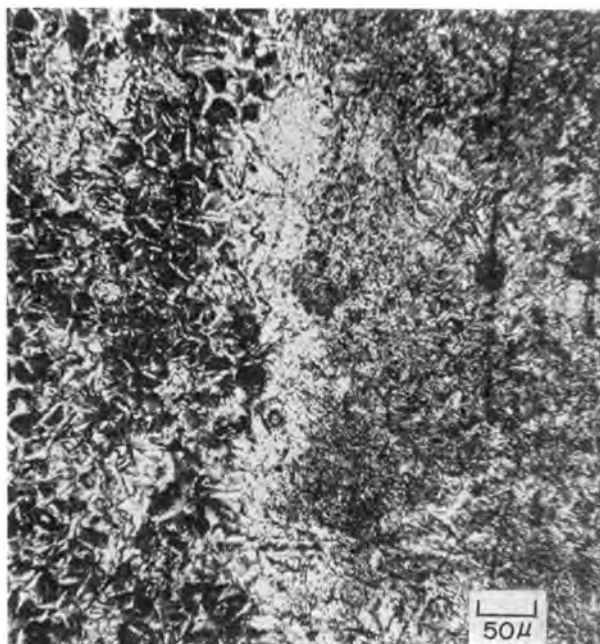


FIG. 4. Surface area from unequally cooled lead-antimony ingot containing 4% antimony showing crest of secondary wave of antimony-rich alloy (left) frozen in the process of covering the original surface film (right) of antimony-rich alloy. (Unetched specimen.) 150X.

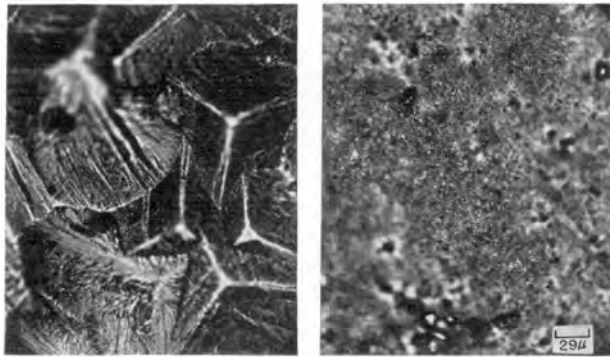


FIG. 5. Surface appearance of chill cast lead-antimony alloy with 9% antimony. (a) Before etching; (b) after etching with acetic acid-hydrogen peroxide solution and subsequent stripping of the surface film of antimony with Scotch tape. The subsurface layer here shown consists of an eutectic mixture of lead and antimony. 150X.

which nevertheless conformed to the general shape of the crystal (Fig. 5).

Taper sectioning confirmed the observations made at the ingot surface. A columnar dendritic growth was revealed a short distance inward from the ingot surface, separated from the surface by a layer of eutectic structure, while at the surface there appeared a very thin layer of antimony.

The appearance of the surface as viewed under the microscope left no doubt that the original frozen surface had withdrawn from the mold face through shrinkage of the ingot surface layer, expansion of the mold, or both. This space then appeared to have been filled by still molten material that flowed to the surface through interdendritic channels or flowed along the mold wall from regions still molten. The surprising feature is that the liquid metal flowing to the surface did not appear to have frozen instantly. Equally surprising is the fact that, when freezing did begin, primary crystallization of antimony should first occur, and to such an extent.

DISCUSSION

The type of inverse segregation that causes exudations of a low-melting point constituent at the surface is common in binary tin bronzes, phosphorus-tin bronzes, zinc-tin bronzes, leaded bronzes, leaded gun metals, and aluminum-copper alloys. For all of these alloys there are certain factors in common from which the following significant observations have been made (1, 3).

(A) Inverse segregation occurs only in alloys with a considerable freezing range.

(B) The exudation type of segregation is observed with alloys in which there separates a low-melting point constituent during solidification.

(C) Inverse segregation occurs only in alloys that contract during solidification.

(D) The presence of gas absorption tends to increase the effect.

(E) Inverse segregation increases with increasing rate of solidification with the exception that very rapidly chilled thin sections fail to exhibit this effect.

(F) Inverse segregation is favored by the formation of coarse columnar grains.

On the basis of these observations a comparatively simple explanation of inverse segregation is possible.

Redistribution of Solute Atoms during Freezing

At the instant a melt is poured into a mold at lower temperature there is formed a surface of intense supercooling and heat begins to flow from the interior of the liquid, through the interface, and into the mold. Immediately after contact is made, the region of supercooling or chill is confined to a very thin section of the melt, parallel to the chill wall, and the balance of the melt is essentially without a thermal gradient (5). After a brief interval a thermal gradient is set up that extends into the interior. When a thermal gradient is established, dendritic growth will proceed simultaneously from a great many points along the dendritic arms that first developed in the undercooled layer (Fig. 6). This secondary dendritic growth will extend along the thermal gradient toward the interior of the melt and the growth rate will depend upon the steepness of the thermal gradient. The steepness of the thermal gradient depends upon the thermal properties of the mold wall, the liquidus to solidus range of the alloy, conductivity of the solidifying metal, and the temperature level of solidification (6).

This growth produces a series of parallel dendritic arms extending from the surface layer well into the interior of the ingot. The spacing of these parallel dendritic arms has been shown (7) to increase with increasing concentration of the solute atoms and with deceleration of growth, and also to vary in the same manner as the ratio of the heat of fusion to the thermal diffusivity. These interrelating factors indicate that each growing dendritic arm of the crystal is surrounded by thermal and concentration gradi-

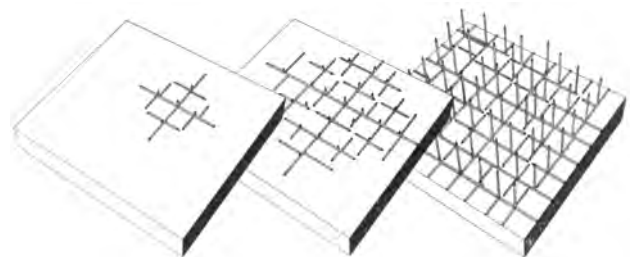


FIG. 6. Dendritic growth from mold wall into interior of melt (a) Initial nucleation in the supercooled layer of melt next to the mold wall; (b) rapid dendritic growth parallel to mold wall to remove initial condition of supercooling in this layer; (c) dendritic growth toward the interior of the melt following the establishment of a temperature gradient.

ents that extend for considerable distances into the surrounding melt.

For the purpose of illustration the space occupied by the growing crystal may be considered as made up of an assemblage of cells (parallelograms) of practically uniform size with a growing dendritic arm occupying the longitudinal axis of each. Dimensions of the cells (spacing of the dendritic arms) are determined by the concentration and thermal gradients set up at the time that the dendritic arms were embryonic. Subsequent radial growth of each dendritic arm is restricted to the confines of the original cell because of the presence of surrounding cells. Conditions existing at successive stages of growth are therefore not exactly as depicted in Fig. 6 because the dendritic arms would not have a uniform thickness throughout their length, as shown, but would also grow in diameter as solidification proceeds.

Normally, in the case of diffusion to an expanding surface, the area of the diffusion field would increase continuously, but under the conditions outlined above the area of the diffusion field cannot increase. The concentration gradient will change continuously, however, affected by the concentration changes at the boundaries of the other cells.

The extent of dendritic growth for any instant can be calculated, if it is assumed that equilibrium conditions exist, by reference to the equilibrium phase diagram and application of the lever rule. The calculation can also be made for nonequilibrium conditions, if the assumption is made that diffusion into the solid is negligible while diffusion throughout the liquid is complete (8). Conditions applying for equilibrium and extreme nonequilibrium can then be compared graphically. All actual freezing conditions will occur somewhere between these extremes.

How this would affect dendritic growth is shown graphically in Fig. 7 for an alloy of 1% antimony in lead. The figure represents three stages in the growth

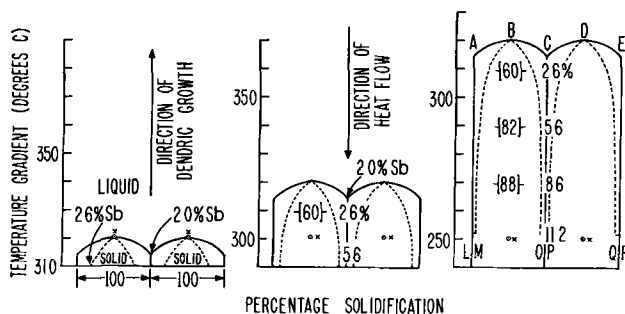


FIG. 7. Graphic representation of growth of parallel dendritic arms toward the interior of a melt under the influence of a temperature gradient. — Solidification under equilibrium conditions; - - - solidification under nonequilibrium conditions; [] - percentage solidified at given temperature.

of two dendritic arms, parallel to a thermal gradient, as the temperature of point x varies from 320.5° to 250.5°C (608.9° to 482.9°F). As the temperature of point x drops there will be a progressive solidification of the remaining liquid portion upon the dendritic arm that includes point x , and the latter will progressively become thicker. At the same time there will be a progressive increase in the antimony concentration of the still liquid portion surrounding point x . The numbers in brackets indicate the percentage solidification at the indicated temperatures, while the unbracketed numbers represent the concentration of the melt at the solid-liquid interface. The dendritic arms are assumed to have equal growth rates and to be surrounded by others with similar conditions of growth.

For equilibrium conditions (solid line), with a temperature gradient as shown, the advancing boundary of solidification would assume in cross section the form indicated by the line ABCDE, and the boundaries AL and ER would be in contact with neighboring dendritic arms. The entire solidification of the dendritic arms would take place in the temperature interval between 320.5° and 314°C (608.9° and 597.2°F), with the composition of the melt at the beginning being 1% and increasing to 2% just prior to final solidification. The composition of the solid would approach 1.0% as a limit and at the moment of final solidification would have a uniform composition of 1.0%. At 314°C (597.2°F) there would be no gap remaining between the dendritic arms.

The boundary condition between solid and liquid metal for conditions of extreme nonequilibrium (broken line) are represented by the line LMBOP-DQR. Solidification in this case begins at the same temperature but extends over a much larger interval, reaching the eutectic temperature of 252°C (485.6°F). The melt also varies in composition along the interface, approaching the eutectic composition of 11.2% antimony just prior to final solidification. With a considerable gap still remaining between

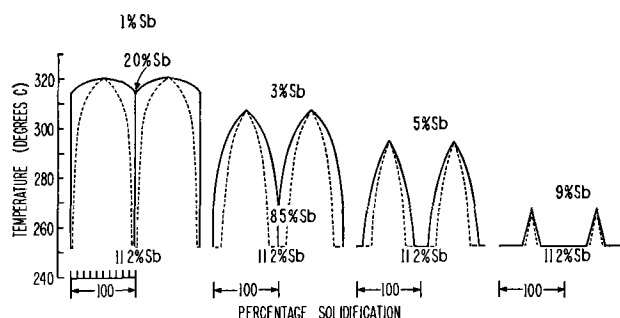


FIG. 8. Graphic representation of change in interdendritic channels for increase in antimony concentration. — Solidification under equilibrium conditions; - - - solidification under nonequilibrium conditions.

the dendritic arms even at the eutectic temperature, there is a definite possibility of interdendritic flow through the porous surface crust.

The space remaining between solidifying dendritic arms at the eutectic temperature increases as the amount of antimony in the alloy is increased (Fig. 8). This is true not only because of the decreased solidification taking place but also because the spacing increases with increasing concentration of the solute atoms (7). The length of the dendritic arms as compared with their thickness is dependent upon the steepness of the temperature gradient so that in chill casting quite long dendrites are possible before the surface layer is completely frozen. Fig. 7 and 8 are two-dimensional graphic representations of a three-dimensional effect. For any actual cross section the total solidification would therefore appear greater and the liquid layer surrounding each dendrite would actually appear thinner than represented here.

The assumption that diffusion in the liquid layer is complete, used here in the calculation of nonequilibrium conditions and previously by others (9-12), has been attacked (13) on the grounds that a diffusion coefficient of 1-10 cm²/day for liquid metals (14, 15) would be entirely inadequate to insure uniform composition of the melt during freezing. That the entire melt is not of a uniform composition is undoubtedly true, as witness the concentration gradient that exists between the tip and base of a growing dendritic arm. If the diffusion coefficient was sufficiently high, there would be diffusion from regions of higher concentration to lower with uniform solidification and elimination of dendritic growth. For actual dendritic growth, however, where the mass of liquid metal is, figuratively speaking, divided into many small cells in which diffusion distances are small, the assumption can be made without serious error that complete diffusion has occurred in the liquid cross section under consideration. Spacing between dendritic arms has been measured to be about 0.001 mm for cubic metals (7) and a large portion of this space is filled with solidified metal in the first part of the freezing interval when there is but slight change in the liquid concentration. In the final part of the freezing interval when concentration gradients are large, the diffusion would be operating through such short distances that the diffusion coefficient of 1 to 10 cm²/day would seem adequate.

However, if the above rate of diffusion is not sufficient to produce uniform concentration in the remaining molten layer, the argument is not basically altered. The effect of an inadequate diffusion rate would be to pile up an excess of solute atoms at the solidifying interface. This, in turn, would result in a

lower percentage of solidification at a given temperature and result in a larger space between dendritic arms when the eutectic temperature was reached. The net effect would be to push nonequilibrium conditions to a greater extreme than discussed above and thus increase the possibility of interdendritic channels in the outer crust.

Interdendritic Flow

While the interdendritic flow theory now seems to be generally accepted, the exact reason for an outward flow of metal between the solidifying dendrites has been the subject of some dispute. It has been suggested (16) that, as solidification proceeds, dissolved gases become increasingly concentrated in the residual liquid until the saturation point is exceeded, whereupon the gas is liberated and forces the liquid metal along the interdendritic passages toward the ingot exterior. Exudation in an 11% tin bronze does not occur when melting is performed in an oxidizing atmosphere, but becomes very noticeable in a reducing atmosphere (17, 18). Inverse segregation is greatest under atmospheres of hydrogen, water vapor, hydrogen sulfide, or methane (19). Similar results have been found for aluminum alloys (20). This evidence suggests that dissolved hydrogen causes severe segregation.

However, gas is not the sole factor or even a necessary one as demonstrated by experiments which show that inverse segregation can occur in alloys melted in a vacuum (21-25).

Lead reportedly dissolves less than 0.1 ml of hydrogen per 100 g of lead when near the melting point of the liquid metal (26). For oxygen a solubility of 0.2 ml per 100 g of lead has been reported (27), with a marked decrease in solubility for increasing additions of antimony. This volume of gas, while small, nevertheless constitutes better than 1% of the alloy by volume so that its liberation in the later stages of freezing could have an appreciable effect. However, it has been shown (25) that inverse segregation occurs in lead-antimony even when vacuum cast. One alloying constituent has been experimentally substituted for another in the interdendritic channels of a semisolid metal (28) thus proving that interdendritic flow is possible when motivated by purely gravitational forces. In the present investigation no internal porosity was found. Such porosity would be expected if gas was the motivator of interdendritic flow to the surface. The behavior of very slowly cooled ingots in which the low melting constituent withdrew from between the primary lead dendrites at the side surfaces and concentrated at the bottom surface of the ingot indicated an interdendritic flow caused by hydro-

static pressure of the still molten metal and the simple effort of a liquid to seek the lowest level.

In the case of steels cast in chill molds an air gap has been found to form between the mold wall and the frozen crust of the alloy (5). Microscopic examination of the surface of the lead-antimony alloys indicates that a gap is formed in this case also. Whether the gap was formed due to shrinkage of the original dendritic crust or expansion of the mold was not determined. Both factors probably occur to some extent and reinforce each other. Existence of an actual air gap such as occurs in steel appears to be unlikely. Instead the gap is probably filled continuously as it is produced by an inflow of molten metal. Whether or not the supercooled conditions survive long enough to cause complete filling will depend upon the conditions at the mold surface.

From the foregoing discussion it may be seen that no special force is necessary to cause interdendritic flow of metal after a gap is formed. The melt remaining between the solidifying dendrites will be near the eutectic composition. As this metal is forced into the gap by the hydrostatic pressure of the liquid interior, that portion of the liquid moving toward the surface from more remote regions will be brought to the eutectic composition. The metal flowing to fill the gap would therefore be expected to have essentially eutectic composition, whatever the composition of the original hypoeutectic melt.

Primary Crystallization of Antimony

Presence of a surface layer of antimony-rich phase in which lead appears as only a minor constituent is surprising. From the foregoing discussion a eutectic composition would be expected at the surface, but the interdendritic flow theory is inadequate to explain a structure in which antimony is plainly far in excess of the eutectic amount. In addition, antimony shows unmistakable evidence of primary dendritic crystallization and has the same crystal structure as it exhibits in the hypereutectic alloys where primary crystallization of antimony is to be expected.

Primary crystallization of antimony could occur in either of two possible ways. Either primary crystallization of antimony has occurred at the mold surface at the moment of initial chill or antimony has formed primary crystals from the eutectoid solution that flows into the air gap subsequent to the initial freezing at the mold face.

Primary crystallization of antimony at the surface in the initial chill could only occur by some process of phase inversion whereby the antimony crystals were momentarily precipitated before the expected and usual crystallization of lead crystals. Such a condition might be brought about by the extreme condition of chill and resultant super-

cooling produced at the moment of first contact of molten metal with mold surface. This would imply a change in the liquid prior to solidification. Theories of this type have been advanced and were considered as a possible cause of the primary crystallization of antimony.

Re-examination of Smith's theory of mobile equilibrium (29), Benedick's theory of the Ludwig-Soret effect (30), Hanson's (31) and Johnson's (32) theory of undercooling, and Ubblohde's (33) theory of minimum volume change do not suggest any mechanism that would so completely invert the normal order of precipitation as to allow primary crystallization of antimony prior to the solidification of the α phase crystals. In addition, the above theories have been more or less discredited either because of lack of favorable evidence or actual conflict with observed phenomena. Recent demonstrations (34-36) that metals can undergo extensive supercooling in the absence of nucleating agents, however, suggest a possible mechanism of phase inversion. If the molten metal were to be heated to a temperature sufficient to destroy all nuclei for lead nucleation but insufficient to destroy those effective for antimony, then the liquidus curve for the hypereutectic alloys could conceivably be extended into the hypoeutectic region, provided the lead remained supercooled and did not precipitate. Primary crystallization of antimony could then occur in regions where lead would normally be expected to appear.

Careful investigation, however, leads to the conclusion that antimony crystals were formed subsequent to the formation of the metal crust of primary lead crystallization and not at the instant that the molten metal first contacted the mold face. This conclusion is based upon the following considerations.

(A) In alloys of low antimony concentration, primary crystals of antimony (surface film) did not completely cover the surface but were concentrated at grain boundaries and interdendritic boundaries. If initial precipitation of antimony (inverse chill) occurred at the mold face, the distribution of the primary crystals would be expected to be random. Concentration at grain and dendritic boundaries indicates prior formation of a primary lead dendritic structure.

(B) The greater the differential between mold temperature and alloy freezing point the less the amount of antimony film present at the surface. Extremely rapid chill produced practically no exudations in alloys with low concentration of antimony. This is the opposite effect to that expected from an initial freezing of antimony due to surface chill.

(C) In the ingots that were adjusted for conditions

of unequal cooling, the greatest exudation of antimony and the appearance of well-formed tetrahedral crystals of antimony occurred at the face of lesser chill which is likewise contrary to a concept of surface chill.

(D) In very slowly cooled ingots, exudations occurred as a result of drainage, and primary antimony crystals were present only at the bottom of the mold which was also the last surface to cool (mold heated from below). In such slowly cooled ingots (mold and melt both originally above the freezing point of the melt) surface chill should be absent and the presence of primary crystallization of antimony at the warmest point of the mold suggests the alternate mechanism.

(E) In those cases where visible flow of metal could be traced across the original surface, the number, size, and perfection of the antimony crystals was greater on the secondary surface than on the primary.

(F) If primary crystallization of antimony is due to supercooling of lead at the initial chill surface, then the presence of nuclei for the crystallization of lead should prevent this supercooling and lead should precipitate first, in the normal manner. The ability of solid metal or metal powder to promote homogeneous nucleation of its own melt has been demonstrated (37). Castings made in a lead mold, however, continued to show primary crystallization of antimony at the surface.

(G) It has been demonstrated (36) that the more complex type of crystal structures show a greater tendency to supercool and that antimony shows a greater tendency to supercool than lead. Considering also that at the moment of initial chill large masses of metal are involved, it does not seem likely that lead could be supercooled to any such extent that antimony would first precipitate. More logically, antimony could be expected to supercool in the solution of eutectic composition that is extruded at the surface. In such a solution most of the heterogeneous nucleating agents would have been filtered out by passage through the narrow channel between solidifying dendrites. The mass of metal would also be separated into small droplets, a necessary condition for extreme supercooling (36). Due to a difference in crystal structure and lattice spacing the lead could not act as a nucleating agent for the antimony (37). Primary crystallization of lead could continue upon existing lead surfaces until the antimony became sufficiently supercooled to precipitate or until the molten solution was brought into contact with the mold face where nucleating agents might be present.

The primary crystallization of antimony is therefore considered to take place as a consequence of interdendritic flow of a melt of practically eutectic

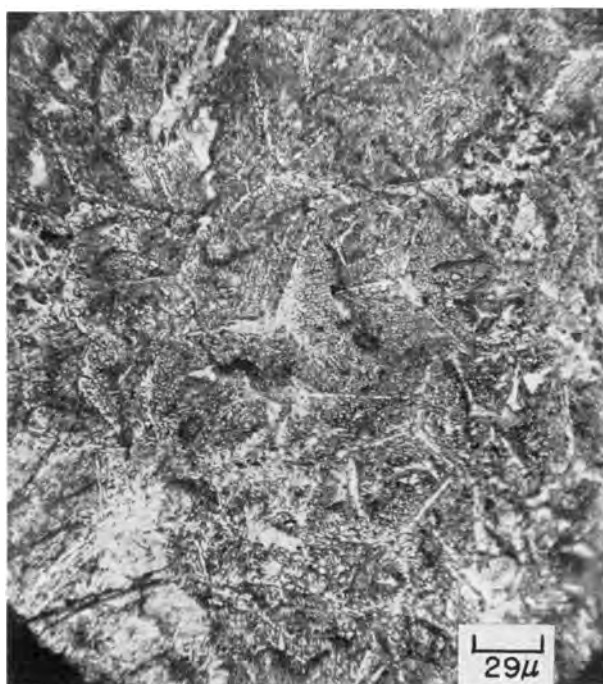


FIG. 9. A portion of the field of view to the left of the center of Fig. 4, considerably magnified. The tetrahedral shape of the individual crystals and the nature of the dendritic structure indicate oriented primary growth of antimony in the surface layer 300X.

composition into the gap left by the cooling of the metal. Lack of nucleating agents produces supercooling of the antimony while the lead continues to precipitate with consequent enrichment of the remaining metal in antimony. The primary dendritic crystallization of antimony apparently occurs at the colder mold surface, and dendritic arms extend through the still liquid melt filling the gap to the original metal crust. The observed appearance of small tetrahedra in the new surface with the dendritic arms extending along the tetrahedra edges in the [100] directions (Fig. 9) agrees with the report that surface crystals of castings of rhombohedral metals usually have a preferred orientation with the [111] direction normal to the cold surface (38). Solidification of the antimony in the layer brings the remaining melt to the eutectic composition and eutectic crystallization occurs within the primary antimony dendritic structure. Continued solidification of the liquid eutectic causes a volume decrease and the metal recedes from the mold face and the sides of the tetrahedra so that they become exposed in relief at the surface.

SUMMARY AND CONCLUSIONS

Inspection of commercially cast lead-antimony battery grids revealed the same phenomenon of excessive antimony at the surface as was found in all laboratory experiments. Laboratory experiments show that the excess amount of antimony in the sur-

face layer increases with increasing antimony content of the alloy and decreases with increasing chill. The observation that exudations decrease with increasing chill does not appear to check with previous reports. However, the terms slow chill and fast chill are relative. Castings referred to herein were made in small molds, of which at least two sides were aluminum, while some of the previous work is based on very large ingots cast in sand molds. Exudations observed on the very slowly cooled ingots (in metal molds) although highly localized in one portion of the casting probably represented as great a degree of segregation as did the more uniformly distributed (and much more noticeable) exudations of the more rapidly cooled specimens. Unequal cooling at various mold faces appeared to be as important a factor on inverse segregation behavior as was rate of chill.

Whether considered to be beneficial or harmful, inverse segregation in the lead-antimony alloys is a factor of importance. For some applications, inverse segregation may have advantages. Improved brightness and tarnish resistance result from the presence of a surface layer of antimony, and the effect of the phenomenon is to seal off and prevent any surface appearance of shrinkage cavities (except on the last surface to cool, which acts as a feeder). Whether such a layer would contribute to the physical properties of the alloy is problematical. The antimony layer is very thin and would not be expected to contribute materially to hardness or wear resistance, but the layer of eutectic material beneath it may reach a considerable thickness. Interdendritic flow of still molten alloy into the cavity left by shrinkage of the original frozen crust makes possible close casting tolerances and undoubtedly is in part responsible for the onetime belief that lead-antimony alloys expanded during freezing.

Inverse segregation may prove detrimental in applications involving corrosion resistance, such as storage battery grids. Preferential leaching out of antimony from the surface of lead-antimony alloys when subjected to anodic corrosion in sulfuric acid has been previously reported (39). Such action will have a twofold effect: (A) the surface antimony and eutectic structure extend from the surface into the interior of the casting along the interdendritic channels so that a penetrating type of corrosion may occur; (B) if the battery paste is applied to the as-cast surface, subsequent forming will remove the thin antimony layer and the exposed antimony in the surface eutectic so that poor electrical conductance and poor adherence of the active material would seem likely. Since the resulting surface will be much rougher, however, the active material may tend to adhere more firmly. Which effect pre-

dominates remains to be determined from future investigation.

The effect of inverse segregation on casting should also be pointed out. As already stated, formation of a second surface film tends to cover over any defects in the original frozen surface so that sound, pore-free castings of close dimensional tolerance are possible when the temperatures at the various mold faces are properly regulated and a proper feeding head of molten metal is provided. If all mold faces are equally chilled, however, then internal porosity should result.

The phenomenon of inverse segregation appears to be intimately associated with dendritic growth. Factors that tend to prevent dendritic growth should also tend to eliminate inverse segregation. While there is a possibility that supercooling of the eutectic and primary crystallization of the antimony could be prevented by the use of proper nucleating agents incorporated in the mold facing (37) or in the melt, there would still be a layer of eutectic structure and composition formed at the surface.

In some cases where excess antimony at the surface may be detrimental, as possibly for battery grids, the simplest solution would appear to be the removal of the surface film by chemical or electrochemical means before subsequent operations are undertaken.

Any discussion of this paper will appear in a Discussion Section to be published in the June 1955 issue of the JOURNAL

REFERENCES

1. N. B. VAUGHAN, *J. Inst. Metals*, **61**, 35 (1937).
2. W. T. PELL-WALPOLE, *Metal Treatment*, **16**, 103, 171 (1949).
3. D. HANSON AND W. T. PELL-WALPOLE, "Chill Cast Tin Bronzes," Chapter IX, Arnold and Co., London (1951).
4. A. J. MOORE, *Metallurgia*, **38**, 71 (1948).
5. H. F. BISHOP, F. A. BRANDT, AND W. S. PELLINI, *Trans. Am. Foundrymen's Soc.*, **59**, 435 (1951).
6. H. F. BISHOP AND W. S. PELLINI, *Foundry*, **80**, 86 (1952).
7. B. H. ALEXANDER AND F. N. RHINES, *J. Metals*, **188**, 1267 (1950).
8. A. C. SIMON AND E. L. JONES, *This Journal*, **100**, 1 (1953).
9. W. G. PFANN, *J. Metals*, **4**, 747 (1952).
10. G. H. GULLIVER, "Metallic Alloys," Appendix, C. Griffin and Co., London (1922).
11. E. SCHEUER, *Z. Metallkunde*, **23**, 237 (1931).
12. A. HAYES AND J. CHIPMAN, *Trans. Am. Inst. Mining Met. Engrs.*, **135**, 85 (1939).
13. W. A. TILLER, K. A. JACKSON, J. W. RUTTER, AND B. CHALMERS, *Acta Metallurgica*, **1**, 428 (1953).
14. J. FRENKEL, "Kinetic Theory of Liquids," p. 201, Oxford University Press, Oxford (1946).
15. W. JOST, "Diffusion," p. 479, Academy Press, New York (1952).
16. R. GENDERS, *J. Inst. Metals*, **37**, 241 (1927).

17. C. H. BIERBAUM, *ibid.* **37**, 281 (1927).
18. F. HÖHNE, *Giesserei*, **20**, 523 (1953).
19. W. CLAUS AND F. W. BAUER, *Metallwirtschaft*, **15**, 587 (1936).
20. G. MASING AND O. DAHL, *Z. anorg. Chem.*, **154**, 189 (1926).
21. W. FRAENKEL AND W. GÖDECKE, *Z. Metallkunde*, **21**, 322 (1929).
22. M. V. L. GAYLER, *J. Inst. Metals*, **44**, 97 (1930).
23. H. BOHNER, *Metallwirtschaft*, **11**, 437 (1932).
24. K. IOKIBE, *Science Repts. Tôhoku Univ.*, **20**, 608 (1931).
25. L. JACOBY AND A. VERO, *Roy. Hung. Palatine-Joseph Univ. Tech. Econ. Sci. Soprom Pubs. Dept. Mining Met.*, **14**, 347 (1942).
26. W. R. OPIE AND N. J. GRANT, *J. Metals*, **3**, 244 (1951).
27. H. W. WÖRNER, *J. Inst. Metals*, **66**, 131 (1940).
28. M. L. SAMUELS, A. R. ELSEA, AND K. GRUBE, *Trans. Am. Soc. Metals*, **31**, 459 (1943).
29. S. W. SMITH, *Bull. Inst. Mining Met.*, **35**, 248 (1926).
30. C. BENEDICKS, *Trans. Am. Inst. Mining Met. Engrs.*, **71**, 597 (1925).
31. D. HANSON, Communication on paper by S. Smith, *J. Inst. Metals*, **17**, 112 (1917).
32. F. JOHNSON, Communication on paper by R. T. Rolfe, *J. Inst. Metals*, **20**, 274 (1918); **21**, 413 (1919).
33. UBBELOHDE, Discussion on paper by N. B. Vaughan, Ref. (1).
34. M. D. EBERALL, *J. Inst. Metals*, **76**, 295 (1949).
35. A. CIBULA, *ibid.*, **76**, 321 (1949).
36. D. TURNBULL AND R. E. CECIL, *J. Appl. Phys.*, **21**, 804 (1950).
37. J. A. REYNOLDS AND C. R. TOTTLE, *J. Inst. Metals*, **80**, 93 (1951).
38. F. C. NIX AND E. SCHMID, *Z. Metallkunde*, **21**, 286 (1929).
39. J. B. BURBANK AND A. C. SIMON, *This Journal*, **100**, 11 (1953).

Electroluminescence with Nonsinusoidal Fields¹

SOL NUDELMAN² AND FRANK MATOSSI

U. S. Naval Ordnance Laboratory, White Oak, Maryland

ABSTRACT

Electric fields in the form of square or rectangular waves, saw-tooth waves, and exponential waves were applied to an electroluminescent phosphor. The light output contained green and blue luminescence bands, which were examined separately by means of filters, a photomultiplier, and an oscilloscope. Square wave fields produce luminescence peaks whenever the field is changing, followed by a decline in luminescence when the field is steady. Peak heights increase proportionally to about the fourth power of the field strength. They decrease with increasing frequency for the green band, while for the blue band they first increase up to about 2000 cps and then decrease. The decay obeys power laws with different exponents before and after a critical time of about 0.7 msec. A rectangular field pulse of greater duration than the critical time produces, in the green band, peaks of equal total intensity at the field reversals; in the blue band, the same excitation produces peaks with equal changes in intensity. Other field shapes produce peaks of luminescence whose heights and shapes depend on field shape and duration of the steady field before it is changed. Additional peaks in the green band appear whenever the field begins to decrease.

Observations are interpreted by using the following assumptions: excitation is due to collision processes of accelerated electrons; green luminescence involves transitions to the conduction band and to traps; blue luminescence is caused by transitions within a luminescence center; the effective field changes in time because of the development of polarization charges. Additional peaks in the green band are due to recombination processes of the polarization charges.

INTRODUCTION

In general, experiments on electroluminescent phosphors have been conducted with d-c or sinusoidally varying electric fields. These investigations have already offered valuable information and have led to conjectures on the mechanisms involved in electroluminescence (1). Additional information on the fundamental processes can be expected from application of nonsinusoidal field changes, particularly in the form of square waves, since in these cases all effects related to duration of the field show up more clearly, and the influence of the field as such can be better separated from the influence of the manner of its application. Here, therefore, fields have been applied in the form of square pulses, saw-tooth waves, rectangular pulses variable in width and repetition rate, and exponential waves to an electroluminescent ZnS:Cu, Pb-phosphor.³ It was necessary to make the observations separately for the green and the blue luminescence bands (2) of this phos-

phor since characteristic differences in the electroluminescence properties of these two regions were found.

Quantitative measurements with respect to field dependence, frequency dependence, and decay laws were made on the electroluminescence patterns [brightness waves (3)] obtained by using square wave electric fields. For other field shapes only qualitative observations are reported.

Work related to this has recently been published on the influence of step functions on the time-average light output (4), on oscillograms obtained with trapezoidal waves (5) and other field shapes (6).

Although a complete and quantitative interpretation of every experimental detail is as yet impossible, sufficient information seems to be available to justify a discussion of some mechanisms contributing to electroluminescence in the light of the present observations. Other workers have suggested basic mechanisms that are relevant to some of the results of this study (1-3, 7-11). These proposals, either in their original or in a modified form, are incorporated with those given here in order to obtain an integrated picture.

EQUIPMENT AND PROCEDURE

The fields were produced by using generators giving a variety of signal wave shapes. The genera-

¹ Manuscript received March 8, 1954. This paper was presented at the meetings of the Swiss and German Physical Societies in Lugano, Switzerland, September 5, 1953, and Innsbruck, Austria, September 20, 1953, respectively; and at the Chicago Meeting of The Electrochemical Society May 2 to 6, 1954.

² Also at the University of Maryland, College Park, Maryland.

³ *Sylvania Electric Products Inc., Bayside, N. Y.*

tors for square waves and saw-tooth waves were variable from 10 to 10,000 cps, while a pulse generator variable in pulse width and repetition rate had a range of 100–1000 cps. A direct coupled amplifier with a rise time under load of less than 10 μ sec supplied an output peak to peak voltage of 0–320 volts. Exponential wave shapes were obtained by feeding a square wave into a square wave amplifier with a large RC time constant in its output circuit. This unit had a rise time under load of 250 μ sec, which could be increased still more by appropriate condensers. It supplied a continuously variable peak to peak voltage of 0–4000 volts.

Light output from the phosphor was observed by a 1P21 photomultiplier tube followed by a direct coupled oscilloscope. In general, data were obtained by taking pictures of the signal trace on the oscilloscope, then reading these films with an optical comparator.

The electroluminescent phosphor investigated was in the form of a cell containing a ZnS:Cu, Pb-phosphor³ exhibiting predominantly green light at excitation (12). Different samples of these green cells gave essentially equal results. In order to separate observations for the blue and the green luminescence band of this phosphor, a Wratten filter No. 21, which transmits wave lengths above 5300 \AA , or No. 36, which transmits between 3700 and 4600 \AA , was used.

EXPERIMENTAL RESULTS

Square waves.—When a square pulse of about 10 μ sec rise time is applied to the electroluminescent phosphor, the light output exhibits sharply rising peaks at the time of every field change. The peaks are followed by decreasing light output or “decay”, which generally does not have time to reach zero light output before the appearance of the next peak. The resultant luminescence pattern contains, therefore, a varying component or “ripple” superimposed on a steady background. All measurements of luminescence intensity, as peak heights or decay curves, are taken from the level of zero light output (“reference level”), which corresponds to the oscilloscope trace obtained without field.

For the same potential difference, the luminescence pattern is generally the same, whether the field is reversed in direction or simply applied and then removed.

Fig. 1 is a reproduction of an oscillogram made with three exposures for different field strengths. Besides illustrating the general peak pattern obtained with square wave fields, this figure also shows that with increasing field it takes less time for the luminescence to reach the maximum of the peak.

Dependence of height of luminescence peaks on

the repetition rate of square pulses is shown in Fig. 2. As the frequency increases, green peaks decrease in height, while blue peaks increase to a maximum value, then decrease. Experiments with manually switched D. C. indicate, however, that green peaks also decrease at extremely low frequencies, i.e., below about 2 cps. Voltage at the cell was maintained constant for these measurements.

The frequency dependence of the peak heights can be described empirically by a formula like

$$\dot{I}_p = A + B \log f$$

over the frequency range 10–10,000 cps for the green peaks, and up to about 2000 cps for the blue peaks. I_p is peak height, f , frequency; A and B are constants.

Dependence of the steady background on repetition rate is also shown in Fig. 2. These curves appear to have some of the characteristics of the curves shown by Waymouth (2), obtained for the time-average light output with sinusoidal fields. There, too, the green electroluminescence increases with frequency from zero to a steady maximum value in the vicinity of 1000 cps, while the blue intensity is still growing in a nearly linear manner at about 2000 cps; but, in addition, a decrease is found in the mag-



FIG. 1. Triply exposed oscillogram for blue electroluminescence, square wave fields, 90 cps, 250 μ sec rise time.

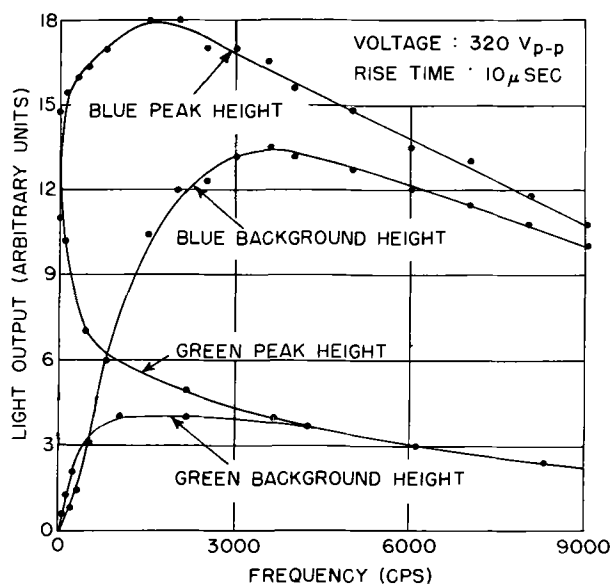


FIG. 2. Peak and steady background heights vs. repetition rate. Curves for green luminescence not drawn to same scale as for blue luminescence. Ordinates are measured from the reference ordinate for zero light output.

nitude of the steady background for both blue and green luminescence at sufficiently high frequencies. The analogy to Waymouth's results is understandable since the time-average light output is determined, to an appreciable extent, by the steady background.

Dependence of the height of the luminescence peaks on the field strength is shown in Fig. 3. Green and blue peaks grow with increasing field strength, although the green peaks do so at a more rapid rate. The curves of Fig. 3 may be described by power laws in the form $I_p = AE^n$, except for the low field region

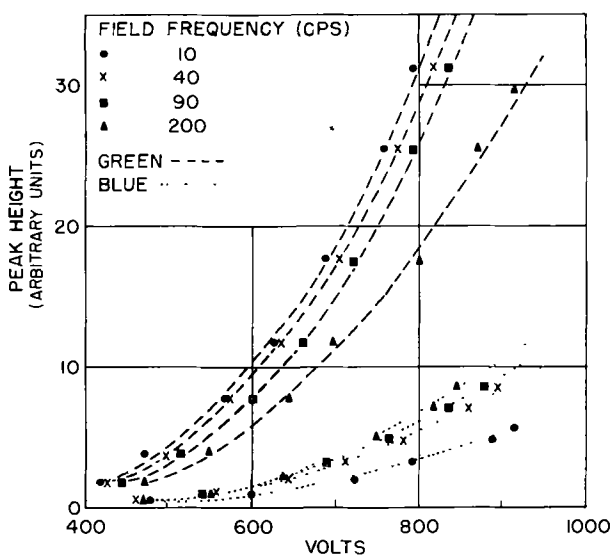


FIG. 3. Peak height vs. applied voltage. Curves for green luminescence not drawn to same scale as for blue luminescence.

of the curves for the blue peaks. The values of n obtained are 4.3 and 3.8 for the green and blue peak heights, respectively. It is also possible to represent the curves by a law of the form $I_p = aE^2 \exp(-b/E)$ as is found also by Destriau (3), with the exception that at frequencies higher than about 100 cps experimental curves of the blue luminescence depart from this relationship.

Fig. 4 shows decay curves in semi-log or log-log representation. Since the longest linear region appears in the log-log representation, it is preferable to describe the electroluminescent decay by power laws of the form $I = At^{-m}$. Furthermore, the early "linear" region of the semi-log plots is still more complex when observed with an enlarged time scale.

"Natural decay" was obtained after exposing the phosphor to weak radiation from an Argon lamp.

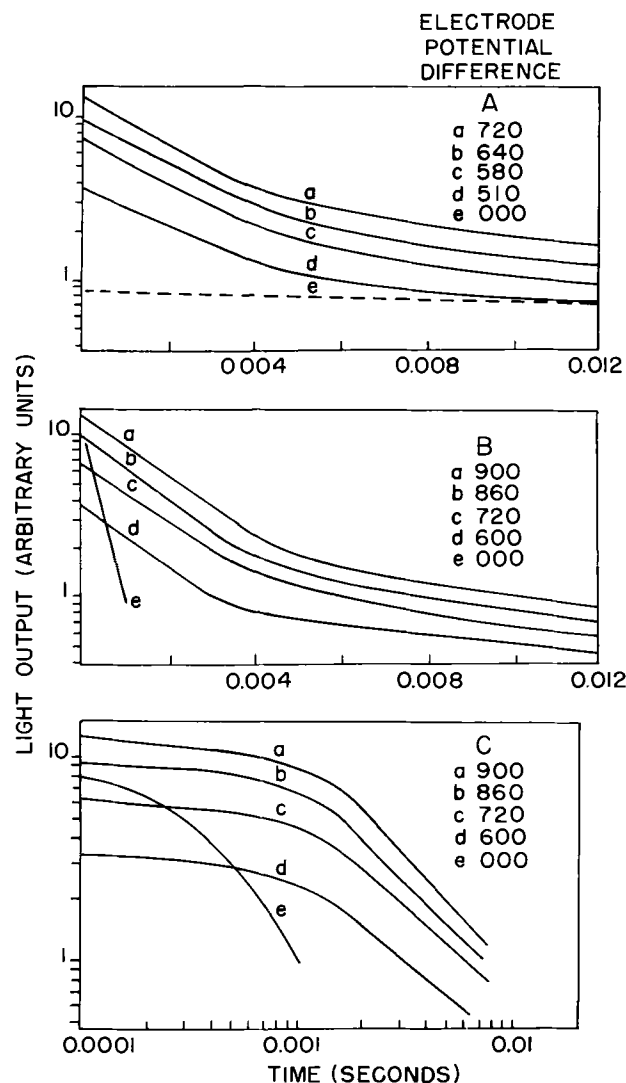


FIG. 4. Decay curves, 10 cps, 250 μ sec rise time. (A) Green luminescence, semi-log; (B) blue luminescence, semi-log; (C) blue luminescence, log-log.

The natural decay curve for the blue luminescence appears to be strictly exponential, while that for the green band is more complex. The blue natural decay is much faster than decay of the blue electroluminescence, while the natural decay curve for the green band declines at a slower rate than the corresponding electroluminescence decay.

Slopes of the decay curves vary somewhat with the field. This is particularly noticeable in Fig. 4c for the late decay of the blue band. However, for higher frequencies and for decay curves of the green luminescence in general, there is much less change, if any, of the slopes. There is also a variation of the slopes with frequency for constant field strength, particularly for the late decay of the blue luminescence where, for example, values of m vary from about 0.72 at 10 cps to 0.95 at 90 cps (at about 800 volts) (13). If the rise time of the field was changed, there was again a distinct change of m . Similar remarks would apply to the constants of an exponential decay law.

Rectangular pulses.—When fields of rectangular pulses like those indicated in Fig. 5 are applied to the phosphor, with different times t_1 and t_2 , observations reveal a marked qualitative difference between the green and the blue luminescence.

The significant features are: if t_1 is larger than about 0.7 msec, the blue electroluminescence peak increments, P_1 and P_2 in Fig. 5, are about equal, while for the green luminescence the heights H_1 and H_2 are of about the same magnitude. If t_1 is decreased to less than about 0.7 msec, the increment P_2 of the blue peaks becomes smaller. This critical time is of the same order of magnitude as the

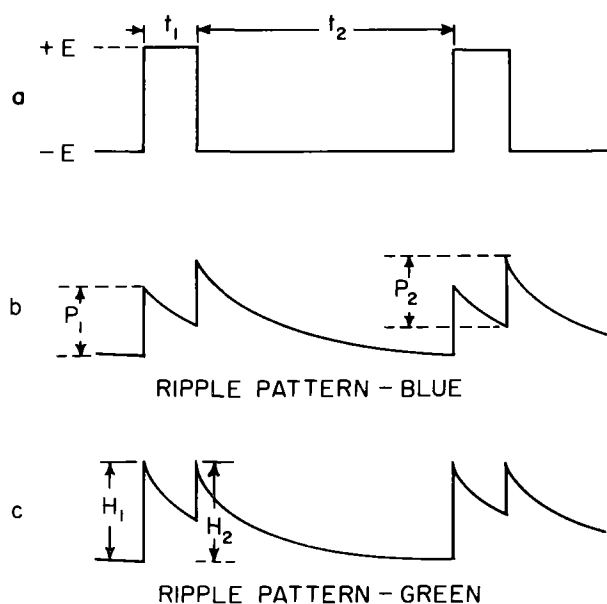


FIG. 5. Luminescence patterns for rectangular wave shapes.

transition time observed between the two linear decay regions in Fig. 4c.

Also, H_2 of the green luminescence begins to change its value if t_1 becomes smaller than the critical time. The complex quantitative details of the electroluminescence observed at small pulse time are the subject of a separate investigation and are not relevant to the discussions of this paper.

The patterns illustrated in Fig. 5 were produced by electric fields of 10 μ sec rise time. Fields with longer rise times give similar results although they are not as well defined.

Exponential and saw-tooth fields.—Fig. 6, 7, and 8 are examples of oscillograms taken with a dual beam d-c oscilloscope showing a variety of electric field wave shapes and corresponding electroluminescent patterns. These oscillograms have peaks labeled by different letters. General observations pertaining to these peaks are as follows.

The A and B peaks begin to grow whenever the applied field starts to grow from zero. The A peaks, observed at sudden field reversals, have the same appearance as peaks for square wave fields. D peaks are essentially identical with A peaks, except that they occur on sudden field removals.

The C and C' peaks appear when the applied field starts to change from some steady value. They exist in the green band only and are observable only on relatively slow field changes since, for rapid field changes, A peaks would hide the C peaks. C peaks

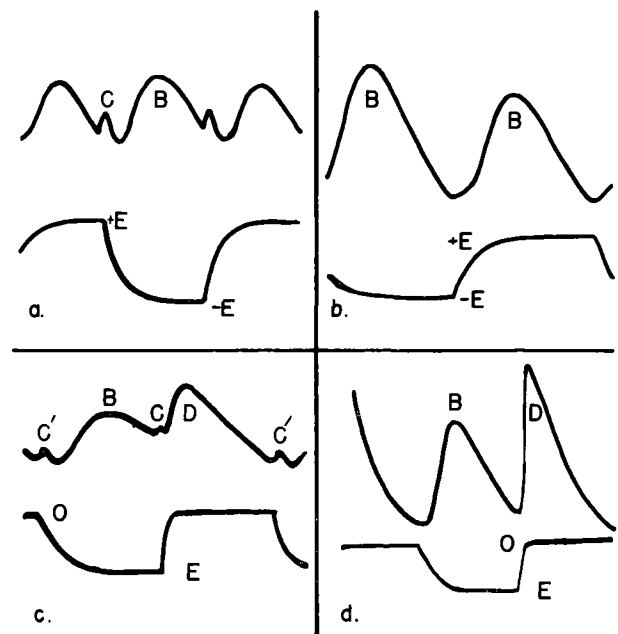


FIG. 6. Exponential fields, 500 cps, reversed and unidirectionally pulsed. (In the oscillograms in Fig. 6, 7, and 8, pictures a and c refer to green luminescence; b and d to blue luminescence. In each picture, the upper curve shows the ripple pattern; the lower curves, the corresponding applied fields.)

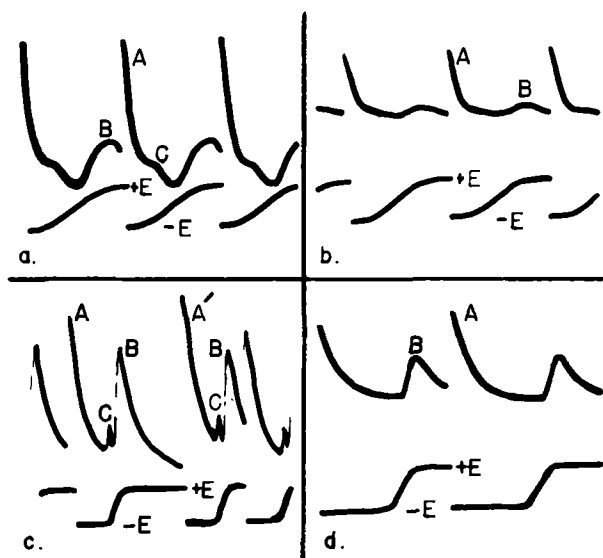


FIG. 7. Saw-tooth fields. (a) 100 cps; (b) 250 cps; (c) modified saw-tooth, rise time, 2.8 msec; (d) rise time, 2 msec.

occur when the field starts to decrease, while C' peaks appear when the field starts to rise in the case of uni-directional pulsing.

C and C' peaks decay rapidly compared with the corresponding B peaks. The C' peaks become smaller relative to the B peaks at lower frequencies. If the field strength is raised, the B peaks grow faster than the C peaks, indicating that B peaks are sensitive to the rate of growth of the applied field while C peaks are not.

Zalm and coworkers (5, 6) also report the appearance of C -like peaks under similar circumstances.

Intensity of the peaks seems to depend on the rate of growth of the field and on the time of steady field before or after field reversals (A' and B' peaks).

At very high frequencies (higher than the reciprocal of the critical time) still more complicated details appear, in particular a general decrease of the height of succeeding peaks in the green band as long as field reversals are going on (Fig. 8). This is much more conspicuous at still higher frequencies.

Finally, it should be pointed out that the patterns

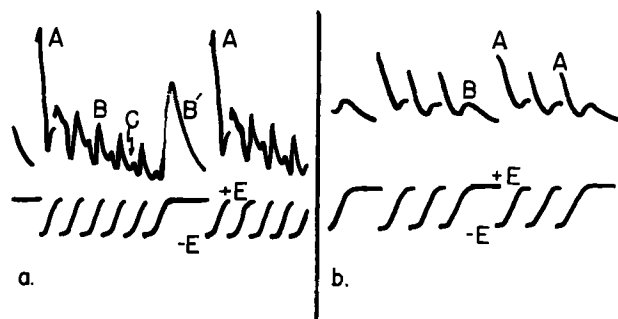


FIG. 8. Interrupted saw-tooth fields. (a) 1000 cps; (b) 1100 cps.

obtained for square pulses may be considered as simplifications of those described here inasmuch as only A -type peaks would be present.

Extinguishing effect.—If the cell is first exposed to near ultraviolet radiation and then, in addition, is placed under the influence of an electric field that is too weak to produce electroluminescence, the luminescence excited by ultraviolet radiation is diminished (14). The behavior resembles that observed for a long decay nonelectroluminescent ZnS:Cu-phosphor (15). This extinguishing effect seems to exist only in the green band. It appears with fields produced by potential differences as low as 2 volts.

INTERPRETATION

Basic assumptions.—A satisfactory basis for an interpretation must include, even if only in general terms, a description of the excitation mechanism, the luminescence processes for green and blue emission bands, and the properties of the effective internal field as distinguished from the applied external field.

Although there is no general agreement on a definite solution of the problem of the excitation mechanism, it is reasonable to assume some collision process between electrons accelerated by the field and luminescence centers. The details of such collision excitation are irrelevant as far as these considerations are concerned. The picture proposed by Curie (7) and Piper and Williams (11) (field excitation of donors, creating conduction electrons being accelerated to impact ionize or excite activators) may be accepted readily. In any case, the assumption of collision processes certainly implies that excitation must depend on the field strength, the number of electrons available for acceleration in the conduction band, and the number of centers available for excitation.

The rapid natural decay of blue luminescence, which can be described by an exponential law (Fig. 4), suggests the assumption that the blue luminescence is probably due to excitation of electrons from the ground level to some excited level within the same center, followed by an almost immediate direct transition to the ground level. Decay of the phosphor's green luminescence, however, is much slower and follows a more complicated law. The green luminescence, therefore, is probably due to some phosphorescence process with a delaying mechanism such as traps or metastable states and with transitions involving the conduction band. Similar assumptions are made by Burns (8). Also, the strong extinguishing effect observed for green luminescence only is evidence that electrons excited from green centers reach the conduction band where they can be removed by the field and made ineffective by

nonradiative transitions as considered in another case (16).

It is further assumed that green centers are excited with high efficiency, so that the number of excitable green centers strongly depends on the rate at which they are refilled. The efficiency of exciting blue centers may or may not be high. In any case, the number of excitable blue centers will remain practically unchanged because of the fast rate of refilling indicated by fast natural decay. The term "excitable center" shall indicate that the total number of centers may be much larger, but that for every field strength there may be a certain limit as to how many centers can be excited out of the total. This limit may be related to the energy level of the center.

The effective field strength in a semiconducting particle embedded in a dielectric material between metal electrodes may be expected to be different from the field applied to the electrodes. At any one instant, the effective field may be different in various regions of the phosphor particle, since strong fields are probably concentrated near the surface. One should also expect that the effective field changes in time as space charges or polarization charges build up. Thus, the field in the interior of the particle will diminish because of the polarization charges drawn to the surface by the field. If the applied field is suddenly removed after the polarization charges have accumulated, these charges themselves should create a field whose strength would decrease as the charges flow back to a neutral distribution. Therefore, if the applied field is removed or reversed faster than the polarization charges would disperse, one would expect an effective field with a maximum value shortly after application of the field reversal or removal. For slower changes of the external field, this maximum would shift to longer times. The rates of change of field and accumulation and dispersal of space charges, therefore, determine the growth and decay of the internal field.

This picture is essentially identical with ideas proposed by Kallmann (10) to explain photoconductivity experiments. He infers from his observations that at least some part of the polarization charge is trapped so that a quasi-persistent polarization of the phosphor particle is produced, which builds up and decays very slowly. Waymouth and Bitter (4) arrived at similar conclusions from electroluminescence experiments.

If the field is only removed or diminished and not reversed, the polarization charges not only provide the effective field at the removal time, but also act as an additional supply of electrons released for recombination with holes.

There is evidence that electroluminescence is restricted to small regions of the phosphor particle

(6, 17). The discussion applies to this sensitive region only. However the variation of luminescence in time is of more concern than its location.

General discussion.—The basic assumptions enumerated above appear sufficient to account for most of the observations, at least qualitatively. The general mechanism responsible for the production of peaks like those in Fig. 1 may be described as follows. At the time the field is suddenly applied or reversed, electrons in the conduction band are accelerated by the field and excite luminescence centers by some collision process. In due time, conduction electrons pile up near one surface, weakening the effective field in the interior of the particle (or its sensitive region) with a corresponding decrease of the phosphor light output. The break in decay curves at the critical time of about 0.7 msec indicates two polarization processes, a fast one and a slow one which may be identified with the piling up of electrons held either in the conduction band by the field alone or in traps producing the "persistent" polarization.

At removal of the field, the polarization charges for some time provide the field necessary for occurrence of the peaks. Similarly, at field reversals the effective field is, for the first moment, the sum of the applied field and the field of the polarization charges, after which the effective field decays again.

It is easily understood that the shape of the luminescence peaks depends on the manner of growth and decay of the internal field which itself is determined by the wave shape of the applied field. Therefore, the *B* peaks and *D* peaks in Fig. 6 to 8 are considered generally to be of the same origin as the *A* peaks, the difference in shape being due only to the difference in field shapes.

Results obtained with rectangular field pulses (Fig. 5) furnish further information that shall be used to specify the model presented here in some respect and to test its applicability.

Events leading to the blue curve of Fig. 5 may be described as follows. At some field reversal, blue centers are excited, but the excited electrons return almost immediately to their ground levels so that there is always a sufficient number of excitable centers. Decay of the blue luminescence must, therefore, be considered as being due to decay of the effective field, although the intensity may not be a direct measure of the field strength. If the field is reversed again, the situation is the same as before: a sufficient number of excitable centers and an effective field that decays from a maximum value at the time of reversal. Therefore, an intensity increase equal to that observed before is found.

For intervals shorter than the critical time, polarization charges apparently do not have sufficient time to accumulate so that the effective field con-

tributed by these charges at the time of reversal is smaller than it would have been for longer time intervals, with a corresponding decrease of the light output so that P_2 decreases as it is observed.

The typical green curve of Fig. 5 can also be understood on the basis of these general assumptions. The centers excited at some field reversal are refilled relatively slowly since the green luminescence involves trapping. A subsequent field reversal, therefore, does not find the same number of excitable centers as before, but, because one assumed the field excitation of green centers to be very efficient, all the refilled centers will be excited again. This brings the number of empty centers, the number of excited electrons, and the luminescence intensity to the same absolute value as at the previous field reversal.

While the effective field lasts, i.e., within the critical time, green decay is much faster than natural decay. This indicates an additional loss of electrons from the conduction band caused by the field. This may be due to the same kind of "field-induced non-radiative transitions" that had to be introduced (16) for the interpretation of the quenching effect of the field on a phosphor during ultraviolet excitation, but there may be still another mechanism involved. During the short time of excitation by the field pulse, the traps, which are essential for the slow natural decay, may not fill as completely as in the case of the continuous ultraviolet excitation; but, in any case, the quenching effect, for whose existence there is independent evidence, should be a contributing factor.

The critical time, interpreted here as the time necessary to pile up polarization charges, is of the same order of magnitude as the lifetime of an electron in the conduction band as determined by Curie (18). This is plausible since, on the one hand, a much shorter lifetime would make it impossible to collect a sufficient number of electrons in the cloud of drifting polarization charges; and since, on the other hand, a much longer lifetime would leave so many electrons in the conduction band that polarization charges could not be restricted to a relatively small region near the surface. In order that phenomena as described above can be observed, the indicated relation between lifetime and piling-up time should, therefore, be obeyed in the particular phosphor.

As pointed out further above, the dependence of C and C' peaks on field strength is different from that observed for B peaks. The mechanism for C and C' peaks should, therefore, be of a different kind. It is assumed that recombination of excess electrons released whenever the external field is diminished after polarization charges had time to pile up is responsible for the appearance of C peaks. Polarization charges flowing back during a time of "field

off" will be stopped suddenly when the field is applied again before they have been neutralized. They will then have an additional change of transitions, which may produce the C' peaks. At low frequencies, these peaks should disappear, as is observed, since the flow of the polarization charges has ceased before renewed field application. Both C and C' peaks should be absent for the blue band since the blue luminescence does not involve transitions from the conduction band.

The foregoing discussion provides an adequate description of the more important qualitative features of the electroluminescence patterns. Further details are considered below.

Details.—The difference between A and A' peaks in the green band is assumed to be due to the difference in numbers of excitable centers at the respective times of field reversal. For the A' peaks there is much more time for centers to be filled before the field is reversed than for the A peaks. Consequently, A' peaks are larger. There is no corresponding phenomenon for the blue peaks since the blue centers are filled much faster.

The pattern of Fig. 8 can be understood as being due to a combination of the effects previously considered, but already, without any reference to a mechanism, one should expect a decrease of the heights of subsequent B peaks in the green band since the green B peaks, according to experience, need a relatively long time to develop up to their maximum. This time is cut short while the high frequency field reversals are going on. The height of the B' peak, however, is normal again since there is sufficient time available.

The frequency dependence of the peak heights shown in Fig. 2 may also be understood on the basis of the picture developed here. Since, with increasing frequency, fewer electrons get back to the green centers before the beginning of the next half period, the number of electrons available for acceleration at this moment increases. Therefore, peaks of the blue luminescence should grow initially with frequency because of the increase in the number of accelerated electrons, but eventually the influence of the decrease of the effective field at field reversal because of the decrease of the number of polarization charges piled up during one half period must prevail. For the heights of the green peaks, it is necessary to take into account the fact that the number of filled green centers decreases with increasing frequency. This effect becomes unimportant only at extremely low frequencies. The fact that the frequency dependence follows empirically a logarithmic law is not yet understood. It may be purely fortuitous.

Finally, the general features of the electroluminescence patterns obtained with sinusoidal fields should also be governed by the processes consid-

ered here. In particular, one would expect *C*-like and *B*-like peaks, which may be distorted and shifted because of the different time characteristics of the fields. Indeed, the usually observed two peaks per half period may be identified with such peaks. The "in-phase" peaks correspond to *B* peaks, the "out-of-phase" peaks are equivalent to *C* peaks. A similar interpretation has recently been given by Curie (18).

The discussion above corroborates and supplements the general picture outlined in the previous sections, although not every detail has been treated. Thus, general aspects of the observed electroluminescence phenomena can be understood in terms of a few plausible assumptions on excitation, luminescence processes, and internal field.

ACKNOWLEDGMENTS

The authors would like to thank Dr. R. M. Talley for helpful discussions, and Mr. W. W. Talbert and Mr. P. N. Buford for their assistance in matters dealing with experimental design. They also thank the Sylvania Electric Company for supplying them with electroluminescent lamps, and Dr. J. F. Waymouth for information about the phosphors.

Any discussion of this paper will appear in a Discussion Section to be published in the June 1955 JOURNAL.

REFERENCES

1. W. W. PIPER AND F. E. WILLIAMS, *Phys. Rev.*, **87**, 151 (1952); C. W. JEROME AND W. C. GUNGLE, *This Journal*, **100**, 34 (1953).
2. J. F. WAYMOUTH, *ibid.*, **100**, 81 (1953).
3. G. DESTRIAU, *Phil. Mag.*, **38**, 700 (1947).
4. J. F. WAYMOUTH AND F. BITTER, *Electrochem. Soc.*, Enlarged Abstracts of Papers Presented by the Electronics Division, April 1953, Abstract No. 27.
5. P. ZALM, H. A. KLASSENS, AND G. DIEMER, *ibid.*, Abstract No. 28.
6. P. ZALM, G. DIEMER, AND H. A. KLASSENS, *Philips Research Repts.*, **9**, 81 (1954).
7. D. CURIE, *J. phys. radium*, **13**, 317 (1952); **14**, 135, 510, 672 (1953).
8. L. BURNS, *This Journal*, **100**, 572 (1953).
9. G. DÉCHÈNE, *J. phys. radium*, **9**, 109 (1938).
10. H. KALLMAN, Progress Reports, Contract No. DA 36-0398c-15297, U. S. Signal Corps, SCEL, Little Silver, N. J., September, 1952 and May, 1953.
11. W. W. PIPER AND F. E. WILLIAMS, *Bull. Am. Phys. Soc.*, **29**, 40 (1954).
12. H. H. HOMER, R. H. RULON, AND K. H. BUTLER, *This Journal*, **100**, 566 (1953).
13. E. KRAUTZ, *Z. Naturforschg.*, **4a**, 284 (1949). (Krautz has found similar values of *m* for the decay of Gudden-Pohl flashes.)
14. G. DESTRIAU, Private communication; T. MILLER, *J. Appl. Phys.*, **23**, 1289 (1952); M. UETA, *J. Phys. Soc. Japan*, **8**, 429 (1953).
15. G. DESTRIAU AND J. MATTLER, *J. phys. radium*, **11**, 529 (1950); F. MATOSSI AND S. NUDELMAN, *Phys. Rev.*, **89**, 660 (1953).
16. F. MATOSSI, *Naturwiss.*, **40**, 239 (1953); *ibid.*, **94**, 1151 (1954).
17. J. F. WAYMOUTH AND F. BITTER, Private communication.
18. D. CURIE, *J. phys. radium*, **14**, 672 (1953).

Measuring Problems and Techniques at A-C Furnace Arcs¹

W. E. SCHWABE

National Carbon Research Laboratories, Cleveland, Ohio

ABSTRACT

A quantitative investigation of an a-c electric furnace arc is dependent upon measurement of the true arc voltage. The electrical resistance of an a-c arc is a function of many variables including current, arc length, electrode composition, furnace atmosphere, and temperature. Experimental procedures specially adapted to arc voltage measurement have been evolved and are described, together with a unique circuit which automatically compensates an inherent measurement error.

INTRODUCTION

The electric arc furnace and its power supply circuit form a costly tool of production and must be constructed with the rugged simplicity necessary to continuous trouble-free operation. Such construction does not provide for the wide variation of circuit parameters desirable from a research viewpoint. In a three-phase furnace, electrophysical investigations of the arc are further complicated by the interaction of the three phases.

To facilitate a practical small-scale approach to fundamental investigations of the electric furnace arc, a laboratory size, single-phase experimental arc furnace was constructed. The furnace is rated at 100 kva and was built for operation with two graphite electrodes permitting a steel capacity of 250 lb. However, to permit a more accurate control of arc length, the furnace has been adapted to single electrode operation for electrodes up to three inches in diameter. The electrical circuit is completed to the furnace shell by means of a bottom electrode. An independent electrode-positioning mechanism permits push-button control of the arc length. Power is supplied from a 440-v a-c line through a 100-kva power transformer tapped and regulated to provide a continuous variation of secondary voltage up to 280 v. Current limitation is accomplished with a number of variable resistance and inductance elements, which may be connected individually or in combination to provide the ballast desired. Fig. 1 is a schematic diagram of the experimental arc furnace circuit.

In addition to a variety of conventional electrical meters, special photographic and high-speed recording equipment is used in studies of the arc.

An extremely important parameter in an a-c electric arc furnace circuit is the arc voltage, i.e.,

the voltage drop between the electrode tip and the melt surface.

Measuring the arc voltage is a problem from both a technical and physical viewpoint. It is the objective of this paper to describe problems associated with the measurement of arc voltage, to discuss measuring techniques together with experimental results, and to propose a standard terminology for certain electrical quantities heretofore classified as arc voltage.

MEASUREMENT OF A-C ARC VOLTAGE

Measurement errors may be roughly divided into two groups as follows:

(a) external errors—introduced by the inclusion in the measurement of arc voltage, unwanted voltage drops across circuit elements adjacent to the arc; such elements include the electrode, the melt, and the furnace shell;

(b) internal errors—due to the electrophysical characteristics of arc conduction.

External errors.—An ideal measurement of arc voltage would be accomplished by connecting the leads of a suitable measuring device to the terminal points of the arc, the so-called anode and cathode spots. From a practical viewpoint such direct measurements are impossible, due to the high temperature existing inside the furnace, particularly in the arc zone. Even probe measurements, normally restricted to a short time interval, may not be applied because of the erratic travel of anode and cathode spots, characteristic of an open arc. Fig. 2 is a sequence of three photographs taken at an open arc and shows the successive half cycle locations of the arc stream occurring during each film exposure of approximately 1/30 sec (four electrical half cycles based on 60-cycle supply frequency).

In order to permit practical arc voltage measurements, meter connections have been established at the electrode clamp and on the arc furnace shell. Such measurements include the unwanted series voltage drops previously described.

¹ Manuscript received March 1, 1954. This paper was prepared for delivery before the Chicago Meeting, May 2 to 6, 1954.

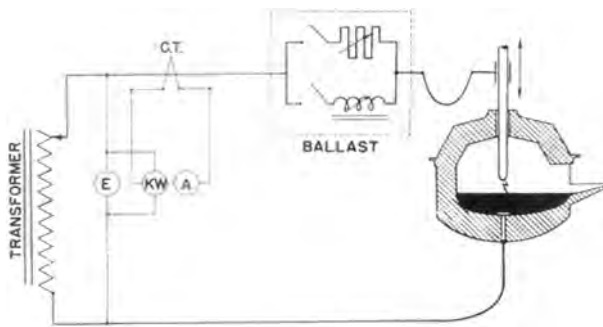


FIG. 1. Schematic diagram of experimental circuit

It is well to point out that in submerged arc furnaces the problem of measuring the arc voltage is further complicated by the contact between charge and electrode which forms parallel current paths shunting the arc, and so increasing the current through the series elements. The author's investigations have dealt primarily with the open arc, excluding detailed studies of the parallel resistance effect.



FIG. 2. Arc in a melting furnace. Three consecutive frames of a movie taken at a speed of 16 frames/sec.

The magnitude of the inherent series error has been determined for the author's circuit by lowering the electrode into the melt and measuring the short-circuit current as well as the voltage drop across the included circuit elements.

Fig. 3 is an oscillogram taken from such a test. One cycle of short-circuit current and the associated

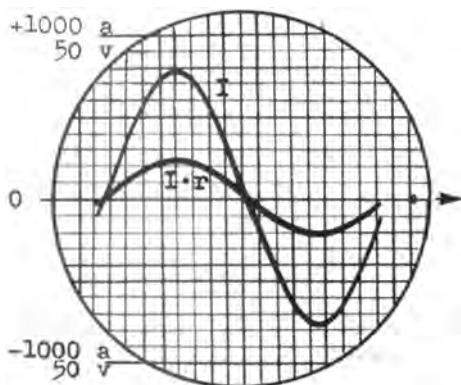


FIG. 3. Oscillogram showing the current I and the associated voltage drop $I \cdot r$ of an electrode being short-circuited with the melt.

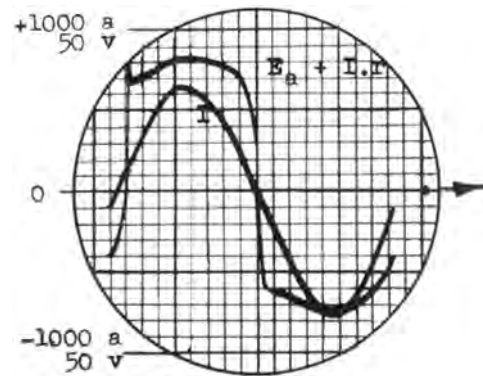


FIG. 4. Oscillogram of arc current I and arc voltage E_a including $I \cdot r$ drop.

voltage drop are plotted vs. time on the screen of a cathode-ray oscilloscope. One scale division represents 100 amp and 5 v. Peak values are 780 amp and 12 v, respectively.

An arc is established by raising the electrode from the short-circuit position, this operation being characterized by a decrease in current from its short-circuit magnitude to a value governed by the arc length and the parameters of the external circuit. Fig. 4 illustrates one cycle of current with the uncorrected arc voltage, which includes the drop previously discussed. The voltage trace is a combination of a square and a sinusoidal wave.

The error made by including the series $I \cdot r$ drop may be eliminated through a tedious point-by-point subtraction based on a knowledge of the instantaneous values of I and R . To overcome the necessity of such an operation, however, a relatively simple circuit arrangement has been developed which automatically eliminates the unwanted $I \cdot r$ drop from the recorded values of arc voltage. Both the arc and the electrode-melt-shell combination are considered to be purely noninductive resistance elements, and each in simple series circuit with the arc. Therefore, if a voltage equivalent to that across these elements, but of opposite polarity, be impressed in the metering circuit, the error is automatically canceled at every instant. The necessary voltage

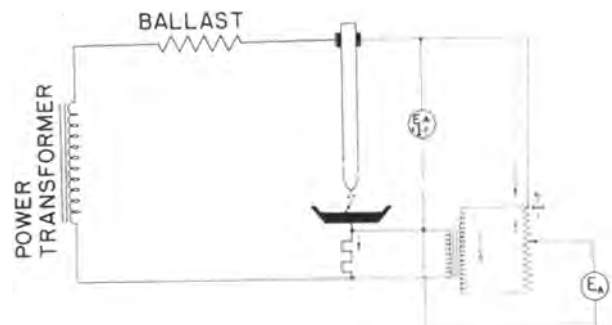


FIG. 5. Negative feedback circuit applied to measurement of arc voltage.

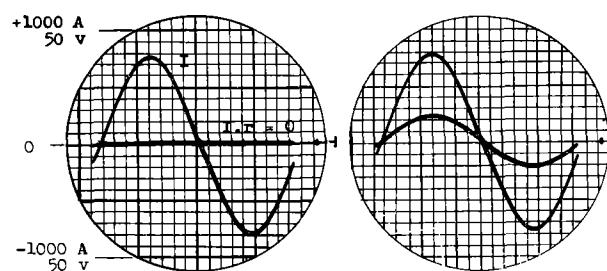


FIG. 6. Oscillograms of short circuit current and $I \cdot r$ voltage drop. *Left*, $I \cdot r$ drop cancelled; *right*, $I \cdot r$ drop present as shown in Fig. 3.

drop is readily obtained from a noninductive shunt in series with the arc, and the reversal of polarity is accomplished with a transformer. Fig. 5 illustrates the essential features of such a negative feedback circuit.²

The negative feedback circuit is very easily calibrated by establishing a short circuit between electrode and melt, and adjusting the potentiometer to precisely compensate the inherent $I \cdot r$ drop. Fig. 6 illustrates one cycle of short-circuit current and the compensated $I \cdot r$ drop. For purpose of comparison, the short circuit current and uncorrected $I \cdot r$ traces of Fig. 3 are also shown.

Fig. 7 is an arc voltage and current trace in which the $I \cdot r$ drop has been compensated by the negative feedback circuit. The uncorrected trace of Fig. 4 has been inserted for comparison. Note that the sinusoidal cap on the voltage trace of Fig. 4 has been eliminated with the negative feedback circuit, and that the voltage trace of Fig. 6 now approaches a square wave. Other changes in the voltage and current wave forms of the two oscillograms are attributed to changes in the arc during the time elapsed between the two photographs.

It is of interest at this point to call attention to the fact that in Fig. 7 peak values of both voltage and current differ in each half cycle, the voltage reaching peak values of 33 and 25 v, respectively, with current peaks of 660 and 630 amp, respectively.

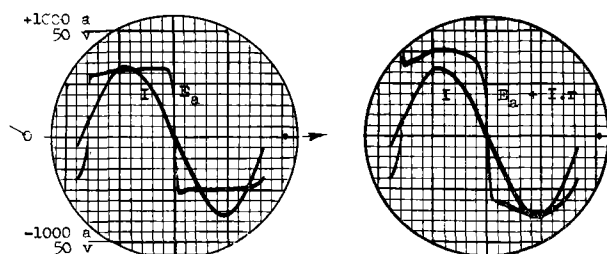


FIG. 7. Oscillograms of current I and arc voltage. *Left*, corrected arc voltage; *right*, uncorrected arc voltage as shown in Fig. 4.

² It is conceivable that this circuit be modified to compensate the true impedance drop given by $I \cdot z$, where $z = \sqrt{r^2 + x_L^2}$, in cases where the inductive component assumes significant proportions.

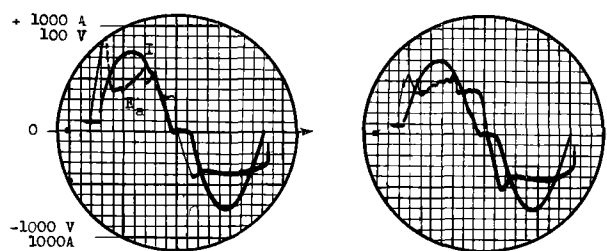


FIG. 8. Disturbance of the arc voltage during melt-down of steel. Upper half-cycles: melt = cathode, lower half-cycles graphite-electrode = cathode.

This effect is primarily due to differences between the cathode behavior of graphite and iron, as the polarity reverses with the alternating current. During the first half cycle when the graphite is cathode, a better arc conductivity is shown by the higher current and lower arc voltage. During the succeeding half cycle the converse is true.

The arc studied in Fig. 4 and 7 was struck between a graphite electrode and a slag-covered melt. Presence of a slag on the surface of the melt has a smoothing effect on the arc voltage wave form. In the case of an arc between a graphite electrode and liquid metal in the absence of slag, the arc voltage wave form is distorted by an erratic high-frequency disturbance in the half cycle during which the melt is cathode. This disturbance also deforms the current trace. The oscillograms of Fig. 8a and b were taken at an arc struck directly to liquid steel and illustrate the effect of this disturbance on the arc voltage wave forms.

Finally, it should be mentioned that, as an alternate source, the opposing voltage for the negative feedback circuit may be obtained from the secondary circuit of a current transformer connected in the furnace circuit, and that a calculation of the required opposing voltage may be made if the circuit parameters are known. Such a calculation eliminates the necessity of conducting a short-circuit test.

This negative feedback principle is readily adaptable to measurements of arc power and resistance and may find application in the precise determination of maximum arc power occurring at optimum current as well as in automatic electrode regulating systems.

Internal errors.—Having eliminated external errors with the negative feedback circuit, calculations of arc power based on independent measurements of arc voltage and current are still in error by a varying positive quantity. Through an oscillographic analysis of individual half cycles of arc voltage and current, it was concluded that conventional voltmeters indicating either rms or average values receive a positive influence from a portion of each half cycle of voltage which does not contribute to arc power,

so that arc power computations based on independent voltage and current measurements are necessarily in error.

Each half cycle of arc voltage is characterized by an initial period during which the open-circuit voltage rises to the value necessary to re-ignite the arc. As soon as the arc strikes, the voltage drops suddenly to a relatively constant value for the remainder of the half cycle. Compared with submerged arc, the open arc of an electric steel furnace is subject to a more rapid heat dissipation accompanied by a more rapid cooling of both anode and cathode spots, and so necessitating a relatively higher ignition voltage in each half cycle. The time delay until this ignition voltage is reached varies with the nature of the circuit. In a circuit containing little reactance, the time delay between zero voltage and ignition voltage is increased, whereas the phase displacement between current and voltage due to the inductance in a conventional arc furnace circuit promotes arc re-ignition by delivering an additional voltage of self-induction, $L di/dt$, which reaches its maximum when the current is near zero.

The oscillograms of Fig. 9 were taken at an arc circuit containing very little inherent reactance and demonstrate two extremes of ignition peak and correlated time delay. Fig. 9a shows the arc voltage and current at the beginning of a half cycle. The arc was struck between a graphite electrode and a slag-covered melt. Some time elapses before the current increases; this represents the ignition delay and, in this case, may be expressed as approximately five electrical degrees. Fig. 9a was taken at a short arc, the graphite electrode having been cathode in this particular half cycle. When the input voltage, governed by its sinusoidal variation, reaches the arc ignition value of approximately 15 v, a current flows.

In this case of short arc, there is no clearly defined ignition peak, and the arc voltage actually rises from its ignition value to remain almost constant

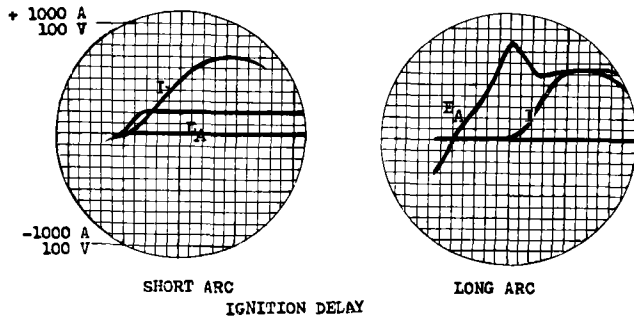


FIG. 9. Oscillograms showing parts of one half-cycle of arc current I and corrected arc voltage E_a . Left, short arc, current flow starts immediately; right, long arc, current flow delayed.

at twenty volts. This phenomenon is attributed to the superior conductivity of the short arc. In Fig. 9b the arc length has been increased, the other circuit parameters having been unchanged. In this case, the ignition delay is almost 45 electrical degrees, and the current flows only when an ignition voltage of about 90 v is reached. When the current flow is established, the voltage drops from its ignition value to 60 v and remains almost constant.

The time portion of the arc voltage from its intersection with the zero axis to the ignition peak is essentially the open-circuit voltage, and does not contribute significantly to the power of the arc. For this reason, it is referred to as the *passive* arc voltage. The time portion of the arc voltage during which a current flows has been designated the *active* arc voltage.

It is apparent that a conventional voltmeter responds to the passive as well as to the active arc voltage and that its over-all indication is higher than it should be. Arc power computations based on independent measurements of arc voltage and current are, therefore, in error by this varying positive value.

It should also be noted that in the case of prolonged ignition delay, the current does not reach its maximum at 90 electrical degrees as with a sine wave, but somewhat later. Although Fig. 9a and b illustrate the usual extremes of ignition delay, occasional delays of 55-60 electrical degrees have been observed.

Fig. 10 is a simplified reconstruction of another arc voltage trace. The input voltage in this case is 50 v rms (70.7 v peak). The ignition delay is 30 electrical degrees, and the ignition voltage is 35 v. The active arc voltage is 23.3 v and remains constant from 30 electrical degrees to 160 electrical degrees

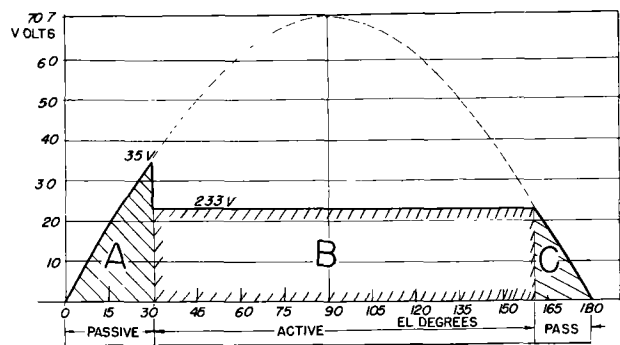


FIG. 10 Reconstruction of a typical arc voltage half-cycle. Areas A and C are passive; area B is active. Calculated meter readings of rms and average values:

Meter type	Indication	Active arc voltage (B)	Apparent arc voltage (A + B + C)	Error %
Dynamometer or thermo.	RMS	19.3	21.8	+13
Rectifier	Avg	16.4	19.3	+18

at which point it breaks down to zero. Areas A and C are passive, only area B being active in contributing to arc power.

The average and rms values for the entire voltage curve as well as for the active portion have been calculated. Both sets of calculations are based on a full half cycle (180 electrical degrees). The results of the calculations are listed in the table of Fig. 10 and indicate errors of +13 and +18% in the conventional meter readings of rms and average arc voltage, respectively. The error values calculated in this particular case are only indicative, since they apply only to the particular half cycle in question, although they do demonstrate the existence of a very considerable error.

MEASUREMENT OF ACTIVE A-C ARC VOLTAGE

It is apparent from the foregoing discussions that the active arc voltage for any short period may be measured by oscillographic means, provided that the negative feedback principle is applied. A much more desirable arrangement would provide a continuous rms meter reading of the active arc voltage. An intermediate solution may be based upon the ratio of watts to rms amperes to give the effective rms voltage. It can be assumed that the arc is a pure resistance, so that the power factor is unity. A major disadvantage of this wattmeter-ammeter method lies in the fact that two simultaneous readings are necessary. These readings are difficult to obtain, especially at melting furnaces during the melt down period, when current and arc power fluctuate rapidly.

To overcome the necessity of making two simultaneous readings, it is conceivable that the watt-

meter and ammeter indications might be combined in a single instrument so calibrated that its resultant continuous indication is watt/amp, or active rms arc voltage. Such a circuit has not been developed. A relatively simple electronic circuit is also conceivable, by means of which the voltmeter circuit is only closed when current is flowing.

The ratio of the active part of the arc voltage to the apparent arc voltage expressed as a percentage may be designated an *arc form factor*. Having measured the active and apparent arc voltage by means of the previously described wattmeter-ammeter method and an electrodynamicometer voltmeter, respectively, arc form factors of 80–90% at an open arc between a graphite electrode and steel have been determined.

Lower values between 60 and 70% were found at arcs with a more pronounced rectifying effect.

It is essential to keep in mind that such meter readings average the conditions of both half waves.

DISCUSSION

As previously stated, electrophysical investigations of the electric furnace arc conducted at producing installations have many practical limitations. Therefore, small-scale investigations utilizing an experimental furnace have been undertaken in preliminary studies of this important arc.

In the past, a considerable obstacle to the efficient collection of comparison data has been a certain ambiguity of terms commonly used in reference to the electrical operating characteristics of industrial arc furnaces. Clarification and standardization of these terms is considered to be of importance with respect to continued investigations of the complex physics of the electric furnace arc.

It is pointed out that the indications or reactions of many conventional electrical or electromechanical devices depend to some degree on the arc voltage as an activating impulse, and are positively influenced by both external and internal errors as described in the foregoing sections. The following definitions of terms related to a-c arc voltage are offered as a step toward a more thorough understanding of the electric furnace arc.

1. Gross A-C Arc Voltage

The alternating potential difference existing between the two nearest convenient points of the arc furnace circuit including the arc. This includes the voltage drop between the anode and cathode spots as well as that across resistance elements external to the arc, e.g., the potential difference between electrode clamp and furnace shell as measured by a voltmeter indicating rms or average values (see Fig. 11a).

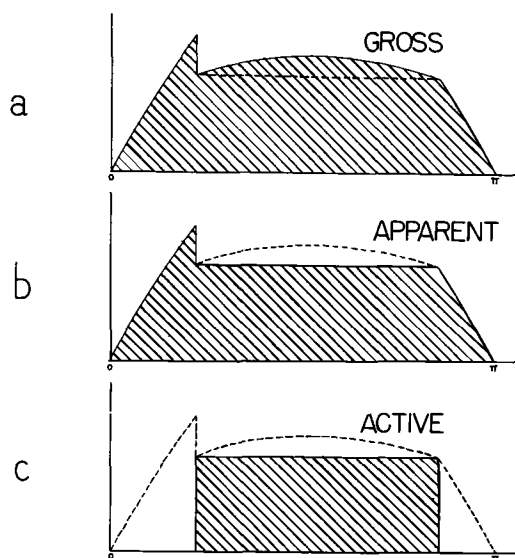


FIG. 11. Schematic definition of gross, apparent, and active a-c voltage.

2. *Apparent A-C Arc Voltage*

The alternating potential difference existing between the anode and cathode spots of an a-c arc. This can be measured either by connecting adequate probe contacts directly to the anode and cathode spots or, more practically, by making connections at external points and correcting the indication by means of a feedback circuit (see Fig. 11b).

3. *Active A-C Arc Voltage*

That portion of each individual half cycle of ap-

parent arc voltage contributing to arc power. The rms value of active arc voltage can be calculated from simultaneous wattmeter and ammeter readings (see Fig. 11c).

4. *Arc Form Factor*

The per cent ratio between the active and the apparent arc voltage.

Any discussion of this paper will appear in a Discussion Section to be published in the June 1955 issue of the JOURNAL.

Diffusion of Hydrogen and Deuterium in High Purity Zirconium¹

EARL A. GULBRANSEN AND KENNETH F. ANDREW

Westinghouse Research Laboratories, East Pittsburgh, Pennsylvania

ABSTRACT

Kinetics of the reaction of zirconium with pure hydrogen and deuterium was studied for 60°–250°C, H₂ pressures of 1.1–5.0 cm Hg, and composition range Zr–ZrH_{1.70}, using a vacuum microbalance method. The reaction was shown to be diffusion-controlled with diffusion occurring from a surface of constant concentration into a heterogeneous system.

The diffusion equation was solved for these conditions using the method originally developed by Neuman and recently applied by Wagner to this type of problem. Average concentration according to this view is given by

$$\bar{C} = 2.845 \frac{D^{1/2} t^{1/2}}{h}$$

where D is diffusion coefficient in cm²/sec, t is time in seconds, and h is specimen thickness in centimeters.

Plots of \bar{C} vs $t^{1/2}$ show this relationship to hold over wide variations in time, temperature, pressure, and specimen thickness. Diffusion coefficients were calculated and when plotted against $1/T$ on a logarithmic plot gave a heat of activation of 11,400 cal/mole. The corresponding entropy of activation was 2.7 cal/mole/°C.

The following equation expresses data for diffusion of hydrogen in zirconium:

$$D = 1.09 \times 10^{-3} e^{-11,400/RT} \text{ cm}^2/\text{sec}$$

For the composition range of Zr to ZrH_{1.6}, experimental data fit the proposed explanation for the reaction. At higher compositions, deviations were observed.

Diffusion of deuterium in zirconium was also studied and data found to fit the equation:

$$D_{D_2} = 0.73 \times 10^{-3} e^{-11,400/RT} \text{ cm}^2/\text{sec}$$

The relationship between the diffusion coefficient of hydrogen and deuterium was found to be 1.5. The theoretical value should be $\sqrt{2}$.

The diffusion mechanism proposed was verified by experimental results.

INTRODUCTION

Much of the work on the reaction of zirconium with hydrogen was reviewed by Smith in 1948 (1) and by Gulbransen in 1954 (2). Two studies have been made of the kinetics of the reaction with hydrogen. Gulbransen and Andrew (3) studied the rate of hydriding between 200° and 300°C using high purity metal and a source of highly purified hydrogen. Although some kinetic data were obtained, the rate of reaction was difficult to reproduce and appeared to be sensitive to pretreatment and to surface films. Since the initial surface oxide film was not removed and its importance was not recognized at that time, these kinetic results must

be interpreted in terms of an oxide-contaminated surface.

Bernstein and Cubicciotti (4) studied the permeation of zirconium by hydrogen at 545°–920°C. Again, results were difficult to reproduce, and evidence for a contaminating film was observed in all experiments.

Recent studies by Gulbransen and Andrew (5) showed that the room temperature surface oxide film has a remarkable inhibiting effect on rate of hydriding. Unless great care was taken to remove the initial oxide film and to purify the hydrogen, the rate of hydriding was limited by a surface reaction.

Since the mechanism of hydriding of zirconium may involve one or more diffusion processes, precise information on the phase diagram of zirconium-hydrogen alloys is required. Although Hägg (6)

¹ Manuscript received March 29, 1954. This paper was prepared for delivery before the Chicago Meeting, May 2–6, 1954.

studied the system earlier and showed the existence of several hydride phases, the ranges of homogeneity of these phases were not established.

To supplement this work, Gulbransen and Andrew (7) determined ranges of homogeneity of several phases from thermodynamic studies and from x-ray diffraction studies. In brief, for temperatures below 500°C, the ϵ -phase of Hägg was shown to have a composition range of $\text{ZrH}_{1.965}$ to $\text{ZrH}_{1.64}$, while the δ -phase has a range from $\text{ZrH}_{1.56}$ to $\text{ZrH}_{1.40}$. A two-phase region of α - and δ -phases exists for all compositions between zirconium saturated with hydrogen in solid solution and $\text{ZrH}_{1.40}$. At 250°C, the maximum temperature used in this work, the solubility of hydrogen in zirconium corresponds to the composition $\text{ZrH}_{0.001}$ (8).

With this new information on the phase diagram, and with techniques available for removing the initial surface oxide film and for purifying hydrogen, it was possible to study the mechanism of the reaction of pure hydrogen with a clean zirconium surface.

ANALYSIS OF DIFFUSION PROBLEMS

Wagner (9) has discussed the general problem of diffusion in binary systems of more than one phase. From a mathematical point of view this problem was similar to that of melting or solidification in which one substance changes into another with emission or absorption of heat. The common feature of these problems was the existence of a moving surface of separation between two phases, at which material or heat was being transferred. The original solution of the heat problem was due to Neuman and was presented in a book by Carslaw and Jaeger (10).

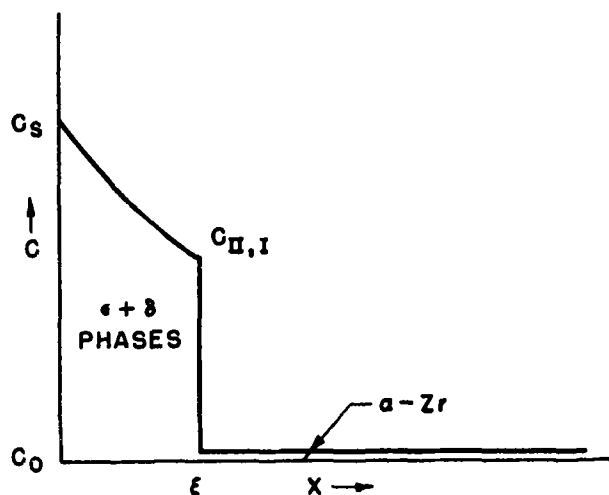


FIG. 1. Diffusion picture, hydrogen in zirconium (after Wagner). $t > 0$; $c_s = \text{ZrH}_{1.965}$; $c_{\text{II,I}} = \text{ZrH}_{1.40}$; $c_0 = \text{ZrH}_{0.001}$ at 250°C.

General picture.—Fig. 1 shows the analysis given by Wagner (9) for diffusion from a surface into a heterogeneous system for a flat plate. c_s is the surface concentration at $x = 0$, c_0 is the concentration at time $t = 0$, and $c_{\text{II,I}}$ is the concentration in phase II at the interface ξ with phase I. Diffusion proceeds from the surface in the homogeneous phase II. At time t the region of phase II extends from $x = 0$ to $x = \xi$.

Since hydrogen reacts with zirconium to form two hydride phases in addition to dissolving in α -zirconium, the validity of the diffusion picture shown in Fig. 1 may be questioned. However, the ϵ and δ hydride phases for most purposes can be considered as one phase, since their ranges of homogeneity are nearly continuous (7) and since their crystal structures are similar. The effect of solution of hydrogen in the metal is negligible since the solubility at 250°C is of the order of $\text{ZrH}_{0.001}$ (8).

General solution.—The following equation governs the diffusion process:

$$\frac{\partial c}{\partial t} = D \frac{\partial^2 c}{\partial x^2} \quad (\text{I})$$

Here the diffusion coefficient, D , is assumed to be independent of concentration. The boundary condition is

$$c = c_s \text{ at } x = 0 \text{ and } t > 0 \quad (\text{II})$$

At the interface $x = \xi$ the concentration of diffusing species in phase II is that relating to the equilibrium value between phases I and II.

$$c = c_{\text{II,I}} \text{ at } x = \xi \quad (\text{III})$$

When the interface is displaced by $d\xi$ for a time dt , the quantity $[c_{\text{II,I}} - c_0] d\xi$ of hydrogen must be supplied from the region $x < \xi$. Thus,

$$[c_{\text{II,I}} - c_0] d\xi = D dt \left(\frac{\partial c}{\partial x} \right)_{\xi=0} \quad (\text{IV})$$

A particular solution of equation (I) for boundary condition (II) is

$$c = c_s - B \operatorname{erf} \left(\frac{x}{2\sqrt{Dt}} \right), \text{ for } 0 < x < \xi \quad (\text{V})$$

Here, B is a constant and erf is the error function.

Wagner (9) assumes as does Neuman (10) that the plane of discontinuity is shifted proportional to $t^{1/2}$. Thus,

$$\xi = \gamma 2\sqrt{Dt} \quad (\text{VI})$$

Here, γ is a dimensionless parameter.

Substituting, one obtains

$$c_s - c_{\text{II,I}} = B \operatorname{erf}(\gamma) \quad (\text{VII})$$

$$c_{\text{II},1} - c_o = \frac{B}{\sqrt{\pi}} \exp(-\gamma^2) \quad (\text{VIII})$$

Eliminating B , one has

$$\frac{c_s - c_{\text{II},1}}{c_{\text{II},1} - c_o} = \sqrt{\pi} \gamma e^{\gamma^2} \operatorname{erf} \gamma \quad (\text{IX})$$

γ can be found from equation (IX) and B from equations (VII) and (VIII).

D is usually found by observing the displacement ξ and by the use of equation (VI). However, if the reaction is followed by a weight gain method, D must be obtained from the average concentration in the sample as a function of time.

Solution for weight gain method.—Let \bar{c} be the average concentration in phase II, $o < x < \xi$. Then,

$$\bar{c} = \frac{1}{\xi} \int_o^\xi c(x, t) dx$$

$$= \frac{1}{\xi} \int_o^\xi \left[c_s - B \operatorname{erf} \frac{x}{2\sqrt{Dt}} \right] dx \quad (\text{X})$$

$$= \frac{1}{\xi} \left[c_s \xi - B \int_o^\xi \operatorname{erf} \frac{\gamma x}{\xi} dx \right] \quad (\text{XI})$$

Integrating,

$$\bar{c} = c_s - B \operatorname{erf} \gamma + \frac{B}{\gamma\sqrt{\pi}} (1 - e^{-\gamma^2}) \quad (\text{XII})$$

This shows that \bar{c} is independent of t .

Substituting (VII) and rearranging,

$$\frac{\bar{c} - c_{\text{II},1}}{c_s - c_{\text{II},1}} = \frac{1 - e^{\gamma^2}}{\gamma\sqrt{\pi} \operatorname{erf} \gamma} \quad (\text{XIII})$$

Using this analysis, equations (IX) and (XIII) are plotted as a function of γ . From the plot of equation (IX) a value for γ is obtained and from a plot of equation (XIII) and this value of γ , a value for

$$\frac{(\bar{c} - c_{\text{II},1})}{(c_s - c_{\text{II},1})}$$

can be obtained.

From these plots $\gamma = 0.425$ and

$$\frac{\bar{c} - c_{\text{II},1}}{c_s - c_{\text{II},1}} = 0.485$$

Now an expression can be written for the average concentration \bar{C} over the whole specimen:

$$\bar{C} \frac{h}{2} = \bar{c} \xi + c_o \left(\frac{h}{2} - \xi \right) \quad (\text{XIV})$$

Here, $h/2$ is the half thickness and c_o the solubility of hydrogen in α -Zr. For temperatures of 250°C and lower, c_o has a value of 0.001 or less in terms of the ratio H/Zr and is, therefore, negligible.

Substituting equation (VI) and (XIV) and the values for γ and \bar{c} ,

$$\bar{C} = 2.845 \frac{D^{1/2} t^{1/2}}{h} \quad (\text{XV})$$

For the 0.0127 cm specimens, this equation becomes

$$\bar{C} = 224 D^{1/2} t^{1/2} \quad (\text{XVI})$$

and for the 0.0508 cm specimens,

$$\bar{C} = 56 D^{1/2} t^{1/2} \quad (\text{XVII})$$

In deriving equation (XV) from (XIV) it is assumed that c_s is constant and independent of pressure. Phase diagram studies by Gulbransen and Andrew (7) show that c_s has a value of 1.965 in terms of the ratio H/Zr, and for temperatures of 250°C and lower, c_s is independent of pressures of the order of 1 cm Hg and higher.

Testing of the mechanism of the reaction.—The reaction mechanism upon which equation (XV) is based can be tested experimentally. First, plots of \bar{C} vs. $t^{1/2}$ can be used to test the square root of time relationship. Second, use of different thicknesses of samples tests the validity of equation (XV). Third, use of both hydrogen and deuterium having different diffusion coefficients gives an additional way of testing equation (XV). Fourth, the analysis assumes a constant value for c_s . The effect of pressure, therefore, should be negligible. Fifth, a plot of $\log D$ vs. $1/T$ should give a straight line and a reasonable heat of activation. Sixth, the entropy of activation of the diffusion process should have a value near zero or slightly positive.

EXPERIMENTAL

A vacuum microbalance was used to determine the rate of reaction of hydrogen with the metal. Its construction and use has been described in previous publications (11, 12). The sensitivity of the balance was 1.25 divisions (0.00125 cm) per microgram for the 0.05 g sample, and the weight change was estimated to $\frac{1}{4}$ of a division (0.20×10^{-6} g).

A mullite furnace tube sealed directly to the Pyrex glass system contained the specimen. The vacuum behavior of this system has been described (13). Special precautions necessary for the study of zirconium have also been described (5). In all experiments described here, the system and specimen were pumped for at least 15 hr to minimize contamination of the gas atmosphere by degassing of the walls of the vacuum system.

Specimens were sheets of zirconium 0.0127 and 0.050 cm thick. Two weights of specimen were used, 0.0486 g or 0.4995 g. The larger specimens were used for experiments at 60°–100°C where the

TABLE I. Analysis of zirconium samples

	Foote Zr typical wt %
Si	0.01
Fe	0.04
Al	0.01
Cu	<0.01
Ti	0.03
Mn	<0.001
Ca	0.01
Mg	<0.003
Pb	<0.001
Mo	<0.001
Ni	0.01
Cr	0.001
Sn	0.001
W	<0.001
N	<0.01
O	<0.01
H	<0.02
C	<0.001
Hf	2.40

amount of reaction was small, while the smaller specimens were used where a large reaction with hydrogen was expected.

Pure hydrogen or deuterium was prepared by diffusing the purified electrolytic hydrogen or high purity grade of deuterium (99.66% D₂) through a palladium tube (11). To minimize contamination the gas was prepared immediately before use.

High purity iodide zirconium was obtained from Foote Mineral Company. The analysis is given in Table I. All specimens were given an abrading and cleaning treatment as previously described (5). They were placed in turn on the balance, and the tube sealed off. The specimen and vacuum system was pumped for 15 hr or longer. Before reacting with hydrogen, each sample was heated to 700°C in high vacuum for 1–2 hr.

RESULTS AND DISCUSSION

General

Fig. 2 shows a series of weight gain vs. time curves for the hydriding of zirconium at 150°–250°C and for a hydrogen pressure of 5 cm Hg. A new specimen was used for each experiment. For the area and weight of the specimens, a weight gain of about 715 $\mu\text{g}/\text{cm}^2$ corresponds to a concentration of $\text{ZrH}_{1.965}$. In several of the experiments shown in Fig. 2, this concentration was achieved. No visual evidence was found for the presence of an oxide film after concluding the experiment.

Fig. 3 shows a similar series of curves for 60°–125°C. The curves were of similar shape to those of Fig. 2. However, the maximum concentration at-

tained in these experiments for one hour of reaction was $\text{ZrH}_{0.2}$.

There is no evidence of an induction period which suggests that the surface was free of oxide film and that the reaction is diffusion-controlled. Previous studies (5) have shown that very thin oxide films (a) exert a strong inhibiting influence on the hydrogen reaction, (b) were responsible for the observed induction period of the reaction, and (c) explain many of the supposedly inert characteristics of the metal to reaction with hydrogen.

Rate law correlation.—To test the mechanism of reaction, the average concentration \bar{C} was plotted against the square root of time according to equation (XV). Fig. 4 shows this type of plot for the 250° and 175°C experiments. The 250°C data follow a straight line relationship up to a concentration corresponding to an H/Zr ratio of 1.60 or the limit of the two-phase region. The 175°C data show a straight line relationship to the concentration limit of the experiment, namely, a value of H/Zr of 0.86.

Fig. 5 shows similar plots for the 60° and 100°C experiments. Although only the initial stage of the reaction was studied, straight line relationships were

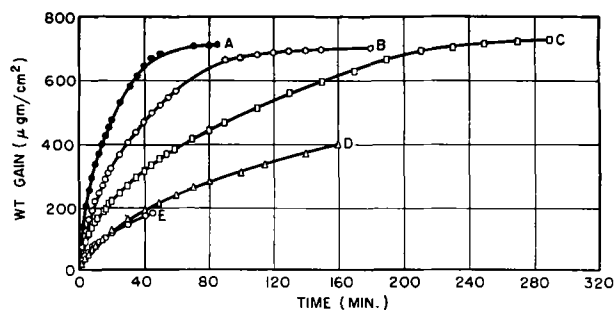


FIG. 2. Effect of temperature on hydriding zirconium. Curve A, 250°C, 5 cm of Hg of H₂; curve B, 225°C, 5 cm of Hg of H₂; curve C, 200°C, 5 cm of Hg of H₂; curve D, 175°C, 5 cm of Hg of H₂; curve E, 150°C, 5 cm of Hg of H₂.

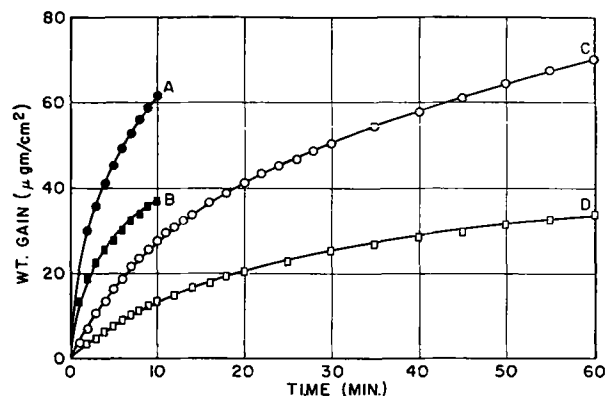


FIG. 3. Effect of temperature on hydriding zirconium. Curve A, 125°C, 2.3 cm of Hg of H₂; curve B, 100°C, 2.4 cm of Hg of H₂; curve C, 80°C, 2.4 cm of Hg of H₂; curve D, 60°C, 2.4 cm of Hg of H₂.

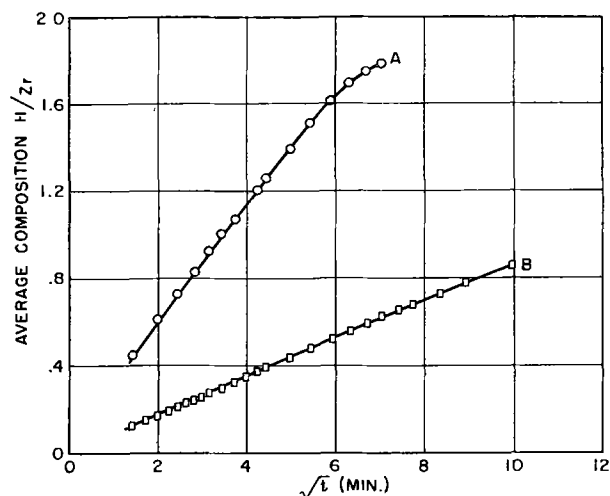


FIG. 4. Effect of temperature on hydriding zirconium. Curve A, 250°C, 5.0 cm of Hg of H₂; curve B, 175°C, 5.0 cm of Hg of H₂.

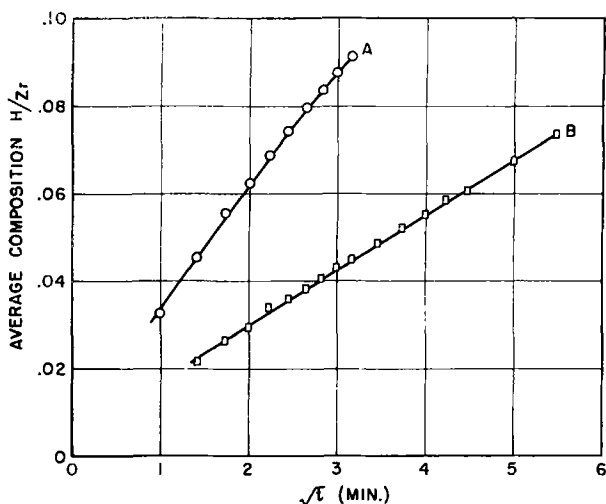


FIG. 5. Effect of temperature on hydriding zirconium. Curve A, 100°C, 2.4 cm of Hg of H₂; curve B, 60°C, 1.4 cm of Hg of H₂.

found. Thus equation (XV) adequately describes the time behavior, including the assumption made by Wagner on the movement of the interface between phases.

Effect of pressure.—Fig. 6 shows \bar{C} vs. $t^{1/2}$ plots of the data for two experiments at 225°C in which the pressure was varied from 1.1 to 5.0 cm of Hg. Slopes of the two plots were identical. The difference between the two curves was due to the fact that the buoyancy correction² was not applied to the data. Hence the effect of pressure on the rate of hydriding was negligible, and the surface concentration c_s was essentially ZrH_{1.965}. This conclusion was also supported by thermodynamic evidence (7).

Effect of sample shape.—According to equation

² This correction was a result of thermal convection currents set up in the furnace tube. It could be evaluated from the final vacuum reading.

(XV) the sample thickness, h , affects the slope of the \bar{C} vs. $t^{1/2}$ plot by the factor $1/h$. Fig. 7 shows a comparison of this type of plot for two thicknesses of metal, 0.0127 and 0.0508 cm. The effect of h on the plots was that predicted by equation (XV).

Calculation of Diffusion Coefficients

Equation (XV) was used to calculate diffusion coefficients from the \bar{C} vs. $t^{1/2}$ plots. These are summarized in Table II. Fig. 8 shows these data on a log D vs. $1/T$ plot, and from the slope a heat of activation of 11,400 cal/mole was calculated. Data for samples of different thicknesses were included.

D_0 was calculated from the equation

$$D = D_0 e^{-\Delta H^*/RT} \quad (\text{XVIII})$$

Here, D_0 was the value of D at infinite temperature, and ΔH^* was the heat of activation of diffusion. The values of D_0 were tabulated and an average value of 1.09×10^{-3} was calculated. The data could be represented by

$$D = 1.09 \times 10^{-3} \times e^{-11,400/RT} \text{ cm}^2/\text{sec} \quad (\text{XIX})$$

The value of 11,400 cal/mole for the heat of activation of diffusion for hydrogen in zirconium

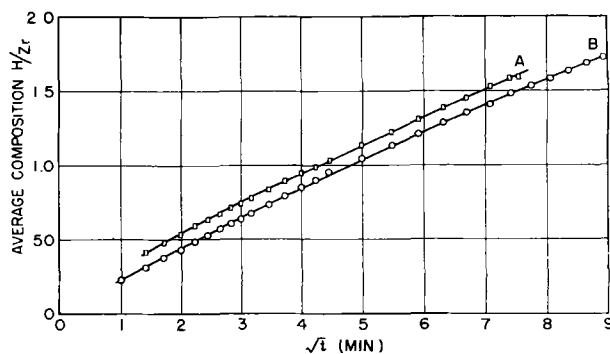


FIG. 6. Effect of pressure on hydriding zirconium. Curve A, 225°C, 5 cm of Hg of H₂; curve B, 225°C, 1.1 cm of Hg of H₂.

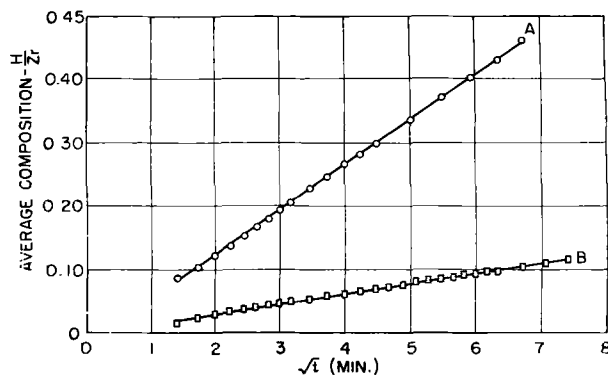


FIG. 7. Effect of sample thickness on hydriding zirconium. Curve A, 0.0127 cm thick, 150°C, 2.4 cm of Hg of H₂; curve B, 0.0508 cm thick, 150°C, 5.0 cm of Hg of H₂.

TABLE II Diffusion data hydrogen in zirconium

$t^{\circ}\text{C}$	$1/T \times 10^3$	D_{avg} cm^2/sec	D_0 cm^2/sec
60	3.0021	4.60×10^{-11}	1.341×10^{-3}
80	2.832	7.09×10^{-11}	0.784×10^{-3}
100	2.680	2.54×10^{-10}	1.178×10^{-3}
120	2.544	3.25×10^{-10}	0.705×10^{-3}
125	2.512	6.43×10^{-10}	1.144×10^{-3}
150	2.360	1.625×10^{-9}	1.26×10^{-3}
175	2.232	2.470×10^{-9}	0.876×10^{-3}
200	2.114	6.02×10^{-9}	1.099×10^{-3}
225	2.008	1.33×10^{-8}	1.33×10^{-3}
250	1.912	2.215×10^{-8}	1.217×10^{-3}
			avg 1.09×10^{-3}

appears to be reasonable since value heats of activation of 5,740-10,100 cal/mole have been observed (14) for the diffusion of hydrogen in palladium. The most reliable work on diffusion of hydrogen in palladium gave a value of 5,740 cal/mole (15, 16).

Calculation of Entropy of Activation

One of the best ways to check on diffusion results is to make an approximate calculation of the entropy of activation using the classical theory of diffusion as restated by Zener (17). According to this theory, D_0 is given by the expression

$$D_0 = ga^2\nu e^{\Delta S^*/R} \quad (\text{XX})$$

Here, a is the distance between sites for diffusion, ν is the frequency of vibration along the path of the

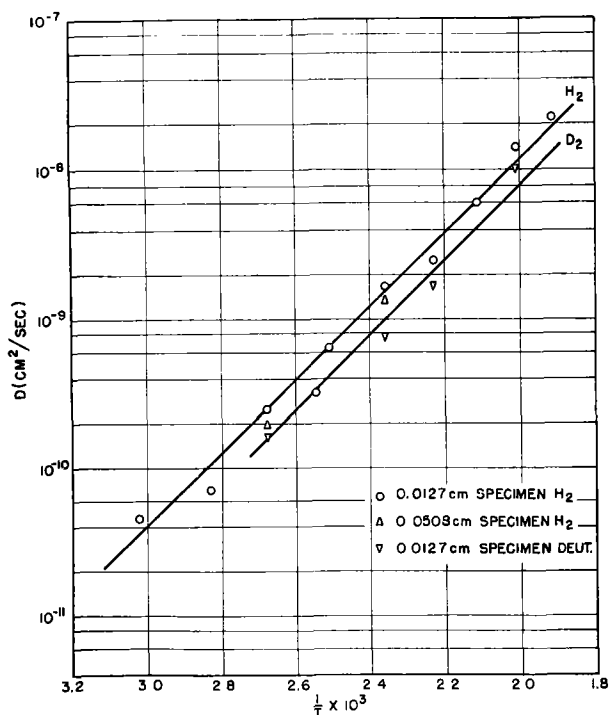


FIG 8. D vs. $1/T$ log plot (60°-250°C). $\Delta H = 11,400$ cal/mole; $P = 1.1-5.0$ cm of Hg of gas

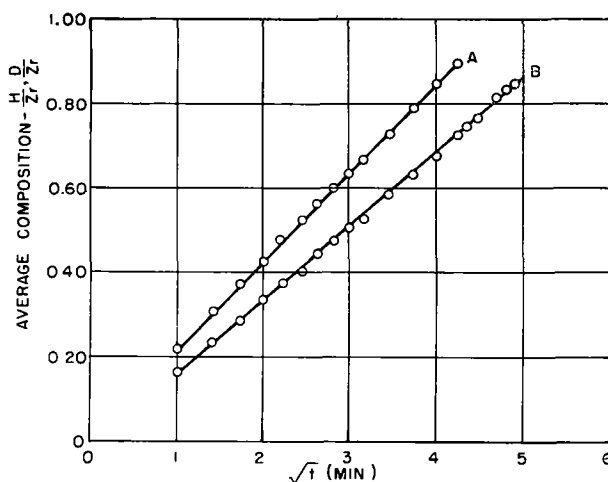


FIG 9 Comparison of reaction of hydrogen and deuterium with zirconium Curve A, H_2 , 225°C, 1.1 cm of Hg; curve B, D_2 , 225°C, 1.8 cm of Hg

TABLE III. Diffusion data deuterium in zirconium

$t^{\circ}\text{C}$	$1/T \times 10^3$	D , cm^2/sec	D_0 , cm^2/sec
100	2.680	1.62×10^{-10}	7.5×10^{-4}
150	2.360	7.70×10^{-10}	6.0×10^{-4}
175	2.232	1.64×10^{-9}	5.8×10^{-4}
225	2.008	1.023×10^{-8}	10.0×10^{-4}
			$D_0 \text{ avg} = 7.3 \times 10^{-4}$

diffusion, ΔS^* is the entropy of activation of diffusion, and g is a constant determined by the geometry of the particular processes of diffusion.

In many diffusion problems the experimentally determined values include entropy and heat of activation terms for the process of forming the defects by which diffusion occurs. For the case of hydrogen in metals, such as zirconium, the tetrahedral sites in the hydride structures are already available for diffusion. Therefore, diffusion of hydrogen in the hydride structures should involve only the entropy and heat of activation terms for diffusion. According to theory, the entropy of activation should have slightly positive values.

The frequency of vibration of hydrogen atoms in the equation has been evaluated from entropy of solution data which will be discussed in a future paper. A value for ν of 4×10^{13} vibrations/sec was found. The distance a between tetrahedral sites in the δ -phase was 2.39 Å.

To evaluate the constant g , the diffusion of hydrogen atoms or ions is assumed to occur through the movement of unoccupied tetrahedral sites. g is evaluated by calculating the probability P_i of an unoccupied site occurring next to a particular hydrogen atom or ion. The probability varies from a value of $\frac{2 - 1.965}{2}$ at the surface to a value of

$\frac{2 - 1.4}{2}$ at the interface $c_{II,I}$. The geometrical mean of these values is 0.072. Since $g = \frac{1}{6} \Sigma P_i$, $g = 0.012$. Substituting the values of D_o , g , a^2 and ν , $\Delta S^* = +2.7$. This value is in agreement with theoretical predictions of Zener (17).

Diffusion of Deuterium

The diffusion of deuterium in zirconium was studied at 100°, 150°, 175°, and 225°C. Weight gain vs. time curves were similar to those seen in Fig. 2 and 3. Fig. 9 shows a comparison of \bar{C} vs. $t^{1/2}$ plots for hydrogen and for deuterium diffusing into the metal at 225°C. A straight line relationship was found for both gases.

Diffusion coefficients are summarized in Table III and plotted in Fig. 8. Although the data were somewhat scattered, the temperature dependence was the same as that found for the case of hydrogen, so the heat of activation for the diffusion process was the same for both gases. Calculated D_o values for hydrogen and for deuterium were 1.09×10^{-3} and 7.3×10^{-4} , respectively. Therefore, the ratio of D_{H_2}/D_{D_2} was independent of temperature and approximately equal to 1.5.

Jost and Widman (15, 16) observed a ratio of 1.3 for $D_{H_2}D_{D_2}$. Using the transition state theory of diffusion, they show that the effect of the mass of the diffusing specie was in the frequency term in the expression for the diffusion coefficient, the frequency of vibration being proportional to $1/\sqrt{m}$ or $1/\sqrt{2}$. Thus, the simple theory gives a ratio of D_{H_2}/D_{D_2} of 1.41. This compares with the experimental value of about 1.5.

A similar analysis could be made using the classical theory of diffusion as expressed in equation (XIX). The major effect appears to be that of mass on frequency of vibration along the path for reaction. Considering the scattering of experimental results, the diffusion of deuterium in zirconium is adequately explained by equation (XV) with the effect of mass on the frequency of vibration of the particular diffusing specie explaining the ratio of D_{H_2}/D_{D_2} .

Limit of Application of Diffusion Equation

Equation (XV) was derived on the basis of the diffusion of hydrogen from the surface through the ϵ and δ hydride phases to form new δ -phase. It was

assumed in the derivation that the plane of discontinuity was shifted proportional to $t^{1/2}$. At some value of the average concentration \bar{C} , the planes of discontinuity meet at the distance $h/2$. Equation (XIV) was used to calculate \bar{C} for this condition, and a value of 1.67 was obtained. Fig. 4 shows a plot of \bar{C} vs. $t^{1/2}$ for the hydrogen reaction at a temperature of 250°C. A straight line was found for concentrations up to 1.6–1.7. This agrees with the prediction of the equation.

ACKNOWLEDGMENT

The authors wish to express their appreciation to Dr. C. Zener and Dr. G. Comenetz for their helpful suggestions on the solution of the diffusion equation.

Any discussion of this paper will appear in a Discussion Section to be published in the June 1955 issue of the JOURNAL.

REFERENCES

1. D. P. SMITH, "Hydrogen in Metals", The University of Chicago Press, Chicago (1948).
2. E. A. GULBRANSEN, Chapter in book, "Zirconium and Its Alloys", to be published.
3. E. A. GULBRANSEN AND K. F. ANDREW, *J. Metals*, **1**, 515 (1949).
4. R. B. BERNSTEIN AND D. CUBICCIOTTI, *J. Phys. and Colloid Chem.*, **55**, 238 (1951).
5. E. A. GULBRANSEN AND K. F. ANDREW, *J. Electrochem. Soc.*, **101**, 348 (1954).
6. G. HÄGG, *Z. physik. Chem.*, **11**, 439 (1930).
7. E. A. GULBRANSEN AND K. F. ANDREW, *J. Electrochem. Soc.*, **101**, 474 (1954).
8. E. A. GULBRANSEN AND K. F. ANDREW, To be published by AIME.
9. C. WAGNER, quoted by W. Jost, "Diffusion in Solids, Liquids and Gases", Academic Press, Inc., New York (1952).
10. H. S. CARSLAW AND J. C. JAEGER, "Conduction of Heat in Solids", Clarendon Press, Oxford (1947).
11. E. A. GULBRANSEN, *Trans. Electrochem. Soc.*, **81**, 327 (1942).
12. E. A. GULBRANSEN, "Advances in Catalysis", 120–174, Academic Press, Inc., New York (1953).
13. E. A. GULBRANSEN AND K. F. ANDREW, *Ind. Eng. Chem.*, **41**, 2762 (1949).
14. R. M. BARRER, "Diffusion in and Through Solids", Cambridge University Press, Cambridge (1951).
15. W. JOST AND A. WIDMAN, *Z. physik. Chem.*, **B29**, 247 (1935).
16. W. JOST AND A. WIDMAN, *Z. physik. Chem.*, **B45**, 285 (1940).
17. C. ZENER, *J. Applied Phys.*, **22**, 372 (1951).

High Temperature Crystal Structure of Thorium¹

PREMO CHIOTTI

Ames Laboratory, Atomic Energy Commission, Iowa State College, Ames, Iowa

ABSTRACT

High temperature x-ray diffraction patterns and electrical resistivity measurements show that thorium of 99.8% purity transforms from face-centered cubic to body-centered cubic on heating to $1400 \pm 25^\circ \text{C}$. At 1450°C the lattice constant of body-centered cubic thorium is $4.11 \pm 0.01 \text{ \AA}$. The extrapolated lattice constant of face-centered cubic thorium at the same temperature is $5.180 \pm 0.005 \text{ \AA}$. The lattice constant of the metal used is $5.089 \pm 0.001 \text{ \AA}$ at room temperature. The transformation temperature is rapidly increased as the amount of carbon in the metal is increased. Zirconium has the opposite effect in that small amounts of it are very effective in lowering the temperature at which the transformation begins.

INTRODUCTION

Thorium at ordinary temperatures has a close-packed face-centered cubic structure. In an earlier investigation (1) some resistance measurements on thorium in the temperature range between 750° and 1700°C gave evidence of a possible allotropic transformation. At about the same time, an investigation of the thorium-zirconium system by Carlson (2) indicated that a complete series of solid solutions is formed between these two elements at elevated temperatures. Since zirconium is body-centered cubic at temperatures above 865°C , the results obtained by Carlson can be explained more satisfactorily on the supposition of the existence of a body-centered cubic form for thorium. In order to resolve this question, further resistance measurements were made and x-ray diffraction patterns were taken in the temperature range in question.

EXPERIMENTAL METHODS

The change in electrical resistance with temperature of thorium was measured over a temperature range of 750°C to its melting point. The method employed and apparatus used have been described in detail elsewhere (3). In this method, a specimen approximately a quarter-inch in diameter and four inches long is clamped between two water-cooled copper electrodes and is heated under vacuum or in an inert atmosphere to various temperatures by passing a 60-cycle alternating current through it. Two thin thorium wires are spot welded one centimeter apart near the middle of the bar where the

temperature is reasonably uniform. The potential developed between these two leads is balanced against the output of a current transformer whose primary is connected in series with the specimen. Since the output of the current transformer is proportional to the current through the primary, and the potential developed across the one-centimeter length of the specimen is the product of the same current and specimen resistance, the change in resistance with temperature is measured directly. Essentially, this is an alternating-current potentiometric null-point method. In order to balance one alternating voltage against another, it is necessary that the two voltages be of identical wave form and 180° out of phase. These conditions can be met quite closely in the method described. However, Corbino (4) has shown that, on heating a metal filament by means of an alternating current, a second harmonic is introduced due to small variations in resistance with temperature in the course of current reversal. This effect could not be readily detected with an oscilloscope in the present investigation and was considered negligible as far as the qualitative course of the resistance vs. temperature curve of thorium is concerned. Temperature measurements were obtained by focusing a disappearing-filament type optical pyrometer onto a small hole drilled into the middle of the specimen.

X-ray diffraction data were obtained with a North American Philips Company high angle goniometer diffractometer which was adapted for high temperature investigations (5). A sketch of the goniometer specimen holder and furnace developed for this purpose is shown in Fig. 1. Both the base and furnace cover are water-cooled. The incident and diffracted x-rays pass through a 2.5-mil aluminum window which extends over a 180°C arc on the furnace cover. The furnace is evacuated through a

¹ Manuscript received May 28, 1954. This paper was prepared for delivery at the Chicago Meeting, May 2 to 6, 1954. Contribution No. 330 from the Institute for Atomic Research and Department of Chemistry, Iowa State College, Ames, Iowa. Work was performed in the Ames Laboratory of the Atomic Energy Commission.

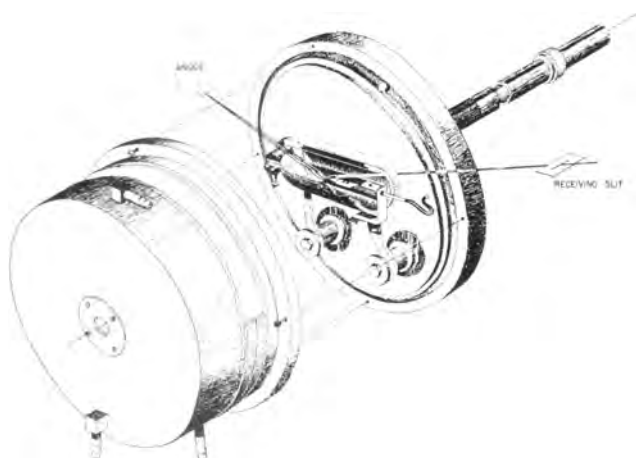


FIG. 1. Isometric projection of furnace and specimen holder attachment for x-ray diffraction goniometer.

hollow stainless steel shaft which extends through the goniometer.

Two types of specimens were used. One consisted of a thorium bar approximately $5\frac{1}{16} \times 3\frac{3}{16} \times 3\frac{1}{2}$ in., held in place by the clamp shown on the left side of the furnace base in Fig. 1. The other consisted of a smaller piece of thorium, $\frac{1}{4} \times \frac{1}{8} \times \frac{3}{4}$ in., supported in an appropriate slot on a tantalum bar, the bar being held in place by the same clamp mentioned above. No appreciable reaction between the tantalum and the thorium was observed at temperatures up to 1575°C. The latter arrangement proved more satisfactory since thorium bars were found to sag when heated to this temperature.

Samples are heated by means of a tantalum sheet resistance element. Radiation shields surround the heating element to reduce radiation losses. The specimen is heated by radiation from the heating element and does not make direct contact with it. Temperature measurements are made by sighting an optical pyrometer on a small hole (No. 65 drill) drilled into the side of the specimen. The hole in the specimen is so arranged that it can be viewed through a glass window sealed onto the furnace cover and through a $\frac{1}{8}$ -in. hole drilled through the radiation shields.

EXPERIMENTAL RESULTS

The first evidence for a transformation in thorium was obtained from electrical resistance measurements. Results of measurements on a thorium specimen taken from cast metal are shown in Fig. 2. The resistance is seen to rise rapidly in the temperature range of 1425° to about 1525°C. The average heating rate through this temperature range was 1.6°/min. There is evidence of a second break in the curve at 1700°C which is believed to be due to incipient fusion; however, the bar did not melt in two until heated to 1740°C. Similar runs on other bars cut from cast metal, bars made from pressed

metal powder, and on Westinghouse metal, all gave a sharp increase in resistance at $1400^\circ \pm 25^\circ\text{C}$. The range of temperature over which this increase takes place is evidently related to the impurities in the metal and to some extent to temperature gradients in the specimen. Carbon is very effective in increasing the temperature at which the transformation begins. Metal containing as little as 0.2 wt % carbon along with the usual impurities no longer gives any definite indication of a transformation.

X-ray diffraction data confirmed the existence of a transformation in thorium. The metal transforms from face-centered cubic to body-centered cubic on heating to above 1400°C. Copper radiation and a nickel foil filter placed in the receiving slit were used in studying the transformation. In some cases where the alpha peaks were particularly strong, the corresponding beta peak was not completely suppressed. The scanning speed in each case was two degrees 2θ per minute. Fig. 3 shows the diffraction peaks of a sample which initially contained approximately 345 ppm carbon, 195 ppm nitrogen, 1000 ppm oxygen, and 1200 ppm metallic impurities. At 1375°C the 111 face-centered cubic peak was very strong. The temperature was then increased to 1415°C. The range from 26° to $33^\circ 2\theta$ was immediately scanned. As may be seen from this figure, a new peak identified as the 110 body-centered cubic peak appeared. This region was then rescanned and the diffraction peaks up to $146^\circ 2\theta$ recorded. The possible identification of the peaks is shown on the figure. The pressure in the system during the run was maintained between

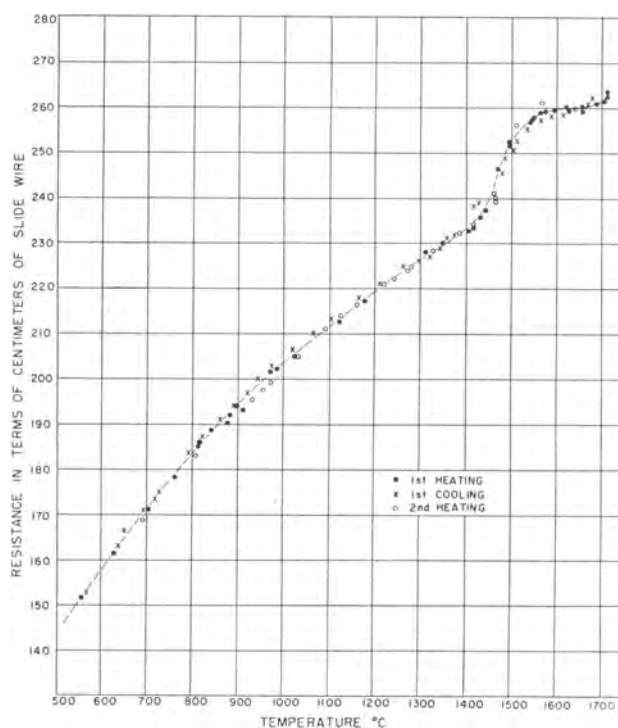


FIG. 2. Temperature dependence of the electrical resistance of thorium.

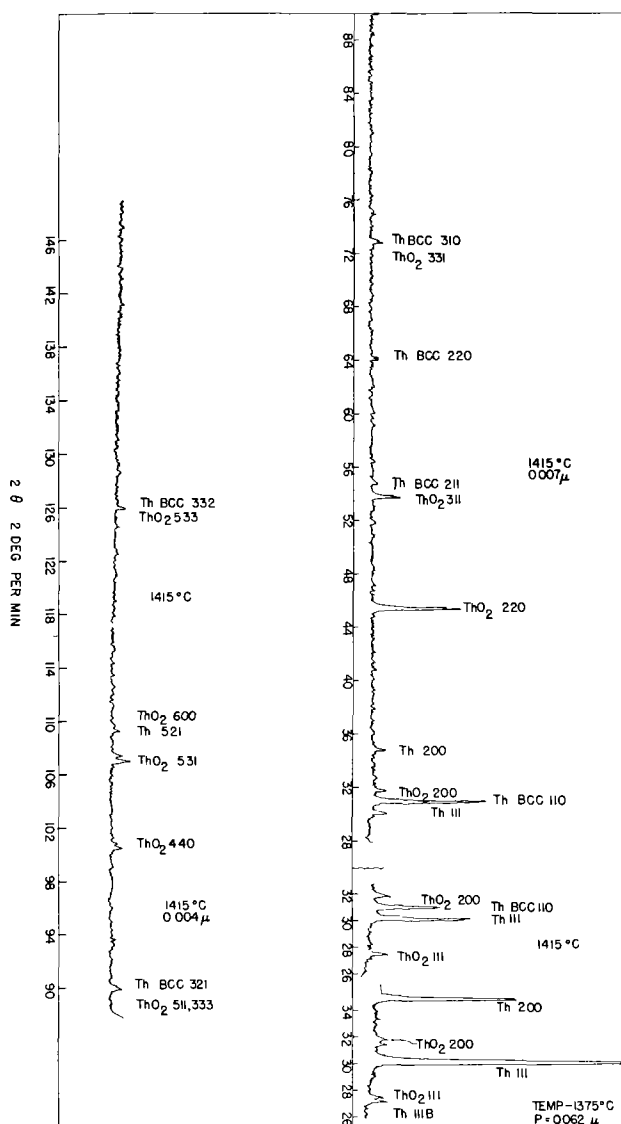


FIG. 3. Diffraction patterns of thorium contaminated with ThO_2 .

2.0×10^{-6} to 7.0×10^{-5} mm of Hg. The missing body-centered cubic peaks and the peculiar relative intensities of the peaks observed is believed to be due to excessively large grains and grain orientation.

Fig. 4 shows the nature of a thorium specimen surface after being heated for about six hours at temperatures between 1200° and 1500°C during the course of x-ray diffraction studies. The large dark spots are believed to be oxide particles in the metal initially. The fine structure is probably due to contamination by oxygen or other gaseous impurities during the heating operation. Large recrystallized grains and the outlines of the old grains are evident.

Fig. 5 shows the front reflection peaks obtained with a sample of iodide crystal bar thorium of unknown purity. At 1440°C only one face-centered cubic peak and two body-centered cubic peaks are present. At 1505°C only two body-centered cubic peaks remain; however, these two peaks are not the

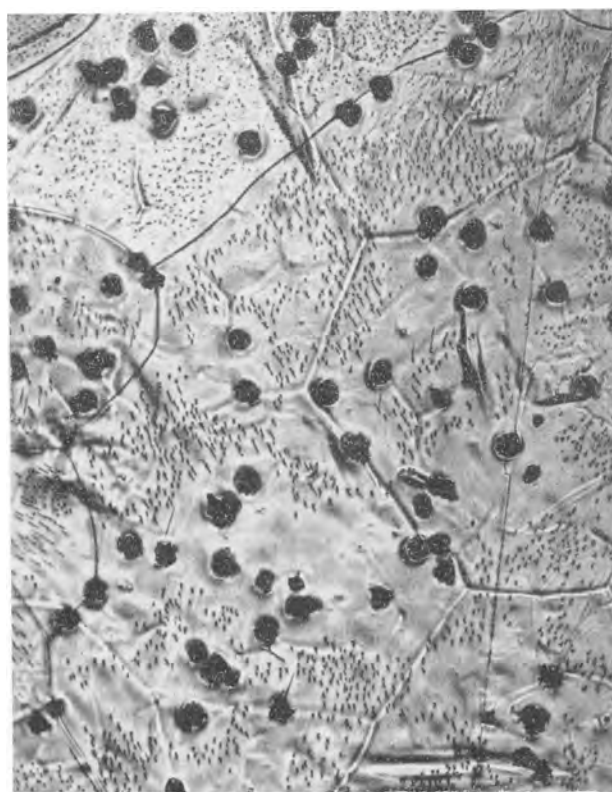


FIG. 4. Surface of thorium sample after about 6 hr at temperatures between 1200° and 1500°C , unetched $100\times$.

same as the body-centered peaks present at 1440°C . A possible explanation for this observation is that a change in orientation of the grains results as the transformation goes to completion. Absence of thorium oxide peaks is noted.

Both tantalum and niobium lower the temperature at which the transformation begins to approximately 1375°C . The lowering of the transformation temperature may be due to solubility of these metals in body-centered thorium or due to removal of impurities which normally increase the stability of the face-centered modification. Tantalum, when added to thorium in small amounts, effectively removes carbon from solid solution to form insoluble Ta_2C . In this case the thorium matrix can be dissolved with nitric acid leaving the insoluble carbide as a residue. Niobium presumably does likewise. The extent of solid solubility of either niobium or tantalum in body-centered thorium is uncertain, but from atomic size considerations it is expected to be small. Zirconium, however, is very effective in lowering the temperature at which thorium transforms. Diffraction peaks obtained from a sample containing 1 wt % each of niobium and zirconium are shown in Fig. 6. It is evident from this figure that some of the body-centered phase is present at 1340°C and that the face-centered cubic phase has disappeared at 1375°C .

Small variations in alignment of the specimens along with the effects of orientation resulted in a

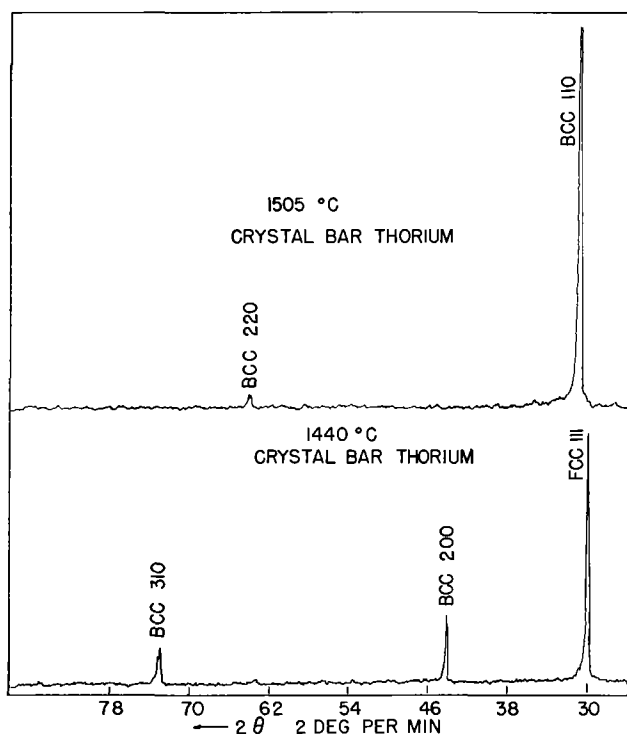


Fig. 5. Diffraction patterns of crystal bar thorium of unknown purity.

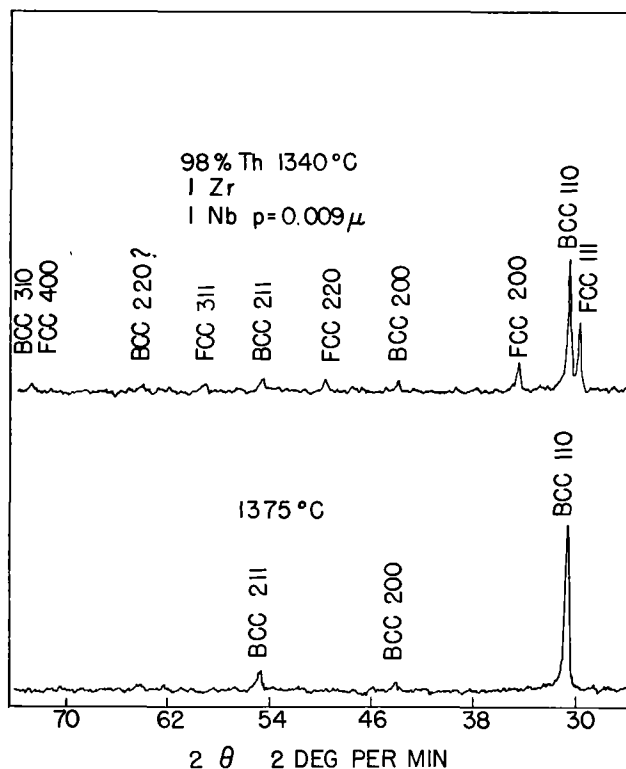


Fig. 6. Diffraction patterns of thorium containing 1 wt % each of niobium and zirconium taken at 1340° and 1375°C.

much greater variation in peak position than is normally obtained with well-aligned samples with small, randomly oriented grains. Nelson and Riley's (6) extrapolation method was used in determining the lattice constants. Individual peaks were also

scanned at one-fourth degree 2θ /min to obtain better resolution of the peaks. The uncertainty in the extrapolated value of the lattice constant of the body-centered thorium was found to be rather large due to the fact that the well defined peaks usually occurred only in the front reflection region and the total number of peaks was generally limited to five or less.

CONCLUSIONS

As a result of a large number of x-ray diffraction measurements on thorium metal containing approximately 345 ppm carbon, 195 ppm nitrogen, 1000 ppm oxygen, and 1200 ppm metallic impurities, it may be concluded that this metal transforms from face-centered cubic to body-centered cubic at $1400 \pm 25^\circ\text{C}$. The lattice constant of the body-centered metal at 1450°C is $4.11 \pm 0.01 \text{ \AA}$, and the extrapolated lattice constant of the face-centered cubic modification at the same temperature is $5.180 \pm 0.005 \text{ \AA}$. At room temperature the lattice constant of the metal used was $5.089 \pm 0.001 \text{ \AA}$.

Some contamination of the specimen surface by carbon on heating at 600° and 900°C was observed. This was probably because of outgassing of rubber vacuum seals or the Apiezon wax used to seal the aluminum window. Prolonged heating in this range usually resulted in the appearance of extraneous peaks which could be indexed as face-centered cubic thorium carbide. At temperatures above 1000°C , no difficulty in this respect was observed, possibly because of the rapid diffusion of carbon into the metal. Possible variation of the carbon content on the surface of the specimens due to these effects probably contributed to the observed variation in the lattice constants.

ACKNOWLEDGMENTS

The author wishes to acknowledge the cooperation and assistance of fellow members of the Ames Laboratory. The high temperature x-ray diffraction patterns were obtained with the assistance of Robert White.

Any discussion of this paper will appear in a Discussion Section to be published in the June 1955 JOURNAL.

REFERENCES

1. P. CHIOTTI, "Thorium-Carbon System," Atomic Energy Commission Report No. AECD-3072 (1950).
2. O. N. CARLSON, "Some Studies on Uranium-Thorium-Zirconium Ternary Alloy Systems," Atomic Energy Commission Report No. AECD-3206 (1950).
3. P. CHIOTTI, "Measurement of the Electrical Resistance of Metals and Alloys at High Temperatures," to appear in *Rev. Sci. Instr.*
4. O. M. CORBINO, *Atti reale accad. Lincei*, Ser. 5, **19**, 133 (1910); *ibid.*, **20**, 222 (1911).
5. P. CHIOTTI, "Adaptation of a Geiger-Counter X-ray Spectrometer for High Temperature Investigations," to appear in *Rev. Sci. Instr.*
6. J. B. NELSON AND D. P. RILEY, *Proc. Phys. Soc. London*, **57**, 160 (1945).

Anodic Behavior of Copper in HCl¹

LEE STEPHENSON² AND J. H. BARTLETT

Department of Physics, University of Illinois, Urbana, Illinois

ABSTRACT

Anodic behavior of copper in 2*N* HCl has been studied by both electrical and optical methods. The temporal behavior of current and voltage have been found, as well as the current vs. voltage characteristics. The anode surface has been observed both visually and photographically with the aid of conventional microscopes, and the anolyte has been photographed cinematographically using a schlieren microscope.

When the current is turned on, a layer, probably CuCl, starts to form at random nucleation spots on the anode. This grows until the whole anode is covered, at which time the current drops abruptly. Up until this time the anolyte becomes less concentrated, but the concentration may increase again after the current has become low.

The anode-calomel voltage may be written as $V = \epsilon(i) + ir$, where $\epsilon(i)$ becomes constant at high current densities. The values of $\epsilon(i)$ have been found by both the interruption and the direct method, and there appear to be at least four of physical significance. These values are -0.35 , -0.27 , -0.05 , and $+0.11$ v.

In general, the current drops twice before reaching its minimum value. If t_I is the time from the make to the first drop, and if $Q = \int_0^{t_I} i dt$, and if i_0 is the "initial" current after the make, then empirically $Q = 24(i_0 - 0.70)^{-0.53}$, where i_0 is in ma.

The anode layer is about 3 μ thick in the steady state. When the circuit is broken, r and ϵ change rather rapidly (in about 0.1 sec), but the layer dissolves off slowly.

INTRODUCTION

In an endeavor to further the understanding of electrochemical phenomena, such as overshoot and oscillations, which occur in biological systems, Bartlett (1) studied the anodic behavior of iron in aqueous H₂SO₄ with special attention to various kinds of transient phenomena which may arise when the applied voltage is changed. The work was continued by Bartlett and Stephenson (2) with emphasis now on the steady-state behavior of passive and active iron, and on the transients resulting from brief interruptions of the active steady state. Microscopic observation of the anode *in situ* revealed that evolution of hydrogen caused disruption of the layer which tended to form, so that this introduced an uncontrollable variation with resulting lack of reproducibility. The conclusion was reached that the Fe | H₂SO₄ system is an undesirable one to use for the study of layer formation, which seems to be basic for any analysis of overshoot and oscillation.

Fortunately, other systems do exhibit these transient phenomena, and these are much more reproducible.³ Bartlett and Stephenson decided to

investigate the system consisting of a copper anode in aqueous HCl. This is admirably suited for the study of layer formation because of the following properties: (a) Cu is attacked only very slowly by 2*N* HCl; (b) the anode layer which is formed is readily detected by simple optical means; (c) rates of reaction are such that the transient phenomena can be followed easily; (d) compositions of the layer and the soluble anode product are known; and (e) no undesirable products are formed during electrolysis. The purpose of the present paper is to report on various physical changes which take place at the surface of a copper anode immersed in HCl, and on changes occurring in the diffusion layer next to this anode. The work may be regarded as a theoretical contribution to the behavior of metal electrodes covered with precipitated salt, as found in corrosion reactions.

Procedure

The experiments to be described fall into two main categories: electrical and optical. The electrical experiments involve studies of temporal behavior of current and voltage, and of the current vs. voltage characteristics. The optical experiments consist of both visual and cinematographic observation of the anode surface with conventional microscopes, and of cinematographic studies of the

¹ Manuscript received December 9, 1953. This paper sums up investigations which have been reported at the Philadelphia Meeting, May 4 to 8, 1952, the Montreal Meeting, October 26 to 30, 1952, and the New York Meeting, April 12 to 16, 1953.

² Present address: California Research Corporation, La Habra, California.

³ The high degree of reproducibility in the system re-

ported on here is evident from Fig. 5-8, 13, and 14, where each point represents one run only and is not an average of several runs.

anolyte using a schlieren microscope. The optical experiments are carried out in conjunction with the electrical experiments so that accurate correlation of all related phenomena is possible.

Apparatus

Cell.—The circuit employed in these experiments is shown semipictorially in Fig. 1. The electrolytic cell consisted of a rectangular box made of glass with an optical window of glass 0.1 mm thick in one face to permit microscopic observation of the anode *in situ*. The inside dimensions of the cell were 2.5 x 7.5 x 7.5 cm. The cell contained 110 ml of an aqueous solution of hydrochloric acid, into which were placed two working electrodes and a reference electrode. Unless otherwise noted, the acid concentration was 2 moles/l (2*N*) and the temperature was 25°C. Preliminary experiments were carried out in both air-saturated and oxygen-free solutions in order to determine the effects of dissolved oxygen on the phenomena to be observed. No differences in the transient behavior were apparent, and microscopic observations failed to show any changes in the anode film due to dissolved oxygen. Consequently, the more convenient air-saturated solutions were used. Because of physical limitations imposed upon the structure and the orientation of the anode by the microscopic experiments and the schlieren experiments, it was decided to conduct all experiments with a vertical anode and to permit free convection of the anolyte. The anode structure consisted of a vertical brass rod with a 1 cm length of # 14 (1.63 mm diameter) copper wire (Anaconda) soldered horizontally into its lower end. Picein 105⁴ covered the entire assembly except for the end cross section, *A*, of the copper wire, which constituted the anode surface. Filed anodes were prepared using a Nicholson "Mill Smooth" file. Electropolished anodes were prepared by mechanical polishing down to 4/0 polishing paper (Norton) followed by electropolishing in 50% orthophosphoric acid. The cathode, *K*, was a 0.005 in. thick platinized platinum sheet, 3.0 x 3.3 cm, supported by a brass rod which was covered with Picein. A 0.1*N* calomel half-cell was used as the reference electrode. Provided the distance between the anode and the cell walls was at least 2 mm, the transient behavior was found to be independent of cell geometry (2).

The potential measurement, source of emf, recording of current and voltage, and interruption techniques were as described in a previous paper (2). In addition, a Brown recording potentiometer (0–10 mv) was used to record slow transients (i.e., those lasting longer than about 20 sec). The external

⁴ Obtained from E. H. Sargent Company, Chicago, Illinois.

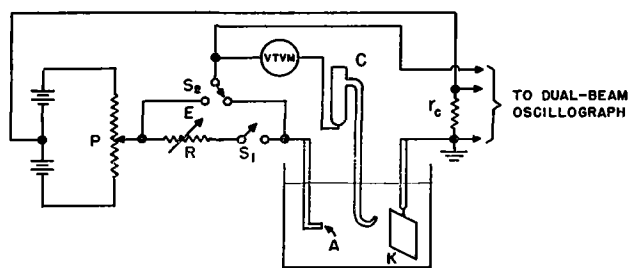


FIG. 1. Basic circuit P, potential divider; R, 200 ohm helipot; VTVM, vacuum tube voltmeter; A, 0.021 cm² copper anode; C, 0.1*N* calomel reference electrode; K, 10 cm² platinized cathode; *r_c*, current resistor.

circuit resistance was controlled by a 200 ohm helipot, *R*.

Microscope and accessories.—For visual observation of the anode surface, a microscope was provided with a special mechanical stage to hold the electrolytic cell, electrodes, etc. For most work, a 16 mm (10×) objective having a numerical aperture of 0.25 and a working distance of 6 mm was used, together with a 10× eyepiece. The anode was illuminated obliquely to obtain maximum contrast. A 35 mm Praktica FX single-lens reflex camera was used to obtain photomicrographs.

Cinematographic microscope.—Cinematography of the anode surface was accomplished with a conventional 8 mm home movie camera, Bell and Howell Model 134-V. The camera lens, an f/1.9 Super Comat, was removed from the camera and mounted backward (in order to preserve the conjugate relationship for which the lens was corrected) on a short extension tube. This arrangement provided an excellent cinematographic microscope having a primary magnification of 3.4 diameters. An auxiliary lens and 45° prism were mounted in the side of the extension tube to permit simultaneous recording of the current and voltage

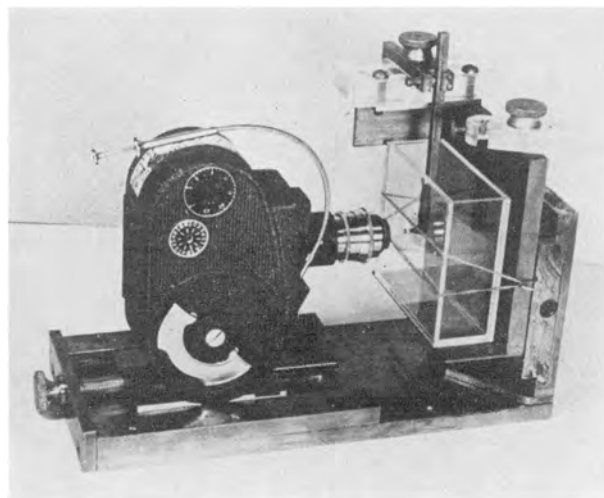


FIG. 2. Cinematographic microscope

deflections on the oscillograph screen. Fig. 2 shows the principal features of this apparatus.

Schlieren photography.—Information about the diffusion layer was obtained by using a specially constructed schlieren microscope (3). This is an optical instrument in which the intensity of light incident on the photographic film at a certain point is a linear function of the gradient of the index of refraction at the corresponding point in the object space. Even though this method has not yet been made quantitative at concentration gradients as high as those occurring in the present work, it still is very helpful in furnishing a general picture of what is occurring. Schlieren motion pictures of the diffusion layer were taken with the aid of the 8 mm camera used for microphotography.

MAKE TRANSIENTS

General nature of transients.—If a freshly filed anode is placed in the solution and the circuit is then closed, the nature of the ensuing current vs. time curve (here designated as a "make transient") will depend on the external emf E and the external resistance R (1).

The complete circuit will be considered as consisting of two parts, the internal part and the external part. The internal part is defined as that part which extends in the cell from the anode metal to the tip of the calomel electrode. Its resistance will be denoted by r . The external part of the circuit is that part which metalically connects the anode to the cathode, plus the part from the cathode to the calomel electrode tip. Its resistance will be termed R . If i is the total cell current measured in the external circuit, the anode-calomel voltage V is given by

$$V = E - iR \quad (I)$$

If E and R are held constant, i can still vary, but V will also vary. In the i - V plane, the above equation will be represented by a straight line, which will be called the load line, in analogy to vacuum tube terminology. (The resistance R consists mainly of the resistance of the helipot, and we shall regard as negligible the resistance of the leads, of the potential divider circuit, and of the solution between cathode and calomel, because these total approximately 1.5 ohms, or only 1% of the minimum resistance employed in the present work.)

A typical make transient for medium R (140 ohms) and high final voltage V is shown in Fig. 3a. At the very beginning, there is a spike (not shown) lasting about 10^{-5} or 10^{-4} sec. The current then falls rapidly from the "initial" value i_0 and becomes approximately independent of time. This region will be called the first plateau. The current actually goes

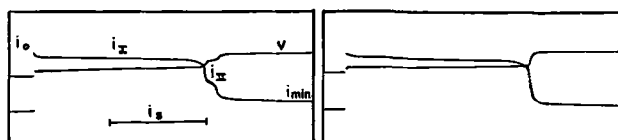


FIG. 3. Make transients. $E = +0.50$ v, $R = 140$ ohms. *a*, Left, freshly filed anode; *b*, right, electropolished anode.

through an inflection point, i_T , decreasing more or less slowly. After a rather abrupt drop to a second plateau (current i_{II}), the current drops again, then varies slowly. For the case shown in the figure, it goes through a minimum i_{min} and then rises to the steady state value i_∞ . If, however, i_0 is sufficiently high, such a minimum is not observed and the current will fall continually until i_∞ is reached. The current may overshoot one or more times before settling down to the steady value, 1.7 ma. This is illustrated in the semilogarithmic plot of Fig. 4.

Electrode potential and resistance.—If an appreciable current flows, the anode-calomel voltage will, in general, differ from the reversible value, V_{rev} . The overvoltage is defined as the difference between the observed voltage (at a given current) and the reversible value. It is regarded as composed of three distinct contributions: resistance overvoltage $V_r = ir$, concentration overvoltage or polarization V_c , and "activation" overvoltage V_a (4).

The anode-calomel voltage may then be written as

$$V = V_{rev} + V_a + V_c + V_r = \epsilon + ir. \quad (II)$$

The quantity $\epsilon = V_{rev} + V_a + V_c$ will be termed the electrode potential for present purposes. If this is constant for a certain set of circumstances, the locus of i vs. V will be a straight line with intercept ϵ and slope $1/r$. This determination is called the direct method (5) of obtaining ϵ and r . Another

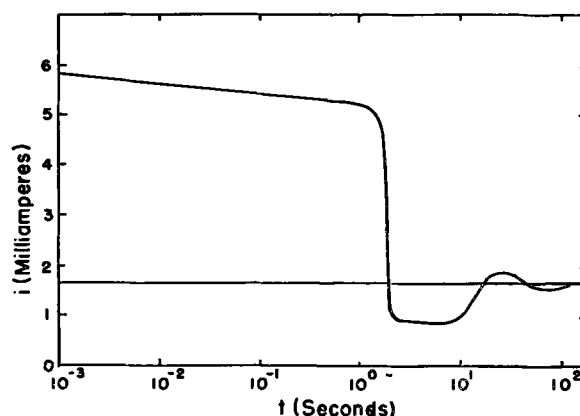


FIG. 4. Make transient for freshly filed anode. The horizontal line at 1.7 ma represents the steady-state current $E = +0.50$ v, $R = 140$ ohms.

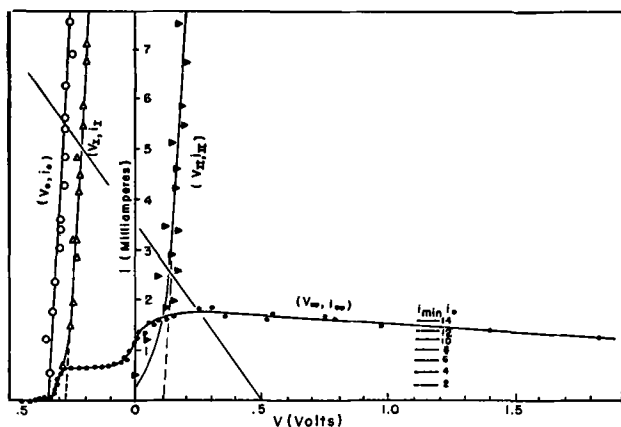


FIG. 5. Characteristic curves for the Cu | HCl (2N) system at 25°C with a freshly filed anode having an area of 2.1 mm².

method which may be used to check or complement this is the interruption method. This consists in breaking the circuit and observing V before and after, as well as i before, the break. Then $\epsilon = V_{\text{cft}}$ and $r = (V_{\text{on}} - V_{\text{off}})/i$. Both methods were used, and they agree in all cases where they are applicable. The interruption method will not be suitable if the recording apparatus is not sufficiently fast, for a rapid decay of ϵ may escape detection. Even where this decay is observed, one must extrapolate back to $t = 0$ in order to find the value of ϵ at the time of the break. The results of Hickling and Salt (6), based on extrapolation, were criticized adversely by Frumkin (7).

For high current densities, the value of ϵ is constant in the steady state (8) and at certain critical points (for the system Cu | HCl), as will now be shown. These critical points occur when i is equal to i_0 , i_I , and i_{II} , respectively. As may be seen from Fig. 5, the loci (V_0, i_0) , (V_I, i_I) , and (V_{II}, i_{II}) , which shall be called "characteristics", become straight, mutually parallel lines above approximately 1 ma. (Similar behavior has been found for the steady state, for Hickling (8) stated that "there is a fairly general tendency for the overvoltage to approach a constant maximum value" at high current densities.) The reciprocal of the common slope of the characteristics equals the resistance, and is 12 ohms for the system (Cu | 2M HCl). Thus, the cell's internal resistance does not change appreciably until after the second plateau has been reached.

The values of ϵ determined by this direct method are $\epsilon_0 = -0.35$ v, $\epsilon_I = -0.27$ v, and $\epsilon_{II} = +0.11$ v. In other words, at high current densities these experiments show that the overvoltage (excluding that due to ohmic resistance) has one constant value for i_0 , another for i_I , and another for i_{II} .

Two of the above values of ϵ were confirmed by

interruption experiments, which resulted in $\epsilon_0 = -0.35$ v and $\epsilon_I = -0.27$ v. However, when the current during the second plateau and later is interrupted, the value of V after 10^{-4} sec is $\epsilon_{II} = -0.05$ v. This is reconcilable with the result of the direct method if it can be assumed that there is a rapid decay ($<10^{-4}$ sec) from $\epsilon_{II} = +0.11$ v to $\epsilon'_{II} = -0.05$ v. (The recording apparatus used in the present experiments was relatively slow, being incapable of detecting decay constants appreciably smaller than 10^{-4} sec.) The value of $\epsilon = 0.11$ v does seem to have physical significance (cf. "Break Transients").

Typical curves showing the variation of ϵ and r with time as determined by the interruption method are given in Fig. 6. Data were obtained for freshly filed anodes with $E = +0.20$ v and $R = 140$ ohms, and are plotted on the assumption that the entire voltage change at the break is due to an ir drop.

On open circuit, the potential of the copper electrode is $\epsilon_{00} = -0.44$ v (with respect to 0.1N calomel). Immediately after the circuit is closed, the potential jumps to $\epsilon_0 = -0.35$ v, as is evidenced by a small dot on the film. (The switch contact S_1 [Fig. 1] bounced for about 10^{-3} sec after closing, and thus provided sufficient break to observe this value of ϵ .) The potential then rises less rapidly to $\epsilon_I = -0.27$ v. It stays at this value until the end of the first plateau, when it changes abruptly to

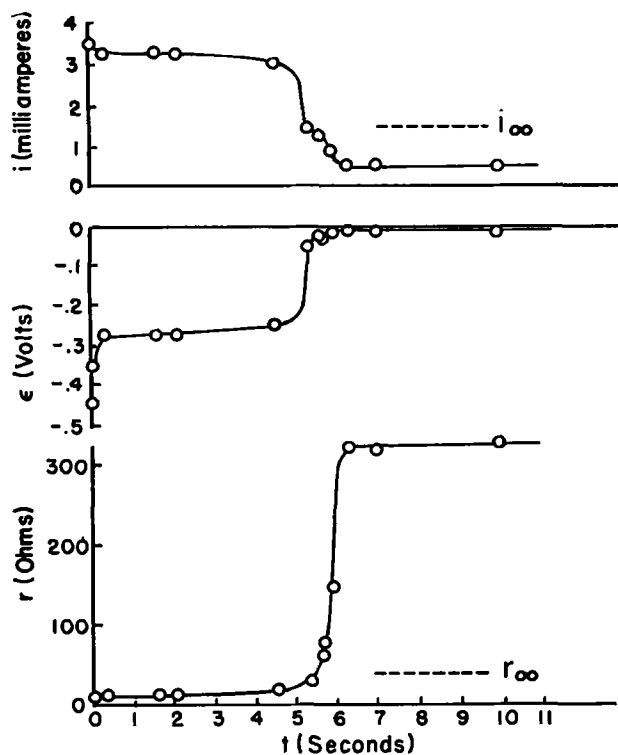


FIG. 6. Temporal behavior of ϵ and r following make. $E = +0.20$ v, $R = 140$ ohms.

$\epsilon'_{II} = -0.05$ v, the potential of the second plateau, where it remains for the rest of the transient.

The resistance r remains essentially constant at its initial value, $r_0 = 12$ ohms, until the end of the first plateau. Then, soon after the ϵ jump, it increases abruptly to a maximum value and decreases slowly toward its steady-state value r_∞ , ϵ staying practically constant⁵ at -0.05 v.

If one now re-examines the i vs. t curve with an eye to stating on what portions ϵ varies and on what portions r varies, the following conclusions are reached:

1. The drop in current from i_0 to i_I and the drop from i_I to i_{II} are due primarily to changes in ϵ , while the drop from i_{II} to i_{min} is due primarily to a change in r . In the case of electropolished anodes where the transition from i_I to i_{min} is relatively smooth, it is presumed that the changes in ϵ and r occur almost simultaneously.

2. Variations of the cell current subsequent to the current drop are due primarily to changes in r , for ϵ remains approximately constant at $\epsilon_{II} = 0.11$ v.

Durations of plateaus.—The duration of the first plateau is found to depend on i_0 . Let t_I be the time from the make to the inflection point at the drop from i_I to i_{II} , and let $Q = \int_0^{t_I} i dt$. Then empirically,

$$Q \approx i_I t_I = 24 (i_0 - 0.70)^{-0.53} \quad (III)$$

(This is shown in Fig. 7.) If E and R be given, then i_0 and i_I can be found from the intersection of the load line with the characteristics. Then, from equation (III), t_I can be estimated. It will decrease as i_0 increases. The value 0.70 in equation (III) corresponds to the steady-state current on the lower plateau (see below).

The duration of the second plateau appears to be affected by the condition of the anode surface, being a maximum for a filed surface and a minimum for an electropolished surface. Indeed, with an electropolished anode the second plateau is sometimes entirely absent, its expected location being marked only by a slight discontinuity in the slope of the i vs. t curve (Fig. 3b).

Prediction of general features of a make transient.—Once the "characteristics", i.e., the straight lines associated with the critical points, have been found, it is an easy matter, knowing equation (III), to give the main features of a transient corresponding to any values of E and R .

⁵ Under similar circumstances, the potential drop across the diffusion layer has been deduced to be negligible. See reference (9).

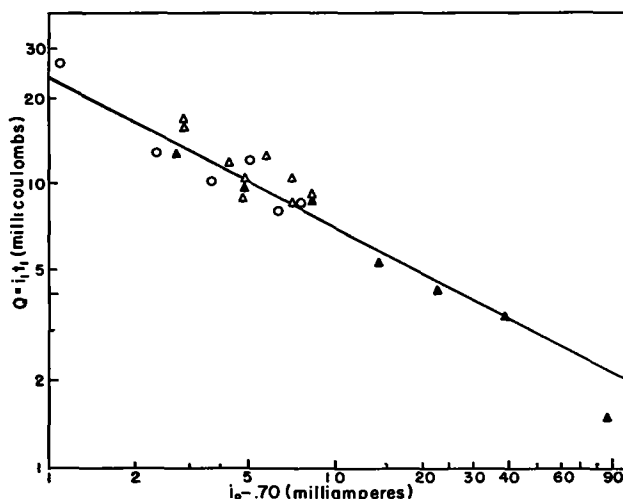


FIG. 7. Q as a function of i_0 for both freshly filed and electropolished anodes. $Q = 24 (i_0 - 0.70)^{-0.53}$

If equations (I) and (II) are solved for i , the result is

$$i = \frac{E - \epsilon}{R + r} \quad (IV)$$

One can substitute in the values of E and R , set $r = 12$ (the value of the solution resistance), and the values ϵ_0 and ϵ_I , to obtain i_0 and i_I . Alternatively, these can be found graphically by letting the load line intersect the characteristics corresponding to ϵ_0 and ϵ_I , respectively. The values of V are dependent on those of i by equation (I).

Once i_0 and i_I are known, t_I can be obtained from equation (III), so that the main features of the make transient up to the time that the current first drops can be given beforehand. Thus it is seen that the characteristic lines, which may be obtained quite easily, are extremely useful in prediction.

The current minimum.—In many cases the current passes through a minimum shortly after the final current drop. For currents up to 15 ma, i_{min} is found to depend mainly upon i_0 , as illustrated in Fig. 8. There is also a dependence of i_{min} on the condition of the anode surface, it being smaller for electropolished anodes than for ground anodes.

Schlieren study of the anolyte.—The qualitative nature of changes occurring in the diffusion layer at the anode was determined with a schlieren microscope. The pictures shown in Fig. 9 were taken using a freshly filed anode, with $E = 0.50$ v and $R = 140$ ohms. The schlieren knife edge was adjusted to show positive and negative gradients with equal clarity, and so oriented with respect to the anode (which appears in silhouetted profile at the left of the photographs) that bright regions corresponded to a refractive index (and concentration) which was increasing toward the anode, and

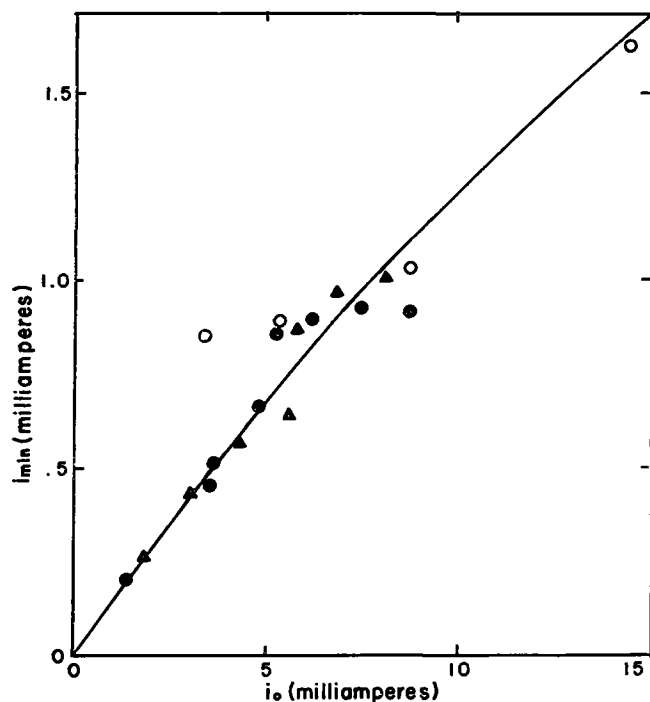


FIG. 8. Minimum current vs. initial current for a freshly filed anode

dark regions corresponded to a refractive index (and concentration) which was decreasing toward the anode.

At $t = 0$, immediately before closing the switch, the anolyte is seen to have a uniform concentration throughout the region in which the diffusion layer is expected to develop. The bright line outlining the face of the anode is due primarily to diffraction (10), but may be enhanced somewhat by the presence of products from the acid's slow attack on the anode. After electrolysis has proceeded for 0.7 sec, a dark region is observed extending out from the anode into the solution approximately 0.15 mm (measured at the center of the anode). Since the refractive index is decreasing toward the anode in this region, it can only be a region in which the HCl concentration is decreasing toward the anode; i.e., Cl^- is being consumed at the anode-solution interface. (Some of the photographs show a brightening of the anolyte nearest the anode which lasts for about one-third the duration of the first plateau. This is as yet not explained, and is not relevant to the present discussion.) At 1.3 sec and 2.0 sec the HCl-depleted region has advanced to approximately 0.27 mm and 0.33 mm, respectively. Comparing the photographs taken at 2.0 sec (near the end of the first plateau), at 2.1 sec (on the second plateau), and at 2.2 sec (near the current minimum), it is seen that no change whatever occurs in the diffusion layer when the current drops. After 4 sec have elapsed, the HCl-depleted region has nearly reached its maximum extent of about 0.48 mm, the reduced

density of this region being evidenced by the fact that it is carried upward by convection. At the same time it is observed that a bright region, corresponding to a refractive index which increases as the anode is approached, has begun to form at the face of the anode. At 6 sec the current has reached its minimum (Fig. 4), the HCl-depleted region has advanced to its maximum extent, and the material of the bright region of the anode product has begun to stream from the bottom of the anode, showing that its density is greater than that of 2*N* HCl. After 10 sec have elapsed, the current has begun to rise toward its steady-state value, the HCl-depleted layer has begun to recede, and the anode product has established a steady downward flow which tends to counteract the upward convection previously established by the HCl-depleted layer. At 300 sec the current has reached its steady-state value. The HCl-depleted region is not only appreciably reduced in extent, but is now being swept downward by the anode product.

The anode reactions.—Since, when current flows, Cl^- disappears from solution and Cl_2 is not observed to be liberated, the Cl^- must be consumed by some reaction involving the oxidation of copper. The resulting products are at least two in number, for it is observed that a layer forms on the anode and a viscous stream pours down from it after the layer has been completed.

Some evidence as to the nature of the anode reactions is furnished by the existence of the two

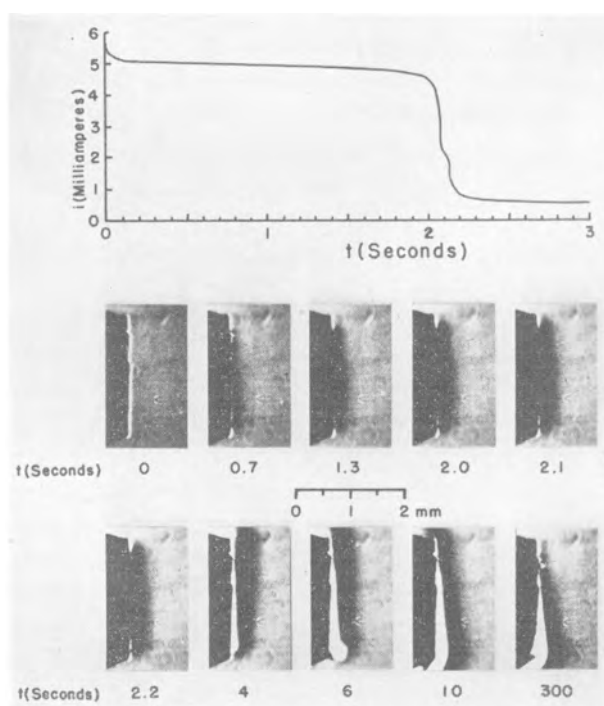
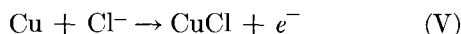


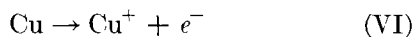
FIG. 9. Schlieren study of the anolyte following make. $E = +0.50$, $R = 140$ ohms.

electrode potentials, $\epsilon_1 = -0.27$ v and $\epsilon'_{11} = -0.05$ v. The former is observed when at least part of the anode surface is exposed to the solution, while the latter potential corresponds to the surface being completely covered with the above-mentioned layer. As will be seen below, ϵ_1 differs from ϵ_0 because of concentration polarization. The potential ϵ_0 is characteristic of the anode before much layer has had time to form. The anode potential ϵ_1 is practically constant until the sudden transition to ϵ'_{11} , or in other words is almost uninfluenced by the layer formation until the layer is about complete.

It is necessary, then, to postulate one type of reaction for the bare surface and another for the covered surface. According to Gatty and Spooner (11), "At the moment of immersion of a Cu electrode in aqueous aerated solution, the electrode is covered with a film of Cu_2O . In concentrated acid chloride solutions, (this) film is readily broken up, (and) the electrode potential will be close to that of the anodic field of bare metal. The electrode tends to establish the $\text{Cu} | \text{CuCl} | \text{Cl}^-$ electrode potential, CuCl being the least soluble of the copper chlorides. Complex ion formation takes place between the anodically formed CuCl and the halide in solution." The picture which the authors have developed, and which is consistent with all the known facts, is as follows: (A) the initial reaction is between chloride ions in solution and copper metal, resulting in the formation of CuCl layer on the anode; the potential ϵ_1 is then associated with the reaction



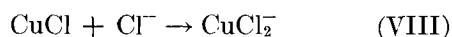
(B) when the surface is covered, this reaction is supplanted by another, to which the potential ϵ'_{11} corresponds. According to Wagner (12) "depletion of chloride ions will yield a rather well-defined electrode potential corresponding to a copper electrode in a solution saturated with CuCl in the absence of excess electrolyte, especially HCl ." This reaction may be



Cuprous ions can diffuse through the CuCl layer until they meet with chloride ions, and then one may have the reaction



Also, CuCl is known to react with excess Cl^- to form the soluble, colorless complexes CuCl_2^- and CuCl_3^- (13-16). It is assumed that the removal reaction is



Layer thickness.—If the anode reaction is as deduced above, then a knowledge of Q affords a

convenient means for estimating the thickness of the anode layer at the time the current drops. Assuming that Faraday's laws apply, Q/zF is the number of moles of CuCl formed up to that time. Assuming further that a negligible amount of CuCl is dissolved before the current drops, the thickness of the layer is given by $\delta = QM/zFd$, where M is the gram-molecular weight of CuCl , $zF = 96,500$ coulombs/mole, A is the anode area, and d is the density of CuCl . Taking, for example, the value $Q = 10.5$ millicoulombs (for $i_0 = 5.6$ ma) it is found that $\delta = 1.5 \times 10^{-4}$ cm. (Clearly, the CuCl layer cannot be expected to appear in the photos of Fig. 9, for its thickness is far beyond the limit of resolution of the schlieren microscope.)

It is also possible to estimate the thickness of the layer in the steady state by breaking the circuit and observing how long it takes for the layer to be removed completely. The rate of removal after interruption is assumed to be the same as the rate of formation in the steady state, namely i_∞/zF moles/sec. The thickness of the steady-state layer will therefore be given by $\delta = i_\infty Mt/zFAd$, t is the time required for removal. With the aid of a microscope equipped with circularly polarizing film to improve image contrast, visual observation of the anode revealed that the time required for complete removal of the layer depends upon the value of V_∞ at the time of interruption, typical values of t and δ calculated from them being as follows:

V_∞ (v)	t (sec)	δ (μ)
+0.20	9.6 (± 0.8)	2.3 (± 0.2)
+0.80	14.9 (± 1.0)	3.3 (± 0.2)
+1.40	18.0 (± 1.6)	3.5 (± 0.3)

These values for δ indicate that the steady-state layer thickness is probably of the same order of magnitude as that found when the current drops from i_1 to i_{\min} .

Layer growth.—Moving pictures of the anode surface taken at 64 frames/sec show that the layer begins to form at many randomly distributed points as soon as electrolysis begins, and that the growth from these nuclei takes place in a sideways manner. The current drops immediately after the pores of the nearly completed layer have been so reduced in size that they are no longer resolvable on the film (i.e., diameters reduced to roughly 5μ or less). Fig. 10 shows a series of photomicrographs of the anode face taken during the initial transient when $E = +0.70$ v and $R = 140$ ohms. Fig. 10(a) shows the electropolished anode immediately before electrolysis begins. Because of the oblique illumination employed, a truly specular surface would be completely dark. The bright spots which are observed are due to tiny pits left by electropolishing

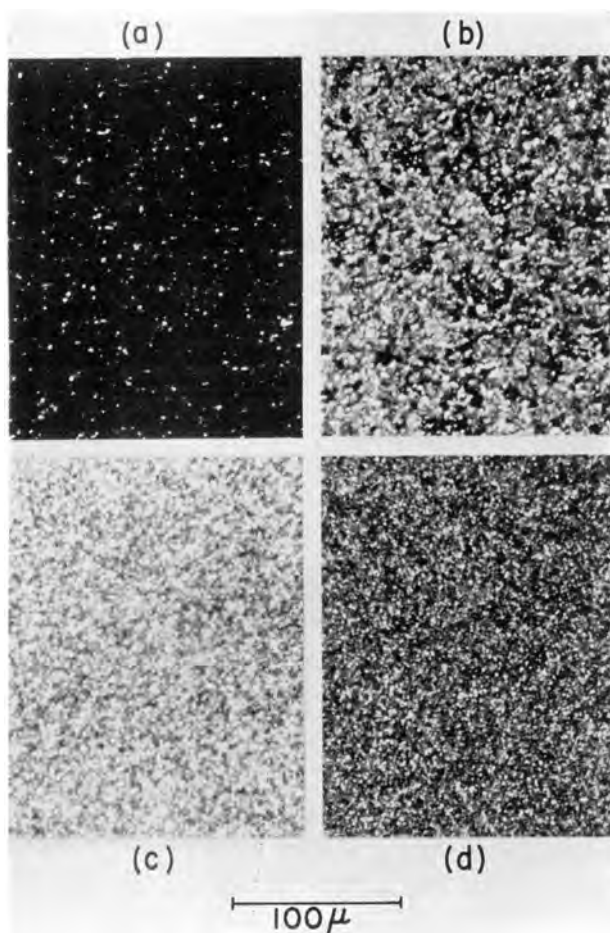


FIG. 10 Photomicrographs of the anode. (a) Before electrolysis; (b) midway on the first plateau; (c) at current minimum; and (d) steady state. $E = +0.70$ v; $R = 140$ ohms.

(17) and to a slight amount of etching which takes place while the microscope is being focused upon the immersed electrode.⁶ Fig. 10(b), taken approximately midway on the first plateau, shows that the free surface (dark areas) is greatly reduced by the sideways growth of the layer although no appreciable change in the cell current has occurred up to this time. Approximately 5 sec after the current drops, it reaches a minimum. At this point, the completed layer appears as in Fig. 10(c). The current then rises until the steady state is reached (after about 5 min of electrolysis) and then the layer appears as shown in Fig. 10(d).

BREAK TRANSIENTS

Dependence of potential decay on steady-state voltage.—Events subsequent to current interruption yield information on the layer removal process

⁶ It was found that the undesired etching could be inhibited by making the electrode cathodic while the necessary optical adjustments were being made (cathodic current density approximately 1 ma/cm²). However, this method was not employed.

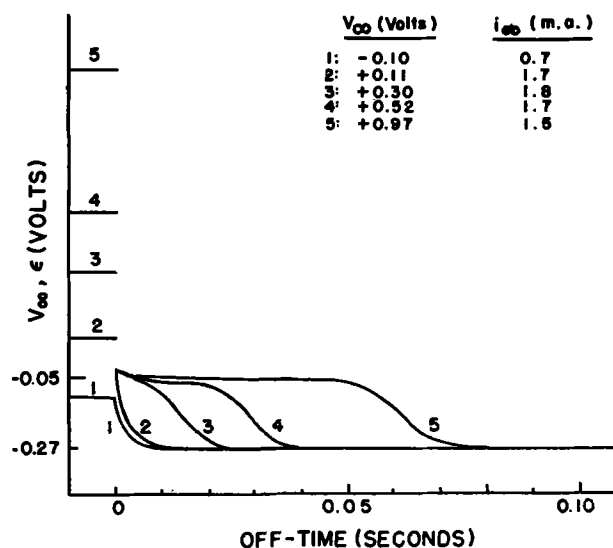


FIG. 11. Potential decay following interruption of the steady-state current, shown for various steady-state conditions.

alone, thus enabling one to separate this from that of layer formation. The curves in Fig. 11 show how the potential V varies after the break has been made, for different initial steady-state voltages V_{∞} . For values of V_{∞} greater than approximately 0 v, ϵ drops quickly to -0.05 v,⁷ remains approximately constant for a brief time depending on V_{∞} , and then drops suddenly to $\epsilon_1 = -0.27$ v. The potential vs. time curve has the same shape for passive iron (Fig. 12) in H_2SO_4 as it does for copper in HCl , which may indicate that similar mechanisms are operative in the two cases. The make curve for the transition from active iron to passive iron has been interpreted in terms of the formation of a layer, and now it is seen that the break curve for the passive-active transition resembles the break curve in copper, where it is known that there is a layer present. The evidence for a layer on passive iron is thus made stronger than ever, and it now remains to identify positively the reactions by which it is formed and removed.

In copper, for $V_{\infty} < -0.05$ v, the potential decay is somewhat like an exponential from V_{∞} to ϵ_1 . From ϵ_1 on, the potential falls slowly to $\epsilon_0 = -0.44$ v, this process lasting many minutes (see Fig. 13). Although this method of recording does not indicate that anything special occurs at $\epsilon_0 = -0.35$ v, still one observes that stirring right after interruption does reduce the potential immediately to this value

⁷ It has already been supposed that this is really composed of two drops, with $\epsilon_{11} = 0.11$ v as the intermediate value. The value -0.05 v is presumably the true electrode potential (i.e., without overvoltage) of the completed layer. The value $\epsilon_1 = -0.27$ v agrees with the potential of Cu in 2N HCl saturated with $CuCl$ (R. S. COOPER, private communication).

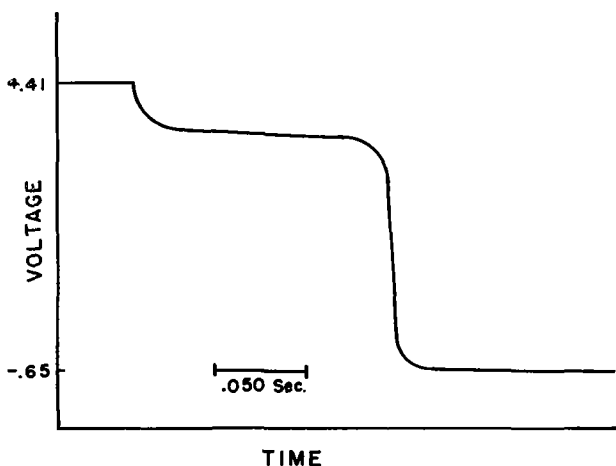
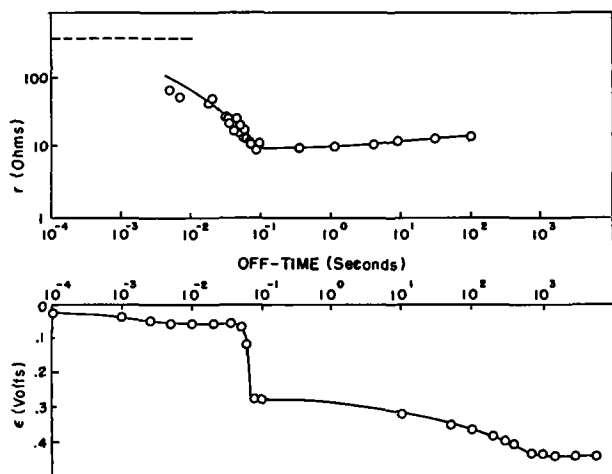
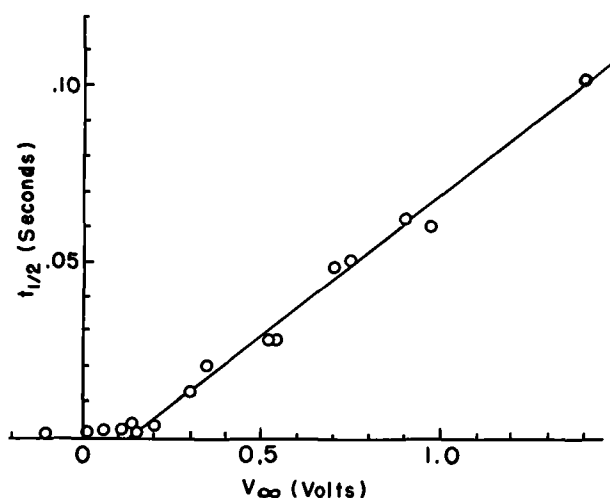


FIG. 12. Break transient for passive iron

of -0.35 v. This suggests that the difference between ϵ_0 and ϵ_I is due to concentration polarization.

The duration of the break plateau ($\epsilon = -0.05$ v) depends linearly upon V_∞ . (The duration is defined arbitrarily as the time from the interruption until the midpoint $\epsilon = -0.16$ v is reached, and will be denoted by $t_{1/2}$.) Fig. 14 is a plot of the duration $t_{1/2}$ against V_∞ . It is a straight line which has an intercept of $+0.11$ v on the V -axis. This is regarded as evidence that $\epsilon = +0.11$ v is the potential of the completed layer, as is also found from the characteristic curves. Below $+0.11$ v, the layer is not complete, so that there is no preparatory time necessary to make part of the surface bare.

Temporal behavior of ϵ and r .—Fig. 13 shows the temporal behavior of ϵ and r following interruption of an arbitrarily chosen steady-state condition, $V_\infty = +0.75$ v and $i_\infty = 1.6$ ma. To obtain these data, the steady-state current was interrupted for a predetermined length of time, at the end of which

FIG. 13 Temporal behavior of ϵ and r following interruption of the steady state. $V_\infty = +0.75$, $i_\infty = 1.6$ ma.FIG. 14. $t_{1/2}$ vs. V_∞

the circuit was closed again. The electrode potential, ϵ , was taken to be the value of V immediately before the circuit was closed, since equation (II) becomes $V = \epsilon$ when the current is interrupted. The resistance r is determined by measuring $V_{on} = \epsilon + ir$ just before the circuit is broken, or just after it is made, and also measuring $V_{off} = \epsilon$ just after the circuit is broken, or just before it is made. Eliminating ϵ and solving for r it is seen that in either case

$$r = (V_{on} - V_{off})/i \quad (\text{VIII})$$

With the apparatus at hand it was not possible to obtain off-times shorter than 0.005 sec. The dashed line at $r = 400$ ohms represents the value of r at the instant of interruption (calculated on the basis that $\epsilon = \epsilon_{II} = +0.11$ v).

The data show that the abrupt drop in ϵ does not begin until the decay of r is more than 96% complete.

Schlieren study after break.—When the steady-state current is interrupted, fairly rapid changes in the anolyte seem to occur, but whether or not they correspond to the sudden drop in ϵ cannot as yet be stated with certainty. The schlieren photographs in Fig. 15 show that 10 sec after interruption the Cl^- gradient is nearly erased, while the stream of anode product continues almost unabated as the layer continues to dissolve. After 20 sec the Cl^- gradient can no longer be detected and the CuCl_2^- gradient has begun to iron out, all of the layer having been removed at this time. After 40 sec the CuCl_2^- is no longer streaming from the anode, and by the time 60 sec have elapsed the anolyte has almost regained the composition of the main body of solution. From Fig. 13 it can be seen that the time required for erasure of the concentration gradients is about the same as the time required for decay from $\epsilon_I = -0.27$ v to $\epsilon_0 = -0.35$ v. This is consistent with

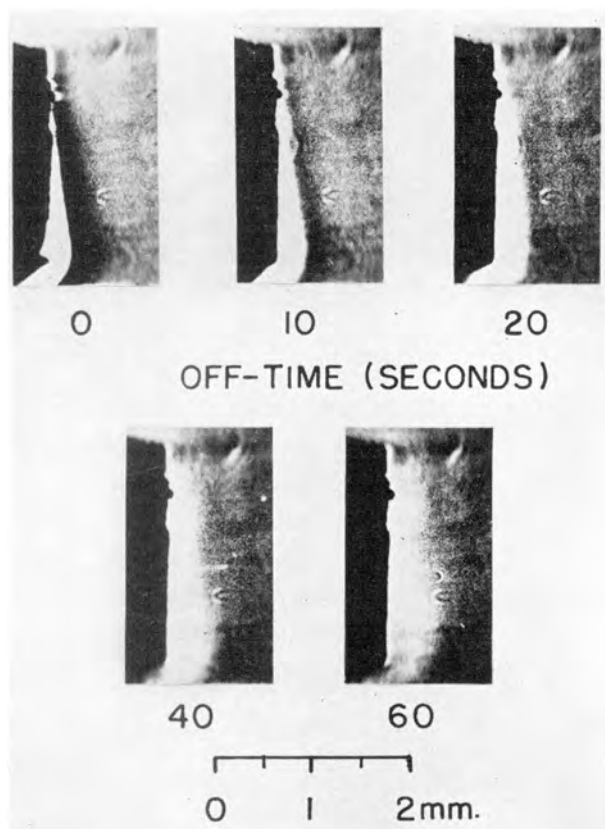


FIG. 15. Schlieren study of the analyte following interruption of the steady state $V_{\infty} = +0.25$ v, $i_{\infty} = 1.8$ ma.

the previous hypothesis that the difference in these two potentials is to be attributed to concentration polarization.

DISCUSSION

The present work has demonstrated the nature of the processes associated with that portion of the make transient up to the current minimum. The early layer growth starts from randomly distributed nuclei on the anode surface and proceeds radially so that little knobs are formed. When these have grown sufficiently, they touch each other. The anode will then have a thin continuous layer upon it, and this needs (18) to be only a few molecules thick (i.e., of the order of 10^{-7} cm) in order to establish the potential characteristic of a copper electrode covered with CuCl. It was found (Fig. 8) that ϵ may increase suddenly without a corresponding change in r , indicating that the portion of the layer responsible for the increase must have negligible resistance and, consequently, be very thin. The subsequent increase in r indicates the completion of a relatively thick layer, because it exhibits a large resistance. It should be emphasized that no sharp distinction or boundary is imagined to exist between the thin ϵ -layer and the thick r -layer. Both are

imagined to grow simultaneously during the course of a transient and to be completed at very nearly the same time, completion of the r -layer usually lagging, but never preceding that of the ϵ -layer.

A kinetic explanation will be achieved when one can predict quantitatively how the electrode potential ϵ and the resistance r will vary with time. At the end of the first plateau, ϵ changes rapidly, and this may indicate the rate at which the surface becomes covered (3). From the beginning of the second plateau, however, ϵ is nearly constant, so that the current changes are due to changes in the resistance r . The detailed mechanism of how these changes occur is still obscure, but it may be possible to learn more about it by suitable make and break experiments. In particular, data are needed for the variation of r with time when the steady state is interrupted for times less than 0.01 sec.

SUMMARY

When the circuit is closed in the Cu | 2N HCl(aq) | H₂(Pt) system, the current exhibits a very brief initial spike. The anode-calomel potential may be represented at all times $>10^{-5}$ sec by $V = \epsilon + ir$, where ϵ , the electrode potential, has no noticeable dependence on i at high currents, and r , the resistance within the cell between anode and calomel, is ohmic in nature. The open circuit voltage is -0.44 v, and has four characteristic values thereafter. Immediately after the spike, $\epsilon = \epsilon_0 = -0.35$ v. The current drops from i_0 to an approximately constant value i_I (first plateau), and ϵ becomes $\epsilon_I = -0.27$ v. (This change is attributed to concentration polarization.) The charge Q which must flow before the current completes its drop to a new constant value i_{II} (second plateau) is connected with i_0 by the empirical relation $Q = 24(i_0 - 0.70)^{-0.53}$. The value of ϵ_{II} as determined by extrapolation of the (V_{II}, i_{II}) plot is $\epsilon_{II} = +0.11$ v; the value found from interruption experiments is $\epsilon'_{II} = -0.05$ v. This could be accounted for by an overvoltage term with a decay time of 10^{-5} sec or less. The value of r is constant up to the second plateau, and corresponds to the resistance of the solution. The second plateau has a duration which is shorter, the smoother the surface. It is followed by a rapid drop in i and the associated rapid increase in resistance. A slower change then occurs, and the current may go through a minimum value i_{min} before reaching the steady state i_{∞} .

From the moment electrolysis begins, an anode layer grows sideways, starting at many randomly spaced points. It is probably composed of CuCl, formed by the reaction $\text{Cu} + \text{Cl}^- \rightarrow \text{CuCl} + e^-$ and removed by the reaction $\text{CuCl} + \text{Cl}^- \rightarrow \text{CuCl}_2^-$. When the anode has become completely covered,

the layer is of the order of 10^{-4} cm in thickness. At this point an abrupt drop in i occurs (due to the sudden ϵ change). This is followed by a rise in resistance, which occurs when the pores are closed, and only slightly more CuCl is deposited than that necessary to cause the ϵ change. During the period when the high current was flowing a steep Cl^- gradient was established. The quick drop in i does not affect the over-all diffusion layer, and so the Cl^- continues to diffuse slowly toward the anode, building up the concentration. This will reduce the resistance of the layer, for it is more soluble in higher concentrations of Cl^- . In the steady state the layer formation reaction proceeds at the same rate as the layer removal reaction, the net reaction being $\text{Cu} + 2\text{Cl}^- \rightarrow \text{CuCl}_2 + e^-$.

When the steady-state current is interrupted (V_∞ assumed to be greater than ϵ_{II}), V drops instantly from V_∞ to ϵ_{II} (an ir drop) then decays very rapidly to $\epsilon = -0.05$ v (an overvoltage decay) where it remains relatively constant. At the interruption r begins to decrease rapidly, presumably due to Cl^- attack on the outer part of the anode layer. When the decay of r is approximately 96% complete, the inner part of the layer apparently ruptures and ϵ drops abruptly from -0.05 v to -0.27 v (ϵ_1). After several seconds, depending on the value of V_∞ before interruption, the layer, whose thickness was of the order of 10^{-4} cm before interruption, is completely dissolved. As the concentration gradients in the anolyte gradually disappear, ϵ drops from ϵ_1 to ϵ_0 . Thereafter ϵ continues to drop slowly until it eventually reaches ϵ_{00} .

ACKNOWLEDGMENTS

This work was supported at the outset by the University of Illinois Research Board and then by the Office of Ordnance Research, and the authors

desire to express their deep appreciation to both organizations for their help. Professor C. Wagner and Dr. A. K. Graham gave them invaluable encouragement and aid. They also wish to thank Mr. Jack Hinde for very competent assistance with the reduction of the data, and Mr. Ralph S. Cooper for his critical reading of the manuscript.

Any discussion of this paper will appear in a Discussion Section to be published in the June 1955 issue of the JOURNAL.

REFERENCES

1. J. H. BARTLETT, *Trans. Electrochem. Soc.*, **87**, 521 (1945).
2. J. H. BARTLETT AND L. STEPHENSON, *This Journal*, **99**, 504 (1952).
3. L. STEPHENSON, Thesis, University of Illinois (1953).
4. F. P. BOWDEN AND J. N. AGAR, *Ann. Repts. Progr. Chem.*, **1938**, 90.
5. A. L. FERGUSON, *Trans. Electrochem. Soc.*, **76**, 113 (1939).
6. A. HICKLING AND F. W. SALT, *Trans. Faraday Soc.*, **37**, 450 (1941); **38**, 474 (1942). See also F. W. SALT, *Disc. Faraday Soc.*, **1**, 169 (1941).
7. A. FRUMKIN, *Acta Physicochim.*, **18**, 23 (1943).
8. A. HICKLING, *Disc. Faraday Soc.*, **1**, 127 (1947).
9. G. E. KIMBALL AND A. GLASSNER, *J. Chem. Phys.*, **8**, 815 (1940).
10. P. FAYOLLE AND P. NASLIN, "Photographie Instantanee et Cinematographie Ultra-rapide," p. 9, Editions de la Revue d'Optique, Paris (1950).
11. O. GATTY AND E. C. R. SPOONER, "The Electrode Potential Behavior of Corroding Metals in Aqueous Solutions," Chap. IV, Clarendon Press, Oxford (1938).
12. C. WAGNER, Private communication.
13. ST. V. NARAY-SZABO AND Z. SZABO, *Z. phys. Chem.*, **166**, 228 (1933).
14. S. R. CARTER AND F. M. LEA, *J. Chem. Soc.*, **127**, 499 (1925).
15. A. A. NOYES AND M. CHOW, *J. Am. Chem. Soc.*, **40**, 739 (1918).
16. G. BODLÄNDER AND O. STORBECK, *Z. anorg. Chem.*, **31**, I, 458 (1902).
17. P. A. JACQUET, *Trans. Electrochem. Soc.*, **69**, 629 (1936).
18. H. MAYER, "Physik dünner Schichten", Wissenschaftliche Verlagsgesellschaft, Stuttgart (1950).

Reaction of Thallium with Oxygen and Moisture¹

J. T. WABER AND G. E. STURDY

Los Alamos Scientific Laboratory of the University of California, Los Alamos, New Mexico

ABSTRACT

Reactions of thallium with water vapor and air were investigated in the range 25°–75°C to throw light on the mechanism of atmospheric corrosion. It was deduced on the basis of changes in the rate laws, and confirmed by x-ray diffraction, that the principal reaction product changes from Tl_2O to $TlOH$ as the relative humidity of air increases. Parabolic and cubic laws, as well as a new growth law, were observed. Effects of carbon dioxide and of preformed sulfide films were also studied. The tentative x-ray structure of $TlOH$ is presented.

INTRODUCTION

Atmospheric attack on thallium is relatively slow (1), the observed initial penetration rate being 2–10 μ /day depending on the aggressiveness of the environment.

Several investigations have been made of the dissolution of thallium in mineral acids (2–8), but only two of them (4, 5) contain information which may be applied to atmospheric corrosion. Plank and Urmanczy (4) concluded that the reaction between thallium and water is determined by hydrogen overvoltage, and that dissolved oxygen has a strong effect on the reaction at 25°C. For example, corrosion of thallium occurs 1.4 times as fast in air-saturated water as in hydrogen-saturated water; with oxygen-saturated water the reaction takes place 12.2 times as rapidly. In a later paper (5) they present evidence that thallium does not react with water at 25°C in the absence of oxygen. From these data the rate is probably less than 3 mg/cm²/hr at 25°C.

The data of this paper are divided into five groups; (a) oxidation of thallium in dry oxygen and dry air; (b) effect of humidity and temperature on the change of mechanism; (c) x-ray study of products formed under different conditions; (d) effect of a preformed sulfide film; and (e) a brief evaluation of the effect of carbon dioxide. Surprisingly, the cubic growth law was observed in addition to the more usual parabolic one. A hitherto unreported time dependence (growth law) was observed, and it plays an important role in the over-all picture of corrosion of this metal.

EXPERIMENTAL DETAILS AND RESULTS

High purity thallium metal was rolled to form 2-mil and 20-mil foils, then stored in mineral oil. Before use, the metal foil was degreased with petroleum ether and immersed in a warm perchloric

acid solution (11% by volume) to remove surface oxide. The metal remained bright when stored in the cold acid.

At the beginning of each run, samples were cut to the desired size, immersed in acid, then washed with alcohol, acetone, and finally with ethyl ether. They were put in numbered porcelain crucibles which were placed in desiccators containing different saturated salt solutions. The salt solutions were selected to maintain certain constant humidities throughout the run. The desiccators and their contents were then placed in constant temperature ovens. For runs in which a gas other than air was used, the desiccator was purged for 10 min before it was returned to the oven. Periodically, the samples were removed for weighing. The crucible and specimen were weighed together on an Ainsworth Type FDJ microbalance. After weighing, the specimen and crucible were returned to the desiccator, and the desiccator was again purged.

In a few additional runs, samples were weighed by measuring the extension of silica helixes from which samples were suspended within the corrosive medium. Thus, samples were not exposed to air during weighing. This technique did not yield results significantly different from those obtained by the microbalance technique; however, due to certain inherent features of the silica helix method, the data showed more scatter than did those obtained with the microbalance. Since the value of the silica helix data lies only in showing that significantly different products were not formed when air was excluded during the weighings, these data are not included here.

Test periods during which weighings were carried out lasted from 210 to 240 hr. Specimens for x-ray work were repeatedly examined for periods up to 750 hr without detectable change in identity of the products. Although these are not long-term experiments when compared with conventional weathering tests, it was felt that observations were continued

¹ Manuscript received August 20, 1953.

TABLE I. Reaction parameters for dry oxygen

Run No.	Temp, °C	Gas present	Time slope, n	Rate constant, k_n
13	38	oxygen	0.56	2.82
14	38	oxygen	0.58	2.97
21	57	oxygen	0.53	1.77
23	57	oxygen	0.53	1.77
19	75	oxygen	0.66	2.81
20	75	oxygen	0.76	0.93
17	38	air	0.59	2.06
18	38	air	0.59	1.65

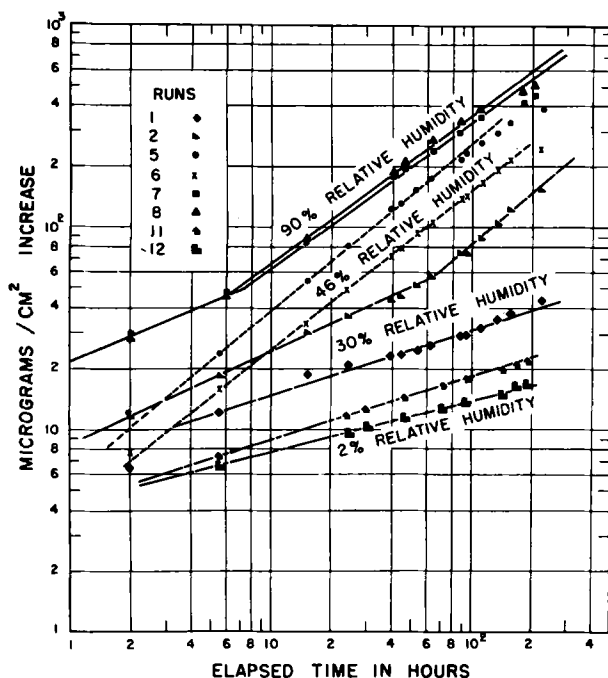


FIG. 1. Graphical summary illustrating the effect of the moisture content of air on the corrosion rates and the rate laws.

TABLE II. Effect of relative humidity on rate constants and time dependences at 38°C

Run No.	Relative humidity	Gas present	Time slope, n	Rate constant, k_n
11	2	air	0.31	4.38
12	2	air	0.25	4.34
1	30	air	0.33	6.25
2*	30	air	{0.46 0.84}	{8.40 1.70}
15	30	helium	0.36	5.24
16	30	helium	0.36	5.24
5	46	air	0.76	7.2
6	46	air	0.78	4.1
7	90	air	0.70	13.2
8	90	air	0.70	13.2

* Two values of n and k occur successively during this run as shown in Fig. 2.

long enough to give a reasonable idea of corrosion behavior.

X-ray diffractometer patterns of the fresh metal surface were taken with a General Electric XRD-3 instrument. After exposure the samples were again

examined. X-ray spectra of pure compounds were obtained wherever possible.

Treatment of Data

Experimental weight gains, w , were plotted on log-log coordinate paper as $\mu\text{g}/\text{cm}^2$ vs. elapsed time, t , in hours. When a straight line results, one may conclude that the corrosion reaction follows a rate law such as

$$W = k_n t^n \quad (\text{I})$$

On such a log-log plot the slope of the line is equal to n , and the rate constant, k_n , is equal to the weight gain at the end of 1 hr. Values of n and k_n are tabulated and discussed for each run. Exponents are, respectively, one-half and one-third for the parabolic and cubic laws (9).

Reaction with Dry Oxygen and Dry Air

Rate parameters of metal specimens exposed to oxygen in contact with dry P_2O_5 are listed in Table I. The time dependence is quite different from average values observed for tests with water present, especially at lower temperatures.

In addition, several runs were made in air dried with MgClO_4 for x-ray work. Reliable weight gain data could not be obtained in these cases because oxide was lost occasionally during the frequent manipulation necessary to align the specimen in the x-ray diffractometer.

Reaction with Moist Air

In contrast to the parabolic time dependence observed with dry oxygen, the cubic law is followed at low relative humidities and temperatures. However, a new rate law was obtained under more aggressive conditions. This observation led to the conclusion that a change in mechanism was involved. Much of this report is devoted to clarifying what reactions are involved.

The bulk of the data relating to the effect of humidity was obtained at 38°C. This temperature is a practical upper limit for atmospheric corrosion tests. Some of the data are presented graphically in log-log form in Fig. 1. Values of n and k_n for each run were calculated from the lines shown in Fig. 1 and are listed in Table II.

Curves in Fig. 1 show that two different average slopes are needed to describe the whole set of data. Table II shows that the slopes, n (time dependences) are generally greater at higher humidities. At lower humidities (runs 1, 2, 11, 12, 15, 16) the average value² of n is 0.34, whereas n increases to an average value of 0.74 for higher humidities. This observation suggests that the mechanism changes significantly in the vicinity of 30% relative humidity. The amount of metal consumed after 200-hr ex-

² Excluding the second higher n value for run 2.

posure to low humidities is significantly less than if the 4/3 law had been followed for the same period. Clearly, then, moisture increases the rate of attack.

At higher temperatures the time dependence increases at 30% relative humidity. Corresponding rates and time dependences for temperatures between 38° and 75°C are listed in Table III.

These data suggest that nucleation and growth of the hydroxide are more rapid as the temperature increases, despite a lower degree of supersaturation. The equilibrium pressure, as shown in Appendix A, corresponds to 8 and 11% relative humidity at 57° and 75°C.

Significantly the time dependences in runs 3 and 4 changed from 0.814 and 0.805 to 0.3 and 0.35, respectively, at about 40 hr. This phenomenon is illustrated in Fig. 2. Cubic rate constants are 35 and 28, respectively. At 39 hr, corroded specimens had changed color from rust to chocolate brown. The rust color was commonly observed in tests made at low humidities.

On the basis of x-ray studies, it is probable that the high values of n for 75°C are due to formation of Tl_2O_3 from $TlOH$.

Rate of Hydration

To substantiate the deduction that the 4/3-law, which is dominant at higher humidities, corresponds to the reaction of the oxide (already formed) with water vapor, the rate of hydration of thallos oxide was studied directly. A specimen of metal was converted to oxide by exposing it to dry oxygen at 75°C. The oxide sample was exposed to air containing 30% relative humidity at 35°C, and weight changes were determined by the microbalance technique.

The resulting time dependence was 0.75 and the rate constant was 1.2, based on the area of the metal specimen. These rate parameters are in reasonably good agreement with results shown in Table III, and in particular with the values $n = 0.84$ and $k_n = 1.7$ found in run 2 (for 38°C).

Dissolution in Boiling Water

Two tests were run in vigorously boiling water. The flask containing the specimens was equipped with a reflux condenser which was loosely stoppered. Reasonably large quantities of thallium dissolved despite the reduced oxygen content of the boiling water. In the first case, 0.57 mg/cm² dissolved in 4.5 hr. In the second, 6.3 mg/cm² dissolved in 2 hr. However, in the second run, the rather adherent hydroxide was removed from the specimen before weighing. Assuming that a linear rate law was followed, these data compute to 130 and 3100 $\mu\text{g}/\text{cm}^2/\text{hr}$ for 92°C. These rates are very large in com-

TABLE III. Effect of temperature on rate constants and time dependences at 30% relative humidity

Run No.	Relative humidity	Gas present	Time slope, n	Rate constant, k_n
1	38	air	0.33	6.25
2	38	air	{ 0.46 0.84	{ 8.40 1.70
15	38	helium	0.36	5.24
16	38	helium	0.36	5.24
3	57	air	0.81	5.87
4	57	air	0.80	4.80
9	75	air	0.95	7.98
10	75	air	0.95	7.98

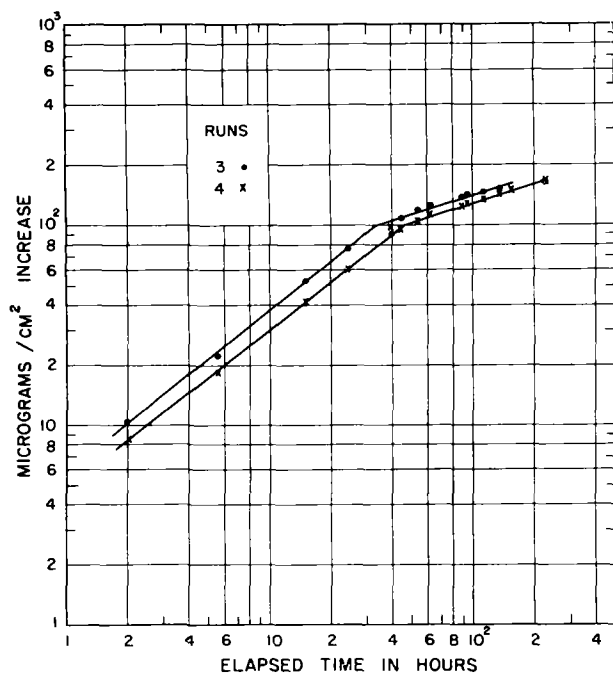


FIG. 2. Unexplained decrease in time dependence with increasing time. Possibly it indicates a change to oxide formation.

parison with those shown in Table II. Certainly the dissolution of thallium proceeds rapidly in the presence of very little air.

X-Ray Studies

Positive identification of products was hampered by a lack of published x-ray diffraction data for the hydroxide. Some preparative chemistry was necessary to connect observed patterns with this product. The crystal structure of $TlOH$ was determined during this investigation.

Two pieces of thallium metal were exposed to dry air at 35° to 70°C in desiccators containing $MgClO_4$. Periodically x-ray diffractograms were taken. The resulting patterns agree quite well with regard to the line positions reported by Halla, Tompa, and Zimmerman (10) for thallos oxide. However, significant differences in line intensities

TABLE IV. Effectiveness of sulfide films in reducing corrosion

Run No.	Temp, °C	Gas present	Relative humidity	Time slope, n	Rate constant, k_n
29	38	oxygen	P ₂ O ₅	0.35	15.4
30	38	oxygen	P ₂ O ₅	0.35	12.2
31	38	helium	30	0.81	3.2
32	38	helium	30	0.78	4.55

TABLE V. Rate parameters for attack by moist and dry carbon dioxide

Run No.	Relative humidity	Temp, °C	Time slope, n	Rate constant, k_n
23	P ₂ O ₅	38	0.41	5.40
24	P ₂ O ₅	38	0.41	5.40
25	30	38	0.18	27.0
26	30	38	0.18	27.0
27	30	38	0.02	53.0
28	30	38	0.03	36.8

were noticed.³ A very plausible explanation is that the oxide pattern formed on the heavily rolled (and thus strongly oriented) metal was itself strongly oriented. Such orientation alters the relative intensities from those observed for a random powder sample. Further investigation of the orientation relationship has been deferred.

Because the equilibrium pressure of the thallos hydroxide-oxide reaction varies from 10 to 30% relative humidity over a range of temperatures, as shown in Appendix A, x-ray diffraction patterns of corrosion products formed at two temperatures were studied using humidities above and below this equilibrium value. In agreement with conclusions drawn from reaction rates, Tl₂O is formed in dry air and TlOH is formed in high-humidity air.

Several diffractometer traces were made of a specimen exposed to 50% relative humidity at 70°C. The changes in pattern strongly suggested that TlOH was being oxidized to Tl₂O₃ as time increased. After 233 hr exposure, when the product was mainly Tl₂O₃, the specimen was placed in dry air at 70°C. Diffractograms indicate that TlOH was converted to Tl₂O and that Tl₂O₃ was unaffected.

To confirm this deduction, the specimen, which had been exposed only to dry air at 70°C and which exhibited at Tl₂O pattern, was placed in a desiccator containing air of approximately 20% relative humidity at 70°C. After 10 hr exposure, the x-ray diffractogram indicated formation of TlOH plus some Tl₂O₃. Further exposure indicated the growth of Tl₂O₃.

³ In addition, there was some evidence to indicate that line positions changed slightly with time in such a way as to suggest a decrease in cell size.

Sulfide Films

Gibney (11) suggested that since thallium is somewhat similar to lead in its behavior and both readily form sulfides, a thin coating of thallos sulfide might be protective. In order to investigate this possibility, samples were dipped into a strong ammonium polysulfide solution for several minutes until a uniform thin coating of the sulfide had formed. The specimens were then washed, dried, and treated as described previously. It was found that the corrosion rate apparently increases in the presence of the sulfide film. Ultimately, in dry oxygen it would appear to be advantageous to use sulfide films since the cubic growth law corresponds to a protective film more than does the parabolic law ($n = 1/2$). Table I shows that the parabolic law is characteristic of the reaction with dry oxygen. However, the benefits of using such sulfide films are slight at best (Table IV).

Reaction with Carbon Dioxide

Thallium carbonate was found in corrosion products which had been allowed to stand in the laboratory for years. To ascertain whether carbon dioxide was contributing to atmospheric attack, tests were run in dry and in moist carbon dioxide (Table V). Aside from water and unintentional impurities, the gas was 100% carbon dioxide.

Samples used in four runs with moist carbon dioxide showed very little increase in weight after the large initial increase which had occurred by the end of 1 hr. Inasmuch as the metal samples were not consumed during exposure, it appears that attack is virtually stopped by a protective film formed after the initial rapid attack.

The time dependence observed in runs 25–28 appear sufficiently different from 0.34 and 0.74 to justify the conclusion that carbon dioxide is not contributing significantly to the corrosion mechanism in laboratory atmospheres.

However, 0.41 lies between the values of 0.33 and 0.50 which are characteristic of low humidities and dry air. The rate constant 5.40 for carbon dioxide in contact with phosphorus pentoxide, is larger than those shown in Table IV for phosphorus pentoxide-dried oxygen. Thus, it is possible that carbon dioxide might contribute to weight gain in the low-humidity region. The rate constant for approximately 100% carbon dioxide is only 35% greater than that for runs in air ($n \approx 1/3$) extrapolated to zero humidity. Considering that the carbon dioxide content of air is seldom greater than a few percent, it is reasonable to conclude that direct reaction of the metal with carbon dioxide from laboratory atmospheres is probably unimportant. One cannot conclude that its reaction with the oxide is of neg-

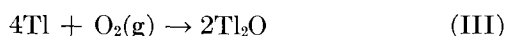
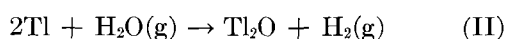
ligible influence on the over-all reaction kinetics. In fact, it is very difficult to prepare carbonate-free thallos oxide by wet chemical methods. However, x-ray patterns of the two specimens exposed to laboratory air contained no lines which could be attributed definitely to thallium carbonate.

When one of these specimens was subsequently exposed to 50% relative humidity at 35°C it exhibited several unidentified lines and gave off gas when immersed in 10% by volume perchloric acid. These observations suggest thallos bicarbonate may form from the hydroxide.⁴

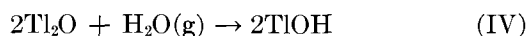
DISCUSSION

The principal conclusions of this paper were deduced from rate data confirmed by x-ray diffraction. The corrosion product is mainly thallos oxide or hydroxide depending on humidity.

On the basis of rate parameter data, the effects of humidity can be explained if one of the two reactions:



occurs in the low-humidity range and if either



occurs in the high-humidity range. Although Plank and Urmanczy (6) state that reaction (II) will not occur in the absence of oxygen, data to the contrary have been presented here.

Runs 15 and 16, made in moist helium, show that direct reaction with water to form thallos oxide occurs at 38°C in the absence of oxygen. Similarly, oxidation of thallium by boiling water occurs in the virtual absence of dissolved oxygen. The rate of reaction with water is small in comparison to the rates Plank and Urmanczy initially observed in aerated solutions (4) and the limit (ca. 3 $\mu\text{g}/\text{cm}^2/\text{hr}$ at 25°C) set later by how much thallium they could detect by titration does not seriously disagree with rates from Tables II and III.

The effect of dissolved oxygen is probably one of depolarization rather than direct reaction. Hence, their statement that rate is strongly dependent upon oxygen content is correct, but the statement that reaction will not occur in the absence of oxygen is in contradiction to the present data, and a slow reaction cannot be excluded by their experiment. In experiments using silica springs, reaction occurred, although oxygen was carefully excluded.

One may estimate the depolarizing effect of aera-

⁴The x-ray pattern for TlHCO_3 is apparently not known.

tion by comparing the average value of k_n for runs 1 and 2 and for runs 15 and 16. The ratio is 1.4 in agreement with the figure cited by Plank and Urmanczy (4).

It is interesting to note that at lower humidities (runs 1, 2, 11, 12, 15, and 16) the average value⁵ of n is 0.34, whereas n increased to an average value⁶ of 0.74 for higher humidities. This observation suggests that the mechanism changes significantly around 30% relative humidity. The rate constant, k_n , is roughly proportional to the relative humidity. A line drawn through k_n values for $n = 0.74$ passes close to the origin. In contrast, the few values available for the cubic law ($n \simeq 1/3$) extrapolate to $k_n \simeq 4$ at 0% relative humidity.

It was not clear from data in Tables II and III whether the reaction to form hydroxide proceeded by steps, such as reaction (II) followed by reaction (IV), or by the over-all reaction (V). Thus the hydration reaction (IV) was studied by using a specimen of thallos oxide. The resulting time dependence and rate constant were almost equal to the average values found for high-humidity runs. One might note that the weight change accompanying formation of hydroxide from a given amount of metal is 2.13 times as great as that for oxide formation. Thus, the hydration reaction would appear to be dominant and rate-controlling in the over-all reaction, even if the rates for reaction (II) and (IV) were approximately equal.

Since the time dependence of reaction (III), $n \simeq 1/2$, is different from that observed at low humidity, $n \simeq 1/3$, it is concluded that reaction (II) is dominant. The hydration reaction (IV) has a time dependence of $n = 3/4$, which is in agreement with that found in the high-humidity range. Therefore, it was concluded that the sequence of reactions, (III) plus (IV), accounts for the over-all behavior represented by equation (V).

The equilibrium water pressure of a thallos-oxide-hydroxide mixture amounts to a relative humidity of 5% or more at 38°C, as shown in Appendix A. Thus, the change from reaction (III) to reactions (III) plus (IV), as relative humidity is increased, is consistent with the change in thermodynamic stability. As humidity is decreased from 30%, it becomes less likely that the hydroxide product is formed by reaction (III) plus (IV), and in dry air this over-all reaction would nearly cease as evidenced by k_n approaching zero. At low humidity-

⁵ Excluding the second higher n value for run 2.

⁶ In 8 of 26 runs, n was found to be in the range 0.70 to 0.84 and to have a mean value of 0.74. To the best of the authors' knowledge, such a time dependence has not been previously reported. Although no theoretical justification for this time dependence or slope is readily evident, its use appears to be empirically justified.

ties, however, a different reaction is responsible. Even at 30% relative humidity the product is apparently mainly the compound Tl_2O .

It appears that since 30% relative humidity is substantially greater than 5.5% (the equilibrium water pressure estimated from Appendix A at 38°C) one might expect the change in mechanism to occur at somewhat lower humidities. Undoubtedly the formation of $TlOH$ does occur occasionally at humidities near 15 or 20%. The limiting factor is nucleation of the hydroxide.

As Langmuir (12) pointed out, heterogeneous chemical reactions can occur only at the interface between two reacting phases. Numerous examples of hydration and decomposition reactions have supported this hypothesis. Thus nuclei of the hydroxide must either be present or be formed before reaction (IV) can continue.

It is well known that large supersaturations are required to nucleate heterogeneous reactions. One such reaction, a phase change, is formation of drops of moisture from water vapor. The ΔH of formation of the hydroxide from the oxide is balanced by the energy required to form the oxide-hydroxide interface. With the heat of formation (13.6 kcal) having the same magnitude as the latent heat of condensation of water (10.6 kcal/mole), it might be expected that a large degree of supersaturation would be required to nucleate the hydroxide. Of course, for this argument it is assumed that the magnitude of surface energy at the solid interface is comparable to that of the steam-water interface. Experience indicates that solid interfacial energies are large. Thus, a reasonable explanation appears to be that the hydroxide does not form below 30% relative humidity because it cannot be nucleated easily in this humidity range. The rate of formation of hydroxide in comparison with that of the oxide would probably be slow until supersaturation became relatively large.

During run 2, made at 30% relative humidity, the time dependence changed abruptly from 0.46 to 0.84. A reasonable explanation is that the hydroxide was locally nucleated and spread rapidly across the specimen surface.

CONCLUSION

In the corrosion of thallium the observed change in growth law from the cubic to the $\frac{4}{3}$ -power time dependence as the relative humidity is increased is associated with a change from formation of thallose oxide to formation of the hydroxide as the principal product. The reaction of thallium with water vapor in the low humidity range, and the hydration of thallose oxide in the higher humidity range are concluded to be the dominant reactions.

ACKNOWLEDGMENTS

The assistance in this investigation of many members of the staff is greatly appreciated. Especially helpful were E. Staritzky's chemical microscopy studies, C. F. Stambaugh's and D. D. Whyte's preliminary x-ray diffraction studies and R. N. R. Mulford's work in preparing and analyzing several compounds. The author is indebted to J. Singer for making available his unpublished results on the crystal structure of thallose hydroxide.

Any discussion of this paper will appear in a Discussion Section to be published in the June 1955 JOURNAL.

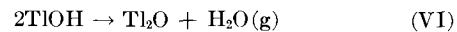
REFERENCES

1. H. E. HOWE AND A. A. SMITH, JR., *This Journal*, **97**, 167C (1950).
2. J. PLANK AND A. URMANCZY, *Z. anorg. Chem.*, **238**, 51 (1938).
3. M. CENTNERSZSER, *Atti Congr. intern. chim. 10th Congr. Rome*, **3**, 555 (1939).
4. J. PLANK AND A. URMANCZY, *Z. anorg. Chem.*, **241**, 158 (1939).
5. J. PLANK AND A. URMANCZY, *ibid.*, **241**, 416 (1939).
6. J. PLANK AND A. URMANCZY, *Korrosion u. Metallschutz*, **16**, 33 (1940).
7. J. PLANK AND A. URMANCZY, *Magyar Kém. Folyóirat*, **46**, 113 (1940).
8. J. PLANK AND A. URMANCZY, *Korrosion u. Metallschutz*, **17**, 141 (1941).
9. J. T. WABER, *Metal Prog.*, **62**, 76 (1952).
10. F. HALLA, H. TOMPA AND L. ZIMMERMAN, *Z. Krist.*, **86**, 303 (1933).
11. R. B. GIBNEY, Private communication.
12. I. LANGMUIR, *J. Am. Chem. Soc.*, **38**, 2263 (1916).
13. F. BAHR, *Z. anorg. Chem.*, **71**, 93 (1911).
14. R. DE FORCRAND, *Compt. rend.*, **176**, 873 (1923).
15. J. SINGER, Unpublished work (1951).

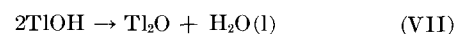
APPENDIX A

Equilibrium Decomposition Pressure of Thallose Hydroxide

The equilibrium pressure of water vapor over a mixture of thallose oxide and hydroxide has been studied by Bahr (13). His data are plotted both as the pressure in millimeters of mercury and as relative humidity vs. the reciprocal absolute temperature. From such a slope, since the equilibrium constant is proportional to pressure for such a heterogeneous reaction, one calculates ΔH for the reaction



to be 13.64 kcal. Heats of solution have been determined by De Forcrand (14) to be 28.327 kcal and 25.210 kcal for $2TlOH$. The difference, 3.117 kcal, is the heat of reaction using liquid water. Employing the latent heat of vaporization of water at 10°C as 10.627 kcal/mole, the difference, 3.02 kcal, is the heat of reaction using liquid water. That is, the heat change for the reaction



is 3.02 determined from vapor pressures and 3.117 determined calorimetrically. The two values agree well enough to justify the conclusion that the line representing the data in Fig 3 is correct. The ΔH from this graph is the average

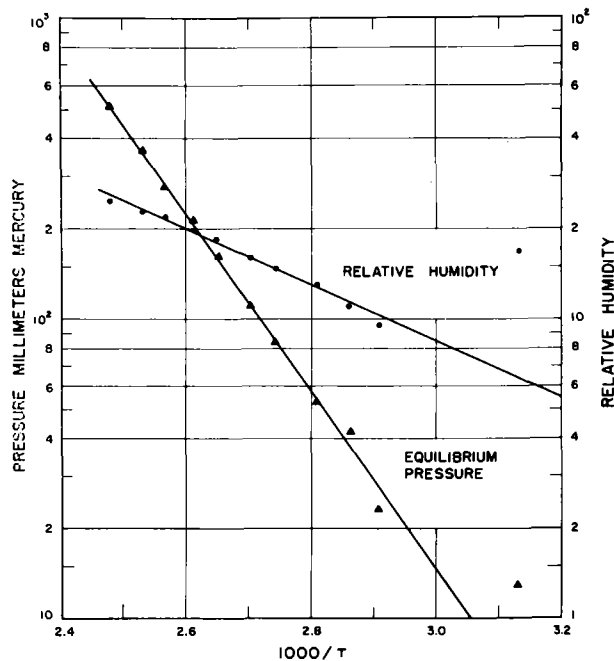


FIG. 3. Variation in equilibrium decomposition pressure of thallos hydroxide with temperature. These pressures correspond to the indicated equivalent relative humidities.

determined for the range 60°–130°C and has not been corrected to 10°C. The effect of ΔC_p , as can be seen from the slight downward concavity of the data, would be to increase the difference slightly and to bring it into better agreement.

APPENDIX B

Crystal lattice parameters and the space group of thallos hydroxide have been determined by Singer (15) from Weissenberg patterns.

The cell is hexagonal with the parameters

$$\begin{aligned} c &= 3.90 \text{ } kx \\ a &= 9.72 \text{ } kx \\ c/a &= 0.402 \end{aligned}$$

and contains 6 molecules per unit cell with the Laue symmetry $6/m$. The space group is $C6_3/m$. The six thallium ions are at:

$$\begin{array}{ll} x, y, \frac{1}{4} & \bar{x}, \bar{y}, \frac{3}{4} \\ \bar{y}, x - y, \frac{1}{4} & y, y - x, \frac{3}{4} \\ y - x, \bar{x}, \frac{1}{4} & x - y, x, \frac{3}{4} \end{array}$$

with $x = 0.312 \pm 0.001$ and $y = 0.350 \pm 0.001$.

The oxygen ions are in the same sixfold set, namely $6h$. Here the parameters are $x = 0.165 \pm 0.004$ and $y = 0.530 \pm 0.004$. The Tl-OH distance is $2.65 \pm 0.05 \text{ } kx$.

Some refinement in parameters may occur in the course of further detailed Fourier analysis.

The Effect of Ultrasonic Waves on the Electrodeposition of Copper^{1,2}

W. R. WOLFE,³ HYMAN CHESSIN,⁴ ERNEST YEAGER, AND FRANK HOVORKA

Department of Chemistry, Western Reserve University, Cleveland, Ohio

ABSTRACT

Effects of ultrasonic waves on the electrodeposition of copper have been determined at frequencies of 200 and 1000 kc/sec with acid-sulfate plating baths of various concentrations. Polarization measurements indicate that ultrasonic waves produce a marked decrease in polarization, while x-ray diffraction studies indicate that ultrasonic waves increase the tendency for preferred orientation. These effects are correlated with disruption of concentration gradients at the electrode surface by ultrasonic waves. Schlieren photographs of the gradients support these conclusions. Microagitation associated with moderately intense ultrasonic waves seems considerably more effective than ordinary mechanical stirring in breaking up concentration gradients at an electrode.

INTRODUCTION

Various workers (1-9) have reported⁵ the effects of ultrasonic waves on electrodeposition of metals. These effects extend from the improvement of the metal structure (3-5) to formation of colloidal suspensions of the metal instead of coherent deposits (7, 8). Relatively little specific information is available, however, with the exception of the work of Roll (5, 6) as to the effects of ultrasonic waves on polarization and structure of electrodeposits, particularly under controlled acoustical and electrochemical conditions.

As part of the present investigation, effects of ultrasonic waves on electrodeposition of copper have been ascertained in terms of polarization measurements and x-ray diffraction data. Copper has been chosen for this study because the activation polarization is small, simultaneous deposition of hydrogen is minor, and concentration polarization is significant in determining properties of the deposit. Microagitation associated with moderately intense ultrasonic waves (1 watt/cm²) should be effective in disrupting concentration gradients normally present adjacent to the cathode surface.

EXPERIMENTAL TECHNIQUES

Measurements have been made with ultrasonic waves at frequencies of 200 and 1000 kc/sec, with

¹ Manuscript received March 11, 1954. This paper was prepared for delivery before the Montreal Meeting, October 26-30, 1952.

² Work partially supported by the Office of Naval Research.

³ Present address: Experimental Station, E. I. du Pont de Nemours, Wilmington, Delaware.

⁴ Present address: Research Institute, University of Arkansas, Fayetteville, Arkansas.

⁵ For a review of the electrochemical applications of ultrasonic waves, see reference (9).

most of the research at the latter. The acoustical system used for the work at 1000 kc/sec is shown in Fig. 1. A circular, X-cut, quartz plate of 3 in. diameter was used to convert electrical energy from a 1000-watt, radio-frequency generator to acoustical energy. The quartz transducer was mounted in an underwater housing which permitted propagation of ultrasonic waves horizontally into the 80-gal, glass, thermostatic tank (Fig. 1). A similar arrangement was used for the measurements at 200 kc/sec. Acoustical intensities of as much as 20 watts/cm² were available directly in front of the quartz transducer, provided the water in the tank was relatively air-free and the unidirectional flow of the water associated with acoustical streaming was not impeded. Otherwise, gas-type cavitation bubbles would accumulate in the sound field and limit the intensity of ultrasonic waves which could be propagated a few centimeters to a few watts/cm² or less. Water in the glass tank was partially degassed by boiling under reduced pressure in a separate steel tank then pumping into the tank under a layer of oil to retard resaturation by air.

For part of the work, a reflector was placed at an oblique angle in the tank at the end opposite the transducer. This prevented formation of standing waves and greatly reduced complications associated with reflections from the back of the tank.

Electrochemical measurements were made in the glass cell shown in Fig. 2. This cell was located in the tank so that the cathode-containing section was in the ultrasonic field at a distance of 10 cm or less from the surface of the quartz transducer. Glass walls of the bulb containing the cathode were of the order of 10⁻³ in. in thickness, and hence did not scatter or reflect ultrasonic waves to any appreciable extent. A fritted glass plug was sealed into the bottom of the cell in order that the solutions might be

saturated with hydrogen gas when desired. The cathode surface was normally oriented at an angle of approximately 15° with respect to the wave front in order to avoid formation of standing waves. In addition, with the 15° angle, gas bubbles resulting from gas-type cavitation did not accumulate on the cathode surface but were swept away by unidirectional flow associated with ultrasonic waves of appreciable intensity.

Acoustical intensities have been calculated⁶ from pressure amplitudes as determined with a barium titanate hydrophone (10).⁷ Prior to electrochemical measurements, transmission characteristics of the glass bulb were checked by pressure amplitude measurements both inside and in front of the cell when it was filled with solutions similar to those used in actual electrodeposition. These data permitted calculation of acoustical amplitudes in the cell from acoustical measurements outside the cell. During electrochemical measurements, acoustical amplitudes were determined by moving the hydrophone momentarily to a point directly in front of the cell in the ultrasonic field. As a check, the hydrophone was placed in the cell in the position normally occupied by the cathode after electrochemical measurements had been completed. Response of the hydrophone was measured with a Ballantine vacuum tube voltmeter, Model 304. The hydrophone was calibrated by means of radiation pressure measurements over the range of acoustical parameters involved in the experimental work. This calibration was subsequently checked at intensities below cavitation levels against a similar hydrophone which had been previously calibrated by the U.S. Navy Underwater Sound Reference Laboratory at Orlando, Florida.

Absolute accuracy of the pressure amplitude measurements at or near the cathode surface for intensities of the order 1 watt/cm^2 or less was limited to a probable error of $\pm 15\%$ because of nonhomogeneity of the acoustical field as a result of refraction and diffraction effects as well as the gas-type cavitation bubbles which formed in the cell. At higher intensities the absolute accuracy became progressively less because of acoustical complications associated with pressure amplitude measurements in the presence of gas-type cavitation bubbles.

Polarization measurements were made by the direct method. The Luggin capillary was introduced

⁶ The acoustical intensity (I) is related to the rms pressure (p_o) by the equation $I = (p_o)^2/\rho c$ where ρ and c are the density and the velocity of sound in the solution.

⁷ For details concerning construction and performance characteristics of this type of hydrophone, see reference (10).

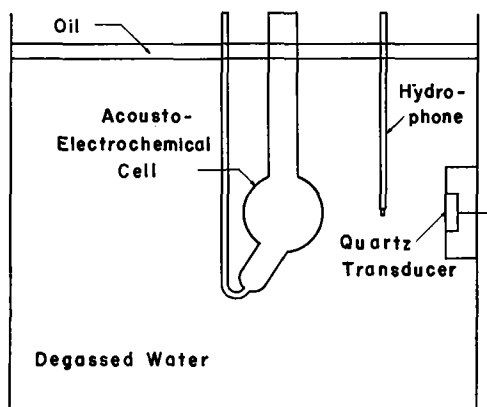


FIG. 1. Acoustical apparatus

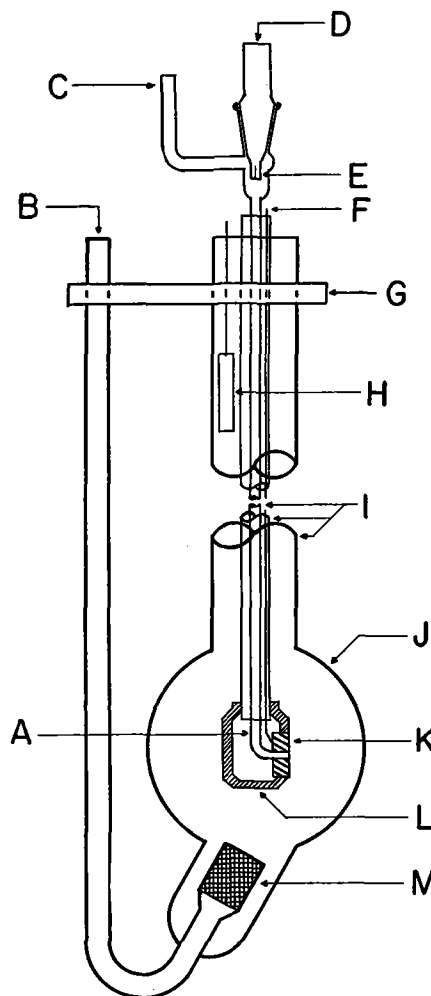


FIG. 2. Acousto-electrochemical cell. A—Luggin capillary; B—hydrogen gas; C—for filling capillary tube; D—solution bridge; E—asbestos; F—cathode lead; G—clamp; H—anode; I—glass; J—glass 0.001 in. wall; K—cathode; L—Lucite; M—glass frit.

through a hole in the back of the cathode in such a fashion that the tip was flush with the cathode surface (Fig. 2). This avoided acoustical complications which would have arisen if the Luggin capil-

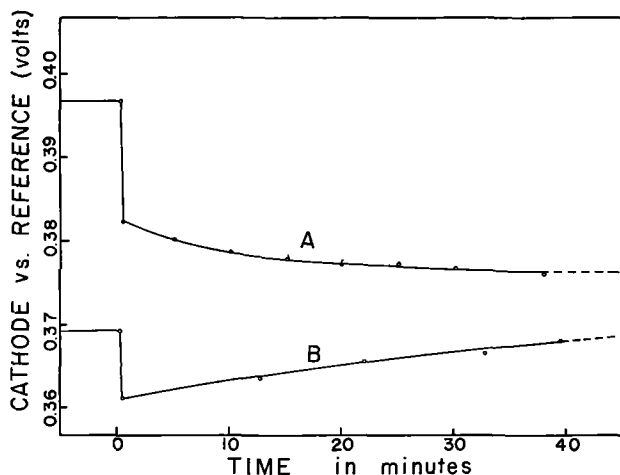


FIG. 3. Effect of ultrasonic waves on polarization as a function of time. Electrolyte: 0.17M CuSO_4 + 0.02M H_2SO_4 ; current density: 8 ma/cm²; temperature: 25° C; ultrasonic frequency: 1000 kc/sec; acoustical intensity: 0.8 watts/cm². Curve A: preplate below limiting current density; curve B: preplate above limiting current density.

lary had been placed in front of the cathode. From the Luggin capillary extended a solution bridge which connected with a saturated mercurous sulfate reference electrode. The part of the solution bridge adjacent to the Luggin capillary was filled with the plating solution, while the section of the bridge leading to the reference electrode was filled with a saturated potassium sulfate solution. A constricted capillary containing asbestos fiber was used to separate the two sections of the solution bridge as shown in Fig. 2. Apparent surface area of the copper cathode was 1 cm² for all measurements. The arrangement shown in Fig. 2 permitted removal of cathodes from the plastic holder for x-ray diffraction examination.

The copper anode used in polarization measurements was located in the neck of the glass cell as shown in Fig. 2. A voltage-regulated power supply (300 volts) was used as a source of current with a large resistance in series with the cell. Current was determined in terms of the IR drop across a standard 10-ohm resistance in series with the cell. Potential differences between the cathode and the reference electrode were measured with a Leeds and Northrup potentiometer, Type K-2. A Brown Elektronik recording potentiometer with a response time of 2 sec for 90% deflection was used to follow small changes in voltage of the polarized cathode as a function of time.

Prior to each series of measurements, the copper cathode was polished with 2/0, 3/0, and finally 4/0 emery paper. In the polishing process the glass end of the Luggin capillary was also polished flush with the metal surface. The cathode was then placed in approximately 1*N* nitric acid for 60 sec. A preplate

was deposited at a current density of 16 ma/cm² for 15 min in the solution subsequently used for polarization measurements. This current density was less than the limiting current density for all acid-sulfate plating baths used with the vertical cathode. Unless otherwise stated, polarization measurements were generally made with increasing current density by recording the potential approximately 30 sec after adjustment of the polarizing current to a specific value. This was immediately increased to a higher value and the procedure repeated.

One of the criteria for successful polarization measurements is reproducibility. Consistently lower and more reproducible polarization values were obtained with hydrogen-saturated solutions than with air-saturated solutions. Hence, subsequent measurements were made with hydrogen-saturated solutions. Hydrogen was purified by passing it through a conventional purification train.

EXPERIMENTAL RESULTS

Data presented in Fig. 3 were obtained with ultrasonic waves at a frequency of 1000 kc/sec and an intensity of 0.8 watt/cm². The apparent current density was 8 ma/cm², while the solution was 0.17M CuSO_4 and 0.02M H_2SO_4 . Curves A and B differ in that the former is for a cathode prepared in the manner described previously, while the latter is for a cathode prepared with part of the preplate at 30 ma/cm² for 10 min, then 16 ma/cm² for 15 min. The ratio of true to apparent surface area for the cathode represented by curve B was probably much greater than for that represented by curve A, since deposition above the limiting current density favors a porous, relatively high area deposit.

The immediate effect of ultrasonic waves in both cases was an almost instantaneous decrease in cathode potential. This initial change occurred so quickly that the recording potentiometer could not follow it. The rapid decrease in polarization results from disruption of concentration gradients by the ultrasonic waves.

Subsequent changes in cathode potential after the initial decrease are attributed to changes in the effective surface area of the cathode in both cases. Even in the absence of ultrasonic waves, the cathode polarization represented by curve A showed a slight tendency to decrease, while that represented by curve B tended to increase with time. These trends appear to be promoted by ultrasonic waves with both curves approaching some limiting value. Similar effects, although less marked, could be produced by ordinary agitation of the solution near the cathode.

In Fig. 4 data are presented for polarization immediately after introduction of the ultrasonic waves

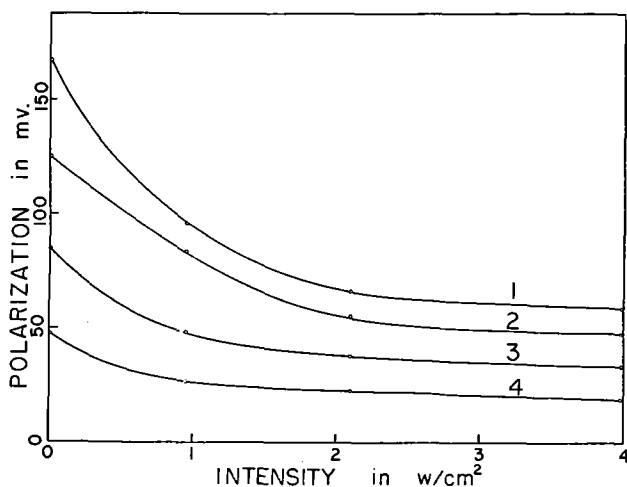


FIG. 4. Dependence of polarization on acoustical intensity and current density. Electrolyte: 0.17M CuSO_4 + 0.02M H_2SO_4 ; temperature: 25° C; ultrasonic frequency: 1000 kc/sec. Current densities: curve 1, 25 ma/cm²; curve 2, 20 ma/cm²; curve 3, 14 ma/cm²; curve 4, 8 ma/cm².

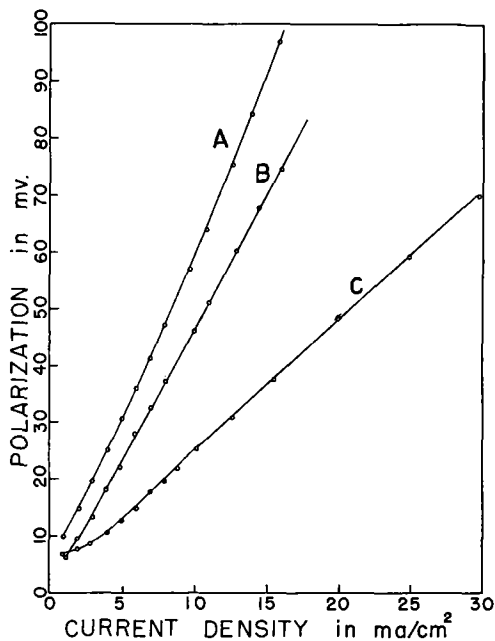


FIG. 5. Polarization at various current densities without ultrasonic waves (curve A), with ultrasonic waves at 1000 kc/sec and 4 watts/cm² (curve C), and with directional flow past the cathode surface (curve B). Electrolyte: 0.17M CuSO_4 + 0.02M H_2SO_4 ; temperature: 25° C.

(1000 kc/sec) as a function of acoustical intensity. Results in this graph as well as those in all subsequent graphs were obtained with a cathode preplated at current densities below the limiting value. The approach of the polarization to a limiting value with increasing acoustical intensity probably indicates that almost all of the concentration polarization has been removed. The evidence is not completely conclusive, however, inasmuch as intensity of the ultrasonic waves at the cathode surface could

not be determined with sufficient certainty at higher intensities (e.g., 4 watts/cm²) because of gas-type cavitation bubbles. Similar results have been obtained with solutions of both higher copper sulfate concentration and lower pH. Polarization is most marked with solutions of lowest concentration, i.e., the solution represented in Fig. 4.

Fig. 5 represents polarization at various current densities in a 0.17M CuSO_4 , 0.02M H_2SO_4 solution with ultrasonic waves (curve C), without ultrasonic waves (curve A), and with ordinary unidirectional flow of solution (curve B). The latter polarization measurements were made with a flow of approximately 1 m/sec parallel to the cathode surface in a specially constructed cell described elsewhere (11). While the effects of stirring and of ultrasonic waves are comparable, it is apparent that the ultrasonic waves are more effective in the present case.

The graph in Fig. 6 represents the effects of ultrasonic waves on polarization in a more concentrated solution: 0.86M CuSO_4 and 0.02M H_2SO_4 . Polarizing as well as depolarizing effects of ultrasonic waves are less in the case of this solution than that represented in Fig. 5, as might be anticipated on the basis of concentration polarization. It is interesting to note that, in the case of curve C in Fig. 6, for the range 30–100 ma/cm² the polarization is a reasonably linear function of the logarithm of current density with a Tafel slope of approximately 0.08.

In Fig. 7 effects of ultrasonic waves (1000 kc/sec) on polarization are compared in hydrogen-saturated solution (B) and in degassed solution (A) in which there was insufficient dissolved gas to support gas-type cavitation. While there was appreciable depolarization in the degassed solution, the effect was greater in the hydrogen-saturated solution, particularly at high current densities. Thus, gas-type

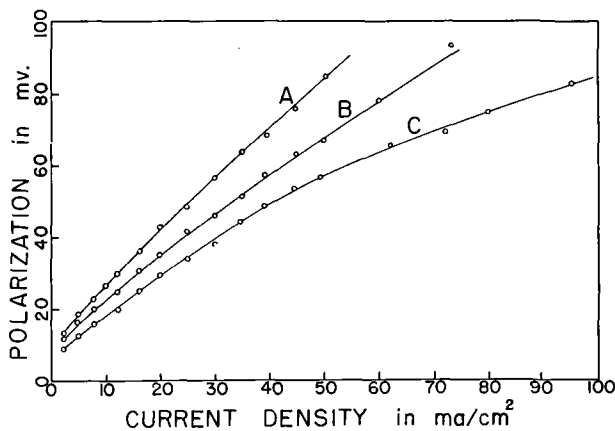


FIG. 6. Polarization at various current densities without ultrasonic waves (curve A) and with ultrasonic waves at a frequency of 1000 kc/sec and 0.9 watts/cm² (curve B) and 4 watts/cm² (curve C). Electrolyte: 0.86M CuSO_4 + 0.02M H_2SO_4 ; temperature: 25° C.

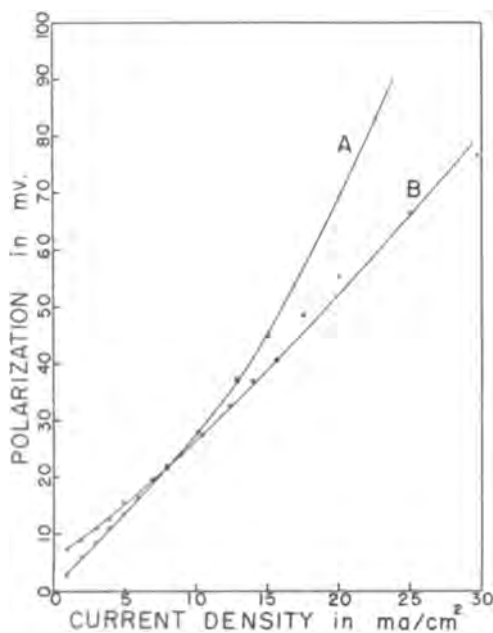


FIG. 7. Polarization at various current densities with ultrasonic waves in degassed solutions (curve A) and in hydrogen saturated solutions (curve B). Electrolyte: 0.17M CuSO_4 + 0.02M H_2SO_4 ; temperature: 25° C; ultrasonic frequency: 1000 kc/sec; acoustical intensity: 4 watts/cm².



FIG. 8. X-ray diffraction patterns of copper deposits. Electrolyte: 0.17M CuSO_4 + 0.02M H_2SO_4 ; current density: 20 ma/cm²; plating time: approx. 70 min. Pattern *a* (left), with quiescent solution; pattern *b* (center), with stirring; pattern *c* (right), with progressive ultrasonic waves (1000 kc/sec, 4 watts/cm²).

cavitation contributes appreciably to depolarization. The smaller, but nevertheless appreciable, depolarizing effect observed in the degassed solution can be explained at least partially in terms of unidirectional streaming effects associated with intense sound waves.

A sufficient number of polarization measurements also have been made with ultrasonic waves at a frequency of 200 kc/sec to establish that ultrasonic effects at this lower frequency are substantially the same as at 1000 kc/sec with respect to order of magnitude. At the lower frequency, however, the wave length was comparable to the cathode dimensions; hence, the associated acoustical diffraction effects rendered the quantitative aspects of the measurements somewhat questionable at 200 kc/sec.

Polarization measurements support the conclusion that the predominate effect of the ultrasonic waves is disruption of the concentration gradients. If this

TABLE I. Crystallographic results

Condition	Solution concentration: molarity		Current density ma/cm ²	Time of deposition min	Relative orientation
	CuSO_4	H_2SO_4			
Static*	0.17	0.02	8	80	2
Stirred					4
Ultrasonics†					4
Static	0.17	0.02	20	75	1
Stirred					4
Ultrasonics					4
Static	0.86	0.02	20	72	5
Stirred					5
Ultrasonics					5
Static	0.86	0.2	20	72	2
Stirred					2
Ultrasonics					2

* No stirring or ultrasonic waves.

† Acoustical intensity: approximately 2.5 watts/cm²; frequency 1000 kc/sec.



FIG. 9. Schlieren photographs of concentration gradients at copper cathode. Electrolyte: 0.86M CuSO_4 + 0.02M H_2SO_4 ; current density: 25 ma/cm². Fig. 9a (left): vertical cathode without ultrasonic waves. Fig. 9b (center): vertical cathode with progressive ultrasonic waves (1 watt/cm² at 1000 kc/sec). Fig. 9c (right): horizontal cathode with standing waves (\approx 0.1 watt/cm² at 1000 kc/sec).

is the case, changes in crystallographic properties of the electrodeposits should be comparable to those produced by ordinary mechanical agitation or stirring. A typical set of x-ray diffraction patterns of deposits with and without ultrasonic waves (1000 kc/sec) and with stirring are shown in Fig. 8a, b, and c. A glancing-beam technique similar to that of Hume-Rothery (12), and Wyllie (13) was used to obtain these diffraction patterns. In this part of the work, stirring was accomplished by passing a stream of hydrogen bubbles past the cathode in the cell shown in Fig. 2. It is apparent that both ultrasonic waves and stirring favored the preferred orientation of the 110 plane parallel to the electrode surface.⁸ Grain-size changes were minor. In Table I, changes in the tendency for preferred orientation are compared on a relative basis in terms of an arbitrary scale extending from 1, for the least tendency for orientation, to 5 for the maximum tendency observed. From Table I it is evident that the ultrasonic waves produced an appreciable increase in the

⁸ Other x-ray diffraction patterns, together with additional polarization data, are presented in reference (17).

tendency for preferred orientation only in the most dilute solutions in which concentration polarization was most marked. Furthermore, the effects of the ultrasonic waves and the unidirectional stirring on the preferred orientation are comparable.

Fig. 9 shows Schlieren photographs which indicate directly the effect of ultrasonic waves on the concentration gradient adjacent to the cathode surface. These photographs were obtained by optical techniques similar to those described by Bartlett (14). The darkest area in each photograph represents the cathode. The light region adjacent to the cathode surface in Fig. 9a is associated with the concentration gradient. The absence of this region in Fig. 9b demonstrates the effectiveness of ultrasonic waves at cavitation levels in disrupting concentration gradients. The Schlieren technique as used in this work was probably sufficient to reveal a diffusion layer of the order of 0.001 cm in thickness. Fig. 9 indicates the action of low intensity ultrasonic waves on the concentration gradients in a standing wave with the cathode surface perpendicular to the wave front. Experimental work in progress indicates that the regions of demarcation between the light and black areas in Fig. 9c probably correspond to the pressure loops or displacement nodes of the standing waves in the solution. This effect can be used to explain the half wave length ripples obtained by Young and Kersten (15) on the surfaces of metals electrodeposited in a standing wave.

The effects of ultrasonic waves on the electrodeposition of copper were examined at acoustical intensities as high as 100 watts/cm² in a converging sound field from a focusing type transducer. At these intensities, copper was not deposited in a coherent plate; rather a colloidal suspension of copper was produced. Even the base plate was appreciably eroded.

SIGNIFICANCE OF RESULTS

On the basis of experimental results previously described, the following conclusions were reached concerning copper deposition in the presence of ultrasonic waves:

1. The depolarizing action of ultrasonic waves is primarily associated with the interaction of acoustical waves with concentration gradients at the cathode surface.

2. Ultrasonic waves at cavitation levels seem considerably more effective than conventional mechanical agitation in breaking up these gradients.

3. Structural changes at intensities of the order of a few watts/cm² or less generally reflect acoustically produced changes in concentration gradients at the electrode surface.

The effectiveness of ultrasonic waves in disrupting concentration gradients may be explained, at least in part, in terms of a microagitation effect. Conventional stirring can be used to reduce the effective thickness of the concentration gradient to 10⁻³ cm. Surface conditions at distances less than 10⁻³ cm are relatively unchanged even in the case of high speed unidirectional flow. Disturbances are produced at the electrode surface by ultrasonic waves, however, as the acoustical waves encounter a phase discontinuity and are largely reflected. Cavitation phenomena right at the electrode surface are particularly significant. As a result, the effective thickness of concentration gradients is reduced to a value considerably smaller than that obtained with stirring.

An accurate prediction of concentration polarization even in unstirred solutions is not readily made because of convection currents associated with the vertical cathode and because of edge effects. These convection currents were very evident in Schlieren photographs of the concentration gradients at the top and bottom of the cathode. On the basis of simple equations (16) for diffusion and electrolyte transport, the limiting current density in the unstirred solution represented in Fig. 5 should be approximately 15 ma/cm², whereas the actual value was approximately 30 ma/cm². Thus, it is not possible at this time to compare the depolarizing action of ultrasonic waves with the concentration polarization in a quantitative fashion.

While not likely, it is possible that the relatively large depolarizing effect of ultrasonic waves may not be entirely associated with concentration polarization; some decrease in activation polarization may occur. At higher current densities in more dilute solutions, there also may have been some *IR* drop included in polarization measurements even with this type of Luggin capillary. Preliminary measurements by the commutator technique with electrodes of similar construction and solutions of comparable concentrations lead to the conclusion that *IR* drop was not more than a few millivolts in dilute solutions.

Ultrasonic or sonic waves may have possible application in specialized plating processes where ordinary stirring is not sufficiently effective in breaking up concentration gradients. Such might be the case with small objects of irregular contour. The best way to introduce sound waves would probably be to drive the whole object being plated at a sonic or ultrasonic frequency. Ultrasonic waves should also prove significant in laboratory investigations of electrode processes where it is desirable to minimize the effects of concentration gradients.

ACKNOWLEDGMENTS

The authors are pleased to acknowledge the assistance of Dr. John F. Yeager in obtaining polarization measurements with unidirectional flow, and Mr. Robert W. Penn in obtaining the Schlieren photographs.

Any discussion of this paper will appear in a Discussion Section to be published in the June 1955 JOURNAL.

REFERENCES

1. T. RUMMEL AND K. SCHMITT, *Korrosion u. Metallschutz*, **19**, 101 (1943).
2. F. LEVI, *Ricerca Sci.*, **19**, 887 (1949).
3. F. MULLER AND H. KUSS, *Helv. Chim. Acta*, **33**, 217 (1950).
4. F. MULLER, *Angew. Chem.*, **62**, 25 (1950).
5. A. ROLL, *Z. Metallkunde*, **41**, 339, 413 (1950); *ibid.*, **42**, 238, 271; *Metalloberfläche*, **6B**, 49 (1952).
6. A. ROLL AND G. SCHRAG, *Z. Metallkunde*, **42**, 197 (1951).
7. B. CLAUS, *Z. tech. Phys.*, **16**, 80, 202 (1935).
8. B. CLAUS AND E. SCHMIDT, *Kolloid-Beih.*, **45**, 41 (1936).
9. E. YEAGER AND F. HOVORKA, *J. Acoust. Soc. Amer.*, **25**, 443 (1953).
10. E. YEAGER, H. DIETRICK, AND F. HOVORKA, *ibid.*, **25**, 456 (1953).
11. J. YEAGER, Ph.D. Thesis, Western Reserve University, 1953.
12. W. HUME-ROTHERY AND M. WYLLIE, *Proc. Roy. Soc.*, **A181**, 331 (1943).
13. M. WYLLIE, *Rev. Sci. Instr.*, **18**, 426 (1947).
14. J. H. BARTLET AND L. STEPHENSON, *This Journal*, **101**, 571 (1954).
15. W. YOUNG AND H. KERSTEN, *J. Chem. Phys.*, **4**, 426 (1936).
16. See, for example, G. KORTUM AND J. BOCKRIS, "Textbook of Electrochemistry," Vol. II, pp. 402-7, Elsevier Publishing Co., New York (1951).
17. W. WOLFE, E. YEAGER, AND F. HOVORKA, Technical Report No. 10, Contract N7 onr 47002, Western Reserve University, December, 1952.

Kilogram Scale Reductions of Vanadium Pentoxide to Vanadium Metal¹

ARTHUR P. BEARD AND DONALD D. CROOKS

Knolls Atomic Power Laboratory, General Electric Company, Schenectady, New York

ABSTRACT

The reduction of V_2O_5 with calcium to give 750-1000 gram buttons of massive ductile vanadium has been accomplished. Using an iodine igniter-booster and an optimum amount of excess calcium, the authors obtained 84% yields of metal. In this process oxygen impurity seems to be the main embrittling agent, while silicon impurity up to 0.2 wt % has no apparent effect on the vanadium.

INTRODUCTION

The production of vanadium metal by reduction of vanadium pentoxide with calcium, as reported by McKechnie and Seybolt in earlier work (1), was undertaken in order to provide material of sufficient purity and ductility for use in studies of its reactions with gases (2), methods of fabrication, and physical properties. In addition, it was desirable to determine if product purity could be retained in reactions yielding 750 to 1000 grams (instead of 125 g) and if yields could be increased substantially above the 74% value reported earlier.

EXPERIMENTAL PROCEDURE

Equipment.—In the small scale bomb reductions of vanadium pentoxide with calcium, using an iodine igniter-booster charge, McKechnie and Seybolt obtained small, ductile buttons of about 125 g (74% yield). The steel container, lined with a magnesia crucible, was 4 in. in diameter, 11 in. high, with $\frac{3}{8}$ in. wall. This reaction vessel was made tight by compression of a steel cover on an annealed copper gasket. It was found that yields of about 270 g (about 78% of theoretical) of massive metal could be obtained by taking a reaction charge of 600 g V_2O_5 , 1057 g calcium, and 300 g iodine, pressing the mixture into 3 in. diameter disks with 80 tons pressure, and performing the reduction in the described bomb. The amount of excess calcium needed to give ductile metal was also decreased from about 60% to about 53% excess. However, the frequency of explosive burnouts of the steel bombs increased when using this technique.

A new reduction vessel was designed and fabricated for producing vanadium. It was made from steel pipe, 6.6 in. O.D., with about $\frac{1}{16}$ in. wall, and was about 20 in. tall. Six $\frac{1}{2}$ in. diameter bolts were

used to compress the steel cover on an annealed copper gasket to make the bomb tight. A flare fitting was brazed in the cover for flushing the bomb with dry inert gas.

A tapered magnesia liner, 5 in. at the top, $4\frac{1}{2}$ in. at the bottom, 18 in. high, with $\frac{1}{4}$ in. wall was slipped into the steel container. Coarse grained magnesia was used between the liner and inside of the bomb for centering and support of the crucible. This type of liner proved to be quite successful since it could be removed easily from the steel bomb after a reduction was made. Liners formed directly in the bomb were unsatisfactory.

A 15-kw, 10,000 cycle, motor generator was used as the source of power for heating the bombs. An optimum heating rate of 50° - 60° /min was used until the rapid temperature rise caused by reaction inside the bomb was detected by a thermocouple on the outside of the bomb. This temperature rise generally was noticed after about 12 min of heating. The maximum temperature reached on the outside of the bombs, in reductions using iodine boosters, was around 900°C about 19 min after the start of heating.

Chemicals.—The high purity vanadium pentoxide used in this work was obtained from the Electro Metallurgical Division of Union Carbide and Carbon. A typical analysis (figures are weight percentages) is given in Table I. Before being used in a reduction, the oxide was dried in air at 200°C .

Calcium, similar to that used by McKechnie and Seybolt (1), was used in this work. Iodine, used as an igniter-booster, was Eimer and Amends C. P. grade.

A series of reductions were made, varying the amounts of V_2O_5 , excess calcium, and the iodine igniter-booster, in order to determine the optimum charge for the designed bomb. The V_2O_5 , magnesia liner and cover, coarse magnesia grain and steel bomb were air-dried at $\sim 200^{\circ}\text{C}$. After the liner had

¹ Manuscript received September 17, 1953. This paper was prepared for delivery before the New York Meeting, April 12 to 16, 1953.

TABLE I. Analysis of high purity V_2O_5

Element	Weight %	Remarks
C	0.003	Chemical analyses
H ₂	0.047	
N ₂	0.0114	
Si	0.30	
Be	<0.0005	
Mn	<0.005	
Al	<0.1	
Mg	0.003	
Pb	<0.05	
Cr	0.05	
Ca	<0.1	Spectrographic analyses are approximate and may be in error by a factor of 3.
Sm	<0.02	
Mo	<0.02	
Co	<0.04	
Fe	0.08	
Cu	0.0005	
Na	0.05	
Zn	<0.1	
Ni	<0.01	
Ti	0.02	

FIG. 1. Vanadium button produced by bomb reduction of V_2O_5 with calcium.

cooled, it was filled with a well-mixed composition of calcium, iodine, and V_2O_5 , and placed in the steel bomb. Coarse magnesia grain was jolted into the space between the bomb wall and liner. The space above the magnesia cover of the liner was also filled with magnesia grain. The steel lid was bolted down with six $\frac{1}{2}$ in. diameter bolts by means of a torque wrench to insure uniform pressure on the copper gasket. After being evacuated and flushed several times with argon or helium, the reaction vessel was sealed under an atmosphere of inert gas. It was then

heated by induction behind a concrete wall which was a safety shield for the experimenter.

RESULTS

In preliminary work on making large scale reductions, a number of attempts were made to form dense magnesia liners in the bomb. Reductions, using these liners, resulted in slag absorption from the reduction to such an extent that the molten vanadium button would wet and react with the liner. The dense, high-fired preformed magnesia crucibles absorbed some slag but a layer always separated the conglomerated metal from the liner proper. Also, as mentioned previously, this type of liner facilitated the removal of the reaction products after a reduction.

Pressed charges of 2180 g of V_2O_5 , 3840 g of Ca, and 1090 g of I_2 , and unpressed charges of 1635 g of V_2O_5 , 2880 g of Ca, 818 g of I_2 were found to be optimum for the bomb size and heating cycle employed. An excess of calcium of 53–54% resulted in an optimum yield of metal of 84%. At 40% and 60% excesses the yields dropped 10% to 5%, respectively. Below about 40% excess calcium, the amount of oxygen in the vanadium button increases to more than 0.05 wt %, thus embrittling the metal beyond cold workability. The effect of changing the amount of iodine booster-igniter was not as apparent. Using half the amount considered optimum decreased the yield of about 4%. Using twice the amount influenced the yield very little.

The vanadium buttons obtained in this process are 770–1020 g, depending on size of charge used. The metal conglomerated quite nicely as shown in Fig. 1. Slag inclusions however were present and could not be completely leached out of the as-reduced button. The latter can be cold-rolled down to sheet without annealing. Comparison of typical analysis of vanadium produced in this work with other reported materials is given in Table II.

No direct correlation of oxygen content of the vanadium buttons with Vickers Hardness Number was found (2). This is understandable considering the variance in carbon, nitrogen, and silica contents of the buttons. All of these and other elements could influence the hardness. However, oxygen content above about 0.05% generally rendered the vanadium too brittle for cold working. This was first observed by McKechnie and Seybolt.

Some visual evidence of the constituent present at the grain boundaries of as-reduced vanadium is shown in Fig. 2, 3, and 4 as being carbide.

The silicon content of most of the metal produced in this work ran higher than in metal reported by McKechnie and Seybolt (1). It was thought that it could cause embrittlement, but up to concentrations

TABLE II. Comparative analyses of vanadium

Reported by	Oxygen	Nitrogen	Hydrogen	Carbon	Iron	Silicon	Calcium
	%	%	%	%	%	%	%
McKechnie and Seybolt (1)	0.031	0.016	0.005	0.21	<0.01	0.04	0.023
	0.017	0.013	0.002	0.20	<0.01	0.001	0.014
Kinzel (3)	0.05-0.12	0.02-0.04	0.001-0.004	0.03-0.07	—	—	—
Gregory, Lilliendahl, and Wroughton (4)	0.1-0.25	0.01-0.015	—	0.05	0.01	—	0.05
Beard and Crooks, this paper	0.028	0.005	0.001	0.126	—	0.065	<0.1*
	0.033	0.013	0.002	0.102	—	0.04	<0.1

* Spectrographic analyses of calcium are approximate and may be in error by a factor of 3.

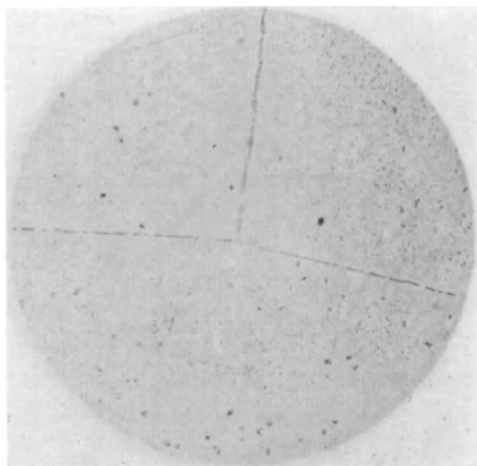


FIG. 2. As-reduced vanadium. % oxygen = 0.047, % nitrogen = 0.009, % carbon = 0.092, and VHN = 134. Etchant 10% hydrochloric acid. 250× B.F. before reduction for publication.

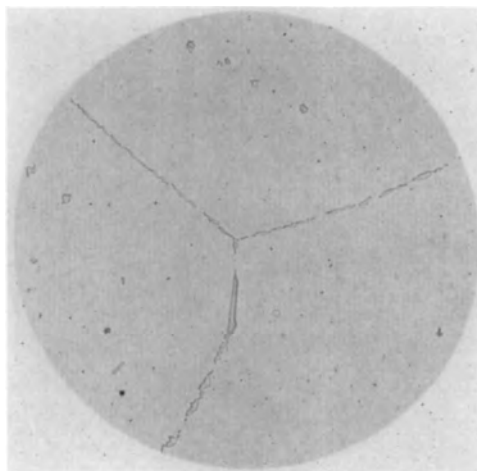


FIG. 4. As-reduced vanadium. % oxygen = 0.049, % nitrogen = 0.009, % carbon = 0.175, and VHN = 131. Etchant 10% hydrochloric acid. 250× B.F. before reduction for publication.

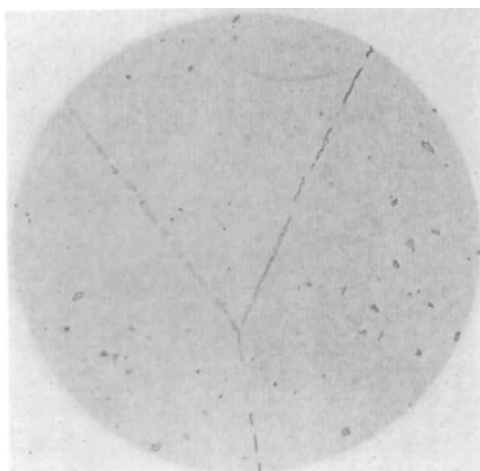


FIG. 3. As-reduced vanadium. % oxygen = 0.047, % nitrogen = 0.009, % carbon = 0.125, and VHN = 136. Etchant 10% hydrochloric acid. 250× B.F. before reduction for publication.

of 0.2 wt % no correlation between silicon concentration and increased hardness of the vanadium could be found. This silicon impurity was traced directly to the V_2O_5 . The amounts of nitrogen in various

buttons were found generally to be less than one half that expected from analyses of the starting materials.

CONCLUSIONS

The feasibility of producing 750-1000 gram buttons of vanadium by reduction of V_2O_5 with calcium, using an iodine igniter-booster, and still retain the purity found in material produced on a 125 g scale by McKechnie and Seybolt has been shown. The percentage yield of massive metal has been increased from 74% to 84%. The amount of excess calcium necessary to give highest yield of ductile metal was reduced from about 60% to 54%.

Oxygen impurity in vanadium seems to be the main embrittling agent in this process. Silicon impurity up to 0.2 wt % does not seem to cause embrittlement of the vanadium.

ACKNOWLEDGMENTS

The authors wish to express their appreciation for assistance in this work by coworkers and for dis-

cussions with A. U. Seybolt. Analyses in Tables I and II are by courtesy of L. P. Pepkowitz, W. S. Horton, and F. P. Landis of the General Electric Company.

Any discussion of this paper will appear in a Discussion Section to be published in the June 1955 JOURNAL.

REFERENCES

1. R. K. McKECHNIE AND A. U. SEYBOLT, *This Journal*, **97**, 311 (1950).
2. A. U. SEYBOLT AND H. T. SUMSION, *Trans. Am. Inst. Mining Met. Engrs.*, **197**, 292 (1953).
3. A. B. KINZEL, *Metal Prog.*, **58**, 315 (1950).
4. E. D. GREGORY, W. C. LILLIENDAHL, AND D. M. WROUGHTON, *This Journal*, **98**, 295 (1951).

Inert-Gas Forging¹

CARL L. KOLBE

Research Laboratory, General Electric Company, Schenectady, New York

ABSTRACT

Apparatus has been designed and operated to enable a metal specimen to remain in argon gas during an entire heating and forging operation. A furnace capable of operating to 2500°C is coupled to a 250-lb pneumatic air hammer, so that materials may be forged at extremely high temperatures with a minimum of oxidation. Molybdenum and tungsten alloys have been forged between 1750° and 2200°C without visible surface oxidation. A titanium alloy was forged at 1500°C.

With this equipment there can be less diffusion of gases into the material, minor slippery oxide films, less surface cracking, easier deformation at higher forging temperatures than ever before possible.

INTRODUCTION

To obtain the best mechanical properties of a metal, deformation by forging, rolling, swaging, or extruding is usually required. These operations generally involve heating in air or in some protective atmosphere, followed by deforming in air. However, metals and alloys which have a great affinity for gases at high temperatures are now being fabricated and, as a result, new methods must be employed to reduce successfully the harmful effects obtained from heating or forging in air, hydrogen, or nitrogen. Pure beryllium, titanium, zirconium, and uranium may be deformed at moderately low temperatures and rolled in steel packs. These packs are excellent for keeping the material hot and reducing oxidation. However, this method has disadvantages. The working range is limited to a temperature below the melting point of the sheathing material; the material being worked is hidden from view; there is a probability of welding and sticking to the sheath material; and the cost of fabrication is high. Inert-gas forging helps eliminate these problems.

Refractory metals are being considered as base materials for high temperature applications, so it seems reasonable that higher forging temperatures will be needed if these materials are to be deformed successfully. Inert-gas forging can help protect metals from gross oxidation while at high temperatures, thereby reducing scaling and the loss of valuable material and ductility by oxidation.

EXPERIMENTAL PROCEDURE

Apparatus.—The apparatus included a forging hammer (250-lb Nazel pneumatic air hammer capable of 210 strokes/min), a furnace (with a graphite tube as the heating element and powdered

graphite as insulation), and metal work chamber. A 3000 cycle, 100 kw induction coil was used to induce temperatures to 2500°C. The graphite tube had an inside diameter of 10.3 cm and was 91.5 cm long. The entire furnace was placed in a gas-tight aluminum box (Fig. 1). The work chamber connected the hammer to the furnace, so that the three pieces of equipment became an integral unit. In order that the hammer could be operated in its usual manner, the hammer die and anvil were connected to the chamber with rubber bellows (Fig. 2). The front of the work chamber had a partial glass top section so that the interior could be observed. The bottom of the front section consisted of a rubber apron and rubber bellows-type gloves for manipulation of the material from the furnace to the hammer. An additional chamber small enough to be flushed clear of air in a short time was used to introduce or remove specimens or equipment from the work chamber after the regular operation began. A molybdenum boat was placed in the furnace and could be shoved in and out with a molybdenum poker. The specimens could be placed on the boat for heating to temperature. In case of danger of reaction with the boat, a stabilized zirconia block or a pure magnesia block was used between the specimens and the boat. In all of the work described here, welding-grade argon was used. No further attempt to purify the gas was made. Argon was introduced through the rear of the furnace and out into the work chamber where it was intermittently removed through a valve whenever pressure on the rubber apron became too high.

Material.—Table I gives complete information on materials used and their conditions and temperatures of forging.

Procedure.—After the equipment was assembled, a Freon-gas detector was used to reveal leaks. The whole unit was partially evacuated and filled with

¹ Manuscript received September 14, 1953. This paper was prepared for delivery before the New York Meeting, April 12 to 16, 1953.

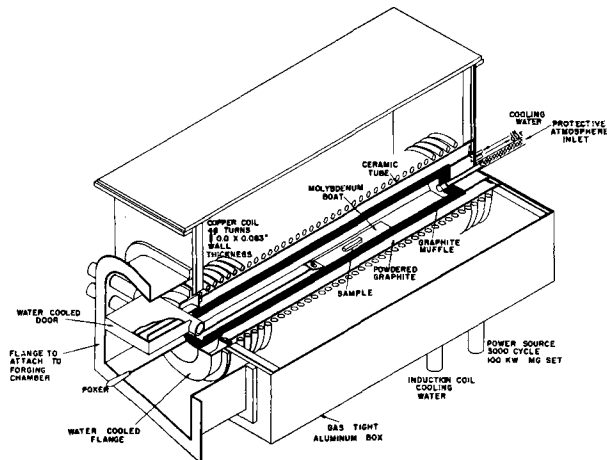


Fig. 1. Induction furnace details

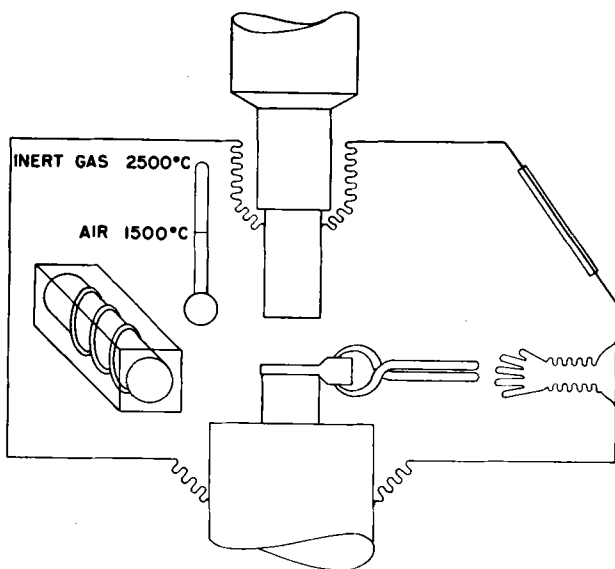


Fig. 2. Schematic drawing of the work chamber attached to the forging hammer and induction furnace.

TABLE I

Material	Condition	Forging temp (°C)
Mo	Arc-cast	1775
Mo-2.66Ti-0.084C	Arc-cast	1750, 1830, 1920
Mo-0.85V	Arc-cast	1800, 1920
W-30Mo-1.5Th	Sintered	2100, 2200
Ti alloy	Arc-cast	1500

argon. This operation was repeated three times. As the argon gas was being admitted for the final flushing treatment, the furnace was heated to temperature. Readings were taken from the furnace wall with an optical pyrometer. Specimens to be forged were placed directly on the molybdenum boat or on a ceramic slab and heated to temperature. The molybdenum boat was pulled forward in the furnace so that the specimen could be gripped with

a pair of tongs and placed under the hammer. This final operation had to be performed quickly, since heat loss can be very great at such high temperatures.

EXPERIMENTAL RESULTS

A high degree of success was obtained in working all of the materials studied, but molybdenum-base alloys gave the best results. Pure molybdenum reduced to test-specimen size without any difficulty. Mo-Ti alloys could be reduced from 1.27 cm² to 6.4 mm² in one heat after some initial working. Weight losses on these small specimens were less than 0.5% when worked in argon atmosphere. Specimen surfaces were still bright, showing these losses were not caused by oxidation, but by small sections breaking off.

Mo-V alloys required temperatures above 1800°C for best results. Original work at 1800°C produced some edging cracks, but after these cracks were ground out and the temperature raised to 1920°C, no further edge cracks appeared. Some of this material was later reduced between 1200° and 800°C to 3.2 mm wire, which did not fracture after a 180-degree bend. This same alloy was later forged in air between 1800° and 2035°C with a 12% loss due to oxidation. Tensile tests showed no appreciable difference between the two materials. The W-Mo-Th alloy was forged from a 8.0 mm² sintered bar to a flat sheet 1.8 mm thick by 3.18 cm wide. This piece was later rolled in air to a sheet 0.36 mm thick by 3.8 cm wide with great difficulty and much edge cracking. Despite its reduction, the sheet was very brittle and could not be bent without heating.

An arc-cast button of Ti alloy was forged at 1500°C from 6.35 mm to 1.5 mm for tensile specimens and metallographic examination. Attempts to work this material in air previously had not been successful.

Temperatures reported throughout this paper must be considered as maximum temperatures, with the working range at the higher temperatures varying as much as 300°-400°C. For example, an alloy being reduced as much as 75% in one heat from a temperature of 1830°C may drop to a temperature as low as 1400°C before this operation is completed.

The atmosphere obtained during this work was inert enough to keep molybdenum alloys from oxidizing, but titanium alloys were slightly discolored.

Whenever possible, molybdenum alloys were forged as squares rather than the generally recommended octagons. The usual difficulty of developing a diamond shape during deformation was not encountered.

CONCLUSIONS

With the equipment described, materials can be worked at very high temperatures without the usual gross oxidation. For some alloys, this means less diffusion of gases into the material, minor slippery oxide films, less surface cracking, and easier deformation at higher temperature. Consequently, increased material recovery and improved forgeability are obtained.

ACKNOWLEDGMENTS

Specimens for this work have come from various sources. Arc-melted molybdenum was from P. C.

Rossin, General Electric Research Laboratory; the Mo-Ti-C was a salvage section of ingot No. 4-887 from Climax Molybdenum Company; the Mo-V alloy was purchased from the Climax Molybdenum Company; the W-Mo-Th alloy was from bar X51-3-11, Cleveland Wire Works, through J. Slivka; Ti alloy was furnished by J. McMullin, General Electric Research Laboratory. My gratitude to J. Nisbet, T. Doig, E. Jones, and other members of the Metal Processing Laboratory who have aided in this work.

Any discussion of this paper will appear in a Discussion Section, to be published in the June 1955 JOURNAL.

Room-Temperature Ductile Chromium¹

H. JOHANSEN² and G. ASAI

U. S. Bureau of Mines, Northwest Electrodevelopment Laboratory, Albany, Oregon

ABSTRACT

Development of the effort to find room-temperature ductile chromium is reviewed. Preparation and some mechanical properties of ductile chromium are described, as are techniques of making brittle chromium ductile by removal of surface layers. Reasons for the ductility, or lack of it, are advanced on the basis of experiments showing the effect of certain impurities, mechanical working, and heat treatment. No clear explanation for the surface phenomenon was obtained. Possible future uses of ductile chromium are discussed.

INTRODUCTION

The search for room-temperature ductile chromium has involved many investigators whose efforts have been summarized recently (1). Results of these investigations, until quite recently, were uniformly unsuccessful in obtaining room-temperature ductile metal.

Recently, room-temperature ductile sheet was produced from arc-melted electrolytic chromium (2) by a process described by Greenaway (3). Simultaneously, it was independently discovered at this laboratory that swaged chromium rod, pointed by an electrolytic etching process was ductile (4), and that ductility was dependent on removal of certain surface layers from the chromium.

Preparation and some mechanical properties of ductile chromium are the subject of the present paper. "Ductile" implies room-temperature ductility, unless otherwise specified.

PREPARATION OF DUCTILE METAL

Preparation of ductile chromium has depended on at least two factors: production of metal of high purity, particularly with regard to oxygen, and discovery of certain techniques in hot and cold working of the metal.

Although first indications of ductility were observed in chromium produced by magnesium reduction of chromium chlorides, two other methods may be depended on for more certain results. One method is electrolysis of high purity chromic acid under special conditions of bath temperature and current density to produce electrolytic plate of very low impurity content—especially oxygen. This method has been described by Blum (5) and Greenaway (3, 6). Certain modifications in the method were developed

at this laboratory (4) to enable greater production, since the electrolytic method suffers from a very low efficiency.

The second method is to reduce residual oxygen in commercial electrolytic chromium with hydrogen. A listing of the many earlier investigations of this method has been published (7).

The hydrogen reduction apparatus described in reference (8) has allowed production of chromium sufficiently pure to be made into ductile metal. In this process, powdered chromium metal is deoxidized with high purity hydrogen at 1200°C for 16 hr. Hydrogen is purified by a system using a cold trap, phosphorous pentoxide, and a zirconium getter.

Of the two methods, electrolysis gives the purer product; indeed, electrolytic plate made by this method, arc-melted and sheath-rolled at 850°C has given indication of ductility even without special surface preparation.

The hydrogen treatment method, however, lends itself to production of larger amounts, and, in addition to lowering the oxygen content, simultaneously lowers nitrogen, sulfur, and carbon contents.

One other method of production of chromium metal, the iodide dissociation method (9), should probably furnish ductile metal, although so far only individual grains have been reported as possessing ductility. The extreme difficulty of producing significant amounts of chromium metal by the iodide process seriously limits the usefulness of the technique.

Since the chief impurity remaining in electrolytic chromium is oxygen, purification attempts necessarily have revolved around removal of this element. In addition to the problem of removal, a reliable analysis for oxygen was sought. The method of Adcock (10), in which chromium is dissolved in hydrochloric acid and the residue considered to be the oxide, has been the standard method of oxygen analysis. For the lowest oxygen ranges, however, neither vacuum fusion nor the method of Adcock

¹ Manuscript received June 14, 1954. This paper was prepared for delivery before the Chicago Meeting, May 2 to 6, 1954.

² Present address: Department of Chemistry, University of Oregon, Eugene, Oregon.

give reliable results, and for the present work the appearance of the microstructure of a specimen of arc-melted chromium was used as the criterion of oxygen content.

Except where noted, all chromium tested in this work was purified by hydrogen treatment of commercial electrolytic chromium.³ Purities have been better than 99.9% and usually better than 99.95%.

MECHANICAL WORKING

Techniques of working chromium from powder compacts have been described previously (7). The present investigation indicates that ductile sheet may be made by powder metallurgy, but with somewhat more difficulty than the arc-melting process (8). In general, hot work at a temperature of 1100°C is necessary while handling the arc-cast metal. After reductions of a minimum of 50%, cold work in the region of 800°C is required. As more cold work is done, the recrystallization temperature steadily declines so that final passes in swaging or rolling should be done from a furnace at less than 700°C.

SWAGING

The following procedure has been used to produce 0.125 in. diameter rods from 2 in. diameter ingots by sheath swaging. Swaging unsheathed has been generally unsuccessful.

1. A 2 in. diameter arc-melted ingot was sheathed in stainless iron and swaged to 1 in. diameter at temperatures starting at 1100° and finishing at 900°C.

2. Recrystallization was accomplished by heating the swaging to 1200°C in hydrogen.

3. The swaging was resheathed in mild steel and swaged at 800°C to 0.5 in. diameter.

4. This was followed by recrystallization at 1200°C in hydrogen, resheathed, and swaged at 700°C to 0.125 in. diameter.

The as-swaged 0.125 in. diameter rods produced in this fashion are quite brittle to rapid bending at room temperature, although it was found that all would bend at very low strain rates. Typical examples of swaged rod are shown in Fig. 1.

Rolling

Attempts have been made in the past to roll powder-compacted chromium in air directly. These attempts failed. All successful rolling was done with mild-steel sheathing which protected the chromium powder compacts from the chilling effect of the rolls and from air contamination. With the production of dense metal from the arc-melting process, protection from the atmosphere was not so crucial. In

³ Purchased from Electro Metallurgical Company.

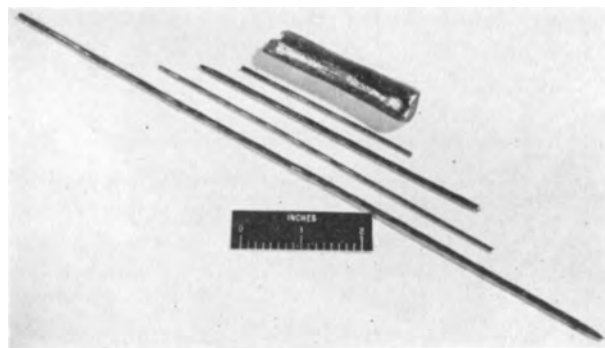


FIG. 1. Swaged rods

addition, with higher purity chromium, the brittle-to-ductile transition temperature was lowered so that rolling could safely proceed at lower temperatures; consequently the chilling effect was not so pronounced.

For preparation of thin, ductile sheet, rolling unsheathed with the resultant close control on dimension, surface finish, and extent of work, was a necessity.

Good quality sheet was prepared by the following procedures:

1. The arc-cast ingot, after a stress-relief anneal of 1200°C in hydrogen, was quartered longitudinally and hammer- or press-forged at 1100°C. Quartering of the ingot was found to eliminate a tendency of ingots to center burst on forging. Upset forging of arc-cast ingots has shown promise of being superior to the quartering method. Press forging was preferred for the smaller sizes.

2. The forging was recrystallized by heating to 1200°C in hydrogen. Again it was sheathed in mild steel and rolled at 700°–800°C to a reduction of about 50% in thickness. The chromium at this stage was very sensitive to surface chilling, hence the sheath was retained for the initial rolling step.

3. After desheathing, the sheet was rolled directly in air from an 800°C furnace to any thickness desired. The rolling temperature was gradually decreased so that final passes were made at an estimated sheet temperature of 400°C.

Reductions in rolling were moderate, of the order of 10%/pass initially, ending with 2%. Chromium

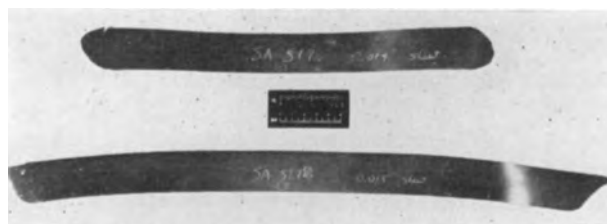


FIG. 2. Air-rolled sheet

sheet as thin as 0.01 in. thickness was made by this procedure. Thinner sheet may be made by pack-rolling. Fig. 2 shows specimens of sheet rolled in air.

Wire Drawing

Chromium wire has been drawn at 600°C using swaged rod as starting material, and as low as room temperature on small wire diameters. Reductions in area per pass were of the order of 6% at a starting size of 0.25 in. diameter using tungsten carbide dies in a lead-antimony bath. The smallest finished wire made by drawing had a 0.025 in. diameter. The following procedure has been found to produce consistent success in drawing wire: (A) the as-swaged rod at a starting size of about 0.25 in. is recrystallized by heating to 1200°C in hydrogen; (B) the rod is then drawn at 350°–400°C in a lead-antimony eutectic bath using Oildag⁴ as a die lubricant.

Extrusion

Hot extrusion of 2 in. diameter ingots has proved successful. The ingots were sheathed in mild steel. Five ingots were extruded at 1100°C and all showed excellent results. Reductions in area were of the order of 80%. The grain size of these extrusions after recrystallization was much smaller than that in swaged rods of equal reduction. Extruded material has been processed to ductile wire. Extrusion shows much promise in that extruded rods may be worked at lower temperatures on larger diameters; thus it offers hope for larger sections having ductility.

SURFACE PHENOMENON

As noted above, removal of the surface layers of a swaged rod resulted in a remarkable increase in ductility of the specimen. It was soon established that the same technique applied to sheet and drawn wire as well.

The effect was first noticed while tipping rods for wire drawing in which a 250 g/l chromic acid-2.5 g/l sulfuric acid solution was used as an electrolyte. Chromium was made the anode and a strip of copper served as cathode. A current of 5–10 amp was passed through the cell for perhaps half a minute, or until a sufficient amount had been removed, sometimes as little as 0.002 in. in depth. Usually 0.005–0.01 in. on the diameter was removed.

The mode of removal of the surface layer does not appear to be significant. Mechanical, chemical, and electrolytic methods all confer the beneficial effect. However, electrolytic etching was found to give superior results, as well as the smoothest, brightest surface, so this method was usually employed.

Wain and Henderson (2) have reported ductility in chromium sheet as a result of chemical etching of

⁴ Produced by Acheson Colloids, Port Huron, Michigan.

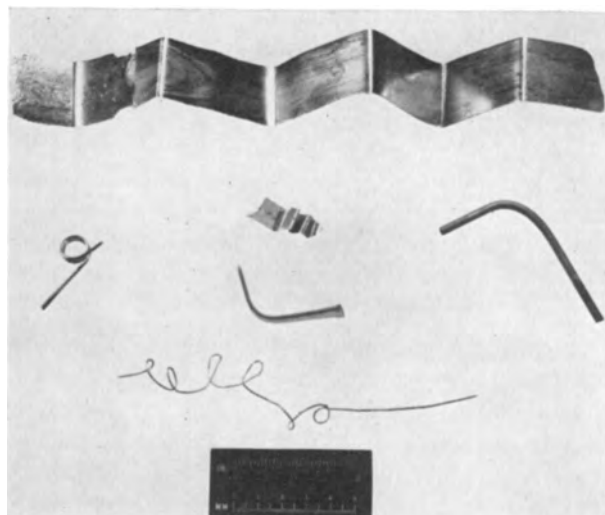


FIG. 3. Cold ductile wire, rod, and sheet

the surface, and their results have been confirmed here using hydrochloric acid as the etchant. Mechanical removal of metal by use of polishing papers also serves to induce ductility, but it is somewhat less effective than chemical or electrolytic treatment. Fig. 3 shows typical specimens of room-temperature ductile chromium rod, wire, and sheet.

The phenomenon of dependency of ductility in chromium on the removal of certain surface layers has been anticipated in a British patent (11) obtained for a method of rendering brittle tungsten ductile by electrolytic removal of the surface layers. Shortly thereafter, this laboratory made tests on chromium sheet using conditions stated in the patent with entirely negative results.

Annealing appeared to improve bendability of unetched sheet slightly, but all test specimens annealed above 500°C broke at the slowest strain rate available. The etched specimens, however, continued to show excellent ductility in exploratory tests through 600°C when the number of reverse bends before failure began to fall off, until a specimen which had been heated to 900°C, then etched, could be bent only 10 times before failure. Since the recrystallization temperature was found by x-ray examination to be between 700° and 800°C, it was evident that chromium sheet may show some ductility in the recrystallized condition. Curiously, ductility in the recrystallized state could be produced in sheet, but not in wire.

Transition Temperature

The transition temperature of ductile wire was found to be in the range of 0° to –10°C as tested in bending with a ram speed of 60 in./min and as low as –66°C when tested with a ram speed of 0.079 in./min.

Tensile Tests

The tensile strength of electrolytic chromium at room temperature has been reported (15), as has that of sintered powder compacts (1), and of wrought and recrystallized chromium (16).

Room-temperature tensile tests were made on etched drawn wire in various conditions of heat treatment. A test of surface-treated wire was also carried out at 240°C. Specimens were prepared for testing by an initial etch of the entire wire, then the grip-ends were stopped off, and a center gauge section was reduced by further etching to insure fracture occurring in the gauge length. Specimens were held in Templin grips or modified Jacobs chucks. The loading rate was 0.02 in./min.

MECHANICAL TESTING

The effect of temperature and purity on ductility and other properties of brittle chromium has been summarized for tests carried out exclusively on sintered powder compacts (1). High porosity of such test specimens leads to serious doubt of the validity of results recorded for mechanical properties as determined by bend, impact, and tensile tests. The present investigation gave quite different results, and the differences may be ascribed, in part at least, to the use of wrought chromium rather than sintered powder compacts, somewhat purer chromium, and surface preparation.

Bend Tests

Bend tests were made using equipment previously described (14) for testing brittle chromium to find the ductile-to-brittle transition temperature. One bender consisted of a simple two-point suspension so arranged that a manually depressed ram would strike the center of the test coupon or wire and rapidly bend or break it. The other bender operated in a similar fashion except that the rate of ram advance was adjustable by means of a variable speed drive mechanism.

A further test was frequently employed on thin specimens as a criterion of ductility: the number of times a specimen could be reverse bent rapidly by hand, before failure.

Results of bend testing air-rolled chromium sheet at room temperature (25°C) are shown in Table I. One sample as-rolled was shown to be bendable, but only at a slow strain rate. The same sheet after removal of 0.003 in. from each surface still had not broken after 50 reverse bends. After subsequent discovery of the present conditions for ductility, the treatment recommended in the patent was repeated and this time found to give full ductility. The explanation must be that the earlier chromium did not

TABLE I. Bend testing of Cr sheet S-1

Condition of sheet	Max. strain rate* (in./in./sec) 10 ⁶	Knoop hardness	Thickness after pickling	Reverse bends before failure
°C				
As-worked (0.013 in. thick)	12.8	255	0.007 in.	>50 times
200 Anneal	24	261	Not determined	
300 Anneal	24	255	Not determined	
400 Anneal	<7	255	Not determined	
500 Anneal	12.63	246	Not determined	
		271†		
600 Anneal	<2.9	252	0.0075	55
700 Anneal	<2.9	243	0.007	33
800 Anneal	<2.9	181	0.008	22
900 Anneal	<2.9	157	0.005	10

* Maximum strain rate for successful bending.

† On bend after bending.

have proper characteristics for being made ductile, since careful etching to various depths did not produce ductile sheet. No specimen of the older chromium could be made ductile regardless of the extent of surface removal. This indicated that improved techniques for producing purer metal and for mechanical working to suitable structure were responsible for the improvement necessary to reach full ductility.

Further indication of the surface removal effect has been noted for beryllium and vanadium. Kaufman, Gordon, and Lillie (12) reported that hot ductility in beryllium was improved by deep etching. Kinzel (13) noted the necessity for quite drastic surface removal to obtain vanadium sufficiently ductile for cold rolling.

The full explanation for the phenomenon of ductility obtained by surface removal techniques is lacking. Two possible causes are suggested immediately: contamination during the mechanical working steps, and/or a surface structure condition which may contain microcracks as a result of working. Fig. 4 shows on the left an as-drawn wire specimen which was deeply etched on one half and was

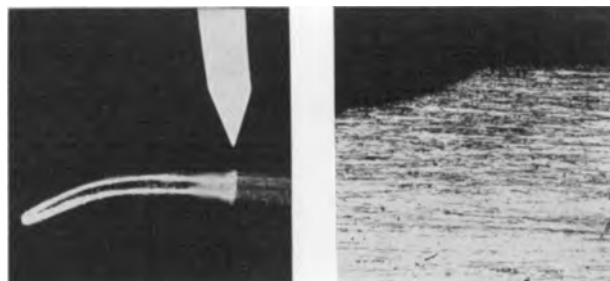


FIG. 4. Etched and bent wire on left (5X), arrow points to same zone in photomicrograph on right. 150X before reduced for publication.

bent cold. The arrow points to the boundary between the etched and unetched portions. The microstructure of the region indicated by the arrow is shown on the right. While the unetched zone undoubtedly shows a more strongly worked structure, the difference appears to be only a matter of degree. Hardness values taken across this specimen from outside edge to center showed that the average hardness (Knoop) in the edge region was 308 and the average for the interior was 246. No indication of a particular inclusion was visible.

As-worked.—The increased ductility of molybdenum and tungsten as a result of cold working is well known. Significant tensile test results are given in Table II and are plotted in Fig. 5 to show the effect of increasing cold work on the tensile properties of chromium wire. The results show that chromium work hardens to some extent, and that the rate of work hardening increases slightly with increased working beyond 80% reduction in area. However, wires drawn at 350°–400°C to result in a reduction in area of 95% without intermediate heat treatment, have very good bending properties in the as-worked conditions. The per cent elongation showed a variation which is to be expected considering the different diameters used and the short gauge lengths. However, a general lowering of per cent elongation with increase in work was indicated.

Two different types of fractures were exhibited by the as-worked specimens. There was the brittle, flat-granular failure which showed zero elongation, and there was a cup-cone fracture for the ductile failures. Test number 6 gave a 25% elongation and failed with a double cup-cone fracture as illustrated in Fig. 6.

Annealed.—The effect of heat treatment on the

TABLE II. Tensile strength of cold* worked chromium
Load rate = 0.02 in./min.

Test No.	Diameter at start (in.)	Diameter of test sample (in.)	%Red'n in area from drawing	Ult. str. 1000 psi	Elongation % in 1 in.
5	0.223	0.062	92.1	100.6	3†
26	0.216	0.062	91.8	100.6	2†
27	0.216	0.062	91.8	98.2	10
4	0.223	0.078	87.8	97.4	9
20	0.223	0.078	87.8	97.2	7
14	0.216	0.078	86.9	94.0	8
8	0.232	0.105	79.6	85.8	10
3	0.223	0.105	78.1	85.6	15
19	0.223	0.105	78.1	87.5	12
18	0.223	0.135	63.5	75.8	16
12	0.216	0.135	60.8	76.6	24
23	0.216	0.135	60.8	78.3	14
6	0.232	0.180	39.7	70.4	25

* Cold working was by drawing at 400°C.

† Broke outside gauge length; elongation due to "necking" not included in elongation values.

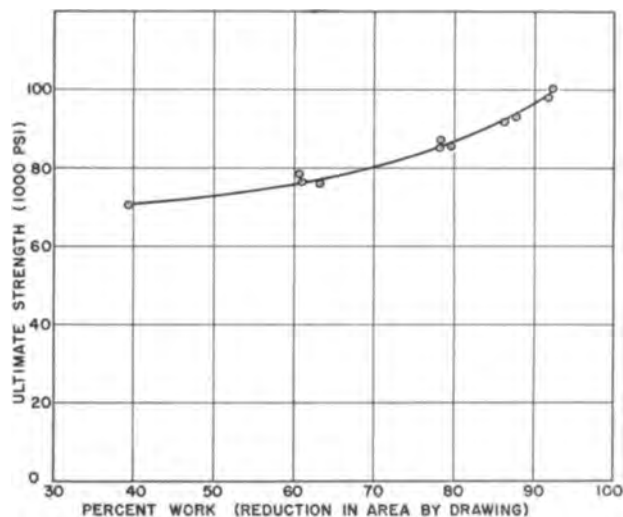


FIG. 5. Effect of cold work on ultimate strength

tensile strengths of 0.060 in. diameter wires was noted by comparing the as-worked wires with those annealed at 700°, 800°, and 900°C. The 700°C annealing was to represent stress relief, the 800°C anneal was to represent recrystallization, and the 900°C was to represent recrystallization and slight grain growth. All annealing was done in purified hydrogen or helium atmosphere. Since tensile strength of individual wires varied somewhat, annealed wires were compared with other portions of the same wire when possible. Results of these tests are given in Table III and show that: (A) annealing $\frac{3}{4}$ hr at 700° appears to reduce the ultimate strength by about 15% and correspondingly increases the elongation; (B) recrystallization by heating for $\frac{3}{4}$ hr at 800°C embrittled the specimens to the extent that they could not be held in the tensile grips to obtain a test.

Test at 240°C.—Three as-worked specimens were tested in tension at 240°C and the results compared with those tested at room temperature. Table IV

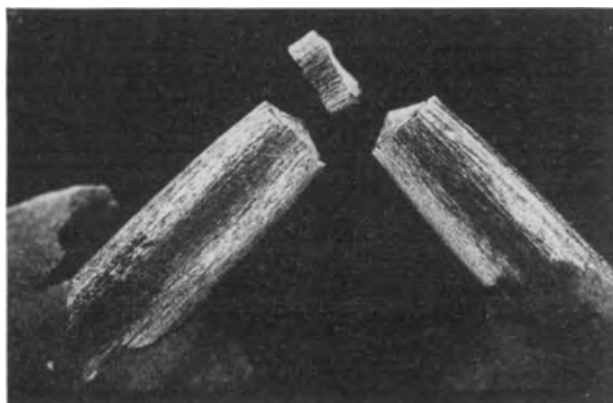


FIG. 6. Cup-cone tensile failure. 10X before reduced for publication.

TABLE III. *Tensile strength of as-worked and annealed wires*

Load rate 0.02 in./min.

Test No.	Material	Condition	Test diam. (in.)	Ult. str. 1000 psi	Elong. % in 1 in.	Remarks
32	W-28	As-worked	0.062	100.6	3*	
33	W-28	700°C-¾ hr	0.062	85.5	6*	
34	W-32	As-worked	0.062	100.6	2*	
35	W-32	As-worked	0.062	98.2	10	
36	W-32	700°C-¾ hr	0.062	85.5	7*	
37	W-38A	As-worked	0.062	112.1	7	
38	W-38A	As-worked	0.062	106.1	10	
39	W-38A	As-worked	0.062	106.9	9	
40	W-38A	700°C-¾ hr	0.062	91.7	12	
41	W-38A	700°C-¾ hr	0.062	90.0	12	
42	W-38A	800°C-¾ hr	0.062	Broke in grips		Recrystallized
43	W-38A	800°C-¾ hr	0.062	Broke in grips		Recrystallized
44	W-38A	900°C-5 hr	0.062	Broke in grips		Recrystallized with slight grain growth
45	W-38A	900°C-5 hr	0.062	Broke in grips		Recrystallized with slight grain growth
46	W-38B	As-worked	0.062	100.8	8	
47	W-38B	700°C-20 hr	0.062	95.3	0	
48	W-38B	700°C-20 hr	0.062	Broke in grips		

* Broke outside of gauge length; elongation due to "necking" not included in elongation value.

shows test results. Fracture of the 240°C tests were typified by smoother "necking" and a definite silky cup-cone failure. The ultimate strengths were lowered by 5-10% with some reduction in corresponding elongations.

Impact Tests

Chromium has been reported to have extremely low impact values (1). This also is a matter of common experience to those who have attempted to work chromium cold. At temperatures up to 325°C values did not exceed 0.5 ft lb, and at 700°C the values were only about 8 ft lb, so that chromium was considered to lack toughness even at temperatures well above the transition temperature.

While not a test of ductile chromium, data on a few specimens of as-cast chromium are included to show that above the transition temperature of about 350°C chromium displays excellent impact strength.

Tests were made on unnotched Charpy specimens to compare better with other values (1). The 400°C test was made by removing the specimen from a furnace slightly above the test temperature and quickly placing it in the impact machine. Data are shown in Table V.

Room temperature impact values on as-cast material were so low as to be scarcely measurable. Results at a nominal 400°C, however, showed the large value of 118 ft lb. The specimens did not fracture, so a valid test was not obtained.

Lack of a suitable impact testing procedure for the smaller ductile rods and wires prevented inclusion of comparable data on ductile material.

TABLE IV. *Tensile strength of wire at 240°C*

Material	Test diameter	U. T. S. 1000 psi		Elongation % in 1 in.	
		25°C	240°C	25°C	240°C
W-29	0.135	79	71	16	16
W-29	0.104	86	78	10	7
W-29	0.078	93	88	8	5

TABLE V. *Impact test on as-cast chromium*

Specimen Number	Temp, °C (Nominal)	Impact ft lb
1	Room	1.5
2	400	119
3	400	128
4	400	106
		Avg. 118

Torsion Test

No values for torsional strength of chromium have been noted in the literature. Excellent ductility in tension contrasts strongly with lower resistance to impact. Light peening with a hammer on ductile wire is sufficient to cause the wire to crumble. For that reason, behavior of ductile wire in torsion was of some interest.

A small torsion testing apparatus was constructed having a variable speed mechanism arranged to turn a chuck at a prearranged rate. Specimens were prepared by etching chromium wire which had been drawn as described, and all were in the as-worked condition. The specimen was placed between this chuck and another which was prevented from rotating by a lever arm with a weight attached. From the angle and weight needed to counterbalance the tor-

TABLE VI. *Torsion test*

Run No.	Mean diameter (in.)	Gauge length (in.)	Ult. strength psi	Ult. strain rev./in. (gauge)
T-2	0.055	2.75	92,200	9.35
T-3	0.051	2.50	93,000	10.4
T-4	0.051	2.88	95,100	20.5
T-6	0.051	1.75	94,800	19.0
T-10	0.051	3.00	92,400	23.4

sion the torsional strength was computed. All tests were at 25°C. Results of the tests are shown in Table VI. A typical torsion failure is shown in Fig. 7.

The results show an unexpected strength and ductility in torsion. A maximum ultimate strength of about 95,100 psi and a strain of 23.4 turns to the inch was obtained.

Creep Rupture

A creep rupture value for vacuum-cast electrolytic chromium has been recorded at 1 min for 20,000 psi and 871°C (17).

A single creep rupture test was carried out on a recrystallized specimen of high purity chromium swaged rod. The load was initially 10,000 psi at a temperature of 500°C. No creep was noted over a period of one week, so the load was raised to 15,000 psi. The specimen had 0.01 in. elongation in 1.53 in. at the end of 1000 hr when the test was discontinued.

EFFECT ON DUCTILITY OF ADDED IRON OR NICKEL

Regarding the effect of added elements on transition temperatures of chromium, it has been reported that iron and particularly nickel raise it (1).

To test the effect of added iron and nickel in making alloyed chromium wire using production techniques known to produce ductility in chromium

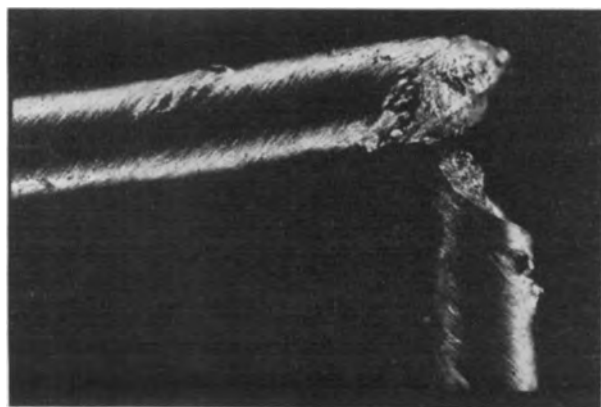


Fig. 7. Torsion failure. Protuberances are lead-chromium compound remaining from incomplete etching. 10X before reduced for publication.

alone, 1% alloys each of iron and nickel were made with high purity chromium. The powders were mixed, pressed into bars, sintered in hydrogen, and consumable arc-melted. The ingots were sheathed and swaged at 1000°C. The 1% nickel addition was found to be unusually hard in the as-cast condition (R_b88 , while pure as-cast chromium is about R_b55) and shattered badly upon swaging at 1000°C. Remelting and reswaging of this ingot at 1250°C showed little improvement.

The case with the 1% iron alloy was different. Working to finished wire was accomplished with little difficulty, and the wire was ductile after surface removal. Hardness of the 1% iron alloy was about the same as that of pure chromium, i.e., about R_b55 . One per cent iron increased the work hardening during wire drawing. Permissible reduction in area with the iron alloy during wire drawing at 400°C was about one-half that allowed with pure chromium, or about 45% and 95%, respectively, before annealing at 1200°C.

EFFECT OF DIFFERENT GASES ON BENDING OF WIRE

As has been noted, chromium wire (hot worked from high purity, arc-melted ingots) in the as-worked condition is brittle at room temperature. Removal of a very thin surface layer renders the chromium ductile. The question was raised whether the embrittling was due to contamination of the surface by gases during processing and working. Hydrogen, oxygen, and nitrogen were encountered in the normal processing of ductile wire or sheet. Samples of ductile chromium wire were treated at various temperatures for 1 hr in the various gases including helium as a control. After heat treatment, the specimens were bent manually to test for ductility.

Three or four etched wire specimens, each about 2 in. long and about 0.040 in. in diameter, were placed in a closed end Pyrex tube which was evacuated to less than 1μ and backfilled with purified gas.⁵ This was repeated twice, then the tube containing specimens was drawn off and inserted in a furnace at the desired temperature. After heat treatment the ampoule was broken open and the wires tested. Results of the tests with the different gases at the different temperatures are given in Table VII and show that:

⁵ Cylinder nitrogen was purified by passing the gas through pyrogallol absorbers followed by a phosphorus pentoxide dryer. Cylinder oxygen was treated by passing the gas through a train consisting of 0.2N $KMnO_4$, 0.1N KOH, and a phosphorus pentoxide dryer. Helium and hydrogen were both purified by passing through a Zr-Ti getter furnace at 850°C.

TABLE VII. *Effect of different gases on ductility*

Run	Ingot or wire	Diam	Gas	Temp, °C	Time (hr)	Color	Ductility as treated	Diameter as etched, in.	Ductility as etched	Remarks
0-1	SA4595	0.051	O ₂	700	1	Scaly and green	Brittle	0.035	Bent	
0-4	SA5031	0.051	O ₂	600	1	Scaly and green	Bent			
0-2	SA4595	0.051	O ₂	500	1	Scaly and green	Bent			
0-3	SA5031	0.051	O ₂	400	1	Slight green	Bent	0.034	Bent	
N-4	SA5031	0.054	N ₂	600	1	Black and tan	Brittle			
N-5	W-23	0.052	N ₂	500	1	Blue and tan	Brittle	0.045	Bent	
		0.036								
N-3	W-24	0.057	N ₂	400	1	Slightly spotty	Bent and broke	0.040	Bent and broke	
		0.036								
N-1	W-24	0.057	N ₂	400	4¼	Spots of pale blue	Bent and broke	0.045	Bent and broke	Bad sample Bad sample
N-6	W-29	0.052	Cyl. N ₂	400	1	None	Bent			
N-7	W-29	0.052	Cyl. N ₂	400	1	Slight tan	Bent			
N-8	W-36	0.052	Cyl. N ₂	700	6	Gray and black	Brittle	0.048	Bent	
V-1	W-36	0.057	Vacuum	700	1	Metallic gray	Brittle	0.045	Bent	

1. Oxygen became harmful somewhere between 600° and 700°C.

2. Nitrogen became harmful somewhere between 400° and 500°C.

3. Hydrogen and helium gases gave inconclusive results since observations indicated that the embrittling effect may have been due to traces of nitrogen.

4. Only one sample⁶ was tested in vacuum. Annealing at 700°C for 1 hr resulted in a surface disturbance which rendered it unbendable in the as-annealed surface condition.

5. Oxidation at 700°C seemed to be more penetrating than nitriding at 700°C, due possibly to the nature of the surface layer, the oxide being rather scale like and nonadherent as compared to the nitrided layer.

6. Metallographic examination of four other samples⁷ showed that there was no perceivable difference in nature or depth of the corrosion layer.

Gaseous exposure tests indicated that the influence of nitrogen might bear more attention, and attempts were made to compare nitrogen contents in the surface layer and the body of the material. In one case, the surface layer of a 0.250 in. diameter swaging was turned off and its nitrogen content compared with the interior of the swaging.

R-1040 body 0.002% N
R-1042 outer layer 0.02% N

In the other case, ductile 0.052 in. diameter wire was exposed to cylinder nitrogen at 700°C for 6 hr. The thickness of removal required to render it bendable again was estimated to be 0.00175–0.0015 in. Know-

⁶ (V-1), Vycor enclosed.

⁷ O-1, O-5, N-5, and N-3, Table VIII.

ing this, the entire sample was sent for nitrogen analysis and compared with nitrogen content of another section of the same wire which was not exposed to nitrogen. The discolored layer (0.00075 in.) was removed before sampling.

R-1086 nonexposed 0.0228% N
R-1087 entire exposed wire 0.0298% N

By calculation, concentration of nitrogen in the brittle layer was found to be approximately 0.1%.

DISCUSSION

Previous attempts to explain the brittle-ductile phenomenon in chromium have relied to a large extent on the presence of certain impurities, principally oxygen since it is usually the impurity present in largest amount. Pursuit of the highest purity chromium possible was a logical approach to the question of ductility in chromium, but as purer metal was made, it became apparent that purity was not the whole story. Kind and extent of deformation were found to play a role. It has been asserted that oxygen has relatively little influence on the transition temperature (1), and the theory has been advanced that iron on the surface of chromium obtained from the steel sheath in rolling operations may be the cause of the brittleness (2). This is supported by investigators who found that iron raised the ductile-to-brittle transition temperature (1).

Results of the present investigation do not agree with these findings concerning oxygen and iron. It is agreed that oxygen may not be the sole cause of brittleness, but it is considered to be a contributing factor. The fact remains that to date the only room-temperature ductile chromium has also been low oxygen chromium. It is possible that iron in high

concentration on the surface, as from sheath rolling, may contribute to the brittleness, but the present experiment with a 1% iron alloy appeared to give material as ductile at room temperature as pure chromium.

Experiments with various gaseous atmospheres and the influence on the ductility showed several unexplained features. Oxygen was not found to be injurious up to 600°C, while hydrogen, helium, and vacuum gave results similar to nitrogen. From appearances of the specimens it was suspected that traces of nitrogen present in the other gases may have been the embrittling agent. The concentration of nitrogen in the brittle layer was found to be about 0.1%, considerably higher than expected. At temperatures below 800°C (approximate recrystallization temperature) all specimens were ductile after etching, and oxygen specimens were ductile below 700°C without etching. Specimens heated in air to 600°C, however, were brittle before etching.

No explanation for the brittle behavior can be advanced on the basis of the present work. A cold-ductile wire can be made brittle by heating in gettered hydrogen to 600°C. By removing as little as 0.002 in. from the radius, the wire can be made completely cold-ductile again. These results suggest that brittleness in chromium may be due to any one or a combination of several factors. Impurities such as oxygen, nitrogen, and nickel are considered to have possible influence, and the extent of cold work may be a factor. Cold-ductile wire heated above the recrystallization temperature is completely and permanently embrittled. However, one sample⁸ showed an elongation of 25% after only a 40% reduction in area, and a portion of the worked area was removed by etching. So it was apparent that a completely cold-worked structure was not absolutely necessary for maximum cold-ductility as was considered previously.

Possible uses for fully ductile chromium will certainly be in the field of heat engines, where as an alloying agent its properties of heat, corrosion, and wear resistance are already utilized. Full use of the pure metal will not be possible, however, until the impact strength at room temperature is increased. Nevertheless, in view of the present relative ease of hot-forgeability and the good hot impact strength, a possible use is for turbine-bucket material.

Potential electronic uses for ductile wire are anticipated where the high vapor pressure at temperatures above 800°C would not be a disadvantage. Use as

a thermocouple element may be possible. The excellent oxygen gettering property would be of advantage for some uses.

The achievement of room-temperature ductile chromium leads to the confident expectation that further investigation may unlock all the secrets of ductility dependence, not only for chromium, but for other body-center cubic metals as well.

ACKNOWLEDGMENT

Acknowledgment is made to W. J. Knapp who designed and carried out the torsion tests, and to R. G. Nelson who reviewed the manuscript.

Acknowledgment is also made to A. U. Seybolt and C. E. Lacy of Knolls Laboratory who performed the hot-extrusion of chromium.

Any discussion of this paper will appear in a Discussion Section to be published in the June 1955 JOURNAL.

REFERENCES

1. A. H. SULLY, E. A. BRANDES, AND K. W. MITCHELL, *J. Inst. Metals*, **81**, 585 (1953).
2. H. L. WAIN AND F. HENDERSON, *Proc. Phys. Soc. (London)*, **66**, 515 (1953).
3. H. T. GREENAWAY, "Pure Chromium, Its Production and Freezing Point," Report SM 163, Department of Supply, Aeronautical Research Laboratories, Melbourne, Australia, January 1951.
4. G. ASAI AND H. JOHANSEN, "Massive Chromium," Final Report to Army Ordnance Corps, Watertown Arsenal Laboratory, Watertown, Mass., September 15, 1953.
5. W. BLUM, *Trans. Electrochem. Soc.*, **90**, 87 (1946).
6. H. T. GREENAWAY, S. T. JOHNSTONE, AND M. K. MCQUILLAN, *J. Inst. Metals*, **80**, 109 (1951).
7. W. J. KROLL, W. F. HERBERT, AND L. A. YERKES, *This Journal*, **97**, 258 (1950).
8. H. L. GILBERT, H. A. JOHANSEN, AND R. G. NELSON, *J. Metals*, **5**, 63 (1953).
9. H. B. GOODWIN, R. A. GILBERT, C. M. SCHWARTZ, AND C. T. GREENIDGE, *This Journal*, **100**, 152 (1953).
10. F. ADCOCK, *J. Iron Steel Inst.*, **115**, 369 (1927).
11. F. G. VAN DEN BORSCH, D. J. C. PURSER, D. S. B. SHANNON, AND VACUUM SCIENCE LTD., British Pat. 554,829, November 1941.
12. A. R. KAUFMAN, P. GORDON, AND D. W. LILLIE, *Trans. Am. Soc. Metals*, **42**, 785 (1950).
13. A. B. KINZEL, *Metal Progr.*, **58**, 315 (1950).
14. H. L. GILBERT, H. A. JOHANSEN, AND R. G. NELSON, "Malleable Chromium and Its Alloys," U. S. Bur. Mines Rept. Invest. 4905, September 1952.
15. A. BRENNER, P. BURKHEAD, AND C. JENNINGS, *J. Res. Nat. Bur. Standards*, **40**, 31 (1948).
16. H. A. JOHANSEN, H. L. GILBERT, R. G. NELSON, AND R. L. CARPENTER, "Tensile Properties of Pure Chromium at Elevated Temperatures," U. S. Bur. Mines Rept. Invest. 5058, May 1954.
17. R. M. PARKE AND F. P. BENS, "Chromium Base Alloys," Symposium on Materials for Gas Turbines, *ASTM*, Nov., 80 (1946).

⁸ Tensile test No. 6, Table II.

The Role of the Electric Arc Furnace in Utilizing Some Strategic Off-Grade Ores¹

LLOYD H. BANNING

Ferrous Metals Branch, Region II, U. S. Bureau of Mines, Albany, Oregon

ABSTRACT

A dry-top, arc-resistance, electric smelting technique for recovering strategic metals from off-grade ores is described. Advantages of using a bulky form of reductant such as hogged wood waste in the furnace charge are pointed out. Smelting test data on nickel ores, a siliceous manganese ore, off-grade chromite concentrates, a fine grained chromite ore, and aluminum silicates are presented. The relationship between a theoretical smelting efficiency and slag-to-metal ratio is shown. The possibility of applying this dry-top, arc-resistance, electric smelting technique to other ores is indicated.

INTRODUCTION

It has been estimated that the United States consumed 2,300,000 short tons of manganese ore, 1,334,000 tons of chromite, 106,000 tons of nickel, and 6,000,000 tons of bauxite in 1953 (1). Unfortunately, our country is largely dependent on foreign sources for these vital ores. Approximately 7% of the manganese ore, 4% of the chromite, and 28% of the bauxite was produced from domestic deposits. About 1% of the nickel consumed in the country was produced as a by-product of the domestic copper refining industry. Stockpiling programs for manganese and chromite have materially increased the domestic production of these ores in the last two years. Domestic nickel production will also be increased when the Hanna Nickel Smelting Company starts operation of their new electric ferronickel smelter near Riddle, Oregon, late in 1954. Since 1947 the domestic production of bauxite decreased from 39% to its estimated present proportion of 28% of domestic consumption.

There are many known off-grade deposits of nickel, chromium, manganese, and aluminum ores in continental United States which are not amenable to conventional mineral dressing and chemical treatment processes. The Bureau of Mines began investigations several years ago to determine the feasibility of treating some of these off-grade ores by electric smelting processes. Ravitz and coworkers at the Intermountain Experiment Station, Salt Lake City, Utah, have published results of some of the Bureau's early smelting investigations on smelting off-grade nickel ores (2, 3). Torgeson and coworkers at the Boulder City, Nevada, station, have published results of matte smelting tests on Chamberlain,

South Dakota, manganese nodules (4). Batch smelting tests on Mouat, Montana, and Coquille, Oregon, chromite concentrates have been described by Wessel and Rasmussen (5). The practicability of using hogged fuel in electric smelting charges when smelting Pacific Northwest ores was pointed out by Rasmussen (6). Cremer's report on nickel smelting investigations at the Northwest Electrodevelopment Laboratory was released in January 1954 (7).

Electric smelting research is being continued at the Northwest Electrodevelopment Laboratory, Albany, Oregon, on "selective reduction" operations where only part of the metal oxides are reduced to metal, on "nonselective reduction" operations where almost all of the metal oxides are reduced to metal, and on "complete reduction" operations where all of the oxides charged to the furnace are reduced and no slag is produced. This paper describes these various smelting techniques.

FUNDAMENTALS OF ARC FURNACE SMELTING

In arc furnace smelting operations carbon is added to the charge only to reduce the oxides to metal. The degree of reduction is dependent on the quantity of reductant in the charge. The heat for the reduction reaction is generated either by arcing on the molten bath, or by passage of the current through the molten slag, or by a combination of both. When an arc is maintained between the molten bath and the electrodes the operation is usually referred to as arc-resistance smelting; when the electrodes contact the slag the operation is referred to as slag-resistance smelting. Both roofed furnaces and open-top furnaces are used. Most of the smelting research at Albany has been carried out in open-top furnaces using a dry-top, arc-resistance, smelting technique.

In dry-top, arc-resistance smelting operations reductants and usually fluxes are mixed with the ore and charged to the furnace. The reductant may

¹ Manuscript received April 9, 1954. This paper was prepared for delivery before the Chicago Meeting, May 2 to 6, 1954.

be coke, charcoal, sawdust, hogged fuel, metallic reductants such as ferrosilicon, or mixtures of these materials. When fluxes are used, fluxing reagents such as limestone or quartz are mixed with the charge so that the resulting slag will be fluid enough to tap from the furnace. When the furnace is operating normally, the charge is kept at a uniform thickness; the electrodes extend through the charge, and the useful heat for conducting the smelting is generated by arcing from the electrode tips to the molten bath and by the current passing through the slag; gas produced by the reaction escapes through the porous charge as it feeds continually into the smelting zone. Metal and slag are tapped from the furnace at regular intervals.

The most noteworthy feature of the smelting method employed at Albany, Oregon, is the use of hogged fuel in the charge. Hogged fuel, a by-product of Oregon's extensive lumber industry, is a mixture of wood chips, splinters, and sawdust resulting from feeding slabs, edgings, and other saw mill wastes through a machine called a "hog." Some advantages of using hogged fuel in the furnace charge are: (A) it forms a porous charge through which gases can readily escape and prevents crusting of the charge; (B) a hogged fuel charge serves as a heat insulating roof over the smelting zone; (C) the electrical conductivity of the charge is low; (D) vaporization and dust losses are minimized; and (E) the temperature of the smelting zone may be varied by adjustment of the proportion of hogged fuel to other reductants in the charge.

When analyses of the charge materials are known, flux, carbon, and electric energy requirements for conducting any electric smelting operation can be calculated. Three reasons for using fluxes are: (a) to control slag melting temperature; (b) to prevent corrosion to furnace refractories; and (c) to improve recovery of the metallic constituents. The natural slag melting temperature can be determined with the aid of slag-phase diagrams (8). The amount of necessary fluxes to be added to the furnace charge for producing a fluid slag can be determined by the same means. Furnace charges that produce acid slags are usually smelted in carbon lined furnaces; however, such linings cannot be used when carbon is deficient in the charge as in the selective reduction of low-carbon ferronickel from siliceous nickel ores. Usually a high-iron slag is produced and, although the slag is acid, a basic magnesite lining is used because of its resistance to high iron slags. Enough limestone could be used to make the slag basic, but it is generally good practice to keep the slag volume to a minimum.

Carbon requirements may be calculated from molecular weights of the reactants and the equation

for the reaction. An example of a carbon calculation is shown below:



Therefore, 12.01 (mole wt C) lb C are required per 58.69 (mole wt Ni) lb Ni reduced, or 0.204 lb C are required per lb Ni reduced.

In reducing a metal from its oxide it is assumed that the electrical energy required for the reaction is the same quantity as that liberated when the metal is oxidized. When calculating the efficiency of electrical energy utilization in the electric furnace the only energy considered useful is that required for this reaction. The change in heat content (electrical energy) of a given reaction, ΔH , is obtained by subtracting the heats of formation of all the reacting materials from the heats of formation of all the products (9). An example of a calculation for determining the theoretical electrical energy for reducing Ni from NiO is as follows:



$$-57.8 \text{ kcal (NiO heat of formation per mole)} + \text{O} = -26.4 \text{ kcal (CO heat of formation per mole)} + \text{O}$$

$$\Delta H \text{ for producing one mole Ni from NiO} = (-26.4 + \text{O}) - (-57.8 + \text{O}) = 31.4 \text{ kcal}$$

$$\Delta H \text{ for 58.69 g Ni (one mole)} = 31.4 \text{ kcal}$$

$$\Delta H \text{ for 1 g Ni} = 31.4/58.69 = 0.535 \text{ kcal}$$

$$\Delta H \text{ for 1 lb Ni} = 0.535 \times 453.59 = 242.7 \text{ kcal}$$

$$1 \text{ kcal} = 0.0011628 \text{ kw hr}$$

Therefore, $242.7 \times 0.0011628 = 0.282$ kw hr of electrical energy is the theoretical quantity required to reduce 1 lb of Ni from NiO.

The calculated carbon and energy requirements for producing metal from the ores discussed in this paper are:

	Ni	Fe	Mn	Cr	Ti	Al	Si
Lb of C/lb.....	0.204	0.215	0.218	0.346	0.501	0.668	0.856
Kw hr/lb.....	0.282	0.355	0.717	0.952	1.70	3.03	2.80

Slag-to-metal ratio, carbon specification for metal, slag conductivity, charge conductivity, and desired smelting temperature are most of the factors that determine the proper voltage-current relationship to use in a particular electric smelting operation. Although an exact formula for determining this relationship has not been developed, sufficient data are available to indicate certain operating principles. A comparatively high voltage-current relationship is employed where there is a high slag-to-metal ratio. This is especially true when it is desired to produce

a low-carbon metal such as ferronickel from siliceous nickel ores. Slags produced when smelting these ores have comparatively high resistances. Contamination of the metal with carbon and high electrode consumption is prevented by using a voltage-current relationship high enough to prevent the electrodes from contacting the slag. Low-carbon ferronickel can also be produced from ferruginous nickel ores. Slags produced from these ores have a lower electrical resistance, due to the presence of iron oxide in the slag; a lower voltage-current relationship is used.

In operations where no slag is produced, such as the production of aluminum-silicon alloys, a low voltage-current relationship is employed. In this case, it is also important to use a charge having a low electrical conductivity. If either the voltage-current relationship or the charge conductivity is too high, current flows through the charge causing the charge to heat above the smelting zone, the electrodes to rise, and the smelting zone to cool. A continuation of these conditions usually results in an inoperable furnace. Generally these conditions can be corrected by increasing the current to the furnace. However, the current at which the maximum heating occurs is not necessarily the maximum current at which the furnace will operate. The current at which the maximum heating occurs may be called the optimum current. Optimum current in an electric arc furnace can be determined by a method described by Cochran (10). Optimum current differs for each voltage tap in steel-making furnaces; in smelting furnaces, optimum current may differ for each ore being smelted as well as for each voltage tap.

DESCRIPTION OF SMELTING FURNACES

Two 3-phase, cylindrical, stationary, pit-type, electric arc furnaces are available for making continuous experimental smelting tests at the Northwest Electrodevelopment Laboratory. The large furnace, designated ESB, using 8-in. or 6-in. graphite electrodes has a shell 96 in. in diameter and 78 in. high. Diameter inside the refractory is 67 in.; the height is 58 in. The small furnace designated ESA, using either 3-in. or 4-in. graphite electrodes, has a shell 50 in. in diameter and 55 in. high. Diameter inside the refractory is 32 in., and the height is 39 in. Carbon brick or magnesite brick are used for furnace linings. Furnace hearths are usually rammed with carbon paste or periclase. Both furnaces are used as open-top furnaces; however, provisions have been made for using a roof on the smaller furnace.

The electrode clamp arm assemblies are cable-suspended with provisions for readily changing electrode spacing. Graphite electrodes are placed at the corners of an equilateral triangle. Electrode current is automatically controlled by a balanced-

beam type regulator. Either furnace when in use is connected to a 1000-kva Westinghouse transformer which has six voltage taps. The secondary busses of the transformer may be connected in series or parallel; when connected in series the voltage is approximately twice the parallel connection voltage. The open circuit phase-to-phase voltage ranges from 38 to 106 volts on the parallel connection and from 80 to 220 volts on the series connection.

SELECTIVE REDUCTION SMELTING TECHNIQUES

Selective reduction smelting techniques have been employed to recover low-carbon ferronickel from off-grade nickel ores, high-purity iron from high-phosphorous iron ore, and to remove iron from manganese slags. The selective reduction technique is best illustrated by the results of a few of the tests on nickel ores. Table I shows the results of two smelting tests on Riddle ore from Douglas County, Oregon, two smelting tests on Cle Elum ore from Kittitas County, Washington, and one on Red Flat ore from Curry County, Oregon. All ores were treated under dry-top smelting conditions. In addition, open-arc smelting was employed in one test on Riddle ore. In this test the molten pool between electrodes was never allowed to become covered with raw charge. Also, a roofed furnace was used in one test on Cle Elum ore. In this test coke was the only reductant.

A cooperative agreement for conducting smelting research on Riddle nickel ore was entered into by the M. A. Hanna Company and the Bureau of Mines in 1951. Smelting tests on Riddle ore, discussed in this paper, were made while the cooperative agreement was in effect. Although the results were promising, the Hanna Nickel Smelting Company chose another process for ferronickel production at their new plant.

Examination of Table I indicates that higher proportions of carbon are required in the charge when smelting an ore high in iron. Only 3.92 times the carbon required to reduce the nickel oxide in the ore was used in the test on Riddle ore. The alloy product contained about twice as much iron as nickel. In the test on Red Flat ore, 12.8 times the stoichiometric proportion of carbon was used to produce an alloy containing about 8.5 times as much iron as nickel and, in the test on Cle Elum ore to produce a similar alloy, 32.5 times as much carbon was added to the charge as was theoretically required to reduce the nickel in the ore. Part of the carbon was undoubtedly consumed in reducing the Fe_2O_3 to FeO . Analyses indicate that more nickel is lost in the slag when a higher grade nickel metal is produced. The calculated nickel recovery for the tests on Red Flat and Cle Elum ore were both higher than the recovery on

TABLE I. Selective reduction tests on nickel ores

Type of smelting	Riddle		Cle Elum		Red Flat Dry-top
	Dry-top	Open-arc	Dry-top	Roofed	
Ore analyses, %					
Ni	1.5	1.5	1.19	1.19	0.74
Fe	15.2	15.2	45.9	45.9	28.2
C,* ratio to stoich. prop.	3.92	3.92	46.7	32.5	12.8
Lb of limestone/100 lb of ore.	None	None	12.0	12.0	None
Time of test, hr.	88	20	27	53	72
Feed rate, lb ore/hr.	471	343	460	266	409
Electrical conditions:					
Voltage, phase-to-phase.	205	158	120	120	200
Current, amp.	400	700	1600	1000	653
Kw input.	206	197	300	200	225
Kilowatt-hours:					
Per ton dry ore.	875	1145	1335	1580	1072
Per lb of Ni in metal.	47.9	67.0	72.1	84.5	88.1
Per lb of metal,					
Theoretical.	0.34	0.32	0.35	0.35	0.34
Actual.	15.4	23.6	5.7	9.4	13.2
Efficiency, %.	2.18	1.37	6.17	3.68	2.57
Electrode consumption, lb/ton dry ore.	12.2	32.0	9.2	18.4	10.5
Slag-to-metal ratio.	15.9	19.5	6.3	9.6	14.9
Typical metal analysis:					
Ni, %.	32.2	35.2	7.85	11.12	10.8
Fe, %.	69.2	63.1	—	—	86.8
C, %	0.05	0.05	0.05	0.10	0.06
Slag analysis, %					
Ni.	0.22	0.21	0.04	0.05	0.08
Fe.	15.0	15.7	39.8	42.5	33.0
Ni recovery in metal, %†.	83.3	83.4	96.2	96.0	87.1

* Carbon required for NiO only.

† Recovery figures based on weights and analyses of slag and metal products.

Riddle ore mainly because lower grade ferronickel alloys were produced.

The highest voltage tap was used in the tests on Riddle and Red Flat ores. Lower voltage was employed in the tests on Cle Elum ore. The operation indicated that the high-iron slag from the Cle Elum ore was a better conductor of electricity than the slags produced from Riddle and Red Flat ore. Therefore, to maintain stable arcs in the furnace, a lower voltage was employed.

Calculations indicate that higher efficiencies were obtained at higher kilowatt inputs. Electrode consumption appeared to be inversely proportional to kilowatt input. Results also indicate that efficiency, which is the percentage relationship between the theoretical electrical energy requirement and the actual requirement, increased as the slag-to-metal ratio decreased. Perhaps, the most significant figure in Table I is the kilowatt hour consumption per pound of nickel recovered. This figure, inversely proportional to the nickel content of the ore, varied from 47.9 for 1.5% Ni Riddle ore to 88.1 for 0.74% Ni Red Flat ore.

NONSELECTIVE REDUCTION SMELTING

Nonselective reduction smelting may be defined as smelting operations in which no attempt is made to prevent small amounts of carbon, silicon, and other impurities from reducing into the metal product. The quantity of carbon added to the charge is not as critical as in selective reduction smelting or in complete reduction smelting, and the slag-to-metal ratio is much lower than in selective reduction smelting. Typical examples of nonselective smelting operations are the production of pig iron, high-carbon ferrochrome, and silicomanganese.

Smelting Tests on a Siliceous Manganese Ore

Present General Service Administration stockpile specifications limit the SiO_2 plus Al_2O_3 content of manganese ores to 15%. Smelting tests at the Northwest Electrodevelopment Laboratory have shown that this limitation on SiO_2 and Al_2O_3 has little bearing on the usefulness of manganese ore for the manufacture of silicomanganese. Table II shows the results of four dry-top smelting tests on a siliceous manganese ore, rhodonite, from southern Oregon.

TABLE II. Smelting tests on a siliceous manganese ore

	Test No.				
	71-1	68-1	68-3	5-3	85-2
Furnace used	Small	Small	Small	Large	Small
Ore analysis, %					
Mn	24.8	24.8	24.8	27.2	32.4
Fe	2.06	2.06	2.06	2.1	3.2
SiO ₂	45.5	45.5	45.5	45.2	40.7
C,* ratio to stoich. prop.	1.43	1.38	1.20	1.34	1.20
Lb of limestone/100 lb ore	12	23	36	42	42
Time of test, hr	7.8	8.6	11	8.5	6.6
Feed rate, lb ore/hr	239	210	191	471	167
Electrical conditions:					
Voltage, phase-to-phase	124	110	110	124	120
Current, amp	870	1,000	1,000	2,300	960
Kw input	190	200	200	500	200
Kilowatt-hours:					
Per ton ore	1,610	2,000	2,040	2,080	2,460
Per lb metal					
Theoretical	1.04	1.05	1.03	1.07	0.96
Actual	5.43	5.11	4.13	2.94	3.53
Efficiency, %	19.1	20.5	24.9	36.4	27.2
Electrode consumption, lb					
Per ton ore	23.0	37.0	37.0	23.6	35.6
Per ton metal	148.4	134.0	134.0	80.8	110
Slag-to-metal ratio	3.80	3.31	2.96	2.01	2.14
Metal analysis, %					
Mn	64.7	65.9	63.8	66.3	73.7
Fe	8.6	8.5	7.7	6.9	6.0
Si	19.3	19.5	19.6	20.2	14.8
Slag analysis, %					
Mn	15.6	12.2	8.4	6.8	4.1
Fe	0.25	0.33	2.0	0.4	0.70
SiO ₂	52.3	51.2	48.0	46.0	40.0
CaO	12.5	22.3	30.0	33.4	40.0
MgO	1.2	1.81	2.77	1.3	4.2
Basicity of slag**	0.29	0.52	0.76	0.82	1.24
Mn recovery in metal, %†	52.0	62.0	71.4	86.1	89.2

* Theoretical carbon required to produce silicomanganese.
 ** Basicity is the mole ratio of the basic constituents to the acid constituents.
 † Manganese recovery based on weights and analyses of metal and slag products.

This ore contained more than 45 % silica. The fifth test was made on a sink-float concentrate from this same ore. These particular smelting tests were selected to show the relationship between the basicity of the slag and the manganese recovery in the silico-manganese product. Limestone was used in all the tests for control of basicity. One of the tests, 5-3, was conducted in the large furnace, the remainder being conducted in the small furnace. Carbon varied between 1.30 and 1.43 times the stoichiometric proportion, the highest proportion being used in the test in which the smallest amount of limestone was added to the charge. The highest manganese recovery was made on the sink-float concentrate. The relationship between the basicity of the slag and the manganese recovery is plotted in Fig. 1.

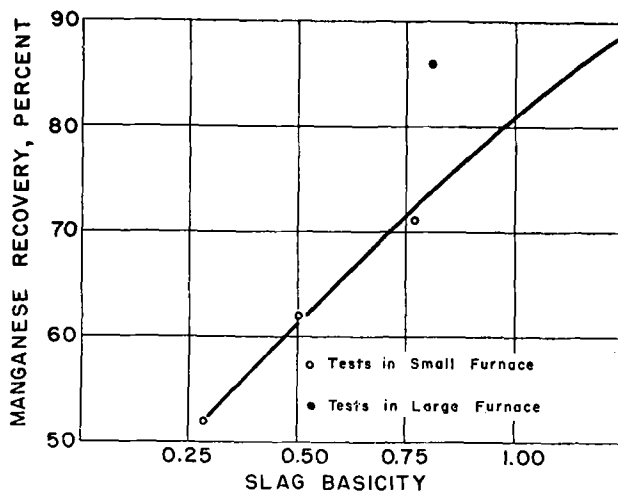


FIG. 1. Relationship between slag basicity and manganese recovery.

Results of smelting tests show a more efficient use of electrical energy and electrodes in the large furnace than in the small furnace. The calculated efficiency was up to 36.4% for the test in the large furnace and varied between 19 and 27% for tests in the small furnace.

Smelting Tests on Off-grade Chromites

Results of two smelting tests each on off-grade chromite concentrates from Mouat, Montana, and Coquille, Oregon, and one test on Iron King, Grant County, Oregon, chromite ore are shown in Table III. Quartz was the only flux used in the furnace charges. Hogged fuel and coke, correctly proportioned, were the reductants. The use of hogged fuel made it practical to smelt the chromite concentrates without previous agglomeration.

Four of the five smelting tests on chromite, shown in Table III, were made in the small furnace. One

of the tests on Coquille concentrates was made at a phase-to-phase voltage of 158, the other three tests were made at a voltage of 200. The kilowatt input varied between 185 and 280, and was highest at the higher voltage. Electrode consumption was less and the reductant requirement was more when operating at the high voltage.

One smelting test on Mouat chromite concentrates was made in the large furnace. Results again indicated a more efficient use of electrical energy in the large furnace. Average calculated efficiency was higher for the chromite smelting tests than for the siliceous manganese smelting tests. The lower slag-to-metal ratio and the higher kilowatt input were factors contributing to the higher smelting efficiency.

The smelting test on Iron King chromite ore is noteworthy. The ore contained only 26.2% Cr_2O_3 and the slag-to-metal ratio was approximately twice as high as when smelting concentrates, but the kilo-

TABLE III. Smelting tests on off-grade chromites

Head sample.....	Mouat conc.		Coquille conc.		Iron King ore
	7	123	91	122	124
Test No.....					
Furnace used.....	Large	Small	Small	Small	Small
Ore analysis, %					
Cr_2O_3	36.4	36.4	33.6	33.6	26.2
Fe.....	18.1	18.1	17.7	17.7	9.58
SiO_2	7.7	7.7	3.0	3.0	16.8
MgO.....	16.0	16.0	9.4	9.4	21.6
Al_2O_3	22.9	22.9	25.2	25.2	12.0
Lb of quartz/100 lb ore.....	20.8	22.0	20.0	20.0	17.0
C,* ratio to stoich. prop.....	1.29	1.81	1.41	1.82	1.65
Time of test, hr.....	73	101.6	25	137	40.7
Feed rate, lb ore/hr.....	487.6	279.5	168	237	309
Electrical conditions					
Voltage, phase-to-phase.....	153	200	158	200	200
Current, amp.....	1800	900	700	900	900
Kw input, avg.....	450	280	185	255	248
Kilowatt-hours:					
Per ton ore.....	1848	2007	2200	2155	1610
Per lb Cr.....	4.33	4.53	4.81	4.53	4.50
Per lb metal					
Theoretical.....	0.766	0.698	0.726	0.718	0.758
Actual.....	2.15	2.24	2.40	2.19	2.65
Efficiency, %.....	35.6	31.2	30.2	32.8	28.6
Electrode consumption, lb					
Per ton ore.....	39.1	11.6	55.1	23.5	10.5
Per lb of Cr.....	0.092	0.026	0.120	0.049	0.029
Slag-to-metal ratio.....	1.41	1.34	1.38	1.08	2.55
Metal analysis, %					
Cr.....	49.8	49.4	49.9	48.3	54.8
Fe.....	36.0	37.4	34.6	34.9	32.5
Si.....	5.90	3.38	4.58	4.82	4.35
C.....	6.53	6.70	7.04	7.37	7.13
Slag analysis, %					
Cr.....	2.64	3.15	2.78	3.59	3.57
Fe.....	2.67	2.44	1.50	2.41	3.31
Cr recovery in metal, %†.....	93.0	92.1	92.9	92.5	87.2

* Percent of theoretical C required to reduce Cr and Fe in charge.

† Cr recovery based on weights and analyses of metal and slag products.

TABLE IV. Complete reduction smelting

Furnace used	Aluminum-silicon alloy		Chrome silicide	
	Small	Small	Large	Large
Materials charged, lb:				
Clay.....	100	74		
Quartz.....		26	100	100
Ferrochrome.....			55 ^a	55 ^b
C, ratio of stoich. prop.....	1.02 ^c	0.95 ^c	1.02 ^d	0.97 ^d
Time of test, hr.....	72	102	91.5	94.4
Feed rate, lb ore/hr.....	53	50	154	190
Electrical conditions:				
Voltage, phase-to-phase.....	52	38	42	54
Current, amp.....	1600	2100	5000	4500
Kw, input.....	135	140	350-400	420
Kilowatt-hours:				
Per ton ore.....	5080	5560	5000 ^e	4321 ^e
Per lb of alloy,				
Theoretical.....	2.67	2.62	2.80	2.80
Actual.....	7.1	6.7	7.34 ^f	5.38 ^f
Efficiency, %.....	37.6	39.1	38.1	52.0
Electrode consumption, lb				
Per ton ore.....	115	150	51.3 ^g	55.14 ^g
Per lb of alloy.....	0.16	0.18	0.067 ^h	0.063 ^h
Alloy analysis, %				
Al.....	46	33	—	—
Si.....	43	55	44.9	47.1
Cr.....	—	—	28.3	30.9
Fe.....	5.8	8	22.1	17.0
Ti.....	3.2	3	—	—
C.....	—	—	0.04	0.035

^a Mouat ferrochrome.

^b Iron King ferrochrome.

^c Theoretical carbon required to reduce the SiO₂ and Al₂O₃ in the charge.

^d Theoretical carbon required to reduce only the SiO₂ in the charge.

^e Kilowatt-hour consumption per ton of quartz in the charge.

^f Kilowatt-hour consumption per pound of silicon produced.

^g Electrode consumption per ton of quartz in the charge.

^h Electrode consumption per pound of silicon produced.

watt-hour consumption per pound of chromium recovered in the ferrochrome product was about the same as when smelting the higher Cr₂O₃ content concentrates. Eighty-seven per cent of the chromium was recovered in the metal product, which was only 5% lower than the recovery obtained when smelting concentrates.

COMPLETE REDUCTION SMELTING

Production of aluminum-silicon alloys, silicon, chrome silicide, and ferrosilicon are examples of complete reduction smelting processes. In these operations, all oxides charged to the furnace are reduced. No slag is tapped from the furnace unless there is a deficiency of reductant in the smelting charge. Electrodes are directly on the molten metal bath and a much lower voltage is used than when conducting a smelting operation in which slag is produced. Use of hogged fuel in the charge is especially beneficial in controlling the feed rate to the smelting zone and maintaining a continuous smelting operation.

Tests on the production of aluminum-silicon alloys containing from 33 to 46% aluminum, and on the production of chrome silicide are shown in Table IV. Tests on production of aluminum-silicon alloys were made in the small furnace; those on production of chrome silicide were made in the large furnace.

Tests on Aluminum-Silicon Alloy

The first research program on production of aluminum-silicon alloys was conducted in cooperation with the Apex Smelting Company of Chicago. It was during this smelting campaign that hogged fuel was first used in furnace charges. Promising test results obtained at that time have led to commercialization of the aluminum-silicon, 3-phase electric furnace, smelting process by the National Metallurgical Corporation at Springfield, Oregon.

Production of aluminum-silicon alloy in an electric arc furnace is probably the most difficult smelting operation conducted at the Northwest Electrodevelopment Laboratory. The correct quantity of

reductants properly proportioned is necessary to maintain a continuous smelting operation. A deficiency of carbon results in a selective reduction of silicon from the aluminum silicates and formation of a slag high in alumina. Unless tapping temperatures are extremely high, this slag cannot be drained from the furnace. An excess of carbon in the charge promotes formation of carbides which accumulate on the furnace hearth causing the electrodes to rise and eventually prevents tapping of the furnace. Data presented in Table IV indicate that an almost stoichiometric proportion of reductant was used.

In one test, only calcined clay and reductant were used in the furnace charge and a phase-to-phase voltage of 52 was employed; in the other test, quartz was mixed with the charge and the voltage was reduced to 38. The latter test was the easier operation. The difficulty of smelting aluminum silicates increases as the aluminum content of the charge increases. Efficiencies for these tests were considerably higher than for nonselective reduction smelting tests.

Tests on Production of Chrome Silicide

The silicon content of the chrome silicide product may be controlled by proportioning of quartz and ferrochrome in the charge. Standard grades of chrome silicide contain from 42 to 49% silicon, 34 to 41% chromium, and not over 0.05% carbon. Chrome silicide products containing less silicon usually exceed the maximum specifications for carbon.

Both chrome silicide smelting tests were conducted in the large furnace. The proportion of reductant used is comparable to that used in the production of aluminum-silicon alloys. Voltages used and electrical energy consumption per ton of oxides reduced were also comparable, although electrode consumption was considerably less. Results of these tests are shown in Table IV.

EFFECT OF SLAG-TO-METAL RATIO ON SMELTING EFFICIENCY

Efficiencies of all smelting tests presented in this paper are shown in the tables. These efficiencies have been calculated from theoretical electrical energy requirements and actual electrical energy requirements for production of the various alloys. For example, the theoretical electrical energy requirement for the production of ferrochrome from Iron King ore, shown in Table III, is calculated as follows:

$$\begin{aligned}
 54.8 \text{ (Cr content)} &\times 0.952 \\
 &\text{(kwhr for production of 1 lb Cr)} = 0.521 \\
 32.5 \text{ (Fe content)} &\times 0.355 \\
 &\text{(kwhr for production of 1 lb Fe)} = 0.115 \\
 4.35 \text{ (Si content)} &\times 2.80 \\
 &\text{(kwhr for production of 1 lb Si)} = 0.122
 \end{aligned}$$

Theoretical kwhr requirement per lb alloy produced 0.758

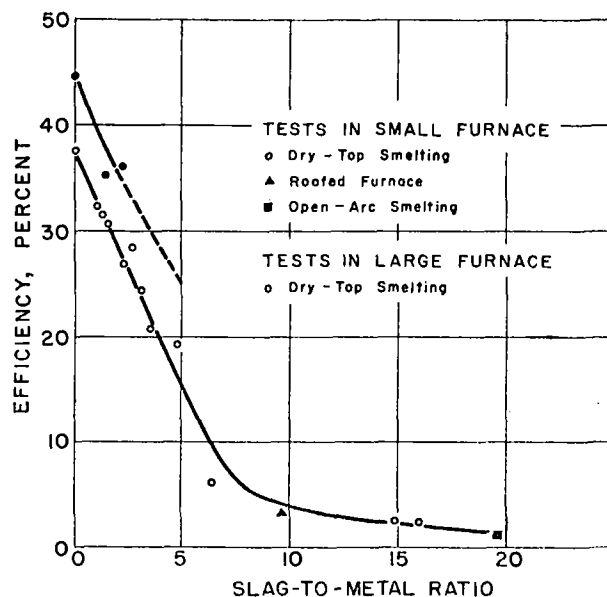


FIG. 2. Relationship between slag-to-metal ratio and smelting efficiency.

The actual electrical energy requirement for the production of 1 lb alloy was 2.65 kwhr. Using these data the efficiency of utilization of electrical energy is calculated to be 28.6%.

The relationship between the efficiency of electrical energy utilization and the slag-to-metal ratio for tests described in this paper is plotted in Fig. 2. The curves show how the efficiency of an electric smelting operation increases as the slag-to-metal ratio decreases, and indicate that this relationship is not materially affected by the type of material being smelted. Admittedly, other factors effect the efficiency of electrical energy utilization, for instance, the curves indicate that the efficiency is higher in a large furnace than in a small furnace. In one test on production of chrome silicide in the large furnace, the efficiency was calculated to be 52%. This efficiency is believed to be comparable to that attained in many commercial furnaces.

CONCLUSIONS

Smelting research in electric arc furnaces has indicated that some off-grade ores are amenable to treatment by smelting processes for the production of strategic metals. These investigations have led to some commercial developments. The National Metallurgical Corporation has begun production of aluminum-silicon alloys in an electric arc furnace at Springfield, Oregon. These alloys will be used to supply silicon for, and supplement aluminum in, commercial aluminum alloys. The Hanna Smelting Company plans to start production of ferronickel in electric arc furnaces near Riddle, Oregon, late this year. Previous to the initiation of these enterprises, the Bureau of Mines at Albany, Oregon, had

conducted smelting tests in cooperation with both companies.

Smelting tests have shown that a commercial grade silicomanganese can be produced from a siliceous manganese ore containing over three times the SiO_2 plus Al_2O_3 content acceptable under GSA stockpile specifications. Smelting tests on chromites have indicated that concentrates can be smelted without agglomeration and that a high recovery of chromium can be made by smelting a fine-grained chromite directly. These results indicate that production of silicomanganese from off-grade manganese ores, and ferrochrome and chrome silicide from off-grade chromites is commercially feasible.

Results of these tests indicate that the efficiency of electrical energy utilization is mainly dependent on the slag-to-metal ratio. A method has been described for determining this efficiency. Also, methods used in determining flux requirements, reductant requirements, and in selecting the proper electrical conditions for smelting operations have been described. These methods may be applied in selecting

the proper conditions for carrying out electric smelting operations on ores other than those reported.

Any discussion of this paper will appear in a Discussion Section to be published in the June 1955 JOURNAL.

REFERENCES

1. *Eng. Mining J.*, **155**, No. 2, pp. 88-89, 99-100, 101, and 102 (1954).
2. S. F. RAVITZ, V. MILLER, AND F. B. PETERMANN, *Trans. Am. Inst. Mining Met. Engrs.*, **159**, 442 (1944).
3. S. F. RAVITZ, U. S. Bureau Mines Repts. Invest. 4122, September 1947.
4. D. R. TORGESON, T. E. EVANS, J. L. MORNING, F. W. WESSEL, AND R. G. KNICKERBOCKER, U. S. Bureau Mines Repts. Invest. 3917, September 1946.
5. F. W. WESSEL AND R. T. C. RASMUSSEN, *J. Metals*, **2**, 984 (1950).
6. R. T. C. RASMUSSEN, *J. Metals*, **4**, 1273 (1952).
7. H. CREMER, U. S. Bureau Mines Repts. Invest. 5021, January 1954.
8. E. F. OSBORN, R. C. DEVRIES, K. H. GEE, AND H. M. KRANER, *J. Metals*, **6**, 33 (1954).
9. F. H. GETMAN AND F. DANIELS, "Outlines of Physical Chemistry," 7th ed., p. 115, John Wiley & Sons, Inc., New York (1941).
10. D. R. COCHRAN, *Blast Furnace Steel Plant*, **41**, 1031 (1953).

A New Furnace for Production of Calcium Carbide and Other Products¹

MARVIN J. UDY

546 Portage Road, Niagara Falls, New York

ABSTRACT

A new type of furnace has been developed for the manufacture of calcium carbide and high melting metals, alloys, and metallic carbides. The furnace is designed to move under the electrodes continuously, thus removing products as they are made. A large pilot plant furnace is needed to determine fully its advantages or disadvantages.

INTRODUCTION

The manufacture of CaC_2 had its beginning at the turn of the century, and many pertinent patents were issued between 1898 and 1908 (1-9).

Most early furnaces utilized single-phase power with top and bottom electrodes or with two suspended electrodes. Two of the most successful furnaces produced by these early workers were the continuous Horry furnace (1), and one presented by Leleux (6).

The Horry furnace, in operation at Niagara Falls during the period 1910-1915, was a rotary type, using single-phase power with two electrodes. The electrodes were suspended in a cast iron receptacle that moved away from the electrodes on the circumference of a vertical rotating wheel. To remove the carbide formed, segments on the circumference of the receptacle were removed when the carbide was cool enough. The segments were then used to extend the section of the receptacle around the electrodes, thereby forming a new section into which the charge was fed. Considerable early success was attained with this furnace as well as with the batch-type furnace.

The common drawback of all these early furnaces was the use of single-phase power, and this fact alone made it necessary to operate in small multiple units. Operating and maintenance costs were generally high. It was logical, therefore, that as the demand for calcium carbide grew, furnaces designed to use three-phase power were necessary. By 1915, or soon after, practically all CaC_2 was being produced in three-phase tapping furnaces.

In the operation of a three-phase tapping furnace for making CaC_2 , there are difficulties in operation that have never been overcome, although calcium carbide furnaces have been increased in size to as much as 30,000 kva. A study of the melting point

diagram of CaC_2 (10) will show clearly the reason for such difficulties in spite of furnace size, excellent electrical equipment and refractories, and greater technological skill.

Melting Point of Calcium Carbide and Its Effect on Furnace Operation

Pure CaC_2 melts at approximately 2300°C. Seventy per cent CaC_2 melts at approximately 1780°C, and 35% CaC_2 melts at approximately 1800°C.

The general practice today is to operate as close to 85% CaC_2 as possible, because this is the highest grade that can be successfully tapped from the furnace. Actually, commercial carbide averages about 80% CaC_2 . Operating temperature of the present carbide furnace is, therefore, somewhat higher than 2100°C. The nominal 85% grade of CaC_2 yields 4.7 ft³ C_2H_2 /lb CaC_2 . U. S. specifications are as follows:

Size designation	Minimum average volume of acetylene gas evolved per lb at 60°F and 30 in. barometric pressure
Lump	4.5
Egg	4.5
Nut	4.5
½ by ¼	4.5
¼ by ¼	4.5
Rice	4.3
14 ND	4.3

Rarely, however, does CaC_2 reach the customer with a yield as high as 4.7 ft³/lb CaC_2 . Large producers are now making and selling acetylene directly to the user. However, carbide of less than 4.7 ft³/lb increases the ultimate cost.

Due to the high melting point of 85% CaC_2 , operating problems are severe. Because there is 15% excess lime in 85% CaC_2 , the problem of carbon balance is of prime importance. When the furnace is over-coked and purer carbide made, difficulty immediately results from higher conductivity of the

¹ Manuscript received March 19, 1954. This paper was prepared for delivery before the Chicago Meeting, May 2 to 6, 1954.

charge resulting in loss of control of electrode position. This difficulty usually shows itself in higher positions of electrode tips in the furnace and frozen CaC_2 on the bottom. Careful weighing of both carbon and lime is absolutely necessary. Segregation often takes place in getting the charge to the furnace, and unless the lime is really hard burned, lime air slakes, producing excessive dust. This inability to maintain proper carbon balance results in additional coke or lime being added from the working floor of the furnace. If the electrodes are high, lime is added, and if the electrodes are low, coke is added. In some cases, it has been the custom to add as much as 30% of the lime at the furnace working floor to keep the electrode tips in proper working position, in order to tap the carbide properly. This is quite a burden on the operators and demands considerable skill on their part. In some cases, 15% or more of the lime has been wasted as dust blown from the furnace. Electrode tip position in the charge is affected by the size of the lime and coke. Also, when a higher gas yield carbide is produced, tapping difficulties result.

Tapping of Calcium Carbide

Molten CaC_2 usually is tapped into cast metal molds or cars. While 85% CaC_2 chills rapidly on the surface, there is, nevertheless, considerable wear and tear on the molds. This comes chiefly from impurities like ferrosilicon which is reduced from silica in the lime and coke. The investment in molds for carbide is high. There has been some change in recent years, and some of the larger companies are now using casting wheels and casting into thinner ingots; however, casting wheels are expensive and require considerable maintenance. On larger furnaces when continuous tapping is approached, and on smaller furnaces where intermittent tapping is practiced, higher labor and maintenance costs are involved.

DEVELOPMENT OF NEW PROCESS AND NEW TYPE FURNACE

Operational difficulties of a CaC_2 furnace and increasing labor costs led to re-examination of furnaces for the manufacture of calcium carbide. From a careful study of the CaC_2 production process and application of accumulated experience, an improved furnace, which seems feasible for commercial purposes, has been developed on a laboratory scale.

It appeared from a study of the melting point diagram for CaC_2 and lime that CaC_2 should be made readily at temperatures below the melting point of 85% CaC_2 , or even down to 1800°C . It was reasoned, therefore, that high purity CaC_2

could be made directly in ingot form at a temperature below the melting point of 100% CaC_2 . Also, if a furnace could be designed to use three-phase power, and at the same time operate with a carbon-to-lime ratio to produce high purity CaC_2 using 100% of the CaO present in the lime, the control of the carbon balance would be less critical. In addition, each unit of pure CaC_2 should be made with little or no increased power cost over the standard carbide made today. Dust losses could be reduced if the charge around the electrodes were reduced to a minimum.

In order to operate with the slight excess of coke required to make CaC_2 from 100% of the CaO , calcium carbide should be removed immediately from the vicinity of the electrode as fast as it is formed. This immediate removal of carbide would also remove excess coke, which in a normal furnace affects the position of the electrodes. In the proposed furnace, excess coke would have little effect on the electrode position. Also, less energy would be required since the CaC_2 would not need to be superheated for tapping. In addition, carbide is produced in ingot form continuously and is automatically removed from the furnace. This reduces labor costs in tapping. Furthermore, the furnace adapts itself to a low chargehead around the electrodes. Because of lower pressure in the low chargehead, dust losses are minimized. Under these conditions of lower pressure and lower temperature above the charge, a simple roof construction for recovery and control of fumes is possible. Early experimental work gave proof that these surmises were true and indicated that 100% CaC_2 can be made in place with little, if any, increased power cost per unit of pure CaC_2 over that required for the usual 85% max. CaC_2 .

EXPERIMENTAL FURNACES

Two experimental furnaces using 150 kva were built,² one of the horizontal moving type and one of the vertical moving type in which the carbide was formed in place and removed as made. The horizontal type furnace differs radically from any previous furnace for CaC_2 production. Both furnaces show definitely that heat transfer from the arcs to the carbide and to the charge can be accomplished in very thin layers of charge (6–12 in.) above the tips of the electrodes. Reduced dust losses and cleaner carbon monoxide were observed. In the horizontal moving type, the electrode tips may be carried at the same level or at different levels. In the vertical type furnace, the electrode tips are at a constant level with the furnace moving down as the

²The work was carried out at Battelle Memorial Institute for the Research Development Corporation of Hamilton, Ontario, Canada.

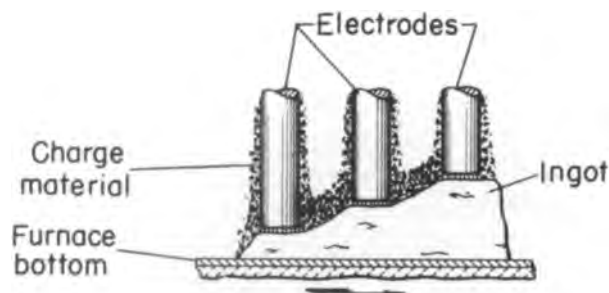


FIG. 1. Staggered electrode position of horizontal-type furnace.

CaC_2 is formed, thus removing the finished carbide out of the smelting zone.

The small horizontal laboratory furnace uses two $\frac{1}{2}$ -in. graphite electrodes placed at different levels and spaced so that the active areas around the electrodes do not quite touch. Under these conditions, the electrodes maintain their relative vertical position when on the automatic regulators. If spacing is too close, the electrodes take the same vertical position, the furnace is required to move faster, and the ingot of CaC_2 has less depth. Sufficient work has not been done to determine the relative values of these two types of operation.

Fig. 1 illustrates the electrode position and direction of movement of the car or furnace, also the different levels of the electrodes in the horizontal-type furnaces. This furnace body moved approximately $\frac{1}{2}$ in./min. The voltage was 45–52 volts, electrode to ground.

In the vertical version, the furnace moves down away from the electrode. This furnace body moved at approximately $\frac{3}{4}$ in./min. In application, the furnace would be made of short vertical sections which would be removed from the ingot and returned to a position at top of the furnace around the electrodes.

Fig. 2 is an ingot of carbide produced in the horizontal furnace. It shows the beginning of the test run with the ingot coming up to approximately 1 ft in depth and then maintaining this depth until the test was stopped. The carbide averaged well above $5 \text{ ft}^3 \text{ C}_2\text{H}_2$ per lb.

One example of the vertical-type furnace is shown in Fig. 3. In this version, the short section of the



FIG. 2. Photograph of an ingot of calcium carbide produced in the horizontal continuous-ingot furnace. (Ingot was moved from right to left under the electrodes.)

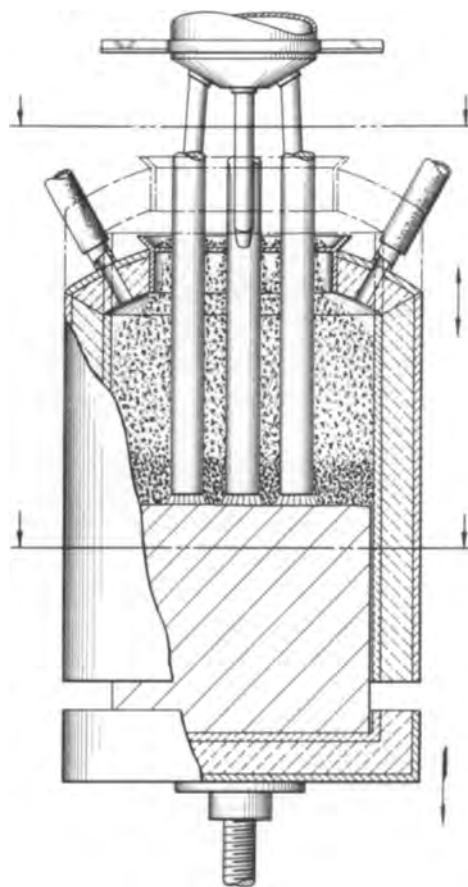


FIG. 3. Vertical furnace with reciprocating movement

furnace would be given a short reciprocating up and down movement to keep the ingot of CaC_2 free so that it can be lowered slowly.

Fig. 4 is an artist's drawing of a proposed 3000 kva horizontal furnace.

In general, it is believed at this time that for large furnaces of the order of 3000–30,000 kva, the horizontal version as shown in Fig. 4 will probably prove best from an engineering, cost, operating, and safety standpoint. The vertical furnace definitely has possibilities in smaller scale operations such as silicon carbide, aluminum carbide, ferrocabo titanium, titanium carbonitride, calcium silicate, zir-

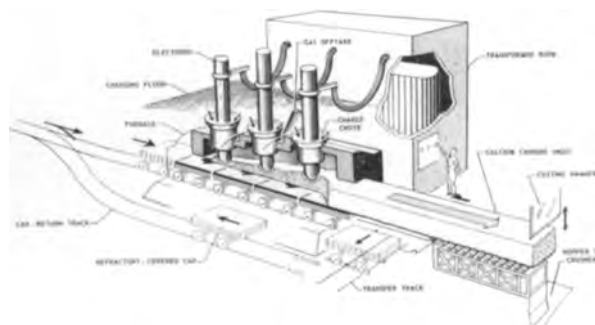


FIG. 4. Sketch of proposed 3000 kw furnace

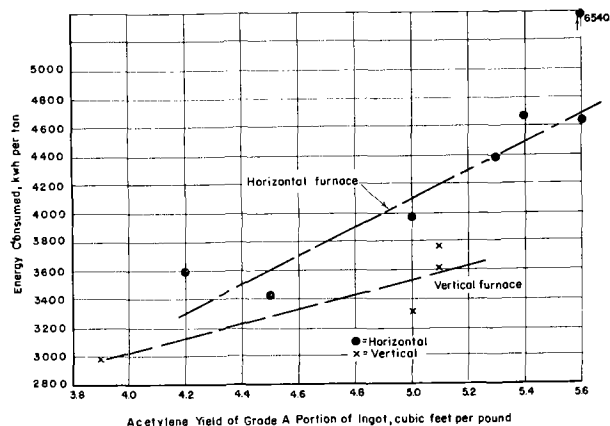


FIG. 5. Relationship of electrical energy consumed to acetylene yield of calcium carbide produced in laboratory furnace.

conium carbide, barium oxide, silicon metal, and other carbides, nitrides, and metals produced at high temperatures. Most of these products have already been made experimentally in the furnace.

Power Consumption Expected

The relationship of electrical energy consumed to acetylene yield of the carbide produced in the 150 kva furnaces is shown in Fig. 5. These data are based on short experimental runs. Conditions of starting and stopping undoubtedly influenced the results. Both furnaces would show greater efficiency when operated continuously, 24 hr/day.

With the 150 kva ingot furnace, the power consumption for CaC_2 yielding $4.7 \text{ ft}^3/\text{lb}$ was indicated at about 3600 kwhr/ton, and for carbide yielding $5.6 \text{ ft}^3/\text{lb}$, the power consumption was indicated at about 4200 kwhr/ton. The high yield carbide was made from Mississippi lime and petroleum coke. It utilized 100% of the CaO present. A yield of 5.6 ft^3 acetylene/lb CaC_2 is approximately 19% more gas than obtained from the usual 85% CaC_2 .

In any electric furnace scaled up from 150 kva to 3000–6000 kva or more, a decrease of 25% in power consumption can be expected. This would indicate

about 3140 kwhr/ton CaC_2 having a 5.6 gas yield or a little more power than required in the present carbide furnace making CaC_2 with a gas yield of only $4.7 \text{ ft}^3/\text{lb}$.

Likewise, with 3600 kwhr for 80–85% CaC_2 , one should expect a 25% decrease in power or approximately 2700 kwhr/ton of 80–85% CaC_2 . However, these projected estimates of power consumption in large continuous ingot furnaces require substantiation in a pilot plant. It is felt that power consumption will be less per pound of acetylene than in present furnaces.

Dust losses are greatly reduced since the electrode tips are never submerged more than 6–12 in. in the charge. Under these conditions, carbon monoxide is freely evolved, eliminating formation of high pressure areas under the electrodes which causes blowing with resultant heavy dust losses.

In summation, the proposed furnaces appear to have a place in the manufacture of calcium carbide and allied products. Further development of the continuous-ingot type of furnace should result in a process with lower operating costs including less power consumption, lower labor costs, better operating conditions, easier material supply, minimized dust hazards, less air pollution, simpler roof construction, simplified gas collection, and possibly other advantages.

Any discussion of this paper will appear in a Discussion Section, to be published in the June 1955 JOURNAL.

REFERENCES

1. W. S. HARRY, U. S. Pat. 657,736, September 11, 1900.
2. J. ZIMMERMAN AND I. S. PRENNER, U. S. Pat. 671,008, April 2, 1901.
3. W. BORCHERS, U. S. Pat. 660,043, Oct. 16, 1900.
4. C. L. WILSON, C. MUMA, J. W. UNGER, *et al.*, U. S. Pat. 601,367, March 29, 1898.
5. J. M. MOORHEAD, U. S. Pat. 664,333, Dec. 18, 1900.
6. H. LELEUX, U. S. Pat. 654,463, July 24, 1900.
7. E. F. PRICE, U. S. Pat. 826,742, July 24, 1906.
8. J. C. KING, U. S. Pat. 872,352, Dec. 3, 1907.
9. C. E. WILSON, U. S. Pat. 943,290, Dec. 14, 1909.
10. C. H. AAL, *Chemistry and Industry*, 1950, 830.

Explosive Limits of Hydrogen-Chlorine Mixtures¹

A. W. UMLAND

The Dow Chemical Company, The Texas Division, Freeport, Texas

ABSTRACT

The lower explosive limit concentration of hydrogen (with upward flame propagation) in mixtures of chlorine containing oxygen, nitrogen, and carbon dioxide in proportions typical of electrolytic chlorine were determined at pressures from 0 to 135 psig. The explosive limit was found to be quite sensitive to variations of pressure and composition. It varied from about 3.1 to about 8.1% hydrogen depending on pressure and chlorine concentration.

INTRODUCTION

In the production of chlorine by the electrolysis of salt there are always a few per cent of other gases. These gases are made up of leakage air plus small amounts of hydrogen, oxygen, carbon dioxide, and carbon monoxide formed by secondary reactions occurring at the anodes and diaphragms. In a chlorine consuming process, as the chlorine is removed, these gases remain and increase in concentration. Ultimately the hydrogen concentration may increase until the mixture becomes potentially explosive. Therefore, in the interest of safety, it is desirable that explosive limits of hydrogen be accurately known in atmospheres of chlorine containing the usual impurities in the ratios present in cell gas at various pressures.

There have been few papers (1-5) published on the explosive limits of hydrogen and chlorine mixtures. Weisweiler (2) gives some explosive limits for pure hydrogen and chlorine. Lindeijer (3) gives the explosive limits with downward flame propagation at atmospheric pressure for three component systems of hydrogen and chlorine with nitrogen, carbon dioxide, oxygen, air, carbon monoxide, and nitric oxide. Since there has been no previous work published on the explosive limits of hydrogen in chlorine containing the usual impurities in cell gas at various pressures this work was undertaken.

The direction of flame propagation has a very marked effect upon explosive limits. Limits obtained when the column of gas is ignited at the bottom of the column allowing the flame to travel up (upward flame propagation) are less than those obtained with downward propagation. In fact, a downward limit mixture of some gases will give a severe explosion with upward flame propagation. Consequently, limits determined in this work are for upward flame propagation.

¹ Manuscript received May 5, 1954. This paper was prepared for delivery before the Chicago Meeting, May 2 to 6, 1954.

The definitions in the literature of explosive limits have been quite varied. A number of criteria have been proposed, among these are per cent combustion of gases, presence of flame, pressure rise, and velocity of flame propagation. The most acceptable definition is the lowest concentration of the gas in which a flame will continuously propagate through the entire volume of gas. The definition used for this work is the lowest concentration of hydrogen that will give an appreciable pressure rise. This was adopted because a flame can seldom be seen in a near limit explosion of a hydrogen-chlorine mixture even in a darkened room.

To obtain satisfactory explosive limits the experimental apparatus must meet certain requirements. The bomb should have an inside diameter of at least 5 cm (6, 7) to minimize wall effects. The source of ignition must have sufficient energy for positive ignition of the gases yet not high enough to cause disruptive effects in the bomb or give a partial ignition in the immediate vicinity of the ignitor (8).

EXPERIMENTAL

Explosive limits were determined in a stainless steel bomb having an inside diameter of 5 cm and a length of 20 cm. The volume of the bomb was 432 ml. A cross section of the bomb is shown in Fig. 1. The bomb was closed at one end with a high-pressure sight glass to permit visual observation of the determination. The opposite end was closed with a piece of 0.003 in. thick brass shim stock to serve as a safety rupture disk. A magnetically driven stirrer was provided for mixing the gases in the bomb. The stirrer was essentially a small centrifugal blower drawing the gases downward through the bomb and discharging into a 1 cm x 2 cm duct extending along one side of the bomb to the top of the bomb, thus providing positive circulation of the gases in the bomb.

A modified "spark plug" with a variable spark gap was provided for igniting the gases. The high voltage

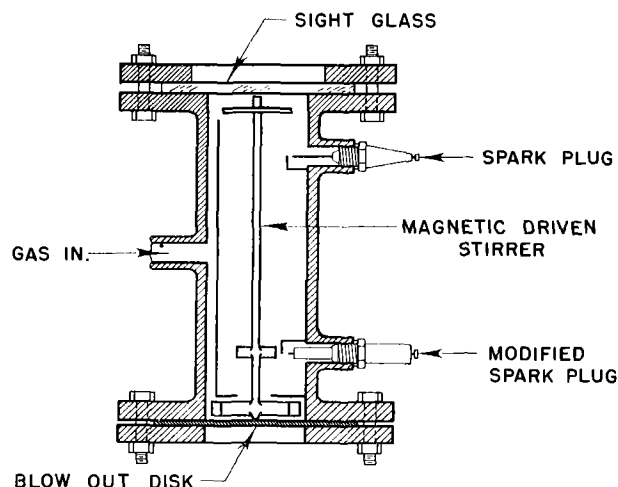


FIG. 1. Cross section of the bomb used for the determination of explosive limits.

electrode was fixed and used Teflon insulation. The other electrode was an eccentric metal plate on the shaft of the stirrer. The spark gap was varied by turning the stirrer shaft.

The assembled bomb was mounted vertically behind a heavy wood shield. A mirror was provided for viewing the bomb through a safety glass window in the shield.

A Foxboro recording pressure gauge with a range of 0–150 psi and having a 24-min clock was provided for recording the pressure wave of an explosion.

A high-pressure measuring buret was provided for measuring the volume of hydrogen added. This consisted of two graduated tubes, connected at the bottom, containing a confining liquid (hexachlorobutadiene). By proper setting of the valves at the top of the buret, hydrogen can be added to one tube to force the hydrogen in the other tube into the bomb as shown in Fig. 2. The connecting tubing between the bomb, gauges, etc., was made of $\frac{1}{8}$ in. O.D. copper capillary tubing.

The electric spark for ignition was supplied by a high voltage power supply consisting of two model "T" Ford coils having their secondary windings in series feeding a rectifier doubler. The output of the power supply was 35,000 v D.C. A battery of 12 500 mmfd 25,000 v condensers were connected in series—parallel with the output of the power supply by a switch giving five steps of capacitance varying from 250 to 1500 mmfd. This provided a means of varying the intensity or energy of the spark.

The gas mixtures tested were mixed from commercially available gases. First, a stock gas containing the desired proportion of oxygen, nitrogen, and carbon dioxide was prepared. From this stock gas, mixtures containing approximately 5, 10, 20, 30, 40, and 50% chlorine were prepared. The lower explosive

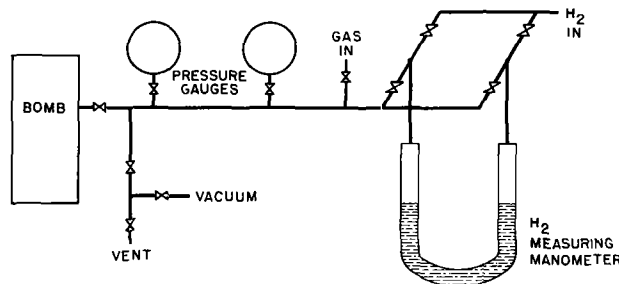


FIG. 2. Schematic diagram of the apparatus

limits of these mixtures with hydrogen were determined at pressure increments of 20 psi.

A gas mixture to be tested was placed in the bomb at the desired pressure (the bomb was first thoroughly evacuated). The valve at the bomb was closed, and the connecting tubing was evacuated and then filled with hydrogen to the same pressure. A measured volume of hydrogen at this same pressure was added to the bomb and mixed for ten minutes. The mixture was sparked, and any pressure rise from an explosion was recorded on the pressure recorder.

The per cent hydrogen added was calculated from the volume added using the ideal gas equation by the following equations:

$$\% \text{ Hydrogen} = \frac{H_1}{B + H_1} \times 100$$

$$H_1 = V_1 - V - (L + M + G - V_1)$$

$$\left(\frac{B + L + M + G - V}{B + L + M + G - V_1} - 1 \right)$$

If more than 28 ml of hydrogen was required, then:

$$\% \text{ Hydrogen} = \frac{\left(\frac{H_1 B}{B + H_1} + H_2 \right) 100}{B + H_2}$$

$$H_2 = V_1 - V_2 - [L + M + G + V_2 - T]$$

$$\left[\frac{B + L + M + G - T + V_1}{B + L + M + G - T + V_2} - \frac{(M + G - T + V_1)(T - 2V_1)K}{(B + L + M + G - T + V_2)P_1} - 1 \right]$$

$$- [M + G - T + V_1] [T - 2V_1] \frac{K}{P_1}$$

B = Volume of bomb = 432 ml.

L = Volume of connecting tubing and gauges = 42 ml.

M = Volume of dead space above graduation of buret = 6 ml.

P = Initial pressure of charged gas in bomb psia.

P_1 = Pressure of gas after addition of hydrogen from side 1 of buret, psia.

P_2 = Pressure of gas after addition of hydrogen from side 2 of buret, psia.

h = Height of calibrated portion of buret = 6.75 in.
 G = Volume of buret at top graduation = 28 ml.
 V = Initial reading of buret 1.
 V_1 = Reading of buret after addition of hydrogen from side 1.
 V_2 = Final reading of buret 1 after addition of hydrogen from side 2.
 T = Total volume of liquid in buret.
 S = Specific gravity of seal liquid = 1.664.
 $K = \frac{Sh}{27.7 G} = 0.01448$.
 H_1 = Volume of hydrogen added to bomb from side 1 of buret.
 H_2 = Volume of hydrogen added to bomb from side 2 of buret.

RESULTS

Approximately 1800 individual runs were made to determine the lower explosive limits with upward flame propagation of hydrogen with 30 mixtures of chlorine, oxygen, nitrogen, and carbon dioxide at pressure increments of 20 psi up to about 135 psig. These results are tabulated in Table I and are shown plotted vs. the pressure in Fig. 3, 4, 5, and 6. Each point shown is the result of from four to ten or more individual runs. The standard deviation of a single run is about 0.1%; consequently, the probability of the error of a single point being not greater than $\pm 0.2\%$ is about 90–95%.

The effect of pressure on explosive limits varies with each gas mixture and is unpredictable. Comparatively small changes in pressure or composition of the gas may make marked changes in the explosive limits; consequently, extrapolation or interpolation from the observed data can lead to large errors.

The effect of variation of chlorine concentration on the explosive limit of a typical cell gas mixture is shown in Fig. 7. The explosive limit reaches a maximum between 10 and 30% chlorine. This indicates that explosions with low chlorine concentrations are primarily hydrogen-oxygen explosions. The high heat capacity of the chlorine tends to increase the limit until the chlorine concentration is high enough for the "mass action" to shift to a hydrogen-chlorine explosion.

Increasing the temperature of the gas in general lowers the explosive limit, while decreasing the temperature raises the limit (Fig. 8). The explosive limit decreases with increasing oxygen concentration (Fig. 9). Replacing part of the nitrogen of air with carbon dioxide raises the explosive limit.

Fig. 10, 11, 12, and 13 give calculated curves for obtaining the safe operating limits of a chlorine consuming process. Final chlorine concentration is plotted vs. initial hydrogen concentration for various initial chlorine concentrations. For a given initial chlorine and hydrogen concentration the curve gives the final chlorine concentration at the explosion limit. All points to the left of the initial chlorine con-

TABLE I. Typical results²

Composition of the gas mixtures before addition of H₂ and the % H₂ at the lower explosive limit with upward flame propagation:

Gas No.		% Cl ₂		Balance	
1		0		A mixture of:	
10		11.1		46.5% N ₂	
12		29.8		32.5% CO ₂	
13		5.7		21.1% O ₂	
14		19.1			
15		40.4			
17		52.5			
Pure Chlorine		Gas No. 1		Gas No. 10	
psig	% H ₂	psig	% H ₂	psig	% H ₂
103	3.2	127	6.0	135	5.6
81	3.2	106	5.9	127	5.8
61	3.7	85	5.9	107	6.7
41	3.6	64	5.8	86	6.7
21	4.0	43	5.4	64	6.9
1	4.1	21	5.3	43	6.6
		11	5.3	22	6.4
		1	5.4	1	5.8
Gas No. 12		Gas No. 13		Gas No. 14	
psig	% H ₂	psig	% H ₂	psig	% H ₂
138	6.4	138	6.6	139	7.3
128	6.5	128	6.4	130	8.1
106	6.4	107	6.9	108	7.8
85	6.0	86	6.2	87	7.3
64	6.0	64	5.8	65	7.8
43	5.8	44	6.2	44	7.9
21	5.4	21	5.8	22	7.2
1	6.0	1	5.2	1	6.8
Gas No. 15		Gas No. 17			
psig	% H ₂	psig	% H ₂		
135	5.0	134	4.4		
126	4.8	124	4.6		
104	4.8	103	4.2		
84	4.8	82	4.2		
63	4.8	62	4.4		
43	5.0	42	4.2		
22	5.2	21	4.6		
1	5.6	1	5.0		

centration line are safe mixtures while points to the right of the line are explosive.

DISCUSSION

Typical data for determinations of explosive limits are given in Table II. An indication of the pre-

² An extended version of this table has been deposited as Document 4400 with the ADI Auxiliary Publications Project, Photoduplication Service, Library of Congress, Washington 5, D. C. A copy may be secured by citing the Document number and by remitting \$1.25 for a photoprint or for a 35-mm microfilm. Advance payment is required. Make check payable to: Chief, Photoduplication Service, Library of Congress.

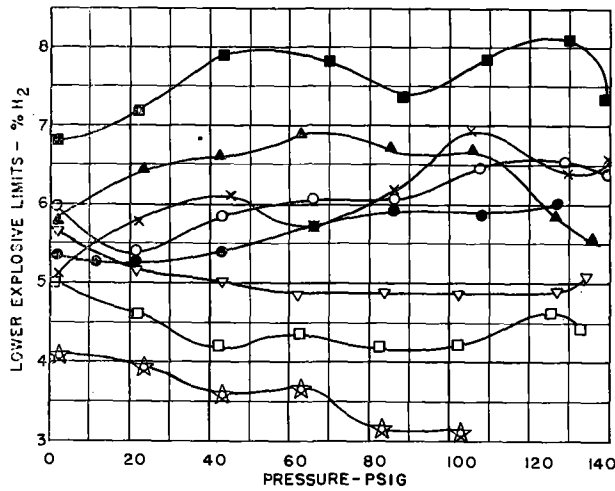


FIG. 3. Effect of pressure on the lower explosive limit of H₂-Cl₂ mixtures. Analysis of the gases before the addition of H₂ was: —●— 0.0% Cl₂; —×— 5.7% Cl₂; —▲— 11.1% Cl₂; —■— 19.1% Cl₂; —○— 29.8% Cl₂; —▽— 40.4% Cl₂; —□— 52.5% Cl₂; —☆— 100% Cl₂; balance a mixture of 46.5% N₂, 32.5% CO₂, and 21.1% O₂.

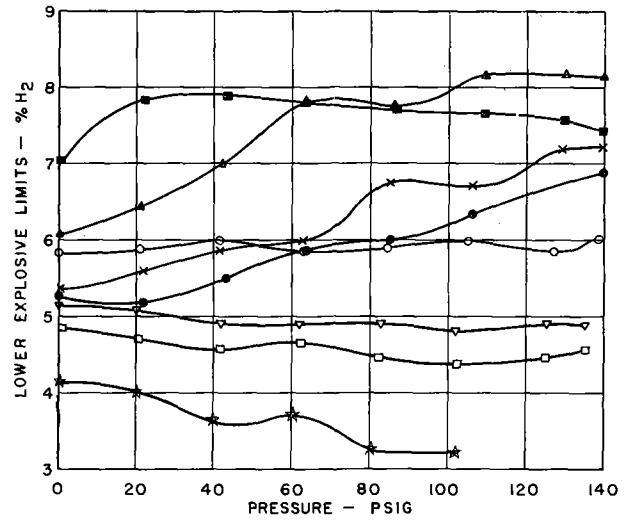


FIG. 6. Effect of pressure on the lower explosive limit of H₂-Cl₂ mixtures. Analysis of the gases before the addition of H₂ was: —●— 0.0% Cl₂; —×— 3.9% Cl₂; —▲— 9.4% Cl₂; —■— 19.5% Cl₂; —○— 29.1% Cl₂; —▽— 40.1% Cl₂; —□— 49.0% Cl₂; —☆— 100% Cl₂; balance of 38.3% CO₂, 14.3% O₂, and 48.4% N₂.

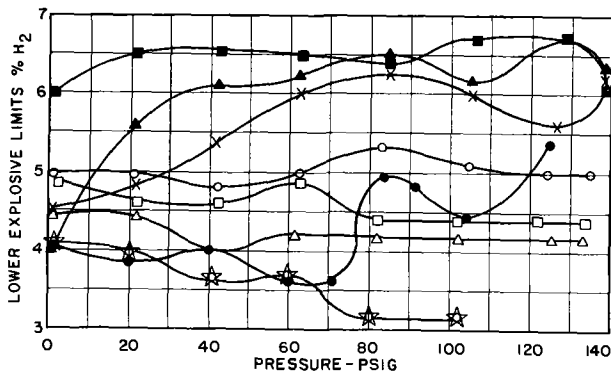


FIG. 4. Effect of pressure on the lower explosive limit of H₂-Cl₂ mixtures. Analysis of the gases before the addition of H₂ was: —●— 0.0% Cl₂; —×— 5.2% Cl₂; —▲— 11.1% Cl₂; —■— 17.3% Cl₂; —○— 29.8% Cl₂; —□— 41.2% Cl₂; —△— 53.9% Cl₂; —☆— 100% O₂; balance a mixture of 79.1 N₂ and 20.9% O₂.

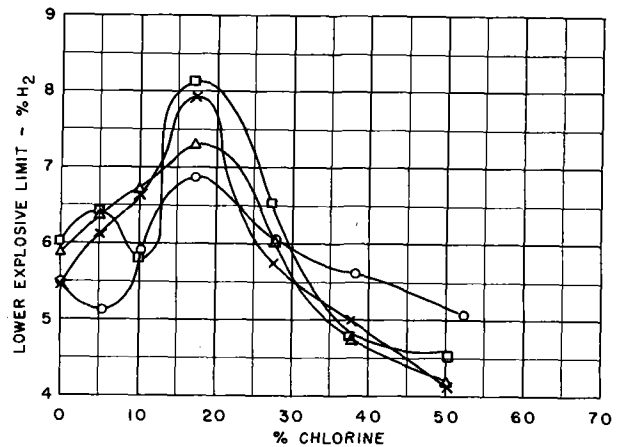


FIG. 7. Effect of chlorine concentration on the lower explosive limit: —□— 130 psig; —△— 90 psig; —×— 40 psig; —○— 0 psig. The inert gas contained 46.5% N₂, 32.5% CO₂, and 21.1% O₂.

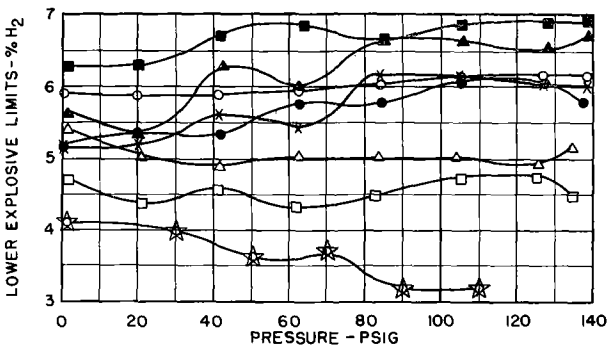


FIG. 5. Effect of pressure on the lower explosive limit of H₂-Cl₂ mixtures. Analysis of the gases before the addition of H₂ was: —●— 0.0% Cl₂; —×— 4.8% Cl₂; —▲— 8.9% Cl₂; —■— 21.8% Cl₂; —○— 29.3% Cl₂; —△— 40.4% Cl₂; —□— 54.0% Cl₂; —☆— 100% Cl₂; balance a mixture of 34.7% CO₂, 30.6% O₂, and 34.7% N₂.

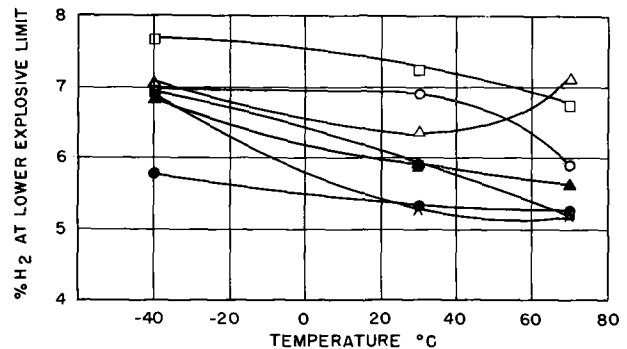


FIG. 8. Effect of temperature on the lower explosive limit at various pressures. Analysis of the gases before the addition of H₂ was: —×— 0.0 psig, 0.0% Cl₂; —●— 40 psig, 0.0% Cl₂; —▲— 90 psig, 0.0% Cl₂; —■— 130 psig, 0.0% Cl₂; —△— 0 psig, 10.4% Cl₂; —○— 40 psig, 10.4% Cl₂; —□— 90 psig, 10.4% Cl₂; balance a mixture of 46.5% N₂, 32.5% CO₂, and 21.1% O₂.

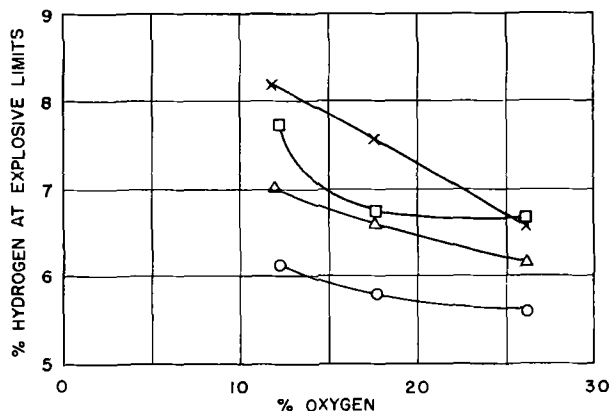


FIG. 9. Effect of oxygen concentration on the lower explosive limit of a mixture of 10% Cl₂, 30% CO₂, balance N₂ with upward flame propagation: —○— 0 psig; —△— 40 psig; —□— 90 psig; —×— 130 psig.

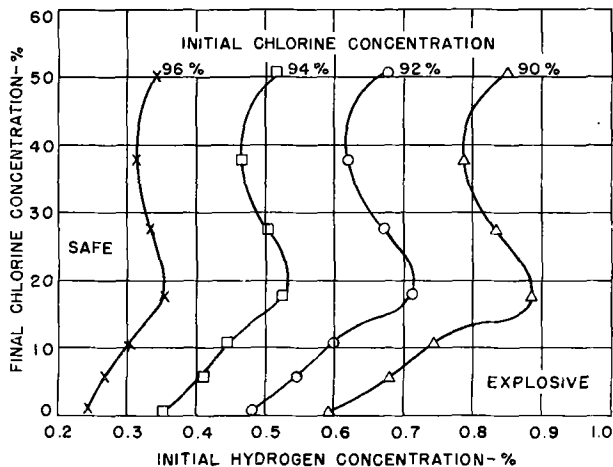


FIG. 12. Safe operating range for a chlorine consuming process at 90 psig. Analysis of the inert gas was 46.5% nitrogen, 32.5% carbon dioxide, and 21.1% oxygen.

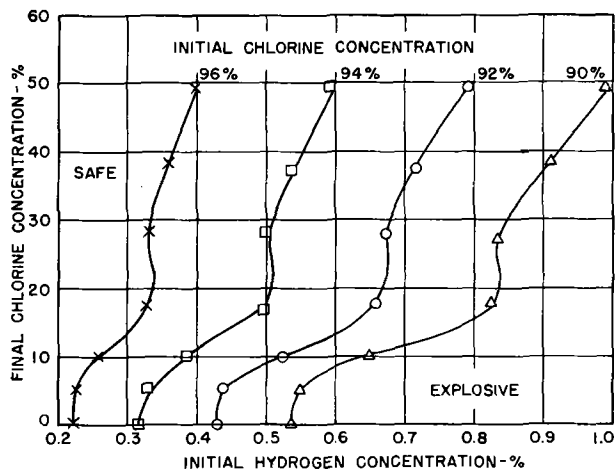


FIG. 10. Safe operating range for a chlorine consuming process at 0 psig. Analysis of the inert gas was 46.5% nitrogen, 32.5% carbon dioxide, and 21.1% oxygen.

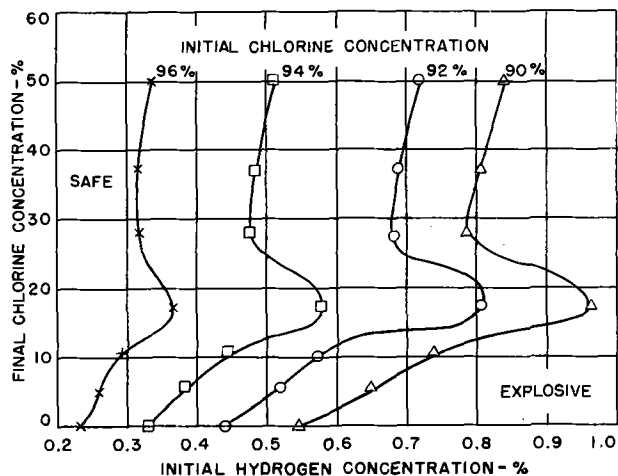


FIG. 11. Safe operating range for a chlorine consuming process at 40 psig. Analysis of the inert gas was 46.5% nitrogen, 32.5% carbon dioxide, and 21.1% oxygen.

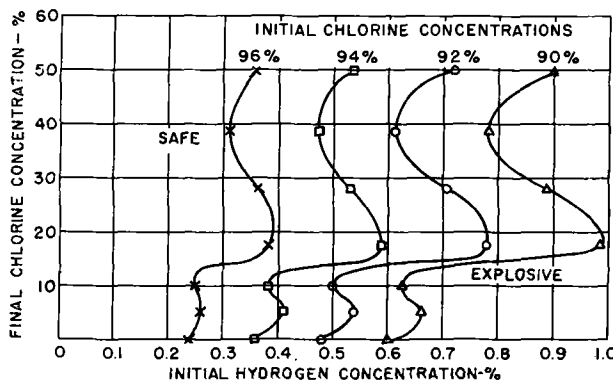


FIG. 13. Safe operating range for a chlorine consuming process at 130 psig. Analysis of the inert gas was 46.5% nitrogen, 32.5% carbon dioxide, and 21.9% oxygen.

cision of the determinations was obtained by plotting the hydrogen concentration vs. the pressure rise for individual runs. A statistical analysis of this plot was made by calculating the "least squares" regression line of the data (ignoring those points that had no pressure rise) and determining the standard error of the intercept on the hydrogen concentration axis. The standard error was found to range from 0.05 to 0.1%. Therefore reasonable confidence limits (90-95%) of a determination would be $\pm 0.2\%$ hydrogen. Since the values reported in this paper were the lowest values at which an explosion occurred, the distribution of errors will be somewhat skewed. The probability that the true value is less than the observed value is somewhat less than the probability of it being greater than the observed value. The larger standard errors were found with the gas mixtures which gave the smaller change in pressure rise with change in hydrogen concentration. This was caused by errors in the observed pressure rise from damping, friction, hysteresis, inertia, etc., in the pressure

TABLE II. *Typical data*

Run No.	Initial pres. psig	Final pressure after adding H ₂ psig	Vol. H ₂ added ml	% H ₂	Pressure rise psi
<i>Gas No. 2:</i>					
558	80	84	20.0	4.0	0
559	80	84	24.0	4.8	0
560	80	84	25.0	4.9	6
561	80	85	28.0	5.5	24
562	80	85	26.0	5.1	9
563	80	84	25.0	4.9	4
564	80	84	24.0	4.8	0
565	80	84	24.5*	4.9*	5
<i>Gas No. 4:</i>					
1395	130	138	30.0	5.9	0
1396	130	139	34.0	6.7	0
1397	130	140	38.0	7.4	>20
1398	130	139	35.0	6.9	0
1399	130	139	36.0	7.0	>20
1400	130	139	35.5	7.0	>20
1401	130	139	35.0	6.9	>20
1402	130	138	33.0	6.5	0
1403	130	139	34.0	6.7	0
1404	130	139	34.5*	6.8*	15
1405	130	139	34.0	6.7	0
<i>Gas No. 31:</i>					
1469	20	23	36.0	7.1	9
1470	20	22	35.0	6.9	9
1471	20	22	34.0	6.7	6
1472	20	22	33.0	6.5	6
1473	20	22	31.0	6.1	0
1474	20	22	31.5	6.2	0
1475	20	22	32.0	6.3	0
1476	20	22	32.5*	6.4*	5

* Explosive limit.

recorder. These errors probably could have been minimized by using a strain gauge on the bomb with a suitable high speed recorder for the pressure recorder.

Extremely erratic results were obtained on the first determinations on this project. These were found to be caused by poor gas mixing and improper ignition. The ignition problem was solved by increasing the voltage of the power supply. The first bomb used was provided with a swinging metal vane inside the bomb for mixing the gases. The vane was moved by rocking the bomb. This would not give satisfactory mixing of the gases in any reasonable time. A new bomb was made of stainless steel and had a magnetically coupled stirrer. This stirrer had three propeller blades on a single shaft and could be operated at 3000 rpm for 30 min without having satisfactory mixing. For example, analyses of successive samples taken from a mixture theoretically containing 10% hydrogen varied from 7 to 12%. The final design of the stirrer gave satisfactory gas mixing after 10 min

TABLE III. *Check analyses on hydrogen addition and mixing*

Initial pres. N ₂ , psig	Final pres. after addition of H ₂ , psig	Vol. H ₂ added, ml	Calc. % H ₂	% H ₂ analyzed
100	107	35	6.9	7.0
100	104	22	4.4	4.5
130	143	50	9.6	9.6
60	68	50	9.6	9.5
10	13	50	9.7	9.6

Hydrogen was added to nitrogen in the bomb and mixed for 10 min. Analyses were made using a mass spectrometer.

at 3000 rpm. Table III gives some check analyses on hydrogen addition and mixing. Hydrogen was added to nitrogen in the bomb and mixed for 10 min. Analyses were made using a mass spectrometer. The analyses check the calculated concentration of hydrogen with the experimental error of the analyses ($\pm 0.1\%$ hydrogen).

Some of the points on the calculated curves on Fig. 7, 8, and 9 appear inconsistent. These errors were caused by the necessity of interpolating between some of the observed data in order to have them at the same pressure. The data in Fig. 8 showing the effect of temperature on the explosive limits do not have the precision of the other data in this paper. They were obtained as an afterthought, and there was not enough gas for the desired degree of replication of the determinations. Also, the temperatures varied $\pm 10^\circ\text{C}$ from the desired value.

Since there have been no published data comparable to most of the data presented in this paper, there can be no comparison of results with those obtained by others. However, the explosive limit of hydrogen with air (4.1% H₂) determined in this paper checks with the value obtained by others (7).

Any discussion of this paper will appear in a Discussion Section to be published in the June 1955 JOURNAL.

REFERENCES

1. P. MATHIEU, *J. phys.*, **7**, 166 (1917).
2. A. WEISWEILER, *Z. Elektrochem.*, **42**, 499 (1936).
3. E. W. LINDEIJER, *Rec. trav. chim.*, **56**, 105 (1937).
4. T. I. KUNIN AND V. I. SERDYUKOV, *J. Gen. Chem. (U.S.S.R.)*, **16**, 1421 (1946).
5. E. A. MASON, W. C. BAUER, AND R. R. QUINCY, "Explosions in Chlorine Absorption Systems," Item No. 53-23, Industrial Liaison Office, Massachusetts Institute of Technology, Cambridge (1953).
6. G. W. JONES, *Chem. Rev.*, **22**, 1 (1938).
7. H. F. COWARD AND G. W. JONES, "Limits of Flammability of Gases and Vapors," Bull. 503, U.S. Bureau of Mines (1952).
8. E. W. LINDEIJER, *Rec. trav. chim.*, **56**, 97 (1937).

Discussion Section



THE REACTION OF SILVER ALLOYS WITH SULFUR IN MINERAL OIL

II. Examination of Reaction Films and Mechanism of Reaction

H. O. Spauschus, R. W. Hardt, and R. T. Foley
(pp. 6-9)

J. T. WABER¹: The authors have presented a very interesting paper. There is, I believe, an alternate mechanism which might be proposed which will lead to a linear growth law. When the surface reaction is slow in comparison with diffusion, a constant reaction rate will obtain. Recent detailed theoretical calculations briefly reported by Williams and Wallace² showed that at temperatures below 135°F the rate of formation of chloride ions at the silver chloride-solution interphase was slow in comparison with the rate of arrival of Ag ions.

In the case of the alloys at hand, there can be changes in the concentration and mobility of free electrons due to the presence of alloy atoms dissolved in the sulfide film. Such a change in the availability of electrons would affect the rate of sulfide ion formation and, hence, an effect on the linear rate would be expected. If such a mechanism does operate, the rate law will change to a parabolic one at moderately higher temperatures.

A strained sulfide layer of constant thickness next to the metal was proposed to account for the linear law. Presumably this layer restricted diffusion so as to be rate-controlling: it was not clear from the presentation whether x-ray changes attributed to strain were not due to shifts in the lattice parameter which, in turn, were due to alloy atoms dissolved in the Ag₂S.

R. T. FOLEY: If a boundary reaction as described by Williams and Wallace² were the rate-determining step, the linear rate behavior would be accounted for. The case discussed involves silver chloride which is almost a pure ionic conductor. Thus, electronic conductivity would control the reaction rate.

On the other hand, silver sulfide is an *N*-type semiconductor. We may assume that lattice defects consist of metal ions and quasi-free electrons. [There are reports indicating a sulfur excess (silver deficit), but in view of several recent studies,³ this does not appear reasonable.] Solution of a divalent or trivalent cation sulfide in the silver sulfide would tend to increase the number of free electrons and decrease the number of silver ions. The concentration gradient and, thus, the reaction rate would be decreased. This has been shown, in an earlier paper,⁴ to

This Discussion Section includes discussion of papers appearing in the JOURNAL OF THE ELECTROCHEMICAL SOCIETY, 101, No. 7-12 (January-June 1954).

¹ Los Alamos Scientific Laboratory, Los Alamos, N. Mex.

² WILLIAMS AND WALLACE, *J. Chem. Phys.*, **21**, 1294 (1953).

³ M. H. HEBB, *J. Chem. Phys.*, **20**, 185 (1952).

⁴ See Fig. 3, R. T. FOLEY, M. J. BOLTON, AND W. MORRILL, *This Journal*, **100**, 538 (1953).

be the case qualitatively. The authors contend that the alloying sulfide in solution is concentrated in the first formed film. Thus, the observed rate is linear because the controlling step is diffusion through a layer of constant thickness rather than an increasing thickness of reaction product.

We do not believe that the strains arise from coherency stresses. One would expect the same stresses in silver, silver-thallium alloys, and silver-cadmium alloys. Only the latter gave appreciable distortions and lowered reaction rates.

The explanation for the lower rate must be based on a difference on valency.

The authors thank Dr. Waber for his stimulating suggestions.

THE ELECTROLYTIC PREPARATION OF MOLYBDENUM FROM FUSED SALTS

II. Preparation of Reduced Molybdenum Halides

Seymour Senderoff and Abner Brenner (pp. 28-30)

A. C. LOONAM⁵: How much of the molybdenum gets through the diaphragm and is oxidized at the anode?

S. SENDEROFF: In preparing K₃MoCl₆ by electrolysis of a solution of K₂MoO₄ in strong hydrochloric acid, followed by precipitation of the salt with HCl gas, an over-all yield of 70% was obtained. While some of the loss was due to solubility of the K₃MoCl₆, most of it was probably the result of loss of molybdenum through the diaphragm. However, no attempt was made in this work to minimize this loss by improvement of the diaphragm. Undoubtedly, a thicker diaphragm with finer pores would reduce the loss of molybdenum to the anolyte. Further, it should be noted that the anolyte remaining at the end of a run can be added to the catholyte of succeeding runs to recover the molybdenum which passes through the diaphragm.

M. A. STEINBERG⁶: Can you describe the type of Mo crystals produced?

S. SENDEROFF: The type of crystals produced varies with current density, temperature, and other operating conditions, as described in the first paper in this series.⁷

THE ELECTROLYTIC PREPARATION OF MOLYBDENUM FROM FUSED SALTS

III. Studies of Electrode Potentials

Seymour Senderoff and Abner Brenner (pp. 31-38)

M. A. STEINBERG⁸: 1. What is the cathode material for coherent Mo deposits at 600°C?

2. How do you visualize the transport of oxygen ions to the cathode in oxygenated salt baths?

S. SENDEROFF: 1. For the deposit shown in Fig. 9 of an

⁵ 70 East 45th Street, New York 17, N. Y.

⁶ Horizons, Inc., Cleveland, Ohio.

⁷ S. SENDEROFF AND A. BRENNER, *This Journal*, **101**, 16 (1954).

⁸ Horizons, Inc., Cleveland, Ohio.

earlier paper,⁷ the cathode was a silver-plated steel tube. A tungsten cathode was used for the deposit shown in Fig. 7 and 8.⁷

2. One need not consider the oxygen or oxygen-containing ions as involved in electrical transport at all. Most of the current through the bath is probably carried by the potassium and chloride ions. Since both the oxygen and molybdenum in the bath probably are contained in complex ions of low mobility and low concentration, the transfer of both the oxygen and the molybdenum to the cathode is probably governed by diffusion and not greatly dependent upon the charge of the ions in which they appear.⁹

L. M. LITZ¹⁰: It is of interest to note in connection with your emf measurements in molten salts certain measurements reported by Rempel and Ozeryanya.¹¹ These authors used the reversible chlorine electrode and obtained the following potentials in equimolar NaCl-KCl baths containing 0.1M concentration of the metal chloride at 690°C: Zn, 1.883; Fe, 1.582; Co, 1.514; Cu, 1.414; Pb, 1.390; Ag, 1.287; Bi, 1.181; Ni, 1.179. The position of Ni in this series is particularly interesting.

S. SENDEROFF: We have not measured the potential of nickel under the conditions described in Table I, but preliminary experiments on electrochemical replacement indicate that nickel has a potential in this system close to that of silver. Verdieck and Yntema¹² also found that nickel is more noble than copper in molten AlCl₃-KCl-NaCl.

MORRIS EISENBERG¹³: Dr. Senderoff's choice of Ag/AgCl as a reference electrode is certainly a wise one. However, this raises a few questions.

1. What is the potential of this reference electrode relative to the normal hydrogen electrode?

2. What is the temperature coefficient of the Ag/AgCl reference electrode in this temperature range?

3. How significant are the liquid junction potentials in your baths?

S. SENDEROFF: 1. I don't know. An approximate value of this potential may be obtained by measuring the potential of a chain of cells with progressively lower-melting electrolytes with molten AgCl at one end and aqueous HCl at the other, but such a value would have little or no thermodynamic significance.

2. Again, I don't know. If the reference electrode is kept at the same temperature as the electrode under study during potential measurements, the temperature coefficient of the potential of the reference electrode is not needed for thermodynamic calculations. Furthermore, the temperature coefficient of a half-cell is not determinable by strictly thermodynamic measurements.

3. In the systems under study, the current across the boundary of the liquid junction is probably carried largely by potassium and chloride ions. This situation is analogous to the use of a KCl bridge when measuring potentials in aqueous systems. We believe, therefore, that the liquid

junction potentials are small enough to be ignored in the experiments we have described.

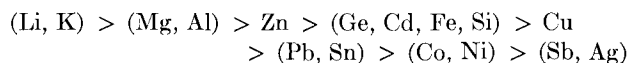
F. TRUMBORE¹⁴ AND G. C. FRYBURG¹⁵: The statement of Senderoff and Brenner that nickel may be more noble than copper in the KCl-LiCl system was of especial interest to us. A few years ago at the Lewis Flight Propulsion Laboratory we were engaged in an attempt to determine the thermodynamic properties of the copper-nickel alloy system by the emf method and found that cells of the type



gave voltages opposite in sign to that expected and showed very erratic behavior. It was noticed that the alloy electrode lost copper during the course of an experiment and became coated with small crystals of nickel. Moreover, cells of the type

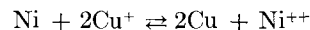


gave reasonable voltages of the expected sign. These facts indicated a reversal or near reversal of nobility of the two metals in going from the aqueous to the fused salt system. In connection with these and other studies conducted by one of us at the Bell Telephone Laboratories a number of crude experiments were performed to get some idea of the relative nobilities of various elements in the KCl-LiCl system. These experiments consisted simply of adding a given metal to a solution of the chloride of a second metal in KCl-LiCl and observing the presence or absence of displacement of the second metal from the solution. These experiments indicated the following "nobility" series (elements to the left of > will displace those to the right):



This series is, of course, qualitative and may not represent the true order of the standard electrode potentials because of the various ion species, activities of the ions in the melts, etc. However, the relative positions of Zn, Fe, Cu, and Ag agree with those of Senderoff and Brenner.

Quantitative data on standard electrode potentials of other metals in the KCl-LiCl and other fused salt systems should be of considerable value to workers in the emf field. The stability of emf cells of the type mentioned above depends to a large degree on the difference in nobility of the two metals because the magnitude of this difference determines the equilibrium constant of the exchange reaction



(in the copper-nickel case), and may control the rate of transfer of the metals between the electrodes. Statements have appeared in the literature that in order for the emf method to be applicable to a given alloy system the nobility differences based on the emf series in aqueous solutions should be on the order of 0.2 volt¹⁶ to 0.7 volt.¹⁷ Such

¹⁴ Bell Telephone Laboratories, Inc., Murray Hill, N. J.

¹⁵ National Advisory Committee for Aeronautics, Lewis Flight Propulsion Laboratory, Cleveland, Ohio.

¹⁶ N. W. TAYLOR, *J. Am. Chem. Soc.*, **45**, 2865 (1923).

¹⁷ O. KUBASCHEWSKI AND O. VON GOLDBECK, *Trans. Faraday Soc.*, **45**, 948 (1949).

⁹ C. WAGNER, *This Journal*, **101**, 181 (1954).

¹⁰ National Carbon Company, Cleveland, Ohio.

¹¹ REMPEL AND OZERYANYA, *Z. Fiz. Khim.*, **25**, 1181 (1951).

¹² VERDIECK AND YNTEMA, *J. Phys. Chem.*, **48**, 268 (1944).

¹³ Stanford Research Institute, Menlo Park, Calif.

statements neglect the possibility that considerable changes may occur in the relative values of electrode potentials in going to fused salt electrolytes, as indicated above in the qualitative series. Furthermore, simple consideration of the equilibrium constant for the exchange reaction shows that, in certain cases, even if the two metals have the same standard electrode potential in the fused salt system it should be possible, by proper choice of the concentration of the ion of the less noble metal and of other conditions, to minimize metal transfer to the extent that reliable data could be obtained. Thus, data on electrode potentials in fused salt systems might show that certain alloy systems could be studied for which the emf method was formerly thought to be unsuitable.

S. SENDEROFF: Since making the measurements described in the paper, we have done some calculations which indicate that the inversion of the positions of copper and nickel in the emf series should not have been so surprising to us and to others who have observed it. We calculated the equilibrium constants, K , at 730°C for the reaction, $MCl_n + n/2H_2(g) \rightarrow M + nHCl(g)$ from Brewer's thermodynamic data for the metal halides at elevated temperatures. When $\log K$ thus calculated was tabulated for about a dozen metals, a list was obtained which is equivalent to the idealized emf series to be expected at that temperature, since $\log K$ for the reaction is proportional to E^0 against a hypothetical hydrogen electrode at that temperature. Negative values of $\log K$ would correspond to the "active" metals above hydrogen, and positive values to the "noble" metals below hydrogen. It turns out that on the basis of this strictly thermodynamic calculation, Cu^+ and nickel are both below hydrogen, and nickel is below copper. Some other metals whose potentials have been measured fall in the correct order.

While we have not carried this further as yet, it seems that as more thermodynamic data at high temperatures become available, it will be interesting to compare such calculations with potential measurements to throw light on the state of the electrolyte in molten salts, and to judge the reversibility of electrode systems.

ANODIC BEHAVIOR OF ALUMINUM AND ITS ALLOYS IN SULFURIC ACID ELECTROLYTES

Ralph B. Mason and Phyllis E. Fowle (pp. 53-59)

R. C. SPOONER¹⁸: The authors are to be congratulated on a clear and interesting presentation of their investigation of conditions governing the anodizing of aluminum and its alloys. It is regretted that the paper does not discuss in detail the voltages required under the various conditions employed, since this information is essential for consideration of the coating formation mechanism.

The coating ratio-metal loss curves in Fig. 2 and 3 at 72 amp/ft² which tilt upward are of special interest. Their shape is attributed to a decreased rate of solution of the coating at the bottom of the pores because of a build-up of solution products within the pore channels. Later in the paper, the possibility is mentioned that the

"pores are fewer in number because of a higher voltage across the primary or barrier layer." In view of the noted abnormal increase in voltage accompanying rises in coating ratio, this suggests that the larger ratios may be due, in part at least, to a reduction in the number of pores so lowering the surface area exposed to electrolyte attack and thus decreasing the amount of coating dissolved.

The authors' comments would be appreciated on the following two queries: 1. Did the proportionately large edge effect with the small panels employed at the higher current densities (e.g., 2 in.² at 72 amp/ft²) cause "burning"? 2. What was the effect on the voltage required for a fixed current density of the addition of 2% oxalic acid to the 12% sulfuric acid solution?

RALPH B. MASON AND PHYLLIS E. FOWLE: 1. No trouble with "burning" was encountered with the small aluminum samples at the high current densities except in the case of 24S-T at a temperature of 34°F. In this case it was not possible to use a current density higher than 24 amp/ft². In the oral presentation of the paper it was pointed out that it is usually impractical to use current densities as high as 48 or 72 amp/ft². In the laboratory, small samples can be readily coated provided there is adequate cooling and agitation of the electrolyte.

2. There was no significant change in voltage when 2% oxalic acid was added to the 12% sulfuric acid solution. It is to be regretted that certain papers discussing the mechanism of coating formation have overstressed the importance of voltage. In the case of the sulfuric acid electrolytes, the voltage data and theory will not stand up under a rigid analysis.

EXTRACTIVE METALLURGY OF ZIRCONIUM BY THE ELECTROLYSIS OF FUSED SALTS

II. Process Development of the Electrolytic Production of Zirconium from K_2ZrF_6

M. A. Steinberg, M. E. Sibert, and E. Wainer
(pp. 63-78)

N. F. MURPHY¹⁹: Did the graphite electrode give off powdered graphite to the melt which would codeposit with the zirconium? Did the graphite porosity decrease on pre-baking?

M. E. SIBERT: There was no evidence of any loss of graphite from the graphite anode. The only carbon contamination encountered has resulted from accidental breakage of the protecting graphite sleeve on the cathode support rod.

There is no notable change in porosity of the graphite regardless of treatment. Leakage develops after a number of runs when the crucible becomes saturated with salts.

MORRIS EISENBERG²⁰: Do you need a protective atmosphere for the storage of the zirconium powders?

M. E. SIBERT: A protective atmosphere is not required for storage of this electrolytic zirconium powder. We have had no instances of spontaneous ignition of this powder when stored in air. Apparently either a protective oxide film is formed in the aqueous recovery procedure, or the

¹⁸ Chemical Division, Aluminium Laboratories Ltd., Kingston, Ontario, Canada.

¹⁹ Virginia Polytechnic Institute, Blacksburg, Va.

²⁰ Stanford Research Institute, Menlo Park, Calif.

hydrogen content is appreciably less than those powders which are subject to this hazard.

CORROSION INHIBITION IN ACID SOLUTION

Cecil V. King and Edward Hillner (pp. 79-83)

A. C. MAKRIDES²¹: The experiments reported by the authors are interesting in more than one connection. It appears from their results that complexing or chelating agents are excellent inhibitors of the dissolution of iron under strongly oxidizing conditions. This suggests that the mechanism by which organic inhibitors function is not "poisoning" of hydrogen evolution as proposed by Elze and Fischer²² and by Bockris and Conway.²³ These same compounds have no effect or actually accelerate dissolution of zinc (with the exception of sodium gluconate which shows about 50% inhibition). This further suggests that inhibition by organic compounds is directly related to the stability of the adsorption complex formed between the metal and the inhibitor, and the consequent decrease in dissolution rate of the surface layers of the metal, rather than to any mechanical blockage of hydrogen ion discharge. As pointed out elsewhere²⁴ recent theories of chemisorption on metals lead to the prediction that chemisorption of such compounds would be stronger on iron, which has *d*-bond character, than on zinc.

Inhibition by $K_2Cr_2O_7$ is known to be dependent on the *pH* of the solution.²⁵ The *pH* of the reference corroding solution was about 1.7; addition of the complexing agent generally raised this by 0.4, or more, *pH* units. The observed increase in effectiveness of inhibition by $K_2Cr_2O_7$ in these solutions could, therefore, be caused by the higher *pH*. In two cases out of three where the *pH* of the solution was adjusted to 1.7, or close to this, after addition of the complexing agent, the complexing agent appears to have decreased rather than increased the inhibition effectiveness of $K_2Cr_2O_7$.²⁶ It would be helpful in the interpretation of results to know if this point has been checked by the authors.

C. V. KING AND E. HILLNER: Essentially Dr. Makrides raises three pertinent questions. They are:

1. Do complexing agents in general inhibit iron dissolution (in the reference solution with no dichromate), and is the inhibition due to adsorption?

2. Do most complexing agents accelerate the dissolution of zinc in the same solution?

3. Is the main effect of the complexing agents on dichromate inhibition due to raising the *pH*?

These questions can be answered as follows:

1. The inhibition by gluconic and citric acids and by

²¹ Department of Chemistry, University of Texas, Austin, Texas.

²² J. ELZE AND F. FISCHER, *This Journal*, **99**, 259 (1952).

²³ J. O'M. BOCKRIS AND B. E. CONWAY, *J. Phys. & Colloid Chem.*, **53**, 527 (1949).

²⁴ N. HACKERMAN AND A. C. MAKRIDES, *Ind. Eng. Chem.*, In press.

²⁵ See, for example, G. G. BERWICK, *Chemistry & Industry*, **1953**, 408.

²⁶ See Table III, Zinc and EDTA, and Table IV, Iron and citric acid, C. V. KING AND E. HILLNER, *This Journal*, **101**, 79 (1954).

EDTA may be due to adsorption on iron; no experimental evidence is available. It is certainly not due to blocking or "poisoning" hydrogen evolution, but may be due to blocking the formation of atomic hydrogen, or some step in the reduction of nitrate. We now have evidence that other chelating agents are poor inhibitors without dichromate, and that neocupferron, which forms insoluble chelates with ferrous and ferric ions, inhibits, but not by adsorption.

2. The dissolution of zinc appears to be diffusion controlled in all the solutions without dichromate. Gluconate lowered the rate because the molecular acid diffuses more slowly than hydrogen ion. EDTA increased the rate because of the extra acid present (molecular acid as well as hydrogen ion). Citric acid, as reported, seemed to have little effect because less HCl was present; the diffusion coefficient of citric acid is smaller but it dissolves more equivalents per molecule. These effects are independent of *pH* within wide limits.

3. The *pH* of the reference solution is 1.8 rather than 1.7; the activity coefficient of HCl at these ionic strengths is very close to 0.80. Actually only one case is shown²⁷ where corrosion is smaller (at the same or a lower *pH*) than in the reference solution. The effect of dichromate should have been shown at several HCl concentrations to cover the *pH* range, or it should have been stated that dichromate enhances inhibition by the complexing agent, at the same *pH*. Actually, later experiments show more conclusively that these and other complexing agents do enhance dichromate inhibition at the reference *pH*.

THE PROTECTIVE ACTION OF PIGMENTS ON STEEL

M. J. Pryor (pp. 141-148)

U. R. EVANS²⁸: Dr. Pryor's study of aqueous extracts of lead and zinc pigments is most welcome, and adds greatly to our knowledge. Where it overlaps with earlier work, the facts are in general accord. It must, however, be remembered that the poor showing of red lead in aqueous extract is no argument against red lead paints, where inhibition is largely due to the degradation products of lead soaps—many of which have been identified and estimated in this laboratory by van Rooyen and Mayne;²⁹ they are mostly salts of dibasic organic acids. However, even in red lead oil paints, the addition of litharge consistently improves performance, as shown in the seven-year outdoor tests organized from Cambridge.³⁰

Earlier laboratory tests³¹ showed clearly that, in the absence of oil, litharge is highly superior to red lead. The following are the losses of weight (in units of 10^{-4} gram)

²⁷ See Table III, Iron, C. V. KING AND E. HILLNER, *This Journal*, **101**, 79 (1954).

²⁸ Department of Metallurgy, University of Cambridge, Cambridge, England.

²⁹ D. VAN ROOYEN AND J. E. O. MAYNE, *J. Appl. Chem.*, *London*, **4**, 384 (1954).

³⁰ S. C. BRITTON AND U. R. EVANS, *J. Soc. Chem. Ind.*, *London*, **58**, 90 (1939).

³¹ K. G. LEWIS AND U. R. EVANS, *J. Soc. Chem. Ind.*, *London*, **53**, 25T (1934).

obtained when steel (or iron) specimens are rotated for 20 hr at 25°C in tubes partly filled with liquid, with or without pigment, but also containing air or oxygen.

In the oxygen experiments, pure litharge was used; in the air experiments, pigment-type litharge or red lead was used. The numbers for percentage areas visibly corroded are also shown. Each experiment with pigment is the mean of two measurements; those for experiments without pigment are mostly the mean of 3 or 4 measurements. The specimens were rectangles of sheet measuring 3 x 1 cm.

molecules are continually attaching and detaching themselves, and it is unlikely that protection can be explained by assuming that the whole metallic surface becomes covered with attached litharge molecules; there will always be some gaps. Oxygen at high pressure will arrive quickly enough to build a passivating film; but at low pressure it will not arrive quickly enough to prevent iron entering the liquid at sensitive spots as cations, electrical neutrality being maintained by the cathodic reduction of oxygen on the area between the sensitive spots. If, however

Material	Gas	Liquid	Weight loss			Percentage of area visibly corroded		
			No pigment	Litharge	Red Lead	No pigment	Litharge	Red Lead
Steel MS2.....	Air	Distilled water	44	1	9	17	0	3
Steel MS2.....	Air	0.001M NaCl	45	1	21	10	0	5
Steel MS2.....	Air	0.001M Na ₂ SO ₄	122	4	52	29	1	6
Steel MS2.....	Air	Sea water	124	16	38	80	2	35
Electrolytic Iron.....	Oxygen	0.001M Na ₂ SO ₄	78	0	—	17	0	—
Steel H33.....	Oxygen	0.001M Na ₂ SO ₄	206	4	—	65	0	—
Steel P1.....	Oxygen	0.001M Na ₂ SO ₄	117	10	—	20	3	—

The tentative explanation offered in 1935, emphasizing pH values and the basic character of inhibitive pigments, was not very unlike Dr. Pryor's theory which emphasizes reserve alkalinity. Neither seems entirely satisfactory today; one would like to know whether a buffer system of the same reserve alkalinity, based on soluble salts, would inhibit corrosion to the same extent in presence of chlorides.

Without finally rejecting reserve alkalinity as an explanation, it is well to explore alternatives. The rise of potential with time, which is attributed by Dr. Pryor to litharge acting as an anodic inhibitor, could also be attributed to an increase in rate of supply of oxygen per unit area of bare metal (an increase which is to be expected if a film is gradually spreading over the surface). It is well known that increased oxygen supply, whether obtained by increased pressure or by movement of the liquid, will render the cathodic polarization curve less steep, and thus raise the value of the potential at which it intersects the anodic curve. Furthermore, the increased oxygen supply improves the chance of obtaining passivity instead of corrosion.

If, in completely stagnant liquid, a metal surface is completely covered with a film except for small gaps of radius r and area a , separated by distances large compared to r , the rate of arrival of oxygen is approximately proportional to $a^{1/2}$ so that the rate per unit area of bare metal is proportional to $a^{-1/2}$. As the area of the gaps becomes small the supply per unit area of gap becomes better, although (for a fixed number of gaps per unit area) the supply per unit area of specimen becomes worse.³²

If we postulate that litharge is adsorbed on metal, but not on iron oxide, the facts are easily explained. Adsorbed

³² It is assumed that the oxygen is used up on arrival, so that the rate of arrival is $CD/\int_r^\infty dr/2\pi r^2 = 2\pi CDr = 2\pi^{1/2}CDa^{1/2}$ where C is the oxygen concentration in the body of the liquid and D the diffusivity.

there is adsorption of litharge molecules (however partial and transitory), the increased rate of arrival of oxygen at points where it is required may suffice to cause film building to predominate over film breakdown, and since lead oxide is postulated to be not adsorbed on iron oxide, the final film will be iron oxide free from lead.

M. J. PRYOR: Dr. Evans' comments and his experimental data are greatly appreciated. It is agreed that the relatively poor showing of a red lead in these experiments does not necessarily imply that it is a poor paint pigment since, if vehicles of the linseed oil type are used, inhibiting lead soaps can be formed. This probably applies also to basic lead carbonate which had no detectable inhibitive action in the form of an aqueous extract. The usefulness of these pigments in paint systems is affected by such factors as the nature of the vehicle and the geometry of the pigment particles which were not considered in this investigation.

Dr. Evans raises the question of whether a buffer system of similar reserve alkalinity based on soluble salts inhibits corrosion to the same extent in the presence of chlorides as the aqueous pigment extracts under similar conditions. Chlorides break down the protection afforded by aqueous pigment extracts relatively easily, and similar buffer systems based on soluble salts are generally more effective inhibitors in chloride containing solutions. Since buffering action is presumably required mainly at the small anodic areas rather than in the bulk of the solution, the rate of transport of the ions responsible for buffering to the anodic areas is clearly important. It is reasonable to suppose that soluble anions would migrate to the anodic areas more rapidly than colloidal or massive lead hydroxide or a positively charged $Pb(OH)^+$ ion of presumably low transport number and thus provide better buffering at the points where this property is most urgently required.

The alternative explanation of the mechanism of inhibition by litharge extracts advanced by Dr. Evans is a reasonable one but falls somewhat outside the scope of present experimental work. For instance, the writer's investigation was mainly an attempt to clarify some of the macro-

chemical reactions occurring during interaction of aqueous pigment extracts and steel. However, such detailed consideration of inhibitor mechanisms is clearly in order and the theory of reserve alkalinity can be extended as follows to provide such a picture. The potential of steel in a litharge extract is a mixed polarized potential and it can be determined from the Nernst equilibrium potentials of the individual anodic and cathodic reactions that very high polarization of both reactions occurs. High polarization of the cathodic reaction is normally observed on steel in somewhat alkaline solutions, but a high degree of anodic polarization is dependent on the presence of an inhibitor. The structure of many passivity films formed in anodic inhibitors has been shown to be duplex^{33, 34} and to consist of small inclusions of corrosion product in a matrix of $\gamma\text{-Fe}_2\text{O}_3$. According to the concepts of Müller,³⁵ anodic polarization is dependent on the resistance and, hence, on the size of these pores in the oxide film. If the pores (which are filled with corrosion product) are very small, the anodic polarization and thus the potential will be very high and the rate of corrosion very low whereas, if the pores are larger, the anodic polarization and the potential will be lower. In inhibitor solutions a localized production of hydrogen ions at the anodic areas occurs due to the formation of hydrated oxide. If the solution in the region of the anodic areas is unbuffered, the pH will fall and low pH values are detrimental to the formation of protective films of oxide and corrosion product; consequently, the size of the anodic areas will tend to increase. If, however, the solution at the anodic areas is buffered, protective films of oxide and corrosion product may form at these points and the size of the anodic areas will tend to remain small. This also implies that buffering action at the small anodic areas is more important than buffering action in the bulk of the solution.

At the present time, there appears to be insufficient direct experimental evidence to distinguish between these views. Thus Dr. Evans' comments emphasize the need for further experimental study of these points.

DIAPHRAGM TYPE AMALGAM CAUSTIC-CHLORINE CELL

Chas. Potter and A. L. Bisio (pp. 158-161)

RALPH M. HUNTER³⁶: A study of the construction of this cell would lead one to suspect that the lower voltage could have been caused by a current leak between the cathode lead and the amalgam. Such leak could give the authors the benefit of the amalgam decomposition potential. Are they sure that this did not happen?

A. L. BISIO AND C. POTTER: The lower voltage is caused by operation of the cell as a Sorensen cell, amalgam decomposition occurring as a result of a local cell set up between the amalgam and the graphite. We doubt whether any leakage of current occurred.

³³ J. E. O. MAYNE, J. W. MENTER, AND M. J. PRYOR, *J. Chem. Soc.*, **1950**, 3229.

³⁴ M. J. PRYOR, M. COHEN, AND F. BROWN, *This Journal*, **99**, 263 (1951).

³⁵ W. J. MÜLLER, *Trans. Electrochem. Soc.*, **76**, 167 (1939).

³⁶ Dow Chemical Company, Midland, Mich.

EFFECT OF CHAIN BRANCHING ON ELECTRO-CHEMICAL CARBON-HALOGEN BOND FISSION. POSSIBLE MECHANISM FOR THE PROCESS

Philip J. Elving, Joseph M. Markowitz, and Isadore Rosenthal (pp. 195-202)

GARRETT W. THIESSEN³⁷: In the macroelectrolysis³⁸ of α -bromopropionic acid, (watery solution, K-salt) the main yield appears to be ethylidene bromide, i. e., 1,2-dibromoethane. This is (R + Br) if the acid is R·COOH, and an unusual result. Identification has been handicapped by (a) decomposition with evolution of HBr on distilling; (b) lack of existence of a suitable derivative in literature. The constants agree approximately, most significant being density greater than that of concentrated H_2SO_4 . Br analysis close, but not quite high enough.

No unsaturation was found in the escaping electrolysis gases.

PHILIP J. ELVING, JOSEPH M. MARKOWITZ, AND ISADORE ROSENTHAL: The result described by Dr. Thiessen is most interesting, and, as he implies, quite unexpected. It would seem that any mechanism which could be contrived to account for his result would necessarily involve decomposition of the carboxylate group.

Of course, there is no necessary relation between this result and the result of the polarographic reduction of 2-bromopropanoic acid. Dr. Thiessen describes his experimental conditions as "macro-electrolysis" (with platinum electrodes). One assumes that he did not control the cathode potential, but used constant current. Consequently, a variety of products might be formed at potentials much greater than those encountered in polarographic work.

It is virtually certain that no ethylidene bromide is produced in the polarographic reduction of 2-bromopropanoic acid. The former substance has a half-wave potential of -1.31 v vs. S.C.E. at 25° in $0.5M$ $\text{NH}_3\text{-NH}_4\text{Cl}$ buffer at pH 8.3. Under the same conditions, 2-bromopropanoic acid exhibits only one wave with a half-wave potential of -1.14 v. If ethylidene bromide were a product, a second wave would appear when 2-bromopropanoic acid is electrolyzed under these experimental conditions; such a wave is not observed.

PREPARATION AND EXAMINATION OF BERYLLIUM CARBIDE

M. W. Mallett, E. A. Durbin, M. C. Udy, D. A. Vaughan, and E. J. Center (pp. 298-305)

J. A. UPPER³⁹: In this paper under Hardness Measurements, it was stated that "Readings of 2678, 2520, and 2613 were obtained with a 50-gram load and 2740 with a 25-gram load. It appears that the hardness of Be_2C is greater than that of silicon carbide and approaches the hardness of boron carbide." These statements were made regarding Knoop hardness measurements made on a Tukon hardness tester.

³⁷ Monmouth College, Monmouth, Ill.

³⁸ Unpublished research at Monmouth College; Pt electrodes.

³⁹ Norton Company, Niagara Falls, Canada.

Regarding the above statements, we would like to submit the following information.

From observations made in the Norton Research Laboratory in Worcester, Massachusetts, it does not appear that Be_2C is as hard as silicon carbide. Typical Knoop hardness data for the very hardest materials are:

Material	Knoop hardness (100-gram load)
B_4C	2800
B	2500
SiC	2500
TiC	2500
Be_2C	2300
ZrC	2100
Al_2O_3	2050
WC	1900

The Knoop hardness determinations set forth above (excepting Be_2C) were obtained from a paper by Thibault and Nyquist.⁴⁰ Values for Be_2C were more recently obtained.

The paper under discussion also quotes Knoop hardness readings obtained at both 50- and 25-gram loads on the Tukon tester. In the paper by Thibault and Nyquist⁴⁰ it is pointed out that the Knoop numbers obtained at different loadings are not directly comparable. In order to obtain comparable data, all tests must be conducted at a common load. The cause of the variation of the measured Knoop hardness with indenting load is discussed in a paper by Tarasov and Thibault.⁴¹

MANLEY W. MALLETT: We wish to thank Mr. Upper for drawing our attention to the fact that Knoop hardness numbers based on indentations made by a 25- or 50-gram load are not directly comparable with numbers determined from indentations made at higher loads. Accordingly, we should revise our statement on the hardness of Be_2C to read that it lies between those of zirconium carbide and silicon carbide.

THE NATURE OF THE ZINC-CONTAINING ION IN STRONGLY ALKALINE SOLUTIONS

Theodora P. Dirkse (pp. 328-331)

J. J. LANDER⁴²: The author is probably aware that, be-

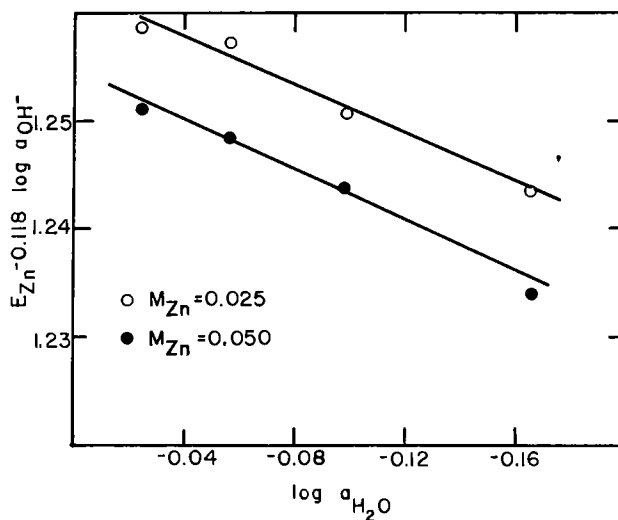
⁴⁰ N. W. THIBAUT AND H. L. NYQUIST, "The Measured Knoop Hardness of Hard Substances and Factors Affecting Its Determination," 28th annual convention, American Society for Metals, Atlantic City, November 1946.

⁴¹ L. P. TARASOV AND N. W. THIBAUT, paper delivered at 28th annual convention, American Society for Metals, Atlantic City, November 1946.

⁴² Naval Research Laboratory, Washington, D. C.

cause x and y are known with certainty, perhaps z might be determined by a plot similar to that with which the value of y was determined, i.e., by graphing $E_{\text{Zn}} - 0.0295 y \log a_{\text{OH}^-}$ vs. $\log a_{\text{H}_2\text{O}}$ and determining the slopes of the resultant curves at several values of M_{Zn} . The results should be interesting, because if the experimental data are of sufficient precision, they should show whether z has an integral value or whether it varies over a rather wide range of a_{OH^-} . Thus his data itself might possibly determine whether or not degree of hydration can be expressed exactly. Evidently, determination of z has been ruled out on the basis of *a priori* considerations, which, even if based on previous experimental evidence, do not necessarily apply to this work which seems to be of high quality.

T. P. DIRKSE: A plot such as that suggested by Dr. Lander can be prepared from the data used in the paper referred to. Using two different concentrations of zinc such a plot gives reasonably straight lines (see accompanying



Variation of $[E_{\text{Zn}} - 0.118 \log a_{\text{OH}^-}]$ with $\log a_{\text{H}_2\text{O}}$

graph). The two lines are parallel and the slope of each is 0.114. This is reasonably close to 0.118 which corresponds to a value of four for z . It is striking that there is a regularity of behavior and that the plot gives an integral value for z . It is possible that this indicates that four water molecules are specially bound in each zinc complex although there is a tendency at present to discount the significance of such hydration numbers.



Coulometry—Related Phenomena of Electrolysis and Current-Sweep Polarography¹

N. Howell Furman²

Introduction

For several recent years, a number of new or modified aspects of electroanalytical methods have been studied in our laboratories. Recently, emphasis has shifted to the determination of substances in the milligram range and lower, down even to the submicrogram range. Our first war-time research in 1942 evolved a procedure that consisted in the electrolysis of traces of metals such as copper, lead, cobalt, cadmium, iron, nickel, zinc, etc., into a small mercury cathode, followed by removal of the mercury by distillation and polarographic or spectrophotometric examination of the residue (1). During war-time, it was not possible to explore other techniques for estimating the metals that were present in the mercury cathode. It was recognized that, without exceedingly careful technique and proper admission of air (oxygen) during the distillation, the more volatile metals such as cadmium might be lost. Subsequently, Cooper (2) investigated the determination of other metals amalgamated with mercury by making the amalgam the anode in a capillary dropping assembly and taking polarograms. This technique gave good qualitative information and semiquantitative results, even on five-component mixtures. The results with simpler amalgams appear to be of interest in connection with the determination of the diffusion coefficients of metals in mercury as solvent medium (3).

Recently, Rogers and coworkers (4) and Cooke (5) have had good success in using coulometric or polarographic techniques of combined methods in estimating submicrogram amounts of metals electrolyzed into mercury.

Schmidt (6) has found that controlled potential electrolysis of a dilute amalgam as anode permits one to electrolyze out and determine elements such as copper, lead, cadmium, and zinc, whereas the passive metals, cobalt and nickel, in presence of excess of iron do not electrolyze out. He has demonstrated that amounts of the first four metals ranging from a few micrograms up to several milligrams may be removed from the mercury and then estimated polarographically. Presumably the passive metals may then be recovered by distillation of the mercury and estimated by polarographic, spectrophotometric, or other methods.

The developments thus far mentioned have been concerned primarily with electrolysis and polarography. The present paper is concerned primarily with coulometry.

Coulometry

Coulometric methods have been open for development since the publication by Faraday of his fundamental laws of electrolysis. For a great many years, the classical coulometric method with cells in series has been studied in courses in physical chemistry, or for fundamental standardization purposes (7).

¹ Palladium Medal Address delivered at the Wrightsville Beach Meeting, September 15, 1953.

² Princeton University, Department of Chemistry, Princeton, New Jersey.

The technique has been advocated for the precise determination of equivalent weights (8). Recently there has been a very decided increase in interest in various coulometric methods for analytical and other purposes.

Controlled potential electrolysis in conjunction with series oxyhydrogen coulometers has been developed by Hickling (9) and by Lingane (10).

A fundamental idea that is essential to a number of modern developments in coulometry for analytical purposes is that of the addition of a substance to a solution for the purpose of generating therefrom at 100% current efficiency a reagent to carry out a definite chemical reaction, thus dispensing with the necessity of preparing and storing standard solutions. This mode of approach seems to be due to Szebelledy and Somogyi (11) who studied brominations and neutralizations in this fashion. They did not appear to realize the full advantages and simplicity of the approach since they used indicators to detect end points and a series silver coulometer for current integration. They achieved a high degree of precision.

It is of interest that some of the present popularity of the coulometric method is due, in part at least, to early studies on surface coatings and corrosion films. Among the earliest of modern studies along this line is one by Grower (12) on the thickness of tin coatings on copper wires. His apparatus is represented schematically in Fig. 1. He was able to differentiate between the pure tin layer and the underlying layer, and also visually when the intermediate layer of copper-tin alloy was dissolved and the pure copper color appeared. Gas coulometers were used for the quantitative measurements.

A very significant development is contained in a study by Campbell and Thomas (13) on the thickness of experimental corrosion or tarnish films of oxide of sulfide or mixtures of oxide and sulfide on pure copper or silver foils. This paper clearly demonstrates the principle of electrolysis at constant current with simple measurement of time to a potentiometric end point or a succession of such points. This type of study has recently been repeated by Allen (14) who found that purest copper, after cleaning by electrolytic polishing and transfer to a system that could be evacuated, developed a film of cuprous oxide of average thickness of 6.5 Å, whereas exposure to air from 0.5 hr typically developed a 15 Å film, whereas after several hours in dry air the films grew to 20–25 Å thickness. The effect of different techniques of washing after polishing could be clearly examined.

The anodic stripping of electrolytic coatings by a constant current to a potentiometric cutoff point was developed by Francis (15) as a convenient method for estimating the thicknesses of electrodeposited coatings of one metal on another.

The evolution of the modern application of the coulometric method to general classes of reactions in solution received its major recent advance from the extensive series of researches by Swift and his associates (16) who have given the name "coulometric titration" to the process of development of a

reagent at constant current to a determinable end point. Other similar developments that should be mentioned are by Trishin (17) who measured amounts of dissolved metals in mercury at constant current by time measurement to a determinable cutoff point. Epstein, Sober, and Silver (18) neutralized acids to an end point by generating alkali from potassium bromide at constant current. Trishin has used the name electrochronometric analysis for the constant-current process with measurement of time to an end point. This name covers both titrations of soluble systems as well as the deposit on, or removal from, electrodes at constant current.

Our own contributions to the field have included the development of a convenient electronic apparatus for providing constant current (19) and an exploration of the electrogeneration of ferrous (20) or ceric (21) ion. In these studies potentiometric technique with a vacuum-tube voltmeter or a

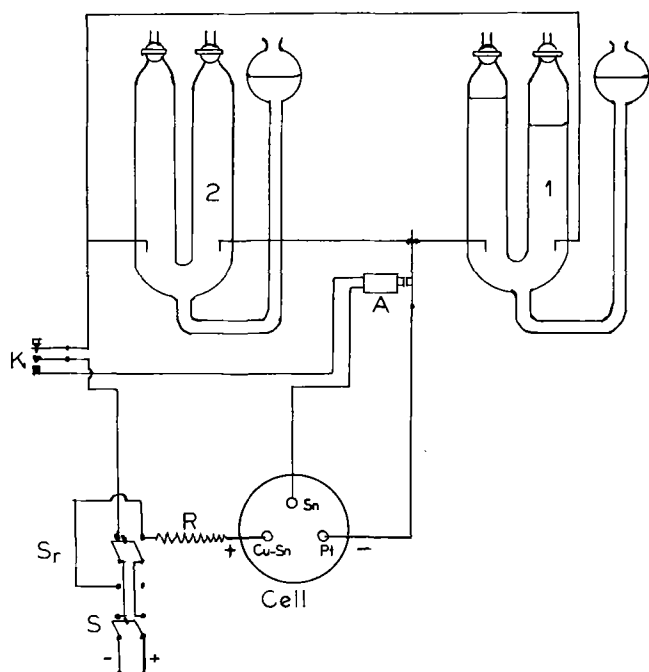


FIG. 1. Grower's thickness tester. Oxyhydrogen coulometer, [1], is in series until the anode Cu-Sn is electrolyzed away until its surface is substantially different from that of the pure tin indicator electrode, Sn. Relay, [A], then throws coulometer [2], into the circuit. The current is stopped when the copper-tin surface of electrode Cu-Sn changes visually to pure copper. The circuit is opened manually.

pH meter was used to detect the end point. In the course of this work it was realized that the amperometric technique with polarized electrodes, used by Swift and associates, was more sensitive and that a compensated potentiometric end point or titration to a suitable potential of a potentiometric system might be adaptable to work in the low microgram range.

This sensitive compensated end point (22) was applied to the estimation of vanadium (V) in presence of uranium (VI) by electrolytically generated ferrous ion in the vanadium range 400 down to 2 micrograms in the presence of a large excess of uranium (23). In the range from 20 to 2 micrograms, the average error was about 1%.

When applied to the coulometric determination of uranium that had been reduced to the quadrivalent state by cadmium amalgam coulometric titrations with electrolytically generated ceric ion (24) in sulfuric acid medium, the errors were larger

and of the order of 2.6% in the estimation of 10 micrograms of uranium or 4.8% (avg) when 5 micrograms were estimated.

Thus far the most sensitive method that we have tested has consisted in the coulometric estimation of permanganate (25). This process as used probably consisted in the storage of a slight amount of pregenerated ferrous ion in the ferric reagent, reaction of the ferrous with the added permanganate, and restoration of the ferrous ferric equilibrium that existed prior to addition of the permanganate. The average error in estimating 0.1 to 0.2 micrograms of manganese in this fashion was 3.5% (9 determinations). In the range from 0.08 down to 0.01 microgram, the average error was not appreciably larger, but from 0.08 down to 0.003 microgram the average error was 9%.

The indication in all these sensitive determinations is essentially amperometric in character with a passage of the galvanometer through zero current reading at the end point. This research indicates that the concentration range that is accessible for titrations by essentially the classical compensated end point (equal and opposite potential to indicator

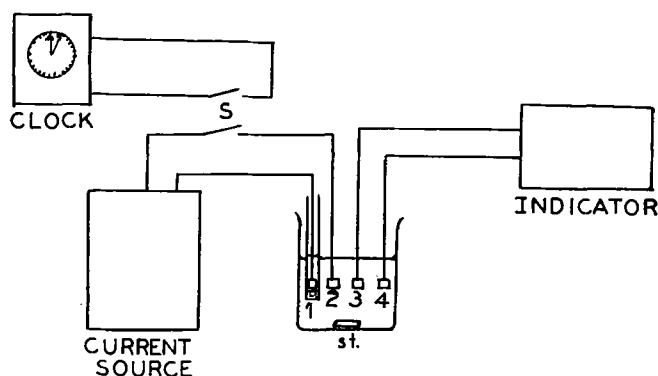


FIG. 2. Coulometric circuit with electrometric indicator. A constant current from the current source and the precision electric time clock are thrown into the circuit simultaneously by the switch, [S], electrode, [1], is sheltered from the solution by a porous diaphragm, and the reagent is generated at electrode, [2]. The electrodes [3], [4] serve to indicate the end point either by potentiometric, amperometric, or other feasible type of indication. St. represents a stirrer bar driven by a magnetic stirrer.

system) of Müller (26) is very far down in the micro region, and it is probable that with an adequate microburet the lower range of titrations could be extended appreciably.

The major limitations to the extension of the coulometric titration process to the submicrogram range seem to lie in kinetic factors at extreme dilutions, slow electrode processes, and adsorption phenomena. Our observations appear to indicate that the slow approach toward equilibrium that one encounters wherever intermittent potentiometric balancing is practiced is largely eliminated by allowing the indicator electrode to take up or deliver an infinitesimal continuous current near the end point.

In the majority of applications that have been made with electrolytically generated ceric ion, the precision and accuracy appear to be less satisfactory than with processes in which a reversible system is involved in the final part of the titration. An interesting feature of these sensitive methods is that no elaborate temperature control nor very exacting experimental conditions have been involved. Purity of reagents and removal of dissolved air (oxygen) have been important.

When oxidation by ceric ion is applied to organic substances, it is necessary to use fresh cerous solution for each

determination, whereas in many inorganic estimations small samples can be added to the solution and titrated without adding a fresh generating solution. Hydroquinone has been titrated successfully with errors averaging 0.5% in the range 100–300 micrograms of hydroquinone, 2% in the 12–90 microgram range, and 3% in the 1–3 microgram range (27).

Determinations with photometric indication in the ultraviolet range have been made by J. W. Handleman (unpublished) for the bromination process. The coulometric generator electrodes were inserted in the solution that was contained in the special cell described by Bricker and Sweetser (28). The bottom of this cell was of dimensions to fit the 1-cm compartment of the Beckman DU spectrophotometer. Brominations of 60–80 micrograms of resorcinol gave an average error of 0.4%. These studies make it apparent that one might combine all the advantages of photometric estimations with the coulometric determination principle, such as generation of successive known amounts of reagent beyond the end point.

Current-Sweep or Potentiometric Polarography

Polarization curves on background medium and medium plus reagent are useful in coulometry as well as in various electrometric methods. It was found profitable to build a number of resistor decades of such characteristics that current could be increased by definite increments. Current voltage curves were then taken by reading emf between reference electrode and generator electrode positioned to avoid or minimize IR drop (29). Later, a continuously variable current was applied more conveniently with the aid of a triode, the grid of which was varied in voltage to give an essentially linear current in the plate circuit. The actual electrode and cell to be used in a coulometric process could be thus used to determine current efficiency for the generation of a reagent. This procedure gives a conservative estimate of the permissible conditions for generation with substantially 100% efficiency. A comprehensive discussion and analysis of the utilization of polarization curves in analytical electrochemistry has recently appeared from the Ecole Supérieure laboratory in Paris (30).

In sweeping the current it was observed that polarograms could be constructed manually at rotating platinum electrodes with less tendency to form time maxima or rounded humps at the usual point where maxima are apt to occur when the voltage is increased point by point. Later experiments (unpublished) with automatic current-sweep were disappointing with solid electrodes, but preliminary observations indicate that there may be desirable features in the current-sweep idea as applied to the dropping capillary mercury electrode. These possibilities are being explored further by R. N. Adams.

Other Coulometric Techniques

The coulometric titration technique may obviously be utilized with any valid type of end-point indication. Various potentiometric, amperometric, and photometric procedures have been tested and there are many other possibilities which have already been used or will lend themselves to give automatic end points, actuate control devices, etc. Carson has developed automatic devices (31) and has used the derivative polarographic idea (32) in good advantage for indication when the solution must be heated during coulometric titration.

Automatic methods.—Analysis and probably control of gas or liquid streams is possible by mixing sample and reagent in a fixed ratio by a proper pump or other mixing device. The current that is needed to keep the mixture continually titrated to a definite index point may be calibrated in terms

of concentration of the substance titrated. The general form of apparatus is indicated schematically in Fig. 3. This type of coulometric application was first described by Shaffer and coworkers (33).

Automatic titration to an end point is possible in batch operations, and a suitable analytical system has been described by Carson (34).

Coulometric generation of standard solutions.—It is possible to generate certain solutions coulometrically at constant current in a portion of the apparatus that is external to the solution to be titrated. DeFord and associates (35) have demonstrated the desirability of this procedure by generating alkali from sodium sulfate, the cathode and anode process being separated by a diaphragm of glass wool in an inverted U-tube with inlet tube at the bottom of the U. This mode of procedure obviously is capable of extension through many branches of volumetric analysis. The resultant change in volume of the solution titrated is a possible unfavorable factor for micro applications.

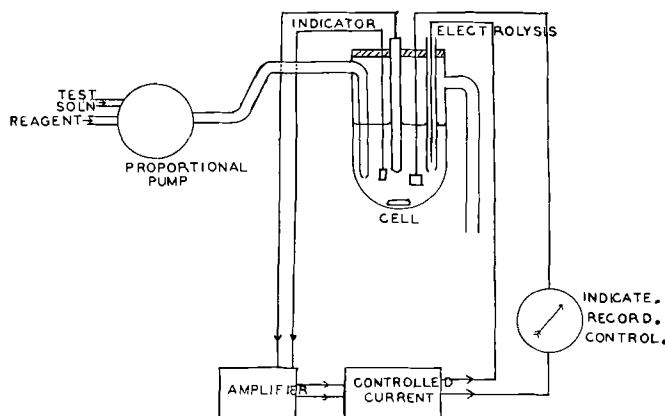


Fig. 3. Coulometric indication in testing flow systems. The indicator circuit activates the current control so that the mixture of reagent and test solution or gas is titrated constantly to maintain a predetermined value of the indicating system.

The constant current-time principle has been used from time to time to generate hydrogen or oxygen to be added as a known component of a gaseous mixture, to prepare dilute standard solutions of various sorts, and probably for other uses.

This review has not been designed to be all-inclusive but rather to describe some recent developments that have made coulometry of increasing analytical usefulness. The majority of papers that have not been mentioned here can be readily located through the papers cited or through a review paper that appeared recently (36).

Acknowledgment

This award of the Palladium Medal is obviously in recognition of a long-continued group effort involving colleagues and students. It is a pleasure to acknowledge the writer's thorough training in research in analytical electrodeposition under the guidance of the late Professor L. W. McCay, and the excellent instruction in electrochemistry, especially potentiometry, conductometry, and classical coulometry that was given by Professor Emeritus G. A. Hulett in his graduate laboratory course. This instruction led to association with Dr. I. M. Kolthoff in the authorship of "Potentiometric Titrations." With few exceptions, the doctoral theses of the writer's graduate students have been in the field of electrochemical studies as applied in chemical analysis. A number of

undergraduate researches of supervisees have also been in this field, and a number of these have been published. These various efforts have served as the basis for the award.

REFERENCES

1. N. H. FURMAN, C. E. BRICKER, AND B. McDUFFIE, *J. Wash. Acad. Sci.*, **38**, 159 (1948).
2. N. H. FURMAN AND W. C. COOPER, *J. Am. Chem. Soc.*, **72**, 5667 (1950).
3. W. C. COOPER AND N. H. FURMAN, *ibid.*, **74**, 6183 (1952).
4. S. S. LORD, JR., R. C. O'NEILL, AND L. B. ROGERS, *Anal. Chem.*, **24**, 209 (1952).
5. W. D. COOKE, *ibid.*, **25**, 512 (1953).
6. W. E. SCHMIDT, Dissertation, Princeton University, Princeton, N. J. (1953).
7. E. B. ROSA AND G. W. VINAL, *Bull. Bur. Standards*, **13**, 479 (1916); *Proc. Nat. Acad. Sci. U. S.*, **3**, 59 (1917).
8. E. L. QUINN AND G. A. HULETT, *J. Phys. Chem.*, **17**, 770 (1914); an illustration of this type of research is given in this work.
9. A. HICKLING, *Trans. Faraday Soc.*, **38**, 27 (1942).
10. J. J. LINGANE, *J. Am. Chem. Soc.*, **67**, 1916 (1945).
11. S. SZEDELLEDY AND Z. SOMOGYI, *Z. anal. Chem.*, **112**, 313, 323, 332, 385, 391, 395, 400 (1938).
12. G. G. GROWER, *Am. Soc. Testing Materials, Proc.*, **II**, **17**, 129 (1917).
13. W. E. CAMPBELL AND U. B. THOMAS, *Trans. Electrochem. Soc.*, **76**, 303 (1939).
14. J. A. ALLEN, *Trans. Faraday Soc.*, **48**, 273 (1952).
15. H. T. FRANCIS, *This Journal*, **93**, 79 (1948), C. T. KUNZE AND A. R. WILEY, *ibid.*, **99**, 354 (1952).
16. S. W. SEASE, C. NIEMANN, AND E. H. SWIFT, *Anal. Chem.*, **19**, 197 (1947).
R. J. MYERS AND E. H. SWIFT, *J. Am. Chem. Soc.*, **70**, 1047 (1948).
D. J. MEIER, R. J. MYERS, AND E. H. SWIFT, *ibid.*, **71**, 2341 (1949).
R. A. BROWN AND E. H. SWIFT, *ibid.*, **71**, 2717 (1949).
W. S. WOOSTER, P. S. FARRINGTON, AND E. H. SWIFT, *Anal. Chem.*, **21**, 1457 (1949).
W. J. RAMSAY, P. S. FARRINGTON, AND E. H. SWIFT, *ibid.*, **22**, 332 (1950).
P. S. FARRINGTON AND E. H. SWIFT, *ibid.*, **22**, 889 (1950).
17. F. I. TRISHIN, *Zhur. Anal. Khim.*, **3**, 21 (1948).
18. J. EPSTEIN, H. A. SOBER, AND S. D. SILVER, *Anal. Chem.*, **19**, 675 (1947).
19. C. N. REILLEY, W. D. COOKE, AND N. H. FURMAN, *ibid.*, **23**, 1030 (1951); *ibid.*, **24**, 1044 (1952).
20. W. D. COOKE AND N. H. FURMAN, *ibid.*, **22**, 896 (1950).
21. N. H. FURMAN, W. D. COOKE, AND C. N. REILLEY, *ibid.*, **23**, 945 (1951).
22. W. D. COOKE, C. N. REILLEY, AND N. H. FURMAN, *ibid.*, **23**, 1662 (1951).
23. N. H. FURMAN, C. N. REILLEY, AND W. D. COOKE, *ibid.*, **23**, 1665 (1951).
24. N. H. FURMAN, C. E. BRICKER, AND R. V. DILTS, *ibid.*, **25**, 482 (1953).
25. W. D. COOKE, C. N. REILLEY, AND N. H. FURMAN, *ibid.*, **24**, 205 (1952).
26. E. MÜLLER, "Elektrometrische (potentiometrische) Massanalyse," 6th ed., p. 52, Steinkopf (1942); lithoprinted by Edwards Bros., Ann Arbor, Mich. (1945).
27. R. N. ADAMS AND N. H. FURMAN, *Anal. Chem.*, **25**, 1564 (1953).
28. C. E. BRICKER AND P. B. SWEETSER, *Anal. Chem.*, **24**, 409 (1952).
29. R. N. ADAMS, C. N. REILLEY, AND N. H. FURMAN, *ibid.*, **25**, 1160 (1953).
30. R. GAUGUIN, *Anal. Chim. Acta*, **7**, 172 (1952).
R. GAUGUIN, *ibid.*, **7**, 360 (1952).
R. GAUGUIN AND G. CHARLOT, *ibid.*, **7**, 408 (1952).
R. GAUGUIN AND G. CHARLOT, *ibid.*, **8**, 65 (1953).
J. BADOZ-LAMBING, *ibid.*, **7**, 585 (1952).
31. W. N. CARSON, JR., *Anal. Chem.*, **25**, 466 (1953).
32. C. N. REILLEY, W. D. COOKE, AND N. H. FURMAN, *ibid.*, **23**, 1223 (1951).
33. P. A. SHAFER, JR., A. BRIGLIO, AND J. A. BROCKMAN, JR., *ibid.*, **20**, 1008 (1948).
34. W. N. CARSON, JR., *ibid.*, **25**, 226 (1953).
35. D. D. DEFORD, J. N. PITTS, AND C. J. JOHNS, *ibid.*, **23**, 938 (1951); *ibid.*, **23**, 941 (1951).
36. P. S. TUTUNDZIC, *Anal. Chim. Acta*, **8**, 168 (1953); *ibid.*, **8**, 182, 184 (1953).

Nathaniel Howell Furman—The Man and His Work

R. M. Burns¹

I can think of no more agreeable way to end a vacation in Maine than to fly down here today to tell you what I know about the 1953 Palladium Medalist. I first met Howell Furman in 1919 upon my return to Princeton from the war. He too was out of uniform and had joined the Princeton faculty as assistant professor after having taught at Stanford University. A native of New Jersey, his trip to California had impressed him with the wild and Gargantuan qualities of the West. He has been satisfied ever since to live in the East.

Our medalist's choice of New Jersey as a state in which to be born may be considered as very early evidence of prophetic vision, for New Jersey with its billion dollar chemical industry leads the nation in chemical manufacture and in number of chemists. The village of Lawrenceville, near Princeton, has the distinction of claiming him as a native son. Here as a

boy, he worked summers in his father's old fashioned general store, the town's headquarters, which also housed the post office. An additional source of income was the sale of lost golf balls which, in spare moments, he hunted on the Lawrenceville School golf course across the street from his home. No doubt it was this early acquaintance with golf balls that led to his later addiction to the game. Not that he has ever let golf seriously interfere with chemistry. Indeed he originated the saying that: "He who shoots 100 has no business playing golf; he who shoots 80 has no business." I am not sure where this leaves President Eisenhower.

To go back to Lawrenceville, it was natural that he should go to the well-known boy's school there and on to Princeton. At the latter, he impressed both teachers and members of the class of 1913, and was thought likely to succeed.

Another important vital statistic concerns Lawrenceville, for there lived in that town the attractive Hannah Henderickson, sister to Furman's close companion at Lawrenceville

¹ Bell Telephone Laboratories, Inc., Murray Hill, New Jersey.



The Problem of Correct Thermal Insulation of Bottom Linings of Aluminum Furnaces

J. Wleugel¹ and O. C. Böckman²

Introduction

Designers of aluminum furnaces are well aware that the thermal insulation of bottom linings for aluminum furnaces must be adjusted to the intended operating conditions of the furnaces, viz., current density of the anode, furnace voltage, and the distance between the anode and the metal bath acting as cathode. In this paper, a theoretical analysis of the problem is attempted, based on some measurements on operating furnaces and on thermochemical data for the reduction of alumina to aluminum metal.

Stating the Problem

The main characteristics of furnace operation are: (a) furnace voltage, in this paper designated E ; (b) total direct current I , and the current density of the anode I/A ; (c) distance between the anode and metal bath, designated d ; (d) current efficiency, designated s ; (e) specific energy consumption, expressed in kwhr/kg metal produced, designated r .

These five quantities are naturally interrelated and their relationships involve certain electrochemical and physical quantities: (f) heat of reaction, or change of enthalpy, of the cell reaction



(g) change of free energy, or equivalently, the equilibrium decomposition voltage of Al_2O_3 under operating conditions; (h) effects of irreversibilities, or overvoltage; (i) different ohmic voltage drops: in the outer circuit (bus bars), in the anode and cathode, and in the electrolytic bath between the anode and cathode; (j) heat generation accompanying these different ohmic voltage drops; and (k) different heat losses of the furnace: heat conducted through the furnace bottom lining, through the anode, radiant heat losses from the bath especially when charging the alumina, and the heat content of anode gases and metal produced.

Two main aspects of the problem have to be discussed: (A) the energy balance of the furnace, and (B) actual voltage drops.

While a knowledge of the actual voltage drops is required to arrive at a true picture of the electrolytic process, the problem of correct heat insulation is solved mainly by proper application of the energy balance.

Heat losses represent a waste of energy, and any reduction in the heat losses per kg metal produced naturally turns out to be a gain in the energy efficiency of the process. By increasing the thermal insulation, heat losses may be reduced. However, the practical operation of the furnace imposes certain limitations as to the amount of insulation that may be applied.

A reduction in heat losses requires an equivalent reduction

in heat generation in order to maintain the correct temperature of the bath. Generation of heat may be regulated mainly by regulating the distance between anode and cathode, and by regulating the total current, or, equivalently, the current density of the anode.

With a given current density, the effect of a reduction of heat generation by reducing the anode-cathode distance is complicated by a second phenomenon, viz., the current efficiency will simultaneously be reduced, especially at low values of anode-cathode distances. A reduction in current efficiency naturally will result in an increase in specific energy consumption.

Thus we find that two effects are opposed: when reducing the anode-cathode distance, the heat generated is reduced, which permits an increase in thermal insulation, but, at the same time, the current efficiency is reduced. It will be demonstrated that minimum specific energy consumption is obtained when these two opposing effects are properly balanced. Calculation of the conditions for the proper balancing of the two opposing effects provides means for the determination of the correct thermal insulation of aluminum furnaces.

In the discussions to follow, actual voltage drops will be calculated to arrive at a true picture of the process. Aspects of current efficiency have then to be considered, and lastly an energy balance will be set up to demonstrate the conditions for the minimum specific energy consumption.

Actual Voltage Drops

Actual voltage drops of a number of 33-kamp and 18-kamp furnaces have been determined in the following manner.

By constant current the anode is lowered successively until complete short-circuiting and the furnace voltage at different positions of the anode is noted. It is presumed that measurements are carried out so rapidly that the cell does not change its temperature during measurements. Measurements of different furnaces, all of them operating at the same current density, show a remarkable conformity. A good average of the measurements is given in Fig. 1.

It is seen that at first the furnace voltage decreases along a straight line as the anode is lowered. At a certain point, a sudden voltage drop of about 1.6 volts is observed. By further lowering the anode, a slight decrease in furnace voltage is noted until a constant value of about 1.4 volts is obtained.

This voltage characteristic of the furnace may be explained by assuming that direct contact between the anode and the metal bath at first is obtained in a single point, or at least in a restricted area. When this contact is established, electrolysis is interrupted and the voltage drop observed corresponds roughly to the decomposition voltage of the electrolysis. Complete short-circuiting is obtained when the total working surface of the anode is in direct contact with the metal bath, this condition being established by further lowering of the anode. The short-circuiting voltage of the furnace thus pro-

¹ A/S Norsk Aluminium Company, Oslo, Norway.

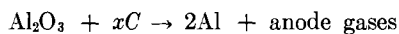
² Elektrokemisk A/S, Oslo, Norway.

Energy Balance

When setting up an energy balance with the aim of providing means for calculating the conditions of minimum specific energy consumption, three main groups of energy dissipations must be distinguished.

Heat of Reaction

Energy consumed by the electrode reaction is equivalent to the heat of the net cell reaction



The heat of reaction depends on the composition of anode gases. With a gas composition of 65% CO₂ and 35% CO, the authors have calculated the heat of reaction at 1000°C to be 276.0 kcal/gram mole of alumina (7). This corresponds to 5.94 kwhr/kg Al. The sensible heat content of anode gases and of produced metal is a permanent loss and may logically be added to the heat of reaction. This addition amounts to 0.73 kwhr/kg Al under the assumed operating conditions, giving a total of 6.67 kwhr/kg Al.

For any furnace operating under these conditions, the energy consumed by the electrochemical reaction may be found by multiplying the number of kg metal produced with 6.67 kwhr/kg Al. To be correct, for furnaces operating under other conditions, viz., with other anode gas compositions, a slight correction of this value has to be introduced. This correction, however, is so small that in this paper it is neglected.

Actual decomposition voltage, multiplied by total direct current through the furnace, and by current efficiency, may be interpreted as the power input to the furnace directly converted to chemical energy. This power input may, by dividing with the metal production, be expressed as a specific energy consumption, and gives the figure 4.77 kwhr/kg Al. This figure, being less than the energy requirements of reaction, shows that a part of the energy requirements of the reaction must be supplied from other sources. Assuming that the power input associated with the current losses is fully recovered as useful heat and a current efficiency of 85%, which gives an additional energy supply, corresponding to 0.83 kwhr/kg, we get a total of 5.60 kwhr/kg. Even this figure is less than the energy requirements of the reaction. The difference, or 1.07 kwhr/kg, must then be supplied by heat generated by ohmic resistance, mainly in the bath.

This comparison of energy requirements of the reaction with actual decomposition voltage is demonstrated in Fig. 2.

Generation of "Useless Heat"

The power input to the furnace, not required for covering the heat of reaction and the sensible heat of anode gases and metal produced, is dissipated to the surroundings as heat losses. The power input, which corresponds to the voltage drops in the anode and cathode, in part contributes toward heating the electrolytic bath, and in part it is generated where it may be considered to be of no use. The short-circuiting voltage of the furnaces measured is 1.4 volts, which corresponds to the combined voltage drops of anode and cathode. Of this, we may estimate that 0.4 volt will contribute to the heating of the bath and 1.0 volt generates useless heat.

For measured furnaces we get the power input generating useless heat by multiplying this 1.0 volt by the total current.

Generation of "Useful Heat"

Total power input to the furnace may be calculated by multiplying the total furnace voltage by the total furnace current. By subtracting from the total power input the items

calculated under heat of reaction and generation of useless heat, we get the heat generation necessary to maintain the correct temperature of the bath. This power input is dissipated as heat losses from the furnace bottom by heat conduction through the furnace lining and by radiant heat losses from the bath, especially during the charging of alumina.

The heat generation equivalent to this power input may be called the generation of "useful heat," as this heat generation is effectively utilized in keeping the bath at correct temperature.

It will be seen that we now have arrived at a quantity very important for our reasoning. By using data from furnaces in actual operation, the generation of useful heat may be calculated for this particular installation and operating conditions. We may then calculate the effect of changing the operating conditions, or of changing the heat insulation of the furnace bottom on the specific energy consumption.

Specific Energy Consumption

The following data serve as basis for our calculations.

A number of 33-kamp furnaces of the same design operating under the same conditions have for a long period of operation produced metal with a specific energy consumption of 19.1 kwhr/kg, as calculated from the weight of metal produced and the readings of the kwhr-meter of the series. Unfortunately, no kamp hr- or kvolt hr-meter were used, but frequent readings of the total series current and voltage established a reasonable value for the current efficiency to be 83.0%.

It may be shown that current efficiency s , specific energy consumption r , and furnace voltage E are related to each other by the equation

$$E = 0.3354 \cdot r \cdot s$$

when E and r are expressed in volts and kwhr/kg, respectively, and s is given as a fraction. The measured values given above then correspond to an average furnace voltage of 5.31 volts, which checks well with the average voltage of the series according to the frequent readings.

These figures, by the nature of their derivation, include the time when anode effects occur. During the anode effects the power input to the furnace is greatly increased, which, to a large extent, is converted into useful heat. For our purpose then it seems logical to include the time when anode effects occur, and the figure 5.31 volts will be used as an average furnace voltage.

According to the voltage characteristic of the furnace (Fig. 1), this average furnace voltage corresponds to an average distance between anode and cathode of 3.75 cm. This checks well with actual measurements of this distance for the furnaces in question as measured by lowering of the anode until the first contact with the metal bath.

It is not quite correct to use the average furnace voltage in combination with the voltage characteristic of Fig. 1 since the former includes anode effects and the latter is based on the normal operation of the furnaces. The main purpose of our investigation is, however, to demonstrate the effect of changing the operating conditions on specific energy consumption. It is felt that, although theoretically not correct, this simplification does not invalidate our conclusions as to the effects of changing the operating conditions. It must be stressed, however, that the actual figures given refer to this particular installation and the general methods of attendance used. For other installations and methods of attendance, other figures will result. It is thought, however, that the trend

of the figures may be more generally valid. To demonstrate this trend is the main purpose of our investigation.

We then arrive at the following fundamental data for the furnaces measured:

Furnace voltage, E	5.31 volts
Current, I	33.0 kampf
Current density, I/A	0.91 amp/cm ²
Current efficiency, s	83.0 %
Specific energy consumption, r	19.1 kw/hr/kg
Average anode-cathode distance, d	3.75 cm

By using these data and the furnace characteristic shown in Fig. 1, together with the relationship found between current efficiency and anode-cathode distance, we may construct lines showing the specific energy consumption at different total currents, or, equivalently, at different current densities. Thermal insulation is supposed to be unaltered. To maintain the correct temperature of the bath, the change in total current has to be compensated for by an equivalent change in anode-cathode distance, to give a constant generation of useful heat.

Suppose the thermal insulation is changed to give a different loss of heat at correct temperature of the bath. We may then repeat our calculations with the new value for the generation of useful heat.

In the calculations to follow, the 33-kampf furnaces, which have supplied the fundamental data, are supposed to operate at different operating conditions and with different thermal insulation of the furnace bottom. Similar calculations may be performed using data obtained from the operation of furnaces of other designs and of other sizes, generation of necessary useful heat being naturally dependent on furnace design and on furnace size as well as on the method of furnace attendance.

To carry out these calculations, we must first determine the generation of useful heat with the normal heat insulation of the furnace. This is done in the following manner:

Furnace current	= 33.0 kampf
Current efficiency	= 83.0%
Metal production 33.0 kampf · 0.83 · 0.3354 kg/kampf hr	= 9.18 kg/hr
Heat of reaction 9.18 kg/h · 6.67 kw/hr/kg	= 61.1 kw
"Useless heat" generation 1.00 volt · 33.0 kampf	= 33.0 kw
<hr/>	
By addition	94.1 kw
Furnace voltage	= 5.31 volt
Total power input 5.31 volts · 33.0 kampf	= 175.2 kw
Useful heat generation by difference 175.2 - 94.1	= 81.1 kw
<hr/>	
Specific energy consumption 175.2 kw/9.18 kg/h	= 19.1 kw/hr/kg.

Our calculations are carried out for five different cases:

(A) The insulation of the furnace bottom is reduced, necessitating 40% increase in the generation of useful heat, or a total generation of useful heat of 81.1 · 1.40 = 113.7 kw.

(B) 20% increase of said heat generation, or 81.1 · 1.20 = 97.4 kw.

(C) Normal insulation.

(D) 20% reduction of said heat generation by properly increased insulation, giving 81.1 · 0.80 = 64.9 kw.

(E) 40% reduction of said heat generation, giving 81.1 · 0.60 = 48.7 kw.

The voltage characteristic is naturally influenced by the current density of the electrolysis. The observed voltage characteristic, at a current density of 0.91 amp/cm², therefore has to be transformed to voltage characteristics at other current densities.

This transformation raises the problem of the choice of correct zero point for the distance between the anode and the metal bath. Obviously, the first point of contact is not the correct zero point because this point indicates the minimum distance which is less than the average distance.

A reasonable correction for the zero point may be obtained

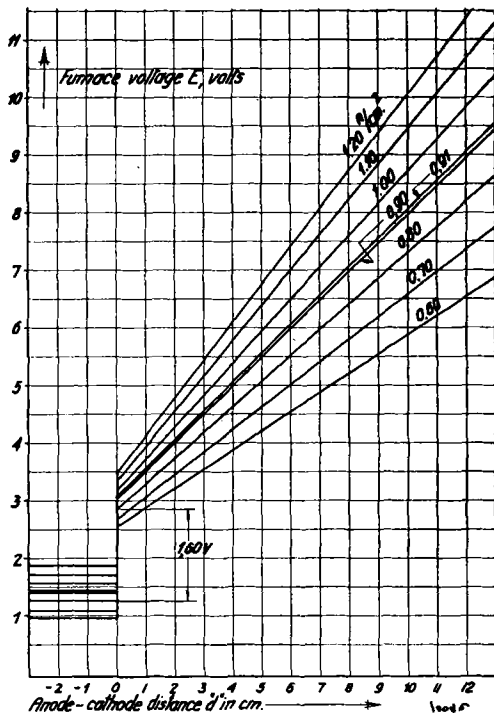


FIG. 3. Voltage characteristics of different current densities, corrected zero point.

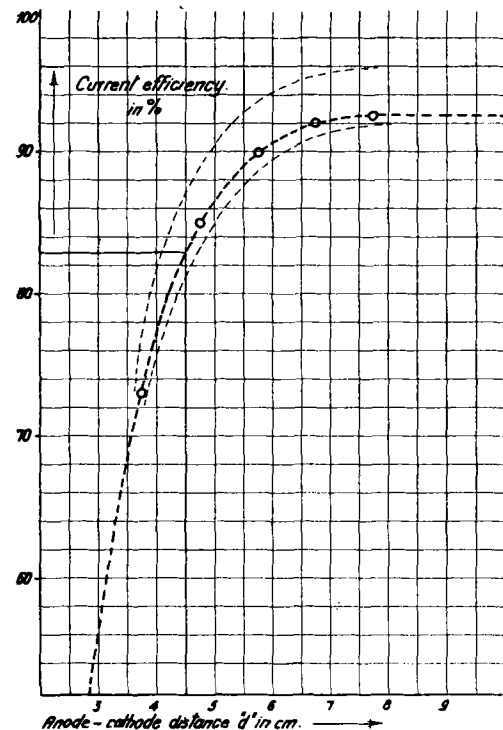


FIG. 4. Current efficiency, viz., anode-cathode distance, corrected zero point.

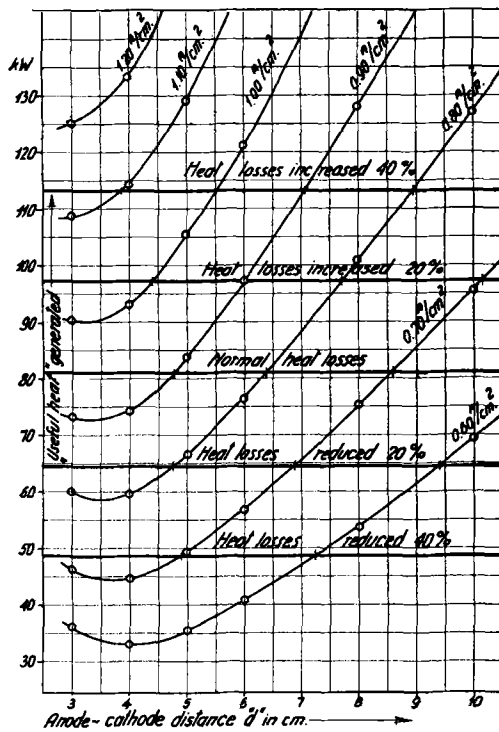


FIG. 5. Comparison of useful heat generated and heat losses from bottom lining.

in the following manner. The short-circuiting voltage may be considered as representing the voltage drops in the current supply under normal operating conditions. By adding the actual decomposition voltage, we arrive at $1.4 + 1.6 = 3.0$ volts, which should be the furnace voltage at zero distance just before contact between anode and metal is obtained, assuming plane surfaces. By extrapolating the straight line of the voltage characteristic (Fig. 1) down to 3.0 volts, we arrive at a zero point correction of 0.75 cm. This correction is applied in all the later calculations.

The voltage characteristics at different current densities are given in Fig. 3. It may be seen from this figure that the short-circuiting voltage too is influenced by a change in current density. It is assumed that a constant proportion of the short-circuiting voltage is contributing to the generation of useful heat.

The current efficiency at different distances between the anode and metal bath with zero point correction introduced is given diagrammatically in Fig. 4.

By repeating the calculation of useful heat generation, assuming different current densities and different anode-cathode distances, we arrive at Fig. 5. From this graph, the correct anode-cathode distance may be found for different values of useful heat generation, corresponding to different thermal insulations of the furnace.

In this manner, an energy balance is set up for every hypothetical operation of the furnace indicated by the circles of Fig. 5. For the same hypothetical operating conditions, the specific energy consumption is calculated as given by the open circles in Fig. 6. The dotted lines indicate the current densities.

For each current density and furnace insulation (Fig. 5) the correct anode-cathode distance giving the correct generation of useful heat is noted and these values are introduced into Fig. 6, black circles. The circles representing the same furnace insulation are connected by fully drawn lines. These

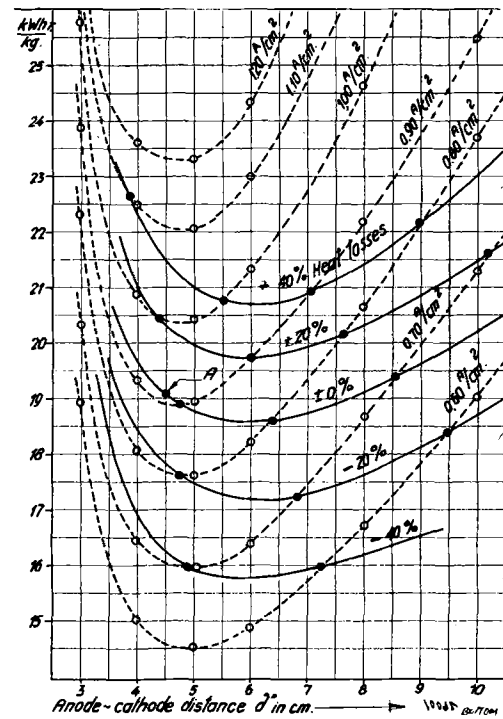


FIG. 6. Specific energy consumption at different current densities and different heat losses from furnace bottom.

lines then represent the actually possible operating conditions of the furnace without altering the insulation.

The operating conditions of the furnaces that have provided the fundamental data are represented in Fig. 6 by the black circle marked A.

Discussion

From Fig. 6 it may be seen how the two opposing effects act. At small distances between the anode and the metal bath the specific energy consumption increases rapidly with a decrease in this distance. This effect is caused by the rapid decrease in current efficiency with a decrease in the anode-cathode distance at low values of this distance.

On the other hand, specific energy consumption increases but slowly with an increase in the anode-cathode distance above 6-7 cm, at constant insulation.

It may be seen further that an increase or a decrease in the amount of insulation applied imposes a change in operating conditions with accompanying changes in specific energy consumption. An increase in furnace insulation generally tends to reduce specific energy consumption. This increase in furnace insulation has to be compensated for by a decrease in anode-cathode distance or in current density. If the anode-cathode distance, however, turns out to be small, the increased insulation may result in an increase in specific energy consumption, as indicated by the left side of Fig. 6. This fact points to the danger of overinsulating the furnaces.

For a given installation, a change in current density results in a change in metal production. When considering the application of the relationship given in Fig. 6 to an installation actually operating, the problem of total metal production must be paid due attention.

When planning new installations, however, the relationships given may serve as a guide in the choice of proper operating data. With a given total metal production, the choice of current density will influence the linear dimensions of the furnaces, and consequently the installation costs. A

balance must here be struck on economic considerations of installation cost, viz., cost of operation.

Results of this analysis may, naturally, be anticipated by common sense and practical experience. It is thought, however, to be of some value to give a quantitative evaluation of the relationships to supplement the qualitative reasoning of common sense and practical experience.

References

1. M. DE K. THOMPSON AND R. G. SEYL, *Trans. Electrochem. Soc.*, **64**, 321 (1933).
2. I. W. CUTHBERTSON AND J. WADDINGTON, *Trans. Faraday Soc.*, **32**, 745 (1936).
3. G. MORITZ, U. S. Dept. of Commerce PB 70023, March 8, 1944.
4. P. DROSSBACH, *Z. Elektrochem.*, **34**, 206 (1928).
5. P. DROSSBACH, *ibid.*, **36**, 179 (1930).
6. W. D. TREADWELL AND L. TEREBSI, *Helv. Chim. Acta*, **16**, 922 (1933).
7. National Bureau of Standards, Selected Values of Chemical Thermodynamic Properties, Series III.
8. P. DROSSBACH, *Z. Elektrochem.*, **40**, 605 (1934).
9. T. G. PEARSON AND J. WADDINGTON, *Discussions Faraday Soc.*, **1**, 307 (1947).
10. E. GRÜNERT, *Z. Elektrochem.*, **48**, 393 (1942).



Report of the Chlor-Alkali Committee of the Industrial Electrolytic Division for the Year 1953

William Cecil Gardiner¹

Production Capacity

The last report of this committee was on May 5, 1952 so this report covers events of 1952 and 1953. The estimated capacity at the end of 1951 was 7200 tons of chlorine per day, but at the end of 1953 it was 9800 tons. This capacity was 0.8% by the nitrosyl chloride process, at one plant, 6.5% from sodium cells, at four plants, 16.0% from mercury cells, at eleven plants, and the remaining 76.7% from diaphragm cells. There are now 63 operating chlorine plants with two more to be completed soon.

Caustic soda production capacity at the end of 1953 was estimated to be 12,155 tons, of which 18.5% was by the lime-soda process and the rest electrolytic.

Actual chlorine production was 2,517,913 tons in 1951, 2,608,690 tons in 1952, and 2,794,320 tons in 1953 or 6900, 7100, and 7640 average daily tons, respectively. Production averaged 7450 tons per day in January 1953, increased to 7840 tons per day in June. In December, production decreased to a daily average of 7330 tons.

New Facilities

Expansions started in the past two years were all completed by the end of 1953 except the Wichita, Kansas, plant of Frontier Chemical Company, the Montague, Michigan, plant of Hooker Electrochemical Company, and the Brunswick, Georgia, plant of Hercules Power Company. These should be in operation in 1954. This expansion has been with seven mercury cell plants using three types of cells, 17 diaphragm cell plants using four types of cells, and two chemical chlorine processes.

The following new electrolytic chlor-alkali plants have been completed in this period:

- Allied Chemical & Dye Corporation, Solway Process Division, Moundsville, W. Va.* (Solvay mercury cells)
- Frontier Chemical Company, Wichita, Kans.* (moved Hooker cells from Pittsfield, Mass., also expanding)
- Mathieson Alabama Chemical Corporation, McIntosh, Ala.* (Mathieson mercury cells)
- North Carolina Pulp & Paper Company, Plymouth, N. C.* (deNora mercury cells)
- Pennsylvania Salt Manufacturing Company, Calvert City, Ky.* (deNora mercury cells)
- Monsanto Chemical Corporation, Muscle Shoals, Tenn., and Anniston, Ala.* (deNora mercury cells)

Expansions have been completed at the following:

- Allied Chemical & Dye Corporation, Hopewell, Va.* (oxidation of by-product NOCl to release Cl₂ and regenerate HNO₃)
- Allied Chemical & Dye Corporation, Solway Process Division, Baton Rouge, La.* (diaphragm cells), Syracuse, N. Y. (mercury cells)

¹ Divisional Editor, Industrial Electrolytic Division. Mathieson Chemical Corporation, Niagara Falls, New York. Prepared for delivery before the Chicago Meeting, May 2 to 6, 1954.

- Brown Company, Berlin, N. H.* (Hooker diaphragm cells)
- Columbia-Southern Chemical Corporation, Barberton, Ohio, Corpus Christi, Texas, Lake Charles, La., and Natrium, W. Va.* (Hooker diaphragm cells)
- Diamond Alkali Corporation, Houston, Texas, Painesville, Ohio, and Pine Bluff, Ark.* (Diamond diaphragm cells)
- Dow Chemical Company, Freeport, Texas, and Midland, Mich.* (Dow diaphragm cells)
- Hooker Electrochemical Company, Niagara Falls, N. Y., and Tacoma, Wash.* (Hooker diaphragm cells)
- Niagara Alkali Company, Niagara Falls, N. Y.* (Niagara Alkali round type diaphragm cells)
- Velsicol Corporation, Memphis, Tenn.* (Hooker diaphragm cells)
- Wyandotte Chemical Corporation, Wyandotte, Mich.* (Hooker diaphragm cells)

A sodium plant under construction at Ashtabula, Ohio, for National Distillers was stopped because a major customer changed plans.

Two Canadian plants, previously announced, are producing. The Marathon Paper Company built a plant at Marathon, Ontario, using deNora mercury cells and Western Chemicals Ltd. built a plant at Duvernay, Alberta, using Hooker Type S diaphragm cells.

An interesting process development to watch will be the Hercules Powder Company's plant at Brunswick, Georgia. The process is licensed from Dow and Grosvenor Laboratories for the indirect oxidation of HCl in a ferric oxide-ferric chloride mass. HCl is a by-product of toxaphene manufacture.

The Muscle Shoals plant operated by Monsanto for the U. S. Corps of Engineers has been kept in stand-by condition. Late in 1953 it was offered for lease by private industry.

The new mercury cell plants have been felt in the mercury market. The 1953 industrial consumption of mercury rose 23% above 1952 largely because three mercury cell plants were opened and capacity at another was expanded. Mercury was returned to the market from a plant closed down in Jersey City, New Jersey. In spite of this, mercury prices dropped during 1952 from \$217-219 to \$187-189 per flask (\$2.85-\$2.88 to \$2.46-\$2.49 per lb). Annual mercury consumption by the chlor-alkali industry in 1949 was 755 flasks. This increased to 2507 flasks in 1952 and 2378 in 1953. This last figure was 4.5% of the U. S. consumption.

Chlorine End Use

The estimated end use of chlorine is as follows:

	%
Solvents	25
Plastics and fibers	15
Pesticides and herbicides	15
Pulp and paper	14
Automotive fluids	13
Refrigerants and propellants	11
Sanitation	4
Miscellaneous	2
	—
	100

Future Outlook for Chlorine

Considering the broad and expanding end uses of chlorine, the yearly chlorine consumption is expected to show an annual increase of 7.9% up to 1960.

The chlorinated solvents, carbon tetrachloride, chloroform, methylene chloride, trichloroethylene, perchloroethylene, etc., should remain over the next ten years as the major outlets for chlorine.

The growing acceptance of fibers and plastics derived from chlorine will make a major contribution to chlorine expansion. Foremost are vinyl chloride and vinylidene chloride polymers used in household floor tile, curtains, seat covers, etc. Phenolics for foundry shell molds and for bonding wood waste will show conservative gains. Chlorine use in phenolics will be limited by the competition of the Raschig process to make phenol (benzene, HCl, and air) with the chlorination of benzene process. Likewise the meteoric rise in ethylene glycol-terephthalates and acrylonitrile for synthetic fibers will augment chlorine consumption only where the chlorohydrin process is used to make ethylene oxide. Kel-F growth is a certainty. The rising acceptance of the silicones will reflect in turn a greater need for methyl chloride.

Indications are that the herbicide 2,4-D demand will level off and 2,4,5-T will continue to grow at its current rate. The phenomenal rise in the use of chlorinated insecticides (BHC, DDT, chlorodane, aldrin, and toxaphene) will be difficult to match in the future. Lindane, the 100% gamma isomer of BHC, is currently the fastest growing. Pentachlorophenol, mainly used as a wood preservative, should show gains over its past record.

Pulp and paper requirements for chlorine are expected to remain at about the present level over the next few years.

Growth in automotive fluids, ethylene glycol, and tetraethyl lead will increase the chlorine demand moderately. Chlorine for manufacture of glycol will be limited to the chlorohydrin process. TEL fluid contains or requires for its production ethyl chloride and ethylene dichloride. The greater number of automobiles and the trend toward higher compression engines tend to increase the use of TEL and glycol. The shift to jet engines for aircraft and the increasing use of aromatics offsets this trend somewhat. Milder winters and the suggestion (by car manufacturers) to use glycol antifreeze for several winters are affecting the market.

The market for ethylene glycol is growing outside its use as antifreeze. *Chemical Week* reports that over 70% of the glycol produced in the past few years has gone into such end uses as plasticizers and synthetic rubber. The trend toward direct

oxidation of ethylene rather than the chlorohydrin process to obtain ethylene oxide means that chlorine requirements will not keep pace with these new glycol outlets.

Refrigerants and propellants consisting of du Pont's Freons and General Chemical's Genetrons, a series of fluoro-organics, should maintain their annual growth. Methyl chloride used as a refrigerant should bolster chlorine consumption in this application.

The Caustic Soda Picture

The growth curve for chlorine consumption has been at a faster rate than for caustic soda. At this time, electrolytic caustic soda capacity comes very close to being able to supply the market. Lime-soda plants make up the difference. Favorable location and high quality of product provide outlets for some lime-soda producers even when electrolytic caustic is difficult to sell. This causes a prospective chlorine producer to study well how new caustic soda is to be handled.

Use of by-product HCl from the chlorination of organics is a growing factor in balancing the chlorine-caustic soda situation. Some of the means being used or considered are:

1. The conversion of by-product HCl to chlorine. Hercules is building a plant for doing this at its Brunswick, Georgia, toxaphene plant.
2. The Raschig process makes phenol from benzene, HCl, and air in competition with the direct chlorination of benzene.
3. The manufacture of ethyl and vinyl chloride from ethylene-HCl and acetylene-HCl, respectively.

Acknowledgment

Mr. Axel Heilborn, Niagara Alkali Company, Mr. Morton S. Kircher, Hooker Electrochemical Company, Mr. Robert B. MacMullin, R. B. MacMullin Associates, and Mr. Warren D. Sherrow, Great Lakes Carbon Corp., assisted in this report.

REFERENCES

Several review items appeared in the past two years that are of interest to the chlor-alkali industry.

D. O. HUBBARD, "The Chlor-Alkali Industry, 1902-52," *This Journal*, **99**, 307C (1952)

Two Staff-Industry Reports appeared in *Industrial and Engineering Chemistry* [**45**, 1162 and 1824 (1953)] describing mercury cell plants in Italy and at McIntosh, Ala., respectively

M. S. KIRCHER, "Postwar Industrial Electrochemical and Related Chemical Developments in the Niagara Area," *This Journal*, **100**, 58C (1953).

F. CHRENCIK, "Electrochemical Chlorine-Caustic Soda Production in the Gulf Coast Area," *ibid.*, **100**, 182C (1953)



The Utility of Thermodynamic Interpretation of Polarization Curves

Marcel Pourbaix¹

Abstract

A description is given of several principles related to the thermodynamic interpretation of polarization curves: reaction potential, equilibrium potential, affinity, overvoltage, direction in which an electrochemical reaction occurs, and polarization curves of an electrochemical reaction.

Applications to some particular cases are given: (a) experimental determination of the thermodynamic equilibrium potential of an irreversible reaction; (b) determination of oxidation reduction catalysts; (c) prediction of conditions of corrosion and passivity of metals and alloys; behavior of mild steel in a bicarbonate medium; behavior of stainless steel in acetate buffer, influence of chlorides; action of chlorides on the corrosion of iron and the remedy for this action; prevention of localized corrosion.

Principles

Reaction potential and equilibrium potential, affinity, overvoltage, direction in which an electrochemical reaction occurs, and polarization curve of an electrochemical reaction (1).—The direction in which a thermodynamically possible electrochemical reaction, r , occurs at the interface between a metal and an aqueous solution is determined by relative values of the reaction potential E' of the metal surface and of the equilibrium potential E_r of the reaction. When the potential E' of the metallic surface is higher than the equilibrium potential E_r of the reaction, this reaction can be brought about only in the direction of an oxidation; when the potential E' is lower than the equilibrium potential E_r , the reaction can be brought about only in the direction of a reduction.

It should be understood that these potentials are both computed with respect to the same reference electrode and are related to the same physicochemical state of the substances taking part in the reaction; that is to say, particularly to the same conditions of temperature, fugacity (for the gaseous reaction products), and activity (for dissolved reaction products). Reaction potential E' can be measured experimentally according to the classical method of Haber and Luggin,² utilizing a siphon whose capillary extremity dips into the solution in the immediate proximity of the metallic surface; equilibrium potential E_r of the reaction can be calculated thermodynamically.³

¹ Belgian Center for the Study of Corrosion, University of Brussels, Brussels, Belgium. Paper prepared for delivery before the Philadelphia Meeting, May 4 to 8, 1952.

² Haber (2) seems to have been the first to recognize, in 1898, the great importance of electrode potential on the course of electrochemical reactions; Haber, in collaboration with Luggin in 1900 (3), has indicated a method for the measurement of this potential.

³ If one takes arbitrarily as equal to zero the equilibrium potential of the electrochemical reaction of the reference electrode (e.g., $H_2 = 2H^+_{aq} + 2e^-$ in the case of the hydrogen electrode) and the free energies of formation of H_2 at one atmosphere and H^+_{aq} at $pH = 0$, the equilibrium potential E_r

If one uses for electrochemical reactions the relation of de Donder (5)

$$A \cdot V \geq 0$$

which relates the direction of the reaction (determined by the sign of the rate V) to the sign of its affinity A , one obtains the relation (6)

$$(E' - E_r) \cdot i_r \geq 0$$

where the difference $E' - E_r$ between the potential E' of the metallic surface and the equilibrium potential E_r of the reaction is in quantity and in sign the affinity divided by n Faradays or the overvoltage⁴ of this reaction on this surface; the reaction current i_r , which measures, according to Faraday's law, the rate of reaction r is to be considered as positive in the case of oxidation and as negative in the case of reduction. Relation $(E' - E_r) \cdot i_r \geq 0$ states, in short, that the rate of an electrochemical reaction is always either zero or of the same sign as its overvoltage.

The characteristics of irreversibility of an electrochemical reaction brought about at the interface between a metal and an aqueous solution can be represented by a polarization curve $E' = f(i_r)$. This curve expresses in short the relation $E' - E_r = \varphi(i_r)$ between the affinity $E' - E_r$ and the rate i_r of the reaction, if this curve is determined by avoiding any concentration polarization, i.e., if the equilibrium potential E_r of the reaction is maintained practically at the same value for the different reaction rates i_r (this can then be the case generally only when experiments are made in solutions which are sufficiently agitated and buffered).

If one plots positive potentials in ordinates upward and in volts of an electrochemical reaction of the type $\sum \nu M + ne^- = 0$, of which the constituents M have free energies of formation μ (in calories), has the value:

$$E = \frac{\sum \nu \mu}{23,060 n} \quad [\text{see (4)}]$$

⁴ Thus defined, the overvoltage corresponds to the "Fehlspannung," an idea proposed by Lange and Nagel in 1937 (7).

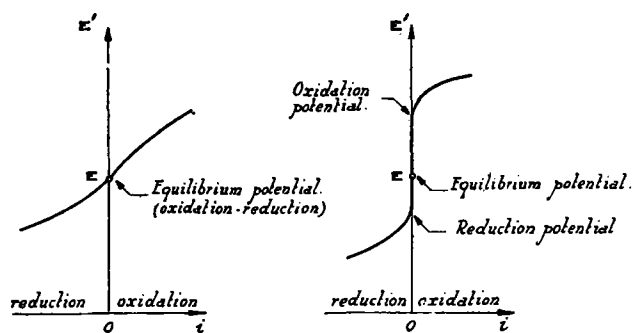


FIG. 1a and 1b. Types of polarization curves. Fig. 1a, left, reversible reaction in the two directions; Fig. 1b, right, irreversible reaction in the two directions.

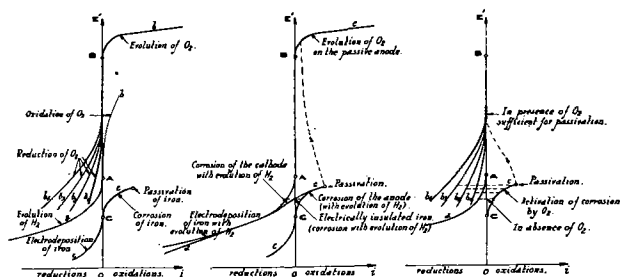


FIG. 2a, 2b, and 2c. Polarization curves and behavior of iron. Fig. 2a, left, polarization curves, curve a, $H_2 = 2H^+ + 2e^-$, curve b, $2H_2O = O_2 + 4H^+ + 4e^-$, curve c, $Fe = Fe^{++} + 2e^-$; Fig. 2b, center, behavior of iron electrode in a solution initially free from hydrogen and oxygen; Fig. 2c, right, action of increasing quantities of oxygen on the behavior of electrically insulated iron.

the positive currents, or rates of oxidation, in abscissas toward the right, polarization curves are, according to relation $(E' - E_r) \cdot i_r \geq 0$, ascending from left to right and intersect the axis of ordinates at a point corresponding to the equilibrium potential E_r of the reaction (Fig. 1).

According to this method of representation, in the case of reactions which are reversible in both directions (Fig. 1a), for which a small affinity $E' - E_r$ (positive or negative) is sufficient in order to bring about an appreciable rate (in the direction of oxidation or reduction), the polarization curve intersects the axis of ordinates at a point where $E' = E_r$ (equilibrium potential of the reaction). In this case, an electrode in contact with the oxidation-reduction system acquires the equilibrium potential; the value of this potential is the thermodynamic equilibrium potential. This equilibrium potential is measurable, e.g., Pt in the presence of $Fe^{++}_{aq}/Fe^{+++}_{aq}$, platinumized Pt in the presence of H_2/H^+_{aq} , Tl in the presence of Tl^+_{aq} .

In the case of reactions which are practically irreversible in both directions (Fig. 1b), rate of reaction remains practically zero for measurable values of the affinity (positive and negative), the polarization curve coincides practically with the ordinate axis on each side of the point representing the equilibrium potential E_r . The curve departs from this axis only when the overvoltage exceeds in absolute value a certain critical value which measures the potential barrier or the "activation overvoltage" relative to the reaction. There exists, then, according to definitions proposed by Van Rysseberghe (8), an oxidation potential above which the reaction actually occurs in the direction of oxidation, and a reduction potential below which the reaction occurs in the direction of reduction; the potential E_r corresponding to thermodynamic equilibrium of oxidation-reduction is situated

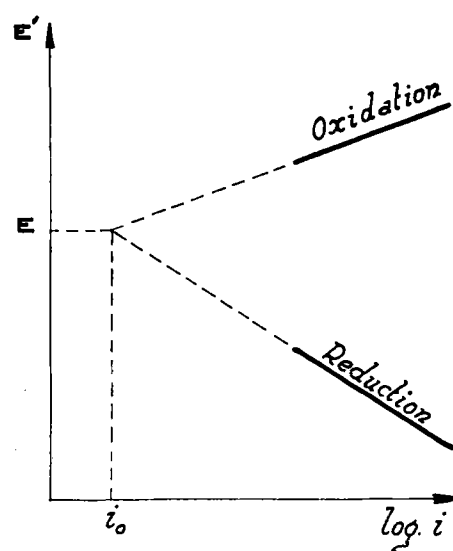


FIG. 3. Catalysis of electrochemical reaction

between these two potentials. In the case of such irreversible reactions, one electrode placed in contact with the oxidation-reduction system shows a potential generally unstable which can vary between the oxidation potential and the reduction potential; the equilibrium potential is not experimentally measurable directly (e.g., Pt in the presence of O_2/H_2O).

In the very frequent case of simultaneous electrochemical reactions occurring on the same metallic surface, analysis of the complex phenomena which result may be generally effected in a sufficiently approximate manner by means of a simple superposition of polarization curves corresponding to each of the reactions. Fig. 2, on the subject of which discussion appears elsewhere (1), illustrates an example of the use of polarization curves in the behavior of iron. The classical work of Evans in the use of polarization curves in the study of "local elements" in corrosion (9) may be considered as the basis of the science of corrosion of metals in aqueous solutions. Wagner has shown in a fundamental treatment of the corrosion of zinc amalgams (10) that the method of superposition of polarization curves is applicable even in the absence of local action. Pourbaix has applied this method in the study of different electrochemical phenomena related in particular to the corrosion of iron (11) [see also Reference (1), p. 471]. Bonhoeffer has demonstrated experimentally the validity of this method of superposition of polarization curves in the corrosion of iron in the presence of H_2SO_4 (12).

Applications

Four cases in which the thermodynamic interpretation of polarization curves has been useful are discussed.

Experimental Determination of Thermodynamic Equilibrium of an Irreversible Reaction⁵

It is well known that polarization curves generally follow Tafel's law, $E' = a + b \log i$, where i is the absolute value of the reaction current.

In the case of the reaction $O_2 + 4H^+ + 4e^- = 2H_2O$ on Pt and on Au, Hoar (13) observed that, if one extrapolates logarithmically according to Tafel's law, the oxygen polarization curve $2H_2O \rightarrow O_2 + 4H^+ + 4e^-$ and that related to the reduction $O_2 + 4H^+ + 4e^- \rightarrow 2H_2O$, these curves intersect at the thermodynamic equilibrium potential of the reaction (Fig. 3). Bowden and Agar (14) have suggested a considera-

⁵ See Reference (1), p. 14.

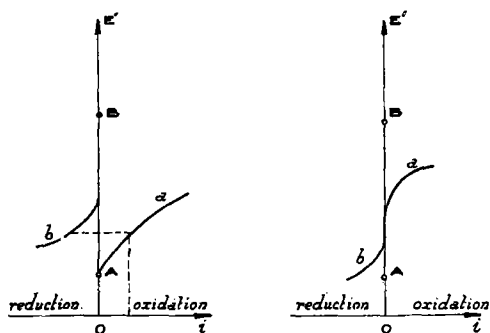


Fig. 4a and 4b. Polarization curves and electrochemical catalysis of chemical reaction. Fig. 4a, left, catalysis; curve a, $2\text{H}_2 = 4\text{H}^+ + 4\text{e}^-$, curve b, $2\text{H}_2\text{O} = \text{O}_2 + 4\text{H}^+ + 4\text{e}^-$; Fig. 4b, right, no catalysis; curve a, $2\text{H}_2 = 4\text{H}^+ + 4\text{e}^-$, curve b, $2\text{H}_2\text{O} = \text{O}_2 + 4\text{H}^+ + 4\text{e}^-$.

tion of the two reaction currents thus extrapolated at the equilibrium potential as a measure of the catalytic activity of the electrode for the reaction. In the case of the reaction $\text{O}_2 + 4\text{H}^+ + 4\text{e}^- = 2\text{H}_2\text{O}$ studied by Hoar, this current was from 10^{-13} to 10^{-12} amp/cm².

Prediction of Oxidation-Reduction Catalysts⁶

When, for a same metallic surface, two polarization curves related, respectively, to (a) an oxidation reaction, e.g., $2\text{H}_2 \rightarrow 4\text{H}^+ + 4\text{e}^-$, and (b) a reduction reaction, e.g., $\text{O}_2 + 4\text{H}^+ + 4\text{e}^- \rightarrow 2\text{H}_2\text{O}$, are such that values of the potential exist for which both reactions take place with measurable rates (Fig. 4a), it follows⁷ that the metallic surface is likely to catalyze electrochemically the resulting chemical reaction ($2\text{H}_2 + \text{O}_2 \rightarrow 2\text{H}_2\text{O}$) if the reaction medium contains simultaneously the oxidant (O_2) and⁷ the reducing agent (H_2). The metal then acquires, if electrochemically insulated, the potential at which the two reaction currents are equal in absolute value. This value of the current measures the rate of the over-all catalyzed reaction. On the other hand, when polarization curves are such that there is no potential at which both reactions occur with a measurable rate (Fig. 4b), the metal surface is not likely to catalyze the resulting reaction. As far as is known, this interpretation has not yet been the object of any experimental work.

Prediction of Corrosivity and Passivity of Metals and Alloys⁸

Here again are given, with some modifications and developments, considerations previously presented in collaboration with Van Rysselberghe (16), with the object, in part, of determining under what conditions a particular metal or alloy is corroded or not corroded by a given solution, and also of

⁶ See Reference (1), p. 466.

⁷ Unpublished discussion among J. Weydema, W. G. Burgers, and M. Pourbaix.

⁸ Assume that there is immunity, or cathodic protection, of a metal when this metal, although presenting a real metallic surface, is thermodynamically stable; all corrosion of the metal is then thermodynamically impossible. Consider that there is passivation when the surface of the metal is not really metallic, but is covered by a film or deposit of oxide, salt, or some extraneous material. Consider that there is passivity when, although thermodynamically unstable, the metal does not corrode practically; there is passivity by inertia when the absence of corrosion is due to irreversibility of the corrosion reaction, as could be the case with zinc and nickel; there is passivity resulting from coating when the absence of corrosion is due to a passivation, by the formation of a film or deposit of an oxide or salt or extraneous material (15).

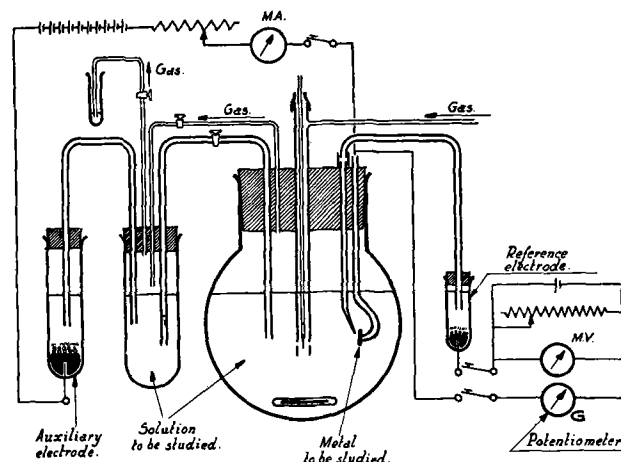


Fig. 5. Apparatus

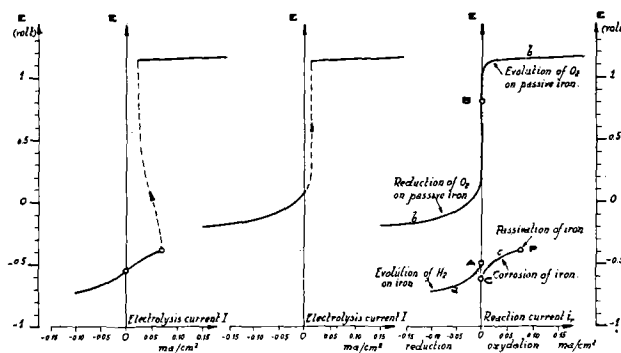


Fig. 6. Behavior of mild steel in a solution of NaHCO_3 0.10 mole, pH 8.6. Left, degassed solution; center, solution saturated under 1 atm; right, polarization curves, curve a, $\text{H}_2 = 2\text{H}^+ + 2\text{e}^-$, curve b, $2\text{H}_2\text{O} = \text{O}_2 + 4\text{H}^+ + 4\text{e}^-$, curve c, $\text{Fe} = \text{Fe}^{++} + 2\text{e}^-$.

determining which modifications in the composition of an alloy or metal or solution may prevent corrosion. Three cases will be given as examples.

Behavior of mild steel in a bicarbonate solution⁹.—By means of the experimental arrangement shown in Fig. 5, an ordinary mild steel electrode, previously descaled, is polarized cathodically and anodically and placed in a solution of NaHCO_3 0.1M of pH 8.6 strongly stirred and rendered free of oxygen by degassing under vacuum. The electrolysis curve shown on the left side of Fig. 6 is obtained. The anodic curve is composed of two stable branches, one at a low and the other at a high potential. If the same electrode placed in the same solution saturated with oxygen at a pressure of one atmosphere is polarized, electrolysis curves shown in the center of Fig. 6 are obtained.

Knowing the pH of the solution (8.6), one is able to determine easily the points A and B of the right part of Fig. 6 which correspond, respectively, to the equilibrium potential of the reaction $\text{H}_2 = 2\text{H}^+ + 2\text{e}^-$ (-0.51 v) and to the equilibrium potential of the reaction $2\text{H}_2\text{O} = \text{O}_2 + 4\text{H}^+ + 4\text{e}^-$ ($+0.72$ v). In the case of a solution practically free from iron, the equilibrium potential C relative to the reaction $\text{Fe} = \text{Fe}^{++} + 2\text{e}^-$ is about -0.60 v. It is now easy to trace the polarization curves of these three reactions (right part of Fig. 6).

⁹ See Reference (16), p. 220. The author's experiments mentioned in (1) and (2) were made in August 1949 in the laboratories of the National Bureau of Standards, with the collaboration of I. A. Denison, B. J. Mair, and W. J. Schwerdtfeger.

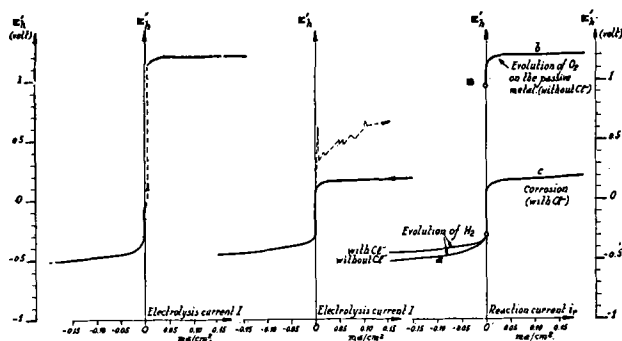


FIG. 7. Behavior of 18/8 stainless steel in degassed solution of $\text{CH}_3\text{COOH} + \text{CH}_3\text{COONa}$, 0.10 mole ($\text{pH} = 4.9$) in absence of NaCl and in presence of NaCl . Left, solution without chloride; center, solution with chloride, right, polarization curves; curve a, $\text{H}_2 = 2\text{H}^+ + 2e^-$; curve b, $2\text{H}_2\text{O} = \text{O}_2 + 4\text{H}^+ + 4e^-$; curve c, $\text{Fe} = \text{Fe}^{++} + 2e^-$.

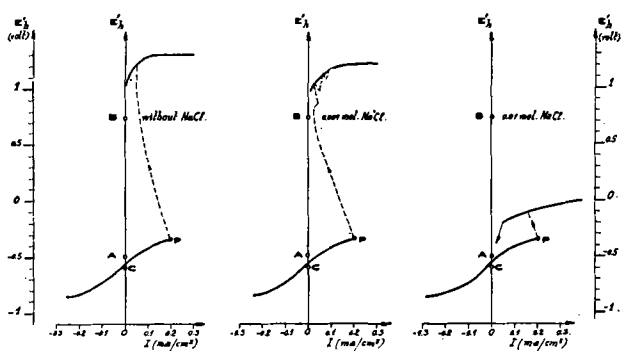


FIG. 8a, 8b, and 8c. Influence of chloride on the behavior of mild steel in a solution of NaHCO_3 , 0.10 molar ($\text{pH} 8.4$) in absence of oxygen (degassed solutions).

The result shows that if the passive film which is formed at point P prevents completely corrosion (which, in a solution free from any trace of reducing agent, is shown by the absence of any stable anodic current between the points P and B), the corrosion of steel is possible only for potentials between C and P; corrosion is impossible for potentials below C, in which case there is immunity or cathodic protection; corrosion is impossible for potentials above P. These general conditions of corrosion hold whatever the reason for which a metal acquires any particular potential.

It is easy on this basis to determine the conditions under which differential aeration occurs (as elucidated by Evans), to explain the activating or passivating effect of oxidizing inhibitors (17), and, in a general way, to predict the treatments to be employed to protect mild steel in bicarbonate solutions.

Behavior of "stainless steel" in acetic solution—influence of chlorides¹⁰.—If 18-8 stainless steel is polarized cathodically or anodically, as indicated above, in a solution of acetic acid and sodium acetate of $\text{pH} 4.9$, strongly stirred and degassed, electrolysis curves shown on the left side of Fig. 7 are obtained. The anodic curve presents only one stable branch which is observed at potentials more positive than the equilibrium potential (+0.94 v) of an oxygen electrode immersed in the solution (reaction $2\text{H}_2\text{O} = \text{O}_2 + 4\text{H}^+ + 4e^-$). As a result, no oxidation is possible in the potential range (below +0.94 v) exhibited by electrically insulated steel. This steel is therefore corrosion resistant under these conditions.

If the same electrode is polarized in the solution obtained

¹⁰ See Reference (16), p. 227.

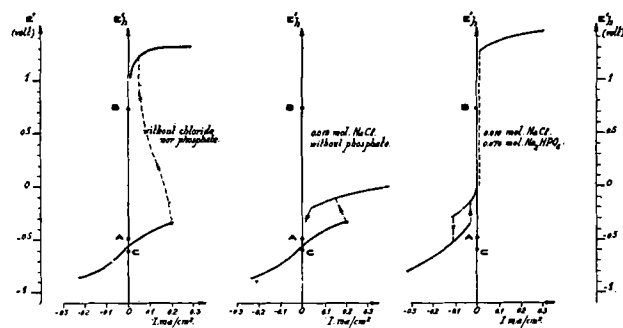


FIG. 9a, 9b, and 9c. Influence of chloride and of phosphate on the behavior of mild steel in a solution of NaHCO_3 , 0.10 molar in absence of oxygen (degassed solution).

by the addition of sodium chloride to the acetic solution above, the anodic polarization curve instead of being located entirely above the equilibrium potential of the oxygen electrode is located below this potential. This indicates an oxidation of the metal and a high corrosion rate. When the polarization curve at increasing current densities is determined, irregularities connected with the local formation and destruction of a film which leads to localized corrosion are observed. Such tests readily show that 18-8 steel, which does not corrode in pure acetate solutions, is strongly corroded by acetate solutions containing chlorides.

Action of chloride on the corrosion of iron and remedy for this action.—In collaboration with Feron, the author investigated, by means of the above-mentioned method, the influence of chlorides on the electrochemical behavior of mild steel in degassed solutions 0.10M of sodium bicarbonate (18). Results obtained are shown on Fig. 8.

In the absence of chloride, the anodic polarization curve shows two stable branches represented in Fig. 8a. One of these branches, in the range of potentials between the equilibrium potential of the metal C (about -0.60 v), and its passivation potential, P (-0.35 v), corresponds to the corrosion of the metal. The other branch, at potentials above the equilibrium potential of the oxygen electrode, B (+0.72 v), corresponds to the evolution of oxygen without corrosion. Corrosion of the metal is, therefore, possible only between -0.60 v (C) and -0.35 v (P); below -0.60 v, the metal is cathodically protected; above -0.35 v the metal is protected by passivation.

Incorporation of increasing quantities of chloride in the solution (Fig. 8b and 8c) does not modify the circumstances of cathodic protection nor the value of the passivation potential P, but the result is that it permits the flow of more and more current between the passivation potential P and the potential of the oxygen electrode B. This is related to the appearance of strong local corrosive attack.

Consequently, it is among the anions likely to stabilize the protective oxide film with the formation of slightly soluble ferric salt that a remedy for the activity of chlorides may be discovered. Furthermore, the effectiveness of this remedy will be such that all current between potentials P and B will be suppressed and that the type of anodic polarization curve existing in the absence of chloride (Fig. 8a) is again observed. This remedy will be completely effective if it enables one to obtain polarization curves similar to those in Fig. 7a, i.e., oxidation curve which presents only one branch located entirely above the potential B of the oxygen electrode. In this case, no corrosion is possible and the remedy is perfect.

Preliminary experiments were carried out on the effect of the addition of increasing quantities of disodium phosphate

in degassed solutions of 0.10M sodium bicarbonate and 0.010M sodium chloride. It was observed that, for additions at least 0.07M in Na_2HPO_4 , the anodic polarization curve corresponds to the above condition (Fig. 9c). All corrosion is avoided, at least by potentials above the passivation potential P (-0.35 v).

Consider the fact that cathodic polarization of iron in such solutions reveals an activation of the metal below the passivation potential. It seems, therefore, that even in the absence of phosphate (19) the protective oxide film is dissolved by reduction at such potentials. It has not yet been determined whether phosphate also protects the metal in these reducing conditions and it is possible that danger of corrosion exists under these conditions. In the present state of these studies, it seems that, in order to protect iron and unalloyed steels completely by passivation in the presence of chloride solutions, it is necessary to use mixed inhibitors containing a substance like phosphate which prevents all oxidation current at potential higher than the passivation potential, and an oxidant (chromate, nitrite, etc.) preventing the existence of potentials below the passivation potential.

Since chlorides do not modify the potential at which iron is protected cathodically, cathodic protection of iron and ordinary steel is possible in the presence of, as well as in the absence of, chloride, provided that in both cases the potential be decreased below a well-defined value (-0.60 v for pH below 10).

Prevention of Localized Corrosion

One important question concerning the protection of iron and nonalloyed steel remains unsolved, that is, how to avoid localized corrosion due to chlorides and to unsafe inhibitors (pitting).

This pitting seems to be caused in the majority of cases by phenomena of differential oxidation which, as Evans has shown in the case of oxygen, result in local currents between cathodes (where the potential is higher than the passivation potential and at which the oxidizing agent is reduced) and anodes (where the potential is below the passivation potential and at which the metal corrodes).

Two groups of remedies are possible for this type of corrosion. Cathodic protection can be applied by bringing the potential of all parts of the surface below -0.60 v (for pH below 10); or mixed inhibitors can be used, for instance, the mixture of phosphate and oxidant mentioned above, which prevents any oxidation of the metal below the equilibrium potential of the oxygen electrode. Systematic researches concerning the determination and thermodynamic interpretation of polarization curves are likely to lead to a satisfactory solution of this problem.

REFERENCES

1. M. POURBAIX, Mechanism of Electrochemical Oxidation, 8th Congress, Inst. Intern. chim. Solvay, Brussels, September 1950, Stoops, Brussels (1951).
2. F. HABER, Z. Elektrochem., **4**, 506 (1898).
3. F. HABER, Z. physik. Chem., **32**, 193, 270 (1900).
4. M. POURBAIX, Thermodynamics of Dilute Aqueous Solutions; Graphic Representation of Role of pH and Potential, (Delft Thesis 1945), Preface by F. E. C. Scheffer, Beranger, Paris-Liege (1946); English translation by J. N. Agar, preface by U. R. Evans, Arnold, London (1949).
5. TH. DE DONDER AND P. VAN RYSSELBERGHE, "Affinity," Gauthier Villars, Paris (1936); also, Stanford University Press, Stanford, Calif. (1936).
6. M. POURBAIX, Corrosion, **6**, 395 (1950).
7. E. LANGE AND K. NAGEL, Z. physik. Chem., **A181**, 19 (1937).
8. P. VAN RYSSELBERGHE, Proc. Intern. Comm. Electrochem. Thermodynam. and Kinet., CITCE Milan, September 1950, p. 392, Tamburini, Milan (1951).
9. U. R. EVANS, "Metallic Corrosion, Passivity and Protection," Arnold, London (1946).
10. C. WAGNER AND W. TRAUD, Z. Elektrochem., **44**, 391 (1938).
11. M. POURBAIX, Metaux & Corrosion, **17**, 189 (1938); Contribution to the Study of the Corrosion of Iron, Thesis, Brussels, 1945; Chim. peintures, **8**, 262 (1945); Rev. Ecole Polytech. Univ. Brussels, **25**, 143 (1945); *ibid.*, **26**, 40 (1946); Metaux & Corrosion, **21**, 121 (1946); Bull. Techn. Assoc. Ing. Brussels, 167 (1946); *ibid.*, 109 (1947); Corrosion, Passivity and Passivation of Iron; Influence of pH and Potential, and Speed and Manner of Corrosion of Iron; Influence of pH, Chlorides and Chromates, Mem. Soc. Roy. Belge Ing. Ind., March 1951.
12. K. F. BONHOEFFER, Z. Elektrochem., **55**, 151 (1951).
13. T. P. HOAR, Proc. Roy. Soc., London, **A142**, 642 (1933).
14. F. P. BOWDEN AND J. N. AGAR, Ann. Repts. on Progr. Chem., **35**, 90 (1938).
15. M. POURBAIX, Inhibition, Passivity and Passivation, Proc., 3rd meeting, Intern. Comm. Electrochem. Thermodynam. Kinet., CITCE Bern, August 1951, p. 464, Manfredi, Milan.
16. M. POURBAIX AND P. VAN RYSSELBERGHE, Comments on Corrosion and Passivation of Metals, Proc., 2nd meeting, Intern. Comm. Electrochem. Thermodynam. Kinet., CITCE Milan, September 1950, p. 219, Tamburini, Milan (1951).
17. M. POURBAIX AND P. VAN RYSSELBERGHE, Corrosion, **6**, 313 (1950).
18. M. POURBAIX AND J. FERON, Passivation of Iron in the Presence of Chlorides, Proc., 3rd meeting, Intern. Comm. Electrochem. Thermodynam. Kinet., CITCE Bern, August 1951, p. 135, Manfredi, Milan.
19. M. POURBAIX AND J. FERON, Passivation and Activation Potentials of Iron; Cathodic Corrosion of Iron in the Presence of Oxygen, *ibid.*, p. 128.